# INTRUMENTAL ANALYSIS



*David Harvey*
DePauw University

LibreTexts™

# Instrumental Analysis

David Harvey

DePauw University

This text is disseminated via the Open Education Resource (OER) LibreTexts Project (https://LibreTexts.org) and like the thousands of other texts available within this powerful platform, it is freely available for reading, printing, and "consuming."

The LibreTexts mission is to bring together students, faculty, and scholars in a collaborative effort to provide an accessible, and comprehensive platform that empowers our community to develop, curate, adapt, and adopt openly licensed resources and technologies; through these efforts we can reduce the financial burden born from traditional educational resource costs, ensuring education is more accessible for students and communities worldwide.

Most, but not all, pages in the library have licenses that may allow individuals to make changes, save, and print this book. Carefully consult the applicable license(s) before pursuing such effects. Instructors can adopt existing LibreTexts texts or Remix them to quickly build course-specific resources to meet the needs of their students. Unlike traditional textbooks, LibreTexts' web based origins allow powerful integration of advanced features and new technologies to support learning.




LibreTexts is the adaptable, user-friendly non-profit open education resource platform that educators trust for creating, customizing, and sharing accessible, interactive textbooks, adaptive homework, and ancillary materials. We collaborate with individuals and organizations to champion open education initiatives, support institutional publishing programs, drive curriculum development projects, and more.

The LibreTexts libraries are Powered by NICE CXone Expert and was supported by the Department of Education Open Textbook Pilot Project, the California Education Learning Lab, the UC Davis Office of the Provost, the UC Davis Library, the California State University Affordable Learning Solutions Program, and Merlot. This material is based upon work supported by the National Science Foundation under Grant No. 1246120, 1525057, and 1413739.

Any opinions, findings, and conclusions or recommendations expressed in this material are those of the author(s) and do not necessarily reflect the views of the National Science Foundation nor the US Department of Education.

Have questions or comments? For information about adoptions or adaptions contact info@LibreTexts.org or visit our main website at https://LibreTexts.org.

This text was compiled on 05/09/2026

# TABLE OF CONTENTS


Licensing

About the Author

## 1: Introduction

- 1.1: Classification of Analytical Methods
- 1.2: Types of Instrumental Methods
- 1.3: Instruments For Analysis
- 1.4: Selecting an Analytical Method
- 1.5: Calibration of Instrumental Methods

## 2: Electrical Components and Circuits

- 2.1: Basic Terminology and Laws of Electricity
- 2.2: Direct Current (DC) Circuits
- 2.3: Alternating Current Circuits
- 2.4: Semiconductors

## 3: Operational Amplifiers

- 3.1: Operational Amplifiers
- 3.2: Operational Amplifier Circuits
- 3.3: Amplification and Measurement of Signals
- 3.4: Mathematical Operations Using Operational Amplifiers

## 4: Analog and Digital Data

- 4.1: Analog and Digital Data
- 4.2: Working With Binary Numbers
- 4.3: Cleaning Up Signals and Counting Events

## 5: Signals and Noise

- 5.1: The Signal-to-Noise Ratio
- 5.2: Sources of Instrumental Noise
- 5.3: Signal-to-Noise Enhancement

## 6: An Introduction to Spectrophotometric Methods

- 6.1: General Properties of Electromagnetic Radiation
- 6.2: Wave Properties of Electromagnetic Radiation
- 6.3: Quantum Mechanical Properties of Electromagnetic Radiation
- 6.4: Emission and Absorbance Spectra
- 6.5: Quantitative Considerations

## 7: Components of Optical Instruments

- 7.1: General Design of Optical Instruments
- 7.2: Sources of Radiation

- 7.3: Wavelength Selectors
- 7.4: Sample Containers
- 7.5: Radiation Transducers
- 7.6: Fiber Optics
- 7.7: Fourier Transform Optical Spectroscopy

## 8: An Introduction to Optical Atomic Spectroscopy

- 8.1: Optical Atomic Spectra
- 8.2: Atomization Methods
- 8.3: Sample Introduction Methods

## 9: Atomic Absorption Spectrometry

- 9.1: Sample Atomization Techniques
- 9.2: Atomic Absorption Instrumentation
- 9.3: Interferences in Absorption Spectroscopy
- 9.4: Atomic Absorption Techniques

## 10: Atomic Emission Spectrometry

- 10.1: Emission Spectroscopy Based on Flame and Plasma Sources
- 10.2: Emission Spectroscopy Based on Arc and Spark Sources

## 11: Atomic Mass Spectrometry

- 11.1: General Features of Atomic Mass Spectrometry
- 11.2: Mass Spectrometers
- 11.3: Inductively Coupled Plasma Mass Spectrometer
- 11.4: Other Forms of Atomic Mass Spectrometry

## 12: Atomic X-Ray Spectrometry

- 12.1: Fundamental Principles
- 12.2: Instrument Components
- 12.3: Atomic X-Ray Fluorescence Methods
- 12.4: Other X-Ray Methods

## 13: Introduction to Ultraviolet/Visible Absorption Spectrometry

- 13.1: Transmittance and Absorbance
- 13.2: Beer's Law
- 13.3: Effect of Noise on Transmittance and Absorbance Measurements
- 13.4: Instrumentation

## 14: Applications of Ultraviolet/Visible Molecular Absorption Spectrometry

- 14.1: What is Molar Absorptivity?
- 14.2: Absorbing Species
- 14.3: Qualitative and Characterization Applications
- 14.4: Quantitative Applications
- 14.5: Photometric Titrations

## 15: Molecular Luminescence

- 15.1: Theory of Fluorescence and Phosphorescence
- 15.2: Instruments for Measuring Fluorescence and Phosphorescence
- 15.3: Applications and Photoluminescence methods
- 15.4: Chemiluminscence
- 15.5: Evaluation of Molecular Luminescence

## 16: An Introduction to Infrared Spectrometry

- 16.1: Theory of Infrared Absorption Spectrometry
- 16.2: Infrared Sources and Transducers
- 16.3: Infrared Instruments

## 17: Applications of Infrared Spectrometry

- 17.1: Mid-Infrared Absorption Spectometry
- 17.2: Mid-Infrared Reflection Spectrometry
- 17.3: Near-Infrared and Far-Infrared Spectroscopy

## 18: Raman Spectroscopy

- 18.1: Theory of Raman Spectroscopy
- 18.2: Instrumentation
- 18.3: Applications of Raman Spectroscopy
- 18.4: Other Types of Raman Spectroscopy

## 19: Nuclear Magnetic Resonance Spectroscopy

- 19.1: Theory of Nuclear Magnetic Resonance
- 19.2: Environmental Effects on NMR Spectra
- 19.3: NMR Spectrometers
- 19.4: Applications of Proton NMR
- 19.5: Carbon-13 NMR
- 19.6: Two-Dimensional Fourier Transform NMR

## 20: Molecular Mass Spectrometry

- 20.1: Molecular Mass Spectra
- 20.2: Ion Sources
- 20.3: Mass Spectrometers
- 20.4: Applications of Molecular Mass Spectrometry

## 21: Surface Characterization by Spectroscopy and Microscopy

- 21.1: Introduction to the Study of Surfaces
- 21.2: Spectroscopic Surface Methods
- 21.3: Scanning Electron Microscopy
- 21.4: Scanning Probe Microscopes

## 22: An Introduction to Electroanalytical Chemistry

- 22.1: Electrochemical Cells
- 22.2: Potentials in Electroanalytical Cells

- 22.3: Electrode Potentials
- 22.4: Calculation of Cell Potentials from Electrode Potentials
- 22.5: Currents in Electrochemical Cells
- 22.6: Types of Electroanalytical Methods

## 23: Potentiometry

- 23.1: Reference Electrodes
- 23.2: Metallic Indicator Electrodes
- 23.3: Membrane Ion-Selective Electrodes
- 23.4: Molecular-Selective Electrode Systems
- 23.5: Instruments for Measuring Cell Potentials
- 23.6: Quantitative Potentiometry

## 24: Coulometry

- 24.1: Introduction to Coulometry
- 24.2: Controlled-Potential Coulometry
- 24.3: Controlled-Current Coulometry

## 25: Voltammetry

- 25.1: Potential Excitation Signals and Currents in Voltammetry
- 25.2: Voltammetric Instrumentation
- 25.3: Linear Sweep Voltammetry
- 25.4: Cyclic Voltammetry
- 25.5: Polarography
- 25.6: Stripping Methods
- 25.7: Applications of Voltammetry

## 26: Introduction to Chromatographic Separations

- 26.1: A General Description of Chromatography
- 26.2: Migration Rates of Solutes
- 26.3: Zone Broadening and Column Efficiency
- 26.4: Optimization and Column Performance
- 26.5: Summary of Important Relationships for Chromatography
- 26.6: Applications of Chromatography

## 27: Gas Chromatography

- 27.1: Principles of Gas Chromatography
- 27.2: Instruments for Gas Chromatography
- 27.3: Gas Chromatographic Columns and Stationary Phases
- 27.4: Applications of Gas Chromatography

## 28: High-Performance Liquid Chromatography

- 28.1: Scope of HPLC
- 28.2: Column Efficiency in Liquid Chromatography
- 28.3: Instruments for Liquid Chromatography
- 28.4: Partition Chromatography
- 28.5: Adsorption Chromatography

- 28.6: Ion-Exchange Chromatography
- 28.7: Size-Exclusion Chromatography

## 29: Supercritical Fluid Chromatography

- 29.1: Properties of Supercritical Fluids
- 29.2: Supercritical Fluid Chromatography

## 30: Capillary Electrophoresis and Capillary Electrochromatography

- 30.1: An Overview of Electrophoresis
- 30.2: Capillary Electrophoresis
- 30.3: Applications of Capillary Electrophoresis

## 31: Thermal Methods

- 31.1: Thermogravimetry
- 31.2: Differential Thermal Analysis and Differential Scanning Calorimetry

## 32: Radiochemical Methods

- 32.1: Radioactive Isotopes
- 32.2: Instrumentation
- 32.3: Neutron Activation Methods
- 32.4: Isotope Dilution Methods

## 33: Automated Methods of Analysis

- 33.1: Overview of Automated Methods of Analysis
- 33.2: Flow-Injection Analysis
- 33.3: Other Automated Methods of Analysis

## 34: Particle Size Determination

- 34.1: Overview
- 34.2: Measuring Particle Size Using Sieves
- 34.3: Measuring Particle Size by Sedimentation
- 34.4: Measuring Particle Size Using Image Analysis
- 34.5: Measuring Particle Size Using Light Scattering

## 35: Appendicies

- 35.1: Evaluation of Analytical Data
- 35.2: Single-Sided Normal Distribution
- 35.3: Critical Values for t-Test
- 35.4: Critical Values for F-Test
- 35.5: Critical Values for Dixon's Q-Test
- 35.6: Critical Values for Grubb's Test
- 35.7: Activity Coefficients
- 35.8: Standard Reduction Potentials & Polarographic Half-wave Potentials
- 35.9: Recommended Primary Standards
- 35.10: Acronyms and Abbreviations

Index

Glossary

Detailed Licensing

# Licensing

*A detailed breakdown of this resource's licensing can be found in **Back Matter/Detailed Licensing**.*

## About the Author

**David Harvey**, professor of chemistry and biochemistry at DePauw University, is the recipient of the 2016 American Chemical Society Division of Analytical Chemistry J. Calvin Giddings Award for Excellence in Education. The national award recognizes a scientist who has enhanced the professional development of analytical chemistry students, developed and published innovative experiments, designed and improved equipment or teaching labs and published influential textbooks or significant articles on teaching analytical chemistry.



# CHAPTER OVERVIEW

## 1: Introduction

Analytical chemistry is the science of how to make good measurements that we can use to solve a chemical problem. Many problems in analytical chemistry begin with the need to identify what is present in a sample. This is the scope of a qualitative analysis, examples of which include identifying the products of a chemical reaction, screening an athlete's urine for a performance-enhancing drug, or determining the spatial distribution of Pb on the surface of an airborne particulate. An early challenge for analytical chemists was developing simple chemical tests to identify inorganic ions and organic functional groups. The classical laboratory courses in inorganic and organic qualitative analysis, still taught at some schools, are based on this work.

Perhaps the most common analytical problem is a quantitative analysis, examples of which include the elemental analysis of a newly synthesized compound, measuring the concentration of glucose in blood, or determining the difference between the bulk and the surface concentrations of Cr in steel. Much of the analytical work in clinical, pharmaceutical, environmental, and industrial labs involves developing new quantitative methods to detect trace amounts of chemical species in complex samples. Most of the examples in this text are of quantitative analyses.

Another important area of analytical chemistry, which receives more limited attention in this text, are methods for characterizing physical and chemical properties. The determination of chemical structure, particle size, and surface structure are examples of a characterization analysis.

The purpose of a qualitative, a quantitative, or a characterization analysis is to solve a problem associated with a particular sample. The purpose of a fundamental analysis, on the other hand, is to improve our understanding of the theory that supports an analytical method and to understand better an analytical method's limitations.

Like all areas of chemistry, analytical chemistry is so broad in scope and so much in flux that it is difficult to find a simple definition more revealing than this quote attributed to C. N. Reilly (1925-1981), who was a professor of chemistry at the University of North Carolina at Chapel Hill and one of the most influential analytical chemists of the last half of the twentieth century:

"*Analytical chemistry is what analytical chemists do*."

In this chapter we expand upon this simple definition by introducing approaches to making analytical measurements and by developing a shared language for discussing analytical chemistry, more generally, and instrumentation, more specifically.


1.1: Classification of Analytical Methods

1.2: Types of Instrumental Methods

1.3: Instruments For Analysis

1.4: Selecting an Analytical Method

1.5: Calibration of Instrumental Methods



This page titled 1: Introduction is shared under a CC BY-NC-SA 4.0 license and was authored, remixed, and/or curated by David Harvey.

# 1.1: Classification of Analytical Methods

Analytical chemistry has a long history. On the bookshelf of my office, for example, there is a copy of the first American edition of Fresenius's *A System of Instruction in Quantitative Chemical Analysis*, which was published by John Wiley & Sons in 1886. Nearby are many newer texts, such as Bard and Faulkner's *Electrochemical Methods: Fundamentals and Applications*, the most recent edition of which was published by Wiley in 2000. In 883 pages, Fresnius's text covers essentially all that was known in the 1880s about analytical chemistry and what we now call classical methods of analysis. Bard and Faulkner's text, which is 864 pages, covers just one category of what we now call modern instrumental methods of analysis. Whether a classical method of analysis or a modern instrumental method analysis, the species of interest, which we call the analyte, is probed in a way that provides qualitative or quantitative information.

## Classical Methods of Analysis

The distinguishing feature of a classical method of analysis is that the principal measurements are observations of reactions (Did a precipitate form? Did the solution change color?) or the measurement of one of a small number of physical properties, such as mass or volume. Because these measurements are not selective for a single analyte, a classical method of analysis usually required extensive work to isolate the analyte of interest from other species that would interfere in the analysis. As we see in Figure 1.1.1, Fresenius's method for determining the amount of nickel in ores required 58 hours, most of which was spent bringing the ore into solution and then isolating the analyte from interferents by a sequence of precipitations and filtrations. The final determination of the amount of nickel in the ore was derived from two measurements of mass: the combined mass of Co and Ni, and the mass of Co. Although of historic interest, we will not consider further classical methods of analysis in this text.

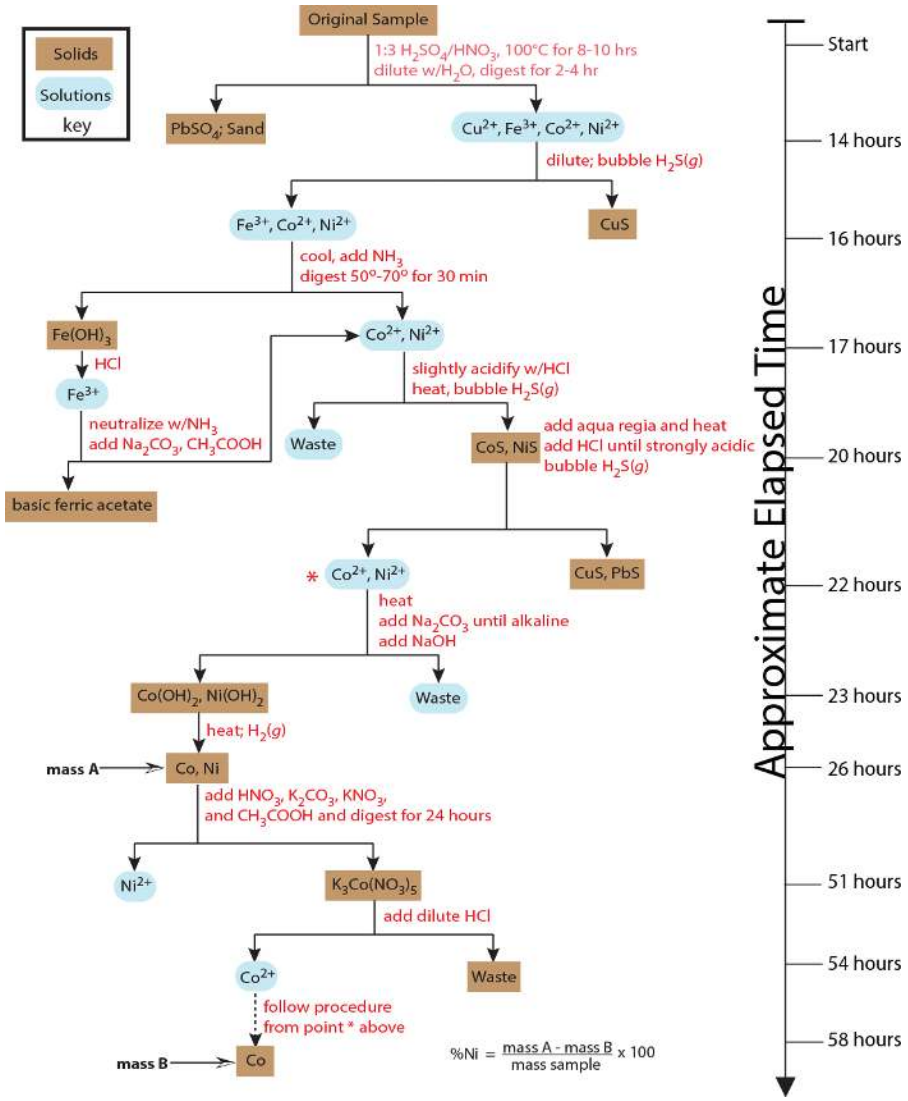



Figure 1.1.1: Fresenius' analytical scheme for the gravimetric analysis of Ni in ores. After each step, the solid and the solution are separated by gravity filtration. Note that the mass of nickel is not determined directly. Instead, Co and Ni first are isolated and weighed together (**mass A**), and then Co is isolated and weighed separately (**mass B**). The timeline shows that it takes approximately 58 hours to analyze a single sample; although several sample could be prepared in parallel, the throughput of samples was limited to just a few per day.

## Modern Instrumental Methods of Analysis

The distinguishing feature of modern instrumental methods of analysis is that it extends measurements to many more physical properties, such as current, potential, the absorption or emission of light, and mass-to-charge ratios, to name a few. Instrumental methods for separating analytes, such as chromatographic separations, and instrumental methods that allow for the simultaneous analysis of multiple analytes make for a much more rapid analysis. By the 1970s, flame atomic absorption spectrometry (FAAS) replaced gravimetry as the standard method for analyzing nickel in ores [see, for example, Van Loon, J. C. *Analytical Atomic Absorption Spectroscopy*, Academic Press: New York, 1980]. Because FAAS is much more selective than precipitation, there is less need to chemically isolate the analyte; as a result, the time to analyze a single sample decreased to a few hours and the throughput of samples increased to hundreds per day.

This page titled 1.1: Classification of Analytical Methods is shared under a CC BY-NC-SA 4.0 license and was authored, remixed, and/or curated by David Harvey.

# 1.2: Types of Instrumental Methods

It is useful to organize instrumental methods of analysis into several groups based on the chemical or physical properties that we use to generate a signal that we can measure and relate to the analyte of interest to us. One group of instrumental methods is based on the interaction of photons of electromagnetic radiation with matter, which we call collectively spectroscopy. We can divide spectroscopy into two broad classes of techniques. In one class of techniques there is a transfer of energy between the photon and the sample. Table 1.2.1 provides a list of several representative examples.

Table 1.2.1. Examples of Spectroscopic Instrumental Methods That Involve an Exchange of Energy Between a Photon and the Sample

| type of energy transfer | region of electromagnetic spectrum | spectroscopic technique |
|---|---|---|
| absorption | $\gamma$-ray | Mossbauer spectroscopy |
| | X-ray | X-ray absorption spectroscopy |
| | UV/Vis | UV/Vis spectroscopy |
| | IR | infrared spectroscopy |
| | microwave | raman spectroscopy |
| | radio wave | electron spin resonance<br>nuclear magnetic resonance |
| emission (thermal excitation) | UV/Vis | atomic emission spectroscopy |
| photoluminescence | X-ray | X-ray fluorescence |
| | UV/Vis | fluorescence spectroscopy<br>phosphorescence spectroscopy<br>atomic fluorescence spectroscopy |
| chemiluminescence | UV/Vis | chemiluminescence spectroscopy |

In the second broad class of spectroscopic techniques, the electromagnetic radiation undergoes a change in amplitude, phase angle, polarization, or direction of propagation as a result of its refraction, reflection, scattering, diffraction, or dispersion by the sample. Several representative spectroscopic techniques are listed in Table 1.2.2.

Table 1.2.2. Examples of Other Spectroscopic Instrumental Methods

| region of electromagnetic spectrum | type of interaction | spectroscopic technique |
|---|---|---|
| X-ray | diffraction | X-ray diffraction |
| UV/Vis | refraction | refractrometry |
| | scattering | nephelometry<br>turbidimetry |
| | dispersion | optical rotary dispersion |

A second group of instrumental methods is based on the measurement of current, charge, or potential at the surface of an electrode, sometimes while controlling one or both of the other two variables, and sometime while stirring the solution. Figure 1.2.1 provides a visual introduction to these methods.

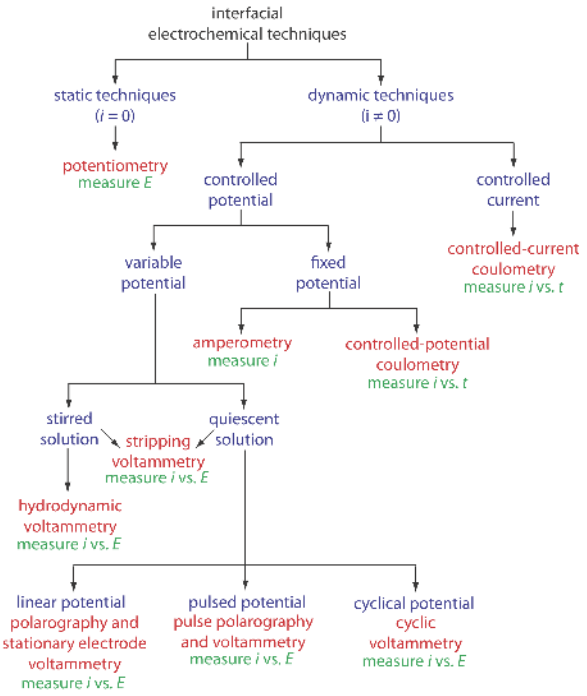



Figure 1.2.1 Family tree that highlights the similarities and differences between a number of interfacial electrochemical techniques. The specific instrumental methods are shown in red, the experimental conditions are shown in blue, and the analytical signals are shown in green.

Our third group of instrumental methods gathers together a variety of other measurements that can provide a useful analytical signal; these are summarized in Table 1.2.3.

Table 1.2.3. Additional Examples of Instrumental Methods of Analysis

| type of measurement or phenomenon | instrumental method |
|---|---|
| piezoelectric effect | quartz crystal microbalance |
| mass-to-charge ratio | mass spectrometry |
| rate of chemical reaction or physical process | kinetic methods<br>flow injection analysis<br>neutron activation analysis<br>isotope diution analysis |
| thermal energy | thermal gravimetry<br>differential thermal analysis<br>differential scanning calorimetry |

Our last group of instrumental methods are used to separate mixtures based on either the equilibrium partitioning of species between two phases or the migration of species in response to an applied electrical field. These methods usally are paired with a suitable instrumental method from Table 1.2.1, Table 1.2.2, Table 1.2.3, or Figure 1.2.1 to provide a way to follow the separation.

Table 1.2.4. Examples of Instrumental Methods for Separating Mixtures.

| basis of separation | instrumental method |
|---|---|
| equilibrium partitioning between two phases | gas chromatography<br>liquid chromatography<br>supercritical fluid chromatography |
| migration in response to applied electrical field | electrophoresis |

This page titled 1.2: Types of Instrumental Methods is shared under a CC BY-NC-SA 4.0 license and was authored, remixed, and/or curated by David Harvey.

# 1.3: Instruments For Analysis

An early example of a colorimetric analysis is Nessler's method for ammonia, which was introduced in 1856. Nessler found that adding an alkaline solution of $HgI_2$ and KI to a dilute solution of ammonia produced a yellow-to-reddish brown colloid in which the colloid's color depended on the concentration of ammonia. In addition to the sample, Nessler prepared a series of standard solutions, each containing a known amount of ammonia, and placed each in a glass tube with a flat bottom. Allowing sunlight to pass through the tubes from bottom-to-top, Nessler observed them from above, as seen in Figure 1.3.1. By visually comparing the color of the sample to the colors of the standards, Nessler was able to estimate the concentration of ammonia in the sample.

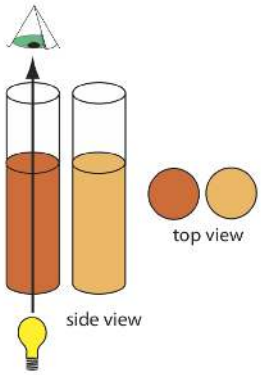



Figure 1.3.1. Nessler's original method for comparing the color of two solutions. Natural sunlight passes upwards through the samples and standards and the analyst views the solutions by looking down toward the light source. The top view, shown on the right, is what the analyst sees. To estimate the analyte's concentration, the analyst exchanges standards until the sample's color falls between the color of two standards.

Nessler's method converts a sample's chemical and/or physical properties—the color that forms when $NH_3$ reacts with $HgI_2$ and KI—into a signal that we can detect, process, and report as a relative measure of the amount of $NH_3$ in the sample. Although we might not think of a Nessler tube as an instrument, the process of probing a sample in a way that converts its chemical or physical properties into a form of information that we can report is the essence of any instrument.

The basic components of an instrument include a probe that interacts with the sample, an input transducer that converts the sample's chemical and/or physical properties into an electrical signal, a signal processor that converts the electrical signal into a form that an output transducer can convert into a numerical or visual output that we can understand. We can represent this as a sequence of actions that take place within the instrument

$$\text{probe} \rightarrow \text{sample} \rightarrow \text{input transducer} \rightarrow \text{raw data} \rightarrow \text{signal processor} \rightarrow \text{output transducer}$$

and as a general flow of information

$$\text{chemical and/or physical information} \rightarrow \text{electrical information} \rightarrow \text{numerical or visual response}$$

In Nessler's method, the probe is sunlight, the analyst's eye is the input transducer, the raw data is the response of the eye's optic nerve to the attenuation of light, the signal processor is the brain, and the output is a visual report of the sample's color relative to the standards.

$$\text{sunlight} \rightarrow \text{sample} \rightarrow \text{eye} \rightarrow \text{response of optic nerve} \rightarrow \text{brain} \rightarrow \text{visual report of color}$$

## Ways to Encode Information

As suggested above, information is encoded in two broad ways: as electrical information (such as currents and potentials) and as information in other, non-electrical forms (such as chemical and physical properties).

## Non-electrical Information

Nessler's method begins and ends with non-electrical forms of information: the sample has a color and we use that color to report that the concentration of $NH_3$ in our sample is greater than 0.50 mg/L and less than 1.00 mg/L. Other non-electrical ways to encode information are the observation that a precipitate forms when we add $Ag^+$ to a solution of NaCl, the balance beam scale that my

doctor uses to measure my weight, the percentage of light that passes through a sample, and the volume and moles of $Cu(NO_3)_2$ in a graduated cylinder.

## Electrical Information

Although my doctor's balance beam scale encodes my mass by the position of two movable weights along a signal arm–a decidedly non-electrical means of encoding information—the electronic analytical balance that is found in almost all chemistry labs encodes the mass in the form of electrical information (Figure 1.3.1). An electromagnet levitates the sample pan above a permanent cylindrical magnet. When we place an object on the sample pan, it displaces the sample pan downward by a force equal to the product of the sample's mass and its acceleration due to gravity. The balance detects this downward movement and generates a counterbalancing force by increasing the current to the electromagnet. The current needed to return the balance to its original position is proportional to the object's mass.



Figure 1.3.1: The photo shows a typical electronic balance capable of determining mass to the nearest ±0.1 mg. The sticker inside the balance's wind shield is its annual calibration certification. For a review of other types of electronic balances, see Schoonover, R. M. *Anal. Chem.* **1982**, *54*, 973A-980A.

Although we tend to use interchangeably, the terms "weight" and "mass," there is an important distinction between them. Mass is the absolute amount of matter in an object, measured in grams. Weight, *W*, is a measure of the gravitational force, *g*, acting on that mass, *m*:

$$W = m \times g$$

An object has a fixed mass but its weight depends upon the acceleration due to gravity, which varies subtly from location-to-location.

A balance measures an object's weight, not its mass. Because weight and mass are proportional to each other, we can calibrate a balance using a standard weight whose mass is traceable to the standard prototype for the kilogram. A properly calibrated balance gives an accurate value for an object's mass.

Electrical information comes in three domains: analog, time, and digital. In the analog domain, the signal shows the amplitude of the electrical signal—say current or potential—as a function of an independent variable, which might be wavelength when recording a spectrum, applied potential in a cyclic voltammetry experiment, or time when separating a mixture by gas chromatography. A time domain signal shows the frequency with which the electrical signal rises above or below a threshold value, as when counting the rate at which ionizing radiation, such as alpha or beta particles, are detected by a Geiger counter. Finally, in the digital domain, the signal is a count of discrete events, such as counting the number of drops dispensed by an autotitrator by allowing the drops to disrupt a beam of light.

## Input Transducers, Detectors, and Sensors

As defined above, a transducer is a device that converts information from a non-electrical form to an electrical form (the input transducer) or from an electrical form to a non-electrical form (the output transducer). Detector is a much broader term that includes all aspects of the instrument from the input transducer to the output transducer; thus, a visible spectrometer is a detector that uses an input transducer to convert the attenuation of the source radiation to a reported absorbance. A sensor is a detector designed to monitor a particular analyte, such as a pH electrode.

# Output Transducers and Readout Devices

An instrument's output transducer converts the information carried in electrical form into a non-electrical form that we can understand. Common examples of output transducers, or readout devices, are a simple meter, a digital display, a physical trace of the signal as a function of a dependent variable, such as a spectrum or a chromatogram, or a photographic plate.

## Computers in Instruments

Many instruments include a computer that provides us with the ability to control the instrument and, perhaps of greater importance, to process the data both by modifying the electrical signal as it passes from the input transducer to the output transducer, and by providing tools for processing the data after it leaves the output transducer.

---

This page titled 1.3: Instruments For Analysis is shared under a CC BY-NC-SA 4.0 license and was authored, remixed, and/or curated by David Harvey.

# 1.4: Selecting an Analytical Method

The analysis of a sample generates a chemical or a physical signal that is proportional to the amount of analyte in the sample. This signal may be anything we can measure, such the examples described in Section 1.2. It is convenient to divide analytical techniques into two general classes based on whether the signal is directly proportional to the mass or moles of analyte, or is directly proportional to the analyte's concentration.

Consider the two graduated cylinders in Figure 1.4.1, each of which contains a solution of 0.010 M $Cu(NO_3)_2$. The cylinder on the left contains 10 mL, or $1.0 \times 10^{-4}$ moles of $Cu^{2+}$, and the cylinder on the right contains 20 mL, or $2.0 \times 10^{-4}$ moles of $Cu^{2+}$. If a technique responds to the absolute amount of analyte in the sample, then the signal due to the analyte $S_A$ is given as

$$S_A = k_A n_A \tag{1.4.1}$$

where $n_A$ is the moles or grams of analyte in the sample, and $k_A$ is a proportionality constant. Because the cylinder on the right contains twice as many moles of $Cu^{2+}$ as the cylinder on the left, analyzing its contents gives a signal twice as large as that for the other cylinder.



Figure 1.4.1: Two graduated cylinders, each containing 0.10 M $Cu(NO_3)_2$. Although the cylinders contain the same concentration of $Cu^{2+}$, the cylinder on the left contains $1.0 \times 10^{-4}$ mol $Cu^{2+}$ and the cylinder on the right contains $2.0 \times 10^{-4}$ mol $Cu^{2+}$.

A second class of analytical techniques are those that respond to the analyte's concentration, $C_A$

$$S_A = k_A C_A \tag{1.4.2}$$

In this case, an analysis of the contents of the two cylinders gives the same result. As most instruments respond to the analyte's concentration, we will imit ourselves to using Equation 1.4.2 for the remainder of this section.

## Defining the Problem

To select an appropriate analytical method for a particular problem we need to consider our needs and compare them to the strengths and weaknesses of the available analytical methods. If we are screening samples on a production line to determine if an analyte exceeds a threshold so that we can set them aside for a more careful analysis, then we may wish to give more consideration to speed than to accuracy or precision. On the other hand, if we our analyte is part of a complex mixture, then we may wish to give more consideration to analytical methods that provide for greater selectivity. Or, if we expect that our samples will vary substantially in the concentration of analyte, then we may give more consideration to an analytical method for which Equation 1.4.2 applies over a wide range of concentrations.

## Performance Characteristics of Instruments

As suggested above, when we choose an analytical method, we match the its performance characteristics (or figures of merit) to our needs. Some of these characteristics are quantitative (accuracy, precision, sensitivity, detection limit, selectivity, dynamic range, and selectivity) and others are more qualitative (robustness, ruggedness, scale of operation, time, and cost).

### Accuracy

Accuracy, or bias, is a measure of how close the result of an experiment is to the "true" or expected result. We can express accuracy as an absolute error, $e$

$$e = x - \mu$$

where $x$ is the experimental result and $\mu$ is the expected result, or as a percentage relative error, $\%e_r$

$$\%e_r = \frac{x - \mu}{\mu} \times 100$$

A method's accuracy depends on many things, including the signal's source, the value of $k_A$ in Equation 1.4.2, and the ease of handling samples without loss or contamination.

> Because it is unlikely that we know the true result, we can use an expected or accepted result to evaluate accuracy. For example, we might use a standard reference material, which has an accepted value for our analyte, to establish the analytical method's accuracy. You will find a more detailed treatment of accuracy in, including a discussion of sources of errors, in Appendix 1.

### Precision

When we analyze a sample several times, the individual results vary from trial-to-trial. Precision is a measure of this variability. The closer the agreement between individual analyses, the more precise the results. For example, the results shown in the upper half of Figure 1.4.2 for the concentration of potassium in a sample of serum are more precise than those in the lower half of Figure 1.4.2. It is important to understand that precision does not imply accuracy. That the data in the upper half of Figure 1.4.2 are more precise does not mean that the first set of results is more accurate. In fact, neither set of results may be accurate.

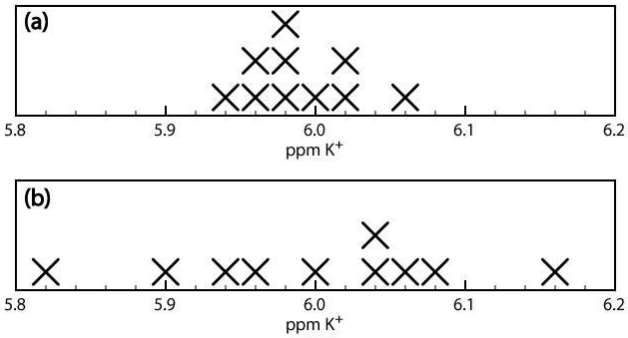



Figure 1.4.2: Two determinations of the concentration of potassium in serum, showing the effect of precision on the distribution of individual results. The data in (a) are less scattered and, therefore, more precise than the data in (b).

A method's precision depends on several factors, including the uncertainty in measuring the signal and the ease of handling samples reproducibly, and is reported as an absolute standard deviation, $s$

$$s = \sqrt{\frac{\sum_{i=1}^{n} (X_i - \overline{X})^2}{n - 1}} \tag{1.4.3}$$

or a relative standard deviation, $s_r$

$$s_r = \frac{s}{\overline{X}} \tag{1.4.4}$$

where $\overline{X}$ is the average, or mean value of the individual measurements.

$$\overline{X} = \frac{\sum_{i=1}^{n} X_i}{n} \tag{1.4.5}$$

> Confusing accuracy and precision is a common mistake. See Ryder, J.; Clark, A. *U. Chem. Ed.* **2002**, *6*, 1–3, and Tomlinson, J.; Dyson, P. J.; Garratt, J. *U. Chem. Ed.* **2001**, *5*, 16–23 for discussions of this and other common misconceptions about the

meaning of error. You will find a more detailed treatment of precision in Appendix 1, including a discussion of sources of errors.

### Sensitivity

The ability to demonstrate that two samples have different amounts of analyte is an essential part of many analyses. A method's sensitivity is a measure of its ability to establish that such a difference is significant. Sensitivity is often confused with a method's detection limit, which is the smallest amount of analyte we can determine with confidence.

See Pardue, H. L. *Clin. Chem.* **1997**, *43*, 1831-1837 for an explanation for why a method's sensitivity is not the same as its detection limit.

Sensitivity is equivalent to the proportionality constant, $k_A$, in Equation 1.4.2 [IUPAC Compendium of Chemical Terminology, Electronic version]. If $\Delta S_A$ is the smallest difference we can measure between two signals, then the smallest detectable difference in the analyte's concentration is

$$\Delta C_A = \frac{\Delta S_A}{k_A}$$

Suppose, for example, that our analytical signal is a measurement for which the smallest detectable increment is ±0.001 (arbitrary units). If our method's sensitivity is $0.200\text{M}^{-1}$, then our method can conceivably detect a difference in concentration of as little as

$$\Delta C_A = \frac{\pm 0.001}{0.200\ \text{M}^{-1}} = \pm 0.005\ \text{M}^{-1}$$

For two methods with the same $\Delta S_A$, the method with the greater sensitivity—that is, the method with the larger $k_A$—is better able to discriminate between smaller amounts of analyte.

### Detection Limit

The International Union of Pure and Applied Chemistry (IUPAC) defines a method's detection limit as the smallest concentration or absolute amount of analyte that has a signal significantly larger than the signal from a suitable blank [IUPAC Compendium of Chemical Technology, Electronic Version]. Although our interest is in the amount of analyte, in this section we will define the detection limit in terms of the analyte's signal. Knowing the signal, we can calculate the analyte's concentration, $C_A$, using Equation 1.4.2, $S_A = k_A C_A$ where $k$ is the method's sensitivity.

Let's translate the IUPAC definition of the detection limit into a mathematical form by letting $S_{mb}$ represent the average signal for a method blank, and letting $\sigma_{mb}$ represent the method blank's standard deviation. To detect the analyte, its signal must exceed $S_{mb}$ by a suitable amount; thus,

$$(S_A)_{DL} = S_{mb} \pm z\sigma_{mb} \tag{1.4.6}$$

where $(S_A)_{DL}$ is the analyte's detection limit.

The value we choose for $z$ depends on our tolerance for reporting the analyte's concentration even if it is absent from the sample (what is called a type 1 error). Typically, $z$ is set to three, which corresponds to a probability, $\alpha$, of 0.00135, or 0.135%. As shown in Figure 1.4.3a, there is only a 0.135% probability of detecting the analyte in a sample that actually is analyte-free.

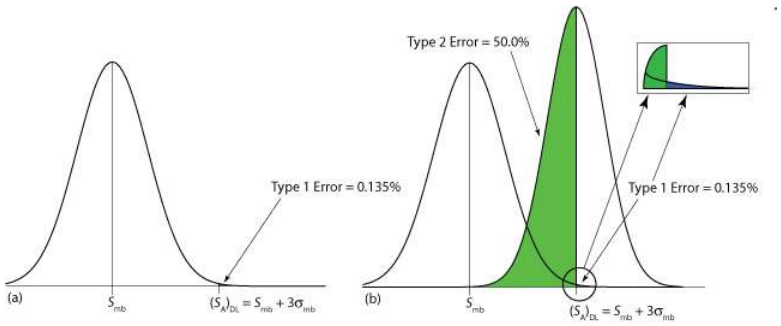



Figure 1.4.3: Normal distribution curves showing the probability of type 1 and type 2 errors for the IUPAC detection limit. (a) The normal distribution curve for the method blank, with $S_{mb}$ = 0 and $\sigma_{mb}$ = 1. The minimum detectable signal for the analyte, $(S_A)_{DL}$, has a type 1 error of 0.135%. (b) The normal distribution curve for the analyte at its detection limit, $(S_A)_{DL}$= 3, is superimposed on the normal distribution curve for the method blank. The standard deviation for the analyte's signal, $\sigma_A$, is 0.8, The area in green represents the probability of a type 2 error, which is 50%. The inset shows, in blue, the probability of a type 1 error, which is 0.135%.

A detection limit also is subject to a type 2 error in which we fail to find evidence for the analyte even though it is present in the sample. Consider, for example, the situation shown in Figure 1.4.3b where the signal for a sample that contains the analyte is exactly equal to $(S_A)_{DL}$. In this case the probability of a type 2 error is 50% because half of the sample's possible signals are below the detection limit. We correctly detect the analyte at the IUPAC detection limit only half the time. The IUPAC definition for the detection limit is the smallest signal for which we can say, at a significance level of $\alpha$, that an analyte is present in the sample; however, failing to detect the analyte does not mean it is not present in the sample.

The detection limit often is represented, particularly when discussing public policy issues, as a distinct line that separates detectable concentrations of analytes from concentrations we cannot detect. This use of a detection limit is incorrect [Rogers, L. B. *J. Chem. Educ.* **1986**, *63*, 3–6]. As suggested by Figure 1.4.3, for an analyte whose concentration is near the detection limit there is a high probability that we will fail to detect the analyte.

An alternative expression for the detection limit, the limit of identification, minimizes both type 1 and type 2 errors [Long, G. L.; Winefordner, J. D. *Anal. Chem.* **1983**, *55*, 712A–724A]. The analyte's signal at the limit of identification, $(S_A)_{LOI}$, includes an additional term, $z\sigma_A$, to account for the distribution of the analyte's signal.

$$(S_A)_{LOI} = (S_A)_{DL} + z\sigma_A = S_{mb} + z\sigma_{mb} + z\sigma_A \tag{1.4.7}$$

As shown in Figure 1.4.4, the limit of identification provides an equal probability of a type 1 and a type 2 error at the detection limit. When the analyte's concentration is at its limit of identification, there is only a 0.135% probability that its signal is indistinguishable from that of the method blank.

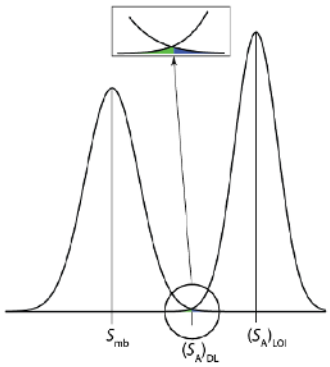


Figure 1.4.4: Normal distribution curves for a method blank and for a sample at the limit of identification: $S_{mb}$ = 0; $\sigma_{mb}$ = 1; $\sigma_A$ = 0.8; and $(S_A)_{LOI}$ = 0 + 3 × 1 + 3 × 0.8 = 5.4. The inset shows that the probability of a type 1 error (0.135%) is the same as the probability of a type 2 error (0.135%).

The ability to detect the analyte with confidence is not the same as the ability to report with confidence its concentration, or to distinguish between its concentration in two samples. For this reason the American Chemical Society's Committee on

Environmental Analytical Chemistry recommends the limit of quantitation, $(S_A)_{LOQ}$ ["Guidelines for Data Acquisition and Data Quality Evaluation in Environmental Chemistry," *Anal. Chem.* **1980**, *52*, 2242–2249 ].

$$(S_A)_{LOQ} = S_{mb} + 10\sigma_{mb} \tag{1.4.8}$$

### Dynamic Range

A method's dynamic range (or linear range) runs from its limit of quantication, (Equation 1.4.8, to the highest concentration for which the sensitivity, $k_A$, remains constant, resulting in a straight-line relationship between $S_A$ and $C_A$. This upper limit is called the limit of linearity, LOL. Between the LOQ and the LOL we can use Equation 1.4.2 to convert a measured signal into the corresponding concentration of the analyte. Above the LOQ the relationship between the signal and the analyte's concentration no longer is a straight-line.

### Selectivity

An analytical method is specific if its signal depends only on the analyte [Persson, B-A; Vessman, J. *Trends Anal. Chem.* **1998**, *17*, 117–119; Persson, B-A; Vessman, J. *Trends Anal. Chem.* **2001**, *20*, 526–532]. Although specificity is the ideal, few analytical methods are free from interferences. When an interferent, *I*, contributes to the signal, we expand 1.4.1 and Equation 1.4.2 to include its contribution to the sample's signal, $S_{samp}$

$$S_{samp} = S_A + S_I = k_A C_A + k_I C_I \tag{1.4.9}$$

where $S_I$ is the interferent's contribution to the signal, $k_I$ is the interferent's sensitivity, and $C_I$ is the concentration of interferent in the sample.

Selectivity is a measure of a method's freedom from interferences [Valcárcel, M.; Gomez-Hens, A.; Rubio, S. *Trends Anal. Chem.* **2001**, *20*, 386–393]. A method's selectivity for an interferent relative to the analyte is defined by a selectivity coefficient, $K_{A,I}$

$$K_{A,I} = \frac{k_I}{k_A} \tag{1.4.10}$$

which may be positive or negative depending on the signs of $k_I$ and $k_A$. The selectivity coefficient is greater than +1 or less than –1 when the method is more selective for the interferent than for the analyte.

> Although $k_A$ and $k_I$ usually are positive, they can be negative. For example, some analytical methods work by measuring the concentration of a species that remains after is reacts with the analyte. As the analyte's concentration increases, the concentration of the species that produces the signal decreases, and the signal becomes smaller. If the signal in the absence of analyte is assigned a value of zero, then the subsequent signals are negative.

Determining the selectivity coefficient's value is easy if we already know the values for $k_A$ and $k_I$. As shown by Example 1.4.1, we also can determine $K_{A,I}$ by measuring $S_{samp}$ in the presence of and in the absence of the interferent.

**Example 1.4.1**

A method for the analysis of $Ca^{2+}$ in water suffers from an interference in the presence of $Zn^{2+}$. When the concentration of $Ca^{2+}$ is 100 times greater than that of $Zn^{2+}$, an analysis for $Ca^{2+}$ has a relative error of +0.5%. What is the selectivity coefficient for this method?

**Solution**

Since only relative concentrations are reported, we can arbitrarily assign absolute concentrations. To make the calculations easy, we will let $C_{Ca}$ = 100 (arbitrary units) and $C_{Zn}$ = 1. A relative error of +0.5% means the signal in the presence of $Zn^{2+}$ is 0.5% greater than the signal in the absence of $Zn^{2+}$. Again, we can assign values to make the calculation easier. If the signal for $Cu^{2+}$ in the absence of $Zn^{2+}$ is 100 (arbitrary units), then the signal in the presence of $Zn^{2+}$ is 100.5.

The value of $k_{Ca}$ is determined using Equation 1.4.2

$$k_{Ca} = \frac{S_{Ca}}{C_{Ca}} = \frac{100}{100} = 1$$

In the presence of $Zn^{2+}$ the signal is given by Equation 1.4.9; thus

$$S_{samp} = 100.5 = k_{\text{Ca}}C_{\text{Ca}} + k_{\text{Zn}}C_{\text{Zn}} = (1 \times 100) + k_{\text{Zn}} \times 1$$

Solving for $k_{\text{Zn}}$ gives its value as 0.5. The selectivity coefficient is

$$K_{\text{Ca,Zn}} = \frac{k_{\text{Zn}}}{k_{\text{Ca}}} = \frac{0.5}{1} = 0.5$$

If you are unsure why, in the above example, the signal in the presence of zinc is 100.5, note that the percentage relative error for this problem is given by

$$\frac{\text{obtained result} - 100}{100} \times 100 = +0.5\%$$

Solving gives an obtained result of 100.5.

A selectivity coefficient provides us with a useful way to evaluate an interferent's potential effect on an analysis. Solving Equation 1.4.10 for $k_I$

$$k_I = K_{A,I} \times k_A \tag{1.4.11}$$

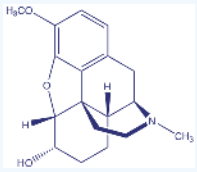
and substituting in Equation 1.4.2 and simplifying gives

$$S_{samp} = k_A\{C_A + K_{A,I} \times C_I\} \tag{1.4.12}$$

An interferent will not pose a problem as long as the term $K_{A,I} \times C_I$ in Equation 1.4.12 is significantly smaller than than $C_A$.

## Example 1.4.2

Barnett and colleagues developed a method to determine the concentration of codeine (structure shown below) in poppy plants [Barnett, N. W.; Bowser, T. A.; Geraldi, R. D.; Smith, B. *Anal. Chim. Acta* **1996**, *318*, 309– 317]. As part of their study they evaluated the effect of several interferents. For example, the authors found that equimolar solutions of codeine and the interferent 6-methoxycodeine gave signals, respectively of 40 and 6 (arbitrary units).




(a) What is the selectivity coefficient for the interferent, 6-methoxycodeine, relative to that for the analyte, codeine.

(b) If we need to know the concentration of codeine with an accuracy of ±0.50%, what is the maximum relative concentration of 6-methoxy-codeine that we can tolerate?

### Solution

(a) The signals due to the analyte, $S_A$, and the interferent, $S_I$, are

$$S_A = k_A C_A \qquad S_I = k_I C_I$$

Solving these equations for $k_A$ and for $k_I$, and substituting into Equation 1.4.10 gives

$$K_{A,I} = \frac{S_I/C_I}{S_A/C_I}$$

Because the concentrations of analyte and interferent are equimolar ($C_A = C_I$), the selectivity coefficient is

$$K_{A,I} = \frac{S_I}{S_A} = \frac{6}{40} = 0.15$$

(b) To achieve an accuracy of better than ±0.50% the term $K_{A,I} \times C_I$ in Equation 1.4.12 must be less than 0.50% of $C_A$; thus

$$K_{A,I} \times C_I \leq 0.0050 \times C_A$$

Solving this inequality for the ratio $C_I/C_A$ and substituting in the value for $K_{A,I}$ from part (a) gives

$$\frac{C_I}{C_A} \leq \frac{0.0050}{K_{A,I}} = \frac{0.0050}{0.15} = 0.033$$

Therefore, the concentration of 6-methoxycodeine must be less than 3.3% of codeine's concentration.

Problems with selectivity also are more likely when the analyte is present at a very low concentration [Rodgers, L. B. *J. Chem. Educ.* **1986**, *63*, 3–6].

## Robustness and Ruggedness

For a method to be useful it must provide reliable results. Unfortunately, methods are subject to a variety of chemical and physical interferences that contribute uncertainty to the analysis. If a method is relatively free from chemical interferences, we can use it to analyze an analyte in a wide variety of sample matrices. Such methods are considered robust.

Random variations in experimental conditions introduces uncertainty. If a method's sensitivity, *k*, is too dependent on experimental conditions, such as temperature, acidity, or reaction time, then a slight change in any of these conditions may give a significantly different result. A rugged method is relatively insensitive to changes in experimental conditions.

## Scale of Operation

Another way to narrow the choice of methods is to consider three potential limitations: the amount of sample available for the analysis, the expected concentration of analyte in the samples, and the minimum amount of analyte that will produce a measurable signal. Collectively, these limitations define the analytical method's scale of operations.

We can display the scale of operations visually (Figure 1.4.5) by plotting the sample's size on the *x*-axis and the analyte's concentration on the *y*-axis. For convenience, we divide samples into macro (>0.1 g), meso (10 mg–100 mg), micro (0.1 mg–10 mg), and ultramicro (<0.1 mg) sizes, and we divide analytes into major (>1% w/w), minor (0.01% w/w–1% w/w), trace ($10^{-7}$% w/w–0.01% w/w), and ultratrace (<$10^{-7}$% w/w) components. Together, the analyte's concentration and the sample's size provide a characteristic description for an analysis. For example, in a microtrace analysis the sample weighs between 0.1 mg and 10 mg and contains a concentration of analyte between $10^{-7}$% w/w and $10^{-2}$% w/w.

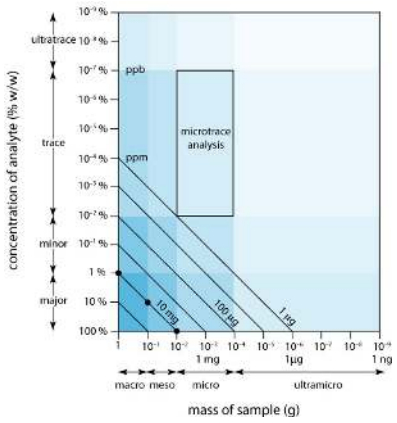



Figure 1.4.5: Scale of operations for analytical methods. The shaded areas define different types of analyses. The boxed area, for example, represents a microtrace analysis. The diagonal lines show combinations of sample size and analyte concentration that contain the same mass of analyte. The three filled circles (•), for example, indicate analyses that use 10 mg of analyte. See Sandell, E. B.; Elving, P. J. in Kolthoff, I. M.; Elving, P. J., eds. *Treatise on Analytical Chem-istry*, Interscience: New York, Part I, Vol. 1, Chapter 1, pp. 3–6; (b) Potts, L. W. *Quantitative Analysis–Theory and Practice*, Harper and Row: New York, 1987, pp. 12 for more details.

The diagonal lines connecting the axes show combinations of sample size and analyte concentration that contain the same absolute mass of analyte. As shown in Figure 1.4.5, for example, a 1-g sample that is 1% w/w analyte has the same amount of analyte (10 mg) as a 100-mg sample that is 10% w/w analyte, or a 10-mg sample that is 100% w/w analyte.

We can use Figure 1.4.5 to establish limits for analytical methods. If a method's minimum detectable signal is equivalent to 10 mg of analyte, then it is best suited to a major analyte in a macro or meso sample. Extending the method to an analyte with a

concentration of 0.1% w/w requires a sample of 10 g, which rarely is practical due to the complications of carrying such a large amount of material through the analysis. On the other hand, a small sample that contains a trace amount of analyte places significant restrictions on an analysis. For example, a 1-mg sample that is $10^{-4}$% w/w in analyte contains just 1 ng of analyte. If we isolate the analyte in 1 mL of solution, then we need an analytical method that reliably can detect it at a concentration of 1 ng/mL.

## Equipment, Time, and Cost

Finally, we can compare analytical methods with respect to their equipment needs, the time needed to complete an analysis, and the cost per sample. Methods that rely on instrumentation are equipment-intensive and may require significant operator training. For example, the graphite furnace atomic absorption spectroscopic method for determining lead in water requires a significant capital investment in the instrument and an experienced operator to obtain reliable results. Other methods, such as titrimetry, require less expensive equipment and less training.

The time to complete an analysis for one sample often is fairly similar from method-to-method. This is somewhat misleading, however, because much of this time is spent preparing samples, preparing reagents, and gathering together equipment. Once the samples, reagents, and equipment are in place, the sampling rate may differ substantially. For example, it takes just a few minutes to analyze a single sample for lead using graphite furnace atomic absorption spectroscopy, but several hours to analyze the same sample using gravimetry. This is a significant factor in selecting a method for a laboratory that handles a high volume of samples.

The cost of an analysis depends on many factors, including the cost of equipment and reagents, the cost of hiring analysts, and the number of samples that can be processed per hour. In general, methods that rely on instruments cost more per sample then other methods.

## Making the Final Choice

Unfortunately, the design criteria discussed in this section are not mutually independent [Valcárcel, M.; Ríos, A. *Anal. Chem.* **1993**, *65*, 781A–787A]. Working with smaller samples or improving selectivity often comes at the expense of precision. Minimizing cost and analysis time may decrease accuracy. Selecting a method requires carefully balancing the various design criteria. Usually, the most important design criterion is accuracy, and the best method is the one that gives the most accurate result. When the need for a result is urgent, as is often the case in clinical labs, analysis time may become the critical factor.

In some cases it is the sample's properties that determine the best method. A sample with a complex matrix, for example, may require a method with excellent selectivity to avoid interferences. Samples in which the analyte is present at a trace or ultratrace concentration usually require a concentration method. If the quantity of sample is limited, then the method must not require a large amount of sample.

---

This page titled 1.4: Selecting an Analytical Method is shared under a CC BY-NC-SA 4.0 license and was authored, remixed, and/or curated by David Harvey.

# 1.5: Calibration of Instrumental Methods

To standardize an analytical method we also must determine the analyte's sensitivity, $k_A$, in the following equation

$$S_{total} = k_A C_A + S_{blank} \tag{1.5.1}$$

where $S_{total}$ is the measured signal, $C_A$ is the analyte's concentration, and $S_{reag}$ is the signal in the absence of the analyte. In principle, it is possible to derive the value of $k_A$ for any analytical method if we understand fully all the chemical reactions and physical processes responsible for the signal. Unfortunately, such calculations are not feasible if we lack a sufficiently developed theoretical model of the physical processes or if the chemical reaction's evince non-ideal behavior. In such situations we must determine the value of $k_A$ by analyzing one or more standard solutions, each of which contains a known amount of analyte. In this section we consider several approaches for determining the value of $k_A$. For simplicity we assume that $S_{blank}$ is accounted for by a proper reagent blank, allowing us to replace $S_{total}$ in with the analyte's signal, $S_A$.

$$S_A = k_A C_A \tag{1.5.2}$$

## Single-Point Versus Multiple-Point Standardization

The simplest way to determine the value of $k_A$ in Equation 1.5.2 is to use a single-point standardization in which we measure the signal for a standard, $S_{std}$, that contains a known concentration of analyte, $C_{std}$. Substituting these values into Equation 1.5.2 and rearrange

$$k_A = \frac{S_{std}}{C_{std}} \tag{1.5.3}$$

to give us the value for $k_A$. Having determined $k_A$, we can calculate the concentration of analyte in a sample by measuring its signal, $S_{samp}$, and calculate $C_A$ *as*

$$C_A = \frac{S_{samp}}{k_A} \tag{1.5.4}$$

A single-point standardization is the least desirable method for standardizing a method. There are two reasons for this. First, any error in our determination of $k_A$ carries over into our calculation of $C_A$. Second, our experimental value for $k_A$ is based on a single concentration of analyte. To extend this value of $k_A$ to other concentrations of analyte requires that we assume a linear relationship between the signal and the analyte's concentration, an assumption that often is not true [Cardone, M. J.; Palmero, P. J.; Sybrandt, L. B. *Anal. Chem.* **1980**, *52*, 1187–1191]. Figure 1.5.1 shows how assuming a constant value of $k_A$ leads to a determinate error in $C_A$ if $k_A$ becomes smaller at higher concentrations of analyte. Despite these limitations, single-point standardizations find routine use when the expected range for the analyte's concentrations is small. Under these conditions it often is safe to assume that $k_A$ is constant (although you should verify this assumption experimentally). This is the case, for example, in clinical labs where many automated analyzers use only a single standard.

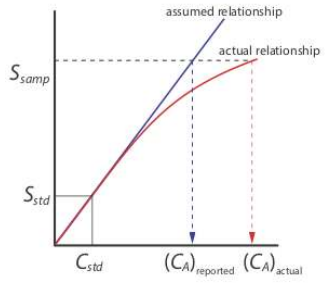



Figure 1.5.1: Example showing how a single-point standardization leads to a determinate error in an analyte's reported concentration if we incorrectly assume that $k_A$ is constant. The assumed relationship between $S_{samp}$ and $C_A$ is based on a single standard and is a straight-line; the actual relationship between $S_{samp}$ and $C_A$ becomes curved for larger concentrations of analyte.

The better way to standardize a method is to prepare a series of standards, each of which contains a different concentration of analyte. Standards are chosen such that they bracket the expected range for the analyte's concentration. A multiple-point

standardization should include at least three standards, although more are preferable. A plot of $S_{std}$ versus $C_{std}$ is called a calibration curve. The exact standardization, or calibration relationship, is determined by an appropriate curve-fitting algorithm.

> Linear regression, which also is known as the method of least squares, is one such algorithm. Its use is covered in Appendix 1.

There are two advantages to a multiple-point standardization. First, although a determinate error in one standard introduces a determinate error, its effect is minimized by the remaining standards. Second, because we measure the signal for several concentrations of analyte, we no longer must assume $k_A$ is independent of the analyte's concentration. Instead, we can construct a calibration curve similar to the "actual relationship" in Figure 1.5.1.

## External Standards

The most common method of standardization uses one or more external standards, each of which contains a known concentration of analyte. We call these standards "external" because they are prepared and analyzed separate from the samples.

> Appending the adjective "external" to the noun "standard" might strike you as odd at this point, as it seems reasonable to assume that standards and samples are analyzed separately. As we will soon learn, however, we can add standards to our samples and analyze both simultaneously.

### Single External Standard

With a single external standard we determine $k_A$ using EEquation 1.5.3 and then calculate the concentration of analyte, $C_A$, using Equation 1.5.4.

**Example 1.5.1**

A spectrophotometric method for the quantitative analysis of $Pb^{2+}$ in blood yields an $S_{std}$ of 0.474 for a single standard for which the concentration of lead is 1.75 ppb. What is the concentration of $Pb^{2+}$ in a sample of blood for which $S_{samp}$ is 0.361?

**Solution**

Equation 1.5.3 allows us to calculate the value of $k_A$ using the data for the single external standard.

$$k_A = \frac{S_{std}}{C_{std}} = \frac{0.474}{1.75 \text{ ppb}} = 0.2709 \text{ ppb}^{-1}$$

Having determined the value of $k_A$, we calculate the concentration of $Pb^{2+}$ in the sample of blood is calculated using Equation 1.5.4.

$$C_A = \frac{S_{samp}}{k_A} = \frac{0.361}{0.2709 \text{ ppb}^{-1}} = 1.33 \text{ ppb}$$

### Multiple External Standards

Figure 1.5.2 shows a typical multiple-point external standardization. The volumetric flask on the left contains a reagent blank and the remaining volumetric flasks contain increasing concentrations of $Cu^{2+}$. Shown below the volumetric flasks is the resulting calibration curve. Because this is the most common method of standardization, the resulting relationship is called a normal calibration curve.

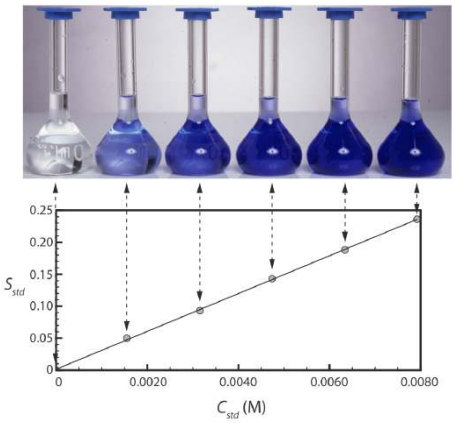



Figure 1.5.2: The photo at the top of the figure shows a reagent blank (far left) and a set of five external standards for $Cu^{2+}$ with concentrations that increase from left-to-right. Shown below the external standards is the resulting normal calibration curve. The absorbance of each standard, $S_{std}$, is shown by the filled circles.

When a calibration curve is a straight-line, as it is in Figure 1.5.2, the slope of the line gives the value of $k_A$. This is the most desirable situation because the method's sensitivity remains constant throughout the analyte's concentration range. When the calibration curve is not a straight-line, the method's sensitivity is a function of the analyte's concentration. In Figure 1.5.1, for example, the value of $k_A$ is greatest when the analyte's concentration is small and it decreases continuously for higher concentrations of analyte. The value of $k_A$ at any point along the calibration curve in Figure 1.5.1 is the slope at that point. In either case, a calibration curve allows to relate $S_{samp}$ to the analyte's concentration.

### Example 1.5.2

A second spectrophotometric method for the quantitative analysis of $Pb^{2+}$ in blood has a normal calibration curve for which

$$S_{std} = (0.296\ \text{ppb}^{-1} \times C_{std}) + 0.003$$

What is the concentration of $Pb^{2+}$ in a sample of blood if $S_{samp}$ is 0.397?

#### Solution

To determine the concentration of $Pb^{2+}$ in the sample of blood, we replace $S_{std}$ in the calibration equation with $S_{samp}$ and solve for $C_A$.

$$C_A = \frac{S_{samp} - 0.003}{0.296\ \text{ppb}^{-1}} = \frac{0.397 - 0.003}{0.296\ \text{ppb}^{-1}} = 1.33\ \text{ppb}$$

It is worth noting that the calibration equation in this problem includes an extra term that does not appear in Equation 1.5.4. Ideally we expect our calibration curve to have a signal of zero when $C_A$ is zero. This is the purpose of using a reagent blank to correct the measured signal. The extra term of +0.003 in our calibration equation results from the uncertainty in measuring the signal for the reagent blank and the standards.

An external standardization allows us to analyze a series of samples using a single calibration curve. This is an important advantage when we have many samples to analyze. Not surprisingly, many of the most common quantitative analytical methods use an external standardization.

There is a serious limitation, however, to an external standardization. When we determine the value of $k_A$ using Equation 1.5.3, the analyte is present in the external standard's matrix, which usually is a much simpler matrix than that of our samples. When we use an external standardization we assume the matrix does not affect the value of $k_A$. If this is not true, then we introduce a proportional determinate error into our analysis. This is not the case in Figure 1.5.3, for instance, where we show calibration curves for an analyte in the sample's matrix and in the standard's matrix. In this case, using the calibration curve for the external standards leads to a negative determinate error in analyte's reported concentration. If we expect that matrix effects are important, then we try to match the standard's matrix to that of the sample, a process known as matrix matching. If we are unsure of the sample's matrix,

then we must show that matrix effects are negligible or use an alternative method of standardization. Both approaches are discussed in the following section.

> The matrix for the external standards in Figure 1.5.2, for example, is dilute ammonia. Because the $Cu(NH_3)_4^{2+}$ complex absorbs more strongly than $Cu^{2+}$, adding ammonia increases the signal's magnitude. If we fail to add the same amount of ammonia to our samples, then we will introduce a proportional determinate error into our analysis.

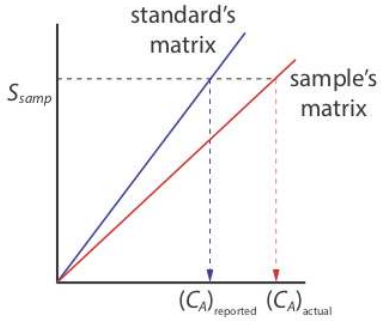



Figure 1.5.3: Calibration curves for an analyte in the standard's matrix and in the sample's matrix. If the matrix affects the value of $k_A$, as is the case here, then we introduce a proportional determinate error into our analysis if we use a normal calibration curve.

## Standard Additions

We can avoid the complication of matching the matrix of the standards to the matrix of the sample if we carry out the standardization in the sample. This is known as the method of standard additions.

### Single Standard Addition

The simplest version of a standard addition is shown in Figure 1.5.4. First we add a portion of the sample, $V_o$, to a volumetric flask, dilute it to volume, $V_f$, and measure its signal, $S_{samp}$. Next, we add a second identical portion of sample to an equivalent volumetric flask along with a spike, $V_{std}$, of an external standard whose concentration is $C_{std}$. After we dilute the spiked sample to the same final volume, we measure its signal, $S_{spike}$.

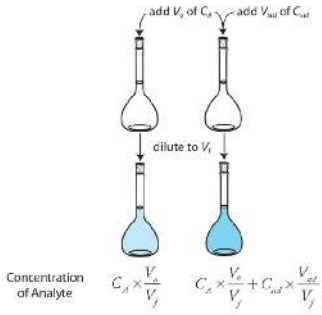



Figure 1.5.4: Illustration showing the method of standard additions. The volumetric flask on the left contains a portion of the sample, $V_o$, and the volumetric flask on the right contains an identical portion of the sample and a spike, $V_{std}$, of a standard solution of the analyte. Both flasks are diluted to the same final volume, $V_f$. The concentration of analyte in each flask is shown at the bottom of the figure where $C_A$ is the analyte's concentration in the original sample and $C_{std}$ is the concentration of analyte in the external standard.

The following two equations relate $S_{samp}$ and $S_{spike}$ to the concentration of analyte, $C_A$, in the original sample.

$$S_{samp} = k_A C_A \frac{V_o}{V_f} \tag{1.5.5}$$

$$S_{spike} = k_A \left( C_A \frac{V_o}{V_f} + C_{std} \frac{V_{std}}{V_f} \right) \tag{1.5.6}$$

As long as $V_{std}$ is small relative to $V_o$, the effect of the standard's matrix on the sample's matrix is insignificant. Under these conditions the value of $k_A$ is the same in Equation 1.5.5 and Equation 1.5.6. Solving both equations for $k_A$ and equating gives

$$\frac{S_{samp}}{C_A \frac{V_o}{V_f}} = \frac{S_{spike}}{C_A \frac{V_o}{V_f} + C_{std} \frac{V_{std}}{V_f}} \tag{1.5.7}$$

which we can solve for the concentration of analyte, $C_A$, in the original sample.

## Example 1.5.3

A third spectrophotometric method for the quantitative analysis of $Pb^{2+}$ in blood yields an $S_{samp}$ of 0.193 when a 1.00 mL sample of blood is diluted to 5.00 mL. A second 1.00 mL sample of blood is spiked with 1.00 mL of a 1560-ppb $Pb^{2+}$ external standard and diluted to 5.00 mL, yielding an $S_{spike}$ of 0.419. What is the concentration of $Pb^{2+}$ in the original sample of blood?

### Solution

We begin by making appropriate substitutions into Equation 1.5.7 and solving for $C_A$. Note that all volumes must be in the same units; thus, we first covert $V_{std}$ from 1.00 mL to $1.00 \times 10^{-3}$ mL.

$$\frac{0.193}{C_A \frac{1.00 \text{ mL}}{5.00 \text{ mL}}} = \frac{0.419}{C_A \frac{1.00 \text{ mL}}{5.00 \text{ mL}} + 1560 \text{ ppb} \frac{1.00 \times 10^{-3} \text{ mL}}{5.00 \text{ mL}}}$$

$$\frac{0.193}{0.200 C_A} = \frac{0.419}{0.200 C_A + 0.3120 \text{ ppb}}$$

$$0.0386 C_A + 0.0602 \text{ ppb} = 0.0838 C_A$$

$$0.0452 C_A = 0.0602 \text{ ppb}$$

$$C_A = 1.33 \text{ ppb}$$

The concentration of $Pb^{2+}$ in the original sample of blood is 1.33 ppb.

It also is possible to add the standard addition directly to the sample, measuring the signal both before and after the spike (Figure 1.5.5). In this case the final volume after the standard addition is $V_o + V_{std}$ and Equation 1.5.5, Equation 1.5.6, and Equation 1.5.7 become

$$S_{samp} = k_A C_A \tag{1.5.8}$$

$$S_{spike} = k_A \left( C_A \frac{V_o}{V_o + V_{std}} + C_{std} \frac{V_{std}}{V_o + V_{std}} \right) \tag{1.5.9}$$

$$\frac{S_{samp}}{C_A} = \frac{S_{spike}}{C_A \frac{V_o}{V_o + V_{std}} + C_{std} \frac{V_{std}}{V_o + V_{std}}} \tag{1.5.10}$$

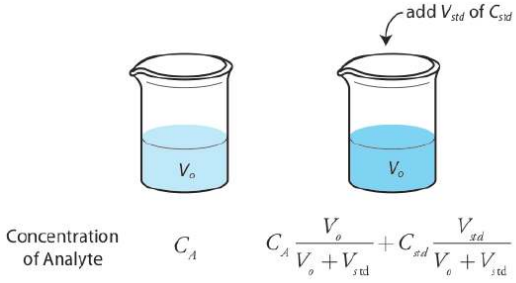



Figure 1.5.5: Illustration showing an alternative form of the method of standard additions. In this case we add the spike of external standard directly to the sample without any further adjust in the volume.

## Example 1.5.4

A fourth spectrophotometric method for the quantitative analysis of $Pb^{2+}$ in blood yields an $S_{samp}$ of 0.712 for a 5.00 mL sample of blood. After spiking the blood sample with 5.00 mL of a 1560-ppb $Pb^{2+}$ external standard, an $S_{spike}$ of 1.546 is measured. What is the concentration of $Pb^{2+}$ in the original sample of blood?

**Solution**

$$\frac{0.712}{C_A} = \frac{1.546}{C_A \frac{5.00\text{ mL}}{5.005\text{ mL}} + 1560\text{ ppb}\frac{5.00\times10^{-3}\text{ mL}}{5.005\text{ mL}}}$$

$$\frac{0.712}{C_A} = \frac{1.546}{0.9990C_A + 1.558\text{ ppb}}$$

$$0.7113C_A + 1.109\text{ ppb} = 1.546C_A$$

$$C_A = 1.33\text{ ppb}$$

The concentration of $Pb^{2+}$ in the original sample of blood is 1.33 ppb.

### Multiple Standard Additions

We can adapt a single-point standard addition into a multiple-point standard addition by preparing a series of samples that contain increasing amounts of the external standard. Figure 1.5.6 shows two ways to plot a standard addition calibration curve based on Equation 1.5.6. In Figure 1.5.6a we plot $S_{spike}$ against the volume of the spikes, $V_{std}$. If $k_A$ is constant, then the calibration curve is a straight-line. It is easy to show that the *x*-intercept is equivalent to $-C_AV_o/C_{std}$.

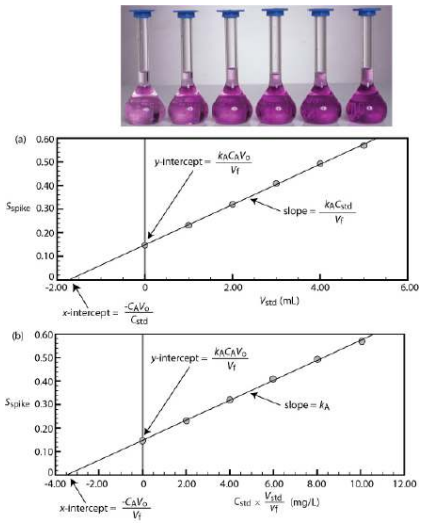



Figure 1.5.6: Shown at the top of the figure is a set of six standard additions for the determination of $Mn^{2+}$. The flask on the left is a 25.00 mL sample diluted to 50.00 mL with water. The remaining flasks contain 25.00 mL of sample and, from left-to-right, 1.00, 2.00, 3.00, 4.00, and 5.00 mL spikes of an external standard that is 100.6 mg/L $Mn^{2+}$. Shown below are two ways to plot the standard additions calibration curve. The absorbance for each standard addition, $S_{spike}$, is shown by the filled circles.

## Example 1.5.5

Beginning with Equation 1.5.6 show that the equations in Figure 1.5.6a for the slope, the *y*-intercept, and the *x*-intercept are correct.

**Solution**

We begin by rewriting Equation 1.5.6 as

$$S_{spike} = \frac{k_AC_AV_o}{V_f} + \frac{k_AC_{std}}{V_f} \times V_{std}$$

which is in the form of the equation for a straight-line

$$y = y\text{-intercept} + \text{slope} \times x\text{-intercept}$$

where $y$ is $S_{spike}$ and $x$ is $V_{std}$. The slope of the line, therefore, is $k_A C_{std}/V_f$ and the $y$-intercept is $k_A C_A V_o/V_f$. The $x$-intercept is the value of $x$ when $y$ is zero, or

$$0 = \frac{k_A C_A V_o}{V_f} + \frac{k_A C_{std}}{V_f} \times x\text{-intercept}$$

$$x\text{-intercept} = -\frac{k_A C_A V_o / V_f}{K_A C_{std}/V_f} = -\frac{C_A V_o}{C_{std}}$$

Because we know the volume of the original sample, $V_o$, and the concentration of the external standard, $C_{std}$, we can calculate the analyte's concentrations from the $x$-intercept of a multiple-point standard additions.

**Example 1.5.6**

A fifth spectrophotometric method for the quantitative analysis of $Pb^{2+}$ in blood uses a multiple-point standard addition based on Equation 1.5.6. The original blood sample has a volume of 1.00 mL and the standard used for spiking the sample has a concentration of 1560 ppb $Pb^{2+}$. All samples were diluted to 5.00 mL before measuring the signal. A calibration curve of $S_{spike}$ versus $V_{std}$ has the following equation

$$S_{spike} = 0.266 + 312\ \text{mL}^{-1} \times V_{std}$$

What is the concentration of $Pb^{2+}$ in the original sample of blood?

**Solution**

To find the $x$-intercept we set $S_{spike}$ equal to zero.

$$S_{spike} = 0.266 + 312\ \text{mL}^{-1} \times V_{std}$$

Solving for $V_{std}$, we obtain a value of $-8.526 \times 10^{-4}$ mL for the $x$-intercept. Substituting the $x$-intercept's value into the equation from Figure 1.5.6a

$$-8.526 \times 10^{-4}\ \text{mL} = -\frac{C_A V_o}{C_{std}} = -\frac{C_A \times 1.00\ \text{mL}}{1560\ \text{ppb}}$$

and solving for $C_A$ gives the concentration of $Pb^{2+}$ in the blood sample as 1.33 ppb.

Since we construct a standard additions calibration curve in the sample, we can not use the calibration equation for other samples. Each sample, therefore, requires its own standard additions calibration curve. This is a serious drawback if you have many samples. For example, suppose you need to analyze 10 samples using a five-point calibration curve. For a normal calibration curve you need to analyze only 15 solutions (five standards and ten samples). If you use the method of standard additions, however, you must analyze 50 solutions (each of the ten samples is analyzed five times, once before spiking and after each of four spikes).

### Using a Standard Addition to Identify Matrix Effects

We can use the method of standard additions to validate an external standardization when matrix matching is not feasible. First, we prepare a normal calibration curve of $S_{std}$ versus $C_{std}$ and determine the value of $k_A$ from its slope. Next, we prepare a standard additions calibration curve using Equation 1.5.6, plotting the data as shown in Figure 1.5.6b. The slope of this standard additions calibration curve provides an independent determination of $k_A$. If there is no significant difference between the two values of $k_A$, then we can ignore the difference between the sample's matrix and that of the external standards. When the values of $k_A$ are significantly different, then using a normal calibration curve introduces a proportional determinate error.

## Internal Standards

To use an external standardization or the method of standard additions, we must be able to treat identically all samples and standards. When this is not possible, the accuracy and precision of our standardization may suffer. For example, if our analyte is in a volatile solvent, then its concentration will increase if we lose solvent to evaporation. Suppose we have a sample and a standard with identical concentrations of analyte and identical signals. If both experience the same proportional loss of solvent, then their

respective concentrations of analyte and signals remain identical. In effect, we can ignore evaporation if the samples and the standards experience an equivalent loss of solvent. If an identical standard and sample lose different amounts of solvent, however, then their respective concentrations and signals are no longer equal. In this case a simple external standardization or standard addition is not possible.

We can still complete a standardization if we reference the analyte's signal to a signal from another species that we add to all samples and standards. The species, which we call an **internal standard**, must be different than the analyte.

Because the analyte and the internal standard receive the same treatment, the ratio of their signals is unaffected by any lack of reproducibility in the procedure. If a solution contains an analyte of concentration $C_A$ and an internal standard of concentration $C_{IS}$, then the signals due to the analyte, $S_A$, and the internal standard, $S_{IS}$, are

$$S_A = k_A C_A$$

$$S_{IS} = k_{SI} C_{IS}$$

where $k_A$ and $k_{IS}$ are the sensitivities for the analyte and the internal standard, respectively. Taking the ratio of the two signals gives the fundamental equation for an internal standardization.

$$\frac{S_A}{S_{IS}} = \frac{k_A C_A}{k_{IS} C_{IS}} = K \times \frac{C_A}{C_{IS}} \tag{1.5.11}$$

Because $K$ is a ratio of the analyte's sensitivity and the internal standard's sensitivity, it is not necessary to determine independently values for either $k_A$ or $k_{IS}$.

### Single Internal Standard

In a single-point internal standardization, we prepare a single standard that contains the analyte and the internal standard, and use it to determine the value of $K$ in Equation 1.5.11.

$$K = \left(\frac{C_{IS}}{C_A}\right)_{std} \times \left(\frac{S_A}{S_{IS}}\right)_{std} \tag{1.5.12}$$

Having standardized the method, the analyte's concentration is given by

$$C_A = \frac{C_{IS}}{K} \times \left(\frac{S_A}{S_{IS}}\right)_{samp}$$

**Example 1.5.7**

A sixth spectrophotometric method for the quantitative analysis of $Pb^{2+}$ in blood uses $Cu^{2+}$ as an internal standard. A standard that is 1.75 ppb $Pb^{2+}$ and 2.25 ppb $Cu^{2+}$ yields a ratio of $(S_A/S_{IS})_{std}$ of 2.37. A sample of blood spiked with the same concentration of $Cu^{2+}$ gives a signal ratio, $(S_A/S_{IS})_{samp}$, of 1.80. What is the concentration of $Pb^{2+}$ in the sample of blood?

*Solution*

Equation 1.5.12 allows us to calculate the value of $K$ using the data for the standard

$$K = \left(\frac{C_{IS}}{C_A}\right)_{std} \times \left(\frac{S_A}{S_{IS}}\right)_{std} = \frac{2.25 \text{ ppb } Cu^{2+}}{1.75 \text{ ppb } Pb^{2+}} \times 2.37 = 3.05 \frac{\text{ppb } Cu^{2+}}{\text{ppb } Pb^{2+}}$$

The concentration of $Pb^{2+}$, therefore, is

$$C_A = \frac{C_{IS}}{K} \times \left(\frac{S_A}{S_{IS}}\right)_{samp} = \frac{2.25 \text{ ppb } Cu^{2+}}{3.05 \frac{\text{ppb } Cu^{2+}}{\text{ppb } Pb^{2+}}} \times 1.80 = 1.33 \text{ ppb } Pb^{2+}$$

### Multiple Internal Standards

A single-point internal standardization has the same limitations as a single-point normal calibration. To construct an internal standard calibration curve we prepare a series of standards, each of which contains the same concentration of internal standard and

a different concentrations of analyte. Under these conditions a calibration curve of $(S_A/S_{IS})_{std}$ versus $C_A$ is linear with a slope of $K/C_{IS}$.

> Although the usual practice is to prepare the standards so that each contains an identical amount of the internal standard, this is not a requirement.

**Example 1.5.8**

A seventh spectrophotometric method for the quantitative analysis of $Pb^{2+}$ in blood gives a linear internal standards calibration curve for which

$$\left(\frac{S_A}{S_{IS}}\right)_{std} = (2.11\ \text{ppb}^{-1} \times C_A) - 0.006$$

What is the ppb $Pb^{2+}$ in a sample of blood if $(S_A/S_{IS})_{samp}$ is 2.80?

**Solution**

To determine the concentration of $Pb^{2+}$ in the sample of blood we replace $(S_A/S_{IS})_{std}$ in the calibration equation with $(S_A/S_{IS})_{samp}$ and solve for $C_A$.

$$C_A = \frac{\left(\frac{S_A}{S_{IS}}\right)_{samp} + 0.006}{2.11\ \text{ppb}^{-1}} = \frac{2.80 + 0.006}{2.11\ \text{ppb}^{-1}} = 1.33\ \text{ppb Pb}^{2+}$$

The concentration of $Pb^{2+}$ in the sample of blood is 1.33 ppb.

In some circumstances it is not possible to prepare the standards so that each contains the same concentration of internal standard. This is the case, for example, when we prepare samples by mass instead of volume. We can still prepare a calibration curve, however, by plotting $(S_A/S_{IS})_{std}$ versus $C_A/C_{IS}$, giving a linear calibration curve with a slope of $K$.

> You might wonder if it is possible to include an internal standard in the method of standard additions to correct for both matrix effects and uncontrolled variations between samples; well, the answer is yes as described in the paper "Standard Dilution Analysis," the full reference for which is Jones, W. B.; Donati, G. L.; Calloway, C. P.; Jones, B. T. *Anal. Chem.* **2015**, *87*, 2321-2327.

This page titled 1.5: Calibration of Instrumental Methods is shared under a CC BY-NC-SA 4.0 license and was authored, remixed, and/or curated by David Harvey.

# CHAPTER OVERVIEW

## 2: Electrical Components and Circuits


2.1: Basic Terminology and Laws of Electricity

2.2: Direct Current (DC) Circuits

2.3: Alternating Current Circuits

2.4: Semiconductors


---

This page titled 2: Electrical Components and Circuits is shared under a CC BY-NC-SA 4.0 license and was authored, remixed, and/or curated by David Harvey.

# 2.1: Basic Terminology and Laws of Electricity

Current, $I$, is a movement of charge over time and is expressed in amperes, $A$, where 1 ampere is equivalent to 1 coulomb/sec. In this section we review the convention used to describe currents in electrical circuits and review four laws of electricity.

## Conventional Currents

If we connect one end of a wire to the positive terminal of a battery and connect the other end to the negative terminal of the same battery, then electrons will move through the and a current will flow through the wire. The electrons move from the battery's negative terminal through the wire to the battery's positive terminal. The direction of the current, however, runs from the battery's positive terminal to the battery's negative terminal; that is, current is treated as if it is the movement of positive charge. This probably strikes you as odd, but it simply reflects the original understanding of current from a time before the electron was identified. Figure 2.1.1 shows the difference between these two ways of thinking about current.

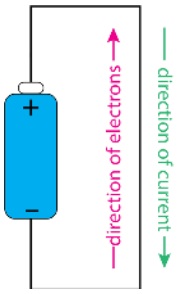



Figure 2.1.1. Two descriptions of current in an electrical circuit. The convention for currents is

## Laws of Electricity

There are four basic laws of electricity that are important to us in this chapter: Ohm's law, Kirchhoff's laws, and the power law. Let's take a brief look at each.

### Ohm's Law

Ohm's law explains the relationship between current, $I$, measured in amps ($A$), resistance, $R$, measured in ohms ($\Omega$), and potential, $V$, measured in volts ($V$), and is written as

$$V = I \times R \tag{2.1.1}$$

The voltage is measured between any two points in a circuit using a voltmeter.

### Kirchhoff's Two Laws

The first of Kirchoff's two laws states that the sum of the currents at any point in a circuit must equal zero.

$$\sum I = 0 \tag{2.1.2}$$

The second law states that the sum of the voltages in a closed loop must equal zero.

$$\sum V = 0 \tag{2.1.3}$$

### Power Law

When a current passes through a resistor, the temperature of the resistor increases and power (energy per unit time) is lost. The amount of power lost, $P$, is the product of current and voltage, with units of joules/sec

$$P = I \times V \tag{2.1.4}$$

or, substituting in Ohm's law (Equation 2.1.1), we can express power as

$$P = I^2 \times R = \frac{V^2}{R} \tag{2.1.5}$$

Note

An excellent resource for this section and other sections in this chapter is **Principles of Electronic Instrumentation** by A. James Diefenderfer and published by W. B. Saunders Company, 1972.

This page titled 2.1: Basic Terminology and Laws of Electricity is shared under a CC BY-NC-SA 4.0 license and was authored, remixed, and/or curated by David Harvey.

# 2.2: Direct Current (DC) Circuits

A direct current, which is the focus of this section, is one that flows in one direction. An alternating current, which is the focus of the next section, is one that periodically switches direction.

## Basic Direct Current (DC) Circuits

There are two basic direct current circuits of importance to us: those with two or more resistors connected in a series, and those with two or more resistors arranged parallel to each other. Other direct current circuits can be understood in terms of these two basic circuits.

### Resistors in Series

Figure 2.2.1 shows an example of a simple DC circuit in which three resistors, with resistances of $R_1$, $R_2$, and $R_3$, are connected in series to the two ends of battery that has a potential of $V$. A switch is included in the circuit that is used to close the loop and allow a current to flow from the battery's positive terminal to its negative terminal.

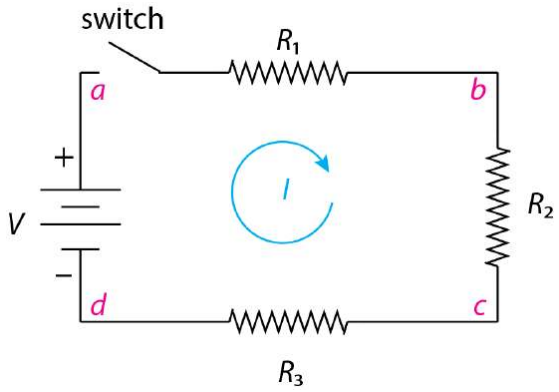



Figure 2.2.1. Example of a DC circuit that consists of three resistors in series.

Kirchoff's first law requires that the sum of the currents at any point in the circuit is zero. Consider point *b*. If the current that arrives from point *a* is $I$, then the current that leaves *b* is $-I$, where the sign tells us about the direction of the current with respect to the point. This requires that $I_a - I_c = 0$, which means that the current has the same absolute value at all points in the circuit.

Application of Kirchhoff's second law requires that the sum of the voltages in this circuit equal 0, which is true if the sum of the voltage across each of the three resistors is equal to the voltage of the battery. The voltage across each resistor is given by Ohm's law

$$V = IR_1 + IR_2 + IR_3 \tag{2.2.1}$$

If we divide both sides of Equation 2.2.1 by the current, then we have

$$V = I \times (R_1 + R_2 + R_3) = IR_s \tag{2.2.2}$$

where $R_s$ is the circuit's effective resistance, which is the sum of the resistances of the individual resistors.

One of the useful properties of this circuit is that the voltage drop across an individual resistor is proportional to that resistor's contribution to $R_s$. Consider the points in Figure 2.2.1 labeled $a$ and $b$ that are on opposite sides of the first resistor in this series. The drop in voltage across this resister, $V_{ab}$, is

$$V_{ab} = IR_1 \tag{2.2.3}$$

Dividing Equation 2.2.3 by Equation 2.2.1

$$\frac{V_{ab}}{V} = \frac{IR_1}{IR_s} = \frac{R_1}{R_s} \tag{2.2.4}$$

and

$$V_{ab} = V \times \frac{R_1}{R_s} \tag{2.2.5}$$

The circuit in Figure 2.2.1 is an example of a simple voltage divider in that it divides the battery's voltage into parts and allows us to use a single battery to select one of several possible voltages. For example, the voltage at between points *a* and *b* is

$$V_{ab} = V \times \frac{R_1}{R_s} \tag{2.2.6}$$

the voltage at between points *a* and *c* is

$$V_{ac} = V \times \frac{R_1 + R_2}{R_s} \tag{2.2.7}$$

and the voltage at between points *a* and *d* is

$$V_{ad} = V \times \frac{R_1 + R_2 + R_3}{R_s} = V \times \frac{R_s}{R_s} = V \tag{2.2.8}$$

## Parallel Circuits

Figure 2.2.2 shows an example of a simple DC circuit in which three resistors, with resistances of $R_1$, $R_2$, and $R_3$, are connected parallel to each other. A switch is included in the circuit that is used to close the loop and allow a current to flow from the battery's positive terminal to its negative terminal.

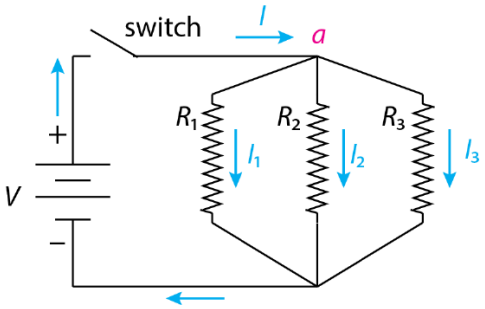



Figure 2.2.2. Example of a DC circuit that consists of three resistors in parallel.

If we apply Kirchoff's first law to the current at the point identified as *a*, then the sum of the currents must equal zero and

$$\sum I = 0 = I - I_1 - I_2 - I_3 \tag{2.2.9}$$

where $I$ is the current entering point *a* and $I_1$, $I_2$, and $I_3$ are the currents passing through the three resistors. Rearranging Equation 2.2.9 and substituting into Ohm's law gives

$$\frac{V}{R_p} = \frac{V}{R_1} + \frac{V}{R_2} + \frac{V}{R_3} \tag{2.2.10}$$

where $R_p$ is the circuit's effective resistance, which is equivalent to

$$\frac{1}{R_p} = \frac{1}{R_1} + \frac{1}{R_2} + \frac{1}{R_3} \tag{2.2.11}$$

or to

$$G_p = G_1 + G_2 + G_3 \tag{2.2.12}$$

where $G$ is a resistor's conductance, which is the inverse of its resistance.

One of the useful properties of this circuit is that it serves as a current divider. The current passing through the resistor $R_1$ is

$$\frac{I_1}{I} = \frac{V/R_1}{V/R_p} = \frac{1/R_1}{1/R_p} = \frac{G_1}{G_p} \tag{2.2.13}$$

Multiplying through by the total current gives

$$I_1 = I \times \frac{G_1}{G_p} \tag{2.2.14}$$

### More Complex Circuits

The treatment above considers circuits that contain only resistors in series or resistors in parallel. A circuit that contains both resistors in series and resistors in parallel can often be simplified to an equivalent circuit that has only resistors in series or in parallel, or that consists of single resistor. Figure 2.2.3 provides an example. The circuit at the far left shows two parallel resistors, $R_2$ and $R_3$, that, together, are in series with a third resistor, $R_1$.

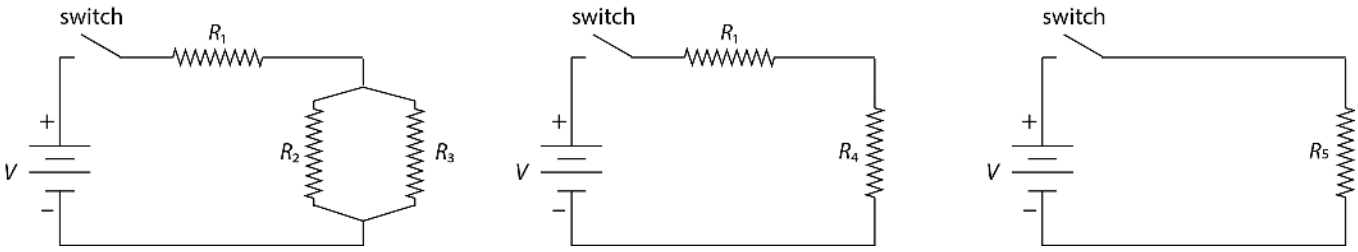



Figure 2.2.3. Example (on left) of a DC circuit that has both resistors in series and in parallel, and two equivalent circuits.

Using Equation 2.2.11 we can replace the two resistors in parallel with a single resistor, $R_4$, where

$$\frac{1}{R_4} = \frac{1}{R_2} + \frac{1}{R_3} \tag{2.2.15}$$

giving the equivalent circuit shown in the middle. Finally, we can use Equation 2.2.2 to replace the two resistors in series with the single resistor, $R_5$, as shown on the far right, where

$$R_5 = R_1 + R_4 \tag{2.2.16}$$

## Measuring Voltage and Current

Figure 2.2.4 shows a digital multimeter that is used to measure voltage or current (amongst other possible measurements that we will not consider here). The measurement of voltages and currents always contains some error, the magnitude of which we consider here.

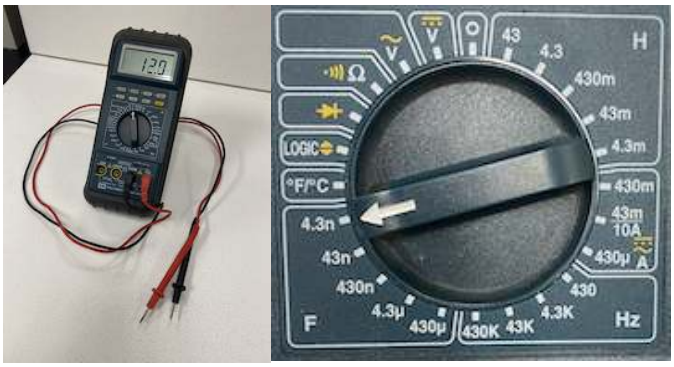



Figure 2.2.1. Photos of (left) a digital multimeter and (right) a close-up of the digital multimeter's dial. Symbols: V is voltage, Ω is resistance, F is capacitance, Hz is frequency, A is current, H is inductance. Symbols with a wavy line on top (~) are for AC circuits and symbols with solid or dashed lines (— or ---) on top are for DC circuits.

### Errors in Measuring Voltage

To measure an unknown voltage of $V_x$ with an internal resistance of $R_x$, we include the meter with its internal resistance of $R_m$ as part of a voltage divider circuit. We read the voltage displayed on the meter, $V_m$, and use Equation 2.2.5 to determine $V_x$

$$V_m = V_x \times \frac{R_m}{R_m + R_x} \tag{2.2.17}$$

If we do not know the value of $R_x$, which is often the case, then we can still report an accurate value for $V_x$ if $R_m >> R_x$, as we can then write

$$V_m = V_x \times \frac{R_m}{R_m + R_x} \approx V_x \times \frac{R_m}{R_m} \approx V_x \tag{2.2.18}$$

The percent error, $E_x$, in $V_x$

$$E_x = \frac{V_m - V_x}{V_x} \times 100 = -\frac{R_m}{R_m + R_x} \times 100 \tag{2.2.19}$$

For example, suppose that $R_m = 10^3 \times R_x$, then the measurement error is

$$E = -\frac{R_x}{(10^3 \times R_x) + R_x} \times 100 = -\frac{1}{10^3 + 1} \times 100 = -0.0999\% \tag{2.2.20}$$

or approximately –0.1%.

### Errors in Measuring Current

To measure an unknown current, $I_x$, we include the meter in a current divider circuit in which some of $I_x$ is drawn through a load resistor, $R_l$, of known value, and the remaining current is drawn through a known standard resistance set by the meter, $R_m$. Using Equation 2.2.13 for a current divider, the fraction of $I_x$ that passes through the meter is

$$\frac{I_m}{I_x} = \frac{R_m + R_l}{R_m} \tag{2.2.21}$$

Solving for $I_x$ gives

$$I_x = I_m \times \left(\frac{R_m}{R_m + R_l}\right) = I_m \times \left(1 + \frac{R_m}{R_l}\right) \tag{2.2.22}$$

If the resistors are selected such that $\frac{R_m}{R_l} << 1$, then the current displayed on the meter, $I_m$, is an accurate measure of $I_x$. The percent error in the reported current is

$$E_x = -\frac{R_m}{R_m + R_l} \times 100 \tag{2.2.23}$$

For example, suppose that $R_m = 10^{-3} \times R_l$, then the measurement error is

$$E = -\frac{10^{-3} \times R_l}{(10^{-3} \times R_l) + R_l} \times 100 = -\frac{10^{-3}}{10^{-3} + 1} \times 100 = -0.0999\% \tag{2.2.24}$$

or approximately $-0.1\%$.

This page titled 2.2: Direct Current (DC) Circuits is shared under a CC BY-NC-SA 4.0 license and was authored, remixed, and/or curated by David Harvey.

# 2.3: Alternating Current Circuits

A direct current has a fixed value that is independent of time. An alternating current, on the other hand, has a value that changes with time. This change in current follows a pattern that we can characterize by it period—the time, $t_p$, for one complete cycle—or by its frequency, $f$, which is the reciprocal of its period

$$f = \frac{1}{t_p} \tag{2.3.1}$$

Frequency is reported in hertz (Hz), which is equivalent to one cycle per second.

## Sinusoidal Currents and Voltages

Although we can draw many periodic signals—and will do so in later chapters—the simplest periodic signal is a sine wave: as shown on the right side of Figure 2.3.1, the sine is a propagating wave whose amplitude, $A$, is a function of time, $t$, which we write as $a(t)$.

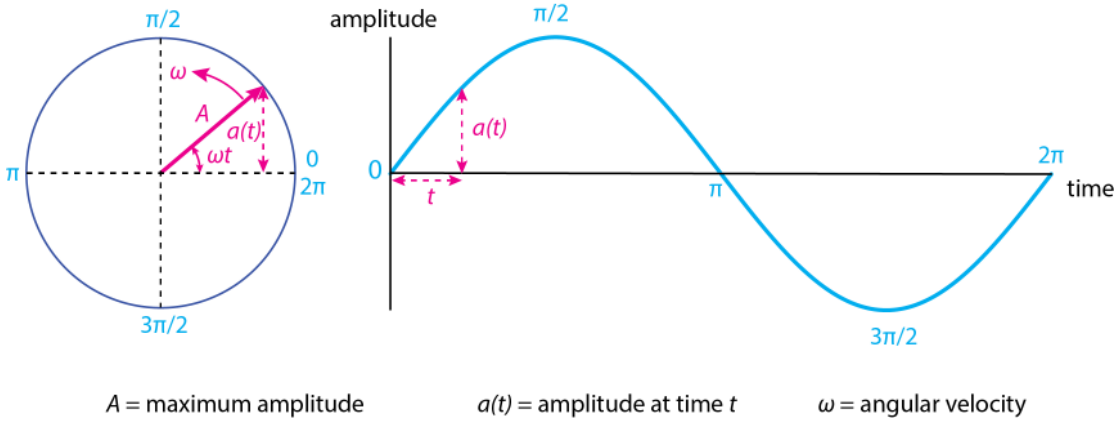



Figure 2.3.1. Illustration showing how a sine wave can be explained by a rotating vector. See text for an explanation of the symbols.

The left side of Figure 2.3.1 provides a rotating vector representation of the sine wave (a representation we will encounter again in Chapter 19 on NMR spectroscopy). The vector is the arrow that extends from the center of the circle to the circle's edge. It is rotating to the left with an angular velocity given by $\omega$ and that is expressed in radians per the sine wave's period, $t_p$; thus

$$\omega = \frac{2\pi}{t_p} = 2\pi f \tag{2.3.2}$$

where $f$ is the frequency. The amplitude of the sine wave as a function of time, $a(t)$, is equivalent to the projection of the rotating vector onto the *x*-axis; thus

$$a(t) = A \sin \omega t = A \sin 2\pi f t \tag{2.3.3}$$

In the context of this chapter, the amplitude is either a current, $i$, or a voltage, $v$.

$$i(t) = I \sin \omega t = I \sin 2\pi f t \tag{2.3.4}$$

$$v(t) = V \sin \omega t = V \sin 2\pi f t \tag{2.3.5}$$

where $I$ is the maximum, or peak current, and $V$ is the maximum, or peak voltage.

Equations 2.3.4 and 2.3.5 require that a sine wave's time-dependent amplitude, $a(t)$, has a value of zero when $t = n\pi$, where $n$ is an integer. There is no reason to insist on this and two sine waves can be separated from each other in time, as shown in Figure 2.3.2, by a phase angle, $\Phi$. The equation for the sine wave when $\Phi \neq 0$ becomes

$$a(t) = A \sin (\omega t + \Phi) = A \sin (2\pi f t + \Phi) \tag{2.3.6}$$

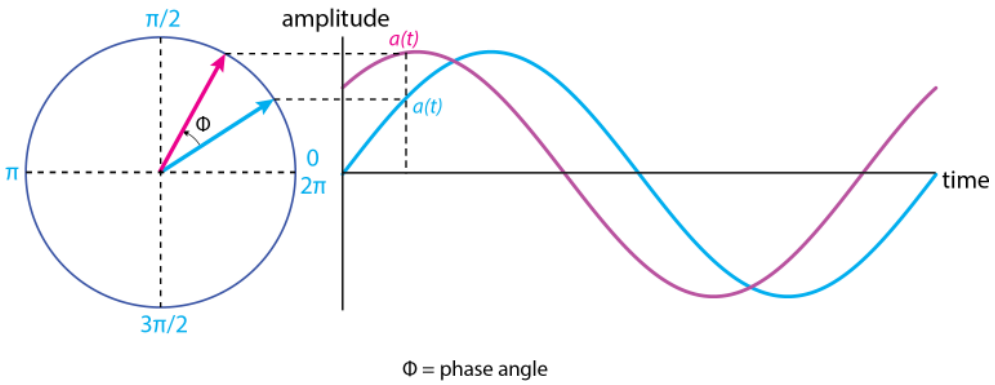



Figure 2.3.2. Two sine waves that are out-of-phase with each other. The angle, Φ, between the two rotating vectors is the phase angle.

One complication of an alternating current is that the net current over the course of a single cycle is zero. This is a problem for us because the equation for power in a resistor is

$$P = \frac{I^2}{R} \neq 0 \tag{2.3.7}$$

Figure 2.3.3 shows several ways to report current in AC circuits.

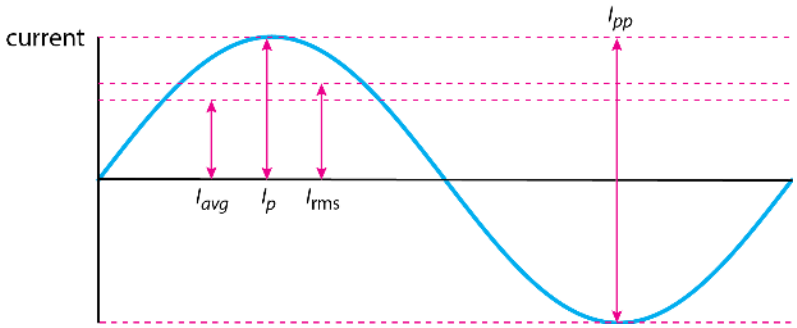



Figure 2.3.3. Different ways to report current: $I_p$ is the maximum absolute current, or peak current; $I_{pp}$ is the peak-to-peak current; $I_{rms}$ is the root-mean-square current; and $I_{avg}$ is the numerical average current.

The root-mean-square current, $I_{rms}$, is defined as

$$I_{rms} = \sqrt{\frac{I_p^2}{2}} = \sqrt{2} \times \frac{I_p}{2} = 0.707 \times I_p \tag{2.3.8}$$

and yields the same power in an AC circuit as a direct current of equal value in a DC circuit. The average current, $I_{avg}$, is

$$I_{avg} = \frac{1}{\pi} \int_0^{\pi} I_p \sin \omega t \, dt = \frac{2I_p}{\pi} = 0.6371 \times I_p \tag{2.3.9}$$

## Capacitors

A capacitor is a component of circuits that is capable of storing charge. Figure 2.3.4 shows the design of a typical capacitor and its symbol when constructing an electrical circuit. The capacitor consists of two conducting plates separated by a thin layer of an insulating, or dielectric material. The plates have areas of $A$ and are separated by a distance, $d$. The dielectric material has a dielectric constant, $\epsilon$. A simple capacitor might consist of two pieces of a metal foil separated by air, which serves as as the dielectric material. A capacitor's ability to store charge, $Q$, is given by

$$Q = C \times V \tag{2.3.10}$$

where $V$ is the voltage applied across the two plates and where $C$ is the capacitor's capacitance, which, in turn, is defined as

$$C = \frac{\epsilon A}{d} \tag{2.3.11}$$

Capacitance is measured in units of farads, where one farad is equal to one coulomb per volt.

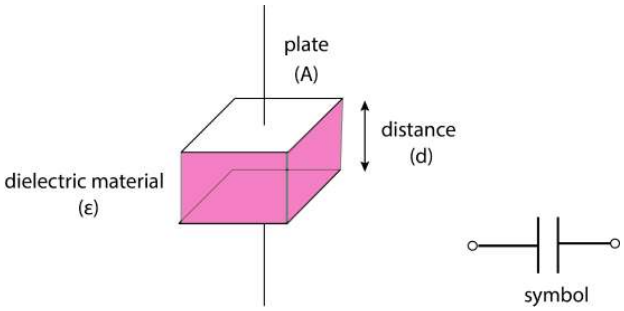



Figure 2.3.4. Schematic diagram of a capacitor. In an electrical circuit, a capacitor is represented by the symbol at the lower right.

## Resistor and Capacitor in Series

Figure 2.3.5 shows a resistor, with a resistance of $R$, and a capacitor, with a capacitance of $C$, in series with a voltage source, with a voltage of $V$.

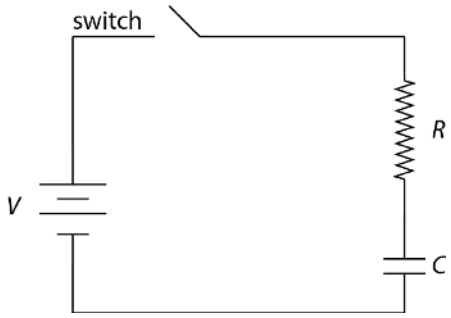



Figure 2.3.5. A simple circuit that consists of a resistor and capacitor in series.

When the switch it closed, current flows as the capacitor builds up a charge. From Kirchoff's laws, we know that

$$V = v_R + v_C = iR + \frac{Q}{C} \tag{2.3.12}$$

where $v_R$ and $v_C$ are, respectively, the time-dependent voltages across the resistor and the capacitor. Because $V$ has a fixed value, any increase in $v_C$ as the capacitor is charged is offset by a decrease in $V_r$. Given that the values of $v_C$ and $v_R$—and the associated currents—are time-dependent, we can differentiate Equation 2.3.12 with respect to time

$$\frac{dV}{dt} = 0 = \left(R \times \frac{di}{dt}\right) + \left(\frac{1}{C} \times \frac{dq}{dt}\right) = \left(R \times \frac{di}{dt}\right) + \frac{i}{C} \tag{2.3.13}$$

Rearranging Equation 2.3.13 gives

$$\frac{di}{i} = -\frac{1}{RC}dt \tag{2.3.14}$$

Integrating both sides of this equation

$$\int_{I_0}^{i} \frac{1}{i} di = -\frac{1}{RC} \int_{0}^{t} dt \tag{2.3.15}$$

leads to the following relationship between the current at time $t$ and the initial current, $I_0$

$$i_t = I_0 \times e^{-t/RC} \tag{2.3.16}$$

which tells us that the current decreases exponentially as the capacitor becomes fully charged. Replacing the current in equation 2.3.16 with $\frac{V}{R}$ and substituting back into Equation 2.3.12

$$v_C = V_0 \left(1 - e^{-t/RC}\right) \tag{2.3.17}$$

shows us that during the time the capacitor is being charged, the current flowing through the capacitor is decreasing exponentially to its limit of zero, and the voltage across the capacitor is increasing exponentially to its limit of the applied voltage.

### Time Constant

The value $RC$ in Equation 2.3.16 and in Equation 2.3.17 is the circuit's time constant. It takes approximately five time constants for the capacitor to fully charge or fully discharge. Figure 2.3.6 shows the voltage across the capacitor, $v_C$, as it is allowed to charge and to discharge. Time is shown in terms of the number of elapsed time constants, and voltage is expressed as a fraction of the maximum voltage. The dashed line shows that the time constant, $RC$, is equivalent to $0.63\times$ the maximum voltage.

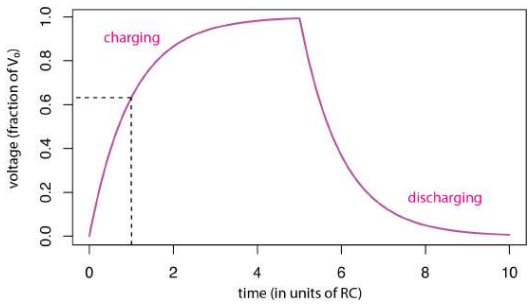



Figure 2.3.6. Voltage across a capacitor as it is charged and then discharged. The scale on the *x*-axis is time in increments of the time constant, $RC$, and the scale on the *y*-axis is the fraction of the applied voltage. The dashed line shows that the time constant is equivalent to $0.63\times$ the applied voltage.

## Response of a Series RC Circuit to a Sinusoidal Input

If we replace the DC voltage source in Figure 2.3.5 with an AC source, then the capacitor will undergo a continuous fluctuation in its voltage and current as a function of time. We know, form Equation 2.3.10 that charge, $Q$, is the product of capacitance, $C$, and voltage,$V$, which we can write as a derivative with respect to time.

$$\frac{dq}{dt} = C \times \frac{dv}{dt} \tag{2.3.18}$$

### Phase Shift in an AC Circuit

In an AC circuit, as we learned earlier in Equation 2.3.4, the current, which is equivalent to $dq/dt$ is

$$i = I_p \sin 2\pi ft \tag{2.3.19}$$

where $I_p$ is the peak current. Substituting into Equation 2.3.18 gives

$$i = I_p \sin 2\pi ft = C \times \frac{dv}{dt} \tag{2.3.20}$$

Rearranging this equation and integrating over time gives the time-dependent voltage across the capacitor, $v_C$, as

$$v_C = \frac{I_p}{2\pi fC}\left(-\cos 2\pi ft\right) \tag{2.3.21}$$

We can rewrite this equation in terms of a sine function instead of a cosine function by recognizing that the two are 90° out of phase with each other; thus

$$v_C = \frac{I_p}{2\pi fC}\left(\sin 2\pi ft - 90\right) = V_p\left(\sin 2\pi ft - 90\right) \tag{2.3.22}$$

Comparing Equation 2.3.19 and Equation 2.3.22, we see that the current and the voltage are 90° out-of-phase with each other; Figure 2.3.7 shows this visually.

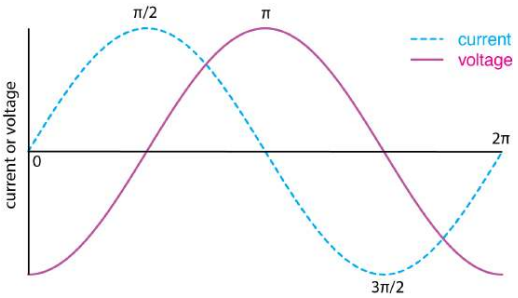



Figure 2.3.7. Response of a capacitor's voltage to a sinusoidal input current showing that they are 90° ($\pi/2$) out-of-phase.

## Capacitive Reactance, Resistance, and Impedence

From Equation 2.3.22 we see that

$$V_p = \frac{I_p}{2\pi ft} \tag{2.3.23}$$

Dividing both sides by $I_p$ gives

$$\frac{V_p}{I_p} = X_C = \frac{1}{2\pi ft} \tag{2.3.24}$$

where $X_C$ is the capacitor's reactance, which, like a resistor's resistance, has units of ohms. Unlike a resistor, however, a capacitor's reactance is frequency dependent and, given the reciprocal relationship between $X_C$ and $f$, it becomes smaller at higher frequencies.

In a RC circuit, both the resistor and the capacitor contribute to the circuit's impedence of the alternating current. Because the contribution of the capacitor is 90° out-of-phase to the contribution from the resistor, the net impedence, $Z$, is

$$Z = \sqrt{R^2 + X_C^2} \tag{2.3.25}$$

as shown in Figure 2.3.8 where the vector that represents $Z$ is the hypotonus of a right triangle defined by the resistor's resistance and the capacitor's reactance.

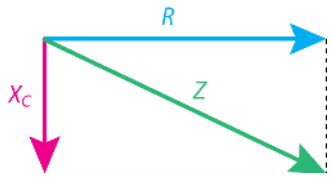



Figure 2.3.8: The relationship between a resistor's resistance, a capacitor's reactance, and the impedence of the RC circuit.

Substituting in Equation 2.3.24 shows the effect of frequency on impedence.

$$Z = \sqrt{R^2 + \left(\frac{1}{2\pi ft}\right)^2} \tag{2.3.26}$$

Writing Ohm's law in terms of impedence, $V_p = I_p \times Z$, and substituting it into Equation 2.3.26, defines $I_p$ and $V_p$ in terms of impedence.

$$V_p = I_p \times \sqrt{R^2 + \left(\frac{1}{2\pi ft}\right)^2} \tag{2.3.27}$$

$$I_p = \frac{V_p}{\sqrt{R^2 + \left(\frac{1}{2\pi ft}\right)^2}} \tag{2.3.28}$$

## Filters Based on RC Circuits

The frequency dependence of an RC circuit provides us with the ability to attenuate some frequencies and to pass other frequencies. This allows for the selective filtering of an input signal. Here we consider the design of a low-pass filter that removes higher frequency signals, and the design of a high-pass filter that removes lower frequency signals. Figure 2.3.9 shows that (a) a low-pass filter places the resistor before the capacitor and measures the output voltage, $V_{out}$, across the capacitor, and that (b) a high-pass filter places the capacitor before the resistor and measures the output voltage, $V_{out}$, across the resistor.

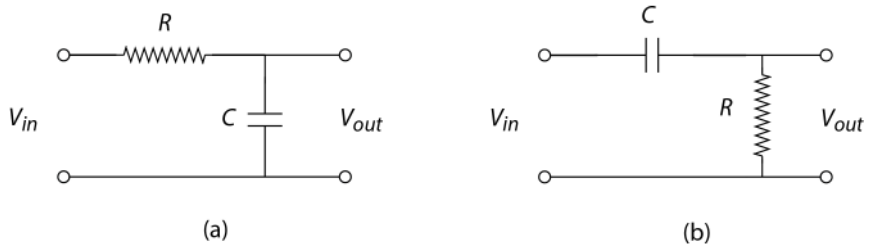



Figure 2.3.9. Circuits for (a) a low-pass filter and (b) a high-pass filter.

### Low-Pass Filter

For the low-pass filter in Figure 2.3.9$a$, the ratio of the voltage across the capacitor, $(V_p)_{out}$, to the peak input voltage, $(V_p)_{in}$, is equal to the fraction of the circuit's impedence, $Z$, attributed to the capacitor's reactance, $X_C$, as expected for a voltage divider that consist of elements in series.

$$\frac{(V_p)_{out}}{(V_p)_{in}} = \frac{X_C}{Z} = \frac{(2\pi fC)^{-1}}{\sqrt{R^2 + \left(\frac{1}{2\pi fC}\right)^2}} \tag{2.3.29}$$

Figure 2.3.10$a$ shows the frequency response for a low-pass filter with a $1 \times 10^6$ Hz resistor and a $1 \times 10^{-6}$ F capacitor, removing all frequencies greater than approximately $10^1$ Hz.

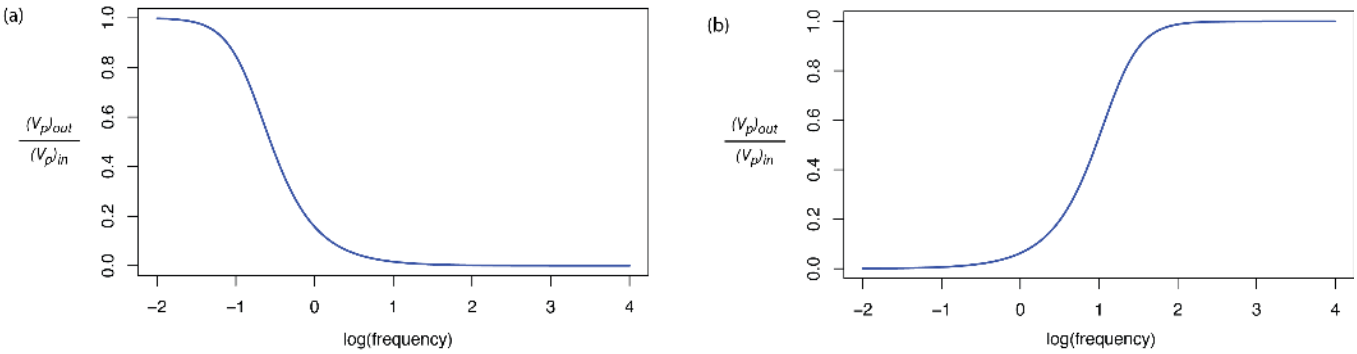



Figure 2.3.10. The output of (a) a low-pass filter and (b) a high-pass filter.

### High-Pass Filter

For the high-pass filter in Figure 2.3.9$b$, the ratio of the voltage across the resistor, $(V_p)_{out}$, to the peak input voltage, $(V_p)_{in}$, is equal to the fraction of the circuit's impedence, $Z$, attributed to the resistor's resistance, $R$, as expected for a voltage divider that consist of elements in series.

$$\frac{(V_p)_{out}}{(V_p)_{in}} = \frac{R}{Z} = \frac{R}{\sqrt{R^2 + \left(\frac{1}{2\pi fC}\right)^2}} \tag{2.3.30}$$

Figure 2.3.10$b$ shows the frequency response for a low-pass filter with a $1 \times 10^5$ Hz resistor and a $1 \times 10^{-7}$ F capacitor, removing all frequencies less than approximately $10^{-1}$.

This page titled 2.3: Alternating Current Circuits is shared under a CC BY-NC-SA 4.0 license and was authored, remixed, and/or curated by David Harvey.

# 2.4: Semiconductors

A semiconductor is a material whose resistivity to the movement of charge falls somewhere between that of a conductor, through which we can move a charge easily, and an insulator, which resists the movement of charge. Some semiconductors are elemental, such as silicon and germanium (both of which we examine more closely in this section) and some are multielemental, such as silicon carbide.

## Properties of Silicon and Germanium Semiconductors

A conductor, such as aluminum or copper, has a resistivity on the order of $10^{-8} - 10^{-6}\ \Omega \cdot m$, which means that its resistance to the movement of electrons is sufficiently small that it carries a current without much effort. An insulator, such as the mineral quartz, $SiO_2$, has a resistivity on the order of $10^{15} - 10^{19}\ \Omega \cdot m$. Silicon, on the other hand, has a resistivity of approximately $640\ \Omega \cdot m$ and germainum has a resistivity of about $0.46\ \Omega \cdot m$.

> **Note**
>
> The inverse of resistivity is conductivity.

Silicon and germanium are in the same group as carbon. If we use a simplified view of atoms, we can treat silicon and germanium as having four valence electrons and an effective nuclear charge, $Z_{eff}$, of

$$\begin{aligned}(Z_{eff})_{\text{Si}} &= Z - \text{ number of core electrons} \\ &= 14 - 10 \\ &= +4 \\ (Z_{eff})_{\text{Ge}} &= Z - \text{ number of core electrons} \\ &= 32 - 28 \\ &= +4\end{aligned}$$

We can increase the conductivity of silicon and germanium by adding to them—this is called doping—a small amount of an impurity. Adding a small amount of In or Ga, which have three valence electrons instead of four valence electrons, leaves a small number of vacancies, or holes, in which an electron is missing. Adding a small amount of As or Sb, which have five valence electrons instead of four valence electrons, leaves a small number of extra electrons. Figure 2.4.1 shows all three possibilities.

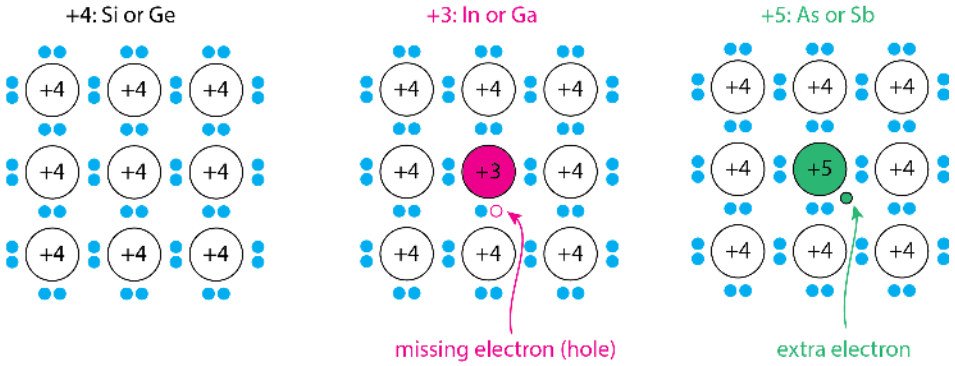



Figure 2.4.1. Illustration showing a two-dimensional cross-section through (left) a single crystal of silicon or germanium; (middle) a single crystal of silicon or germanium doped with indium or gallium; and (right) a single crystal of silicon or germanium doped with arsenic or antimony. Doping with indium or gallium leaves a hole where an electron is missing, and doping with arsenic or antimony leaves an extra electron. Patterned after figures in Diefenderfer, A. J. **Principles of Electronic Instrumentation**, W. B. Saunders (1972).

If we apply a potential across the semiconductor doped with As or Sb, the extra electron moves toward the positive pole, creating a small current, and leaving behind a vacancy, or hole. If we apply a potential across the semiconductor doped with In or Ga, electrons enter the semiconductor from the negative pole, occupying the vacancies, or holes, and creating a small current. In both cases, electrons move toward the positive pole and holes move toward the negative pole. We call an As or Sb doped semiconductor

an *n*-type semiconductor because the primary carrier of charge is an electron; we call an In or Ga doped semiconductor an *p*-type semiconductor because the primary carrier of charge is the hole.

## Semiconductor Diodes

A diode is an electrical device that is more conductive in one direction than in the opposite direction. A diode takes advantage of the properties of the junction between a *p*-type and an *n*-type semiconductor.

### Properties of *pn* Junctions

Let's use Figure 2.4.2 to make sense of how a semiconductor diode works. The figure is divided into two parts: the left side of the figure, parts (a), (b), and (c), show the behavior of the semiconductor diode when a foward bias is applied, and the right side of the figure, parts (d), (e), and (f), show its behavior when a reverse bias is applied. For both, the semiconductor diode consists of a junction between a *n*-type semiconductor, which has an excess of electrons and carries a negative charge, and a *p*-type semiconductor, which has an excess of holes and, thus, a positive charge; this is shown in (a) and (d). How the semiconductor is manufactured is not of important to us.

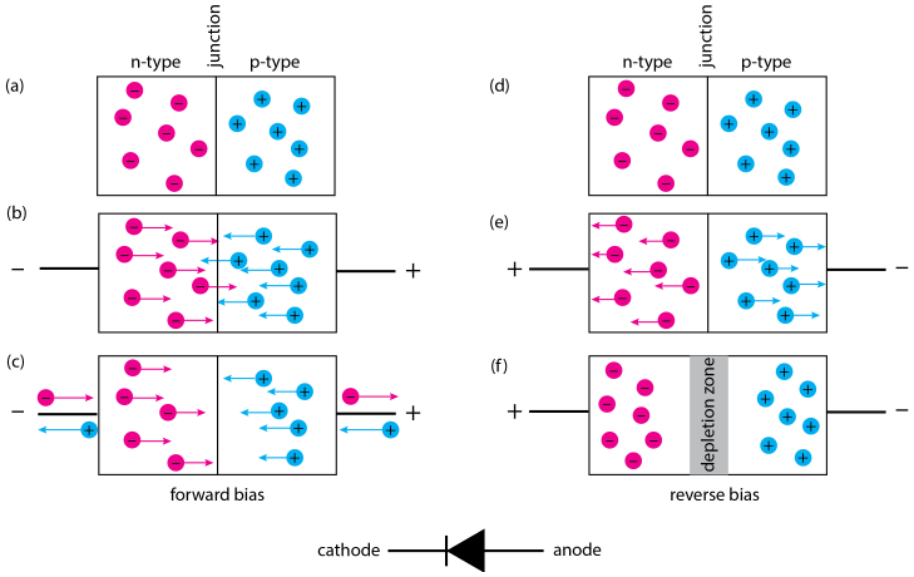



Figure 2.4.2. The behavior of a semiconductor diode under forward bias and reverse bias, and symbol for a semiconductor diode. See the text for additional details.

To effect a forward bias, we apply a positive potential to the *p*-type region and apply a negative potential to the *n*-type region. As we see in (b), the holes in the *p*-region move toward the junction and the electrons in the *n*-region move toward the junction as well. When holes and electrons meet they combine and are eliminated, which is why we see fewer holes and electrons in (c). Additional electrons flow into the *n*-region and electrons are pulled away from the *p*-region, as seen in (c), resulting in a current. To effect a reverse bias, we switch the applied potentials so that the *p*-region has the negative potential and the *n*-region has the positive potential. The result, as seen in (e) is a brief current as the holes and electrons move away from each other. leaving behind, in (f), a depletion zone that has essentially no electrons or holes.

### Current-Voltage Curves for Semiconductor Diodes

Figure 2.4.3 shows a plot of current as a function of voltage for a semiconductor diode. In forward bias mode the current increases exponentially with an increase in applied voltage, but remains at essentially zero when operated under a reverse bias. The use of a sufficiently large negative potential, however, does result in an sudden and dramatic increase in current; the potential at which this happens is called the breakdown voltage.

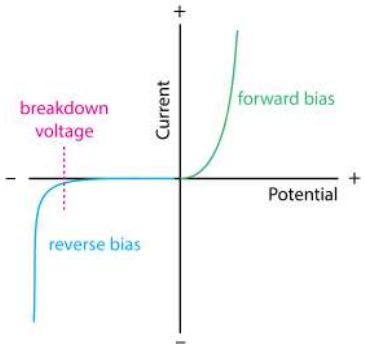



Figure 2.4.3. Current-voltage curve for a semiconductor diode under forward bias and under reverse bias.

---

This page titled 2.4: Semiconductors is shared under a CC BY-NC-SA 4.0 license and was authored, remixed, and/or curated by David Harvey.

# CHAPTER OVERVIEW

## 3: Operational Amplifiers


3.1: Operational Amplifiers

3.2: Operational Amplifier Circuits

3.3: Amplification and Measurement of Signals

3.4: Mathematical Operations Using Operational Amplifiers


---

This page titled 3: Operational Amplifiers is shared under a CC BY-NC-SA 4.0 license and was authored, remixed, and/or curated by David Harvey.

# 3.1: Operational Amplifiers

An operational amplifier (or op amp, for short) is an electrical circuit that has a variety of uses, a few of which we consider in this section: how to amplify and measure the signal from a transducer (detector), and how to perform mathematical operations on signals. In this section we will provide a basic overview of operational amplifiers without worrying about the specific internal details of its electrical circuit.

> **Note**
>
> An excellent resource for this section and other sections in this chapter is **Principles of Electronic Instrumentation** by A. James Diefenderfer and published by W. B. Saunders Company, 1972.

## Symbolic Representation of an Operational Amplifier

Figure 3.1.1 provides a symbolic representation of an operational amplifier. The large triangular shape is the operational amplifier, which is an extensive circuit whose exact design is not of interest to us; thus, the simple shape. The operational amplifier has two voltage inputs that are identified as $v_-$ and as $v_+$ and labeled as $-$ and $+$ on the op amp. The difference between $v_-$ and $v_+$ is defined as $v_s$. The operational amplifier also has a single voltage output that is identified as $v_{out}$. All voltages are measured relative to a circuit common of 0 V, represented by the small triangle at the bottom of the figure, that provides a shared reference; the circuit common is understood to be present even when it is not shown. Not included in this figure are the connections to a power supply, which are necessary for its operation.

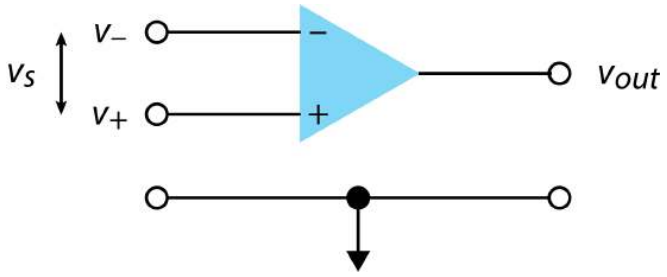



Figure 3.1.1. Representation of an operational amplifier. See the text for details.

## Inverting and Noninverting Inputs

The minus sign and the plus sign that appear as labels on the op amp in Figure 3.1.1 do not mean that one input has a positive value and that the other input has a negative value. Instead, an input to the lead with a negative sign is inverted: if $v_-$ is a negative DC voltage, then the output voltage, $v_{out}$, is a positive DC voltage, and if $v_-$ is a positive DC voltage, then the output voltage, $v_{out}$, is a negative DC voltage. For an AC input to $v_-$, the output is 180° out-of-phase, which implies a reversal in sign. The other input to the op amp is noninverting, which means that applying a positive voltage to $v_+$ results in a positive signal at $v_{out}$.

## Key Properties of Operational Amplifiers

The ideal operational amplifier has several important properties that derive from its internal circuitry. The first of these properties is that the op amp's gain, $A$, which is defined as the ratio of the output voltage to the input voltage

$$A_{op} = -\frac{v_{out}}{v_s} = -\frac{v_{out}}{v_- - v_+} \tag{3.1.1}$$

is very large, typically on the order of $10^4$ – $10^6$. We need to be careful when we use the term gain as there can be a significant difference between the gain of the operational amplifier and the gain of the circuit that contains the operational amplifier. The gain of the operational amplifier, which is what we mean by Equation 3.1.1, is called the open-loop gain. The gain of a circuit that contains an operational amplifier is called a closed-loop gain. Where there is ambiguity, we will be careful to refer to the op amp's gain, $A_{op}$, or to the circuit's gain, $A_c$, as these are more descriptive.

A second property of an operational amplifier is that regardless of the specific values of $v_-$ and $v_+$, the op amp's internal circuitry is designed such that the current between the two inputs is effectively zero; in essence, the impedence, $Z$, between the two inputs is so

large that from Ohm's law, $V = I \times Z$, the current between these two inputs is $I \approx 0$. A large input impedence means we can connect our op amp to a high voltage source and know that it will draw a small current instead of overloading the circuit that includes the op amp.

A third property of an operational amplifier is that its output impedence is very small, which means we can draw a current from the circuit that meets our needs—this current is drawn from the op amp's power supply—even if the current into the op amp is zero. For example, if the circuit's gain is small, we can use the operational amplifier to provide a large gain in current.

---

This page titled 3.1: Operational Amplifiers is shared under a CC BY-NC-SA 4.0 license and was authored, remixed, and/or curated by David Harvey.

# 3.2: Operational Amplifier Circuits

In the last section we noted that an operational amplifier magnifies the difference between two voltage inputs

$$A_{op} = -\frac{v_{out}}{v_- - v_+} \tag{3.2.1}$$

where the gain, $A_{op}$, is typically between $10^4$ and $10^6$. To better control the gain—that is, to make the gain something we can adjust to meet our needs—the operational amplifier is incorporated into a circuit that allows for feedback between the output and the inputs. In this section, we examine two feedback circuits.

## The Inverting Amplifier Circuit

Figure 3.2.1 is an example of an operational amplifier circuit with a negative feedback loop that consists of a resistor, $R_f$, that connects the op amp's output to its input at a summing point, $S$. Because the feedback loop is connected to the op amp's inverting input, the effect is called negative feedback.

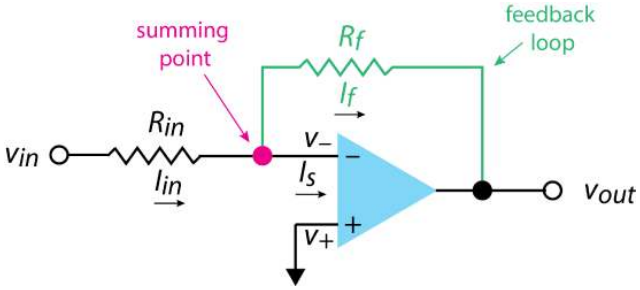



Figure 3.2.1. Operational amplifier circuit with a negative feedback loop.

We can analyze this circuit using the laws of electricity from Chapter 2. Let's begin by rearranging Equation 3.2.1 to solve for $v_{out}$

$$v_{out} = -A_{op} \times (v_- - v_+) \tag{3.2.2}$$

and then expand the right side of this equation

$$v_{out} = -A_{op} \times (v_- - v_+) = -A_{op} \times v_- + A_{op} \times v_+ \tag{3.2.3}$$

and solve for $v_-$

$$v_- = v_+ - \frac{v_{out}}{A_{op}} \tag{3.2.4}$$

Because the op amp's gain $A_{op}$ is so large—recall that it is typically in the range $10^4$ and $10^6$—we can simplify Equation 3.2.4 to

$$v_- \approx v_+ \tag{3.2.5}$$

One consequence of Equation 3.2.5 is that for this circuit $v_- \approx 0$ V as it is at the circuit common.

From Kirchoff's laws, we know that the total current that enters the summing point must equal the total current that leaves the summing point, or

$$I_{in} = I_s + I_f \tag{3.2.6}$$

where $I_s$ is the current between the op amp's two inputs. As we noted in Chapter 3.1, an operational amplifier's internal circuitry is designed such at $I_s \approx 0$; thus

$$I_{in} = I_f \tag{3.2.7}$$

Substituting in Ohm's law ($V = I \times R$) gives

$$\frac{v_{in} - v_-}{R_{in}} = \frac{v_- - v_{out}}{R_f} \tag{3.2.8}$$

From Equation 3.2.5, we know that $v_- \approx 0$, which allows us to simplify Equation 3.2.8 to

$$\frac{v_{in}}{R_{in}} = -\frac{v_{out}}{R_f} \tag{3.2.9}$$

Rearranging, we find that the gain for the circuit, $A_c$, is

$$A_c = \frac{v_{out}}{v_{in}} = -\frac{R_f}{R_{in}} \tag{3.2.10}$$

Equation 3.2.10 shows us that circuit in Figure 3.2.1 returns a voltage, $v_{out}$, that has the opposite sign of $v_{in}$ with a gain for the circuit that depends on only the relative values of the two resistors, $R_f$ and $R_{in}$.

## The Voltage-Follower Circuit

Figure 3.2.2 shows another operational amplifier with a feedback loop. In this case the input to the op amp, $v_{in}$, is made to the noninverting lead and the output is feed back into the op amp's inverting lead.

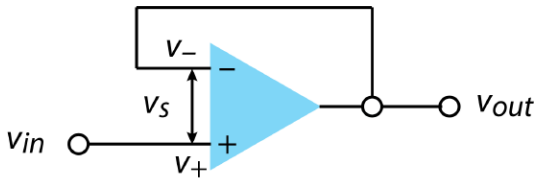



Figure 3.2.2. Operational amplifier circuit for a voltage follower.

From Kirchoff's voltage law, we know that the op amp's output voltage is equal to the sum of the input voltage and the difference, $v_s$ between the voltage applied to the op amp's two leads; thus

$$V_{out} = v_{in} + v_s \tag{3.2.11}$$

The op amp's gain, $A_{op}$, is defined in terms of $v_s$ and $v_{out}$

$$-A_{op} = \frac{v_{out}}{v_s} \tag{3.2.12}$$

where the minus sign is due to the change in sign between the output voltage and the voltage applied to the inverting lead. Substituting Equation 3.2.12 into Equation 3.2.11 gives

$$V_{in} - \frac{V_{out}}{A_{op}} = V_{out} \tag{3.2.13}$$

Because the operational amplifier's gain—which is not the same thing as the circuit's gain—is large, Equation 3.2.13 becomes

$$v_{in} = v_{out} \tag{3.2.14}$$

Our analysis of this circuit shows that it returns the original voltage without any gain. It does, however, allow us to draw that voltage from the circuit with more current than the original voltage source might be able to handle.

This page titled 3.2: Operational Amplifier Circuits is shared under a CC BY-NC-SA 4.0 license and was authored, remixed, and/or curated by David Harvey.

# 3.3: Amplification and Measurement of Signals

In Chapter 1.3 we identified the basic components of an instrument as a probe that interacts with the sample, an input transducer that converts the sample's chemical and/or physical properties into an electrical signal, a signal processor that converts the electrical signal into a form that an output transducer can convert into a numerical or a visual output that we can understand. We can represent this as a sequence of actions that take place within the instrument

$$\text{probe} \rightarrow \text{sample} \rightarrow \text{input transducer} \rightarrow \text{raw data} \rightarrow \text{signal processor} \rightarrow \text{output transducer}$$

creating the following general flow of information

$$\text{chemical and/or physical information} \rightarrow \text{electrical information} \rightarrow \text{numerical or visual response}$$

As suggested above, information is encoded in two broad ways: as electrical information (such as currents and potentials) and as information in other, non-electrical forms (such as chemical and physical properties). In this section we will consider how we can measure electrical signals.

## Current Measurements

In Chapter 7 we will introduce the phototube, seen here in Figure 3.3.1, as a transducer for converting photons of light into an electrical current that we can measure. A photon of light strikes a photoemissive cathode and ejects an electron that is then drawn to an anode that is held a positive potential. The resulting current is our analytical signal. As each photon generates a single electron, the resulting current is small and needs amplifying if it is to be useful to us. Operational amplifiers provide a way to accomplish this amplification.

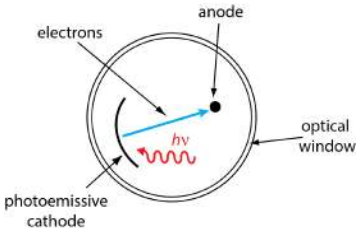



Figure 3.3.1. Schematic illustration of a phototube. See Chapter 7 for additional details.

Figure 3.3.2 shows a simple electrical circuit that we can use to amplify and measure a small current. If you compare this to the inverting amplifier circuit in Chapter 3.2, you will see that we are replacing the input voltage and input resistor with the input current, $I_x$, that we wish to measure.

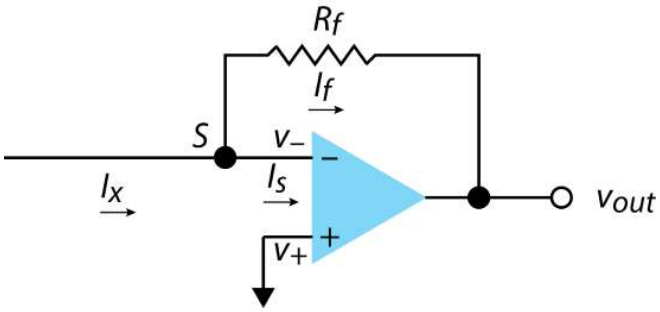



Figure 3.3.2. Operational amplifier circuit for converting a current into a voltage.

From Kirchoff's current law, we know that at the summing point, $S$, the current from the transducer is equal to the sum of the current through the feedback loop, $I_f$, and the current to the op amp's inverting input, $I_s$.

$$I_x = I_s + I_f \tag{3.3.1}$$

As we learned in the last section, $I_s \approx 0$, which means $I_x \approx I_f$. From Ohm's law, we have

$$V_{out} = -I_f \times R_f = -I_x \times R_f \tag{3.3.2}$$

Rearranging to solve for $I_x$

$$I_x = -\frac{V_{out}}{R_f} = kV_{out} \tag{3.3.3}$$

shows us that there is a linear relationship between the voltage we measure from the circuit's output and the current that enters the circuit. By choosing to make $R_f$ large, a small current is converted into a voltage that is easy to measure. In addition, we know from Chapter 2 that the error in measuring the current from the transducer, $E_x$, is

$$E_x = -\frac{R_m}{R_m + R_l} \times 100 \tag{3.3.4}$$

where $R_m$ is the resistance of the measuring circuit and $R_l$ is the resistance of the source, which generally is large. The resistance of the measuring circuit is

$$R_m = \frac{R_r}{A_{op}} \tag{3.3.5}$$

If we choose $R_f$ such that it is similar in magnitude to the op amp's gain, $A_{op}$, then $R_m$ is small and the relative error is small as well.

## Potential Measurements

From Chapter 2 we know that the error in measuring voltage, $E_x$, is a function of the resistance of the measuring circuit, $R_m$, and the resistance of the source, $R_x$.

$$E_x = \frac{V_m - V_x}{V_x} \times 100 = -\frac{R_m}{R_m + R_x} \times 100 \tag{3.3.6}$$

To maintain a small measurement error requires that $R_x << R_m$. This creates a complication when the voltage source has a high internal resistance, as is the case, for example, when we measure pH using a glass electrode where the internal resistance is on the order of $10^7 - 10^8 \Omega$ (see Chapter 23 for details about glass electrodes). The inverting amplifier circuit discussed in Chapter 3.2 has a resistance of perhaps $10^5 \Omega$. To increase $R_m$, the voltage we wish to measure, $V_x$, is first run through a voltage follower circuit, where the internal resistance is on the order of $10^{12} \Omega$, and the output is then run through the inverting amplifier, as seen in Figure 3.3.3. The result is an amplified output voltage measured under conditions where the relative error is small.

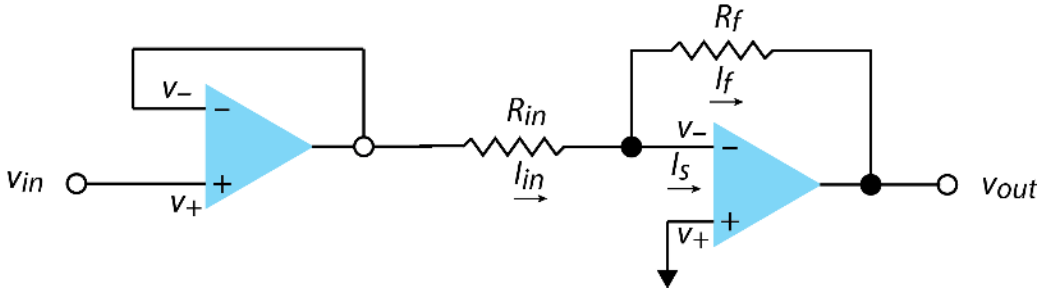



Figure 3.3.3. Circuit for measuring voltage that combines a voltage follower and an inverting amplifier.

## Comparison of Transducer Outputs

In Chapter 13 we will cover molecular absorption spectroscopy in which we measure the absorbance of sample relative to the absorbance of a reference. A difference amplifier, such as that shown in Figure 3.3.4, allows us to amplify and measure the difference between two voltages. In this circuit, the two voltages, $v_1$ and $v_2$, are fed into the op amp's two inputs, $v_-$ and $v_+$, passing through identical resistors. A feedback loop with a resistor connects $v_1$ to $v_{out}$ and a resistor identical to that in the feedback loop connects $v_2$ to the circuit common.

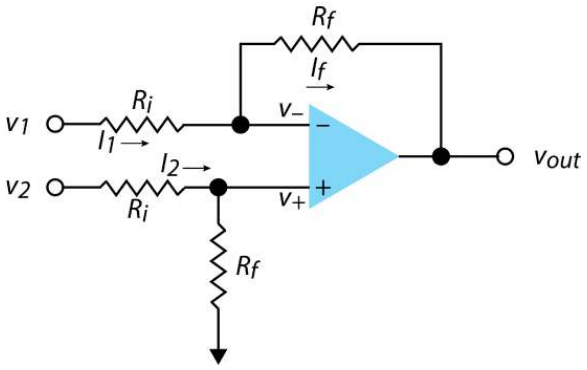



Figure 3.3.4. Circuit used to amplify and measure the difference between two voltages.

We can use Ohm's law to define the currents $I_1$ and $I_f$ as

$$I_1 = \frac{v_1 - v_-}{R_i} \tag{3.3.7}$$

$$I_f = \frac{v_- - v_{out}}{R_f} \tag{3.3.8}$$

By now you should see that the currents $I_1$ and $I_f$ are approximately the same because the op amp's high internal impedence prevents current from flowing into the op amp. Combining Equation 3.3.7 and Equation 3.3.8 gives

$$\frac{v_1 - v_-}{R_i} = \frac{v_- - v_{out}}{R_f} \tag{3.3.9}$$

which we can solve for the voltage at the op amp's inverting input

$$R_f v_1 - R_f v_- = R_i v_- - R_i V_{out} \tag{3.3.10}$$

$$R_i v_- + R_f v_- = R_f v_1 + R_i v_{out} \tag{3.3.11}$$

$$v_- = \frac{R_f v_1 + R_i v_{out}}{R_i + R_f} \tag{3.3.12}$$

The input to the op amp's noniverting lead is the output of a voltage divider (see Chapter 2) acting on $v_2$

$$v_+ = v_2 \times \left( \frac{R_f}{R_i + R_f} \right) \tag{3.3.13}$$

The feedback loop works to ensure that the inputs to $v_-$ and to $v_+$ are identical; thus

$$\frac{R_f v_1 + R_i v_{out}}{R_i + R_f} = v_2 \times \left( \frac{R_f}{R_i + R_f} \right) \tag{3.3.14}$$

which we can simply to

$$V_1 R_f + V_{out} R_i = V_2 R_f \tag{3.3.15}$$

$$V_{out} = \frac{R_f}{R_i} \times (V_2 - V_1) \tag{3.3.16}$$

The output voltage from the circuit is equal to the difference between the two input voltages, but amplified by the ratio of the resistance of $R_f$ to $R_i$.

---

This page titled 3.3: Amplification and Measurement of Signals is shared under a CC BY-NC-SA 4.0 license and was authored, remixed, and/or curated by David Harvey.

# 3.4: Mathematical Operations Using Operational Amplifiers

The circuit for comparing two voltages is an example of using an operational amplifier to complete a mathematical operation. In this section we will examine several additional examples of mathematical operations completed using operational amplifiers.

## Multiplication and Division by a Constant

The inverting amplifier that we considered earlier, and that is reproduced here in Figure 3.4.1, returns an output voltage, $v_{out}$ that multiplies the input voltage by an amount that depends on the ratio of the resistors $R_{in}$ and $R_f$.

$$v_{out} = -v_{in} \times \frac{R_f}{R_{in}} \tag{3.4.1}$$

Multiplication takes place when $R_f > R_{in}$ and division takes place when $R_{in} > R_f$. Note that there is a reversal in the sign of the voltage.

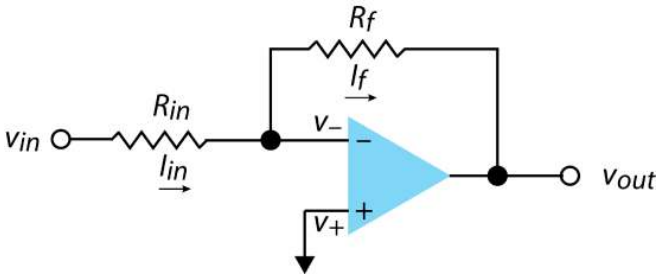



Figure 3.4.1. Operational amplifier circuit that multiples or divides an input voltage by a constant.

## Addition or Subtraction

Figure 3.4.2 shows an operational amplifier circuit that adds together four separate input voltages. From our earlier analysis of circuits, you should see that

$$I_f = I_1 + I_2 + I_3 + I_4 \tag{3.4.2}$$

We can replace $I_f$ in this equation using Ohm's law; thus

$$v_{out} = -R_f \times \left( \frac{v_1}{R_1} + \frac{v_2}{R_2} + \frac{v_3}{R_3} + \frac{v_4}{R_4} \right) \tag{3.4.3}$$

If all five of the resistors are identical, then $v_{out}$ is a simple summation of the four input voltages.

$$v_{out} = -(v_1 + v_2 + v_3 + v_4) \tag{3.4.4}$$

If we choose $R_f$ such that it is $0.25 \times R_1$ and set $R_1 = R_2 = R_3 = R_4$, then the output voltage is the average of the input voltages

$$v_{out} = -\frac{v_1 + v_2 + v_3 + v_4}{4} \tag{3.4.5}$$

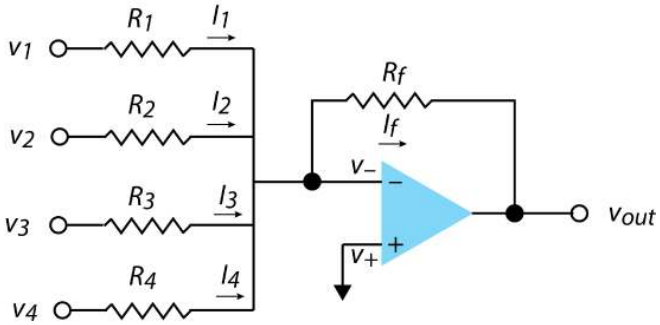



Figure 3.4.2. Operational amplifier circuit that adds together four voltages.

The voltage comparator covered in the last section subtracts one voltage from another. When more than two voltages are involved, then we can adapt the voltage adder circuit in Figure 3.4.2 to include subtraction by first running the voltage we wish to subtract

through the inverting amplifier introduced in Chapter 3.2. Figure 3.4.3 shows this where $v_{out} = -(v_4 + v_3 + v_2 - v_1)$.

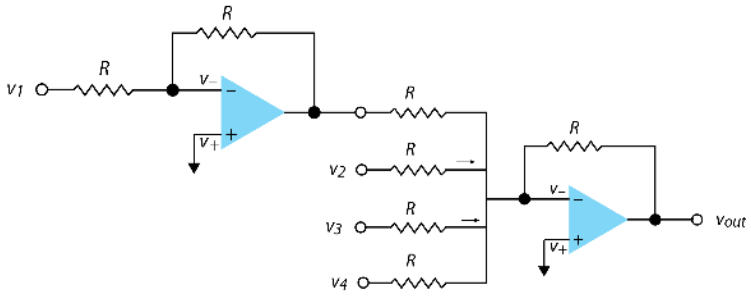



Figure 3.4.3. Operational amplifier circuit that adds together three voltages and subtracts a fourth voltage from the sum.

## Integration

Figure 3.4.4 shows an operational amplifier circuit that we can use to integrate a time-dependent signal. The circuit has a feedback loop, but it is built around a capacitor instead of a resistor because it stores charge over time. The circuit also has two switches that allow us to use the circuit over a specific period of time. When the hold switch is open, the input voltage cannot enter the circuit. Closing the hold switch sets $t = t_0$. As long as the reset switch is open, current moves through the feedback loop. Opening the hold switch sets $t = t_f$, where $t_f$ is the total elapsed time. When this cycle is over, closing the reset switch drains the capacitor so that it is ready for its next use.

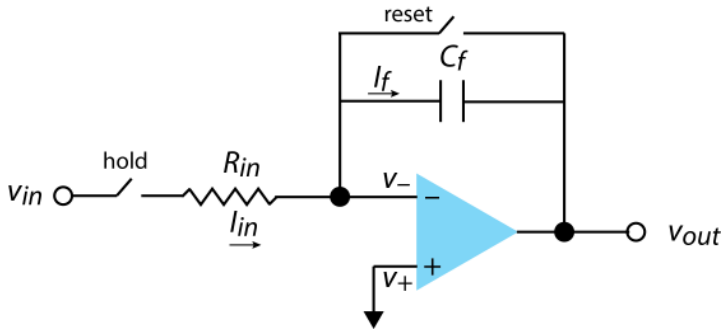



Figure 3.4.4. Operational amplifier circuit that integrates the input signal.

As we have seen several times, the current into the summing point, $I_{in}$ is equal to the current in the feedback loop.

$$I_{in} = I_f \tag{3.4.6}$$

From Chapter 2, we know that the current in the feedback loop is $I_f = -C_f \frac{dv_{out}}{dt}$ and, we know from Ohm's law that $i_{in} = \frac{V_{in}}{R_{in}}$. Substituting both relationships into Equation 3.4.6 gives

$$\frac{V_{in}}{R_{in}} = -C_f \frac{dv_{out}}{dt} \tag{3.4.7}$$

Rearranging this equation

$$dv_{out} = -\frac{v_{in}}{R_i C_f} dt \tag{3.4.8}$$

and integrating over time gives

$$\int_{v_{out,1}}^{v_{out,2}} dv_{out} = -\frac{1}{R_{in} C_f} \int_{t_1}^{t_2} v_{in} dt \tag{3.4.9}$$

If we begin the integration having previously discharged the capacitor and define $t_1$ as the the moment we close the hold switch and define $t_2$ as the moment we reopen the hold switch, then Equation 3.4.9 becomes

$$v_{out} = -\frac{1}{R_{in} C_f} \int_0^t v_{in} dt \tag{3.4.10}$$

and the output voltage is the integral of the input voltage multiplied by $(-R_{in} C_f)^{-1}$.

## Differentiation

Reversing the capacitor and the resistor in the circuit in Figure 3.4.4 coverts the circuit from one that returns the integral of the input signal, into one that returns the derivative of the input signal; Figure 3.4.5 shows the resulting circuit.

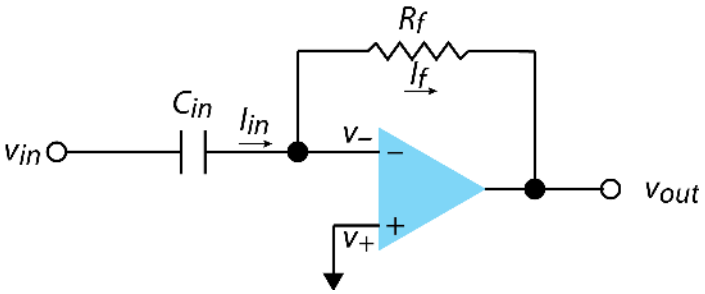



Figure 3.4.5. Operational amplifier circuit that returns the derivative of the input signal.

For this circuit we have $I_{in} = C \times \frac{dv_{in}}{dt}$ and $I_f = -\frac{V_{out}}{R}$. Given that $I_{in} = I_f$, we are left with

$$-\frac{V_{out}}{R} = C \times \frac{dv_{in}}{dt} \tag{3.4.11}$$

$$v_{out} = -RC \times \frac{dv_{in}}{dt} \tag{3.4.12}$$

This page titled 3.4: Mathematical Operations Using Operational Amplifiers is shared under a CC BY-NC-SA 4.0 license and was authored, remixed, and/or curated by David Harvey.

# CHAPTER OVERVIEW

## 4: Analog and Digital Data


4.1: Analog and Digital Data

4.2: Working With Binary Numbers

4.3: Cleaning Up Signals and Counting Events


---

This page titled 4: Analog and Digital Data is shared under a CC BY-NC-SA 4.0 license and was authored, remixed, and/or curated by David Harvey.

# 4.1: Analog and Digital Data

Figure 4.1.1 shows an *xy*-recorder that we can use to provide a permanent record of a cyclic voltammetry experiment. In this particular experiment, we apply a variable potential to an electrochemical cell and measure the current that flows in response to this potential (see Chapter 25 for a discussion of cyclic voltammetry). The potential and the current, which is converted into a voltage for the purpose of recording the cyclic voltammogram, are fed into the recorder using the cables on the right side of the recorder. The Y1 Range and the X Range controls allow us to adjust the scales of the axes.

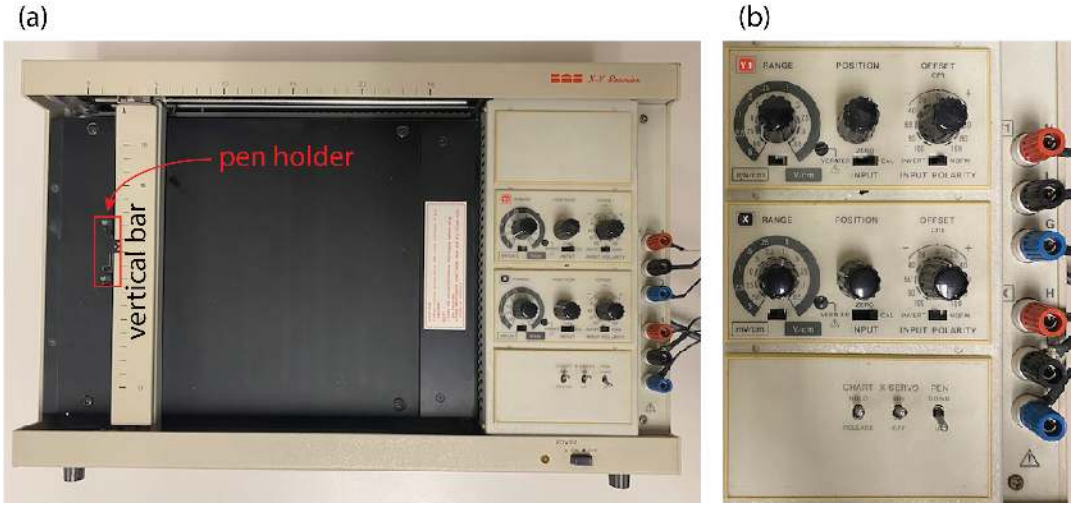



Figure 4.1.1. Photograph (a) of an *xy*-recorder and (b) close-up view of the recorder's controls.

The vertical bar on the *xy*-recorder moves toward the recorder's left or right based on the applied potential, and a pen attached to the vertical bar moves toward the recorder's top or bottom based on the measured current. The applied potential and the current are continuous variables within the instrument's range; the resulting cyclic voltammogram in Figure 4.1.2 is an analog record of the experiment.

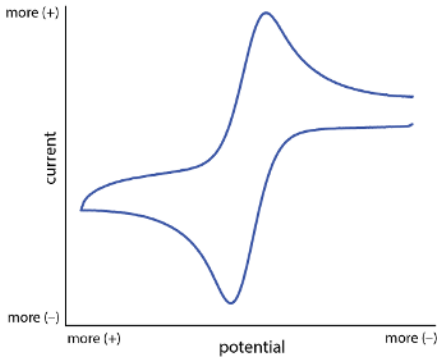



Figure 4.1.2. Example of the type of output obtained with the *xy*-recorder for a cyclic voltammetry experiment.

Although the analog trace in Figure 4.1.2 provides a permanent record of an experiment, it is not in form that gives us access to the raw data. We can take the image and use digitizing software (see here for an open-source digitizer) to extract a digital version of the data, or we can design our instruments to collect the data in digital form by sampling the analog signal at preset intervals and then saving the data. Such files often are in a format that includes metadata that explains how to extract the data from the file. For example, *xy*-coordinate data for a wide variety of spectroscopy experiments is often stored digitally using a format established by the Joint Committee on Atomic and Molecular Physical Data (JCAMP). Such files have the extension .jdx and can be opened using a variety of different software programs.

Figure 4.1.3 is a screenshot that illustrates how we can work with digitized data using data analysis software, such as R and RStudio. The upper left panel shows some of the contents of a .jdx file that contains the IR spectrum of methanol (in this case, digitized by NIST from an analog hard copy). The lines preceded by double hashtags (##) are metadata that provide information about the *x*-axis scale (minimum and maximum limits and increments between values), the *y*-axis scale (minimum and maximum

values), and the number of data points. This is followed by multiple lines of digitized data. Each line of data contains one value of *x* and five values of *y*. The R package readJDX was used to extract the information from the .jdx file and to store it in a variable given the name methanol (see upper right panel). Code written in R (see lower left panel) was used to plot (see lower right panel) the spectrum.

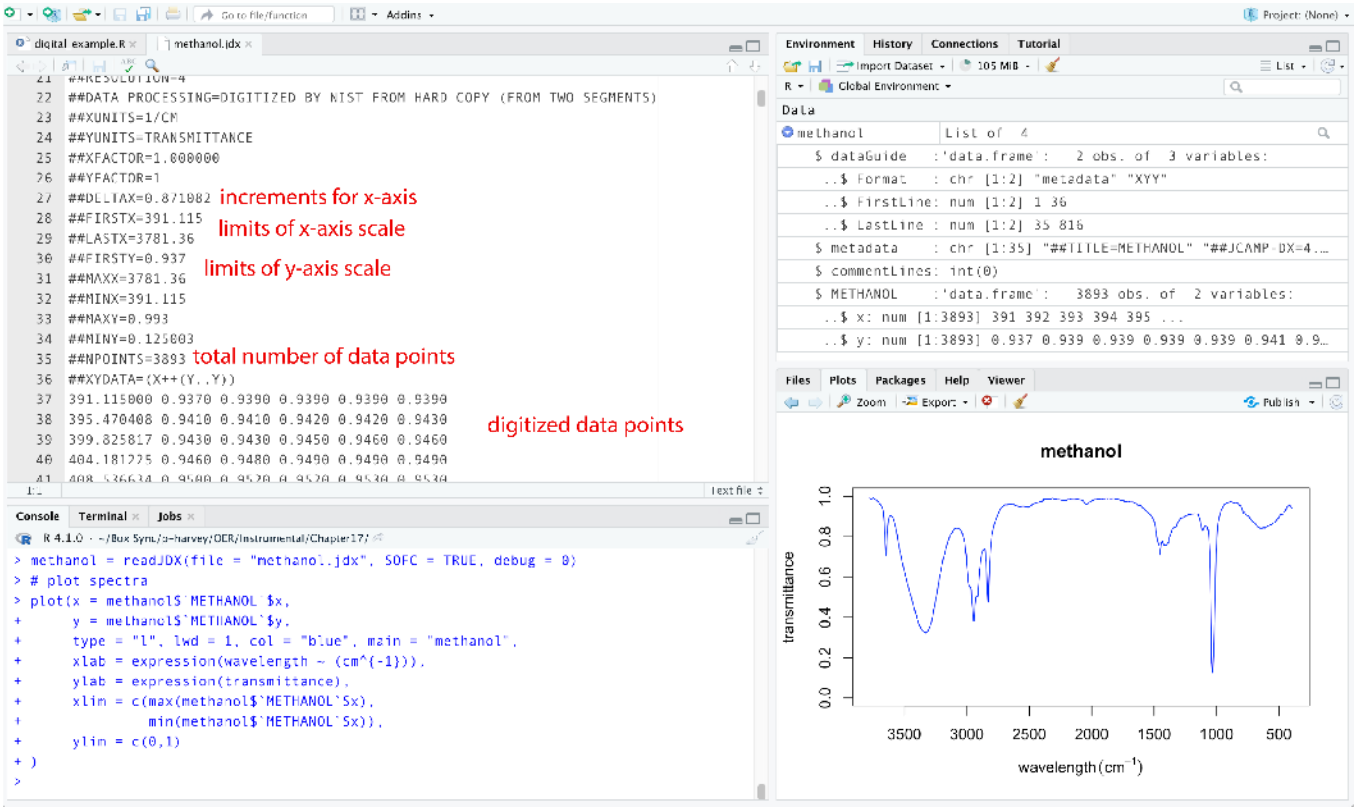



Figure 4.1.3: Screenshot from RStudio showing the analysis of a digitized spectrum. See text for details.

Although the spectrum for methanol in Figure 4.1.4—with its smooth, continuous line—looks like an analog spectrum, this is a result of choosing to plot the data as a sequence of lines that connect individual points without actually displaying the individual points themselves. Figure 4.1.4, in which we plot only the individual data points, shows us that the spectrum actually consists of discrete, digitized data.

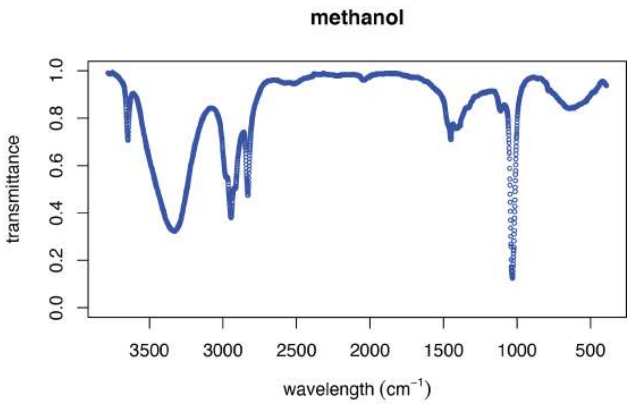



Figure 4.1.4. The IR spectrum for methanol from the .jdx data in Figure 4.1.2 plotted here using individual points instead of a line that connects the individual points.

This page titled 4.1: Analog and Digital Data is shared under a CC BY-NC-SA 4.0 license and was authored, remixed, and/or curated by David Harvey.

# 4.2: Working With Binary Numbers

In Chapter 7 we will examine several transducers for counting photons. The transducers are made of an array—some use a linear array and some use a two-dimensional array—of individual detecting units. We will worry about the details of how these transducers work in Chapter 7, but if you take a quick look at Figure 7.5.4 – 7.5.6 you will see that the number of individual detecting units are interesting: a linear array of 1024 individual units; another linear array, but with 2048 units, and a two-dimensional array that has $1024 \times 1024 = 1,048,576$ individual units. What is interesting about these numbers is that each is a power of two: $1024 = 2^{10}$, $2048 = 2^{11}$, and $1,048,576 = 10^{20}$.

Humans are comfortable working with numbers expressed using a decimal notation that relies on 10 unique digits (0, 1, 2, 3, 4, 5, 6, 7, 8, and 9), but computers work with information using a binary notation that is limited to just two unique digits (0 and 1). Although we will not complete calculations using binary numbers, you will see examples of instrumental methods, such as FT-NMR, where the data analysis algorithms (the Fourier transform in this case) require that the number of data points be a power of two. It is useful, therefore, to be familiar with how we represent numbers in both decimal and binary form.

## Decimal Representation of Numbers

My university was founded in 1837, which is a decimal expression of the year. Each of these four digits represents a power of 10, a fact that is clear when we read the number out loud: one thousand—eight hundred— thirty—seven, or, when we write it out this way

$$(1 \times 1000) + (8 \times 100) + (3 \times 10) + (7 \times 1) = 1837$$

or this way

$$(1 \times 10^3) + (8 \times 10^2) + (3 \times 10^1) + (7 \times 10^0) = 1837$$

We refer to the 7 being in the ones place ($10^0 = 1$), the 3 in the tens place ($10^1 = 10$), the 8 in the hundreds place ($10^2 = 100$), and the 1 in the thousands place ($10^3 = 1000$). Figure $4.2.1a$ shows these three ways of representing a number using a decimal notation.

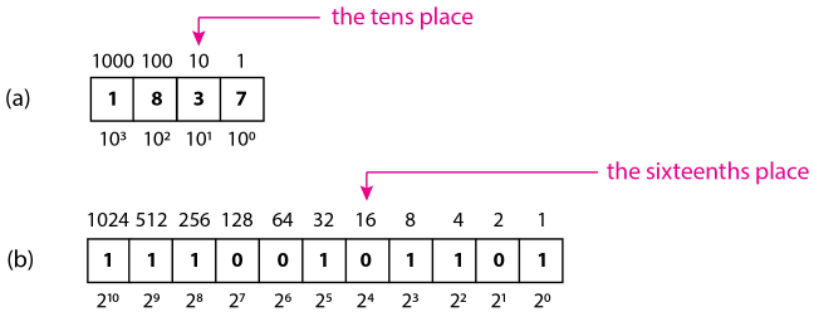



Figure 4.2.1. Three notations used to represent a number using (a) decimal digits and powers of 10 and (b) binary digits and powers of 2. The same number is represented in both (a) and (b).

## Binary Representation of Numbers

The decimal number 1837 is 11100101101 in binary notation. We can see that this is true if we follow the pattern for decimal numbers in reverse. There are eleven binary digits, so we begin by expressing the number as multiples of the powers of two from $2^{10}$ to $2^0$, beginning with the digit furthest to the left and moving to the right

$$(1 \times 2^{10}) + (1 \times 2^9) + (1 \times 2^8) + (0 \times 2^7) + (0 \times 2^6) + (1 \times 2^5) + (0 \times 2^4) + (1 \times 2^3) + (1 \times 2^2) + (0 \times 2^1) + (1 \times 2^0) = 1837$$

Each power of two has a decimal equivalent—$2^4$ is the same as $2 \times 2 \times 2 \times 2 = 16$, for example—which we can express here as

$$(1 \times 1024) + (1 \times 512) + (1 \times 256) + (0 \times 128) + (0 \times 64) + (1 \times 32) + (0 \times 16) + (1 \times 8) + (1 \times 4) + (0 \times 2) + (1 \times 1) = 1837$$

Each power of two represents a place as well; thus, the second 0 from the right is in the sixteenths place. Figure $4.2.1b$ provides a visual representation of these ways of expressing a binary number.

## Converting Between Decimal and Binary Representations of Numbers

There are lots of on-line calculators that you can use to convert between decimal and binary representations of numbers, such as the one here. Still, it is useful to be comfortable with converting numbers by hand. Converting a binary number into its decimal equivalent is straightforward, as we showed above for the binary representation of the year in which my university was founded

$$11100101101 = (1 \times 1024) + (1 \times 512) + (1 \times 256) + (0 \times 128) + (0 \times 64) + (1 \times 32) + (0 \times 16) + (1 \times 8) + (1 \times 4) + (0 \times 2) + (1 \times 1) = 1837$$

Converting a decimal number, such as 1837, into its binary equivalent requires a bit more work; Table 4.2.1 will help us organize the conversion. We begin by writing the dividend, which is 1837, in the left-most column and divide it by 2, writing the quotient of 918 in the second column and the remainder of 1 in the third column; note that dividing by 2 gives a remainder of 0 if the dividend is even or a remainder of 1 if the dividend is odd. The remainder is the exponent for the first place in the binary notation. In this case, we have $2^0 = 1$. The quotient becomes the dividend for the next cycle, with the process continuing until we achieve a quotient of 0. The binary equivalent of the original decimal is given by reading the remainders from bottom-to-top as 11100101101.

Table 4.2.1. Converting a binary number into its decimal equivalent.

| dividend | quotient | remainder | binary notation |
|---|---|---|---|
| 1837 | 918 | 1 | $2^0 = 1$ |
| 918 | 459 | 0 | $2^1 = 1$ |
| 459 | 229 | 1 | $2^2 = 1$ |
| 229 | 114 | 1 | $2^3 = 1$ |
| 114 | 57 | 0 | $2^4 = 1$ |
| 57 | 28 | 1 | $2^5 = 1$ |
| 28 | 14 | 0 | $2^6 = 1$ |
| 14 | 7 | 0 | $2^7 = 1$ |
| 7 | 3 | 1 | $2^8 = 1$ |
| 3 | 1 | 1 | $2^9 = 1$ |
| 1 | 0 | 1 | $2^{10} = 1$ |

This page titled 4.2: Working With Binary Numbers is shared under a CC BY-NC-SA 4.0 license and was authored, remixed, and/or curated by David Harvey.

# 4.3: Cleaning Up Signals and Counting Events

How an instrument handles signals depends on what is being measured, so we cannot develop here a single model that applies to all instruments. Broadly speaking, however, an instrument is likely to include one or more of the following: the ability to clean up the raw signal and convert it into a form that we can analyze; the ability to count events in binary form; the ability to convert binary information into a digital information; and the ability to convert between digital and analog signals. In this section we will cover the first two of these topics.

## Cleaning Up a Signal

Suppose our instrument is designed to count discrete events, perhaps a Geiger counter that detects the emission of $\beta$ particles, or a photodiode that detects photons. Even though a time-dependent count of particles is a digital signal, the raw signal (a voltage) likely consists of digital pulses superimposed on a background signal that contains noise, as seen in Figure 4.3.1. The total signal, therefore, is in analog form.

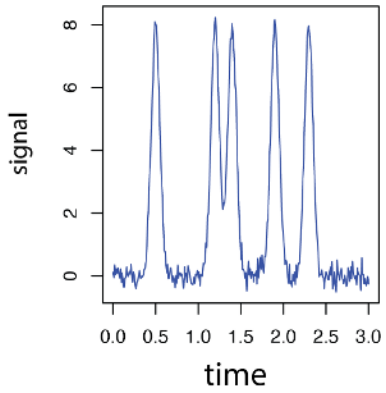



Figure 4.3.1. The raw signal (voltage) for an experiment in which we are interested in counting the number of events in a defined period of time. In this case, there are five discrete pulses, two of which partially overlap each other. The individual pulses are superimposed on a background signal that shows a modest amount of random noise.

To clean up this signal we want to accomplish two things: remove the noise and ensure that each pulse is counted. A simple way to accomplish this is to set a threshold signal and use a voltage follower operational amplifier (see Chapter 3) to set all voltages below the threshold to a logical value of 0 and all voltages above the threshold to a logical value of 1. As seen in Figure 4.3.2, the choice of the threshold voltage must be chosen carefully if we are to resolve closely spaced pulses and discriminate against noise. Note that the peak-shaped pulses become rectangular pulses.

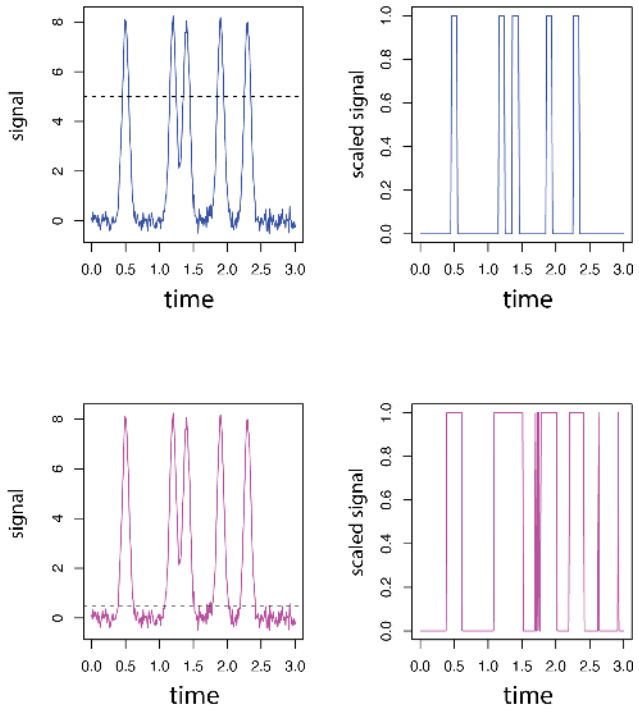



Figure 4.3.2. Two attempts at cleaning up the data from Figure 4.3.1. At the top, setting the threshold voltage to 5 results in a noise-free set of rectangular pulses that are well-separated from each other. Setting the threshold to 0.5 volts merges the two separate pulses at times between 1.0 and 1.5 into a single pulse and captures a number of noise spikes between times of 1.5 and 2.0, and between times of 2.5 and 3.0.

## Binary Pulse Counter

To count the pulses in Figure 4.3.2 we can send them though a binary pulse counter (BPC). Figure 4.3.3 shows how such a counter works. In this case, the BPC has three registers, each of which can be in a logical state of 0 or 1. With three registers, we are limited to counting no more than $2^3 = 8$ pulses; a more useful BPC would have more registers. We can treat the pulses as entering the BPC from the right. When a pulse enters a register, it flips each register from 1 to 0 or from 0 to 1, stopping after if first flips a register from 0 to 1. For example, the second pulse flips the right-most register from 1 to 0 and the middle register from 0 to 1; because the middle register initially was at 0, the counting of this pulse comes to an end.

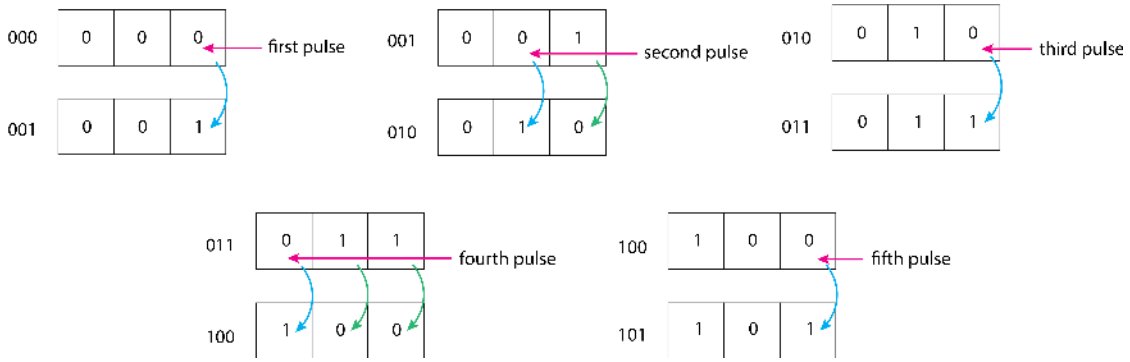



Figure 4.3.3. Operation of a binary pulse counter showing how the contents of three registers respond to the measurement of five pulses.

This page titled 4.3: Cleaning Up Signals and Counting Events is shared under a CC BY-NC-SA 4.0 license and was authored, remixed, and/or curated by David Harvey.

# CHAPTER OVERVIEW

## 5: Signals and Noise

When we try to calibrate an analytical method or to optimize an analytical system, our ability to do so successfully is limited by the uncertainty, or noise, in our measurements and by background signals that interfere with our ability to measure the signal of interest to us. In this chapter we will consider how we characterize noise, example of sources of noise, and ways to clean up our data by decreasing the contribution of noise to our measurements and by correcting for the presence of background signals.


5.1: The Signal-to-Noise Ratio

5.2: Sources of Instrumental Noise

5.3: Signal-to-Noise Enhancement


---

This page titled 5: Signals and Noise is shared under a CC BY-NC-SA 4.0 license and was authored, remixed, and/or curated by David Harvey.

# 5.1: The Signal-to-Noise Ratio

When we make a measurement it is the sum of two parts, a determinate, or fixed contribution that arises from the analyte and an indeterminate, or random, contribution that arises from uncertainty in the measurement process. We call the first of these the signal and we call the latter the noise. There are two broad categories of noise: that associated with obtaining samples and that associated with making measurements. Our interest here is in the latter.

## What is Noise?

Noise is a random event characterized by a mean and standard deviation. There are many types of noise, but we will limit ourselves for now to noise that is stationary, in that its mean and its standard deviation are independent of time, and that is heteroscedastic, in that its mean and its variance (and its standard deviation) are independent of the signal's magnitude. Figure 5.1.1$a$ shows an example of a noisy signal that meets these criteria. The *x*-axis here is shown as time—perhaps a chromatogram—but other units, such as wavelength (spectroscopy) or potential (electrochemistry), are possible. Figure 5.1.1$b$ shows the underlying noise and Figure 5.1.1$c$ shows the underlying signal. Note that the noise in Figure 5.1.1$b$ appears consistent in its central tendency (mean) and its spread (variance) along the *x*-axis and is independent of the signal's strength.

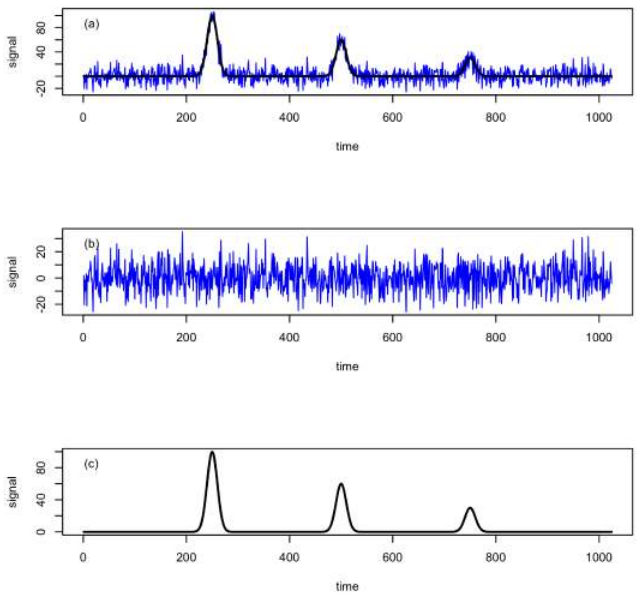



Figure 5.1.1: Plots showing (a) the signal and the noise in blue with the signal superimposed as a smooth line; (b) the noise only; and (c) the signal only. The signal consists of three peaks at times of 250, 500, and 750, and with maximum values of 100, 60, and 30, respectively. The noise is drawn at random from a normal distribution with a mean of 0 and a standard deviation of 10.

## How Do We Characterize the Signal and the Noise?

Although we characterize noise by its mean and its standard deviation, the most important benchmark is the signal-to-noise ratio, $S/N$, which we define as

$$S/N = \frac{S_{\text{analyte}}}{s_{\text{noise}}}$$

where $S_{\text{analyte}}$ is the signal's value at particular location on the *x*-axis and $s_{\text{noise}}$ is the standard deviation of the noise using a signal-free portion of the data. As general rules-of-thumb, we can measure the signal with some confidence when $S/N \geq 3$ and we can detect the signal with some confidence when $3 \geq S/N \geq 2$. For the data in Figure 5.1.1, and using the information in the figure caption, the signal-to-noise ratios are, from left-to-right, 10, 6, and 3.

Note

To measure the signal with confidence implies we can use the signal's value in a calculation, such as constructing a calibration curve. To detect the signal with confidence means we are certain that a signal is present (and that an analyte responsible for the signal is present) even if we cannot measure the signal with sufficient confidence to allow for a meaningful calculation.

This page titled 5.1: The Signal-to-Noise Ratio is shared under a CC BY-NC-SA 4.0 license and was authored, remixed, and/or curated by David Harvey.

# 5.2: Sources of Instrumental Noise

When we make an analytical measurement, we are interested in both the accuracy and the precision of our results. Noise, as we learned in the previous section, is a random fluctuation in the signal that limits our ability to detect the presence of the underlying signal. There are a variety of ways in which noise can enter into our measurements. Some of these sources of noise are related to the process of collecting and processing samples for analysis; these sources of noise, which we might collectively call chemical sources of noise, are important and receive consideration in those sections of this textbook that consider the application of analytical methods. In this chapter, we will limit ourselves to considering sources of noise that arise from the instruments we use to make measurements. We call these sources of instrumental noise.

## Thermal Noise

Even when an external voltage is not applied to an electrical circuit, a small current is present due to the random motion of electrons that arises from the temperature of the surroundings; we can this thermal (or, sometimes, Johnson) noise. The magnitude of this noise in any electrical element increases with temperature, of course, but it also is affected by its resistance, and by how quickly it responds to a change in the signal. Mathematically, we express this as the root-mean-square voltage, $\nu_{\text{rms}}$, which is given as

$$\nu_{\text{rms}} = \sqrt{4kTR\Delta f} \tag{5.2.1}$$

where $k$ is Boltzmann's constant, $T$ is the temperature in Kelvin, $R$ is the resistance in ohms, and $\Delta f$ is the bandwidth. The latter term is a measure of how quickly the electrical element responds to a change in its input by changing its output from 10% to 90% of its final value, which is called the rise time, $t_r$, where

$$\Delta f = \frac{1}{3t_r}$$

For example, if a change in the input increases the output by 1, then the rise time is how long it takes the output to increase from 0.1 to 0.9.

A close look at Equation 5.2.1 shows that we can reduce thermal noise by decreasing the temperature, by decreasing the resistance of the electrical circuit, and by decreasing the bandwidth; the latter, of course, comes at the cost of an increase in the response time, which means the instrument responds more slowly to a change in the signal. Of these, it is often easiest to reduce the temperature by cooling, for example, the instrument's detector.

## Shot Noise

As its name implies, shot noise is a discrete event that happens in response to an event, such as the movement of an electron through the space between two surfaces of opposite charge. These events are random and quantized, and generate random furcations in the current that have a root-mean-square value, $i_{\text{rms}}$, which is given by

$$i_{\text{rms}} = \sqrt{2Ie\Delta f} \tag{5.2.2}$$

where $I$ is the average current, $e$ is the charge on the electron in Coulombs, and $\Delta f$ is the bandwidth. Of these terms, the only one under our control is the bandwidth; again, decreasing the bandwidth comes at the cost of an instrument that responds more slowly to a change in the signal.

## Flicker Noise

Unlike thermal noise or shot noise, flicker noise is related to the frequency of the signal being measured, $f$, instead of the signal's bandwidth. The sources of flicker noise are not well understood, but it is known that it is inversely proportional to the signal's frequency; thus, flicker noise is sometimes called $1/f$ noise. Because of the inverse relationship, flicker noise is more important at low frequencies, where it appears as a long-term drift in the signal. It is less important at higher frequencies where thermal noise and shot noise are more important.

## Environmental Noise

Our instruments normally do not operate in an environment free from external signals, each of which has a frequency that can be picked up by the instrument. Television signals, cell-phone signals, radio signals, power lines are obvious examples of high-to-moderate frequencies that can serve as noise. Less obvious are lower frequency sources of noise, such as the change in temperature during the day or through the year.

---

This page titled 5.2: Sources of Instrumental Noise is shared under a CC BY-NC-SA 4.0 license and was authored, remixed, and/or curated by David Harvey.

# 5.3: Signal-to-Noise Enhancement

There are two broad approaches we can use to improve the signal-to-noise ratio: hardware and software. Hardware approaches are built into the instrument and include decisions on how the instrument is set-up for making measurements (for example, the choice of a scan rate or a slit width), and how the signal is processed by the instrument (for example, using electronic filters). A few approaches are briefly considered here; others are included with the discussion of individual instruments. Software solutions are computational approaches in which we manipulate the data either while we are collecting it or after data acquisition is complete.

## Hardware Solutions

One way to reduce noise is to focus on the circuitry, or hardware, used to measure the signal.

### Shielding

One way to reduce environmental noise is to prevent it from entering into the instrument's electronic circuitry. One approach is to use a Faraday cage in which the instrument sits within a room or space covered with a conductive material. Electromagnetic radiation from the environment is absorbed by the conductive material and then shunted away to the ground. Rather than encasing the entire instrument in a Faraday cage, particularly sensitive portions of the circuitry can be shielded.

### Differential Amplifier

A difference amplifier (see Chapter 3) is an electrical circuit used to determine the difference between two input voltages or currents and to return that difference as a larger voltage or current. As the magnitude of the noise in the two input signals is generally similar in value—that is, it is in phase—while the signal of interest is not, much of the noise's contribution to the signal is subtracted out.

### Filtering

When the frequency of the noise is quite different from the frequency of the signal, a simple electrical circuit can be used to remove the high frequency noise and pass the low frequency signal; this is called a low-pass filter. See Chapter 2 for details on low-pass filters.

### Modulation

When the signal of interest has a low frequency, the effect of flicker noise becomes significant because a technique that removes low frequency noise will remove the signal as well. Modulation is a process of increasing the frequency of the signal. When complete, a high-pass filter is used to remove the noise. Reversing the modulation returns the original signal, but with much of the noise removed.

## Software Solutions

In this section we will consider three common computational tools for improving the signal-to-noise ratio: signal averaging, digital smoothing, and Fourier filtering.

### Signal Averaging

The most important difference between the signal and the noise is that a signal is determinate (fixed in value) and the noise is indeterminate (random in value). If we measure a pure signal several times, we expect its value to be the same each time; thus, if we add together *n* scans, we expect that the net signal, $S_n$, is defined as

$$S_n = nS$$

where $S$ is the signal for a single scan. Because noise is random, its value varies from one run to the next, sometimes with a value that is larger and sometimes with a value that is smaller, and sometimes with a value that is positive and sometimes with a value that is negative. On average, the standard deviation of the noise increases as we make more scans, but it does so at a slower rate than for the signal

$$s_n = \sqrt{n}s$$

where $s$ is the standard deviation for a single scan and $s_n$ is the standard deviation after *n* scans. Combining these two equations, shows us that the signal-to-noise ratio, $S/N$, after *n* scans increases as

$$(S/N)_n = \frac{S_n}{s_n} = \frac{nS}{\sqrt{n}s} = \sqrt{n}(S/N)_{n=1}$$

where $(S/N)_{n=1}$ is the signal-to-noise ratio for the initial scan. Thus, when $n = 4$ the signal-to-noise ratio improves by a factor of 2, and when $n = 16$ the signal-to-noise ratio increases by a factor of 4. Figure 5.3.1 shows the improvement in the signal-to-noise ratio for 1, 2, 4, and 8 scans.

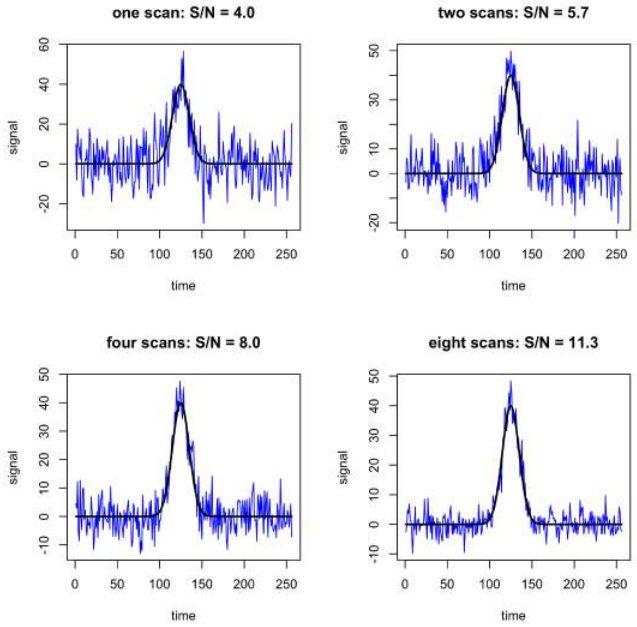



Figure 5.3.1: Improvement in the signal-to-noise ratio through signal averaging using 1, 2, 4, and 8 scans. Each plot shows the noisy signal in blue with the pure signal superimposed in black. The total signal is divided by the number of scans so that each *y*-axis has the same scale.

Signal averaging works well when the time it takes to collect a single scan is short and when the analyte's signal is stable with respect to time both because the sample is stable and the instrument is stable; when this is not the case, then we risk a time-dependent change in $S_{\text{analyte}}$ and/or $s_{\text{noise}}$ Because the equation for $(S/N)_n$ is proportional to the $\sqrt{n}$, the relative improvement in the signal-to-noise ratio decreases as $n$ increases; for example, 16 scans gives a $4\times$ improvement in the signal-to-noise ratio, but it takes an additional 48 scans (for a total of 64 scans) to achieve a $8\times$ improvement in the signal-to-noise ratio.

## Digital Smoothing Filters

One characteristic of noise is that its magnitude fluctuates rapidly in contrast to the underlying signal. We see this, for example, in Figure 5.3.1 where the underlying signal either remains constant or steadily increases or decreases while the noise fluctuates chaotically. Digital smoothing filters take advantage of this by using a mathematical function to average the data for a small range of consecutive data points, replacing the range's middle value with the average signal over that range.

## Moving Average Filters

For a moving average filter, also called a boxcar filter, we replace each point by the average signal for that point and an equal number of points on either side; thus, a moving average filter has a width, $w$, of 3, 5, 7, ... points. For example, suppose the first five points in a sequence are

| | | | | |
|---|---|---|---|---|
| 0.80 | 0.30 | 0.80 | 0.20 | 1.00 |

then a three-point moving average ($w = 3$) returns values of

| | | | | |
|---|---|---|---|---|
| NA | 0.63 | 0.43 | 0.67 | NA |

where, for example, 0.63 is the average of 0.80, 0.30, and 0.80. Note that we lose $(w - 1)/2 = (3 - 1)/2 = 1$ points at each end of the data set because we do not have a sufficient number of data points to complete a calculation for the first and the last point. Figure 5.3.2 shows the improvement in the $S/N$ ratio when using moving average filters with widths of 5, 9, and 13.

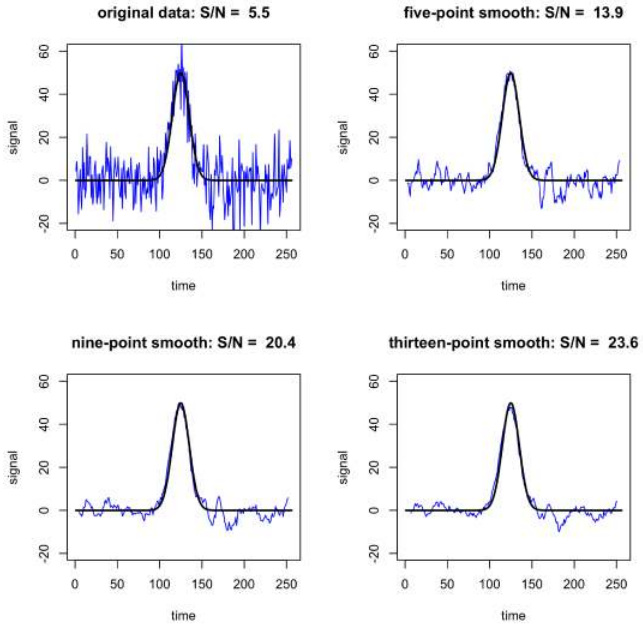



Figure 5.3.2: Improvement in the signal-to-noise ratio using moving average filters with ranges of 5, 9, and 13 on the original data shown in the upper left quadrant. Each plot shows the noisy signal in blue with the pure signal superimposed in black.

One limitation to a moving average filter is that it distorts the original data by removing points from both ends, although this is not a serious concern if the points in question are just noise. Of greater concern is the distortion in a signal's height if we use a range that is too wide; for example, Figure 5.3.3, shows how a 23-point moving average filter (shown in blue) applied to the noisy signal in the upper left quadrant of Figure 5.3.2, reduces the height of the original signal (shown in black). Because the filter's width—shown by the red bar—is similar to the peak's width, as the filter passes through the peak it systematically reduces the signal by averaging together values that are mostly smaller than the maximum signal.

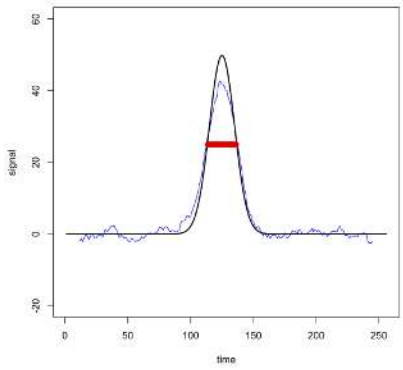



Figure 5.3.3: Example that shows how a moving average filter can distort the signal when applied to the noisy signal in the upper left quadrant of Figure 5.3.2. The original pure signal is shown in black and the signal after applying a 23-point moving average filter is shown in blue. The width of the moving average filter is shown by the red bar.

## Savitzky-Golay Filters

A moving average filter weights all points equally; that is, points near the edges of the filter contribute to the average as a level equal to points near the filter's center. A Savitzky-Golay filter uses a polynomial model that weights each point differently, placing more weight on points near the center of the filter and less weight on points at the edge of the filter. Specific values depend on the size of the window and the polynomial model; for example, a five-point filter using a second-order polynomial has weights of

$$-3/35 \quad 12/35 \quad 17/35 \quad 12/35 \quad -3/35$$

For example, suppose the first five points in a sequence are

| | | | | |
|---|---|---|---|---|
| 0.80 | 0.30 | 0.80 | 0.20 | 1.00 |

then this Savitzky-Golay filter returns values of

| | | | | |
|---|---|---|---|---|
| NA | NA | 0.41 | NA | NA |

where, for example, the value for the middle point is

$$0.80 \times \frac{-3}{35} + 0.30 \times \frac{12}{35} + 0.80 \times \frac{17}{35} + 0.20 \times \frac{12}{35} + 1.00 \times \frac{-3}{35} = 0.406 \approx 0.41$$

Note that we lose $(w-1)/2 = (5-1)/2 = 2$ points at each end of the data set, where *w* is the filter's range, because we do not have a sufficient number of data points to complete the calculations. For other Savitzky-Golay smoothing filters, see Savitzky, A.; Golay, M. J. E. *Anal Chem*, **1964**, *36*, 1627-1639. Figure 5.3.4 shows the improvement in the $S/N$ ratio when using Savitzky-Golay filters using a second-order polynomial with 5, 9, and 13 points.

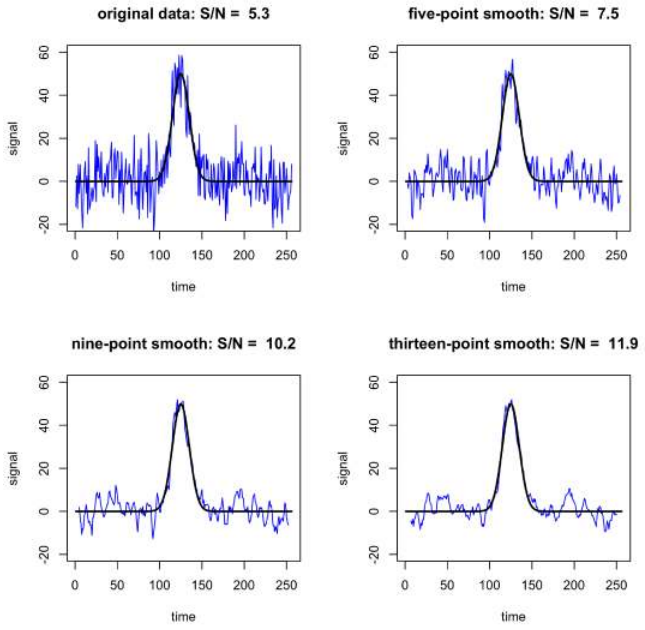



Figure 5.3.4: Improvement in the signal-to-noise ratio using Savitzky-Golay filters of ranges of 5, 9, and 13 on the original data shown in the upper left quadrant. Each plot shows the noisy signal in blue with the pure signal superimposed in black.

Because a Savitzky-Golay filter weights points differently than does a moving average smoothing filter, a Savitzky-Golay filter introduces less distortion to the signal, as we see in the following figure.

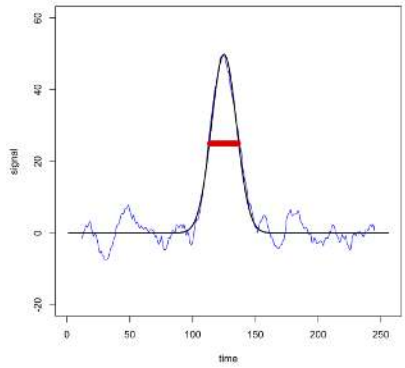



Figure 5.3.5: A Savitzky-Golay filter is less aggressive than a moving average filter. Applying a 23-point Savitzky-Golay filter to the noisy signal in the upper left quadrant of Figure 5.3.4 results in little distortion of the signal. Contrast this with Figure 5.3.3 where a 23-point moving average filter results in substantial distortion of the signal. The original pure signal is shown in black and the signal after applying a 23-point Savitzky-Golay filter is shown in blue. The width of the Savitzky-Golay filter is shown by the red bar.

## Fourier Filtering

This approach to improving the signal-to-noise ratio takes advantage of a mathematical technique called a Fourier transform (FT). The basis of a Fourier transform is that we can express a signal in two separate domains. In the first domain the signal is characterized by one or more peaks, each defined by its position, its width, and its area; this is called the frequency domain. In the second domain, which is called the time domain, the signal consists of a set of oscillations, each defined by its frequency, its amplitude, and its decay rate. The Fourier transform—and the inverse Fourier transform—allow us to move between these two domains.

**Note**

The mathematical details behind the Fourier transform are beyond the level of this textbook; for a more in-depth treatment, consult this series of articles from the *Journal of Chemical Education*:

- Glasser, L. "Fourier Transforms for Chemists: Part I. Introduction to the Fourier Transform," *J. Chem. Educ.* **1987**, *64*, A228–A233.
- Glasser, L. "Fourier Transforms for Chemists: Part II. Fourier Transforms in Chemistry and Spectroscopy," *J. Chem. Educ.* **1987**, *64*, A260–A266.
- Glasser, L. "Fourier Transforms for Chemists: Part III. Fourier Transforms in Data Treatment," *J. Chem. Educ.* **1987**, *64*, A306–A313.

Figure 5.3.6*a* shows a single peak in the frequency domain and Figure 5.3.6*b* shows its equivalent time domain signal. There are correlations between the two domains:

- the further a peak in the frequency domain is from the origin, the greater it corresponding oscillation frequency in the time domain
- the broader a peak's width in the frequency domain, the faster its decay rate in the time domain
- the greater the area under a peak in the frequency domain, the higher its initial intensity in the time domain

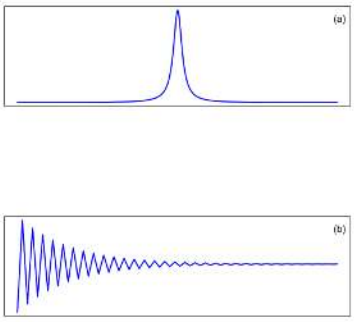



Figure 5.3.6: The plot in (a) shows a frequency domain consisting of a single peak defined by its position along the *x*-axis, its width, and its area. The plot in (b) shows the corresponding time domain that consists of a single oscillating signal defined by its oscillation frequency, its initial intensity, and its decay rate.

We can use a Fourier transform to improve the signal-to-noise ratio because the signal is a single broad peak and the noise appears as a multitude of very narrow peaks. As noted above, a broad peak in the frequency domain has a fast decaying signal in the time domain, which means that while the beginning of the time domain signal includes contributions from the signal and the noise, the latter part of the time domain signal includes contributions from noise only. The figure below shows how we can take advantage of this to reduce the noise and improve the signal-to-noise ratio for the noisy signal in Figure 5.3.7*a*, which has 256 points along the *x*-axis and has a signal-to-noise ratio of 5.1. First, we use the Fourier transform to convert its original domain into the new domain, the first 128 points of which are shown in Figure 5.3.7*b* (note: the first half of the data contains the same information as the second half of the data, so we only need to look at the first half of the data). The points at the beginning are dominated by the signal, which is why there is a systematic decrease in the intensity of the oscillations; the remaining points are dominated by noise, which is why the variation in intensity is random. To filter out the noise we retain the first 24 points as they are and set the intensities of the remaining points to zero (the choice of how many points to retain may require some adjustment). As shown in Figure 5.3.7*c*, we repeat this for the remaining 128 points, retaining the last 24 points as they are. Finally, we use an inverse Fourier transform to return to our original domain, with the result in Figure 5.3.7*d*, with the signal-to-noise ratio improving from 5. 1 for the original noisy signal to 11.2 for the filtered signal.

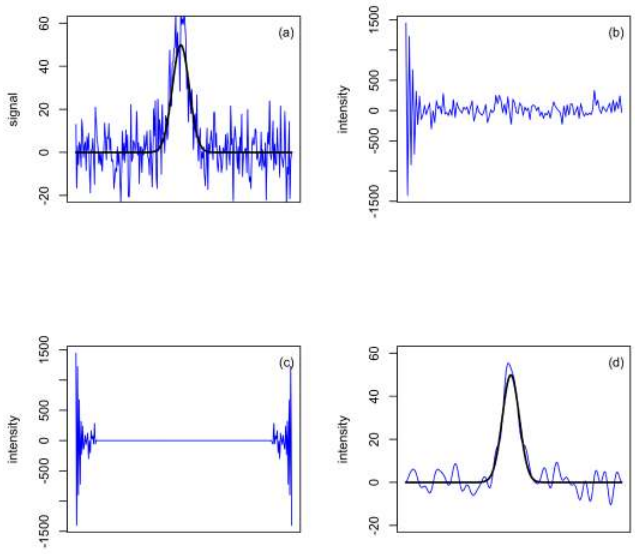



Figure 5.3.7: Example of removing noise using a Fourier filter. The original noisy signal with $S/N = 5.1$ is shown in (a) and is similar to the noisy signal in Figure 5.3.2$a$ and Figure 5.3.4$a$. The first half of the Fourier transformed data is shown in (b). The Fourier transformed data is shown in (c) after zeroing out all but the first and the last 24 points. Returning to the original domain gives the final filtered signal with $S/N = 11.1$.

This page titled 5.3: Signal-to-Noise Enhancement is shared under a CC BY-NC-SA 4.0 license and was authored, remixed, and/or curated by David Harvey.

# CHAPTER OVERVIEW

## 6: An Introduction to Spectrophotometric Methods


6.1: General Properties of Electromagnetic Radiation

6.2: Wave Properties of Electromagnetic Radiation

6.3: Quantum Mechanical Properties of Electromagnetic Radiation

6.4: Emission and Absorbance Spectra

6.5: Quantitative Considerations


---


This page titled 6: An Introduction to Spectrophotometric Methods is shared under a CC BY-NC-SA 4.0 license and was authored, remixed, and/or curated by David Harvey.

# 6.1: General Properties of Electromagnetic Radiation

Electromagnetic radiation—light—is a form of energy whose behavior is described by the properties of both waves and particles. Some properties of electromagnetic radiation, such as its refraction when it passes from one medium to another ($Figure 6.1.1$), are explained best when we describe light as a wave. Other properties, such as absorption and emission, are better described by treating light as a particle. The exact nature of electromagnetic radiation remains unclear, as it has since the development of quantum mechanics in the first quarter of the 20th century [Home, D.; Gribbin, J. *New Scientist* 1991, 2 Nov. 30–33]. Nevertheless, this dual model of wave and particle behavior provides a useful description for electromagnetic radiation.



Figure 6.1.1. The Golden Gate bridge as seen through rain drops. Refraction of light by the rain drops produces the distorted images. Source: Brocken Inaglory (commons. Wikipedia.org).

## The Electromagnetic Spectrum

The frequency and the wavelength of electromagnetic radiation vary over many orders of magnitude. For convenience, we divide electromagnetic radiation into different regions—the electromagnetic spectrum—based on the type of atomic or molecular transitions that gives rise to the absorption or emission of photons (Figure 6.1.2). The boundaries between the regions of the electromagnetic spectrum are not rigid and overlap between spectral regions is possible.

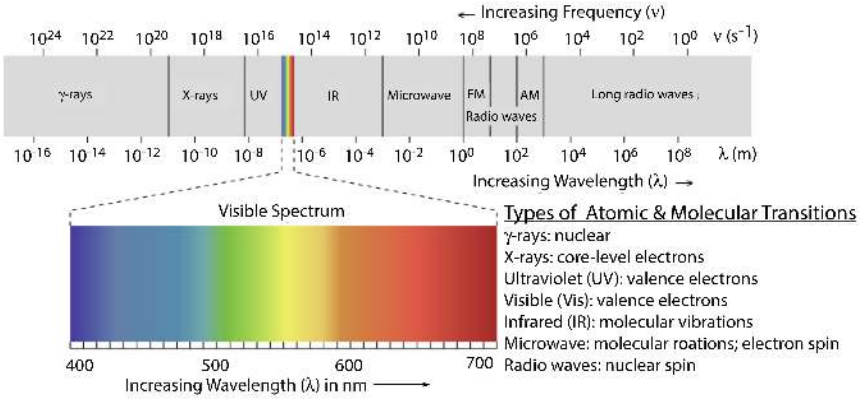



Figure 6.1.2. The electromagnetic spectrum showing the boundaries between different regions and the type of atomic or molecular transitions responsible for the change in energy. The colored inset shows the visible spectrum. Source: modified from Zedh (www.commons.Wikipedia.org).

This page titled 6.1: General Properties of Electromagnetic Radiation is shared under a CC BY-NC-SA 4.0 license and was authored, remixed, and/or curated by David Harvey.

# 6.2: Wave Properties of Electromagnetic Radiation

## Ways to Characterize a Wave

Electromagnetic radiation consists of oscillating electric and magnetic fields that propagate through space along a linear path and with a constant velocity. The oscillations in the electric field and the magnetic field are perpendicular to each other and to the direction of the wave's propagation. Figure 6.2.1 shows an example of plane-polarized electromagnetic radiation, which consists of a single oscillating electric field and a single oscillating magnetic field.

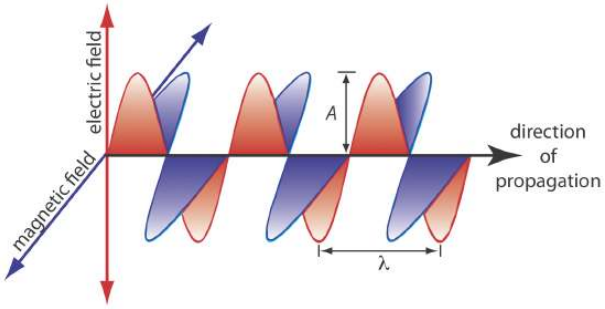



Figure 6.2.1. Plane-polarized electromagnetic radiation showing the oscillating electric field in blue and the oscillating magnetic field in red. The radiation's amplitude, *A*, and its wavelength, $\lambda$, are shown. Normally, electromagnetic radiation is unpolarized, with oscillating electric and magnetic fields present in all possible planes perpendicular to the direction of propagation.

### Measurable Properties

An electromagnetic wave is characterized by several fundamental properties, including its velocity, amplitude, frequency, phase angle, polarization, and direction of propagation [Ball, D. W. *Spectroscopy* **1994**, *9(5)*, 24–25]. Focusing on the oscillations in the electric field, amplitude is the maximum displacement of the electrical field. The wave's frequency, $\nu$, is the number of oscillations in the electric field per unit time. Wavelength, $\lambda$ is defined as the distance between successive maxima . Figure 6.2.1 shows the initial amplitude as 0; the phase angle $\Phi$ accounts for the fact that the initial amplitude need not be zero, which we can accomplish by shifting the wave along the direction of propagation.

There is a relationship between wavelength and frequency, which is

$$\lambda = \frac{c}{\nu}$$

where $c$ is the speed of light in a vacuum. Another unit useful unit is the wavenumber, $\overline{\nu}$, which is the reciprocal of the wavelength

$$\overline{\nu} = \frac{1}{\lambda}$$

Wavenumbers frequently are used to characterize infrared radiation, with the units given in $cm^{-1}$. Power, $P$, and intensity, $I$, are two additional properties of light, both related to the square of the amplitude; power is the energy transferred per second and intensity is the power transferred to a given area.

In a vacuum, electromagnetic radiation travels at the speed of light, *c*, which is $2.99792 \times 10^8$ m/s. When electromagnetic radiation moves through a medium other than a vacuum, its velocity, *v*, is less than the speed of light in a vacuum. The difference between *v* and *c* is sufficiently small (<0.1%) that the speed of light to three significant figures, $3.00 \times 10^8$ m/s, is accurate enough for most purposes.

> When electromagnetic radiation moves between different media—for example, when it moves from air into water—its frequency, $\nu$, remains constant. Because its velocity depends upon the medium in which it is traveling, the electromagnetic radiation's wavelength, $\lambda$, changes. If we replace the speed of light in a vacuum, *c*, with its speed in the medium, $v$, then the wavelength is
>
> $$\lambda = \frac{v}{\nu}$$

This change in wavelength as light passes between two media explains the refraction of electromagnetic radiation seen in the photograph of light passing through rain drop, what was included in the previous section. This is discussed in more detail later in this section.

### Example 6.2.1

In 1817, Josef Fraunhofer studied the spectrum of solar radiation, observing a continuous spectrum with numerous dark lines. Fraunhofer labeled the most prominent of the dark lines with letters. In 1859, Gustav Kirchhoff showed that the D line in the sun's spectrum was due to the absorption of solar radiation by sodium atoms. The wavelength of the sodium D line is 589 nm. What are the frequency and the wavenumber for this line?

**Solution**

The frequency and wavenumber of the sodium D line are

$$\nu = \frac{c}{\lambda} = \frac{3.00 \times 10^{8}\ \text{m/s}}{589 \times 10^{-9}\ \text{m}} = 5.09 \times 10^{14}\ \text{s}^{-1}$$

$$\overline{\nu} = \frac{1}{\lambda} = \frac{1}{589 \times 10^{-9}\ \text{m}} \times \frac{1\ \text{m}}{100\ \text{cm}} = 1.70 \times 10^{4}\ \text{cm}^{-1}$$

### Exercise 6.2.1

Another historically important series of spectral lines is the Balmer series of emission lines from hydrogen. One of its lines has a wavelength of 656.3 nm. What are the frequency and the wavenumber for this line?

**Answer**

The frequency and wavenumber for the line are

$$\nu = \frac{c}{\lambda} = \frac{3.00 \times 10^{8}\ \text{m/s}}{656.3 \times 10^{-9}\ \text{m}} = 4.57 \times 10^{14}\ \text{s}^{-1}$$

$$\overline{\nu} = \frac{1}{\lambda} = \frac{1}{656.3 \times 10^{-9}\ \text{m}} \times \frac{1\ \text{m}}{100\ \text{cm}} = 1.524 \times 10^{4}\ \text{cm}^{-1}$$

## Polarization

Figure 6.2.1 shows a single oscillating electrical field and, perpendicular to that, a single oscillating magnetic field. This is an example of plane polarized light in which oscillation of the electrical field occurs at just one angle. Normally electromagnetic radiation oscillates simultaneously at all possible angles. Figure 6.2.2 shows the difference in these two cases. If we observe the plane polarized light as it oscillates toward us, we see the single line at the top of the figure where blue indicates a positive amplitude and red indicates a negative amplitude, and where the opacity of the shading shows the change in the amplitudes. The vertical dashed lines show nodes where the amplitude is zero and where no light is seen. With ordinary light, we see a circular beam of radiation because the electrical field is oscillating at all angles. The amplitude's sign and magnitude, and the presence of nodes where the amplitude is zero, remain evident to us. Note that if we observe the source's intensity, then the each of the lines and circles in Figure 6.2.2 will appear blue (positive values as intensity is proportion to the square of the amplitude); we continue to observe fluctuations in the intensity and the presence of the nodes.

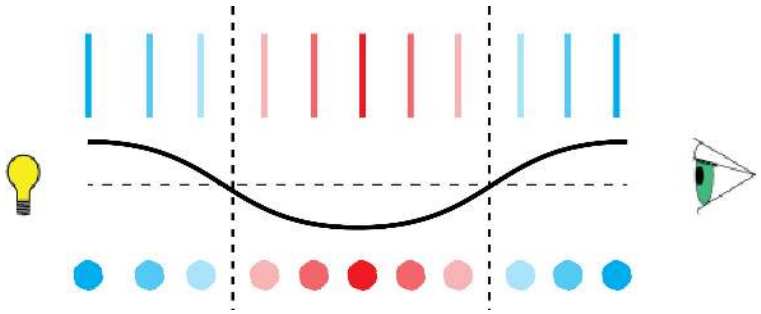


Figure 6.2.2: Illustration showing the difference between plane polarized light (top) and ordinary light (bottom). Blue is used to show positive amplitudes and red is used to show negative amplitudes. The opacity of the colors—which have values of 100%, 67%, 33%, and 0%—indicate the relative magnitudes of the amplitudes. When the opacity is 0%, the amplitude is zero and there is a node.

## Mathematical Representation of Waves

We can describe the oscillations in the electric field as a sine wave

$$A_t = A_e \sin(2\pi\nu t + \Phi)$$

where $A_t$ is the magnitude of the electric field at time $t$, $A_e$ is the field's maximum amplitude, $\nu$ is the wave's frequency, and $\Phi$ is a phase angle that accounts for the fact that $A_t$ need not have a value of zero at time $t = 0$. The identical equation for the magnetic field is

$$A_t = A_m \sin(2\pi\nu t + \Phi)$$

where $A_m$ is the magnetic field's maximum amplitude.

One of the important features of waves is that adding or subtracting together two (or more) gives a new wave. Figure 6.2.3 shows one example. The superposition of waves explains why two identical waves that are completely out-of-phase with each other produce a signal in which the amplitude is zero at all points.

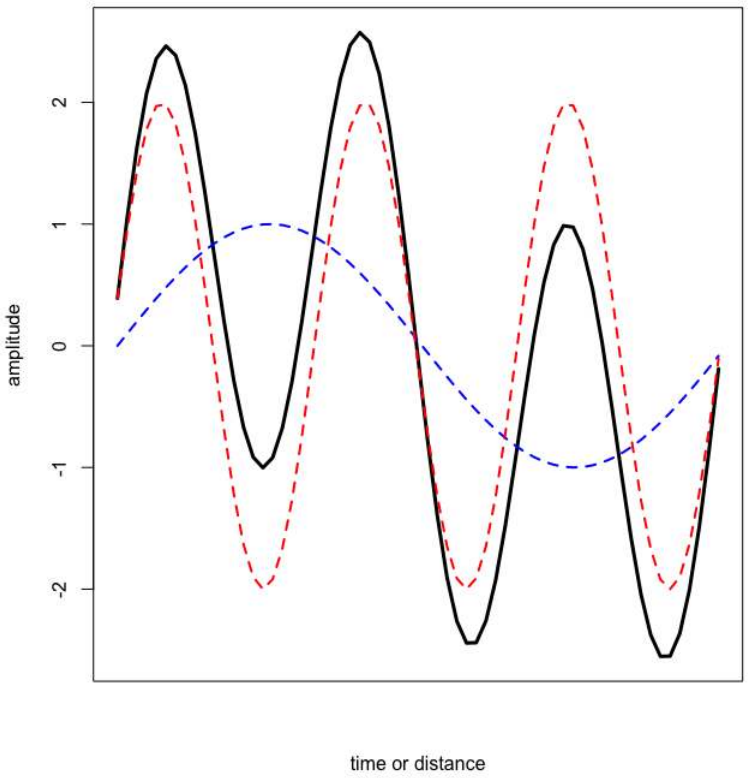



Figure 6.2.3: Illustration of the principle of superposition. The x-axis scale runs from zero to $2\pi$. The equation for the wave shown as a dashed blue line is $y = sin(x)$ and the equation for the wave shown as a dashed red line is $y = 2sin(\pi/16 + 3x)$. The sum of these two waves is the solid black line.

Another important consequence of the superposition of waves is that if we can add together a series of waves to produce a new wave, then there is a corresponding mathematical process that takes a complex wave and determines the underlying set of sine waves of which it is comprised. This process is called a Fourier transform, which we will revisit in later chapters.

## Interactions of Waves With Matter

When light encounters matter—perhaps a particle, a solution, or a thin film—it can interact with it in several ways. In this section we consider two such interactions: refraction and reflection. Three additional types of interactions—the scattering of light, the diffraction of light, and the transmission of light—are considered in later chapters where they play an important role in specific instrumental methods of analysis.

### Refraction

When light passes from one medium (perhaps air) into another medium (perhaps water) that has a different density, the light experiences a change in direction that is a consequence of a difference in its velocity in the two media. This bending of light is called refraction, the extent of which is given by Snell's law

$$\frac{\sin \theta_1}{\sin \theta_2} = \frac{\eta_2}{\eta_1} = \frac{v_1}{v_2}$$

where $\eta_i$ is the refractive index of a medium and $v_i$ is the velocity in a medium, and where the angles, $\theta_i$, are shown in Figure 6.2.4.

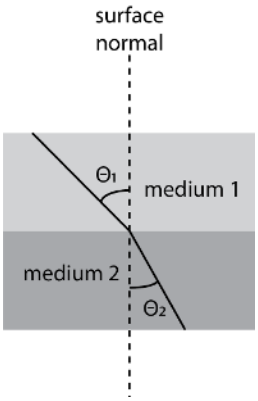



Figure 6.2.4: Illustration of the refraction of light as it moves across the interface of two media with different refractive indexes. The angles of the light are given by $\theta$ and are measured relative to a surface normal, which is shown by the dashed line. The denser medium has the smaller value of $\theta$ and the larger the refractive index.

## Reflection

In addition to refraction, when light crosses an interface that separates media with different refractive indexes, some of the light is reflected back. When then angle of incidence is 0° (that is, the light is perpendicular to the interface), then the fraction of light that is reflected is given by

$$\frac{I_r}{I_0} = \frac{(\eta_2 - \eta_1)^2}{(\eta_2 + \eta_1)^2}$$

where $I_r$ is the intensity of light that is reflected, $I_0$ is the intensity of light from the source that enters the interface, and $\eta_i$ is the refractive index of the media. If light crosses more than one interface—as is the case when light passes through a sample cell—then the total fraction of reflected light is the sum of the fraction of light reflected at each interface.

---

This page titled 6.2: Wave Properties of Electromagnetic Radiation is shared under a CC BY-NC-SA 4.0 license and was authored, remixed, and/or curated by David Harvey.

# 6.3: Quantum Mechanical Properties of Electromagnetic Radiation

In the last section, we considered properties of electromagnetic radiation that are consistent with identifying light as a wave. Other properties of light, however, cannot be explained by a model that treats it as a wave; instead, we need to consider a model that treats light as a system of discrete particles, which we call photons.

## The Photoelectric Effect

As shown in Figure 6.3.1, in a photoelectric cell, a metal, such as sodium, is held under vacuum and exposed to electromagnetic radiation, which enters the cell through an optical window. If the frequency of the radiation is sufficient, electrons escape from the metal with a kinetic energy that we can measure; we call these photoelectrons. If the photocell's anode is held at a potential that is positive relative to the potential applied to the cathode, the photoelectrons move from the cathode to the anode, generating a current that is measured by an ammeter. If the voltage applied to the anode is made sufficiently negative, the electrons eventually fail to reach the anode and the current decreases to zero. The voltage needed to stop the flow of electrons is called the stopping voltage.

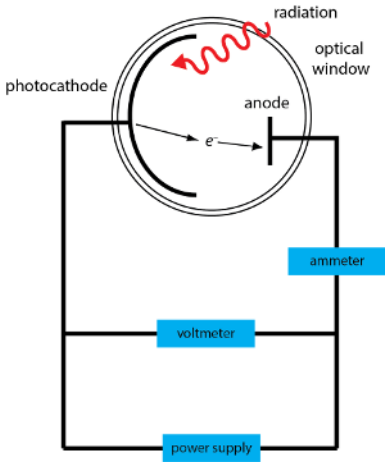



Figure 6.3.1: Illustration of a photoelectric cell. The photocathode is fashioned from or coated with a metal and placed in an evacuated cell along with an anode. Electromagnetic radiation is focused on the photocathode and, if it has sufficient energy, the metal emits electrons with a kinetic energy that depends on the metal and the frequency of the electromagnetic radiation. The potential applied to the photocathode and the anode determine whether the electrons reach the anode; if they do, then a current flows, which is measured by the ammeter.

In a photoelectron spectrum we vary the frequency and intensity of the electromagnetic radiation and observe their effect on either the number of photoelectrons released (measured as a current) or the energy of the photoelectrons released (measured by their kinetic energy). A typical set of experiments are shown in Figure 6.3.2$a$ using Na and in Figure 6.3.2$b$ using Na, Zn, and Cu. The data show several interesting features. First, we see in Figure 6.3.2$a$ that the intensity of the light source has no effect on the minimum frequency of light needed to eject a photoelectron from Na—we call this the threshold frequency—but that a high intensity source of electromagnetic radiation results in the release of a greater number of photoelectrons and, therefore, a greater current than for a lower intensity source. Second, we see in Figure 6.3.2$b$ that different metals have different threshold frequencies, but that once we exceed each metal's threshold frequency, the change in the kinetic energy of the photoelectrons with increasing frequency yields lines of equal slopes.

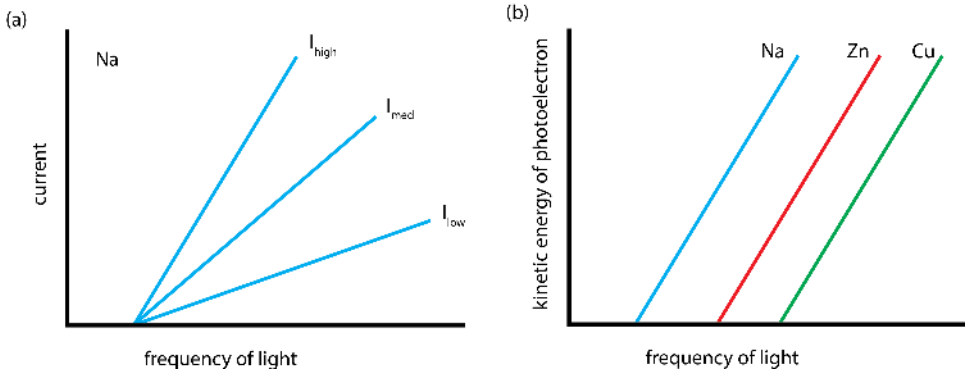



Figure 6.3.2: The two types of photoelectric effect experiments. In (a) we measure the current that flows as we change the intensity and the frequency of the electromagnetic radiation. In (b) we measure the kinetic energy of the photoelectrons as a function of the frequency of the electromagnetic radiation.

We can explain these experimental observations if we assume that the source of electromagnetic energy has an energy, $E_{\text{ER}}$, that does two things: it overcomes the energy that binds the photoelectron to the metal, $E_{\text{BE}}$, and it imparts the remaining energy into the photoelectron's kinetic energy, $E_{\text{KE}}$, where ER means electromagnetic radiation, BE means binding energy and KE means kinetic energy.

$$E_{\text{KE}} = E_{\text{ER}} - E_{\text{BE}}$$

A wave model for electromagnetic radiation is insufficient to explain the photoelectric effect because when it strikes the metal the radiation's energy would be distributed across all atoms on the surface, none of which would then receive an energy that exceeds the photoelectron's binding energy. Instead, the results in Figure 6.3.2 make sense only if we assume that light consists of discrete particles with energies that are a function of frequency or wavelength

$$E_{\text{ER}} = h\nu = \frac{hc}{\lambda} \tag{6.3.1}$$

where $h$ is Plank's constant. This leave us with the following equation relating kinetic energy, the energy of the photon, and the binding energy of the electron.

$$E_{\text{KE}} = h\nu - E_{\text{BE}}$$

Note that the slope of the lines in Figure 6.3.2*b* is Plank's constant.

## Energy States

Equation 6.3.1 is central to the particle, or quantum mechanical model of the atom in which we understand that chemical species—atoms, ions, molecules—exist only in discrete states, each with a single, well-defined energy. A wave, on the other hand, can take on any energy. A simple image is the possible energies of a ball as it rolls down a ramp (wave) or a staircase (particle), as in Figure 6.3.3.

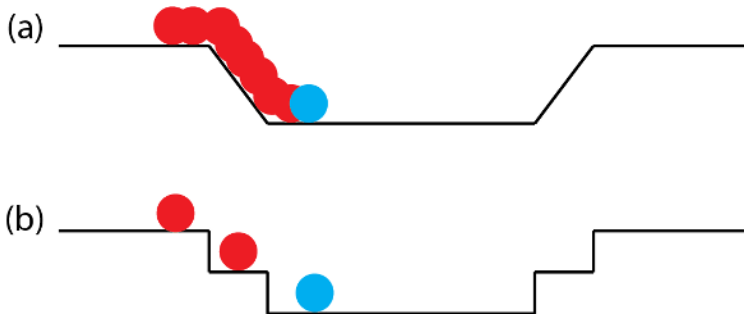



Figure 6.3.3. The energy of a ball is measured by its height relative to its final position, shown in blue. When a ball rolls down a ramp, as in (a), it can take on any energy between its initial and final energies. When a ball rolls down a staircase, as in (b), it can take only certain discrete energies. The ball in (b) is said to be quantized.

When an atom, ion, or molecule moves between two of these discrete states, the difference in energy, $\Delta E$, is given by

$$\Delta E = h\nu = \frac{hc}{\lambda}$$

In absorption spectroscopy a photon is absorbed by an atom, ion, or molecule, which undergoes a transition from a lower-energy state to a higher-energy, or excited state (Figure 6.3.4*a*). The reverse process, in which an atom, ion, or molecule emits a photon as it moves from a higher-energy state to a lower energy state (6.3.4*b*), is called emission.

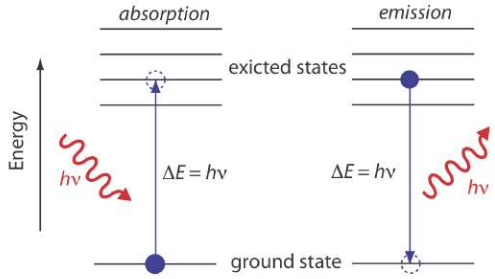



Figure 6.3.4. A simplified energy diagram that shows the absorption and emission of a photon by an atom or a molecule. When a photon of energy $h\nu$ strikes the atom, ion, or molecule, absorption may occur if the difference in energy, $\Delta E$, between the ground state and the excited state is equal to the photon's energy. An atom, ion, or molecule in an excited state may emit a photon and return to the ground state. The photon's energy, $h\nu$, equals the difference in energy, $\Delta E$, between the two states.

The types of energy states involved in emission and absorption depend on the energy of the electromagnetic radiation. In general, $\gamma$ -rays involve transitions between nuclear states, X-rays probe the energies of core-level electrons, ultraviolet-visible radiation probes the energies of valence electrons, infrared radiation provides information on vibrational energy states, microwave radiation probes rotational energy levels and electron spins, and radio waves provide information on nuclear spins. While infrared spectroscopy may provide information on a molecule's vibrational energy states, the energies available in ultraviolet-visible spectroscopy provide information on both the molecule's electronic states and its vibrational states, as shown in Figure 6.3.5.

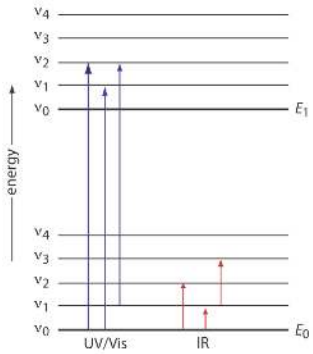



Figure 6.3.5. Diagram showing two electronic energy levels ($E_0$ and $E_1$), each with five vibrational energy levels $\nu_{0-4}$. Absorption of ultraviolet and visible radiation (shown by the blue arrows) leads to a change in the analyte's electronic energy levels and, possibly, a change in vibrational energy as well. A change in vibrational energy without a change in electronic energy levels occurs with the absorption of infrared radiation (shown by the red arrows).

This page titled 6.3: Quantum Mechanical Properties of Electromagnetic Radiation is shared under a CC BY-NC-SA 4.0 license and was authored, remixed, and/or curated by David Harvey.

# 6.4: Emission and Absorbance Spectra

In the last section we considered the source of emission and absorption. In this section we consider the types of emission and absorbance spectra that we will form the basis for many of the chapters that follow.

## Emission Spectra

When an atom, ion, or molecule moves from a higher-energy state to a lower-energy state it emits photons with energies equal to the difference in energy between the two states. The result is an emission spectrum that shows the intensity of emission as a function of wavelength. The shapes of these emission spectra fall into two broad types: line spectra and band spectra.

### Line Spectra

When the energy states are well separated from each other, and when there is just one type of transition between the energy states, the result is a line spectrum that consists of a small number of narrow bands. Figure 6.4.1, for example, shows the emission spectrum from gas phase Cu atoms, which consists of seven lines, two of which are too close to each other to resolve them from each other. The individual emissions lines are very narrow, as we might expect, because the atom's energy levels have precise values.

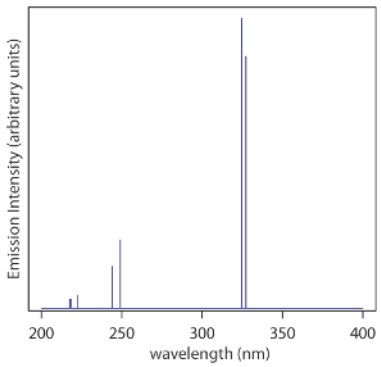



Figure 6.4.1. Emission spectrum from a Cu hollow cathode lamp in which Cu atoms are present in the gas phase. This spectrum consists of seven distinct emission lines (the first two differ by only 0.4 nm and are not resolved at the scale shown in this spectrum). Each emission line has a width of approximately 0.01 nm at 1⁄2 of its maximum intensity. See Chapter 9 for more information on hollow cathode lamps.

### Band Spectra

The emission spectrum for a gas phase atom is relatively simple because the number of possible transitions is small and because their individuals energies are well-separated from each other. When a molecule in a solvent emits light, the number of possible changes in energy levels can be quite large if the molecule undergoes transitions between electronic, vibrational, and rotational energy levels. The resulting spectrum has so many emission individual emission lines that we see a single broad peak, or band, that we call a band spectrum. Figure 6.4.2 shows the emission spectrum for the dye coumarin 343, which is incorporated in a reverse micelle and suspended in cyclohexanol.

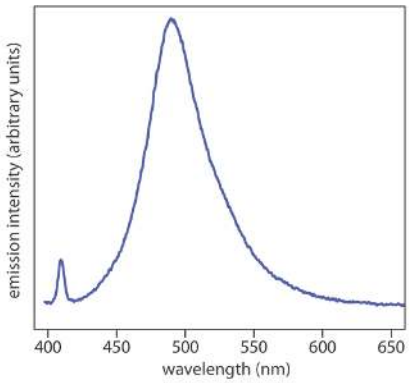



Figure 6.4.2. Emission spectrum of the dye coumarin 343, which is incorporated in a reverse micelle suspended in cyclohexanol. The sharp peak at 409 nm is from the laser source used to excite coumarin 343. The broad band centered at approximately 500 nm is the dye's emission band. Source: data from Bridget Gourley, Department of Chemistry & Biochemistry, DePauw University.

**Note**

When considering sources of electromagnetic radiation for spectroscopic instruments, we usually describe them as line sources and continuous sources depending on on whether they emit discrete lines, as is the case for the hollow cathode lamp in Figure 6.4.1, or exhibit emission over a broad range of wavelengths without any gaps, as is the case for a green light-emitting diode (LED), whose spectrum is shown in Figure 6.4.3.

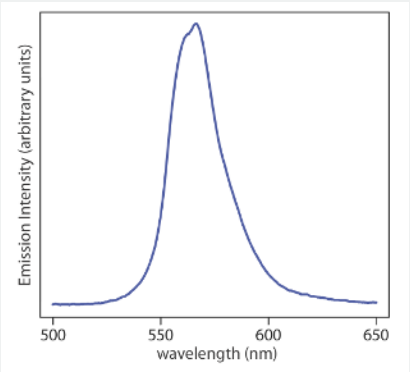



Figure 6.4.3. Spectrum showing the emission from a green LED, which provides continuous emission over a wavelength range of approximately 530–640 nm.

## Absorbance Spectra

When an atom, ion, or molecule moves from a lower-energy state to a higher-energy state it absorbs photons with energies equal to the difference in energy between the two states. The result is an absorbance spectrum that shows the intensity of emission as a function of wavelength. As is the case for emission spectra, absorbance spectra range from narrow lines to broad bands. The atomic absorption spectrum for Na is shown in Figure 6.4.4, and is typical of that found for most atoms. The most obvious feature of this spectrum is that it consists of a small number of discrete absorption lines that correspond to transitions between the ground state (the 3*s* atomic orbital) and the 3*p* and the 4*p* atomic orbitals.

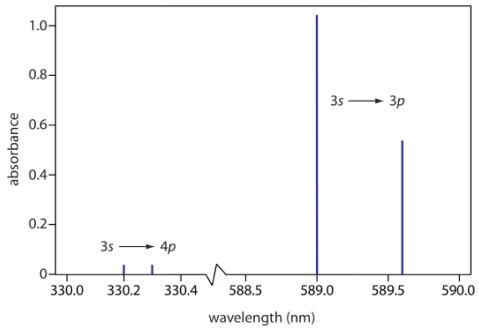



Figure 6.4.4. Atomic absorption spectrum for sodium. Note that the scale on the *x*-axis includes a break.

Another feature of the atomic absorption spectrum in Figure 6.4.4 is the narrow width of the absorption lines, which is a consequence of the fixed difference in energy between the ground state and the excited state, and the lack of vibrational and rotational energy levels. Natural line widths for atomic absorption, which are governed by the uncertainty principle, are approximately $10^{-5}$ nm. Other contributions to broadening increase this line width to approximately $10^{-3}$ nm.

The absorbance spectra for molecules consists of broad bands for the same reasons discussed above for emission spectra. The UV/Vis spectrum for cranberry juice in Figure 6.4.5 shows a single broad band for the anthocyanin dyes that are responsible for its red color. The IR spectrum for ethanol in Figure 6.4.6 shows multiple absorption bands, some broader and some narrower. The narrow bands, however, are still much broader than the lines in the atomic absorption spectrum for Na.

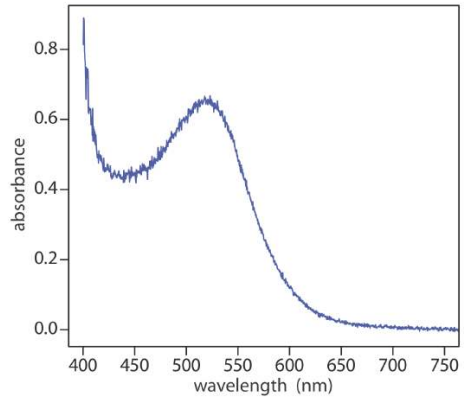



Figure 6.4.5. Visible absorbance spectrum for cranberry juice. The anthocyanin dyes in cranberry juice absorb visible light with blue, green, and yellow wavelengths; as a result, the juice appears red.

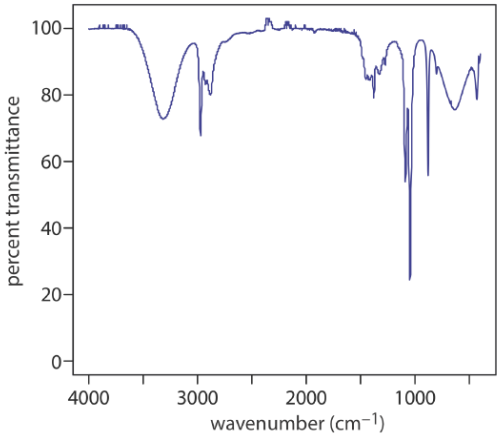



Figure 6.4.6. Infrared spectrum of ethanol.

This page titled 6.4: Emission and Absorbance Spectra is shared under a CC BY-NC-SA 4.0 license and was authored, remixed, and/or curated by David Harvey.

# 6.5: Quantitative Considerations

An important part of the chapters that follow is a consideration of how we can use the emission or absorbance of photons to determine the concentration of an analyte in a sample. Here we provide a brief summary of quantitative spectroscopic methods of analysis in Table 6.5.1, leaving more specific details for later chapters.

Table 6.5.1. Quantitative spectroscopic methods of analysis.

| What happens to the photons? | What do we measure? | What is the relationship between what we measure and concentration, $C$? | What are some examples? |
|---|---|---|---|
| emitted | the power, $P_e$, of emitted light | $P_e = kC$ | flame atomic emission, molecular fluorescence and phosphorescence |
| scattered | the power, $P_{sc}$, of scattered light | $P_{sc} = kC$ | nephelometry, turbidity, Raman spectroscopy |
| absorbed | the power, $P_t$, of transmitted light relative to the power, $P_0$, of the light source | $-\log\left(\frac{P_t}{P_0}\right)$ | flame atomic absorbance, molecular absorbance |

This page titled 6.5: Quantitative Considerations is shared under a CC BY-NC-SA 4.0 license and was authored, remixed, and/or curated by David Harvey.

# CHAPTER OVERVIEW

## 7: Components of Optical Instruments

An early example of a colorimetric analysis is Nessler's method for ammonia, which was introduced in 1856. Nessler found that adding an alkaline solution of $HgI_2$ and KI to a dilute solution of ammonia produced a yellow-to-reddish brown colloid, in which the colloid's color depended on the concentration of ammonia. By visually comparing the color of a sample to the colors of a series of standards, Nessler was able to determine the concentration of ammonia. Colorimetry, in which a sample absorbs visible light, is one example of a spectroscopic method of analysis. At the end of the nineteenth century, spectroscopy was limited to the absorption, emission, and scattering of visible, ultraviolet, and infrared electromagnetic radiation. Since then, spectroscopy has expanded to include other forms of electromagnetic radiation—such as X-rays, microwaves, and radio waves—and other energetic particles—such as electrons and ions.


7.1: General Design of Optical Instruments

7.2: Sources of Radiation

7.3: Wavelength Selectors

7.4: Sample Containers

7.5: Radiation Transducers

7.6: Fiber Optics

7.7: Fourier Transform Optical Spectroscopy


Thumbnail: A diffraction grating monochromator.


This page titled 7: Components of Optical Instruments is shared under a CC BY-NC-SA 4.0 license and was authored, remixed, and/or curated by David Harvey.

# 7.1: General Design of Optical Instruments

The spectroscopic techniques in the chapters that follow use instruments that share several common basic components: a source of energy; a means for holding the sample of interest to us; a device that can isolate a narrow range of wavelengths; a detector for measuring the signal; and a signal processor that displays the signal in a form convenient for the analyst. Figure 7.1.1 shows four common ways of stringing together these units.

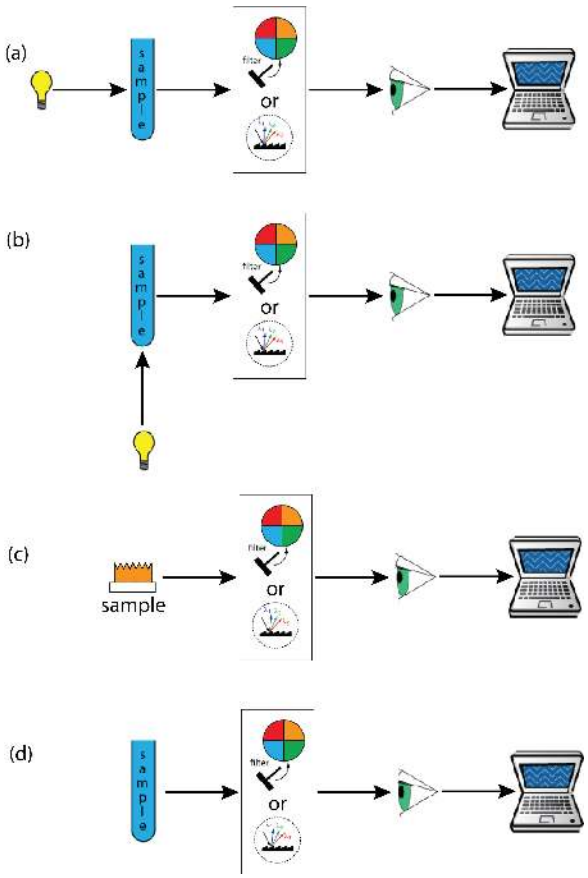



Figure 7.1.1: Four common optical benches for spectroscopy. Each of (a), (b), and (c) includes a source of energy either in the form of electromagnetic radiation (a, b) or thermal energy (c), a means for introducing the sample, a means for selecting the wavelengths of electromagnetic radiation to monitor, a detector, and a signal processor. In (d), the source of energy comes from a chemical reaction. The optical bench in (a) is suitable for absorbance measurements; the optical bench in (b) is suitable for fluorescence measurements; the optical bench in (c) is suitable for emission measurements, and the optical bench in (d) is suitable for chemiluminescence measurements.

The remaining sections of this chapter provide general information on each of these units. More specific details appear in the chapters on individual methods.

This page titled 7.1: General Design of Optical Instruments is shared under a CC BY-NC-SA 4.0 license and was authored, remixed, and/or curated by David Harvey.

# 7.2: Sources of Radiation

All forms of spectroscopy require a source of energy to place the analyte in an excited state. In absorption and scattering spectroscopy this energy is supplied by photons. Emission and photoluminescence spectroscopy use thermal energy, radiant (photon) energy, or chemical energy to promote the analyte to a suitable excited state. In this section we consider the sources of radiant energy.

## Sources of Electromagnetic Radiation

A source of electromagnetic radiation must provide an output that is both intense and stable in the region of interest. Sources of electromagnetic radiation are classified as either continuum or line sources. Table 7.2.1 provides a list of some common sources of electromagnetic radiation.

Table 7.2.1. Common sources of electromagnetic radiation.

| source | wavelength region | useful for... |
|---|---|---|
| $H_2$ and $D_2$ lamp | continuum source from 160–380 nm | molecular absorption |
| tungsten lamp | continuum source from 320–2400 nm | molecular absorption |
| Xe arc lamp | continuum source from 200–1000 nm | molecular fluorescence |
| nernst glower | continuum source from 0.4–20 μm | molecular absorption |
| globar | continuum source from 1–40 μm | molecular absorption |
| nichrome wire | continuum source from 0.75–20 μm | molecular absorption |
| hollow cathode lamp | line source in UV/Vis | atomic absorption |
| Hg vapor lamp | line source in UV/Vis | molecular fluorescence |
| laser | line source in UV/Vis/IR | atomic and molecular absorption, fluorescence, and scattering |

Continuum sources emits radiation over a broad range of wavelengths, with a relatively smooth variation in intensity (Figure 7.2.1), and are used for molecular absorbance using UV/Vis and IR radiation. Further details on these sources are in Chapters 13 and 16, respectively.

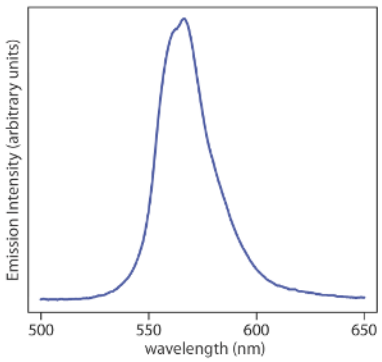



Figure 7.2.1. Spectrum showing the emission from a green LED, which provides continuous emission over a wavelength range of approximately 530–640 nm.

A line source, on the other hand, emits radiation at discrete wavelengths, with broad regions showing no emission lines (Figure 7.2.2), and are used for atomic absorption, atomic and molecular fluorescence, and Raman spectroscopy. Further details on hollow cathode lamps are included in Chapter 9.

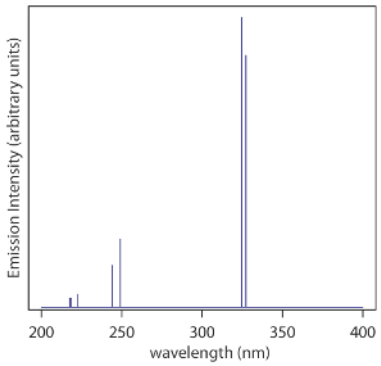



Figure 7.2.2. Emission spectrum from a Cu hollow cathode lamp. This spectrum consists of seven distinct emission lines (the first two differ by only 0.4 nm and are not resolved at the scale shown in this spectrum). Each emission line has a width of approximately 0.01 nm at 1⁄2 of its maximum intensity.

## Laser Sources

An important line source of radiation is a laser, which is an acronym for **l**ight **a**mplification by **s**timulated **e**mission of **r**adiation. Laser emission is monochromatic with a narrow bandwidth of just a few micrometers. As suggested by the term amplification, a laser provides a source of high intensity emission. The source of this intensity is embedded in the term stimulated emission, to which we now turn our attention.

### How a Laser Works

To understand how a laser works, we need to consider four key ideas: pumping, population inversion, stimulated emission, and light amplification.

### Pumping

Emission cannot occur unless we first populate higher energy levels with electrons, which we can accomplish by, for example, the absorption of photons, as shown in Figure 7.2.3. Emission occurs when an electron in a higher energy state relaxes back to a lower energy state by emitting a photon with an energy equal to the difference in the energy between these two states. The process of populating the excited states with electrons is called pumping and is accomplished by using an electrical discharge, by passing an electrical current through the lasing medium, or by absorption of high energy photons. The goal of pumping is to create a large population of excited states.

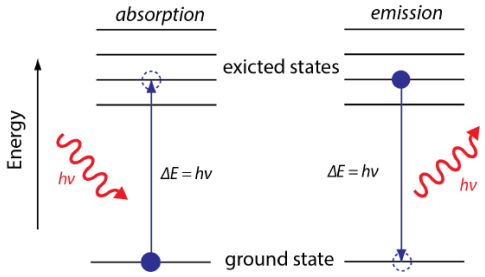



Figure 7.2.3. A general scheme showing the difference between absorption (on the left) and emission (on the right).

### Population Inversion

Normally the majority of the species we are studying are in their ground electronic state with only a small number of species in an excited electronic state. For a laser to achieve a high intensity of emission, it is necessary to create a situation in which there are more species in the excited state than in the ground state, as shown in Figure 7.2.4 where the non-inverted population has four species in the ground state and two species in the excited state, and where the inverted population has four species in the excited state and two species in the ground state.

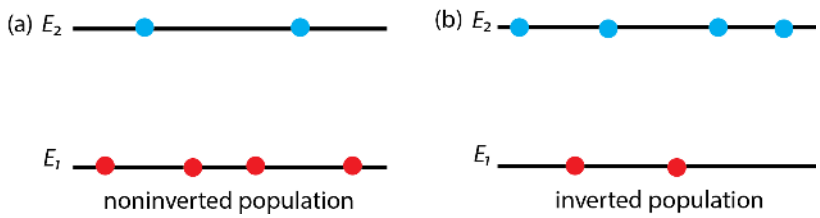



Figure 7.2.4. Illustration of (a) a non-inverted population and (b) an inverted population. In the non-inverted population there are four electrons with energies of $E_1$ and two electrons with energies of $E_2$; for the inverted population there are four electrons with energies of $E_2$ and two electrons with energies of $E_1$.

## Stimulated Emission and Light Amplification

Figure 7.2.3 shows emission of a photon following absorption of a photon of equal energy. No more than one photon is emitted for each photon that is absorbed, with some species in an excited state relaxing to the ground state through non-radiative pathways. This spontaneous emission is a random process, which means that the timing of emission and the direction in which emission occurs are random.

Emission in a laser, as depicted in Figure 7.2.5, is stimulated by a photon with an energy equal to that of the difference in energy between the excited state and the ground state. The interaction of the incoming photon with the excited state results in the excited state's immediate relaxation to the ground state by the emission of a photon. The original photon and the emitted photon are coherent, with identical energies, identical directions, and identical phases. Because two coherent photons are emitted, the amplitude of the emitted radiation is doubled, as we see in Figure 7.2.5; this is what we mean by light amplification.

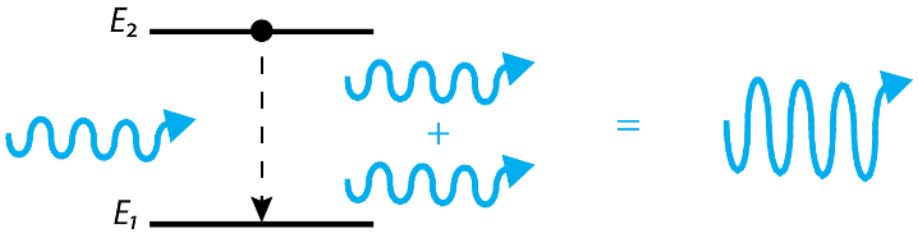



Figure 7.2.5. In stimulated emission, a photo with an energy equivalent to $E_2 - E_1$ stimulates the emission of a photon of equal energy. The two photons are coherent with each other, producing an emission with an amplitude that is double that of the individual photons.

## Laser Systems

As the previous sections suggest, creating a population inversion is the limiting factor in generating radiation from a laser. The two-level system in Figure 7.2.5, which involves a single excited state and a single ground state, cannot create a population inversion because when the ground state and excited state are equal in population, the rate at which excited states are produced through pumping equals the rate at which excited states are lost through emission. To achieve stimulated emission, laser systems use three-level or four-level systems, as outlined in Figure 7.2.6.

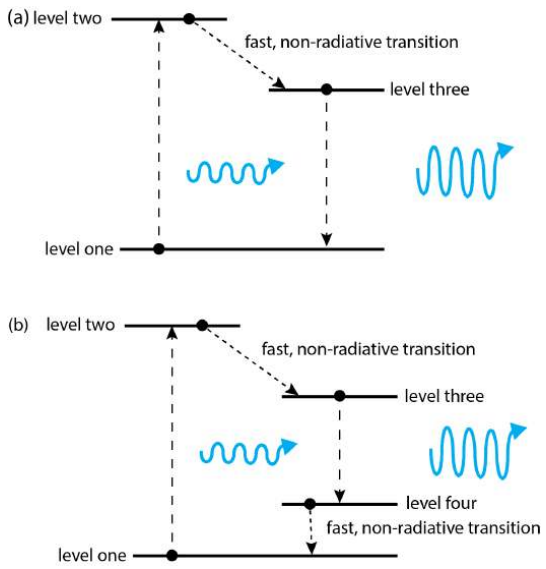



Figure 7.2.6. Examples of (a) a three-level system and (b) a four-level system for generating emission from a laser.

In a three-level system, pumping is used to populate the excited states in level two. From level two, an efficient pathway for non-radiative relaxation populates the excited state in level three, which is sufficiently stable to allow for a population inversion. In a four-level system, the population inversion is achieved between level three and level four.

## Types of Lasers

Lasers are categorized by the nature of the lasing medium: solid-state crystals, gases, dyes, and semiconductors. Solid-state lasers use a crystalline material, such as aluminum oxide, that contains trace amounts of an element, such as chromium or neodymium, which serves as the actual lasing medium. Gas lasers use gas phase atoms, ions, or molecules as a lasing medium. The lasing medium in a dye laser is a solution of an organic dye molecule. A dye laser typically is capable of emitting light over a broad range of wavelengths, but is tunable to a specific wavelength within that range. Finally, a semiconductor laser uses modified light-emitting diodes as a lasing medium.

Table 7.2.2. Examples of Lasers.

| category | lasing medium | wavelengths |
|---|---|---|
| solid state | ruby (0.05% Cr(III) in $Al_2O_3$) | 694.3 nm |
| | Nd:YAG (neodymium ion in yttrium aluminum garnet | 1054 nm; 532 nm |
| gas | He/Ne | 632.8 nm |
| | $Ar^+$ | 514.5 nm, 488 nm |
| | $N_2$ | 337.1 nm |
| | $CO_2$ | 10.6 µm |
| dye | rhodamine | 540–680 nm |
| | fluorescein | 530–560 nm |
| | cumarin | 490–620 nm |
| semiconductor | indium gallium nitride | 405 nm |
| | aluminum gallium indium phosphide | 635 nm |

This page titled 7.2: Sources of Radiation is shared under a CC BY-NC-SA 4.0 license and was authored, remixed, and/or curated by David Harvey.

# 7.3: Wavelength Selectors

In Nessler's original colorimetric method for ammonia, which was described at the beginning of the chapter, the sample and several standard solutions of ammonia are placed in separate tall, flat-bottomed tubes. As shown in Figure 7.3.1, after adding the reagents and allowing the color to develop, the analyst evaluates the color by passing ambient light through the bottom of the tubes and looking down through the solutions. By matching the sample's color to that of a standard, the analyst is able to determine the concentration of ammonia in the sample.

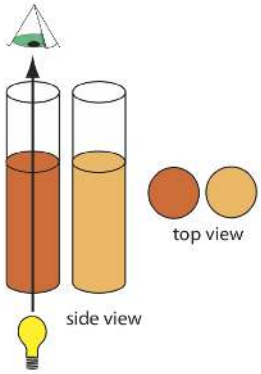



Figure 7.3.1. Nessler's original method for comparing the color of two solutions. Natural light passes upwards through the samples and standards and the analyst views the solutions by looking down toward the light source. The top view, shown on the right, is what the analyst sees. To determine the analyte's concentration, the analyst exchanges standards until the two colors match.

In Figure 7.3.1 every wavelength of light from the source passes through the sample. This is not a problem if there is only one absorbing species in the sample. If the sample contains two components, then a quantitative analysis using Nessler's original method is impossible unless the standards contains the second component at the same concentration as in the sample.

To overcome this problem, we want to select a wavelength that only the analyte absorbs. Unfortunately, we can not isolate a single wavelength of radiation from a continuum source, although we can narrow the range of wavelengths that reach the sample. As seen in Figure 7.3.2, a wavelength selector always passes a narrow band of radiation characterized by a nominal wavelength, an effective bandwidth, and a maximum throughput of radiation. The effective bandwidth is defined as the width of the radiation at half of its maximum throughput.

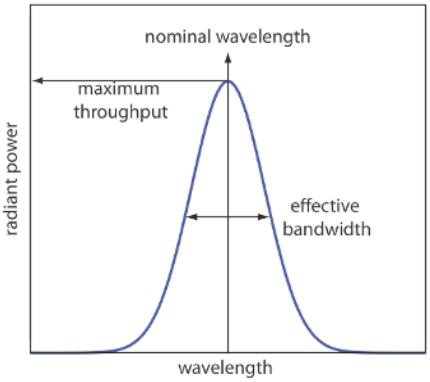



Figure 7.3.2. Radiation exiting a wavelength selector showing the band's nominal wavelength and its effective bandwidth.

The ideal wavelength selector has a high throughput of radiation and a narrow effective bandwidth. A high throughput is desirable because the more photons that pass through the wavelength selector, the stronger the signal and the smaller the background noise. A narrow effective bandwidth provides a higher resolution, with spectral features separated by more than twice the effective bandwidth being resolved. As shown in Figure 7.3.3, these two features of a wavelength selector often are in opposition. A larger effective bandwidth favors a higher throughput of radiation, but provide less resolution. Decreasing the effective bandwidth improves resolution, but at the cost of a noisier signal [Jiang, S.; Parker, G. A. *Am. Lab.* **1981**, October, 38–43]. For a qualitative analysis, resolution usually is more important than noise and a smaller effective bandwidth is desirable; however, in a quantitative analysis less noise usually is desirable.

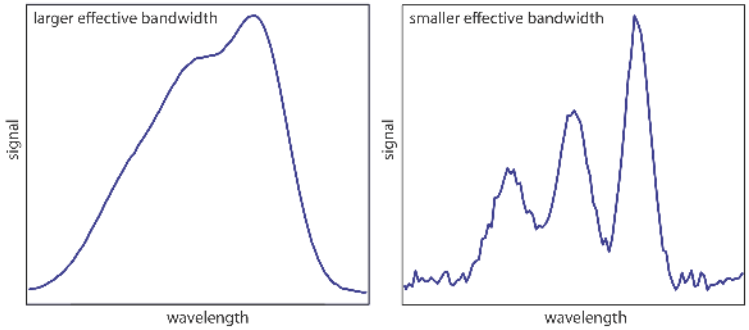



Figure 7.3.3. Example showing the effect of the wavelength selector's effective bandwidth on resolution and noise. The spectrum with the smaller effective bandwidth (on the right) has a better resolution, allowing us to see the presence of three peaks, but at the expense of a noisier signal. The spectrum with the larger effective bandwidth (on the left) has less noise, but at the expense of less resolution between the three peaks.

## Filters

The simplest method for isolating a narrow band of radiation is to use an absorption or interference filter.

### Absorption Filters

As their name suggests, absorption filters work by selectively absorbing radiation from a narrow region of the electromagnetic spectrum. A simple example of an absorption filter is a piece of colored glass or polymer film. A purple filter, for example, removes the complementary color green from 500–560 nm. Commercially available absorption filters provide effective bandwidths of 30–250 nm, although the throughput at the low end of this range often is only 10% of the source's emission intensity. Interference filters are more expensive than absorption filters, but have narrower effective bandwidths, typically 10–20 nm, with maximum throughputs of at least 40%. The latter value suggests that an important limitation to an absorption filter is that it may significantly reduce the amount of light from the source that reaches the sample and the detector. Figure 7.3.4 shows an example of a filter holder with filters that pass bands of light centered at 440 nm, 490 nm, or 550 nm.

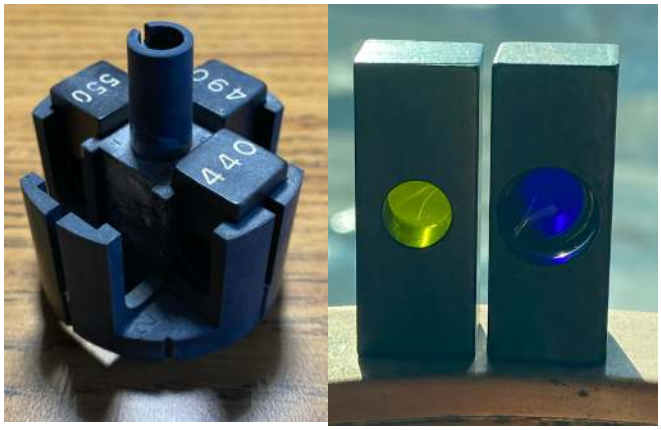



Figure 7.3.4: The photo on the left shows a filter holder with three filters in place. The photo on the right shows a filter that passes green light centered at 550 nm and a filter that passes blue light centered at 440 nm.

### Interference Filters

An **interference filter** consists of a transparent dielectric material, such as $CaF_2$, which is sandwiched between two glass plates, each coated with a thin, semitransparent metal film (7.3.5$a$). When a continuous source of light passes through the interference filter it undergoes constructive and destructive interference that isolates and passes a narrow band of light centered at a wavelength that satisfies Equation 7.3.1

$$\lambda = \frac{2nb}{m} \tag{7.3.1}$$

where $n$ is the refractive index of the dielectric material, $b$ is the thickness of the dielectric material, and $m$ is the order of the interference (typically first-order). Figure 7.3.5$b$ shows the result of passing the emission from a green LED—a continuous source

that emits light from approximately 500 nm to 650 nm—through an interference filter that produces an effective bandwidth of a few nanometers. In this case, a 210 nm thick film with a refractive index of 1.35 passes light centered at a wavelength of

$$\lambda = \frac{2 \times 1.35 \times 210 \text{ nm}}{1} = 567 \text{ nm}$$

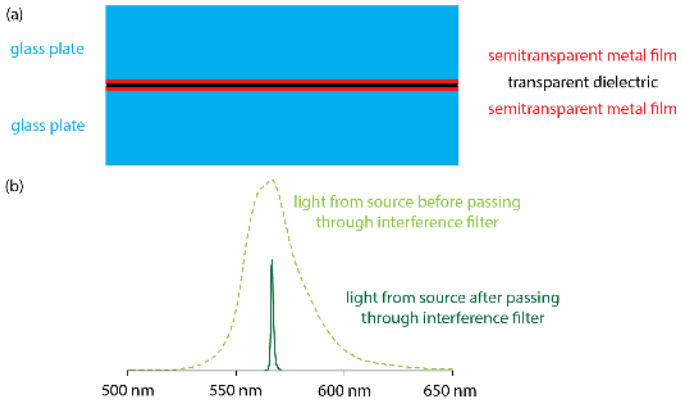



Figure 7.3.5. The structure of an Interference filter is shown in (a) and consists of a thin dielectric film sandwiched between two glass plates coated with a thin metal film that allows some of the source's light to pass through the film while reflecting the remainder of the light. Because the light traverses different distances through the dielectric, only light with a wavelength that satisfies Equation 7.3.1 passes through the filter, resulting in a narrow effective bandwith.

## Monochromators

A filter has one significant limitation—because a filter has a fixed nominal wavelength, if we need to make measurements at two wavelengths, then we must use two filters. A monochromator is an alternative method for selecting a narrow band of radiation that also allows us to continuously adjust the band's nominal wavelength. Monochromators are classified as either fixed-wavelength or scanning. In a fixed-wavelength monochromator we select the wavelength by manually rotating the grating. Normally a fixed-wavelength monochromator is used for a quantitative analysis where measurements are made at one or two wavelengths. A scanning monochromator includes a drive mechanism that continuously rotates the grating, which allows successive wavelengths of light to exit from the monochromator. A scanning monochromator is used to acquire a spectrum, and, when operated in a fixed-wavelength mode, for a quantitative analysis.

The construction of a typical monochromator is shown in Figure 7.3.6. Radiation from the source enters the monochromator through an entrance slit. The radiation is collected by a collimating mirror or lens, which focuses a parallel beam of radiation to a diffraction grating (left) or a prism (right), that disperses the radiation in space. A second mirror or lens focuses the radiation onto a planar surface that contains an exit slit. Radiation exits the monochromator and passes to the detector. As shown in Figure 7.3.6, a monochromator converts a polychromatic source of radiation at the entrance slit to a monochromatic source of finite effective bandwidth at the exit slit. The choice of which wavelength exits the monochromator is determined by rotating the diffraction grating or prism. A narrower exit slit provides a smaller effective bandwidth and better resolution than does a wider exit slit, but at the cost of a smaller throughput of radiation.

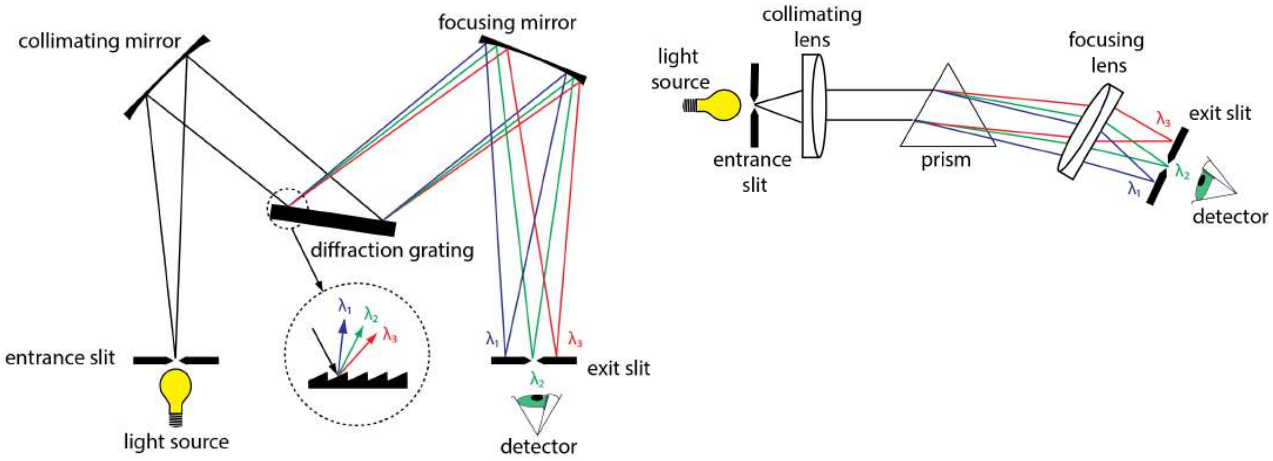



Figure 7.3.6. Examples of two types of monochromators: a diffraction grating monochromator an the left and a prism monochromator on the right.

Polychromatic means many colored. Polychromatic radiation contains many different wavelengths of light. Monochromatic means one color, or one wavelength. Although the light exiting a monochromator is not strictly of a single wavelength, its narrow effective bandwidth allows us to think of it as monochromatic.

## Monochromators Based on Prisms

Although prism monochromators were once in common use, they have mostly been replaced by diffraction gratings. There are several reasons for this. One reason is that diffraction gratings are much less expensive to manufacture. A second reason is that a diffraction grating provides a linear dispersion of of wavelengths along the focal plane of the exit slit, which means the resolution between adjacent wavelengths is the same throughout the source's optical range. A prism, on the other hand, provides a greater resolution at shorter wavelengths than it does a longer wavelengths.

## Monochromators Based on Diffraction Gratings

The inset in the diffraction grating monochromator in Figure 7.3.6 shows the general saw-toothed pattern of a diffraction grating, which consists of a series of grooves with broad surfaces exposed to light from the source. As shown in Figure 7.3.7, parallel beams of source radiation (shown in blue) from the monochromator's collimating mirror strike the surface of the diffraction grating and are reflected back (shown in green) toward the monochromator's focusing mirror and the detector. The parallel beams from the source strike the diffraction grating at an incident angle $i$ relative to the grating normal, which is a line perpendicular to the diffraction grating's base. The parallel beams bounce back toward the detector do so at a reflected angle $r$ to the grating normal.

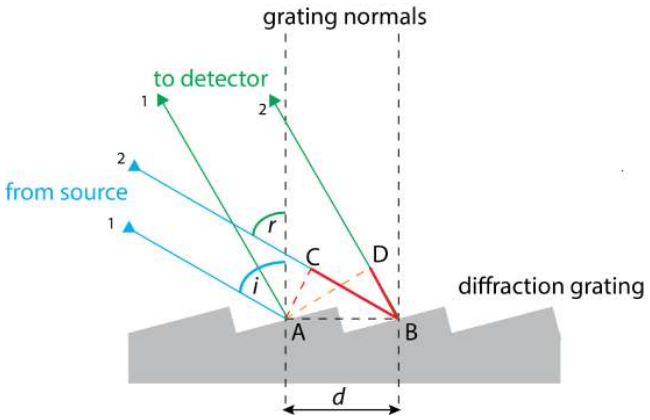



Figure 7.3.7. Illustration of how a monochromator's diffraction grating works to convert a beam of polychromatic light at the monochromator's entrance slit into a monochromatic beam of light at the monochromator's exit slit. Rotating the diffraction grating, changes the angles $i$ and $r$ and, therefore, the wavelength of light that exits the monochromator. The diffraction grating illustrated here is known as an echellette-type grating.

Constructive interference between the reflected beams occurs if their path lengths differ by an integer multiple of the incident beam's wavelength ($n\lambda$), where $n$ is the diffraction order. A close examination of Figure 7.3.7 shows that the difference in the distance traveled by two parallel beams of light, identified as 1 and 2, that strike adjacent grooves on the diffraction grating is equal to the sum of the line segments $\overline{CB}$ and $\overline{BD}$, both shown in red; thus

$$n\lambda = \overline{CB} + \overline{BD} \tag{7.3.2}$$

The incident angle, $i$, is equal to the angle CAB and the reflected angle, $r$, is equal to the angle DAB, which means we can write the following two equations

$$\overline{CB} = d \sin i \tag{7.3.3}$$

$$\overline{BD} = d \sin r \tag{7.3.4}$$

where $d$ is the distance between the diffraction grating's grooves. Substituting back gives

$$n\lambda = d(\sin i + \sin r) \tag{7.3.5}$$

which allows us to calculate the angle at which we can detect a wavelength of interest, $r$, given the angle of incidence from the source, $i$, and the number of grooves per mm (or the distance between grooves).

### Example 7.3.1

At what angle can we detect light of 650 nm using a diffraction grating with 1500 gooves per mm if the incident radiation is at an angle of $50^\circ$ to the grating normal? Assume that this is a first-order diffraction.

**Solution**

The distance between the grooves is

$$d = \frac{1 \text{ mm}}{1500 \text{ grooves}} \times \frac{10^6 \text{ nm}}{\text{mm}} = 666.7 \text{ nm}$$

To find the angle, we begin with

$$n\lambda = 1 \times 650 \text{ nm} = d(\sin i + \sin r) = 666.7 \text{ nm} \times (\sin(50) + \sin r)$$

$$0.9750 = 0.7660 + \sin r$$

$$0.2090 = \sin r$$

$$r = 12.1^\circ$$

## Performance Characteristics of a Monochromator

The quality of a monochromator depends on several key factors: the purity of the light that emerges from the exit slit, the power of the light that emerges from the exit slit, and the resolution between adjacent wavelengths.

### Spectral Purity

The radiation that emerges from a monochromator is pure if it (a) arises from the source and if it (b) follows the optical path from the entrance slit to the exit slit. Stray radiation that enters the monochromator from openings other than the entrance slit—perhaps through small imperfections in the joints—or that reaches the exit slit after scattering from imperfections in the optical components or dust, serves as a contaminant in that the power measured at the detector has a component at the monochromator's analytical wavelength and a component from the stray radiation that includes radiation at other wavelengths.

### Power

The amount of radiant energy that exits the monochromator and reaches the detector in a unit time is power. The greater the power, the better the resulting signal-to-noise ratio. The more radiation that enters the monochromator and is gathered by the collimating mirror, the greater the amount of radiation that exits the monochromator and the greater the power at the detector. The ability of a monochromator to collect radiation is defined by its $f/number$. As shown in Figure 7.3.8, the smaller the $f/number$, the greater the area and the greater the power. The light-gathering power increases as the inverse square of the $f/number$; thus, a monochromator rated as $f/2$ gathers $4\times$ as much radiation as a monochromator rated as $f/4$.

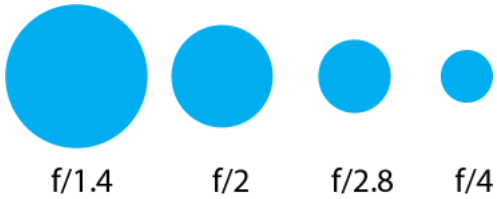



Figure 7.3.8. Relationship between the light-gathering power of a monochromator and its $f/number$.

### Resolution

To separate two wavelengths of light and detect them separately, it is necessary to to disperse them over a sufficient distance. The angular dispersion of a monochromator is defined as the change in the angle of reflection (see the angle $r$ in Figure 7.3.7) for a change in wavelength, or $dr/d\lambda$. Taking the derivative of Equation 7.3.5 for a fixed angle of incidence (see the angle $i$ in Figure 7.3.7) gives the angular dispersion as

$$\frac{dr}{d\lambda} = \frac{n}{d\cos r} \tag{7.3.6}$$

where $n$ is the diffraction order. The linear dispersion of radiation, $D$, gives the change in wavelength as a function of $y$, the distance along the focal plane of the monochromator's exit slit; this is related to the angular dispersion by

$$D = \frac{dy}{d\lambda} = \frac{F dr}{d\lambda} \tag{7.3.7}$$

where $F$ is the focal length. Because we are interested in wavelength, it is convenient to take the inverse of Equation 7.3.7

$$D^{-1} = \frac{d\lambda}{dy} = \frac{1}{F} \times \frac{d\lambda}{dr} \tag{7.3.8}$$

where $D^{-1}$ is the reciprocal linear dispersion. Substituting Equation 7.3.6 into Equation 7.3.8 gives

$$D^{-1} = \frac{d\lambda}{dy} = \frac{d\cos r}{nF} \tag{7.3.9}$$

which simplifies to

$$D^{-1} = \frac{d}{nF} \tag{7.3.10}$$

for angles $r < 20^\circ$ where $\cos r \approx 1$. Because the linear dispersion of radiation along the monochromator's exit slit is independent of wavelength, the ability to resolve two wavelengths is the same across the spectrum of wavelengths.

Another way to report a monochromator's ability to distinguish between two closely spaced wavelengths is its resolving power, $R$, which is defined as

$$R = \frac{\lambda}{\Delta\lambda} = nN$$

where $\lambda$ is the average of the two wavelengths, $\Delta\lambda$ is the difference in their values and $N$ is the number of grooves on the diffraction grating that are exposed to the radiation from the collimating mirror. The greater the number of grooves, the greater the resolving power.

## Monochromator Slits

A monochromator has two sets of slits: an entrance slit that brings radiation from the source into the monochromator and an exit slit that passes the radiation from the monochromator to the detector. Each slit consists of two metal plates with sharp, beveled edges separated by a narrow gap that forms a rectangular window and which is aligned with the focal plane of the collimating mirror. Figure 7.3.9 shows a set of four slits from a monochromator taken from an atomic absorption spectrophotometer. From bottom-to-top, the slits have widths, $w$, of 2.0 mm, 1.0 mm, 0.5 mm, and 0.2 mm.



Figure 7.3.9. Photo showing a set of four entrance slits to a monochromator from an atomic absorption spectrometer. From bottom-to-top they have widths of 2.0 mm, 1.0 mm, 0.5 mm, and 0.2 mm. The monochromator's exit slits are identical and. For this monochromator, the operator selects the slit width for the entrance slits and the exit is automatically set to the same width.

### Effect of Slits on Monochromatic Radiation

Suppose we have a source of monochromatic radiation with a wavelength of 400.0 nm and that we pass this beam of radiation through a monochromator that has entrance and exit slits with a width, $w$, of 1.0 mm and a reciprocal linear dispersion of 1.2 nm/mm. The product of these two variables is called the monochromator's effective bandwidth, $\Delta\lambda_{\text{eff}}$, and is given as

$$\Delta\lambda_{\text{eff}} = wD^{-1} = 1.0 \text{ mm} \times 1.2 \text{ nm/mm} = 1.2 \text{ nm} \tag{7.3.11}$$

The width of the beam in units of wavelength, therefore, is 1.2 nm. In this case, as shown in Figure 7.3.10, if we scan the monochromator, our beam of monochromatic radiation will first enter the exit slit at a wavelength setting of 398.8 nm and will fully exit the slit at a wavelength setting of 401.2 nm. In between these limits a portion of the beam is blocked and only a portion of the beam passes through the exit slit and reaches the detector. For example, when the monochromator is set to 399.4 nm or 400.6 nm, half of ther beam reaches the detector with a power of $0.5 \times P$. If we monitor the power at the detector as a function of wavelength, we obtain the profile shown at the bottom of Figure 7.3.10. The monochromator's bandwidth encompasses the range of wavelengths over which some portion of the beam of radiation passes through the exit slit.

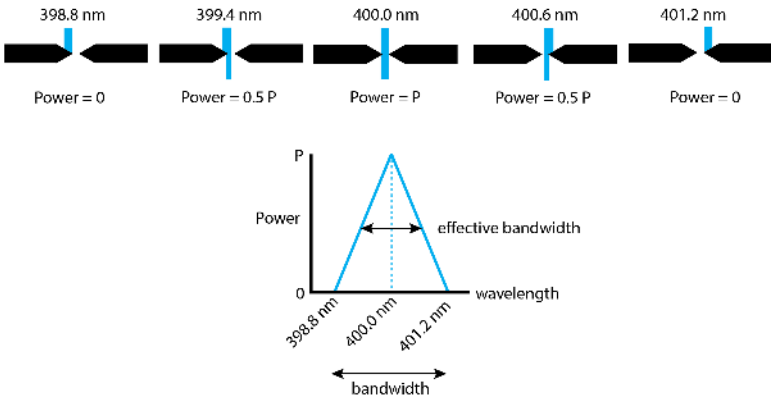



Figure 7.3.10: Illustration showing the relationship between effective bandwidth of a monochromatic source of radiation and the width of a monochromator's exit slit.

## Effect of Slit Width on Resolution

Suppose we have a source of radiation that consists of precisely three wavelengths—399.4 nm, 400.0 nm, and 400.6 nm—and we pass them through a monochromator with an effective bandwidth of 1.2 nm. Using the analysis from the previous section, the radiation with a wavelength of 399.4 nm passes through the monochromator's exit slit for any wavelength setting between 398.8 and 400.0 nm, which means it overlaps with the radiation with a wavelength of 400.0 nm. The same is true for the radiation with a wavelength of 400.6 nm, which also overlaps with the radiation with a wavelength of 400.0 nm. As shown in Figure 7.3.11$a$, we cannot resolve the three monochromatic sources of radiation, which appear as a single broad band of radiation. Decreasing the effective bandwidth to one-half of the difference in the wavelengths of the adjacent sources of radiation produces, as shown in Figure 7.3.11$b$, baseline resolution of the individual sources of wavelength. To resolve the sources of radiation with wavelengths of 399.4 nm and 400.0 nm using a monochromator with a reciprical linear dispersion of 1.2 nm/mm requires an effective bandwidth of

$$\Delta\lambda_{\text{eff}} = 0.5 \times (400.0 \text{ nm} - 399.4 \text{ nm}) = 0.3 \text{ nm}$$

and a slit width of

$$w = \frac{\Delta\lambda_{\text{eff}}}{D^{-1}} = \frac{0.3 \text{ nm}}{1.2 \text{nm/mm}} = 0.25 \text{ mm}$$

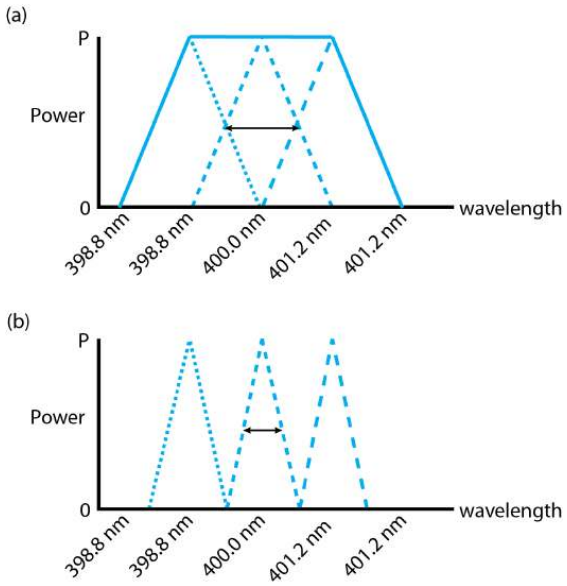



Figure 7.3.11: Illustration showing (a) the inability of a monochromator with an effective bandwidth of 1.2 nm to resolve three lines with wavelengths of 399.4 nm, 400.0 nm, and 400.6 nm. Decreasing the effective bandwidth to 0.3 nm, as in (b), allows for complete resolution of the three lines.

## Choosing a Slit Width

The choice of slit width always involves a trade-off between increasing the radiant power that reaches the detector by using a wide slit width, which improves the signal-to-noise ratio, and improving the resolution between closely spaced peaks, which requires a narrow slit width. Figure 7.3.3 illustrates this trade-off. Ultimately, the needs of the analyst will dictate the choice of slit width.

---

This page titled 7.3: Wavelength Selectors is shared under a CC BY-NC-SA 4.0 license and was authored, remixed, and/or curated by David Harvey.

# 7.4: Sample Containers

The sample compartment provides a light-tight environment that limits stray radiation. Samples normally are in a liquid or solution state, and are placed in cells constructed with UV/Vis transparent materials, such as quartz, glass, and plastic (Figure 7.4.1). A quartz or fused-silica cell is required when working at a wavelength <300 nm where other materials show a significant absorption. The most common pathlength is 1 cm (10 mm), although cells with shorter (as little as 0.1 cm) and longer pathlengths (up to 10 cm) are available. Longer pathlength cells are useful when analyzing a very dilute solution or for gas samples. The highest quality cells allow the radiation to strike a flat surface at a $90^o$ angle, minimizing the loss of radiation to reflection. A test tube often is used as a sample cell with simple, single-beam instruments, although differences in the cell's pathlength and optical properties add an additional source of error to the analysis.

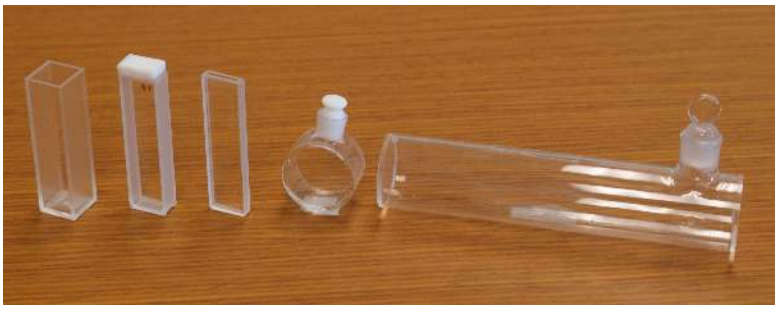


Figure 7.4.1. Examples of sample cells for UV/Vis spectroscopy. From left to right (with path lengths in parentheses): rectangular plastic cuvette (10.0 mm), rectangular quartz cuvette (5.000 mm), rectangular quartz cuvette (1.000 mm), cylindrical quartz cuvette (10.00 mm), cylindrical glass cuvette with quartz windows (100.0 mm). Cells often are available as a matched pair, which is important when using a double-beam instrument.

Infrared spectroscopy routinely is used to analyze gas, liquid, and solid samples. Sample cells are made from materials, such as NaCl and KBr, that are transparent to infrared radiation. Gases are analyzed using a cell with a pathlength of approximately 10 cm. Longer pathlengths are obtained by using mirrors to pass the beam of radiation through the sample several times.

A liquid sample may be analyzed using a variety of different sample cells (Figure 7.4.2). For non-volatile liquids a suitable sample is prepared by placing a drop of the liquid between two NaCl plates, forming a thin film that typically is less than 0.01 mm thick. Volatile liquids are placed in a sealed cell to prevent their evaporation.

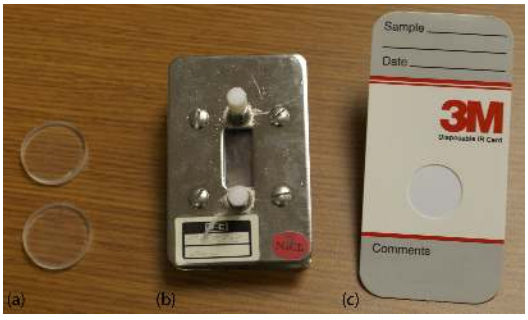



Figure 7.4.2. Three examples of IR sample cells: (a) NaCl salts plates; (b) fixed pathlength (0.5 mm) sample cell with NaCl windows; (c) disposable card with a polyethylene window that is IR transparent with the exception of strong absorption bands at 2918 $cm^{-1}$ and 2849 $cm^{-1}$.

This page titled 7.4: Sample Containers is shared under a CC BY-NC-SA 4.0 license and was authored, remixed, and/or curated by David Harvey.

# 7.5: Radiation Transducers

## Introduction

In Nessler's original method for determining ammonia (see Section 7.4) the analyst's eye serves as the detector, matching the sample's color to that of a standard. The human eye, of course, has a poor range—it responds only to visible light—and it is not particularly sensitive or accurate. Modern detectors use a sensitive transducer to convert a signal consisting of photons into an easily measured electrical signal. Ideally the detector's signal, *S*, is a linear function of the electromagnetic radiation's power, *P*,

$$S = kP + D \tag{7.5.1}$$

where *k* is the detector's sensitivity, and *D* is the detector's dark current, or the background current when we prevent the source's radiation from reaching the detector. There are two broad classes of spectroscopic transducers: photon transducers and thermal transducers, although we will subdivide the photon transducers given their rich variety. Table 7.5.1 provides several representative examples of each class of transducers.

> Transducer is a general term that refers to any device that converts a chemical or a physical property into an easily measured electrical signal. The retina in your eye, for example, is a transducer that converts photons into an electrical nerve impulse; your eardrum is a transducer that converts sound waves into a different electrical nerve impulse.

Table 7.5.1. Examples of Transducers for Spectroscopy

| transducer | class | wavelength range | output signal |
|---|---|---|---|
| photovoltaic cell | photon | 350–750 nm | current |
| phototube | photon | 200–1000 nm | current |
| photomultiplier | photon | 110–1000 nm | current |
| Si photodiode | photon | 250–1100 nm | current |
| photoconductor | photon | 750–6000 nm | change in resistance |
| photovoltaic cell | photon | 400–5000 nm | current or voltage |
| thermocouple | thermal | 0.8–40 μm | voltage |
| thermistor | thermal | 0.8–40 μm | change in resistance |
| pneumatic | thermal | 0.8–1000 μm | membrane displacement |
| pyroelectric | thermal | 0.3–1000 μm | current |

## Photon Transducers

A photon transducer takes a photon and converts it into an electrical signal, such as a current, a change in resistance, or a voltage. Many such detectors use a semiconductor as the photosensitive surface. When the semiconductor absorbs photons, valence electrons move to the semiconductor's conduction band, producing a measurable current.

### Photovoltaic Cells

A photovoltaic cell (Figure 7.5.1) consists of a thin film of a semiconducting material, such as selenium sandwiched between two electrodes: a base electrode of iron or copper and a thin semi-transparent layer of silver or gold that serves as the collector electrode. When a photon of visible light falls on the photovoltaic cell it generates an electron and a hole with a positive charge within the semiconductor. Movement of the electrons from the collector electrode to the base electrode generates a current that is proportional to the power of the incoming radiation and that serves as the signal.

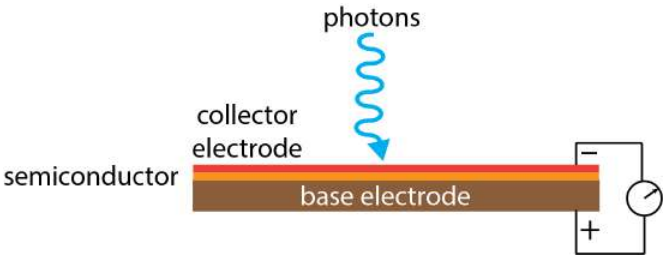



Figure 7.5.1: Schematic diagram of a photovoltaic cell that consists of a semiconducting thin film of selenium placed between two electrodes. When a photon strikes the semiconductor, it generates an electron and a hole that carries a positive charge. The movement of the electron from the collector electrode to the base electrode generates a measureable current.

## Phototubes and Photomultipliers

Phototubes and photomultipliers use a photosensitive surface that absorbs radiation in the ultraviolet, visible, or near IR to produce an electrical current that is proportional to the number of photons that reach the transducer (see Figure 7.5.2). The current results from applying a negative potential to the photoemissive surface and a positive potential to a wire that serves as the anode. In a photomultiplier tube, a series of positively charged dynodes serves to amplify the current, producing $10^6$–$10^7$ electrons per photon.

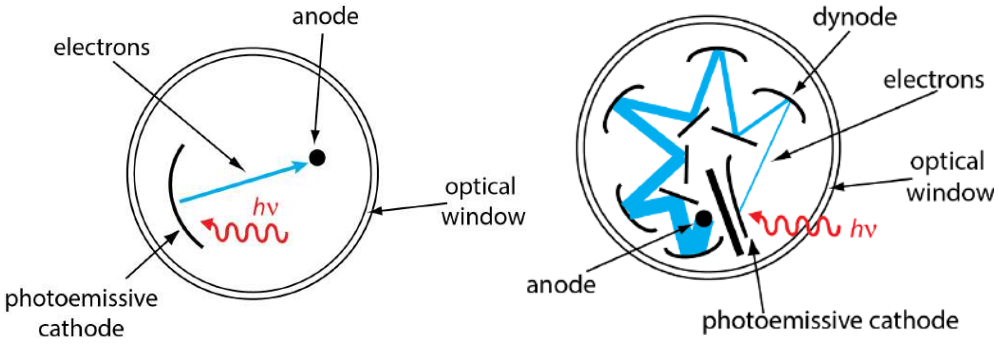



Figure 7.5.2.Schematic of a phototube (left) and a photomultiplier tube (right). In both, a photon strikes the photoemissive cathode producing electrons. In the phototube, the electrons that are drawn toward a positively charged anode, generating a current. In the photomultiplier tube, the electrons accelerate toward a positively charged dynode. Collision of these electrons with the dynode generates additional electrons, which accelerate toward the next dynode. A total of $10^6$–$10^7$ electrons per photon eventually reach the anode, generating an electrical current.

## Silicon Photodiodes

Applying a reverse biased voltage to the *pn* junction of a silicon semiconductor creates a depletion zone in which conductance is close to zero (see Chapter 2 for an earlier discussion of semiconductors). When a photon of light of sufficient energy impinges on the depletion zone, an electron-hole pair is formed. Movement of the electron through the *n*–region and of the hole through the *p*–region generates a current that is proportional to the number of photons reaching the detector. A silicon photodiode has a wide spectral range from approximately 190 nm to 1100 nm, which makes it versatile; however, a photodiode is less sensitive than a photomultiplier.

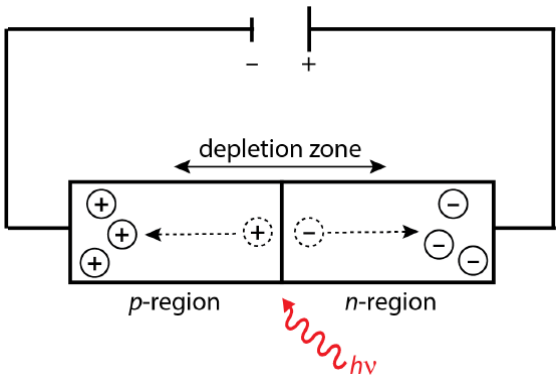



Figure 7.5.3: Illustration of silicon photodiode. See the text for a description of how the deterctor works.

## Multichannel Photon Transducers

The photon transducers discussed above detect light at a single wavelength passed by the monochromator to the detector. If we wish to record a complete spectrum then we must continually adjust the monochromator either manually or by using a servo motor. In a multichannel instrument we create a one-dimensional or two-dimensional array of detectors that allow us to monitor simultaneously radiation spanning a broad range of wavelengths.

### Photodiode Arrays

An individual silicon photodiode is quite small, typically with a width of approximately 0.025 mm. As a result, a linear (one-dimensional) array that consists of 1024 individual photodiodes has a width of just 25.6 mm. Figure 7.5.4, for example, shows the UV detector from an HPLC. Light from the deuterium lamp passes through a flow cell, is dispersed by a diffraction grating, and then focused onto a linear array of photodiodes. The close-up on the right shows the active protion of the photodiode array covered by an optical window. The active width of this photodiode array is approximately 6 mm and includes more than 200 individual photodiodes, sufficient to provide 1 nm resolution from 180 nm to 400 nm.

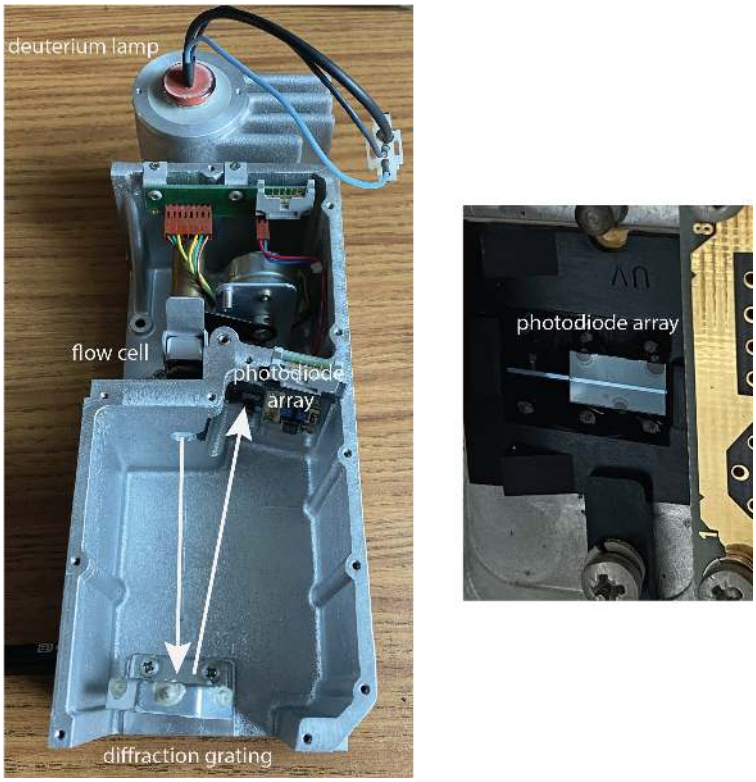



Figure 7.5.4: The photo on the left shows the UV detector from an HPLC and the photo on the right shows a close-up view of the its linear photodiode array deterctor. The bright line, from reflected light, is the photodiode array. The active portion of this detector is covered by an optically transparent window.

### Charge-Transfer Devices

One way to increase the sensitivity of a detector is to collect and store charges before counting them. This is the approach taken with two types of charge-transfer devices: charged-coupled detectors and charge-injection detectors. Individual detectors, or pixels, consist of a layer of silicon dioxide coated on top of semiconductor. When a photon impinges on the detector it creates an electron-hole pair. An electrode on top of the silicon dioxide layer collects and stores either the negatively charged electrons or the positively charged holes. After a sufficient time, during which 10,000-100,000 charges are collected, the total accumulated charge is measured. Because individual pixels are small, typically 10 µm, they can be arranged in either a linear, one-dimensional array or a two-dimensional array. A charge-transfer device with 1024 x 1024 pixels will be approximately 10 mm x 10 mm in size.

Note

There are two important charge-transfer devices used as detectors: a charge-coupled device (CCD), which is discussed below, and a charge-injection device (CID), which is discussed in Chapter 10. Both types of devices use a two-dimensional arrays of individual detectors that store charge. The two devices differ primarily in how the accumulated charges are read.

Figure 7.5.5 shows a cross-section of a single detector (pixel) in a charge-coupled device (CCD) where individual pixels are arranged in a two-dimensional array. Electron-hole pairs are created in a layer of *p*-doped silicon. The holes migrate to the *n*-doped silicon layer and the electrons are drawn to the area below a positively charged electrode. When it is time to record the accumulated charges, the charge is read in the upper-right corner of the array with charges in the same row measured by shifting them from left-to-right. When the first row is read, the charges in the remaining rows are shifted up and recorded. In a charge-injection device, the roles of the electrons and holes are reversed and the accumulated positive charged are recorded.

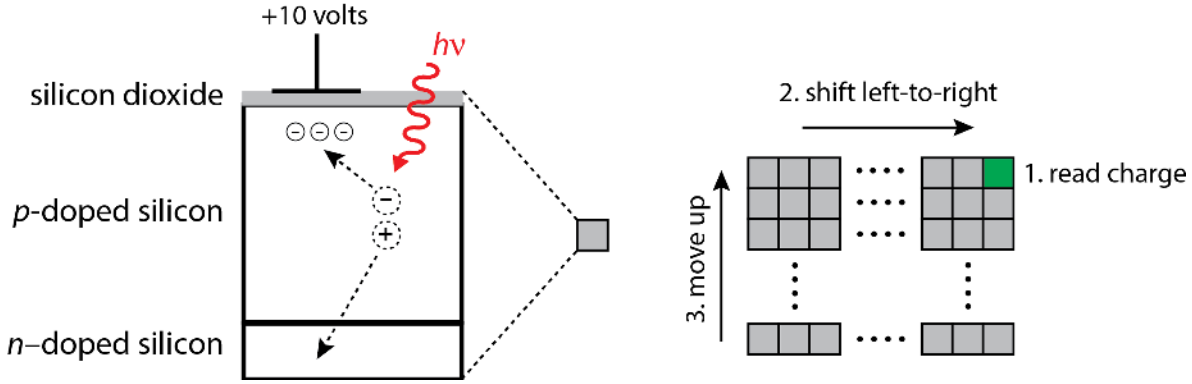



Figure 7.5.5: Schematic diagram of a charge-coupled device (CCD). The figure on the left shows a single detector, or pixel. When a photon impinges on the detector it generates an electron-hole pair in the *p*-doped layer. The electrons migrate and accumulate beneath a positively charged electrode. Individual pixels are arranged in an array, as shown on the right. This array may be a single row (a linear, or one-dimensional array) or in a series of rows. The charge in each pixels is recorded by shifting the pixels from left-to-right and by moving rows of pixels up.

Figure 7.5.6 shows an example of spectrophotometer equipped with a linear CCD detector that includes 2048 individual elements with a wavelength range from 200 nm to 1100 nm. The spectrometer is housed in a compact space of 90 mm x 60 mm




Figure 7.5.6: Example of a spectrophotometer equipped with a linear CCD detector.

## Thermal Transducers

Infrared photons do not have enough energy to produce a measurable current with a photon transducer. A thermal transducer, therefore, is used for infrared spectroscopy. The absorption of infrared photons increases a thermal transducer's temperature, changing one or more of its characteristic properties. A pneumatic transducer, for example, is a small tube of xenon gas with an IR transparent window at one end and a flexible membrane at the other end. Photons enter the tube and are absorbed by a blackened surface, increasing the temperature of the gas. As the temperature inside the tube fluctuates, the gas expands and contracts and the flexible membrane moves in and out. Monitoring the membrane's displacement produces an electrical signal.

---

This page titled 7.5: Radiation Transducers is shared under a CC BY-NC-SA 4.0 license and was authored, remixed, and/or curated by David Harvey.

# 7.6: Fiber Optics

If we need to monitor an analyte's concentration over time, it may not be possible to remove samples for analysis. This often is the case, for example, when monitoring an industrial production line or waste line, when monitoring a patient's blood, or when monitoring an environmental system, such as stream. With a **fiber-optic** probe we can analyze samples *in situ*. An example of a remote sensing fiber-optic probe is shown in Figure 7.6.1. The probe consists of two bundles of fiber-optic cable. One bundle transmits radiation from the source to the probe's tip, which is designed to allow the sample to flow through the sample cell. Radiation from the source passes through the solution and is reflected back by a mirror. The second bundle of fiber-optic cable transmits the nonabsorbed radiation to the wavelength selector. Another design replaces the flow cell shown in Figure 7.6.1 with a membrane that contains a reagent that reacts with the analyte. When the analyte diffuses into the membrane it reacts with the reagent, producing a product that absorbs UV or visible radiation. The nonabsorbed radiation from the source is reflected or scattered back to the detector. Fiber optic probes that show chemical selectivity are called optrodes.

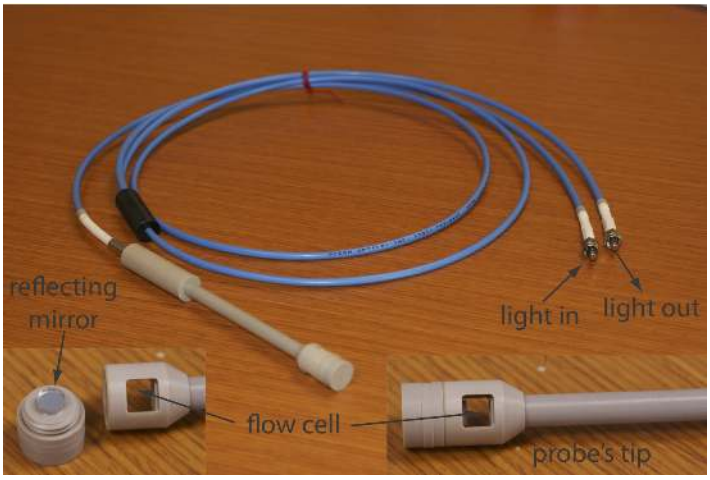



Figure 7.6.1: Example of a fiber-optic probe. The inset photographs at the bottom of the figure provide close-up views of the probe's flow cell and the reflecting mirror.

This page titled 7.6: Fiber Optics is shared under a CC BY-NC-SA 4.0 license and was authored, remixed, and/or curated by David Harvey.

# 7.7: Fourier Transform Optical Spectroscopy

Thus far, the optical benches described in this chapter either use a single detector and a monochromator to pass a single wavelength of light to the detector, or use a multichannel array of detectors and a diffraction grating to disperse the light across the detectors. Both of these approaches have advantages and limitations. For the first of these designs, we can improve resolution by using a smaller slit width, although this comes with a decrease in the throughput of light that reaches the detector, which increases noise. Recording a complete spectrum requires scanning the monochromator; a slow scan rate can improve resolution by reducing the range of wavelengths reaching the detector per unit time, but at the expense of a longer analysis time, which is a problem if the composition of our samples changes with time. For the second of these designs, resolution is limited by the size of the array; for example, a spectral range of 190 nm to 800 nm and a photodiode array with 512 individual elements has a digital resolution of

$$\frac{800 - 190}{512} = 1.2 \text{ nm/diode}$$

although the optical resolution—defined by the actual number of individual diodes over which a wavelength of light is dispersed—is greater and may vary with wavelength. Because a photodiode array allows for the simultaneous detection of radiation by each diode in the array, data acquisition is fast and a complete spectrum is acquired in approximately one second.

## Interferometers

We can overcome the limitations described above if we can find a way to avoid dispersing the source radiation in time by scanning the monochromator, or dispersing the source radiation in space across an array of sensors. An interferometer, Figure 7.7.1, provides one way to accomplish this. Radiation from the source is collected by a collimating mirror and passed to a beam splitter where half of the radiation is directed toward a mirror set at a fixed distance from the beam splitter, and the other half of the radiation is passed through to a mirror that moves back and forth. The radiation from the two mirrors is recombined at the beam splitter and half of it is passed along to the detector.

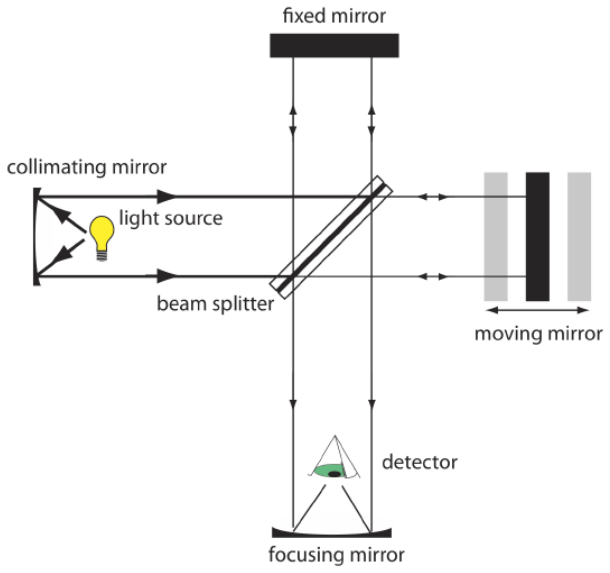



Figure 7.7.1: Schematic diagram of an interferometer for use in optical spectroscopy. The distance of the fixed mirror and the moving mirror from the beam splitter is the same when the moving mirror is in the position shown in black.

### Time Domain and Frequency Domain

When the radiation recombines at the beam splitter, constructive and destructive interference determines, for each wavelength, the intensity of light that reaches the detector. As the moving mirror changes position, the wavelength of light that experiences maximum constructive interference and maximum destructive interference also changes. The signal at the detector shows intensity as a function of the moving mirror's position, expressed in units of distance or time. The result is called an interferogram or a time domain spectrum. The time domain spectrum is converted mathematically, by a process called a Fourier transform, to a spectrum (a frequency domain) that shows intensity as a function of the radiation's frequency.

Figure 7.7.2 shows the relationship between the time domain spectrum and the frequency domain spectrum. The spectra in the first row show the relationship between (a) the time domain spectrum and (b) the corresponding frequency domain spectrum for a monochromatic source of radiation with a frequency, $\nu_1$, of 1 and an amplitude, $A_1$, of 1.0. In the time domain we see a simple cosine function with the general form

$$S = A_1 \times \cos\left(2\pi\nu_1 t\right) \tag{7.7.1}$$

where $S$ is the signal and $t$ is the time. The spectra in the second row show the same information for a second monochromatic source of radiation with a frequency, $\nu_2$, of 1.2 and an amplitude, $A_2$, of 1.5, which is given by the equation

$$S = A_2 \times \cos\left(2\pi\nu_2 t\right) \tag{7.7.2}$$

If we have a source that emits just these two frequencies of light, then the corresponding time domain and frequency domain spectra in the last row, where

$$S = A_1 \times \cos\left(2\pi\nu_1 t\right) + A_2 \times \cos\left(2\pi\nu_2 t\right) \tag{7.7.3}$$

Although the time domain spectrum in panel (e) is more complex than those in panels (a) and (c), there is a clear repeating pattern, one cycle of which is shown by the arrow. Note that for each of these three examples, the time domain spectrum and the frequency domain spectrum encode the same information about the source radiation.

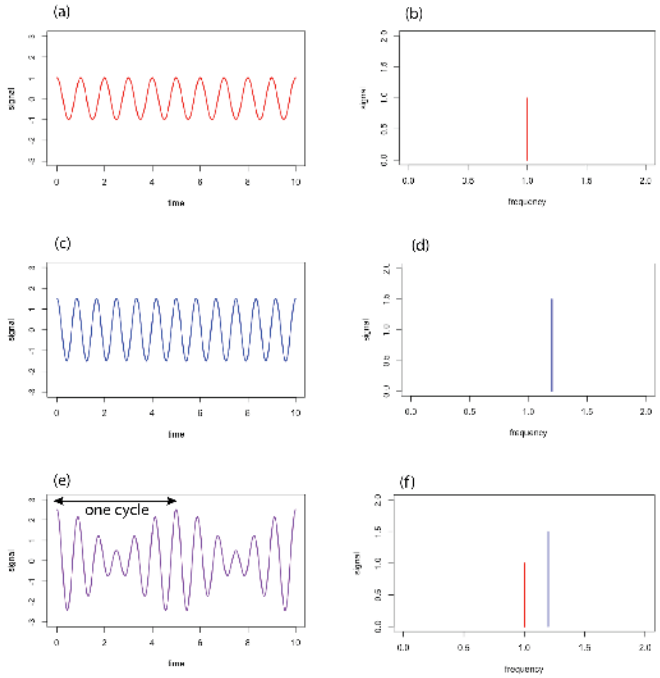



Figure 7.7.2: Time domain and frequency domain spectra for (a) and (b) a monochromatic source with a frequency of $\nu_1$ and an amplitude of $A_1$, for (c) and (d) a monochromatic source with a frequency of $\nu_2$ and an amplitude of $A_2$, and (e) and (f) a polychromatic source that consists of the two monochromatic sources.

The two monochromatic signals in Figure 7.7.2 are line spectra with line widths that are essentially zero. But what if our signal has a measurable linewidth? We might consider such a signal to be the sum of a series of cosine functions, each with an amplitude and a frequency. Figure 7.7.3$a$ shows a frequency domain that contains a single peak with a finite width and Figure 7.7.3$b$ shows the corresponding time domain spectrum, which consists of an oscillating signal with an amplitude that decays over time. In general, Figure 7.7.2 and Figure 7.7.3 show that

- the further a peak in the frequency domain is from the origin, the greater its corresponding oscillation frequency in the time domain
- the broader a peak's width in the frequency domain, the faster its decay rate in the time domain
- the greater the area under a peak in the frequency domain, the higher its initial intensity in the time domain

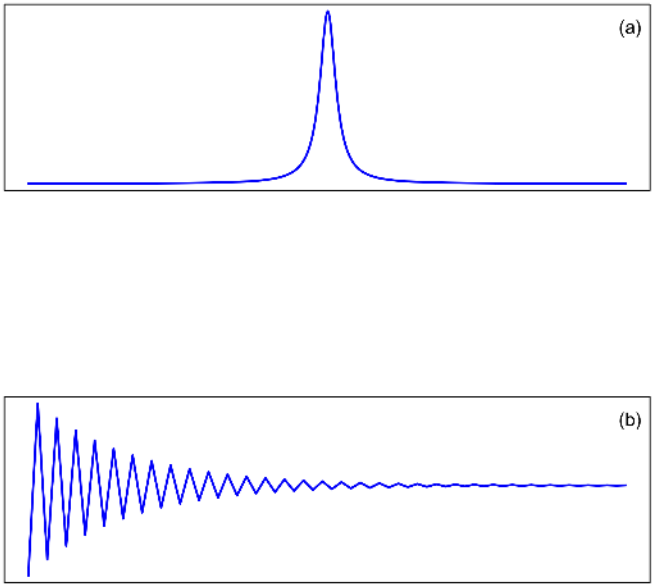



Figure 7.7.3: The plot in (a) shows a frequency domain consisting of a single peak defined by its position along the *x*-axis, its width, and its area. The plot in (b) shows the corresponding time domain that consists of a single oscillating signal defined by its oscillation frequency, its initial intensity, and its decay rate.

The mathematical process of converting between the time domain and the frequency domain is called a Fourier transform. The details of the mathematics are sufficiently complex that calculations by hand are impractical.

## Advantages of Fourier Transform Spectrometry

In comparison to a monochromator, an interferometer has several significant advantages. The first advantage, which is termed Jacquinot's advantage, is the greater throughput of source radiation. Because an interferometer does not use slits and has fewer optical components from which radiation is scattered and lost, the throughput of radiation reaching the detector is $80 - 200\times$ greater than that for a monochromator. The result is less noise. A second advantage, which is called Fellgett's advantage, is a savings in the time needed to obtain a spectrum. Because the detector monitors all frequencies simultaneously, a spectrum takes approximately one second to record, as compared to 10–15 minutes when using a scanning monochromator. A third advantage is that increased resolution is achieved by increasing the distance traveled by the moving mirror, which we can achieve without the need to decrease a scanniing monochromator's slit width or without increasing the size of an array detector.

This page titled 7.7: Fourier Transform Optical Spectroscopy is shared under a CC BY-NC-SA 4.0 license and was authored, remixed, and/or curated by David Harvey.

# CHAPTER OVERVIEW

## 8: An Introduction to Optical Atomic Spectroscopy


8.1: Optical Atomic Spectra

8.2: Atomization Methods

8.3: Sample Introduction Methods


---

This page titled 8: An Introduction to Optical Atomic Spectroscopy is shared under a CC BY-NC-SA 4.0 license and was authored, remixed, and/or curated by David Harvey.

# 8.1: Optical Atomic Spectra

## Energy Level Diagrams

The energy of ultraviolet and visible electromagnetic radiation is sufficient to cause a change in an atom's valence electron configuration. Sodium, for example, has a single valence electron in its 3*s* atomic orbital. As shown in Figure 8.1.1, unoccupied, higher energy atomic orbitals also exist. The valence shell energy level diagram in Figure 8.1.1 might strike you as odd because it shows the 3*p* orbitals split into two groups of slightly different energy (the two lines differ by just 0.6 nm). The cause of this splitting is a consequence of an electron's angular momentum and its spin. When these two are in the opposite direction, then the energy is slightly smaller than when the two are in the same direction. The effect is largest for *p* orbitals and sufficiently smaller for *d* and *f* orbitals that we do not bother to show the difference in their energies in this diagram.

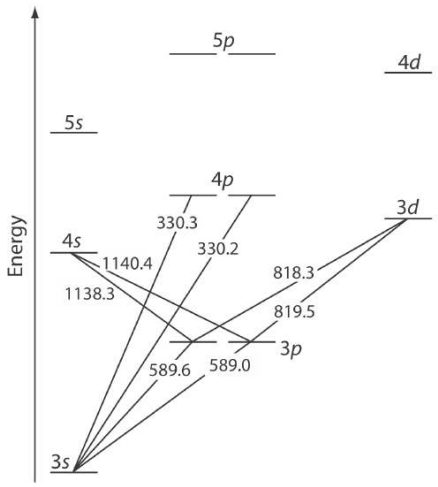



Figure 8.1.1. Valence shell energy level diagram for sodium. The wavelengths (in nm) corresponding to several transitions are shown.

Absorption of a photon is accompanied by the excitation of an electron from a lower-energy atomic orbital to an atomic orbital of higher energy. Not all possible transitions between atomic orbitals are allowed. For sodium the only allowed transitions are those in which there is a change of ±1 in the orbital quantum number (*l*); thus transitions from $s \rightarrow p$ orbitals are allowed, but transitions from $s \rightarrow s$ and from $s \rightarrow d$ orbitals are forbidden.

## Atomic Absorption Spectra

The atomic absorption spectrum for Na is shown in Figure 8.1.2, and is typical of that found for most atoms. The most obvious feature of this spectrum is that it consists of a small number of discrete absorption lines that correspond to transitions between the ground state (the 3*s* atomic orbital) and the 3*p* and the 4*p* atomic orbitals. Absorption from excited states, such as the $3p \rightarrow 4s$ and the $3p \rightarrow 3d$ transitions included in Figure 8.1.1, are too weak to detect. Because an excited state's lifetime is short—an excited state atom typically returns to a lower energy state in $10^{-7}$ to $10^{-8}$ seconds—an atom in the exited state is likely to return to the ground state before it has an opportunity to absorb a photon.

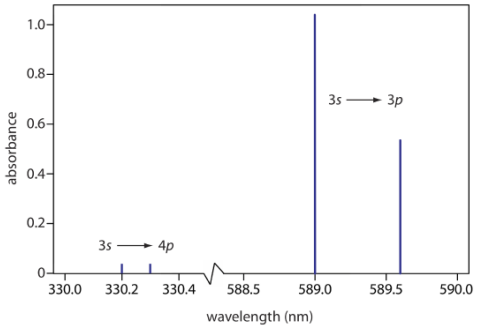



Figure 8.1.2. Atomic absorption spectrum for sodium. Note that the scale on the *x*-axis includes a break.

## Atomic Emission Spectra

Atomic emission occurs when electrons in higher energy orbitals return to a lower energy state, releasing the excess energy as a photon. The ground state electron configuration for Na of $1s^2 2s^2 2p^6 3s^1$ places a single electron in the $3s$ valence shell. Introducing a solution of NaCl to a flame results in the formation of Na atoms (more on this in Chapter 9) and provides sufficient energy to promote the valence electron in the $3s$ orbital to higher energy excited states, such as the $3p$ orbitals identified in the energy level diagram for sodium in Figure 8.1.1. When an electron returns to its ground state, the excess energy is released as a photon. As seen in Figure 8.1.3, the emission spectrum for Na is dominated by the pair of lines with wavelengths of 589.0 and 589.6 nm.

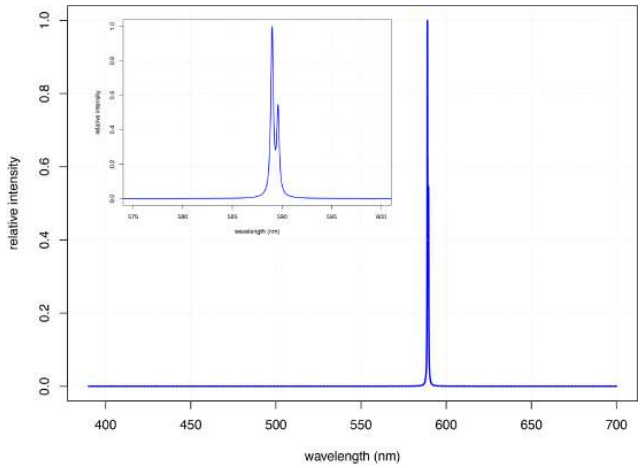



Figure 8.1.3: Atomic emission spectrum for Na at a temperature of 3000 K. The inset shows that there are two closely spaced emission lines with wavelengths of 589.0 and 589.6 nm. The spectra were simulated using the R package atomicEmission.

## Atomic Fluorescence Spectra

When an atom in an excited state emits a photon as a means of returning to a lower energy state, how we describe the process depends on the source of energy creating the excited state. When excitation is the result of thermal energy, as is the case for the spectrum in Figure 8.1.3, we call the process atomic emission spectroscopy. When excitation is the result of the absorption of a photon, we call the process atomic fluorescence spectroscopy. The absorption spectrum for Na in Figure 8.1.2 and its emission spectrum in Figure 8.1.2 shows that Na has both strong absorption and emission lines at 589.0 and 589.6 nm. If we use a source of light at 589.6 nm to move the 3*s* valence electron to a 3*p* excited state, we can then measure the emission of light at the same wavelength, making the measurement at 90° to avoid an interference from the original light source.

Fluorescence also may occur when an electron in an excited state first loses energy by a process other than the emission of a photon—we call this a radiationless transition—reaching a lower energy excited state from which it then emits a photon. For example, a ground state Na atom may first absorb a photon with a wavelength of 330.2 nm (a $3s \rightarrow 4p$ transition), which then loses energy through a radiationless transition to the 3*p* orbital where it then emits a photon to reach the 3*s* orbital.

## Atomic Line Widths

Another feature of the atomic absorption spectrum in Figure 8.1.2 and the atomic emission spectrum in Figure 8.1.3 is the narrow width of the absorption and emission lines, which is a consequence of the fixed difference in energy between the ground state and the excited state, and the lack of vibrational and rotational energy levels. The width of an atomic absorption or emission line arises from several factors that we consider here.

### Broadening Due to Uncertainty Principle

From the uncertainty principle, the product of the uncertainty of the frequency of light and the uncertainty in time must be greater than 1.

$$\Delta\nu \times \Delta t > 1$$

To determine the frequency with infinite precision, $\Delta\nu = 0$, requires that the lifetime of an electron in a particular orbital must be infinitely large. While this may be essentially true for an electron in the ground state, it is not true for an electron in an excited state where the average lifetime—how long it takes before it returns to the ground state—may be on the order of $10^{-7}$ to $10^{-8}$ s. For example, if $\Delta t = 5 \times 10^{-8}$ s for the emission of a photon with a wavelength of 500.0 nm, then

$$\Delta\nu = 2 \times 10^{7}\ \text{s}^{-1}$$

To convert this an uncertainty in wavelength, $\Delta\lambda$, we begin with the relationship

$$\nu = \frac{c}{\lambda}$$

and take the derivative of $\nu$ with respect to wavelength

$$d\nu = -\frac{c}{\lambda^2} d\lambda$$

Rearranging to solve for the uncertainty in wavelength, and letting $\Delta\nu$ and $\Delta\lambda$ serve as estimates for $d\nu$ and $d\lambda$ leaves us with

$$|\Delta\lambda| = \frac{\Delta\nu \times \lambda^2}{c} = \frac{(500.0 \times 10^{-9}\ \text{m}^2) \times (2 \times 10^{7}\text{s}^{-1})}{2.998 \times 10^{8}\ \text{m/s}} = 1.7 \times 10^{-14}\ \text{m}$$

or $1.7 \times 10^{-5}$ nm. Natural line widths for atomic spectra are approximately $10^{-5}$ nm.

## Doppler Broadening and Pressure Broadening

When an atom emits a photon, the frequency (and, thus, the wavelength) of the photon depends on whether the emitting atom is moving toward the detector or moving away from the detector. When the atom is moving toward the detector, as in Figure 8.1.4*a*, its emitted light reaches the detector at a greater frequency—a shorter wavelength—than when the light source is stationary, as in Figure 8.1.4*b*. An atom moving away from the detector, as in Figure 8.1.4*c* emits light that reaches the detector with a smaller frequency and a longer wavelength.

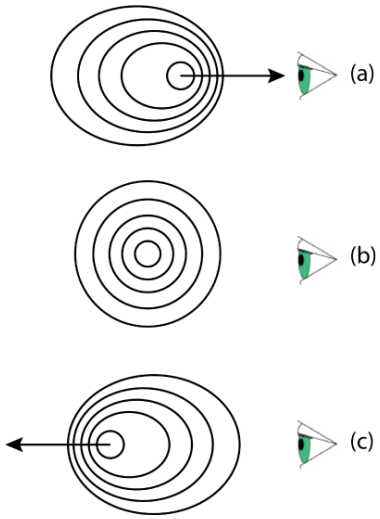



Figure 8.1.4: Illustration showing the original of Doppler broadening. In (a) and (c) the atom is moving toward or away from the detector, respectively. In (b), the atom is stationary relative to the detector.

Atoms are in constant motion, which means that they also experience constant collisions, each of which results in a small change in the energy of an electron in the ground state or in an excited state, and a corresponding change in the wavelength emitted or absorbed. This effect is called pressure (or collisional) broadening. As is the case for Doppler broadening, pressure broadening increases with temperature. Together, Doppler broadening and pressure broadening result in an approximately 100-fold increase in line width, with line widths on the order of approximately $10^{-3}$ nm.

## Effect of Temperature on Atomic Spectra

As noted in the previous section, temperature contributes to the broadening of atomic absorption and atomic emission lines. Temperature also has an effect on the intensity of emission lines as it determines the relative population of an atom's various excited states. The Boltzmann distribution

$$\frac{N_i}{N_0} = \frac{P_i}{P_0} e^{-E_i/kT}$$

gives the relative number of atoms in a specific excited state, $N_i$, relative to the number of atoms in the ground state, $N_0$, as a function of the difference in their energies, $E_i$, Boltzmann's constant, $k$, the temperature in Kelvin, $T$, and $P_i$ and $P_0$ are statistical factors that account for the number of equivalent energy states for the excited state and the ground state. Figure 8.1.5 shows how temperature affects the atomic emission spectrum for sodium's two intense emission lines at 589.0 and 589.6 nm for temperatures from 2500 K to 7500 K. Note that the emission at 2500 K is too small to appear using a *y*-axis scale of absolute intensities. A change in temperature from 5500 K to 4500 K reduces the emission intensity by 62%. As you might guess from this, a small change in temperature—perhaps as little as 10 K can result in a measurable decrease in emission intensity of a few percent.

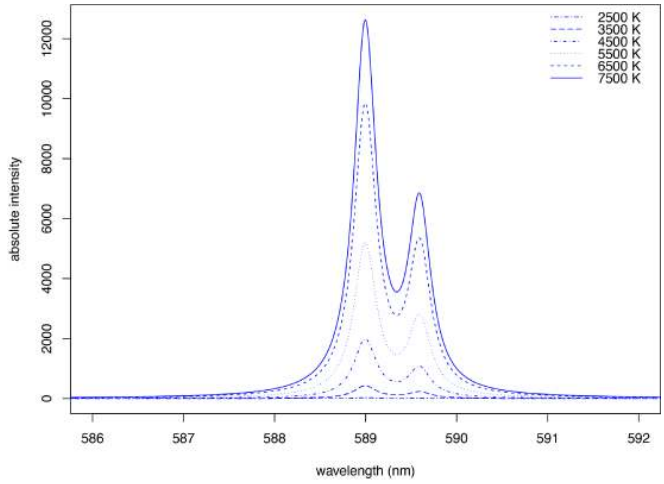



Figure 8.1.5: Atomic emission spectra for Na as a function of temperature. The spectra were simulated using the R package atomicEmission.

An increase in temperature may also change the relative emission intensity of different lines. Figure 8.1.6, for example, shows the atomic emission spectra for copper at 5000 K and 7000 K. At the higher temperature, the most intense emission line changes from 510.55 nm to 521.82 nm, and several additional peaks between 400 nm and 500 nm become more intense.

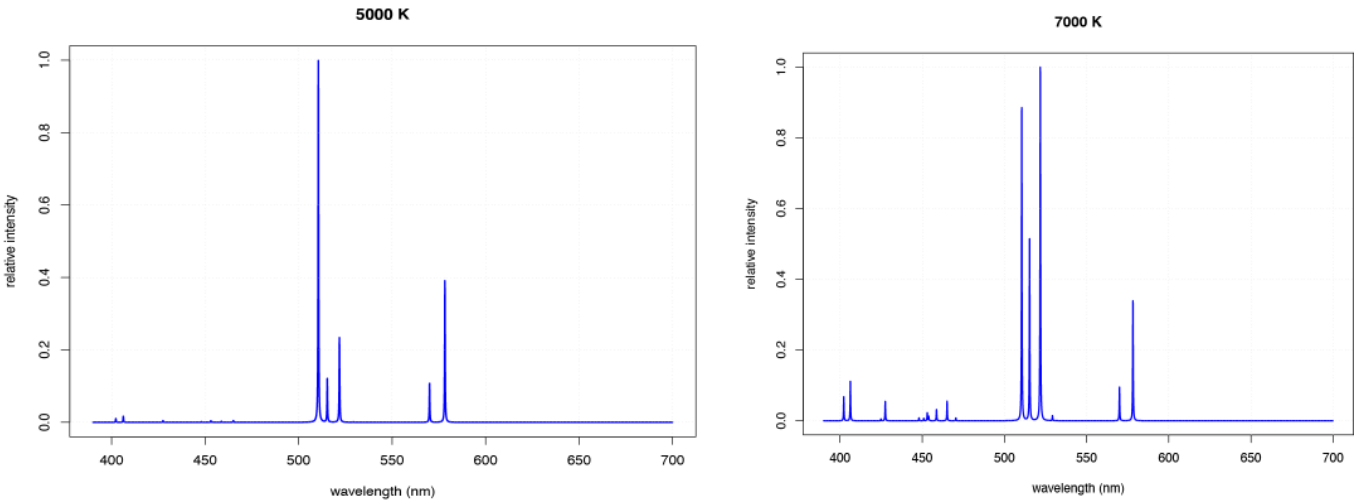



Figure 8.1.6: Atomic emission spectra for Cu at 5000 K and 7000 K. The spectra were simulated using the R package atomicEmission.

## Band and Continuum Spectra

The atomic emission spectra for sodium in Figure 8.1.3 consists of discrete, narrow lines because they arise from the transition between the discrete, well-defined energy levels seen in Figure 8.1.1. Atomic emission from a flame also include contributions from two additional sources: the emission from molecular species that form in the flame and emission from the flame. A sample of water, for example, is likely to contain a variety of ions, such as $Ca^{2+}$, that form molecular species, such as CaOH in the flame, and that emit photon over a much broader range of wavelengths than do atoms. The flame, itself, emits photons throughout the range of wavelengths used in UV/Vis atomic emission.

---

This page titled 8.1: Optical Atomic Spectra is shared under a CC BY-NC-SA 4.0 license and was authored, remixed, and/or curated by David Harvey.

# 8.2: Atomization Methods

Atomic methods require that the sample consist of individual gas phase atoms or gas phase atomic ions. With rare exceptions, this is not the form in which we obtain samples. If we are interested in analyzing seawater for the concentration of sodium, we need to find a way to convert the solution of aqueous sodium ions, $Na^+(aq)$, into gas phase sodium atoms, $Na(g)$, or gas phase sodium ions, $Na^+(g)$. The process by which this happens is called atomization and requires a source of thermal energy. Examples of atomization methods include the use of flames, resistive heating, plasmas, and electric arcs and sparks. More details on specific atomization methods appear in the chapters that follow.

This page titled 8.2: Atomization Methods is shared under a CC BY-NC-SA 4.0 license and was authored, remixed, and/or curated by David Harvey.

# 8.3: Sample Introduction Methods

In addition to a method of atomization, atomic spectroscopic methods require a means of placing the sample within the device used for atomization. The analysis of seawater for sodium ions requires a means for working with a sample that is in solution. The analysis of a salt-substitute for sodium, on the other hand, requires a means for working with solid samples, which could be first bringing it into solution or working directly with the solid. How a sample is introduced also depends on the method of atomization. Examples of different methods of sample introduction include aspirating a solution directly into a flame, injecting a small aliquot of solution onto a resistive heating mechanism, or exposing a solid sample to a laser or electric spark. More details on specific methods for introducing samples appear in the chapters that follow.

This page titled 8.3: Sample Introduction Methods is shared under a CC BY-NC-SA 4.0 license and was authored, remixed, and/or curated by David Harvey.

# CHAPTER OVERVIEW

## 9: Atomic Absorption Spectrometry


9.1: Sample Atomization Techniques

9.2: Atomic Absorption Instrumentation

9.3: Interferences in Absorption Spectroscopy

9.4: Atomic Absorption Techniques


---


This page titled 9: Atomic Absorption Spectrometry is shared under a CC BY-NC-SA 4.0 license and was authored, remixed, and/or curated by David Harvey.

# 9.1: Sample Atomization Techniques

The process of converting an analyte to a free gaseous atom is called atomization. Converting an aqueous analyte into a free atom requires that we strip away the solvent, volatilize the analyte, and, if necessary, dissociate the analyte into free atoms. Desolvating an aqueous solution of $CuCl_2$, for example, leaves us with solid particulates of $CuCl_2$. Converting the particulate $CuCl_2$ to gas phases atoms of Cu and Cl requires thermal energy.

$$CuCl_2(aq) \rightarrow CuCl_2(s) \rightarrow Cu(g) + 2Cl(g)$$

There are two common atomization methods: flame atomization and electrothermal atomization, although a few elements are atomized using other methods.

## Flame Atomization

Figure 9.1.1 shows a typical flame atomization assembly with close-up views of several key components. In the unit shown here, the aqueous sample is drawn into the assembly by passing a high-pressure stream of compressed air past the end of a capillary tube immersed in the sample. When the sample exits the nebulizer it strikes a glass impact bead, which converts it into a fine aerosol mist within the spray chamber. The aerosol mist is swept through the spray chamber by the combustion gases—compressed air and acetylene in this case—to the burner head where the flame's thermal energy desolvates the aerosol mist to a dry aerosol of small, solid particulates. The flame's thermal energy then volatilizes the particles, producing a vapor that consists of molecular species, ionic species, and free atoms.

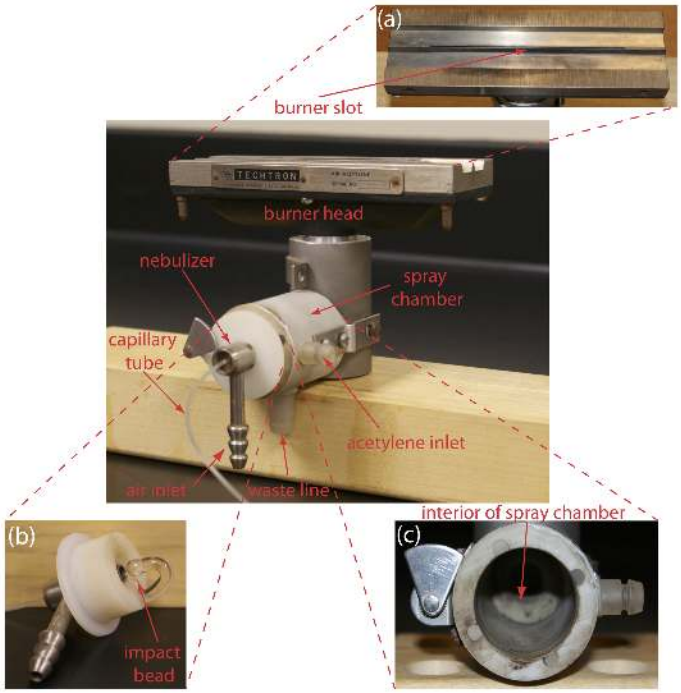



Figure 9.1.1. Flame atomization assembly with expanded views of (a) the burner head showing the burner slot where the flame is located; (b) the nebulizer's impact bead; and (c) the interior of the spray chamber. Although the unit shown here is from an instrument dating to the 1970s, the basic components of a modern flame AA spectrometer are the same.

***Burner.*** The slot burner in Figure 9.1.1$a$ provides a long optical pathlength and a stable flame. Because absorbance is directly proportional to pathlength, a long pathlength provides greater sensitivity. A stable flame minimizes uncertainty due to fluctuations in the flame.

The burner is mounted on an adjustable stage that allows the entire assembly to move horizontally and vertically. Horizontal adjustments ensure the flame is aligned with the instrument's optical path. Vertical adjustments change the height within the flame from which absorbance is monitored. This is important because two competing processes affect the concentration of free atoms in the flame. The more time an analyte spends in the flame the greater the atomization efficiency; thus, the production of free atoms

increases with height. On the other hand, a longer residence time allows more opportunity for the free atoms to combine with oxygen to form a molecular oxide. As seen in Figure 9.1.2, for a metal this is easy to oxidize, such as Cr, the concentration of free atoms is greatest just above the burner head. For a metal, such as Ag, which is difficult to oxidize, the concentration of free atoms increases steadily with height.

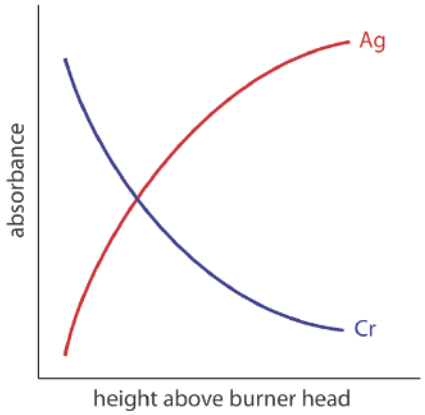



Figure 9.1.2. Absorbance versus height profiles for Ag and Cr in flame atomic absorption spectroscopy.

***Flame.*** The flame's temperature, which affects the efficiency of atomization, depends on the fuel–oxidant mixture, several examples of which are listed in Table 9.1.1. Of these, the air–acetylene and the nitrous oxide–acetylene flames are the most popular. Normally the fuel and oxidant are mixed in an approximately stoichiometric ratio; however, a fuel-rich mixture may be necessary for easily oxidized analytes.

Table 9.1.1. Fuels and Oxidants Used for Flame Combustion

| fuel | oxidant | temperature range (°C) |
|---|---|---|
| natural gas | air | 1700–1900 |
| hydrogen | air | 2000–2100 |
| acetylene | air | 2100–2400 |
| acetylene | nitrous oxide | 2600–2800 |
| acetylene | oxygen | 3050–3150 |

Figure 9.1.3 shows a cross-section through the flame, looking down the source radiation's optical path. The primary combustion zone usually is rich in gas combustion products that emit radiation, limiting is useful- ness for atomic absorption. The interzonal region generally is rich in free atoms and provides the best location for measuring atomic absorption. The hottest part of the flame typically is 2–3 cm above the primary combustion zone. As atoms approach the flame's secondary combustion zone, the decrease in temperature allows for formation of stable molecular species.

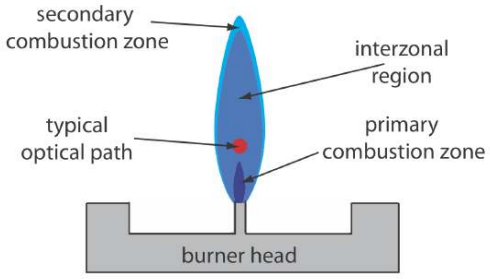



Figure 9.1.3. Profile of typical flame using a slot burner. The relative size of each zone depends on many factors, including the choice of fuel and oxidant, and their relative proportions.

***Sample Introduction.*** The most common means for introducing a sample into a flame atomizer is a continuous aspiration in which the sample flows through the burner while we monitor absorbance. Continuous aspiration is sample intensive, typically requiring from 2–5 mL of sample.

Flame microsampling allows us to introduce a discrete sample of fixed volume, and is useful if we have a limited amount of sample or when the sample's matrix is incompatible with the flame atomizer. For example, continuously aspirating a sample that has a high concentration of dissolved solids—sea water, for example, comes to mind—may build-up a solid de- posit on the burner head that obstructs the flame and that lowers the absorbance. Flame microsampling is accomplished using a micropipet to place 50–250 μL of sample in a Teflon funnel connected to the nebulizer, or by dipping the nebulizer tubing into the sample for a short time. Dip sampling usually is accomplished with an automatic sampler. The signal for flame microsampling is a transitory peak whose height or area is proportional to the amount of analyte that is injected.

***Advantages and Disadvantages of Flame Atomization.*** The principal advantage of flame atomization is the reproducibility with which the sample is introduced into the spectrophotometer; a significant disadvantage is that the efficiency of atomization is quite poor. There are two reasons for poor atomization efficiency. First, the majority of the aerosol droplets produced during nebulization are too large to be carried to the flame by the combustion gases. Consequently, as much as 95% of the sample never reaches the flame, which is the reason for the waste line shown at the bottom of the spray chamber in Figure 9.1.1. A second reason for poor atomization efficiency is that the large volume of combustion gases significantly dilutes the sample. Together, these contributions to the efficiency of atomization reduce sensitivity because the analyte's concentration in the flame may be a factor of $2.5 \times 10^{-6}$ less than that in solution [Ingle, J. D.; Crouch, S. R. *Spectrochemical Analysis*, Prentice-Hall: Englewood Cliffs, NJ, 1988; p. 275].

## Electrothermal Atomization

A significant improvement in sensitivity is achieved by using the resistive heating of a graphite tube in place of a flame. A typical electrothermal atomizer, also known as a graphite furnace, consists of a cylindrical graphite tube approximately 1–3 cm in length and 3–8 mm in diameter. As shown in Figure 9.1.4, the graphite tube is housed in an sealed assembly that has an optically transparent window at each end. A continuous stream of inert gas is passed through the furnace, which protects the graphite tube from oxidation and removes the gaseous products produced during atomization. A power supply is used to pass a current through the graphite tube, resulting in resistive heating.

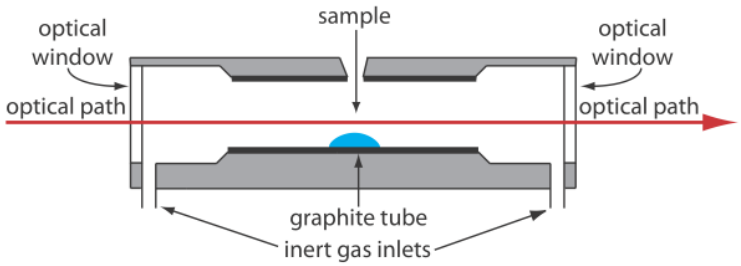



Figure 9.1.4. Diagram showing a cross-section of an electrothermal atomizer, which also is known as a graphite furnace.

Samples of between 5–50 μL are injected into the graphite tube through a small hole at the top of the tube. Atomization is achieved in three stages. In the first stage the sample is dried to a solid residue using a current that raises the temperature of the graphite tube to about 110°C. In the second stage, which is called ashing, the temperature is increased to between 350–1200°C. At these temperatures organic material in the sample is converted to $CO_2$ and $H_2O$, and volatile inorganic materials are vaporized. These gases are removed by the inert gas flow. In the final stage the sample is atomized by rapidly increasing the temperature to between 2000–3000°C. The result is a transient absorbance peak whose height or area is proportional to the absolute amount of analyte injected into the graphite tube. Together, the three stages take approximately 45–90 s, with most of this time used for drying and ashing the sample.

Electrothermal atomization provides a significant improvement in sensitivity by trapping the gaseous analyte in the small volume within the graphite tube. The analyte's concentration in the resulting vapor phase is as much as $1000\times$ greater than in a flame atomization [Parsons, M. L.; Major, S.; Forster, A. R. *Appl. Spectrosc.* **1983**, *37*, 411–418]. This improvement in sensitivity—and the resulting improvement in detection limits—is offset by a significant decrease in precision. Atomization efficiency is influenced strongly by the sample's contact with the graphite tube, which is difficult to control reproducibly.

## Specialized Atomization Techniques

A few elements are atomized by using a chemical reaction to produce a volatile product. Elements such as As, Se, Sb, Bi, Ge, Sn, Te, and Pb, for example, form volatile hydrides when they react with $NaBH_4$ in the presence of acid. An inert gas carries the volatile hydride to either a flame or to a heated quartz observation tube situated in the optical path. Mercury is determined by the cold-vapor method in which it is reduced to elemental mercury with $SnCl_2$. The volatile Hg is carried by an inert gas to an unheated observation tube situated in the instrument's optical path.

## Flame or Electrothermal Atomization?

The most important factor in choosing a method of atomization is the analyte's concentration. Because of its greater sensitivity, it takes less analyte to achieve a given absorbance when using electrothermal atomization. Table 9.1.2 which compares the amount of analyte needed to achieve an absorbance of 0.20 when using flame atomization and electrothermal atomization, is useful when selecting an atomization method. For example, flame atomization is the method of choice if our samples contain 1–10 mg $Zn^{2+}$/L, but electrothermal atomization is the best choice for samples that contain 1–10 µg $Zn^{2+}$/L.

Table 9.1.2. Concentration of Analyte (in mg/L) That Yields an Absorbance of 0.20

| element | flame atomization | electrothermal atomization |
|---|---|---|
| Ag | 1.5 | 0.0035 |
| Al | 40 | 0.015 |
| As | 40 | 0.050 |
| Ca | 0.8 | 0.003 |
| Cd | 0.6 | 0.001 |
| Co | 2.5 | 0.021 |
| Cr | 2.5 | 0.0075 |
| Cu | 1.5 | 0.012 |
| Fe | 2.5 | 0.006 |
| Hg | 70 | 0.52 |
| Mg | 0.15 | 0.00075 |
| Mn | 1 | 0.003 |
| Na | 0.3 | 0.00023 |
| Ni | 2 | 0.024 |
| Pb | 5 | 0.080 |
| Pt | 70 | 0.29 |
| Sn | 50 | 0.023 |
| Zn | 0.3 | 0.00071 |

Source: Varian Cookbook, SpectraAA Software Version 4.00 Pro.
As: 10 mg/L by hydride vaporization; Hg: 11.5 mg/L by cold-vapor; and Sn:18 mg/L by hydride vaporization

This page titled 9.1: Sample Atomization Techniques is shared under a CC BY-NC-SA 4.0 license and was authored, remixed, and/or curated by David Harvey.

# 9.2: Atomic Absorption Instrumentation

Atomic absorption spectrophotometers use optical benches similar to those described earlier in Chapter 7, including a source of radiation, a method for introducing the sample (covered in the previous section), a means for isolating the wavelengths of interest, and a way to measure the amount of light absorbed or emitted.

## Radiation Sources

Because atomic absorption lines are narrow, we need to use a line source instead of a continuum source to record atomic absorption spectra. Figure 9.2.1 will help us understand why this is necessary. As discussed in Chapter 7, a typical continuum source has an effective bandwidth on the order of 1 nm after passing through a monochromator. An atomic absorption line, as we learned in Chapter 8, has an effective line width on the order of 0.002 nm due to Doppler broadening and pressure broadening that takes place in a flame. If we pass the radiation from a continuum source through the flame, the incident power from the source, $P_0$, and the power that reaches the detector, $P_t$, are essentially identical, leading to an absorbance of zero. A line source, which operates a temperature that is lower than a flame, has a line width on the order of 0.001 nm. Passing this source radiation through the flame results in a measurable $P_T$ and a measurable absorbance.

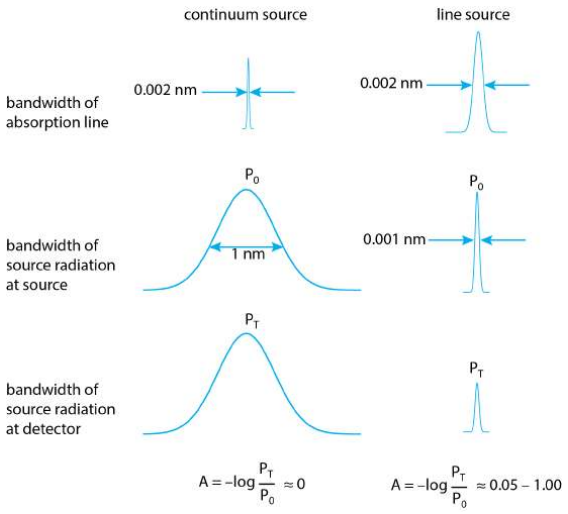



Figure 9.2.1: Illustration showing the effect on absorbance of using a continuum source and a line source for atomic absorption. Note that the peaks in the top row have the same width; thus, the x-axis scale is different for the continuum spectra than for the line source spectra.

The source for atomic absorption is a hollow cathode lamp that consists of a cathode and anode enclosed within a glass tube filled with a low pressure of an inert gas, such as Ne or Ar (Figure 9.2.2). Applying a potential across the electrodes ionizes the filler gas. The positively charged gas ions collide with the negatively charged cathode, sputtering atoms from the cathode's surface. Some of the sputtered atoms are in the excited state and emit radiation characteristic of the metal(s) from which the cathode is manufactured. By fashioning the cathode from the metallic analyte, a hollow cathode lamp provides emission lines that correspond to the analyte's absorption spectrum.

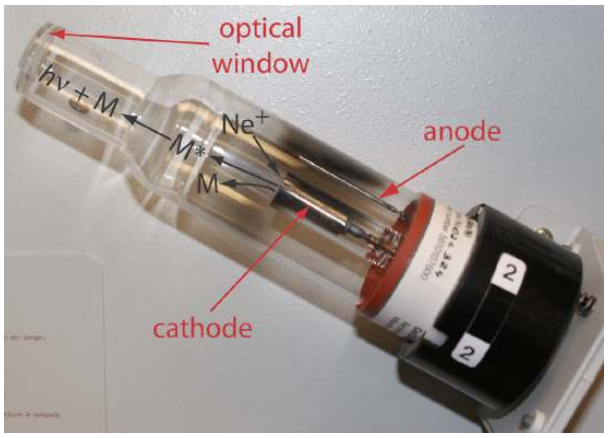



Figure 9.2.2. Photo of a typical multielemental hollow cathode lamp. The cathode in this lamp is fashioned from an alloy of Co, Cr, Cu, Fe, Mn, and Ni, and is surrounded by a glass shield that isolates it from the anode. The lamp is filled with Ne gas. Also shown is the process that leads to atomic emission. Note the black deposit of sputtered metal on the outer wall of the hollow cathode lamp. See the text for additional details.

Each element in a hollow cathode lamp provides several atomic emission lines that we can use for atomic absorption. Usually the wavelength that provides the best sensitivity is the one we choose to use, although a less sensitive wavelength may be more appropriate for a sample that has higher concentration of analyte. For the Cr hollow cathode lamp in Table 9.2.1, the best sensitivity is obtained using a wavelength of 357.9 nm as this line requires the smallest concentration of analyte to achieve an absorbance of 0.20.

Table 9.2.1. Atomic Emission Lines for a Cr Hollow Cathode Lamp

| wavelength (nm) | slit width (nm) | mg Cr/L giving $A$ = 0.20 | $P_0$ (relative) |
|---|---|---|---|
| 357.9 | 0.2 | 2.5 | 40 |
| 425.4 | 0.2 | 12 | 85 |
| 429.0 | 0.5 | 20 | 100 |
| 520.5 | 0.2 | 1500 | 15 |
| 520.8 | 0.2 | 500 | 20 |

Another consideration is the emission line's intensity, $P_0$. If several emission lines meet our requirements for sensitivity, we may wish to use the emission line with the largest relative $P_0$ because there is less uncertainty in measuring $P_0$ and $P_T$. When analyzing a sample that is ≈10 mg Cr/L, for example, the first three wavelengths in Table 9.2.1 provide good sensitivity; the wavelengths of 425.4 nm and 429.0 nm, however, have a greater $P_0$ and will provide less uncertainty in the measured absorbance.

The emission spectrum for a hollow cathode lamp includes, in addition to the analyte's emission lines, additional emission lines from impurities present in the metallic cathode and from the filler gas. These additional lines are a potential source of stray radiation that could result in an instrumental deviation from Beer's law. The monochromator's slit width is set as wide as possible to improve the throughput of radiation and narrow enough to eliminate these sources of stray radiation.

## Optical Benches

Atomic absorption spectrometers are available using either a single-beam and a double-beam optical bench. Figure 9.2.3 shows a typical single-beam spectrometer, which consists of a hollow cathode lamp as a source, a flame, a grating monochromator, a detector (usually a photomultiplier tube), and a signal processor. Also included in this design is a chopper that periodically blocks light from the hollow cathode lamp from passing through the flame and reaching the detector. The purpose of the chopper is to provide a means for discriminating against the emission of light from the flame, which will otherwise contribute to the total amount of light that reaches the detector. As shown in Figure 9.2.3, when the chopper is closed, the only light reaching the detector is from the flame; emission from the flame and light from the lamp after it passes through the flame reach the detector when the chopper is open. The difference between the two signals gives the amount of light that reaches the detector after being absorbed by the sample.

An alternative method that accomplishes the same thing is to modulate the amount of radiation emitted by the hollow cathode lamp.

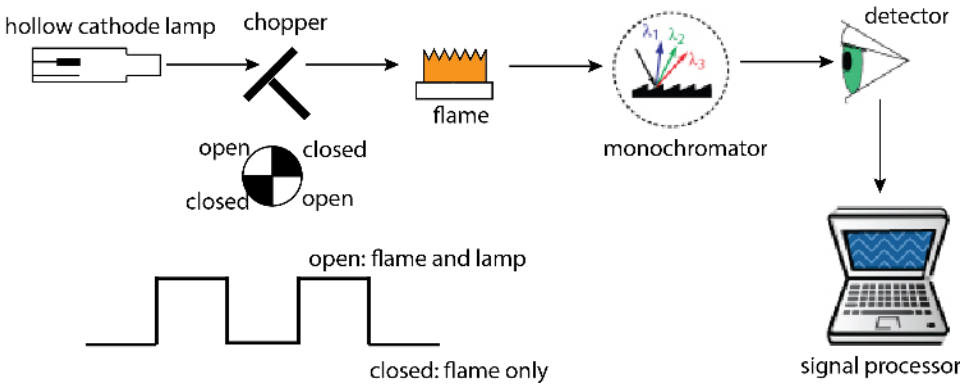



Figure 9.2.3: Typical single-beam optical bench for atomic absorption.

Figure 9.2.4 shows the typical arrangement of a double-beam instrument for atomic absorption spectroscopy. In this design, the chopper alternates between two optical paths: one in which light from the hollow cathode lamp bypasses the flame and that measures the total emission of radiation from the flame and the lamp, and one that passes the hollow light from the hollow cathode lamp through the flame and that measures the emission of light from the flame and the amount of light from the hollow cathode lamp that is not absorbed by the sample. The difference between the two signals gives the amount of light that reaches the detector after being absorbed by the sample.

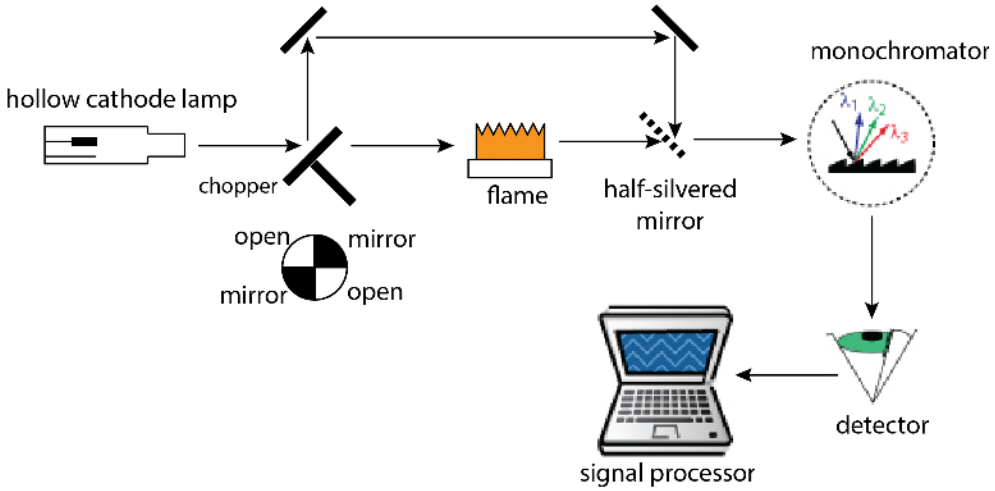



Figure 9.2.4: Typical double-beam optical bench for atomic absorption.

This page titled 9.2: Atomic Absorption Instrumentation is shared under a CC BY-NC-SA 4.0 license and was authored, remixed, and/or curated by David Harvey.

# 9.3: Interferences in Absorption Spectroscopy

In describing the optical benches for atomic absorption spectroscopy, we noted the need to modulate the radiation from the source in order to discriminate against emission of radiation from the flame. In this section we consider additional sources of interference and discuss ways to compensate for them.

## Spectral Interferences

A spectral interference occurs when an analyte's absorption line overlaps with an interferent's absorption line or band. Because atomic absorption lines are so narrow, the overlap of two such lines seldom is a problem. On the other hand, a molecule's broad absorption band or the scattering of source radiation is a potentially serious spectral interference.

An important consideration when using a flame as an atomization source is its effect on the measured absorbance. Among the products of combustion are molecular species that exhibit broad absorption bands and particulates that scatter radiation from the source. If we fail to compensate for these spectral interferences, then the intensity of transmitted radiation is smaller than expected. The result is an apparent increase in the sample's absorbance. Fortunately, absorption and scattering of radiation by the flame are corrected by analyzing a blank that does not contain the sample.

Spectral interferences also occur when components of the sample's matrix other than the analyte react to form molecular species, such as oxides and hydroxides. The resulting absorption and scattering constitutes the sample's background and may present a significant problem, particularly at wavelengths below 300 nm where the scattering of radiation becomes more important. If we know the composition of the sample's matrix, then we can prepare our samples using an identical matrix. In this case the background absorption is the same for both the samples and the standards. Alternatively, if the background is due to a known matrix component, then we can add that component in excess to all samples and standards so that the contribution of the naturally occurring interferent is insignificant. Finally, many interferences due to the sample's matrix are eliminated by increasing the atomization temperature. For example, switching to a higher temperature flame helps prevents the formation of interfering oxides and hydroxides.

If the identity of the matrix interference is unknown, or if it is not possible to adjust the flame or furnace conditions to eliminate the interference, then we must find another method to compensate for the background interference. Several methods have been developed to compensate for matrix interferences, and most atomic absorption spectrophotometers include one or more of these methods.

One of the most common methods for background correction is to use a continuum source, such as a $D_2$ lamp. Because a $D_2$ lamp is a continuum source, absorbance of its radiation by the analyte's narrow absorption line is negligible. Only the background, therefore, absorbs radiation from the $D_2$ lamp. Both the analyte and the background, on the other hand, absorb the hollow cathode's radiation. Subtracting the absorbance for the $D_2$ lamp from that for the hollow cathode lamp gives a corrected absorbance that compensates for the background interference. Although this method of background correction is effective, it does assume that the background absorbance is constant over the range of wavelengths passed by the monochromator. If this is not true, then subtracting the two absorbances underestimates or overestimates the background. A typical optical arrangement is shown in Figure 9.3.1.

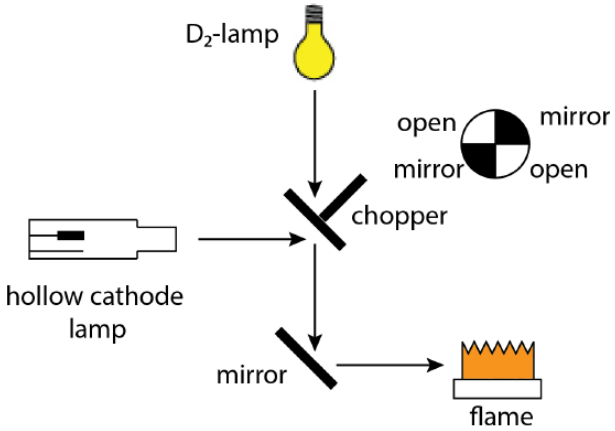



Figure 9.3.1: Illustration showing a modification to the optical bench to allow for background correction using a continuous source, such as a $D_2$-lamp. The chopper alternates between allowing light from the hollow cathode lamp and light from the $D_2$-lamp to pass through the flame and reach the detector.

Another approach to removing the background is to take advantage of the Zeeman effect. The basis of the technique is outlined in Figure 9.3.2 and described below in more detail. In the absence of an applied magnetic field—B = 0, where B is the strength of the magnetic field—a $p \rightarrow d$ absorbance by the analyte takes place between two well-defined energy levels and yields a single well-defined absorption line, as seen on the left side of panel (a). When a magnetic field is applied, B > 0, the three equal energy *p*-orbitals split into three closely spaced energy levels and the five equal energy *d*-orbitals split into five closely spaced energy levels. The allowed transitions between these energy levels of $\Delta M_l = 0, \pm 1$ yields three well-defined absorption lines, as seen on the right-side of panel (a), the central one of which ($\Delta M_l = 0$) is at the same wavelength as the absorption line in the absence of the applied magnetic field. This central band is the only wavelength at which the analyte absorbs.

As we see in Figure $9.3.2b, c$, we apply a magnetic field to the instrument's electrothermal atomizer and place a rotating polarizer between it and the hollow cathode lamp. When the rotating polarizer is in one position, radiation from the hollow cathode light is absorbed only by the central absorption line, giving a measure of absorption by both the background and the analyte. when the rotating polarizer is in the other position, radiation from the hollow cathode lamp is absorbed only by the two outside lines, providing a measure of absorption by the background only. The difference in these two absorption values is a function of the analyte's concentration.

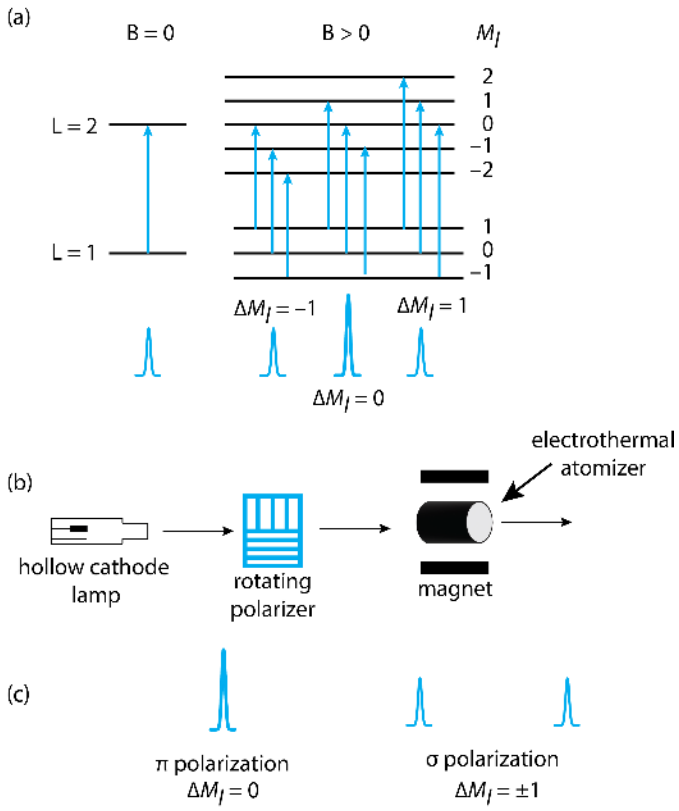



Figure 9.3.2: Illustration of using the Zeeman effect to compensate for background absorption when using an electrothermal atomizer: panel (a) explains the origin of the Zeemen effect; panel (b) shows the modification to the instrument; and panel (c) shows the resulting absorption lines. See the text for more details.

A third method for compensating for background absorption is to take advantage of what happens to the emission intensity of a hollow cathode lamp when it is operated at a high current. As seen in Figure 9.3.3, when using a high current the emission band become significantly broader than when using a normal (low) current and, at the analytical wavelength, the emission intensity from the lamp decreases due to self-absorption, a process in which the ground state atoms in the hollow cathode lamp absorb photons emitted by the excited state atoms in the hollow cathode lamp. When using a low current we measure absorption from both the analyte and the background; when using a high current, absorption is due almost exclusively to the background. This approach is called Smith-Hieftje background corrections.

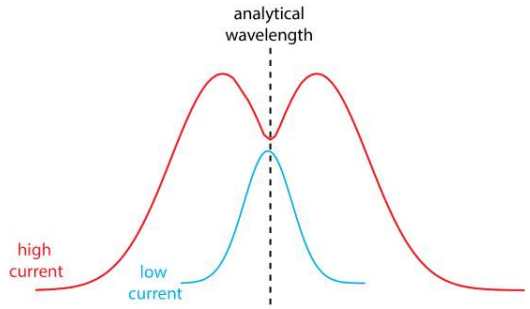



Figure 9.3.1: Illustration showing the basis of Smith-Hieftje background correction.

## Chemical Interferences

The quantitative analysis of some elements is complicated by chemical interferences that occur during atomization. The most common chemical interferences are the formation of nonvolatile compounds that contain the analyte and ionization of the analyte.

One example of the formation of a nonvolatile compound is the effect of $PO_4^{3-}$ or $Al^{3+}$ on the flame atomic absorption analysis of $Ca^{2+}$. In one study, for example, adding 100 ppm $Al^{3+}$ to a solution of 5 ppm $Ca^{2+}$ decreased calcium ion's absorbance from 0.50 to 0.14, while adding 500 ppm $PO_4^{3-}$ to a similar solution of $Ca^{2+}$ decreased the absorbance from 0.50 to 0.38. These interferences are attributed to the formation of nonvolatile particles of $Ca_3(PO_4)_2$ and an Al–Ca–O oxide [Hosking, J. W.; Snell, N. B.; Sturman, B. T. *J. Chem. Educ.* **1977**, *54*, 128–130].

When using flame atomization, we can minimize the formation of non-volatile compounds by increasing the flame's temperature by changing the fuel-to-oxidant ratio or by switching to a different combination of fuel and oxidant. Another approach is to add a releasing agent or a protecting agent to the sample. A releasing agent is a species that reacts preferentially with the interferent, releasing the analyte during atomization. For example, $Sr^{2+}$ and $La^{3+}$ serve as releasing agents for the analysis of $Ca^{2+}$ in the presence of $PO_4^{3-}$ or $Al^{3+}$. Adding 2000 ppm $SrCl_2$ to the $Ca^{2+}$/ $PO_4^{3-}$ and to the $Ca^{2+}$/$Al^{3+}$ mixtures described in the previous paragraph increased the absorbance to 0.48. A protecting agent reacts with the analyte to form a stable volatile complex. Adding 1% w/w EDTA to the $Ca^{2+}$/ $PO_4^{3-}$ solution described in the previous paragraph increased the absorbance to 0.52.

An ionization interference occurs when thermal energy from the flame or the electrothermal atomizer is sufficient to ionize the analyte

$$M(s) \rightleftharpoons M^+(aq) + e^- \tag{9.3.1}$$

where M is the analyte. Because the absorption spectra for M and $M^+$ are different, the position of the equilibrium in reaction 9.3.1 affects the absorbance at wavelengths where M absorbs. To limit ionization we add a high concentration of an ionization suppressor, which is a species that ionizes more easily than the analyte. If the ionization suppressor's concentration is sufficient, then the increased concentration of electrons in the flame pushes reaction 9.3.1 to the left, preventing the analyte's ionization. Potassium and cesium frequently are used as an ionization suppressor because of their low ionization energy.

This page titled 9.3: Interferences in Absorption Spectroscopy is shared under a CC BY-NC-SA 4.0 license and was authored, remixed, and/or curated by David Harvey.

# 9.4: Atomic Absorption Techniques

## Preparing the Sample

Flame and electrothermal atomization require that the analyte is in solution. Solid samples are brought into solution by dissolving in an appropriate solvent. If the sample is not soluble it is digested, either on a hot-plate or by microwave, using $HNO_3$, $H_2SO_4$, or $HClO_4$. Alternatively, we can extract the analyte using a Soxhlet extractor. Liquid samples are analyzed directly or the analytes extracted if the matrix is in- compatible with the method of atomization. A serum sample, for instance, is difficult to aspirate when using flame atomization and may produce an unacceptably high background absorbance when using electrothermal atomization. A liquid–liquid extraction using an organic solvent and a chelating agent frequently is used to concentrate analytes. Dilute solutions of $Cd^{2+}$, $Co^{2+}$, $Cu^{2+}$, $Fe^{3+}$, $Pb^{2+}$, $Ni^{2+}$, and $Zn^{2+}$, for example, are concentrated by extracting with a solution of ammonium pyrrolidine dithiocarbamate in methyl isobutyl ketone.

## Standardizing the Method

Because Beer's law also applies to atomic absorption, we might expect atomic absorption calibration curves to be linear. In practice, however, most atomic absorption calibration curves are nonlinear or linear over a limited range of concentrations. Nonlinearity in atomic absorption is a consequence of instrumental limitations, including stray radiation from the hollow cathode lamp and the variation in molar absorptivity across the absorption line. Accurate quantitative work, therefore, requires a suitable means for computing the calibration curve from a set of standards.

When possible, a quantitative analysis is best conducted using external standards. Unfortunately, matrix interferences are a frequent problem, particularly when using electrothermal atomization. For this reason the method of standard additions often is used. One limitation to this method of standardization, however, is the requirement of a linear relationship between absorbance and concentration.

> Most instruments include several different algorithms for computing the calibration curve. The instrument in my lab, for example, includes five algorithms. Three of the algorithms fit absorbance data using linear, quadratic, or cubic polynomial functions of the analyte's concentration. It also includes two algorithms that fit the concentrations of the standards to quadratic functions of the absorbance.

## Evaluation of Atomic Absorption Spectroscopy

### Scale of Operation

Atomic absorption spectroscopy is ideally suited for the analysis of trace and ultratrace analytes, particularly when using electrothermal atomization. For minor and major analytes, sample are diluted before the analysis. Most analyses use a macro or a meso sample. The small volume requirement for electrothermal atomization or for flame microsampling, however, makes practical the analysis of micro and ultramicro samples.

### Accuracy

If spectral and chemical interferences are minimized, an accuracy of 0.5–5% is routinely attainable. When the calibration curve is nonlinear, accuracy is improved by using a pair of standards whose absorbances closely bracket the sample's absorbance and assuming that the change in absorbance is linear over this limited concentration range. Determinate errors for electrothermal atomization often are greater than those obtained with flame atomization due to more serious matrix interferences.

### Precision

For an absorbance greater than 0.1–0.2, the relative standard deviation for atomic absorption is 0.3–1% for flame atomization and 1–5% for electrothermal atomization. The principle limitation is the uncertainty in the concentration of free analyte atoms that result from variations in the rate of aspiration, nebulization, and atomization for a flame atomizer, and the consistency of injecting samples for electrothermal atomization.

## Sensitivity

The sensitivity of a flame atomic absorption analysis is influenced by the flame's composition and by the position in the flame from which we monitor the absorbance. Normally the sensitivity of an analysis is optimized by aspirating a standard solution of analyte and adjusting the fuel-to-oxidant ratio, the nebulizer flow rate, and the height of the burner, to give the greatest absorbance. With electrothermal atomization, sensitivity is influenced by the drying and ashing stages that precede atomization. The temperature and time at each stage is optimized for each type of sample.

Sensitivity also is influenced by the sample's matrix. We already noted, for example, that sensitivity is decreased by a chemical interference. An increase in sensitivity may be realized by adding a low molecular weight alcohol, ester, or ketone to the solution, or by using an organic solvent.

## Selectivity

Due to the narrow width of absorption lines, atomic absorption provides excellent selectivity. Atomic absorption is used for the analysis of over 60 elements at concentrations at or below the level of μg/L.

## Time, Cost, and Equipment

The analysis time when using flame atomization is short, with sample throughputs of 250–350 determinations per hour when using a fully automated system. Electrothermal atomization requires substantially more time per analysis, with maximum sample throughputs of 20–30 determinations per hour. The cost of a new instrument ranges from between $10,000– $50,000 for flame atomization, and from $18,000–$70,000 for electrothermal atomization. The more expensive instruments in each price range include double-beam optics, automatic samplers, and can be programmed for multielemental analysis by allowing the wavelength and hollow cathode lamp to be changed automatically.

---

This page titled 9.4: Atomic Absorption Techniques is shared under a CC BY-NC-SA 4.0 license and was authored, remixed, and/or curated by David Harvey.

# CHAPTER OVERVIEW

## 10: Atomic Emission Spectrometry

10.1: Emission Spectroscopy Based on Flame and Plasma Sources
10.2: Emission Spectroscopy Based on Arc and Spark Sources

This page titled 10: Atomic Emission Spectrometry is shared under a CC BY-NC-SA 4.0 license and was authored, remixed, and/or curated by David Harvey.

# 10.1: Emission Spectroscopy Based on Flame and Plasma Sources

## What is Emission?

An analyte in an excited state possesses an energy, $E_2$, that is greater than its energy when it is in a lower energy state, $E_1$. When the analyte returns to its lower energy state—a process we call relaxation—the excess energy, $\Delta E$, is

$$\Delta E = E_2 - E_1$$

There are several ways in which an atom may end up in an excited state, including thermal energy, which is the focus of this chapter. The amount of time an atom, *A*, spends in its excited state—what we call the excited state's lifetime—is short, typically $10^{-5}$ to $10^{-9}$ s for an electronic excited state. Relaxation of the atom's excited state, *A**, occurs through several mechanisms, including collisions with other species in the sample and the emission of photons. In the first process, which we call nonradiative relaxation, the excess energy is released as heat.

$$A^* \longrightarrow A + \text{ heat}$$

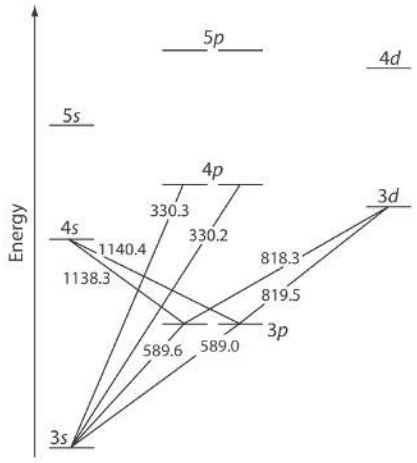
In the second mechanism, the excess energy is released as a photon of electromagnetic radiation.

$$A^* \longrightarrow A + h\nu$$

The release of a photon following thermal excitation is called emission. The focus of this chapter is on the emission of ultraviolet and visible radiation following the thermal excitation of atoms. Atomic emission spectroscopy has a long history. Qualitative applications based on the color of flames were used in the smelting of ores as early as 1550 and were more fully developed around 1830 with the observation of atomic spectra generated by flame emission and spark emission [Dawson, J. B. *J. Anal. At. Spectrosc.* **1991**, *6*, 93–98]. Quantitative applications based on the atomic emission from electric sparks were developed by Lockyer in the early 1870 and quantitative applications based on flame emission were pioneered by Lundegardh in 1930. Atomic emission based on emission from a plasma was introduced in 1964.

## Atomic Emission Spectra

Atomic emission occurs when a valence electron in a higher energy atomic orbital returns to a lower energy atomic orbital. Figure 10.1.1 shows a portion of the energy level diagram for sodium, which consists of a series of discrete lines at wavelengths that correspond to the difference in energy between two atomic orbitals.




FFigure 10.1.1. Valence shell energy level diagram for sodium. The wavelengths corresponding to several transitions are shown.

The intensity of an atomic emission line, $I_e$, is proportional to the number of atoms, $N^*$, that populate the excited state

$$I_e = kN^* \tag{10.1.1}$$

where *k* is a constant that accounts for the efficiency of the transition. If a system of atoms is in thermal equilibrium, the population of excited state *i* is related to the total concentration of atoms, *N*, by the Boltzmann distribution. For many elements at temperatures of less than 5000 K the Boltzmann distribution is approximated as

$$N^* = N\left(\frac{g_i}{g_0}\right)e^{-E_i/kT} \tag{10.1.2}$$

where $g_i$ and $g_0$ are statistical factors that account for the number of equivalent energy levels for the excited state and the ground state, $E_i$ is the energy of the excited state relative to the ground state, $E_0$, $k$ is Boltzmann's constant ($1.3807 \times 10^{-23}$ J/K), and $T$ is the temperature in Kelvin. From Equation 10.1.2 we expect that excited states with lower energies have larger populations and more intense emission lines. We also expect emission intensity to increase with temperature. The emission spectrum for sodium is shown in Figure 10.1.2

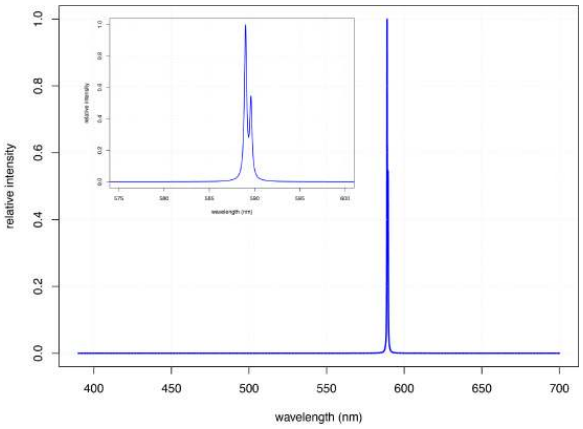



Figure 10.1.2: Visible emission spectrum for sodium. The inset shows a close up of the emission lines at 589.0 and 589.6 nm that appear in the energy level diagram in Figure 10.1.1.

An atomic emission spectrometer is similar in design to the instrumentation for atomic absorption. In fact, it is easy to adapt most flame atomic absorption spectrometers for atomic emission by turning off the hollow cathode lamp and monitoring the difference between the emission intensity when aspirating the sample and when aspirating a blank. Many atomic emission spectrometers, however, are dedicated instruments designed to take advantage of features unique to atomic emission, including the use of plasmas, arcs, sparks, and lasers as atomization and excitation sources, and an enhanced capability for multielemental analysis.

## Flames as a Source

Atomization and excitation in flame atomic emission is accomplished with the same nebulization and spray chamber assembly used in atomic absorption (see Chapter 9). The burner head consists of a single or multiple slots, or a Meker-style burner. Older atomic emission instruments often used a total consumption burner in which the sample is drawn through a capillary tube and injected directly into the flame.

> A Meker burner is similar to the more common Bunsen burner found in most laboratories; it is designed to allow for higher temperatures and for a larger diameter flame.

## The Inductively Coupled Plasma Source

A plasma is a hot, partially ionized gas that contains an abundant concentration of cations and electrons. The plasma used in atomic emission is formed by ionizing a flowing stream of argon gas, producing argon ions and electrons. A plasma's high temperature results from resistive heating as the electrons and argon ions move through the gas. Because a plasma operates at a much higher temperature than a flame, it provides for a better atomization efficiency and a higher population of excited states.

A schematic diagram of the inductively coupled plasma source (ICP) is shown in Figure 10.1.3. The ICP torch consists of three concentric quartz tubes, surrounded at the top by a radio-frequency induction coil. The sample is mixed with a stream of Ar using a nebulizer, and is carried to the plasma through the torch's central capillary tube. Plasma formation is initiated by a spark from a Tesla coil. An alternating radio-frequency current in the induction coil creates a fluctuating magnetic field that induces the argon ions and the electrons to move in a circular path. The resulting collisions with the abundant unionized gas give rise to resistive heating, providing temperatures as high as 10000 K at the base of the plasma, and between 6000 and 8000 K at a height of 15–20

mm above the coil, where emission usually is measured. At these high temperatures the outer quartz tube must be thermally isolated from the plasma. This is accomplished by the tangential flow of argon shown in the schematic diagram. Samples are brought into the ICP using the same basic types of nebulization described in Chapter 8 for flame atomic absorption spectroscopy.

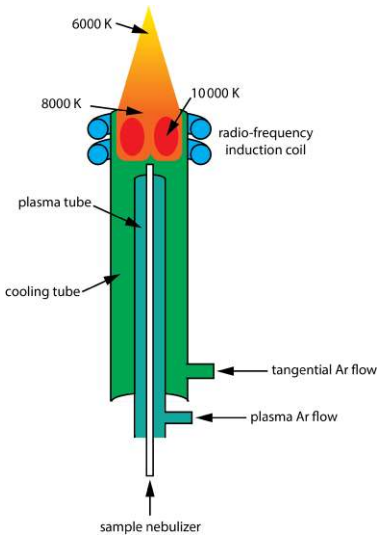



Figure 10.1.3. Schematic diagram of an inductively coupled plasma torch for atomic emission.

## The Direct Current Plasma Source

An alternative to the inductively coupled plasma source is the direct current (dc) plasma jet, one example of which is illustrated in Figure 10.1.4. The argon plasma (shown here in blue) forms between two graphite anodes and a tungsten cathode. The sample is aspirated into the plasma's excitation region where it undergoes atomization, excitation, and emission at temperatures of 5000 K.

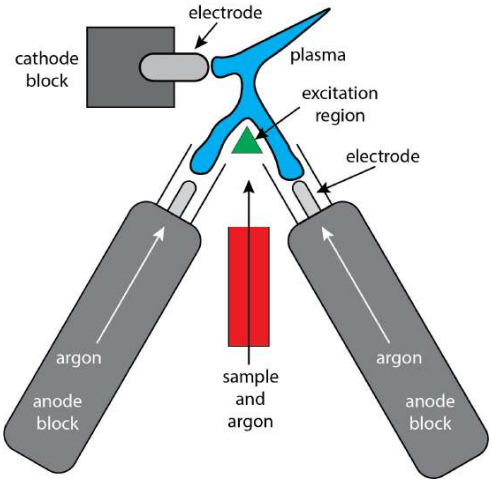



Figure 10.1.4: Illustration showing a schematic diagram of a direct current plasma source of atomic emission.

## Flame and Plasma Spectrometers

One advantage of atomic emission over atomic absorption is the ease of analyzing samples for multiple analytes. This additional capability arises because atomic emission, unlike atomic absorption, does not need an analyte-specific source of radiation. The two most common types of spectrometers are sequential and multichannel. In a sequential spectrometer the instrument has a single detector and uses the monochromator to move from one emission line to the next. A multichannel spectrometer uses the monochromator to disperse the emission across a field of detectors, each of which measures the emission intensity at a different wavelength.

## Sequential Instruments

A sequential instrument uses a programmable scanning monochromator, such as those described in Chapter 7, to rapidly move the monochromator's grating over wavelength regions that are not of interest, and then pauses and scans slowly over the emission lines of the analytes. Sampling rates of 300 determinations per hour are possible with this configuration. Another option, which is less common, is to move the exit slit and the detector across the monochromator's focal plane, pausing and recording the emission at the desired wavelengths.

## Multichannel Instruments

Another approach to a multielemental analysis is to use a multichannel instrument that allows us to monitor simultaneously many analytes. A simple design for a multichannel spectrometer, shown in Figure 10.1.5, couples a monochromator with multiple detectors that are positioned in a semicircular array around the monochromator at positions that correspond to the wavelengths for the analytes. A sample throughput of 3000 determinations per hour are possible using a multichannel ICP.

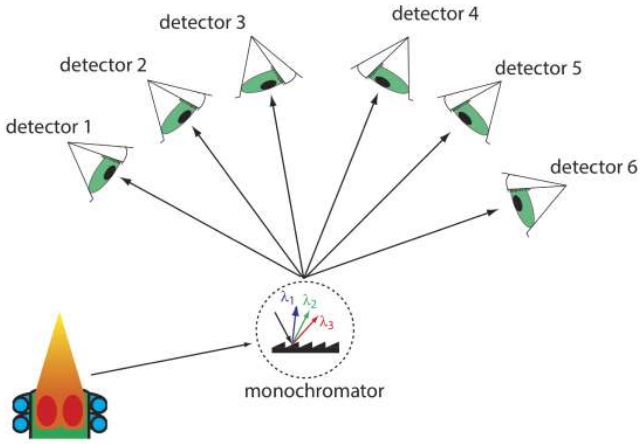



Figure 10.1.5. Schematic diagram of a multichannel atomic emission spectrometer for the simultaneous analysis of several elements. Instruments may contain as many as 48–60 detectors.

Another option for a multichannel instrument takes advantage of the charge-injection device, or CID, as a detector (see Chapter 7 for discussion of the charge-coupled device, another type of charge-transfer device used as a detector). Light from the plasma source is dispersed across the CID in two dimensions. The surface of the CID has in excess of 90000 detecting elements, or pixels, that allows for a resolution between detecting elements on the order of 0.04 nm. Light from the atomic emission source is distributed across the detector's surface by a diffraction grating such that each element of interest is detected using its own set of pixels, called a read window. Figure 10.1.6 shows that individual read windows consist of a set of detecting elements, nine of which collect photons from the spectral line and 30 of which provide a measurement of the source's background.

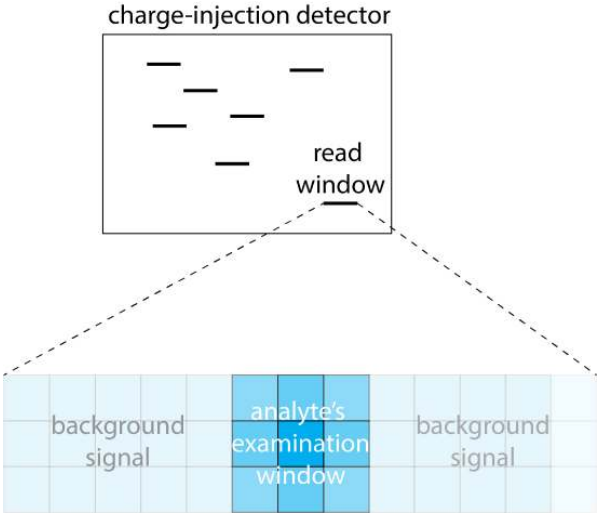



Figure 10.1.6: Illustration showing a charge-injection detector. The read window consists of nine central elements that measure the analyte's emission intensity (shown here using blue shading) and 30 of which measure the background emission from the plasma source.

## Application of Flame and Plasma Sources

Atomic emission is used widely for the analysis of trace metals in a variety of sample matrices. The development of a quantitative atomic emission method requires several considerations, including choosing a source for atomization and excitation, selecting a wavelength and slit width, preparing the sample for analysis, minimizing spectral and chemical interferences, and selecting a method of standardization.

## Choice of Atomization and Excitation Source

Except for the alkali metals, detection limits when using an ICP are significantly better than those obtained with flame emission (Table 10.1.1). Plasmas also are subject to fewer spectral and chemical interferences. For these reasons a plasma emission source is usually the better choice.

Table 10.1.1. Detection Limits for Atomic Emission

| element | detection limit (µg/mL): flame emission | detection limit (µg/mL): ICP |
|---|---|---|
| Ag | 2 | 0.2 |
| Al | 3 | 0.2 |
| As | 2000 | 2 |
| Ca | 0.1 | 0.0001 |
| Cd | 300 | 0.07 |
| Co | 5 | 0.1 |
| Cr | 1 | 0.08 |
| Fe | 10 | 0.09 |
| Hg | 150 | 1 |
| K | 0.01 | 30 |
| Li | 0.001 | 0.02 |
| Mg | 1 | 0.02 |
| Mn | 1 | 0.01 |
| Na | 0.01 | 0.1 |
| Ni | 10 | 0.2 |
| Pb | 0.2 | 1 |
| Pt | 2000 | 0.9 |
| Sn | 100 | 3 |
| Zn | 1000 | 0.1 |

Source: Parsons, M. L.; Major, S.; Forster, A. R.; App. Spectrosc. 1983, 37, 411–418.

### Selecting the Wavelength and Slit Width

The choice of wavelength is dictated by the need for sensitivity and the need to avoid interferences from the emission lines of other constituents in the sample. Because an analyte's atomic emission spectrum has an abundance of emission lines—particularly when using a high temperature plasma source—it is inevitable that there will be some overlap between emission lines. For example, an analysis for Ni using the atomic emission line at 349.30 nm is complicated by the atomic emission line for Fe at 349.06 nm.

A narrower slit width provides better resolution, but at the cost of less radiation reaching the detector. The easiest approach to selecting a wavelength is to record the sample's emission spectrum and look for an emission line that provides an intense signal and is resolved from other emission lines.

### Preparing the Sample

Flame and plasma sources are best suited for samples in solution and in liquid form. Although a solid sample can be analyzed by directly inserting it into the flame or plasma, they usually are first brought into solution by digestion or extraction.

### Minimizing Spectral Interferences

The most important spectral interference is broad, background emission from the flame or plasma and emission bands from molecular species. This background emission is particularly severe for flames because the temperature is insufficient to break down refractory compounds, such as oxides and hydroxides. Background corrections for flame emission are made by scanning over the emission line and drawing a baseline (Figure 10.1.7). Because a plasma's temperature is much higher, a background interference

due to molecular emission is less of a problem. Although emission from the plasma's core is strong, it is insignificant at a height of 10–30 mm above the core where measurements normally are made.

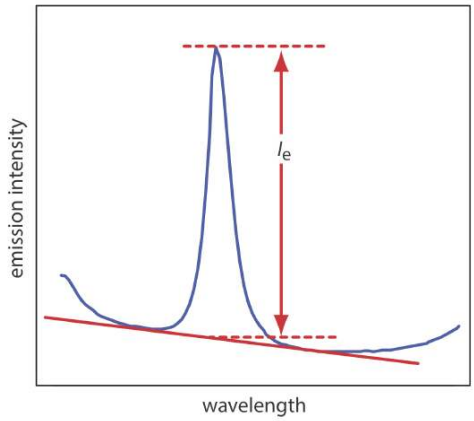



Figure 10.1.7. Method for correcting an analyte's emission for the flame's background emission.

## Minimizing Chemical Interferences

Flame emission is subject to the same types of chemical interferences as atomic absorption; they are minimized using the same methods: by adjusting the flame's composition and by adding protecting agents, releasing agents, or ionization suppressors. An additional chemical interference results from self-absorption. Because the flame's temperature is greatest at its center, the concentration of analyte atoms in an excited state is greater at the flame's center than at its outer edges. If an excited state atom in the flame's center emits a photon, then a ground state atom in the cooler, outer regions of the flame may absorb the photon, which decreases the emission intensity. For higher concentrations of analyte self-absorption may invert the center of the emission band (Figure 10.1.8).

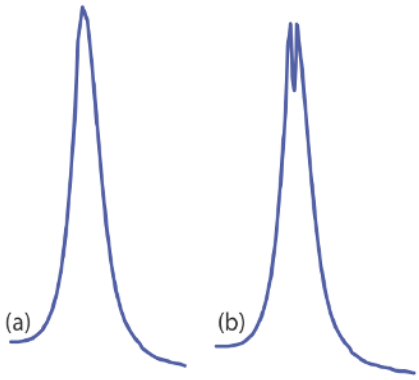



Figure 10.1.8. Atomic emission lines for (a) a low concentration of analyte, and (b) a high concentration of analyte showing the effect of self-absorption.

Chemical interferences when using a plasma source generally are not significant because the plasma's higher temperature limits the formation of nonvolatile species. For example, $PO_4^{3-}$ is a significant interferent when analyzing samples for $Ca^{2+}$ by flame emission, but has a negligible effect when using a plasma source. In addition, the high concentration of electrons from the ionization of argon minimizes ionization interferences.

## Standardizing the Method

From Equation 10.1.1 we know that emission intensity is proportional to the population of the analyte's excited state, $N^*$. If the flame or plasma is in thermal equilibrium, then the excited state population is proportional to the analyte's total population, $N$, through the Boltzmann distribution (Equation 10.1.2).

A calibration curve for flame emission usually is linear over two to three orders of magnitude, with ionization limiting linearity when the analyte's concentrations is small and self-absorption limiting linearity at higher concentrations of analyte. When using a

plasma, which suffers from fewer chemical interferences, the calibration curve often is linear over four to five orders of magnitude and is not affected significantly by changes in the matrix of the standards.

Emission intensity is affected significantly by many parameters, including the temperature of the excitation source and the efficiency of atomization. An increase in temperature of 10 K, for example, produces a 4% increase in the fraction of Na atoms in the 3*p* excited state, an uncertainty in the signal that may limit the use of external standards. The method of internal standards is used when the variations in source parameters are difficult to control. To compensate for changes in the temperature of the excitation source, the internal standard is selected so that its emission line is close to the analyte's emission line. In addition, the internal standard should be subject to the same chemical interferences to compensate for changes in atomization efficiency. To accurately correct for these errors the analyte and internal standard emission lines are monitored simultaneously.

---

This page titled 10.1: Emission Spectroscopy Based on Flame and Plasma Sources is shared under a CC BY-NC-SA 4.0 license and was authored, remixed, and/or curated by David Harvey.

# 10.2: Emission Spectroscopy Based on Arc and Spark Sources

## Arc Source

An arc source consists of two electrodes separated by a gap of up to 20 mm (see Figure 10.2.1 for one configuration). A potential of 50 V (or more) is applied and a continuous current in the range of 2–30 A is maintained throughout the analysis. If the sample is a metal, then it can be fashioned into the electrodes. For nonmetallic samples, the electrodes typically are fashioned from graphite and a cup-like depression is drilled into one of the electrodes. The sample is ground into a powder and packed into the sample cup. The plasma generated by an arc source typically has a temperature of 4000 K to 5000 K and has an abundance of emission lines for the analyte with a relatively small background emission.

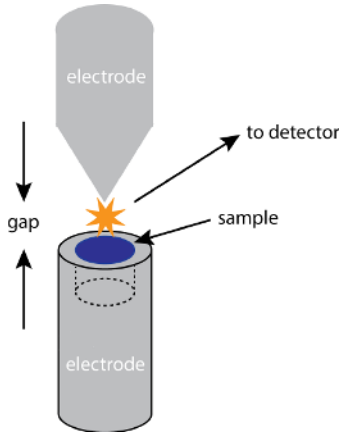



Figure 10.2.1: Example of an arc source in which the electrodes are fashioned from graphite. The lower electrode is fashioned to contain a cup-like depression in which a sample can be placed. The orange starburst shows the location where the plasma forms and where emission takes place.

## Spark Source

Unlike an arc source, which generates a continuous emission of electromagnetic radiation, a spark source generates a series of short emissions, each lasting on the order of a few μs. The sample serves as one of the two electrodes, with the other electrode fashioned from tungsten (see Figure 10.2.2). The two electrodes are separated by a gap of 3–6 mm. A potential as small as 300–500 V and as large as 1020 KV. The frequency of the spark is in the range of 100–500 per second. The temperature within the plasma can be quite intense, which gives rise to both emission lines from the atoms, but also emission from ions formed in the plasma.

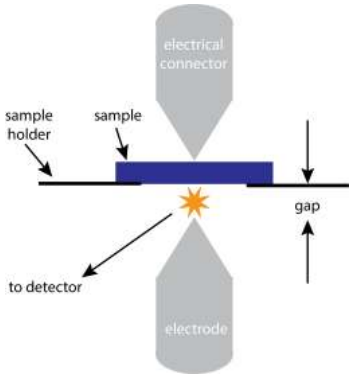



Figure 10.2.2: Example of spark source. The orange starburst shows the location where the plasma forms and where emission takes place.

## Instrumentation

For both the arc source and the spark source, emission from the plasma is collected and analyzed using the same types of optical benches discussed in the previous section on atomic emission from flames and plasma sources. Figure 10.2.3 shows an emission

spectrum for a sample of the alkaline earth metals, which shows a single intense emission line for Ca at 422.673nm and a single intense emission line for Sr at 460.7331 nm. Mg exhibits three closely spaced emission lines at 516.7322 nm, 517.2684 nm, and 518.3604 nm. Finally, Ba has a single strong emission line at 553.5481 nm, but also many less intense emission lines above 600 nm. The presence of faint, but measurable emission lines can create complications when trying to identify the elements present in a sample.

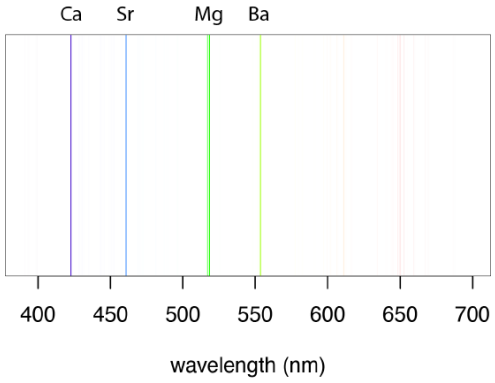



Figure 10.2.3: Simulated emission spectrum using an arc source. The sample shows strong emission lines for Ca, Sr, Mg, and Ba that can serve for qualitative identification of these elements. The faint lines above 600 nm—you may have difficulty seeing that they are there—are additional emission lines from Ba. What appears as a single line for Mg is actually three closely spaced emission lines at 516.7322 nm, 517.2684 nm, and 518.3604 nm.

---

This page titled 10.2: Emission Spectroscopy Based on Arc and Spark Sources is shared under a CC BY-NC-SA 4.0 license and was authored, remixed, and/or curated by David Harvey.

# CHAPTER OVERVIEW

## 11: Atomic Mass Spectrometry


11.1: General Features of Atomic Mass Spectrometry

11.2: Mass Spectrometers

11.3: Inductively Coupled Plasma Mass Spectrometer

11.4: Other Forms of Atomic Mass Spectrometry


---


This page titled 11: Atomic Mass Spectrometry is shared under a CC BY-NC-SA 4.0 license and was authored, remixed, and/or curated by David Harvey.

# 11.1: General Features of Atomic Mass Spectrometry

In mass spectrometry—whether of atoms, which is covered in this chapter, or of molecules, which is covered in Chapter 20—we convert the analyte into ions and then separate these ions based on the ratio of their masses to their charges. In this section we give careful attention to what we mean by mass, by charge, and by mass-to-charge ratio. We also give brief consideration to how we generate and measure ions, topics covered in greater detail in subsequent sections.

## Atomic Weights in Mass Spectrometry

We trace the modern era of chemistry to John Dalton's development of atomic theory, which made three hypotheses:

1. Elements, which are the smallest division of matter with distinct chemical properties, are composed of atoms. All atoms of a given element are identical—This is not strictly true, as we will see shortly, but we won't hold that against Dalton!—and different from the atoms of other elements. The element carbon is made of carbon atoms, which are different from the atoms of oxygen that make up elemental oxygen.
2. Compounds are composed of atoms from two or more elements. Because atoms cannot be subdivided, the elements that make up a compound are always present in ratios of whole numbers. A compound containing carbon and oxygen, for example, can have 1 carbon atom and 1 oxygen atom (CO) or 1 carbon atom and 2 oxygen atoms ($CO_2$), but it cannot have 1.5 carbon atoms.
3. In a chemical reaction, the elements that make up the reactants rearrange to make new compounds as products. The atoms that make up these compounds, however, are not destroyed, nor are new atoms created.

Dalton's first hypothesis simply recognized the atom as the basic building block of chemistry. Water, for example, is made from atoms of hydrogen and oxygen. The second hypothesis recognizes that for every compound there is a fixed combination of atoms. Regardless of its source (rain, tears, or a bottle of Evian) a molecule of water always consists of two hydrogen atoms for every atom of oxygen. Dalton's third hypothesis is a statement that atoms are conserved in a reaction; this is more commonly known as the conservation of mass.

### The Structure of the Atom

Although Dalton believed that atoms were indivisible, we know now that they are made from three smaller subatomic particles: the electron, the proton, and the neutron. The atom, however, remains the smallest division of matter with distinct chemical properties.

**Electrons, Protons, and Neutrons**. The characteristic properties of electrons, protons, and neutrons, are shown in Table 11.1.1.

Table 11.1.1. Mass and Charge of Subatomic Particles

| particle | mass (g) | unit charge | charge (in Coulombs, C) |
|---|---|---|---|
| electron | $9.10939 \times 10^{-28}$ | $-1$ | $-1.6022 \times 10^{-19}$ |
| proton | $1.67262 \times 10^{-24}$ | $+1$ | $+1.6022 \times 10^{-19}$ |
| neutron | $1.67493 \times 10^{-24}$ | 0 | 0 |

The proton and the neutron make up the atom's nucleus, which is located at the center of the atom and has a radius of approximately $5 \times 10^{-3}$ pm. The remainder of the atom, which has radius of approximately 100 pm, is mostly empty space in which the electrons are free to move. Of the three subatomic particles, only the electron and the proton carry a charge, which we can express as a relative unit charge, such as $+1$ or $-2$, or as an absolute charge in Coulombs. Because elements have no net charge (that is, they are neutral), the number of electrons and protons in an element must be the same.

**Atomic Numbers**. Why is an atom of carbon different from an atom of hydrogen or helium? One possible explanation is that carbon and hydrogen and helium have different numbers of electrons, protons, or neutrons; Table 11.1.2 provides the relevant numbers.

Table 11.1.2. Comparison of the Elements Hydrogen, Helium, and Carbon

| element | number of protons | number of neutrons [1] | number of electrons |
|---|---|---|---|
| hydrogen | 1 | 0, 1, or 2 | 2 |
| helium | 2 | 2 | 2 |
| carbon | 6 | 6, 7, or 8 | 6 |

[1] Only the number of neutrons for the most important naturally occurring forms of these elements are shown here.

Note that although Table 11.1.2 shows that a helium atom has two neutrons, an atom of hydrogen or carbon has three possibilities for the numbers of neutrons. It is even possible for a hydrogen atom to exist without a neutron. Clearly the number of neutrons is not crucial to determining if an atom is carbon, hydrogen, or helium. Although hydrogen, helium, and carbon have different numbers of electrons, the number is not critical to an element's identity. For example, it is possible to strip an electron away from helium to form a helium ion with a charge of $+1$ that has the same number of electrons as hydrogen; nevertheless, it is still helium.

What makes an atom carbon is the presence of six protons, whereas every atom of hydrogen has one proton and every atom of helium has two protons. The number of protons in an atom is called its atomic number, which we represent as *Z*.

**Atomic Mass and Isotopes**. Protons and neutrons are of similar mass and much heavier than electrons (see Table 11.1.1); thus, most of an atom's mass is in its nucleus. Because not all of an element's atoms necessarily have the same number of neutrons, it is possible for two atoms of an element to differ in mass. For this reason, the sum of an atom's protons and neutrons is known as its mass number (*A*). Carbon, for example, can have a mass number of 12, 13, or 14 (six protons and six, seven, or eight neutrons), and hydrogen can have a mass number of 1, 2, or 3 (one proton and zero, one, or two neutrons).

Atoms of the same element (same *Z*), but with a different number of neutrons (different *A*) are called isotopes. Hydrogen, for example has three isotopes (see Table 11.1.2). The isotope with 0 neutrons is the most abundant, accounting for 99.985% of all stable hydrogen atoms, and is known, somewhat self-referentially, as hydrogen. Deuterium, which accounts for 0.015% of all stable hydrogen atoms, has 1 neutron. The isotope of hydrogen with two neutrons is called tritium. Because tritium is radioactive it is unstable and disappears with time.

The usual way to represent isotopes is with the symbol ${}^{A}_{Z}X$ where *X* is the atomic symbol for the element. The three isotopes of hydrogen, which has an elemental symbol of H, are ${}^{1}_{1}\mathrm{H}$, ${}^{2}_{1}\mathrm{H}$, and ${}^{3}_{1}\mathrm{H}$. Because the elemental symbol (*X*) and the atomic number (*Z*) provide redundant information, we often omit the atomic number; thus, deuterium becomes ${}^{2}\mathrm{H}$. Unlike hydrogen, the isotopes of other elements do not have specific names. Instead they are named by taking the element's name and appending the atomic mass. For example, the isotopes of carbon are called carbon-12, carbon-13, and carbon-14.

### Atomic Mass

Individual atoms weigh very little, typically about $10^{-24}$ g to $10^{-22}$ g. This amount is so small that there is no easy way to measure the mass of a single atom. To assign masses to atoms it is necessary to assign a mass to one atom and to report the masses of all other atoms relative to that absolute standard. By agreement, atomic mass is stated in terms of atomic mass units (amu) or Daltons (Da), where 1 amu and 1 Da are defined as 1/12 of the mass of an atom of carbon-12. The atomic mass of carbon-12, therefore, is exactly 12 amu. The atomic mass of carbon-13 is 13.00335 amu because the mass of an atom of carbon-13 is $1.0836125\times$ greater than the mass of an atom of carbon-12.

**Note**

If you calculate the masses of carbon-12 and carbon-13 by adding together the masses of each isotope's electrons, neutrons, and protons from Table 11.1.1 you will obtain a mass ratio of 1.08336, not 1.0836125. The reason for this is that the masses in Table 11.1.1 are for "free" electrons, protons, and neutrons; that is, for electrons, protons, and neutrons that are not in an atom. When an atom forms, some of the mass is lost. "Where does it go?," you ask. Remember Einstein and $E = mc^2$? Mass can be converted to energy and the lost mass is the nuclear binding energy that holds the nucleus together.

**Average Atomic Mass**. Because carbon exists in several isotopes, the atomic mass of an "average" carbon atom is not exactly 12 amu. Instead it is usually reported on periodic tables as 12.01 or 12.011, values that are closer to 12.0 because 98.90% of all carbon

atoms are carbon-12. The IUPAC's Commission on Isotopic Abundances and Atomic Weights currently reports its mass as [12.0096, 12.0116] amu where the values in the brackets are the lower and the upper estimates for the average mass in a variety of naturally occurring materials. As shown in the following example, if you know the percent abundance and atomic masses of an element's isotopes, then you can calculate it's average atomic mass.

### Example 11.1.1

The element magnesium, Mg, has three stable isotopes with the following atomic masses and percent abundances:

| isotope | mass (amu) | percent abundance |
|---|---|---|
| $^{24}Mg$ | 23.9924 | 78.70 |
| $^{25}Mg$ | 24.9938 | 10.13 |
| $^{26}Mg$ | 25.9898 | 11.17 |

Calculate the average atomic mass for magnesium.

**Solution**

To find the average atomic mass we multiply each isotopes' atomic mass by its fractional abundance (the decimal equivalent of its percent abundance) and add together the results; thus

$$\text{avg. amu} = (0.7870)(23.994\ \text{amu}) + (0.1013)(24.9938\ \text{amu}) + (0.1117)(25.9898\ \text{amu})\ \text{avg. amu} = 24.32\ \text{amu}$$

As the next example shows, we also can work such problems in reverse, using an element's average atomic mass and the atomic masses of its isotopes to find each isotope's percent abundance.

### Example 11.1.2

The element gallium, Ga, has two naturally occurring isotopes. The isotope $^{69}Ga$ has an atomic mass of 68.926 amu and the isotope $^{71}Ga$ has an atomic mass of 70.926 amu. The average atomic mass for gallium is 69.723. Find the percent abundances for gallium's two isotopes.

**Solution**

If we let $x$ be the fractional abundance of $^{69}Ga$, then the fractional abundance of $^{71}Ga$ is $1 - x$ (that is, the total amounts of $^{69}Ga$ and $^{71}Ga$ must add up to one). Usingthe same general approach as Example 11.1.1, we find that

$$69.723\ \text{amu} = (x)(68.926\ \text{amu}) + (1 - x)(70.926\ \text{amu})$$

$$69.723\ \text{amu} = 68.926x\ \text{amu} + 70.926\ \text{amu} - 70.926x\ \text{amu}$$

$$2.000x\ \text{amu} = 1.203\ \text{amu}$$

$$x = 0.6015$$

$$1 - x = 1 - 0.6015 = 0.3985$$

Thus, 60.15% of naturally occurring gallium is $^{69}Ga$ and 39.85% is $^{71}Ga$.

### Note

Although many periodic tables report atomic masses to two decimal places—the periodic table I consult most frequently, for example gives the average atomic mass of carbon as 12.01 amu—the high resolving power of some mass spectrometers allows us to report masses to three or four decimal places.

## Mass-to-Charge Ratio

As we will learn later, a mass spectrometer separates ions on the basis of their mass-to-charge ratio ($m/z$), and not on their mass only or their charge only. As most ions that form during mass spectrometry are singly charged, spectra are often reported using masses ($m$) instead of mass-to-charge ratios; be sure to remain alert for this when looking at mass spectra.

---

This page titled 11.1: General Features of Atomic Mass Spectrometry is shared under a CC BY-NC-SA 4.0 license and was authored, remixed, and/or curated by David Harvey.

# 11.2: Mass Spectrometers

A mass spectrometer has three essential needs: a means for producing ions, in this case (mostly) singly charged atoms; a means for separating these ions in space or in time by their mass-to-charge ratios; and a means for counting the number of ions for each mass-to-charge ratio. Figure 11.2.1 provides a general view of a mass spectrometer in the same way that we first introduced optical instruments in Chapter 7. The ionization of the sample is analagous to the source of photons in optical spectroscopy as it generates the particles (ions, instead of photons) that ultimately make up the measured signal. The separation of the resulting ions by their mass-to-charge ratios, which is accomplished using a mass analyzer, is analagous to the role of a monochromator in optical spectroscopy. The means for counting ions serves the same role as, for example, a photomultiplier tube in optical spectroscopy. Note that the mass spectrometer is held under vacuum as this allows the ions to travel great distances without undergoing collisions that might alter their charge or energy.

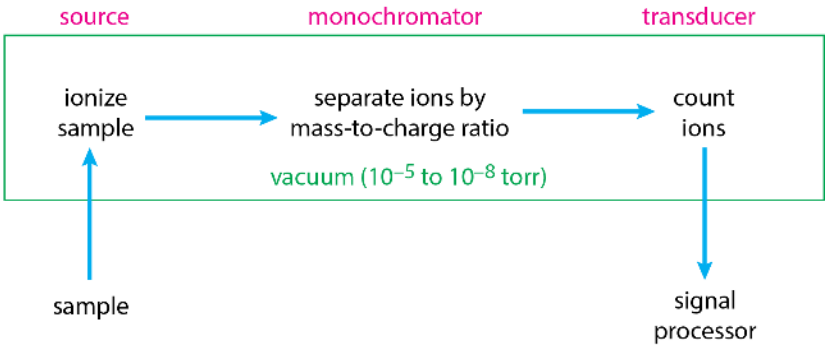



Figure 11.2.1: The basic components of a mass spectrometer. The blue arrows show the direction of sample-to-signal in which the sample is ionized, the ions separated by their mass-to-charge ratio, and ions with the same mass-to-charge ratio counted. The text in red at the top of the figure relates these components to their equivalent in optical spectroscopy.

## Sources of Ionization

The most common means for generating ions are plasmas of various sorts, lasers, electrical sparks, and other ions. We will give greater attention to these in the next several sections as we consider specific examples of atomic mass spectrometry.

## Transducers for Counting Ions

The transducer for mass spectrometry must be able to report the number of ions that emerge from the mass analyzer. Here we consider two common types of transducers.

### Electron Multipliers

In Chapter 7 we introduced the photomultiplier tube as a way to convert photons into electrons, amplifying the signal so that a single photon produces $10^6$ to $10^7$ electrons, which generates a measurable current. An electron multiplier serves the same role in mass spectrometry. Figure 11.2.2 shows two versions of this transducer. The electron multiplier in Figure 11.2.2*a* uses a set of individual dynodes. When an ion strikes the first dynode, it generates several electrons, each of which is passed along to the next dynode before arriving at a collecting plate where the current is measured. The result is an amplification, or gain, in the signal of approximately $10^7\times$. The electron multiplier in Figure 11.2.2*b* uses a horn-shaped cylinder—typically made from glass coated with a thin layer of a semiconducting material—whose surface acts as a single, continuous dynode. When an ion strikes the continuous dynode it generates several electrons that are reflected toward the collector plate where the current is measured. The result is an amplification of $10^5$ to $10^8\times$.

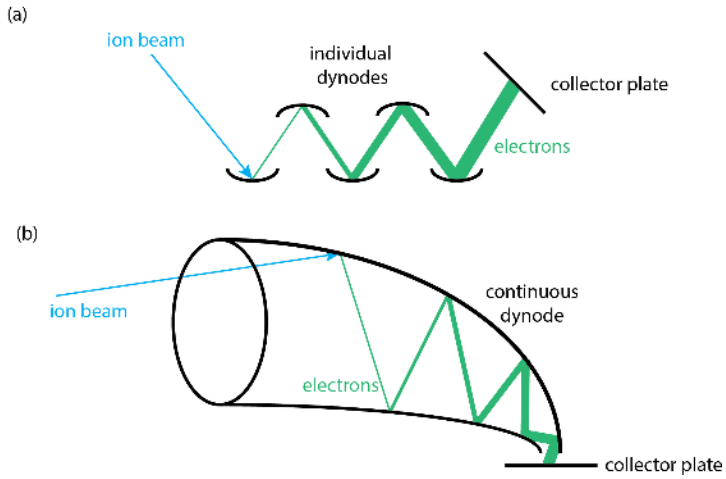



Figure 11.2.2: Electron multipliers using (a) individual, or discrete dynodes, and (b) a single, continuous dynode. The ion beam is represented by the blue arrows and the electrons are represented by the green lines. The increasing thickness of the green lines shows the amplification of the signal.

### Faraday Cup

A Faraday cup, as its name suggests, is a simple device shaped like a cup. Ions enter the cup where they strike a collector electrode. A current is directed to the collector plate that is sufficient to neutralize the charge of the ions. The magnitude of this current is proportional to the number of ions. A Faraday cup has the advantage of simplicity, but is less sensitive than an electron multiplier because it lacks the amplification provided by the dynodes.

## Separating Ions

Before we can detect the ions, we need to separate them so that we can generate a spectrum that shows the intensity of ions as a function of their mass-to-charge ratio. In this section we consider the three most common mass analyzers for atomic mass spectrometry.

### Quadrupole Mass Analyzers

The quadrupole mass analyzer is the most important of the mass analyzers included in this chapter: it is compact in size, low in cost, easy to use, and easy to maintain. As shown in Figure 11.2.3, a quadrapole mass analyzer consists of four cylindrical rods, two of which are connected to the positive terminal of a variable direct current (dc) power supply and two of which are connected to the power supply's negative terminal; the two positive rods are positioned opposite of each other and the two negative rods are positioned opposite of each other. Each pair of rods is also connected to a variable alternating current (ac) source operated such that the alternating currents are 180° out-of-phase with each other. An ion beam from the source is drawn into the channel between the quadrupoles and, depending on the applied dc and ac voltages, ions with only one mass-to-charge ratio successfully travel the length of the mass analyzer and reach the transducer; all other ions collide with one of the four rods and are destroyed.

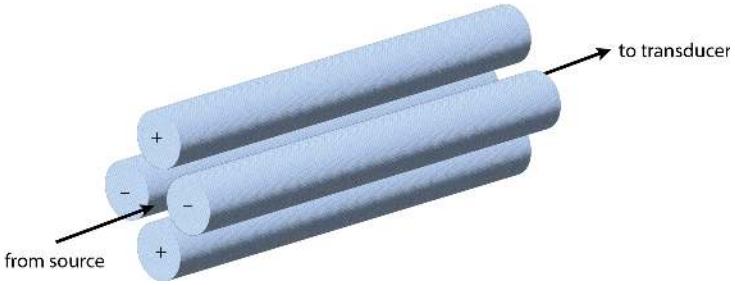



Figure 11.2.3: Basic arrangement of the quadrupole mass analyzer. The plus and the minus signs on each rod indicate which are connected to the positive terminal of the dc power supply. Not shown here is the circuitry for applying the alternating current. The ion beam enters the channel between the quadrupoles. Depending on the applied dc and ac voltages, some of the ions emerge from this channel and reach the transducer.

To understand how a quadrupole mass analyzer achieves this separation of ions, it helps to consider the movement of an ion relative to just two of the four rods, as shown in Figure 11.2.4 for the poles that carry a positive dc voltage. When the ion beam

enters the channel between the rods, the ac voltage causes the ion to begin to oscillate. If, as in the top diagram, the ion is able to maintain a stable oscillation, it will pass through the mass analyzer and reach the transducer. If, as in the middle diagram, the ion is unable to maintain a stable oscillation, then the ion eventually collides with one of the rods and is destroyed. When the rods have a positive dc voltage, as they do here, ions with larger mass-to-charge ratios will be slow to respond to the alternating ac voltage and will pass through the transducer. The result is shown in the figure at the bottom (and repeated in Figure 11.2.5$a$) where we see that ions with a sufficiently large mass-to-charge ratios successfully pass through the transducer; ions with smaller mass-to-charge ratios do not. In this case, the quadrupole mass analyzer acts as a high-pass filter.

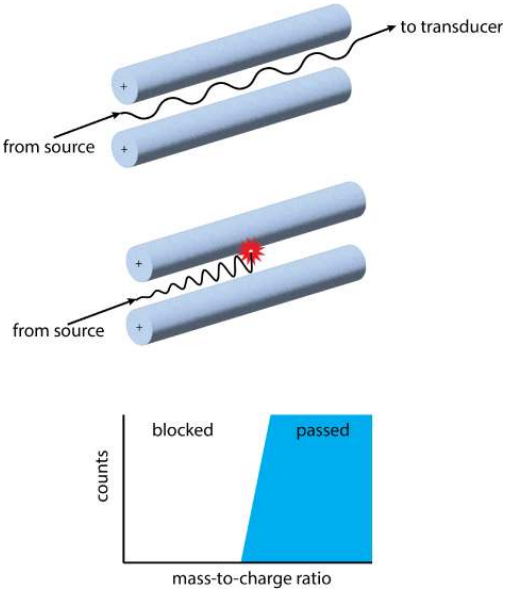



Figure 11.2.4: Illustration of how a quadrupole mass analyzer achieves separation of ions by their mass-to-charge ratio. See the text for additional details.

We can extend this to the behavior of the ions when they interact with rods that carry a negative dc voltage. In this case, the ions are attracted to the rods, but those ions that have a sufficiently small mass-to-charge ratio are able to respond to the alternating current's voltage and remain in the channel between the rods. The ions with larger mass-to-charge ratios move more sluggishly and eventually collide with one of the rods. As shown in Figure 11.2.5$b$, in this case, the quadrupole mass analyzer acts as a low-pass filter. Together, as we see in Figure 11.2.5$c$, a quadrupole mass analyzer operates as both a high-pass and a low-pass filter, allowing a narrow band of mass-to-charge ratios to pass through the transducer. By varying the applied dc voltage and the applied ac voltage, we can obtain a full mass spectrum.

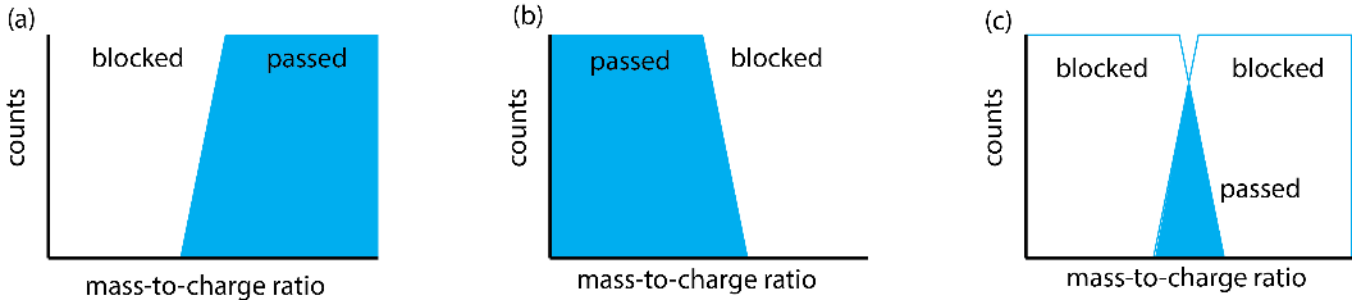



Figure 11.2.5: Illustration that shows how a quadrupole mass analyzer acts as both (a) a high-pass filter and (b) a low pass filter, with the result that it passes only ions with a narrow range of mass-to-charge ratios.

Quadrupole mass analyzers provide a modest mass-to-charge resolution of about 1 amu and extend to $m/z$ ratios of approximately 2000. Quadrupole mass analyzers are particularly useful for sources based on plasmas.

### Time-of-Flight (TOF) Mass Analyzers

In a time-of-flight mass analyzers, ions are created in small clusters by applying a periodic pulse of energy to the sample using a laser beam or a beam of energetic particles to ionize the sample. The small cluster of ions are then drawn into a tube by applying an

electric field and then allowed to drift through the tube in the absence of any additional applied field; the tube, for obvious reasons, is called a drift tube. All of the ions in the cluster enter the drift tube with the same kinetic energy, KE, which means, given

$$\text{KE} = \frac{1}{2}mv^2 \tag{11.2.1}$$

that the square of an ion's velocity is inversely proportional to the ion's mass. As a result, lighter ions move more quickly than heavier ions. Flight times are typically less than 30 μs. A time-of-flight mass analyzer provide better resolution than a quadrupole mass analyzer, but is limited to sources that can be pulsed.

### Double-Focusing Mass Analyzers

In a double-focusing mass analyzer, two mechanisms are used to focus a beam of ions onto the transducer. One of the mechanisms is an electrotatic analyzer that serves to confine the kinetic energy of the ions to a narrow range of energies. The second mechanism is a magnetic sector analyzer that uses an applied magnetic field to separate the ions by their mass-to-charge ratio. The combination of two analyzers allows for a significant resolution. More details on this type of mass analyzer is included in Chapter 20.

---

This page titled 11.2: Mass Spectrometers is shared under a CC BY-NC-SA 4.0 license and was authored, remixed, and/or curated by David Harvey.

# 11.3: Inductively Coupled Plasma Mass Spectrometer

In Chapter 10 we introduced the inductively coupled plasma (ICP) as a source for atomic emission. The plasma in ICP is formed by ionizing a flowing stream of argon gas, producing argon ions and electrons. The sample is introduced into the plasma where the high operating temperature of 6000–8000 K is sufficient to atomize and ionize the sample. In optical ICP we measure the emission of photons from the atoms and ions that are in excited states. In ICP-MS we use the plasma as a source of ions that we can send to a mass spectrometer for analysis.

## Instrumentation for ICP-MS

An ICP torch operates at room pressure and at an elevated temperature, and a mass spectrometer, as noted in Section 11.2, operates under a vacuum and at room temperature. This difference in pressure and temperature means that a coupling together of these two instrument requires an interface than can bring the pressure and temprature in line with the demands of the mass spectrometer. Figure 11.3.1 provides a schematic diagram of a typical ICP-MS instrument with the ICP torch on the right and the mass spectrometer's quadrupole mass analyzer and a continuous electron multiplier on the left. In between the two is a two-stage interface. Note that none of the components in Figure 11.3.1 are drawn to scale.

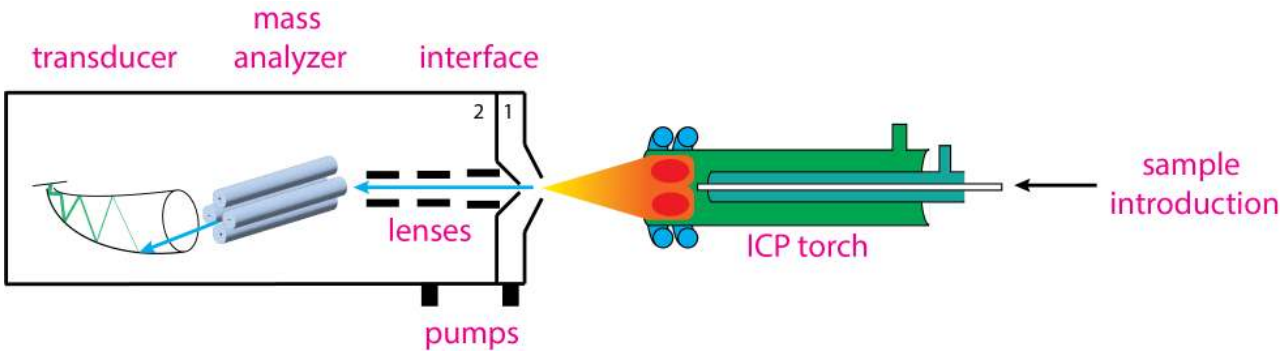



Figure 11.3.1. Schematic diagram of an instrument for an inductively coupled plasma mass spectrometer (ICP-MS), showing the torch and the sample nebulizer that make up the ICP on the right, and the mass analyzer and the transducer that make up the MS on the left. Also shown is the interface between the two. The first stage of the interface (1) samples the plasma from the ICP torch and then further reduces the number of particles that are passed along to the second stage (2) a set of ion lenses are used to remove electrons, neutral species, and photons and to focus the ion beam onto the quadrupole.

The first stage of the interface consists of two cone-shaped openings: a sampler cone and a skimmer cone. The hot plasma from the ICP torch enters the first stage of the interface through the sampler cone, which is a pin-hole with a diameter of approximately 1 mm. Samples in solution form are drawn directly into the ICP torch using a nebulizer. Solid samples are vaporized using a laser (a process called laser ablation) and the vapor drawn directly into the ICP torch.

A pump is used to drop the pressure in the first stage to approximately 1 torr. The expansion of the plasma as it enters the first stage results in some cooling of the plasma. The skimmer cone allows a small portion of the plasma in the first stage to pass into the second stage, which is held at the mass spectrometer's operating pressure of approximately $10^{-5}$ torr. A series of ion lenses are used to narrow the conical dispersion of the plasma, to isolate positive ions from electrons, neutral species, and photons—all of which will generate a signal if they reach the transducer—and to focus the ion beam onto the quadrupole's entrance.

## Atomic Mass Spectra and Interferences

Figure 11.3.2 shows an example of an ICP-MS spectrum for the analysis of a metal coating using laser ablation to volatilize the sample. The quadrupole mass analyzer operates over a mass-to-charge range of approximately 3 to 300 and can resolve lines that differ by $\pm 1$ m/z. Data are collected either by scanning the quadrupole to provide a survey spectrum of all ions generated in the plasma, as is the case in Figure 11.3.2, or by peak hopping in which we gather data for just a few discrete mass-to-charge ratios,

adjusting the quadrupole so that it passes only a single mass-to-charge ratio and count the ions for a set period of time before moving to the next mass-to-charge ratio.

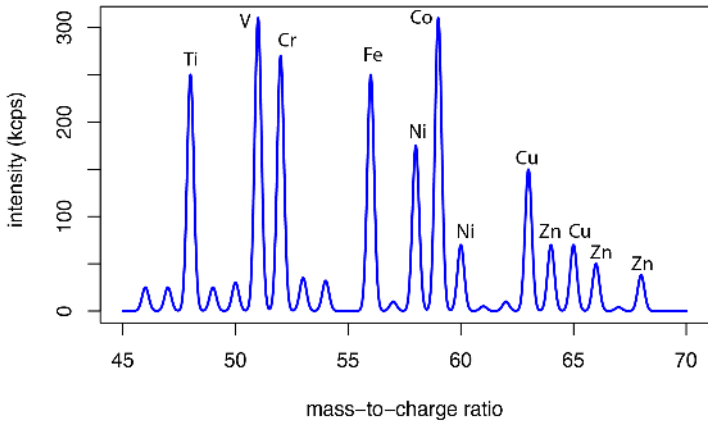



Figure 11.3.2. Example of an ICP-MS spectrum of a metal coating using laser ablation to vaporize the sample before drawing it into the ICP torch. The intensity of ions is reported in kilocounts per seconds. The major peaks are identified by element. The data used to construct this figure were extrapolated from the source linked to here.

## Spectroscopic Interferences

An ICP-MS spectrum is much simpler than the corresponding ICP atomic emission spectrum because each element in the latter has many emission lines and because the plasma itself has many emission lines. Still, an ICP-MS is not free from interferences, the two most important of which are isobaric ions and polyatomic ions.

**Isobaric Ions**. Iso- means same and -baric means weight; thus, isobaric means same weight and refers to two (or more) species that have—within the resolution of the mass spectrometer—identical weights and that both contribute to the same peak in the mass spectrum. The source of this interference is the existence of isotopes. For example, the most abundant ions for argon and for calcium are $^{40}$Ar and $^{40}$Ca, and, given the resolving power of a quadrupole mass analyzer, the two ions appear as a single peak at $m/z = 40$ even though the mass of $^{40}$Ar is 39.962383 amu and the mass of $^{40}$Ca is 39.962591 amu. We can correct for this interference because the second most abundant isotope of calcium, $^{44}$Ca, does not share a $m/z$ with argon (or with another element). Figure 11.3.3 shows the ICP-MS spectrum for a sample that contains calcium and argon, and Example 11.3.1 shows how we can use this spectrum to determine the contribution of each element.

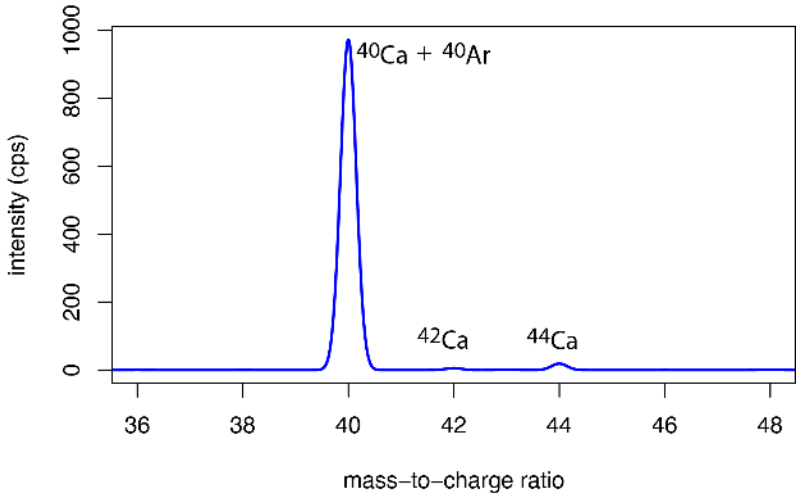



Figure 11.3.3: ICP-MS spectrum for a mixture of calcium and argon. The peak at $m/z = 40$ includes contributions from both $^{40}$Ca and $^{40}$Ar. The other two peaks are for $^{42}$Ca and for $^{44}$Ca and do not include contributions from argon. The peaks for $^{36}$Ar, $^{38}$Ar, $^{43}$Ca, $^{46}$Ca, and $^{48}$Ca are too small to appear as peaks in this spectrum.

**Example 11.3.1**

For the spectrum in Figure 11.3.3, the intensity at $m/z = 40$ is 972.07 cps and the intensity at $m/z = 44$ is 18.77 cps. Given that the istopic abundance of $^{40}$Ca is 96.941% and the isotopic abundance of $^{44}$Ca is 2.086%, what is the counts-per-second at $m/z = 40$ for Ca and for Ar.

**Solution**

Given that only $^{44}$Ca contributes to the peak at $m/z = 44$ we can use the relative abundances of $^{40}$Ca and $^{44}$Ca to determine the expected contribution of $^{40}$Ca to the total intensity at $m/z = 40$.

$$18.77 \text{ cps} \times \frac{96.941}{2.086} = 872.28 \text{ cps}$$

Subtracting this result from the total intensity gives the intensity at $m/z = 40$ for argon as

$$972.07 \text{ cps} - 872.28 \text{ cps} = 99.79 \text{ cps}$$

**Polyatomic Ions**. Compensating for isobaric ions is relatively straightforward because we can rely on the known isotopic abundances of the elements. A more difficult problem is an interference between the isotope of an elemental analyte and a polyatomic ion that has the same mass. Such polyatomic ions may arise from the sample's matrix or from the plasma. For example, the ion $^{40}Ar^{16}O^+$ has a mass-to-charge ratio of 56, which overlaps with peak for $^{56}$Fe, the most abundant isotope of iron. Although we could choose to monitor iron at a different mass-to-charge ratio, we will lose sensitivity as we are using a less abundant isotope. Corrections can be made using the method outlined in Example 11.3.1, although it may require using multiple peaks, which increases the uncertainty of the final result.

### Matrix Effects

A matrix effect occurs when the sample's matrix affects the relationship between the signal and the concentration of the analyte. Matrix effects are common in ICP-MS and may lead to either a suppression or an enhancement in the signal. Although not always well understood, matrix effects likely result from how easily an ionizable element affects the ability to ionize other elements. Matrix matching, using the method of standard additions, or using an internal standard can help minimize matrix effects for quantitative work.

## Applications of ICP-MS

ICP-MS finds application for analytes in a wide variety of matrices, including both solutions and solids. Solution samples with high concentrations of dissolved ions may present problems due to the deposition of the salts onto the sampler and skimmer cones, which reduces the size of the pinhole that provides entry into the interface between the ICP torch and the mass spectrometer. The use of laser ablation makes it possible to analyzer surfaces—such as glasses, metals, and ceramics—without additional sample preparation.

**Qualitative and Semiquantitative Applications**. One of the strengths of ICP-MS is its ability to provide a survey scan, such as that in Figure 11.3.1, that allows for the identification of the elements present in a sample. Analysis of a single sample that contains known concentrations of these elements is suitable for providing a rough estimate of their concentration in the sample.

**Quantitative Analysis**. For a more accurate and precise quantitative analysis, one can prepare multiple external standards and prepare a calibration curve. Linearly across approximately six orders of magnitude with detection limits of less than 1 ppb. Including an internal standard in the external standards can help reduce matrix effects. The ideal internal standard will not produce isobaric ions and its primary ionization potential should be similar to that for the analyte; when working with several analytes, it may be necessary to choose a different internal standard for each analyte.

**Isotope Ratios**. An important advantage of ICP-MS over other analytical methods is its ability to monitor multiple isotopes for a single element.

This page titled 11.3: Inductively Coupled Plasma Mass Spectrometer is shared under a CC BY-NC-SA 4.0 license and was authored, remixed, and/or curated by David Harvey.

# 11.4: Other Forms of Atomic Mass Spectrometry

Although ICP-MS is the most widely used method of atomic mass spectrometry, there are other forms of atomic mass spectrometry, three of which we highlight here.

## Spark Source Mass Spectrometry (SSMS)

In SSMS, a solid sample is vaporized using a spark source, as described in Chapter 10.2 for atomic emission. Because the spark is generated in an evacuated housing the interface between the spark source and the mass spectrometer is simpler. Because the spark generates ions with a large distribution of kinetic energies a quadrupole mass analyzer is not practicable; instead, the mass spectrum is recorded using a double-focusing mass analyzer (see Chapter 20 for more details about this type of mass spectrometer). One advantage of the double-focusing mass analyzer is that it is capable or resolving small differences in masses. For example, in ICP-MS the peaks for $^{56}Fe^{+}$ and the polyatomic ion $^{40}Ar^{16}O^{+}$ overlap, appearing as a single peak. A double-focusing mass analyzer can separate these two ions, which have, respectively, masses of 55.934942 amu and 55.957298 amu.

## Glow Discharge Mass Spectrometry (GDMS)

A glow discharge source generates ions in manner similar to that used to generate the emission of photons in a hollow cathode lamp (see Chapter 9.2 for a discussion of the hollow cathode lamp). The sample serves as the cathode in a cell that contains a very low pressure of argon gas. The application of a high voltage pulse between the cathode and an anode that also is in the cell, converts some of the Ar to $Ar^{+}$ ion, which then collide with the cathode, sputtering some of the solid sample into a mixture of gas-phase atoms and ions, the later of which are drawn into the mass spectrometer for analysis.

## Elemental Surface Analysis by Mass Spectrometry

When analyzing a solid sample, we often are interested in how its composition varies either across the surface or as a function of depth. We can gather information across a surface if we can focus the ion source to a small spot and then raster that spot across the surface, and we can gather information as a function of depth if we can use sputter away a portion of the surface. See Chapter 21 for a discussion of two such techniques: secondary ion mass spectometry (SIMS) and laser microprove mass spectrometry.

This page titled 11.4: Other Forms of Atomic Mass Spectrometry is shared under a CC BY-NC-SA 4.0 license and was authored, remixed, and/or curated by David Harvey.

# CHAPTER OVERVIEW

## 12: Atomic X-Ray Spectrometry


12.1: Fundamental Principles

12.2: Instrument Components

12.3: Atomic X-Ray Fluorescence Methods

12.4: Other X-Ray Methods


---

This page titled 12: Atomic X-Ray Spectrometry is shared under a CC BY-NC-SA 4.0 license and was authored, remixed, and/or curated by David Harvey.

# 12.1: Fundamental Principles

In Chapter 6 we introduced the electromagnetic spectrum and the characteristic properties of photons, such as the wavelengths, the frequencies, and the energies of ultraviolet, visible, and infrared light. The wavelength range for photons of X-ray radiation extends from approximately 0.01 nm to 10 nm. Although we are used to reporting a photon's wavelength in nanometers, for historical reasons the wavelength of an X-ray photon usually is reported in angstroms (for which the symbol is Å) where 1 Å = 0.1 nm; thus the wavelength range of 0.01 nm to 10 nm for X-ray radiation also is expressed as 0.1 Å to 100 Å. This range of wavelengths corresponds to a range of frequencies from approximately $3 \times 10^{19}$ $s^{-1}$ to $3 \times 10^{16}$ $s^{-1}$, and a range of energies from $2 \times 10^{-19}$ J to $2 \times 10^{-17}$ J.

## Sources of X-Rays

There are three routine ways to generate X-rays, each of which is covered in this section: we can bombard a suitable metal with a beam of high-energy electrons, we can use one X-ray to stimulate the emission of additional X-rays through fluorescence, and we can use a radioactive isotope that emits X-rays as it decays.

### Obtaining X-Rays From Electron Beam Sources

An electron beam is created by heating a tungsten wire filament to a temperature at which it releases electrons. These electrons are pulled toward a metal target by applying an accelerating voltage between the metal target and the tungsten wire. The result is the broad continuum of X-ray emission in Figure 12.1.1. The source of this continuous emission spectrum is the reduction in the kinetic energy of the electrons as they collide with the metal target. The loss of kinetic energy results in the production of photons over a broad range of wavelengths and is known as Bremsstrahlung, or braking radiation.

**Note**

In earlier chapters we divided the sources of photons into two broad groups: continuous sources, such as a tungsten lamp, that produce photons at all wavelengths between a lower limit and an upper limit, and line sources, such as a hollow cathode lamp, that produce photons for one or more discrete wavelengths. The sources used to generate X-rays also generate continuum and/or line spectra.

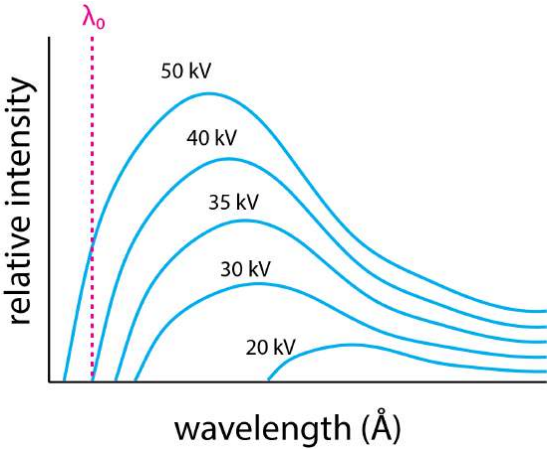



Figure 12.1.1: X-ray emission from a metal target using an electron beam. The voltage listed above each curve is the accelerating voltage used to create the electron beam. Each accelerating voltage has a minimum wavelength, $\lambda_0$, below which emission does not occur. The dashed line shows $\lambda_0$ for an accelerating voltage of 40 kV.

The lower wavelength limit for X-ray emission, identified here as $\lambda_0$, is the maximum possible loss of kinetic energy, *KE*, and is equal to

$$KE = \frac{hc}{\lambda_0} = Ve \tag{12.1.1}$$

where $h$ is Planck's constant, $c$ is the speed of light, $V$ is the accelerating voltage, and $e$ is the charge on the electron. The product of the accelerating voltage and the charge on the electron is the kinetic energy of the electrons. Solving Equation 12.1.1 for $\lambda_0$ gives

$$\lambda_0 = \frac{hc}{Ve} = \frac{12.398 \text{ kV Å}}{V} \tag{12.1.2}$$

where $\lambda_0$ is in angstroms and $V$ is in kilovolts. Note that Equation 12.1.1 and Equation 12.1.2 do not include any terms that depend on the target metal, which means that for any accelerating voltage, $\lambda_0$ is the same for all metal targets. Table 12.1.1 gives values of $\lambda_0$ that span the range of accelerating voltages in Figure 12.1.1.

Table 12.1.1. Shortest wavelength of continuous X-ray emission when using an electron beam as a function of its accelerating voltage.

| accelerating voltage (kV) | $\lambda_0$ (Å) |
|---|---|
| 20 | 0.62 |
| 25 | 0.50 |
| 30 | 0.41 |
| 35 | 0.35 |
| 40 | 0.31 |
| 45 | 0.28 |
| 50 | 0.25 |

If we apply a sufficiently large accelerating voltage, then the emission spectrum will consist of both a continuum spectrum and a line spectrum, as we see in Figure 12.1.2 with molybdenum as the target metal. The spectrum consists of both a continuum similar to that in Figure 12.1.1, and two lines, one at a wavelength of 0.63 Å and one at a wavelength of 0.71 Å. The source of these lines is the emission of X-rays from excited state ions that form when a sufficiently high-energy electron from the electron beam removes an electron from an atomic orbital close to the nucleus. As electrons in atomic orbitals at a greater distance from the nucleus drop into the atomic orbital with a vacancy, they release their extra energy as a photon.

Although the background emission from the continuum is the same for all metal targets, the energy for the lines have values that are characteristic for different metals because the energy to remove an electron varies from element-to-element, increasing with atomic number. For example, an accelerating voltage of at least

$$V = \frac{12.398 \text{ kV Å}}{0.61 Å} = 20 \text{ kV}$$

is needed to generate the line spectrum for molybdenum in Figure 12.1.2.

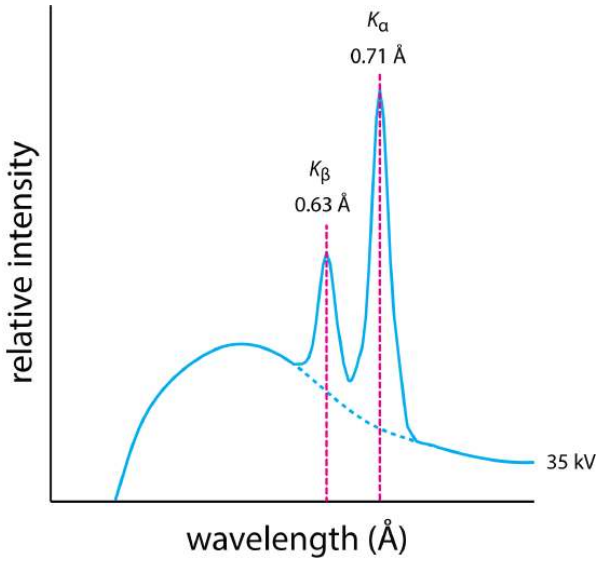



Figure 12.1.2: The X-ray emission spectrum for molybdenum using an electron beam with an accelerating voltage of 35 kV. The spectrum consists of both a continuum similar to that in Figure 12.1.1 and two lines, one at a wavelength of 0.63 Å and one at a wavelength of 0.71 Å.

The characteristic emission lines for molybdenum in Figure 12.1.2 are identified as $K_\alpha$ and $K_\beta$, a notation with which you may not be familiar. The simplified energy level diagram in Figure 12.1.3 will help us understand this notation. Each arrow in this energy-level diagram shows a transition in which an electron moves from an orbital at greater distance from the nucleus to an orbital closer to the nucleus. The letters K, L, and M correspond to the principal quantum number *n*, which has values of 1, 2, 3... that indicate the initial vacancy created by the collision of the ion beam with the target metal. The Greek symbols $\alpha$, $\beta$, and $\gamma$ indicate the source of the electron that fills this vacancy in terms of its change in the principal quantum number, $\Delta n$. An electron moving from $n = 2$ to $n = 1$ and an electron moving from $n = 4$ to $n = 3$ have the same designation of $\alpha$. The emission line in Figure 12.1.2 identified as $K_\beta$, therefore, is the result of an electron in the $n = 3$ shell moving into a vacancy in the $n = 1$ shell $K$.

Figure 12.1.3: Simplified energy-level diagram showing the nomenclature for identifying characteristic X-ray lines.

**Note**

Why is Figure 12.1.3 a simplified energy-level diagram? For each $n > 1$ there is more than one atomic orbital. When $n = 2$ there are three energy levels: one that corresponds to $l = 0$, one that corresponds to $l = 1$ and $m_l = 0$, and one that corresponds to $l = 1$ and $m_l = \pm 1$. The allowed transitions to the $n = 1$ energy levels requires a change in the value for $l$; thus, we expect to find two emission lines from $n = 2$ to $n = 1$ instead of the one shown in Figure 12.1.3. These two lines, which we can identify as $K_{\alpha 1}$ and

$K_{\alpha 2}$, generally are sufficiently close in value that they are not resolved in the X-ray emission spectrum. For example, $K_{\alpha 1} = 0.709$ and $K_{\alpha 2} = 0.714$ for molybdenum. You can find a table of X-ray emission lines here.

### Obtaining X-Rays From Fluorescent Sources

When an atom in an excited state emits a photon as a means of returning to a lower energy state, how we describe the process depends on the source of energy that created the excited state. When excitation is the result of thermal energy, we call the process atomic emission. When excitation is the result of the absorption of a photon, we call the process atomic fluorescence. In X-ray fluorescence, excitation is brought about using photons from a source of continuous X-ray radiation. More details on X-ray fluorescence are provided later in this chapter.

### Obtaining X-Rays From Radioactive Sources

Atoms that have the same number of protons but a different number of neutrons are isotopes. To identify an isotope we use the notation ${}^{A}_{Z}E$, where $E$ is the element's atomic symbol, $Z$ is the element's atomic number, and $A$ is the element's atomic mass number. Although an element's different isotopes have the same chemical properties, their nuclear properties are not identical. The most important difference between isotopes is their stability. The nuclear configuration of a stable isotope remains constant with time. Unstable isotopes, however, disintegrate spontaneously, emitting radioactive decay particles as they transform into a more stable form.

An element's atomic number, $Z$, is equal to the number of protons and its atomic mass, $A$, is equal to the sum of the number of protons and neutrons. We represent an isotope of carbon-13 as ${}^{13}_{6}C$ because carbon has six protons and seven neutrons. Sometimes we omit $Z$ from this notation—identifying the element and the atomic number is repetitive because all isotopes of carbon have six protons and any atom that has six protons is an isotope of carbon. Thus, $^{13}$C and C–13 are alternative notations for this isotope of carbon.

Radioactive particles can decay in several ways, one of which results in the emission of X-rays. For example, $^{55}$Fe can capture an electron and undergo a process in which a proton becomes a neutron, becoming $^{55}$Mn and releasing the excess energy as a $K_{\alpha}$ X-ray. We will not give further consideration to radioactive sources of atomic X-ray emission; see Chapter 32, however, for a further discussion of radioactive methods of analysis.

## X-Ray Absorption

Figure 12.1.4 shows a portion of molybdenum's X-ray absorption spectrum over the same range of wavelengths as shown in Figure 12.1.2 for its emission spectrum. Both spectra are relatively simple: the emission spectrum consists of two lines superimposed on a continuum background, and the absorbance spectrum consists of a single line, identified here as the K edge.

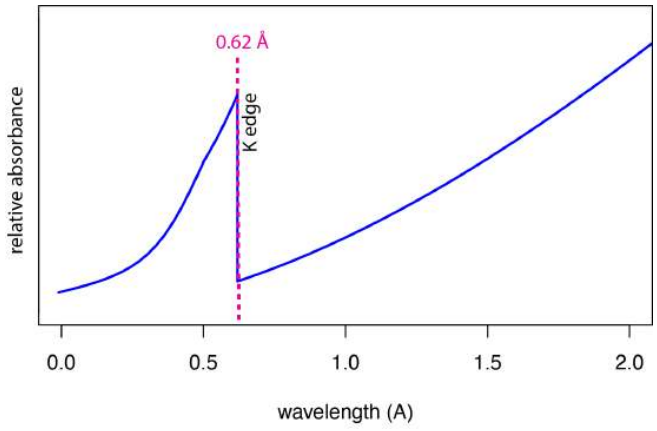



Figure 12.1.4: A portion of the X-ray absorption spectrum for molybdenum.

### The Absorption Process

If an X-ray photon is of sufficient energy, then its absorbance by an atom results in the ejection of an electron from one of the atom's innermost atomic orbitals, which you may recognize as the production of a photoelectron. For molybdenum, a wavelength of 0.62 Å (an energy of 20.0 kV) is needed to eject a photoelectron from the K shell ($n$ = 1). At this wavelength the probability of absorption is at is greatest. At shorter wavelengths (greater energies) there is sufficient energy to eject the electron, however, the probability of absorption decreases and the relative absorbance decreases slowly. The abrupt decrease in absorbance for wavelengths larger than 0.62 Å—this abrupt decrease is the source of the term edge—happens because the photons no longer have sufficient energy to eject an electron from the K shell. The slow increasing absorbance at wavelengths greater than the K edge is the result of ejecting electrons from the L shell, which has edges at 4.3 Å, 4.7 Å, and 4.9 Å.

**Note**

The simplified energy level diagram in 12.1.3 shows only one energy level for $n$ = 2 (the L shell). As we noted earlier, there are three energy levels when $n$ = 2: one that corresponds to $l$ = 0, one that corresponds to $l$ = 1 and $m_l$ = 0, and one that corresponds to $l$ = 1 and $m_l$ = ±1. The three edges corresponding to these energy levels are identified as $L_I$, $L_{II}$, and $L_{III}$.

### Beer's Law and X-Ray Absorption

When a source of X-rays passes through a sample with a thickness of $x$, the following equation holds

$$A = -\ln \frac{P}{P_0} = \mu_M \rho x \tag{12.1.3}$$

where A is the absorbance, $P_0$ is the power of the X-ray source incident on the sample, $P$ is the power of the X-ray source after it passes through the sample, $\mu_M$ is the sample's mass absorption coefficient and $\rho$ is the sample's density. You may have noticed the similarity between this equation and the equation for Beer's law that we first encountered in Chapter 6

$$A = -\ln \frac{P}{P_0} = \epsilon b C \tag{12.1.4}$$

where $\epsilon$ is the molar absorptivity, $b$ is the pathlength, and $C$ is molar concentration. Note that both density (g/mL) and molarity (mol/L) are a measure of concentration that expresses the amount of the absorbing material present in the sample.

## X-Ray Fluorescence

When an electron is ejected from a shell near the nucleus by the absorption of an X-ray, the vacancy created is eventually filled when an electron at a greater distance from the nucleus moves down. Because it takes more energy to eject an electron and create a vacancy than is returned by the movement of other electrons into the vacancy, the resulting fluorescent emission of X-rays is always at wavelengths that are longer (lower energy) than the wavelength that was absorbed. We see this in Figure 12.1.4 and Figure 12.1.1 for molybdenum where it absorbs an X-ray with a wavelength of 0.62 Å and emits X-rays with wavelengths of 0.63 Å and 0.71 Å.

## X-Ray Diffraction

When an X-ray beam is focused onto a sample that has a regular (crystalline) pattern of atoms in three dimensions, some of the radiation scatters from the surface and some of the radiation passes through to the next layer of atoms where the combination of scattering and passing through continues. As a result of this process, the radiation undergoes diffraction in which X-rays of some wavelengths appear to reflect off the surface while X-rays of other wavelengths do not. The conditions the result in diffraction are easy to understand using the diagram in Figure 12.1.5.

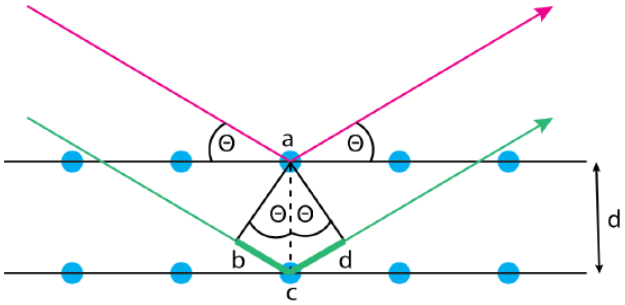



Figure 12.1.5: Illustration showing the diffraction of X-rays from an ordered crystalline sample. See the text for additional details.

The red and green arrows are two parallel beams of X-rays that are focused on an ordered crystalline solid that consists of a layered repeatable pattern of atoms shown by the blue circles. The two beams of X-rays encounter the solid at an angle of $\theta$. The X-ray shown in red scatters off of the first layer, exiting at the same angle of $\theta$. The X-ray shown in green penetrates to the second layer where it undergoes scattering, exiting at the same angle of $\theta$. We know from the superposition of waves (see Chapter 6) that the two beams of X-rays will remain in phase, and thus experience constructive interference, only if the additional distance traveled by the green wave—the sum of the line segments $\overline{bc}$ and $\overline{cd}$—is an integer multiple of the wavelength; thus

$$\overline{bc} + \overline{cd} = n\lambda \tag{12.1.5}$$

We also know that the length of the line segments $\overline{bc}$ and $\overline{cd}$ are given by

$$\overline{bc} = \overline{cd} = d \sin\theta \tag{12.1.6}$$

where $d$ is the distance between the crystal's layers. Combining Equation 12.1.5 and Equation 12.1.6 gives

$$n\lambda = 2d \sin\theta \tag{12.1.7}$$

Rearranging Equation 12.1.7 shows that we will observe diffraction only at angles that satisfy the equation

$$\sin\theta = \frac{n\lambda}{2d} \tag{12.1.8}$$

This page titled 12.1: Fundamental Principles is shared under a CC BY-NC-SA 4.0 license and was authored, remixed, and/or curated by David Harvey.

# 12.2: Instrument Components

Atomic X-ray spectrometry has the same needs as other forms of optical spectroscopy: a source of X-rays, a means for isolating a desired range of wavelengths of X-rays, a means for detecting the X-rays, and a means for converting the signal at the transducer into a meaningful number.

## X-Ray Sources

The most important source of X-rays is the X-ray tube, a basic diagram of which is shown in Figure 12.2.1. A beam of electrons (shown in red) from a heated tungsten filament (shown in orange) serves as a cathode with a negative potential. The electrons are drawn toward an anode that has a positive potential. The tip of the anode is made from a metal target (shown in blue) that will produce X-rays (shown in green) with the desired wavelengths when struck by the electron beam. Typical metal targets include tungsten, molybdenum, silver, copper, iron, and cobalt. The filament and the target metal are housed inside an evacuated tube. The emitted X-rays exit the tube through an optical window.

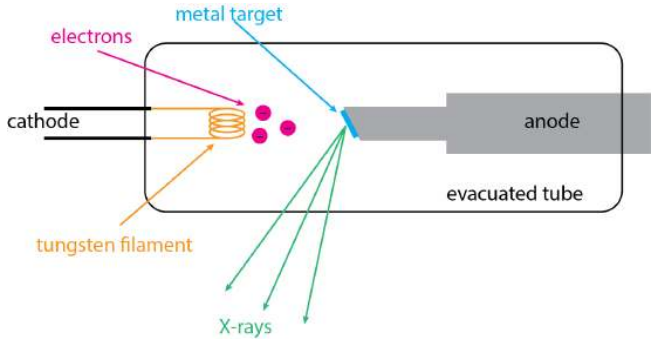



Figure 12.2.1: Schematic diagram showing the key parts of an X-ray tube. See text for details.

Any material that is naturally radioactive emits characteristic X-rays that potentially can serve as a source of X-rays that another species can absorb. For example, in the absorption spectrum for molybdenum (see Figure 18.1.4) the $K_\alpha$ line has a wavelength of 0.62 Å, which corresponds to an energy of 20.0 kV. A radioactive source with an emission line that has a wavelength slightly longer than 0.62 Å (between, for example, 0.5 Å and 0.6 Å) is sufficient. One possibility is $^{109}$Cd, which emits X-rays with a wavelength of 0.56 Å, or an energy of 22 kV.

## X-Ray Filters and Monochromators

A filter and a monochromator are designed to take a broad range of emission from a source and narrow the range of wavelengths that reach the sample. Figure 12.2.2 shows how to accomplish this using an absorption filter. The blue line shows the emission spectrum for a sample that includes two lines—the $K_\alpha$ line and the $K_\beta$ line—superimposed on a broad continuum. The green line shows the absorption spectrum for a different element whose K edge falls in between the sample's $K_\alpha$ and $K_\beta$ lines. In this case the K edge filter removes most of the continuum and the $K_\beta$ line, allowing just the $K_\alpha$ line and a small amount of the continuum to reach the sample.

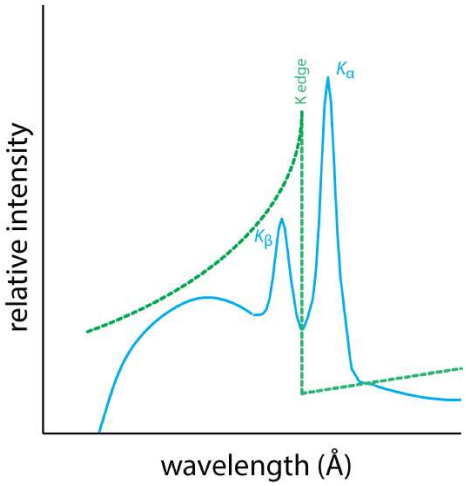



Figure 12.2.2: Illustration of how an X-ray filter works by comparing the absorbance spectrum for the filter (in green) to the emission spectrum of the source (in blue). See the text for additional details.

Figure 12.2.3 shows the basic design for an X-ray monochromator, which can operate in either an absorption mode, in which X-rays from the source pass through the sample before entering the monochromator, or in an emission mode, in which X-rays from the source excite the sample and fluorescent emission is sampled at 90°.

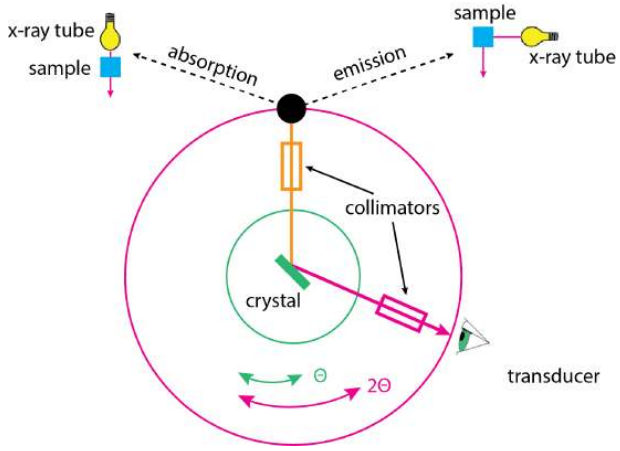



Figure 12.2.3: Illustration of an X-ray monochromator. The black circle shows the location of the sample and the X-ray source, which can take one of two configurations and experiments: absorption mode or emission mode. See text for additional details.

In either mode, the X-rays pass through a collimator that focuses them onto a crystal where the X-rays undergo diffraction. X-rays are collected by a second collimator before arriving at the transducer. To scan the source, the crystal rotates through an angle of $\theta$; the transducer must rotate twice as fast, traversing an angle of $2\theta$ to maintain an identical angle between the source and the transducer.

An X-ray monochromator's effective range is determined by the properties of the crystal used for diffraction. We know from Chapter 12.1 that

$$n\lambda = 2d\sin\theta \tag{12.2.1}$$

where $n$ is the diffraction order, $\lambda$ is the wavelength, $\theta$ is the X-ray's angle of incidence, and $d$ is the spacing between the crystal's layers. The practical limit for the angle depends on the monochromator's design, but typically $\theta$ is 7.5° to 75° (or $2\theta$ angles of 15° to 150°). A common crystal is LiF, which has a spacing of 2.01 Å; thus, it provides a wavelength range from a lower limit of

$$\lambda = 2d\sin\theta = 2 \times 2.01 \text{ Å} \times \sin(7.5^\circ) = 0.52 \text{ Å}$$

to an upper limit of

$$\lambda = 2d\sin\theta = 2 \times 2.01 \text{ Å} \times \sin(75^\circ) = 3.9 \text{ Å}$$

when $n = 1$. This range of wavelengths is sufficient to study the elements K to Cd using their $K_\alpha$ lines.

## X-Ray Transducers

The most common transducers for atomic X-ray spectrometry are the flow proportional counter, the scintillation counter, and the Si(Li) semiconductor. All three transducers act as photon counters.

### Photon Counting

The most common transducer for measuring atomic absorbance and atomic emission of ultraviolet and visible light is a photomultiplier tube. As we learned in Chapter 7, a photon strikes a photosensitive surface and generates several electrons. These electrons collide with a series of dynodes, each collision of which generates additional electrons. This amplification of one photon into $10^6$–$10^7$ electrons results in a steady-state current that we can measure. When the intensity of radiation from the source is smaller, as it is with X-rays, then it is possible to store the electrons in a capacitor that, when discharged, provides a pulsed signal that carries information about the photons.

### Flow Proportional Counters

Figure 12.2.4 shows the basic structure of a flow proportional counter. The transducer's cell has an inlet and an outlet for creating the flow of argon gas. The cell has windows made from an X-ray transparent materials, such as beryllium. X-rays enter the cell and, as shown by the reaction in the upper left, ionizes the argon, generating a photoelectron. This photoelectron is sufficiently energetic that it further ionizes the argon, as shown by the reaction in the lower right. The result is an amplification of a single photon into as many as 10,000 electrons. These electrons are drawn to a tungsten wire that is held at a positive charge, and then flow into a capacitor. Discharging the capacitor gives a pulsed signal whose height is proportional to the initial number of electrons and, therefore, to the energy, frequency, and wavelength of the photons.

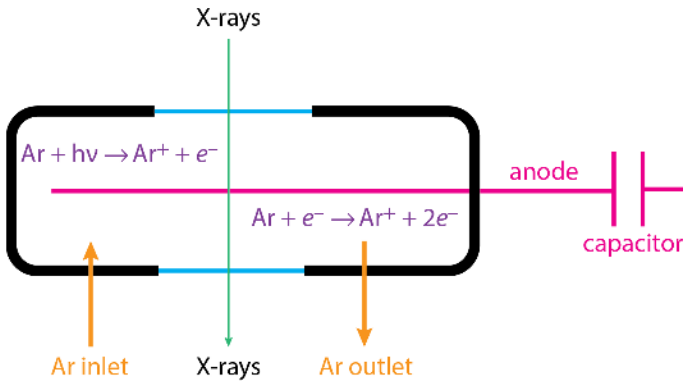



Figure 12.2.4: Schematic diagram of a flow proportional cell for photon counting. See text for details.

### Scintillation Counters

A flow proportional counter is not an efficient transducer for shorter wavelength (lower energy) X-rays that are likely to pass through the cell without being absorbed by the argon gas, leading to a reduction in the signal. In this case we can use a scintillation counter. Figure 12.2.5 shows how this works. X-ray photons are focused onto a single crystal of NaI that is doped with a small amount, approximately 0.2%, of $Tl^+$ as an iodide salt. Absorption of the X-rays results in the fluorescent emission of multiple photons of visible light with a wavelength of 410 nm. Each of these photons falls on the photocathode of a photomultiplier, eventually producing a voltage pulse. Each pulse corresponds to a single photon with an energy that is proportional to the pulse's height.

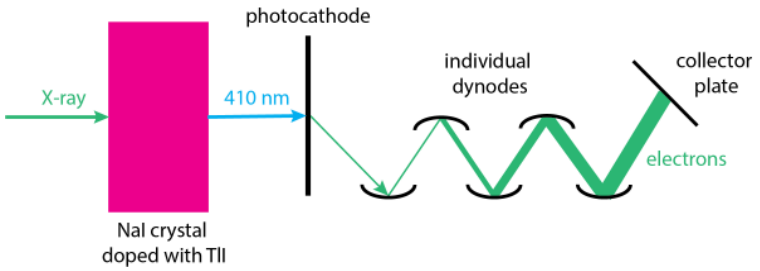


Figure 12.2.5: Schematic diagram of a scintillation counter. See text for details.

### Semiconductor Transducers

In Chapter 7.5 we introduced the use of the *pn* junction of a silicon semiconductor as a transducer for optical spectroscopy. Absorption of a photon of sufficient energy results in the formation of an electron-hole pair. Movement of the electron through the *n*-layer and movement of the hole through the *p*-region generates a current that is proportional to the number of photons reaching the detector. Figure 12.2.6 shows the structure of the semiconductor used in monitoring X-rays, which consists of a *p*-type layer and an *n*-type layer on either side of single crystal of silicon doped with lithium or germanium. The Si(Li) layer has the same role here as Ar has in the flow proportional counter. An X-ray photon that enters into the Si(Li) layer generates electron-hole pairs leading to a measurable current that is proportional to the energy of the X-ray.

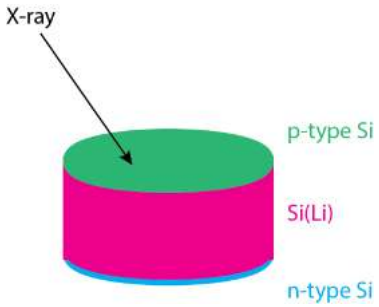


Figure 12.2.6: Structure of a Si(Li) semiconductor transducer.

## X-Ray Signal Processors

The flow proportional counter, scintillation counter, and semiconductor transducers pass a stream of pulses to the signal processor where pulse-height selector is used to isolate only those pulses of interest and a pulse-height analyzer is used to summarize the distribution of pulses.

### Pulse-Height Selectors

Not all pulses measured by the transducer are of interest. For example, pulses with small heights are likely to be noise and pulses with large heights may be a higher-order ($n > 1$) diffraction of shorter, and more energetic wavelengths. Figure 12.2.7 shows the basic details of how pulse-height selector works. The pulse-height selector is set to pass only those pulse heights that are between a lower limit and an upper limit. The figure shows three pulses, one that is too small (in blue), one that is too large (in red), and one that we wish to keep (in green). The pulses run through two channels, one that removes only the blue signal and one that retains only the red signal. The latter signal is inverted and combined with the signal from the other channel. Because the red signal has a different sign in the two channels, it, too, is removed, leaving only the one pulse height that meets the criteria for selection.

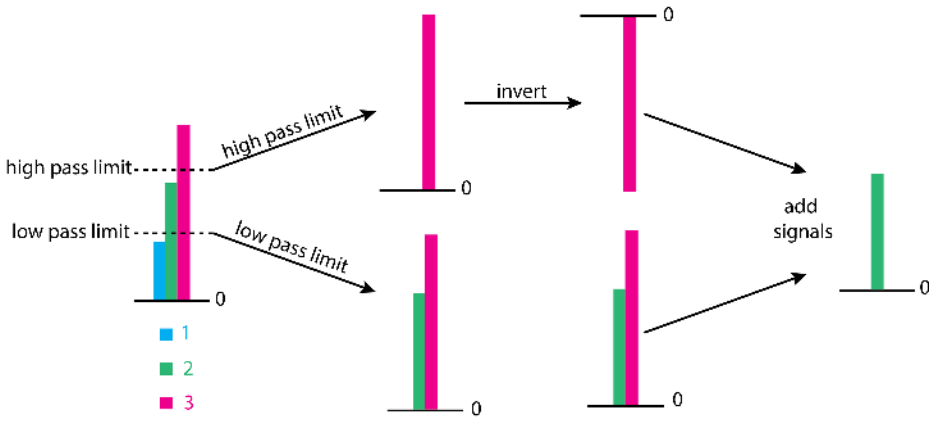



Figure 12.2.7: Illustration of how a pulse-height selector works. Three pulses arrive at the signal processor shown in blue, green, and red with heights greater than the baseline (shown as 0). The pulse-height selector is set to remove all pulses that have a height less than that shown by the low pass limit, and to remove all pulses that have a height greater than the high pass limit. In this case, the low pass filter removes the pulse in blue, and the high pass filter removes all but the pulse in green. The latter is then inverted and then added to the former giving a final signal that contains the one pulse that falls within the two limits.

Having removed pulses with heights that are too small or too large, the remaining pulses are analyzed by counting the number of pulses that share a range of pulse heights. Each unique range of pulse heights is called a channel and corresponds to a specific energy of the photons. A spectrum is a plot showing the count of pulses as function of the energy of the photons.

---

This page titled 12.2: Instrument Components is shared under a CC BY-NC-SA 4.0 license and was authored, remixed, and/or curated by David Harvey.

# 12.3: Atomic X-Ray Fluorescence Methods

In X-ray fluorescence a source of X-rays—emission from an X-ray tube or emission from a radioactive element—is used to excite the atoms of an analyte in a sample. These excited-state atoms return to their ground state by emitting X-rays, the process we know as fluorescence. The wavelengths of these emission lines are characteristic of the elements that make up the sample; thus, atomic X-ray fluorescence is a useful method for both a qualitative analysis and a quantitative analysis.

## Instruments

In the previous section we covered the basic components that make up an atomic X-ray spectrometer: a source of X-rays, a means for isolating those wavelengths of interest, a transducer to measure the intensity of fluorescence, and a signal processor to convert the transducer's signal into a useful measurement. How we string these units together is the subject of this section in which we consider two ways to acquire a sample's spectrum: wavelength dispersive instruments and energy dispersive instruments.

### Wavelength Dispersive Instruments

A wavelength dispersive instrument relies on diffraction using a monochromator, such as that in Figure 12.2.3, to select the analytical wavelength. A sequential wavelength dispersive instrument uses a single monochromator. The monochromator's crystal and transducer are set to the desired angles—$\theta$ for the diffracting crystal and $2\theta$ for the transducer—for the analyte of interest and the fluorescence intensity measured for 1-100 s. The monochromator is adjusted for the next analyte and the process repeated until the analysis for all analytes is complete. Analyzing a sample for 20 analytes may take 30 min or more.

A simultaneous, or multichannel, wavelength dispersive instrument contains as many as 30 crystals and transducers, each at a fixed angle that is preset for an analyte of interest. Each individual channel has a dedicated transducer and pulse-height selector and analyzer. Analysis of a complex sample with many analytes requires less than a minute. This is similar to the multichannel ICP used in atomic emission (see Figure 10.1.5).

### Energy Dispersive Instruments

An energy dispersive instrument eschews a scanning monochromator and, instead, uses a semiconductor transducer to analyze the fluorescent emission by the determining the energies of the emitted photons. As each photon reaches the transducer as a pulse of electrons, its height is measured and converted into the photon's energy. The result is a spectrum showing a count of photons with the same energy as a function of the energy. The collection of data is very fast: if it takes 25 μs to complete the collection and processing of a single photon, then the instrument can count 40,000 photons each second (40 kcps, or kilo counts per second). One limitation to an energy dispersive instrument is its limited resolution with respect to energy. An instrument that operates with 2048 channels—that is, an instrument that divides the energies into 2048 bins—and that processes photons with energies up to 20 keV, has a resolution of approximately 10 eV per channel. Because it does not rely on a monochromator, an energy dispersive instrument occupies a smaller footprint, and portable, hand-held versions are available.

## Qualitative Analysis

Figure 12.3.1 shows the X-ray fluorescence spectrum for the yellow pigment known as naples yellow, the major elements of which are zinc, lead, and antimony. It is easy to identify the major elements in the sample by matching the energies of the individual lines to the published emission lines of the elements, which are available in many on-line sources. For example, the first line highlighted in this spectrum is at an energy of 8.66 KeV, which is close to the $K_\alpha$ line for Zn at 8.64 KeV, and the last highlighted line is at an energy of 29.97 KeV, which is close to the $K_\beta$ line for Sb of 29.7 KeV.

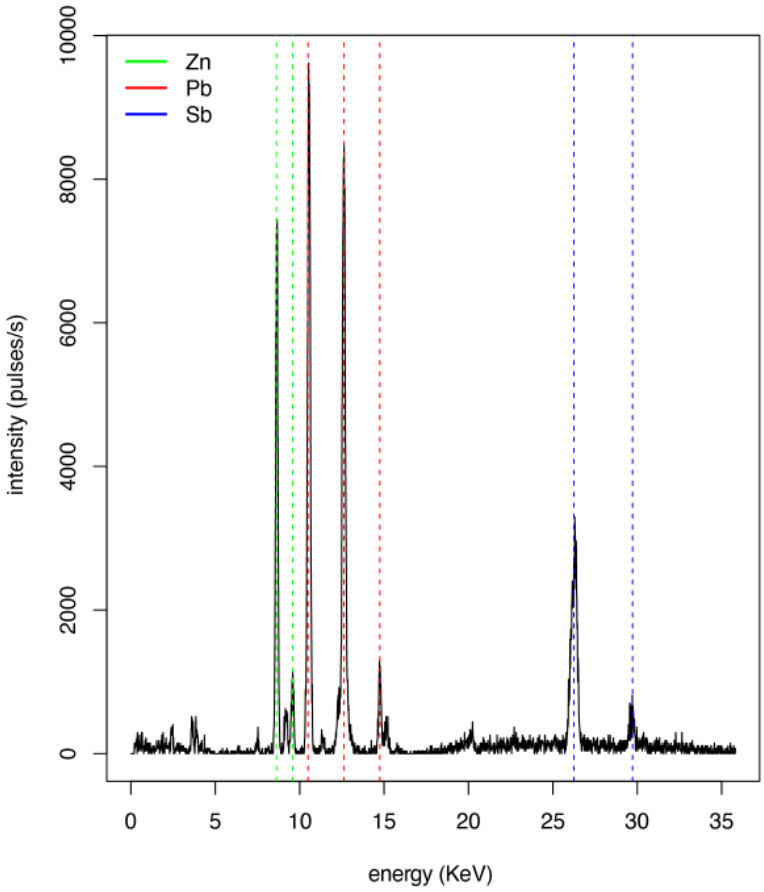



Figure 12.3.1: Energy dispersive XRF of the pigment naples yellow, a lead antimonate that also contains zinc. The spectrometer's energy scale was calibrated using the $\mathrm{K}_\alpha$ line for $^{26}$Fe at 6.4 KeV and the $\mathrm{K}_\alpha$ line for $^{42}$Mo at 17.44 eV. The emission lines for zinc ($\mathrm{K}_\alpha$ and $\mathrm{K}_\beta$) are shown in green, the lines for lead ($\mathrm{L}_\alpha$, $\mathrm{L}_\beta$, and $\mathrm{L}_\gamma$) are shown in red, and the lines for antimony ($\mathrm{K}_\alpha$ and $\mathrm{K}_\beta$) are shown in blue. The original data is available here.

## Quantitative Analysis

A semi-quantitative analysis is possible if we assume that there is a linear relationship between the intensity of an element's emission line and its %w/w concentration in the sample. The intensity of emission from a pure sample or the element, $I_{\text{pure}}$, is measured along with the intensity of emission for the element in a sample, $I_{\text{sample}}$, and the %w/w calculated as

$$\%\mathrm{w/w} = \frac{I_{\text{sample}}}{I_{\text{pure}}} \tag{12.3.1}$$

Equation 12.3.1 is essentially a one-point standardization that makes the significant assumption that the intensity of fluorescent emission is independent of the matrix in which the analyte sits. When this is not true, then errors of 2-3$\times$ are likely.

### Matrix Effects

For fluorescent emission to occur, the analyte must first absorb a photon that can eject a photoelectron. For Equation 12.3.1 to hold, the photons that initiate the fluorescent emission must come from the source only. If other elements within the sample's matrix produced fluorescent emission with sufficient energy to eject photoelectrons from the analyte, then the total fluorescence increases and we overestimate the analyte's concentration. If an element in the matrix absorbs the X-rays from the source more strongly than the analyte, then the analyte's total fluorescence becomes smaller and we underestimate the analyte's concentration. There are three common strategies for compensating for matrix effects.

**External Standards with Matrix Matching**. Instead of using a single, pure sample for the calibration, we prepare a series of standards with different concentrations of the analyte. By matching, as best we can, the matrix of the standards to the matrix of the samples, we can improve the accuracy of a quantitative analysis. This assumes, of course, that we have sufficient knowledge of our sample's matrix.

**Internal Standards**. An internal standard is an element that we add to the standards and samples so that its concentration is the same in each. If the analyte and the internal standard experience similar matrix effects, then the ratio of their intensities is proportional to the ratio of their concentrations

$$\frac{I_{\text{analyte, sample}}}{I_{\text{int std, sample}}} = K \times \frac{C_{\text{analyte, sample}}}{C_{\text{int std, sample}}} \tag{12.3.2}$$

**Dilution**. A third approach is to dilute the samples and standards by adding a quantity of non-absorbing or poorly absorbing material. Dilution has the effect of minimizing the difference in the matrix of the original samples and standards.

---

This page titled 12.3: Atomic X-Ray Fluorescence Methods is shared under a CC BY-NC-SA 4.0 license and was authored, remixed, and/or curated by David Harvey.

# 12.4: Other X-Ray Methods

The application of X-rays to the analysis of materials can take forms other than X-ray fluorescence. In X-ray absorption spectrometry, the ability of a sample to absorb radiation from an X-ray source is measured. Absorption follows Beer's law (see Section 12.1) and, compared to emission, is relatively free of matrix effects. X-ray absorption, however, is a less selective technique than atomic fluorescence because we are not measuring the emission from an analyte's characteristic lines. X-ray absorption finds its greatest utility for the quantitative analysis of samples that contain just one or two major analytes.

In powder X-ray diffraction we focus the radiation from an X-ray tube line source on a powdered sample and measure the intensity of diffracted radiation as a function of the transducer's angle ($2\theta$). A typical powder X-ray diffraction spectrum is in Figure 12.4.1 for the mineral calcite ($CaCO_3$). Qualitative identification is obtained by matching the $2\theta$ peaks to those in published databases. A quantitative analysis for the compound—not the elements that make up the compound—is possible using the intensity of a unique diffraction line in a sample to that for a pure sample. Figure 12.4.2 for a mixture of calcite and magnesite ($MgCO_3$) shows that a simultaneous quantitative analysis for both compounds is possible using the diffraction line at a $2\theta$ of 29.44 for calcite and of 32.65 for magnesite.

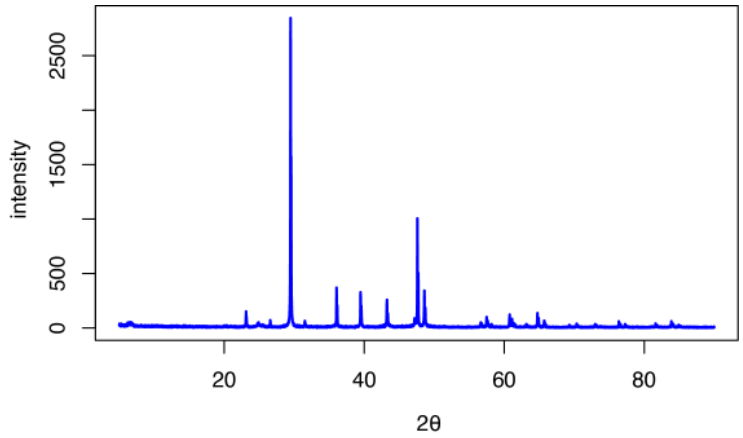



Figure 12.4.1: Powder X-ray diffraction spectrum for the mineral calcite ($CaCO_3$). The original data used to construct this spectrum is here.

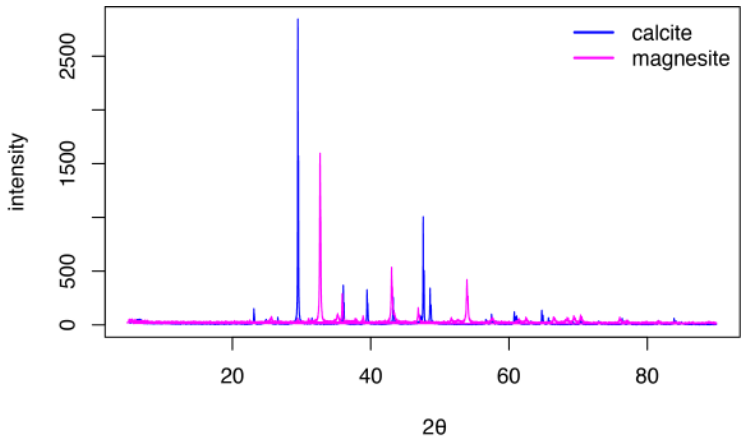



Figure 12.4.2: Powder diffraction spectra for calcite ($CaCO_3$) and magnesite ($MgCO_3$). A quantitative analysis for calcite is possible using its most intense line at a $2\theta$ of 29.44 and a quantitative analysis for magnesite is possible using its most intense line at a $2\theta$ of 32.65. The original data for calcite is here and that for magnesite is here.

This page titled 12.4: Other X-Ray Methods is shared under a CC BY-NC-SA 4.0 license and was authored, remixed, and/or curated by David Harvey.

# CHAPTER OVERVIEW

## 13: Introduction to Ultraviolet/Visible Absorption Spectrometry


13.1: Transmittance and Absorbance

13.2: Beer's Law

13.3: Effect of Noise on Transmittance and Absorbance Measurements

13.4: Instrumentation


---

This page titled 13: Introduction to Ultraviolet/Visible Absorption Spectrometry is shared under a CC BY-NC-SA 4.0 license and was authored, remixed, and/or curated by David Harvey.

# 13.1: Transmittance and Absorbance

As light passes through a sample, its power decreases as some of it is absorbed. This attenuation of radiation is described quantitatively by two separate, but related terms: transmittance and absorbance. As shown in Figure 13.1.1*a*, transmittance is the ratio of the source radiation's power as it exits the sample, $P_T$, to that incident on the sample, $P_0$.

$$T = \frac{P_T}{P_0} \tag{13.1.1}$$

Multiplying the transmittance by 100 gives the percent transmittance, %*T*, which varies between 100% (no absorption) and 0% (complete absorption). All methods of detecting photons—including the human eye and modern photoelectric transducers—measure the transmittance of electromagnetic radiation.

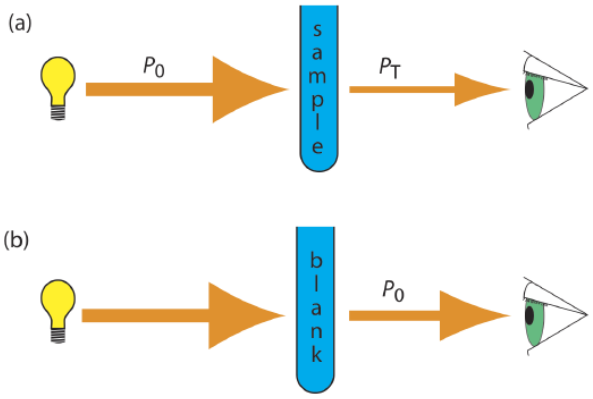



Figure 13.1.1*b*. (a) Schematic diagram showing the attenuation of radiation passing through a sample; $P_0$ is the source's radiant power and $P_T$ is the radiant power transmitted by the sample. (b) Schematic diagram showing how we redefine $P_0$ as the radiant power transmitted by the blank. Redefining $P_0$ in this way corrects the transmittance in (a) for the loss of radiation due to scattering, reflection, absorption by the sample's container, and absorption by the sample's matrix.

Equation 13.1.1 does not distinguish between different mechanisms that prevent a photon emitted by the source from reaching the detector. In addition to absorption by the analyte, several additional phenomena contribute to the attenuation of radiation, including reflection and absorption by the sample's container, absorption by other components in the sample's matrix, and the scattering of radiation. To compensate for this loss of the radiation's power, we use a method blank. As shown in Figure 13.1.1*b*, we redefine $P_0$ as the power exiting the method blank.

An alternative method for expressing the attenuation of electromagnetic radiation is absorbance, *A*, which we define as

$$A = -\log T = -\log \frac{P_T}{P_0} \tag{13.1.2}$$

Absorbance is the more common unit for expressing the attenuation of radiation because—as we will see in the next section—it is a linear function of the analyte's concentration.

## ✔ Example 13.1.1

A sample has a percent transmittance of 50%. What is its absorbance?

### Solution

A percent transmittance of 50.0% is the same as a transmittance of 0.500. Substituting into Equation 13.1.2 gives

$$A = -\log T = -\log(0.500) = 0.301$$

## ? Exercise 13.1.1

What is the %*T* for a sample if its absorbance is 1.27?

**Answer**

To find the transmittance, $T$, we begin by noting that

$$A = 1.27 = -\log T$$

Solving for $T$

$$-1.27 = \log T$$
$$10^{-1.27} = T$$

gives a transmittance of 0.054, or a %T of 5.4%.

This page titled 13.1: Transmittance and Absorbance is shared under a CC BY-NC-SA 4.0 license and was authored, remixed, and/or curated by David Harvey.

# 13.2: Beer's Law

## Absorbance and Concentration

When monochromatic electromagnetic radiation passes through an infinitesimally thin layer of sample of thickness *dx*, it experiences a decrease in its power of *dP* (Figure 13.2.1).

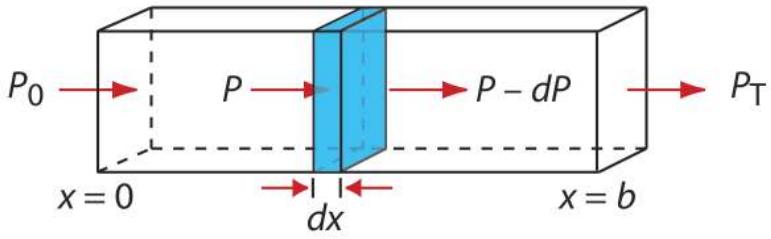



Figure 13.2.1. Factors used to derive the Beer's law.

This fractional decrease in power is proportional to the sample's thickness and to the analyte's concentration, *C*; thus

$$-\frac{dP}{P} = \alpha C dx \tag{13.2.1}$$

where *P* is the power incident on the thin layer of sample and $\alpha$ is a proportionality constant. Integrating the left side of Equation 13.2.1 over the sample's full thickness

$$-\int_{P=P_0}^{P=P_t} \frac{dP}{P} = \alpha C \int_{x=0}^{x=b} dx$$

$$\ln \frac{P_0}{P_T} = \alpha b C$$

converting from ln to log, and substituting into the equation relating transmittance to absorbance

$$A = -\log T = -\log \frac{P_T}{P_0}$$

gives

$$A = abC \tag{13.2.2}$$

where *a* is the analyte's absorptivity with units of $cm^{-1}$ $conc^{-1}$. If we express the concentration using molarity, then we replace *a* with the molar absorptivity, $\varepsilon$, which has units of $cm^{-1}$ $M^{-1}$.

$$A = \varepsilon bC \tag{13.2.3}$$

The absorptivity and the molar absorptivity are proportional to the probability that the analyte absorbs a photon of a given energy. As a result, values for both *a* and $\varepsilon$ depend on the wavelength of the absorbed photon.

### Example 13.2.1

A $5.00 \times 10^{-4}$ M solution of analyte is placed in a sample cell that has a pathlength of 1.00 cm. At a wavelength of 490 nm, the solution's absorbance is 0.338. What is the analyte's molar absorptivity at this wavelength?

**Solution**

Solving Equation 13.2.3 for $\epsilon$ and making appropriate substitutions gives

$$\varepsilon = \frac{A}{bC} = \frac{0.338}{(1.00 \text{ cm})\left(5.00 \times 10^{-4} \text{ M}\right)} = 676 \text{ cm}^{-1} \text{ M}^{-1}$$

### Exercise 13.2.1

A solution of the analyte from Example 13.2.1 has an absorbance of 0.228 in a 1.00-cm sample cell. What is the analyte's concentration?

**Answer**

Making appropriate substitutions into Beer's law

$$A = 0.228 = \varepsilon bC = \left(676\ \text{M}^{-1}\ \text{cm}^{-1}\right)(1\ \text{cm})C$$

and solving for $C$ gives a concentration of $3.37 \times 10^{-4}$ M.

Equation 13.2.2 and Equation 13.2.3, which establish the linear relationship between absorbance and concentration, are known as Beer's law. Calibration curves based on Beer's law are common in quantitative analyses.

As is often the case, the formulation of a law is more complicated than its name suggests. This is the case, for example, with Beer's law, which also is known as the Beer-Lambert law or the Beer-Lambert-Bouguer law. Pierre Bouguer, in 1729, and Johann Lambert, in 1760, noted that the transmittance of light decreases exponentially with an increase in the sample's thickness.

$$T \propto e^{-b}$$

Later, in 1852, August Beer noted that the transmittance of light decreases exponentially as the concentration of the absorbing species increases.

$$T \propto e^{-C}$$

Together, and when written in terms of absorbance instead of transmittance, these two relationships make up what we know as Beer's law.

## Beer's Law and Multicomponent Samples

We can extend Beer's law to a sample that contains several absorbing components. If there are no interactions between the components, then the individual absorbances, $A_i$, are additive. For a two-component mixture of analyte's $X$ and $Y$, the total absorbance, $A_{tot}$, is

$$A_{tot} = A_X + A_Y = \varepsilon_X bC_X + \varepsilon_Y bC_Y$$

Generalizing, the absorbance for a mixture of $n$ components, $A_{mix}$, is

$$A_{mix} = \sum_{i=1}^{n} A_i = \sum_{i=1}^{n} \varepsilon_i bC_i \tag{13.2.4}$$

## Limitations to Beer's Law

Beer's law suggests that a plot of absorbance vs. concentration—we will call this a Beer's law plot—is a straight line with a $y$-intercept of zero and a slope of $ab$ or $\varepsilon b$. In some cases a Beer's law plot deviates from this ideal behavior (see Figure 13.2.2), and such deviations from linearity are divided into three categories: fundamental, chemical, and instrumental.

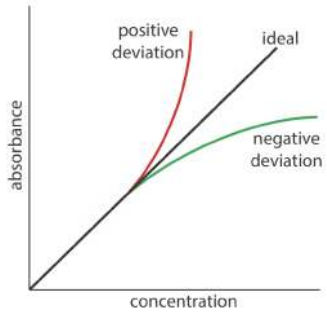



Figure 13.2.2. Plots of absorbance vs. concentration showing positive and negative deviations from the ideal Beer's law relationship, which is a straight line.

## Fundamental Limitations to Beer's Law

Beer's law is a limiting law that is valid only for low concentrations of analyte. There are two contributions to this fundamental limitation to Beer's law. At higher concentrations the individual particles of analyte no longer are independent of each other. The resulting interaction between particles of analyte may change the analyte's absorptivity. A second contribution is that an analyte's absorptivity depends on the solution's refractive index. Because a solution's refractive index varies with the analyte's concentration, values of *a* and $\varepsilon$ may change. For sufficiently low concentrations of analyte, the refractive index essentially is constant and a Beer's law plot is linear.

## Chemical Limitations to Beer's Law

A chemical deviation from Beer's law may occur if the analyte is involved in an equilibrium reaction. Consider, for example, the weak acid, HA. To construct a Beer's law plot we prepare a series of standard solutions—each of which contains a known total concentration of HA—and then measure each solution's absorbance at the same wavelength. Because HA is a weak acid, it is in equilibrium with its conjugate weak base, $A^-$.

> In the equations that follow, the conjugate weak base $A^-$ is sometimes written as A as it is easy to mistake the symbol for anionic charge as a minus sign; thus, we will write $C_A$ instead of $C_{A^-}$.

$$HA(aq) + H_2O(l) \rightleftharpoons H_3O^+(aq) + A^-(aq)$$

If both HA and $A^-$ absorb at the selected wavelength, then Beer's law is

$$A = \varepsilon_{HA} b C_{HA} + \varepsilon_A b C_A \tag{13.2.5}$$

Because the weak acid's total concentration, $C_{total}$, is

$$C_{total} = C_{HA} + C_A$$

we can write the concentrations of HA and $A^-$ as

$$C_{HA} = \alpha_{HA} C_{total} \tag{13.2.6}$$

$$C_A = (1 - \alpha_{HA}) C_{total} \tag{13.2.7}$$

where $\alpha_{HA}$ is the fraction of weak acid present as HA. Substituting Equation 13.2.6 and Equation 13.2.7 into Equation 13.2.5 and rearranging, gives

$$A = (\varepsilon_{HA}\alpha_{HA} + \varepsilon_A - \varepsilon_A\alpha_{HA})\, b C_{total} \tag{13.2.8}$$

To obtain a linear Beer's law plot, we must satisfy one of two conditions. If $\varepsilon_{HA}$ and $\varepsilon_A$ have the same value at the selected wavelength, then Equation 13.2.8 simplifies to

$$A = \varepsilon_A b C_{total} = \varepsilon_{HA} b C_{total}$$

Alternatively, if $\alpha_{HA}$ has the same value for all standard solutions, then each term within the parentheses of Equation 13.2.8 is constant—which we replace with *k*—and a linear calibration curve is obtained at any wavelength.

$$A = kbC_{\text{total}}$$

Because HA is a weak acid, the value of $\alpha_{\text{HA}}$ varies with pH. To hold $\alpha_{\text{HA}}$ constant we buffer each standard solution to the same pH. Depending on the relative values of $\alpha_{\text{HA}}$ and $\alpha_{\text{A}}$, the calibration curve has a positive or a negative deviation from Beer's law if we do not buffer the standards to the same pH.

### Instrumental Limitations to Beer's Law

There are two principal instrumental limitations to Beer's law: stray radiation and non-polychromatic radiation.

Stray radiation is the first contribution to instrumental deviations from Beer's law. Stray radiation arises from imperfections in the wavelength selector that allow light to enter the instrument and to reach the detector without passing through the sample. Stray radiation adds an additional contribution, $P_{\text{stray}}$, to the radiant power that reaches the detector; thus

$$A = -\log \frac{P_{\text{T}} + P_{\text{stray}}}{P_0 + P_{\text{stray}}}$$

For a small concentration of analyte, $P_{\text{stray}}$ is significantly smaller than $P_0$ and $P_{\text{T}}$, and the absorbance is unaffected by the stray radiation. For higher concentrations of analyte, less light passes through the sample and $P_{\text{T}}$ and $P_{\text{stray}}$ become similar in magnitude. This results is an absorbance that is smaller than expected, and a negative deviation from Beer's law.

The second limitation is that Beer's law assumes that radiation reaching the sample is of a single wavelength—that is, it assumes a purely monochromatic source of radiation. Even the best wavelength selector, however, passes radiation with a small, but finite effective bandwidth. Let's assume we have a line source that emits light at two wavelengths, $\lambda'$ and $\lambda''$. When treated separately, the absorbances at these wavelengths, $A'$ and $A''$, are

$$A' = -\log \frac{P'_{\text{r}}}{P'_0} = \varepsilon' bC \qquad A'' = -\log \frac{P''_{\text{T}}}{P''_0} = \varepsilon'' bC$$

If both wavelengths are measured simultaneously the absorbance is

$$A = -\log \frac{(P'_{\text{T}} + P''_{\text{T}})}{(P'_0 + P''_0)}$$

Expanding the logarithmic function of the equation's right side gives

$$A = \log(P'_0 + P''_0) - \log(P'_{\text{T}} + P''_{\text{T}}) \tag{13.2.9}$$

Next, we need to find a relationship between $P_{\text{T}}$ and $P_0$ for any wavelength. To do this, we start with Beer's law

$$A = -\log \frac{P_{\text{T}}}{P_0} = \epsilon bC$$

and then solve for $P_{\text{T}}$ in terms of $P_0$

$$\log \frac{P_{\text{T}}}{P_0} = -\epsilon bC$$

$$\frac{P_{\text{T}}}{P_0} = 10^{-\epsilon bC}$$

$$P_{\text{T}} = P_0 \times 10^{-\epsilon bC}$$

Substituting this general relationship back into our wavelength-specific equation for absorbance, 13.2.9, we obtain

$$A = \log(P'_0 + P''_0) - \log(P'_0 \times 10^{-\epsilon bC} + P''_0 \times 10^{-\epsilon bC}) \tag{13.2.10}$$

For monochromatic radiation, we have $\epsilon' = \epsilon'' = \epsilon$ and Equation 13.2.10 simplifies to Beer's law

$$A = -\log(10^{-\epsilon bC}) = \epsilon bC$$

For non-monochromatic radiation, Equation 13.2.10 predicts that the absorbance is smaller than expected if $\epsilon' > \epsilon''$. Polychromatic radiation always gives a deviation from Beer's law, but the effect is smaller if the value of $\varepsilon$ essentially is constant over the wavelength range passed by the wavelength selector. For this reason, as shown in Figure 13.2.3, it is better to make absorbance

measurements at the top of a broad absorption peak. In addition, the deviation from Beer's law is less serious if the source's effective bandwidth is less than one-tenth of the absorbing species' natural bandwidth [(a) Strong, F. C., III *Anal. Chem.* **1984**, *56*, 16A–34A; Gilbert, D. D. *J. Chem. Educ.* **1991**, *68*, A278–A281]. When measurements must be made on a slope, linearity is improved by using a narrower effective bandwidth.

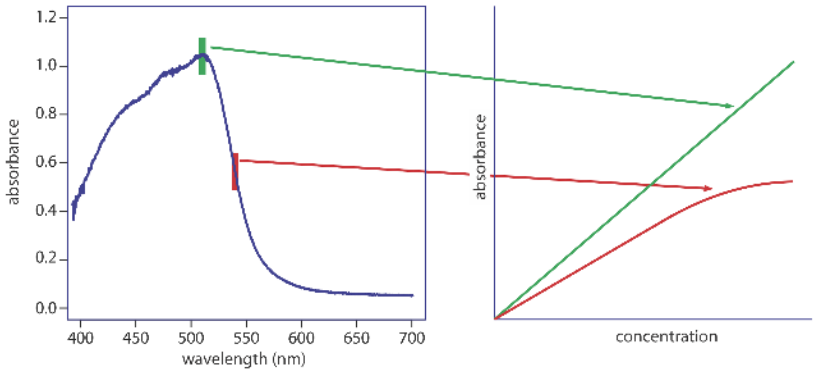



Figure 13.2.3. Effect of wavelength selection on the linearity of a Beer's law plot. Another reason for measuring absorbance at the top of an absorbance peak is that it provides for a more sensitive analysis. Note that the green Beer's law plot has a steeper slope—and, therefore, a greater sensitivity—than the red Beer's law plot. A Beer's law plot, of course, is equivalent to a calibration curve.

This page titled 13.2: Beer's Law is shared under a CC BY-NC-SA 4.0 license and was authored, remixed, and/or curated by David Harvey.

# 13.3: Effect of Noise on Transmittance and Absorbance Measurements

In absorption spectroscopy, precision is limited by indeterminate errors—primarily instrumental noise—which are introduced when we measure absorbance. Precision generally is worse for low absorbances where $P_0 \approx P_T$, and for high absorbances where $P_T$ approaches 0. We might expect, therefore, that precision will vary with transmittance.

We can derive an expression between precision and transmittance by rewriting Beer's law as

$$C = -\frac{1}{\varepsilon b}\log T \tag{13.3.1}$$

and completing a propagation of uncertainty (see the Appendicies for a discussion of propagation of error), which gives

$$s_c = -\frac{0.4343}{\varepsilon b} \times \frac{s_T}{T} \tag{13.3.2}$$

where $s_T$ is the absolute uncertainty in the transmittance. Dividing Equation 13.3.2 by Equation 13.3.1 gives the relative uncertainty in concentration, $s_C/C$, as

$$\frac{s_c}{C} = \frac{0.4343 s_T}{T \log T}$$

If we know the transmittance's absolute uncertainty, then we can determine the relative uncertainty in concentration for any measured transmittance.

Determining the relative uncertainty in concentration is complicated because $s_T$ is a function of the transmittance. As shown in Table 13.3.1, three categories of indeterminate instrumental error are observed [Rothman, L. D.; Crouch, S. R.; Ingle, J. D. Jr. *Anal. Chem.* **1975**, *47*, 1226–1233].

Table 13.3.1. Effect of Indeterminate Errors on Relative Uncertainty in Concentration

| category | sources of indeterminate error | relative uncertainty in concentration |
|---|---|---|
| $s_T = k_1$ | %T readout resolution<br>noise in thermal detectors | $\frac{s_C}{C} = \frac{0.4343 k_1}{T \log T}$ |
| $s_T = k_2\sqrt{T^2 + T}$ | noise in photon detectors | $\frac{s_C}{C} = \frac{0.4343 k_2}{\log T}\sqrt{1 + \frac{1}{T}}$ |
| $s_T = k_3 T$ | positioning of sample cell<br>fluctuations in source intensity | $\frac{s_C}{C} = \frac{0.4343 k_3}{\log T}$ |

A constant $s_T$ is observed for the uncertainty associated with reading %$T$ on a meter's analog or digital scale, both common on less-expensive spectrophotometers. Typical values are ±0.2–0.3% (a $k_1$ of ±0.002–0.003) for an analog scale and ±0.001% a ($k_1$ of ±0.00001) for a digital scale. A constant $s_T$ also is observed for the thermal transducers used in infrared spectrophotometers. The effect of a constant $s_T$ on the relative uncertainty in concentration is shown by curve A in Figure 13.3.1. Note that the relative uncertainty is very large for both high absorbances and low absorbances, reaching a minimum when the absorbance is 0.4343. This source of indeterminate error is important for infrared spectrophotometers and for inexpensive UV/Vis spectrophotometers. To obtain a relative uncertainty in concentration of ±1–2%, the absorbance is kept within the range 0.1–1.

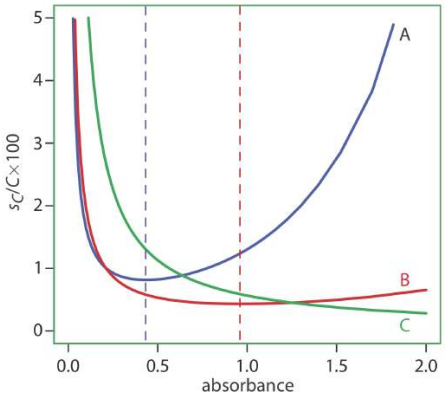



Figure 13.3.1. Percent relative uncertainty in concentration as a function of absorbance for the categories of indeterminate errors in Table 13.3.10.3. A: $k_1$ = ±0.0030; B: $k_2$ = ±0.0030; and C: $k_3$= ±0.0130. The dashed lines correspond to the minimum uncertainty for curve A (absorbance of 0.4343) and for curve B (absorbance of 0.963).

Values of $s_T$ are a complex function of transmittance when indeterminate errors are dominated by the noise associated with photon detectors. Curve B in Figure 13.3.1 shows that the relative uncertainty in concentration is very large for low absorbances, but is smaller at higher absorbances. Although the relative uncertainty reaches a minimum when the absorbance is 0.963, there is little change in the relative uncertainty for absorbances between 0.5 and 2. This source of indeterminate error generally limits the precision of high quality UV/Vis spectrophotometers for mid-to-high absorbances.

Finally, the value of $s_T$ is directly proportional to transmittance for indeterminate errors that result from fluctuations in the source's intensity and from uncertainty in positioning the sample within the spectrometer. The latter is particularly important because the optical properties of a sample cell are not uniform. As a result, repositioning the sample cell may lead to a change in the intensity of transmitted radiation. As shown by curve C in Figure 13.3.1, the effect is important only at low absorbances. This source of indeterminate errors usually is the limiting factor for high quality UV/Vis spectrophotometers when the absorbance is relatively small.

When the relative uncertainty in concentration is limited by the %*T* readout resolution, it is possible to improve the precision of the analysis by redefining 100% T and 0% T. Normally 100% T is established using a blank and 0% T is established while preventing the source's radiation from reaching the detector. If the absorbance is too high, precision is improved by resetting 100% T using a standard solution of analyte whose concentration is less than that of the sample (Figure 13.3.2*a*). For a sample whose absorbance is too low, precision is improved by redefining 0% T using a standard solution of the analyte whose concentration is greater than that of the analyte (Figure 13.3.2*b*). In this case a calibration curve is required because a linear relationship between absorbance and concentration no longer exists. Precision is further increased by combining these two methods (Figure 13.3.2*c*). Again, a calibration curve is necessary since the relationship between absorbance and concentration is no longer linear.

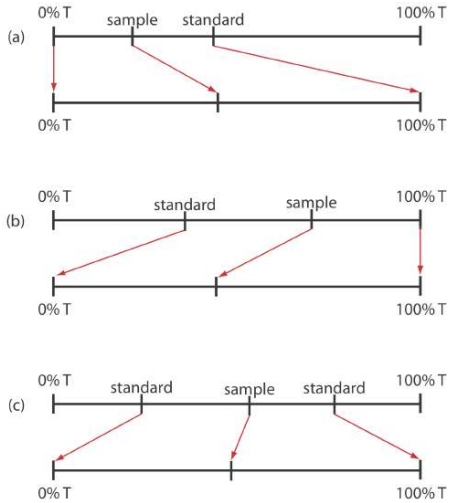



Figure 13.3.17 . Methods for improving the precision of absorption methods: (a) high-absorbance method; (b) low-absorbance method; (c) maximum precision method.

This page titled 13.3: Effect of Noise on Transmittance and Absorbance Measurements is shared under a CC BY-NC-SA 4.0 license and was authored, remixed, and/or curated by David Harvey.

# 13.4: Instrumentation

## Basic Components

As covered in Chapter 7, the basic instrumentation for absorbance measurements consists of a source of radiation, a means for selecting the wavelengths to use, a means for detecting the amount of light absorbed by the sample, and a means for processing and displaying the data. In this section we consider two other essential components of an instrument for measuring the absorbance of UV/Vis radiation by molecules: the optical path that connects the source to the detector and a means for placing the sample in this optical path.

## Instrument Designs for Molecular UV/Vis Absorption

Frequently an analyst must select from among several different optical paths, the one that is best suited for a particular analysis. In this section we examine several different instruments for molecular absorption spectroscopy with an emphasis on their advantages and limitations.

### Filter Photometer

The simplest instrument for molecular UV/Vis absorption is a filter photometer (Figure 13.4.1), which uses an absorption or interference filter to isolate a band of radiation. The filter is placed between the source and the sample to prevent the sample from decomposing when exposed to higher energy radiation. A filter photometer has a single optical path between the source and detector, and is called a single-beam instrument. The instrument is calibrated to 0% T while using a shutter to block the source radiation from the detector. After opening the shutter, the instrument is calibrated to 100% T using an appropriate blank. The blank is then replaced with the sample and its transmittance measured. Because the source's incident power and the sensitivity of the detector vary with wavelength, the photometer is recalibrated whenever the filter is changed. Photometers have the advantage of being relatively inexpensive, rugged, and easy to maintain. Another advantage of a photometer is its portability, making it easy to take into the field. Disadvantages of a photometer include the inability to record an absorption spectrum and the source's relatively large effective bandwidth, which limits the calibration curve's linearity.

> The percent transmittance varies between 0% and 100%. We use a blank to determine $P_0$, which corresponds to 100%T. Even in the absence of light the detector records a signal. Closing the shutter allows us to assign 0%T to this signal. Together, setting 0% T and 100%T calibrates the instrument. The amount of light that passes through a sample produces a signal that is greater than or equal to 0%T and smaller than or equal to 100%T.

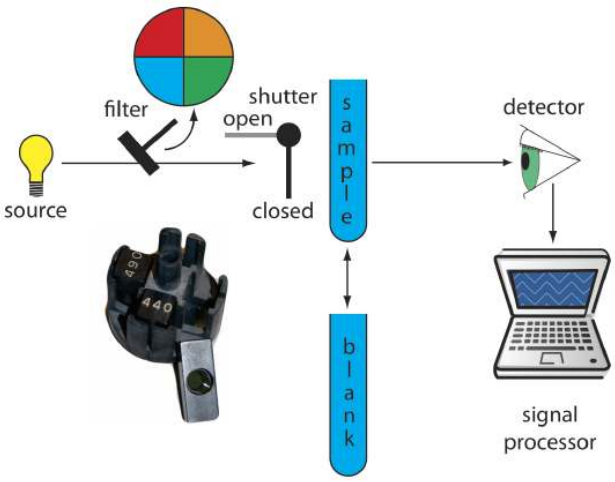



Figure 13.4.1. Schematic diagram of a filter photometer. The analyst either inserts a removable filter or the filters are placed in a carousel, an example of which is shown in the photographic inset. The analyst selects a filter by rotating it into place.

## Single-Beam Spectrophotometer

An instrument that uses a monochromator for wavelength selection is called a spectrophotometer. The simplest spectrophotometer is a single-beam instrument equipped with a fixed-wavelength monochromator (Figure 13.4.2). Single-beam spectrophotometers are calibrated and used in the same manner as a photometer. One example of a single-beam spectrophotometer is Thermo Scientific's Spectronic 20D+, which is shown in the photographic insert to Figure 13.4.2. The Spectronic 20D+ has a wavelength range of 340–625 nm (950 nm when using a red-sensitive detector), and a fixed effective bandwidth of 20 nm. Battery-operated, hand-held single-beam spectrophotometers are available, which are easy to transport into the field. Other single-beam spectrophotometers also are available with effective bandwidths of 2–8 nm. Fixed wavelength single-beam spectrophotometers are not practical for recording spectra because manually adjusting the wavelength and recalibrating the spectrophotometer is awkward and time-consuming. The accuracy of a single-beam spectrophotometer is limited by the stability of its source and detector over time.

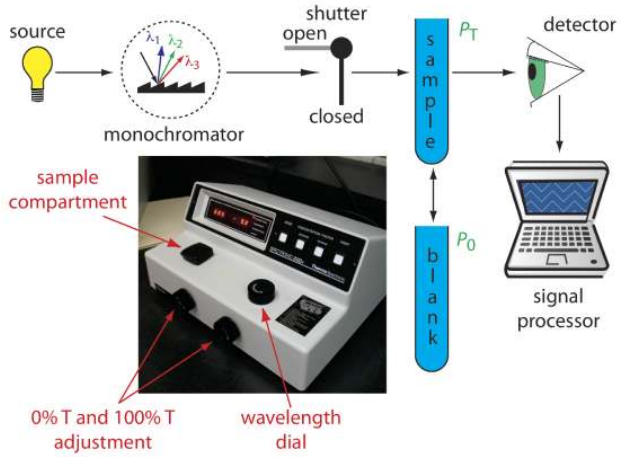



Figure 13.4.2. Schematic diagram of a fixed-wavelength, single-beam spectrophotometer. The photographic inset shows a typical instrument. The shutter remains closed until the sample or blank is placed in the sample compartment. The analyst manually selects the wavelength by adjusting the wavelength dial. Inset photo modified from: Adi (www.commons.Wikipedia.org).

## Double-Beam Spectrophotometer

The limitations of a fixed-wavelength, single-beam spectrophotometer is minimized by using a double-beam spectrophotometer (Figure 13.4.3). A chopper controls the radiation's path, alternating it between the sample, the blank, and a shutter. The signal processor uses the chopper's speed of rotation to resolve the signal that reaches the detector into the transmission of the blank, $P_0$, and the sample, $P_T$. By including an opaque surface as a shutter, it also is possible to continuously adjust 0%T. The effective bandwidth of a double-beam spectrophotometer is controlled by adjusting the monochromator's entrance and exit slits. Effective bandwidths of 0.2–3.0 nm are common. A scanning monochromator allows for the automated recording of spectra. Double-beam instruments are more versatile than single-beam instruments, being useful for both quantitative and qualitative analyses, but also are more expensive and not particularly portable.

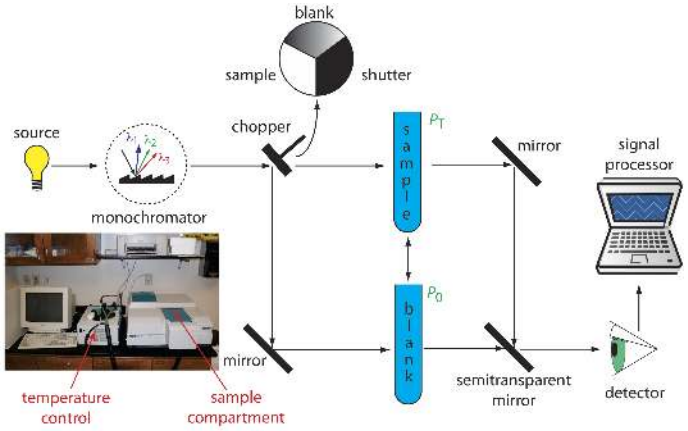



Figure 13.4.3. Schematic diagram of a scanning, double-beam spectrophotometer. A chopper directs the source's radiation, using a transparent window to pass radiation to the sample and a mirror to reflect radiation to the blank. The chopper's opaque surface serves as a shutter, which allows for a constant adjustment of the spectrophotometer's 0%T. The photographic insert shows a typical instrument. The module in the middle of the photo is a temperature control unit that makes it possible to heat or cool the sample to a constant temperature.

## Diode Array Spectrometer

An instrument with a single detector can monitor only one wavelength at a time. If we replace a single photomultiplier with an array of photodiodes, we can use the resulting detector to record a full spectrum in as little as 0.1 s. In a diode array spectrometer the source radiation passes through the sample and is dispersed by a grating (Figure 13.4.4). The photodiode array detector is situated at the grating's focal plane, with each diode recording the radiant power over a narrow range of wavelengths. Because we replace a full monochromator with just a grating, a diode array spectrometer is small and compact.

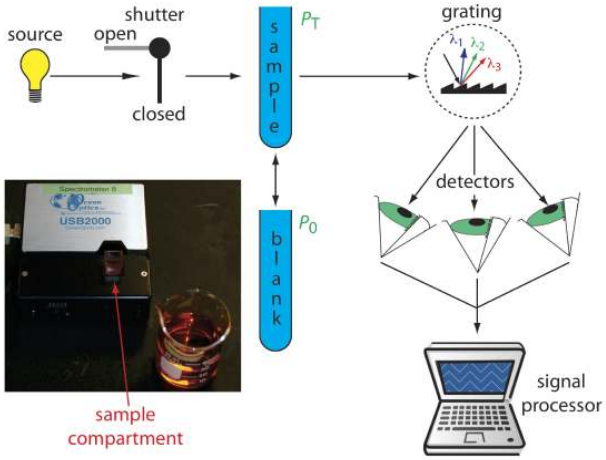



Figure 13.4.4. Schematic diagram of a diode array spectrophotometer. The photographic insert shows a typical instrument. Note that the 50-mL beaker provides a sense of scale. Because the spectrometer is small and compact, it is easy to transport into the field.

One advantage of a diode array spectrometer is the speed of data acquisition, which allows us to collect multiple spectra for a single sample. Individual spectra are added and averaged to obtain the final spectrum. This ***signal averaging*** improves a spectrum's signal-to-noise ratio. If we add together $n$ spectra, the sum of the signal at any point, $x$, increases as $nS_x$, where $S_x$ is the signal. The noise at any point, $N_x$, is a random event, which increases as $\sqrt{n}N_x$ when we add together $n$ spectra. The ***signal-to-noise ratio*** after $n$ scans, $(S/N)_n$ is

$$\left(\frac{S}{N}\right)_n = \frac{nS_x}{\sqrt{n}N_x} = \sqrt{n}\frac{S_x}{N_x}$$

where $S_x/N_x$ is the signal-to-noise ratio for a single scan. The impact of signal averaging is shown in Figure 13.4.5. The first spectrum shows the signal after one scan, which consists of a single, noisy peak. Signal averaging using 4 scans and 16 scans

decreases the noise and improves the signal-to-noise ratio. One disadvantage of a photodiode array is that the effective bandwidth per diode is roughly an order of magnitude larger than that for a high quality monochromator.

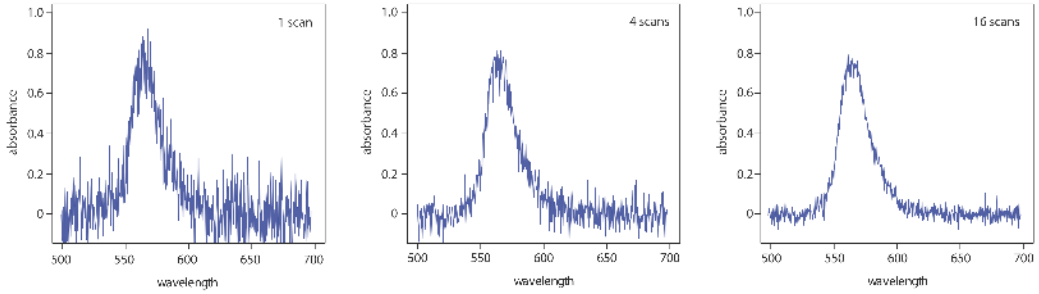
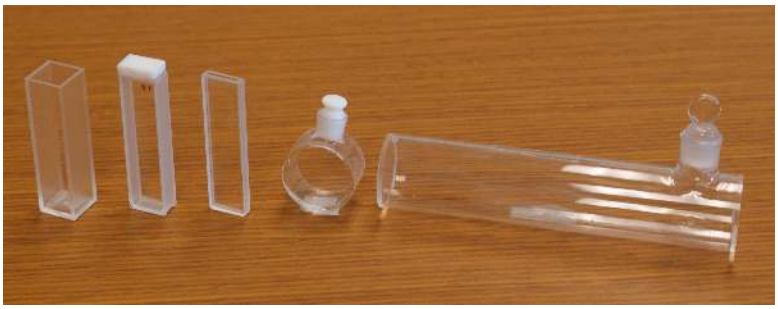



Figure 13.4.5. Effect of signal averaging on a spectrum's signal-to-noise ratio. From top to bottom: spectrum for a single scan; average spectrum after four scans; and average spectrum after adding 16 scans.

## Sample Cells

The sample compartment provides a light-tight environment that limits stray radiation. Samples normally are in a liquid or solution state, and are placed in cells constructed with UV/Vis transparent materials, such as quartz, glass, and plastic (Figure 13.4.6). A quartz or fused-silica cell is required when working at a wavelength <300 nm where other materials show a significant absorption. The most common pathlength is 1 cm (10 mm), although cells with shorter (as little as 0.1 cm) and longer pathlengths (up to 10 cm) are available. Longer pathlength cells are useful when analyzing a very dilute solution or for gas samples. The highest quality cells allow the radiation to strike a flat surface at a $90^o$ angle, minimizing the loss of radiation to reflection. A test tube often is used as a sample cell with simple, single-beam instruments, although differences in the cell's pathlength and optical properties add an additional source of error to the analysis.



FFigure 13.4.6. Examples of sample cells for UV/Vis spectroscopy. From left to right (with path lengths in parentheses): rectangular plastic cuvette (10.0 mm), rectangular quartz cuvette (5.000 mm), rectangular quartz cuvette (1.000 mm), cylindrical quartz cuvette (10.00 mm), cylindrical glass cuvette with quartz windows (100.0 mm). Cells often are available as a matched pair, which is important when using a double-beam instrument.

If we need to monitor an analyte's concentration over time, it may not be possible to remove samples for analysis. This often is the case, for example, when monitoring an industrial production line or waste line, when monitoring a patient's blood, or when monitoring an environmental system, such as stream. With a fiber-optic probe we can analyze samples *in situ*. An example of a remote sensing fiber-optic probe is shown in FFigure 13.4.7. The probe consists of two bundles of fiber-optic cable. One bundle transmits radiation from the source to the probe's tip, which is designed to allow the sample to flow through the sample cell. Radiation from the source passes through the solution and is reflected back by a mirror. The second bundle of fiber-optic cable transmits the nonabsorbed radiation to the wavelength selector. Another design replaces the flow cell shown in Figure 13.4.7 with a membrane that contains a reagent that reacts with the analyte. When the analyte diffuses into the membrane it reacts with the reagent, producing a product that absorbs UV or visible radiation. The nonabsorbed radiation from the source is reflected or scattered back to the detector. Fiber optic probes that show chemical selectivity are called optrodes [(a) Seitz, W. R. *Anal. Chem.* **1984**, *56*, 16A–34A; (b) Angel, S. M. *Spectroscopy* **1987**, *2(2)*, 38–48].

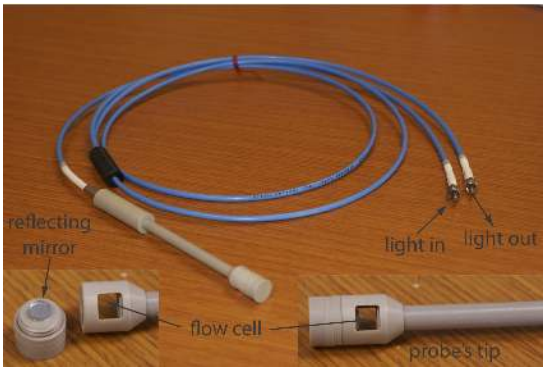



Figure 13.4.7. Example of a fiber-optic probe. The inset photographs at the bottom of the figure provide close-up views of the probe's flow cell and the reflecting mirror.

This page titled 13.4: Instrumentation is shared under a CC BY-NC-SA 4.0 license and was authored, remixed, and/or curated by David Harvey.

# CHAPTER OVERVIEW

## 14: Applications of Ultraviolet/Visible Molecular Absorption Spectrometry


14.1: What is Molar Absorptivity?

14.2: Absorbing Species

14.3: Qualitative and Characterization Applications

14.4: Quantitative Applications

14.5: Photometric Titrations


---

This page titled 14: Applications of Ultraviolet/Visible Molecular Absorption Spectrometry is shared under a CC BY-NC-SA 4.0 license and was authored, remixed, and/or curated by David Harvey.

# 14.1: What is Molar Absorptivity?

Beer's law, as we learned in Chapter 13, gives the relationship between the amount of light absorbed by a sample, $A$, the concentration of the species absorbing light, $C$, the distance (path length) the light travels through the sample, $b$, and the molar absorptivity of the species absorbing light, $\epsilon$

$$A = \epsilon bC$$

The meaning of path length and concentration are self-evident, and their effect on the extent of absorbance also are self-evident: the more absorbing species that are present (concentration) and the more opportunity for any one molecule to absorb light (path length), the greater the absorbance. The meaning of molar absorptivity—what it represents—is less intuitive. It is, of course, a proportionality constant that converts the product of path length and concentration, $bC$, into absorbance, but that is not a particularly satisfying definition. Maximum values for $\epsilon$ are on the order of $10^5$ L/(mol•cm) for simple molecules. and are proportional to the cross-sectional area of the absorbing species and the probability that a photon passing through this cross-sectional area is absorbed. Here we have a self-evident relationship: the greater the cross-sectional area—the more space occupied by the absorbing species—the greater the opportunity for absorbance; and the more favorable the probability of absorption—with probabilities ranging from 0 to 1—the greater the absorbance.

Although molar absorptivity values are often reported in the literature, their values usually vary significantly from study-to-study, presumably due to differences in the purity of the reagents, the solvents used to prepare solutions, the precision with which path length is measured, and the instrument used for the measurements. For this reason, molar absorptivity values are usually calculated as needed by making careful measurements of $A$, $b$, and $C$, or by simply reducing Beer's law to $A = kC$ where $k$ is determined from a calibration curve.

This page titled 14.1: What is Molar Absorptivity? is shared under a CC BY-NC-SA 4.0 license and was authored, remixed, and/or curated by David Harvey.

# 14.2: Absorbing Species

There are two general requirements for an analyte's absorption of electromagnetic radiation. First, there must be a mechanism by which the radiation's electric field or magnetic field can interact with the analyte. For ultraviolet and visible radiation, absorption of a photon changes the energy of the analyte's valence electrons. The second requirement is that the photon's energy, $h\nu$, must exactly equal the difference in energy, $\Delta E$, between two of the analyte's quantized energy states. We can use the energy level diagram in Figure 14.2.1 to explain an absorbance spectrum. The lines labeled $E_0$ and $E_1$ represent the analyte's ground (lowest) electronic state and its first electronic excited state. Superimposed on each electronic energy level is a series of lines representing vibrational energy levels.

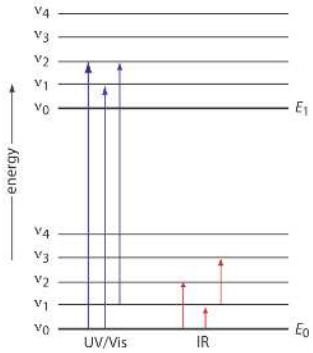



Figure 14.2.1. Diagram showing two electronic energy levels ($E_0$ and $E_1$), each with five vibrational energy levels $\nu_{0-4}$. Absorption of ultraviolet and visible radiation (shown by the blue arrows) leads to a change in the analyte's electronic energy levels and, possibly, a change in vibrational energy as well. A change in vibrational energy without a change in electronic energy levels occurs with the absorption of infrared radiation (shown by the red arrows).

## UV/Vis Spectra for Molecules and Ions

The valence electrons in organic molecules and polyatomic ions, such as $CO_3^{2-}$, occupy quantized sigma bonding ($\sigma$), pi bonding ( $\pi$), and non-bonding ($n$) molecular orbitals (MOs). Unoccupied sigma antibonding ($\sigma^*$) and pi antibonding ($\pi^*$) molecular orbitals are slightly higher in energy. Because the difference in energy between the highest-energy occupied molecular orbitals (HOMO) and the lowest-energy unoccupied molecular orbitals (LUMO) corresponds to ultraviolet and visible radiation, absorption of a photon is possible.

Four types of transitions between quantized energy levels account for most molecular UV/Vis spectra. Table 14.2.1 lists the approximate wavelength ranges for these transitions, as well as a partial list of bonds, functional groups, or molecules responsible for these transitions. Of these transitions, the most important are $n \rightarrow \pi^*$ and $\pi \rightarrow \pi^*$ because they involve important functional groups that are characteristic of many analytes and because the wavelengths are easily accessible. The bonds and functional groups that give rise to the absorption of ultraviolet and visible radiation are called chromophores.

Table 14.2.1. Electronic Transitions Involving n, $\sigma$, and $\pi$ Molecular Orbitals

| transition | wavelength range | examples |
|---|---|---|
| $\sigma \rightarrow \sigma^*$ | <200 nm | C—C, C—H |
| $n \rightarrow \sigma^*$ | 160–260 nm | $H_2O$, $CH_3OH$, $CH_3Cl$ |
| $\pi \rightarrow \pi^*$ | 200–500 nm | C=C, C=O, C=N, C≡C |
| $n \rightarrow \pi^*$ | 250–600 nm | C=O, C=N, N=N, N=O |

Many transition metal ions, such as $Cu^{2+}$ and $Co^{2+}$, form colorful solutions because the metal ion absorbs visible light. The transitions that give rise to this absorption are valence electrons in the metal ion's *d*-orbitals, which are shown in Figure 14.2.2. For a free metal ion, the five *d*-orbitals are of equal energy.

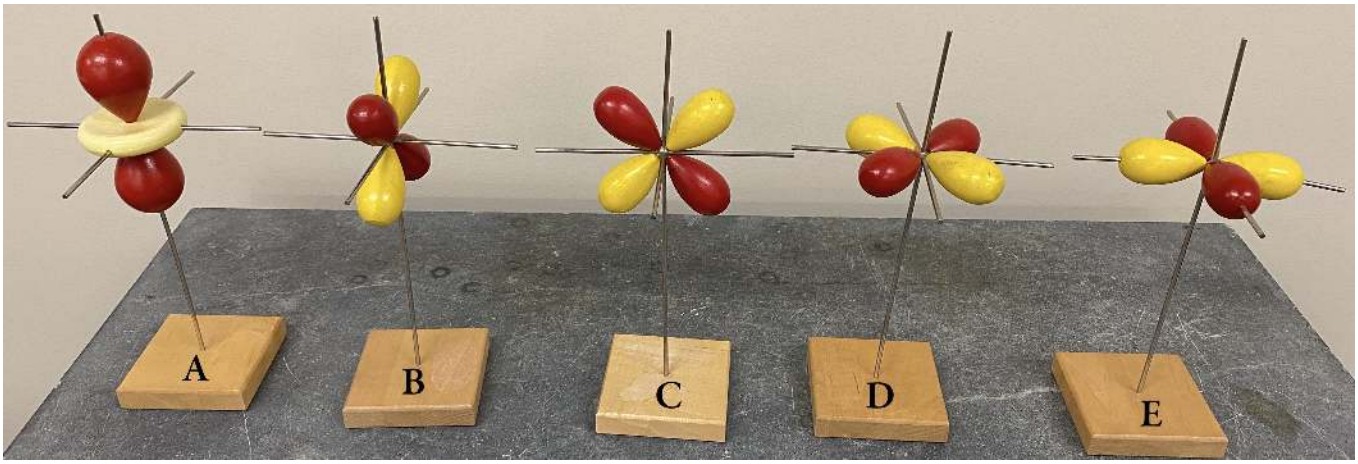



Figure 14.2.2: Models showing the 3*d* orbitals: (A) $d_{z^2}$; (B) $d_{xz}$; (C) $d_{yz}$; (D) $d_{xy}$; and (E) $d_{x^2-y^2}$. The first and last of these orbitals have electron density aligned along the x-, y-, and z-axes.

In the presence of a complexing ligand or solvent molecule, however, the *d*-orbitals split into two or more groups that differ in energy. For example, in an octahedral complex of $Cu(H_2O)_6^{2+}$ the six water molecules, which are aligned with the metal rods in Figure 14.2.2, perturb the *d*-orbitals into the two groups shown in Figure 14.2.3. The magnitude of the splitting of the $d$-orbitals is called the octahedral field strength, $\Delta_{oct}$.

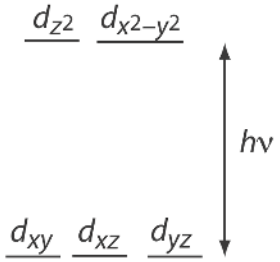



Figure 14.2.3. Splitting of the *d*-orbitals in an octahedral field. The energy gap, $h\nu$, is called $\Delta_{oct}$.

Although the magnitude of the resulting $d \rightarrow d$ transitions for transition metal ions are relatively weak, solutions of the metal-ligand complexes show distinct colors that depend on the metal ion and the ligand, which affect the magnitude of $\Delta_{oct}$. Figure 14.2.4 shows the variation in color for a series of seven octahedral complexes of $Co^{3+}$. The spectra for three of these complexes are shown in Figure 14.2.5, which we can use to estimate the relative size of $\Delta_{oct}$. Each of the spectra shows two absorption bands, one near 400 nm and one a somewhat longer wavelength: a shoulder at about 470 nm for phenanthroline, a peak at about 550 nm for glycine, and a peak at about 620 nm for oxalate. Because $\Delta_{oct}$ is inversely proportional to wavelength, the relative magnitude of $\Delta_{oct}$ increases from $Co(phen)_3^{3+}$ to $Co(glycine)_3^{3+}$ to $Co(oxalate)_3^{3-}$. In Figure 14.2.4, the octahedral field strengths of the ligands decrease from $Co(NO2)_6^{3-}$ to $Co(CO3)_3^{3-}$.




Figure 14.2.4: Metal-ligand complexes of $Co^{3+}$ with nitrite, phenanthroline, ethylenediamine, glycine, water, oxalate, and carbonate. The ligands are arranged from largest octahedral field strength on the left to the smallest on the right.

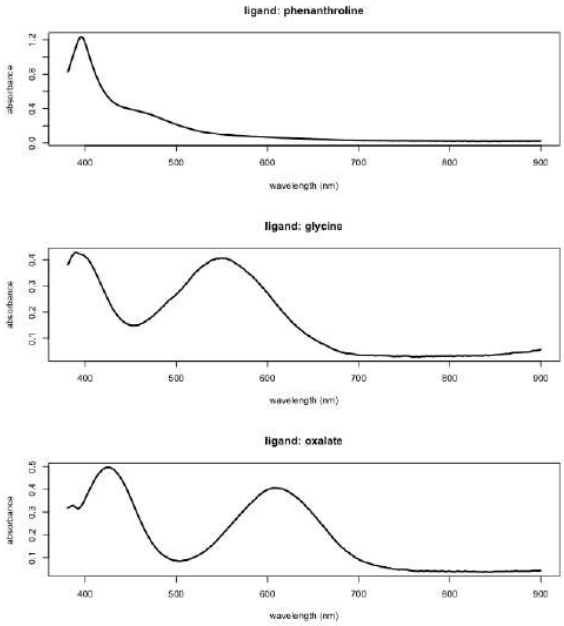



Figure 14.2.5: Visible spectra for the metal-ligand complexes of $Co^{3+}$ with phenanthroline, glycine, and oxalate. See Figure 14.2.4 to see the solution colors.

A more important source of UV/Vis absorption for inorganic metal–ligand complexes is charge transfer, in which absorption of a photon produces an excited state in which there is transfer of an electron from the metal, *M*, to the ligand, *L*.

$$M - L + h\nu \rightarrow \left(M^{+} - L^{-}\right)^{*}$$

Charge-transfer absorption is important because it produces very large absorbances. One important example of a charge-transfer complex is that of *o*-phenanthroline with $Fe^{2+}$, the UV/Vis spectrum for which is shown in Figure 14.2.7. Charge-transfer absorption in which an electron moves from the ligand to the metal also is possible.

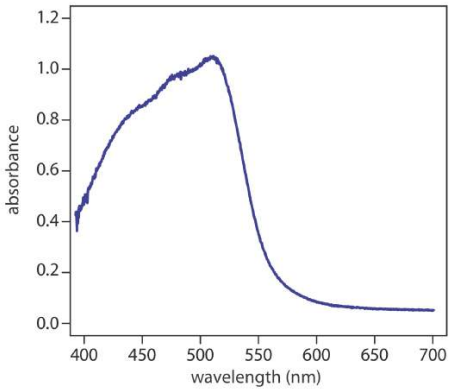



Figure 14.2.6. UV/Vis spectrum for the metal–ligand complex $\mathrm{Fe(phen)_3^{2+}}$, where phen is the ligand *o*-phenanthroline.

This page titled 14.2: Absorbing Species is shared under a CC BY-NC-SA 4.0 license and was authored, remixed, and/or curated by David Harvey.

# 14.3: Qualitative and Characterization Applications

## Qualitative Applications

As discussed in Chapter 14.2, ultraviolet, visible, and infrared absorption bands result from the absorption of electromagnetic radiation by specific valence electrons or bonds. The energy at which the absorption occurs, and the intensity of that absorption, is determined by the chemical environment of the absorbing moiety. For example, benzene has several ultraviolet absorption bands due to $\pi \rightarrow \pi^*$ transitions. The position and intensity of two of these bands, 203.5 nm ($\epsilon$ = 7400 $M^{-1}cm^{-1}$) and 254 nm ($\epsilon$ = 204 $M^{-1}$ $cm^{-1}$), are sensitive to substitution. For benzoic acid, in which a carboxylic acid group replaces one of the aromatic hydrogens, the two bands shift to 230 nm ($\epsilon$ = 11600 $M^{-1}$ $cm^{-1}$) and 273 nm ($\epsilon$ = 970 $M^{-1}$ $cm^{-1}$). A variety of rules have been developed to aid in correlating UV/Vis absorption bands to chemical structure. With the availability of computerized data acquisition and storage it is possible to build digital libraries of standard reference spectra. The identity of an a unknown compound often can be determined by comparing its spectrum against a library of reference spectra, a process known as spectral searching.

## Characterization Applications

Molecular absorption, particularly in the UV/Vis range, has been used for a variety of different characterization studies, including determining the stoichiometry of metal–ligand complexes and determining equilibrium constants. Both of these examples are examined in this section.

### Stoichiometry of a Metal-Ligand Complex

We can determine the stoichiometry of the metal–ligand complexation reaction

$$\mathrm{M} + y\mathrm{L} \rightleftharpoons \mathrm{ML}_y$$

using one of three methods: the method of continuous variations, the mole-ratio method, and the slope-ratio method. Of these approaches, the method of continuous variations, also called Job's method, is the most popular. In this method a series of solutions is prepared such that the total moles of metal and of ligand, $n_{\text{total}}$, in each solution is the same. If $(n_{\mathrm{M}})_i$ and $(n_{\mathrm{L}})_i$ are, respectively, the moles of metal and ligand in solution $i$, then

$$n_{\text{total}} = (n_{\mathrm{M}})_i + (n_{\mathrm{L}})_i$$

The relative amount of ligand and metal in each solution is expressed as the mole fraction of ligand, $(X_{\mathrm{L}})_i$, and the mole fraction of metal, $(X_{\mathrm{M}})_i$,

$$(X_{\mathrm{L}})_i = \frac{(n_{\mathrm{L}})_i}{n_{\text{total}}}$$

$$(X_M)_i = 1 - \frac{(n_{\mathrm{L}})_i}{n_{\text{ total}}} = \frac{(n_{\mathrm{M}})_i}{n_{\text{ total}}}$$

The concentration of the metal–ligand complex in any solution is determined by the limiting reagent, with the greatest concentration occurring when the metal and the ligand are mixed stoichiometrically. If we monitor the complexation reaction at a wavelength where only the metal–ligand complex absorbs, a graph of absorbance versus the mole fraction of ligand has two linear branches—one when the ligand is the limiting reagent and a second when the metal is the limiting reagent. The intersection of the two branches represents a stoichiometric mixing of the metal and the ligand. We use the mole fraction of ligand at the intersection to determine the value of $y$ for the metal–ligand complex $\mathrm{ML}_y$.

$$y = \frac{n_{\mathrm{L}}}{n_{\mathrm{M}}} = \frac{X_{\mathrm{L}}}{X_{\mathrm{M}}} = \frac{X_{\mathrm{L}}}{1 - X_{\mathrm{L}}}$$

> You also can plot the data as absorbance versus the mole fraction of metal. In this case, $y$ is equal to $(1 - X_{\mathrm{M}})/X_{\mathrm{M}}$.

**Example 14.3.1**

To determine the formula for the complex between $Fe^{2+}$ and *o*-phenanthroline, a series of solutions is prepared in which the total concentration of metal and ligand is held constant at $3.15 \times 10^{-4}$ M. The absorbance of each solution is measured at a wavelength of 510 nm. Using the following data, determine the formula for the complex.

| $X_L$ | absorbance | $X_L$ | absorbance |
|---|---|---|---|
| 0.000 | 0.000 | 0.600 | 0.693 |
| 0.100 | 0.116 | 0.700 | 0.809 |
| 0.200 | 0.231 | 0.800 | 0.693 |
| 0.300 | 0.347 | 0.900 | 0.347 |
| 0.400 | 0.462 | 1.000 | 0.000 |
| 0.500 | 0.578 | | |

### Solution

A plot of absorbance versus the mole fraction of ligand is shown in Figure 14.3.1. To find the maximum absorbance, we extrapolate the two linear portions of the plot. The two lines intersect at a mole fraction of ligand of 0.75. Solving for *y* gives

$$y = \frac{X_L}{1 - X_L} = \frac{0.75}{1 - 0.75} = 3$$

The formula for the metal–ligand complex is $Fe(phen)_3^{2+}$.

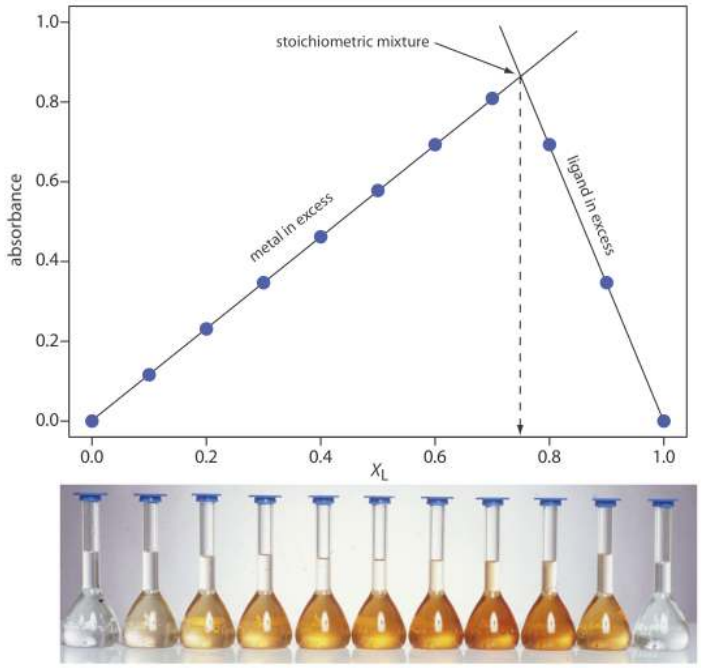



Figure 14.3.1. Continuous variations plot for Example 14.3.1 . The photo shows the solutions used to gather the data. Each solution is displayed directly below its corresponding point on the continuous variations plot. To prepare these solutions I first prepared a solution of $3.15 \times 10^{-4}$ M $Fe^{2+}$ and a solution of $3.15 \times 10^{-4}$ M *o*-phenanthroline. Because the two stock solutions have the same concentration, diluting a portion of one solution with the other solution gives a mixture in which the combined concentration of *o*-phenanthroline and $Fe^{2+}$ is $3.15 \times 10^{-4}$ M. Because each solution has the same volume, each solution also contains the same total moles of metal and ligand.

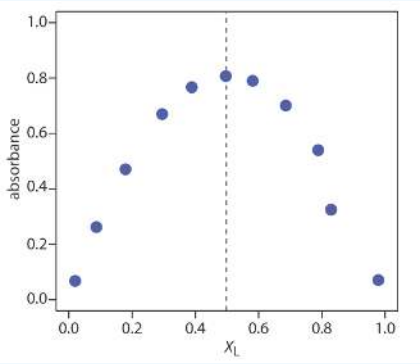
## ? Exercise 14.3.1

Use the continuous variations data in the following table to determine the formula for the complex between $Fe^{2+}$ and $SCN^-$. The data for this problem is adapted from Meloun, M.; Havel, J.; Högfeldt, E. *Computation of Solution Equilibria*, Ellis Horwood: Chichester, England, 1988, p. 236.

| $X_L$ | absorbance | $X_L$ | absorbance | $X_L$ | absorbance | $X_L$ | absorbance |
|---|---|---|---|---|---|---|---|
| 0.0200 | 0.068 | 0.2951 | 0.670 | 0.5811 | 0.790 | 0.8923 | 0.324 |
| 0.0870 | 0.262 | 0.3887 | 0.767 | 0.6860 | 0.701 | 0.9787 | 0.071 |
| 0.1792 | 0.471 | 0.4964 | 0.807 | 0.7885 | 0.540 | | |

**Answer**

The figure below shows a continuous variations plot for the data in this exercise. Although the individual data points show substantial curvature—enough curvature that there is little point in trying to draw linear branches for excess metal and excess ligand—the maximum absorbance clearly occurs at $X_L \approx 0.5$. The complex's stoichiometry, therefore, is $Fe(SCN)^{2+}$.




Several precautions are necessary when using the method of continuous variations. First, the metal and the ligand must form only one metal–ligand complex. To determine if this condition is true, plots of absorbance versus $X_L$ are constructed at several different wavelengths and for several different values of $n_{total}$. If the maximum absorbance does not occur at the same value of $X_L$ for each set of conditions, then more than one metal–ligand complex is present. A second precaution is that the metal–ligand complex's absorbance must obey Beer's law. Third, if the metal–ligand complex's formation constant is relatively small, a plot of absorbance versus $X_L$ may show significant curvature. In this case it often is difficult to determine the stoichiometry by extrapolation. Finally, because the stability of a metal–ligand complex may be influenced by solution conditions, it is necessary to control carefully the composition of the solutions. When the ligand is a weak base, for example, each solutions must be buffered to the same pH.

In the mole-ratio method the moles of one reactant, usually the metal, is held constant, while the moles of the other reactant is varied. The absorbance is monitored at a wavelength where the metal–ligand complex absorbs. A plot of absorbance as a function of the ligand-to-metal mole ratio, $n_L/n_M$, has two linear branches that intersect at a mole–ratio corresponding to the complex's formula. Figure 14.3.2*a* shows a mole-ratio plot for the formation of a 1:1 complex in which the absorbance is monitored at a wavelength where only the complex absorbs. Figure 14.3.2*b* shows a mole-ratio plot for a 1:2 complex in which all three species—the metal, the ligand, and the complex—absorb at the selected wavelength. Unlike the method of continuous variations, the mole-ratio method can be used for complexation reactions that occur in a stepwise fashion if there is a difference in the molar absorptivities of the metal–ligand complexes, and if the formation constants are sufficiently different. A typical mole-ratio plot for the step-wise formation of ML and $ML_2$ is shown in Figure 14.3.2*c*.

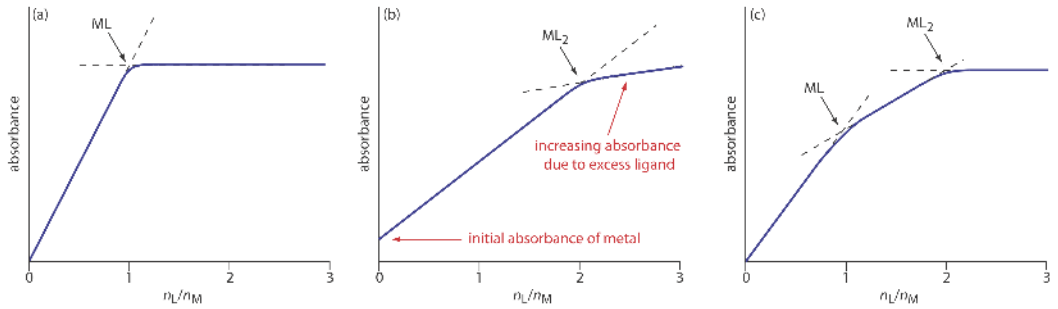



Figure 14.3.2*a*. Mole-ratio plots for: (a) a 1:1 metal–ligand complex in which only the complex absorbs; (b) a 1:2 metal–ligand complex in which the metal, the ligand, and the complex absorb; and (c) the stepwise formation of a 1:1 and a 1:2 metal–ligand complex.

For both the method of continuous variations and the mole-ratio method, we determine the complex's stoichiometry by extrapolating absorbance data from conditions in which there is a linear relationship between absorbance and the relative amounts of metal and ligand. If a metal–ligand complex is very weak, a plot of absorbance versus $X_L$ or $n_L/n_M$ becomes so curved that it is impossible to determine the stoichiometry by extrapolation. In this case the slope-ratio is used.

In the slope-ratio method two sets of solutions are prepared. The first set of solutions contains a constant amount of metal and a variable amount of ligand, chosen such that the total concentration of metal, $C_M$, is much larger than the total concentration of ligand, $C_L$. Under these conditions we may assume that essentially all the ligand reacts to form the metal–ligand complex. The concentration of the complex, which has the general form $M_xL_y$, is

$$[\mathrm{M}_x\mathrm{L}_y] = \frac{C_\mathrm{L}}{y}$$

If we monitor the absorbance at a wavelength where only $M_xL_y$ absorbs, then

$$A = \varepsilon b\,[\mathrm{M}_x\mathrm{L}_y] = \frac{\varepsilon b C_\mathrm{L}}{y}$$

and a plot of absorbance versus $C_L$ is linear with a slope, $s_L$, of

\[s_{\mathrm{L}}=\frac{\varepsilon b}{y}\ ]

A second set of solutions is prepared with a fixed concentration of ligand that is much greater than a variable concentration of metal; thus

$$[\mathrm{M}_x\mathrm{L}_y] = \frac{C_\mathrm{M}}{x}$$

$$A = \varepsilon b\,[\mathrm{M}_x\mathrm{L}_y] = \frac{\varepsilon b C_\mathrm{M}}{x}$$

$$s_M = \frac{\varepsilon b}{x}$$

A ratio of the slopes provides the relative values of *x* and *y*.

$$\frac{s_\mathrm{M}}{s_\mathrm{L}} = \frac{\varepsilon b/x}{\varepsilon b/y} = \frac{y}{x}$$

An important assumption in the slope-ratio method is that the complexation reaction continues to completion in the presence of a sufficiently large excess of metal or ligand. The slope-ratio method also is limited to systems in which only a single complex forms and for which Beer's law is obeyed.

## Determination of Equilibrium Constants

Another important application of molecular absorption spectroscopy is the determination of equilibrium constants. Let's consider, as a simple example, an acid–base reaction of the general form

$$\mathrm{HIn}(aq) + \mathrm{H_2O}(l) \rightleftharpoons \mathrm{H_3O^+}(aq) + \mathrm{In^-}(aq)$$

where HIn and $In^-$ are the conjugate weak acid and weak base forms of an acid–base indicator. The equilibrium constant for this reaction is

$$K_a = \frac{[H_3O^+]\,[A^-]}{[HA]}$$

To determine the equilibrium constant's value, we prepare a solution in which the reaction is in a state of equilibrium and determine the equilibrium concentration for $H_3O^+$, HIn, and $In^-$. The concentration of $H_3O^+$ is easy to determine by measuring the solution's pH. To determine the concentration of HIn and $In^-$ we can measure the solution's absorbance.

If both HIn and $In^-$ absorb at the selected wavelength, then, from Beer's law, we know that

$$A = \varepsilon_{HIn} b[HIn] + \varepsilon_{In} b[In^-] \tag{14.3.1}$$

where $\varepsilon_{HIn}$ and $\varepsilon_{In}$ are the molar absorptivities for HIn and $In^-$. The indicator's total concentration, $C$, is given by a mass balance equation

$$C = [HIn] + [In^-] \tag{14.3.2}$$

Solving Equation 14.3.2 for [HIn] and substituting into Equation 14.3.1 gives

$$A = \varepsilon_{HIn} b\,(C - [In^-]) + \varepsilon_{In} b\,[In^-]$$

which we simplify to

$$A = \varepsilon_{HIn} bC - \varepsilon_{HIn} b\,[In^-] + \varepsilon_{In} b\,[In^-]$$

$$A = A_{HIn} + b\,[In^-]\,(\varepsilon_{In} - \varepsilon_{HIn}) \tag{14.3.3}$$

where $A_{HIn}$, which is equal to $\varepsilon_{HIn} bC$, is the absorbance when the pH is acidic enough that essentially all the indicator is present as HIn. Solving Equation 14.3.3 for the concentration of $In^-$ gives

$$[In^-] = \frac{A - A_{HIn}}{b\,(\varepsilon_{In} - \varepsilon_{HIn})} \tag{14.3.4}$$

Proceeding in the same fashion, we derive a similar equation for the concentration of HIn

$$[HIn] = \frac{A_{In} - A}{b\,(\varepsilon_{In} - \varepsilon_{HIn})} \tag{14.3.5}$$

where $A_{In}$, which is equal to $\varepsilon_{In} bC$, is the absorbance when the pH is basic enough that only $In^-$ contributes to the absorbance. Substituting Equation 14.3.4 and Equation 14.3.5 into the equilibrium constant expression for HIn gives

$$K_a = \frac{[H_3O^+][In^-]}{[HIn]} = [H_3O^+] \times \frac{A - A_{HIn}}{A_{In} - A} \tag{14.3.6}$$

We can use Equation 14.3.6 to determine $K_a$ in one of two ways. The simplest approach is to prepare three solutions, each of which contains the same amount, $C$, of indicator. The pH of one solution is made sufficiently acidic such that [HIn] >> [$In^-$]. The absorbance of this solution gives $A_{HIn}$. The value of $A_{In}$ is determined by adjusting the pH of the second solution such that [$In^-$] >> [HIn]. Finally, the pH of the third solution is adjusted to an intermediate value, and the pH and absorbance, $A$, recorded. The value of $K_a$ is calculated using Equation 14.3.6.

### Example 14.3.2

The acidity constant for an acid–base indicator is determined by preparing three solutions, each of which has a total concentration of indicator equal to $5.00 \times 10^{-5}$ M. The first solution is made strongly acidic with HCl and has an absorbance of 0.250. The second solution is made strongly basic and has an absorbance of 1.40. The pH of the third solution is 2.91 and has an absorbance of 0.662. What is the value of $K_a$ for the indicator?

#### Solution

The value of $K_a$ is determined by making appropriate substitutions into 10.20 where $[H_3O^+]$ is $1.23 \times 10^{-3}$; thus

$$K_a = \left(1.23 \times 10^{-3}\right) \times \frac{0.662 - 0.250}{1.40 - 0.662} = 6.87 \times 10^{-4}$$

## Exercise 14.3.2

To determine the $K_a$ of a merocyanine dye, the absorbance of a solution of $3.5 \times 10^{-4}$ M dye was measured at a pH of 2.00, a pH of 6.00, and a pH of 12.00, yielding absorbances of 0.000, 0.225, and 0.680, respectively. What is the value of $K_a$ for this dye? The data for this problem is adapted from Lu, H.; Rutan, S. C. *Anal. Chem.*, **1996**, *68*, 1381–1386.

**Answer**

The value of $K_a$ is

$$K_a = \left(1.00 \times 10^{-6}\right) \times \frac{0.225 - 0.000}{0.680 - 0.225} = 4.95 \times 10^{-7}$$

A second approach for determining $K_a$ is to prepare a series of solutions, each of which contains the same amount of indicator. Two solutions are used to determine values for $A_{HIn}$ and $A_{In}$. Taking the log of both sides of Equation 14.3.6 and rearranging leave us with the following equation.

$$\log \frac{A - A_{Hin}}{A_{In^-} - A} = \text{pH} - \text{p}K_a \tag{14.3.7}$$

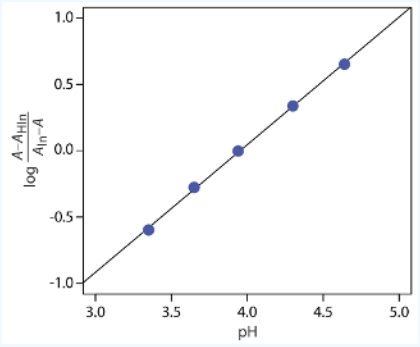
A plot of $\log[(A - A_{HIn})/(A_{In} - A)]$ versus pH is a straight-line with a slope of +1 and a *y*-intercept of $-\text{p}K_a$.

## Exercise 14.3.3

To determine the $K_a$ for the indicator bromothymol blue, the absorbance of each a series of solutions that contain the same concentration of bromothymol blue is measured at pH levels of 3.35, 3.65, 3.94, 4.30, and 4.64, yielding absorbance values of 0.170, 0.287, 0.411, 0.562, and 0.670, respectively. Acidifying the first solution to a pH of 2 changes its absorbance to 0.006, and adjusting the pH of the last solution to 12 changes its absorbance to 0.818. What is the value of $K_a$ for bromothymol blue? The data for this problem is from Patterson, G. S. *J. Chem. Educ.*, **1999**, *76*, 395–398.

**Answer**

To determine $K_a$ we use Equation 14.3.7, plotting $\log[(A - A_{HIn})/(A_{In} - A)]$ versus pH, as shown below.




Fitting a straight-line to the data gives a regression model of

$$\log \frac{A - A_{HIn}}{A_{In} - A} = -3.80 + 0.962\text{pH}$$

The *y*-intercept is $-\text{p}K_a$; thus, the p$K_a$ is 3.80 and the $K_a$ is $1.58 \times 10^{-4}$.

In developing these approaches for determining $K_a$ we considered a relatively simple system in which the absorbance of HIn and $In^-$ are easy to measure and for which it is easy to determine the concentration of $H_3O^+$. In addition to acid–base reactions, we can

adapt these approaches to any reaction of the general form

$$X(aq) + Y(aq) \rightleftharpoons Z(aq)$$

including metal–ligand complexation reactions and redox reactions, provided we can determine spectrophotometrically the concentration of the product, *Z*, and one of the reactants, either *X* or *Y*, and that we can determine the concentration of the other reactant by some other method. With appropriate modifications, a more complicated system in which we cannot determine the concentration of one or more of the reactants or products also is possible [Ramette, R. W. *Chemical Equilibrium and Analysis*, Addison-Wesley: Reading, MA, 1981, Chapter 13].

---

This page titled 14.3: Qualitative and Characterization Applications is shared under a CC BY-NC-SA 4.0 license and was authored, remixed, and/or curated by David Harvey.

# 14.4: Quantitative Applications

## Scope

The determination of an analyte's concentration based on its absorption of ultraviolet or visible radiation is one of the most frequently encountered quantitative analytical methods. One reason for its popularity is that many organic and inorganic compounds have strong absorption bands in the UV/Vis region of the electromagnetic spectrum. In addition, if an analyte does not absorb UV/Vis radiation—or if its absorbance is too weak—we often can react it with another species that is strongly absorbing. For example, a dilute solution of $Fe^{2+}$ does not absorb visible light. Reacting $Fe^{2+}$ with *o*-phenanthroline, however, forms an orange–red complex of $\mathrm{Fe(phen)}_3^{2+}$ that has a strong, broad absorbance band near 500 nm. An additional advantage to UV/Vis absorption is that in most cases it is relatively easy to adjust experimental and instrumental conditions so that Beer's law is obeyed.

### Environmental Applications

The analysis of waters and wastewaters often relies on the absorption of ultraviolet and visible radiation. Many of these methods are outlined in Table 14.4.1. Several of these methods are described here in more detail.

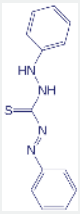
Table 14.4.1. Examples of Molecular UV/Vis Analysis of Waters and Wastewaters

| analyte | method | $\lambda$ (nm) |
|---|---|---|
| trace metals | | |
| aluminum | react with Eriochrome cyanide R dye at pH 6; forms red to pink complex | 535 |
| arsenic | reduce to $AsH_3$ using Zn and react with silver diethyldithiocarbamate; forms red complex | 535 |
| cadmium | extract into $CHCl_3$ containing dithizone from a sample made basic with NaOH; forms pink to red complex | 518 |
| chromium | oxidize to Cr(VI) and react with diphenylcarbazide; forms 540 red-violet product | 540 |
| copper | react with neocuprine in neutral to slightly acid solution and extract into $CHCl_3/CH_3OH$; forms yellow complex | 457 |
| iron | reduce to $Fe^{2+}$ and react with *o*-phenanthroline; forms orange-red complex | 510 |
| lead | extract into $CHCl_3$ containing dithizone from sample made basic with $NH_3$/ $NH_4^+$ buffer; forms cherry red complex | 510 |
| manganese | oxidize to $MnO_4^-$ with persulfate; forms purple solution | 525 |
| mercury | extract into $CHCl_3$ containing dithizone from acidic sample; forms orange complex | 492 |
| zinc | react with zincon at pH 9; forms blue complex | 620 |
| inorganic nonmetals | | |
| ammonia | reaction with hypochlorite and phenol using a manganous 630 salt catalyst; forms blue indophenol as product | 630 |
| cyanide | react with chloroamine-T to form CNCl and then with a pyridine-barbituric acid; forms a red-blue dye | 578 |
| fluoride | react with red Zr-SPADNS lake; formation of $ZrF_6^{2-}$ decreases color of the red lake | 570 |
| chlorine (residual) | react with leuco crystal violet; forms blue product | 592 |
| nitrate | react with Cd to form $NO_2^-$ and then react with sulfanilamide and *N*-(1-napthyl)-ethylenediamine; forms red azo 543 dye | 543 |
| phosphate | react with ammonium molybdate and then | 690 |

| analyte | method | λ (nm) |
|---|---|---|
| | reduce with $SnCl_2$; forms molybdenum blue | |
| organics | | |
| phenol | react with 4-aminoantipyrine and $K_3Fe(CN)_6$; forms yellow antipyrine dye | 460 |
| anionic surfactants | react with cationic methylene blue dye and extract into $CHCl_3$; forms blue ion pair | 652 |

Although the quantitative analysis of metals in waters and wastewaters is accomplished primarily by atomic absorption or atomic emission spectroscopy, many metals also can be analyzed following the formation of a colorful metal–ligand complex. One advantage to these spectroscopic methods is that they easily are adapted to the analysis of samples in the field using a filter photometer. One ligand used for the analysis of several metals is diphenylthiocarbazone, also known as dithizone. Dithizone is not soluble in water, but when a solution of dithizone in $CHCl_3$ is shaken with an aqueous solution that contains an appropriate metal ion, a colored metal–dithizonate complex forms that is soluble in $CHCl_3$. The selectivity of dithizone is controlled by adjusting the sample's pH. For example, $Cd^{2+}$ is extracted from solutions made strongly basic with NaOH, $Pb^{2+}$ from solutions made basic with an $NH_3$/ $NH_4^+$ buffer, and $Hg^{2+}$ from solutions that are slightly acidic.

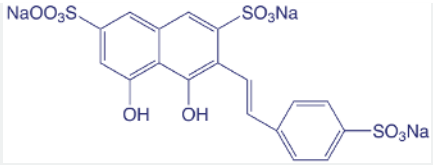
The structure of dithizone is shown below.



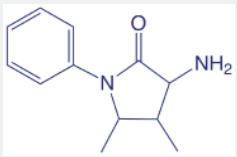

When chlorine is added to water the portion available for disinfection is called the chlorine residual. There are two forms of chlorine residual. The free chlorine residual includes $Cl_2$, HOCl, and $OCl^-$. The combined chlorine residual, which forms from the reaction of $NH_3$ with HOCl, consists of monochloramine, $NH_2Cl$, dichloramine, $NHCl_2$, and trichloramine, $NCl_3$. Because the free chlorine residual is more efficient as a disinfectant, there is an interest in methods that can distinguish between the total chlorine residual's different forms. One such method is the leuco crystal violet method. The free residual chlorine is determined by adding leuco crystal violet to the sample, which instantaneously oxidizes to give a blue-colored compound that is monitored at 592 nm. Completing the analysis in less than five minutes prevents a possible interference from the combined chlorine residual. The total chlorine residual (free + combined) is determined by reacting a separate sample with iodide, which reacts with both chlorine residuals to form HOI. When the reaction is complete, leuco crystal violet is added and oxidized by HOI, giving the same blue-colored product. The combined chlorine residual is determined by difference.

The concentration of fluoride in drinking water is determined indirectly by its ability to form a complex with zirconium. In the presence of the dye SPADNS, a solution of zirconium forms a red colored compound, called a lake, that absorbs at 570 nm. When fluoride is added, the formation of the stable $ZrF_6^{2-}$ complex causes a portion of the lake to dissociate, decreasing the absorbance. A plot of absorbance versus the concentration of fluoride, therefore, has a negative slope.

SPADNS, the structure of which is shown below, is an abbreviation for the sodium salt of 2-(4-sulfophenylazo)-1,8-dihydroxy-3,6-napthalenedisulfonic acid, which is a mouthful to say.




Spectroscopic methods also are used to determine organic constituents in water. For example, the combined concentrations of phenol and ortho- and meta-substituted phenols are determined by using steam distillation to separate the phenols from nonvolatile impurities. The distillate reacts with 4-aminoantipyrine at pH 7.9 ± 0.1 in the presence of $K_3Fe(CN)_6$ to a yellow colored antipyrine dye. After extracting the dye into $CHCl_3$, its absorbance is monitored at 460 nm. A calibration curve is prepared using only the unsubstituted phenol, $C_6H_5OH$. Because the molar absorptivity of substituted phenols generally are less than that for phenol, the reported concentration represents the minimum concentration of phenolic compounds.




4-aminoantipyrene

Molecular absorption also is used for the analysis of environmentally significant airborne pollutants. In many cases the analysis is carried out by collecting the sample in water, converting the analyte to an aqueous form that can be analyzed by methods such as those described in Table 14.4.1. For example, the concentration of $NO_2$ is determined by oxidizing $NO_2$ to $NO_3^-$. The concentration of $NO_3^-$ is then determined by first reducing it to $NO_2^-$ with Cd, and then reacting $NO_2^-$ with sulfanilamide and *N*-(1-naphthyl)-ethylenediamine to form a red azo dye. Another important application is the analysis for $SO_2$, which is determined by collecting the sample in an aqueous solution of $HgCl_4^{2-}$ where it reacts to form $Hg(SO_3)_2^{2-}$. Addition of *p*-rosaniline and formaldehyde produces a purple complex that is monitored at 569 nm. Infrared absorption is useful for the analysis of organic vapors, including HCN, $SO_2$, nitrobenzene, methyl mercaptan, and vinyl chloride. Frequently, these analyses are accomplished using portable, dedicated infrared photometers.

## Clinical Applications

The analysis of clinical samples often is complicated by the complexity of the sample's matrix, which may contribute a significant background absorption at the desired wavelength. The determination of serum barbiturates provides one example of how this problem is overcome. The barbiturates are first extracted from a sample of serum with $CHCl_3$ and then extracted from the $CHCl_3$ into 0.45 M NaOH (pH ≈ 13). The absorbance of the aqueous extract is measured at 260 nm, and includes contributions from the barbiturates as well as other components extracted from the serum sample. The pH of the sample is then lowered to approximately 10 by adding $NH_4Cl$ and the absorbance remeasured. Because the barbiturates do not absorb at this pH, we can use the absorbance at pH 10, $A_{\text{pH 10}}$, to correct the absor-ance at pH 13, $A_{\text{pH 13}}$

$$A_{\text{barb}} = A_{\text{pH 13}} - \frac{V_{\text{samp}} + V_{\text{NH}_4\text{Cl}}}{V_{\text{samp}}} \times A_{\text{pH 10}}$$

where $A_{\text{barb}}$ is the absorbance due to the serum barbiturates and $V_{\text{samp}}$ and $V_{\text{NH}_4\text{Cl}}$ are the volumes of sample and $NH_4Cl$, respectively. Table 14.4.2 provides a summary of several other methods for analyzing clinical samples.

Table 14.4.2. Examples of the Molecular UV/Vis Analysis of Clinical Samples

| analyte | method | $\lambda$ (nm) |
|---|---|---|
| total serum protein | react with NaOH and $Cu^{2+}$; forms blue-violet complex | 540 |
| serum cholesterol | react with $Fe^{3+}$ in presence of isopropanol, acetic acid, and $H_2SO_4$; forms blue-violet complex | 540 |
| uric acid | react with phosphotungstic acid; forms tungsten blue | 710 |
| serum barbituates | extract into $CHCl_3$ to isolate from interferents and then extract into 0.45 M NaOH | 260 |
| glucose | react with *o*-toludine at 100°C; forms blue-green complex | 630 |
| protein-bound iodine | decompose protein to release iodide, which catalyzes redox reaction between $Ce^{3+}$ and $As^{3+}$; forms yellow colored $Ce^{4+}$ | 420 |

### Industrial Applications

UV/Vis molecular absorption is used for the analysis of a diverse array of industrial samples including pharmaceuticals, food, paint, glass, and metals. In many cases the methods are similar to those described in Table 14.4.1 and in Table 14.4.2. For example, the amount of iron in food is determined by bringing the iron into solution and analyzing using the *o*-phenanthroline method listed in Table 14.4.1.

Many pharmaceutical compounds contain chromophores that make them suitable for analysis by UV/Vis absorption. Products analyzed in this fashion include antibiotics, hormones, vitamins, and analgesics. One example of the use of UV absorption is in determining the purity of aspirin tablets, for which the active ingredient is acetylsalicylic acid. Salicylic acid, which is produced by the hydrolysis of acetylsalicylic acid, is an undesirable impurity in aspirin tablets, and should not be present at more than 0.01% w/w. Samples are screened for unacceptable levels of salicylic acid by monitoring the absorbance at a wavelength of 312 nm. Acetylsalicylic acid absorbs at 280 nm, but absorbs poorly at 312 nm. Conditions for preparing the sample are chosen such that an absorbance of greater than 0.02 signifies an unacceptable level of salicylic acid.

### Forensic Applications

UV/Vis molecular absorption routinely is used for the analysis of narcotics and for drug testing. One interesting forensic application is the determination of blood alcohol using the Breathalyzer test. In this test a 52.5-mL breath sample is bubbled through an acidified solution of $K_2Cr_2O_7$, which oxidizes ethanol to acetic acid. The concentration of ethanol in the breath sample is determined by a decrease in the absorbance at 440 nm where the dichromate ion absorbs. A blood alcohol content of 0.10%, which is above the legal limit, corresponds to 0.025 mg of ethanol in the breath sample.

## Developing a Quantitative Method for a Single Component

To develop a quantitative analytical method, the conditions under which Beer's law is obeyed must be established. First, the most appropriate wavelength for the analysis is determined from an absorption spectrum. In most cases the best wavelength corresponds to an absorption maximum because it provides greater sensitivity and is less susceptible to instrumental limitations. Second, if the instrument has adjustable slits, then an appropriate slit width is chosen. The absorption spectrum also aids in selecting a slit width by choosing a width that is narrow enough to avoid instrumental limitaions to Beer's law, but wide enough to increase the throughput of source radiation. Finally, a calibration curve is constructed to determine the range of concentrations for which Beer's law is valid. Additional considerations that are important in any quantitative method are the effect of potential interferents and establishing an appropriate blank.

## Quantitative Analysis for a Single Sample

To determine the concentration of an analyte we measure its absorbance and apply Beer's law using any of the standardization methods described in Chapter 5. The most common methods are a normal calibration curve using external standards and the method of standard additions. A single point standardization also is possible, although we must first verify that Beer's law holds for the concentration of analyte in the samples and the standard.

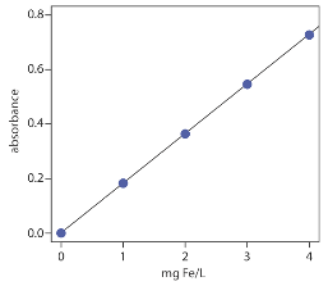
### Example 14.4.1

The determination of iron in an industrial waste stream is carried out by the *o*-phenanthroline described in Representative Method 10.3.1. Using the data in the following table, determine the mg Fe/L in the waste stream.

| mg Fe/L | absorbance |
|---|---|
| 0.00 | 0.000 |
| 1.00 | 0.183 |
| 2.00 | 0.364 |
| 3.00 | 0.546 |
| 4.00 | 0.727 |
| sample | 0.269 |

**Solution**

Linear regression of absorbance versus the concentration of Fe in the standards gives the calibration curve and calibration equation shown here




$$A = 0.0006 + \left(0.1817\ \text{mg}^{-1}\text{L}\right) \times (\text{mgFe/L})$$

Substituting the sample's absorbance into the calibration equation gives the concentration of Fe in the waste stream as 1.48 mg Fe/L

### Exercise 14.4.1

The concentration of $Cu^{2+}$ in a sample is determined by reacting it with the ligand cuprizone and measuring its absorbance at 606 nm in a 1.00-cm cell. When a 5.00-mL sample is treated with cuprizone and diluted to 10.00 mL, the resulting solution has an absorbance of 0.118. A second 5.00-mL sample is mixed with 1.00 mL of a 20.00 mg/L standard of $Cu^{2+}$, treated with cuprizone and diluted to 10.00 mL, giving an absorbance of 0.162. Report the mg $Cu^{2+}$/L in the sample.

**Answer**

For this standard addition we write equations that relate absorbance to the concentration of $Cu^{2+}$ in the sample before the standard addition

$$0.118 = \varepsilon b \left[C_{\text{Cu}} \times \frac{5.00\ \text{mL}}{10.00\ \text{mL}}\right]$$

and after the standard addition

$$0.162 = \varepsilon b \left( C_{Cu} \times \frac{5.00 \text{ mL}}{10.00 \text{ mL}} + \frac{20.00 \text{ mg Cu}}{\text{L}} \times \frac{1.00 \text{ mL}}{10.00 \text{ mL}} \right)$$

in each case accounting for the dilution of the original sample and for the standard. The value of $\varepsilon b$ is the same in both equation. Solving each equation for $\varepsilon b$ and equating

$$\frac{0.162}{C_{Cu} \times \frac{5.00 \text{ mL}}{10.00 \text{ mL}} + \frac{20.00 \text{ mg Cu}}{\text{L}} \times \frac{1.00 \text{ mL}}{10.00 \text{ mL}}} = \frac{0.118}{C_{Cu} \times \frac{5.00 \text{ mL}}{10.00 \text{ mL}}}$$

leaves us with an equation in which $C_{Cu}$ is the only variable. Solving for $C_{Cu}$ gives its value as

$$\frac{0.162}{0.500 \times C_{Cu} + 2.00 \text{ mg Cu/L}} = \frac{0.118}{0.500 \times C_{Cu}}$$

$$0.0810 \times C_{Cu} = 0.0590 \times C_{Ca} + 0.236 \text{ mg Cu/L}$$

$$0.0220 \times C_{Cu} = 0.236 \text{ mg Cu/L}$$

$$C_{Cu} = 10.7 \text{ mg Cu/L}$$

## Quantitative Analysis of Mixtures

Suppose we need to determine the concentration of two analytes, *X* and *Y*, in a sample. If each analyte has a wavelength where the other analyte does not absorb, then we can proceed using the approach in Example 14.4.1 . Unfortunately, UV/Vis absorption bands are so broad that frequently it is not possible to find suitable wavelengths. Because Beer's law is additive the mixture's absorbance, $A_{mix}$, is

$$(A_{mix})_{\lambda_1} = (\varepsilon_x)_{\lambda_1} bC_X + (\varepsilon_Y)_{\lambda_1} bC_Y \tag{14.4.1}$$

where $\lambda_1$ is the wavelength at which we measure the absorbance. Because Equation 14.4.1 includes terms for the concentration of both *X* and *Y*, the absorbance at one wavelength does not provide enough information to determine either $C_X$ or $C_Y$. If we measure the absorbance at a second wavelength

$$(A_{mix})_{\lambda_2} = (\varepsilon_x)_{\lambda_2} bC_X + (\varepsilon_Y)_{\lambda_2} bC_Y \tag{14.4.2}$$

then we can determine $C_X$ and $C_Y$ by solving simultaneously Equation 14.4.1 and Equation 14.4.2. Of course, we also must determine the value for $\varepsilon_X$ and $\varepsilon_Y$ at each wavelength. For a mixture of *n* components, we must measure the absorbance at *n* different wavelengths.

### Example 14.4.2

The concentrations of $Fe^{3+}$ and $Cu^{2+}$ in a mixture are determined following their reaction with hexacyanoruthenate (II), $Ru(CN)_6^{4-}$, which forms a purple-blue complex with $Fe^{3+}$ ($\lambda_{max}$ = 550 nm) and a pale-green complex with $Cu^{2+}$ ($\lambda_{max}$ = 396 nm) [DiTusa, M. R.; Schlit, A. A. *J. Chem. Educ.* **1985**, *62*, 541–542]. The molar absorptivities ($M^{-1}$ $cm^{-1}$) for the metal complexes at the two wavelengths are summarized in the following table.

| analyte | $\varepsilon_{550}$ | $\varepsilon_{396}$ |
|---|---|---|
| $Fe^{3+}$ | 9970 | 84 |
| $Cu^{2+}$ | 34 | 856 |

When a sample that contains $Fe^{3+}$ and $Cu^{2+}$ is analyzed in a cell with a pathlength of 1.00 cm, the absorbance at 550 nm is 0.183 and the absorbance at 396 nm is 0.109. What are the molar concentrations of $Fe^{3+}$ and $Cu^{2+}$ in the sample?

**Solution**

Substituting known values into Equation 14.4.1 and Equation 14.4.2 gives

$$A_{550} = 0.183 = 9970C_{Fe} + 34C_{Cu}$$
$$A_{396} = 0.109 = 84C_{Fe} + 856C_{Cu}$$

To determine $C_{Fe}$ and $C_{Cu}$ we solve the first equation for $C_{Cu}$

$$C_{Cu} = \frac{0.183 - 9970C_{Fe}}{34}$$

and substitute the result into the second equation.

$$0.109 = 84C_{Fe} + 856 \times \frac{0.183 - 9970C_{Fe}}{34}$$
$$= 4.607 - \left(2.51 \times 10^{5}\right) C_{Fe}$$

Solving for $C_{Fe}$ gives the concentration of $Fe^{3+}$ as $1.8 \times 10^{-5}$ M. Substituting this concentration back into the equation for the mixture's absorbance at 396 nm gives the concentration of $Cu^{2+}$ as $1.3 \times 10^{-4}$ M.

Another approach to solving Example 14.4.2 is to multiply the first equation by 856/34 giving

$$4.607 = 251009C_{Fe} + 856C_{Cu}$$

Subtracting the second equation from this equation

$$4.607 = 251009C_{Fe} + 856C_{Cu}$$
$$-0.109 = 84C_{Fe} + 856C_{Cu}$$

gives

$$4.498 = 250925C_{Fe}$$

and we find that $C_{Fe}$ is $1.8 \times 10^{-5}$. Having determined $C_{Fe}$ we can substitute back into one of the other equations to solve for $C_{Cu}$, which is $1.3 \times 10^{-5}$.

## ? Exercise 14.4.2

The absorbance spectra for $Cr^{3+}$ and $Co^{2+}$ overlap significantly. To determine the concentration of these analytes in a mixture, its absorbance is measured at 400 nm and at 505 nm, yielding values of 0.336 and 0.187, respectively. The individual molar absorptivities ($M^{-1}$ $cm^{-1}$) for $Cr3^{+}$ are 15.2 at 400 nm and 0.533 at 505 nm; the values for $Co^{2+}$ are 5.60 at 400 nm and 5.07 at 505 nm.

**Answer**

Substituting into Equation 14.4.1 and Equation 14.4.2 gives

$$A_{400} = 0.336 = 15.2C_{Cr} + 5.60C_{Co}$$

$$A_{400} = 0187 = 0.533C_{Cr} + 5.07C_{Co}$$

To determine $C_{Cr}$ and $C_{Co}$ we solve the first equation for $C_{Co}$

$$C_{Co} = \frac{0.336 - 15.2C_{Co}}{5.60}$$

and substitute the result into the second equation.

$$0.187 = 0.533C_{Cr} + 5.07 \times \frac{0.336 - 15.2C_{Co}}{5.60}$$

$$0.187 = 0.3042 - 13.23C_{Cr}$$

Solving for $C_{Cr}$ gives the concentration of $Cr^{3+}$ as $8.86 \times 10^{-3}$ M. Substituting this concentration back into the equation for the mixture's absorbance at 400 nm gives the concentration of $Co^{2+}$ as $3.60 \times 10^{-2}$ M.

To obtain results with good accuracy and precision the two wavelengths should be selected so that $\varepsilon_X > \varepsilon_Y$ at one wavelength and $\varepsilon_X < \varepsilon_Y$ at the other wavelength. It is easy to appreciate why this is true. Because the absorbance at each wavelength is dominated by one analyte, any uncertainty in the concentration of the other analyte has less of an impact. Figure 14.4.*q* shows that the choice of wavelengths for Practice Exercise 14.4.2 are reasonable. When the choice of wavelengths is not obvious, one method for locating the optimum wavelengths is to plot $\varepsilon_X/\varepsilon_y$ as function of wavelength, and determine the wavelengths where $\varepsilon_X/\varepsilon_y$ reaches maximum and minimum values [Mehra, M. C.; Rioux, J. *J. Chem. Educ.* **1982**, *59*, 688–689].

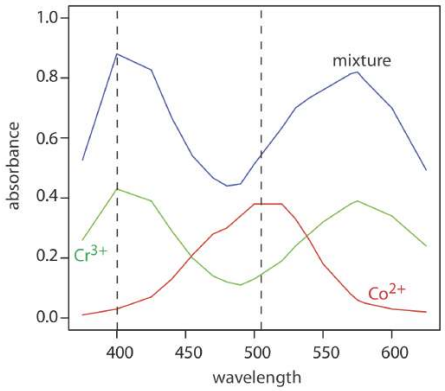



Figure 14.4.1. Visible absorption spectra for 0.0250 M $Cr^{3+}$, 0.0750 M $Co^{2+}$, and for a mixture of $Cr^{3+}$ and $Co^{2+}$. The two wavelengths used to analyze the mixture of $Cr^{3+}$ and $Co^{2+}$ are shown by the dashed lines. The data for the two standards are from Brewer, S. *Solving Problems in Analytical Chemistry*, John Wiley & Sons: New York, 1980.

When the analyte's spectra overlap severely, such that $\varepsilon_X \approx \varepsilon_Y$ at all wavelengths, other computational methods may provide better accuracy and precision. In a multiwavelength linear regression analysis, for example, a mixture's absorbance is compared to that for a set of standard solutions at several wavelengths [Blanco, M.; Iturriaga, H.; Maspoch, S.; Tarin, P. *J. Chem. Educ.* **1989**, *66*, 178–180]. If $A_{SX}$ and $A_{SY}$ are the absorbance values for standard solutions of components *X* and *Y* at any wavelength, then

$$A_{SX} = \varepsilon_X b C_{SX} \tag{14.4.3}$$

$$A_{SY} = \varepsilon_Y b C_{SY} \tag{14.4.4}$$

where $C_{SX}$ and $C_{SY}$ are the known concentrations of *X* and *Y* in the standard solutions. Solving Equation 14.4.3 and Equation 14.4.4 for $\varepsilon_X$ and for $\varepsilon_Y$, substituting into Equation 14.4.1, and rearranging, gives

$$\frac{A_{\text{mix}}}{A_{SX}} = \frac{C_X}{C_{SX}} + \frac{C_Y}{C_{SY}} \times \frac{A_{SY}}{A_{SX}}$$

To determine $C_X$ and $C_Y$ the mixture's absorbance and the absorbances of the standard solutions are measured at several wavelengths. Graphing $A_{\text{mix}}/A_{SX}$ versus $A_{SY}/A_{SX}$ gives a straight line with a slope of $C_Y/C_{SY}$ and a *y*-intercept of $C_X/C_{SX}$. This approach is particularly helpful when it is not possible to find wavelengths where $\varepsilon_X > \varepsilon_Y$ and $\varepsilon_X < \varepsilon_Y$.

The approach outlined here for a multiwavelength linear regression uses a single standard solution for each analyte. A more rigorous approach uses multiple standards for each analyte. The math behind the analysis of such data—which we call a multiple linear regression—is beyond the level of this text. For more details about multiple linear regression see Brereton, R. G. *Chemometrics: Data Analysis for the Laboratory and Chemical Plant*, Wiley: Chichester, England, 2003.

## Example 14.4.3

Figure 14.4.1 shows visible absorbance spectra for a standard solution of 0.0250 M $Cr^{3+}$, a standard solution of 0.0750 M $Co^{2+}$, and a mixture that contains unknown concentrations of each ion. The data for these spectra are shown here.

| λ (nm) | $A_{Cr}$ | $A_{Cu}$ | $A_{mix}$ | λ (nm) | $A_{Cr}$ | $A_{Cu}$ | $A_{mix}$ |
|---|---|---|---|---|---|---|---|
| 375 | 0.26 | 0.01 | 0.53 | 520 | 0.19 | 0.38 | 0.63 |
| 400 | 0.43 | 0.03 | 0.88 | 530 | 0.24 | 0.33 | 0.70 |
| 425 | 0.39 | 0.07 | 0.83 | 540 | 0.28 | 0.26 | 0.73 |
| 440 | 0.29 | 0.13 | 0.67 | 550 | 0.32 | 0.18 | 0.76 |
| 455 | 0.20 | 0.21 | 0.54 | 570 | 0.38 | 0.08 | 0.81 |
| 470 | 0.14 | 0.28 | 0.47 | 575 | 0.39 | 0.06 | 0.82 |
| 480 | 0.12 | 0.30 | 0.44 | 580 | 0.38 | 0.05 | 0.79 |
| 490 | 0.11 | 0.34 | 0.45 | 600 | 0.34 | 0.03 | 0.70 |
| 500 | 0.13 | 0.38 | 0.51 | 625 | 0.24 | 0.02 | 0.49 |

Use a multiwavelength regression analysis to determine the composition of the unknown.

### Solution

First we need to calculate values for $A_{mix}/A_{SX}$ and for $A_{SY}/A_{SX}$. Let's define $X$ as $Co^{2+}$ and $Y$ as $Cr^{3+}$. For example, at a wavelength of 375 nm $A_{mix}/A_{SX}$ is 0.53/0.01, or 53 and $A_{SY}/A_{SX}$ is 0.26/0.01, or 26. Completing the calculation for all wavelengths and graphing $A_{mix}/A_{SX}$ versus $A_{SY}/A_{SX}$ gives the calibration curve shown in Figure 14.4.2. Fitting a straight-line to the data gives a regression model of

$$\frac{A_{mix}}{A_{SX}} = 0.636 + 2.01 \times \frac{A_{SY}}{A_{SX}}$$

Using the *y*-intercept, the concentration of $Co^{2+}$ is

$$\frac{C_X}{C_{SX}} = \frac{[Co^{2+}]}{0.0750 M} = 0.636$$

or $[Co^{2+}]$ = 0.048 M; using the slope the concentration of $Cr^{3+}$ is

$$\frac{C_Y}{C_{SY}} = \frac{[Cr^{3+}]}{0.0250 M} = 2.01$$

or $[Cr^{3+}]$ = 0.050 M.

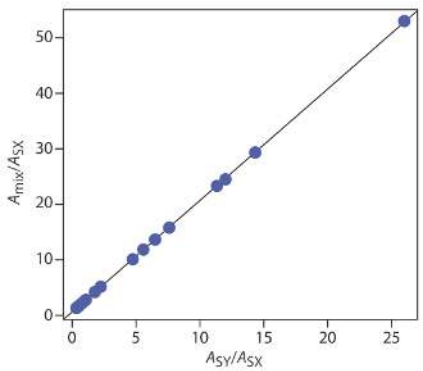



Figure 14.4.2. Multiwavelength linear regression analysis for the data in Example 14.4.3 .

## Exercise 14.4.3


https://chem.libretexts.org/@go/page/365739

A mixture of $MnO_4^-$ and $Cr_2O_7^{2-}$, and standards of 0.10 mM $KMnO_4$ and of 0.10 mM $K_2Cr_2O_7$ give the results shown in the following table. Determine the composition of the mixture. The data for this problem is from Blanco, M. C.; Iturriaga, H.; Maspoch, S.; Tarin, P. *J. Chem. Educ.* **1989**, *66*, 178–180.

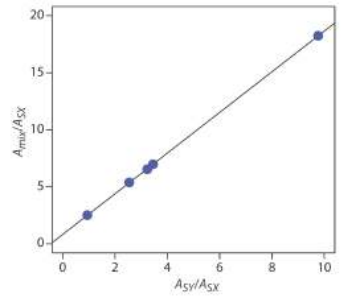
| λ (nm) | $A_{Mn}$ | $A_{Cr}$ | $A_{mix}$ |
|---|---|---|---|
| 266 | 0.042 | 0.410 | 0.766 |
| 288 | 0.082 | 0.283 | 0.571 |
| 320 | 0.168 | 0.158 | 0.422 |
| 350 | 0.125 | 0.318 | 0.672 |
| 360 | 0.036 | 0.181 | 0.366 |

**Answer**

Letting *X* represent $MnO_4^-$ and letting *Y* represent $Cr_2O_7^{2-}$, we plot the equation

$$\frac{A_{mix}}{A_{SX}} = \frac{C_X}{C_{SX}} + \frac{C_Y}{C_{SY}} \times \frac{A_{SY}}{A_{SX}}$$

placing $A_{mix}/A_{SX}$ on the *y*-axis and $A_{SY}/A_{SX}$ on the *x*-axis. For example, at a wavelength of 266 nm the value $A_{mix}/A_{SX}$ of is 0.766/0.042, or 18.2, and the value of $A_{SY}/A_{SX}$ is 0.410/0.042, or 9.76. Completing the calculations for all wavelengths and plotting the data gives the result shown here




Fitting a straight-line to the data gives a regression model of

$$\frac{A_{\text{mix}}}{A_{\text{SX}}} = 0.8147 + 1.7839 \times \frac{A_{SY}}{A_{SX}}$$

Using the *y*-intercept, the concentration of $MnO_4^-$ is

$$\frac{C_X}{C_{SX}} = 0.8147 = \frac{[MnO_4^-]}{1.0 \times 10^{-4}\ \text{M}\ MnO_4^-}$$

or $8.15 \times 10^{-5}$ M $MnO_4^-$, and using the slope, the concentration of $Cr_2O_7^{2-}$ is

$$\frac{C_Y}{C_{SY}} = 1.7839 = \frac{[Cr_2O_7^{2-}]}{1.00 \times 10^{-4}\ \text{M}\ Cr_2O_7^{2-}}$$

or $1.78 \times 10^{-4}$ M $Cr_2O_7^{2-}$.

## Derivative Spectroscopy

Sometimes our signal is superimposed on a background signal, which complicates our analysis because the measure absorbance has contributions from both our analyte and from the background. For example, the following figure shows a Gaussian signal with a maximum value of 50 centered at $x = 125$ that is superimposed on an exponential background. The dotted line is the Gaussian

signal, which has a maximum value of 50 at $x = 125$, and the solid line is the signal as measured, which has a maximum value of 57 at $x = 125$.

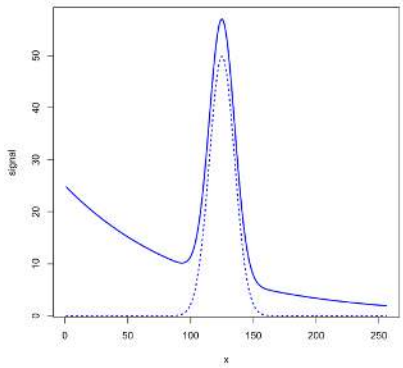



Figure 14.4.3: A Gaussian signal (dotted line) superimposed on an exponential background, which gives rise to the measured signal (solid line).

If the background signal is consistent across all samples, then we can analyze the data without first removing its contribution. For example, the following figure shows a set of calibration standards and their resulting calibration curve, for which the *y*-intercept of 7 gives the offset introduced by the background.

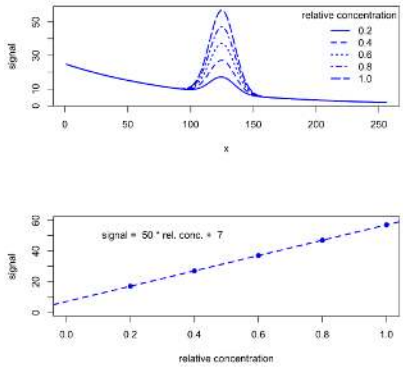



Figure 14.4.4: When the background is the same for all calibration standards and samples, then we can construct a calibration curve without taking into account the presence of the background.

But background signals often are not consistent across samples, particularly when the source of the background is a property of the samples we collect (natural water samples, for example, may have variations in color due to differences in the concentration of dissolved organic matter) or a property of the instrument we are using (such as a variation in source intensity over time). When true, our data may look more like what we see in the following figure, which leads to a calibration curve with a greater uncertainty.

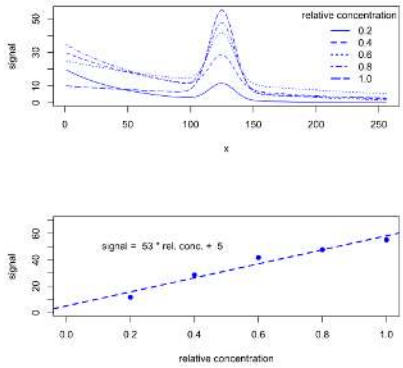



Figure 14.4.5: When the background is not the same for all calibration standards, the quality of the calibration curves suffers, making it less useful for the analysis of samples.

Because the background changes gradually with the values for *x* while the analyte's signal changes quickly, we can use a derivative to the distinguish between the two. One approach is to calculate and plot the derivative, $\frac{\Delta y}{\Delta x}$, as a function of $x$, as shown in Figure 14.4.6. The calibration signal in this case is the difference between the maximum signal and the minimum signal, which are shown by the dotted red lines in the top part of the figure. The fit of the calibration curve to the data and the calibration curve's *y*-intercept of zero shows that we have successfully compensated for the background signals.

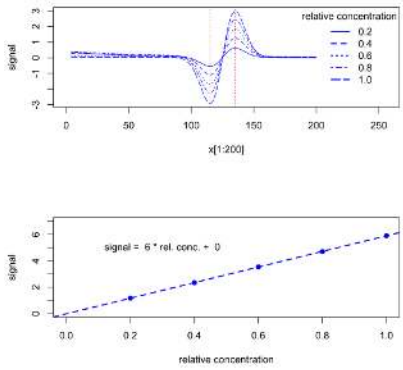



Figure 14.4.6: Taking the derivative of the data in Figure 14.4.5 removes the background signal.

This page titled 14.4: Quantitative Applications is shared under a CC BY-NC-SA 4.0 license and was authored, remixed, and/or curated by David Harvey.

# 14.5: Photometric Titrations

If at least one species in a titration absorbs electromagnetic radiation, then we can identify the end point by monitoring the titrand's absorbance at a carefully selected wavelength. For example, we can identify the end point for a titration of $Cu^{2+}$ with EDTA in the presence of $NH_3$ by monitoring the titrand's absorbance at a wavelength of 745 nm, where the $Cu(NH_3)_2^{4+}$ complex absorbs strongly. At the beginning of the titration the absorbance is at a maximum. As we add EDTA, however, the reaction

$$Cu(NH_3)_4^{2+}(aq) + Y^{4-} \rightleftharpoons CuY^{2-}(aq) + 4NH_3(aq)$$

decreases the concentration of $Cu(NH_3)_2^{4+}$ and decreases the absorbance until we reach the equivalence point. After the equivalence point the absorbance essentially remains unchanged. The resulting spectrophotometric titration curve is shown in Figure $14.5.1a$. Note that the titration curve's *y*-axis is not the measured absorbance, $A_{meas}$, but a corrected absorbance, $A_{corr}$

$$A_{corr} = A_{meas} \times \frac{V_{EDTA} + V_{Cu}}{V_{Cu}}$$

where $V_{EDTA}$ and $V_{Cu}$ are, respectively, the volumes of EDTA and Cu. Correcting the absorbance for the titrand's dilution ensures that the spectrophotometric titration curve consists of linear segments that we can extrapolate to find the end point. Other common spectrophotometric titration curves are shown in Figures $14.5.1b-f$.

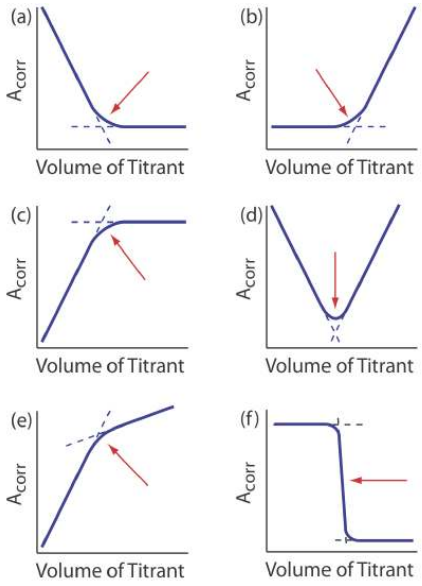



Figure 14.5.1. Examples of spectrophotometric titration curves: (a) only the titrand absorbs; (b) only the titrant absorbs; (c) only the product of the titration reaction absorbs; (d) both the titrand and the titrant absorb; (e) both the titration reaction's product and the titrant absorb; (f ) only the indicator absorbs. The red arrows indicate the end points for each titration curve.

This page titled 14.5: Photometric Titrations is shared under a CC BY-NC-SA 4.0 license and was authored, remixed, and/or curated by David Harvey.

# CHAPTER OVERVIEW

## 15: Molecular Luminescence


15.1: Theory of Fluorescence and Phosphorescence

15.2: Instruments for Measuring Fluorescence and Phosphorescence

15.3: Applications and Photoluminescence methods

15.4: Chemiluminscence

15.5: Evaluation of Molecular Luminescence


---


This page titled 15: Molecular Luminescence is shared under a CC BY-NC-SA 4.0 license and was authored, remixed, and/or curated by David Harvey.

# 15.1: Theory of Fluorescence and Phosphorescence

The use of molecular fluorescence for qualitative analysis and for semi-quantitative analysis dates to the early to mid 1800s, with more accurate quantitative methods appearing in the 1920s. Instrumentation for fluorescence spectroscopy using a filter or a monochromator for wavelength selection appeared in, respectively, the 1930s and 1950s. Although the discovery of phosphorescence preceded that of fluorescence by almost 200 years, qualitative and quantitative applications of molecular phosphorescence did not receive much attention until after the development of fluorescence instrumentation.

## Source of Fluorescence and Phosphorescence

Photoluminescence is divided into two categories: fluorescence and phosphorescence. A pair of electrons that occupy the same electronic ground state have opposite spins and are in a singlet spin state (Figure 15.1.1*a*).

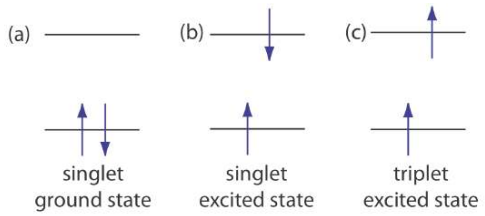



Figure 15.1.1*a*. Electron configurations for (a) a singlet ground state; (b) a singlet excited state; and (c) a triplet excited state.

When an analyte absorbs an ultraviolet or a visible photon, one of its valence electrons moves from the ground state to an excited state with a conservation of the electron's spin (Figure 15.1.1*b*). Emission of a photon from a singlet excited state to the singlet ground state—or between any two energy levels with the same spin—is called fluorescence. The probability of fluorescence is very high and the average lifetime of an electron in the excited state is only $10^{-5}$–$10^{-8}$ s. Fluorescence, therefore, rapidly decays once the source of excitation is removed.

In some cases an electron in a singlet excited state is transformed to a triplet excited state (Figure 15.1.1*c*) in which its spin no is longer paired with the ground state. Emission between a triplet excited state and a singlet ground state—or between any two energy levels that differ in their respective spin states–is called phosphorescence. Because the average lifetime for phosphorescence can be quite long—it ranges from $10^{-4}$–$10^{4}$ seconds—phosphorescence may continue for some time after we remove the excitation source.

To appreciate the origin of fluorescence and phosphorescence we must consider what happens to a molecule following the absorption of a photon. Let's assume the molecule initially occupies the lowest vibrational energy level of its electronic ground state, which is the singlet state labeled $S_0$ in Figure 15.1.2. Absorption of a photon excites the molecule to one of several vibrational energy levels in the first excited electronic state, $S_1$, or the second electronic excited state, $S_2$, both of which are singlet states. Relaxation to the ground state occurs by a number of mechanisms, some of which result in the emission of a photon and others that occur without the emission of a photon. These relaxation mechanisms are shown in Figure 15.1.2. The most likely relaxation pathway from any excited state is the one with the shortest lifetime.

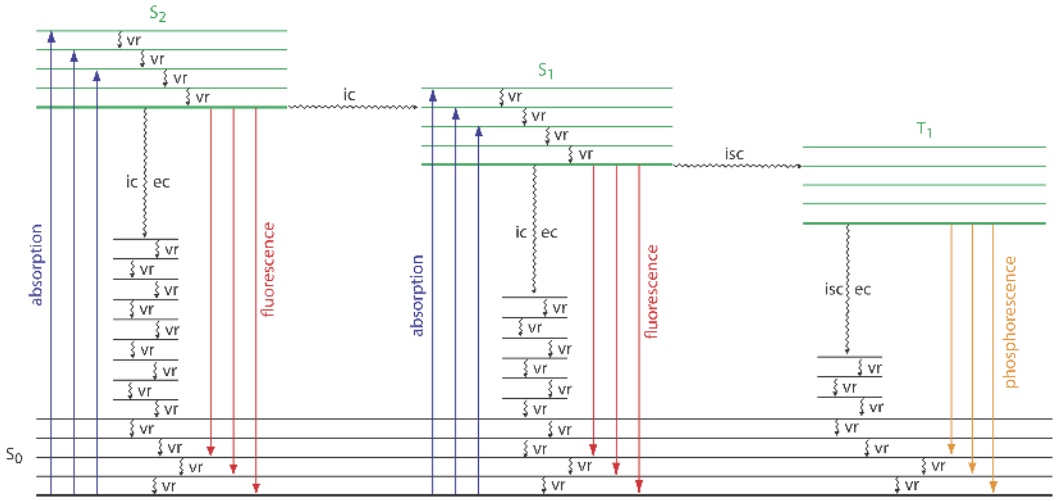



Figure 15.1.2. Energy level diagram for a molecule that shows pathways for the deactivation of an excited state: ***vr*** is vibrational relaxation; ***ic*** is internal conversion; ***ec*** is external conversion; and ***isc*** is an intersystem crossing. The lowest vibrational energy for each electronic state is indicated by the thicker line. The electronic ground state is shown in black and the three electronic excited states are shown in green. The absorption, fluorescence, and phosphorescence of photons also are shown.

## Deactivation Processes

A molecule in an excited state can return to its ground state in a variety of ways that we collectively call deactivation processes.

### Radiationless Deactivation

When a molecule relaxes without emitting a photon we call the process radiationless deactivation. One example of radiationless deactivation is vibrational relaxation, in which a molecule in an excited vibrational energy level loses energy by moving to a lower vibrational energy level in the same electronic state. Vibrational relaxation is very rapid, with an average lifetime of $<10^{-12}$ s. Because vibrational relaxation is so efficient, a molecule in one of its excited state's higher vibrational energy levels quickly returns to the excited state's lowest vibrational energy level.

Another form of radiationless deactivation is an internal conversion in which a molecule in the ground vibrational level of an excited state passes directly into a higher vibrational energy level of a lower energy electronic state of the same spin state. By a combination of internal conversions and vibrational relaxations, a molecule in an excited electronic state may return to the ground electronic state without emitting a photon. A related form of radiationless deactivation is an external conversion in which excess energy is transferred to the solvent or to another component of the sample's matrix.

> Let's use Figure 15.1.2 to illustrate how a molecule can relax back to its ground state without emitting a photon. Suppose our molecule is in the highest vibrational energy level of the second electronic excited state. After a series of vibrational relaxations brings the molecule to the lowest vibrational energy level of $S_2$, it undergoes an internal conversion into a higher vibrational energy level of the first excited electronic state. Vibrational relaxations bring the molecule to the lowest vibrational energy level of $S_1$. Following an internal conversion into a higher vibrational energy level of the ground state, the molecule continues to undergo vibrational relaxation until it reaches the lowest vibrational energy level of $S_0$.

A final form of radiationless deactivation is an intersystem crossing in which a molecule in the ground vibrational energy level of an excited electronic state passes into one of the higher vibrational energy levels of a lower energy electronic state with a different spin state. For example, an intersystem crossing is shown in Figure 15.1.2 between the singlet excited state $S_1$ and the triplet excited state $T_1$.

## Variables that Affect Fluorescence

Fluorescence occurs when a molecule in an excited state's lowest vibrational energy level returns to a lower energy electronic state by emitting a photon. Because molecules return to their ground state by the fastest mechanism, fluorescence is observed only if it is a more efficient means of relaxation than a combination of internal conversions and vibrational relaxations.

A quantitative expression of fluorescence efficiency is the fluorescent quantum yield, $\Phi_f$, which is the fraction of excited state molecules that return to the ground state by fluorescence. The fluorescent quantum yields range from 1 when every molecule in an excited state undergoes fluorescence, to 0 when fluorescence does not occur.

The intensity of fluorescence, $I_f$, is proportional to the amount of radiation absorbed by the sample, $P_0 - P_T$, and the **fluorescence quantum yield**

$$I_f = k\Phi_f (P_0 - P_T) \tag{15.1.1}$$

where $k$ is a constant that accounts for the efficiency of collecting and detecting the fluorescent emission. From Beer's law we know that

$$\frac{P_T}{P_0} = 10^{-\varepsilon bC} \tag{15.1.2}$$

where $C$ is the concentration of the fluorescing species. Solving Equation 15.1.2 for $P_T$ and substituting into Equation 15.1.1 gives, after simplifying

$$I_f = k\Phi_f P_0 \left(1 - 10^{-\varepsilon bC}\right) \tag{15.1.3}$$

When $\varepsilon bC < 0.01$, which often is the case when the analyte's concentration is small, Equation 15.1.3 simplifies to

$$I_f = 2.303k\Phi_f \varepsilon bCP_0 = k'P_0 \tag{15.1.4}$$

where $k'$ is a collection of constants. The intensity of fluorescence, therefore, increases with an increase in the quantum efficiency, the source's incident power, and the molar absorptivity and the concentration of the fluorescing species.

Fluorescence generally is observed when the molecule's lowest energy absorption is a $\pi \rightarrow \pi^*$ transition, although some $n \rightarrow \pi^*$ transitions show weak fluorescence. Many unsubstituted, nonheterocyclic aromatic compounds have a favorable fluorescence quantum yield, although substitutions on the aromatic ring can effect $\Phi_f$ significantly. For example, the presence of an electron-withdrawing group, such as $-NO_2$, decreases $\Phi_f$, while adding an electron-donating group, such as –OH, increases $\Phi_f$. Fluorrescence also increases for aromatic ring systems and for aromatic molecules with rigid planar structures. Figure 15.1.3 shows the fluorescence of quinine under a UV lamp.




Figure 15.1.3. Tonic water, which contains quinine, is fluorescent when placed under a UV lamp. Source: Splarka (commons.Wikipedia.org).

A molecule's fluorescent quantum yield also is influenced by external variables, such as temperature and solvent. Increasing the temperature generally decreases $\Phi_f$ because more frequent collisions between the molecule and the solvent increases external conversion. A decrease in the solvent's viscosity decreases $\Phi_f$ for similar reasons. For an analyte with acidic or basic functional groups, a change in pH may change the analyte's structure and its fluorescent properties.

As shown in Figure 15.1.3, fluorescence may return the molecule to any of several vibrational energy levels in the ground electronic state. Fluorescence, therefore, occurs over a range of wavelengths. Because the change in energy for fluorescent emission generally

is less than that for absorption, a molecule's fluorescence spectrum is shifted to higher wavelengths than its absorption spectrum.

## Variables that Affect Phosphorescence

A molecule in a triplet electronic excited state's lowest vibrational energy level normally relaxes to the ground state by an intersystem crossing to a singlet state or by an external conversion. Phosphorescence occurs when the molecule relaxes by emitting a photon. As shown in Figure 15.1.2, phosphorescence occurs over a range of wavelengths, all of which are at lower energies than the molecule's absorption band. The intensity of phosphorescence, $I_p$, is given by an equation similar to Equation 15.1.4 for fluorescence

$$\begin{aligned} I_P &= 2.303k\Phi_P\varepsilon bCP_0 \\ &= k'P_0 \end{aligned} \tag{15.1.5}$$

where $\Phi_p$ is the **phosphorescence quantum yield**.

Phosphorescence is most favorable for molecules with $n \rightarrow \pi^*$ transitions, which have a higher probability for an intersystem crossing than $\pi \rightarrow \pi^*$ transitions. For example, phosphorescence is observed with aromatic molecules that contain carbonyl groups or heteroatoms. Aromatic compounds that contain halide atoms also have a higher efficiency for phosphorescence. In general, an increase in phosphorescence corresponds to a decrease in fluorescence.

Because the average lifetime for phosphorescence can be quite long, ranging from $10^{-4}$–$10^4$ s, the phosphorescent quantum yield usually is quite small. An improvement in $\Phi_p$ is realized by decreasing the efficiency of external conversion. This is accomplished in several ways, including lowering the temperature, using a more viscous solvent, depositing the sample on a solid substrate, or trapping the molecule in solution. Figure 15.1.4 shows an example of phosphorescence.

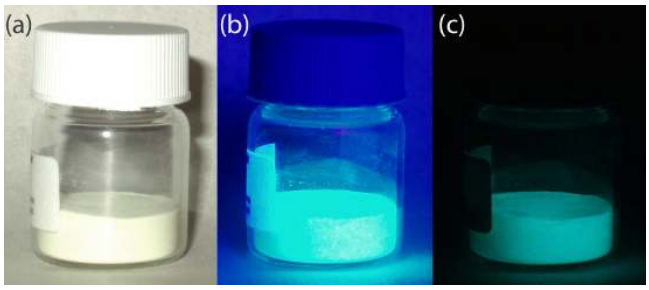



Figure 15.1.4. An europium doped strontium silicate-aluminum oxide powder under (a) natural light, (b) a long-wave UV lamp, and (c) in total darkness. The photo taken in total darkness shows the phosphorescent emission. Source: modified from Splarka (commons.Wikipedia.org).

## Emission and Excitation Spectra

Photoluminescence spectra are recorded by measuring the intensity of emitted radiation as a function of either the excitation wavelength or the emission wavelength. An excitation spectrum is obtained by monitoring emission at a fixed wavelength while varying the excitation wavelength. When corrected for variations in the source's intensity and the detector's response, a sample's excitation spectrum is nearly identical to its absorbance spectrum. The excitation spectrum provides a convenient means for selecting the best excitation wavelength for a quantitative or qualitative analysis.

In an emission spectrum a fixed wavelength is used to excite the sample and the intensity of emitted radiation is monitored as function of wavelength. Although a molecule has a single excitation spectrum, it has two emission spectra, one for fluorescence and one for phosphorescence. Figure 15.1.5 shows the UV absorption spectrum and the UV fluorescence emission spectrum for quinine.

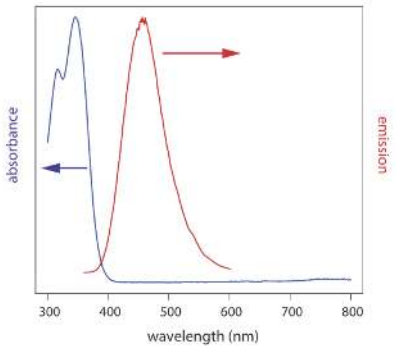



Figure 15.1.5. Absorbance spectrum and fluorescence emission spectrum for quinine in 0.05 M $H_2SO_4$. The emission spectrum uses an excitation wavelength of 350 nm with a bandwidth of 20 nm. Both spectra are normalized so that the maximum absorbance is 1.00 and the maximum emission is 1.00. The actual maximum absorbance is 0.444 and the actual maximum emission is 126747. Source: data from Daniel Scott, Department of Chemistry & Biochemistry, DePauw University.

This page titled 15.1: Theory of Fluorescence and Phosphorescence is shared under a CC BY-NC-SA 4.0 license and was authored, remixed, and/or curated by David Harvey.

# 15.2: Instruments for Measuring Fluorescence and Phosphorescence

## Instrumentation

The basic instrumentation for monitoring fluorescence and phosphorescence—a source of radiation, a means of selecting a narrow band of radiation, and a detector—are the same as those for absorption spectroscopy. The unique demands of fluorescence and phosphorescence, however, require some modifications to the instrument designs discussed in earlier chapters: the filter photometer, the single-beam spectrophotometer, the double-beam spectrophotometer, and the diode array spectrometer. The most important difference is that the detector cannot be placed directly across from the source. Figure 15.2.1 shows why this is the case. If we place the detector along the source's axis it receives both the transmitted source radiation, $P_T$, and the fluorescent, $I_f$, or phosphorescent, $I_p$, radiation. Instead, we rotate the director and place it at 90$^o$ to the source.

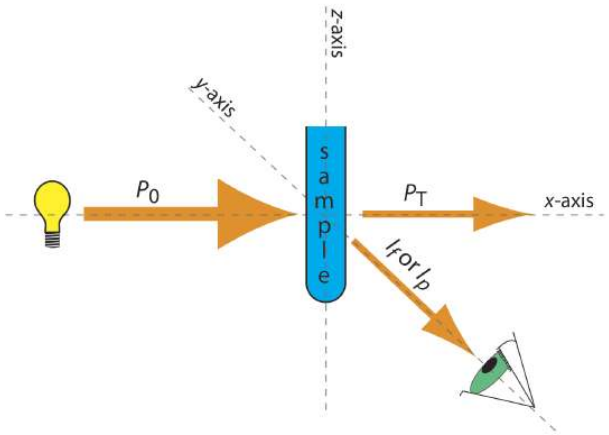



Figure 15.2.1. Schematic diagram showing the orientation of the source and the detector when measuring fluorescence and phosphorescence. Contrast this to Figure 13.4.2, which shows the orientation for absorption spectroscopy.

### Instruments for Measuring Fluorescence

Figure 15.2.2 shows the basic design of an instrument for measuring fluorescence, which includes two wavelength selectors, one for selecting the source's excitation wavelength and one for selecting the analyte's emission wavelength. In a fluorometer the excitation and emission wavelengths are selected using absorption or interference filters. The excitation source for a fluorometer usually is a low-pressure Hg vapor lamp that provides intense emission lines distributed throughout the ultraviolet and visible region. When a monochromator is used to select the excitation and the emission wavelengths, the instrument is called a spectrofluorometer. With a monochromator the excitation source usually is a high-pressure Xe arc lamp, which has a continuous emission spectrum. Either instrumental design is appropriate for quantitative work, although only a spectrofluorometer can record an excitation or emission spectrum.

> A Hg vapor lamp has emission lines at 254, 312, 365, 405, 436, 546, 577, 691, and 773 nm.

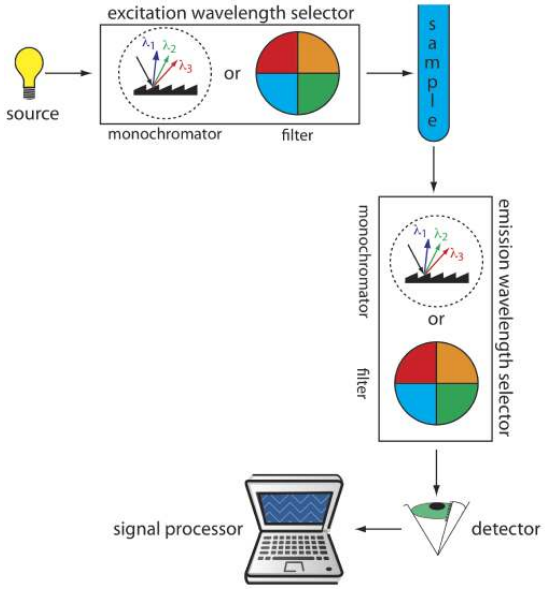



Figure 15.2.2. Schematic diagram for measuring fluorescence showing the placement of the wavelength selectors for excitation and emission. When a filter is used the instrument is called a fluorometer and when a monochromator is used the instrument is called a spectrofluorometer.

The sample cells for molecular fluorescence are similar to those for molecular absorption. Remote sensing using a fiber optic probe is possible using with either a fluorometer or spectrofluorometer. An analyte that is fluorescent is monitored directly. For an analyte that is not fluorescent, a suitable fluorescent probe molecule is incorporated into the tip of the fiber optic probe. The analyte's reaction with the probe molecule leads to an increase or decrease in fluorescence.

## Instruments for Measuring Phosphorescence

An instrument for molecular phosphorescence must discriminate between phosphorescence and fluorescence. Because the lifetime for fluorescence is shorter than that for phosphorescence, discrimination is achieved by incorporating a delay between exciting the sample and measuring the phosphorescent emission. Figure 15.2.3 shows how two out-of-phase choppers allow us to block fluorescent emission from reaching the detector when the sample is being excited and to prevent the source radiation from causing fluorescence when we are measuring the phosphorescent emission.

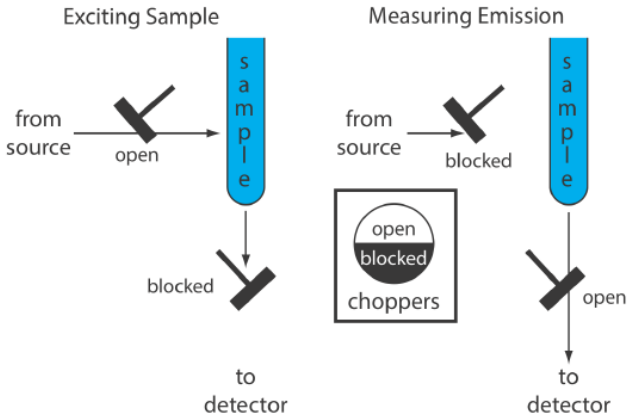



Figure 15.2.3. Schematic diagram showing how choppers are used to prevent fluorescent emission from interfering with the measurement of phosphorescent emission.

Because phosphorescence is such a slow process, we must prevent the excited state from relaxing by external conversion. One way this is accomplished is by dissolving the sample in a suitable organic solvent, usually a mixture of ethanol, isopentane, and diethylether. The resulting solution is frozen at liquid-$N_2$ temperatures to form an optically clear solid. The solid matrix minimizes external conversion due to collisions between the analyte and the solvent. External conversion also is minimized by immobilizing the sample on a solid substrate, making possible room temperature measurements. One approach is to place a drop of a solution

that contains the analyte on a small disc of filter paper. After drying the sample under a heat lamp, the sample is placed in the spectrofluorometer for analysis. Other solid substrates include silica gel, alumina, sodium acetate, and sucrose. This approach is particularly useful for the analysis of thin layer chromatography plates.

---

This page titled 15.2: Instruments for Measuring Fluorescence and Phosphorescence is shared under a CC BY-NC-SA 4.0 license and was authored, remixed, and/or curated by David Harvey.

# 15.3: Applications and Photoluminescence methods

## Quantitative Applications

Molecular fluorescence and, to a lesser extent, phosphorescence are used for the direct or indirect quantitative analysis of analytes in a variety of matrices. A direct quantitative analysis is possible when the analyte's fluorescent or phosphorescent quantum yield is favorable. If the analyte is not fluorescent or phosphorescent, or if the quantum yield is unfavorable, then an indirect analysis may be feasible. One approach is to react the analyte with a reagent to form a product that is fluorescent or phosphorescent. Another approach is to measure a decrease in fluorescence or phosphorescence when the analyte is added to a solution that contains a fluorescent or phosphorescent probe molecule. A decrease in emission is observed when the reaction between the analyte and the probe molecule enhances radiationless deactivation or results in a nonemitting product. The application of fluorescence and phosphorescence to inorganic and organic analytes are considered in this section.

### Inorganic Analytes

Except for a few metal ions, most notably $UO_2^+$, most inorganic ions are not sufficiently fluorescent for a direct analysis. Many metal ions are determined indirectly by reacting with an organic ligand to form a fluorescent or, less commonly, a phosphorescent metal–ligand complex. One example is the reaction of $Al^{3+}$ with the sodium salt of 2, 4, 3′-trihydroxyazobenzene-5′-sulfonic acid —also known as alizarin garnet R—which forms a fluorescent metal–ligand complex (Figure 15.3.1). The analysis is carried out using an excitation wavelength of 470 nm, with fluorescence monitored at 500 nm. Table 15.3.1 provides additional examples of chelating reagents that form fluorescent metal–ligand complexes with metal ions. A few inorganic nonmetals are determined by their ability to decrease, or quench, the fluorescence of another species. One example is the analysis for $F^-$ based on its ability to quench the fluorescence of the $Al^{3+}$–alizarin garnet R complex.

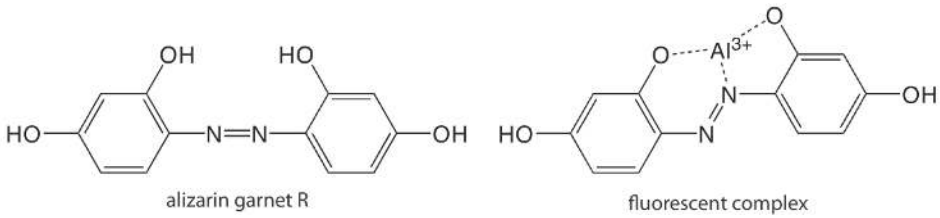



Figure 15.3.1. Structure of alizarin garnet R and its metal–ligand complex with $Al^{3+}$.

Table 15.3.1. Chelating Agents for the Fluorescent Analysis of Metal Ions

| chelating agent | metal ions |
|---|---|
| 8-hydroxyquinoline | $Al^{3+}$, $Be^{2+}$, $Zn^{2+}$, $Li^+$, $Mg^{2+}$ (and others) |
| flavonal | $Zr^{2+}$, $Sn^{4+}$ |
| benzoin | $B_4O_6^{2-}$, $Zn^{2+}$ |
| $2',3',4',5,7-\text{pentahydroxylflavone}$ | $Be^{2+}$ |
| 2-(*o*-hydroxyphenyl) benzoxazole | $Cd^{2+}$ |

### Organic Analytes

As noted earlier, organic compounds that contain aromatic rings generally are fluorescent and aromatic heterocycles often are phosphorescent. Table 15.3.2 provides examples of several important biochemical, pharmaceutical, and environmental compounds that are analyzed quantitatively by fluorimetry or phosphorimetry. If an organic analyte is not naturally fluorescent or phosphorescent, it may be possible to incorporate it into a chemical reaction that produces a fluorescent or phosphorescent product. For example, the enzyme creatine phosphokinase is determined by using it to catalyze the formation of creatine from phosphocreatine. Reacting the creatine with ninhydrin produces a fluorescent product of unknown structure.

Table 15.3.2. Examples of Naturally Photoluminescent Organic Analytes

| class | compounds (F = fluorescence, P = phosphorescence) |
|---|---|
| aromatic amino acids | phenylalanine (F)<br>tyrosine (F)<br>tryptophan (F, P) |
| vitamins | vitamin A (F)<br>vitamin B2 (F)<br>vitamin B6 (F)<br>vitamin B12 (F)<br>vitamin E (F)<br>folic acid (F) |
| catecholamines | dopamine (F)<br>norepinephrine (F) |
| pharmaceuticals and drugs | quinine (F)<br>salicylic acid (F, P)<br>morphine (F)<br>barbiturates (F)<br>LSD (F)<br>codeine (P)<br>caffeine (P)<br>sulfanilamide (P) |
| environmental pollutants | pyrene (F)<br>benzo[a]pyrene (F)<br>organothiophosphorous pesticides (F)<br>carbamate insecticides (F)<br>DDT (P) |

### Standardizing the Method

In Section 15.1 we showed that the intensity of fluorescence or phosphorescence is a linear function of the analyte's concentration provided that the sample's absorbance of source radiation ($A = \varepsilon bC$) is less than approximately 0.01. Calibration curves often are linear over four to six orders of magnitude for fluorescence and over two to four orders of magnitude for phosphorescence. For higher concentrations of analyte the calibration curve becomes nonlinear because the assumption that absorbance is negligible no longer apply. Nonlinearity may be observed for smaller concentrations of analyte fluorescent or phosphorescent contaminants are present. As discussed earlier, quantum efficiency is sensitive to temperature and sample matrix, both of which must be controlled when using external standards. In addition, emission intensity depends on the molar absorptivity of the photoluminescent species, which is sensitive to the sample matrix.

### Representative Method: Determination of Quinine in Urine

The best way to appreciate the theoretical and the practical details discussed in this section is to carefully examine a typical analytical method. Although each method is unique, the following description of the determination of quinine in urine provides an instructive example of a typical procedure. The description here is based on Mule, S. J.; Hushin, P. L. *Anal. Chem.* **1971**, *43*, 708–711, and O'Reilly, J. E.; *J. Chem. Educ.* **1975**, *52*, 610–612.

#### Description of the Method

Quinine is an alkaloid used to treat malaria. It is a strongly fluorescent compound in dilute solutions of $H_2SO_4$ ($\Phi_f = 0.55$). Quinine's excitation spectrum has absorption bands at 250 nm and 350 nm and its emission spectrum has a single emission band at 450 nm. Quinine is excreted rapidly from the body in urine and is determined by measuring its fluorescence following its extraction from the urine sample.

## Procedure

Transfer a 2.00-mL sample of urine to a 15-mL test tube and use 3.7 M NaOH to adjust its pH to between 9 and 10. Add 4 mL of a 3:1 (v/v) mixture of chloroform and isopropanol and shake the contents of the test tube for one minute. Allow the organic and the aqueous (urine) layers to separate and transfer the organic phase to a clean test tube. Add 2.00 mL of 0.05 M $H_2SO_4$ to the organic phase and shake the contents for one minute. Allow the organic and the aqueous layers to separate and transfer the aqueous phase to the sample cell. Measure the fluorescent emission at 450 nm using an excitation wavelength of 350 nm. Determine the concentration of quinine in the urine sample using a set of external standards in 0.05 M $H_2SO_4$, prepared from a 100.0 ppm solution of quinine in 0.05 M $H_2SO_4$. Use distilled water as a blank.

## Questions

1. Chloride ion quenches the intensity of quinine's fluorescent emission. For example, in the presence of 100 ppm NaCl (61 ppm $Cl^-$) quinine's emission intensity is only 83% of its emission intensity in the absence of chloride. The presence of 1000 ppm NaCl (610 ppm $Cl^-$) further reduces quinine's fluorescent emission to less than 30% of its emission intensity in the absence of chloride. The concentration of chloride in urine typically ranges from 4600–6700 ppm $Cl^-$. Explain how this procedure prevents an interference from chloride.

> The procedure uses two extractions. In the first of these extractions, quinine is separated from urine by extracting it into a mixture of chloroform and isopropanol, leaving the chloride ion behind in the original sample.

2. Samples of urine may contain small amounts of other fluorescent compounds, which will interfere with the analysis if they are carried through the two extractions. Explain how you can modify the procedure to take this into account?

> One approach is to prepare a blank that uses a sample of urine known to be free of quinine. Subtracting the blank's fluorescent signal from the measured fluorescence from urine samples corrects for the interfering compounds.

3. The fluorescent emission for quinine at 450 nm can be induced using an excitation frequency of either 250 nm or 350 nm. The fluorescent quantum efficiency is the same for either excitation wavelength. Quinine's absorption spectrum shows that $\varepsilon_{250}$ is greater than $\varepsilon_{350}$. Given that quinine has a stronger absorbance at 250 nm, explain why its fluorescent emission intensity is greater when using 350 nm as the excitation wavelength.

> We know that $I_f$ is a function of the following terms: $k$, $\Phi_f$, $P_0$, $\varepsilon$, $b$, and $C$. We know that $\Phi_f$, $b$, and $C$ are the same for both excitation wavelengths and that $\varepsilon$ is larger for a wavelength of 250 nm; we can, therefore, ignore these terms. The greater emission intensity when using an excitation wavelength of 350 nm must be due to a larger value for $P_0$ or $k$ . In fact, $P_0$ at 350 nm for a high-pressure Xe arc lamp is about 170% of that at 250 nm. In addition, the sensitivity of a typical photomultiplier detector (which contributes to the value of $k$) at 350 nm is about 140% of that at 250 nm.

### 15.3.1 Example

To evaluate the method described iabove, a series of external standard are prepared and analyzed, providing the results shown in the following table. All fluorescent intensities are corrected using a blank prepared from a quinine-free sample of urine. The fluorescent intensities are normalized by setting $I_f$ for the highest concentration standard to 100.

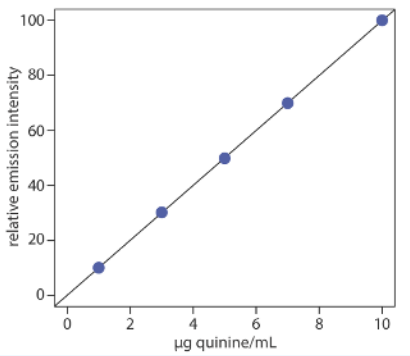
| [quinine] (μg/mL) | $I_f$ |
|---|---|
| 1.00 | 10.11 |
| 3.00 | 30.20 |
| 5.00 | 49.84 |
| 7.00 | 69.89 |
| 10.00 | 100.0 |

After ingesting 10.0 mg of quinine, a volunteer provides a urine sample 24-h later. Analysis of the urine sample gives a relative emission intensity of 28.16. Report the concentration of quinine in the sample in mg/L and the percent recovery for the

ingested quinine.

### Solution

Linear regression of the relative emission intensity versus the concentration of quinine in the standards gives the calibration curve shown below and the following calibration equation.




$$I_f = 0.122 + 9.978 \times \frac{\text{g quinine}}{\text{mL}}$$

Substituting the sample's relative emission intensity into the calibration equation gives the concentration of quinine as 2.81 µg/mL. Because the volume of urine taken, 2.00 mL, is the same as the volume of 0.05 M $H_2SO_4$ used to extract the quinine, the concentration of quinine in the urine also is 2.81 µg/mL. The recovery of the ingested quinine is

$$\frac{\frac{2.81\ \mu\text{g quinine}}{\text{mL urine}} \times 2.00\ \text{mL urine} \times \frac{1\text{mg}}{1000\ \mu\text{g}}}{10.0\ \text{mg quinine ingested}} \times 100 = 0.0562\%$$

It can take 10–11 days for the body to completely excrete quinine so it is not surprising that such a small amount of quinine is recovered from this sample of urine.

This page titled 15.3: Applications and Photoluminescence methods is shared under a CC BY-NC-SA 4.0 license and was authored, remixed, and/or curated by David Harvey.

# 15.4: Chemiluminscence

The focus of this chapter has been on molecular luminescence methods in which emission from the analyte's excited state is achieved following its absorption of a photon. In Chapter 10 we considered atomic emission following excitation of the analyte by thermal energy. An exothermic reaction may also serve as a source of energy. In **chemiluminescence** the analyte is raised to a higher-energy state by means of a chemical reaction, emitting characteristic radiation when it returns to a lower-energy state. When the chemical reaction results from a biological or enzymatic reaction, the emission of radiation is called bioluminescence. Commercially available “light sticks” and the flash of light from a firefly are examples of chemiluminescence and bioluminescence.

The intensity of emitted light, $I$, is proportional to the quantum yield for chemiluminescent emission, $\Phi_{CL}$, which is, itself the product of the quantum yield for creating excited states, $\Phi_{EX}$, and the quantum yield for emission through emission of a photon, $\Phi_{EM}$. The intensity also depends on the rate of the chemical reaction(s) responsible for creating the excited state; thus

$$I = \Phi_{Cl} \times \frac{dC}{dt}$$

where $dC/dt$ is the rate of the chemical reaction.

Chemiluminescent measurements require less equipment than do other forms of molecular emission because there is no need for a source of photons and no need for a monochromator as the only source of photons are those arising from the chemiluminescent reaction. A sample cell to hold the reaction mixture and a photomultiplier tube may be sufficient for the optical bench. Because chemiluminescent emission depends on the reaction's rate, and because the rate decreases with time, the intensity of emission is time-dependent. As a result, the analytical signal is often the integrated emission intensity over a fixed interval of time.

This page titled 15.4: Chemiluminscence is shared under a CC BY-NC-SA 4.0 license and was authored, remixed, and/or curated by David Harvey.

# 15.5: Evaluation of Molecular Luminescence

## Scale of Operation

Photoluminescence spectroscopy is used for the routine analysis of trace and ultratrace analytes in macro and meso samples. Detection limits for fluorescence spectroscopy are influenced by the analyte's quantum yield. For an analyte with $\Phi_f > 0.5$, a picomolar detection limit is possible when using a high quality spectrofluorometer. For example, the detection limit for quinine sulfate, for which $\Phi$ is 0.55, generally is between 1 part per billion and 1 part per trillion. Detection limits for phosphorescence are somewhat higher, with typical values in the nanomolar range for low-temperature phosphorimetry and in the micromolar range for room-temperature phosphorimetry using a solid substrate.

## Accuracy

The accuracy of a fluorescence method generally is between 1–5% when spectral and chemical interferences are insignificant. Accuracy is limited by the same types of problems that affect other optical spectroscopic methods. In addition, accuracy is affected by interferences that affect the fluorescent quantum yield. The accuracy of phosphorescence is somewhat greater than that for fluorescence.

## Precision

The relative standard deviation for fluorescence usually is between 0.5–2% when the analyte's concentration is well above its detection limit. Precision usually is limited by the stability of the excitation source. The precision for phosphorescence often is limited by reproducibility in preparing samples for analysis, with relative standard deviations of 5–10% being common.

## Sensitivity

The sensitivity of a fluorescent or a phosphorescent method is affected by a number of parameters. We already have considered the importance of quantum yield and the effect of temperature and solution composition on $\Phi_f$ and $\Phi_p$. Besides quantum yield, sensitivity is improved by using an excitation source that has a greater emission intensity, $P_0$, at the desired wavelength, and by selecting an excitation wavelength for which the analyte has a greater molar absorptivity, $\varepsilon$. Another approach for improving sensitivity is to increase the volume from which emission is monitored. Figure 15.5.1 shows how rotating a monochromator's slits from their usual vertical orientation to a horizontal orientation increases the sampling volume. The result can increase the emission from the sample by $5 - 30\times$.

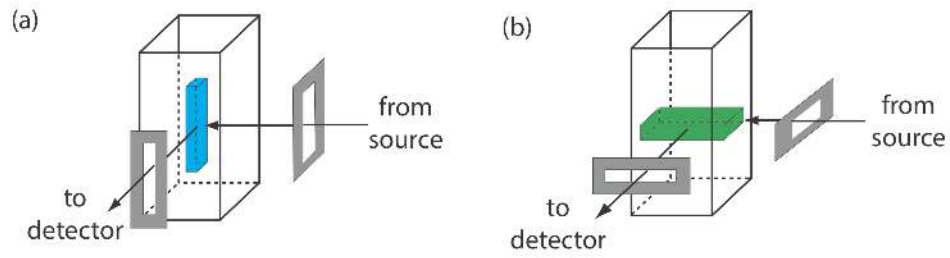



Figure 15.5.1. Use of slit orientation to change the volume from which fluorescence is measured: (a) vertical slit orientation; (b) horizontal slit orientation. Suppose the slit's dimensions are 0.1 mm × 3 mm. In (a) the dimensions of the sampling volume are 0.1 mm × 0.1 mm × 3 mm, or 0.03 $mm^3$. For (b) the dimensions of the sampling volume are 0.1 mm × 3 mm × 3 mm, or 0.9 $mm^3$, a 30-fold increase in the sampling volume.

## Selectivity

The selectivity of fluorescence and phosphorescence is superior to that of absorption spectrophotometry for two reasons: first, not every compound that absorbs radiation is fluorescent or phosphorescent; and, second, selectivity between an analyte and an interferent is possible if there is a difference in either their excitation or their emission spectra. The total emission intensity is a linear sum of that from each fluorescent or phosphorescent species. The analysis of a sample that contains *n* analytes, therefore, is accomplished by measuring the total emission intensity at *n* wavelengths.

## Time, Cost, and Equipment

As with other optical spectroscopic methods, fluorescent and phosphorescent methods provide a rapid means for analyzing samples and are capable of automation. Fluorometers are relatively inexpensive, ranging from several hundred to several thousand dollars, and often are satisfactory for quantitative work. Spectrofluorometers are more expensive, with models often exceeding $50,000.

---

This page titled 15.5: Evaluation of Molecular Luminescence is shared under a CC BY-NC-SA 4.0 license and was authored, remixed, and/or curated by David Harvey.

# CHAPTER OVERVIEW

## 16: An Introduction to Infrared Spectrometry

16.1: Theory of Infrared Absorption Spectrometry
16.2: Infrared Sources and Transducers
16.3: Infrared Instruments

---

This page titled 16: An Introduction to Infrared Spectrometry is shared under a CC BY-NC-SA 4.0 license and was authored, remixed, and/or curated by David Harvey.

# 16.1: Theory of Infrared Absorption Spectrometry

## Understanding the IR Spectrum

Figure 16.1.1 shows the infrared spectrum for ethanol. Unlike a UV/Vis absorbance spectrum, the *y*-axis is displayed as percent transmittance (%T) instead of absorbance, reflecting the fact that IR is used more for qualitative purposes than for quantitative purposes, where Beer's law, which is a linear function of concentration ($A = \epsilon bC$) makes absorbance the more useful measurement. The *x*-axis for an IR spectrum usually is given in wavenumbers, $\overline{\nu} = \lambda^{-1}$, with units of $cm^{-1}$. The peaks in an IR spectrum are inverted relative to absorbance spectrum; that is, they descend from a baseline of 100%T instead of rising from a baseline of zero absorbance.

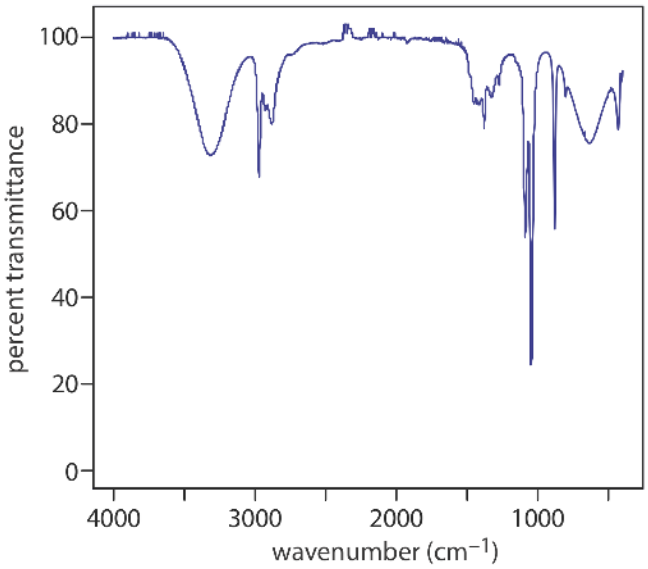



Figure 16.1.1: Infrared (IR) spectrum for ethanol.

### Dipole Changes

The energy of a photon of infrared radiation (see Figure 16.1.2) is not sufficient to affect a change in the electronic energy levels of electrons, as in the UV/Vis atomic or molecular absorption or emission spectroscopies covered in Chapters 9, 10, and 12–15. Instead, infrared radiation is confined to changes in the vibrational energy states of molecules and molecular ions. To absorb an IR photon, the absorbing species must experience a change in its dipole moment, which allows the oscillation in the photon's electrical field to interact with an oscillation in charge within the absorbing species. If the two oscillations have the same frequency, then absorption is possible.

**Note**

Each vibrational energy state in Figure 16.1.2 also has a set of rotational energy states, which means that the peak for a particular change in vibrational energy levels may consist of a series of closely spaced lines, one for each of several changes in rotational energy. Because rotation is difficult for analytes that in liquid or solid forms, we usually see just a single, broad absorption line; for this reason, we will consider only vibrational transitions in this chapter.

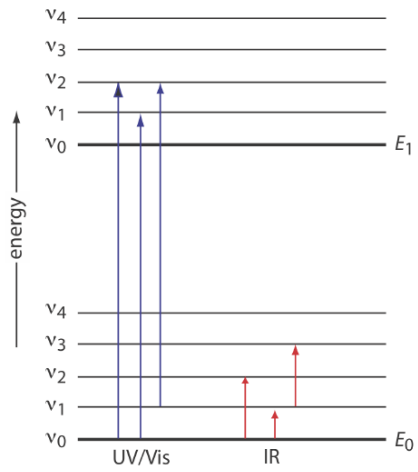



Figure 16.1.2: Diagram showing two electronic energy levels, $E_0$ and $E_1$, each with five vibrational energy levels, $\nu_0 - \nu_1$. Absorption of ultraviolet and visible radiation (shown by the blue arrows) leads to a change in the analyte's electronic energy levels and, possibly, a change in vibrational energy as well. A change in vibrational energy without a change in electronic energy levels occurs with the absorption of infrared radiation (shown by the red arrows).

## Types of Molecular Vibrations

Although we tend to think of the atoms in a molecule as being rigidly fixed in space relative to each other, the individual atoms are in a constant state of motion: bond lengths increase and decrease by stretching and compressing, and bond angles change as the result of the bending of the bonds relative to each other. Figure 16.1.3 shows two different types of stretching (symmetric and asymmetric) and four different types of bending (in-plane rocking, in-plane scissoring, out-of-plane wagging, and out-of-plane twisting).

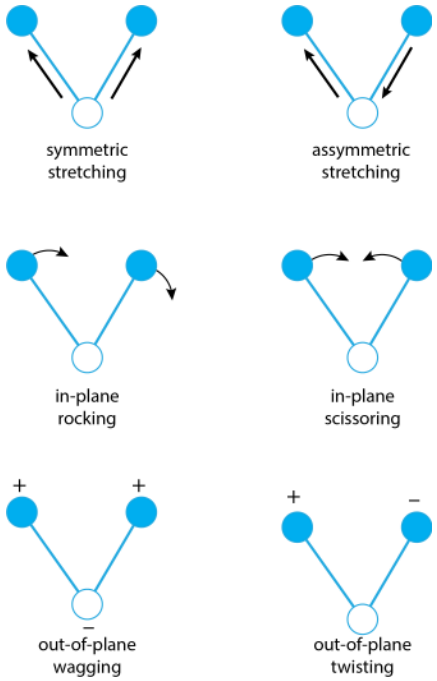



Figure 16.1.3: The six types of stretching and bending motions. For out-of-plane wagging and out-of-plane twisting, the plus sign (+) indicates that the atom is moving toward the viewer and the minus sign (–) indicate that the atom is moving away from the viewer.

Even a simple molecule can have many vibrational modes that give rise to a peak in the IR spectrum, as is the case for ethanol (Figure 16.1.1). The number of possible normal vibrational modes for a linear molecule is $3N - 5$, where $N$ is the number of atoms, and $3N - 6$ for a non-linear molecule. Ethanol, for example, has $3 \times 9 - 6 = 21$ possible vibrational modes. As we will see later in this section, some of these modes may not lead to a change in dipole moment, decreasing the number of peaks in the IR spectrum.

Note

Why does a non-linear molecule have $3N - 6$ vibrational modes? Consider a molecule of methane, $CH_4$. Each of methane's five atoms can move in one of three directions (*x*, *y*, and *z*) for a total of $3 \times 5 = 15$ different ways in which the molecule's atoms can move. A molecule can move in three ways: it can move from one place to another, which we call translational motion; it can rotate around an axis, which we call rotational motion; and its bonds can stretch and bend, which we call vibrational motion. Because the entire molecule can move in the *x*, *y*, and *z* directions, three of methane's 15 different ways of moving are translational. In addition, the molecule can rotate about its *x*, *y*, and *z* axes, accounting for three additional forms of motion. This leaves $15 - 3 - 3 = 9$ vibrational modes. A linear molecule, such as $CO_2$, has $3N - 5$ vibrational modes because it can rotate around only two axes.

## Mechanical Model of Stretching in a Diatomic Molecule

The simplest model system for the the stretching and compressing of a bond is a weight with a mass, *m*, attached to an ideal spring that hangs from the ceiling as shown in Figure 16.1.4*a*. If we pull on the mass and then release it, we initiate a simple oscillating harmonic motion that we can model using Hooke's law. If we displace the weight by a distance, *y*, then the force, *F*, that acts on the weight is

$$F = -ky \tag{16.1.1}$$

where $k$ is the spring's force constant—a measure of the spring's springiness. The negative sign in Equation 16.1.1 indicates that this is the force needed to restore the spring to its original position; that is, the force is in the direction opposite to our action of pulling down on the weight.

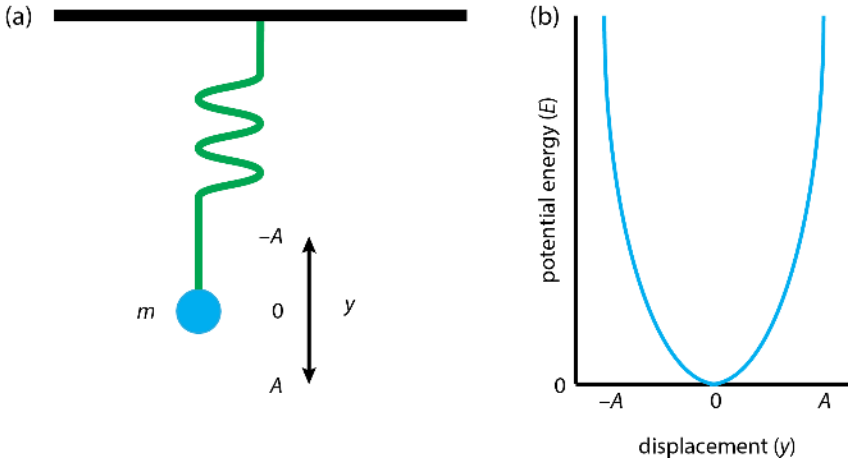



Figure 16.1.4: The model for a simple harmonic oscillator is shown in (a) and its potential energy as a function of displacement is shown in (b).

### Potential Energy of a Harmonic Oscillator

Let's take the potential energy, *E*, of the spring and weight as 0 when they are at rest ($y = 0$). If we pull down on the weight by a distance of $dy$, then the change in the system's potential energy, $dE$, must increase by the product of force and distance

$$dE = -F \times dy = -ky \times dy \tag{16.1.2}$$

Integrating Equation 16.1.2 from $E = 0$ to $E = E$ and from $y = 0$ to $y = y$

$$\int_0^E dE = -k \int_0^y y dy \tag{16.1.3}$$

gives the energy as

$$E = \frac{1}{2} ky^2 \tag{16.1.4}$$

Figure 16.1.4*b* shows the resulting potential energy curve, for which the maximum potential energy is $\frac{1}{2}kA^2$ when the weight is at its maximum displacement. Note that the potential energy curve is a parabola.

### Vibrational Frequency

The simple harmonic oscillator described above and shown in Figure 16.1.4 vibrates with a frequency, $\nu_0$, given by the equation

$$\nu_0 = \frac{1}{2\pi}\sqrt{\frac{k}{m}} \tag{16.1.5}$$

where $k$ is the spring's force constant and $m$ is the weight's mass. We can extend this to a spring that connects two weights to each other by substituting for the mass, $m$, the system's reduced mass, $\mu$

$$\mu = \frac{m_1 \times m_2}{m_1 + m_2} \tag{16.1.6}$$

where $m_1$ and $m_2$ are the masses of the two weights. Substituting Equation 16.1.6 into Equation 16.1.5 gives

$$\nu_0 = \frac{1}{2\pi}\sqrt{\frac{k}{\mu}} = \frac{1}{2\pi}\sqrt{\frac{k(m_1 + m_2)}{m_1 \times m_2}} \tag{16.1.7}$$

If we make the assumption that Equation 16.1.7 applies to simple diatomic molecules, then we can estimate the bond's force constant, $k$, by measuring its vibrational frequency.

## Quantum Treatment of Vibrations

Equations 16.1.4\ and 16.1.7 are based on a classical mechanics treatment of the simple harmonic oscillator in which any displacement, and, thus, any energy is possible. Molecular vibrations, however, are quantized; thus

$$E = \left(v + \frac{1}{2}\right) \times h \times \frac{1}{2\pi}\sqrt{\frac{k}{\mu}} = \left(v + \frac{1}{2}\right) h\nu_0 \tag{16.1.8}$$

where $v$ is the vibrational quantum number, which has allowed values of $0, 1, 2, \ldots$. The difference in energy, $\Delta E$, between any two consecutive vibrational energy levels is $h\nu_0$. As allowed transitions in quantum mechanics are limited to $\Delta\nu = \pm 1$ and as the difference in energy is limited to $\Delta E = h\nu_0$, any particular mode of vibration should give rise to a single peak.

### Anharmonic Behavior

The ideal behavior described in the last section, in which each vibrational motion that produces a change in dipole moment results in a single peak, does not hold due to a variety of reasons, including the coulombic interactions between the atoms as they move toward and away from each other. One result of these non-ideal behaviors is that the value $\Delta E$ does not remain constant for all values of the vibrational quantum number $v$. For larger values of $v$, the value of $\Delta E$ becomes smaller and transitions where $\Delta v = \pm 2$ or $\Delta v = \pm 3$ become possible giving rise to what are called overtone lines at frequencies that are $2\times$ or $3\times$ that for $\nu_0$.

## Why Do We See More or Fewer Vibrational Peaks Than Expected?

Figure 16.1.5 shows the IR spectrum for carbon dioxide, $CO_2$, which consists of three clusters of peaks located at approximately 670 $cm^{-1}$, 2350 $cm^{-1}$, and 3700 $cm^{-1}$. As carbon dioxide is a linear molecule that consists of two carbon-oxygen double bonds (O=C=O), it has $3 \times 3 - 5 = 9 - 5 = 4$ vibrational modes. So why do we see just three clusters of peaks?

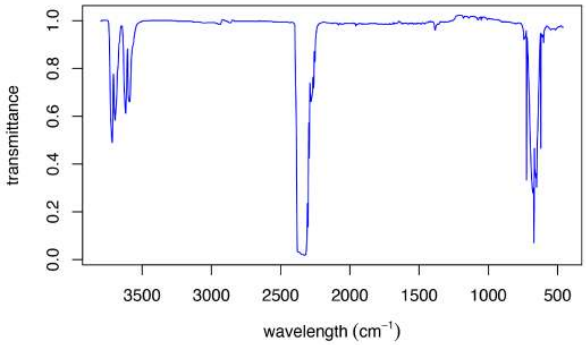



Figure 16.1.5: IR spectrum for $CO_2$. The raw data is from NIST.

One of the requirements for the absorption of infrared radiation, is that the vibrational motion must result in a change in dipole moment. Figure 16.1.6 shows the four vibrational modes for $CO_2$. Of these four vibrational modes, the symmetric stretch does not result in a change in dipole moment. Although this appears to explain why we see just three clusters of peaks, a close examination of the two bending motions in Figure 16.1.6 should convince you that they are identical and, therefore, will appear as a single peak.

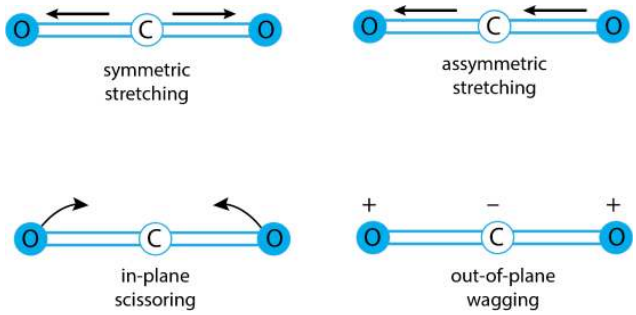



Figure 16.1.6: The four vibrational modes for $CO_2$. The symmetric stretch is not IR active as it does not involve a change in the molecules dipole moment. The asymmetric stretch occurs at 2349 cm$^{-1}$. The two bending motions are identical (or degenerate to each other) and appear at 667 cm$^{-1}$.

So what is the source of the cluster of peaks around 3700 cm$^{-1}$? Sometimes the absorption of a single photon excites two or more vibrational modes. In this case, the wavenumber for this absorption band is equivalent to the sum of the wavenumbers for the asymmetric stretch and the two degenerate bending modes (2349 + 667 = 3016 cm$^{-1}$, and 2349 + 667 + 667 = 3683 cm$^{-1}$). These are called combination bands.

Another source of additional peaks are overtone bands in which $\Delta v = \pm 2$ or $\Delta v = \pm 3$. Figure 16.1.7 shows the IR spectrum for carbonyl sulfide, OCS, which is analagous to $CO_2$ in which one of the oxygens is replaced with sulfur. The peak at 520 cm$^{-1}$ is for its two degenerate bending motions and is labeled $\nu_2$. The asymmetric stretch at 2062 cm$^{-1}$ $(\nu_3)$ and the symmetric stretch at 859 cm$^{-1}$ $(\nu_1)$ are the other two fundamental absorption bands. The remaining peaks are overtones, such as the peak labeled $2\nu_2$ at 1040 cm$^{-1}$, or combination bands, such as the peak labeled $\nu_3 + \nu_1$ at 2921 cm$^{-1}$. Many of the peaks appear as two peaks; this is the result of changes in rotational energy as well.

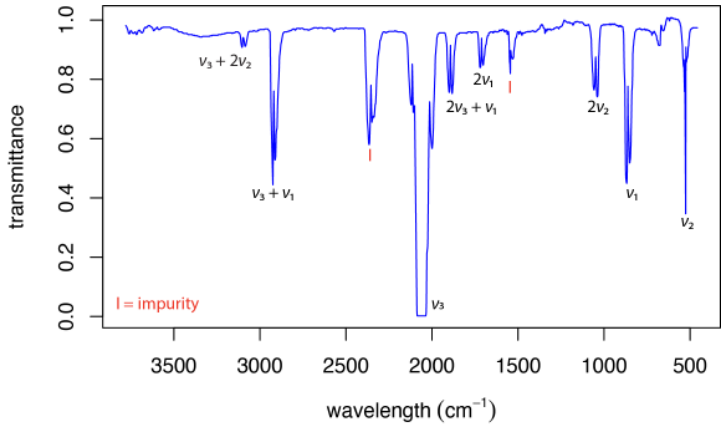



Figure 16.1.7: IR spectrum for OCS. The raw data is form NIST. The peak labeled as I (in red) is an impurity.

---

This page titled 16.1: Theory of Infrared Absorption Spectrometry is shared under a CC BY-NC-SA 4.0 license and was authored, remixed, and/or curated by David Harvey.

# 16.2: Infrared Sources and Transducers

Instrumentation for IR spectroscopy requires a source of infrared radiation and a transducer for detecting the radiation after it passes through the sample.

## Infrared Sources

Most IR sources consist of a solid material that emits radiation when heated by passing a current through the device. The intensity of emitted light typically is greatest at 5900–5000 $cm^{-1}$ and then decreases steadily to 500 $cm^{-1}$. Common examples of IR sources include the Nernst glower (a ceramic rod heated to 1200–2200 K), a globar (a silicon carbide rod heated to 1300–1500 K), an incandescent wire (a nichrome wire heated to approximately 1100 K).

## Infrared Transducers

Because IR radiation has a much lower energy than visible and ultraviolet light, the types of detectors used in UV/Vis spectroscopy are not suitable for recording IR spectra. Most IR detectors measure heat either directly or by a temperature-dependent change in one of its properties.

When two different metals, $M_1$ and $M_2$, are connected to each other in a closed loop, forming two $M_1$–$M_2$ junctions, a potential difference exists between the two junctions. The magnitude of this difference in potential depends on the difference in the temperatures of the two junctions. If the temperature of one junction is held constant or, if the source radiation is chopped—see Chapter 9.2 for a discussion of chopping—then the change in temperature of the other junction can be measured. The active junction is usually coated with a dark material to enhance the absorbance of thermal energy, and is small in size. A high-quality thermocouple is sensitive temperature differences as small as $10^{-6}$ K.

A bolometer is fashioned from materials for which the resistance is temperature dependent. As is true for a thermocouple, the active part of the detector is coated with a dark material and kept small in size.

Triglycerine sulfate, $(NH_2CH_2COOH)_3 \cdot H_2SO_4$, TGS, is a crystalline pyroelectric material. It usually is partially deuterated (DTGS) and, perhaps, doped with *L*-alanine (DLaTGS). The pyroelectric material is placed between two electrodes, one of which is optically transparent to infrared radiation. The absorption of infrared radiation results in a change in temperature and a resulting change in the detector's capacitance and, therefore, the current that flows.

This page titled 16.2: Infrared Sources and Transducers is shared under a CC BY-NC-SA 4.0 license and was authored, remixed, and/or curated by David Harvey.

# 16.3: Infrared Instruments

Instrumentation for infrared spectroscopy use one of three common optical benches: non-dispersive instruments, dispersive instruments, and Fourier transform instruments. As we have already examined non-dispersive and dispersive instruments in Chapter 13, and because they are no longer as common as they once were, we give them only a brief consideration here. Fourier transform instruments, which dominate the current marketplace, receive a more detailed treatment.

## Non-Dispersive Instruments

The simplest instrument for IR absorption spectroscopy is a filter photometer similar to that shown earlier in Figure 13.4.1 for UV/Vis absorption. These instruments have the advantage of portability, which makes the useful in the field, and typically are used as dedicated analyzers for gases such as HCN and CO.

## Dispersive Instruments

Infrared instruments using a monochromator for wavelength selection use double-beam optics similar to that shown earlier in Figure 13.4.3. Double-beam optics are preferred over single-beam optics because the sources and detectors for infrared radiation are less stable than those for UV/Vis radiation. In addition, it is easier to correct for the absorption of infrared radiation by atmospheric $CO_2$ and $H_2O$ vapor when using double-beam optics. Resolutions of 1–3 $cm^{-1}$ are typical for most instruments.

## Fourier Transform Instruments

We covered the basic concepts of the Fourier transform in Chapter 7, which you may wish to review. In this section we take a more detailed look at the application of Fourier transforms to infrared instrumentation.

### Components of a FT-IR

In a Fourier transform infrared spectrometer, or FT–IR, the monochromator is replaced with an interferometer (Figure 16.3.1). There are four key components that make up the interfometer: the drive mechanism that moves the moving mirror, the beam splitter, the light source, and the detector.

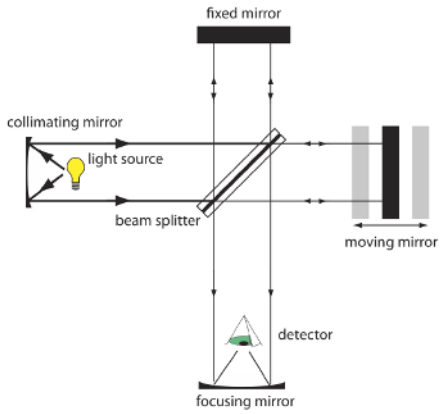



Figure 16.3.1: Schematic diagram of an interferometer. This is the same figure as Figure 7.7.1. The sample is positioned between the beam splitter and the detector.

### Drive Mechanism

As we learned in Chapter 7, the Fourier transform encodes information about the wavelength or frequency of source radiation absorbed by the sample by observing how the signal reaching the detector varies with time. As the moving mirror is displaced in space, some frequencies of light experience complete constructive interference, some frequencies of light experience complete destructive interference, and other frequencies fall somewhere in between giving rise to a time domain spectrum. As the signal is monitored as function of time and the moving mirror is traversing a variable distance, the drive mechanism must allow for a precise and accurate relationship between the two. The mechanism of the moving mirror must be capable of moving the mirror through a distance of up to 20 cm at a scan rate as fast as 10 cm/s; it must also accomplish this while maintaining the mirror's orientation

relative to the axis of its movement. To maintain accuracy, a HeNe laser, which emits visible light with a wavelength of 632.8 nm, is aligned with the light source so that they follow the same optical path.

### Beam Splitter

The beam splitter is designed to reflect 50% of the source radiation to the fixed mirror and to pass the remaining 50% of the source radiation to the moving mirror. The materials used to construct the beam splitter depends on the range of wavelengths being used. The most common range of wavelengths, which is called mid-IR, runs from approximately 670 $cm^{-1}$ to 4000 $cm^{-1}$. Instruments for mid-IR use a beam splitter that consists of silicon or germanium coated onto a substrate of KBr or NaCl.

### Sources and Transducers

The most common sources for FT-IR are those discussed in the previous section, such as a Nernst glower. The most common transducer for FT-IR is pyroelectric triglycine sulfate.

---

This page titled 16.3: Infrared Instruments is shared under a CC BY-NC-SA 4.0 license and was authored, remixed, and/or curated by David Harvey.

# CHAPTER OVERVIEW

## 17: Applications of Infrared Spectrometry

Infrared spectroscopy finds wide use for both qualitative and quantitative analysis. Our organization of IR applications follows that traditionally used by others by dividing the broad range of infrared radiation into three distinct units: the near-IR (4000 $cm^{-1}$ to 14,000 $cm^{-1}$, or 2,500 nm to 700 nm), the mid-IR (670 $cm^{-1}$ to 4000 $cm^{-1}$, or 15 μm to 2.5 μm), and the far-IR (670 $cm^{-1}$ to 10 $cm^{-1}$, or 1000 μm to 15 μm). Note that the near in near-IR means that it is nearest to the visible range of light. Of these, the most important in terms of the breadth of applications is the mid-IR.


17.1: Mid-Infrared Absorption Spectometry

17.2: Mid-Infrared Reflection Spectrometry

17.3: Near-Infrared and Far-Infrared Spectroscopy


---


This page titled 17: Applications of Infrared Spectrometry is shared under a CC BY-NC-SA 4.0 license and was authored, remixed, and/or curated by David Harvey.

# 17.1: Mid-Infrared Absorption Spectometry

Mid-infrared spectrometry is used for the routine qualitative analysis and, to a lesser extent, the quantitative analysis of organic molecules. In this section we consider absorption spectrometry in which we measure the absorbance of IR light as it passes through a gas, solution, liquid, or solid sample. In Section 17.2 we consider reflectance spectrometry in which we measure the absorbance of IR light as it reflects off the surface of a solid sample or a thin film of a liquid sample.

## Sample Handling

Infrared spectroscopy is routinely used to analyze gas, liquid, and solid samples. We know from Beer's law, $A = \epsilon bC$, that absorbance is a linear function of the analyte's concentration, $C$, and the distance, $b$, the light travels through the sample. The challenge with obtaining an IR spectrum, is rarely the analyte's concentration or path length; instead it is finding materials and solvents that are transparent to IR radiation. The optical windows in IR cells are made from materials, such as NaCl and KBr, that are transparent to infrared radiation.

### Gas Phase Samples

The cell for analyzing a sample in the gas phase generally is a 5–10 cm glass cylinder fitted with optically transparent windows. For an analyte with a particularly small concentration, the sample cell is designed with reflective surfaces that allow the infrared radiation to make several passes through the cell before it exits the sample cell, increasing the pathlength and, therefore, the absorbance.

### Solution Solutions

The analysis of a sample in solution is limited by the solvent's IR absorbing properties, with carbon tetrachloride, $CCl_4$, carbon disulfide, $CS_2$, and chloroform, $CHCl_3$, being common solvents. A typical solution cell is shown in Figure 17.1.1. It is fashioned with two NaCl windows separated by a spacer. By changing the spacer, pathlengths from 0.015–1.0 mm are obtained. The sample is introduced into the cell using a syringe and the sample inlet port.

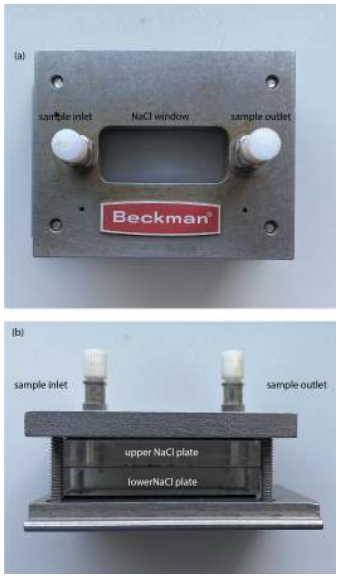



Figure 17.1.1: IR cell for analytes that are in solution. (a) View from above showing the sample inlet, the sample outlet, and the NaCl window. (b) View from the side showing the two NaCl plates.

### Liquid Phase Samples

A sample that is a volatile liquid may be analyzed using the solution cell in Figure 17.1.1. For a non-volatile liquid sample, however, a suitable sample for qualitative work can be prepared by placing a drop of the liquid between the two NaCl plates shown in Figure 17.1.2$a$, forming a thin film that typically is less than 0.01 mm thick. An alternative approach is to place a drop of the sample on a disposable card equipped with a polyethylene "window" that IR transparent with the exception of strong absorption bands at 2918 $cm^{-1}$ and 2849 $cm^{-1}$ (Figure 17.1.2$b$).




Figure 17.1.2: Two examples of IR sample cells for liquid samples: (a) NaCl salts plates; (b) disposable card with a polyethylene window that is IR transparent with the exception of strong absorption bands at 2918 $cm^{-1}$ and 2849 $cm^{-1}$.

## Solid Phase Samples

Transparent solid samples are analyzed by placing them directly in the IR beam. Most solid samples, however, are opaque, and are first dispersed in a more transparent medium before recording the IR spectrum. If a suitable solvent is available, then the solid is analyzed by preparing a solution and analyzing as described above. When a suitable solvent is not available, solid samples are analyzed by preparing a mull of the finely powdered sample with a suitable oil and then smearing it on a NaCl salt plate or a disposable IR card (Figure 17.1.2). Alternatively, the powdered sample is mixed with KBr and pressed, under high pressure, into a thin, optically transparent pellet, as shown in Figure 17.1.3.

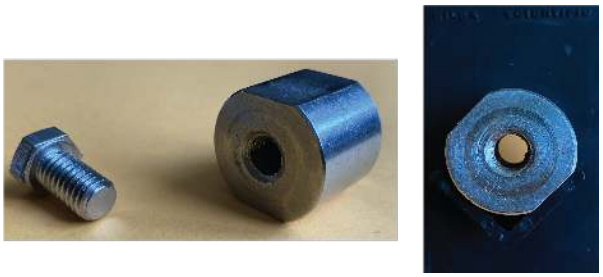


Figure 17.1.3: KBr press for preparing a solid sample for an IR analysis. The photo on the left shows the press. A threaded bolt is screwed into the back of the press (hidden from view). A portion of the sample, mixed with KBr, is added to the press and the second threaded bolt is screwed into the press. The two bolts are tightened by turning against each other, forming an optically transparent pellet, as shown by the photo on the right that looks through the pellet. With the threaded bolts removed, the press sits in a holder and placed in the spectrometer's optical path.

## Qualitative Analysis

The most important application of mid-infrared spectroscopy is in the qualitative identification of organic molecules. Figure 17.1.4 shows mid-IR solution spectra for four simple alcohols: methanol, $CH_3OH$, ethanol, $CH_3CH_2OH$, propanol, $CH_3CH_2CH_2OH$, and isopropanol, $(CH_3)_2CHOH$. Clearly there are similarities and differences in these four spectra: similarities that might lead us to expect that each molecule contains the same functional groups and differences that appear as features unique to a particular molecule. The similarities in these four spectra appear at the higher wavenumber end of the *x*-axis scale; we call the peaks we find there group frequencies. The differences in these four spectra occur below approximately 1500 $cm^{-1}$ in what we call the fingerprint region.

**Note**

The fingerprint region is defined here as beginning at 1500 $cm^{-1}$, extending to the lowest wavenumber shown on the *x*-axis. If you do some searching on the fingerprint region you will see that there is no broad agreement on where it begins. In my searching, I found sources that place the beginning of the fingerprint region as 1500 $cm^{-1}$, 1450 $cm^{-1}$, 1300 $cm^{-1}$, 1200 $cm^{-1}$, and 1000 $cm^{-1}$.

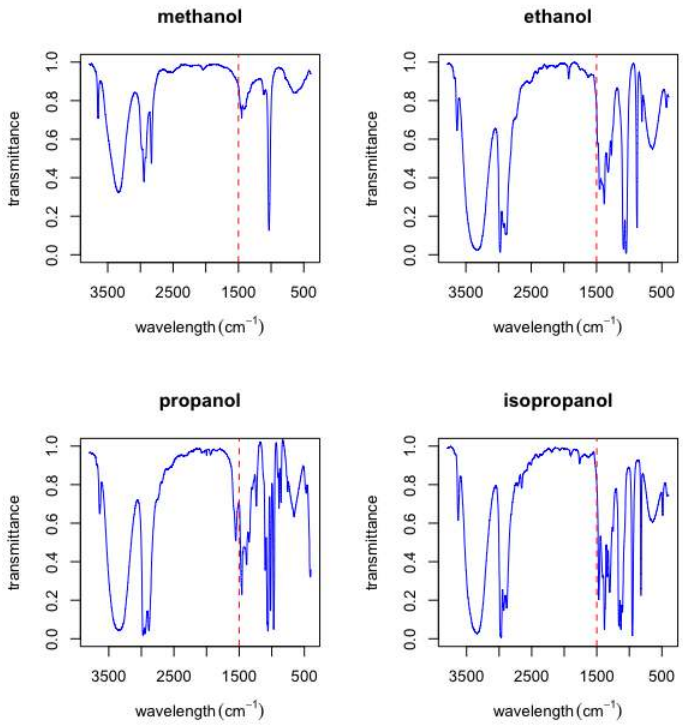



Figure 17.1.4: IR spectra for four simple alcohols: methanol, $CH_3OH$, ethanol, $CH_3CH_2OH$, propanol, $CH_3CH_2CH_2OH$, and isopropanol, $(CH_3)_2CHOH$. Samples were prepared using carbon tetrachloride as a solvent. The vertical dashed red line at 1500 cm$^{-1}$ marks the beginning of the fingerprint region. The original data for these spectra are from NIST.

## Group Frequencies

All four of the spectra in Figure 17.1.4 share a small intensity, sharp peak at approximately 3650 cm$^{-1}$, a strong intensity, broad peak at approximately 3350 cm$^{-1}$, and two medium intensity, sharp peaks at 2950 cm$^{-1}$ and 3850 cm$^{-1}$. By comparing spectra for these and other compounds, we know that the presence of a broad peak between approximately 3200 cm$^{-1}$ and 3600 cm$^{-1}$ is good evidence that the compound contains a hydrogen-bonded –OH functional group. The sharp peak at approximately 3650 cm$^{-1}$ also is evidence of an –OH functional group, but one that is not hydrogen-bonded. The two sharp peaks at 2950 cm$^{-1}$ and 3850 cm$^{-1}$ are consistent with C–H bonds. All four of these peaks are for stretching vibrations. Tables of group frequencies are routinely available.

## The "Fingerprint" Region

Figure 17.1.5 shows a close-up of the fingerprint region for the alcohol samples in Figure 17.1.4. Of particular interest with this set of samples is the increasing complexity of the spectra as we move from the simplest of these alcohols (methanol), to the most complex of these alcohols (propanol and isopropanol). Also of interest is that each spectrum is unique in a way that allows us to confirm a sample by matching it against a library of recorded spectra. There are a number of accessible collections of spectra that are available for this purpose. One such collection of spectra is the NIST Webbook—NIST is the National Institute of Standards and Technology—which is the source of the data used to display the spectra included in this section's figures and which includes spectra for over 16,000 compounds.

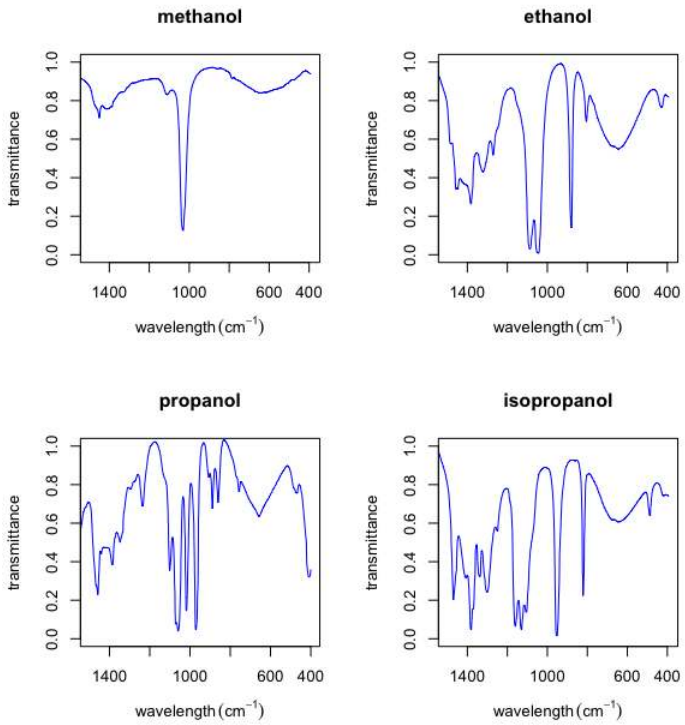



Figure 17.1.5: IR spectra in the fingerprint region for four simple alcohols: methanol, $CH_3OH$, ethanol, $CH_3CH_2OH$, propanol, $CH_3CH_2CH_2OH$, and iso-propanol, $(CH_3)_2CHOH$. Samples were prepared using carbon tetrachloride as a solvent. The original data for these spectra are from NIST.

## Computer Search Systems

With the availability of computerized data acquisition and storage it is possible to build digital libraries of standard reference spectra. The identity of an a unknown compound often can be determined by comparing its spectrum against a library of reference spectra, a process known as spectral searching. Comparisons are made using an algorithm that calculates the cumulative difference between the sample's spectrum and a reference spectrum. For example, one simple algorithm uses the following equation

$$D = \sum_{i=1}^{n} |(A_{sample})_i - (A_{reference})_i| \tag{17.1.1}$$

where $D$ is the cumulative difference, $A_{sample}$ is the sample's absorbance at wavelength or wavenumber $i$, $A_{reference}$ is the absorbance of the reference compound at the same wavelength or wavenumber, and $n$ is the number of digitized points in the spectra. Note that the spectra are defined here by absobrance instead of transmittance as absorbance is directly proportional to concentration. The cumulative absolute difference is calculated for each reference spectrum. The reference compound with the smallest value of $D$ is the closest match to the unknown compound. The accuracy of spectral searching is limited by the number and type of compounds included in the library, and by the effect of the sample's matrix on the spectrum.

Another advantage of computerized data acquisition is the ability to subtract one spectrum from another. When coupled with spectral searching it is possible to determine the identity of several components in a sample without the need of a prior separation step by repeatedly searching and subtracting reference spectra. An example is shown in Figure 17.1.6 in which the composition of a two-component mixture is determined by successive searching and subtraction. Figure 17.1.6$a$ shows the spectrum of the mixture. A search of the spectral library selects cocaine•HCl (Figure 17.1.6$b$) as a likely component of the mixture. Subtracting the reference spectrum for cocaine•HCl from the mixture's spectrum leaves a result (Figure 17.1.6$c$) that closely matches mannitol's reference spectrum (Figure 17.1.6$d$). Subtracting the reference spectrum for mannitol leaves a small residual signal (Figure 17.1.6$e$).

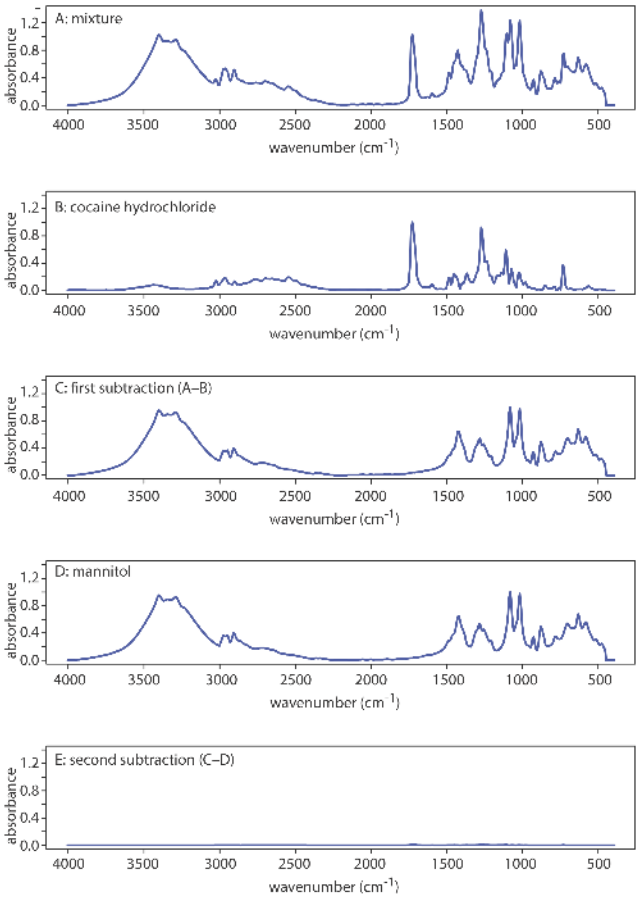



Figure 17.1.6: Identifying the components of a mixture by spectral searching and subtracting. (a) IR spectrum of the mixture; (b) Reference IR spectrum of cocaine•HCl; (c) Result of subtracting the spectrum of cocaine•HCl from the mixture's spectrum; (d) Reference IR spectrum of mannitol; and (e) The residual spectrum after removing mannitol's contribution to the mixture's spectrum. IR spectra traditionally are displayed using percent transmittance, %T, along the *y*-axis. Because absorbance—not percent transmittance—is a linear function of concentration, spectral searching and spectral subtraction, is easier to do when displaying absorbance on the *y*-axis.

## Quantitative Applications

A quantitative analysis based on the absorption of infrared radiation, although important, is encountered less frequently than with UV/Vis absorption, primarily due to the three issues raised here.

### Deviations from Beer's Law

One challenge for quantitative IR is the greater tendency for instrumental deviations from Beer's law when using infrared radiation. Because an infrared absorption band is relatively narrow, any deviation due to the lack of monochromatic radiation is more pronounced. In addition, infrared sources are less intense than UV/Vis sources, which makes stray radiation more of a problem. Differences between the path lengths for samples and for standards when using thin liquid films or KBr pellets are a problem, although an internal standard can correct for any difference in pathlength; alternatively, we can use the cell shown in Figure 17.1.1 to maintain a constant path length.

### Background Correction

The water and carbon dioxide in air have strong absorbances in the mid-IR. A double-beam dispersive instrument corrects for the contributions of $CO_2$ and $H_2O$ vapor because they are present in both pathways through the instrument. An FT-IR, however, includes only a single optical path, so it is necessary to collect a separate spectrum to compensate for the absorbance of atmospheric $CO_2$ and $H_2O$ vapor. This is done by collecting a background spectrum without the sample and storing the result in the instrument's computer memory. The background spectrum is removed from the sample's spectrum by taking the ratio the two signals. Another approach is to flush the sample compartment with nitrogren.

## Measuring Absorbance

Another challenge for quantitative IR is that establishing a 100% T ($A$ = 0) baseline often is difficult because the optical properties of NaCl sample cells may change significantly with wavelength due to contamination and degradation. We can minimize this problem by measuring absorbance relative to a baseline established for the absorption band. Figure 17.1.7 shows how this is accomplished.

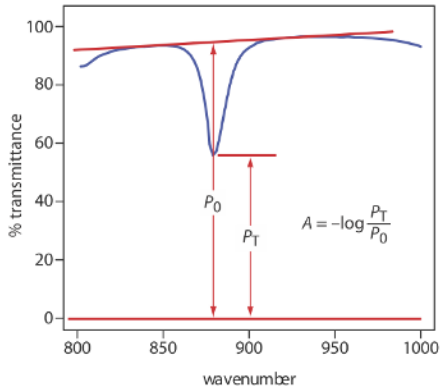



Figure 17.1.7: Method for determining absorbance from an IR spectrum.

## Typical Applications

A recent review paper [Fahelelbom, K. M.; Saleh, A.; Al-Tabakha, M. A.; Ashames, A. A. *Rev. Anal. Chem.* **2022**, *41*, 21–33] summarizes the rich literature in quantitative mid-infrared spectrometry. Among the areas covered are the analysis of pharmaceuticals, including antibiotics, antihypertensives, antivirals, and counterfeit drugs. Mid-infrared spectrometry also finds use for the analysis of environmentally significant gases, such as methane, $CH_4$, hydrogen chloride, HCl, sulfur dioxide, $SO_2$, and nitric oxide, NO.

---

This page titled 17.1: Mid-Infrared Absorption Spectometry is shared under a CC BY-NC-SA 4.0 license and was authored, remixed, and/or curated by David Harvey.

# 17.2: Mid-Infrared Reflection Spectrometry

The first section of this chapter considered mid-IR absorption spectrometry in which we measure the amount of light that is transmitted by the sample, which we can convert, if we wish, into absorbance values. In the process, we examined both transmittance (Figure 7.1.4 and Figure 7.1.5) and absorbance (Figure 7.1.6) spectra. In this section, we consider experiments in which we measure the reflection of infrared radiation by a sample.

## Types of Reflections

There are two broad classes of reflection: internal and external. As shown in Figure 17.2.1, internal reflection occurs when light encounters an interface between two media—here identified as the sample and the support—that have different refractive indicies, *n*. When the refractive index of the support is greater than the refractive index of the sample, then some of the light reflects off the interface. Attenuated total reflectance spectrometry is one example of an instrumental method that relies on internal reflection.

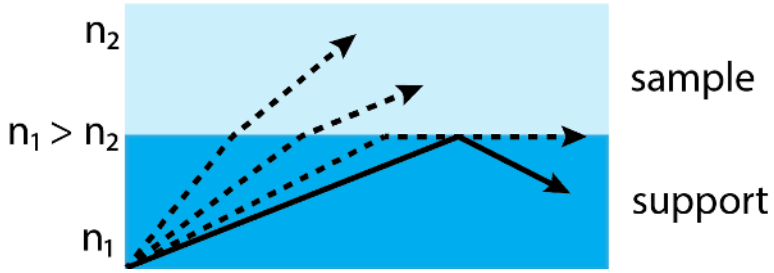



Figure 17.2.1: Internal reflection occurs at the interface between a support that has a greater refractive index than an overlying sample. For small angles of incidence (dashed lines), the light experiences refraction and crosses the interface. For a sufficiently large angle of incidence, the light experiences total reflection, as shown by the solid line.

External reflectance occurs when light reflects off of the sample's surface. As shown in Figure 17.2.2, the way in which light reflects depends on the nature of the sample's surface. In specular reflectance, the angle of reflection is the same at all locations because the sample's surface is smooth; in diffuse reflectance, the angle of reflection varies between locations due to the roughness of the sample's surface. Diffuse reflectance spectrometry is one example of an instrumental method that relies on external reflection.

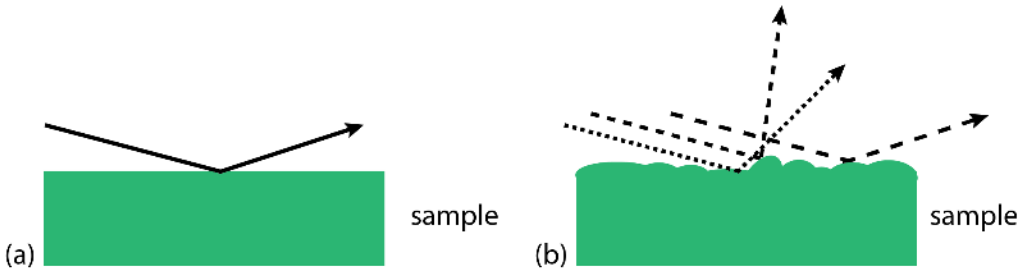



Figure 17.2.2: (a) Specular reflectance at a smooth surface and (b) diffuse reflectance from a rough surface.

## Attenuated Total Reflectance Spectrometry

The analysis of an aqueous sample is complicated by the solubility of the NaCl cell window in water. One approach to obtaining an infrared spectrum of an aqueous solution is to use attenuated total reflectance instead of transmission. Figure 17.2.3 shows a diagram of a typical attenuated total reflectance (ATR) FT–IR instrument. The ATR cell consists of a high refractive index material, such as ZnSe or diamond, sandwiched between a low refractive index substrate and a lower refractive index sample. Radiation from the source enters the ATR crystal where it undergoes a series of internal reflections before exiting the crystal. During each reflection the radiation penetrates a short distance into the sample. This depth of penetration, $d_p$, depends on the wavelength of the light, $\lambda$, the refractive index of the ATR crystal, $n_1$, the refractive index of the sample, $n_2$, and the angle of the incident radiation, $\theta$.

$$d_p = \frac{\lambda}{2\pi\sqrt{n_1^2 \sin^2\theta - n_2^2}} \tag{17.2.1}$$

For example, when using ZnSe as the ATR crystal ($n_1 = 2.4$) and an angle of incidence of $45^\circ$, light of 1000 $cm^{-1}$ penetrates to a depth of 2.0 μm in a sample with a refractive index similar to that for KBr ($n_2 = 1.5$).

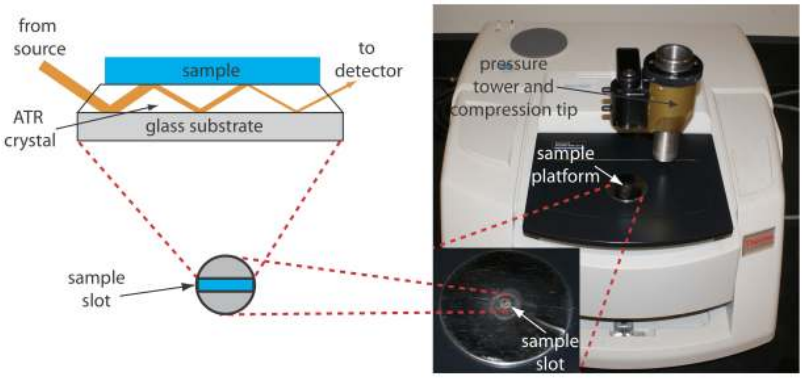



Figure 17.2.3. FT-IR spectrometer equipped with a diamond ATR sample cell. The inserts show a close-up photo of the sample platform, a sketch of the ATR's sample slot, and a schematic showing how the source's radiation interacts with the sample. The pressure tower is used to ensure proper contact of a solid sample with the ATR crystal.

Solid samples also can be analyzed using an ATR sample cell. After placing the solid in the sample slot, a compression tip ensures that it is in contact with the ATR crystal. Examples of solids analyzed by ATR include polymers, fibers, fabrics, powders, and biological tissue samples. ATR spectra are similar, but not identical, to those obtained by measuring transmission. An important contribution to this is the wavelength-dependent depth of penetration of the infrared radiation where a decrease in wavenumber (longer wavelength) results in a greater depth of penetration, which changes the intensity and width of absorption bands.

## Diffuse Reflectance Spectrometry

Another reflectance method is diffuse reflectance, in which radiation is reflected from a rough surface, such as a powder. Powdered samples are mixed with a non-absorbing material, such as powdered KBr, and the reflected light is collected and analyzed. As with ATR, the resulting spectrum is similar to that obtained by conventional transmission methods. Figure 17.2.4 shows the IR spectrum for urea obtained using transmission and diffuse reflectance (both collected using an FT-IR). Both spectra show similar features between 1000 $cm^{-1}$ and 2000 $cm^{-1}$, although there are differences in relative peak heights and background absorption.

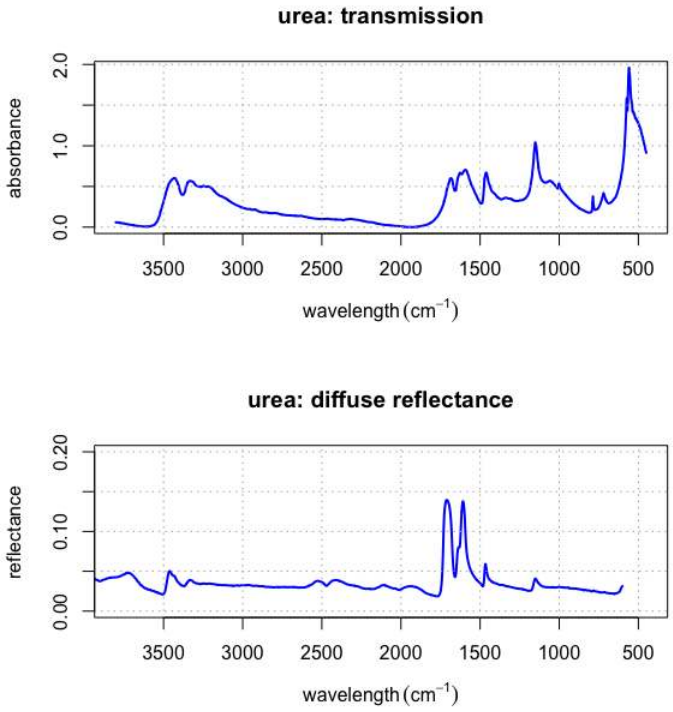



Figure 17.2.4: Diffuse reflection spectra for urea recorded using a FT-IR operating in transmission sample cell (top) or using a diffuse reflectance sample cell (bottom). The *y*-axis for the transmission spectrum is –log(T), where *T* is the transmittance, and the *y*-axis for the diffuse reflectance spectrum is –log(*R*), where *R* is the reflectance.

This page titled 17.2: Mid-Infrared Reflection Spectrometry is shared under a CC BY-NC-SA 4.0 license and was authored, remixed, and/or curated by David Harvey.

# 17.3: Near-Infrared and Far-Infrared Spectroscopy

At the beginning of this chapter we divided infrared radiation into three areas: the near-IR, the mid-IR, and the far-IR. The mid-IR, which runs from 4000 $cm^{-1}$ to 670 $cm^{-1}$ (2.5 μm to 15 μm) is the most analytical useful region and was the subject of the previous two sections. Here we briefly turn our attention to applications using the near-IR and the far-IR.

## Near-Infrared (NIR) Spectroscopy

The near-IR extends from approximately 13,000 $cm^{-1}$ (a wavelength of 770 nm or 0.77 μm, the upper wavelength limit of visible light) to 4000 $cm^{-1}$ (a wavelength of 2,500 nm or 2.5 μm). Earlier we noted that absorption bands in the region that extends from 1500 $cm^{-1}$ to 4000 $cm^{-1}$ are called group frequencies. The absorption bands in the near-infrared often are overtones and combination bands of these group frequencies. Of particular importance are functional groups that include hydrogen: OH, CH, and NH are examples. Absorption bands generally are less intense and less broad. Compared to mid-IR, the NIR is more useful for a quantitative analysis of aqueous samples because the OH absorption bands are much weaker. The instrumentation for NIR spectroscopy, both in transmission mode and in reflectance mode, is similar to that for UV/visible spectrometers and for mid-IR spectrometry.

## Far-Infrared (FIR) Spectroscopy

The far-IR extends from approximately 670 $cm^{-1}$ (a wavelength of 15 μm) to 10 $cm^{-1}$ (a wavelength of 1000 μm or 1 mm). FIR spectroscopy finds applications in the analysis of materials that include metals, including metal oxides, metal sulfides, and metal-ligand complexes. FIR spectroscopy has also been applied to the analysis of polyamides, peptides, and proteins. Because the FIR merges into the microwave region, it also finds use in the analysis of the rotational energies of gases.

This page titled 17.3: Near-Infrared and Far-Infrared Spectroscopy is shared under a CC BY-NC-SA 4.0 license and was authored, remixed, and/or curated by David Harvey.

# CHAPTER OVERVIEW

## 18: Raman Spectroscopy


18.1: Theory of Raman Spectroscopy

18.2: Instrumentation

18.3: Applications of Raman Spectroscopy

18.4: Other Types of Raman Spectroscopy


---


This page titled 18: Raman Spectroscopy is shared under a CC BY-NC-SA 4.0 license and was authored, remixed, and/or curated by David Harvey.

# 18.1: Theory of Raman Spectroscopy

The blue color of the sky during the day and the red color of the sun at sunset are the result of the scattering of light by small particles of dust, by molecules of water vapor, and by other gases in the atmosphere. The efficiency of a photon's scattering depends on its wavelength. We see the sky as blue during the day because violet and blue light scatter to a greater extent than other, longer wavelengths of light. For the same reason, the sun appears red at sunset because red light scatters less efficiently and is more likely to pass through the atmosphere than other wavelengths of light. If we send a focused, monochromatic beam of radiation with a wavelength of $\lambda$ through a medium of particles—whether solid particulates or individual molecules—that have dimensions $< 1.5\lambda$, then the radiation scatters in all directions. For example, infrared light in the near-IR with a wavelength of 700 nm will scatter from any particle whose longest dimension is less than 1,300 nm. Even in an otherwise transparent sample, scattering from molecules occurs.

## Raman Spectra

There are two general classes of scattering: elastic scattering and inelastic scattering. In elastic scattering, a photon is first absorbed by a particle and then emitted without a change in its energy ($\Delta E = 0$); this is called Rayleigh scattering. With inelastic scattering, a photon is first absorbed by a particle and then emitted with a change in its energy ($\Delta E \neq 0$); this is called Raman scattering. A plot that shows the intensity of scattered radiation as a function of the scattered photon's energy, expressed as a change in the wavenumber, $\Delta\overline{\nu}$, is called a Raman spectrum and values of $\Delta\overline{\nu}$ are called Raman shifts.

Figure 18.1.1 shows a portion of the Raman spectrum for carbon tetrachloride and illustrates several important features. First, Rayleigh scattering produces an intense peak at $\Delta\overline{\nu} = 0$. Although the peak is intense, it carries no useful information as the absolute energy is just that for the source. Second, Raman scattering has two components—Stokes lines and the anti-Stokes lines—that have identical absolute shifts relative to the line for Rayleigh scattering, but that have different signs. The Stokes lines have positive values for $\Delta\overline{\nu}$ and the anti-Stokes lines have negative values for $\Delta\overline{\nu}$. Third, each of the Stokes lines is more intense than the corresponding anti-Stokes line. Fourth, because we measure the shift in a peak's wavenumber relative to the source radiation, the spectrum is independent of the source radiation.

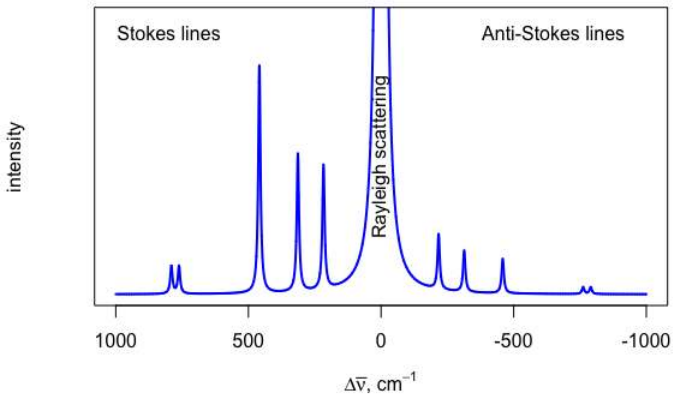



Figure 18.1.1: The Raman spectrum for carbon tetrachloride, $CCl_4$, showing the intense peak for Rayleigh scattering at $\Delta\overline{\nu} = 0$ and five lines each for Stokes and anti-Stokes scattering with $\Delta\overline{\nu} = \pm 217.0\ \text{cm}^{-1}$, $\Delta\overline{\nu} = \pm 313.5\ \text{cm}^{-1}$, $\Delta\overline{\nu} = \pm 458.7\ \text{cm}^{-1}$, $\Delta\overline{\nu} = \pm 761.7\ \text{cm}^{-1}$, and $\Delta\overline{\nu} = \pm 790.4\ \text{cm}^{-1}$. The values for these lines are from NIST; the spectrum itself is simulated.

**Note**

The energy—and, thus, the wavenumber—of a photon that experiences Stokes scattering is less than the energy—and, thus, the wavenumber—of the source radiation, which begs the question of why a Stokes shift is reported as a positive value instead of a negative value. Although you will find most Raman spectra with positive values for the Stokes shift, you also will find examples where Stokes shifts are reported with negative values. Because the Stokes lines are more intense than the anti-Stokes lines, and, therefore, more useful, and because their respective shifts result from the same changes in vibrational energy states

that we find in IR spectroscopy, it is convenient to report the Stokes lines as positive values so that we can align a species's Raman and IR spectra. See the next two sections for additional details.

## Mechanism of Raman and Rayleigh Scattering

In Chapter 6 we examined the mechanism by which absorption and emission occur. In subsequent chapters we explored atomic absorption and atomic emission spectrometry, ultraviolet and visible molecular absorption spectrometry, molecular luminescence spectrometry, and infrared molecular absorption spectrometry. In each case we began by considering an energy level diagram that explains the origin of absorption and emission. Figure 18.1.2 provides an energy diagram that we can use to explain the origin of the lines that make up a Raman spectrum, such as the spectrum for carbon tetrachloride in Figure 18.1.1.

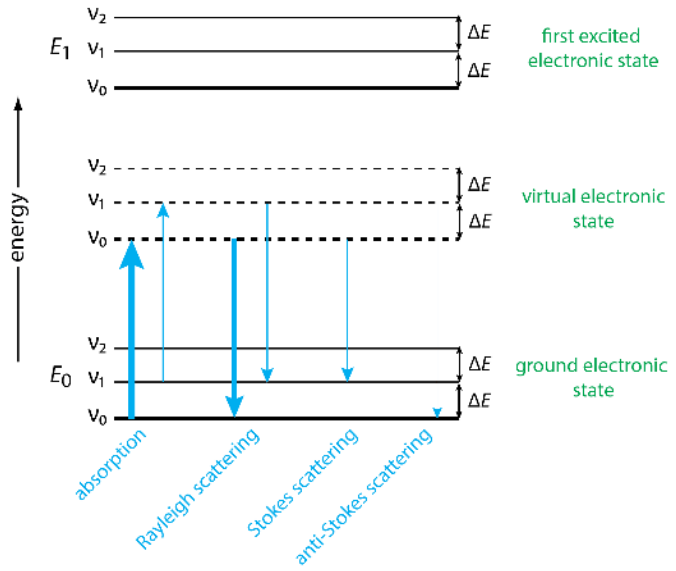



Figure 18.1.2: Energy level diagram that shows the origin of Rayleigh, Stokes, and anti-Stokes scattering. The thickness of the individual arrows provides a sense of the relative number of photons absorbed or emitted—the thicker the arrow, the greater the number of photons—although the individual thicknesses are not to scale.

The first thing to note about the energy level diagram in Figure 18.1.2 is that, in addition to showing the ground electronic state and the first excited electronic state—each with three vibrational energy levels—it also shows a virtual electronic state, something we did not encounter with other methods (see, for example, the energy diagram for UV and IR molecular absorption spectrometry in Figure 6.4.2). The ground and the first excited electronic states are quantized, which means that absorption cannot happen if the source's energy does not match exactly the change in energy between the two electronic states. The energy of an emitted photon also is fixed by the difference in the energy of the two electronic states. A virtual electronic state, however, is not quantized and is determined by the energy of the source radiation. The source of radiation, therefore, does not need to match a particular change in energy.

Absorption of a photon of source radiation moves the analyte from the ground electronic state to a virtual electronic state without a change in vibrational energy state, as seen by the two arrows at the far left of the diagram. Because the ground vibrational energy state, $\nu_0$, is more populated than the vibrational energy state, $\nu_1$, more of the analyte ends up in a virtual electronic state's lowest vibrational energy than in a higher vibrational energy state, which is shown here by the relative thickness of the two arrows.

Once in a virtual electronic state, the analyte can return to the ground excited state in one of three ways. It can do so without a change in the vibrational energy level. In this case, the energy of absorption and the energy of emission are the same and $\Delta E = 0$ and $\Delta \bar{\nu} = 0$. This is Rayleigh scattering and, as suggested by the combined thickness of the two arrows in Figure 18.1.2, it is the most important mechanism of relaxation.

When relaxation includes a change in the vibrational energy level, the result is an absolute change in energy equivalent to the difference in energy, $\Delta E$, between adjacent vibrational energy levels. For Stokes scattering, relaxation is to a higher vibrational energy level, such as $\nu_0 \rightarrow \nu_1$ and, for anti-Stokes scattering, relaxation to a lower vibrational energy level, such as $\nu_1 \rightarrow \nu_0$. As

suggested by the thickness of the lines for Stokes and anti-Stokes scattering in Figure 18.1.2, the Stokes lines are more intense than the anti-Stokes lines because they begin in a more heavily populated excited state.

## Relationship Between IR and Raman Spectra

One important feature of Figure 18.1.2 is that the transition that gives rise to a particular Stokes line or anti-Stokes line is the same transition that will give rise to a corresponding IR band. If the selection rules for these transitions are the same for a particular species, then we expect that its IR spectrum and its Raman spectrum will have peaks at the same (or similar) values of $\overline{\nu}$ and $\Delta\overline{\nu}$ for its fundamental vibrations; however, as we see in Table 18.1.1 for carbon tetrachloride, $CCl_4$, there are five fundamental vibrations in its Raman spectrum, but just three in its IR spectrum.

Table 18.1.1: Fundamental Vibrational Energies for $CCl_4$ (values from NIST).

| Infrared ($\overline{\nu}$, $cm^{-1}$) | Raman ($\Delta\overline{\nu}$, $cm^{-1}$) |
|---|---|
| — | 217.0 (*l*) |
| 309.9 (*l*) weak | 313.5 (*l*) |
| — | 458.7 (*l*) |
| 768 (*g*); very strong | 761.7 (*l*) |
| 789 (*g*); very strong | 790.4 (*l*) |

The designations (*g*) and (*l*) indicate the sample's phase where (*g*) is gas phase and (*l*) is liquid phase. The designations of weak and very strong for the IR peaks indicates the relative extent of absorption: very strong means a relatively small %T (and a strong absorbance) and weak means a relatively large %T (and a weak absorbance). See Figure 18.1.1 for the relative amount of scattering in the Raman spectrum for $CCl_4$.

In Chapter 16 we learned that in IR spectroscopy a compound's fundamental vibrational energy is active—that is, we see a peak in its IR spectrum—only if the corresponding stretch or bend results in a change in the compound's dipole moment. For Raman spectroscopy, a compound's fundamental vibrational energy is active only if the corresponding stretch or bend results in a change in the polarizability of its electrons. Polarizability essentially is a measure of how easy it is to distort a compound's electron cloud by applying an external electric field, such as when a photon from the source is absorbed; in general, polarizability increases when a stretching or bending motion increases the compound's volume as the electrons are then spread over a greater amount of space.

Figure 18.1.3 shows the four stretching and bending modes for $CCl_4$. The stretching motion in (a), in which all four C–Cl bond lengths increase and decrease together, means the molecule's volume increases and decreases; thus, this vibrational mode is Raman active. The symmetry of the stretching motion, however, means there is no change in the molecule's dipole moment and the vibrational mode is IR inactive. The asymmetric stretch in (b), on the other hand, is both IR and Raman active. The bending motion in (c) results in the molecule becoming more or less compact in size, and is Raman active; the symmetry of the scissoring motions, however, means that the vibrational mode is IR inactive. The bending motions in (d) are both IR and Raman active.

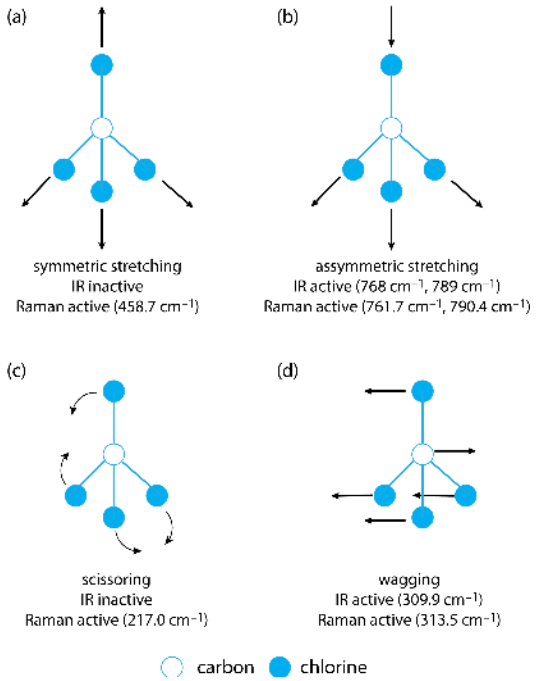



Figure 18.1.3. The four fundamental types of vibrational motions for $CCl_4$. The molecule has a tetrahedral shape. The black arrows show the direction of movement of the individual atoms. A molecule of $CCl_4$ has $3 \times 5 - 6 = 15 - 6 = 9$ vibrational modes. The bending motion in (d) and the stretching motion in (b) are triply degenerate, the bending motion in (c) is doubly degenerate, and the stretching motion in (a) is singly degenerate; this accounts for the nine possible vibrational modes. The asymmetric stretching motion in (b) gives rise to a split peak for reasons we will not consider here.

In general, symmetric stretching and bending modes result in relatively strong Raman scattering peaks, but no absorption in the IR, while symmetric stretching and bending modes result in both IR and Raman peaks. As a result, IR and Raman are complementary techniques.

## Raman Depolarization Ratios

If the source of electromagnetic radiation is plane-polarized, then it is possible to collect a Raman spectrum using light scattered in a plane that is parallel to the source and, separately, in a plane that is perpendicular to the source. The ratio of a line's intensity of scattering in the perpendicular spectrum, $I_{\perp}$, to the intensity of scattering in the parallel spectrum, $I_{||}$, is called the depolarization ratio, $p$.

$$p = \frac{I_{\perp}}{I_{||}} \tag{18.1.1}$$

A Raman line that originates from a vibrational mode that does not change the molecules shape will result in a depolarization ratio close to zero and an absence of the line in the perpendicular spectrum. Figure 18.1.4 shows the Raman spectrum when collecting data parallel (top) and perpendicular (bottom) to the light source. The absence of the peak at 458.7 $cm^{-1}$ in the perpendicular spectrum confirms that this is the symmetric stretch illustrated in Figure 18.1.3$a$.

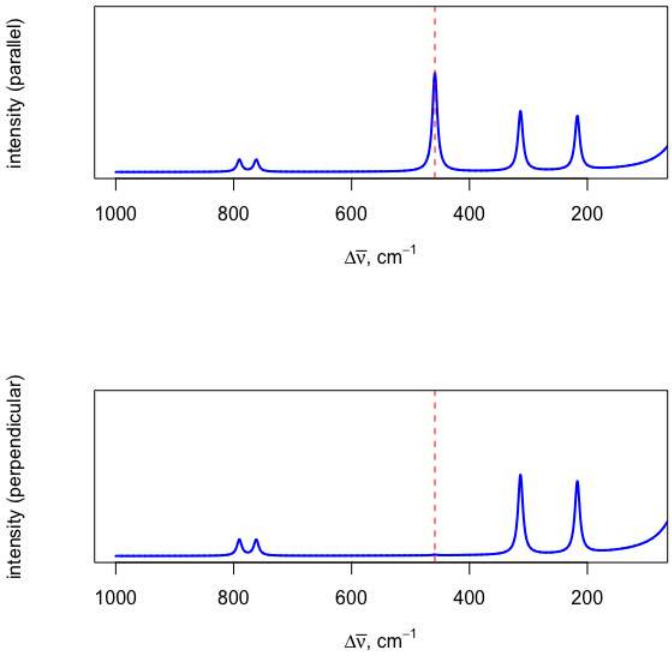



Figure 18.1.4: Raman spectrum for $CCl_4$ measured (top) parallel to the plane-polarized light source and (bottom) perpendicular to the plane-polarized source. The dashed red line shows the position of the symmetric stretch at 458.7 $cm^{-1}$; the absence of this peak in the perpendicular spectrum—the depolarization ratio, $p$ is 0.005—confirms that this is the symmetric stretch. The remaining peaks have depolarization ratios of 0.75. The slope of increasing intensity below 200 $cm^{-1}$ is from the Rayleigh scattering peak. The values for these lines are from NIST; the spectrum itself is simulated.

This page titled 18.1: Theory of Raman Spectroscopy is shared under a CC BY-NC-SA 4.0 license and was authored, remixed, and/or curated by David Harvey.

# 18.2: Instrumentation

The basic instrumentation for Raman spectroscopy is similar to that for other spectroscopic techniques: a source or radiation, an optical bench for bringing the source to the sample, and a suitable detector.

## Sources

One of the notable features of the Raman spectrum for $CCl_4$ (see Figure 18.1.1) is the low intensity of the Stokes lines and the anti-Stokes lines relative to the line for Rayleigh scattering. The low intensity of these lines requires that we use a high intensity source so that there are a sufficient number of scattered photons to collect. For this reason, a laser is the most common source for Raman spectroscopy, providing a high intensity, monochromatic source. Table 18.2.1 summarizes some of the more common lasers.

Table 18.2.1. Examples of Laser Sources for Raman Spectroscopy

| type of laser | wavelengths (nm) |
|---|---|
| Ar ion | 488.0 or 514.5 |
| Kr ion | 530.9 or 647.1 |
| He/Ne | 632.8 |
| Near Infrared (NIR) Diode Laser | 785 or 830 |
| Nd/YAG | 532 or 1064 |

The intensity of Raman scattering is proportional to $\frac{1}{\lambda^4}$, where $\lambda$ is the wavelength of the source radiation; thus, the smaller the wavelength, the more intense the intensity of scattered light. For example, the intensity of scattering using an Ar ion laser at 488.0 nm is almost $23\times$ greater than the intensity of scattering using a Nd/YAG laser at 1064 nm

$$\frac{(1/480)^4}{(1/1064)^4} = 22.6$$

The increased scattering when using a smaller wavelength laser comes at a cost, however, of an interference from fluorescence from species that are promoted into excited electronic states by the source. The NIR diode laser and Nd/YAG laser, when operated at 1064 $cm^{-1}$, discriminate against fluorescence and are useful, therefore, for samples where fluorescence is a problem.

## Samples

Raman spectroscopy has several advantages over infrared spectroscopy. Because water does not exhibit much Raman scattering it is possible to analyze aqueous samples; this is a serious limitation for IR spectroscopy where water absorbs strongly. The ability to focus a laser onto a small area makes it possible to analyze very small samples. A liquid sample, for example, can be held in the tip of a 1-mm inner diameter capillary tube, such as that used for measuring melting points. Solid samples and gaseous samples can be sampled using the same types of cells used in IR and FT-IR (see Chapter 17). Fiber optic probes make it possible to collect samples remotely. Figure 18.2.1 shows the basic set-up. A small bundle of fibers (shown in blue) brings light from the source to the sample where a second bundle of fibers (shown in green) brings the scattered light to the slit that passes light onto the detector.

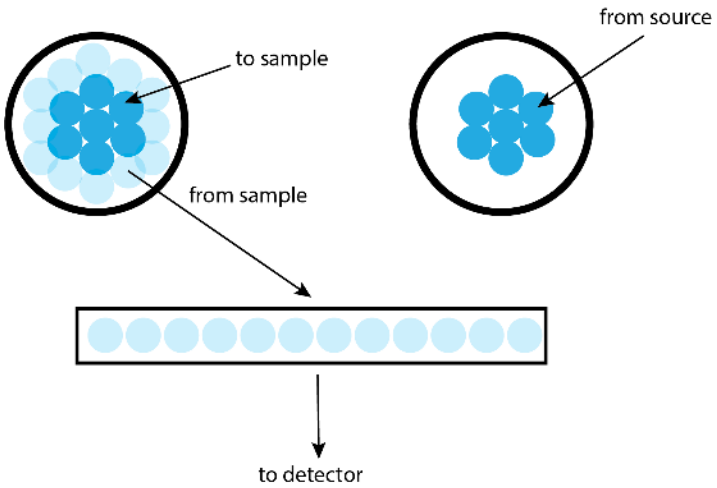



Figure 18.2.1: Illustration of a fiber optic probe for Raman spectroscopy. The darker blue circles are cross-sections of individual fibers that bring light from the source to the sample, and the lighter blue circles are cross-sections of individual fibers that collect scattered light from the sample and bring it to the detector. The circular arrangement of the collection fibers are gathered into a linear array and focused onto the entrance slit of the instrument's detector.

## Optical Bench

Raman spectrometers use optical benches similar to those for UV/Vis or IR spectroscopy, which were covered in Chapter 7. Dispersive instruments place the laser source and the detector at 90° to each other so that any unscattered high intensity emission from the laser source is not collected by the detector. A filter is used to remove the Rayleigh scattering. To record a spectrum one either uses a scanning monochromator or a multichannel detector. Fourier transform instruments are similar to those used in FT-IR and include a filter to isolate the Stokes lines.

---

This page titled 18.2: Instrumentation is shared under a CC BY-NC-SA 4.0 license and was authored, remixed, and/or curated by David Harvey.

# 18.3: Applications of Raman Spectroscopy

Raman spectroscopy is useful for both qualitative and quantitative analyses, examples of which are provided in this section.

## Qualitative Applications

There are numerous databases that provide reference spectra for inorganic compounds, for minerals, for synthetic organic pigments, for natural and synthetic inorganic and organic pigments, and for carbohydrates. Such data bases are often searchable by not only name and formula, but by the prominent Raman scattering lines. Examples of spectra are included here using data from the databases linked to above.

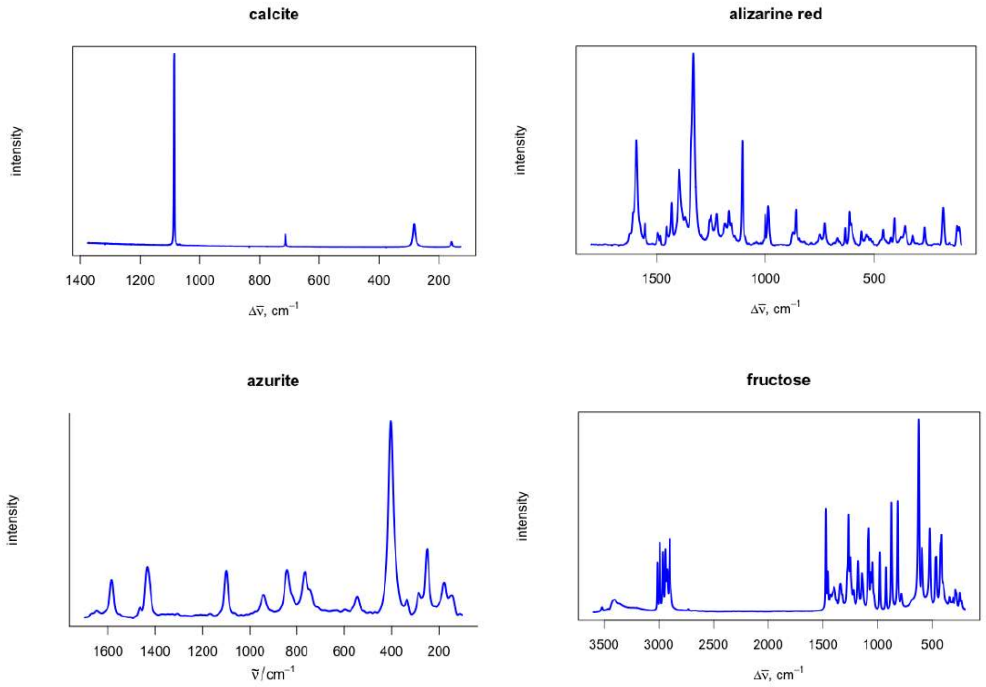



Figure 18.3.1: Examples of Raman spectra for the mineral calcite ($CaCO_3$), the organic pigment alizarine red ($C_{14}H_7NaO_7S$), the inorganic pigment azurite ($Cu_3(CO_3)_2(OH)_2$), and the carbohydrate fructose ($C_6H_{12}O_6$). The data for these spectra were obtained from the databases linked to at the beginning of this section.

## Quantitative Applications

The intensity of Raman scattering, $I(\nu)_R$, is directly proportional to the intensity of the source radiation, $I_l$, and the concentration of the scattering species, $C$. The direct proportionality between $I(\nu)_R$ and $I_l$ is important given that each photon experiencing Raman scattering requires approximately $10^8$ excitation photons. Using a laser as a source of radiation and increasing its power leads to an improvement in sensitivity. The direct proportionality between $I(\nu)_R$ and the concentration of the scattering species means that a calibration curve of band intensity (or band area) is a linear function of concentration, allowing for a quantitative analysis.

This page titled 18.3: Applications of Raman Spectroscopy is shared under a CC BY-NC-SA 4.0 license and was authored, remixed, and/or curated by David Harvey.

# 18.4: Other Types of Raman Spectroscopy

Traditional Raman spectroscopy has several limitations, perhaps the most important of which is that the probability of Raman scattering is much less than that for Rayleigh scattering, which leads to low sensitivity with detection limits often as large as 0.1 M. Here we briefly describe two forms of Raman spectroscopy that allow for significant improvements in detection limits.

## Resonance Raman Spectroscopy (RRS)

If the wavelength of the source is similar to the wavelength needed to move the species from its ground electronic state to its first electronic excited state (not the virtual excited state shown in Figure 18.1.2), then the lines associated with the symmetric fundamental vibrations increase in intensity by a factor of $10^2$ to $10^6$. The improvement in sensitivity results in a substantial reduction in detection limits as low as $10^{-8}$ M. The use of a tunable laser makes it possible to adjust the wavelength of light emitted by the source to maximize the intensity of scattering.

## Surface-Enhanced Raman Spectroscopy (SERS)

For reasons that are poorly understood, the intensity of Raman scattering lines is enhanced when the scattering species is absorbed to the surface of colloidal particles of metals such as Ag, Au, or Cu, or to the surface of etched metals. The phenomenon is not limited to just a few lines—as is the case for RRS—and results in a $10^3$ to $10^6$) improvement in the intensity of scattering. If a tunable laser is used for the source, allowing for both RRS and SERS, detection limits of $10^{-9}$ M to $10^{-12}$ M are possible.

This page titled 18.4: Other Types of Raman Spectroscopy is shared under a CC BY-NC-SA 4.0 license and was authored, remixed, and/or curated by David Harvey.

# CHAPTER OVERVIEW

## 19: Nuclear Magnetic Resonance Spectroscopy


19.1: Theory of Nuclear Magnetic Resonance
19.2: Environmental Effects on NMR Spectra
19.3: NMR Spectrometers
19.4: Applications of Proton NMR
19.5: Carbon-13 NMR
19.6: Two-Dimensional Fourier Transform NMR


---


This page titled 19: Nuclear Magnetic Resonance Spectroscopy is shared under a CC BY-NC-SA 4.0 license and was authored, remixed, and/or curated by David Harvey.

# 19.1: Theory of Nuclear Magnetic Resonance

As is the case with other forms of optical spectroscopy, the signal in nuclear magnetic resonance (NMR) spectroscopy arises from a difference in the energy levels occupied by the nuclei in the analyte. In this section we develop a general theory of nuclear magnetic resonance spectroscopy that draws on quantum mechanics and on classical mechanics to explain these energy levels.

## Quantum Mechanical Description of NMR

The quantum mechanical description of an electron is given by four quantum numbers: the principal quantum number, $n$, the angular momentum quantum number, $l$, the magnetic quantum number, $m_l$, and the spin quantum number, $m_s$. The first three of these quantum numbers tell us something about where the electron is relative to the nucleus and something about the electron's energy. The last of these four quantum numbers, the spin quantum number, tells us something about the ability of an electron to interact with an applied magnetic field. An electron has possible spins of +1/2 or of –1/2, which we often refer to as spin up, using an upwards arrow, ↑, to represent it, or as spin down, using a downwards arrow, ↓, to represent it.

A nucleus, like an electron, carries a charge and has a spin quantum number. The overall spin, $I$, of a nucleus is a function of the number of protons and neutrons that make up the nucleus. Here are three simple rules for nuclear spin states:

- If the number of neutrons and the number of protons are both even numbers, then the nucleus does not have a spin; thus, $^{12}$C, with six protons and six neutrons, has no overall spin and $I = 0$.
- If the number of neutrons plus the number of protons is an odd number, then the nucleus has a half-integer spin, such as 1/2 or 3/2; thus, $^{13}$C, with six protons and seven neutrons, has an overall spin of $I = 1/2$; this also is true for $^{1}$H.
- If the number of neutrons and the number of protons are both odd numbers, then the nucleus has an integer spin, such as 1 or 2; thus, $^{2}$H, with one proton and one neutron, has an overall spin of $I = 1$.

**Note**

Predicting that $^{13}$C has a spin of $I = 1/2$, but that $^{127}$I has a spin of $I = 3/2$ and that $^{17}$O has a spin of $I = 5/2$ is not trivial. A periodic table that provides spin states for elements is available here.

The total number of spin states—that is, the total number of possible orientations of the spin—is equal to $(2 \times I) + 1$. To be NMR active, a nucleus must have at least two spin states so that a change in spin states, and, therefore, a change in energy, is possible; thus, $^{12}$C, for which there are $(2 \times 0) + 1 = 1$ spin states, is NMR inactive, but $^{13}$C, for which there are $(2 \times 1/2) + 1 = 2$ spin states with values of $m = +1/2$ and of $m = -1/2$, is NMR active, as is $^{2}$H for which there are $(2 \times 1) + 1 = 3$ spin states with values of $m = +1/2$, $m = 0$, and $m = -1/2$. As our interest in this chapter is in the NMR spectra for $^{1}$H and for $^{13}$C, we will limit ourselves to considering $I = 1/2$ and spin states of $m = +1/2$ and of $m = -1/2$.

### Energy Levels in an Applied Magnetic Field

Suppose we have a large population of $^{1}$H atoms. In the absence of an applied magnetic field the atoms are divided equally between their possible spin states: 50% of the atoms have a spin of +1/2 and 50% of the atoms have a spin of –1/2. Both spin states have the same energy, as is the case on the left side of Figure 19.1.1, and neither absorption nor emission occurs.

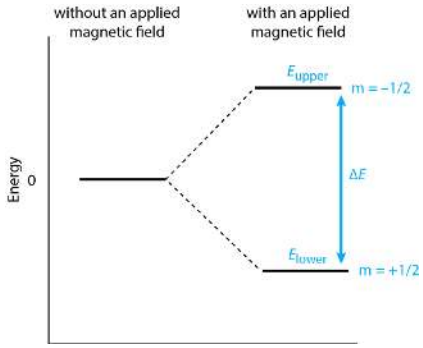



Figure 19.1.1. Energy level diagram for a proton, $^{1}$H, in the absence (left) and in the presence (right) of an applied magnetic field.

In the presence of an applied magnetic field, as on the right side of Figure 19.1.1, the nuclei are either aligned with the magnetic field with spins of $m = +1/2$, or aligned against the magnetic field with spins of $m = -1/2$. The energies in these two spin states, $E_{\text{lower}}$ and $E_{\text{upper}}$, are given by the equations

$$E_{\text{lower}} = -\frac{\gamma h}{4\pi} B_0 \tag{19.1.1}$$

$$E_{\text{upper}} = +\frac{\gamma h}{4\pi} B_0 \tag{19.1.2}$$

where $\gamma$ is the magnetogyric ratio for the nucleus, $h$ is Planck's constant, and $B_0$ is the strength of the applied magnetic field. The difference in energy, $\Delta E$, between the two states is

$$\Delta E = E_{\text{upper}} - E_{\text{lower}} = +\frac{\gamma h}{4\pi} B_0 - \left(-\frac{\gamma h}{4\pi} B_0\right) = \frac{\gamma h}{2\pi} B_0 \tag{19.1.3}$$

Substituting Equation 19.1.3 into the more familiar equation $\Delta E = h\nu$ gives the frequency, $\nu$, of electromagnetic radiation needed to effect a change in spin state as

$$\nu = \frac{\gamma B_0}{2\pi} \tag{19.1.4}$$

This is called the Larmor frequency for the nucleus. For example, if the magnet has a field strength of 11.74 Tesla, then the frequency needed to effect a change in spin state for $^1$H, for which $\gamma$ is $2.68 \times 10^8$ rad $\text{T}^{-1}\text{s}^{-1}$, is

$$\nu = \frac{(2.68 \times 10^8 \text{rad T}^{-1}\text{s}^{-1})(11.74 \text{ T})}{2\pi} = 5.01 \times 10^8 \text{ s}^{-1}$$

or 500 MHz, which is in the radio frequency (RF) range of the electromagnetic spectrum. This is the Larmor frequency for $^1$H.

### Population of Spin States

The relative population of the upper spin state, $N_{\text{upper}}$, and of the lower spin state, $N_{\text{lower}}$, is given by the Boltzmann equation

$$\frac{N_{\text{upper}}}{N_{\text{lower}}} = e^{-\Delta E/kT} \tag{19.1.5}$$

where $k$ is Boltzmann's constant ($1.38066 \times 10^{-23}$ J/K) and $T$ is the temperature in Kelvin. Substituting in Equation 19.1.3 for $\Delta E$ gives this ratio as

$$\frac{N_{\text{upper}}}{N_{\text{lower}}} = e^{-\gamma h B_0/2\pi kT} \tag{19.1.6}$$

IF we place a population of $^1$H atoms in a magnetic field with a strength of 11.74 Tesla, the ratio $\frac{N_{\text{upper}}}{N_{\text{lower}}}$ at 298 K is

$$\frac{N_{\text{upper}}}{N_{\text{lower}}} = e^{-\frac{(2.68\times10^8 \text{ rad s}^{-1})(6.626\times10^{-34} \text{ Js})(11.74 \text{ T})}{(2\pi)(1.38\times10^{-23} \text{ JK}^{-1})(298 \text{ K})}} = 0.99992$$

If this ratio is 1:1, then the probability of absorption and emission are equal and there is no net signal. In this case, the difference in the populations is on the order of 8 per 100,000, or 80 per 1,000,000, or 80 ppm. The small difference in the two populations means that NMR is less sensitive than many other spectroscopic methods.

## Classical Description of NMR

To understand the classical description of an NMR experiment we draw upon Figure 19.1.2. For simplicity, let's assume that in the population of nuclei available to us, there is an excess of just one nucleus with a spin state of +1/2. In Figure 19.1.2*a*, we see that the spin of this nucleus is not perfectly aligned with the applied magnetic field, $B_0$, which is aligned with the *z*-axis; instead the nucleus precesses around the *z*-axis at an angle of theta, Θ. As a result, the net magnetic moment along the *z*-axis, $\mu_z$, is less than the magnetic moment, μ, of the nucleus. The precession occurs with an angular velocity, $\omega_0$, of $\gamma B_0$.

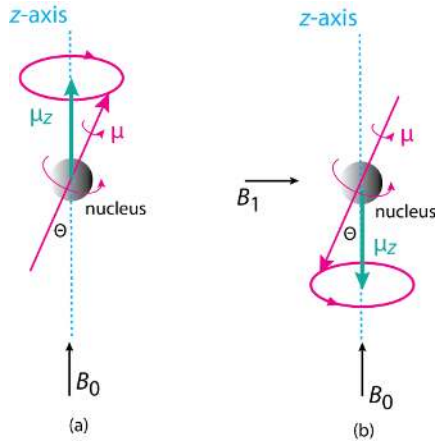



Figure 19.1.2. Illustration that shows in (a) the magnetic moment, μ, of a nucleus whose spin is aligned with the applied magnetic field, $B_0$. Application of the magnetic field, $B_1$ flips the spin of the nucleus, as shown in (b).

If we apply a source of radio frequency (RF) electromagnetic radiation along the *x*-axis such that its magnetic field component, $B_1$, is perpendicular to $B_0$, then it will generate its own angular velocity in the *xy*-plane. When the angular velocity of the precessing nucleus matches the angular velocity of $B_1$, absorption takes place and the spin flips, as seen in Figure 19.1.2*b*.

## Relaxation

When the magnetic field $B_1$ is removed, the nucleus returns to its original state, as seen in Figure 19.1.2*a*, a process called relaxation. In the absence of relaxation, the system is saturated with equal populations of the two spin states and absorption approaches zero. This process of relaxation has two separate mechanisms: spin-lattice relaxation and spin-spin relaxation.

In spin-lattice relaxation the nucleus in its higher energy spin state, Figure 19.1.2*b*, returns to its lower energy state spin state, Figure 19.1.2*a*, by transferring energy to other species present in the sample (the lattice in spin-lattice). Spin-lattice relaxation is characterized by first-order exponential decay with a characteristic relaxation time of $T_1$ that is a measure of the average time the nucleus remains in its higher energy spin state. Smaller values for $T_1$ result in more efficient relaxation.

If two nuclei of the same type, but in different spin states, are in close proximity to each other, they can trades places in which the nucleus in the higher energy spin state gives up its energy to the nucleus in the lower energy spin state. The result is a decrease in the average life-time of an excited state. This is called spin-spin relaxation and it is characterized by a relaxation time of $T_2$.

## Continuous Wave NMR vs. Fourier Transform NMR

In Chapter 16 we learned that we can record an infrared spectrum by using a scanning monochromator to pass, sequentially, different wavelengths of IR radiation through a sample, obtaining a spectrum of absorbance as a function of wavelength. We also learned that we can obtain the same spectrum by passing all wavelengths of IR radiation through the sample at the same time using an interferometer, and then use a Fourier transform to convert the resulting interferogram into a spectrum of absorbance as a function of wavelength. Here we consider their equivalents for NMR spectroscopy.

### Continuous Wave NMR

If we scan $B_1$ while holding $B_0$ constant—or scan $B_0$ while holding $B_1$ constant—then we can identify the Larmor frequencies where a particular nucleus absorbs. The result is an NMR spectrum that shows the intensity of absorption as a function of the frequency at which that absorption takes place. Because we record the spectrum by scanning through a continuum of frequencies, the method is known as continuous wave NMR. Figure 19.1.2 provides a useful visualization for this experiment.

### Fourier Transform NMR

In Fourier transform NMR, the magnetic field $B_1$ is applied as a brief pulse of radio frequency (RF) electromagnetic radiation centered at a frequency appropriate for the nucleus of interest and for the strength of the primary magnetic field, $B_0$. The pulse typically is 1-10 μs in length and applied in the *xy*-plane. From the Heisenberg uncertainty principle, a short pulse of $\Delta t$ results in a broad range of frequencies as $\Delta f = 1/\Delta t$; this ensures that the pulse spans a sufficient range of frequencies such that the nucleus of interest to us will absorb energy and enter into an excited state.

Before we apply the pulse, the population of nuclei are aligned parallel to the applied magnetic field, $B_0$, some with a spin of +1/2 and others with a spin of –1/2. As we learned above, there is a slight excess of nuclei with spins of +1/2, which we can represent as a single vector that shows their combined magnetic moments along the *z*-axis, $\mu_z$, as shown in Figure 19.1.3*a*. When we apply a pulse of RF electromagnetic radiation with a magnetic field strength of $B_1$, the spin states of the nuclei tip away from the *z*-axis by an angle that depends on the nucleus's magnetogyric ratio, $\gamma$, the value of $B_1$, and the length of the pulse. If, for example, a pulse of 5 μs tips the the magnetic vector by 45° (Figure 19.1.3*b*), then a pulse of 10 μs will tip the magnetic vector by 90° degrees (Figure 19.1.3*c*), so that it now lies completely within the *xy*-plane.

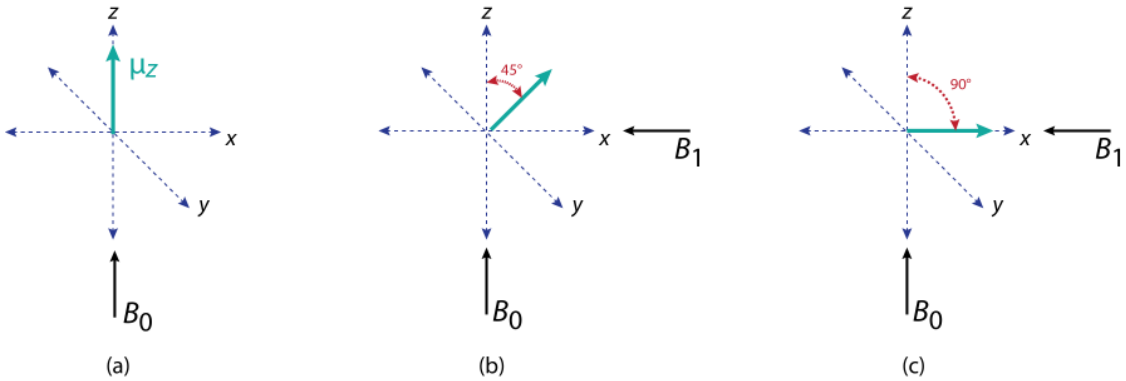



Figure 19.1.3. Illustration that shows (a) the net magnetic moment on the *z*-axis for a population of nuclei in an applied magnetic field with a field strength of $B_0$. Application of a pulsed RF field, $B_1$, tips the magnetic moment (b) away from the *z*-axis. The longer the pulse of RF, the greater the angle of tipping, as shown in (c).

At the end of the pulse, the nuclei begin to relax back to their original state. Figure 19.1.4 shows that this relaxation occurs both in the *xy*-plane (spin-spin relaxation) and along the *z*-axis (spin-lattice relaxation). If we were to trace the path of the magnetic vector with time, we would see that it follows a spiral-like motion as its contribution in the *xy*-plane decreases and its contribution along the *z*-axis increases. We measure this signal—called the free induction decay, or FID—during this period of relaxation.

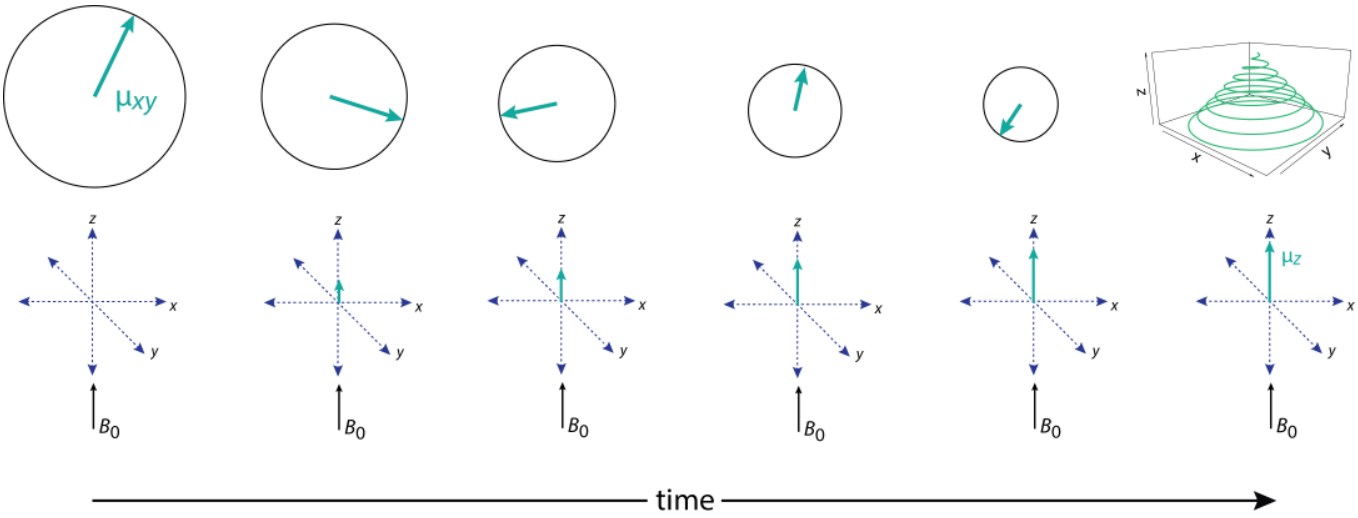



Figure 19.1.4. Illustration showing the process of relaxation during an NMR experiment. The bottom row shows the net magnetic moment aligned with the *z*-axis, $\mu_z$, as a function of time. The top row shows the net magnetic moment in the *xy*-plane with the figure on the top right showing the overall change in the net magnetic moment in three dimensions.

The FID for a system that consists of only one type of nucleus is the simple exponentially damped oscillating signal in Figure 19.1.5*a*. The Fourier transform of this simple FID gives the spectrum in Figure 19.1.5*b* that has a single peak. A sample with a more than one type of nucleus yields a more complex FID pattern, such as that in Figure 19.1.5*c*, and a more complex spectrum, such as the two peaks in Figure 19.1.5*d*. Note that, as we learned in an earlier treatment of the Fourier transform in Chapter 7, a broader peak in the frequency domain results in a faster decay in the time domain.

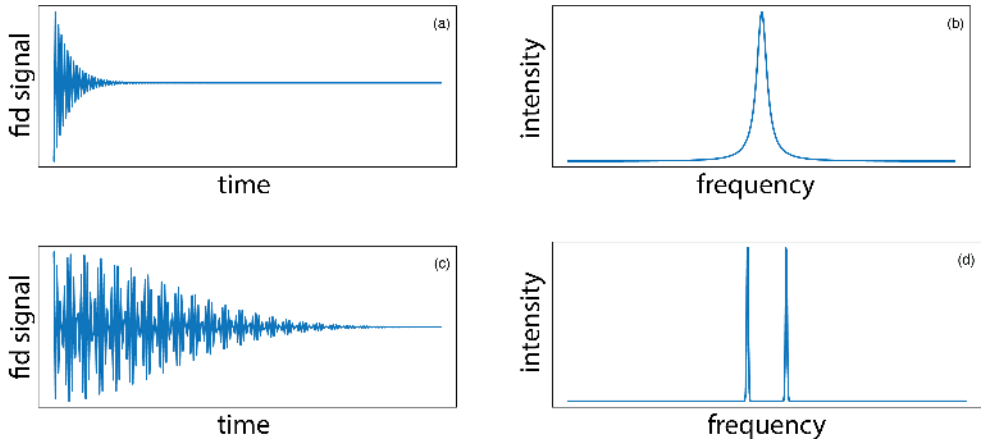



Figure 19.1.5. Panels (a) and (b) show the FID signal for a sample that yields single peak and the result of taking the FT of the FID. Panels (c) and (d) show the FID signal for a sample that consists of two peaks and the result of taking the FT of the FID.

Figure 19.1.6 shows a typical pulse sequence highlighting the total cycle time and its component parts: the pulse width, the acquisition time during which the FID is recorded, and a recycle delay before applying the next pulse and beginning the next cycle.

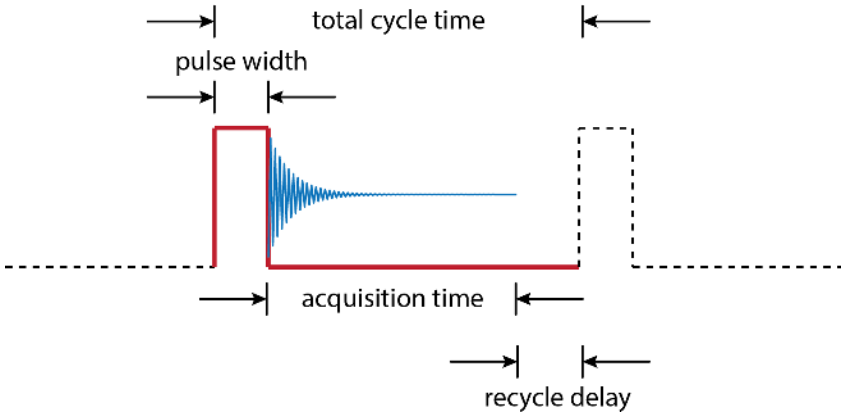



Figure 19.1.1: Example of a pulse sequence.

This page titled 19.1: Theory of Nuclear Magnetic Resonance is shared under a CC BY-NC-SA 4.0 license and was authored, remixed, and/or curated by David Harvey.

# 19.2: Environmental Effects on NMR Spectra

In the previous section we showed that there is a relationship between the Larmor frequency for a nucleus, $\nu$, its magnetogyric ratio, $\gamma$, and the primary applied magnetic field strength, $B_0$

$$\nu = \frac{\gamma B_0}{2\pi} \tag{19.2.1}$$

and we used this equation to show that the Larmor frequency for the $^1$H nucleus in a magnetic field of $B_0 = 11.74$ T is 500 MHz. If this is the only thing that determines the frequency where absorption takes place, then all compounds that contain hydrogens will yield a $^1$H NMR spectrum with a single peak at the same frequency. If all spectra are identical, then NMR provides little in the way of useful information. The NMR spectrum for propane ($CH_3$–$CH_2$—$CH_3$) in Figure 19.2.1 shows two clusters of peaks that give us confidence in the utility of NMR. In this case, it seems likely that the cluster of peaks between 250 Hz and 300 Hz, which have a greater total intensity, are for the six hydrogens in the two methyl groups (–$CH_3$) and that the cluster of peaks around 400 Hz are due to the methylene group (–$CH_2$–). In this section we will consider why the location of a nucleus within a molecule—what we call its environment—might affect the frequency at which it absorbs and why a particular absorption line might appear as a cluster of individual peaks instead of as a single peak.

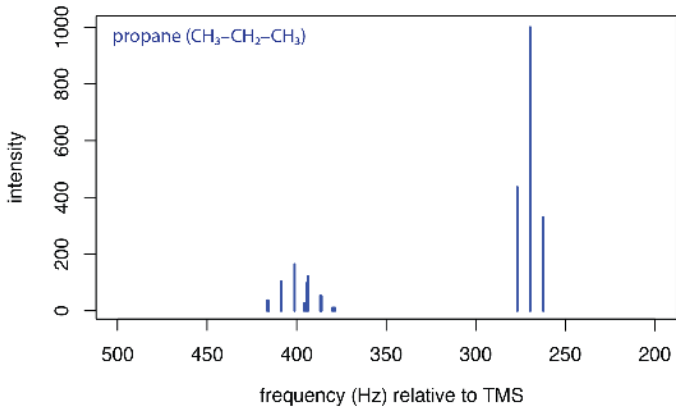



Figure 19.2.1: $^1$H NMR spectrum for propane. The original data used to construct this spectrum is here and was obtained on a 300 MHz instrument.

## The NMR Spectrum's Scale

Before we consider how a nucleus's environment affects the frequencies at which it absorbs, let's take a moment to become familiar with the scale used to plot a NMR spectrum. The label on the *x*-axis of the NMR spectrum for propane in Figure 19.2.1 raises several questions that we will answer here.

### Why is the Scale Relative?

From Equation 19.2.1 we see that the frequency at which a nucleus absorbs is a function of the magnet's field strength, $B_0$. This means the frequency of a peak in an NMR spectrum depends on the value of $B_0$. One complication is that instruments with identical nominal values for $B_0$ likely will have slightly different actual values, which leads to small variations in the frequency at which a particular hydrogen absorbs on different instruments. We can overcome this problem by referencing a hydrogen's measured frequency to a reference compound that is set to a frequency of 0. The difference between the two frequencies should be the same on different instruments. For example, the most intense peak in the NMR spectrum for propane, Figure 19.2.1, has a frequency of 269.57 Hz when measured on an NMR with a nominal field strength of 300 MHz, which means that its frequency is 269.57 Hz greater than the reference, which is identified as TMS.

### What is TMS?

The reference compound is tetramethylsilane, TMS, which has the chemical formula of $(CH_3)_4Si$ in which four methyl groups are in a tetrahedral arrangement about the central silicon. TMS has the advantage of having all of its hydrogens in the same environment, which yields a single peak. Its hydrogen atoms also absorbs at a low frequency that is well removed from the frequency at which most other hydrogen atoms absorb, which makes it easy to identify its peak in the NMR spectrum.

### How Can We Create a Universal Scale?

An additional complication with the spectrum in Figure 19.2.1 is that the frequency at which a particular hydrogen absorbs is different when using a 60 MHz NMR than it is when using a 300 MHz NMR, a consequence of Equation 19.2.1. To create a single scale that is independent of $B_0$ we divide the peak's frequency, relative to TMS, by $B_0$, expressing both in Hz, and then report the result on a part-per-million scale by multiplying by $10^6$. For example, the most intense peak in the NMR spectrum for propane, Figure 19.2.1, has a frequency of 269.57 Hz; the NMR on which the spectrum was recorded had a field strength of 300 MHz. On a parts-per-million scale, which we identify as delta, $\delta$, the peak appears at

$$\delta = \frac{269.57 \text{ Hz}}{300 \times 10^6 \text{ Hz}} \times 10^6 = 0.899 \text{ ppm}$$

If we record the spectrum of propane on a 60 MHz instrument, then we expect that this peak to appear at 0.899 ppm, or a frequency of

$$\nu = \frac{0.899 \text{ ppm} \times (60 \times 10^6 \text{ Hz})}{10^6} = 53.9 \text{ Hz}$$

relative to TMS.

Most hydrogens have values of $\delta$ between 1 and 13. Figure 19.2.2 shows the $^1$H NMR for propane using a ppm scale. The right side of the ppm scale is described as being upfield, with absorption occurring at a lower frequency, and with a smaller difference in energy, $\Delta E$, between the ground state and the excited state. The left side of the ppm scale is described as being downfield, with absorption occurring at a higher frequency, and with a greater difference in energy, $\Delta E$, between the ground state and the excited state.

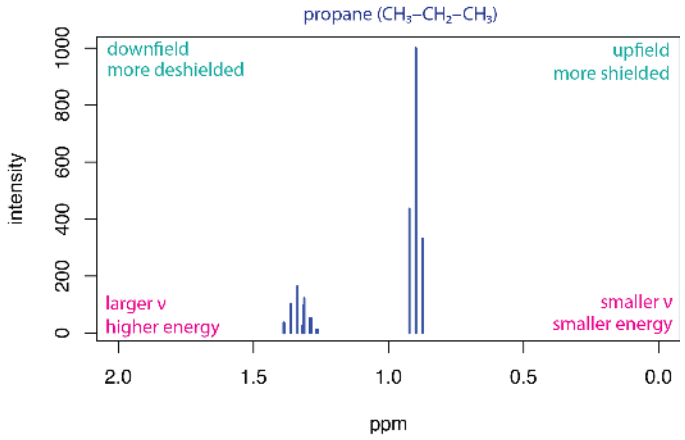



Figure 19.2.2: $^1$H NMR spectrum for propane expressed in ppm. The original data used to construct this spectrum is here and was obtained on a 300 MHz instrument. The peak for TMS is not shown.

## Types of Environmental Effects

The NMR spectrum for propane in Figure 19.2.2 shows two important features: the peaks for the two types of hydrogen in propane are shifted downfield relative to the reference and the methylene hydrogens are shifted further downfield than the methyl hydrogens. Both groups appear as clusters of peaks instead of as single peaks. In this section we consider the source of these two phenomena.

### Chemical Shifts

In the presence of a magnetic field, the electrons in a molecule circulate, generating a secondary magnetic field, $B_e$, that usually, but not always, opposes the primary applied magnetic field, $B_{\text{appl}}$. The result is that the nucleus is partially shielded by the electrons such that the field it experiences, $B_0$, usually is smaller than the applied field and

$$B_0 = B_{\text{appl}} - B_e \tag{19.2.2}$$

The greater the shielding, the smaller the value of $B_0$ and the further to the right the peak appears in the NMR spectrum. For example, in the NMR spectrum for propane in Figure 19.2.2 the cluster of peaks for the –$CH_3$ hydrogens centered at 0.899 ppm

shows greater shielding than the cluster of peaks for the $–CH_2–$ hydogens that is centered at 1.337 ppm.

Chemical shifts are useful for determining structural information for molecules. A few examples are listed in the following table and more extensive tables here. Note that the range of chemical shifts for the methyl and the methylene groups encompass the values for propane in Figure 19.2.2.

Table 19.2.1. $^1H$ Shifts in ppm

| type of hydrogen | example | range of chemical shifts (ppm) |
|---|---|---|
| primary alkyl | $R–CH_3$ | 0.7 – 1.3 |
| secondary alkyl | $R–CH_2–R$ | 1.2 – 1.6 |
| tertiary alkyl | $R_3CH$ | 1.4 – 1.8 |
| methyl ketone | $R–C(=O)–CH_3$ | 2.0 – 2.4 |
| aromatic methyl | $C_6H_5–CH_3$ | 2.4 – 2.7 |
| alkynyl | $R–C\equiv C–H$ | 2.5 – 3.0 |
| alkyl halide (X = F, Cl, Br, I) | $R_2X–CH$ | 2.5 – 4.0 |
| alcohol | $R_3–C–OH$ | 2.5 – 5.0 |
| vinylic | $R_2–C=C(–R)–H$ | 4.5 – 6.5 |
| aryl | $C_6H_5–H$ | 6.5 – 8.0 |
| aldehyde | $R–C(=O)–H$ | 9.7 – 10.0 |
| carboxylic acid | $R–C(=O)–OH$ | 11.0 – 12.0 |

## Spin-Spin Coupling

Chemical shifts are the result of shielding from the magnetic field associated with a molecule's circulating electrons. The splitting of a peak into a multiplet of peaks is the result of the shielding of one nucleus by the nuclei on adjacent atoms, and is called spin-spin coupling. Consider the NMR for propane in Figure 19.2.2, which consists of two clusters of peaks. The six hydrogens in the two methyl groups are sufficiently close to the two hydrogens in the methylene group that the spins of the methylene hydrogens can affect the frequency at which the methyl hydrogens absorb. Figure 19.2.3$a$ shows how this works. Each of the two methylene hydrogens has a spin and those spins can both be aligned with the magnetic field, $B_0$, both be aligned against $B_0$, or two configurations in which one is aligned with $B_0$ and one is aligned against $B_0$, as seen by the arrows. When the two spins are aligned with $B_0$, the frequency at which the methyl hydrogens absorb is shifted downfield, and when the two spins are aligned against $B_0$, the frequency at which the methyl hydrogens absorb is shifted upfield; in the remaining two cases, there is no change in the ferquency at with the methyl hydrogens absorb. The result, as seen in Figure 19.2.3$a$ is a triplet of peaks in a 1:2:1 intensity ratio.

The analysis for the effect of the six methyl hydrogens on the two methylene hydrogens is a bit more complex, but works in the same way. Figure 19.2.3$b$, for example, shows that there are 15 ways to arrange the spins of the six methyl hydrogens such that two are spin down and four are spin up. Figure 19.2.3$c$ show the resulting NMR spectrum, which is a set of seven peaks in a 1:6:15:20:15:6:1 intensity ratio.

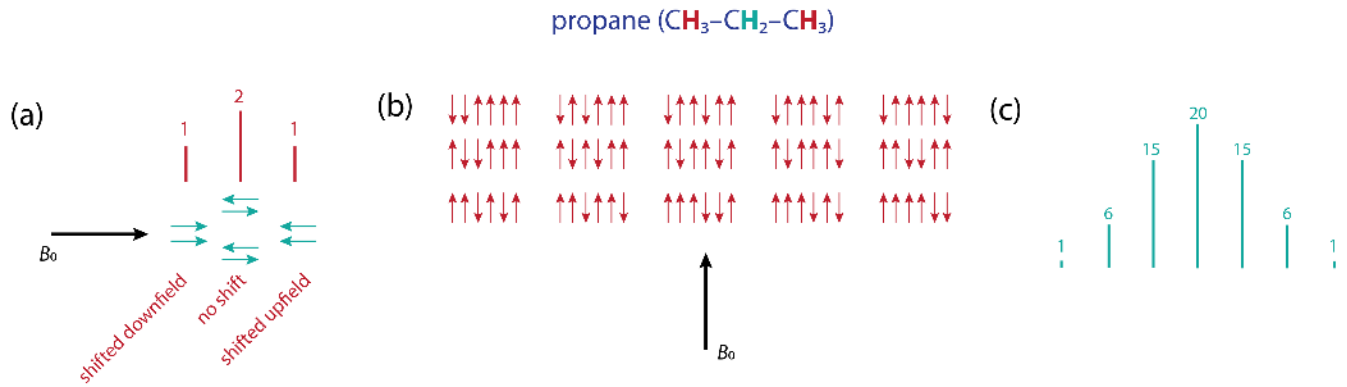



Figure 19.2.3. Illustration that shows the origin of spin-spin splitting: (a) The methyl hydrogens in propone split into three peaks by the spins of the two hydrogens on the adjacent methylene carbon; (b) The 15 different ways in which the six methyl hydrogens in propane have two nuclei that are spin down and four that are spin up; (c) The methylene hydrogens in propane are split into seven peaks by the six methyl hydrogens.

Figure 19.2.4 provides the splitting pattern observed for nuclei with $I = +1/2$, such as $^1$H. The pattern is defined by the coefficients of a binomial distribution—asking how many different ways you can get $X$ outcomes in $Y$ attempts is at the heart of a binomial distribution—this is easy to represent using Pascal's triangle—which shows us that for six equivalent nuclei we expect to find seven peaks with relative peak areas (or other measure of the signal) of 1:6:15:20:15:6:1. Note that the first and the last entry in any row is 1 and that all other entries in a row, as illustrated for the third entry in the seventh row, are the sum of the two entries in the row immediately above. The pattern also is know as the $N + 1$ rule as the $N$ equivalent hydrogens will split the peak for an adjacent hydrogen into $N + 1$ peaks.

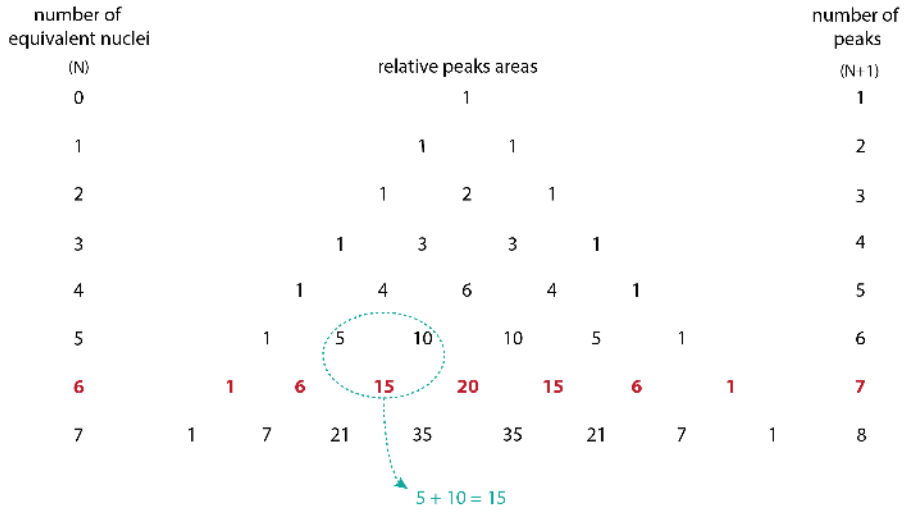



Figure 19.2.4. Pascal's triangle defines the splitting patterns in $^1$H NMR. The annotation shows how the values in any row of Pascal's triangle give are derived from the previous row.

Figure 19.2.5 compares the experimental NMR for propane with its simulatd spectrum based on spin-spin splitting and the 2:6 ratio of methylene hydrogens relative to methyl hydrogens. The overall agreement between the two spectra is pretty good. The splitting of the individual peaks is designated by the coupling constant, $J$, which is shown in Figure 19.2.5 for both the experimental and the calculated spectra. Note that the coupling constant is the same whether we are considering the effect of the methyl hydrogens on the methylene hydrogens, or the effect of the methylene hydrogens on the methyl hydrogens. Values of the coupling constant become smaller the greater the distance between the nuclei.

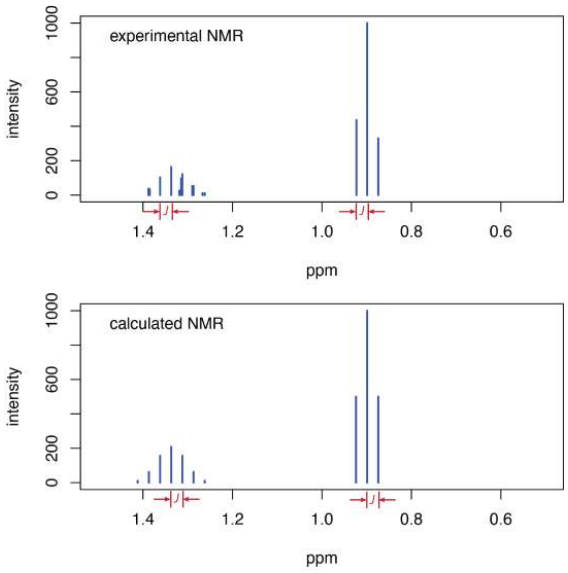



Figure 19.2.5: Experimental and calculated $^{1}$H NMR spectra for propane. The original data used to construct this spectrum is here and was obtained on a 300 MHz instrument. The peak for TMS is not shown.

The treatment of spin-spin coupling above works well if the difference in the chemical shifts for the two nuclei is significantly greater than the magnitude of their coupling constant. When this is not true, the splitting patterns can become much more complex and often are difficult to interpret. There are a variety of to simplify spectra, one of which, decoupling, is outlined in Figure 19.2.6. The original spectrum (top) shows two doublets, suggesting that we have two individual nuclei that are coupled to each other. If we irradiate the nucleus on the right at its frequency, we can saturate its ground and excited states such that it ceases to absorb. As a result, the nucleus on the left no longer shows evidence of spin-spin coupling to the nucleus on the right (middle) and appears as a singlet. When we turn off the decoupler (bottom) the spin-spin coupling between the two nuclei returns more quickly than relaxation returns the signal for the nucleus on the right.

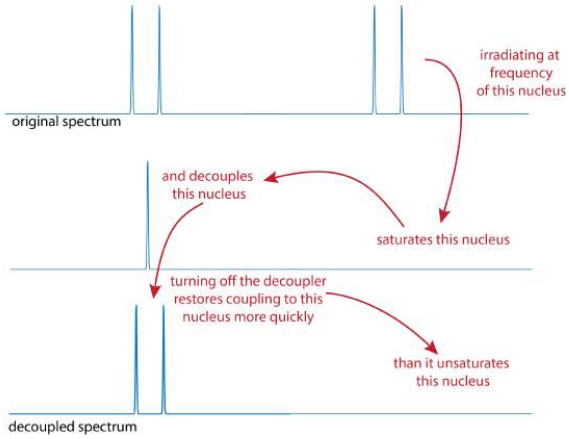



Figure 19.2.6. Illustration showing the effect of decoupling on an NMR spectrum. See the text for additional details.

This page titled 19.2: Environmental Effects on NMR Spectra is shared under a CC BY-NC-SA 4.0 license and was authored, remixed, and/or curated by David Harvey.

# 19.3: NMR Spectrometers

Earlier in this chapter, we noted that there are two basic experimental designs for recording a NMR spectrum. One is a continuous-wave instrument in which the range of frequencies over which the nucleus of interest absorb is scanned linearly, exciting the different nuclei sequentially. Most instruments, however, use pulses of RF radiation to excite all nuclei at the same time and then use a Fourier transform to recover the signals from the individual nuclei. Our attention in this chapter is limited to instruments for FT-NMR.

## Components of Fourier Transform Spectrometers

Figure 19.3.1 includes a photograph of 400 MHz NMR and a cut-away illustration of the instrument; together, these show the key components of a FT-NMR: a magnet that provides the applied magnetic field, $B_0$, a nucleus-dependent probe that provides the radio-frequency signal that yields the magnetic field, $B_1$, and a way to insert the sample into the instrument. The NMR in the photograph also is equipped with a sample changer that allows the user to load 30 or more samples that are analyzed sequentially.

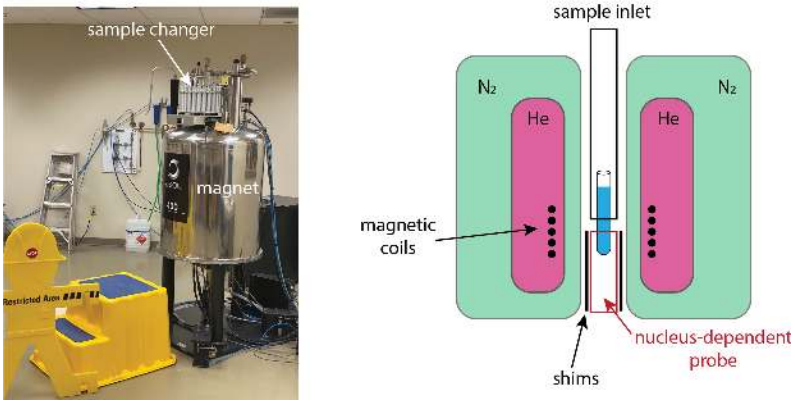



Figure 19.3.1. Photograph of a 400 MHz NMR and an illustration of the magnet's housing and the location of the sample.

## Magnets

The NMR in Figure 19.3.1 is described as having a frequency, $\nu$, of 400 MHz. The relationship between frequency and the magnet's field strength, $B_0$, is given by the equation

$$\nu = \frac{\gamma B_0}{2\pi} \tag{19.3.1}$$

where $\gamma$ is the magnetogyric ratio for the nucleus. A NMR's frequency is defined in terms of a nucleus of $^1$H; thus, a 400 MHz NMR has a magnet with a field strength of

$$B_0 = \frac{(2\pi) \times \nu}{\gamma} = \frac{(2\pi) \times (400 \times 10^6 \text{ s}^{-1})}{2.68 \times 10^8 \text{ rad T}^{-1} \text{ s}^{-1}} = 9.4 \text{ T}$$

Early instruments used a permanent magnet and were limited to field strengths of 0.7, 1.4, and 2.1 T, or 30, 60, and 90 MHz. As higher frequencies provide for greater sensitivity and resolution, modern instruments use a tightly wrapped coil of wire—typically a niobium/tin alloy or a niobium/titanium wire—that becomes superconducting when cooled to the temperature of liquid He (4.2 K). The result is a magnetic field strength of as much as 21 T or 900 MHz for $^1$H NMR. The magnetic coil is held within a reservoir of liquid He, which, itself, is held within a reservoir of liquid $N_2$.

To be useful, the magnetic field must remain stable—that is, it must not drift—and it must be homogeneous throughout the sample. These are accomplished by using a reference to lock the magnetic field in place and by shimming.

### Locking the Magnetic Field

Samples for NMR are prepared using a solvent in which the protons are replaced with deuterium. For example, instead of using chloroform, $CHCl_3$, as a solvent, we use deuterated chloroform, $CDCl_3$, where D is equivalent to $^2$H. This has the benefit of providing a solvent that will not contribute to the signals in the NMR spectrum. It also has the benefit that $^2$H has a spin of $I = 1$,

and a corresponding Larmor frequency. By monitoring the frequency at which $^2H$ absorbs, the instrument can use a feed-back loop to maintain its value by adjusting the magnet's field strength.

### Shimming

A magnetic field that is not homogeneous is like a table with four legs, one of which is just a bit shorter than the others. To balance the table, we place a small wedge, or shim, under the shorter leg. When a magnetic field is not homogeneous, small, localized adjustments are made to the magnetic field using a set of shimming coils arranged around the sample. Shimming can be accomplished by the operator by monitoring the quality of the signal for a particular nucleus, however, most instruments use an algorithm that allows the instrument to shim itself.

## The Sample Inlet and the Sample Probe

The center of the instrument, which runs from the sample input at the top to the sample probe at the bottom, is open to the laboratory environment and is at room temperature. The sample is placed in a cylindrical tube (Figure 19.3.2*a*), that is made from thin-walled borosilicate glass and is 180 mm long and 5 mm in diameter. The tube is then inserted into a teflon sleeve—called a spinner—as shown in Figure 19.3.2*b*, which is designed to both situate the sample at the proper depth within the sample probe, and to spin the sample about its long axis. This spinning is used to ensure that the sample averages out any inhomogeneities in the magnetic field not resovled by shimming.

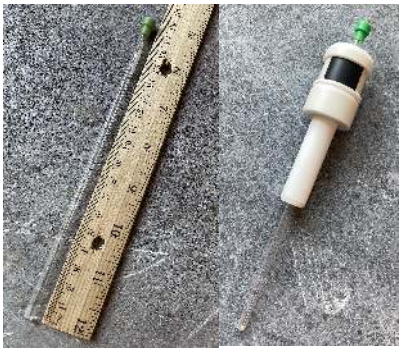


Figure 19.3.2. Photographs showing an NMR sample tube (left) and the spinner assembly (right).

The sample probe contains the coils needed to excite the sample and to detect the NMR signal as the excited states undergo relaxation. Figure 19.3.3 shows two configurations for this; in both configurations, the same coil is used for both excitation and detection. In the design on the left, which uses a permanent magnet, the applied magnetic field, $B_0$, is oriented horizontally across the sample's diameter and the radio frequency electromagnetic radiation and its field, $B_1$ is oriented vertically using a spiral coil. In the design on the right, which is used with a superconducting magnet, the applied magnetic field, $B_0$, is oriented vertically and the pulse of radio frequency electromagnetic radiation and its field, $B_1$, is oriented horizontally using a saddle coil.

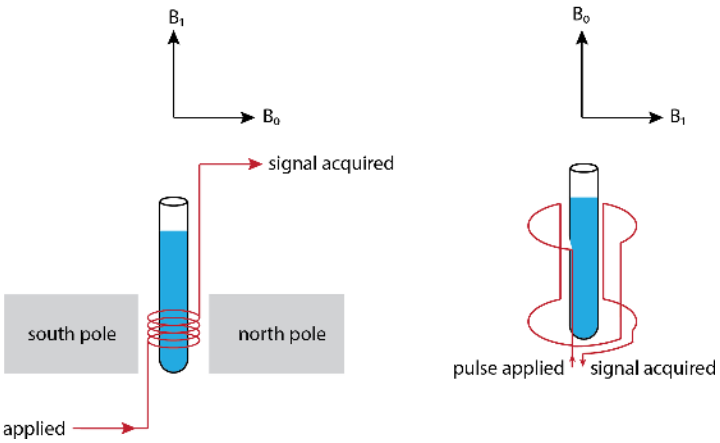



Figure 19.3.3. Two configurations for applying the magnetic fields $B_0$ and $B_1$. The configuration on the left is used with a permanent, such as a continuous wave instrument or a benchtop FT-NMR. The configuration on the right is used with a superconducting magnet, such as the instrument in Figure 19.3.1.

## Data Processing

In Chapter 19.1 we used the following figure to describe a pulse NMR experiment. Following a pulse that is applied for 1–10 μs, the free-induction decay, FID, is recorded for a period of time that may range from as little as 0.1 seconds to as long as 10 seconds, depending on the nucleus being probed.

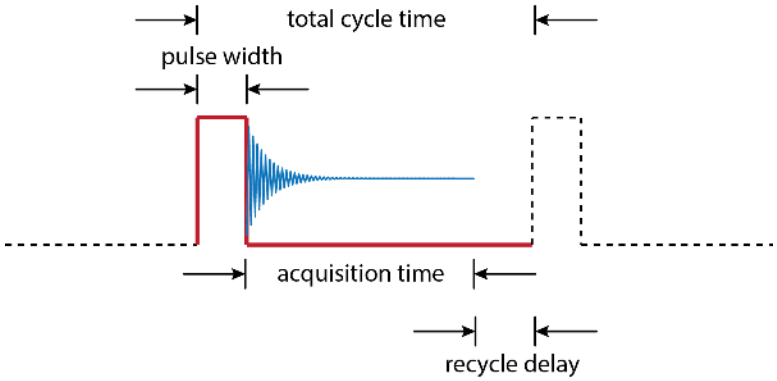



Figure 19.3.4. An example of a pulse sequence for FT-NMR. See the text for a description of the terms shown here.

The FID is an analog signal in the form of a voltage, typically in the μV range. This analog signal must be converted into a digital signal for data processing, which is called an analog-to-digital conversion, ADC. Two important considerations are needed here: how to ensure that the signal—more specifically, the location of the peaks in the NMR spectrum—is not distorted, and how to accomplish the ADC when the frequencies are on the order of hundreds of MHz.

### Analog-to-Digital Conversion

An analog-to-digital converter maps the signal onto a limited number of possible values—expressed in binary notation—and are characterized by the number of available bits. A 2-bit ADC convertor, for example, is limited to $2^2 = 4$ possible binary values of 00, 01, 10, and 11 that correspond to the decimal numbers 1, 2, 3, and 4. Having only four possible values, of course, would distort the FID pattern in Figure 19.3.4 from a smoothly varying oscillating signal into a series of steps. Using an ADC convertor with 16 bits allows for 65,536 unique digital values, a significant improvement. Another form of distortion occurs if we do not sample the FID with sufficient frequency. Consider, for example, the simple sine wave in Figure 19.3.5*a* that is shown as a solid line. If we sample this signal only five times over a period of less than four complete cycles, as shown by the five equally-spaced dots in Figure 19.3.5*a*, then the apparent signal is that shown by the dadshed line.

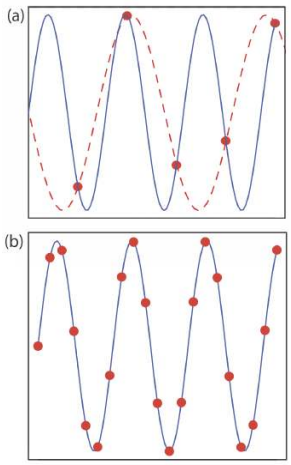



Figure 19.3.5: Effect of sampling frequency when monitoring a periodic signal. Individual samples are shown by the red dots (•). In (a) the sampling frequency is approximately 1.5 samples per period. The dashed red line shows the apparent signal based on five samples and the solid blue line shows the true signal. In (b) a sampling frequency of six samples per period accurately reproduces the true signal.

According to the Nyquist theorem, to determine accurately the frequency of a periodic signal, we must sample the signal at least twice during each cycle or period. Given a sampling rate of $\Delta$, the following equation

$$\Delta = \frac{1}{2\nu_{max}} \tag{19.3.2}$$

defines the highest frequency, $\nu_{max}$, that we can monitor accurately. A sampling rate of six samples per period is more than sufficient to reproduce the real signal in Figure 19.3.5.

A peak with a frequency that is greater than $\nu_{max}$ is not absent from the spectrum; instead, it simply appears at a different location. For example, suppose we can monitor accurately any frequency within the window shown in Figure 19.3.6 and that we only measure frequencies within this window. A peak with a frequency that is greater than what we can measure accurately by $\Delta\nu$ appears at an apparent frequency that is $\Delta\nu$ greater than the frequency window's lower limit. This is called folding.

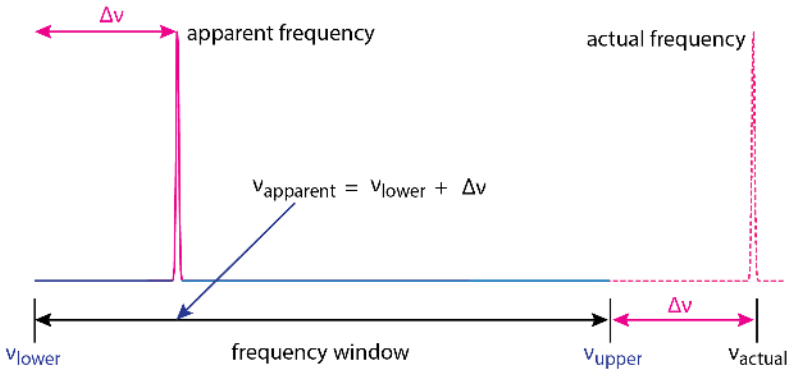



Figure 19.3.6. Illustration showing the origin of folding in which a peak in the NMR spectrum appears at a value of $\delta$ that is different from its actual value.

## Managing MHz Signals

The instrument in Figure 19.3.1 is a 400 MHz NMR. This is a range of frequencies that is too large for an analog-to-digital convertor to handle with accuracy. The frequency window of interest to us, however, is typically 10 ppm for $^1$H NMR (see Chapter 19.2 to review the NMR scale). For a 400 MHz NMR this corresponds to just 4000 Hz, with the useful range running from 400.000 MHz to 400.004 MHz. Subtracting the instrument's frequency of 400 MHz from the signal's frequency limits the latter to the range of 0–4000 Hz, a range that is easy for an ADC to handle.

## Signal Integrators

Integrating to determine the area under the peaks provides a way to gain some quantitative information about the sample. Figure 19.3.7 shows the integration of the NMR of propane first seen in Chapter 19.2. Integration of the peak for the two methyl groups gives a result of 1766 and integration of the peak for the methylene group gives a result of 710. The ratio of the two is

$$\frac{1766}{710} = 2.5$$

which is somewhat smaller than the expected 3:1 ratio.

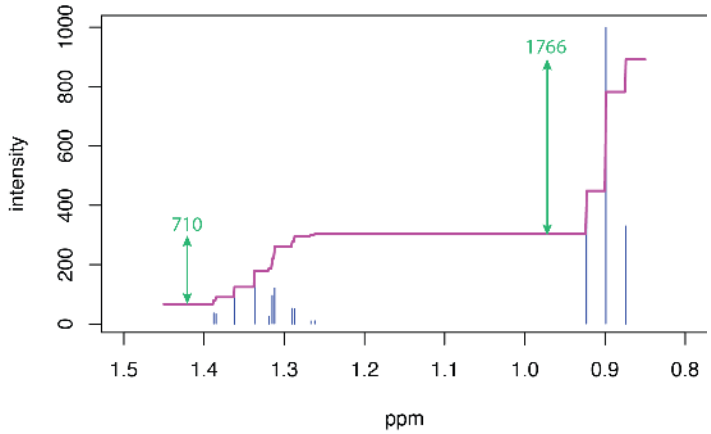



Figure 19.3.1. Illustration of integration. The original data used to construct this spectrum is here and was obtained on a 300 MHz instrument.


https://chem.libretexts.org/@go/page/397288

This page titled 19.3: NMR Spectrometers is shared under a CC BY-NC-SA 4.0 license and was authored, remixed, and/or curated by David Harvey.

# 19.4: Applications of Proton NMR

Proton ($^1$H) NMR finds use for both qualitative analyses and quantitative analyses; in this section we briefly consider each of these areas.

## Identification of Compounds

Proton NMR is an essential tool for the qualitative analysis of organic, inorganic, and biochemical compounds. Figure 19.4.1 provides a simple example that shows the relationship between structure and a $^1$H NMR's peaks. The spectra in this figure are for a set of four simple organic molecules, each of which has a chain of three carbons and an oxygen: 1-propanol, $CH_3CH_2CH_2OH$, 2-propanol, $CH_3CH(OH)CH_3$, propanal, $CH_3CH_2CHO$, and propanoic acid, $CH_3CH_2COOH$. The first two of these molecules are alcohols, the third is an aldehyde, and the last is an acid. The main spectrum runs from 0–14 ppm, with insets showing the spectra over a narrower range of 0–5 ppm.

Each of these molecules has a terminal $–CH_3$ group that is the most upfield peak in its spectrum, appearing between 0.94 – 1.20 ppm. Each of these molecules has a hydrogen that either is bonded to an oxygen or a hydrogen bonded to the same carbon as the oxygen. The hydrogens in the –OH groups of the two alcohols have similar shifts of 2.16 ppm and 2.26 ppm, but the aldehyde hydrogen in the –CHO group and the acid hydrogen in –COOH are shifted further downfield appearing at 9.793 ppm and 11.73 ppm, respectively. The hydrogens in the two $–CH_2–$ groups of 1-propanol have very different shifts, with the one adjacent to the –OH group appearing more downfield at 3.582 ppm than the one next to the $–CH_3$ group at 1.57 ppm. Not surprisingly, the –CH– hydrogen in 2-proponal, which is adjacent to the –OH group appears at 4.008 ppm.

Comparisons such of this make it possible to build tables of chemical shifts—see Table 19.2.1 in Chapter 19.2 for an example—that can help in determining the identify of the molecule giving rise to a particular NMR spectrum. As this receives extensive coverage in other courses, particularly courses in organic chemistry, we will not provide a more extensive coverage here.

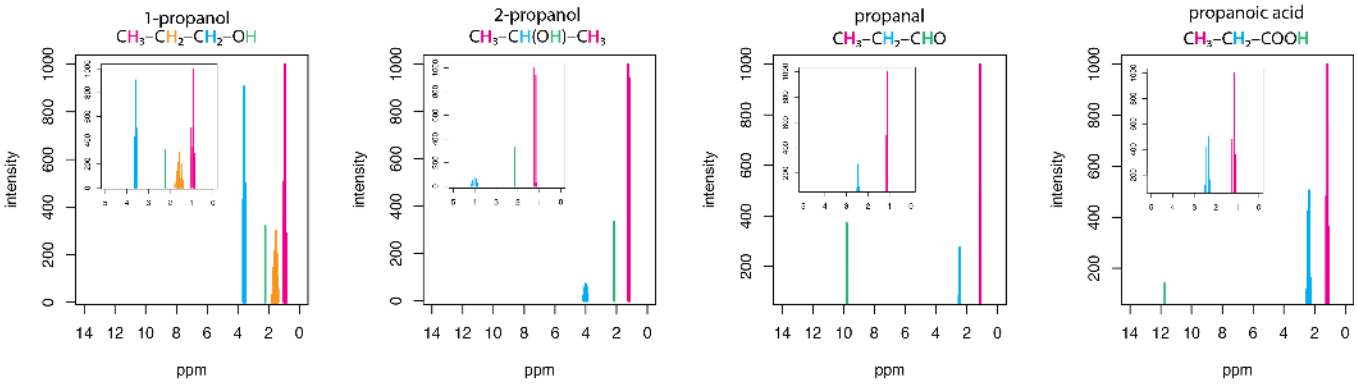



Figure 19.4.1. $^1$H NMR spectra for 1-propanol, 2-propanol, propanal, and propanoic acid. The full spectrum are shown using the scale at the bottom of each figure. The insets show close-ups of the NMR spectra from 0 – 5 ppm. The original data used to construct these spectra are found here. The spectrum for propanal was recorded on a 300 MHz instrument; the other three spectra were recorded on a 90 MHz instrument.

## Quantitative Analysis

A quantitative analysis requires a method of standardization, which for NMR usually makes use of an internal standard. A good internal standard should have high purity and should have a relatively simple NMR spectrum with peaks that do not overlap with the analyte or other species present in the sample. If we are interested in only the relative concentrations of the analyte and the internal standard, then we can use the following formula

$$\frac{M_a}{M_{is}} = \frac{I_a}{I_{is}} \times \frac{N_{is}}{N_a} \tag{19.4.1}$$

where $M$ is the molar concentration of the analyte or internal standard, $I$ is the intensity of the NMR peak for the analyte or internal standard, and $N$ is the number of nuclei giving rise to the NMR peak for the analyte and the internal standard. Even if we don't know the exact concentration of the internal standard, if we know that its concentration is the same in all samples, then we can determine the relative concentration of analyte in a collection of samples.

If we are interested in determining the absolute concentration of analyte in a sample, then we must know the absolute concentration of the internal standared; when true, then Equation 19.4.1 becomes

$$M_a = \frac{I_a}{I_{is}} \times \frac{N_{is}}{N_a} \times M_{is} \tag{19.4.2}$$

Determining the purity of an analyte, $P_a$, in a sample, we can use the equation

$$P_a = \frac{I_a}{I_{is}} \times \frac{N_{is}}{N_a} \times \frac{M_a}{M_{is}} \times \frac{W_{is}}{W_a} \times P_{is} \tag{19.4.3}$$

where $W$ is the weight of the internal standard or the sample that contains our analyte.

---

This page titled 19.4: Applications of Proton NMR is shared under a CC BY-NC-SA 4.0 license and was authored, remixed, and/or curated by David Harvey.

# 19.5: Carbon-13 NMR

The relatively slow development of instrumentation for $^{13}C$ NMR spectra is the result of its limited sensitivity compared to $^{1}H$ NMR. This difference in sensitivity is due to two key differences between the nuclei $^{1}H$ and $^{13}C$: their relative abundances and their relative magnetogyric ratios. While $^{1}H$ comprises 99% of all hydrogen, $^{13}C$ accounts for just 1% of all carbon. The strength of an NMR signal also depends on the difference in energy, $\Delta E$, between the ground state and the excited state, which is a function of the magnetogyric ratio, $\gamma$

$$\Delta E = h\nu = \frac{\gamma B_0}{2\pi} \tag{19.5.1}$$

The greater the difference in energy, the greater the difference in the population between the ground and the excited states, and the greater the signal. The magnetogyric ratio, $\gamma$, for $^{1}H$ is $4\times$ greater than that for $^{13}C$. As a result of these two factors, $^{1}H$ NMR is approximately $6400\times$ more senstitive than $^{13}C$. The development of magnets with higher field strengths and the capabilities of signal averaging (see Chapter 5 on signals and noise) when using Fourier transforms to gather and analyze data, make $^{13}C$ feasible.

Figure 19.5.1 shows $^{13}C$ NMR spectrum for three related molecules: *p*-nitrophenol, *o*-nitrophenol, and *m*-nitrophenol. There are three things to make note of from this figure. First, each spectrum consists of a set of peaks, each of which is a singlet, suggesting that no spin-spin coupling is taking place. Second, the number of peaks in each spectrum is the same as the number of unique types of carbon—four unique carbons for *p*-nitrophenol and six each for *m*-nitrophenol and *o*-nitrophenol—which suggests that chemical shifts in $^{13}C$ provide useful information about the environment of the carbon atoms and, therefore, the molecule's structure. And, third, unlike $^{1}H$, there is no relationship between the intensity of a $^{13}C$ peak and the number of carbon atoms. This is particularly evident when comparing the intensity of the peaks for the carbon bonded to the $–NO_2$ group and the carbon bonded to the –OH group, which are significantly less intense than the peaks for other carbons. We will consider each of these observations in the remainder of this section.

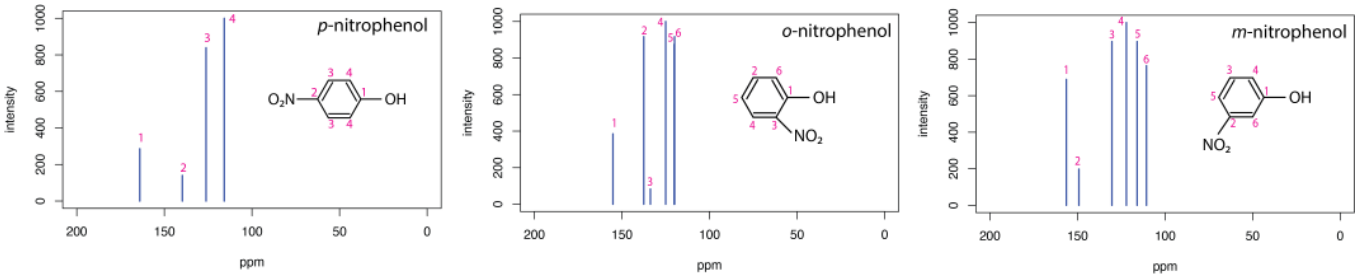



Figure 19.5.1. $^{13}C$ NMR spectra for three nitrophenols. The original data used to construct these spectra are found here. The spectra were recorded on a 15 MHz instrument (with respect to $^{13}C$, or 60 MHz with respect to $^{1}H$).

## Proton Decoupling

In $^{13}C$ NMR there is no coupling between adjacent carbon atoms because it is unlikely that both are $^{13}C$, the only isotope of carbon that is NMR active (the odds that two adjacent carbons are both $^{13}C$ is $0.01 \times 0.01$, or $0.0001$ or $0.010\%$). Coupling does take place between $^{13}C$ and $^{1}H$ when the hydrogen atoms are attached to the carbon atom. Such coupling follows the same N+1 rule as in $^{1}H$ NMR; thus, a quartenary carbon ($R_4C$) appears as a singlet, a methine carbon ($R_3CH$) appears as a doublet, a methylene carbon ($R_2CH_2$) appears as a triplet, and a methyl carbon ($RCH_3$) appears as a quartet. Even with the extensive range of ppm values over which $^{13}C$ peaks appear—chemical shifts for $^{13}C$ spectra run from 250 – 0 ppm instead of 14 – 0 ppm for $^{1}H$ spectra—a compound with many different types of carbon atoms, each with 1 – 3 hydrogen atoms results in a complex spectrum. For this reason, $^{13}C$ NMR spectra are acquired in a way that prevents coupling between $^{13}C$ and $^{1}H$. This is called proton decoupling.

The most common method of proton decoupling is to use a second RF generator to irradiate the sample with a broad-band of RF signals that spans the range of frequencies for the protons. As described earlier in Section 19.3, the effect is to saturate the proton's ground and excited states, which prevents the protons from absorbing energy and from coupling with each other and with the carbons atoms. The $^{13}C$ spectra in Figure 19.5.1 are examples of decoupled spectra.

## Qualitative Applications of $^{13}C$ NMR

Just as with $^{1}H$ NMR spectra, tables of chemical shifts for $^{13}C$ peaks aids in determining a molecules structure. Table 19.5.1 provides ranges of chemical shifts for different types of carbon atom. A set of tables is available here.

Table 19.5.1. $^{13}C$ Shifts in ppm

| type of carbon atom | example | range of chemical shifts (ppm) |
|---|---|---|
| primary alkyl | $R-CH_3$ | 10 – 30 |
| secondary alkyl | $R-CH_2-R$ | 15 – 55 |
| tertiary alkyl | $R_3CH$ | 20 – 60 |
| quaternary alkyl | $R_4C$ | 30 – 40 |
| alkynl | $R-C\equiv C-H$ | 65 – 90 |
| alkenyl | $R-C=C-H$ | 100 – 150 |
| aromatic | $C_6H_6$ | 110 – 170 |
| ester | $R-C(=O)-O-R$ | 165 – 175 |
| amide | $R-C(=O)-N-R_2$ | 165 – 175 |
| carboxylic acid | $R-C(=O)-OH$ | 175 – 185 |
| aldehyde | $R-C(=O)-H$ | 190 – 220 |
| ketone | $R-C(=O)-R$ | 205 – 220 |
| attached to iodine | $C-I$ | 0 – 40 |
| attached to bromine | $C-Br$ | 25 – 65 |
| attached to chlorine | $C-Cl$ | 35 – 80 |
| attached to oxygen | $C-O$ | 40 – 80 |
| attached to nitrogen | $C-N$ | 40 – 60 |

## Nuclear Overhauser Enhancement

The most intense peak in the $^{13}C$ NMR spectrum for *m*-nitrophenol (see Figure 19.5.1 above) is the carbon in the benzene ring labeled as position 4, with an intensity of 1000 (the intensity scale is normalized here to a maximum value of 1000, but for this section, let's take it as an absolute value). Because the spectrum was acquired with proton decoupling turned on, the peak for this carbon appears as a singlet. If we turn proton decoupling off, then we expect the peak to appear as a doublet as this carbon has one hydrogen attached to it. We might reasonably expect to find that each peak has an intensity of 500, giving a total intensity of 1000. The actual intensities of the peaks for this carbon, however, are smaller than expected. Put another way, when we turn proton decoupling on, the intensity of a $^{13}C$ line increases more than expected and the more hydrogens, the greater the effect. This is called nuclear overhauser enhancement (NOE).

NOE is the result of the relative populations of the ground and excited states. The technical details are more than we will consider here, but the extent of the total enhancement of the peak intensities is proportional to the ratio of the magnetogyric ratios of the irradiated nucleus ($^{1}H$) and the observed nucleus ($^{13}C$), which for a $^{1}H$ decoupled $^{13}C$ NMR results in a total enhancement of the intensity of approximately 200%. As magnetogyric ratios can be negative, as is the case for $^{15}N$, a decoupled spectrum can result in less intense peaks. One important consequence of NOE, is that integrated peak areas are not proportional to the number of identical carbon atoms, which is a loss of information.

Note

Although our focus in this chapter is on $^{1}H$ and $^{13}C$ NMR, other nuclei, such as $^{31}P$, $^{19}F$, and $^{15}N$ are useful for the study of chemically and biochemically important molecules.

This page titled 19.5: Carbon-13 NMR is shared under a CC BY-NC-SA 4.0 license and was authored, remixed, and/or curated by David Harvey.

# 19.6: Two-Dimensional Fourier Transform NMR

The $^{1}H$ and $^{13}C$ spectra up to this point are shown in one dimension (1D), which is the frequency absorbed by the analyte's nuclei expressed in ppm. These spectra were acquired by applying a brief RF pulse to the sample, recording the resulting FID, and then using a Fourier transform to obtain the NMR spectrum. In addition to 1D experiments, there are a host of 2D experiments in which we apply a sequence of two or more pulses, recording the resulting FID after applying the last pulse. In this section we will consider one example of a 2D NMR experiment in some detail: $^{1}H$ – $^{1}H$ correlation spectroscopy, or $^{1}H$ – $^{1}H$ COSY.

Figure 19.6.1 shows the basic experimental details for the COSY experiment. The pulse train is shown in (a) and consists of a first pulse that is followed by a delay time, $t_1$, in which the nuclear spins are allowed to precess and relax. This is followed by the application of a second pulse and the measurement of the resulting FID during the acquisition period, $t_2$, that consists of $n_{t_2}$ individual data points. The COSY experiment consists of a sequence of $n_{t_1}$ individual pulse trains, each with a different $t_1$. The result (b) is a matrix with $n_{t_1}$ rows and $n_{t_2}$ columns. To process the data, each row in this matrix is Fourier transformed, the resulting $n_{t_1} \times n_{t_2}$ matrix is transposed to a $n_{t_2} \times n_{t_1}$ matrix and then Fourier transformed again to give (c) a $n_{t_2} \times n_{t_2}$ matrix that shows the intensity of the signal for all possible combinations of applied frequencies.

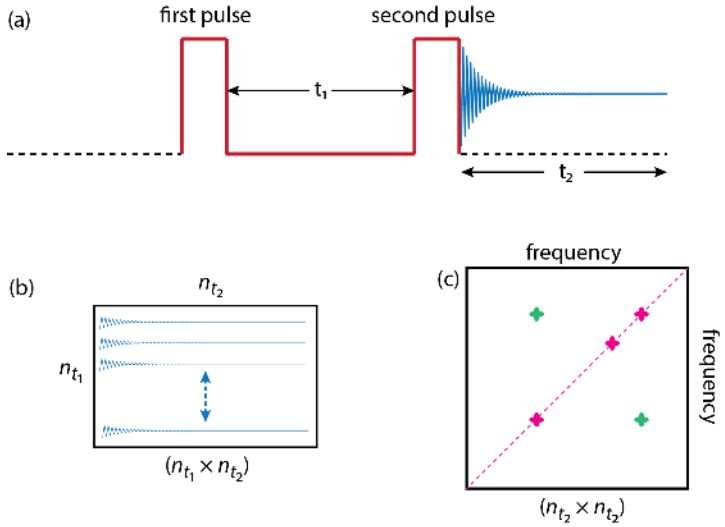



Figure 19.6.1. Details of a COSY experiment: (a) the pulse sequence; (b) the data matrix; and (c) the COSY spectrum. See the text for additional details.

Figure 19.6.2 shows the $^{1}H$ – $^{1}H$ COSY spectrum for ethyl acetate. Instead of just annotating the two axes with numerical values of the frequencies, they are displayed by superimposing the 1D $^{1}H$ NMR spectrum for ethyl acetate in ppm. The points that fall on the diagonal line are just the three frequencies where ethyl acetate has $^{1}H$ peaks. Of more interest are the points that fall on either side of the diagonal line—these are called cross peaks—as these show pairs of hydrogens that are coupled (or correlated) to each other. The cross peaks in the COSY spectrum are symmetrical about the diagonal line and show the correlation between the hydrogens on the methyl carbon and and the methylene carbon that are adjacent to each other (the ethyl part of ethyl acetate). The remaining methyl group is not coupled to the other hydrogen's in the ethyl acetate, so there is no cross peak at the intersection of $\delta = 2.038$ ppm and $\delta = 1.260$ ppm. The information about coupling from cross peaks assists in interpreting complex $^{1}H$ NMR spectra.

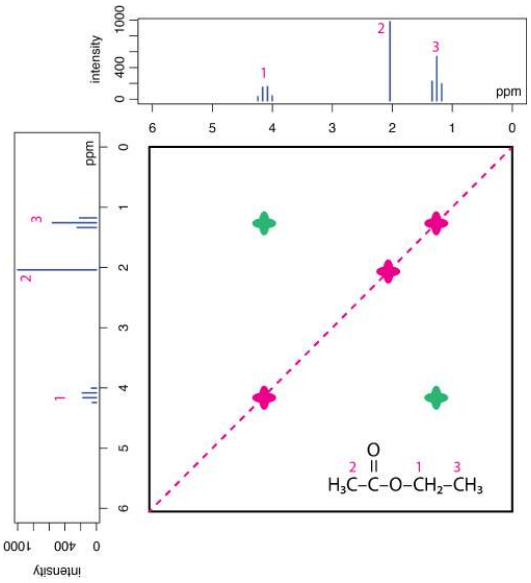



Figure 19.6.2. The COSY spectrum for ethyl acetate. The original data used to create the two $^{1}H$ NMR spectra is available here and was obtained using a 300 MHz NMR. The COSY spectrum is simulated.

COSY is one example of a homonuclear 2D NMR experiment because it examines coupling between identical nuclei, such as $^{1}H$ in Figure 19.6.2. There are many other 2D NMR experiments, each of which uses a sequence of pulses—some that use two pulses, as in COSY, and others that use three or more pulses—and a data analysis algorithm. Table 19.6.1 provides details on some of these methods.

Table 19.6.1. Selected examples of 2D NMR experiments.

| method | information obtained from cross peaks |
|---|---|
| correlation spectroscopy (COSY) | coupling between two protons ($^{1}H$ – $^{1}H$) that are within three chemical bonds of each other |
| total correlation spectroscopy (TOCSY) | coupling between all protons ($^{1}H$) in the molecule |
| heteronuclear correlation spectroscopy (HETCOR) | coupling between a proton ($^{1}H$) and another nucleus, such as carbon ($^{1}H$ – $^{13}C$) or nitrogen ($^{1}H$ – $^{15}N$) |
| nuclear overhauser and exchange spectroscopy (NOESY) | coupling between two protons ($^{1}H$ – $^{1}H$) that are within approximately 5 Å of each other |
| heteronuclear single quantum correlation (HSQC) | coupling between a proton ($^{1}H$) and another nucleus, such as carbon ($^{1}H$ – $^{13}C$) or nitrogen ($^{1}H$ – $^{15}N$) |
| heteronuclear multiple bond coherence spectroscopy (HMBC) | coupling between a proton and a carbon ($^{1}H$ – $^{13}C$) that are two or three bonds apart |
| incredible natural abundance double-quantum transfer (INADEQUATE) | coupling between adjacent carbon atoms ($^{13}C$ – $^{13}C$) |
| double quantum filtered correlation spectroscopy (DQF–COSY) | suppresses signals from water |

This page titled 19.6: Two-Dimensional Fourier Transform NMR is shared under a CC BY-NC-SA 4.0 license and was authored, remixed, and/or curated by David Harvey.

# CHAPTER OVERVIEW

## 20: Molecular Mass Spectrometry


20.1: Molecular Mass Spectra

20.2: Ion Sources

20.3: Mass Spectrometers

20.4: Applications of Molecular Mass Spectrometry


---

This page titled 20: Molecular Mass Spectrometry is shared under a CC BY-NC-SA 4.0 license and was authored, remixed, and/or curated by David Harvey.

# 20.1: Molecular Mass Spectra

Figure 20.1.1 shows a mass spectrum for *p*-nitrophenol, $C_6H_5NO_3$, which has a nominal (integer) mass of 139 daltons. If we send a beam of energetic electrons through a gas phase sample of *p*-nitrophenol, it loses an electron, which we write as the reaction

$$C_6H_5NO_3 + e^- \rightarrow {C_6H_5NO_3}^{+\bullet} + 2e^- \tag{20.1.1}$$

where the product is a radical cation that has a charge of $+1$ and that retains the nominal mass of 139 daltons. We call this the molecular ion—highlighted here in green—and it has a mass-to-charge ratio (*m*/*z*) of 139.

**Note**

Some of the terminology in this chapter was covered earlier in Chapter 11 on atomic mass spectrometry. See the first section of that chapter for a discussion of atomic mass units (amu) and daltons (Da), and of mass-to-charge ratios.

If reaction 20.1.1 is all that happens when *p*-nitrophenol interacts with an energetic electron, then it would not provide much in the way of useful information. The radical cation ${C_6H_5NO_3}^{+\bullet}$, however, retains sufficient excess energy from the initial electron-molecule collision that it is in an excited state. In returning to its ground state, the molecular ion undergoes a series of fragmentations that result in the formation of ions—called daughter ions—with different mass-to-charge ratios. A plot that shows the relative intensity of these ions as a function of their mass-to-charge ratios is called a mass spectrum. The most abundant fragment in the spectrum—shown here in red and which is called the base peak—is assigned a relative intensity of 100; the intensity of all other ions is reported relative to the base perk.

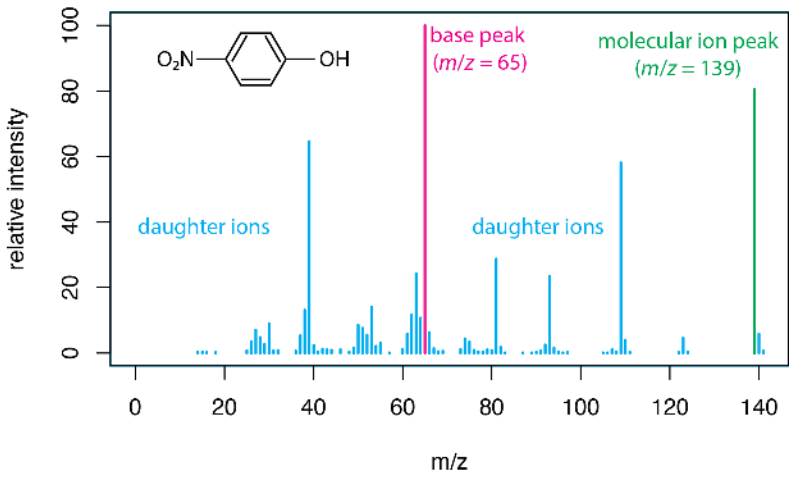



Figure 20.1.1: The mass spectrum for *p*-nitrophenol showing the molecular ion at a m/z of 139 (in green) and the daughter ions (in blue) formed through fragmentation. The most abundant fragment is the base peak at a m/z of 65 (in red). The original data is available here. This particular spectrum was collected using an electron impact source; more on that in Section 20.2.

A molecule's fragmentation patterns provides rich information about its structure. Figure 20.1.2 compares the mass spectra for *o*-nitrophenol, *m*-nitrophenol, and *p*-nitrophenol. All three molecules have clusters of fragment ions at similar mass-to-charge ratios, but the relative abundance of the ions in these clusters varies quite a bit from molecule-to-molecule. For example, the pink rectangle in each spectrum highlights peaks with mass-to-charge ratios from approximately 104 *m*/*z* to 115 *m*/*z*. All three molecules share the property of producing fragment ions with these mass-to-charge ratios; the relative abundance of the fragment ions, however, varies substantially between the three molecules with *o*-nitrophenol and *p*-nitrophenol having a major peak at 109 *m*/*z*, but *m*-nitrophenol showing no more than a trace peak at 109 *m*/*z*. We will return to the use of mass spectrometry for determining structure information later in this chapter.

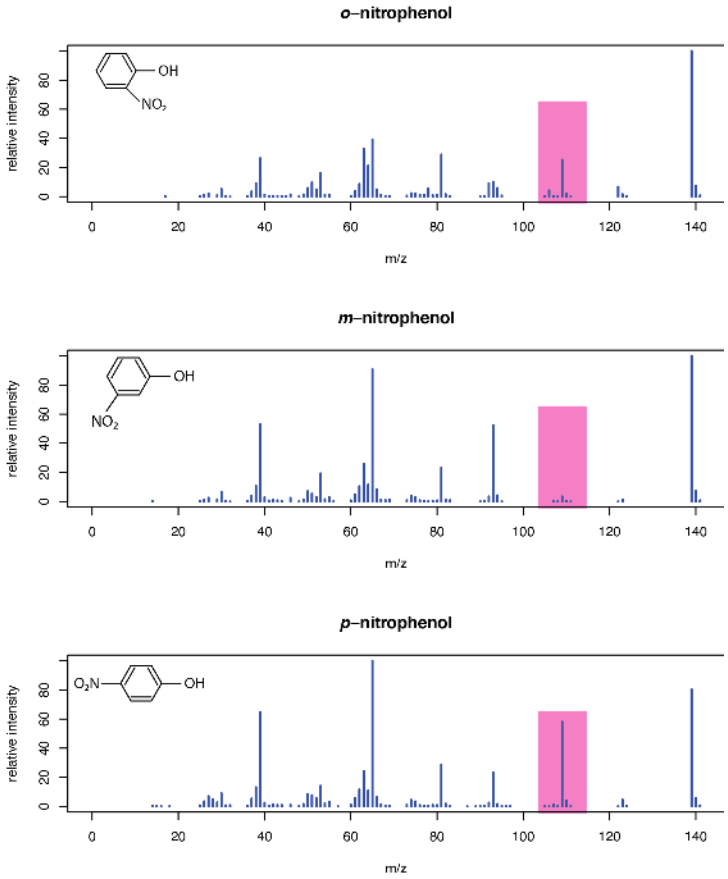



Figure 20.1.2: The mass spectra for *o*-nitrophenol (top), *m*-nitrophenol (middle), and *p*-nitrophenol (bottom). All three molecules show the same pattern of the mass-to-charge ratios where clusters of fragment ions appear; however, the relative abundance of each cluster varies from molecule-to-molecule. The pink rectangle highlights the *m*/*z* values of 104–115. The original data for these spectra are here, here, and here from top-to-bottom.

This page titled 20.1: Molecular Mass Spectra is shared under a CC BY-NC-SA 4.0 license and was authored, remixed, and/or curated by David Harvey.

# 20.2: Ion Sources

Since a mass spectrum shows the relative abundance of ions with different mass-to-charge ratios, a mass spectrometer must include a way to generate ions. More specifically, it needs a method that generates the initial ion as it, once formed, will undergo fragmentation without additional help from the analyst (which does not mean the analyst cannot assist in that fragmentation; see discussion of tandem mass spectrometry in Section 20.4). In this section we consider several common ion sources. We can describe these sources using two characteristic properties: (a) the physical state of the species that is initially ionized (gas, liquid, or solid phase), and (b) whether ionization favors the formation of fragment ions or the formation of molecular ions (hard sources or soft sources).

## Electron Ionization Sources (gas phase/hard source)

The electron ionization (EI) source, also known as an electron impact source, uses a beam of energetic electrons to ionize the analyte. As shown in 20.2.1, the sample is volatilized prior to entering the ion source as gas phase molecules, M(*g*). A heated tungsten filament is used to generate electrons, which are pulled toward a positively charged anode. This electron beam intersects with the gas phase molecules at 90° where ionization occurs

$$\mathrm{M}(g) + e^- \rightarrow \mathrm{M}^{+\bullet}(g) + 2e^- \tag{20.2.1}$$

The molecular ions, $\mathrm{M}^{+\bullet}(g)$, are then swept into the mass analyzer using a set of accelerating plates (not shown here).

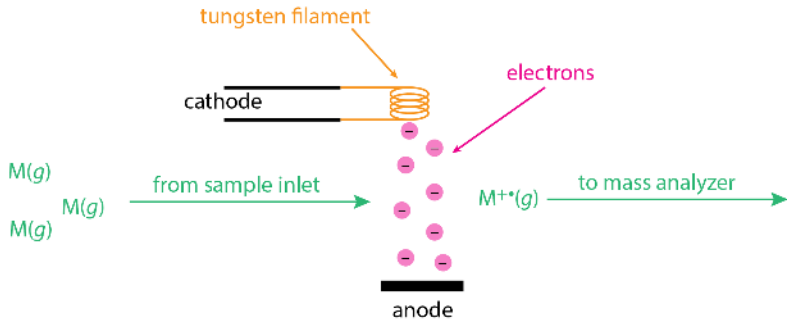



Figure 20.2.1: Illustration of an electron ionization source. The sample is volatilized and brought into the ion source where it intersects with an electron beam, forming the molecular ion, $\mathrm{M}^{+\bullet}$, which is carried on into the mass analyzer.

The electron beam in Figure 20.2.1 has a lot of energy due to the significant potential difference between the cathode and the anode, which may be as much as 70 V. The kinetic energy of these electrons is equivalent to the product of the electron's charge in Coulombs, the applied potential in volts, and Avogadro's number

$$e \times V \times N_A = 1.6 \times 10^{-19} \times 6.022 \times 10^{-23} = 6.7 \times 10^6 \text{ J/mol}$$

or 6,700 kJ/mol. This energy is much greater than typical bond energies, which range from approximately 150–600 kJ/mol for single bonds, from approximately 500–750 kJ/mol for double bonds, and from approximately 800–1100 kJ/mol for triple bonds. The significant difference between the energy of the electrons and bond energies explains why electron ionization spectra are rich in fragment ions, as we saw earlier in Section 20.1 for *o*-nitrophenol, *m*-nitrophenol, and *p*-nitrophenol. This extensive fragmentation is useful in determining an analyte's structure—which is an advantage of a hard ionization method—but at the possible cost of the loss of the molecular ion peak for some analytes. For example, Figure 20.2.2 shows the electron ionization mass spectrum from 1-decanol, $C_{10}H_{22}O$, which has a nominal mass of 158 daltons. The small peak at *m*/*z* = 157 is for the fragment ion $C_{10}H_{21}O^+$; the molecular ion is not observed in this spectrum.

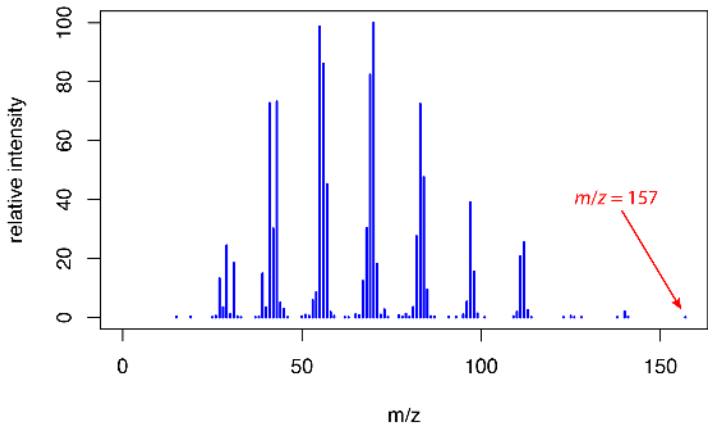



Figure 20.2.2: Mass spectrum for 1-decanol, $C_{10}H_{22}O$, using electron ionization. The peak furthest to the right (*m*/*z* = 157 amu) is one atomic mass unit less than the expected peak for the molecular ion, which does not appear in the spectrum. The original data is available here.

## Chemical Ionization Sources (gas phase/soft source)

Electron ionization is a hard source because the electron beam's energy results in easy fragmentation. In chemical ionization, we introduced a reagent molecule, such as methane, into the electron ionization (CI) source so that it is present at level that is $1000\times$ to $10,000\times$ greater than the analyte. At this higher concentration, it is the reagent molecule that is ionized; for example, when using $CH_4$ as the reagent gas, ions such as $CH_4{}^+$ and $CH_3{}^+$ form. These ions then react with additional methane molecules

$$CH_4{}^+(g) + CH_4(g) \rightarrow CH_5{}^+(g) + CH_3(g) \tag{20.2.2}$$

$$CH_3{}^+(g) + CH_4(g) \rightarrow C_2H_5{}^+(g) + H_2(g) \tag{20.2.3}$$

to form $CH_5{}^+$ and $C_2H_5{}^+$, species that are sufficiently reactive that they easily transfer a hydrogen to a molecule of the analyte, MH

$$CH_5{}^+(g) + MH(g) \rightarrow MH_2{}^+(g) + CH_4(g) \tag{20.2.4}$$

to give a molecular ion that we identify as $[M + H]^+$ and that has a mass that is one amu unit greater than that for M. Alternatively, they can easily remove a hydrogen from a molecule of the analyte, MH

$$C_2H_5{}^+(g) + MH(g) \rightarrow M^+(g) + C_2H_6(g) \tag{20.2.5}$$

to give a molecular ion that we identify as $[M - H]^-$ and that has a mass that is one amu less than that for M. Because formation of the molecular ion occurs indirectly and less energetically, fragmentation is suppressed, leading to a mass spectrum with a molecular ion peak and with only a small number of other ions. Figure 20.2.2 shows the mass spectrum for 1-decanol when using chemical ionization with $CH_4$ as the reagent gas.

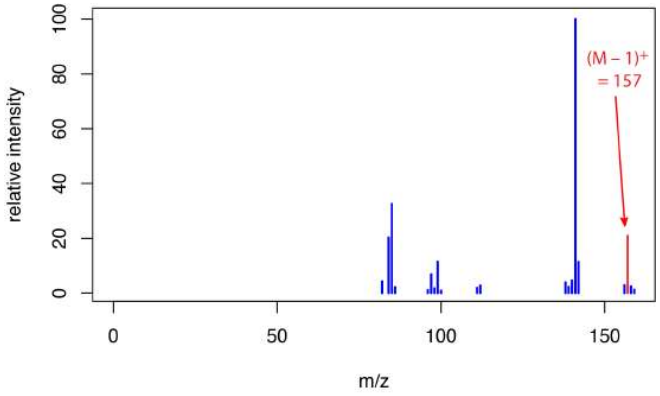



Figure 20.2.3: Mass spectrum for 1-decanol, $C_{10}H_{22}O$, using chemical ionization. The peak highlighted in red is the molecular ion, which has a *m*/*z* ratio of $158 - 1 = 157$ amu. The original data is available here.

## Electrospray Ionization Sources (liquid phase/soft source)

Electron impact and chemical ionization are gas phase sources because the sample is volatilized before it enters the mass spectrometer's inlet. In electrospray ionization (ESI), the sample is a liquid and ions desorb from that matrix in the mass spectrometer's inlet system. The liquid sample is pulled into the spectrometer's inlet through a capillary needle, forming a mist of droplets. The application of a large potential across this inlet assures that the droplets carry positive charges. These charged droplets then enter a chamber where they undergo desolvation, which decreases the size of the droplet and increases their charge density (see Figure 20.2.4). As this charge density increases, the droplets eventually become unstable, for reasons that are not fully understood, and ionized gas-phase ions desorb from the droplets and enter into the mass analyzer.

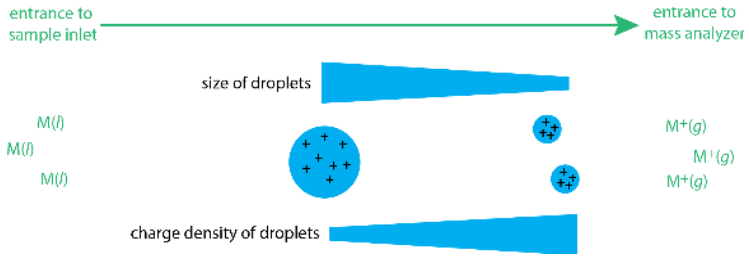



Figure 20.2.4: Illustration showing the change in the size of droplets and the charge density of droplets during electrospray ionization.

A typical electrospray ionization mass spectrum for a small molecule is shown in Figure 20.2.5 for the compound (4-aminophenyl)arsonic acid. As we saw in Figure 20.2.3 for chemical ionization, a soft ionization source results in a limited amount of fragmentation and a strong peak for the molecular ion, which here includes a proton transfer to give the $[M + H]^+$ peak at a *m*/*z* of 218 amu.

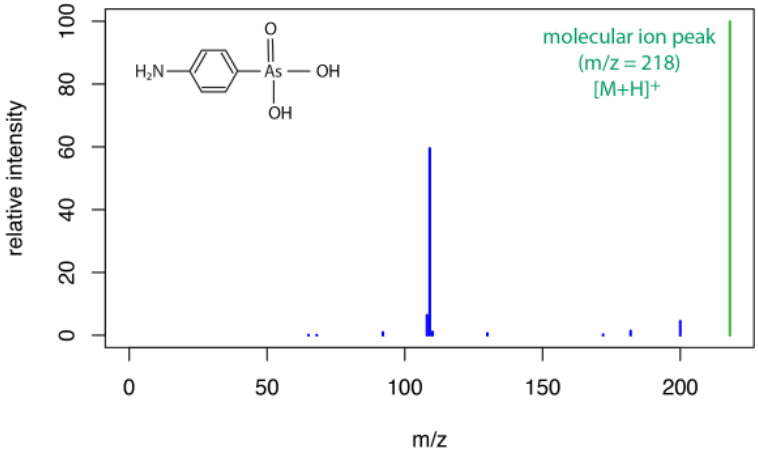



Figure 20.2.5: Mass spectrum for (4-aminophenyl)arsonic acid obtained using electrospray ionization. The spectrum contains only two majors peak: the molecular ion at $m/z = 218$ amu and a fragment at $m/z = 109$ amu. The original data is available here.

Electrospray ionization is particularly useful for biological molecules, such as peptides and proteins, because the soft ionization ensures that molecular weight information is retained. Because these molecules are large, they readily pick up multiple protons, forming multiply charged ions of the general form $[M + zH]^{z+}$ where *z* is the number of protons added. Figure 20.2.6 shows a hypothetical spectrum for the molecule M and Table 20.2.1 provides the corresponding *m*/*z* values for the mass spectrum's peaks.

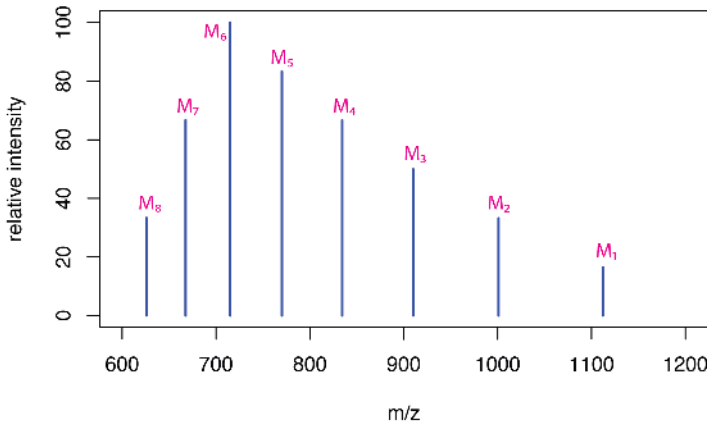



Figure 20.2.6: Simulated electrospray ionization mass spectrum for a molecule, M, that shows eight peaks with mass-to-charge ratios between 600 amu and 1200 amu. The subscripts in the symbols $M_i$ serve to identify the peaks; they are not an indication of charge.

Table 20.2.1. Mass-to-charge ratios for the peaks in Figure 20.2.6.

| peak | *m*/*z* |
|---|---|
| $M_1$ | 1112 |
| $M_2$ | 1001 |
| $M_3$ | 910 |
| $M_4$ | 834 |
| $M_5$ | 770 |
| $M_6$ | 715 |
| $M_7$ | 667 |
| $M_8$ | 626 |

If we take the mass-to-charge ratios for any two adjacent peaks, $M_i$ and $M_j$, where the peak $M_i$ has the greater value for *m*/*z*, and if we assume that $M_j$ has one additional hydrogen atom, giving it a charge that is one unit higher, then

$$Z_i = \frac{M_j - 1}{M_i - M_j} \tag{20.2.6}$$

where $Z_i$ is the charge on the ion $M_i$. Table 20.2.2 shows the calculated charges for the ions $M_1$ to $M_7$.

**Note**

Here is a derivation for Equation 20.2.6. Suppose the molecule of interest has a molecular weight of $m$. If the charge on the ion responsible for peak $M_i$ is $Z$, then it must be the case that the peak's mass is equal to m + Z as it has Z extra hydrogens and it must be the case that its mass-to-charge ratio is

$$M_i = \frac{m + Z}{Z}$$

and its molecular weight, $m$, is

$$m = (M_i \times Z) - Z$$

In the same way, the peak $M_j$ has a charge of $Z + 1$ and

$$M_j = \frac{m + Z + 1}{Z + 1}$$

$$m = (M_j \times Z) + M_j - Z - 1$$

Setting the two equations for $m$ equal to each other and solving for $Z$ gives

$$(M_i \times Z) - Z = (M_j \times Z) + M_j - Z - 1$$

$$(M_i \times Z) = (M_j \times Z) + M_j - 1$$

$$(M_i \times Z) - (M_j \times Z) = M_j - 1$$

$$Z = \frac{M_j - 1}{M_i - M_j}$$

Table 20.2.2. Calculated charges on the ions for peaks $M_1$ to $M_7$

| peak | *m*/*z* | Z |
|---|---|---|
| $M_1$ | 1112 | 9 |
| $M_2$ | 1001 | 10 |
| $M_3$ | 910 | 11 |
| $M_4$ | 834 | 12 |
| $M_5$ | 770 | 13 |
| $M_6$ | 715 | 14 |
| $M_7$ | 667 | 15 |
| $M_8$ | 626 | — |

The molecular weight, $m$, is given by the equation

$$m = (M_i \times Z) - Z \tag{20.2.7}$$

Table 20.2.3 shows the molecular weights for the ions $M_1$ to $M_7$ and their average value. The simulated mass spectrum was created by setting the molecular weight to 10,000 amu and with charges ranging from +9 to +16.

Table 20.2.3. Calculated molecular weights for the ions $M_1$ to $M_7$.

| peak | *m*/*z* | Z | $m$ |
|---|---|---|---|
| $M_1$ | 1112 | 9 | 9,999 |
| $M_2$ | 1001 | 10 | 10,000 |
| $M_3$ | 910 | 11 | 9,999 |
| $M_4$ | 834 | 12 | 9,996 |
| $M_5$ | 770 | 13 | 9,997 |
| $M_6$ | 715 | 14 | 9,996 |
| $M_7$ | 667 | 15 | 10,005 |
| $M_8$ | 626 | — | — |
| | | average molecular weight | 9,999 |

## Matrix-Assisted Laser Desorption/Ionization Sources (solid phase/soft source)

Matrix-assisted laser desorption ionization (MALDI) is a soft ionization source for obtaining the mass spectrum for biologically important molecules, such as proteins and peptides. Figure 20.2.7 illustrates the basic steps in obtaining a MALDI spectrum. The

sample is first mixed with a small molecule—which is called the matrix—to form a solution; the matrix usually is present in a 10:1 ratio. A drop of this mixture is placed on a sample probe and allowed to dry, leaving the sample in a solid form. A pulsed laser beam ($\lambda = 237$ nm is typical) is focused on the solid sample–matrix mixture. The matrix absorbs the laser pulse and the absorption of the laser's energy volatilizes both the matrix and the sample. Ionization of the sample forms molecular ions, usually $[M + H]^+$ ions, which are then swept into the mass analyzer.

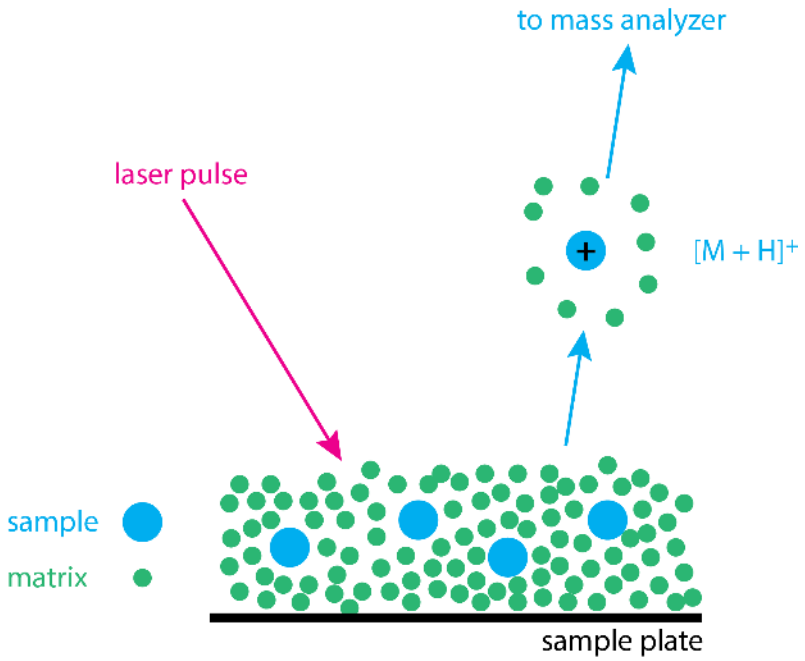



Figure 20.2.7: Illustration of matrix-assisted laser desorption ionization. The sample is dispersed in a liquid matrix and then allowed to dry. A pulsed laser beam is used to vaporize and ionize the sample.

When the sample is a digestion of a protein, then it is a mixture of peptides, each of which appeara as a $[M + H]^+$ peak in the resulting mass spectrum. For example, a peptide with the sequence AWSVAR (alanine–tryptophan–serine–valine–alanine–arginine) will appear as a peak with a mass of 689.8 daltons. To find this value we add together the molecular weights of the amino acids, account for the loss of a molecule of water for each peptide bond that forms, and then account for the hydrogen that gives the $[M + H]^+$ ion. In this case we have

$$[M + H]^+ = 89.1 + 204.2 + 105.1 + 117.1 + 89.1 + 174.2 - (5 \times 18.0) + 1 = 689.8 \text{ amu}$$

where the term $5 \times 18.0$ accounts for the loss of five molecules of $H_2O$ when forming the five peptide bonds.

## Fast Atom Bombardment Sources (liquid phase/soft source)

Fast atom bombardment (FAB) bears some similarity to MALDI: the sample is mixed with a liquid matrix (often glycerol) and bombarded with a beam of xenon or argon atoms (instead of a laser). Desorption of the sample from its matrix forms gas phase ions that are swept into the mass analyzer. Spectra usually contain both a molecular ion and fragmentation patterns.

This page titled 20.2: Ion Sources is shared under a CC BY-NC-SA 4.0 license and was authored, remixed, and/or curated by David Harvey.

# 20.3: Mass Spectrometers

A mass spectrometer has four essential elements: a means for introducing the sample to the instrument, a means for generating a mixture of ions, a means for separating the ions, and a means for counting the ions. In Chapter 20.2 we introduced some of the most important ways to generate ions. In this section we turn our attention to sample inlet systems and to separating and counting ions. You may wish to review Chapter 11 where we considered these topics in the context of atomic mass spectrometry. As we noted in Chapter 11, a mass spectrometer must operate under a vacuum to ensure that ions can travel long distances without undergoing undesired collisions that affect their ion energy.

## Sample Inlet Systems

When the sample is a gas or a volatile liquid, it is easy to transfer a portion of the sample into a reservoir as a gas maintained at a relatively small pressure. The sample is then allowed to enter into the mass spectrometer's ion source through a diaphragm that contains a pin-hole, drawn in by holding the ion source at lower pressure.

Solid and non-volatile liquids are sampled by inserting them directly into the ion source through a vacuum lock that allows the mass spectrometer to remain under vacuum except for the ion source where the sample is inserted. The sample is placed in a capillary tube or a small cup at the end of a sample probe, and then moved into the ion source. The sample probe includes a heating coil that is used, along with the instrument's vacuum, to help volatilize the sample.

Of particular importance are inlet systems that couple a chromatographic or an electrophoretic instrument to a mass spectrometer, providing a way to separate a complex mixture into its individual components and then using the mass spectrometer to determine the composition of those components. The interface between a gas chromatograph and a mass spectrometer (GC-MS) must account for the significant drop in pressure from atmospheric pressure to a pressure of $10^{-8}$ torr; the interface for LC-MS and for EC-MS must provide a way to remove the liquid eluent, to volatilize the samples, and to account for the drop in pressure. See Chapters 27, 28, and 30 for more details.

## Mass Analyzers

The purpose of the mass analyzer is to separate the ions by their mass-to-charge ratios. Ideally we want the mass analyzer to allow us to distinguish between small differences in mass and to do so with a strong signal-to-noise ratio. As we learned in Chapter 7 when introducing optical spectroscopy, these two desires usually are in tension with each other, with improvements in resolution often coming with an increase in noise.

### Resolution

The resolution between two peaks, $R$, in mass spectrometry is defined as the ratio of their average mass to the difference in their masses

$$R = \frac{\overline{m}}{\Delta m} \tag{20.3.1}$$

The following table shows how resolution varies as a function of the average mass and the difference in mass. A resolution of 1,000, for example is sufficient to resolve two ions with an average mass of 100 amu that differ by 0.1 amu, or two ions that have an average mass of 1,000 amu that differ by 1 amu.

Table 20.3.1. Resolution for stated values of $\overline{m}$ and $\Delta m$.

| $\overline{m} \rightarrow$ <br> $\Delta m \downarrow$ | 100 amu | 1000 amu | 10,000 amu |
|---|---|---|---|
| 0.1 amu | 1,000 | 10,000 | 100,000 |
| 1 amu | 100 | 1,000 | 10,000 |
| 10 amu | 10 | 100 | 1,000 |

## Magnetic Sector Mass Analyzers

When a beam of ions passes through a magnetic field, its path is altered, as we see in Figure 20.3.1. The ions experience an acceleration as they exit the ion source and enter the mass analyzer with a kinetic energy that is given by the equations

$$\text{KE} = zeV \tag{20.3.2}$$

$$\text{KE} = \frac{1}{2}mv^2 \tag{20.3.3}$$

where $z$ is the ion's charge (usually +1), $e$ is the electronic charge in Coulombs, $V$ is the applied voltage responsible for the acceleration, $m$ is the ion's mass, and $v$ is the ion's velocity after acceleration. Equation 20.3.2 shows us that all ions with the same charge have the same kinetic energy. Equation 20.3.3, then, tells us that ions with a greater mass will move more slowly.

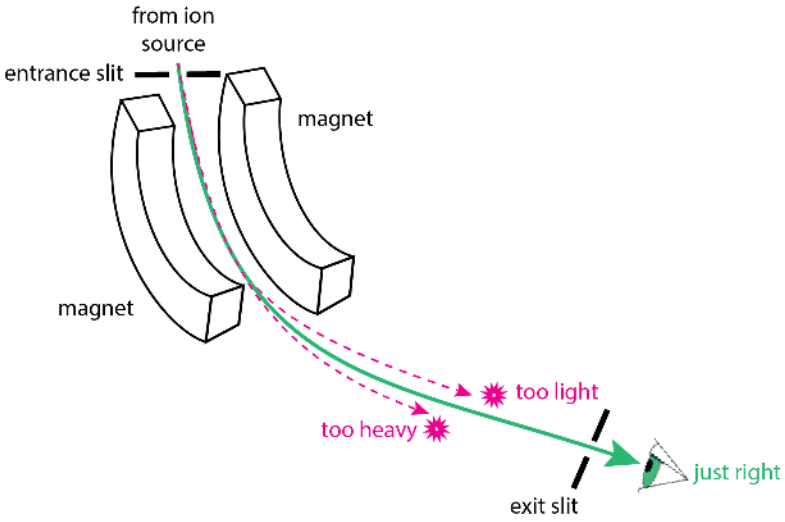



Figure 20.3.1: Illustration of a magnetic sector analyzer for mass spectrometry. Ions from the ion source enter into the mass analyzer. The magnets in the mass analyzer bend the path followed by the ions. For any combination of magnetic field strength and accelerating voltage, only ions with a compatible mass-to-charge ratio are able to leave the mass analyzer through the exit slit; ions that are too heavy or too light, fail to exit the mass analyzer.

An ion's path through the magnetic field is determined by two forces. The first of these forces is the magnetic force, $F_M$, that acts on the ion, which is

$$F_M = Bzev \tag{20.3.4}$$

where $B$ is the magnetic field strength. The second of these forces is the centripetal force, $F_C$, that acts on the ion as it moves along its curved path, which is

$$F_C = \frac{mv^2}{r} \tag{20.3.5}$$

where $r$ is the magnet's radius of curvature. An ion can only navigate these opposing forces if $F_M$ and $F_C$ are equal to each other. This requires that

$$Bzev = \frac{mv^2}{r} \tag{20.3.6}$$

Solving for $v$ gives

$$v = \frac{Bzer}{m} \tag{20.3.7}$$

Substituting back into Equation 20.3.3 and solving for the mass-to-charge ratio gives

$$\frac{m}{z} = \frac{B^2r^2e}{2V} \tag{20.3.8}$$

Equation 20.3.8 tells us that for any combinaton of magnetic field strength, $B$, and accelerating voltage, $V$, only one mass-to-charge ratio has the correct value of $r$ to reach the director. Ions that are too heavy or ions that are too light, will collide with the sides of the mass analyzer before they reach the detector. The mass spectrum is recorded by holding $V$ and $r$ constant and varying the magnetic field strength, $B$. The resolution of a magnetic sector instrument is usually less than 2000.

## Double-Focusing Mass Analyzers

The resolution of a magnetic sector instrument suffers from limitations that affect its ability to narrow the range of kinetic energies—and, thus, velocities—possessed by the ions when they exit the ion source and enter the mass analyzer. The double-focusing mass analyzer in Figure 20.3.2 compensates for this by placing an electrostatic analyzer before the magnetic analyzer, separating the two by a slit. The electrostatic analyzer consists of two curved metal plates, one of which is held at a positive potential and one at a negative potential. As ions pass betweeen the plates, those ions that have too much energy and those that have too little energy fail to pass through the slit that separates the electrostatic analyzer from the magnetic analyzer. In this way, the distribution of energies—and, thus, velocities—is tightened, improving the resolution achieved by the magnetic sector analyzer. Depending on its design, a double-focusing analyzer can achieve a resolution as large as 100,000.

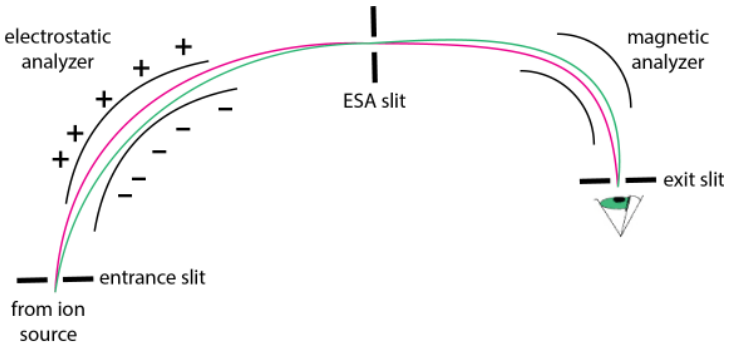



Figure 20.3.2: Illustration of a double-focusing mass analyzer that consists of an electrostatic mass analyzer and a magnetic mass analyzer. Ions that make it through the slit that separates the two analyzers have a smaller range of kinetic energies than the ions in a magnetic sector mass analyzer, which improves resolution.

## Quadrupole Mass Analyzers

The quadrupole mass analyzer was introduced in Chapter 11 and the treatment here is largely the same. A quadupole mass analyzer is compact in size, low in cost, easy to use, and easy to maintain. As shown in Figure 20.3.3, it consists of four cylindrical rods, two of which are connected to the positive terminal of a variable direct current (dc) power supply and two of which are connected to the power supply's negative terminal; the two positive rods are positioned opposite of each other and the two negative rods are positioned opposite of each other. Each pair of rods is also connected to a variable alternating current (ac) source operated such that the alternating currents are 180° out-of-phase with each other. An ion beam from the source is drawn into the channel between the quadrupoles and, depending on the applied dc and ac voltages, ions with only one mass-to-charge ratio successfully travel the length of the mass analyzer and reach the transducer; all other ions collide with one of the four rods and are destroyed.

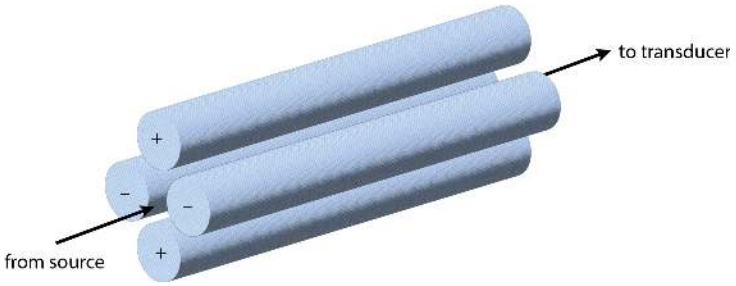



Figure 20.3.3: Basic arrangement of the quadrupole mass analyzer. The plus and the minus signs on each rod indicate which are connected to the positive terminal of the dc power supply. Not shown here is the circuitry for applying the alternating current. The ion beam enters the channel between the quadrupoles. Depending on the applied dc and ac voltages, some of the ions emerge from this channel and reach the transducer.

To understand how a quadrupole mass analyzer achieves this separation of ions, it helps to consider the movement of an ion relative to just two of the four rods, as shown in Figure 20.3.4 for the poles that carry a positive dc voltage. When the ion beam

enters the channel between the rods, the ac voltage causes the ion to begin to oscillate. If, as in the top diagram, the ion is able to maintain a stable oscillation, it will pass through the mass analyzer and reach the transducer. If, as in the middle diagram, the ion is unable to maintain a stable oscillation, then the ion eventually collides with one of the rods and is destroyed. When the rods have a positive dc voltage, as they do here, ions with larger mass-to-charge ratios will be slow to respond to the alternating ac voltage and will pass through the transducer. The result is shown in the figure at the bottom (and repeated in Figure 20.3.5$a$) where we see that ions with a sufficiently large mass-to-charge ratios successfully pass through the transducer; ions with smaller mass-to-charge ratios do not. In this case, the quadrupole mass analyzer acts as a high-pass filter.

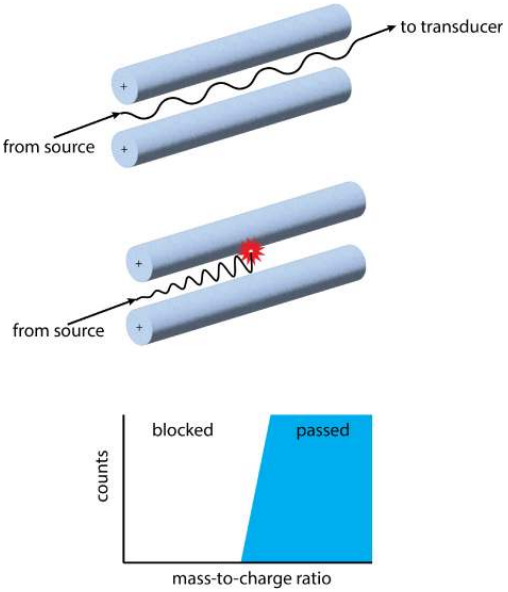



Figure 20.3.4: Illustration of how a quadrupole mass analyzer achieves separation of ions by their mass-to-charge ratio. See the text for additional details.

We can extend this to the behavior of the ions when they interact with rods that carry a negative dc voltage. In this case, the ions are attracted to the rods, but those ions that have a sufficiently small mass-to-charge ratio are able to respond to the alternating current's voltage and remain in the channel between the rods. The ions with larger mass-to-charge ratios move more sluggishly and eventually collide with one of the rods. As shown in Figure 20.3.5$b$, in this case, the quadrupole mass analyzer acts as a low-pass filter. Together, as we see in Figure 20.3.5$c$, a quadrupole mass analyzer operates as both a high-pass and a low-pass filter, allowing a narrow band of mass-to-charge ratios to pass through the transducer. By varying the applied dc voltage and the applied ac voltage, we can obtain a full mass spectrum.

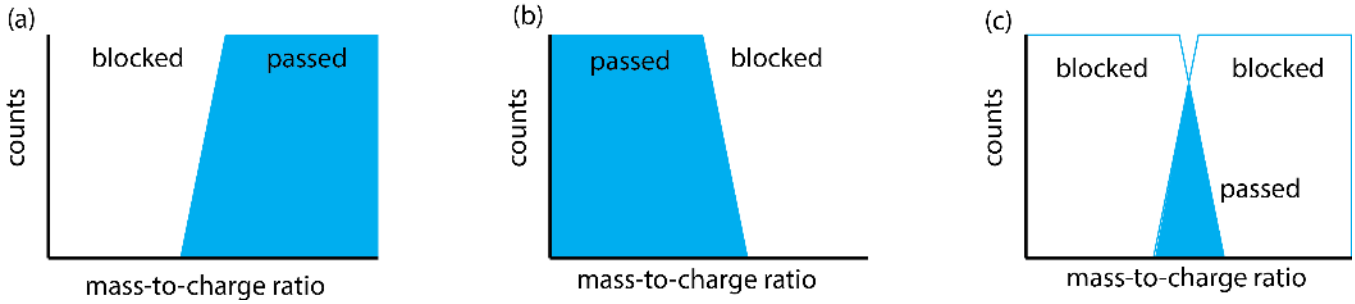



Figure 20.3.5: Illustration that shows how a quadrupole mass analyzer acts as both (a) a high-pass filter and (b) a low pass filter, with the result that it passes only ions with a narrow range of mass-to-charge ratios.

Quadrupole mass analyzers provide a modest mass-to-charge resolution of about 1 amu and extend to $m/z$ ratios of approximately 2000.

## Time-Of-Flight Mass Analyzers

In a time-of-flight mass analyzers, Figure 20.3.6, ions are created in small clusters by applying a periodic pulse of energy to the sample using a laser beam or a beam of energetic particles to ionize the sample. The small cluster of ions are then drawn into a tube

by applying an electric field and then allowed to drift through the tube in the absence of any additional applied field; the tube, for obvious reasons, is called a drift tube. All of the ions in the cluster enter the drift tube with the same kinetic energy, KE, which we define as

$$\text{KE} = \frac{1}{2}mv^2 = zeV \tag{20.3.9}$$

The time, $T$, that it takes the ion to travel the distance, $L$, to the detector is

$$T = \frac{L}{v} \tag{20.3.10}$$

Substituting Equation 20.3.10 into Equation 20.3.9

$$T = \sqrt{\frac{m}{z}} \times \sqrt{\frac{1}{2eV}} \tag{20.3.11}$$

shows us that the time it takes an ion to travel through the drift tube is proportional to the square rate of its mass-to-charge ratio. As a result, lighter ions move more quickly than heavier ions. Flight times are typically less than 30 μs. A time-of-flight mass analyzer provide better resolution than a quadrupole mass analyzer, but is limited to sources that can be pulsed. A linear time-of-flight analyzer, such as that in Figure 20.3.6, provide a resolution of approximately 4,000; other configurations can achieve resolutions of 10,000 or better. The time-of-flight analyzer is well-suited for MALDI ionization as the time between pulses of the laser provides the time needed for detection to occur.

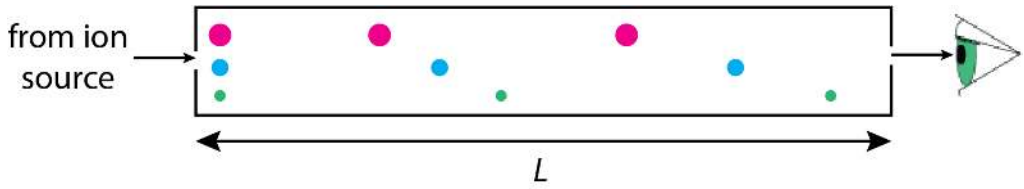



Figure 20.3.6: Illustration of a linear time-of-flight mass analyzer showing three views of the relative positions of three ions with a small (green), medium (blue), and large (red) mass-to-charge ratios as they migrate through the drift tube.

## Ion Trap Mass Analyzers

Figure 20.3.7 provides an illustration of an ion trap mass analyzer, which consists of three electrodes—a central ring electrode and two conical end cap electrodes—that create a cavity into which ions are drawn. The ions in the cavity experience stabilizing and destabilizing forces that affect their movement within the cavity. Ions that adopt stable orbits remain in the cavity. By varying the potentials applied to the electrodes, ions with different mass-to-charge ratios enter into destabilizing orbits and exit through a small hole at the bottom of the trap. An ion trap typcially provides a resolution of 1,000.

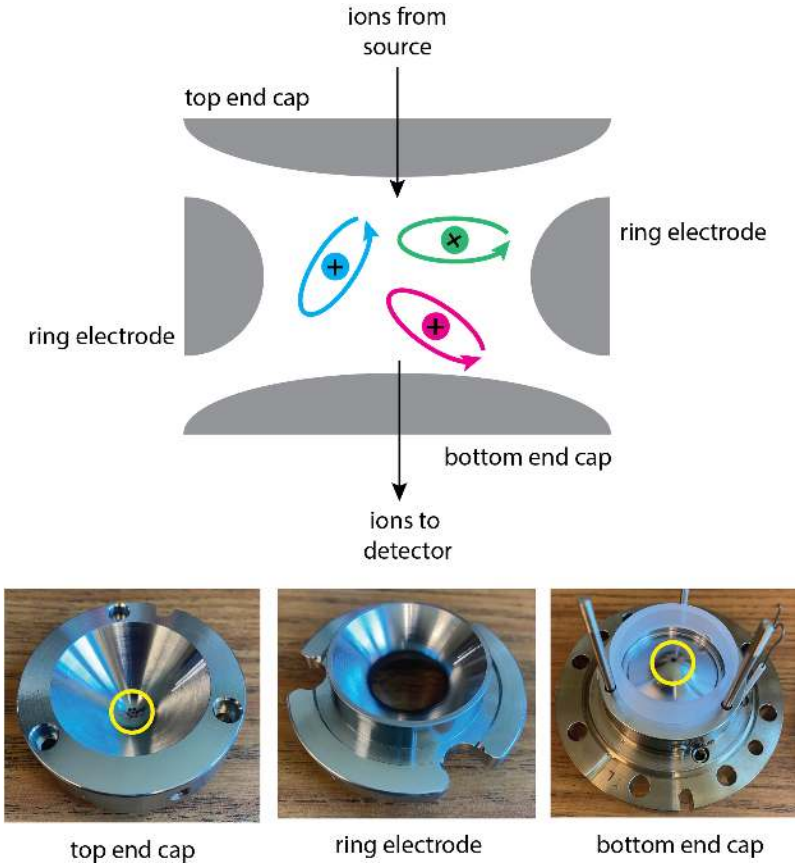



Figure 20.3.7: Illustration of the ion trap mass analyzer showing the cavity defined by the top end cap, the ring electrode, and the bottom end cap. The photographs on the bottom show the conical-shaped top end cap with small holes (inside the yellow circle) that allows ions to enter into the cavity, the ring electrode, and the conical-shaped bottom end cap, which has a small hole (inside the yellow circle) that allows ions to exit the cavity and reach the detector.

## Ion Cyclotron Resonance Mass Analyzer

The ion cyclotron resonance (ICR) analyzer is a form of an ion trap but operates in a way that retains all ions within the trap. When a gas phase ion is placed within an applied magnetic field, the ions move in a circular orbit that is perpendicular to the applied field (Figure 20.3.8). In discussing the magnetric sector analyzer, we showed that the velocity, $v$, of an ion in an applied magnetic field with a strength of $B$ is a function of the radius of the ion's motion, $r$, and its charge

$$v = \frac{Bzer}{m} \tag{20.3.12}$$

Solving for the ratio $v/r$ gives the ion's cyclotron frequency, $w_c$, as

$$w_c = \frac{v}{r} = \frac{zeB}{m} \tag{20.3.13}$$

When an ion moving in a circular orbit, as shown by the smaller of the two circular orbits in Figure 20.3.8$a$, absorbs energy equal to its cyclotron frequency, $w_c$, its velocity, $v$, and the radius of its orbit, $r$ both increase to maintain a constant value for $w_c$; the result is an ion that moves in a circular orbit of greater radius. As $w_c$ depends on the mass-to-charge ratio, all ions of equal $m/z$ experience the same change in their orbit, while ions with other mass-to-charge ratios are unaffected. Ions in the larger orbits eventually return to their original circular orbit as a result of collisions in which they lose energy.

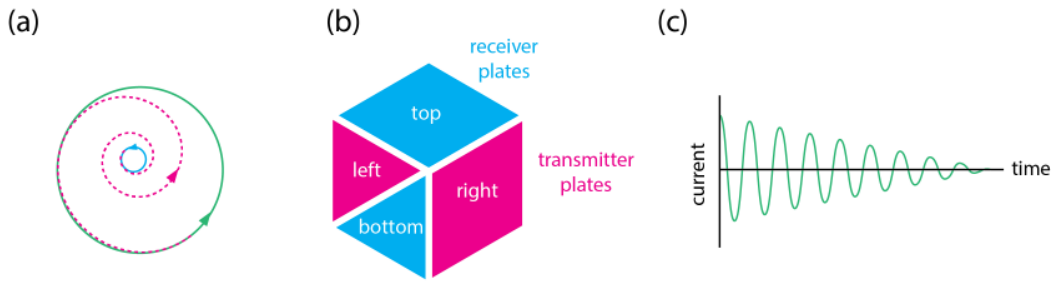



Figure 20.3.8: Illustration of how an ICR mass analyzer works. In (a) an ion originally in a circular orbit with a small radius, shown in blue moves into a circular orbit with a larger radius, shown in green when it absorbs energy equal to its cyclotron frequency, $w_c$, following the path shown in pink. The ICR cell in (b) consists of two transmitter plates that apply the potential that alters each ion's orbit, and two receiver plates that measure the current generated by the ions; there are two additional plates, one in front and one in back, that provide an entrance for bringing ions into the ICR cell from the ion source and for removing the ions in preparation for the next sample. The signal in (c) decays with time as the ions lose energy through collisions.

The trap itself, as seen in Figure 20.3.8*b*, is defined by two pairs of plates (four in all). The transmitter plates are used to apply the potential that alters the orbits of the ions. Movement of the ions generates a current in the receiver plates that serves as the signal, as seen in Figure 20.3.8*c*, that is positive when the ion is closer to one receiver plate and negative when it is closer to the other receiver plate. The initial magnitude of the current is proportional to the number of ions with the mass-to-charge ratio.

The ion cyclotron resonance analyzer is usually operated by applying a short pulse of energy that varies linearly in its frequency. This sets all ions into motion, with each mass-to-charge ratio yielding a current response similar to that in Figure 20.3.8*c*. Collectively, these individual current-time curves gives a time domain spectrum that we can covert into a frequency domain spectrum by taking the Fourier transform. The frequency domain spectrum yields the mass spectrum through Equation 20.3.13. FT-ICR instruments are capable of achieving resolutions of 1,000,000.

---

This page titled 20.3: Mass Spectrometers is shared under a CC BY-NC-SA 4.0 license and was authored, remixed, and/or curated by David Harvey.

# 20.4: Applications of Molecular Mass Spectrometry

## Qualitative Applications

In a qualitative analysis our interest is in determining the identity of a substance of interest to us. By itself, mass spectrometry is a powerful tool for determining the identity of pure compounds. The analysis of mixtures, however, is possible if we use a mass spectrometer as the detector for a separation technique, such as gas chromatography, or if we string together two or more mass analyzers in sequence.

### Identification of Pure Compounds

There are several ways to use a mass spectrum to identify a compound, including identifying its molecular weight, using isotopic ratios, examining fragmentation patterns, and by searching through data bases.

**Using Molecular Weight Information**. A molecular ion peak, $M^{+\bullet}$, when it is present, a $[M + H]^+$ peak or a $[M – H]^+$ peak, provides information about the compound's molecular weight. When using a low resolution mass analyzer, this may be sufficient to distinguish between molecular ions with, for example, a nominal mass of 95 amu and a nominal mass of 96 amu, but insufficient to distinguish between molecular ions with a more precise mass of 96.0399 amu and 96.0575 amu. When using a high resolution mass analyzer, the difference between the last pair of molecular ions may be feasible.

**Using Isotopic Ratios**. The molecule cycloheptene has the formula $C_7H_{12}$ and a nominal mass of 96 amu, and the molecule cyclohexenone has the formula $C_6H_8O$ and a nominal mass of 96 amu. Although both molecules will produce a molecular ion with the same nominal mass-to-charge ratio, each will also have a peak with a nominal mass of M + 1 due to the presence of isotopes of carbon, hydrogen, and oxygen. Because cycloheptene and cyclohexenone have different chemical formulas, the relative heights of their M + 1 peaks are different. Here is how we can work this out.

For every 100 atoms of $^{12}C$ there are 1.08 atoms of $^{13}C$ (that is, 1.08% of the carbon atoms are $^{13}C$), for every 100 atoms of $^{1}H$ there are 0.015 atoms of $^{2}H$, and for every 100 atoms of $^{16}O$ there are 0.04 atoms of $^{17}O$. For cycloheptene, this means that the relative height of its M + 1 peak to its M peak is

$$(7 \times 1.08) + (12 \times 0.015) = 7.74$$

and for cyclohexenone we have

$$(6 \times 1.08) + (8 \times 0.015) + (1 \times 0.04) = 6.64$$

Here we see that a careful examination of the relative height of the M + 1 peak provides a way to distinguish between $C_7H_{12}$ and $C_6H_8O$ even though they have the same nominal masses. On-line calculators are available—this link provides one example—that you can use to calculate the full isotopic abundance patterns, including M + 2, M + 3, and other peaks. Isotopic patterns are particularly useful for identifying the presence of chlorine and bromine in a molecule because each has one isotope with a significant abundance: for chlorine, $^{37}Cl$ has an abundance of 32.5% relative to $^{35}Cl$, and for bromine, $^{81}Br$ has an abundance of 98.0% of $^{79}Br$.

**Using Fragmentation Patterns**. Figure $20.4.1$ shows the mass spectrum of *p*-nitrophenol, which we first considered in Section 20.1. A molecule's mass spectrum is unique and contains information that we can use to deduce its structure. Interpretation of a mass spectrum relies on identifying possible sources for the loss of mass, such as the a $\Delta m$ of 30 amu corresponding to the loss of NO, or a $\Delta m$ of 46 amu corresponding to the loss of $NO_2$. Some mass-to-charge ratios are recognized as evidence for a particular ion, such as $C_5H_5^+$ at a mass-to-charge ratio of 65. The interpretation of fragmentation patterns is covered elsewhere in the curriculum, particularly in organic chemistry, and is not given more consideration here.

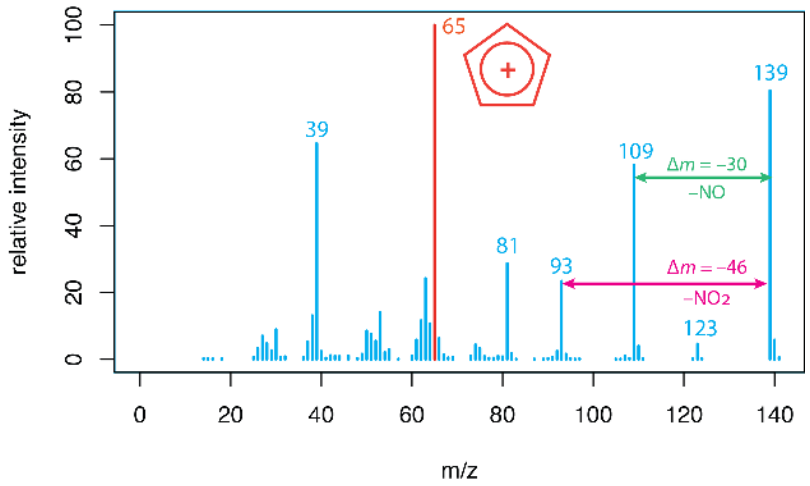



Figure 20.4.1: Mass spectrum of *p*-nitrophenol.

**Using Computer Searching**. Large databases of mass spectra are available (see here for a source from NIST). A peak table of mass-to-charge ratios and peak intensities for a sample is entered into an algorithm that searches the database and identifies the most likely matches.

### Analysis of Mixtures Using MS as a Detector for a GC or LC Separation

Mass spectrometry is a powerful analytical technique when the sample we are analyzing is pure (or if impurities are of sufficiently low concentration that they have little effect on the mass spectrum). For a mixture of two or more analytes, the interpretation of the mass spectrum is difficult, if not impossible. To analyze such a mixture, we need a means of separating the analytes from each other. One approach is to interface a mass spectrometer to a gas chromatograph or a liquid chromatograph. The GC, or LC separates the mixture into its component parts with the mass spectrometer serving as the detector. See Chapter 27 and Chapter 28 for further details about GC-MS and LC-MS.

### Analysis of Mixtures Using Tandem Mass Spectrometry

Another approach to working with a complex sample is to use two or more mass analyzers in what is called tandem mass spectrometry. For example, if we place three quadrupole mass analyzers in a sequence, we can use a soft ionization source to generate mostly molecular ions of the form $[M + H]^+$ for each of the sample's analytes, and then let the first quadrupole separate these molecular ions by the differences in their mass-to-charge ratio. The $[M + H]^+$ molecular ions for one of the analytes is then selectively passed into the second quadrupole where it is allowed to undergo fragmentation by collision with a gas, such as He. Finally, these fragment ions are passed along to the third quadrupole where the mass spectrum is obtained. By sequentially passing each of the molecular ions from the first quadrupole through the second and third quadrupoles, we are able to obtain mass spectra for each molecule in the mixture.

## Quantitative Applications

As a detector for other instrumental methods, such as gas chromatography and liquid chromatography, mass spectrometry provides for a quantitative analysis by monitoring either the total ion count or by monitoring ions of a single mass-to-charge ratio, which is known as selective ion monitoring. As an Independent method for determining an analyte's concentration, mass spectrometry is less attractive due to the difficulty of controlling the amount of sample or standard introduced into the instrument and the affect of the sample's matrix on fragmentation. The use of an internal standard improves precision and accuracy.

This page titled 20.4: Applications of Molecular Mass Spectrometry is shared under a CC BY-NC-SA 4.0 license and was authored, remixed, and/or curated by David Harvey.

# CHAPTER OVERVIEW

## 21: Surface Characterization by Spectroscopy and Microscopy


21.1: Introduction to the Study of Surfaces

21.2: Spectroscopic Surface Methods

21.3: Scanning Electron Microscopy

21.4: Scanning Probe Microscopes


---

This page titled 21: Surface Characterization by Spectroscopy and Microscopy is shared under a CC BY-NC-SA 4.0 license and was authored, remixed, and/or curated by David Harvey.

# 21.1: Introduction to the Study of Surfaces

Thus far we have considered methods for analyzing the bulk properties of samples, such as determining the identity or concentration of an ion in a solution, of a molecule in a gas, or of several elements in a solid. In doing so, we did not concern ourselves with the sample's homogeneity or heterogeneity. In this chapter we give consideration to how we can gather information about the composition of a sample's surface and how it differs from the sample's bulk composition. But first, let's consider several important questions.

## What Is A Surface?

A surface is a boundary, or interface, between two phases, such as a solid and a gas (the type of interface of particular interest to us in this chapter). This is a helpful, but not a sufficient description. Also of interest is the question of depth. Is a surface just the outermost layer of atoms, ions, or molecules, or does it extend several layers into the sample? In what ways might the composition of a sample at the surface differ from its composition in the sample's bulk interior? And, what about variations in composition across a surface? Is the surface itself homogeneous or heterogeneous in its composition? Different analytical methods will sample the surface to different depths and with different surface areas, which means the volume of sample analyzed will vary from method-to-method. For this reason, we usually define a sample's surface as what is analyzed by the analytical method we are using.

## Why Are Surfaces of interest?

Figure 21.1.1 shows the crystal structure of AgCl(*s*), which consists of a repeating pattern of $Ag^+$ ions and $Cl^-$ ions. If you look at the ions in interior of the structure, you will see that each $Ag^+$ ion is surrounded by six $Cl^-$ ions, and each $Cl^-$ ion is surrounded by six $Ag^+$ ions. On the surface, however, we see that $Cl^-$ ions and $Ag^+$ ions no longer are surrounded by six ions of opposite charge. As a result, the $Ag^+$ ions and $Cl^-$ ions on the surface are more chemically reactive than those in the interior and can serve as sites for interesting chemistry. The chemical and physical properties of a sample's surface are likely to be very different than the sample's bulk properties.

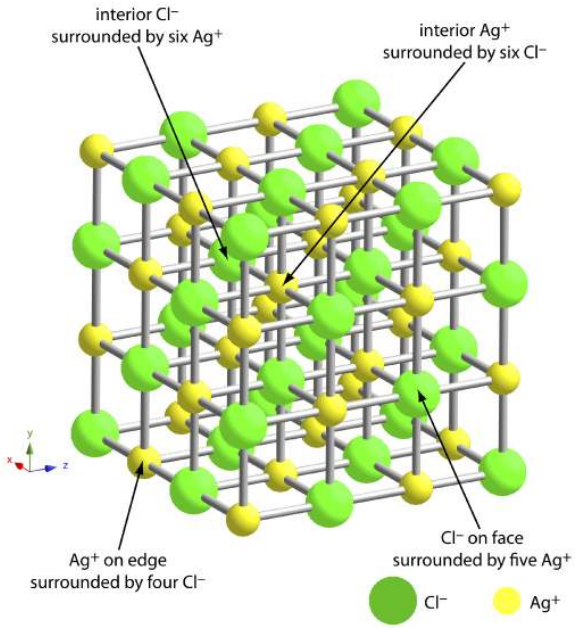



Figure 21.1.1: Ball-and-stick model showing the lattice structure of AgCl. Each silver ion in the lattice's interior binds with six chloride ions and each chloride ion in the interior binds with six silver ions. Those ions on the lattice's surface or edges bind to fewer than six ions and carry a partial charge. A silver ion on the surface, for example, carries a partial positive charge. These charges, for example, make the surface of a precipitate of AgCl an active site for chemical and physical interactions.

## What Challenges Does a Surface Present?

Suppose we are interested in studying the surface of a piece of zinc metal using a probe that samples just the outermost layer of atoms and that samples a circular surface area that is 1 $\mu m^2$. How many atoms of Zn might we expect our probe to encounter? Here

is some useful information about zinc: it has a molar mass of 65.38 g/mol, it has a density of 7.14 g/cm$^3$, and it has an atomic radius of approximately 0.13 nm. From this we calculate the atoms per unit volume as

$$\frac{7.14\text{ g}}{\text{cm}^3}\times\frac{100\text{ cm}}{\text{m}}\times\frac{1\text{m}}{10^9\text{ nm}}\times\frac{1\text{ mol}}{65.38\text{ g}}\times\frac{6.022\times10^{23}\text{ atoms}}{\text{mol}}=\frac{6.6\times10^{15}\text{ atoms}}{\text{cm}^2\text{ nm}}$$

The units in the denominator may look odd to you, but writing them this way emphasizes that we are interested both in the depth from which information is received (given here in nanometers, nm) and in the surface area from which information is received (given here in square centimeters, cm$^2$). Multiplying this value by the thickness of an atomic layer of zinc, which is twice its atomic radius, suggests we are analyzing approximately

$$\frac{6.6\times10^{15}\text{ atoms}}{\text{cm}^2\text{ nm}}\times0.26\text{ nm}=1.7\times10^{15}\frac{\text{atoms}}{\text{cm}^2}$$

If we multiply this value by the surface area that we are sampling from, then we are interacting with approximately

$$1.7\times10^{15}\frac{\text{atoms}}{\text{cm}^2}\times\left(\frac{100\text{ cm}^2}{\text{m}}\right)^2\times\left(\frac{1\text{m}}{10^6\mu\text{m}}\right)^2=1.7\times10^7\text{ atoms of Zn}$$

Although 17 million may seem like a large number, it is not a particularly large number of atoms on which to carry out an analysis. Now, suppose the surface has a 10 ppm impurity of copper atoms; that is, there are 10 copper atoms for every $10^6$ zinc atoms. In this case, our probe of the sample involves just

$$1.7\times10^7\text{ atoms of Zn}\times\frac{10\text{ atoms of Cu}}{10^6\text{ atoms of Zn}}=170\text{ atoms of Cu}$$

As a comparison, if we analyze a sample in which the analyte is present at a concentration that is $1\times10^{-6}$ mol/L using an analytical method that gathers information from a volume that is just 1 mm$^3$, then we are sampling

$$\frac{1\times10^{-6}\text{ mol}}{\text{L}}\times\frac{1\text{L}}{1000\text{ cm}^3}\times\left(\frac{1\text{cm}}{10\text{ mm}}\right)^3\times1\text{ mm}^3\times6.022\times10^{23}\text{ mol}^{-1}$$
$$=6.0\times10^{11}\text{ particles of analyte}$$

An additional challenge when we attempt to analyze a surface is that a freshly exposed surface becomes contaminated with an absorbed layer of gas molecules almost instantly when sitting on a laboratory bench, and in a few seconds to a few minutes at pressures in the range of $10^{-6}$ torr to $10^{-8}$ torr. Analysis of a surface requires careful attention to how the surface is prepared.

## What Opportunities Does a Surface Present?

Compared to many of the methods in Chapters 6–20 and in Chapters 22–34, the use of a probe that samples from a small area allows for moving the probe across the surface—this is called rastering—developing a two-dimensional image of the surface. When using an energetic beam that can etch a hole in the sample, we can obtain information at depth—a process called depth profilling—that provides information in a third dimension. These are particularly important strengths of surface analytical methods.

## How Can We Probe the Surface?

To study a surface, we put energy into it in the form of a beam of photons, electrons, or ions and then we measure the energy that exits the surface in the form of a beam of photons, electrons, or ions. Table 21.1.1 shows some of the possibilities. Also included in this table are methods in which an applied field generates a response from the surface. Entries in **bold** receive attention in this chapter. Surface enhanced Raman spectroscopy received a brief mention in Chapter 18. Note that Auger electron spectroscopy appears twice as the emission of electrons can follow the input of X-ray photons or electrons.

Table 21.1.1. Classifying surface analysis methods based on the input energy and the output energy.

| energy out → energy in ↓ | photon | electron | ion | field |
|---|---|---|---|---|
| photon | surface enhanced Raman spectroscopy (SERS) extended X-ray absorption fine structure (EXAFS) | **X-ray photoelectron spectroscopy (XPS)** **Auger electron spectroscopy (AES)** UV-photoelectron spectroscopy (UPS) | laser-microprobe mass spectrometry (LAMMA) | — |
| electron | energy dispersive X-ray spectroscopy (EDS) electron microprobe (EM) | **Auger electron spectroscopy (AES)** **scanning electron microscopy (SEM)** low energy electron diffraction (LEED) | — | — |
| ion | — | — | Rutherford back scattering (RBS) **secondary ion mass spectrometry (SIMS)** | |
| field | — | **scanning tunneling microscopy (STM)** | — | **atomic force microscopy (AFM)** |

**Note**

There are other ways to probe a surface by putting energy into it, including the application of thermal energy and the use of neutral species. See the text *Methods of Surface Analysis*, Czanderna, A. Editor, Elsevier: Amsterdam (1975) and the article "Analytical Chemistry of Surfaces" by D. M. Hercules and S. H. Hercules, *J. Chem. Educ.* 1984, *61*, 402–409 for detailed reviews. Although neither is a recent publication, both provide an excellent introduction to surface analysis.

This page titled 21.1: Introduction to the Study of Surfaces is shared under a CC BY-NC-SA 4.0 license and was authored, remixed, and/or curated by David Harvey.

# 21.2: Spectroscopic Surface Methods

In this section we consider three representative surface analytical methods: X-ray photoelectron spectroscopy, in which the input is a beam of X-ray photons and the output is electrons; Auger electron spectroscopy, in which the input is either a beam of electrons or of X-ray photons and the output is electrons; and secondary-ion mass spectrometry, in which the input is a beam of ions and the output is ions.

## X-Ray Photoelectron Spectroscopy (XPS)

In X-ray photoelectron spectroscopy, which is also known as electron spectroscopy for chemical analysis (ESCA), we measure the kinetic energy of electrons ejected from a sample following the absorption of X-ray photons. The resulting spectrum is a count of these emitted electrons as a function of their energy.

### Principles of XPS

We can explain the origin of X-ray photoelectron spectroscopy using the photoelectric effect. Figure 21.2.1*a* shows the energy level diagram for an element's 1*s*, 2*s*, and 2*p* core-level electrons along with their KLM designations (see Chapter 12.1 for a previous discussion of this way of designating electrons). A nearly monoenergetic X-ray beam of known energy is focused on the sample, which results in the ejection of a core-level photoelectron, as shown in Figure 21.2.1*b*. The kinetic energy of this emitted electron, $E_{KE}$, is related to its binding energy to the nucleus, $E_{BE}$, by the equation

$$E_{KE} = h\nu - E_{EB} - \Phi_w \tag{21.2.1}$$

where $h\nu$ is the energy of the X-ray photon and $\Phi_w$ is the spectrometer's work function (the energy needed to remove the electron from the surface and into the vacuum). The most common sources of X-rays are the Mg $K_\alpha$ line with an energy of 1253.6 eV or the Al $K\alpha$ line with an energy of 1486.6 eV.

The core-level vacancy created by the photoelectron leaves the atom with an unstable electron configuration. Relaxation to the ground state occurs when this vacancy is filled by an electron from a higher energy shell, with the excess energy released as either the emission of a second electron or the fluorescent emission of a characteristic X-ray, as seen in Figure 21.2.1*c*. The secondary electron in Figure 21.2.1*c* is called an Auger electron.

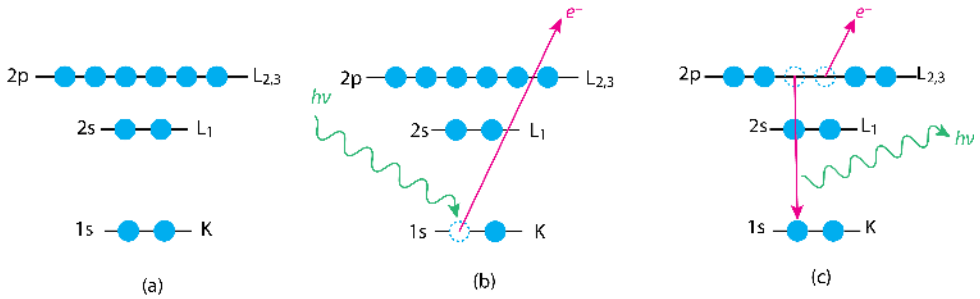



Figure 21.2.1: Energy level diagrams for X-ray photoelectron spectroscopy. In (a) we see the 1*s*, 2*s*, and 2*p* electrons along with their KLM designations. When a photon of sufficient energy is absorbed by the sample (b), a core-level electron is ejected as a photoelectron leaving an unstable electron configuration in which there is a vacancy in the 1s orbital. In (c) an electron from a higher energy orbital moves into the vacancy created by the initial photon with the remaining energy released as a secondary electron or as an X-ray photon.

Figure 21.2.2 provides an example of an XPS survey spectrum for aluminum oxide, $Al_2O_3$, using the $K_\alpha$ line for aluminum as the source of X-rays. The peak table gives the binding energies of the peaks for aluminum and for oxygen using the $K_\alpha$ for Al and, for comparison, the $K_\alpha$ line for Mg. Note the difference in how the major peaks are labeled. The photoelectrons ejected in the process shown in Figure 21.2.1*b* are designated by the element and the *ns* notation that specifies the orbital from which the electron was ejected. Auger electrons are designated using the KLM notation, specifying the initial vacancy created by the absorbed photon, the source of the electron that fills that vacancy, and the source of the ejected Auger electron. The $O_{KLL}$ peak in this spectrum is consistent with the scheme shown in Figure 21.2.1*c*. When the source of the second and third electrons is from the valance shell, then notation is sometimes written as KVV; the $O_{KLL}$ peak here could be designated as $O_{KVV}$.

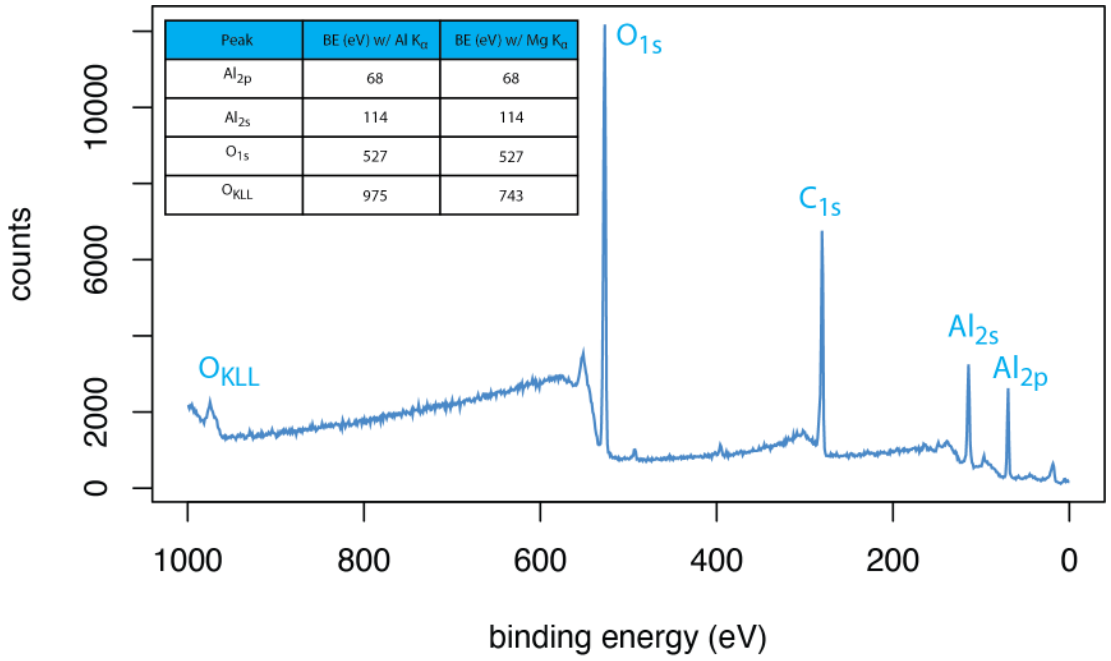



Figure 21.2.2: The XPS spectrum for $Al_2O_3$ using the Al $K_\alpha$ line, with the major peaks labeled. A spectrum such as this, which spans a wide range of energies, is called a survey spectrum. The source of each peak is shown above or next to the spectrum's peaks. The peak table provides the binding energies for aluminum and for oxygen using both the $K_\alpha$ for Al and the $K_\alpha$ for Mg. The original data used to create this figure is from the xpslibrary.

There are a few additional interesting features to note in the survey spectrum for $Al_2O_3$. One is the presence of a peak for carbon even though the sample, $Al_2O_3$, does not contain carbon. The prevalence of carbon in the atmosphere means that trace levels of carbon appear in almost all XPS spectra.

A second feature is the increase in the signal on the high binding energy (low kinetic energy) side of peaks, which is particularly visible here for the $O_{1s}$ peak the $C_{1s}$ peak, and the $Al_{2s}$ peak. The source of this background is electrons that fail to escape the sample without undergoing inelastic collisions that result in a loss of kinetic energy and, given Equation 21.2.1, are recorded as if they have a larger than expected binding energy. Because X-rays penetrate more deeply into the sample than the depth from which electrons can travel without undergoing an inelastic collision, this background is unavoidable. Note that the background is more significant at higher binding energies (smaller kinetic energies).

A third feature is that the binding energy of an XPS peak is independent of the X-ray source, but the binding energy for an Auger peak varies with the X-ray source's energy (see table in Figure 21.2.2). The kinetic energy of the $O_{1s}$, $Al_{2s}$, and $Al_{2p}$ photoelectrons is the difference between the energy of the X-ray photon, $h\nu$, and each electron's binding energy, BE; if we change the X-ray source, then $h\nu$ and KE increase in value, but the BE remains fixed. For the $O_{KLL}$ Auger electron, the kinetic energy depends on the difference in the binding energies of the three electrons involved

$$\text{KE} \approx \text{BE}_K - \text{BE}_L - \text{BE}_L \tag{21.2.2}$$

and is, therefore, independent of the energy of the X-ray source. Given Equation 21.2.1, if the KE remains constant, then an increase in the energy of the X-ray photon, $h\nu$, means that the apparent BE must increase. This shift in binding energy when using a different source is one way to identify a peak as resulting from Auger electrons.

## Instrumentation

The basic instrumentation for XPS is shown in Figure 21.2.3. The most common X-ray sources, as noted above, are Mg (1253.6 eV) and Al (1486.6 ev), which have the advantage of relatively narrow line-widths (0.7 and 0.9 eV, respectively) and, therefore, a relatively narrow range of energies. Higher energy sources are available, such as Ag (2984.4 ev), but at the cost of a wider line-width (2.6 eV). A system of electron lenses collects and focuses the ejected electrons onto the entrance slit of a hemispherical analyzer. The path of an electron through the analyzer depends upon its kinetic energy. By varying the potentials applied to the hemispherical analyzer's inner and outer plates, electrons of different kinetic energies reach the detector. A sputtering gun is an

optional feature that can be used to clean the surface of the sample or to remove successive layers of the sample, allowing for the gathering of spectra at various depths within the sample. Calibration of the spectrometer's binding energy scale, which accounts for the spectrometer's work function, is made using specific lines for one or more conductive metals; examples include Au $4f_{7/2}$ at 83.95 eV and Cu $2p_{3/2}$ at 932.63 ev. The peak for carbon that appears in almost all XPS spectra provides an additional way to check the calibration of the binding energy scale.

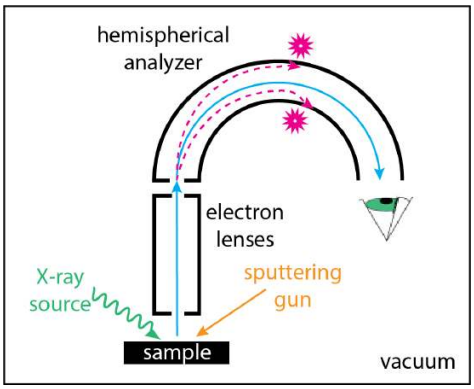



Figure 21.2.3: Schematic diagram of the basic instrumentation for X-ray photoelectron spectroscopy: an X-ray source for generating photoelectrons; a sputtering gun for cleaning the sample's surface or for removing layers of the sample; a set of electron lenses for collecting and focusing the photoelectrons; a hemispherical analyzer for isolating electrons by their kinetic energies; and a transducer to count electrons. The entire instrument is held under a vacuum.

## Applications

X-ray photoelectron spectroscopy is a particularly useful tool for determining the composition and structure of a sample. XPS also can provide information about how the composition of a sample varies with depth and quantitative information about a sample's components.

**Qualitative Analysis**. One of the strengths of X-ray photoelectron spectroscopy is the ability to determine the elements that make up a sample's surface. Figure 21.2.4 shows a survey scan from 0 eV to 1100 eV of a ceramic material. In addition to the O1s peak, we see strong peaks for Si and Al—probably an aluminosilicate ceramic—and small peaks for a variety of elements: La, Ba, Mn, Sn, Ca, Cl, P, and Mg. NIST maintains an extensive, and searchable, database of XPS peaks that help in identifying the elements in a sample.

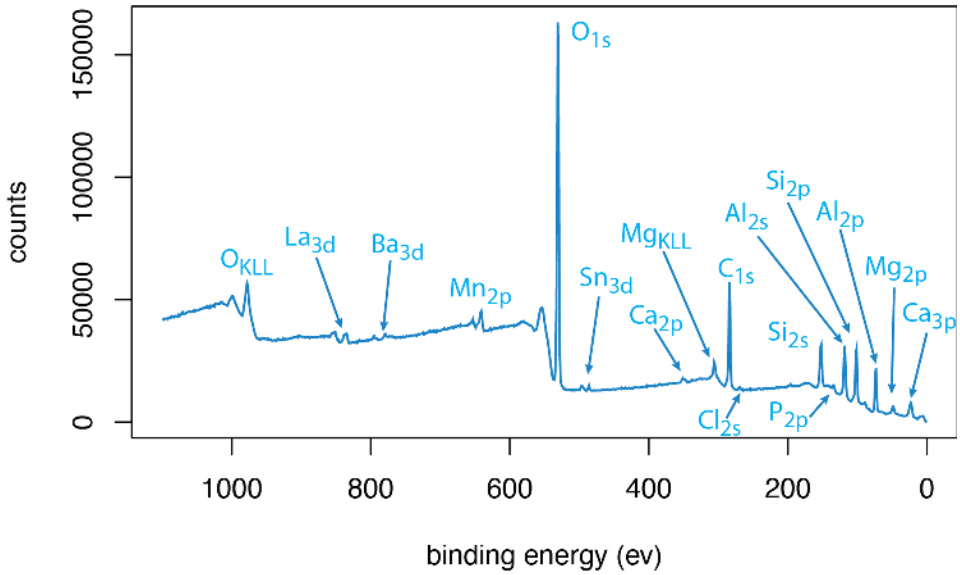



Figure 21.2.4: X-ray photoelectron survey spectrum for an unidentified ceramic material showing the peak assignments, which include major elements that we might reasonably expect from a ceramic (oxygen, magnesium, aluminum, calcium, and silicon) and a variety of trace elements (lanthinum, barium, manganese, tin, chlorine, and phosphorous). The original data used to create this figure is from the xpslibrary.

**Chemical Shifts**. An element's binding energy is sensitive to its chemical environment, particularly with respect to oxidation states and structure. For example, Table 21.2.1 provides the binding energy for chlorine's 2p line in three potassium salts drawn from the NIST database with all values from the same literature source. Using KCl, in which chlorine has an oxidation state of –1, as a baseline, the Cl 2p peak for $KClO_3$ is shifted by +8.4 eV and the Cl 2p peak for $KClO_4$ is shifted by +10.3 eV. The direction of the shift makes sense, as we expect that it will require more energy to remove an electron from an element that has a more positive oxidation state.

Table 21.2.1. Binding energies for the Cl 2p XPS peak as a function of chlorine's oxidation state.

| compound | oxidation state for chlorine | binding energy (eV) for Cl 2p line | ΔBE relative to KCl |
|---|---|---|---|
| KCl | –1 | 198.1 | — |
| $KClO_3$ | +5 | 206.5 | +8.4 |
| $KClO_4$ | +7 | 208.4 | +10.3 |

Chemical shifts also reflect changes in chemical structure. Figure 21.2.5, for example, shows a high resolution scan for the oxygen 2p peak for same sample of aluminum oxide, $Al_2O_3$, in Figure 21.2.1. The surface of a metal oxide often has three distinct sources of oxygen: oxides, which make up the bulk of the sample, hydroxides that form at the surface following the chemisorption of water, and water that is physically absorbed to the surface. Curve-fitting of the raw data shows the contribution of each type of oxygen to the raw data and, through the peak areas, their relative abundance.

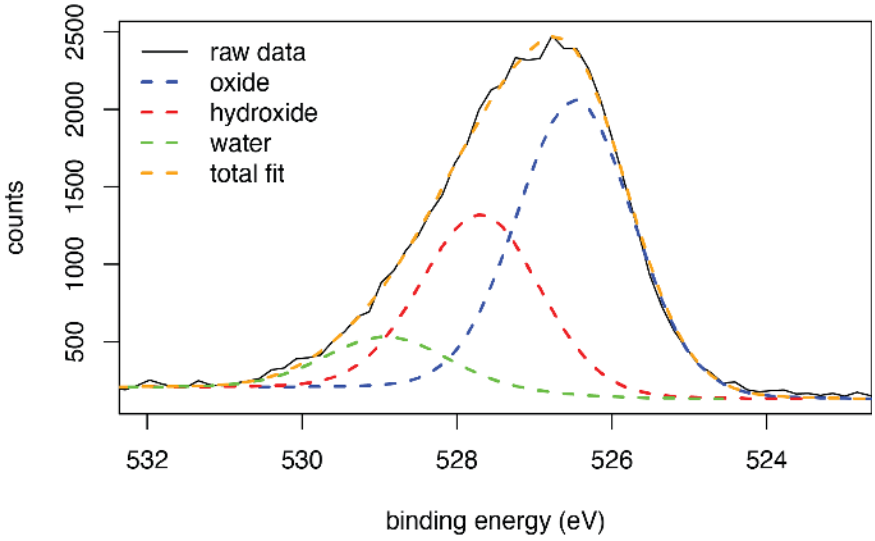



Figure 21.2.5: The results of curve-fitting to determine the relative contribution of different sources of oxygen—oxides, hydroxides, and water—to the $O_{2p}$ peak for aluminum oxide. The original data used to create this figure is from the xpslibrary.

**Wagner Plots**. Both the binding energy of an X-ray photoelectron and the kinetic energy of an Auger electron convey information about the element from which the electrons were emitted. A Wagner plot shows both the binding energy for a photoelectron that leaves a particular core-level vacancy and the kinetic energy of the Auger electron whose origin arises from the filling of this core-level vacancy. Figure 21.2.6 shows an example of a Wagner plot for copper based on its $2p_{3/2}$ X-ray photoelectron and its LMM Auger electron. The diagonal lines are called the modified Auger parameter, which is defined as the sum of the XPS binding energy and the AES kinetic energy. Values for 20 compounds are included in this plot. Of interest here is the clustering of the individual compounds. For example, all of the samples for which copper has an oxidation state of +1 (shown as magenta squares) have similar binding energies between 932 eV and 933 eV, but with more variable kinetic energies, which range from 914 eV to 917 eV. Most of the compounds in which copper has an oxidation state of +2 (shown as blue diamonds) have modified Auger parameters between approximately 1850 eV and 1851 eV, although there is signifiant variation in their individual binding energies and kinetic energies. The two metals (shown as green circles) and the commpounds CuS and CuSe occupy a similar space within the Wagner plot. Interestingly, both CuS and CuSe are transition metal chalcogenides and have semiconducting properties.

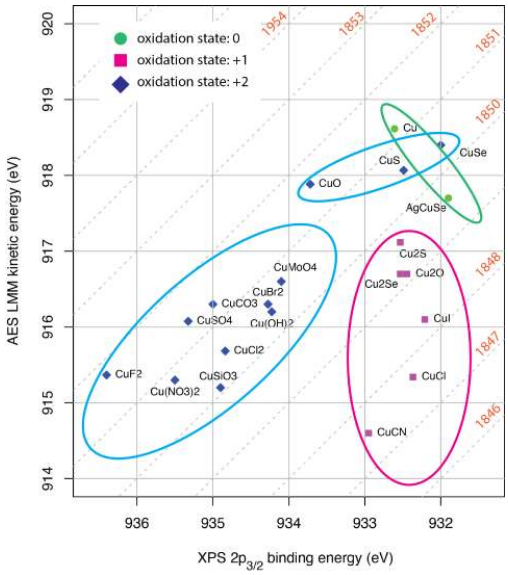



Figure 21.2.6: Wagner plot for 20 copper compounds. The raw data is from https://srdata.nist.gov/xps/Default.aspx and includes 140 measurements of binding energies and 99 measurements of kinetic energies. Compounds are identified by the oxidation state of copper.

**Information at Depth**. X-rays penetrate into a sample to a depth that is greater than the distance the photoelectron can travel without losing energy to inelastic collisions. We can take advantage of this to vary the depth from which we gather information. Figure 21.2.7 shows how this is accomplished by changing the angle from which we collect and analyze photoelectrons. The length of the solid black line is the distance an electron can travel without losing energy in an inelastic collision. When the detector is placed at 90° to the sample's surface, the sampling depth is at its greatest. Adjusting the detector so that it is at 30° to the surface, results in its detecting electrons from a depth that is just half of that when the detector is at 90°.

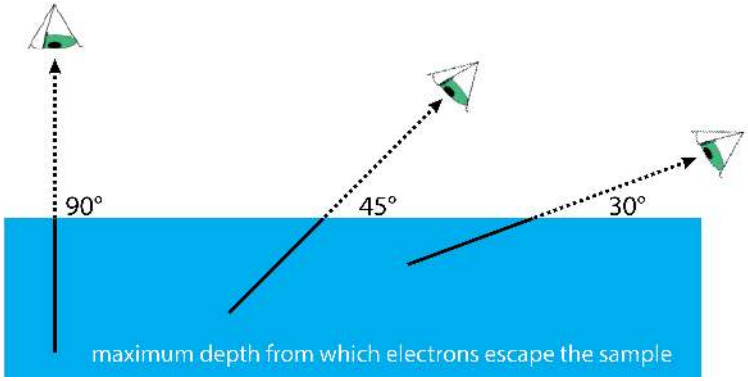



Figure 21.2.7: Illustration showing the measurement of the photoelectron's angle of emission. See text for explanation for how this affects sampling depth.

**Quantitative Analysis**. The intensity of an XPS peak—either is peak height or its peak area—is proportional to the number of atoms of the element responsible for the peak. This allows for determining the relative concentration, $C_x$, of an element in a sample; thus

$$C_x = \frac{I_x/S_x}{\sum (I_i/S_i)} \tag{21.2.3}$$

where $I_x$ is the peak intensity for the element, $S_x$ is the sensitivity factor for the element, and $I_i$ and $S_i$ are the peak intensities and sensitivity factors for all other elements in the sample. Sensitivity factors account for differences in the ease with which photoelectrons are produced and escape from the sample. Published tables of sensitivity factors are available, although they may vary some from instrument-to-instrument. Sensitivity factors are referenced to a standard line, typically $C_{1s}$, which is assigned a sensitivity factor of 1.00.

In many cases we are interested only in the relative concentration of just two elements. In this case, we write Equation 21.2.3 as

$$\frac{C_x}{C_y} = \frac{I_x/S_x}{I_y/S_y} \tag{21.2.4}$$

where $x$ and $y$ are the two elements. For example, using the data in Figure 21.2.4, the $Si_{2p}$ peak has a height of 30 mm and the $Al_{2p}$ peak has a peak height of 20 mm. Their sensitivity factors are, respectively 0.817 and 0.737. Using these values, we find that

$$\frac{C_{Si}}{C_{Al}} = \frac{30/0.817}{20/0.737} = 1.4$$

there are approximately $1.4\times$ as many atoms of silicon as there are atoms of aluminum.

## Auger Electron Spectroscopy (AES)

In Figure 21.2.2 we learned that following the ejection of a photoelectron from an atom's core, the now unstable atom releases energy by either emitting a secondary electron from a higher energy orbital or by releasing a photon. In XPS we measure the intensity of the ejected photoejected electrons as a function of their binding energy; in Auger spectroscopy we measure the intensity of these secondary electrons as a function of their kinetic energies.

The instrumentation for AES can be coupled with an XPS spectrometer or be a stand-alone instrument. In either case, the basic instrumentation is similar to that shown in Figure 21.2.3, although AES spectra are usually initiated using an electron gun as a source instead of an X-ray source. One advantage to using an electron gun is that it can be focused into a smaller beam and can

then easily rastered across a surface, allowing for imaging of the sample's surface. Depth profiling, using an ion beam to remove layers of the sample, is another common use of AES.

Figure 21.2.8 provides an example of a typical AES spectrum, in this case for the mineral calcite, $CaCO_3$. The raw data, on the left, shows the intensity of the signal as a count of electrons with a particular kinetic energy. The large background signal is from electrons that lose kinetic energy as the result of inelastic collisions. The two broad features between approximately 100 eV and 600 eV are the Auger peaks for calcium and for oxygen. The peaks in this case are easy to see because the two analytes are present in bulk. For a trace-level analyte, the Auger peaks in a normal plot may be difficult to see. For this reason, Auger spectra are usually presented by plotting the derivative of the raw data giving the spectrum on the right.

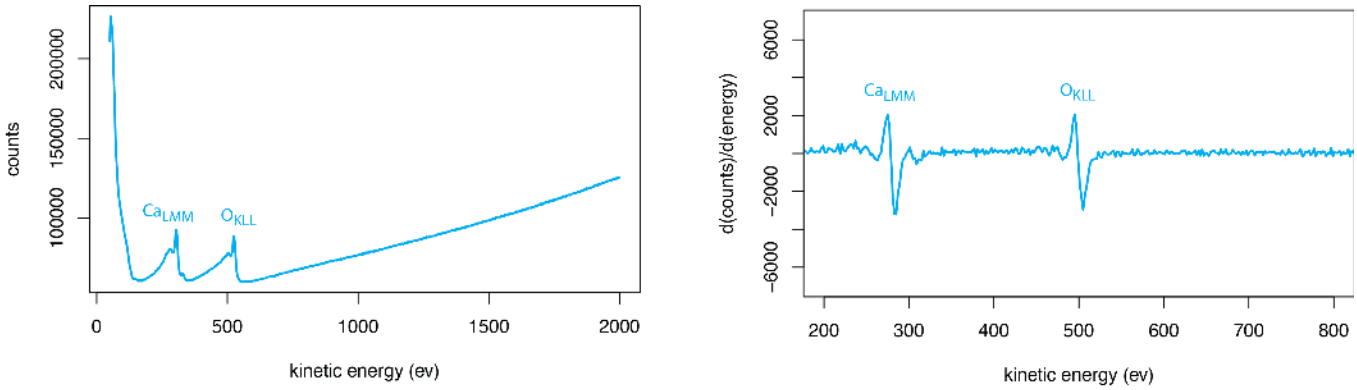



Figure 21.2.8: AES spectrum for the mineral calcite, $CaCO_3$. The figure on the left shows the spectrum as initially recorded and the figure on the right shows the data after taking the derivative of counts as a function of energy. The original data used to create thid figure is from the xpslibrary.

Figure 21.2.9 provides an example of how AES is used to study changes in the composition of a single crystal of $CaCO_3$ that was allowed to equilibrate with a solution containing $Mg^{2+}$ ions. The sample was mounted on a sample probe and the AES spectrum recorded. An $Ar^+$ ion beam was used to remove layers of the sample while the spectrometer was used to record spectra of the sample. As expected, the surface is enriched in $Mg^{2+}$ ions that diffused into the crystal with the relative concentration of $Mg^{2+}$ decreasing. The relative abundance of $Ca^{2+}$ increases with depth; the relative concentration of oxygen remains more or less constant with depth.

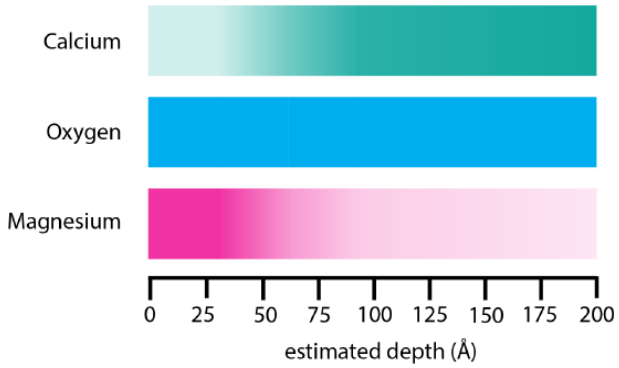



Figure 21.2.9: Depth profiles for calcium, oxygen, and magnesium in a sample of $CaCO_3$ that was suspended in a solution of Mg2+ ion. The shading for each element shows the relative abundance of the element with depth. See Mucci, A.; Morse, J. W.; Kaminsky, M. S. "Auger Spectroscopy Analysis of Magnesian Calcite Overgrowths Precipitated From Seawater and Solutions of Similar Composition," *Am. J. Sci*. **1985**, 289-305 for the paper suggesting this figure.

## Secondary-Ion Mass Spectrometry (SIMS)

In SIMS we bombard the surface of a sample with an energetic primary beam—typically 5-20 keV—of an ion, such as $Ar^+$, $O_2^+$, or $Cs^+$. The primary ion penetrates the sample's surface, ejecting a variety of particles, including neutral atoms, electrons, and, more importantly, secondary ions (singly-charged or multiply charged cations and anions, and clusters of ions). These secondary ions are characterized by their mass-to-charge ratios and by their kinetic energies. The use of a primary ion beam of $Cs^+$ favors the formation of secondary ions that are anions, and a primary beam of $O_2^+$ favors the formation of secondary ions that are cations.

The instrumentation for SIMS includes an ion gun for generating the primary beam and a mass spectrometer for analyzing the secondary ions. In static mode, the primary ion beam is run using a low current density that minimizes the extent to which the sample's outermost layers are removed. In dynamic mode, the primary beam is run at a higher current density that removes more of the sample's surface. Dynamic SIMS is well suited to depth profiling. High mass resolution is obtained using a time-of-flight mass analyzer or a double-focusing mass analyzer; see Chapter 20 for a discussion of different types of mass analyzers.

SIMS is well suited for imaging as the positively charged primary ion can be rastered across the sample's surface. Figure 21.2.10 provides an example of imaging a surface using SIMS by measuring the yield of $^{14}N^{12}C$ ions while rastering the primary ion beam across a 10 μm × 10 μm section of the sample.

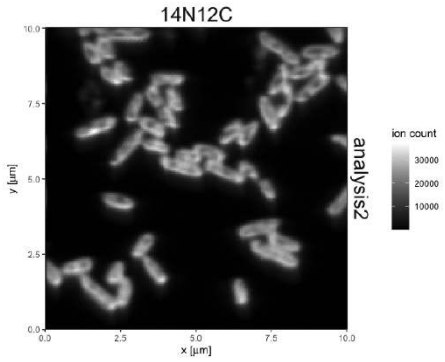



Figure 21.2.10: Image created using the R package lans2r ["lans2r: Work with Look at NanoSims Data in R", Sebastian Kopf, R package version 1.1.0, 2020]. The image shows the analysis of a 10 μm by 10 μm portion of a surface for the $^{14}N^{12}C$ ion, the two major isotopes of carbon and nitrogen. The bright areas have larger total ion counts.

This page titled 21.2: Spectroscopic Surface Methods is shared under a CC BY-NC-SA 4.0 license and was authored, remixed, and/or curated by David Harvey.

# 21.3: Scanning Electron Microscopy

In optical microscopy we use photons to provide images of a sample. Although extraordinarily useful and powerful, the ability to resolve features in optical microscopy is limited by the source of light; in general, we can distinguish between two objects if they are separated by a distance that is greater than the wavelength of the photons being used. The maximum resolution for an optical microscope is about 0.2 μm (200 nm), which means we can use an optical microscope to view a human hair (20-200 μm), an eukaryotic cell (10-100 μm), a chloroplast (5-8 μm), and a mitochondrion (1-3 μm), but not a ribosome (0.01 μm-0.02 μm). In this section we will consider the electron microscope, which has a resolution limit of approximately 0.2 nm, or approximately $1000\times$ more than an optical microscope. In Section 21.4, we will examine two additional types of non-optical microscopy.

## Instrumentation

In scanning electron microscopy we raster a beam of high-energy electrons over a surface using a two-dimensional grid. Figure 21.3.1 shows the basic instrumental needs. The electron gun usually is just a simple tungsten wire that releases electrons when it is heated resistively. Other sources include solid-state crystals of lanthanum hexaboride ($LaB_6$) or cerium hexaboride ($CeB_6$) and the field emission gun, which uses a tungsten wire with a tip that has a radius of about 100 μm. Regardless of their source, these electrons are accelerated to an energy of 1-40 keV and passed through a series of lens that narrow and focus them into a beam with a diameter that falls within a range of 1 nm to 1000 nm (0.001 μm to 1 μm). A set of coiled scan controls deflects the electron beam in a raster pattern across the sample's surface (see inset at the bottom left of Figure 21.3.1). An electron detector monitors the electrons that scatter back from the sample; the type of detector used varies with the type of emission from the sample that we choose to monitor—see the next sub-heading for types of emission—but typically are scintillation devices when monitoring electrons and energy-dispersive detectors when monitoring X-rays.

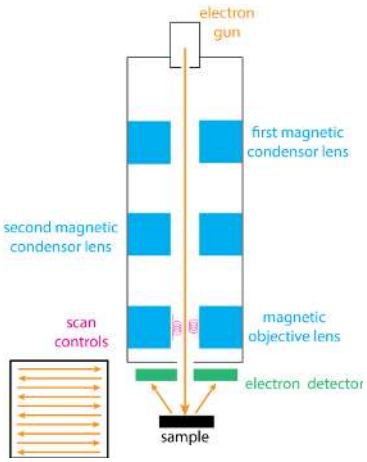



Figure 21.3.1: Schematic diagram of an instrument for scanning electron microscopy, which consists of an electron gun, a system of magnetic lenses, a scan control, and a detector. The inset on the lower left shows a raster pattern in which the electron beam is scanned back-and-forth across the sample's surface.

## Interaction of Electron Beams With Solids

Figure 21.3.1 suggests that the only type of signal is the measurement of electrons that are scattered back toward the detector. The interaction between the electron beam and the sample, however creates a variety of signals, including both electrons and X-rays. Figure 21.3.2 illustrates the types of emission that follows from the interaction of the electron beam with the sample. The electron beam penetrates approximately 1-2 μm into the sample. As you might expect from the previous section on electron spectroscopy, the interaction of an electron beam with a sample results in the emission of some Auger electrons; these electrons come from a volume near the vacuum-sample interface. Of more importance are secondary electrons and backscattered electrons.

As the electron beam penetrates into the sample, the electrons undergo collisions with the sample's atoms. Some of these collisions are elastic in which the electron changes its direction, but retains its kinetic energy. With sufficient time, these electrons eventually undergo a collision in which they cross the sample-vacuum interface and exit the solid. These backscattered electrons are collected and passed along to the detector. Other electrons undergo inelastic collisions, losing kinetic energy and, eventually, become embedded in the sample. Backscattered electrons come from a depth as great as 50% of the depth to which the electron beam

penetrates. Another source of electrons comes from a process in which the electron beam induces the ejection of electrons from the sample's conduction band. These secondary electrons are less numerous than backscattered electrons and they also come from a much shallower depth, typically 5-50 nm.

The electron beam also stimulates the release of X-rays, including the characteristic X-rays of the sample's elements, a broad continuum, and fluorescent X-ray emission. See Chapter 12 for more details about atomic X-ray emission.

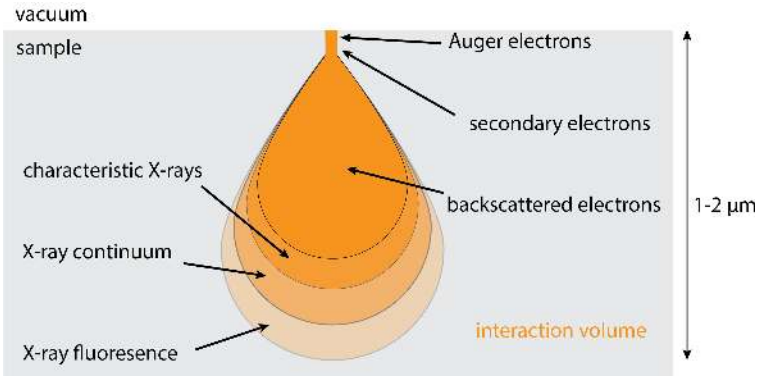



Figure 21.3.2: Illustration showing the types of emission that results from the interaction of an electron beam with a sample. The electron beam penetrates to a depth of approximately 1-2 µm, with the interaction volume increasing with depth. X-rays are emitted from deeper in the sample than are electrons.

As the electron beam is rastered across the sample, the intensity of the backscattered electrons from a specific position on the sample that reaches the detector is stored in the corresponding pixel on the instrument's monitor. The image created in this way is not an optical picture, but a digitized electronic reproduction of the sample's surface. The extent of magnification depends on the length of the detector's monitor relative to the length of a single scan across the sample; scanning a shorter distance results in a greater magnification. An optical microscope usually provides a maximum magnification of $1000\times$; an SEM can achieve a magnification of $1,000,000\times$.

## Applications

Figure 21.3.3 shows four examples of applications of scanning electron microscopy for the measurement of particle size (upper left), for the evaluation of nanowires (upper right), for characterizing the channels in a microfluidic device (lower left), and for examining the tip of a cantilever and tip used for atomic force microscopy. Other applications include biological samples, films and coatings, fibers, and powders, to name a few.

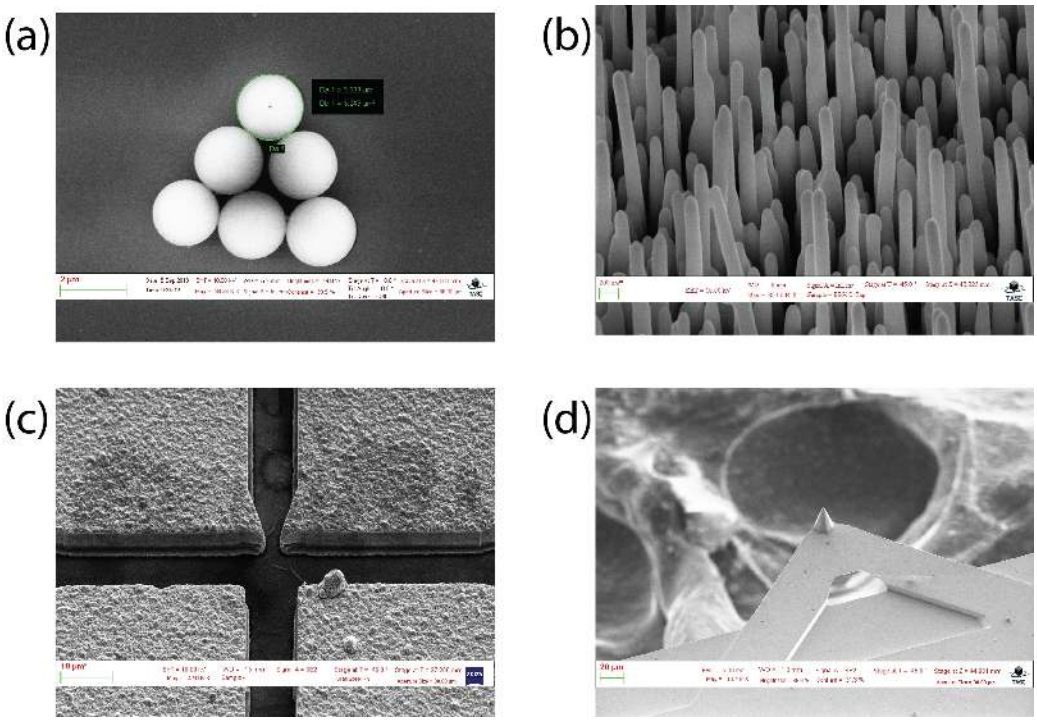



Figure 21.3.3: Scanning electron microscope images. The image in (a) shows six particulate spheres with diameters of about 2 µm each. The image in (b) shows a cluster of nanowires, each with a diameter of approximately 200 nm. The image in (c) shows the intersection of channels in a microfluidic device. The channels have widths of approximately 10 µm, although the upper channel narrows to about 2-4 µm at the intersection of the channels. The image in (d) is the tip of a cantilever used for atomic force microscopy, which we will explore in more detail in Section 21.4. All images are released under a CC-BY license and are available here.

This page titled 21.3: Scanning Electron Microscopy is shared under a CC BY-NC-SA 4.0 license and was authored, remixed, and/or curated by David Harvey.

# 21.4: Scanning Probe Microscopes

in the last section we considered how we can image a surface using an electron beam. In this section we consider a very different approach to developing an image of a surface, one in which we bring a probe close to the surface and examine how the probe interacts with the surface. One advantage of this approach is that the interaction between the probe and the surface can include attraction and repulsion, which opens up a third dimension to the image.

## Scanning Tunneling Microscope (STM)

In the scanning tunneling microscope we take advantage of the ability of a current to pass through the gap between the tip of a conducting probe and a conducting sample when the probe and the sample are held at different potentials. Figure 21.4.1 shows the basic arrangement in which the probe has, ideally, a single atom at its tip. The tunneling current, $I_t$ is given by

$$I_t = Ve^{-Cd} \tag{21.4.1}$$

where $V$ is the applied voltage, $d$ is the distance between the probe's tip and the sample, and $C$ is a constant whose value depends upon the composition of the probe and the sample. The exponential decrease in the tunneling current with distance means that a small change in the position of probe's tip relative to the sample results in a significant change in the signal, providing vertical resolution on the order of 0.1 nm. Probes are fashioned using tungsten wires or platinum-iridium wires.

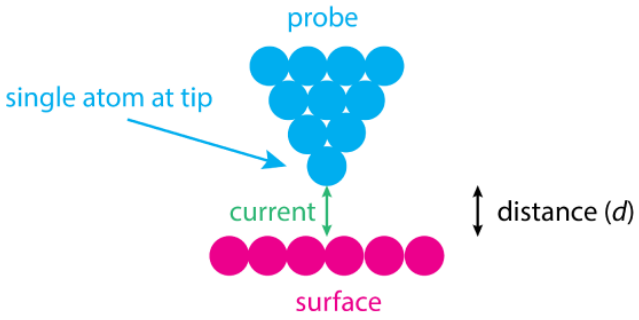



Figure 21.4.1: Illustration showing the relationship between the sample and the tip of the probe in scanning tunneling microscopy.

Scanning tunneling microscopy images are created by moving the probe back-and-forth across the sample while measuring the current. The signal is acquired in one of two modes: constant current or constant height. In constant current mode, the probe's tip is brought near the surface and the current measured, which establishes a setpoint. As the probe moves across the sample, it is raised or lowered to maintain the setpoint current. The result is measure of the distance, $d$, between the probe's tip and the sample along the *z*-axis as a function of the *xy* position of the probe's tip. In constant height mode, the distance, $d$, between the probe's tip and the sample is held constant, and the current, $I_t$, is measured as a function of the *xy* position of the probe's tip. Constant height mode allows for faster data acquisition, but is limited to samples that have flat surfaces.

Positioning of the sample and the probe's tip relative to each other is accomplished by either moving the probe or moving the sample. In either case, the control of movement in accomplished using a piezoelectric scanner. A piezoelectric material, as shown in Figure 21.4.2 experiences a change in its length when a dc potential is applied across its sides, either extending its length or contracting its length.

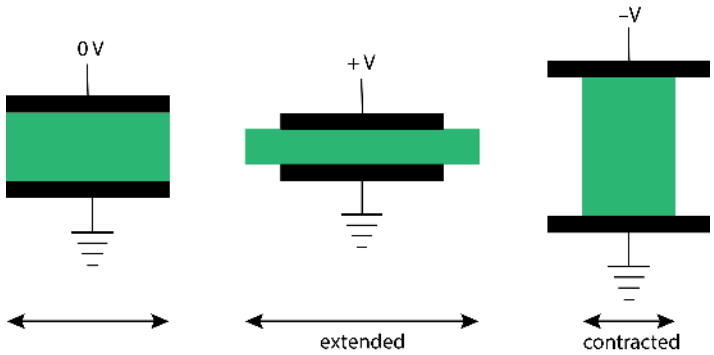



Figure 21.4.2: Illustration showing the behavior of a piezoelectric material when a dc potential is applied to it. The extension and contraction shown here are, of course, exaggerated.

Figure 21.4.3 shows a configuration of cylindrical piezoelectric scanner in which the cylinder's upper half controls movement along the *z*-axis, and the cylinder's lower half is used to control movement along the *x*-axis, the *y*-axis, or both.

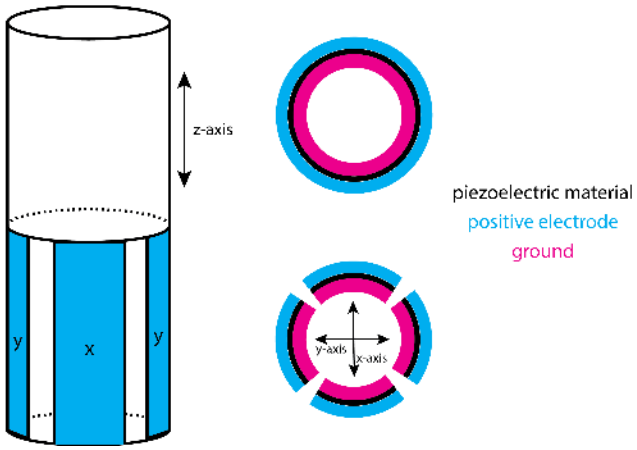



Figure 21.4.3: Illustration that shows the design of a piezoelectric scanner. The top half of the scanner controls movement along the *z*-axis and the lower half of the scanner controls movement along the *x*-axis and the *y*-axis. The piezoelectric material is shown in black, the positive electrodes in blue, and the ground in red.

One limitation of STM is that the sample must be conductive. It is possible to image a non-conducting sample if it first coated with a conductive material, such as gold, although such coatings can mask surface features.

## Atomic Force Microscope (AFM)

Unlike the scanning tunneling microscope, the atomic force microscope does not require a conducting sample and imaging is achieved without a current flowing between the sample and the tip of the probe. Instead, as shown in Figure 21.4.4, the probe is attached to the end of a flexible cantilever. The tip of the probe (see photograph in Figure 21.4.3) is pyramidal in shape and extends about 10 µm from its base on the cantilever. The tip of the probe has a diameter on the order of 10 nm and is made of silicon, Si, or silicon nitride, $Si_3N_4$. The cantilever typically is 100-500 µm in length. The probe is scanned across the sample's surface and the position of the probe relative to the surface is determined by reflecting the beam from a diode laser off the probe-end of the cantilever to a detector.

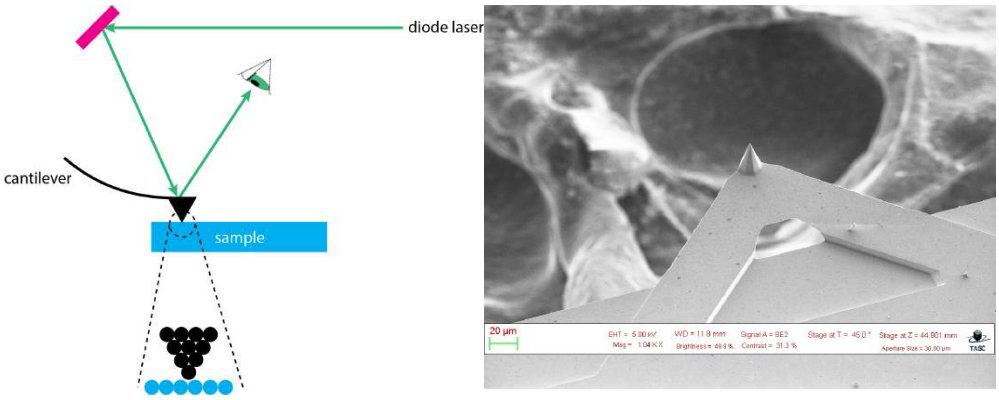



Figure 21.4.4: The figure on the left illustrates how the position of the cantilever and the probe's tip is monitored in atomic force microscopy. The photo on the right shows an SEM image of a typical cantilever and probe tip. The photograph is released under a CC-BY license and is available here.

The force in atomic force is the interaction between the probe's tip and the sample, which may be a force of attraction or a force of repulsion. When the probe's tip is in contact with the sample—known as contact mode—there is a force of repulsion between them. Because the cantilever has a smaller force constant than the atoms in the probe's tip, the cantilever bends. Moving the sample stage to maintain a constant deflection of the laser off of the cantilever provides an image of the sample's surface. Contact mode allows for rapid scanning and work well for samples with rough surfaces, although it may damage samples with softer surfaces.

In non-contact mode, the probe's tip is brought close to the sample's surface, but not allowed to come into contact with it. The cantilever is place into an oscillatory motion. The amplitude of this oscillation is proportional to the force of attraction between the probe's tip and the sample, which varies with the distance between the probe's tip and the sample. Moving the sample stage to maintain a constant oscillation provides an image of the sample's surface. Non-contact mode AFM generally provides lower resolution images, but is less damaging to the sample.

A third mode for collecting data is called intermittent or tapping mode. In this mode the cantilever is set to oscillate at its resonant frequency with the probe's tip coming into contact with the sample's surface when it reaches the bottom of the cantilever's oscillation. The frequency of the oscillation is sensitive to the distance between the probe's tip and the sample. Moving the sample stage to maintain the resonant frequency provides an image of the sample's surface.

You can view a gallery of scanning tunneling microscopy images here, and a gallery of atomic force microscopy images here.

---

This page titled 21.4: Scanning Probe Microscopes is shared under a CC BY-NC-SA 4.0 license and was authored, remixed, and/or curated by David Harvey.

# CHAPTER OVERVIEW

## 22: An Introduction to Electroanalytical Chemistry

In Chapters 6–21 we examined a wide range of spectroscopic techniques that take advantage of the interaction between electromagnetic radiation and matter. In this chapter we turn our attention to electrochemical techniques in which the potential, current, or charge in an electrochemical cell serves as the analytical signal.

Although there are only three fundamental electrochemical signals, there are many possible experimental designs—too many, in fact, to cover adequately in an introductory textbook. The simplest division of electrochemical techniques is between bulk techniques, in which we measure a property of the solution in the electrochemical cell, and interfacial techniques, in which the potential, current, or charge depends on the species present at the interface between an electrode and the solution in which it sits. The measurement of a solution's conductivity, which is proportional to the total concentration of dissolved ions, is one example of a bulk electrochemical technique. A determination of pH using a pH electrode is an example of an interfacial electrochemical technique. Only interfacial electrochemical methods receive further consideration in this textbook. In this chapter we provide an introduction to electrochemistry, introducing ideas relevant to understanding the specific electroanalytical methods introduced in Chapters 23–25.


22.1: Electrochemical Cells

22.2: Potentials in Electroanalytical Cells

22.3: Electrode Potentials

22.4: Calculation of Cell Potentials from Electrode Potentials

22.5: Currents in Electrochemical Cells

22.6: Types of Electroanalytical Methods



This page titled 22: An Introduction to Electroanalytical Chemistry is shared under a CC BY-NC-SA 4.0 license and was authored, remixed, and/or curated by David Harvey.

# 22.1: Electrochemical Cells

A schematic diagram of a typical electrochemical cell is shown in Figure 22.1.1. The electrochemical cell consists of two half-cells, each of which contains an electrode immersed in a solution of ions whose activities determine the electrode's potential. A salt bridge that contains an inert electrolyte, such as KCl, connects the two half-cells. The ends of the salt bridge are fixed with porous frits, which allow the electrolyte's ions to move freely between the half-cells and the salt bridge. This movement of ions in the salt bridge completes the electrical circuit, allowing us to measure the potential using a potentiometer.

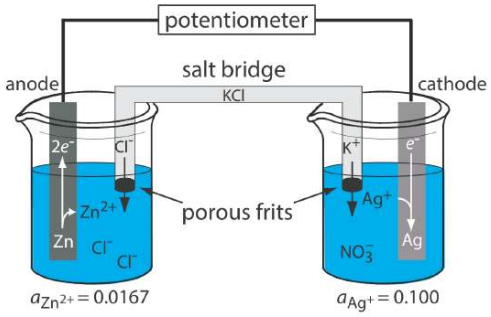



Figure 22.1.1. Example of a potentiometric electrochemical cell. The activities of $Zn^{2+}$ and $Ag^{+}$ are shown below the two half-cells.

The reason for separating the electrodes is to prevent the oxidation reaction and the reduction reaction from occurring at the same electrode. For example, if we place a strip of Zn metal in a solution of $AgNO_3$, the reduction of $Ag^{+}$ to Ag occurs on the surface of the Zn at the same time as a portion of the Zn metal oxidizes to $Zn^{2+}$. Because the transfer of electrons from Zn to $Ag^{+}$ occurs at the electrode's surface, we can not pass them through the potentiometer.

## Conduction in a Cell

Current moves through the cell in Figure 22.1.1 as a result of the movement of two types of charged particles: electrons and ions. First, when zinc, Zn*(s)* underoges an oxidation reaction

$$\mathrm{Zn}(s) \rightleftharpoons \mathrm{Zn}^{2+}(aq) + 2e^{-} \tag{22.1.1}$$

it releases two electrons. These electrons move through the circuit that connects the metallic Zn electrode in the left half-cell to the metallic Ag electrode in the right half-cell, where it effects the reduction of $Ag^{+}$*(aq)*.

$$\mathrm{Ag}^{+}(aq) + e^{-} \rightleftharpoons \mathrm{Ag}(s) \tag{22.1.2}$$

If this is all that happens, then the half-cell on the left will develop an excess of positive charge as $Zn^{2+}$*(aq)* ions accumulate and the half-cell on the right will develop an excess of negative charge due to the loss of $Ag^{+}$*(aq)*. The salt bridge provides a way to continue the movement of charge, and thus the current, with the $K^{+}$ ions moving toward the right half-cell and $Cl^{-}$ ions moving toward the left half-cell.

## Galvanic and Electrolytic Cells

The net reaction for the electrochemical cell in Figure 22.1.1 is

$$\mathrm{Zn}(s) + 2\mathrm{Ag}^{+}(aq) \rightleftharpoons 2\mathrm{Ag}(s) + \mathrm{Zn}^{2+}(\mathrm{aq}) \tag{22.1.3}$$

which simply is the result of adding together the reactions in the two half-cells after adjusting for the difference in electrons. As shown by the arrows in the figure, when we connect the electrodes to the potentiometer, current spontaneously flows from the left half-cell to the right half-cell. We call this a galvanic cell. If we apply a potential sufficient to reverse the direction of the current flow, resulting in a net reaction of

$$2\mathrm{Ag}(s) + \mathrm{Zn}^{2+}(\mathrm{aq}) \rightleftharpoons \mathrm{Zn}(s) + 2\mathrm{Ag}^{+}(aq)$$

then we call the system an electrolytic cell. A galvanic cell produces electrical energy and an electrolytic cell consumes electrical energy.

## Anodes and Cathodes

The half-cell where oxidation takes place is called the anode and, by convention, it is shown on the left for a galvanic cell. The half-cell where reduction takes place is called the cathode and, by convention, it is shown on the right for a galvanic cell.

## Faradaic and Non-Faradaic Currents

When we oxidize or reduce an analyte at the electrode in one half-cell, the electrons pass through the potentiometer to the electrode in the other half-cell where a corresponding reduction or oxidation reaction takes place. In either case, the current from the redox reactions at the two electrodes is called a faradaic current. A faradaic current due to the reduction of an analyte is called a cathodic current and carries a positive sign. An anodic current results from the analyte's oxidation and carries a negative sign.

In addition to the faradaic current from a redox reaction, the current in an electrochemical cell includes non-faradaic sources. Suppose the charge on an electrode is zero and we suddenly change its potential so that the electrode's surface acquires a positive charge. Cations near the electrode's surface will respond to this positive charge by migrating away from the electrode; anions, on the other hand, will migrate toward the electrode. This migration of ions occurs until the electrode's positive surface charge and the excess negative charge of the solution near the electrode's surface are equal. Because the movement of ions and the movement of electrons are indistinguishable, the result is a small, short-lived non-faradaic current that we call the charging current. Every time we change the electrode's potential, a short-lived charging current flows.

Even in the absence of analyte, a small, measurable current flows through an electrochemical cell. This residual current has two components: a faradaic current due to the oxidation or reduction of trace impurities and a non-faradaic charging current. Methods for discriminating between the analyte's faradaic current and the residual current are discussed later in this chapter.

## The Electrical Double Layer

As noted in the previous section, when we apply a potential to an electrode it develops a positive or negative surface charge, the magnitude of which is a function of the metal and the applied potential. Because the surface carries a charge, the composition of the layer of solution immediately adjacent to the electrode changes with, for example, the concentration of cations increasing and the concentration of anions decreasing if the electrode's surface carries a negative charge. As we move away from the electrode's surface, the net potential first decreases in a linear manner, due to the imbalance of the cations and anions, and then in an exponential manner until it reaches zero. This structured surface is called the electrical double layer and consists of an inner layer and a diffuse layer. Anytime we change the potential applied to the electrode, the structure of the electrical double layer changes and a small charging current flows.

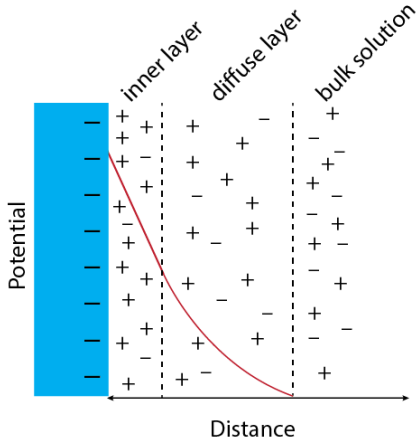



Figure 22.1.2: The electrical double layer. When the electrode carries a negative surface charge, the layer of solution immediately in contact with the electrode, the inner layer, becomes enriched with cations and deficient in anions. At greater distances from the electrode's surface, the concentration of cations and anions become more balanced—this is called the diffuse layer—eventually reaching the bulk solution where the net charge are in balance. The potential decreases linearly through the inner layer and exponentially through the diffuse layer.

## Mass Transfer in Cells with the Passage of Current

The magnitude of a faradaic current is determined by the rate at which the analyte is oxidized at the anode or reduced at the cathode. Two factors contribute to the rate of an electrochemical reaction: the rate at which the reactants and products are transported to and from the electrode—what we call mass transport—and the rate at which electrons pass between the electrode and the reactants and products in solution.

There are three modes of mass transport that affect the rate at which reactants and products move toward or away from the electrode surface: diffusion, migration, and convection. Diffusion occurs whenever the concentration of an ion or a molecule at the surface of the electrode is different from that in bulk solution. For example, if we apply a potential sufficient to completely reduce $Ag^+$ at the electrode surface, the result is a concentration gradient similar to that shown in Figure 22.1.3. The region of solution over which diffusion occurs is the diffusion layer. In the absence of other modes of mass transport, the width of the diffusion layer, $\delta$, increases with time as the $Ag^+$ must diffuse from an increasingly greater distance.

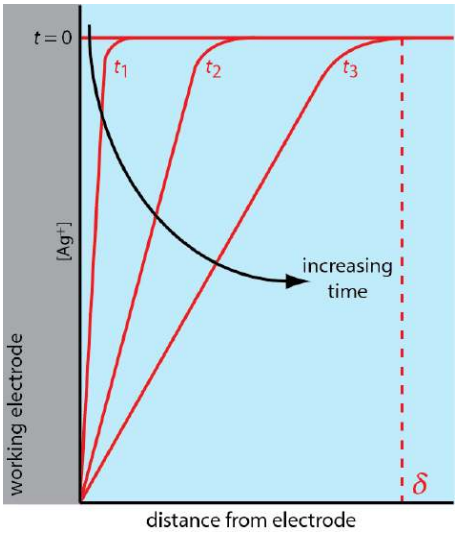



Figure 22.1.3. Concentration gradients (in red) for $Ag^+$ following the application of a potential that completely reduces it to Ag(*s*). Before we apply the potential ($t$ = 0) the concentration of $Ag^+$ is the same at all distances from the electrode's surface. After we apply the potential, its concentration at the electrode's surface decreases to zero and $Ag^+$ diffuses to the electrode from bulk solution. The longer we apply the potential, the greater the distance over which diffusion occurs. The dashed red line shows the extent of the diffusion layer at time $t_3$. These profiles assume that convection and migration do not contribute significantly to the mass transport of $Ag^+$.

Convection occurs when we mix the solution, which carries reactants toward the electrode and removes products from the electrode. The most common form of convection is stirring the solution with a stir bar; other methods include rotating the electrode and incorporating the electrode into a flow-cell.

The final mode of mass transport is migration, which occurs when a charged particle in solution is attracted to or repelled from an electrode that carries a surface charge. If the electrode carries a positive charge, for example, an anion will move toward the electrode and a cation will move toward the bulk solution. Unlike diffusion and convection, migration affects only the mass transport of charged particles.

## Schematic Representations of Cells

Although Figure 22.1.1 provides a useful picture of an electrochemical cell, it is not a convenient way to represent it. Imagine having to draw a picture of each electrochemical cell you are using! A more useful way to describe an electrochemical cell is a shorthand notation that uses symbols to identify different phases and that lists the composition of each phase. We use a vertical slash (|) to identify a boundary between two phases where a potential develops, and a comma (,) to separate species in the same phase or to identify a boundary between two phases where no potential develops. Shorthand cell notations begin with the anode and continue to the cathode. For example, we describe the electrochemical cell in Figure 22.1.1 using the following shorthand notation.

$$\mathrm{Zn}(s)|\mathrm{ZnCl_2}(aq, a_{\mathrm{Zn^{2+}}} = 0.0167)||\mathrm{AgNO_3}(aq, a_{\mathrm{Ag^+}} = 0.100)|\mathrm{Ag}(s)$$

The double vertical slash (||) represents the salt bridge, the contents of which we usually do not list. Note that a double vertical slash implies that there is a potential difference between the salt bridge and each half-cell.

**Example 22.1.1**

What are the anodic, the cathodic, and the overall reactions responsible for the potential of the electrochemical cell in Figure 22.1.4? Write the shorthand notation for the electrochemical cell.

### Solution

The oxidation of Ag to $Ag^+$ occurs at the anode, which is the left half-cell. Because the solution contains a source of $Cl^-$, the anodic reaction is

$$Ag(s) + Cl^-(aq) \rightleftharpoons AgCl(s) + e^-$$

The cathodic reaction, which is the right half-cell, is the reduction of $Fe^{3+}$ to $Fe^{2+}$.

$$Fe^{3+}(aq) + e^- \rightleftharpoons Fe^{2+}(aq)$$

The overall cell reaction, therefore, is

$$Ag(s) + Fe^{3+}(aq) + Cl^-(aq) \rightleftharpoons AgCl(s) + Fe^{2+}(aq)$$

The electrochemical cell's shorthand notation is

$$Ag(s)|HCl(aq, a_{Cl^-} = 0.100), AgCl(\text{sat'd})|$$
$$|FeCl_2(aq, a_{Fe^{2+}} = 0.0100), Fe^{3+}(aq, a_{Fe^{3+}} = 0.0500)|Pt(s)$$

Note that the Pt cathode is an inert electrode that carries electrons to the reduction half-reaction. The electrode itself does not undergo reduction.

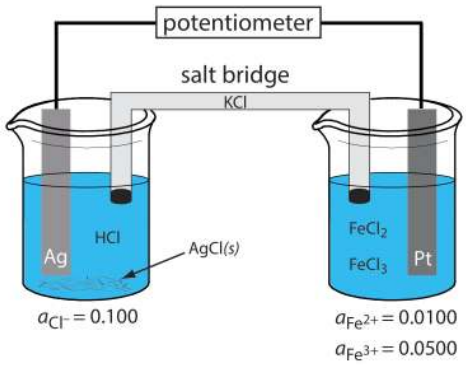



Figure 22.1.4. Potentiometric electrochemical cell for Example 22.1.1.

This page titled 22.1: Electrochemical Cells is shared under a CC BY-NC-SA 4.0 license and was authored, remixed, and/or curated by David Harvey.

# 22.2: Potentials in Electroanalytical Cells

If a Zn*(s)* electrode in a solution of $Zn^{2+}$*(aq)* in an electrochemical cell is at equilibrium, the current is zero and the potential is fixed in value. If we change the potential from its equilibrium value, current will flow as the system moves to its new equilibrium position. Although the initial current is quite large, it decreases over time, reaching zero when the reaction reaches equilibrium. The current, therefore, changes in response to the applied potential. Alternatively, we can pass a fixed current through the electrochemical cell, forcing the oxidation of Zn*(s)* to $Zn^{2+}$*(aq)*, effecting a change in the potential. In short, if we choose to control the potential, then we must accept the resulting current, and we must accept the resulting potential if we choose to control the current.

## The Thermodynamics of Cell Potentials

Because a redox reaction involves a transfer of electrons from a reducing agent to an oxidizing agent, it is convenient to consider the reaction's thermodynamics in terms of the electron. For a reaction in which one mole of a reactant undergoes oxidation or reduction, the net transfer of charge, *q*, in coulombs is

$$q = nF \tag{22.2.1}$$

where *n* is the moles of electrons per mole of reactant, and *F* is Faraday's constant (96485 C/mol). The free energy, Δ*G*, to move this charge given an applied potential, *E*, is

$$\Delta G = Eq \tag{22.2.2}$$

The change in free energy (in kJ/mole) for a redox reaction, therefore, is

$$\Delta G = -nFE \tag{22.2.3}$$

where Δ*G* has units of kJ/mol. The minus sign in Equation 22.2.3 is the result of a different convention for assigning a reaction's favorable direction. In thermodynamics, a reaction is favored when Δ*G* is negative, but a redox reaction is favored when *E* is positive. Substituting Equation 22.2.3 into the thermodynamic equation that relates the free energy to its standard state value

$$\Delta G = \Delta G^\circ + RT \ln Q_r \tag{22.2.4}$$

gives

$$-nFE = -nFE^\circ + RT \ln Q_r \tag{22.2.5}$$

Dividing by –*nF* leads to the Nernst equation

$$E = E^\circ - \frac{RT}{nF} \ln Q_r \tag{22.2.6}$$

where $E^o$ is the potential under standard-state conditions (more on this in Section 22.3). Substituting appropriate values for *R* and *F*, assuming a temperature of 25 $^oC$ (298 K), and switching from the natural logarithm (*ln*) to the base 10 logarithm (*log*) gives the potential in volts as

$$E = E^\circ - \frac{0.05916}{n} \log Q_r \tag{22.2.7}$$

The term $Q_r$ in the previous equations is the reaction quotient, which has the same mathematical form as the reaction's equilibrium constant expression, but uses the instantaneous amounts of reactants and products in place of their equilibrium values. For the cell in Figure 22.1.1, for example, the overall reaction is

$$\mathrm{Zn}(s) + 2\mathrm{Ag}^+(aq) \rightleftharpoons 2\mathrm{Ag}(s) + \mathrm{Zn}^{2+}(\mathrm{aq}) \tag{22.2.8}$$

and Equation 22.2.7 becomes

$$E = E^\circ - \frac{0.05916}{2} \log \frac{[\mathrm{Zn}^{2+}]}{[\mathrm{Ag}^+]^2} \tag{22.2.9}$$

Equation 22.2.9 shows us how the potential changes as the concentrations of $Zn^{2+}$ and $Ag^+$ change.

As we will see in 22.3, 22.2.9 actually is expressed in terms of activities instead of concentrations. The appendix in Chapter 35.7 explains what activity is, why it is important to make a distinction between activity and concentration, and when it is reasonable to use concentrations in place of activities.

## Liquid Junction Potentials

A junction potential develops at the interface between two ionic solutions if there is a difference in the concentration and the mobility of the ions. Consider, for example, a porous membrane that separates a solution of 0.1 M HCl from a solution of 0.01 M HCl (Figure 22.2.1a). Because the concentration of HCl on the membrane's left side is greater than that on the right side of the membrane, $H^+$ and $Cl^-$ will diffuse in the direction of the arrows. The mobility of $H^+$, however, is greater than that for $Cl^-$, as shown by the difference in the lengths of their respective arrows. Because of this difference in mobility, the solution on the right side of the membrane develops an excess concentration of $H^+$ and a positive charge (Figure 22.2.1b). Simultaneously, the solution on the membrane's left side develops a negative charge because there is an excess concentration of $Cl^-$. We call this difference in potential across the membrane a junction potential and represent it as $E_j$.

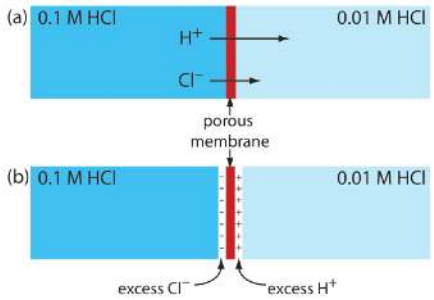



Figure 22.2.1. Origin of the junction potential between a solution of 0.1 M HCl and a solution of 0.01 M HCl.

The magnitude of a junction potential depends upon the difference in the concentration of ions on the two sides of the interface, and may be as large as 30–40 mV. For example, a junction potential of 33.09 mV has been measured at the interface between solutions of 0.1 M HCl and 0.1 M NaCl [Sawyer, D. T.; Roberts, J. L., Jr. *Experimental Electrochemistry for Chemists*, Wiley-Interscience: New York, 1974, p. 22]. A salt bridge's junction potential is minimized by using a salt, such as KCl, for which the mobilities of the cation and anion are approximately equal. We also can minimize the junction potential by incorporating a high concentration of the salt in the salt bridge. For this reason salt bridges frequently are constructed using solutions that are saturated with KCl. Nevertheless, a small junction potential, generally of unknown magnitude, is always present.

This page titled 22.2: Potentials in Electroanalytical Cells is shared under a CC BY-NC-SA 4.0 license and was authored, remixed, and/or curated by David Harvey.

# 22.3: Electrode Potentials

We began this chapter by examining the electrochemical cell in Figure 22.1.1 where $\mathrm{Zn(s)}$ is oxidized to $\mathrm{Zn^{2+}(aq)}$ and $\mathrm{Ag^{+}(aq)}$ is reduced to $\mathrm{Ag(s)}$, as shown by the following reaction.

$$2\mathrm{Ag}(s) + \mathrm{Zn}^{2+}(\mathrm{aq}) \rightleftharpoons \mathrm{Zn}(s) + 2\mathrm{Ag}^{+}(aq)$$

The reaction proceeds as written because the reduction of $\mathrm{Ag^{+}}$*(aq)* to Ag*(s)*

$$\mathrm{Ag}^{+}(aq) + e^{-} \rightleftharpoons \mathrm{Ag}(s) \tag{22.3.1}$$

is more thermodynamically favorable than the reduction of $\mathrm{Zn^{2+}(aq)}$ to $\mathrm{Zn(s)}$

$$\mathrm{Zn}^{2+}(aq) + 2e^{-} \rightleftharpoons \mathrm{Zn}(s) \tag{22.3.2}$$

But, how do we know this is true? In this section we answer this question by taking a close look at electrode potentials.

## Nature of Electrode Potentials

The potential of an electrochemical cell is the difference between the potential at the cathode, $E_{\text{cathode}}$, and the potential at the anode, $E_{\text{anode}}$, where both potentials are defined in terms of a reduction reaction (and are called reduction potentials); thus

$$E_{\text{cell}} = E_{\text{cathode}} - E_{\text{anode}} \tag{22.3.3}$$

$$\mathrm{H}^{+}(aq) + e^{-} = \frac{1}{2}\mathrm{H}_2(g) \tag{22.3.4}$$

which is the reaction that defines the standard hydrogen electrode, or SHE.

## The Standard Hydrogen Electrode (SHE)

The SHE consists of a Pt electrode immersed in a solution in which the activity of hydrogen ion is 1.00 and in which the partial pressure of $\mathrm{H_2}$*(g)* is 1.00 atm (Figure 22.3.1). A conventional salt bridge connects the SHE to the indicator half-cell. The short hand notation for the standard hydrogen electrode is

$$\mathrm{Pt}(s),\ \mathrm{H_2}\,(g, f_{\mathrm{H_2}} = 1.00)\,|\,\mathrm{H^{+}}\,(aq, a_{\mathrm{H^{+}}} = 1.00)\,\| \tag{22.3.5}$$

and the standard-state potential for the reaction 22.3.4 is, by definition, 0.000 V at all temperatures.

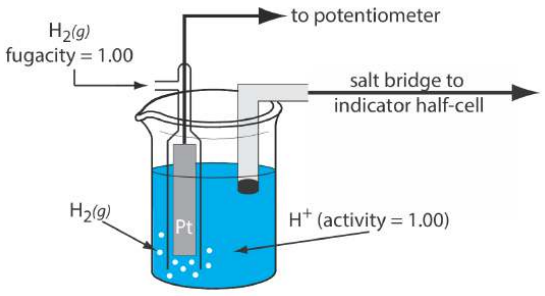



Figure 22.3.1. Schematic diagram showing the standard hydrogen electrode.

## Practical Reference Electrodes

Although the standard hydrogen electrode is the standard against which all other potentials are referenced, it is not practical for routine use as it is difficult to prepare and maintain. Instead, we use one of several other reference electrodes. The two most common of these alternative reference electrodes are the calomel, or $\mathrm{Hg/Hg_2Cl_2}$ electrode, which is based on the following redox couple between $\mathrm{Hg_2Cl_2}$ and Hg (calomel is the common name for $\mathrm{Hg_2Cl_2}$)

$$\mathrm{Hg_2Cl_2}(s) + 2e^{-} \rightleftharpoons 2\mathrm{Hg}(l) + 2\mathrm{Cl}^{-}(aq)$$

and the Ag/AgCl reference electrode, which is based on the reduction of AgCl to Ag

$$\mathrm{AgCl}(s) + e^- \rightleftharpoons \mathrm{Ag}(s) + \mathrm{Cl}^-(aq)$$

A more detailed examination of these two reference electrodes is found in Chapter 23.1.

## Definition of Electrode Potential

To determine the potential for the reduction of $Zn^{2+}$*(aq)* to Zn*(s)* we make it the cathode in the following electrochemical cell

$$\mathrm{Pt}(s),\ \mathrm{H_2}\,(g, P_{\mathrm{H_2}} = 1.00)\,|\,\mathrm{H^+}\,(aq, a_{\mathrm{H^+}} = 1.00)\,\|\mathrm{Zn^{2+}}\,(aq, a_{\mathrm{Zn^{2+}}} = x)\,|\mathrm{Zn}(s) \tag{22.3.6}$$

where *x* is the activity of $Zn^{2+}$ in its half-cell. For example, when $a_{\mathrm{Zn^{2+}}} = 1.00$, the potential of the electrochemical cell is $-0.763\mathrm{V}$. If we find that the potential for the electrochemical cell

$$\mathrm{Zn}(s)|\mathrm{Zn^{2+}}(aq, a_{\mathrm{Zn^{2+}}} = 1.00)\|\mathrm{Ag^+}(aq, a_{\mathrm{Ag^+}} = 1.00)|\mathrm{Ag}(s)$$

is +1.562 V, then knowing that

$$E_{cell} = E_{\mathrm{Ag^+/Ag}} - E_{\mathrm{Zn^{2+}/Zn}} = E_{\mathrm{Ag^+/Ag}} - (-0.763\mathrm{V})$$

gives $E_{\mathrm{Ag^+/Ag}} = +0.799$. In this way, we can build tables of potentials for individual half-reactions.

## Sign Convention for Electrode Potentials

In Section 22.2 we noted the following relationship between an electrochemical potential, $E$, and the Gibbs free energy, $\Delta G$

$$\Delta G = -nFE \tag{22.3.7}$$

which tells us that a positive potential corresponds to a thermodynamically favorable reaction. Knowing that the potential for the electrochemical cell in Equation 22.3.6 is $-0.763\mathrm{V}$ tells us that the reduction of $Zn^{2+}$*(aq)* to Zn*(s)* is not thermodynamically favorable relative to the reduction of $H^+$*(aq)* to $H_2$*(g)*; that is, we do not expect the reaction

$$\mathrm{Zn^{2+}}(aq) + \mathrm{H_2}(g) \rightleftharpoons 2\mathrm{H^+}(aq) + \mathrm{Zn}(s) \tag{22.3.8}$$

to occur; however, with a potential of +0.799 V, we do expect the reaction

$$2\mathrm{Ag^+}(aq) + \mathrm{H_2}(g) \rightleftharpoons 2\mathrm{H^+}(aq) + 2\mathrm{Ag}(s) \tag{22.3.9}$$

to occur. Or, looking at this another way, we expect that Zn*(s)*, but not Ag*(s)*, will dissolve in acid.

## Effect of Activity on Electrode Potentials

In Chapter 22.2 we wrote the Nernst equation for the reaction

$$\mathrm{Zn}(s) + 2\mathrm{Ag^+}(aq) \rightleftharpoons 2\mathrm{Ag}(s) + \mathrm{Zn^{2+}(aq)} \tag{22.3.10}$$

in terms of the concentrations of $Zn^{2+}$*(aq)* and $Ag^+$*(aq)*

$$E = E^\circ - \frac{0.05916}{2}\log\frac{[\mathrm{Zn^{2+}}]}{[\mathrm{Ag^+}]^2} \tag{22.3.11}$$

Although there are times when we will write the Nernst equation in terms of concentrations, thermodynamic functions are more correctly written in terms of the activities of ions. Under ideal conditions, individual ions and molecules of gases behave as independent particles. When this is true, then an ion's activity and concentration are equal and we can write the Nernst equation using concentrations; under other conditions, then the Nernst equation is more correctly written in terms of activities

$$E = E^\circ - \frac{0.05916}{2}\log\frac{a_{\mathrm{Zn^{2+}}}}{(a_{\mathrm{Ag^+}})^2} \tag{22.3.12}$$

where $a_{\mathrm{Zn^{2+}}}$ and $a_{\mathrm{Ag^+}}$ are the activities of $Zn^{2+}$ and $Ag^+$. Equation 22.3.12 shows us how the potential changes as the activities of $Zn^{2+}$ and $Ag^+$ change.

> If you are not familiar with activity, or need a reminder on the relationship between activity and concentration, then see the appendix in Chapter 35.7, which explains what activity is, why it is important to make a distinction between activity and

concentration, and when it is reasonable to use concentrations in place of activities.

## The Standard Electrode Potential $E^\circ$

The standard electrode potential, $E^\circ$, for a half-reaction is the potential when all species are present at unit activity or, for gases, unit fugacity. Its value is independent of how we choose to write the half-reaction; that is, the standard state potential for the reduction of $Ag^+(aq)$ to $Ag(s)$, which is the cathode in the electrochemical cell in Figure 22.1.1, is +0.799 V whether we write the half-reacation as

$$\mathrm{Ag}^+(aq) + e^- \rightleftharpoons \mathrm{Ag}(s) \tag{22.3.13}$$

or as

$$2\mathrm{Ag}^+(aq) + e^- \rightleftharpoons 2\mathrm{Ag}(s) \tag{22.3.14}$$

At first glance, this seems counterintuitive; however, if we calculate the potential when the activity of Ag+ is 0.50 we get

$$E = E^\circ - \frac{0.05916}{1}\log\frac{1}{a_{\mathrm{Ag}^+}} = 0.799 - \frac{0.05916}{1}\log\frac{1}{0.50} = 0.781\mathrm{V}$$

when using reaction 22.3.13, and

$$E = E^\circ - \frac{0.05916}{2}\log\frac{1}{(a_{\mathrm{Ag}^+})^2} = 0.799 - \frac{0.05916}{2}\log\frac{1}{0.50^2} = 0.781\mathrm{V}$$

The appendix in Chapter 35.8 provides a table of standard state reduction potentials for a wide variety of half-reactions at 298 K.

## Some Limitations to the Use of Standard Electrode Potentials

Although standard electrode potentials are valuable, they are several important limitations to their use, which we outline here.

### Substitution of Concentration for Activities

One important limitation is that that the Nernst equation is defined in terms of the activity of ions instead of their concentrations. Although it is easy to prepare a solution for which the concentration of $Na^+$ is 0.100 M using NaCl—just weigh out 5.844 g of NaCl and dissolve in 1.00 L of water—it is much more challenging to prepare a solution for which the activity of $Na^+$ is 0.100. For this reason, in calculations we usually substitute concentrations for activities when using the Nernst equation. This simplification generally is okay for dilute solutions where the difference between activities and concentrations are small.

### Effect of Other Equilibrium Reactions

A standard state potential tells us about the equilibrium position of a redox half-reaction reaction under standard state conditions. If one or more of the species in the half-reaction are involved in other equilibrium reactions, then these reactions will affect the value of the standard potential. For example, $Fe^{2+}$ and $Fe^{3+}$ form a variety of metal-ligand complexes with $Cl^-$ which explains why $E^\circ_{\mathrm{Fe}^{3+}/\mathrm{Fe}^{2+}}$ is 0.771 in the absence of chloride ion, but is 0.70 in 1 M HCl.

### Formal Potentials

One way to compensate for using concentrations and partial pressures in place of activities and fugacities, and to compensate for other equilibrium reactions, is to replace the standard state potentials, $E^\circ$ with a formal potential, $E^{\circ\prime}$, that is measured using concentrations of 1.00 for ions, partial pressures of 1.00 for gases, and for a specific concentration of other reagents. The table below, which is adapted from the appendix in Chapter 35.8, provides formal potentials for $Fe^{3+}/Fe^{2+}$ half-reaction in five different solvents.

| iron | $E^\circ$ (V) | $E^{\circ\prime}$ (V) |
|---|---|---|
| $Fe^{3+} + e^- \rightleftharpoons Fe^{2+}$ | 0.771 | 0.70 in 1 M $HCl$<br>0.767 in 1 M $HClO_4$<br>0.746 in 1 M $HNO_3$<br>0.68 in 1 M $H_2SO_4$<br>0.44 in 0.3 M $H_3PO_4$ |

## Reaction Rates

The reduction of $Fe^{3+}$ to $Fe^{2+}$ consumes an electron, which is drawn from the electrode. The oxidation of another species, perhaps the solvent, at a second electrode is the source of this electron. Because the reduction of $Fe^{3+}$ to $Fe^{2+}$ consumes one electron, the flow of electrons between the electrodes—in other words, the current—is a measure of the rate at which $Fe^{3+}$ is reduced. One important consequence of this observation is that the current is zero when the reaction $Fe^{3+}(aq) \rightleftharpoons Fe^{2+}(aq) + e^-$ is at equilibrium. If redox half-reaction cannot maintain an equilibrium because the reaction in one direction is too slow, then we cannot measure a meaningful standard state potential.

This page titled 22.3: Electrode Potentials is shared under a CC BY-NC-SA 4.0 license and was authored, remixed, and/or curated by David Harvey.

# 22.4: Calculation of Cell Potentials from Electrode Potentials

The potential of an electrochemical cell is the difference between the electrode potentials of the cathode and the anode

$$E_{\text{cell}} = E_{\text{cathode}} - E_{\text{anode}} \tag{22.4.1}$$

where $E_{\text{cathode}}$ and $E_{\text{anode}}$ are both reduction potentials. Given a set of conditions, we can use the Nernst equation to calculate the cell potential, as shown by the following example.

## Example 22.4.1

Calculate (a) the standard state potential and (b) the potential when $[Ag^+]$ = 0.0020 M and $[Cd^{2+}]$ = 0.0050 M, for the following reaction at 25°C.

$$Cd(s) + 2Ag^+(aq) \rightleftharpoons 2Ag(s) + Cd^{2+}(aq)$$

For part (b), calculate the potential twice, once using concentrations and once using activities assuming that the solution's ionic strength is 0.100.

### Solution

(a) In this reaction Cd is oxidized at the anode and $Ag^+$ is reduced at the cathode. Using standard state electrode potentials from Appendix 3, we find that the standard state potential is

$$E^\circ = E^\circ_{Ag^+/Ag} - E^\circ_{Cd^{2+}/Cd} = 0.7996 - (-0.4030) = 1.2026 \text{ V}$$

(b) To calculate the potential when $[Ag^+]$ is 0.0020 M and $[Cd^{2+}]$ is 0.0050 M, we use the appropriate relationship for the reaction quotient, $Q_r$, when writing the Nernst equation

$$E = E^\circ - \frac{0.05916 \text{ V}}{n} \log \frac{[Cd^{2+}]}{[Ag^+]^2}$$

$$E = 1.2026 \text{ V} - \frac{0.05916 \text{ V}}{2} \log \frac{0.050}{(0.020)^2} = 1.14 \text{ V}$$

To calculate the potential using activities, we first calculate the activity coefficients for $Cd^{2+}$ and $Ag^+$. Following the approach outlined in the appendix in Chapter 35.7 gives

$$\log \gamma_{Cd^{2+}} = \frac{-0.51 \times (+2)^2 \times \sqrt{0.100}}{1 + 3.3 \times 0.50 \times \sqrt{0.100}} = -0.2078$$

$$]log\gamma_{Ag^+} = \frac{-0.51 \times (+1)^2 \times \sqrt{0.100}}{1 + 3.3 \times 0.25 \times \sqrt{0.100}} = -0.1279$$

$$a_{Cd^{2+}} = \gamma_{Cd^{2+}} \times [Cd^{2+}] = 0.6197 \times 0.0050 = 0.003098$$

$$a_{Ag^+} = \gamma_{Ag^+} \times [Ag^+] = 7449 \times 0.0020 = 0.00149$$

Finally, we substitute activities for concentrations in the Nernst equation to arrive at a potential of

$$E = 1.2026 \text{ V} - \frac{0.05916 \text{ V}}{2} \log \frac{0.003098}{(0.00149)^2} = 1.11 \text{ V}$$

This page titled 22.4: Calculation of Cell Potentials from Electrode Potentials is shared under a CC BY-NC-SA 4.0 license and was authored, remixed, and/or curated by David Harvey.

# 22.5: Currents in Electrochemical Cells

Most electrochemical techniques rely on either controlling the current and measuring the resulting potential, or controlling the potential and measuring the resulting current; only potentiometry (see Chapter 23) measures a potential under conditions where there is essentially no current. Understanding the relationship between current, *i*, and potential, *E*, is important. Although we learned in Sections 22.3 and 22.4 how to calculated electrode potentials and cell potentials using the Nernst equation, the experimentally measured potentials may differ from their thermodynamic values for a variety of reasons that we outline here.

## iR drop

The movement of an electrical charge in an electrochemical cell generates a potential, $E_{ir}$ defined by Ohm's law

$$E_{ir} = iR \tag{22.5.1}$$

where *i* is the current and *R* is the solution's resistance. To account for this, we can include an additional term to the equation for the electrochemical cell's potential

$$E_{\text{cell}} = E_{\text{cathode}} - E_{\text{anode}} - E_{ir} = E_{\text{Nernst}} - iR \tag{22.5.2}$$

where $E_{\text{Nernst}}$ is the potential from the Nernst equation. The resulting decease in the potential from its idealized value is called the *iR* drop.

## Polarization

Equation 22.5.2 indicates that we expect a linear relationship between an electrochemical cell's potential, $E_{\text{cell}}$. When this is not the case, the electrochemical cell is said to be polarized. There are several sources that contribute to polarization, which we consider in this section; first, however, we define ideal polarized and nonpolarized electrodes.

### Ideal Polarized and Nonpolarized Electrodes and Electrochemical Cells

An ideal polarized electrode is one in which a change in potential over a fairly wide range has no effect on the current that flows through the electrode, as we see in Figure $22.5.1a$ for the range of potentials defined by the solid green line. Such electrodes are useful because they do not themselves undergo oxidation or reduction—they are electrochemically inert—which makes them a good choice for studying the electrochemical behavior of other species.

An ideal nonpolarized electrode is one in which a change in current has no effect on the electrode's potential, as we see in Figure $22.5.1b$ between the limits defined by the solid red line with deviations shown by the dashed red line. Such electrodes are useful because the provided a stable potential against which we can reference the redox potential of other species.

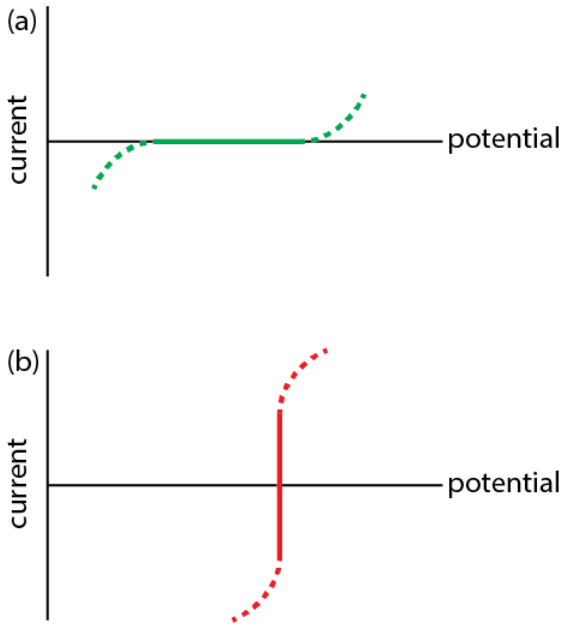



Figure 22.5.1: Current-potential curves for (a) an ideal polarized electrode and for (b) an ideal nonpolarized electrode. For both, the solid line shows the range of (a) potentials or (b) currents where the electrode shows ideal behavior.

## Overpotential

The magnitude of polarization when drawing a current is called the overpotential, $\eta$ and expressed as the difference between the applied potential, *E*, and the potential from the Nernst equation.

$$\eta = E - E_{\text{Nernst}} \tag{22.5.3}$$

The overpotential can be subdivided into a variety of sources, a few of which are discussed below.

## Concentration Polarization

The reduction of $Fe^{3+}$ to $Fe^{2+}$ in an electrochemical cell consumes an electron, which is drawn from the electrode. The oxidation of another species, perhaps the solvent, at a second electrode is the source of this electron. Because the reduction of $Fe^{3+}$ to $Fe^{2+}$ consumes one electron, the flow of electrons between the electrodes—in other words, the current—is a measure of the rate at which $Fe^{3+}$ is reduced.

> The rate of the reaction $\text{Fe}^{3+}(aq) \rightleftharpoons \text{Fe}^{2+}(aq) + e^-$ is the change in the concentration of $Fe^{3+}$ as a function of time.

In order for the reduction of $Fe^{3+}$ to $Fe^{2+}$ to take place, $Fe^{3+}$ must move from the bulk solution into the layer of solution immediately adjacent to the electrode and then diffuse to the electrode's surface; this is called the diffusion layer. Once the reduction takes place, the $Fe^{2+}$ produced must diffuse away from the electrode's surface and enter into the bulk solution. These two processes are called mass transfer and if we try to change the electrode's potential too quickly, mass transfer may result in concentrations of $Fe^{3+}$ to $Fe^{2+}$ at the electrode's surface that are different from that in bulk solution, resulting in concentration polarization.

Let's use the reduction of $Fe^{3+}$ to $Fe^{2+}$ at the cathode of a galvanic cell to think though how concentration polarization affects the potential we measure. From the Nernst equation we know that

$$E = E^\circ_{\text{Fe}^{3+}/\text{Fe}^{2+}} - \frac{0.05916}{1}\log\frac{[\text{Fe}^{2+}]}{[\text{Fe}^{3+}]} = +0.771 - \frac{0.05916}{1}\log\frac{[\text{Fe}^{2+}]}{[\text{Fe}^{3+}]} \tag{22.5.4}$$

If the mass transfer of $Fe^{3+}$ from bulk solution to the electrode's surface is slow and if mass transfer of $Fe^{2+}$ from the electrode's surface to bulk solution is slow, then the concentration of $Fe^{3+}$ at the electrode's surface is smaller than in bulk solution and the concentration of $Fe^{2+}$ at the electrode's surface is greater than in the bulk solution. As a result, the ratio $\frac{[\text{Fe}^{2+}]}{[\text{Fe}^{3+}]}$ is greater than that

predicted by the bulk concentrations of $Fe^{3+}$ and $Fe^{2+}$ and the potential of the cathode is smaller (less positive) than the value +0.771 V predicted by the bulk concentrations of $Fe^{3+}$ and $Fe^{2+}$. The resulting potential of the electrochemical cell

$$E_{\text{cell}} = E_{\text{cathode}} - E_{\text{anode}} \tag{22.5.5}$$

is less positive than that predicted by the bulk concentrations of $Fe^{3+}$ and $Fe^{2+}$ due to this concentration polarization.

Other kinetic processes can contribute to polarization, including the rate of chemical reactions that take place within the layer of solution near the electrode's surface, the kinetics of reactions in which the electroactive species absorb or desorb from the electrode's surface, and the kinetics of the electron transfer process itself. More details on these are included in later chapters covering specific electrochemical techniques.

---

This page titled 22.5: Currents in Electrochemical Cells is shared under a CC BY-NC-SA 4.0 license and was authored, remixed, and/or curated by David Harvey.

# 22.6: Types of Electroanalytical Methods

In the next three chapters we will consider a variety of different interfacial electrochemical experiments; that is, experiments in which the redox reaction takes place at the surface of an electrode. Because electrochemistry is such a broad field, let's use Figure 22.6.1 to organize these techniques by the experimental conditions we choose to use (Do we control the potential or the current? How do we change the applied potential or applied current? Do we stir the solution?) and the analytical signal we decide to measure (Current? Potential?).

At the first level, we divide electrochemical techniques into static techniques and dynamic techniques. In a static technique we do not allow current to pass through the electrochemical cell and, as a result, the concentrations of all species remain constant. Potentiometry, in which we measure the potential of an electrochemical cell under static conditions, is one of the most important quantitative electrochemical methods and is discussed in Chapter 23.

Dynamic techniques, in which we allow current to flow and force a change in the concentration of species in the electrochemical cell, comprise the largest group of interfacial electrochemical techniques. Coulometry, in which we measure current as a function of time, is covered Chapter 24. Voltammetry and amperometry, in which we measure current as a function of a fixed or variable potential, are the subjects of Chapter 25.

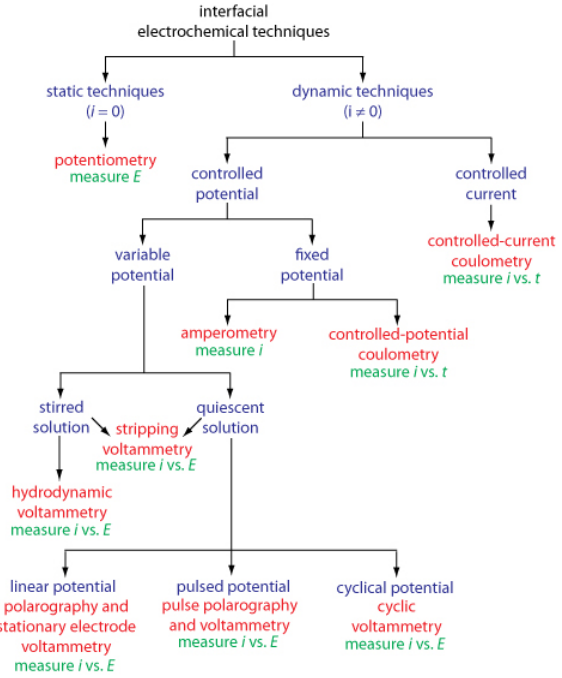



Figure 22.6.1: Family tree that highlights the similarities and differences between a number of interfacial electrochemical techniques. The specific instrumental methods are shown in red, the experimental conditions are shown in blue, and the analytical signals are in green.

This page titled 22.6: Types of Electroanalytical Methods is shared under a CC BY-NC-SA 4.0 license and was authored, remixed, and/or curated by David Harvey.

# CHAPTER OVERVIEW

## 23: Potentiometry

In potentiometry we measure the potential of an electrochemical cell under static conditions. Because no current—or only a negligible current—flows through the electrochemical cell, its composition remains unchanged. For this reason, potentiometry is a useful quantitative method of analysis. The first quantitative potentiometric applications appeared soon after the formulation, in 1889, of the Nernst equation, which relates an electrochemical cell's potential to the concentration of electroactive species in the cell [Stork, J. T. *Anal. Chem.* **1993**, *65*, 344A–351A].

Potentiometry initially was restricted to redox equilibria at metallic electrodes, which limited its application to a few ions. In 1906, Cremer discovered that the potential difference across a thin glass membrane is a function of pH when opposite sides of the membrane are in contact with solutions that have different concentrations of $H_3O^+$. This discovery led to the development of the glass pH electrode in 1909. Other types of membranes also yield useful potentials. For example, in 1937 Kolthoff and Sanders showed that a pellet of AgCl can be used to determine the concentration of $Ag^+$. Electrodes based on membrane potentials are called ion-selective electrodes, and their continued development extends potentiometry to a diverse array of analytes.


23.1: Reference Electrodes
23.2: Metallic Indicator Electrodes
23.3: Membrane Ion-Selective Electrodes
23.4: Molecular-Selective Electrode Systems
23.5: Instruments for Measuring Cell Potentials
23.6: Quantitative Potentiometry


This page titled 23: Potentiometry is shared under a CC BY-NC-SA 4.0 license and was authored, remixed, and/or curated by David Harvey.

# 23.1: Reference Electrodes

In potentiometry we measure the difference between the potential of two electrodes. The potential of one electrode—the working or indicator electrode—responds to the analyte's activity and the other electrode—the counter or reference electrode—has a known, fixed potential. By convention, the reference electrode is the anode; thus, the short hand notation for a potentiometric electrochemical cell is

$$\text{reference electrode} \,||\, \text{indicator electrode}$$

and the cell potential is

$$E_{\text{cell}} = E_{\text{ind}} - E_{\text{ref}}$$

The ideal reference electrode provides a stable, known potential so that we can attribute any change in $E_{\text{cell}}$ to the analyte's effect on the indicator electrode's potential. In addition, the reference electrode should be easy to make and easy to use. Although the standard hydrogen electrode is the reference electrode used to define electrode potentials, it use is not common. Instead, the two reference electrodes discussed in this section find the most applications.

## Calomel Electrodes

A calomel reference electrode is based on the following redox couple between $Hg_2Cl_2$ and Hg (calomel is the common name for $Hg_2Cl_2$)

$$Hg_2Cl_2(s) + 2e^- \rightleftharpoons 2Hg(l) + 2Cl^-(aq)$$

for which the potential is

$$E = E^{\circ}_{Hg_2Cl_2/Hg} - \frac{0.05916}{2}\log\left(a_{Cl^-}\right)^2 = +0.2682\text{V} - \frac{0.05916}{2}\log\left(a_{Cl^-}\right)^2$$

The potential of a calomel electrode, therefore, depends on the activity of $Cl^-$ in equilibrium with Hg and $Hg_2Cl_2$.

As shown in Figure 23.1.1, in a saturated calomel electrode (SCE) the concentration of $Cl^-$ is determined by the solubility of KCl. The electrode consists of an inner tube packed with a paste of Hg, $Hg_2Cl_2$, and KCl, situated within a second tube that contains a saturated solution of KCl. A small hole connects the two tubes and a porous wick serves as a salt bridge to the solution in which the SCE is immersed. A stopper in the outer tube provides an opening for adding addition saturated KCl. The short hand notation for this cell is

$$Hg(l)|Hg_2Cl_2(s), KCl(aq,\ \text{sat'd}\ )\|$$

Because the concentration of $Cl^-$ is fixed by the solubility of KCl, the potential of an SCE remains constant even if we lose some of the inner solution to evaporation. A significant disadvantage of the SCE is that the solubility of KCl is sensitive to a change in temperature. At higher temperatures the solubility of KCl increases and the electrode's potential decreases. For example, the potential of the SCE is +0.2444 V at 25°C and +0.2376 V at 35°C. The potential of a calomel electrode that contains an unsaturated solution of KCl is less dependent on the temperature, but its potential changes if the concentration, and thus the activity of $Cl^-$, increases due to evaporation.

> For example, the potential of a calomel electrode is +0.280 V when the concentration of KCl is 1.00 M and +0.336 V when the concentration of KCl is 0.100 M. If the activity of $Cl^-$ is 1.00, the potential is +0.2682 V.

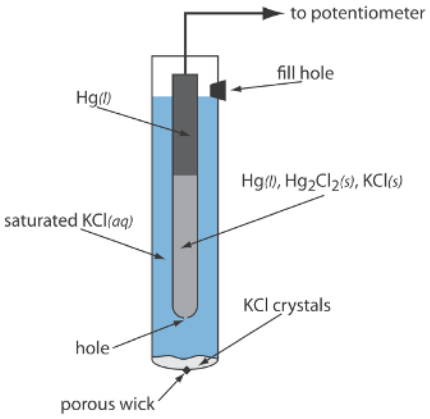



Figure 23.1.1. Schematic diagram showing the saturated calomel electrode.

## Silver/Silver Chloride Electrodes

Another common reference electrode is the silver/silver chloride electrode, which is based on the reduction of AgCl to Ag.

$$\mathrm{AgCl}(s) + e^- \rightleftharpoons \mathrm{Ag}(s) + \mathrm{Cl}^-(aq)$$

As is the case for the calomel electrode, the activity of $Cl^-$ determines the potential of the Ag/AgCl electrode; thus

$$E = E^\circ_{\mathrm{AgCl/Ag}} - 0.05916 \log a_{\mathrm{Cl}^-} = 0.2223 \text{ V} - 0.05916 \log a_{\mathrm{Cl}^-}$$

When prepared using a saturated solution of KCl, the electrode's potential is +0.197 V at 25°C. Another common Ag/AgCl electrode uses a solution of 3.5 M KCl and has a potential of +0.205 V at 25°C. As you might expect, the potential of a Ag/AgCl electrode using a saturated solution of KCl is more sensitive to a change in temperature than an electrode that uses an unsaturated solution of KCl.

A typical Ag/AgCl electrode is shown in Figure 23.1.2 and consists of a silver wire, the end of which is coated with a thin film of AgCl, immersed in a solution that contains the desired concentration of KCl. A porous plug serves as the salt bridge. The electrode's short hand notation is

$$\mathrm{Ag}(s) | \mathrm{Ag\,Cl}(s), \mathrm{KCl}\,(aq, a_{\mathrm{Cl}^-} = x) \,\|$$

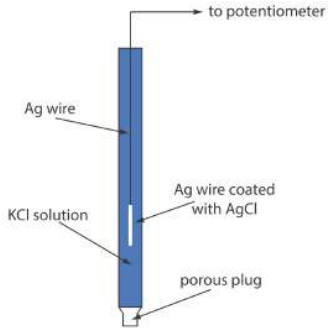



Figure 23.1.2. Schematic diagram showing a Ag/AgCl electrode. Because the electrode does not contain solid KCl, this is an example of an unsaturated Ag/AgCl electrode.

### Converting Potentials Between Reference Electrodes

The standard state reduction potentials in most tables are reported relative to the standard hydrogen electrode's potential of +0.00 V. Because we rarely use the SHE as a reference electrode, we need to convert an indicator electrode's potential to its equivalent value when using a different reference electrode. As shown in the following example, this is easy to do.

## Example 23.1.1

The potential for an $Fe^{3+}/Fe^{2+}$ half-cell is +0.750 V relative to the standard hydrogen electrode. What is its potential if we use a saturated calomel electrode or a saturated silver/silver chloride electrode?

### Solution

When we use a standard hydrogen electrode the potential of the electrochemical cell is

$$E_{\text{cell}} = E_{\text{Fe}^{3+}/\text{Fe}^{2+}} - E_{\text{SHE}} = 0.750\ \text{V} - 0.000\ \text{V} = 0.750\ \text{V}$$

We can use the same equation to calculate the potential if we use a saturated calomel electrode

$$E_{\text{cell}} = E_{\text{Fe}^{3+}/\text{Fe}^{2+}} - E_{\text{SHE}} = 0.750\ \text{V} - 0.2444\ \text{V} = 0.506\ \text{V}$$

or a saturated silver/silver chloride electrode

$$E_{\text{cell}} = E_{\text{Fe}^{3+}/\text{Fe}^{2+}} - E_{\text{SHE}} = 0.750\ \text{V} - 0.197\ \text{V} = 0.553\ \text{V}$$

Figure 23.1.3 provides a pictorial representation of the relationship between these different potentials.

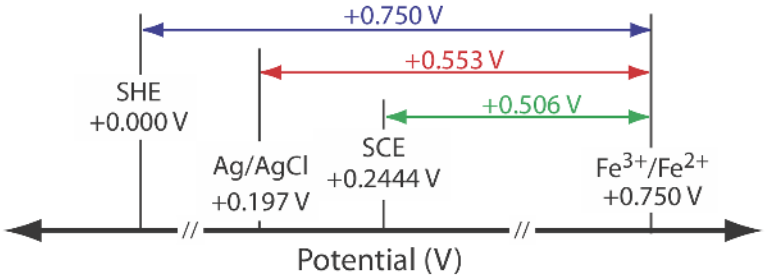



Figure 23.1.3. Relationship between the potential of an $Fe^{3+}/Fe^{2+}$ half-cell relative to the reference electrodes in Example 23.1.1. The potential relative to a standard hydrogen electrode is shown in blue, the potential relative to a saturated silver/silver chloride electrode is shown in red, and the potential relative to a saturated calomel electrode is shown in green.

This page titled 23.1: Reference Electrodes is shared under a CC BY-NC-SA 4.0 license and was authored, remixed, and/or curated by David Harvey.

# 23.2: Metallic Indicator Electrodes

In potentiometry, the potential of the indicator electrode is proportional to the analyte's activity. Two classes of indicator electrodes are used to make potentiometric measurements: metallic electrodes, which are the subject of this section, and ion-selective electrodes, which are covered in the next section.

## Electrodes of the First Kind

If we place a copper electrode in a solution that contains $Cu^{2+}$, the electrode's potential due to the reaction

$$Cu^{2+}(aq) + 2e^- \rightleftharpoons Cu(s)$$

is determined by the activity of $Cu^{2+}$.

$$E = E^{\circ}_{Cu^{2+}/Cu} - \frac{0.05916}{2}\log\frac{1}{a_{Cu^{2+}}} = +0.3419V - \frac{0.05916}{2}\log\frac{1}{a_{Cu^{2+}}}$$

If copper is the indicator electrode in a potentiometric electrochemical cell that also includes a saturated calomel reference electrode

$$SCE\|Cu^{2+}\,(aq, a_{Cu^{2+}} = x)\,|Cu(s)$$

then we can use the cell potential to determine an unknown activity of $Cu^{2+}$ in the indicator electrode's half-cell

$$E_{cell} = E_{\text{ ind}} - E_{SCE} = +0.3419V - \frac{0.05916}{2}\log\frac{1}{a_{Cu^{2+}}} - 0.2224V$$

An indicator electrode in which the metal is in contact with a solution containing its ion is called an electrode of the first kind. In general, if a metal, *M*, is in a solution of $M^{n+}$, the cell potential is

$$E_{call} = K - \frac{0.05916}{n}\log\frac{1}{a_{M^{n+}}} = K + \frac{0.05916}{n}\log a_{M^{n+}}$$

where *K* is a constant that includes the standard-state potential for the $M^{n+}/M$ redox couple and the potential of the reference electrode.

For a variety of reasons—including the slow kinetics of electron transfer at the metal–solution interface, the formation of metal oxides on the electrode's surface, and interfering reactions—electrodes of the first kind are limited to the following metals: Ag, Bi, Cd, Cu, Hg, Pb, Sn, Tl, and Zn.

> Many of these electrodes, such as Zn, cannot be used in acidic solutions because they are easily oxidized by $H^+$.
>
> $$Zn(s) + 2H^+(aq) \rightleftharpoons H_2(g) + Zn^{2+}(aq)$$

## Electrodes of the Second Kind

The potential of an electrode of the first kind responds to the activity of $M^{n+}$. We also can use this electrode to determine the activity of another species if it is in equilibrium with $M^{n+}$. For example, the potential of a Ag electrode in a solution of $Ag^+$ is

$$E = 0.7996V + 0.05916\log a_{Ag^+} \tag{23.2.1}$$

If we saturate the indicator electrode's half-cell with AgI, the solubility reaction

$$AgI(s) \rightleftharpoons Ag^+(aq) + I^-(aq) \tag{23.2.2}$$

determines the concentration of $Ag^+$; thus

$$a_{Ag^+} = \frac{K_{sp,AgI}}{a_{I^-}} \tag{23.2.3}$$

where $K_{sp,AgI}$ is the solubility product for AgI. Substituting Equation 23.2.3 into Equation 23.2.1

$$E = 0.7996 \text{ V} + 0.05916 \log \frac{K_{\text{sp, AgI}}}{a_{\text{I}^-}} \tag{23.2.4}$$

shows that the potential of the silver electrode is a function of the activity of $\text{I}^-$. If we incorporate this electrode into a potentiometric electrochemical cell with a saturated calomel electrode

$$\text{SCE} \| \text{AgI}(s),\ \text{I}^-\ (aq, a_{\text{I}^-} = x)\ | \text{Ag(s)} \tag{23.2.5}$$

then the cell potential is

$$E_{\text{cell}} = K - 0.05916 \log a_{\text{I}^-} \tag{23.2.6}$$

where $K$ is a constant that includes the standard-state potential for the $\text{Ag}^+/\text{Ag}$ redox couple, the solubility product for AgI, and the reference electrode's potential.

If an electrode of the first kind responds to the activity of an ion in equilibrium with $M^{n+}$, we call it an electrode of the second kind. Two common electrodes of the second kind are the calomel and the silver/silver chloride reference electrodes.

> In an electrode of the second kind we link together a redox reaction and another reaction, such as a solubility reaction. You might wonder if we can link together more than two reactions. The short answer is yes. An electrode of the third kind, for example, links together a redox reaction and two other reactions. Such electrodes are less common and we will not consider them in this text.

## Metallic Redox Electrodes

An electrode of the first kind or the second kind develops a potential as the result of a redox reaction that involves the metallic electrode. An electrode also can serve as a source of electrons or as a sink for electrons in an unrelated redox reaction, in which case we call it a redox electrode. The Pt cathode in 23.2.1 is a redox electrode because its potential is determined by the activity of $\text{Fe}^{2+}$ and $\text{Fe}^{3+}$ in the indicator half-cell. Note that a redox electrode's potential often responds to the activity of more than one ion, which limits its usefulness for direct potentiometry.

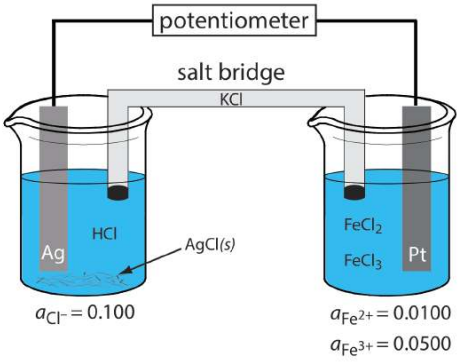



Figure 23.2.1. Potentiometric electrochemical cell in which the anode is a metallic electrode of the first kind (Ag) and the cathode is a metallic redox electrode (Pt).

---

This page titled 23.2: Metallic Indicator Electrodes is shared under a CC BY-NC-SA 4.0 license and was authored, remixed, and/or curated by David Harvey.

# 23.3: Membrane Ion-Selective Electrodes

If metals were the only useful materials for constructing indicator electrodes, then there would be few useful applications of potentiometry. In 1906, Cremer discovered that the potential difference across a thin glass membrane is a function of pH when opposite sides of the membrane are in contact with solutions that have different concentrations of $H_3O^+$. The existence of this membrane potential led to the development of a new class of indicator electrodes, which we call ion-selective electrodes (ISEs). In addition to the glass pH electrode, ion-selective electrodes are available for a wide range of ions. It also is possible to construct a membrane electrode for a neutral analyte by using a chemical reaction to generate an ion that is monitored with an ion-selective electrode. The development of new ion-selective membrane electrodes continues to be an active area of research.

## Classification of Ions-Selective Membranes

There are two broad classes of materials that are used as membranes: crystalline solid-state membranes and non-crystalline membranes. Examples of crystalline solid-state membranes are single crystals of $LaF_3$ and polycrystalline AgS. Examples non-crystalline membranes are glass and hydrophobic membranes that hold a liquid ion-exchanger. Each of these are considered below.

## Properties of Ion-Selective Membranes

To be useful, an ion-selective membrane must be structurally stable (a crystalline membrane that is soluble, for example, is not structurally stable), capable of being machined to a suitable size and shape that can be incorporated into the indicator electrode in a potentiometric electrochemical cell, electrically conductive so it is possible to measure the electrochemical cell's potential, and selective toward the analyte.

### The Membrane's Boundary Potential

Figure 23.3.1 shows a typical potentiometric electrochemical cell equipped with an ion-selective electrode. The short hand notation for this cell is

$$\text{ref (sample)} \;\; \| \text{A}_{\text{samp}} \;\; (aq, a_{\text{A}_{\text{samp}}} = x) \, | \text{membrane} | \text{A}_{\text{int}} \;\; (aq, a_{\text{A}_{\text{int}}} = y) \| \;\; \text{ref (internal)}$$

where the ion-selective membrane separates the two solutions that contain analyte with activities of *x* and *y*: the sample solution and the ion-selective electrode's internal solution. The potential of this electrochemical cell

$$E_{\text{cell}} = E_{\text{ref(int)}} - E_{\text{ref(samp)}} + E_{\text{mem}} \tag{23.3.1}$$

includes the potential of each reference electrode and the difference in potential across the membrane, $E_{\text{mem}}$, which is the membrane's boundary potential. The notations ref(sample) and ref(internal) represent a reference electrode immersed in the sample and a reference electrode immersed in the ion-selective electrode's internal solution. Because the potential of the two reference electrodes are constant, any change in $E_{\text{cell}}$ reflects a change in the membrane's boundary potential.

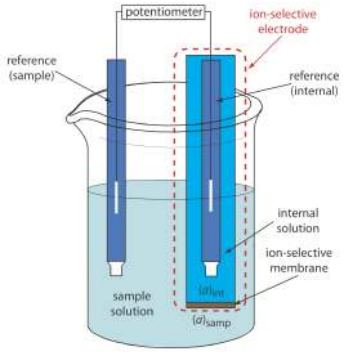



Figure 23.3.1. Schematic diagram that shows a typical potentiometric cell with an ion-selective electrode. The ion-selective electrode's membrane separates the sample, which contains the analyte at an activity of $(a_A)_{\text{samp}}$, from an internal solution that contains the analyte with an activity of $(a_A)_{\text{int}}$.

The analyte's interaction with the membrane generates a boundary potential if there is a difference in its activity on the membrane's two sides. Current is carried through the membrane by the movement of either the analyte or an ion already present in the membrane's matrix. The membrane potential is given by the following Nernst-like equation

$$E_{\text{mem}} = E_{\text{asym}} - \frac{RT}{zF} \ln \frac{(a_A)_{\text{int}}}{(a_A)_{\text{samp}}} \tag{23.3.2}$$

where $(a_A)_{\text{samp}}$ is the analyte's activity in the sample, $(a_A)_{\text{int}}$ is the analyte's activity in the ion-selective electrode's internal solution, and $z$ is the analyte's charge. Ideally, $E_{\text{mem}}$ is zero when $(a_A)_{\text{int}} = (a_A)_{\text{samp}}$. The term $E_{\text{asym}}$, which is an asymmetry potential, accounts for the fact that $E_{\text{mem}}$ usually is not zero under these conditions.

> For now we simply note that a difference in the analyte's activity results in the membrane's boundary potential. As we consider different types of ion-selective electrodes, we will explore more specifically the source of the membrane potential.

Substituting Equation 23.3.2 into Equation 23.3.1, assuming a temperature of 25°C, and rearranging gives

$$E_{\text{cell}} = K + \frac{0.05916}{z} \log (a_A)_{\text{samp}} \tag{23.3.3}$$

where $K$ is a constant that includes the potentials of the two reference electrodes, the asymmetry potential, and the analyte's activity in the internal solution. Equation 23.3.3 is a general equation and applies to all types of ion-selective electrodes.

## Membrane Selectivity

The membrane's boundary potential results from a chemical interaction between the analyte and active sites on the membrane's surface. Because the signal depends on a chemical process, most membranes are not selective toward a single analyte. Instead, the membrane's boundary potential is proportional to the concentration of each ion that interacts with the membrane's active sites. We can rewrite Equation 23.3.3 to include the contribution to the potential of an interferent, $I$

$$E_{\text{cell}} = K + \frac{0.05916}{z_A} \log \left\{ a_A + K_{A,I} (a_I)^{z_A/z_I} \right\} \tag{23.3.4}$$

where $z_A$ and $z_I$ are the charges of the analyte and the interferent, and $K_{A,I}$ is a selectivity coefficient that accounts for the relative response of the interferent. The selectivity coefficient is defined as

$$K_{A,I} = \frac{(a_A)_e}{(a_I)_e^{z_A/z_I}} \tag{23.3.5}$$

where $(a_A)_e$ and $(a_I)_e$ are the activities of analyte and the interferent that yield identical cell potentials. When the selectivity coefficient is 1.00, the membrane responds equally to the analyte and the interferent. A membrane shows good selectivity for the analyte when $K_{A,I}$ is significantly less than 1.00.

Selectivity coefficients for most commercially available ion-selective electrodes are provided by the manufacturer. If the selectivity coefficient is not known, it is easy to determine its value experimentally by preparing a series of solutions, each of which contains the same activity of interferent, $(a_I)_{\text{add}}$, but a different activity of analyte. As shown in Figure 23.3.2, a plot of cell potential versus the log of the analyte's activity has two distinct linear regions. When the analyte's activity is significantly larger than $K_{A,I} \times (a_I)_{\text{add}}$, the potential is a linear function of $\log(a_A)$, as given by Equation 23.3.3. If $K_{\text{A,I}} \times (a_I)_{\text{add}}$ is significantly larger than the analyte's activity, however, the cell's potential remains constant. The activity of analyte and interferent at the intersection of these two linear regions is used to calculate $K_{\text{A,I}}$.

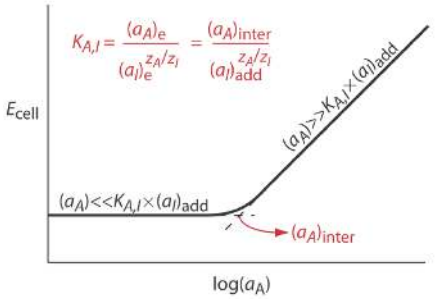



Figure 23.3.2. Diagram showing the experimental determination of an ion-selective electrode's selectivity for an analyte. The activity of analyte that corresponds to the intersection of the two linear portions of the curve, $(a_A)_{inter}$, produces a cell potential identical to that of the interferent. The equation for the selectivity coefficient, $K_{A,I}$, is shown in red.

### Example 23.3.1

Sokalski and co-workers described a method for preparing ion-selective electrodes with significantly improved selectivities [Sokalski, T.; Ceresa, A.; Zwicki, T.; Pretsch, E. *J. Am. Chem. Soc.* **1997**, *119*, 11347–11348]. For example, a conventional $Pb^{2+}$ ISE has a $\log K_{Pb^{2+}/Mg^{2+}}$ of –3.6. If the potential for a solution in which the activity of $Pb^{2+}$ is $4.1 \times 10^{-12}$ is identical to that for a solution in which the activity of $Mg^{2+}$ is 0.01025, what is the value of $\log K_{Pb^{2+}/Mg^{2+}}$ for their ISE?

**Solution**

Making appropriate substitutions into Equation 23.3.5, we find that

$$K_{Pb^{2+}/Mg^{2+}} = \frac{(a_{Pb^{2+}})_e}{(a_{Mg^{2+}})_e^{z_{Pb^{2+}}/z_{Mg^{2+}}}} = \frac{4.1 \times 10^{-12}}{(0.01025)^{+2/+2}} = 4.0 \times 10^{-10}$$

The value of $\log K_{Pb^{2+}/Mg^{2+}}$, therefore, is –9.40.

## The Glass Electrode for pH Measurements

The earliest ion-selective electrodes were based on the observation that a thin glass membrane separating two solutions with different levels of acidity develops a measurable difference in potential on opposite sides of the membrane. Incorporating the glass electrode into a potentiometer along with a reference electrode provides a way to measure the potential. Commercial glass membrane pH electrodes often are available in a combination form that includes both the indicator electrode and the reference electrode. The use of a single electrode greatly simplifies the measurement of pH. An example of a typical combination electrode is shown in Figure 23.3.3.

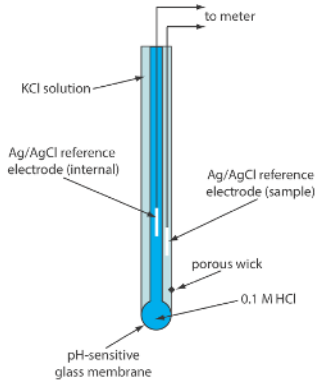



Figure 23.3.3. Schematic diagram showing a combination glass electrode for measuring pH. The indicator electrode consists of a pH-sensitive glass membrane and an internal Ag/AgCl reference electrode in a solution of 0.1 M HCl. The sample's reference electrode is a Ag/AgCl electrode in a solution of KCl (which may be saturated with KCl or contain a fixed concentration of KCl). A porous wick serves as a salt bridge between the sample and its reference electrode.

### The Composition and Structure of Glass Membranes

The first commercial glass electrodes were manufactured using Corning 015, a glass with a composition that is approximately 22% $Na_2O$, 6% CaO, and 72% $SiO_2$. Membranes fashioned from Corning 015 have an excellent selectivity for hydrogen ions, $H^+$, below a pH of 9; above this pH the membrane becomes more selective for other cations and the measured pH value deviates from its actual value. Replacing $Na_2O$ and CaO with $Li_2O$ and BaO extends the useful pH range of glass membranes to pH levels greater than 12.

### Origin of the Boundary Potential for a Glass Membrane

When immersed in an aqueous solution for several hours, the outer approximately 10 nm of the glass membrane's surface becomes hydrated, resulting in the formation of negatively charged sites, —$SiO^-$. Sodium ions, $Na^+$, serve as counter ions. Because $H^+$ binds more strongly to —$SiO^-$ than does $Na^+$, they displace the sodium ions on both sides of the membrane.

$$H^+ + -SiO^-Na^+ \rightleftharpoons -SiO^-H^+ + Na^+ \tag{23.3.6}$$

explaining the membrane's selectivity for $H^+$. The transport of charge across the membrane is carried by the $Na^+$ ions within the glass membrane. The potential of a glass electrode obeys the equation

$$E_{cell} = K + 0.05916 \log a_{H^+} \tag{23.3.7}$$

### Alkaline and Acid Errors

As noted above, at sufficiently basic pH values a glass electrode no longer provides an accurate measure of a sample's pH as the membrane becomes more selective for other monovalent cations, such as $Na^+$ and $K^+$.

**Example 23.3.2**

For a Corning 015 glass membrane, the selectivity coefficient $K_{H^+/Na^+}$ is $\approx 10^{-11}$. What is the expected error if we measure the pH of a solution in which the activity of $H^+$ is $2 \times 10^{-13}$ and the activity of $Na^+$ is 0.05?

**Solution**

A solution in which the activity of $H^+$, $(a_{H^+})_{act}$, is $2 \times 10^{-13}$ has a pH of 12.7. Because the electrode responds to both $H^+$ and $Na^+$, the apparent activity of $H^+$, $(a_{H^+})_{app}$, is

$$(a_{H^+})_{app} = (a_{H^+})_{act} + (K_{H^+/Na^+} \times a_{Na^+}) = 2 \times 10^{-13} + (10^{-11} \times 0.05) = 7 \times 10^{-13}$$

The apparent activity of $H^+$ is equivalent to a pH of 12.2, an error of –0.5 pH units.

Glass pH electrodes also show deviations from ideal behavior at pH levels less than 0.5, although the reasons for this are not clear. Still, a glass electrode has a wide dynamic range for measuring pH.

### Other Limitations to Glass Electrodes

Because an ion-selective electrode's glass membrane is very thin—it is only about 50 µm thick—they must be handled with care to avoid cracks or breakage. Glass electrodes usually are stored in a storage buffer recommended by the manufacturer, which ensures that the membrane's outer surface remains hydrated. If a glass electrode dries out, it is reconditioned by soaking for several hours in a solution that contains the analyte. The composition of a glass membrane will change over time, which affects the electrode's performance. The average lifetime for a typical glass electrode is several years.

## Glass Electrodes for Other Cations

The observation that the Corning 015 glass membrane responds to ions other than $H^+$ led to the development of glass membranes with a greater selectivity for other cations. For example, a glass membrane with a composition of 11% $Na_2O$, 18% $Al_2O_3$, and 71% $SiO_2$ is used as an ion-selective electrode for $Na^+$. Other glass ion-selective electrodes have been developed for the analysis of $Li^+$, $K^+$, $Rb^+$, $Cs^+$, $NH_4^+$, $Ag^+$, and $Tl^+$. Table 23.3.1 provides several examples.

Table 23.3.1. Representative Examples of Glass Membrane Ion-Selective Electrodes for Analytes Other Than $H^+$

| analyte | membrane composition | selectivity coefficients |
|---|---|---|
| $Na^+$ | 11% $Na_2O$, 18% $Al_2O_3$, 71% $SiO_2$ | $K_{Na^+/H^+} = 1000$<br>$K_{Na^+/K^+} = 0.001$<br>$K_{Na^+/Li^+} = 0.001$ |
| $Li^+$ | 15% $Li_2O$, 25% $Al_2O_3$, 60% $SiO_2$ | $K_{Li^+/Na^+} = 0.3$<br>$K_{Li^+/K^+} = 0.001$ |
| $K^+$ | 27% $Na_2O$, 5% $Al_2O_3$, 68% $SiO_2$ | $K_{K^+/Na^+} = 0.05$ |

Selectivity coefficients are approximate; values found experimentally may vary substantially from the listed values. See Cammann, K. *Working With Ion-Selective Electrodes*, Springer-Verlag: Berlin, 1977.

## Crystalline Membrane Electrodes

A solid-state ion-selective electrode has a membrane that consists of either a polycrystalline inorganic salt or a single crystal of an inorganic salt. We can fashion a polycrystalline solid-state ion-selective electrode by sealing a 1–2 mm thick pellet of AgS—or a mixture of AgS and a second silver salt or another metal sulfide—into the end of a nonconducting plastic cylinder, filling the cylinder with an internal solution that contains the analyte, and placing a reference electrode into the internal solution. Figure 23.3.4 shows a typical design.

> The NaCl in a salt shaker is an example of polycrystalline material because it consists of many small crystals of sodium chloride. The NaCl salt plates used in IR spectroscopy, on the other hand, are an example of a single crystal of sodium chloride.

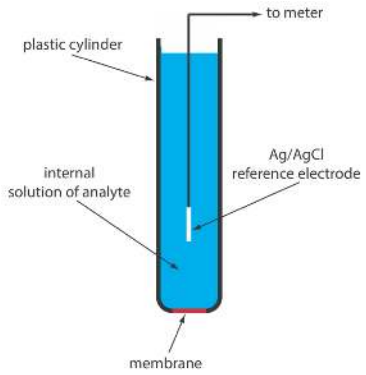



Figure 23.3.4. Schematic diagram of a solid-state electrode. The internal solution contains a solution of analyte of fixed activity.

The membrane potential for a $Ag_2S$ pellet develops as the result of a difference in the extent of the solubility reaction

$$Ag_2S(s) \rightleftharpoons 2Ag^+(aq) + S^{2-}(aq) \tag{23.3.8}$$

on the membrane's two sides, with charge carried across the membrane by $Ag^+$ ions. When we use the electrode to monitor the activity of $Ag^+$, the cell potential is

$$E_{cell} = K + 0.05916 \log a_{Ag^+} \tag{23.3.9}$$

The membrane also responds to the activity of $S^{2-}$, with a cell potential of

$$E_{cell} = K - \frac{0.05916}{2} \log a_{S^{2-}} \tag{23.3.10}$$

If we combine an insoluble silver salt, such as AgCl, with the $Ag_2S$, then the membrane potential also responds to the concentration of $Cl^-$, with a cell potential of

$$E_{cell} = K - 0.05916 \log a_{Cl^-} \tag{23.3.11}$$

By mixing $Ag_2S$ with CdS, CuS, or PbS, we can make an ion-selective electrode that responds to the activity of $Cd^{2+}$, $Cu^{2+}$, or $Pb^{2+}$. In this case the cell potential is

$$E_{\text{cell}} = K + \frac{0.05916}{2} \ln a_{M^{2+}} \tag{23.3.12}$$

where $a_{M^{2+}}$ is the activity of the metal ion.

Table 23.3.2 provides examples of polycrystalline, $Ag_2S$-based solid-state ion-selective electrodes. The selectivity of these ion-selective electrodes depends on the relative solubility of the compounds. A $Cl^-$ ISE using a $Ag_2S$/AgCl membrane is more selective for $Br^-$ ($K_{Cl^-/Br^-} = 10^2$) and for $I^-$ ($K_{Cl^-/I^-} = 10^6$) because AgBr and AgI are less soluble than AgCl. If the activity of $Br^-$ is sufficiently high, AgCl at the membrane/solution interface is replaced by AgBr and the electrode's response to $Cl^-$ decreases substantially. Most of the polycrystalline ion-selective electrodes listed in Table 23.3.2 operate over an extended range of pH levels. The equilibrium between $S^{2-}$ and $HS^-$ limits the analysis for $S^{2-}$ to a pH range of 13–14.

23.3.2. Representative Examples of Polycrystalline Solid-State Ion-Selective Electrodes

| analyte | membrane composition | selectivity coefficients |
|---|---|---|
| $Ag^+$ | $Ag_2S$ | $K_{Ag^+/Cu^{2+}} = 10^{-6}$<br>$K_{Ag^+/Pb^{2+}} = 10^{-10}$<br>$Hg^{2+}$ interferes |
| $Cd^{2+}$ | $CdS/Ag_2S$ | $K_{Cd^{2+}/Fe^{2+}} = 200$<br>$K_{Cd^{2+}/Pb^{2+}} = 6$<br>$Ag^+$, $Hg^{2+}$, and $Cu^{2+}$ must be absent |
| $Cu^{2+}$ | $CuS/Ag_2S$ | $K_{Cu^{2+}/Fe^{3+}} = 10$<br>$K_{Cu^{2+}/Cu^+} = 10^{-6}$<br>$Ag^+$ and $Hg^{2+}$ must be absent |
| $Pb^{2+}$ | $PbS/Ag_2S$ | $K_{Pb^{2+}/Fe^{3+}} = 1$<br>$K_{Pb^{2+}/Cd^{2+}} = 1$<br>$Ag^+$, $Hg^{2+}$, and $Cu^{2+}$ must be absent |
| $Br^-$ | $AgBr/Ag_2S$ | $K_{Br^-/I^-} = 5000$<br>$K_{Br^-/Cl^-} = 0.005$<br>$K_{Br^-/OH^-} = 10^{-5}$<br>$S^{2-}$ must be absent |
| $Cl^-$ | $AgCl/Ag_2S$ | $K_{Cl^-/I^-} = 10^6$<br>$K_{Cl^-/Br^-} = 100$<br>$K_{Cl^-/OH^-} = 0.01$<br>$S^{2-}$ must be absent |
| $I^-$ | $AgI/Ag_2S$ | $K_{I^-/S^{2-}} = 30$<br>$K_{I^-/Br^-} = 10^{-4}$<br>$K_{I^-/Cl^-} = 10^{-6}$<br>$K_{I^-/OH^-} = 10^{-7}$ |
| $SCN^-$ | $AgSCN/Ag_2S$ | $K_{SCN^-/I^-} = 10^3$<br>$K_{SCN^-/Br^-} = 100$<br>$K_{SCN^-/Cl^-} = 0.1 K_{SCN^-/OH^-} = 0.01$<br>$S^{2-}$ must be absent |
| $S^{2-}$ | $Ag_2S$ | $Hg^{2+}$ must be absent |

Selectivity coefficients are approximate; values found experimentally may vary substantially from the listed values. See Cammann, K. *Working With Ion-Selective Electrodes*, Springer-Verlag: Berlin, 1977.

The membrane of a $F^-$ ion-selective electrode is fashioned from a single crystal of $LaF_3$, which usually is doped with a small amount of $EuF_2$ to enhance the membrane's conductivity. Because $EuF_2$ provides only two $F^-$ ions—compared to the three $F^-$ ions in $LaF_3$—each $EuF_2$ produces a vacancy in the crystal's lattice. Fluoride ions pass through the membrane by moving into adjacent vacancies. As shown in Figure 23.3.4, the $LaF_3$ membrane is sealed into the end of a non-conducting plastic cylinder, which contains a standard solution of $F^-$, typically 0.1 M NaF, and a Ag/AgCl reference electrode.

The membrane potential for a $F^-$ ISE results from a difference in the solubility of $LaF_3$ on opposite sides of the membrane, with the potential given by

$$E_{\text{cell}} = K - 0.05916 \log a_{F^-} \tag{23.3.13}$$

One advantage of the $F^-$ ion-selective electrode is its freedom from interference. The only significant exception is $OH^-$ ($K_{F^-/OH^-}$ = 0.1), which imposes a maximum pH limit for a successful analysis. Below a pH of 4 the predominate form of fluoride in solution is HF, which does not contribute to the membrane potential. For this reason, an analysis for fluoride is carried out at a pH greater than 4.

### Example 23.3.3

What is the maximum pH that we can tolerate if we need to analyze a solution in which the activity of $F^-$ is $1 \times 10^{-5}$ with an error of less than 1%?

**Solution**

In the presence of $OH^-$ the cell potential is

$$E_{\text{cell}} = K - 0.05916 \left\{ a_{F^-} + K_{F^-/OH^-} \times a_{OH^-} \right\}$$

To achieve an error of less than 1%, the term $K_{F^-/OH^-} \times a_{OH^-}$ must be less than 1% of $a_{F^-}$; thus

$$K_{F^-/OH^-} \times a_{OH^-} \leq 0.01 \times a_{F^-}$$

$$0.10 \times a_{OH^-} \leq 0.01 \times \left(1.0 \times 10^{-5}\right)$$

Solving for $a_{OH^-}$ gives the maximum allowable activity for $OH^-$ as $1 \times 10^{-6}$, which corresponds to a pH of less than 8.

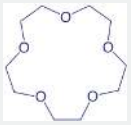
Unlike a glass membrane ion-selective electrode, a solid-state ISE does not need to be conditioned before it is used, and it may be stored dry. The surface of the electrode is subject to poisoning, as described above for a $Cl^-$ ISE in contact with an excessive concentration of $Br^-$. If an electrode is poisoned, it can be returned to its original condition by sanding and polishing the crystalline membrane.

Poisoning simply means that the surface has been chemically modified, such as AgBr forming on the surface of a AgCl membrane.

## Liquid Membrane Electrodes

Another class of ion-selective electrodes uses a hydrophobic membrane that contains a liquid organic complexing agent that reacts selectively with the analyte. Three types of organic complexing agents have been used: cation exchangers, anion exchangers, and neutral ionophores. A membrane potential exists if the analyte's activity is different on the two sides of the membrane. Current is carried through the membrane by the analyte.

An ionophore is a ligand whose exterior is hydrophobic and whose interior is hydrophilic. The crown ether shown here is one example of a neutral ionophore.



One example of a liquid-based ion-selective electrode is that for $Ca^{2+}$, which uses a porous plastic membrane saturated with the cation exchanger di-(*n*-decyl) phosphate. As shown in Figure 23.3.5, the membrane is placed at the end of a non-conducting cylindrical tube and is in contact with two reservoirs. The outer reservoir contains di-(*n*-decyl) phosphate in di-*n*-octylphenylphosphonate, which soaks into the porous membrane. The inner reservoir contains a standard aqueous solution of $Ca^{2+}$ and a Ag/AgCl reference electrode. Calcium ion-selective electrodes also are available in which the di-(*n*-decyl) phosphate is immobilized in a polyvinyl chloride (PVC) membrane that eliminates the need for the outer reservoir.

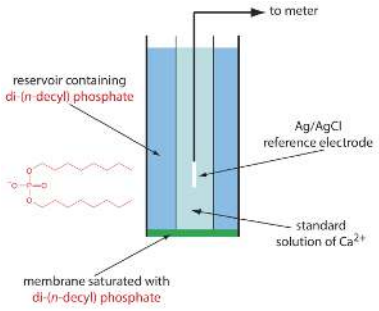



Figure 23.3.5. Schematic diagram showing a liquid-based ion-selective electrode for $Ca^{2+}$. The structure of the cation exchanger, di-(*n*-decyl) phosphate, is shown in red.

The membrane potential for the $Ca^{2+}$ ISE develops as the result of a difference in the extent of the complexation reaction

$$Ca^{2+}(aq) + 2\,(C_{10}H_{21}O)_2\,PO_2^-(mem) \rightleftharpoons Ca\,[(C_{10}H_{21}O)_2\,PO_2]_2\,(mem) \tag{23.3.14}$$

on the two sides of the membrane, where (*mem*) indicates a species that is present in the membrane. The cell potential for the $Ca^{2+}$ ion-selective electrode is

$$E_{cell} = K + \frac{0.05916}{2}\log a_{Ca^{2+}} \tag{23.3.15}$$

The selectivity of this electrode for $Ca^{2+}$ is very good, with only $Zn^{2+}$ showing greater selectivity.

Table 23.3.3 lists the properties of several liquid-based ion-selective electrodes. An electrode using a liquid reservoir can be stored in a dilute solution of analyte and needs no additional conditioning before use. The lifetime of an electrode with a PVC membrane, however, is proportional to its exposure to aqueous solutions. For this reason these electrodes are best stored by covering the membrane with a cap along with a small amount of wetted gauze to maintain a humid environment. Before using the electrode it is conditioned in a solution of analyte for 30–60 minutes.

Table 23.3.3. Representative Examples of Liquid-Based Ion-Selective Electrodes

| analyte | membrane composition | selectivity coefficients |
|---|---|---|
| $Ca^{2+}$ | di-(*n*-decyl) phosphate in PVC | $K_{Ca^{2+}/Zn^{2+}} = 1 - 5$<br>$K_{Ca^{2+}/Al^{3+}} = 0.90$<br>$K_{Ca^{2+}/Mn^{2+}} = 0.38$<br>$K_{Ca^{2+}/Cu^{2+}} = 0.070$<br>$K_{Ca^{2+}/Mg^{2+}} = 0.032$ |
| $K^+$ | valinomycin in PVC | $K_{K^+/Rb^+} = 1.9$<br>$K_{K^+/Cs^+} = 0.38$<br>$K_{K^+/Li^+} = 10^{-4}$ |
| $Li^+$ | ETH 149 in PVC | $K_{Li^+/H^+} = 1$<br>$K_{Li^+/Na^+} = 0.03$<br>$K_{Li^+/K^+} = 0.007$ |
| $NH_4^+$ | nonactin and monactin in PVC | $K_{NH_4^+/K^+} = 0.12$<br>$K_{NH_4^+/H^+} = 0.016$<br>$K_{NH_4^+/Li^+} = 0.0042$<br>$K_{NH_4^+/Na^+} = 0.002$ |
| $ClO_3^-$ | $Fe(o\text{-phen})_3^{3+}$ in *p*-nitrocymene with porous membrane | $K_{ClO_4^-/OH^-} = 1$<br>$K_{ClO_4^-/I^-} = 0.012$<br>$K_{ClO_4^-/NO_3^-} = 0.0015$<br>$K_{ClO_4^-/Br^-} = 5.6 \times 10^{-4}$<br>$K_{ClO_4^-/Cl^-} = 2.2 \times 10^{-4}$ |
| $NO_3^-$ | tetradodecyl ammonium nitrate in pVC | $K_{NO_3^-/Cl^-} = 0.006$<br>$K_{NO_3^-/F^-} = 9 \times 10^{-4}$ |

Selectivity coefficients are approximate; values found experimentally may vary substantially from the listed values. See Cammann, K. *Working With Ion-Selective Electrodes*, Springer-Verlag: Berlin, 1977.

This page titled 23.3: Membrane Ion-Selective Electrodes is shared under a CC BY-NC-SA 4.0 license and was authored, remixed, and/or curated by David Harvey.

# 23.4: Molecular-Selective Electrode Systems

The electrodes in Chapter 23.3 are selective toward ions. In this section we consider how we can incorporate an ion-selective electrode into an electrode that responds to neutral species, such as volatile analytes, such as $CO_2$ and $NH_3$, and biochemically important compounds, such as amino acids and urea.

## Gas-Sensing Membrane Electrodes

A number of membrane electrodes respond to the concentration of a dissolved gas. The basic design of a gas-sensing electrode, as shown in Figure 23.4.1, consists of a thin membrane that separates the sample from an inner solution that contains an ion-selective electrode. The membrane is permeable to the gaseous analyte, but impermeable to nonvolatile components in the sample's matrix. The gaseous analyte passes through the membrane where it reacts with the inner solution, producing a species whose concentration is monitored by the ion-selective electrode. For example, in a $CO_2$ electrode, $CO_2$ diffuses across the membrane where it reacts in the inner solution to produce $H_3O^+$.

$$CO_2(aq) + 2H_2O(l) \rightleftharpoons HCO_3^-(aq) + H_3O^+(aq) \tag{23.4.1}$$

The change in the activity of $H_3O^+$ in the inner solution is monitored with a pH electrode, for which the cell potential, from Chapter 23.3, is

$$E_{\text{cell}} = K + 0.05916 \log a_{H^+} \tag{23.4.2}$$

To find the relationship between the activity of $H_3O^+$ in the inner solution and the activity of $CO_2$ in the inner solution we rearrange the equilibrium constant expression for reaction 23.4.1; thus

$$a_{H_3O^+} = K_a \times \frac{a_{CO_2}}{a_{HCO_3^-}} \tag{23.4.3}$$

where $K_a$ is the equilibrium constant. If the activity of $HCO_3^-$ in the internal solution is sufficiently large, then its activity is not affected by the small amount of $CO_2$ that passes through the membrane. Substituting Equation 23.4.3 into Equation 23.4.2 gives

$$E_{\text{cell}} = K' + 0.05916 \log a_{co_2} \tag{23.4.4}$$

where $K'$ is a constant that includes the constant for the pH electrode, the equilibrium constant for reaction 23.4.1 and the activity of $HCO_3^-$ in the inner solution.

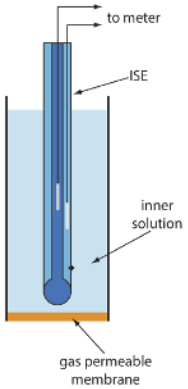



Figure 23.4.1. Schematic diagram of a gas-sensing membrane electrode.

Table 23.4.1 lists the properties of several gas-sensing electrodes. The composition of the inner solution changes with use, and both the inner solution and the membrane must be replaced periodically. Gas-sensing electrodes are stored in a solution similar to the internal solution to minimize their exposure to atmospheric gases.

Table 23.4.1. Representative Examples of Gas-Sensing Electrodes

| analyte | inner solution | reaction in inner solution | ion-selective electrode |
|---|---|---|---|
| $CO_2$ | 10 mM $NaHCO_3$<br>10 mM NaCl | $CO_2(aq) + 2H_2O(l) \rightleftharpoons HCO_3^-(aq) + H_3O^+(aq)$ | glass pH ISE |
| HCN | 10 mM $KAg(CN)_2$ | $HCN(aq) + H_2O(l) \rightleftharpoons CN^-(aq) + H_3O^+(aq)$ | $Ag_2S$ solid-state ISE |
| HF | 1 M $H_3O^+$ | $HF(aq) + H_2O(l) \rightleftharpoons F^-(aq) + H_3O^+(aq)$ | $F^-$ solid-state ISE |
| $H_2S$ | pH 5 citrate buffer | $H_2S(aq) + H_2O(l) \rightleftharpoons HS^-(aq) + H_3O^+(aq)$ | $Ag_2S$ solid state ISE |
| $NH_3$ | 10 mM $NH_4Cl$<br>0.1 M $KNO_3$ | $NH_3(aq) + H_2O(l) \rightleftharpoons NH_4^+(aq) + OH^-(aq)$ | glass pH ISE |
| $NO_2$ | 20 mM $NaNO_2$<br>0.1 M $KNO_3$ | $2NO_2(aq) + 3H_2O(l) \rightleftharpoons NO_3^-(aq) + NO_2^-(aq) + 2H_3O^+(aq)$ | glass pH ISE |
| $SO_2$ | 1 mM $NaHSO_3$<br>pH 5 | $SO_2(aq) + 2H_2O(l) \rightleftharpoons HSO_3^-(aq) + H_3O^+(aq)$ | glass pH ISE |

Source: Cammann, K. *Working With Ion-Selective Electrodes*, Springer-Verlag: Berlin, 1977.

## Biocatalytic Membrane Electrodes

The approach for developing gas-sensing electrodes can be modified to create potentiometric electrodes that respond to a biochemically important species. The most common class of potentiometric biosensors are enzyme electrodes, in which we trap or immobilize an enzyme at the surface of a potentiometric electrode. The analyte's reaction with the enzyme produces a product whose concentration is monitored by the potentiometric electrode. Potentiometric biosensors also have been designed around other biologically active species, including antibodies, bacterial particles, tissues, and hormone receptors.

One example of an enzyme electrode is the urea electrode, which is based on the catalytic hydrolysis of urea by urease

$$CO(NH_2)_2(aq) + 2H_2O(l) \rightleftharpoons 2NH_4^+(aq) + CO_3^-(aq) \tag{23.4.5}$$

Figure 23.4.2 shows one version of the urea electrode, which modifies a gas-sensing $NH_3$ electrode by adding a dialysis membrane that traps a pH 7.0 buffered solution of urease between the dialysis membrane and the gas permeable membrane [(a) Papastathopoulos, D. S.; Rechnitz, G. A. *Anal. Chim. Acta* **1975**, *79*, 17–26; (b) Riechel, T. L. *J. Chem. Educ*. **1984**, *61*, 640–642]. An $NH_3$ electrode, as shown in Table 23.4.1, uses a gas-permeable membrane and a glass pH electrode. The $NH_3$ diffuses across the membrane where it changes the pH of the internal solution.

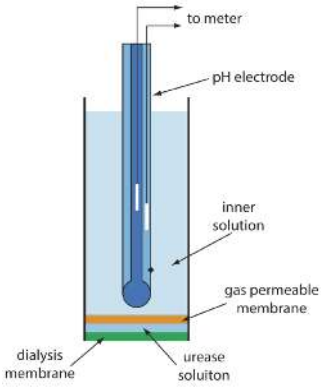



Figure 23.4.2. Schematic diagram showing an enzyme-based potentiometric biosensor for urea. A solution of the enzyme urease is trapped between a dialysis membrane and a gas permeable membrane. Urea diffuses across the dialysis membrane and reacts with urease, producing $NH_3$ that diffuses across the gas permeable membrane. The resulting change in the internal solution's pH is measured with the pH electrode.

When immersed in the sample, urea diffuses through the dialysis membrane where it reacts with the enzyme urease to form the ammonium ion, $NH_4^+$, which is in equilibrium with $NH_3$.

$$NH_4^+(aq) + H_2O(l) \rightleftharpoons H_3O^+(aq) + NH_3(aq) \tag{23.4.6}$$

The $NH_3$, in turn, diffuses through the gas permeable membrane where a pH electrode measures the resulting change in pH. The electrode's response to the concentration of urea is

$$E_{cell} = K - 0.05916 \log a_{urea} \tag{23.4.7}$$

Another version of the urea electrode (Figure 23.4.3) immobilizes the enzyme urease in a polymer membrane formed directly on the tip of a glass pH electrode [Tor, R.; Freeman, A. *Anal. Chem.* **1986**, *58*, 1042–1046]. In this case the response of the electrode is

$$pH = K a_{urea} \tag{23.4.8}$$

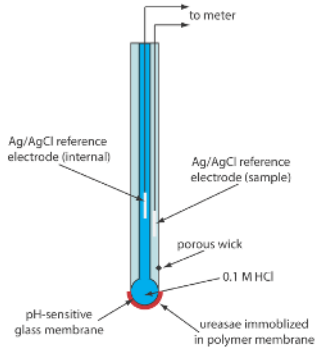



Figure 23.4.3. Schematic diagram of an enzyme-based potentiometric biosensor for urea in which urease is immobilized in a polymer membrane coated onto the pH-sensitive glass membrane of a pH electrode.

Few potentiometric biosensors are available commercially. As shown in Figure 23.4.2 and Figure 23.4.3, however, it is possible to convert an ion-selective electrode or a gas-sensing electrode into a biosensor. Several representative examples are described in Table 23.4.2, and additional examples can be found in this chapter's additional resources.

Table 23.4.2. Representative Examples of Potentiometric Biosensors

| analyte | biologically active phase | substance determined |
|---|---|---|
| 5′-AMP | AMP-deaminase (E) | $NH_3$ |
| L-arginine | arginine and urease (E) | $NH_3$ |
| asparagine | asparaginase (E) | $NH_4^+$ |
| L-cysteine | *Proteus morganii* (B) | $H_2S$ |
| L-glutamate | yellow squash (T) | $CO_2$ |
| L-glutamine | *Sarcina flava* (B) | $NH_3$ |
| oxalate | oxalate decarboxylase (E) | $CO_2$ |
| penicillin | penicllinase (E) | $H_3O^+$ |
| L-phenylalanine | L-amino acid oxidase/horseradish peroxidase (E) | $I^-$ |
| sugars | bacteria from dental plaque (B) | $H_3O^+$ |
| urea | urease (E) | $NH_3$ or $H_3O^+$ |

Source: Complied from Cammann, K. *Working With Ion-Selective Electrodes*, Springer-Verlag: Berlin, 1977 and Lunte, C. E.; Heineman, W. R. “Electrochemical techniques in Bioanalysis,” in Steckham, E. ed. *Topics in Current Chemistry*, Vol. 143, Springer-Verlag: Berlin, 1988, p.8.
Abbreviations for biologically active phase: E = enzyme; B = bacterial particle; T = tissue.

This page titled 23.4: Molecular-Selective Electrode Systems is shared under a CC BY-NC-SA 4.0 license and was authored, remixed, and/or curated by David Harvey.

# 23.5: Instruments for Measuring Cell Potentials

To measure the potential of an electrochemical cell in a way that draws essentially no current we use a potentiometer. To help us understand how a potentiometer accomplishes this, *we will describe the instrument as if the analyst is operating it manually*. To do so the analyst observes a change in the current or the potential and manually adjusts the instrument's settings to maintain the desired experimental conditions. It is important to understand that modern electrochemical instruments provide an automated, electronic means for controlling and measuring current and potential, and that they do so by using very different electronic circuitry than that described here.

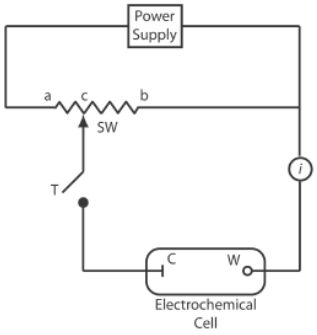



Figure 23.5.1. Schematic diagram of a manual potentiometer: C is the reference electrode; W is the working electrode; SW is a slide-wire resistor; T is a tap key and *i* is an ammeter for measuring current.

Figure 23.5.1 shows a schematic diagram for a manual potentiometer that consists of a power supply, an electrochemical cell with a working electrode and a counter electrode, an ammeter to measure the current that passes through the electrochemical cell, an adjustable, slide-wire resistor, and a tap key for closing the circuit through the electrochemical cell. Using Ohm's law, the current in the upper half of the circuit is

$$i_{\text{upper}} = \frac{E_{\text{PS}}}{R_{ab}} \tag{23.5.1}$$

where $E_{\text{PS}}$ is the power supply's potential, and $R_{ab}$ is the resistance between points *a* and *b* of the slide-wire resistor. In a similar manner, the current in the lower half of the circuit is

$$i_{\text{lower}} = \frac{E_{\text{cell}}}{R_{cb}} \tag{23.5.2}$$

where $E_{\text{cell}}$ is the potential difference between the working electrode and the counter electrode, and $R_{cb}$ is the resistance between the points *c* and *b* of the slide-wire resistor. When $i_{\text{upper}} = i_{\text{lower}} = 0$, no current flows through the ammeter and the potential of the electrochemical cell is

$$E_{\text{coll}} = \frac{R_{cb}}{R_{ab}} \times E_{\text{PS}} \tag{23.5.3}$$

To determine $E_{\text{cell}}$ we briefly press the tap key and observe the current at the ammeter. If the current is not zero, then we adjust the slide wire resistor and remeasure the current, continuing this process until the current is zero. When the current is zero, we use Equation 23.5.3 to calculate $E_{\text{cell}}$.

Using the tap key to briefly close the circuit through the electrochemical cell minimizes the current that passes through the cell and limits the change in the electrochemical cell's composition. For example, passing a current of $10^{-9}$ A through the electrochemical cell for 1 s changes the concentrations of species in the cell by approximately $10^{-14}$ moles.

$$10^{-9}\ \text{A} = 10^{-9}\ \text{C/s} \tag{23.5.4}$$

$$10^{-9}\ \text{C/s} \times 1\ \text{s} \times \frac{1\ \text{mol}}{96485\text{C}} = 1.0 \times 10^{-14}\ \text{mol} \tag{23.5.5}$$

Of course, trying to measure a potential in this way is tedious. Modern potentiometers use operational amplifiers to create a high-impedance voltmeter that measures the potential while drawing a current of less than $10^{-9}$ A. The relative error, $E_r$, in the measured

potential

$$E_r = \frac{R_{\text{cell}}}{R_{\text{meter}} + R_{\text{cell}}} \tag{23.5.6}$$

where $R_{\text{cell}}$ is the resistance of the solution in the electrochemical cell and $R_{\text{meter}}$ is the resistance of the meter. For a solution with a resistance of $10\text{M}\Omega$ to achieve a relative error of $-0.1\%)$ or $-0.001$ requires an $R_{\text{meter}}$ of

$$-0.001 = \frac{-10\ \text{M}\Omega}{R_{\text{meter}} + 10\ \text{M}\Omega}$$

$$-0.001 \times R_{\text{meter}} - 0.01 = -10\ \text{M}\Omega$$

$$-0.001 \times R_{\text{meter}} = -9.990\ \text{M}\Omega$$

$$R_{\text{meter}} = 9990\ \text{M}\Omega$$

---

This page titled 23.5: Instruments for Measuring Cell Potentials is shared under a CC BY-NC-SA 4.0 license and was authored, remixed, and/or curated by David Harvey.

# 23.6: Quantitative Potentiometry

The most important application of potentiometry is determining the concentration of an analyte in solution. Most potentiometric electrodes are selective toward the free, uncomplexed form of the analyte, and do not respond to any of the analyte's complexed forms. This selectivity provides potentiometric electrodes with a significant advantage over other quantitative methods of analysis if we need to determine the concentration of free ions. For example, calcium is present in urine both as free $Ca^{2+}$ ions and as protein-bound $Ca^{2+}$ ions. If we analyze a urine sample using atomic absorption spectroscopy, the signal is propor- tional to the total concentration of $Ca^{2+}$ because both free and bound calcium are atomized. Analyzing urine with a $Ca^{2+}$ ISE, however, gives a signal that is a function of only free $Ca^{2+}$ ions because the protein-bound $Ca^{2+}$ can not interact with the electrode's membrane. In this section, we consider several important aspects of quantiative potentiometry.

## The Relationship Between Concentration and Potential

In Chapter 23.3, we showed that the potential of an ion-selective electrode for an ion with a charge of *z* is

$$E_{\text{cell}} = K + \frac{0.05916}{z} \log \left(a_A\right)_{\text{samp}} \tag{23.6.1}$$

where *K* is a constant that includes the potentials of the ion-selective electrode's internal and external reference electrodes, any asymmetry potential associated with the ion-selective electrode's membrane, and the analyte's activity in the ion-selective electrode's internal solution. Equation 23.6.1 is a general equation and applies to all types of ion-selective electrodes. Note that when the analyte is a cation, an increase in the analyte's activity results in results in an increase in the potential; when the analyte is an anion, which makes *z* a negative number, an increase in the analyte's activity results in a decrease in the potential.

As the concentrations of ions in solution often are reported as pX values, where

$$\text{pX} = -\log a_{\text{X}} \tag{23.6.2}$$

it is convenient to substitute Equation 23.6.2 into Equation 23.6.1

$$E_{\text{cell}} = K - \frac{0.05916}{z}\ \text{pA} \tag{23.6.3}$$

Note that for a cation, an increase in pA results in a decrease in the potential; when the analyte is an anion, an increase in pA results in an increase in the potential.

## Calibrating Potentiometric Electrodes

To use Equation 23.6.3 we need to determine the value of *K*, which we can do using one or more external standards or by the method of standard addition, both of which were covered in Chapter 1.5. One complication, of course, is that potential is a function of the analyte's activity instead of its concentration.

### Activity and Concentration

Equation 23.6.1 is written in terms of the analyte's activity. When we use a potentiometric electrode, however, our goal is to determine the analyte's concentration. As we learned in Chapter 22, an ion's activity is the product of its concentration, $[M^{n+}]$, and a matrix-dependent activity coefficient, $\gamma_{Mn^{n+}}$.

$$a_{M^{n+}} = \left[M^{n+}\right] \gamma_{M^{n+}} \tag{23.6.4}$$

Substituting Equation 23.6.4 into Equation 23.6.1 and rearranging, gives

$$E_{\text{cell}} = K + \frac{0.05916}{n} \log \gamma_{M^{n+}} + \frac{0.05916}{n} \log \left[M^{n+}\right] \tag{23.6.5}$$

We can solve Equation 23.6.5 for the metal ion's concentration if we know the value for its activity coefficient. Unfortunately, if we do not know the exact ionic composition of the sample's matrix—which is the usual situation—then we cannot calculate the value of $\gamma_{Mn^{n+}}$. There is a solution to this dilemma. If we design our system so that the standards and the samples have an identical matrix, then the value of $\gamma_{Mn^{n+}}$ remains constant and Equation 23.6.5 simplifies to

$$E_{\text{cell}} = K' + \frac{0.05916}{n}\log\left[M^{n+}\right] \tag{23.6.6}$$

where $K'$ includes the activity coefficient.

## Calibration Using External Standards

In the absence of interferents, a calibration curve of $E_{\text{cell}}$ versus $\log a_{\text{A}}$, where A is the analyte, is a straight-line. A plot of $E_{\text{cell}}$ versus $\log[A]$, however, may show curvature at higher concentrations of analyte as a result of a matrix-dependent change in the analyte's activity coefficient. To maintain a consistent matrix we add a high concentration of an inert electrolyte to all samples and standards. If the concentration of added electrolyte is sufficient, then the difference between the sample's matrix and the matrix of the standards will not affect the ionic strength and the activity coefficient essentially remains constant. The inert electrolyte added to the sample and the standards is called a total ionic strength adjustment buffer (TISAB).

### Example 23.6.1

The concentration of $Ca^{2+}$ in a water sample is determined using the method of external standards. The ionic strength of the samples and the standards is maintained at a nearly constant level by making each solution 0.5 M in $KNO_3$. The measured cell potentials for the external standards are shown in the following table.

| $[Ca^{2+}]$ (M) | $E_{\text{cell}}$ (V) |
|---|---|
| $1.00 \times 10^{-5}$ | –0.125 |
| $5.00 \times 10^{-5}$ | –0.103 |
| $1.00 \times 10^{-4}$ | –0.093 |
| $5.00 \times 10^{-4}$ | –0.072 |
| $1.00 \times 10^{-3}$ | –0.063 |
| $5.00 \times 10^{-3}$ | –0.043 |
| $1.00 \times 10^{-2}$ | –0.033 |

What is the concentration of $Ca^{2+}$ in a water sample if its cell potential is found to be –0.084 V?

**Solution**

Linear regression gives the calibration curve in Figure 23.6.1, with an equation of

$$E_{\text{cell}} = 0.027 + 0.0303\log\left[Ca^{2+}\right]$$

Substituting the sample's cell potential gives the concentration of $Ca^{2+}$ as $2.17 \times 10^{-4}$ M. Note that the slope of the calibration curve, which is 0.0303, is slightly larger than its ideal value of 0.05916/2 = 0.02958; this is not unusual and is one reason for using multiple standards. One reason that it is not unusual to find that the experimental slope deviates from its ideal value of 0.05916/*n* is that this ideal value assumes that the temperature is 25°C.

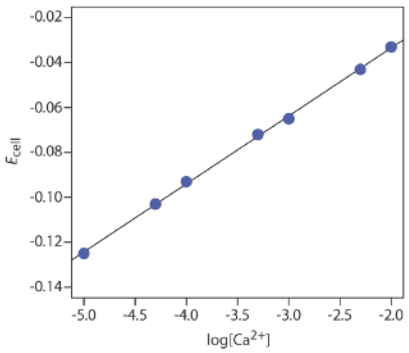



Figure 23.6.1. Calibration curve for the data in Example 23.6.1.

## Calibration Using Standard Additions

Another approach to calibrating a potentiometric electrode is the method of standard additions, which was introduced in Chapter 1.5. First, we transfer a sample with a volume of $V_{samp}$ and an analyte concentration of $C_{samp}$ into a beaker and measure the potential, $(E_{cell})_{samp}$. Next, we make a standard addition by adding to the sample a small volume, $V_{std}$, of a standard that contains a known concentration of analyte, $C_{std}$, and measure the potential, $(E_{cell})_{std}$. If $V_{std}$ is significantly smaller than $V_{samp}$, then we can safely ignore the change in the sample's matrix and assume that the analyte's activity coefficient is constant. Example 23.6.9 demonstrates how we can use a one-point standard addition to determine the concentration of analyte in a sample.

### Example 23.6.2

The concentration of $Ca^{2+}$ in a sample of sea water is determined using a Ca ion-selective electrode and a one-point standard addition. A 10.00-mL sample is transferred to a 100-mL volumetric flask and diluted to volume. A 50.00-mL aliquot of the sample is placed in a beaker with the Ca ISE and a reference electrode, and the potential is measured as –0.05290 V. After adding a 1.00-mL aliquot of a $5.00 \times 10^{-2}$ M standard solution of $Ca^{2+}$ the potential is –0.04417 V. What is the concentration of $Ca^{2+}$ in the sample of sea water?

**Solution**

To begin, we write the Nernst equation before and after adding the standard addition. The cell potential for the sample is

$$(E_{cell})_{samp} = K + \frac{0.05916}{2} \log C_{samp}$$

and that following the standard addition is

$$(E_{cell})_{std} = K + \frac{0.05916}{2} \log \left\{ \frac{V_{samp}}{V_{tot}} C_{samp} + \frac{V_{std}}{V_{tot}} C_{std} \right\}$$

where $V_{tot}$ is the total volume ($V_{samp}$ + $V_{std}$) after the standard addition. Subtracting the first equation from the second equation gives

$$\Delta E = (E_{cell})_{std} - (E_{cell})_{samp} = \frac{0.05916}{2} \log \left\{ \frac{V_{samp}}{V_{tot}} C_{samp} + \frac{V_{std}}{V_{tot}} C_{std} \right\} - \frac{0.05916}{2} \log C_{samp}$$

Rearranging this equation leaves us with

$$\frac{2\Delta E_{cell}}{0.05916} = \log \left\{ \frac{V_{samp}}{V_{tot}} + \frac{V_{std} C_{std}}{V_{tot} C_{samp}} \right\}$$

Substituting known values for $\Delta E$, $V_{samp}$, $V_{std}$, $V_{tot}$ and $C_{std}$,

$$\frac{2 \times \{-0.04417 - (-0.05290)\}}{0.05916} =$$
$$\log \left\{ \frac{50.00 \text{ mL}}{51.00 \text{ mL}} + \frac{(1.00 \text{ mL})(5.00 \times 10^{-2} \text{M})}{(51.00 \text{ mL}) C_{samp}} \right\}$$
$$0.2951 = \log \left\{ 0.9804 + \frac{9.804 \times 10^{-4}}{C_{samp}} \right\}$$

and taking the inverse log of both sides gives

$$1.973 = 0.9804 + \frac{9.804 \times 10^{-4}}{C_{\text{samp}}}$$

Finally, solving for $C_{\text{samp}}$ gives the concentration of $Ca^{2+}$ as $9.88 \times 10^{-4}$ M. Because we diluted the original sample of seawater by a factor of 10, the concentration of $Ca^{2+}$ in the seawater sample is $9.88 \times 10^{-3}$ M.

## The Operational Definition of pH

With the availability of inexpensive glass pH electrodes and pH meters, the determination of pH is one of the most common quantitative analytical measurements. The potentiometric determination of pH, however, is not without complications, several of which we discuss in this section.

One complication is confusion over the meaning of pH [Kristensen, H. B.; Saloman, A.; Kokholm, G. *Anal. Chem.* **1991**, *63*, 885A–891A]. The conventional definition of pH in most general chemistry textbooks is given in terms of the concentration of $H^+$

$$\text{pH} = -\log [H^+] \tag{23.6.7}$$

As we now know, when we measure pH it actually is a measure of the activity of $H^+$.

$$\text{pH} = -\log a_{H^+} \tag{23.6.8}$$

Try this experiment—find several general chemistry textbooks and look up *pH* in each textbook's index. Turn to the appropriate pages and see how it is defined. Next, look up *activity* or *activity coefficient* in each textbook's index and see if these terms are indexed.

Equation 23.6.7 only approximates the true pH. If we calculate the pH of 0.1 M HCl using Equation 23.6.7, we obtain a value of 1.00; the solution's actual pH, as defined by Equation 23.6.8, is 1.1 [Hawkes, S. J. *J. Chem. Educ.* **1994**, *71*, 747–749]. The activity and the concentration of $H^+$ are not the same in 0.1 M HCl because the activity coefficient for $H^+$ is not 1.00 in this matrix. Figure 23.6.2 shows a more colorful demonstration of the difference between activity and concentration.

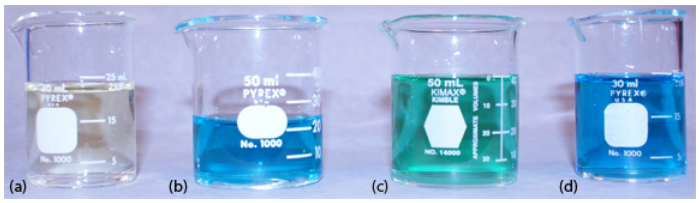



Figure 23.6.2. A demonstration of the difference between activity and concentration using the indicator methyl green. The indicator is pale yellow in its acid form (beaker a: 1.0 M HCl) and is blue in its base form (beaker d: $H_2O$). In 10 mM HCl the indicator is in its base form (beaker b: 20 mL of 10 mM HCl with 3 drops of methyl green). Adding 20 mL of 5 M LiCl to this solution shifts the indicator's color to green (beaker c); although the concentration of HCl is cut in half to 5 mM, the activity of $H^+$ has increased as evidenced by the green color that is intermediate between the indicator's pale yellow, acid form and its blue, base form. The demonstration shown here is adapted from McCarty, C. G.; Vitz, E. "pH Paradoxes: Demonstrating That It Is Not True That pH ≡ –log[$H^+$]," *J. Chem. Educ.* **2006**, *83*, 752–757. This paper provides several additional demonstrations that illustrate the difference between concentration and activity.

A second complication in measuring pH is the uncertainty in the relationship between potential and activity. For a glass membrane electrode, the cell potential, $(E_{\text{cell}})_{\text{samp}}$, for a sample of unknown pH is

$$(E_{\text{cell}})_{\text{samp}} = K - \frac{RT}{F} \ln \frac{1}{a_{H^+}} = K - \frac{2.303RT}{F} \text{pH}_{\text{samp}} \tag{23.6.9}$$

where $K$ includes the potential of the reference electrode, the asymmetry potential of the glass membrane, and any junction potentials in the electrochemical cell. All the contributions to $K$ are subject to uncertainty, and may change from day-to-day, as well as from electrode-to-electrode. For this reason, before using a pH electrode we calibrate it using a standard buffer of known pH. The cell potential for the standard, $(E_{\text{cell}})_{\text{std}}$, is

$$(E_{\text{ccll}})_{\text{std}} = K - \frac{2.303RT}{F}\text{pH}_{\text{std}} \tag{23.6.10}$$

where $\text{pH}_{\text{std}}$ is the standard's pH. Subtracting Equation ??? from Equation 23.6.9 and solving for $\text{pH}_{\text{samp}}$ gives

$$\text{pH}_{\text{samp}} = \text{pH}_{\text{std}} - \frac{\left\{(E_{\text{cell}})_{\text{samp}} - (E_{\text{cell}})_{\text{std}}\right\} F}{2.303RT} \tag{23.6.11}$$

which is the operational definition of pH adopted by the International Union of Pure and Applied Chemistry [Covington, A. K.; Bates, R. B.; Durst, R. A. *Pure & Appl. Chem.* **1985**, *57*, 531–542].

Calibrating a pH electrode presents a third complication because we need a standard with an accurately known activity for $H^+$. Table 23.6.1 provides pH values for several primary standard buffer solutions accepted by the National Institute of Standards and Technology.

Table 23.6.1. pH Values for Selected NIST Primary Standard Buffers

| temp (°C) | saturated (at 25°C) $KHC_4H4O_7$ (tartrate) | 0.05 m $KH_2C_6H_5O_7$ (citrate) | 0.05 m $KHC_8H_4O_4$ (phthlate) | 0.025 m $KH_2PO_4$, 0.025 m $NaHPO_4$ | 0.008695 m $KH_2PO_4$, 0.03043 m $Na_2HPO_4$ | 0.01 m $Na_4B_4O_7$ | 0.025 m $NaHCO_3$, 0.025 m $Na_2CO_3$ |
|---|---|---|---|---|---|---|---|
| 0 | — | 3.863 | 4.003 | 6.984 | 7.534 | 9.464 | 10.317 |
| 5 | — | 3.840 | 3.999 | 6.951 | 7.500 | 9.395 | 10.245 |
| 10 | — | 3.820 | 3.998 | 6.923 | 7.472 | 9.332 | 10.179 |
| 15 | — | 3.802 | 3.999 | 6.900 | 7.448 | 9.276 | 10.118 |
| 20 | — | 3.788 | 4.002 | 6.881 | 7.429 | 9.225 | 10.062 |
| 25 | 3.557 | 3.776 | 4.008 | 6.865 | 7.413 | 9.180 | 10.012 |
| 30 | 3.552 | 3.766 | 4.015 | 6.854 | 7.400 | 9.139 | 9.966 |
| 35 | 3.549 | 3.759 | 4.024 | 6.844 | 7.389 | 9.012 | 9.925 |
| 40 | 3.547 | 3.753 | 4.035 | 6.838 | 7.380 | 9.068 | 9.889 |
| 45 | 3.547 | 3.750 | 4.047 | 6.834 | 7.373 | 9.038 | 9.856 |
| 50 | 3.549 | 3.749 | 4.060 | 6.833 | 7.367 | 9.011 | 9.828 |

Source: Values taken from Bates, R. G. *Determination of pH: Theory and Practice*, 2nd ed. Wiley: New York, 1973. See also Buck, R. P., et. al."Measurement of pH. Definition, Standards, and Procedures," *Pure. Appl. Chem.* **2002**, *74*, 2169–2200. All concentrations are molal (m).

To standardize a pH electrode using two buffers, choose one near a pH of 7 and one that is more acidic or basic depending on your sample's expected pH. Rinse your pH electrode in deionized water, blot it dry with a laboratory wipe, and place it in the buffer with the pH closest to 7. Swirl the pH electrode and allow it to equilibrate until you obtain a stable reading. Adjust the "Standardize" or "Calibrate" knob until the meter displays the correct pH. Rinse and dry the electrode, and place it in the second buffer. After the electrode equilibrates, adjust the "Slope" or "Temperature" knob until the meter displays the correct pH.

Some pH meters can compensate for a change in temperature. To use this feature, place a temperature probe in the sample and connect it to the pH meter. Adjust the "Temperature" knob to the solution's temperature and calibrate the pH meter using the "Calibrate" and "Slope" controls. As you are using the pH electrode, the pH meter compensates for any change in the sample's temperature by adjusting the slope of the calibration curve using a Nernstian response of $2.303RT/F$.

This page titled 23.6: Quantitative Potentiometry is shared under a CC BY-NC-SA 4.0 license and was authored, remixed, and/or curated by David Harvey.

# CHAPTER OVERVIEW

## 24: Coulometry

In a potentiometric method of analysis we determine an analyte's concentration by measuring the potential of an electrochemical cell under static conditions in which no current flows and the concentrations of species in the electrochemical cell remain fixed. Dynamic techniques, in which current passes through the electrochemical cell and concentrations change, also are important electrochemical methods of analysis. In this Chapter we consider coulometry. Voltammetry and amperometry are covered in Chapter 25.


24.1: Introduction to Coulometry

24.2: Controlled-Potential Coulometry

24.3: Controlled-Current Coulometry


---

This page titled 24: Coulometry is shared under a CC BY-NC-SA 4.0 license and was authored, remixed, and/or curated by David Harvey.

# 24.1: Introduction to Coulometry

Coulometry is based on an exhaustive electrolysis of the analyte. By exhaustive we mean the analyte is oxidized or reduced completely at the working electrode, or reacts completely with a reagent generated at the working electrode. There are two forms of coulometry: controlled-potential coulometry, in which we apply a constant potential to the electrochemical cell, and controlled-current coulometry, in which we pass a constant current through the electrochemical cell.

During an electrolysis, the total charge, $Q$, in coulombs, that passes through the electrochemical cell is proportional to the absolute amount of analyte by Faraday's law

$$Q = nFN_A \tag{24.1.1}$$

where $n$ is the number of electrons per mole of analyte, $F$ is Faraday's constant (96 487 C $mol^{-1}$), and $N_A$ is the moles of analyte. A coulomb is equivalent to an A•sec; thus, for a constant current, $i$, the total charge is

$$Q = it_e \tag{24.1.2}$$

where $t_e$ is the electrolysis time. If the current varies with time, as it does in controlled-potential coulometry, then the total charge is

$$Q = \int_0^{t_e} i(t)dt \tag{24.1.3}$$

In coulometry, we monitor current as a function of time and use either Equation 24.1.2 or Equation 24.1.3 to calculate $Q$. Knowing the total charge, we then use Equation 24.1.1 to determine the moles of analyte. To obtain an accurate value for $N_A$, all the current must oxidize or reduce the analyte; that is, coulometry requires 100% current efficiency or an accurate measurement of the current efficiency using a standard.

> Current efficiency is the percentage of current that actually leads to the analyte's oxidation or reduction.

This page titled 24.1: Introduction to Coulometry is shared under a CC BY-NC-SA 4.0 license and was authored, remixed, and/or curated by David Harvey.

# 24.2: Controlled-Potential Coulometry

The easiest way to ensure 100% current efficiency is to hold the working electrode at a constant potential where the analyte is oxidized or reduced completely and where no potential interfering species are oxidized or reduced. As electrolysis progresses, the analyte's concentration and the current decrease. The resulting current-versus-time profile for controlled-potential coulometry is shown in Figure 24.2.1. Integrating the area under the curve from $t = 0$ to $t = t_e$ gives the total charge. In this section we consider the experimental parameters and instrumentation needed to develop a controlled-potential coulometric method of analysis and its applications.

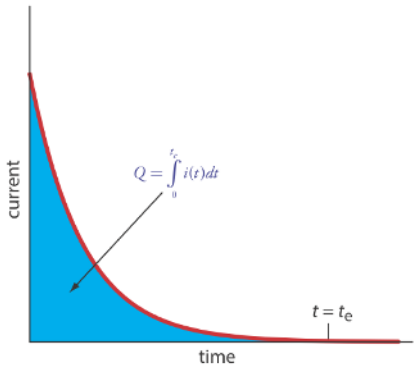



Figure 24.2.1. Current versus time for a controlled-potential coulometric analysis. The measured current is shown by the red curve. The integrated area under the curve, shown in blue, is the total charge.

## Selecting a Constant Potential

To understand how an appropriate potential for the working electrode is selected, let's develop a constant-potential coulometric method for $Cu^{2+}$ based on its reduction to copper metal at a Pt working electrode.

$$Cu^{2+}(aq) + 2e^- \rightleftharpoons Cu(s) \tag{24.2.1}$$

Figure 24.2.2 shows the three reduction reactions that can take place in an aqueous solution of $Cu^{2+}$ and their standard state reduction potentials: the reduction of $O_2$ to $H_2O$, the reduction of $Cu^{2+}$ to Cu, and the reduction of $H_3O^+$ to $H_2$. From the diagram we know that reaction 24.2.1 is favored when the working electrode's potential is more negative than +0.342 V versus the standard hydrogen electrode. To ensure a 100% current efficiency, however, the potential must be sufficiently more positive than +0.000 V so that the reduction of $H_3O^+$ to $H_2$ does not contribute significantly to the total current flowing through the electrochemical cell.

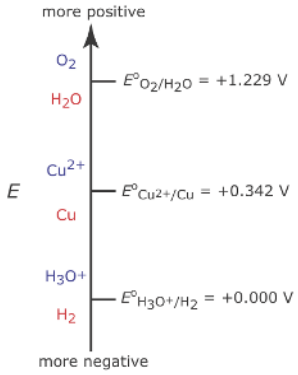



Figure 24.2.2. Standard state reduction potentials for an aqueous solution of $Cu^{2+}$ showing for the reductions of $O_2$ to $H_2O$, of $Cu^{2+}$ to Cu, and of $H_3O^+$ to $H_2$. For each reaction, the oxidized species is in blue and the reduced species is in red.

We can use the Nernst equation for reaction 24.2.1 to estimate the minimum potential for quantitatively reducing $Cu^{2+}$.

$$E = E^\circ_{Cu^{2+}/Cu} - \frac{0.05916}{2} \log \frac{1}{[Cu^{2+}]} \tag{24.2.2}$$

So why are we using the concentration of $Cu^{2+}$ in Equation 24.2.2 instead of its activity as we did in Chapter 23 when we considered potentiometry? In potentiometry we used activity because we used $E_{cell}$ to determine the analyte's concentration. Here we use the Nernst equation to help us select an appropriate potential. Once we identify a potential, we can adjust its value as needed to ensure a quantitative reduction of $Cu^{2+}$. In addition, in coulometry the analyte's concentration is given by the total charge, not the applied potential.

If we define a quantitative electrolysis as one in which we reduce 99.99% of $Cu^{2+}$ to Cu, then the concentration of $Cu^{2+}$ at $t_e$ is

$$\left[Cu^{2+}\right]_{t_e} = 0.0001 \times \left[Cu^{2+}\right]_0 \tag{24.2.3}$$

where $[Cu^{2+}]_0$ is the initial concentration of $Cu^{2+}$ in the sample. Substituting Equation 24.2.3 into Equation 24.2.2 allows us to calculate the desired potential.

$$E = E^\circ_{Cu^{2+}/Cu} - \frac{0.05916}{2}\log\frac{1}{0.0001 \times \left[Cu^{2+}\right]} \tag{24.2.4}$$

If the initial concentration of $Cu^{2+}$ is $1.00 \times 10^{-4}$ M, for example, then the working electrode's potential must be more negative than +0.105 V to quantitatively reduce $Cu^{2+}$ to Cu. Note that at this potential $H_3O^+$ is not reduced to $H_2$, maintaining 100% current efficiency.

Many controlled-potential coulometric methods for $Cu^{2+}$ use a potential that is negative relative to the standard hydrogen electrode—see, for example, Rechnitz, G. A. *Controlled-Potential Analysis*, Macmillan: New York, 1963, p.49. Based on Figure 24.2.2 you might expect that applying a potential <0.000 V will partially reduce $H_3O^+$ to $H_2$, resulting in a current efficiency that is less than 100%. The reason we can use such a negative potential is that the reaction rate for the reduction of $H_3O^+$ to $H_2$ is very slow at a Pt electrode. This results in a significant overpotential—the need to apply a potential more positive or a more negative than that predicted by thermodynamics—which shifts $E^o$ for the $H_3O^+/H_2$ redox couple to a more negative value.

## Minimizing Electrolysis Time

In controlled-potential coulometry, as shown in Figure 24.2.1, the current decreases over time. As a result, the rate of electrolysis—recall from Chapter 22 that current is a measure of rate—becomes slower and an exhaustive electrolysis of the analyte may require a long time. Because time is an important consideration when designing an analytical method, we need to consider the factors that affect the analysis time.

We can approximate how the current changes as a function of time (Figure 24.2.1) as an exponential decay; thus, the current at time $t$ is

$$i_t = i_0 e^{-kt} \tag{24.2.5}$$

where $i_0$ is the current at $t = 0$ and $k$ is a rate constant that is directly proportional to the area of the working electrode and the rate of stirring, and that is inversely proportional to the volume of solution. For an exhaustive electrolysis in which we oxidize or reduce 99.99% of the analyte, the current at the end of the analysis, $t_e$, is

$$i_{t_e} \leq 0.0001 \times i_0 \tag{24.2.6}$$

Substituting Equation 24.2.6 into Equation 24.2.5 and solving for $t_e$ gives the minimum time for an exhaustive electrolysis as

$$t_e = -\frac{1}{k} \times \ln(0.0001) = \frac{9.21}{k} \tag{24.2.7}$$

From this equation we see that a larger value for $k$ reduces the analysis time. For this reason we usually carry out a controlled-potential coulometric analysis in a small volume electrochemical cell, using an electrode with a large surface area, and with a high stirring rate. A quantitative electrolysis typically requires approximately 30–60 min, although shorter or longer times are possible.

## Instrumentation

We can use the three-electrode potentiostat in Figure (24.2.3) to set and control the potential in controlled-potential coulometry . The potential of the working electrode is measured relative to a constant-potential reference electrode that is connected to the working electrode through a high-impedance potentiometer. To set the working electrode's potential we adjust the slide wire resistor that is connected to the auxiliary electrode. If the working electrode's potential begins to drift, we adjust the slide wire resistor to return the potential to its initial value. The current flowing between the auxiliary electrode and the working electrode is measured with an ammeter. Of course, a modern potentionstat uses operational amplifiers to maintain the constant potential without our intervention.

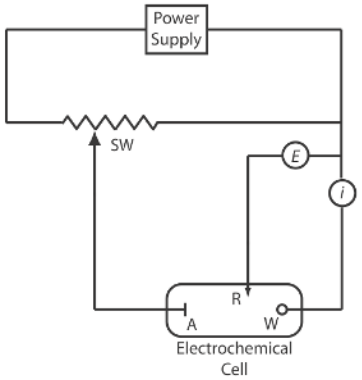



Figure 24.2.3. Schematic diagram for a manual potentiostat: W is the working electrode; A is the auxiliary electrode; R is the reference electrode; SW is a slide-wire resistor, *E* is a high-impendance potentiometer; and *i* is an ammeter.

The working electrode is usually one of two types: a cylindrical Pt electrode manufactured from platinum-gauze (Figure 24.2.4), or a Hg pool electrode. The large overpotential for the reduction of $H_3O^+$ at Hg makes it the electrode of choice for an analyte that requires a negative potential. For example, a potential more negative than –1 V versus the SHE is feasible at a Hg electrode—but not at a Pt electrode—even in a very acidic solution. Because mercury is easy to oxidize, it is less useful if we need to maintain a potential that is positive with respect to the SHE. Platinum is the working electrode of choice when we need to apply a positive potential.



Figure 24.2.4. Example of a cylindrical Pt-gauze electrode used in controlled-potential coulometry. The electrode shown here has a diameter of 13 mm and a height of 48 mm, and was fashioned from Pt wire with a diameter of approximately 0.15 mm. The electrode's surface has 360 openings/$cm^2$ and a total surface area of approximately 40 $cm^2$.

The auxiliary electrode, which often is a Pt wire, is separated by a salt bridge from the analytical solution. This is necessary to prevent the electrolysis products generated at the auxiliary electrode from reacting with the analyte and interfering in the analysis. A saturated calomel or Ag/AgCl electrode serves as the reference electrode.

The other essential need for controlled-potential coulometry is a means for determining the total charge. One method is to monitor the current as a function of time and determine the area under the curve, as shown in Figure 24.2.1. Modern instruments use electronic integration to monitor charge as a function of time. The total charge at the end of the electrolysis is read directly from a digital readout.

## Electrogravimetry

If the product of controlled-potential coulometry forms a deposit on the working electrode, then we can use the change in the electrode's mass as the analytical signal. For example, if we apply a potential that reduces $Cu^{2+}$ to Cu at a Pt working electrode, the difference in the electrode's mass before and after electrolysis is a direct measurement of the amount of copper in the sample. An analytical technique that uses mass as a signal a gravimetric technique; thus, we call this electrogravimetry.

## Quantitative Applications

The majority of controlled-potential coulometric analyses involve the determination of inorganic cations and anions, including trace metals and halides ions. Table 24.2.1 summarizes several of these methods.

Table 24.2.1. Representative Controlled-Potential Coulometric Analyses for Inorganic Ions

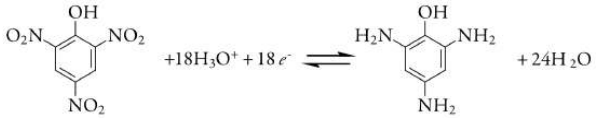
| analyte | electrolytic reaction | electrode |
|---|---|---|
| antimony | $\mathrm{Sb(III)} + 3e^- \rightleftharpoons \mathrm{Sb}$ | Pt |
| arsenic | $\mathrm{As(III)} \rightleftharpoons \mathrm{As(V)} + 2e^-$ | Pt |
| cadmium | $\mathrm{Cd(II)} + 2e^- \rightleftharpoons \mathrm{Cd}$ | Pt or Hg |
| cobalt | $\mathrm{Co(II)} + 2e^- \rightleftharpoons \mathrm{Co}$ | Pt or Hg |
| copper | $\mathrm{Cu(II)} + 2e^- \rightleftharpoons \mathrm{Cu}$ | Pt or Hg |
| halides ($X^-$) | $\mathrm{Ag} + \mathrm{X}^- \rightleftharpoons \mathrm{AgX} + e^-$ | Ag |
| iron | $\mathrm{Fe(II)} \rightleftharpoons \mathrm{Fe(III)} + e^-$ | Pt |
| lead | $\mathrm{Pb(II)} + 2e^- \rightleftharpoons \mathrm{Pb}$ | Pt or Hg |
| nickel | $\mathrm{Ni(II)} + 2e^- \rightleftharpoons \mathrm{Ni}$ | Pt or Hg |
| plutonium | $\mathrm{Pu(III)} \rightleftharpoons \mathrm{Pu(IV)} + e^-$ | Pt |
| silver | $\mathrm{Ag(I)} + 1e^- \rightleftharpoons \mathrm{Ag}$ | Pt |
| tin | $\mathrm{Sn(II)} + 2e^- \rightleftharpoons \mathrm{Sn}$ | Pt |
| uranium | $\mathrm{U(VI)} + 2e^- \rightleftharpoons \mathrm{U(IV)}$ | Pt or Hg |
| zinc | $\mathrm{Zn(II)} + 2e^- \rightleftharpoons \mathrm{Zn}$ | Pt or Hg |

Source: Rechnitz, G. A. *Controlled-Potential Analysis*, Macmillan: New York, 1963.
Electrolytic reactions are written in terms of the change in the analyte's oxidation state. The actual species in solution depends on the analyte.

The ability to control selectivity by adjusting the working electrode's potential makes controlled-potential coulometry particularly useful for the analysis of alloys. For example, we can determine the composition of an alloy that contains Ag, Bi, Cd, and Sb by dissolving the sample and placing it in a matrix of 0.2 M $H_2SO_4$ along with a Pt working electrode and a Pt counter electrode. If we apply a constant potential of +0.40 V versus the SCE, Ag(I) deposits on the electrode as Ag and the other metal ions remain in solution. When electrolysis is complete, we use the total charge to determine the amount of silver in the alloy. Next, we shift the working electrode's potential to –0.08 V versus the SCE, depositing Bi on the working electrode. When the coulometric analysis for bismuth is complete, we determine antimony by shifting the working electrode's potential to –0.33 V versus the SCE, depositing Sb. Finally, we determine cadmium following its electrodeposition on the working electrode at a potential of –0.80 V versus the SCE.

We also can use controlled-potential coulometry for the quantitative analysis of organic compounds, although the number of applications is significantly less than that for inorganic analytes. One example is the six-electron reduction of a nitro group, $–NO_2$,

to a primary amine, $-NH_2$, at a mercury electrode. Solutions of picric acid—also known as 2,4,6-trinitrophenol, or TNP, a close relative of TNT—is analyzed by reducing it to triaminophenol.



Another example is the successive reduction of trichloroacetate to dichloroacetate, and of dichloroacetate to monochloroacetate

$$Cl_3CCOO^-(aq) + H_3O^+(aq) + 2e^- \rightleftharpoons Cl_2HCCOO^-(aq) + Cl^-(aq) + H_2O(l)$$

$$Cl_2HCCOO^-(aq) + H_3O^+(aq) + 2e^- \rightleftharpoons ClH_2CCOO^-(aq) + Cl^-(aq) + H_2O(l)$$

We can analyze a mixture of trichloroacetate and dichloroacetate by selecting an initial potential where only the more easily reduced trichloroacetate reacts. When its electrolysis is complete, we can reduce dichloroacetate by adjusting the potential to a more negative potential. The total charge for the first electrolysis gives the amount of trichloroacetate, and the difference in total charge between the first electrolysis and the second electrolysis gives the amount of dichloroacetate.

### Example 24.2.1

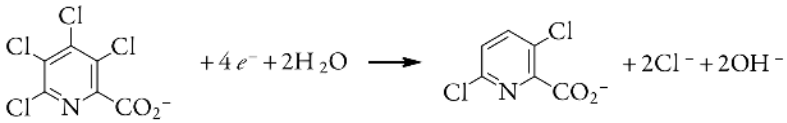
One useful application of controlled-potential coulometry is determining the number of electrons involved in a redox reaction. To make the determination, we complete a controlled-potential coulometric analysis using a known amount of a pure compound. The total charge at the end of the electrolysis is used to determine the value of *n* using Faraday's law. A 0.3619-g sample of tetrachloropicolinic acid, $C_6HNO_2Cl_4$, is dissolved in distilled water, transferred to a 1000-mL volumetric flask, and diluted to volume. An exhaustive controlled-potential electrolysis of a 10.00-mL portion of this solution at a spongy silver cathode requires 5.374 C of charge. What is the value of *n* for this reduction reaction?

#### Solution

The 10.00-mL portion of sample contains 3.619 mg, or $1.39 \times 10^{-5}$ mol of tetrachloropicolinic acid. Solving for *n* gives

$$n = \frac{Q}{FN_A} = \frac{5.374 \text{ C}}{(96478 \text{ C/mol } e^-)\left(1.39 \times 10^{-5} \text{ mol } C_6HNO_2Cl_4\right)} = 4.01 \text{ mol e}^-/\text{mol } C_6HNO_2Cl_4$$

Thus, reducing a molecule of tetrachloropicolinic acid requires four electrons. The overall reaction, which results in the selective formation of 3,6-dichloropicolinic acid, is



This page titled 24.2: Controlled-Potential Coulometry is shared under a CC BY-NC-SA 4.0 license and was authored, remixed, and/or curated by David Harvey.

# 24.3: Controlled-Current Coulometry

A second approach to coulometry is to use a constant current in place of a constant potential, which results in the current-versus-time profile shown in Figure 24.3.1. Controlled-current coulometry has two advantages over controlled-potential coulometry. First, the analysis time is shorter because the current does not decrease over time. A typical analysis time for controlled-current coulometry is less than 10 min, compared to approximately 30–60 min for controlled-potential coulometry. Second, because the total charge is simply the product of current and time, there is no need to integrate the current-time curve in Figure 24.3.1.

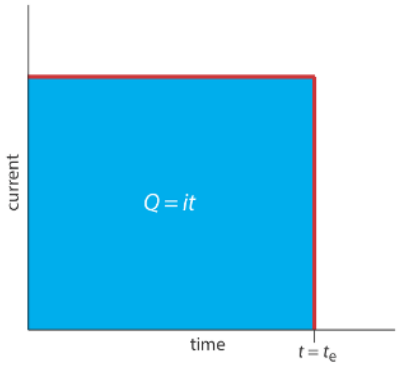



Figure 24.3.1. Current versus time for a controlled-current coulometric analysis. The measured current is shown by the red curve. The integrated area under the curve, shown in blue, is the total charge.

Using a constant current presents us with two important experimental problems. First, during electrolysis the analyte's concentration—and, therefore, the current that results from its oxidation or reduction—decreases continuously. To maintain a constant current we must allow the potential to change until another oxidation reaction or reduction reaction occurs at the working electrode. Unless we design the system carefully, this secondary reaction results in a current efficiency that is less than 100%. The second problem is that we need a method to determine when the analyte's electrolysis is complete. In a controlled-potential coulometric analysis we know that electrolysis is complete when the current reaches zero, or when it reaches a constant background or residual current. In a controlled-current coulometric analysis, however, current continues to flow even when the analyte's electrolysis is complete. A suitable method for determining the reaction's endpoint, $t_e$, is needed.

## Maintaining Current Efficiency

To illustrate why a change in the working electrode's potential may result in a current efficiency of less than 100%, let's consider the coulometric analysis for $Fe^{2+}$ based on its oxidation to $Fe^{3+}$ at a Pt working electrode in 1 M $H_2SO_4$.

$$Fe^{2+}(aq) \rightleftharpoons Fe^{3+}(aq) + e^- \tag{24.3.1}$$

Figure 24.3.2 shows the relevant potentials for this system. At the beginning of the analysis, the potential of the working electrode remains nearly constant at a level near its initial value.

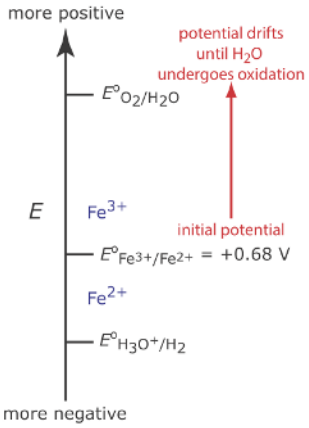



Figure 24.3.2. Potential for the constant-current coulometric analysis of $Fe^{2+}$. The red arrow and text shows how the potential drifts to more positive values, decreasing the current efficiency.

As the concentration of $Fe^{2+}$ decreases and the concentration of $Fe^{3+}$ increases, the working electrode's potential shifts toward more positive values until the oxidation of $H_2O$ begins.

$$2H_2O(l) \rightleftharpoons O_2(g) + 4H^+(aq) + 4e^- \tag{24.3.2}$$

Because a portion of the total current comes from the oxidation of $H_2O$, the current efficiency for the analysis is less than 100% and we cannot use the equation $Q = it$ to determine the amount of $Fe^{2+}$ in the sample.

Although we cannot prevent the potential from drifting until another species undergoes oxidation, we can maintain a 100% current efficiency if the product of that secondary oxidation reaction both rapidly and quantitatively reacts with the remaining $Fe^{2+}$. To accomplish this we add an excess of $Ce^{3+}$ to the analytical solution. As shown in Figure 24.3.3, when the potential of the working electrode shifts to a more positive potential, $Ce^{3+}$ begins to oxidize to $Ce^{4+}$

$$Ce^{3+}(aq) \rightleftharpoons Ce^{4+}(aq) + e^- \tag{24.3.3}$$

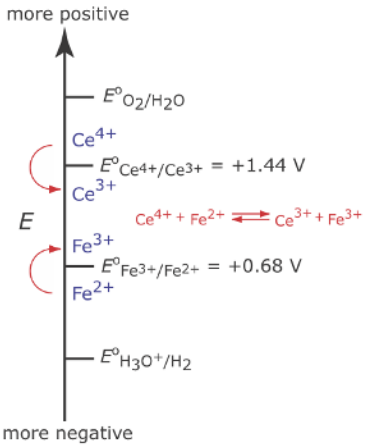



Figure 24.3.3. Standard state reduction potentials for the constant-current coulometric analysis of $Fe^{2+}$ in the presence of a $Ce^{3+}$ mediator. As the potential drifts to more positive values, we eventually reach a potential where $Ce^{3+}$ undergoes oxidation. Because $Ce^{4+}$, the product of the oxidation of $Ce^{3+}$, reacts with $Fe^{2+}$, we maintain current efficiency.

The $Ce^{4+}$ that forms at the working electrode rapidly mixes with the solution where it reacts with any available $Fe^{2+}$.

$$Ce^{4+}(aq) + Fe^{2+}(aq) \rightleftharpoons Ce^{3+}(aq) + Fe^{3+}(aq) \tag{24.3.4}$$

Combining reaction 24.3.3 and reaction 24.3.4 shows that the net reaction is the oxidation of $Fe^{2+}$ to $Fe^{3+}$

$$Fe^{2+}(aq) \rightleftharpoons Fe^{3+}(aq) + e^- \tag{24.3.5}$$

which maintains a current efficiency of 100%. A species used to maintain 100% current efficiency is called a mediator.

## Endpoint Determination

Adding a mediator solves the problem of maintaining 100% current efficiency, but it does not solve the problem of determining when the analyte's electrolysis is complete. Using the analysis for $Fe^{2+}$ in Figure 24.3.3, when the oxidation of $Fe^{2+}$ is complete current continues to flow from the oxidation of $Ce^{3+}$, and, eventually, the oxidation of $H_2O$. What we need is a signal that tells us when no more $Fe^{2+}$ is present in the solution.

For our purposes, it is convenient to treat a controlled-current coulometric analysis as a reaction between the analyte, $Fe^{2+}$, and the mediator, $Ce^{3+}$, as shown by reaction 24.3.4. This reaction is identical to a redox titration; thus, we can use the end points for a redox titration—visual indicators and potentiometric or conductometric measurements—to signal the end of a controlled-current coulometric analysis. For example, ferroin provides a useful visual endpoint for the $Ce^{3+}$ mediated coulometric analysis for $Fe^{2+}$, changing color from red to blue when the electrolysis of $Fe^{2+}$ is complete.

## Instrumentation

We can carry out controlled-current coulometry using the two-electrode galvanostat shown in Figure 24.3.4, which consists of a working electrode and a counter electrode. The working electrode—often a simple Pt electrode—also is called the generator

electrode since it is where the mediator reacts to generate the species that reacts with the analyte. If necessary, the counter electrode is isolated from the analytical solution by a salt bridge or a porous frit to prevent its electrolysis products from reacting with the analyte. The current from the power supply through the working electrode is

$$i = \frac{E_{PS}}{R + R_{cell}} \tag{24.3.6}$$

where $E_{PS}$ is the potential of the power supply, $R$ is the resistance of the resistor, and $R_{cell}$ is the resistance of the electrochemical cell. If $R >> R_{cell}$, then the current between the auxiliary and working electrodes

$$i = \frac{E_{PS}}{R} \approx \text{constant} \tag{24.3.7}$$

maintains a constant value. To monitor the working electrode's potential, which changes as the composition of the electrochemical cell changes, we can include an optional reference electrode and a high-impedance potentiometer.

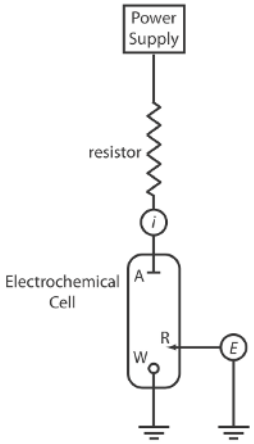



Figure 24.3.4. Schematic diagram of a galvanostat: A is the auxiliary, or counter electrode; W is the working electrode; R is an optional reference electrode, $E$ is a high-impedance potentiometer, and $i$ is an ammeter. The working electrode and the optional reference electrode are connected to a ground. Although a modern galvanostat uses very different circuitry, we can use this figure and the accompanying discussion to understand how we can use the working electrode and the counter electrode to control the current. The galvanostat here includes an optional reference electrode, but its presence or absence is not important if we are not interested in monitoring the working electrode's potential.

Alternatively, we can generate the oxidizing agent or the reducing agent externally, and allow it to flow into the analytical solution. Figure 24.3.5 shows one simple method for accomplishing this. A solution that contains the mediator flows into a small-volume electrochemical cell with the products exiting through separate tubes. Depending upon the analyte, the oxidizing agent or the reducing reagent is delivered to the analytical solution. For example, we can generate $Ce^{4+}$ using an aqueous solution of $Ce^{3+}$, directing the $Ce^{4+}$ that forms at the anode to our sample.

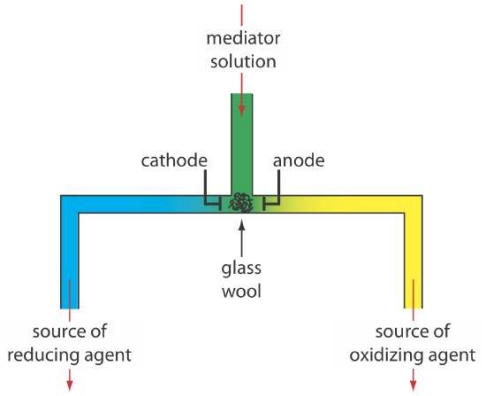



Figure 24.3.5. One example of a device for the external generation of oxidizing agents and reducing agents for controlled-current coulometry. A solution containing the mediator flows into a small-volume electrochemical cell. The resulting oxidation products, which form at the anode, flow to the right and serve as an oxidizing agent. Reduction at the cathode generates a reducing agent.

There are two other crucial needs for controlled-current coulometry: an accurate clock for measuring the electrolysis time, $t_e$, and a switch for starting and stopping the electrolysis. An analog clock can record time to the nearest ±0.01 s, but the need to stop and start the electrolysis as we approach the endpoint may result in an overall uncertainty of ±0.1 s. A digital clock allows for a more accurate measurement of time, with an overall uncertainty of ±1 ms. The switch must control both the current and the clock so that we can make an accurate determination of the electrolysis time.

## Coulometric Titrations

A controlled-current coulometric method sometimes is called a coulometric titration because of its similarity to a conventional titration. For example, in the controlled-current coulometric analysis for $Fe^{2+}$ using a $Ce^{3+}$ mediator, the oxidation of $Fe^{2+}$ by $Ce^{4+}$ (reaction 24.3.4) is identical to the reaction in a redox titration.

There are other similarities between controlled-current coulometry and titrimetry. If we combine the equation $Q = nFN_a$ and the equation $Q = it_e$ and solve for the moles of analyte, $N_A$, we obtain the following equation.

$$N_A = \frac{i}{nF} \times t_e \tag{24.3.8}$$

Compare Equation 24.3.8 to the relationship between the moles of analyte, $N_A$, and the moles of titrant, $N_T$, in a titration

$$N_A = N_T = M_T \times V_T \tag{24.3.9}$$

where $M_T$ and $V_T$ are the titrant's molarity and the volume of titrant at the end point. In constant-current coulometry, the current source is equivalent to the titrant and the value of that current is analogous to the titrant's molarity. Electrolysis time is analogous to the volume of titrant, and $t_e$ is equivalent to the a titration's end point. Finally, the switch for starting and stopping the electrolysis serves the same function as a buret's stopcock.

> For simplicity, we assumed above that the stoichiometry between the analyte and titrant is 1:1. The assumption, however, is not important and does not effect our observation of the similarity between controlled-current coulometry and a titration.

## Quantitative Applications

The use of a mediator makes a coulometric titration a more versatile analytical technique than controlled-potential coulometry. For example, the direct oxidation or reduction of a protein at a working electrode is difficult if the protein's active redox site lies deep within its structure. A coulometric titration of the protein is possible, however, if we use the oxidation or reduction of a mediator to produce a solution species that reacts with the protein. Table 24.3.1 summarizes several controlled-current coulometric methods based on a redox reaction using a mediator.

Table 24.3.1. Representative Examples of Coulometric Redox Titrations

| mediator | electrochemically generated reagent and reaction | representative application |
|---|---|---|
| $Ag^+$ | $Ag^+ \rightleftharpoons \mathbf{Ag^{2+}} + e^-$ | $\mathbf{H_2C_2O_4}(aq) + 2Ag^{2+}(aq) + 2H_2O(l) \rightleftharpoons 2CO_2(g) + 2Ag^+(aq) + 2H_3O^+(aq)$ |
| $Br^-$ | $2Br^- \rightleftharpoons \mathbf{Br_2} + 2e^-$ | $\mathbf{H_2S}(aq) + Br_2(aq) + 2H_2O(l) \rightleftharpoons S(s) + 2Br^-(aq) + 2H_3O^+(aq)$ |
| $Ce^{3+}$ | $Ce^{3+} \rightleftharpoons \mathbf{Ce^{4+}} + e^-$ | $\mathbf{Fe(CN)_6^{4-}}(aq) + Ce^{4+}(aq) \rightleftharpoons Fe(CN)_6^{3-}(aq) + Ce^{3+}(aq)$ |
| $Cl^-$ | $2Cl^- \rightleftharpoons \mathbf{Cl_2} + 2e^-$ | $\mathbf{Ti(I)}(aq) + Cl_2(aq) \rightleftharpoons Ti(III)(aq) + 2Cl^-(aq)$ |
| $Fe^{3+}$ | $Fe^{3+} + e^- \rightleftharpoons \mathbf{Fe^{2+}}$ | $\mathbf{Cr_2O_7^{2-}}(aq) + 6Fe^{2+}(aq) + 14H_3O^+(aq) \rightleftharpoons 2Cr^{3+}(aq) + 6Fe^{3+}(aq) + 21H_2O(l)$ |
| $I^-$ | $3I^- \rightleftharpoons \mathbf{I_3^-} + 2e^-$ | $2\mathbf{S_2O_3^{2-}}(aq) + I_3^-(aq) \rightleftharpoons S_4O_6^{2-}(aq) + 3I^-(aq)$ |
| $Mn^{2+}$ | $Mn^{2+} \rightleftharpoons \mathbf{Mn^{3+}} + e^-$ | $\mathbf{As(III)}(aq) + 2Mn^{3+}(aq) \rightleftharpoons As(V)(aq) + 2Mn^{2+}(aq)$ |

Note: The electrochemically generated reagent and the analyte are shown in **bold**.

For an analyte that is not easy to oxidize or reduce, we can complete a coulometric titration by coupling a mediator's oxidation or reduction to an acid–base, precipitation, or complexation reaction that involves the analyte. For example, if we use $H_2O$ as a mediator, we can generate $H_3O^+$at the anode

$$6H_2O(l) \rightleftharpoons 4H_3O^+(aq) + O_2(g) + 4e^-$$

and generate $OH^-$ at the cathode.

$$2H_2O(l) + 2e^- \rightleftharpoons 2OH^-(aq) + H_2(g)$$

If we carry out the oxidation or reduction of $H_2O$ using the generator cell in Figure 24.3.5, then we can selectively dispense $H_3O^+$ or $OH^-$ into a solution that contains the analyte. The resulting reaction is identical to that in an acid–base titration. Coulometric acid–base titrations have been used for the analysis of strong and weak acids and bases, in both aqueous and non-aqueous matrices. Table 24.3.2 summarizes several examples of coulometric titrations that involve acid–base, complexation, and precipitation reactions.

Table 24.3.2. Representative Coulometric Titrations Using Acid–Base, Complexation, and Precipitation Reactions

| type of reaction | mediator | electrochemically generated reagent and reaction | representative application |
|---|---|---|---|
| acid-base | $H_2O$ | $6H_2O \rightleftharpoons 4\mathbf{H_3O^+} + O_2 + e^-$ | $\mathbf{OH^-}(aq) + H_3O^+(aq) \rightleftharpoons 2H_2O(l)$ |
| acid-base | $H_2O$ | $2H_2O + 2e^- \rightleftharpoons 2\mathbf{OH^-} + H_2$ | $\mathbf{H_3O^+}(aq) + OH^-(aq) \rightleftharpoons 2H_2O(l)$ |
| complexation | $HgNH_3Y^{2-}$ (Y = EDTA) | $HgNH_3Y^{2-} + NH_4^+ + 2e^- \rightleftharpoons \mathbf{HY^{3-}} + Hg + 2NH_3$ | $\mathbf{Ca^{2+}}(aq) + HY^{3-}(aq) + H_2O(l) \rightleftharpoons CaY^{2-}(aq) + H_3O^+(aq)$ |
| precipitation | Ag | $Ag \rightleftharpoons \mathbf{Ag^+} + e^-$ | $\mathbf{I^-}(aq) + Ag^+(aq) \rightleftharpoons AgI(s)$ |
| precipitation | Hg | $2Hg \rightleftharpoons \mathbf{Hg_2^{2+}} + 2e^-$ | $2\mathbf{Cl^-}(aq) + Hg_2^{2+}(aq) \rightleftharpoons Hg_2Cl_2(s)$ |
| precipitation | $Fe(CN)_6^{3-}$ | $Fe(CN)_6^{3-} + e^- \rightleftharpoons \mathbf{Fe(CN)_6^{4-}}$ | $3\mathbf{Zn^{2+}}(aq) + K^+(aq) + 2Fe(CN)_6^{4-}(aq) \rightleftharpoons K_2Zn_3[Fe(CN)_6]_2(s)$ |

Note: The electrochemically generated reagent and the analyte are shown in **bold**.

In comparison to a conventional titration, a coulometric titration has two important advantages. The first advantage is that electrochemically generating a titrant allows us to use a reagent that is unstable. Although we cannot prepare and store a solution of a highly reactive reagent, such as $Ag^{2+}$ or $Mn^{3+}$, we can generate them electrochemically and use them in a coulometric titration. Second, because it is relatively easy to measure a small quantity of charge, we can use a coulometric titration to determine an analyte whose concentration is too small for a conventional titration.

The following example shows the calculations for a typical coulometric analysis.

### Example 24.3.1

To determine the purity of a sample of $Na_2S_2O_3$, a sample is titrated coulometrically using $I^-$ as a mediator and $I_3^-$ as the titrant. A sample weighing 0.1342 g is transferred to a 100-mL volumetric flask and diluted to volume with distilled water. A 10.00-mL portion is transferred to an electrochemical cell along with 25 mL of 1 M KI, 75 mL of a pH 7.0 phosphate buffer, and several drops of a starch indicator solution. Electrolysis at a constant current of 36.45 mA requires 221.8 s to reach the starch indicator endpoint. Determine the sample's purity.

#### Solution

As shown in Table 24.3.1, the coulometric titration of $S_2O_3^{2-}$ with $I_3^-$ is

$$2S_2O_3^{2-}(aq) + I_3^-(aq) \rightleftharpoons S_4O_6^{2-}(aq) + 3I^-(aq)$$

The oxidation of $S_2O_3^{2-}$ to $S_4O_6^{2-}$ requires one electron per $S_2O_3^{2-}$ ($n$ = 1). Combining the equations $Q = nFN_A$ and $Q = it_e$, and solving for the moles and grams of $Na_2S_2O_3$ gives

$$N_A = \frac{it_e}{nF} = \frac{(0.03645\ \text{A})(221.8\ \text{s})}{\left(\frac{1\ \text{mol}\ e^-}{\text{mol}\ Na_2S_2O_3}\right)\left(\frac{96487\ \text{C}}{\text{mol}\ e^-}\right)} = 8.379 \times 10^{-5}\ \text{mol}\ Na_2S_2O_3$$

This is the amount of $Na_2S_2O_3$ in a 10.00-mL portion of a 100-mL sample; thus, there are 0.1325 grams of $Na_2S_2O_3$ in the original sample. The sample's purity, therefore, is

$$\frac{0.1325\ \text{g}\ Na_2S_2O_3}{0.1342\ \text{g sample}} \times 100 = 98.73\%\ \text{w/w}\ Na_2S_2O_3$$

Note that for this calcuation, it does not matter whether $S_2O_3^{2-}$ is oxidized at the working electrode or is oxidized by $I_3^-$.

This page titled 24.3: Controlled-Current Coulometry is shared under a CC BY-NC-SA 4.0 license and was authored, remixed, and/or curated by David Harvey.

# CHAPTER OVERVIEW

## 25: Voltammetry

In voltammetry we apply a time-dependent potential to an electrochemical cell and measure the resulting current as a function of that potential. We call the resulting plot of current versus applied potential a voltammogram, and it is the electrochemical equivalent of a spectrum in spectroscopy, providing quantitative and qualitative information about the species involved in the oxidation or reduction reaction [Maloy, J. T. *J. Chem. Educ.* **1983**, *60*, 285–289]. The earliest voltammetric technique is polarography, developed by Jaroslav Heyrovsky in the early 1920s—an achievement for which he was awarded the Nobel Prize in Chemistry in 1959. Since then, many different forms of voltammetry have been developed. Before we examine some these techniques and their applications in more detail, we must first consider the basic experimental design for voltammetry and the factors influencing the shape of the resulting voltammogram.


25.1: Potential Excitation Signals and Currents in Voltammetry

25.2: Voltammetric Instrumentation

25.3: Linear Sweep Voltammetry

25.4: Cyclic Voltammetry

25.5: Polarography

25.6: Stripping Methods

25.7: Applications of Voltammetry



This page titled 25: Voltammetry is shared under a CC BY-NC-SA 4.0 license and was authored, remixed, and/or curated by David Harvey.

# 25.1: Potential Excitation Signals and Currents in Voltammetry

In voltammetry we apply a time-dependent potential to an electrochemical cell and measure the resulting current as a function of that potential.

## Potential Excitation Signals

As shown in Figure 25.1.1, the potential may consist of (a) a linear scan or (b) a series of pulses. For the linear scan in (a), the direction of the scan can be reversed and repeated for additional cycles. The series of pulses in (b) shows just one of several different pulsed potential excitation signals; we will consider other pulse trains in the section on polarography.

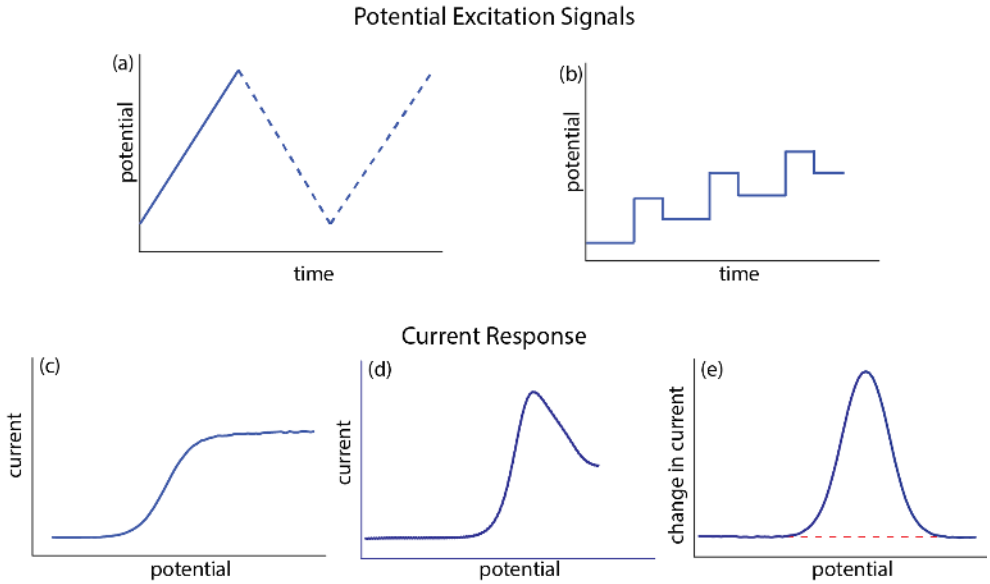



Figure 25.1.1: Two examples of potential excitation signals and three examples of current responses. In (a) the potential varies linearly with time and, as shown by the dashed line, the direction of the scan may be changed and repeated. In (b) the potential is changed by applying a series of pulses. The nature of the current response depends on both the potential excitation signal and other experimental conditions, such as if the solution is stirred.

## Current

The current responses in Figure 25.1.1 show the three common types of signals. In (c) and (d) the current is monitored directly as the potential is changed. In (e) a change in current is recorded using the current immediately before and after the application of a potential pulse. The current itself has three components: faradic current from the oxidation or reduction of the analyte, a charging current, and residual currents.

### Faradaic Current

Faradic current is the result of oxidation or reduction of the analyte at the working electrode. The ease with which electrons move between the electrode and the species that reacts at the electrode affects the faradiac current. When electron transfer kinetics are fast, the redox reaction is at equilibrium. Under these conditions the redox reaction is electrochemically reversible and the Nernst equation applies. If the electron transfer kinetics are sufficiently slow, the concentration of reactants and products at the electrode surface—and thus the magnitude of the faradaic current—are not what is predicted by the Nernst equation. In this case the system is electrochemically irreversible.

### Charging Currents

In addition to the faradaic current from a redox reaction, the current in an electrochemical cell includes other, nonfaradaic sources. Suppose the charge on an electrode is zero and we suddenly change its potential so that the electrode's surface acquires a positive charge. Cations near the electrode's surface will respond to this positive charge by migrating away from the electrode; anions, on the other hand, will migrate toward the electrode. This migration of ions occurs until the electrode's positive surface charge and the negative charge of the solution near the electrode are equal. Because the movement of ions and the movement of electrons are

indistinguishable, the result is a small, short-lived nonfaradaic current that we call the charging current. Every time we change the electrode's potential, a transient charging current flows.

The migration of ions in response to the electrode's surface charge leads to the formation of a structured electrode-solution interface that we call the electrical double layer, or EDL. When we change an electrode's potential, the charging current is the result of a restructuring of the EDL. The exact structure of the electrical double layer is not important in the context of this text, but you can consult this chapter's additional resources for additional information. See Chapter 22.1 for additional details.

### Residual Current

Even in the absence of analyte, a small, measurable current flows through an electrochemical cell. In addition to the charging current discussed above, the residual current includes a faradaic current from the oxidation or reduction of trace impurities in the sample. Methods for discriminating between the analyte's faradaic current and the residual current are discussed later in this chapter.

---

This page titled 25.1: Potential Excitation Signals and Currents in Voltammetry is shared under a CC BY-NC-SA 4.0 license and was authored, remixed, and/or curated by David Harvey.

# 25.2: Voltammetric Instrumentation

Although early voltammetric methods used only two electrodes, a modern voltammeter makes use of a three-electrode potentiostat, such as that shown in Figure 25.2.1. The potential of the working electrode is measured relative to a constant-potential reference electrode that is connected to the working electrode through a high-impedance potentiometer. The auxiliary electrode generally is a platinum wire and the reference electrode usually is a SCE or a Ag/AgCl electrode. We apply a time-dependent potential excitation signal to the working electrode—changing its potential relative to the fixed potential of the reference electrode—and measure the current that flows between the working electrode and the auxiliary electrode. Modern potentiostats include waveform generators that allow us to apply a time-dependent potential profile, such as a series of potential pulses, to the working electrode.

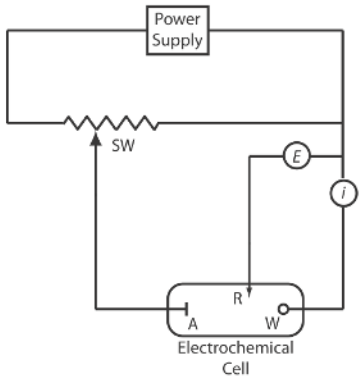



Figure 25.2.1. Schematic diagram for a manual potentiostat: W is the working electrode; A is the auxiliary electrode; R is the reference electrode; SW is a slide-wire resistor, *E* is a high-impendance potentiometer; and *i* is an ammeter.

## Working Electrodes

For the working electrode we can choose among several different materials, including mercury, platinum, gold, silver, and carbon. The earliest voltammetric techniques used a mercury working electrode. Because mercury is a liquid, the working electrode usually is a drop suspended from the end of a capillary tube. In the hanging mercury drop electrode, or HMDE, we extrude the drop of Hg by rotating a micrometer screw that pushes the mercury from a reservoir through a narrow capillary tube (Figure 25.2.2a).

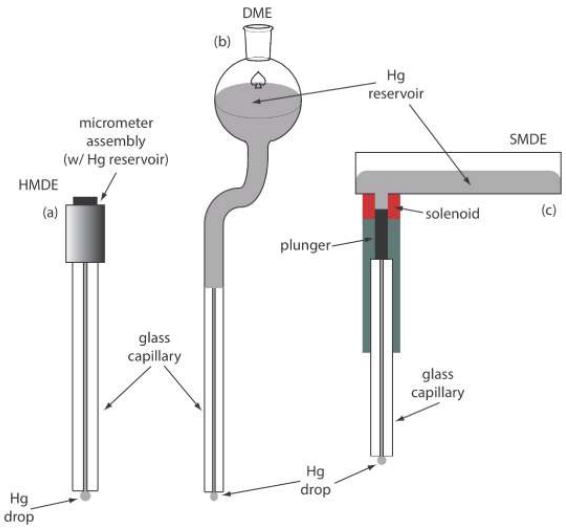



Figure 25.2.2. Three examples of mercury electrodes: (a) hanging mercury drop electrode, or HMDE; (b) dropping mercury electrode, or DME; and (c) static mercury drop electrode, or SMDE.

In the dropping mercury electrode, or DME, mercury drops form at the end of the capillary tube as a result of gravity (Figure 25.2.2 b). Unlike the HMDE, the mercury drop of a DME grows continuously—as mercury flows from the reservoir under the influence of gravity—and has a finite lifetime of several seconds. At the end of its lifetime the mercury drop is dislodged, either manually or on its own, and is replaced by a new drop. The static mercury drop electrode, or SMDE, uses a solenoid driven plunger to control

the flow of mercury (Figure 25.2.2c). Activation of the solenoid momentarily lifts the plunger, allowing mercury to flow through the capillary, forming a single, hanging Hg drop. Repeated activation of the solenoid produces a series of Hg drops. In this way the SMDE may be used as either a HMDE or a DME. There is one additional type of mercury electrode: the mercury film electrode. A solid electrode—typically carbon, platinum, or gold—is placed in a solution of $Hg^{2+}$ and held at a potential where the reduction of $Hg^{2+}$ to Hg is favorable, depositing a thin film of mercury on the solid electrode's surface.

Mercury has several advantages as a working electrode. Perhaps its most important advantage is its high overpotential for the reduction of $H_3O^+$ to $H_2$, which makes accessible potentials as negative as –1 V versus the SCE in acidic solutions and –2 V versus the SCE in basic solutions (Figure 25.2.3). A species such as $Zn^{2+}$, which is difficult to reduce at other electrodes without simultaneously reducing $H_3O^+$, is easy to reduce at a mercury working electrode. Other advantages include the ability of metals to dissolve in mercury—which results in the formation of an amalgam—and the ability to renew the surface of the electrode by extruding a new drop. One limitation to mercury as a working electrode is the ease with which it is oxidized. Depending on the solvent, a mercury electrode can not be used at potentials more positive than approximately –0.3 V to +0.4 V versus the SCE.

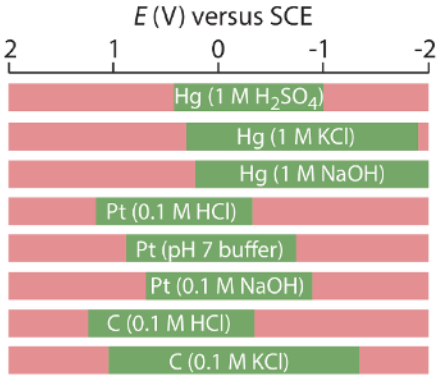



Figure 25.2.3. Approximate potential windows for mercury, platinum, and carbon (graphite) electrodes in acidic, neutral, and basic aqueous solvents. The useful potential windows are shown in green; potentials in red result in the oxidation or the reduction of the solvent or the electrode. Complied from Adams, R. N. *Electrochemistry at Solid Electrodes*, Marcel Dekker, Inc.: New York, 1969 and Bard, A. J.; Faulkner, L. R. *Electro- chemical Methods*, John Wiley & Sons: New York, 1980.

Solid electrodes constructed using platinum, gold, silver, or carbon may be used over a range of potentials, including potentials that are negative and positive with respect to the SCE (Figure 25.2.3). For example, the potential window for a Pt electrode extends from approximately +1.2 V to –0.2 V versus the SCE in acidic solutions, and from +0.7 V to –1 V versus the SCE in basic solutions. A solid electrode can replace a mercury electrode for many voltammetric analyses that require negative potentials, and is the electrode of choice at more positive potentials. Except for the carbon paste electrode, a solid electrode is fashioned into a disk and sealed into the end of an inert support with an electrical lead (Figure 25.2.4). The carbon paste electrode is made by filling the cavity at the end of the inert support with a paste that consists of carbon particles and a viscous oil. Solid electrodes are not without problems, the most important of which is the ease with which the electrode's surface is altered by the adsorption of a solution species or by the formation of an oxide layer. For this reason a solid electrode needs frequent reconditioning, either by applying an appropriate potential or by polishing.

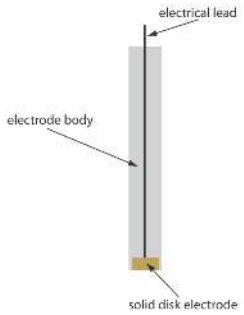



Figure 25.2.4. Schematic showing a solid electrode. The electrode is fashioned into a disk and sealed in the end of an inert polymer support along with an electrical lead.

## Electrochemical Cells

A typical arrangement for a voltammetric electrochemical cell is shown in Figure 25.2.5. In addition to the working electrode, the reference electrode, and the auxiliary electrode, the cell also includes a $N_2$-purge line for removing dissolved $O_2$, and an optional stir bar. Electrochemical cells are available in a variety of sizes, allowing the analysis of solution volumes ranging from more than 100 mL to as small as 50 μL.

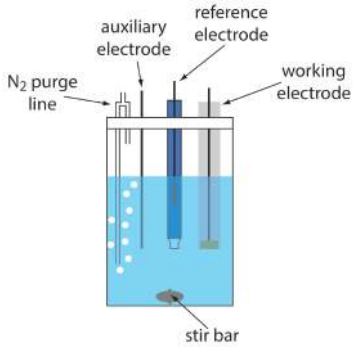



Figure 25.2.5. Typical electrochemical cell for voltammetry.

This page titled 25.2: Voltammetric Instrumentation is shared under a CC BY-NC-SA 4.0 license and was authored, remixed, and/or curated by David Harvey.

# 25.3: Linear Sweep Voltammetry

In the simplest voltammetric experiment we apply a linear potential ramp as an excitation signal and record the current that flows in response to the change in potential. Among the experimental variables under our control are the initial potential, the final potential, the scan rate, and whether we choose to stir the solution or leave it unstirred. We call this linear sweep voltammetry.

To illustrate how linear sweep voltammetry works, let's consider what happens when we reduce $\mathrm{Fe(CN)_6^{3-}}$ to $\mathrm{Fe(CN)_6^{4-}}$ at the working electrode. The relationship between the concentrations of $\mathrm{Fe(CN)_6^{3-}}$, the concentration of $\mathrm{Fe(CN)_6^{4-}}$, and the potential is given by the Nernst equation

$$E = +0.356\ \text{V} - 0.05916 \log \frac{\left[\mathrm{Fe(CN)_6^{4-}}\right]_{x=0}}{\left[\mathrm{Fe(CN)_6^{3-}}\right]_{x=0}} \tag{25.3.1}$$

where +0.356V is the standard-state potential for the $\mathrm{Fe(CN)_6^{3-}/Fe(CN)_6^{4-}}$ redox couple, and $x$ = 0 indicates that the concentrations of $\mathrm{Fe(CN)_6^{3-}}$ and $\mathrm{Fe(CN)_6^{4-}}$ are those at the surface of the working electrode. We use surface concentrations instead of bulk concentrations because the equilibrium position for the redox reaction

$$\mathrm{Fe(CN)_6^{3-}}(aq) + e^- \rightleftharpoons \mathrm{Fe(CN)_6^{4-}}(aq) \tag{25.3.2}$$

is established at the electrode's surface.

Let's assume we have a solution for which the initial concentration of $\mathrm{Fe(CN)_6^{3-}}$ is 1.0 mM and that $\mathrm{Fe(CN)_6^{4-}}$ is absent. Figure 25.3.1 shows the relationship between the applied potential and the species that are stable at the electrode's surface.

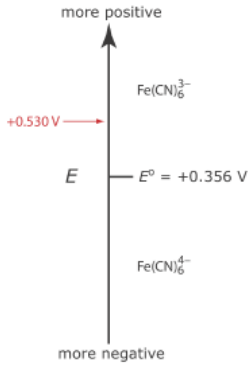



Figure 25.3.1. Potential diagram for the $\mathrm{Fe(CN)_6^{3-}/Fe(CN)_6^{4-}}$ redox half-reaction showing the potentials where $\mathrm{Fe(CN)_6^{3-}}$ and where $\mathrm{Fe(CN)_6^{4-}}$ are the dominate species. At a potential of +0.30 V, only $\mathrm{Fe(CN)_6^{3-}}$ is stable at the electrode's surface.

If we apply a potential of +0.530 V to the working electrode, the concentrations of $\mathrm{Fe(CN)_6^{3-}}$ and $\mathrm{Fe(CN)_6^{4-}}$ at the surface of the electrode are unaffected, and no faradaic current is observed. If we switch the potential to +0.356 V some of the $\mathrm{Fe(CN)_6^{3-}}$ at the electrode's surface is reduced to $\mathrm{Fe(CN)_6^{4-}}$until we reach a condition where

$$\left[\mathrm{Fe(CN)_6^{3-}}\right]_{x=0} = \left[\mathrm{Fe(CN)_6^{4-}}\right]_{x=0} = 0.50\ \text{mM} \tag{25.3.3}$$

If this is all that happens after we apply the potential, then there would be a brief surge of faradaic current that quickly returns to zero, which is not the most interesting of results (although this is the basis for chronoamperometry, an electrochemical method we will not consider in this text). Although the concentrations of $\mathrm{Fe(CN)_6^{3-}}$ and $\mathrm{Fe(CN)_6^{4-}}$ at the electrode surface are 0.50 mM, their concentrations in bulk solution remains unchanged.

Because of this difference in concentration, there is a concentration gradient between the electrode's surface and the bulk solution. This concentration gradient creates a driving force that transports $\mathrm{Fe(CN)_6^{4-}}$ away from the electrode and that transports $\mathrm{Fe(CN)_6^{3-}}$ to the electrode (Figure 25.3.2). As the $\mathrm{Fe(CN)_6^{3-}}$ arrives at the electrode it, too, is reduced to $\mathrm{Fe(CN)_6^{4-}}$. A faradaic current continues to flow until there is no difference between the concentrations of $\mathrm{Fe(CN)_6^{3-}}$ and $\mathrm{Fe(CN)_6^{4-}}$ at the electrode and their concentrations in bulk solution (although this might take a long time!).

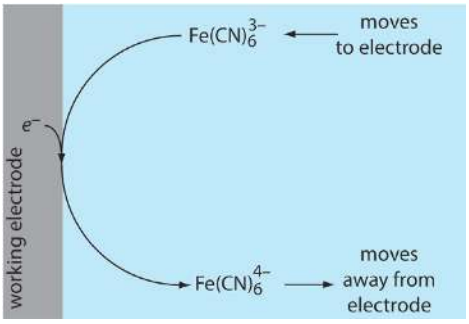



Figure 25.3.2. Schematic diagram showing the transport of $Fe(CN)_6^{4-}$ away from the electrode's surface and the transport of $Fe(CN)_6^{3-}$ toward the electrode's surface following the reduction of $Fe(CN)_6^{3-}$ to $Fe(CN)_6^{4-}$.

Although the potential at the working electrode determines if a faradaic current flows, the magnitude of the current is determined by the rate of the resulting oxidation or reduction reaction. Two factors contribute to the rate of the electrochemical reaction: the rate at which the reactants and products are transported to and from the electrode—what we call mass transport—and the rate at which electrons pass between the electrode and the reactants and products in solution.

## Concentration Profiles at the Working Electrode

There are three modes of mass transport that affect the rate at which reactants and products move toward or away from the electrode surface: diffusion, migration, and convection. Diffusion occurs whenever the concentration of an ion or a molecule at the surface of the electrode is different from that in bulk solution. If we apply a potential sufficient to completely reduce $Fe(CN)_6^{3-}$ at the electrode surface, the result is a concentration gradient similar to that shown in Figure 25.3.3. The region of solution over which diffusion occurs is the diffusion layer. In the absence of other modes of mass transport, the width of the diffusion layer, $\delta$, increases with time as the $Fe(CN)_6^{3-}$ must diffuse from an increasingly greater distance.

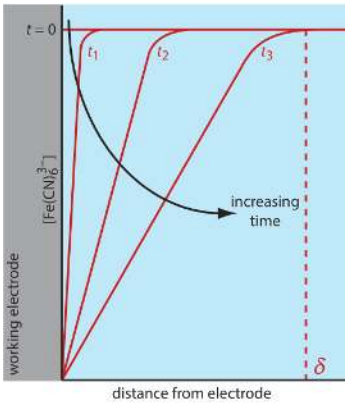



Figure 25.3.3. Concentration gradients (in red) for $Fe(CN)_6^{3-}$ following the application of a potential that completely reduces it to $Fe(CN)_6^{4-}$. Before we apply the potential ($t$ = 0) the concentration of $Fe(CN)_6^{3-}$ is the same at all distances from the electrode's surface. After we apply the potential, its concentration at the electrode's surface decreases to zero and $Fe(CN)_6^{3-}$ diffuses to the electrode from bulk solution. The longer we apply the potential, the greater the distance over which diffusion occurs. The dashed red line shows the extent of the diffusion layer at time $t_3$. These profiles assume that convection and migration do not contribute significantly to the mass transport of $Fe(CN)_6^{3-}$.

Convection occurs when we mix the solution, which carries reactants toward the electrode and removes products from the electrode. The most common form of convection is stirring the solution with a stir bar; other methods include rotating the electrode and incorporating the electrode into a flow-cell.

The final mode of mass transport is migration, which occurs when a charged particle in solution is attracted to or repelled from an electrode that carries a surface charge. If the electrode carries a positive charge, for example, an anion will move toward the electrode and a cation will move toward the bulk solution. Unlike diffusion and convection, migration affects only the mass transport of charged particles.

The movement of material to and from the electrode surface is a complex function of all three modes of mass transport. In the limit where diffusion is the only significant form of mass transport, the current, $i$, in a voltammetric cell is proportional to the slope of

the concentration profile in Figure 25.3.3

$$i \propto \frac{\partial C}{\partial x} \tag{25.3.4}$$

where $C$ is the concentration of $\mathrm{Fe(CN)_6^{3-}}$ and $x$ is distance.

For Equation 25.3.4 to be valid, convection and migration must not interfere with the formation of a diffusion layer. We can eliminate migration by adding a high concentration of an inert supporting electrolyte. Because ions of similar charge are equally attracted to or repelled from the surface of the electrode, each has an equal probability of undergoing migration. A large excess of an inert electrolyte ensures that few reactants or products experience migration. Although it is easy to eliminate convection by not stirring the solution, there are experimental designs where we cannot avoid convection, either because we must stir the solution or because we are using an electrochemical flow cell. Fortunately, as shown in Figure 25.3.4, the dynamics of a fluid moving past an electrode results in a small diffusion layer—typically 1–10 μm in thickness—in which the rate of mass transport by convection drops to zero.

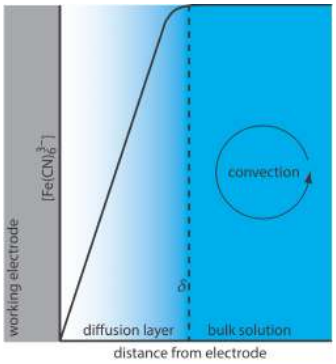



Figure 25.3.4. Concentration gradient for $\mathrm{Fe(CN)_6^{3-}}$ when stirring the solution. Diffusion is the only significant form of mass transport close to the electrode's surface. At distances greater than $\delta$, convection is the only significant form of mass transport, maintaining a homogeneous solution in which the concentration of $\mathrm{Fe(CN)_6^{3-}}$ at $\delta$ is the same as its concentration in bulk solution.

## Concentration Profiles in an Unstirred Solution

Figure 25.3.5 shows the linear sweep voltammogram (the center image, which shows the current as a function of time) and eight snapshots of the concentration profiles for the reduction of $\mathrm{Fe(CN)_6^{3-}}$ to $\mathrm{Fe(CN)_6^{4-}}$ in an unstirred solution. The initial potential was set to +0.530 V and the final potential was set to +0.182 V with a scan rate of 0.050 V/s.

At the initial potential, only $\mathrm{Fe(CN)_6^{3-}}$ is stable at the electrode surface, and no current flows. After 0.696 s the potential is 0.495 V (image to the left of the linear sweep voltammogram) and, because $\mathrm{Fe(CN)_6^{3-}}$ remains stable at the electrode surface, no current flows. Moving clockwise around the linear sweep voltammogram, the applied potential becomes smaller and the concentration of $\mathrm{Fe(CN)_6^{3-}}$ at the electrode surface decreases and the concentration of $\mathrm{Fe(CN)_6^{4-}}$ increases. Initially the slope of the concentration gradient, and, therefore, the current increases; as the concentration of $\mathrm{Fe(CN)_6^{3-}}$ at the electrode surface approaches zero, however, the concentration gradient becomes less steep and the current decreases. The result is the linear sweep voltammogram in the center of the diagram.

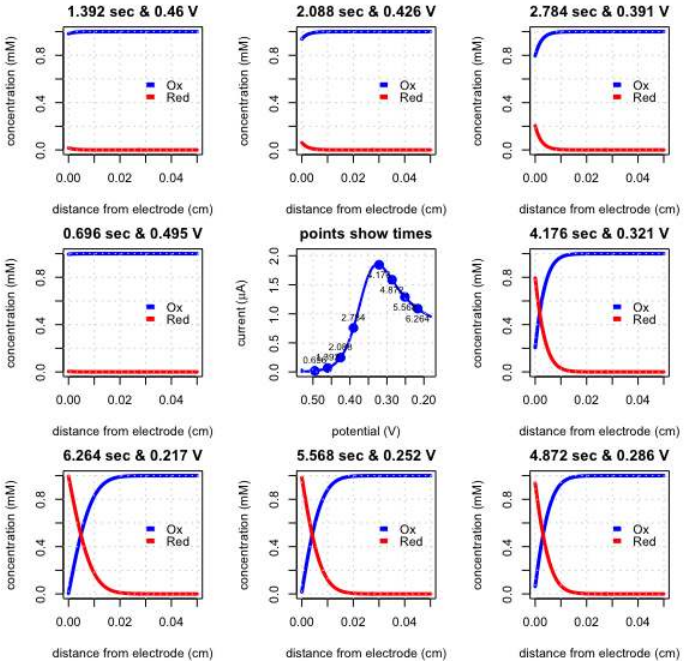



Figure 25.3.5: The central image shows the linear sweep voltammogram in an unstirred solution for the reduction of $\mathrm{Fe(CN)_6^{3-}}$ to $\mathrm{Fe(CN)_6^{4-}}$. The remaining images show the concentration profiles for $\mathrm{Fe(CN)_6^{3-}}$ (in blue) and for $\mathrm{Fe(CN)_6^{4-}}$ (in red) as the potential is swept from +0.530 V to +0.182 V (arranged clockwise, beginning immediately left of the linear sweep voltammogram.

## Concentration Profiles in a Stirred Solution

If we run the same experiment as in Figure 25.3.5, but stir the solution, the resulting linear sweep voltammogram and concentration profiles are those in Figure 25.3.6. Stirring the solution, as we saw in Figure 25.3.4 creates a diffusion layer whose thickness is independent of time.

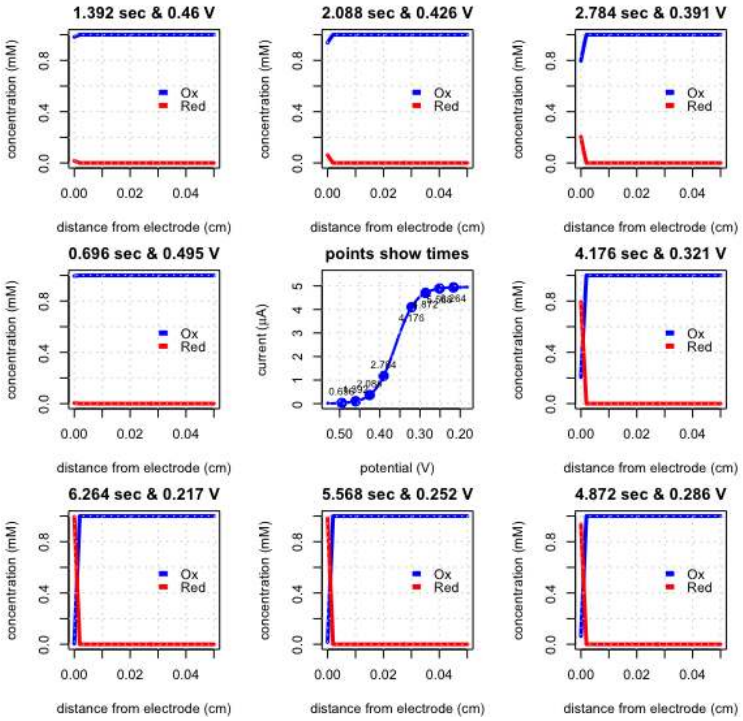



Figure 25.3.6: The central image shows the linear sweep voltammogram in a stirred solution for the reduction of $\mathrm{Fe(CN)_6^{3-}}$ to $\mathrm{Fe(CN)_6^{4-}}$. The remaining images show the concentration profiles for $\mathrm{Fe(CN)_6^{3-}}$ (in blue) and for $\mathrm{Fe(CN)_6^{4-}}$ (in red) as the potential is swept from +0.530 V to +0.182 V (arranged clockwise, beginning immediately left of the linear sweep voltammogram.

As a result, instead of the peak current in Figure 25.3.5, the current reaches a steady-state value, which we call the limiting current, $i_l$. The linear sweep voltammogram also has a characteristic half-wave potential, $E_{1/2}$, when the current is 50% of the limiting current. Figure 25.3.7 shows how the limiting current and half-wave potential are measured.

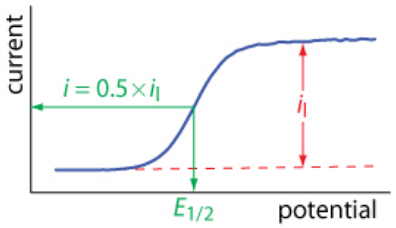



Figure 25.3.7: The limiting current and half-wave potential for a linear sweep voltammetry experiment in a stirred solution.

## Voltammetric Currents

Earlier we noted, in Equation 25.3.4, that the current in linear sweep voltammetry is proportional to the slope of the concentration profile. The current is also a function of other variables, as shown here for the reduction of $\text{Fe(CN)}_6^{3-}$ to $\text{Fe(CN)}_6^{4-}$

$$i = \frac{nFAD\left(\left[\text{Fe(CN)}_6{}^{3-}\right]_{\text{bulk}} - \left[\text{Fe(CN)}_6{}^{3-}\right]_{\text{x = 0}}\right)}{\delta} \tag{25.3.5}$$

where *n* the number of electrons in the redox reaction, *F* is Faraday's constant, *A* is the area of the electrode, *D* is the diffusion coefficient for $\text{Fe(CN)}_6^{3-}$, $\delta$ is the thickness of the diffusion layer, and $\left(\left[\text{Fe(CN)}_6{}^{3-}\right]_{\text{bulk}} - \left[\text{Fe(CN)}_6{}^{3-}\right]_{\text{x = 0}}\right)$ is the difference in the concentration of $\text{Fe(CN)}_6{}^{3-}$ between the bulk solution and the electrode's surface.

Because $n$, $F$, $A$, and $D$ are constants, and because $\delta$ is a constant if we stir the solution, we can write Equation 25.3.5 as

$$i = K_{\text{Fe(CN)}_6{}^{3-}}\left(\left[\text{Fe(CN)}_6{}^{3-}\right]_{\text{bulk}} - \left[\text{Fe(CN)}_6{}^{3-}\right]_{\text{x = 0}}\right) \tag{25.3.6}$$

where $K_{\text{Fe(CN)}_6{}^{3-}}$ is a constant. If we use the limiting current, then $\left[\text{Fe(CN)}_6{}^{3-}\right]_{\text{x = 0}}$ is zero, and Equation 25.3.6 becomes

$$i_l = K_{\text{Fe(CN)}_6{}^{3-}}\left[\text{Fe(CN)}_6{}^{3-}\right]_{\text{bulk}} \tag{25.3.7}$$

### Current/Voltage Relationships for Reversible Reactions

A reversible electrochemical reaction is one in which the concentration of the oxidized and reduced species at the electrode surface remain in thermodynamic equilibrium with each other. When this is true, the Nernst equation explains the relationship between the applied potential, their concentration, and the standard state potential.

Equation 25.3.7 shows us that the limiting current is a measure of the concentration of $\text{Fe(CN)}_6^{3-}$ in bulk solution, which means we can use the limiting current for quantitative work. Figure 25.3.7 also shows that there is a qualitative relationship between the half-wave potential, $E_{1/2}$, and the limiting current; however, it is not yet clear what the half-wave potential represents.

If we solve Equation 25.3.7 for $\left[\text{Fe(CN)}_6{}^{3-}\right]_{\text{bulk}}$ and substitute into Equation 25.3.6 and rearrange, we have

$$\left[\text{Fe(CN)}_6{}^{3-}\right]_{\text{x = 0}} = \frac{i_l - i}{K_{\text{Fe(CN)}_6{}^{3-}}} \tag{25.3.8}$$

If we take the same approach with $\text{Fe(CN)}_6^{4-}$, which forms at the electrode solution, then we have

$$i = -\frac{nFAD\left(\left[\text{Fe(CN)}_6{}^{4-}\right]_{\text{bulk}} - \left[\text{Fe(CN)}_6{}^{4-}\right]_{\text{x = 0}}\right)}{\delta} = K_{\text{Fe(CN)}_6{}^{4-}}\left[\text{Fe(CN)}_6{}^{4-}\right]_{\text{x = 0}} \tag{25.3.9}$$

$$\left[\text{Fe(CN)}_6{}^{4-}\right]_{\text{x = 0}} = \frac{-i}{K_{\text{Fe(CN)}_6{}^{4-}}} \tag{25.3.10}$$

where the minus sign accounts for the concentration profile having a negative slope. Substituting Equation 25.3.9 and Equation 25.3.10 into Equation 25.3.1, which is the Nersnt equation, gives

$$E = E^\circ - 0.05916 \log \frac{-i/K_{\text{Fe(CN)}_6{}^{4-}}}{(i_l - i)/K_{\text{Fe(CN)}_6{}^{3-}}} \tag{25.3.11}$$

$$E = E^\circ + 0.05916 \log \frac{K_{\text{Fe(CN)}_6^{3-}}}{K_{\text{Fe(CN)}_6^{4-}}} - 0.05916 \log \frac{i}{i_l - i} \tag{25.3.12}$$

When $i = \frac{i_l - i}{2}$, which is the definition of $E_{1/2}$, Equation 25.3.12 simplifies to

$$E_{1/2} = E^\circ + 0.05916 \log \frac{K_{\text{Fe(CN)}_6^{3-}}}{K_{\text{Fe(CN)}_6^{4-}}} \tag{25.3.13}$$

The only difference between $K_{\text{Fe(CN)}_6^{3-}}$ and $K_{\text{Fe(CN)}_6^{4-}}$ are the diffusion coefficients, $D$, for $\text{Fe(CN)}_6^{3-}$ and for $\text{Fe(CN)}_6^{4-}$. As these values should be similar, we have

$$E_{1/2} \approx E^\circ \tag{25.3.14}$$

and $E_{1/2}$ provides an estimate for the standard state reduction potential.

### Current/Voltage Relationships for Irreversible Reactions

When an electrochemical reaction is not reversible, the Nernst equation no longer applies, which means we can no longer assume that the half-wave potential provides an estimate for the standard state reduction potential. The relationship between the limiting current and the concentration of the electroactive species in bulk solution still holds true and quantitative work remains possible.

## Oxygen Waves

The presence of dissolved oxygen creates a complication as it is capable of undergoing reduction reactions at the electrode's surface that may interfere with the determination of the analyte's limiting current or half-wave potential. For example, $O_2$ is reduced to $H_2O_2$ with a standard state potential of +0.695 V

$$O_2(g) + 2H^+(aq) + 2e^- \rightleftharpoons H_2O_2(aq) \tag{25.3.15}$$

and $H_2O_2$ subsequently is reduced to $H_2O$ at a standard state potential of +1.763 V.

$$H_2O_2(aq) + 2H^+(aq) + 2e^- \rightleftharpoons 2H_2O(aq) \tag{25.3.16}$$

This is the reason that a typical cell for voltammetry (see Figure 25.2.5) includes the ability to pass $N_2$ through the solution to remove dissolved $O_2$. Once the solution is deaerated, $N_2$ is allowed to flow over the solution to prevent $O_2$ from reentering the solution.

## Applications of Linear Sweep Voltammetry

As we learned in the previous section, the limiting current in linear sweep voltammetry is proportional to the concentration of the species undergoing oxidation or reduction at the electrode surface, which makes it a useful tool for a quantitative analysis. Because we are interested only in the limiting current, most quantitative methods simply hold the potential of the working electrode at a fixed value and measure the limiting current. Because we are measuring the current as a function of time instead of potential, these are called amperometric methods (where ampere is the unit for current). Several examples of amperometic methods are gathered here.

### Amperometric Detectors in Chromatography and Flow-Injection Analysis

One important detector for high-performance liquid chromatography (HPLC) is one in which the mobile phase eluting from the column passes through a small volume electrochemical cell in which the working electrode is held at a potential that will oxidize or reduce the analytes. The resulting current is plotted as function of time to yield the chromatogram. A similar arrangement is used in flow-injection analysis (FIA). See Chapter 28 (HPLC) and Chapter 33 (FIA) for further details.

### Amperometric Senors

One important application of amperometry is in the construction of chemical sensors. One of the first amperometric sensors was developed in 1956 by L. C. Clark to measure dissolved $O_2$ in blood. Figure 25.3.9 shows the sensor's design, which is similar to a potentiometric membrane electrode. A thin, gas-permeable membrane is stretched across the end of the sensor and is separated from the working electrode and the counter electrode by a thin solution of KCl. The working electrode is a Pt disk cathode, and a

Ag ring anode serves as the counter electrode. Although several gases can diffuse across the membrane, including $O_2$, $N_2$, and $CO_2$, only oxygen undergoes reduction at the cathode

$$O_2(g) + 4H_3O^+(aq) + 4e^- \rightleftharpoons 6H_2O(l) \tag{25.3.17}$$

with its concentration at the electrode's surface quickly reaching zero. The concentration of $O_2$ at the membrane's inner surface is fixed by its diffusion through the membrane, which creates a limiting current. The result is a steady-state current that is proportional to the concentration of dissolved oxygen. Because the electrode consumes oxygen, the sample is stirred to prevent the depletion of $O_2$ at the membrane's outer surface.

> The oxidation of the Ag anode is the other half-reaction.
>
> $$Ag(s) + Cl^-(aq) \rightleftharpoons AgCl(s) + e^-$$

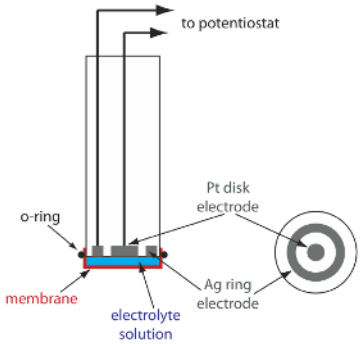



Figure 25.3.9. Clark amperometric sensor for determining dissolved $O_2$. The diagram on the right is a cross-section through the electrode, which shows the Ag ring electrode and the Pt disk electrode.

Another example of an amperometric sensor is a glucose sensor. In this sensor the single membrane in Figure 25.3.10 is replaced with three membranes. The outermost membrane of polycarbonate is permeable to glucose and $O_2$. The second membrane contains an immobilized preparation of glucose oxidase that catalyzes the oxidation of glucose to gluconolactone and hydrogen peroxide.

$$\beta - D - \text{glucose}\ (aq) + O_2(aq) + H_2O(l) \rightleftharpoons \text{gluconolactone}\ (aq) + H_2O_2(aq) \tag{25.3.18}$$

The hydrogen peroxide diffuses through the innermost membrane of cellulose acetate where it undergoes oxidation at a Pt anode.

$$H_2O_2(aq) + 2OH^-(aq) \rightleftharpoons O_2(aq) + 2H_2O(l) + 2e^- \tag{25.3.19}$$

Figure 25.3.10 summarizes the reactions that take place in this amperometric sensor. FAD is the oxidized form of flavin adenine nucleotide—the active site of the enzyme glucose oxidase—and $FADH_2$ is the active site's reduced form. Note that $O_2$ serves a mediator, carrying electrons to the electrode.

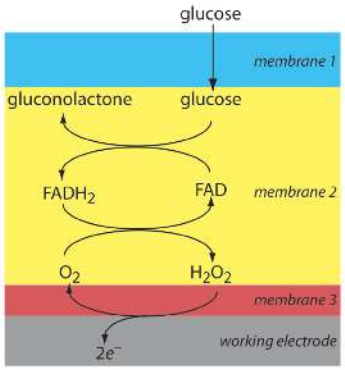



Figure 25.3.10. Schematic showing the reactions by which an amperometric biosensor responds to glucose.

By changing the enzyme and mediator, it is easy to extend to the amperometric sensor in Figure 25.3.10 to the analysis of other analytes. For example, a $CO_2$ sensor has been developed using an amperometric $O_2$ sensor with a two-layer membrane, one of

which contains an immobilized preparation of autotrophic bacteria [Karube, I.; Nomura, Y.; Arikawa, Y. *Trends in Anal. Chem.* **1995**, *14*, 295–299]. As $CO_2$ diffuses through the membranes it is converted to $O_2$ by the bacteria, increasing the concentration of $O_2$ at the Pt cathode.

---

This page titled 25.3: Linear Sweep Voltammetry is shared under a CC BY-NC-SA 4.0 license and was authored, remixed, and/or curated by David Harvey.

# 25.4: Cyclic Voltammetry

In linear sweep voltammetry we scan the potential in one direction, either to more positive potentials or to more negative potentials. In cyclic voltammetry we complete a scan in both directions. Figure 25.4.1a shows a typical potential-excitation signal. In this example, we first scan the potential to more positive values, resulting in the following oxidation reaction for the species *R*.

$$R \rightleftharpoons O + ne^- \tag{25.4.1}$$

When the potential reaches a predetermined switching potential, we reverse the direction of the scan toward more negative potentials. Because we generated the species *O* on the forward scan, during the reverse scan it reduces back to *R*.

$$O + ne^- \rightleftharpoons R \tag{25.4.2}$$

Cyclic voltammetry is carried out in an unstirred solution, which, as shown in Figure 25.4.1b, results in peak currents instead of limiting currents. The voltammogram has separate peaks for the oxidation reaction and for the reduction reaction, each characterized by a peak potential and a peak current.

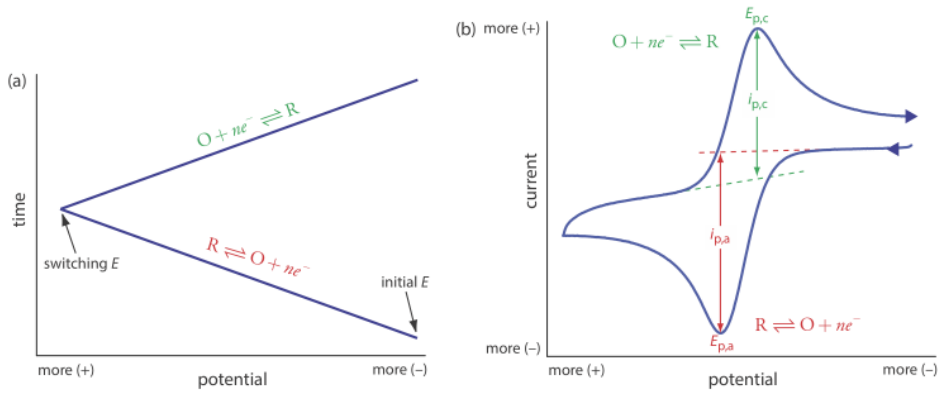



Figure 25.4.1. Details for cyclic voltammetry. (a) One cycle of the triangular potential-excitation signal showing the initial potential and the switching potential. A cyclic voltammetry experiment can consist of one cycle or many cycles. Although the initial potential in this example is the negative switching potential, the cycle can begin with an intermediate initial potential and cycle between two limits. (b) The resulting cyclic voltammogram showing the measurement of the peak currents and peak potentials.

The peak current in cyclic voltammetry is given by the Randles-Sevcik equation

$$i_p = \left(2.69 \times 10^5\right) n^{3/2} A D^{1/2} \nu^{1/2} C_A \tag{25.4.3}$$

where *n* is the number of electrons in the redox reaction, *A* is the area of the working electrode, *D* is the diffusion coefficient for the electroactive species, $\nu$ is the scan rate, and $C_A$ is the concentration of the electroactive species at the electrode. For a well-behaved system, the anodic and the cathodic peak currents are equal, and the ratio $i_{p,a}/i_{p,c}$ is 1.00. The half-wave potential, $E_{1/2}$, is midway between the anodic and cathodic peak potentials.

$$E_{1/2} = \frac{E_{p,a} + E_{p,c}}{2} \tag{25.4.4}$$

Scanning the potential in both directions provides an opportunity to explore the electrochemical behavior of species generated at the electrode. This is a distinct advantage of cyclic voltammetry over other voltammetric techniques. Figure 25.4.2 shows the cyclic voltammogram for the same redox couple at both a faster and a slower scan rate. At the faster scan rate, 25.4.2a, we see two peaks. At the slower scan rate in Figure 25.4.2b, however, the peak on the reverse scan disappears. One explanation for this is that the products from the reduction of *R* on the forward scan have sufficient time to participate in a chemical reaction whose products are not electroactive.

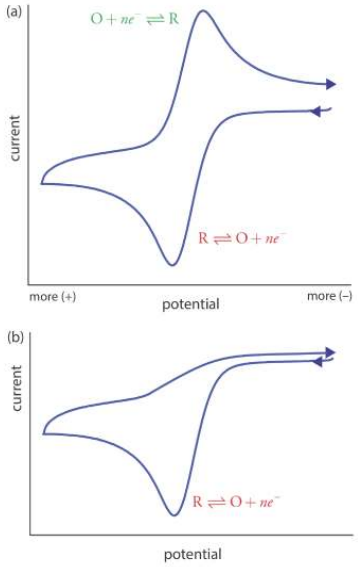



Figure 25.4.2. Cyclic voltammograms for *R* obtained at (a) a faster scan rate and at (b) a slower scan rate. One of the principal uses of cyclic voltammetry is to study the chemical and electrochemical behavior of compounds. See this chapter's additional resources for further information.

---

This page titled 25.4: Cyclic Voltammetry is shared under a CC BY-NC-SA 4.0 license and was authored, remixed, and/or curated by David Harvey.

# 25.5: Polarography

The first important voltammetric technique to be developed—polarography—uses the dropping mercury (DME) electrode as the working electrode (see Figure 25.2.2 for a schematic diagram of the DME as well as two other types of Hg electrodes). In polarography, as in linear sweep voltammetry, we vary the potential and measure the current. The change in potential can be in the form of a linear ramp, as was the case for linear sweep voltammetry, or it can involve a series of pulses.

## Normal Polarography

As shown in Figure 25.5.1, the current is measured while applying a linear potential ramp.

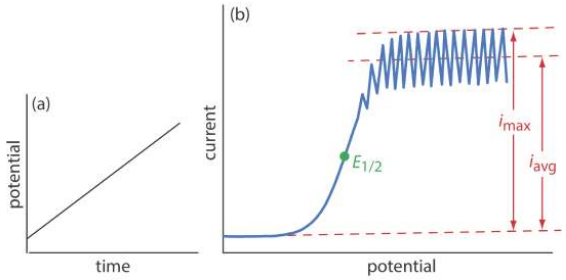



Figure 25.5.1. Details of normal polarography: (a) the linear potential-excitation signal, and (b) the resulting voltammogram.

Although polarography takes place in an unstirred solution, we obtain a limiting current instead of a peak current. When a Hg drop separates from the glass capillary and falls to the bottom of the electrochemical cell, it mixes the solution. Each new Hg drop, therefore, grows into a solution whose composition is identical to the bulk solution. The oscillations in the current are a result of the Hg drop's growth, which leads to a time-dependent change in the area of the working electrode. The limiting current—which also is called the diffusion current—is measured using either the maximum current, $i_{max}$, or from the average current, $i_{avg}$. The relationship between the analyte's concentration, $C_A$, and the limiting current is given by the Ilkovic equations

$$i_{max} = 706nD^{1/2}m^{2/3}t^{1/6}C_A = K_{max}C_A \tag{25.5.1}$$

$$i_{avg} = 607nD^{1/2}m^{2/3}t^{1/6}C_A = K_{avg}C_A \tag{25.5.2}$$

where $n$ is the number of electrons in the redox reaction, $D$ is the analyte's diffusion coefficient, $m$ is the flow rate of Hg, $t$ is the drop's lifetime and $K_{max}$ and $K_{avg}$ are constants. The half-wave potential, $E_{1/2}$, provides qualitative information about the redox reaction.

## Pulse Polarography

Normal polarography has been replaced by various forms of pulse polarography, several examples of which are shown in Figure 25.5.2 [see Osteryoung, J. *J. Chem. Educ.* **1983**, *60*, 296–298 for a comprehensive review]. Normal pulse polarography (Figure 25.5.2a), for example, uses a series of potential pulses characterized by a cycle of time $\tau$, a pulse-time of $t_p$, a pulse potential of $\Delta E_p$, and a scan rate of $\Delta E/\Delta t$. Typical experimental conditions for normal pulse polarography are $\tau \approx 1$ s, $t_p \approx 50$ ms, and $\Delta E/\Delta t \approx 2$ mV/s. The initial value of $\Delta E_p \approx 2$ mV, and it increases by ≈ 2 mV with each pulse. The current is sampled at the end of each potential pulse for approximately 17 ms before returning the potential to its initial value. The shape of the resulting voltammogram is similar to Figure 25.5.1, but without the current oscillations. Because we apply the potential for only a small portion of the drop's lifetime, there is less time for the analyte to undergo oxidation or reduction and a smaller diffusion layer. As a result, the faradaic current in normal pulse polarography is greater than in the polarography, resulting in better sensitivity and smaller detection limits.

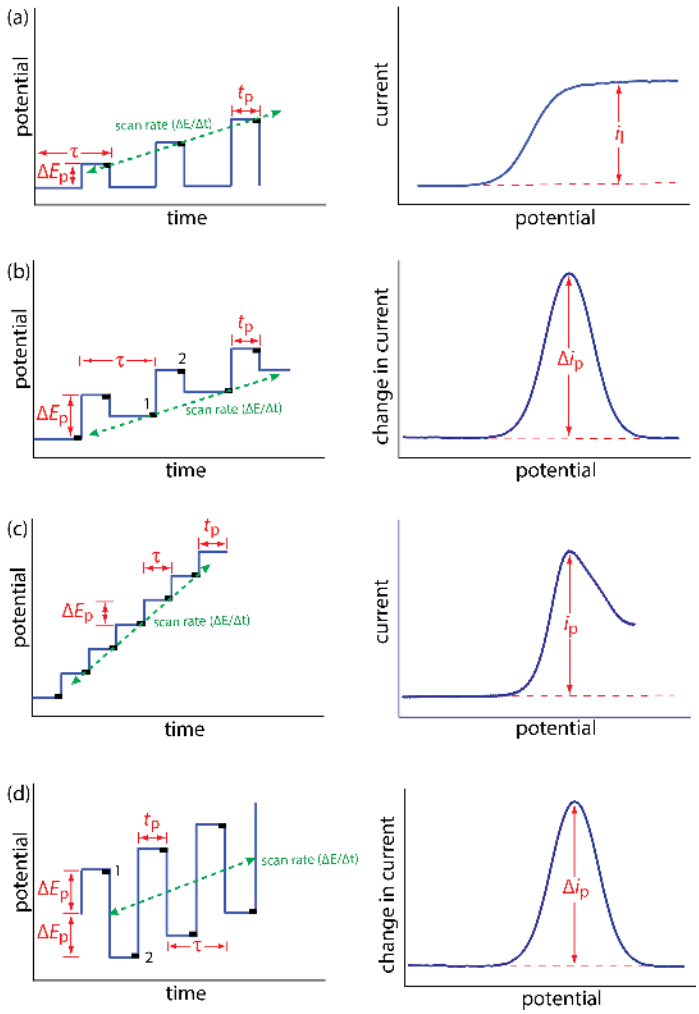



Figure 25.5.2. Potential-excitation signals and voltammograms for (a) normal pulse polarography, (b) differential pulse polarography, (c) staircase polarography, and (d) square-wave polarography. The current is sampled at the time intervals shown by the black rectangles. When measuring a change in current, $\Delta i$, the current at point 1 is subtracted from the current at point 2. The symbols in the diagrams are as follows: $\tau$ is the cycle time; $\Delta E_p$ is a fixed or variable pulse potential relative to the beginning of the cycle; and $t_p$ is the pulse time. The scan rate (change in potential per unit time) is shown by the dashed arrow.

In differential pulse polarography (Figure 25.5.2b) the current is measured twice per cycle: for approximately 17 ms before applying the pulse and for approximately 17 ms at the end of the cycle. The difference in the two currents gives rise to the peak-shaped voltammogram. Typical experimental conditions for differential pulse polarography are $\tau \approx 1$ s, $t_p \approx 50$ ms, $\Delta E_p \approx 50$ mV, and $\Delta E/\Delta t \approx 2$ mV/s.

> The voltammogram for differential pulse polarography is approximately the first derivative of the voltammogram for normal pulse polarography. To see why this is the case, note that the change in current over a fixed change in potential, $\Delta i/\Delta E$, approximates the slope of the voltammogram for normal pulse polarography. You may recall that the first derivative of a function returns the slope of the function at each point. The first derivative of a sigmoidal function is a peak-shaped function.

Other forms of pulse polarography include staircase polarography (Figure 25.5.2c) and square-wave polarography (Figure 25.5.2d). One advantage of square-wave polarography is that we can make $\tau$ very small—perhaps as small as 5 ms, compared to 1 s for other forms of pulse polarography—which significantly decreases analysis time. For example, suppose we need to scan a potential range of 400 mV. If we use normal pulse polarography with a $\Delta E/\Delta t$ of 2 mV/cycle and a $\tau$ of 1 s/cycle, then we need 200 s to complete

the scan. If we use square-wave polarography with a $\Delta E/\Delta t$ of 2 mV/cycle and a $\tau$ of 5 ms/cycle, we can complete the scan in 1 s. At this rate, we can acquire a complete voltammogram using a single drop of Hg!

## Applications

Polarography is used extensively for the analysis of metal ions and inorganic anions, such as $IO_3^-$ and $NO_3^-$. We also can use polarography to study organic compounds with easily reducible or oxidizable functional groups, such as carbonyls, carboxylic acids, and carbon-carbon double bonds.

---

This page titled 25.5: Polarography is shared under a CC BY-NC-SA 4.0 license and was authored, remixed, and/or curated by David Harvey.

# 25.6: Stripping Methods

Another important voltammetric technique is stripping voltammetry, which consists of three related techniques: anodic stripping voltammetry, cathodic stripping voltammetry, and adsorptive stripping voltammetry. Because anodic stripping voltammetry is the more widely used of these techniques, we will consider it in greatest detail.

Anodic stripping voltammetry consists of two steps (Figure 25.6.1). The first step is a controlled potential electrolysis in which we hold the working electrode—usually a hanging mercury drop or a mercury film electrode—at a cathodic potential sufficient to deposit the metal ion on the electrode. For example, when analyzing $Cu^{2+}$ the deposition reaction is

$$Cu^{2+} + 2e^- \rightleftharpoons Cu(Hg) \tag{25.6.1}$$

where Cu(Hg) indicates that the copper is amalgamated with the mercury. This step serves as a means of concentrating the analyte by transferring it from the larger volume of the solution to the smaller volume of the electrode. During most of the electrolysis we stir the solution to increase the rate of deposition. Near the end of the deposition time we stop the stirring—eliminating convection as a mode of mass transport—and allow the solution to become quiescent. Typical deposition times of 1–30 min are common, with analytes at lower concentrations requiring longer times.

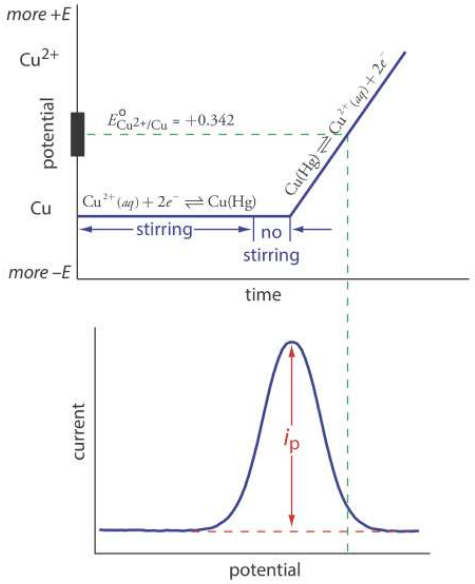



Figure 25.6.1. Potential-excitation signal and voltammogram for anodic stripping voltammetry at a hanging mercury drop electrode or a mercury film electrode.

In the second step, we scan the potential anodically—that is, toward a more positive potential. When the working electrode's potential is sufficiently positive, the analyte is stripped from the electrode, returning to solution in its oxidized form.

$$Cu(Hg) \rightleftharpoons Cu^{2+} + 2e^- \tag{25.6.2}$$

Monitoring the current during the stripping step gives a peak-shaped voltammogram, as shown in Figure 25.6.1. The peak current is proportional to the analyte's concentration in the solution. Because we are concentrating the analyte in the electrode, detection limits are much smaller than other electrochemical techniques. An improvement of three orders of magnitude—the equivalent of parts per billion instead of parts per million—is routine.

## Applications

Anodic stripping voltammetry is very sensitive to experimental conditions, which we must carefully control to obtain results that are accurate and precise. Key variables include the area of the mercury film or the size of the hanging Hg drop, the deposition time, the rest time, the rate of stirring, and the scan rate during the stripping step. Anodic stripping voltammetry is particularly useful for metals that form amalgams with mercury, several examples of which are listed in Table 25.6.1.

Table 25.6.1. Representative Examples of Analytes Determined by Stripping Voltammetry

| anodic stripping voltammetry | cathodic stripping voltammetry | adsorptive stripping voltammetry |
|---|---|---|
| $Bi^{3+}$ | $Br^-$ | bilirubin |
| $Cd^{2+}$ | $Cl^-$ | codeine |
| $Cu^{2+}$ | $I^-$ | cocaine |
| $Ga^{3+}$ | mercaptans (RSH) | digitoxin |
| $In^{3+}$ | $S^{2-}$ | dopamine |
| $Pb^{2+}$ | $SCN^-$ | heme |
| $Tl^+$ | | monesin |
| $Sn^{2+}$ | | testosterone |
| $Zn^{2+}$ | | |

Source: Compiled from Peterson, W. M.; Wong, R. V. *Am. Lab.* November 1981, 116–128; Wang, J. *Am. Lab.* May 1985, 41–50.

The experimental design for cathodic stripping voltammetry is similar to anodic stripping voltammetry with two exceptions. First, the deposition step involves the oxidation of the Hg electrode to $Hg_2^{2+}$, which then reacts with the analyte to form an insoluble film at the surface of the electrode. For example, when $Cl^-$ is the analyte the deposition step is

$$2Hg(l) + 2Cl^-(aq) \rightleftharpoons Hg_2Cl_2(s) + 2e^- \tag{25.6.3}$$

Second, stripping is accomplished by scanning cathodically toward a more negative potential, reducing $Hg_2^{2+}$ back to Hg and returning the analyte to solution.

$$Hg_2Cl_2(s) + 2e^- \rightleftharpoons 2Hg(l) + 2Cl^-(aq) \tag{25.6.4}$$

Table 25.6.1 lists several analytes analyzed successfully by cathodic stripping voltammetry.

In adsorptive stripping voltammetry, the deposition step occurs without electrolysis. Instead, the analyte adsorbs to the electrode's surface. During deposition we maintain the electrode at a potential that enhances adsorption. For example, we can adsorb a neutral molecule on a Hg drop if we apply a potential of –0.4 V versus the SCE, a potential where the surface charge of mercury is approximately zero. When deposition is complete, we scan the potential in an anodic or a cathodic direction, depending on whether we are oxidizing or reducing the analyte. Examples of compounds that have been analyzed by absorptive stripping voltammetry also are listed in Table 25.6.1.

This page titled 25.6: Stripping Methods is shared under a CC BY-NC-SA 4.0 license and was authored, remixed, and/or curated by David Harvey.

# 25.7: Applications of Voltammetry

Voltammetry finds use for both quantitative analyses and characterization analyses. Examples of each are highlighted in this section.

## Quantitative Applications

Voltammetry has been used for the quantitative analysis of a wide variety of samples, including environmental samples, clinical samples, pharmaceutical formulations, steels, gasoline, and oil.

### Selecting the Voltammetric Technique

The choice of which voltammetric technique to use depends on the sample's characteristics, including the analyte's expected concentration and the sample's location. For example, amperometry is ideally suited for detecting analytes in flow systems, including the *in vivo* analysis of a patient's blood or as a selective sensor for the rapid analysis of a single analyte. The portability of amperometric sensors, which are similar to potentiometric sensors, also make them ideal for field studies. Although cyclic voltammetry is used to determine an analyte's concentration, other methods described in this chapter are better suited for quantitative work.

Pulse polarography and stripping voltammetry frequently are interchangeable. The choice of which technique to use often depends on the analyte's concentration and the desired accuracy and precision. Detection limits for normal pulse polarography generally are on the order of $10^{-6}$ M to $10^{-7}$ M, and those for differential pulse polarography, staircase, and square wave polarography are between $10^{-7}$ M and $10^{-9}$ M. Because we concentrate the analyte in stripping voltammetry, the detection limit for many analytes is as little as $10^{-10}$ M to $10^{-12}$ M. On the other hand, the current in stripping voltammetry is much more sensitive than pulse polarography to changes in experimental conditions, which may lead to poorer precision and accuracy. We also can use pulse polarography to analyze a wider range of inorganic and organic analytes because there is no need to first deposit the analyte at the electrode surface.

Stripping voltammetry also suffers from occasional interferences when two metals, such as Cu and Zn, combine to form an intermetallic compound in the mercury amalgam. The deposition potential for Zn is sufficiently negative that any $Cu^{2+}$ in the sample also deposits into the mercury drop or film, leading to the formation of intermetallic compounds such as CuZn and $CuZn_2$. During the stripping step, zinc in the intermetallic compounds strips at potentials near that of copper, decreasing the current for zinc at its usual potential and increasing the apparent current for copper. It is possible to overcome this problem by adding an element that forms a stronger intermetallic compound with the interfering metal. Thus, adding $Ga^{3+}$ minimizes the interference of Cu when analyzing for Zn by forming an intermetallic compound of Cu and Ga.

### Correcting for the Residual Current

In any quantitative analysis we must correct the analyte's signal for signals that arise from other sources. The total current, $i_{tot}$, in voltammetry consists of two parts: the current from the analyte's oxidation or reduction, $i_A$, and a background or residual current, $i_r$.

$$i_{tot} = i_A + i_r \tag{25.7.1}$$

The residual current, in turn, has two sources. One source is a faradaic current from the oxidation or reduction of trace interferents in the sample, $i_{int}$. The other source is the charging current, $i_{ch}$, that accompanies a change in the working electrode's potential.

$$i_r = i_{\text{int}} + i_{ch} \tag{25.7.2}$$

We can minimize the faradaic current due to impurities by carefully preparing the sample. For example, one important impurity is dissolved $O_2$, which undergoes a two-step reduction: first to $H_2O_2$ at a potential of –0.1 V versus the SCE, and then to $H_2O$ at a potential of –0.9 V versus the SCE. Removing dissolved $O_2$ by bubbling an inert gas such as $N_2$ through the sample eliminates this interference. After removing the dissolved $O_2$, maintaining a blanket of $N_2$ over the top of the solution prevents $O_2$ from reentering the solution.

There are two methods to compensate for the residual current. One method is to measure the total current at potentials where the analyte's faradaic current is zero and extrapolate it to other potentials. This is the method shown in Figure 25.3.7. One advantage of extrapolating is that we do not need to acquire additional data. An important disadvantage is that an extrapolation assumes that any

change in the residual current with potential is predictable, which may not be the case. A second, and more rigorous approach, is to obtain a voltammogram for an appropriate blank. The blank's residual current is then subtracted from the sample's total current.

### Analysis for Single Components

The analysis of a sample with a single analyte is straightforward using any of the standardization methods discussed in Chapter 1.

**Example 25.7.1**

The concentration of As(III) in water is determined by differential pulse polarography in 1 M HCl. The initial potential is set to –0.1 V versus the SCE and is scanned toward more negative potentials at a rate of 5 mV/s. Reduction of As(III) to As(0) occurs at a potential of approximately –0.44 V versus the SCE. The peak currents for a set of standard solutions, corrected for the residual current, are shown in the following table.

| [As(III)] (μM) | $i_p$ (μM) |
|---|---|
| 1.00 | 0.298 |
| 3.00 | 0.947 |
| 6.00 | 1.83 |
| 9.00 | 2.72 |

What is the concentration of As(III) in a sample of water if its peak current is 1.37 μA?

**Solution**

Linear regression gives the calibration curve shown in Figure 25.7.1, with an equation of

$$i_p = 0.0176 + 3.01 \times [\text{As(III)}]$$

Substituting the sample's peak current into the regression equation gives the concentration of As(III) as 4.49 μM.

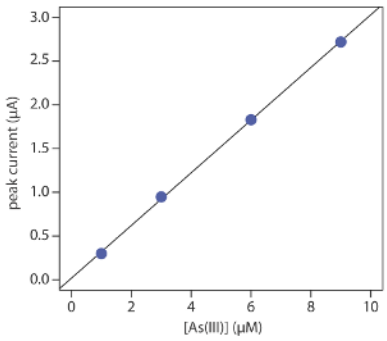



Figure 25.7.1. Calibration curve for the data in Example 25.7.1.

### Multicomponent Analysis

Voltammetry is a particularly attractive technique for the analysis of samples that contain two or more analytes. Provided that the analytes behave independently, the voltammogram of a multicomponent mixture is a summation of each analyte's individual voltammograms. As shown in Figure 25.7.2, if the separation between the half-wave potentials or between the peak potentials is sufficient, we can determine the presence of each analyte as if it is the only analyte in the sample. The minimum separation between the half-wave potentials or peak potentials for two analytes depends on several factors, including the type of electrode and the potential-excitation signal. For normal polarography the separation is at least ±0.2–0.3 V, and differential pulse voltammetry requires a minimum separation of ±0.04–0.05 V.

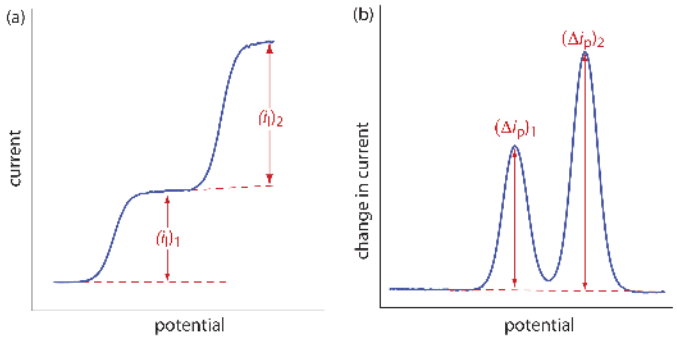



Figure 25.7.2. Voltammograms for a sample that contains two analytes showing the measurement of (a) limiting currents, and (b) peak currents.

If the voltammograms for two analytes are not sufficiently separated, a simultaneous analysis may be possible. An example of this approach is outlined the following example.

**Example 25.7.2**

The differential pulse polarographic analysis of a mixture of indium and cadmium in 0.1 M HCl is complicated by the overlap of their respective voltammograms [Lanza P. *J. Chem. Educ.* **1990**, *67*, 704–705]. The peak potential for indium is at –0.557 V and that for cadmium is at –0.597 V. When a 0.800-ppm indium standard is analyzed, $\Delta i_p$ (in arbitrary units) is 200.5 at –0.557 V and 87.5 at –0.597 V relative to a saturated Ag/AgCl reference electorde. A standard solution of 0.793 ppm cadmium has a $\Delta i_p$ of 58.5 at –0.557 V and 128.5 at –0.597 V. What is the concentration of indium and cadmium in a sample if $\Delta i_p$ is 167.0 at a potential of –0.557 V and 99.5 at a potential of –0.597V.

**Solution**

The change in current, $\Delta i_p$, in differential pulse polarography is a linear function of the analyte's concentration

$$\Delta i_p = k_A C_A$$

where $k_A$ is a constant that depends on the analyte and the applied potential, and $C_A$ is the analyte's concentration. To determine the concentrations of indium and cadmium in the sample we must first find the value of $k_A$ for each analyte at each potential. For simplicity we will identify the potential of –0.557 V as $E_1$, and that for –0.597 V as $E_2$. The values of $k_A$ are

$$k_{\text{In},E_1} = \frac{200.5}{0.800 \text{ ppm}} = 250.6 \text{ ppm}^{-1}$$
$$k_{\text{In},E_2} = \frac{87.5}{0.800 \text{ ppm}} = 109.4 \text{ ppm}^{-1}$$
$$k_{\text{Cd}E_1} = \frac{58.5}{0.793 \text{ ppm}} = 73.8 \text{ ppm}^{-1}$$
$$k_{\text{Cd}E_2} = \frac{128.5}{0.793 \text{ ppm}} = 162.0 \text{ ppm}^{-1}$$

Next, we write simultaneous equations for the current at the two potentials.

$$\Delta i_{E_1} = 167.0 = 250.6 \text{ ppm}^{-1} \times C_{\text{In}} + 73.8 \text{ ppm}^{-1} \times C_{\text{Cd}}$$
$$\triangle i_{E_2} = 99.5 = 109.4 \text{ ppm}^{-1} \times C_{\text{In}} + 162.0 \text{ ppm}^{-1} \times C_{\text{Cd}}$$

Solving the simultaneous equations, which is left as an exercise, gives the concentration of indium as 0.606 ppm and the concentration of cadmium as 0.205 ppm.

## Environmental Samples

Voltammetry is one of several important analytical techniques for the analysis of trace metals in environmental samples, including groundwater, lakes, rivers and streams, seawater, rain, and snow. Detection limits at the parts-per-billion level are routine for many trace metals using differential pulse polarography, with anodic stripping voltammetry providing parts-per-trillion detection limits for some trace metals.

One interesting environmental application of anodic stripping voltammetry is the determination of a trace metal's chemical form within a water sample. Speciation is important because a trace metal's bioavailability, toxicity, and ease of transport through the environment often depends on its chemical form. For example, a trace metal that is strongly bound to colloidal particles generally is not toxic because it is not available to aquatic lifeforms. Unfortunately, anodic stripping voltammetry can not distinguish a trace metal's exact chemical form because closely related species, such as $Pb^{2+}$ and $PbCl^{+}$, produce a single stripping peak. Instead, trace metals are divided into "operationally defined" categories that have environmental significance.

> Operationally defined means that an analyte is divided into categories by the specific methods used to isolate it from the sample. There are many examples of operational definitions in the environmental literature. The distribution of trace metals in soils and sediments, for example, often is defined in terms of the reagents used to extract them; thus, you might find an operational definition for $Zn^{2+}$ in a lake sediment as that extracted using 1.0 M sodium acetate, or that extracted using 1.0 M HCl.

Although there are many speciation schemes in the environmental literature, we will consider one proposed by Batley and Florence [see (a) Batley, G. E.; Florence, T. M. *Anal. Lett.* **1976**, *9*, 379–388; (b) Batley, G. E.; Florence, T. M. *Talanta* **1977**, *24*, 151–158; (c) Batley, G. E.; Florence, T. M. *Anal. Chem.* **1980**, *52*, 1962–1963; (d) Florence, T. M., Batley, G. E.; *CRC Crit. Rev. Anal. Chem.* **1980**, *9*, 219–296]. This scheme, which is outlined in Table 25.7.2, combines anodic stripping voltammetry with ion-exchange and UV irradiation, dividing soluble trace metals into seven groups. In the first step, anodic stripping voltammetry in a pH 4.8 acetic acid buffer differentiates between labile metals and nonlabile metals. Only labile metals—those present as hydrated ions, weakly bound complexes, or weakly adsorbed on colloidal surfaces—deposit at the electrode and give rise to a signal. Total metal concentration are determined by ASV after digesting the sample in 2 M $HNO_3$ for 5 min, which converts all metals into an ASV-labile form.

Table 25.7.1. Operational Speciation of Soluble Trace Metals

| method | speciation of soluble metals | | | | | | |
|---|---|---|---|---|---|---|---|
| ASV | labile metals | | | nonlabile or bound metals | | | |
| Ion-Exchange | removed | not removed | | removed | | not removed | |
| UV Irradiation | | released | not released | released | not released | released | not released |
| Groups | I | II | III | IV | V | VI | VII |
| Group I: free metal ions; weaker labile organic complexes and inorganic complexes | | | | | | | |
| Group II: stronger labile organic complexes; labile metals absorbed on organic solids | | | | | | | |
| Group III: stronger labile inorganic complexes; labile metals absorbed on inorganic solids | | | | | | | |
| Group IV: weaker nonlabile organic complexes | | | | | | | |
| Group V: weaker nonlabile inorganic complexes | | | | | | | |
| Group VI: stronger nonlabile organic complexes; nonlabile metals absorbed on organic solids | | | | | | | |
| Group VII: stronger nonlabile inorganic complexes; nonlabile metals absorbed on inorganic solids | | | | | | | |
| Operational definitions of speciation from (a)Batley,G.E.;Florence,T.M.*Anal.Lett.***1976**,*9*,379–388; (b)Batley,G.E.;Florence,T.M.*Talanta***1977**,*24*,151–158; (c) Batley, G. E.; Florence, T. M. *Anal. Chem.* **1980**, *52*, 1962–1963; (d) Florence, T. M., Batley, G. E.; *CRC Crit. Rev. Anal. Chem.* **1980**, *9*, 219–296. | | | | | | | |

A Chelex-100 ion-exchange resin further differentiates between strongly bound metals—usually metals bound to inorganic and organic solids, but also those tightly bound to chelating ligands—and more loosely bound metals. Finally, UV radiation differentiates between metals bound to organic phases and inorganic phases. The analysis of seawater samples, for example, suggests that cadmium, copper, and lead are present primarily as labile organic complexes or as labile adsorbates on organic colloids (Group II in Table 25.7.1).

Differential pulse polarography and stripping voltammetry are used to determine trace metals in airborne particulates, incinerator fly ash, rocks, minerals, and sediments. The trace metals, of course, are first brought into solution using a digestion or an extraction.

Amperometric sensors also are used to analyze environmental samples. For example, the dissolved $O_2$ sensor described earlier is used to determine the level of dissolved oxygen and the biochemical oxygen demand, or BOD, of waters and wastewaters. The latter test—which is a measure of the amount of oxygen required by aquatic bacteria as they decompose organic matter—is important when evaluating the efficiency of a wastewater treatment plant and for monitoring organic pollution in natural waters. A high BOD suggests that the water has a high concentration of organic matter. Decomposition of this organic matter may seriously deplete the level of dissolved oxygen in the water, adversely affecting aquatic life. Other amperometric sensors are available to monitor anionic surfactants in water, and $CO_2$, $H_2SO_4$, and $NH_3$ in atmospheric gases.

## Clinical Samples

Differential pulse polarography and stripping voltammetry are used to determine the concentration of trace metals in a variety of clinical samples, including blood, urine, and tissue. The determination of lead in blood is of considerable interest due to concerns about lead poisoning. Because the concentration of lead in blood is so small, anodic stripping voltammetry frequently is the more appropriate technique. The analysis is complicated, however, by the presence of proteins that may adsorb to the mercury electrode, inhibiting either the deposition or stripping of lead. In addition, proteins may prevent the electrodeposition of lead through the formation of stable, nonlabile complexes. Digesting and ashing the blood sample mini- mizes this problem. Differential pulse polarography is useful for the routine quantitative analysis of drugs in biological fluids, at concentrations of less than $10^{-6}$ M [Brooks, M. A. “Application of Electrochemistry to Pharmaceutical Analysis,” Chapter 21 in Kissinger, P. T.; Heinemann, W. R., eds. *Laboratory Techniques in Electroanalytical Chemistry*, Marcel Dekker, Inc.: New York, 1984, pp 539–568.]. Amperometric sensors using enzyme catalysts also have many clinical uses, several examples of which are shown in Table 25.7.2.

Table 25.7.2. Representative Amperometric Biosensors

| analyte | enzyme | species detected |
|---|---|---|
| choline | choline oxidase | $H_2O_2$ |
| ethanol | alcohol oxidase | $H_2O_2$ |
| formaldehyde | formaldehyde dehydrogenase | NADH |
| glucose | glucose oxidase | $H_2O_2$ |
| glutamine | glutaminase, glutamine oxidase | $H_2O_2$ |
| glycerol | glycerol dehydrogenase | NADH, $O_2$ |
| lactate | lactate oxidase | $H_2O_2$ |
| phenol | polyphenol oxidase | quinone |
| inorganic phosphorous | nucleoside phosphoylase | $O_2$ |

Source: Cammann, K.; Lemke, U.; Rohen, A.; Sander, J.; Wilken, H.; Winter, B. *Angew. Chem. Int. Ed. Engl.* **1991**, *30*, 516–539.

## Miscellaneous Samples

In addition to environmental samples and clinical samples, differential pulse polarography and stripping voltammetry are used for the analysis of trace metals in other sample, including food, steels and other alloys, gasoline, gunpowder residues, and pharmaceuticals. Voltammetry is an important technique for the quantitative analysis of organics, particularly in the pharmaceutical industry where it is used to determine the concentration of drugs and vitamins in formulations. For example, voltammetric methods are available for the quantitative analysis of vitamin A, niacinamide, and riboflavin. When the compound of interest is not electroactive, it often can be derivatized to an electroactive form. One example is the differential pulse polarographic determination of sulfanilamide, which is converted into an electroactive azo dye by coupling with sulfamic acid and 1-napthol.

In the previous section we learned how to use voltammetry to determine an analyte's concentration in a variety of different samples. We also can use voltammetry to characterize an analyte's properties, including verifying its electrochemical reversibility, determining the number of electrons transferred during its oxidation or reduction, and determining its equilibrium constant in a coupled chemical reaction.

## Characterization Applications

In a characterization application we study the properties of a system. Three examples are described here: determining if a redox reaction is electrochemically reversible, determining the number of electrons involved in the redox reaction, and studying metal-ligand complexation.

### Electrochemical Reversibility and Determination of *n*

Earlier in this chapter we derived a relationship between $E_{1/2}$ and the standard-state potential for a redox couple using the Nernst equation, noting that a redox reaction must be electrochemically reversible. How can we tell if a redox reaction is reversible by looking at its voltammogram? As we learned in Chapter 25.3, for a reversible redox reaction the relationship between potential and current is

$$E = E_{½} - \frac{0.05916}{n} \log \frac{i}{i_l - i} \tag{25.7.3}$$

If a reaction is electrochemically reversible, a plot of $E$ versus $\log \frac{i}{i_l - i}$ is a straight line with a slope of –0.05916/$n$. In addition, the slope should yield an integer value for $n$.

**Example 25.7.3**

The following data were obtained from a linear scan hydrodynamic voltammogram of a reversible reduction reaction.

| $E$ (V vs. SCE) | current (μA) |
|---|---|
| –0.358 | 0.37 |
| –0.372 | 0.95 |
| –0.382 | 1.71 |
| –0.400 | 3.48 |
| –0.410 | 4.20 |
| –0.435 | 4.97 |

The limiting current is 5.15 μA. Show that the reduction reaction is reversible, and determine values for $n$ and for $E_{1/2}$.

**Solution**

Figure 25.7.3 shows a plot of $E$ versus $\log \frac{i}{i_l - i}$. Because the result is a straight-line, we know the reaction is electrochemically reversible under the conditions of the experiment. A linear regression analysis gives the equation for the straight line as

$$E = -0.391\text{V} - 0.0300 \log \frac{i}{i_l - i}$$

From Equation 25.7.3, the slope is equivalent to –0.05916/$n$; solving for $n$ gives a value of 1.97, or 2 electrons. From Equation 25.7.3 we also know that $E_{1/2}$ is the $y$-intercept for a plot of $E$ versus $\log \frac{i}{i_l - i}$; thus, $E_{1/2}$ for the data in this example is –0.391 V versus the SCE.

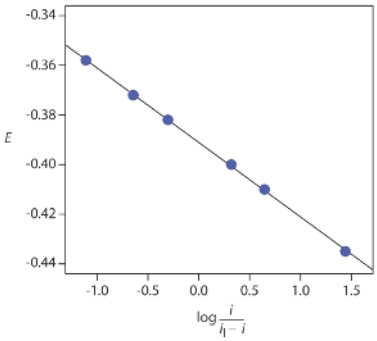



Figure 25.7.3. Determination of electrochemical reversibility for the data in Example 25.7.3.

We also can use cyclic voltammetry to evaluate electrochemical reversibility by looking at the difference between the peak potentials for the anodic and the cathodic scans. For an electrochemically reversible reaction, the following equation holds true.

$$\Delta E_p = E_{p,a} - E_{p,c} = \frac{0.05916 \text{ V}}{n} \tag{25.7.4}$$

As an example, for a two-electron reduction we expect a $\Delta E_p$ of approximately 29.6 mV. For an electrochemically irreversible reaction the value of $\Delta E_p$ is larger than expected.

## Determining Equilibrium Constants for Coupled Chemical Reactions

Another important application of voltammetry is determining the equilibrium constant for a solution reaction that is coupled to a redox reaction. The presence of the solution reaction affects the ease of electron transfer in the redox reaction, shifting $E_{1/2}$ to a more negative or to a more positive potential. Consider, for example, the reduction of *O* to R

$$O + ne^- \rightleftharpoons R \tag{25.7.5}$$

the voltammogram for which is shown in Figure 25.7.4. If we introduce a ligand, *L*, that forms a strong complex with *O*, then we also must consider the reaction

$$O + pL \rightleftharpoons OL_p \tag{25.7.6}$$

In the presence of the ligand, the overall redox reaction is

$$OL_p + ne^- \rightleftharpoons R + pL \tag{25.7.7}$$

Because of its stability, the reduction of the $OL_p$ complex is less favorable than the reduction of *O*. As shown in Figure 25.7.4, the resulting voltammogram shifts to a potential that is more negative than that for *O*. Furthermore, the shift in the voltammogram increases as we increase the ligand's concentration.

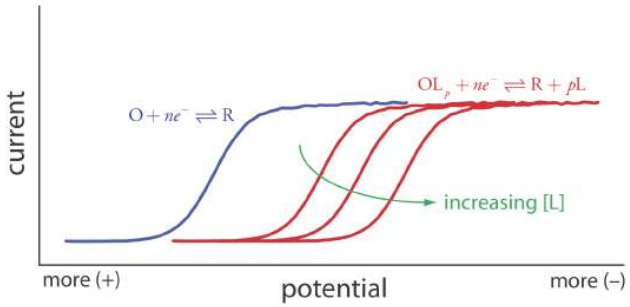



Figure 25.7.4. Effect of a metal-ligand complexation reaction on a voltammogram. The voltammogram in blue is for the reduction of *O* in the absence of ligand. Adding the ligand shifts the potentials to more negative potentials, as shown by the voltammograms in red.

We can use this shift in the value of $E_{1/2}$ to determine both the stoichiometry and the formation constant for a metal-ligand complex. To derive a relationship between the relevant variables we begin with two equations: the Nernst equation for the reduction of *O*

$$E = E^{\circ}_{O/R} - \frac{0.05916}{n} \log \frac{[R]_{x=0}}{[O]_{x=0}} \tag{25.7.8}$$

and the stability constant, $\beta_p$ for the metal-ligand complex at the electrode surface.

$$\beta_p = \frac{[OL_p]_{x=0}}{[O]_{x=0}[L]^p_{x=0}} \tag{25.7.9}$$

In the absence of ligand the half-wave potential occurs when $[R]_{x = 0}$ and $[O]_{x = 0}$ are equal; thus, from the Nernst equation we have

$$(E_{1/2})_{nc} = E^{\circ}_{O/R} \tag{25.7.10}$$

where the subscript "*nc*" signifies that the complex is not present. When ligand is present we must account for its effect on the concentration of *O*. Solving Equation 25.7.9 for $[O]_{x = 0}$ and substituting into the Equation 25.7.8 gives

$$E = E^{\circ}_{O/R} - \frac{0.05916}{n} \log \frac{[R]_{x=0}[L]^p_{x=0}\beta_p}{[OL_p]_{x=0}} \tag{25.7.11}$$

If the formation constant is sufficiently large, such that essentially all *O* is present as the complex $OL_p$, then $[R]_{x=0}$ and $[OL_p]_{x=0}$ are equal at the half-wave potential, and Equation 25.7.11 simplifies to

$$(E_{1/2})_c = E^{\circ}_{O/R} - \frac{0.05916}{n} \log [L]^p_{x=0}\beta_p \tag{25.7.12}$$

where the subscript "*c*" indicates that the complex is present. Defining $\Delta E_{1/2}$ as

$$\triangle E_{1/2} = (E_{1/2})_c - (E_{1/2})_{nc} \tag{25.7.13}$$

and substituting Equation 25.7.10 and Equation 25.7.12 and expanding the log term leaves us with the following equation.

$$\Delta E_{1/2} = -\frac{0.05916}{n} \log \beta_p - \frac{0.05916p}{n} \log [L] \tag{25.7.14}$$

A plot of $\Delta E_{1/2}$ versus log[$L$] is a straight-line, with a slope that is a function of the metal-ligand complex's stoichiometric coefficient, *p*, and a *y*-intercept that is a function of its formation constant $\beta_p$.

### Example 25.7.4

A voltammogram for the two-electron reduction (*n* = 2) of a metal, *M*, has a half-wave potential of –0.226 V versus the SCE. In the presence of an excess of ligand, *L*, the following half-wave potentials are recorded.

| [$L$] (M) | $(E_{1/2})_c$ (V vs. SCE) |
|---|---|
| 0.020 | –0.494 |
| 0.040 | –0.512 |
| 0.060 | –0.523 |
| 0.080 | –0.530 |
| 0.100 | –0.536 |

Determine the stoichiometry of the metal-ligand complex and its formation constant.

#### Solution

We begin by calculating values of $\Delta E_{1/2}$ using Equation 25.7.13, obtaining the values in the following table.

| $[L]$ (M) | $\Delta E_{1/2}$ (V vs. SCE) |
|---|---|
| 0.020 | –0.268 |
| 0.040 | –0.286 |
| 0.060 | –0.297 |
| 0.080 | –0.304 |
| 0.100 | –0.310 |

Figure 25.7.5 shows the resulting plot of $\Delta E_{1/2}$ as a function of log[$L$]. A linear regression analysis gives the equation for the straight line as

$$\triangle E_{1/2} = -0.370\text{V} - 0.0601 \log [L]$$

From Equation 25.7.14 we know that the slope is equal to –0.05916$p$/$n$. Using the slope and $n$ = 2, we solve for $p$ obtaining a value of 2.03 ≈ 2. The complex's stoichiometry, therefore, is $ML_2$. We also know, from Equation 25.7.14, that the $y$-intercept is equivalent to –(0.05916/$n$)log$\beta_p$. Solving for $\beta_2$ gives a formation constant of $3.2 \times 10^{12}$.

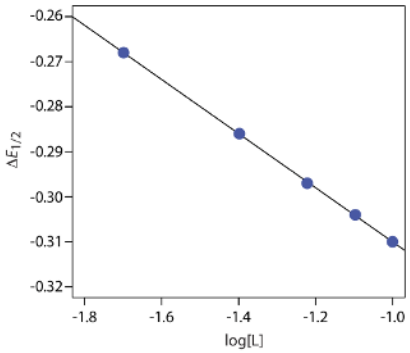



Figure 25.7.5. Determination of the stoichiometry and formation constant for a metal-ligand complex using the data in Example 25.7.4.

Cyclic voltammetry is one of the most powerful electrochemical techniques for exploring the mechanism of coupled electrochemical and chemical reactions. The treatment of this aspect of cyclic voltammetry is beyond the level of this text, although you can consult this chapter's additional resources for additional information.

This page titled 25.7: Applications of Voltammetry is shared under a CC BY-NC-SA 4.0 license and was authored, remixed, and/or curated by David Harvey.

# CHAPTER OVERVIEW

## 26: Introduction to Chromatographic Separations

In previous chapters we explored the application of spectroscopy and electroanalytical chemistry to the quantitative analysis of an analyte in a sample. Despite the power of these instrumental methods of analysis, their use is often limited if the sample contains species that will interfere with the analysis. A UV/Vis analysis, for example, is easy to complete if the analyte is the only species present that absorbs light at the analytical wavelength. If two species contribute to the overall absorbance, a quantitative analysis is still possible if we can measure the sample's absorbance at two wavelengths. Things become more complex, however, as the number of analytes or interferents increase or if we do not know the identity of an intereferent.

Chromatography provides a solution to the analysis of complex samples by providing a way to separate the individual species in a sample prior to their analysis by a spectroscopic or electroanalytical method of analysis. In this chapter we provide a general introduction to chromatographic separations. In the four chapters that follow, we will consider specific chromatographic methods.


26.1: A General Description of Chromatography

26.2: Migration Rates of Solutes

26.3: Zone Broadening and Column Efficiency

26.4: Optimization and Column Performance

26.5: Summary of Important Relationships for Chromatography

26.6: Applications of Chromatography


---


This page titled 26: Introduction to Chromatographic Separations is shared under a CC BY-NC-SA 4.0 license and was authored, remixed, and/or curated by David Harvey.

# 26.1: A General Description of Chromatography

In chromatography we pass a sample-free phase, which we call the mobile phase, over a second sample-free stationary phase that remains fixed in space (Figure 26.1.1). We inject or place the sample into the mobile phase. As the sample moves with the mobile phase, its components partition between the mobile phase and the stationary phase. A component whose distribution ratio favors the stationary phase requires more time to pass through the system. Given sufficient time and sufficient stationary and mobile phase, we can separate solutes even if they have similar distribution ratios.

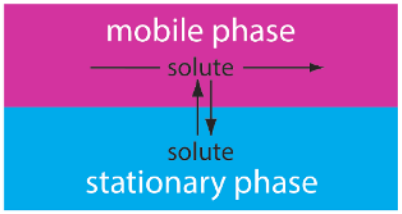



Figure 26.1.1. In chromatography we pass a mobile phase over a stationary phase. When we inject a sample into the mobile phase, the sample's components both move with the mobile phase and partition into the stationary phase. The solute that spends the most time in the stationary phase takes the longest time to move through the system.

## Classification of Chromatographic Methods

There are many ways in which we can identify a chromatographic separation: by describing the physical state of the mobile phase and the stationary phase; by describing how we bring the stationary phase and the mobile phase into contact with each other; or by describing the chemical or physical interactions between the solute and the stationary phase. Let's briefly consider how we might use each of these classifications.

> We can trace the history of chromatography to the turn of the century when the Russian botanist Mikhail Tswett used a column packed with calcium carbonate and a mobile phase of petroleum ether to separate colored pigments from plant extracts. As the sample moved through the column, the plant's pigments separated into individual colored bands. After effecting the separation, the calcium carbonate was removed from the column, sectioned, and the pigments recovered. Tswett named the technique chromatography, combining the Greek words for "color" and "to write." There was little interest in Tswett's technique until Martin and Synge's pioneering development of a theory of chromatography (see Martin, A. J. P.; Synge, R. L. M. "A New Form of Chromatogram Employing Two Liquid Phases," *Biochem. J.* **1941**, *35*, 1358–1366). Martin and Synge were awarded the 1952 Nobel Prize in Chemistry for this work.

### Types of Mobile Phases and Stationary Phases

The mobile phase is a liquid or a gas, and the stationary phase is a solid or a liquid film coated on a solid substrate. We often name chromatographic techniques by listing the type of mobile phase followed by the type of stationary phase. In gas–liquid chromatography, for example, the mobile phase is a gas and the stationary phase is a liquid film coated on a solid substrate. If a technique's name includes only one phase, as in gas chromatography, it is the mobile phase.

### Contact Between the Mobile Phase and the Stationary Phase

There are two common methods for bringing the mobile phase and the stationary phase into contact. In column chromatography we pack the stationary phase into a narrow column and pass the mobile phase through the column using gravity or by applying pressure. The stationary phase is a solid particle or a thin liquid film coated on either a solid particulate packing material or on the column's walls.

In planar chromatography the stationary phase is coated on a flat surface—typically, a glass, metal, or plastic plate. One end of the plate is placed in a reservoir that contains the mobile phase, which moves through the stationary phase by capillary action. In paper chromatography, for example, paper is the stationary phase.

### Interaction Between the Solute and the Stationary Phase

The interaction between the solute and the stationary phase provides a third method for describing a separation (Figure 26.1.2). In adsorption chromatography, solutes separate based on their ability to adsorb to a solid stationary phase. In partition chromatography, the stationary phase is a thin liquid film on a solid support. Separation occurs because there is a difference in the equilibrium partitioning of solutes between the stationary phase and the mobile phase. A stationary phase that consists of a solid support with covalently attached anionic (e.g., $-SO_3^-$ ) or cationic (e.g., $-N(CH_3)_3^+$) functional groups is the basis for ion-exchange chromatography in which ionic solutes are attracted to the stationary phase by electrostatic forces. In size-exclusion chromatography the stationary phase is a porous particle or gel, with separation based on the size of the solutes. Larger solutes are unable to penetrate as deeply into the porous stationary phase and pass more quickly through the column.

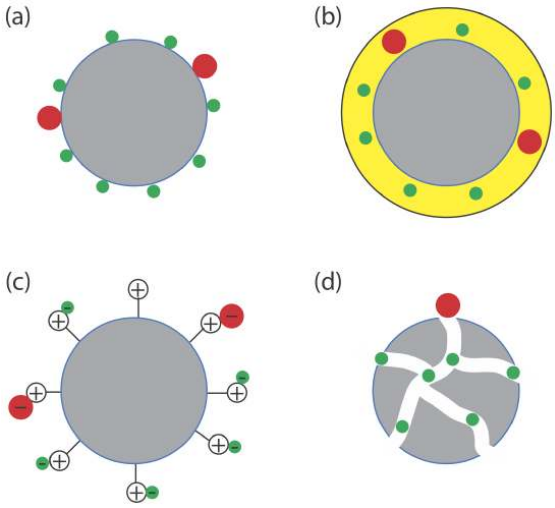



Figure 26.1.2. Four examples of interactions between a solute and the stationary phase: (a) adsorption on a solid surface, (b) partitioning into a liquid phase, (c) ion-exchange, and (d) size exclusion. For each example, the smaller, green solute is more strongly retained than the larger, red solute.

There are other interactions that can serve as the basis of a separation. In affinity chromatography the interaction between an antigen and an antibody, between an enzyme and a substrate, or between a receptor and a ligand forms the basis of a separation.

## Elution Chromatography on Columns

Of the two methods for bringing the stationary phase and the mobile phases into contact, the most important is column chromatography. In this section we develop a general theory that we may apply to any form of column chromatography.

Figure 26.1.3 provides a simple view of a liquid–solid column chromatography experiment. The sample is introduced as a narrow band at the top of the column. Ideally, the solute's initial concentration profile is rectangular (Figure 26.1.4a). As the sample moves down (or throught) the column, the solutes begin to separate (Figure 26.1.3b,c) and the individual solute bands begin to broaden and

develop a Gaussian profile (Figure 26.1.4b,c). If the strength of each solute's interaction with the stationary phase is sufficiently different, then the solutes separate into individual bands (Figure 26.1.3d and Figure 26.1.4d).

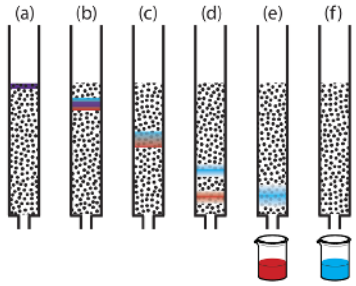



Figure 26.1.3. Progress of a column chromatographic separation of a two-component mixture. In (a) the sample is layered on top of the stationary phase. As mobile phase passes through the column, the sample separates into two solute bands (b–d). In (e) and (f), we collect each solute as it elutes from the column.

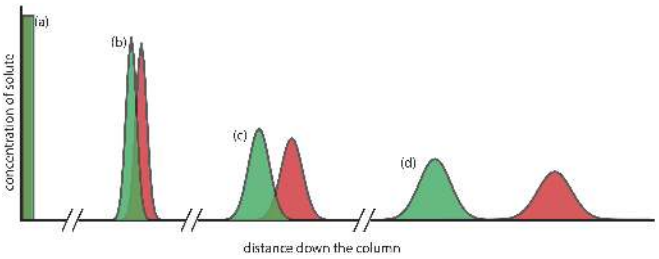



Figure 26.1.4. An alternative view of the separation in Figure 26.1.3 showing the concentration of each solute as a function of distance down the column.

We can follow the progress of the separation by collecting fractions as they elute from the column (Figure 26.1.3e,f), or by placing a suitable detector at the end of the column. A plot of the detector's response as a function of elution time, or as a function of the volume of mobile phase, is known as a chromatogram (Figure 26.1.5), and consists of a peak for each solute.

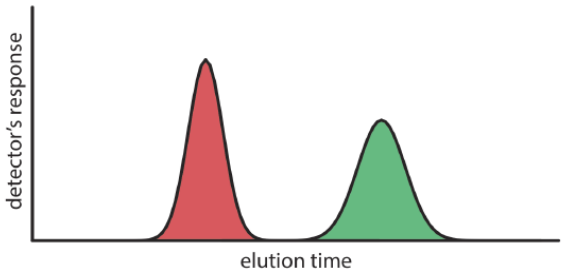



Figure 26.1.5. Chromatogram for the separation shown in Figure 26.1.3 and Figure 26.1.4, showing the detector's response as a function of the elution time.

> There are many possible detectors that we can use to monitor the separation. Later sections of this chapter describe some of the most popular.

This page titled 26.1: A General Description of Chromatography is shared under a CC BY-NC-SA 4.0 license and was authored, remixed, and/or curated by David Harvey.

# 26.2: Migration Rates of Solutes

Our ability to separate two solutes depends on the equilibrium interactions of the solute with the stationary phase and the mobile phase, which effects both the time it takes a solute to travel through the column and the width of the solute's elution profile. In this section we consider the rate at which the solute moves through the column.

## Distribution Constants

Let's assume we can describe a solute's distribution between the mobile phase and stationary phase using the following equilibrium reaction

$$S_{\text{m}} \rightleftharpoons S_{\text{s}} \tag{26.2.1}$$

where $S_{\text{m}}$ is the solute in the mobile phase and $S_{\text{s}}$ is the solute in the stationary phase. The equilibrium constant for this reaction is an equilibrium partition coefficient, $K_{\text{D}}$.

$$K_D = \frac{[S_{\text{s}}]}{[S_{\text{m}}]} \tag{26.2.2}$$

> This is not a trivial assumption. In this section we are, in effect, treating the solute's equilibrium between the mobile phase and the stationary phase as if it is identical to the equilibrium in a simple liquid–liquid extraction carried out in a separatory funnel. You might question whether this is a reasonable assumption. There is an important difference between the two experiments that we need to consider. In a liquid–liquid extraction the two phases remain in contact with each other at all times, allowing for a true equilibrium. In chromatography, however, the mobile phase is in constant motion. A solute that moves into the stationary phase from the mobile phase will equilibrate back into a different portion of the mobile phase; this does not describe a true equilibrium.
>
> So, we ask again: Can we treat a solute's distribution between the mobile phase and the stationary phase as an equilibrium process? The answer is yes, if the mobile phase velocity is slow relative to the kinetics of the solute's movement back and forth between the two phase. In general, this is a reasonable assumption.

## Retention Time

We can characterize a chromatographic peak's properties in several ways, two of which are shown in Figure 26.2.1. Retention time, $t_{\text{r}}$, is the time between the sample's injection and the maximum response for the solute's peak. A chromatographic peak's baseline width, $w$, as shown in Figure 26.2.1, is determined by extending tangent lines from the inflection points on either side of the peak through the baseline. Although usually we report $t_{\text{r}}$ and $w$ using units of time, we can report them using units of volume by multiplying each by the mobile phase's velocity, or report them in linear units by measuring distances with a ruler.

> For example, a solute's retention volume,$V_{\text{r}}$, is $t_{\text{r}} \times u$ where $u$ is the mobile phase's velocity through the column.

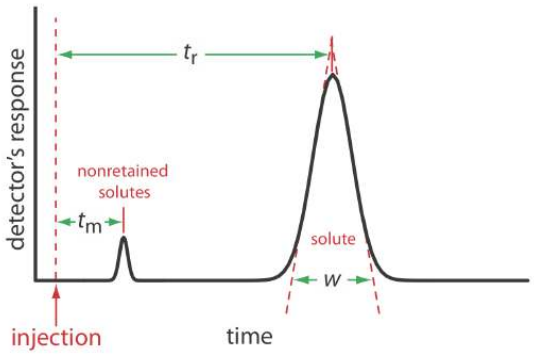



Figure 26.2.1. Chromatogram showing a solute's retention time, $t_r$, and baseline width, $w$, and the column's void time, $t_m$, for nonretained solutes. In this section we focus on retention time; we will consider the width of the solute's peak in Section 26.3.

In addition to the solute's peak, Figure 26.2.1 also shows a small peak that elutes shortly after the sample is injected into the mobile phase. This peak contains all nonretained solutes, which move through the column at the same rate as the mobile phase. The time required to elute the nonretained solutes is called the column's void time, $t_m$.

## The Rate of Solute Migration: The Retention Factor

In the absence of any additional equilibrium reactions in the mobile phase or the stationary phase, $K_D$ is equivalent to the distribution ratio, $D$,

$$D = \frac{[S_0]}{[S_m]} = \frac{(\text{mol S})_s/V_s}{(\text{mol S})_m/V_m} = K_D \tag{26.2.3}$$

where $V_s$ and $V_m$ are the volumes of the stationary phase and the mobile phase, respectively.

A conservation of mass requires that the total moles of solute remain constant throughout the separation; thus, we know that the following equation is true.

$$(\text{mol S})_{tot} = (\text{mol S})_m + (\text{mol S})_s \tag{26.2.4}$$

Solving Equation 26.2.4 for the moles of solute in the stationary phase and substituting into Equation 26.2.2 leaves us with

$$D = \frac{\{(\text{mol S})_{tot} - (\text{mol S})_m\}/V_s}{(\text{mol S})_m/V_m} \tag{26.2.5}$$

Rearranging this equation and solving for the fraction of solute in the mobile phase, $f_m$, gives

$$f_m = \frac{(\text{mol S})_m}{(\text{mol S})_{tot}} = \frac{V_m}{DV_s + V_m} \tag{26.2.6}$$

Because we may not know the exact volumes of the stationary phase and the mobile phase, we simplify Equation 26.2.6 by dividing both the numerator and the denominator by $V_m$; thus

$$f_m = \frac{V_m/V_m}{DV_s/V_m + V_m/V_m} = \frac{1}{DV_s/V_m + 1} = \frac{1}{1+k} \tag{26.2.7}$$

where $k$

$$k = D \times \frac{V_s}{V_m} \tag{26.2.8}$$

is the solute's retention factor. Note that the larger the retention factor, the more the distribution ratio favors the stationary phase, leading to a more strongly retained solute and a longer retention time.

> Other (older) names for the retention factor are capacity factor, capacity ratio, and partition ratio, and it sometimes is given the symbol $k'$. Keep this in mind if you are using other resources. Retention factor is the approved name from the IUPAC Gold Book.

We can determine a solute's retention factor from a chromatogram by measuring the column's void time, $t_m$, and the solute's retention time, $t_r$ (see Figure 26.2.1). Solving Equation 26.2.7 for $k$, we find that

$$k = \frac{1 - f_m}{f_m} \tag{26.2.9}$$

Earlier we defined $f_m$ as the fraction of solute in the mobile phase. Assuming a constant mobile phase velocity, we also can define $f_m$ as

$$f_m = \frac{\text{time spent in the mobile phase}}{\text{time spent in the stationary phase}} = \frac{t_m}{t_r} \tag{26.2.10}$$

Substituting back into Equation 26.2.9 and rearranging leaves us with

$$k = \frac{1 - \frac{t_m}{t_r}}{\frac{t_m}{t_r}} = \frac{t_r - t_m}{t_m} = \frac{t'_r}{t_m} \tag{26.2.11}$$

where $t'_r$ is the adjusted retention time.

**Example 26.2.1**

In a chromatographic analysis of low molecular weight acids, butyric acid elutes with a retention time of 7.63 min. The column's void time is 0.31 min. Calculate the retention factor for butyric acid.

**Solution**

$$k_{but} = \frac{t_r - t_m}{t_m} = \frac{7.63 \text{ min} - 0.31 \text{ min}}{0.31 \text{ min}} = 23.6$$

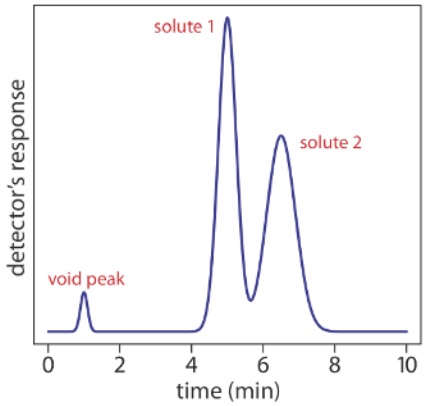



Figure 26.2.2. Chromatogram for Exercise 26.2.1.

## Relative Migration Rates: The Selectivity Factor

Selectivity is a relative measure of the retention of two solutes, which we define using a selectivity factor, $\alpha$

$$\alpha = \frac{k_B}{k_A} = \frac{t_{r,B} - t_m}{t_{r,A} - t_m} \tag{26.2.12}$$

where solute $A$ has the smaller retention time. When two solutes elute with identical retention time, $\alpha = 1.00$; for all other conditions $\alpha > 1.00$.

**Example 26.2.2**

In the chromatographic analysis for low molecular weight acids described in Example 26.2.1, the retention time for isobutyric acid is 5.98 min. What is the selectivity factor for isobutyric acid and butyric acid?

**Solution**

First we must calculate the retention factor for isobutyric acid. Using the void time from Example 26.2.1 we have

$$k_{\text{iso}} = \frac{t_{\text{r}} - t_{\text{m}}}{t_{\text{m}}} = \frac{5.98 \text{ min} - 0.31 \text{ min}}{0.31 \text{ min}} = 18.3$$

The selectivity factor, therefore, is

$$\alpha = \frac{k_{\text{but}}}{k_{\text{iso}}} = \frac{23.6}{18.3} = 1.29$$

This page titled 26.2: Migration Rates of Solutes is shared under a CC BY-NC-SA 4.0 license and was authored, remixed, and/or curated by David Harvey.

# 26.3: Zone Broadening and Column Efficiency

Suppose we inject a sample that has a single component. At the moment we inject the sample it is a narrow band of finite width. As the sample passes through the column, the width of this band continually increases in a process we call band broadening. Column efficiency is a quantitative measure of the extent of band broadening.

## The Shape of Chromatographic Peaks

When we inject a sample onto a column it has a uniform, or rectangular concentration profile with respect to distance down the column. As the sample passes through the column, the individual solute particles move in and out of the stationary phase, remaining in place when in the stationary phase and moving down the column when in the mobile phase. Because some solute particles will, on average, spend more time in the mobile phase and some will, on average, spend more time in the stationary phase, the original rectangular band increases in width and takes on a Gaussian shape, as we see in Figure 26.3.1.

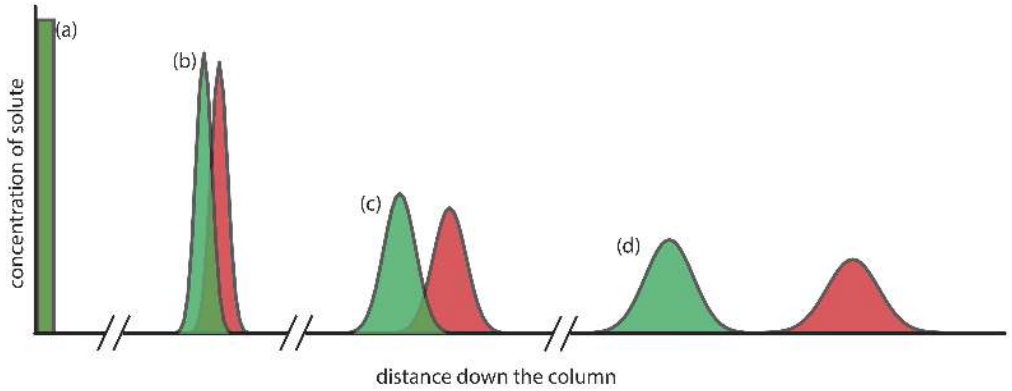



Figure 26.3.1. The initial injection of a sample results in the rectangular band of solutes seen in (a). As the sample migrates through the column, the individual components of the sample take on a Gaussian-shaped band profile, as seen in (b-d).

Our treatment of chromatography in this section assumes that a solute elutes as a symmetrical Gaussian peak, such as that shown in Figure 26.3.1. This ideal behavior occurs when the solute's partition coefficient, $K_D$

$$K_D = \frac{[S_s]}{[S_m]} \tag{26.3.1}$$

is the same for all concentrations of solute. If this is not the case, then the chromatographic peak has an asymmetric peak shape similar to those shown in Figure 26.3.2. The chromatographic peak in Figure 26.3.2a is an example of peak tailing, which occurs when some sites on the stationary phase retain the solute more strongly than other sites. Figure 26.3.2b, which is an example of peak fronting most often is the result of overloading the column with sample.

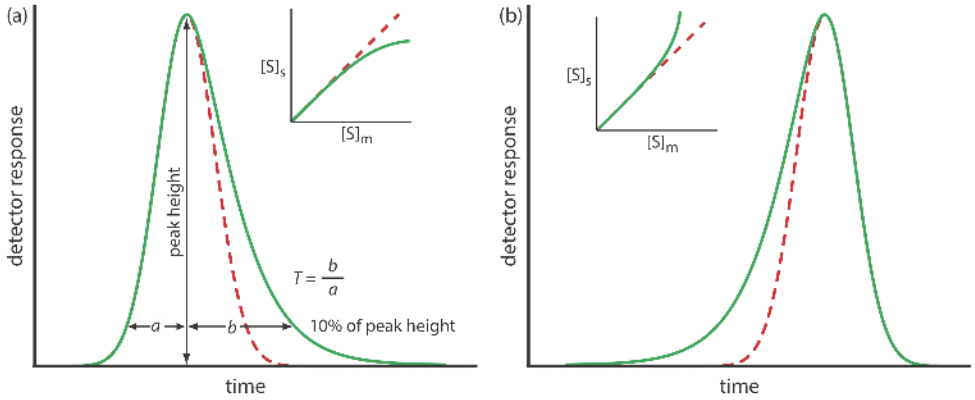



Figure 26.3.2. Examples of asymmetric chromatographic peaks showing (a) peak tailing and (b) peak fronting. For both (a) and (b) the green chromatogram is the asymmetric peak and the red dashed chromatogram shows the ideal, Gaussian peak shape. The insets show the relationship between the concentration of solute in the stationary phase, $[S]_s$, and its concentration in the mobile phase, $[S]_m$. The dashed red lines show ideal behavior ($K_D$ is constant for all conditions) and the green lines show nonideal behavior ($K_D$ decreases or increases for higher total concentrations of solute). A quantitative measure of peak tailing, $T$, is shown in (a).

As shown in Figure 26.3.2a, we can report a peak's asymmetry by drawing a horizontal line at 10% of the peak's maximum height and measuring the distance from each side of the peak to a line drawn vertically through the peak's maximum. The asymmetry factor, $T$, is defined as

$$T = \frac{b}{a} \tag{26.3.2}$$

## Methods for Describing Column Efficiency

In their original theoretical model of chromatography, Martin and Synge divided the chromatographic column into discrete sections, which they called theoretical plates. Within each theoretical plate Martin and Synge assumed that there is an equilibrium between the solute present in the stationary phase and the solute present in the mobile phase [Martin, A. J. P.; Synge, R. L. M. *Biochem. J.* **1941**, *35*, 1358–1366]. They described column efficiency in terms of the number of theoretical plates, $N$,

$$N = \frac{L}{H} \tag{26.3.3}$$

where $L$ is the column's length and $H$ is the height of a theoretical plate. For any given column, the column efficiency improves—and chromatographic peaks become narrower—when there are more theoretical plates.

If we assume that a chromatographic peak has a Gaussian profile, then the extent of band broadening is given by the peak's variance or standard deviation. The height of a theoretical plate is the peak's variance per unit length of the column

$$H = \frac{\sigma^2}{L} \tag{26.3.4}$$

where the standard deviation, $\sigma$, has units of distance. Because retention times and peak widths usually are measured in seconds or minutes, it is more convenient to express the standard deviation in units of time, $\tau$, by dividing $\sigma$ by the solute's average linear velocity, $\overline{u}$, which is equivalent to dividing the distance it travels, $L$, by its retention time, $t_r$.

$$\tau = \frac{\sigma}{\overline{u}} = \frac{\sigma t_r}{L} \tag{26.3.5}$$

For a Gaussian peak shape, the width at the baseline, $w$, is four times its standard deviation, $\tau$.

$$w = 4\tau \tag{26.3.6}$$

Combining Equation 26.3.4, Equation 26.3.5, and Equation 26.3.6 defines the height of a theoretical plate in terms of the easily measured chromatographic parameters $t_r$ and $w$.

$$H = \frac{Lw^2}{16t_r^2} \tag{26.3.7}$$

Combing Equation 26.3.7 and Equation 26.3.3 gives the number of theoretical plates.

$$N = 16\frac{t_r^2}{w^2} = 16\left(\frac{t_r}{w}\right)^2 \tag{26.3.8}$$

**Example 26.3.4**

A chromatographic analysis for the chlorinated pesticide Dieldrin gives a peak with a retention time of 8.68 min and a baseline width of 0.29 min. Calculate the number of theoretical plates? Given that the column is 2.0 m long, what is the height of a theoretical plate in mm?

**Solution**

Using Equation 26.3.8, the number of theoretical plates is

$$N = 16\frac{t_r^2}{w^2} = 16 \times \frac{(8.68\text{ min})^2}{(0.29\text{ min})^2} = 14300\text{ plates}$$

Solving Equation 26.3.3 for $H$ gives the average height of a theoretical plate as

$$H = \frac{L}{N} = \frac{2.00\text{ m}}{14300\text{ plates}} \times \frac{1000\text{ mm}}{\text{m}} = 0.14\text{ mm/plate}$$

It is important to remember that a theoretical plate is an artificial construct and that a chromatographic column does not contain physical plates. In fact, the number of theoretical plates depends on both the properties of the column and the solute. As a result, the number of theoretical plates for a column may vary from solute to solute.

The number of theoretical plates for an asymmetric peak shape is approximately

$$N \approx \frac{41.7 \times \frac{t_r^2}{(w_{0.1})^2}}{T + 1.25} = \frac{41.7 \times \frac{t_r^2}{(a+b)^2}}{T + 1.25} \tag{26.3.9}$$

where $w_{0.1}$ is the width at 10% of the peak's height [Foley, J. P.; Dorsey, J. G. *Anal. Chem.* **1983**, *55*, 730–737].

Asymmetric peaks have fewer theoretical plates, and the more asymmetric the peak the smaller the number of theoretical plates. For example, the following table gives values for $N$ for a solute eluting with a retention time of 10.0 min and a peak width of 1.00 min.

| $b$ | $a$ | $T$ | $N$ |
|---|---|---|---|
| 0.5 | 0.5 | 1.00 | 1850 |
| 0.6 | 0.4 | 1.50 | 1520 |
| 0.7 | 0.3 | 2.33 | 1160 |
| 0.8 | 0.2 | 4.00 | 790 |

## Kinetic Variables That Affect Zone Broadening

Another approach to understanding the broadening of a solute band as it passes through a column is to consider the factors that affect the rate at which a solute moves through the column and how that is affected by the velocity with which the mobile phase moves through the column. We will consider one approach that considers four contributions: variations in path lengths, longitudinal diffusion, mass transfer in the stationary phase, and mass transfer in the mobile phase.

### Multiple Paths: Variations in Path Length

As solute molecules pass through the column they travel paths that differ in length. Because of this difference in path length, two solute molecules that enter the column at the same time will exit the column at different times. The result, as shown in Figure

26.3.3, is a broadening of the solute's profile on the column. The contribution of multiple paths to the height of a theoretical plate, $H_p$, is

$$H_p = 2\lambda d_p \tag{26.3.10}$$

where $d_p$ is the average diameter of the particulate packing material and $\lambda$ is a constant that accounts for the consistency of the packing. A smaller range of particle sizes and a more consistent packing produce a smaller value for $\lambda$. For a column without packing material, $H_p$ is zero and there is no contribution to band broadening from multiple paths.

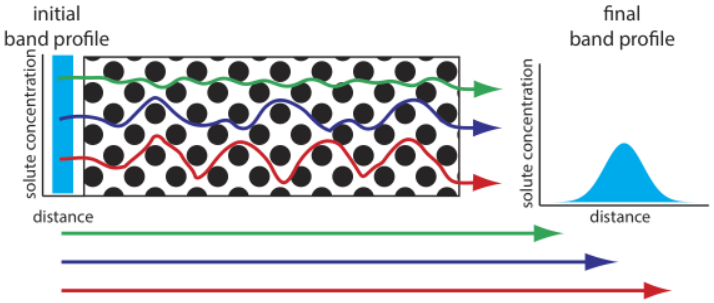



Figure 26.3.3. The effect of multiple paths on a solute's band broadening. The solute's initial band profile is rectangular. As this band travels through the column, individual solute molecules travel different paths, three of which are shown by the meandering colored paths (the actual lengths of these paths are shown by the straight arrows at the bottom of the figure). Most solute molecules travel paths with lengths similar to that shown in blue, with a few traveling much shorter paths (green) or much longer paths (red). As a result, the solute's band profile at the end of the column is broader and Gaussian in shape.

An inconsistent packing creates channels that allow some solute molecules to travel quickly through the column. It also can creates pockets that temporarily trap some solute molecules, slowing their progress through the column. A more uniform packing minimizes these problems.

## Longitudinal Diffusion

The second contribution to band broadening is the result of the solute's longitudinal diffusion in the mobile phase. Solute molecules are in constant motion, diffusing from regions of higher solute concentration to regions where the concentration of solute is smaller. The result is an increase in the solute's band width (Figure 26.3.4). The contribution of longitudinal diffusion to the height of a theoretical plate, $H_d$, is

$$H_d = \frac{2\gamma D_m}{u} \tag{26.3.11}$$

where $D_m$ is the solute's diffusion coefficient in the mobile phase, $u$ is the mobile phase's velocity, and $\gamma$ is a constant related to the efficiency of column packing. Note that the effect of $H_d$ on band broadening is inversely proportional to the mobile phase velocity: a higher velocity provides less time for longitudinal diffusion. Because a solute's diffusion coefficient is larger in the gas phase than in a liquid phase, longitudinal diffusion is a more serious problem in gas chromatography.

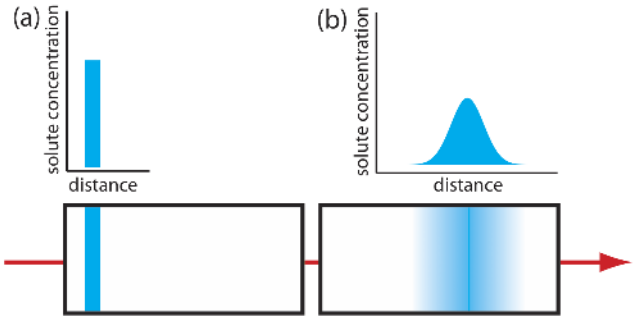



Figure 26.3.4. The effect of longitudinal diffusion on a solute's band broadening. Two horizontal cross-sections through the column and the corresponding concentration versus distance profiles are shown, with (a) being earlier in time. The red arrow shows the direction in which the mobile phase is moving.

## Mass Transfer

As the solute passes through the column it moves between the mobile phase and the stationary phase. We call this movement between phases mass transfer. As shown in Figure 26.3.5, band broadening occurs if the solute's movement within the mobile phase or within the stationary phase is not fast enough to maintain an equilibrium in its concentration between the two phases. On average, a solute molecule in the mobile phase moves some distance down the column before it passes into the stationary phase. A solute molecule in the stationary phase, on the other hand, takes longer than expected to move back into the mobile phase. The contributions of mass transfer in the stationary phase, $H_s$, and mass transfer in the mobile phase, $H_m$, are given by the following equations

$$H_s = \frac{qkd_f^2}{(1+k)^2 D_s} u \tag{26.3.12}$$

$$H_m = \frac{fn\left(d_p^2, d_c^2\right)}{D_m} u \tag{26.3.13}$$

where $d_f$ is the thickness of the stationary phase, $d_c$ is the diameter of the column, $D_s$ and $D_m$ are the diffusion coefficients for the solute in the stationary phase and the mobile phase, $k$ is the solute's retention factor, and $q$ is a constant related to the column packing material. Although the exact form of $H_m$ is not known, it is a function of particle size and column diameter. Note that the effect of $H_s$ and $H_m$ on band broadening is directly proportional to the mobile phase velocity because a smaller velocity provides more time for mass transfer.

> The abbreviation *fn* in Equation 26.3.13 means "is a function of."

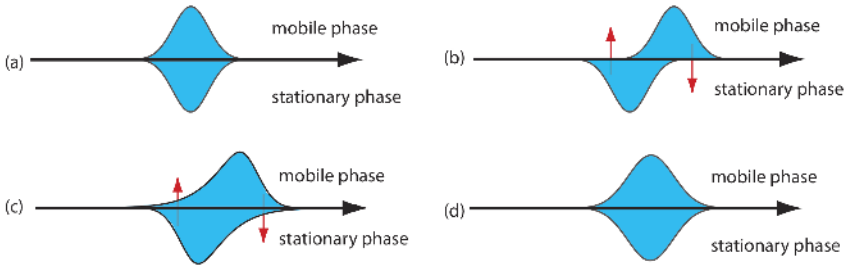



Figure 26.3.5. Effect of mass transfer on band broadening: (a) Ideal equilibrium Gaussian profiles for the solute in the mobile phase and in the stationary phase. (b, c) If we allow the solute's band to move a small distance down the column, an equilibrium between the two phases no longer exits. The red arrows show the movement of solute—what we call the mass transfer of solute—from the stationary phase to the mobile phase, and from the mobile phase to the stationary phase. (d) Once equilibrium is reestablished, the solute's band is now broader.

## Putting It All Together

The height of a theoretical plate is a summation of the contributions from each of the terms that affect band broadening.

$$H = H_p + H_d + H_s + H_m \tag{26.3.14}$$

An alternative form of this equation is the van Deemter equation

$$H = A + \frac{B}{u} + Cu \tag{26.3.15}$$

which emphasizes the importance of the mobile phase's velocity. In the van Deemter equation, $A$ accounts for the contribution of multiple paths ($H_p$), $B/u$ accounts for the contribution of longitudinal diffusion ($H_d$), and $Cu$ accounts for the combined contribution of mass transfer in the stationary phase and in the mobile phase ($H_s$ and $H_m$).

There is some disagreement on the best equation for describing the relationship between plate height and mobile phase velocity [Hawkes, S. J. *J. Chem. Educ.* **1983**, *60*, 393–398]. In addition to the van Deemter equation, other equations include

$$H = \frac{B}{u} + (C_s + C_m)\, u \tag{26.3.16}$$

where $C_s$ and $C_m$ are the mass transfer terms for the stationary phase and the mobile phase and

$$H = Au^{1/3} + \frac{B}{u} + Cu \tag{26.3.17}$$

All three equations, and others, have been used to characterize chromatographic systems, with no single equation providing the best explanation in every case [Kennedy, R. T.; Jorgenson, J. W. *Anal. Chem.* **1989**, *61*, 1128–1135].

To increase the number of theoretical plates without increasing the length of the column, we need to decrease one or more of the terms in Equation 26.3.14. The easiest way to decrease $H$ is to adjust the velocity of the mobile phase. For smaller mobile phase velocities, column efficiency is limited by longitudinal diffusion, and for higher mobile phase velocities efficiency is limited by the two mass transfer terms. As shown in Figure 26.3.6 —which uses the van Deemter equation—the optimum mobile phase velocity is the minimum in a plot of $H$ as a function of $u$.

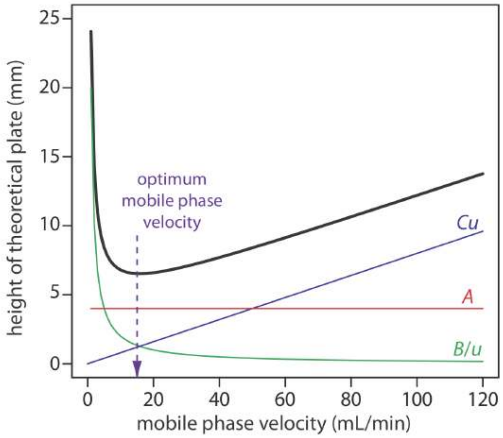



Figure 26.3.6 . Plot showing the relationship between the height of a theoretical plate, $H$, and the mobile phase's velocity, $u$, based on the van Deemter equation.

The remaining parameters that affect the terms in Equation 26.3.14 are functions of the column's properties and suggest other possible approaches to improving column efficiency. For example, both $H_p$ and $H_m$ are a function of the size of the particles used to pack the column. Decreasing particle size, therefore, is another useful method for improving efficiency.

> For a more detailed discussion of ways to assess the quality of a column, see Desmet, G.; Caooter, D.; Broeckhaven, K. "Graphical Data Represenation Methods to Assess the Quality of LC Columns," *Anal. Chem.* **2015**, *87*, 8593–8602.

Perhaps the most important advancement in chromatography columns is the development of open-tubular, or capillary columns. These columns have very small diameters ($d_c \approx$ 50–500 μm) and contain no packing material ($d_p$ = 0). Instead, the capillary column's interior wall is coated with a thin film of the stationary phase. Plate height is reduced because the contribution to $H$ from $H_p$ (Equation 26.3.10) disappears and the contribution from $H_m$ (Equation 26.3.13) becomes smaller. Because the column does not contain any solid packing material, it takes less pressure to move the mobile phase through the column, which allows for longer columns. The combination of a longer column and a smaller height for a theoretical plate increases the number of theoretical plates by approximately $100\times$. Capillary columns are not without disadvantages. Because they are much narrower than packed columns, they require a significantly smaller amount of sample, which may be difficult to inject reproducibly. Another approach to improving resolution is to use thin films of stationary phase, which decreases the contribution to $H$ from $H_s$ (Equation 26.3.12).

> The smaller the particles, the more pressure is needed to push the mobile phase through the column. As a result, for any form of chromatography there is a practical limit to particle size.

This page titled 26.3: Zone Broadening and Column Efficiency is shared under a CC BY-NC-SA 4.0 license and was authored, remixed, and/or curated by David Harvey.

# 26.4: Optimization and Column Performance

The goal of a chromatographic separation is to take a sample with more than one solute and to separate the solutes such that each elutes by itself. Our ability to separate two solutes from each other—to resolve them—is affected by a number of variables; how we can optimize the separation of two solutes is the subject of this section.

## Column Resolution

The goal of chromatography is to separate a mixture into a series of chromatographic peaks, each of which constitutes a single component of the mixture. The resolution between two chromatographic peaks, $R_{AB}$, is a quantitative measure of their separation, and is defined as

$$R_{AB} = \frac{t_{t,B} - t_{t,A}}{0.5\,(w_B + w_A)} = \frac{2\Delta t_r}{w_B + w_A} \tag{26.4.1}$$

where $B$ is the later eluting of the two solutes. As shown in Figure 26.4.1, the separation of two chromatographic peaks improves with an increase in $R_{AB}$. If the areas under the two peaks are identical—as is the case in Figure 26.4.1—then a resolution of 1.50 corresponds to an overlap of only 0.13% for the two elution profiles. Because resolution is a quantitative measure of a separation's success, it is a useful way to determine if a change in experimental conditions leads to a better separation.

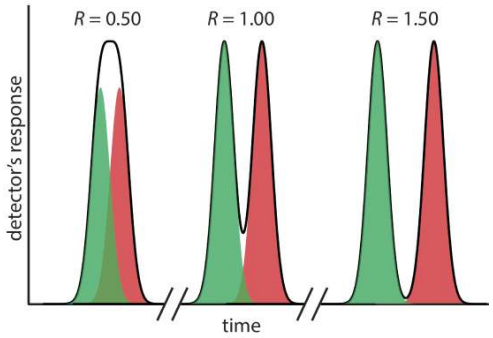



Figure 26.4.1. Three examples that show the relationship between resolution and the separation of a two component mixture. The green peak and the red peak are the elution profiles for the two components. The chromatographic peak—which is the sum of the two elution profiles—is shown by the solid black line.

**Example 26.4.1**

In a chromatographic analysis of lemon oil a peak for limonene has a retention time of 8.36 min with a baseline width of 0.96 min. γ-Terpinene elutes at 9.54 min with a baseline width of 0.64 min. What is the resolution between the two peaks?

**Solution**

Using Equation 26.4.1 we find that the resolution is

$$R_{AB} = \frac{2\Delta t_r}{w_B + w_A} = \frac{2(9.54\text{ min} - 8.36\text{ min})}{0.64\text{ min} + 0.96\text{ min}} = 1.48$$

## The Effect of Retention and Selectivity Factors on Resolution

Now that we have defined the solute retention factor, selectivity, and column efficiency we are able to consider how they affect the resolution of two closely eluting peaks. Because the two peaks have similar retention times, it is reasonable to assume that their peak widths are nearly identical. If the number of theoretical plates is the same for all solutes—not strictly true, but not a bad assumption—then the ratio $t_r/w$ is a constant. If two solutes have similar retention times, then their peak widths must be similar. Equation 26.4.1, therefore, becomes

$$R_{AB} = \frac{t_{r,B} - t_{r,A}}{0.5\,(w_B + w_A)} \approx \frac{t_{r,B} - t_{r,A}}{0.5\,(2w_B)} = \frac{t_{r,B} - t_{r,A}}{w_B} \tag{26.4.2}$$

where $B$ is the later eluting of the two solutes. Solving equation 26.3.8 for $w_B$ and substituting into Equation 26.4.2 leaves us with the following result.

$$R_{AB} = \frac{\sqrt{N_B}}{4} \times \frac{t_{r,B} - t_{r,A}}{t_{r,B}} \tag{26.4.3}$$

Rearranging equation 26.2.11 provides us with the following equations for the retention times of solutes $A$ and $B$.

$$t_{r,A} = k_A t_{\mathrm{m}} + t_{\mathrm{m}} \tag{26.4.4}$$

$$t_{\mathrm{r},B} = k_B t_{\mathrm{m}} + t_{\mathrm{m}} \tag{26.4.5}$$

After substituting these equations into Equation 26.4.3 and simplifying, we have

$$R_{AB} = \frac{\sqrt{N_B}}{4} \times \frac{k_B - k_A}{1 + k_B} \tag{26.4.6}$$

Finally, we can eliminate solute $A$'s retention factor by substituting in equation 26.2.12. After rearranging, we end up with the following equation for the resolution between the chromatographic peaks for solutes A and B.

$$R_{AB} = \frac{\sqrt{N_B}}{4} \times \frac{\alpha - 1}{\alpha} \times \frac{k_B}{1 + k_B} \tag{26.4.7}$$

> Although Equation 26.4.7 is useful for considering how a change in $N$, $\alpha$, or $k$ qualitatively affects resolution—which suits our purpose here—it is less useful for making accurate quantitative predictions of resolution, particularly for smaller values of $N$ and for larger values of $R$. For more accurate predictions use the equation
>
> $$R_{AB} = \frac{\sqrt{N}}{4} \times (\alpha - 1) \times \frac{k_B}{1 + k_{\mathrm{avg}}}$$
>
> where $k_{\mathrm{avg}}$ is ($k_{\mathrm{A}}$ + $k_{\mathrm{B}}$)/2. For a derivation of this equation and for a deeper discussion of resolution in column chromatography, see Foley, J. P. "Resolution Equations for Column Chromatography," *Analyst*, **1991**, *116*, 1275-1279.

Equation 26.4.7 contains terms that correspond to column efficiency, selectivity, and the solute retention factor. We can vary these terms, more or less independently, to improve resolution and analysis time. The first term, which is a function of the number of theoretical plates (for Equation 26.4.7), accounts for the effect of column efficiency. The second term is a function of $\alpha$ and accounts for the influence of column selectivity. Finally, the third term in both equations is a function of $k_B$ and accounts for the effect of solute $B$'s retention factor. A discussion of how we can use these parameters to improve resolution is the subject of the remainder of this section.

## The Effect of Resolution on Retention Time

In addition to resolution, another important factor in chromatography is the amount of time needed to elute a pair of solutes, which we can approximate using the retention time for solute $B$.

$$t_{r,B} = \frac{16 R_{AB}^2 H}{u} \times \left(\frac{\alpha}{\alpha - 1}\right)^2 \times \frac{(1 + k_B)^3}{k_B^2} \tag{26.4.8}$$

where $u$ is the mobile phase's velocity.

## Variables That Affect Column Performance

### Using the Retention Factor to Optimize Resolution

One of the simplest ways to improve resolution is to adjust the retention factor for solute $B$. If all other terms in Equation 26.4.7 remain constant, an increase in $k_B$ will improve resolution. As shown by the green curve in Figure 26.4.2 , however, the improvement is greatest if the initial value of $k_B$ is small. Once $k_B$ exceeds a value of approximately 10, a further increase produces only a marginal improvement in resolution. For example, if the original value of $k_B$ is 1, increasing its value to 10 gives an 82% improvement in resolution; a further increase to 15 provides a net improvement in resolution of only 87.5%.

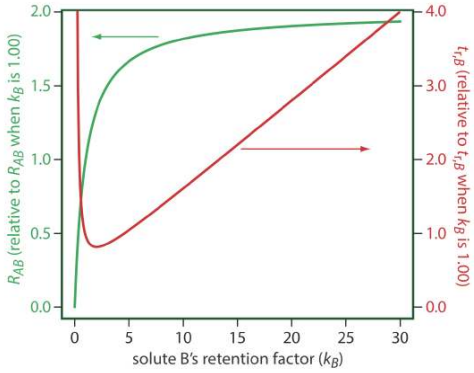



Figure 26.4.2 . Effect of $k_B$ on the resolution for a pair of solutes, $R_{AB}$, and the retention time for the later eluting solute, $t_{r,B}$. The *y*-axes display the resolution and retention time relative to their respective values when $k_B$ is 1.00.

Any improvement in resolution from increasing the value of $k_B$ generally comes at the cost of a longer analysis time. The red curve in Figure 26.4.2 shows the relative change in the retention time for solute *B* as a function of its retention factor. Note that the minimum retention time is for $k_B = 2$. Increasing $k_B$ from 2 to 10, for example, approximately doubles solute B's retention time.

> The relationship between retention factor and analysis time in Figure 26.4.2 works to our advantage if a separation produces an acceptable resolution with a large $k_B$. In this case we may be able to decrease $k_B$ with little loss in resolution and with a significantly shorter analysis time.

To increase $k_B$ without changing selectivity, $\alpha$, any change to the chromatographic conditions must result in a general, nonselective increase in the retention factor for both solutes. In gas chromatography, we can accomplish this by decreasing the column's temperature. Because a solute's vapor pressure is smaller at lower temperatures, it spends more time in the stationary phase and takes longer to elute. In liquid chromatography, the easiest way to increase a solute's retention factor is to use a mobile phase that is a weaker solvent. When the mobile phase has a lower solvent strength, solutes spend proportionally more time in the stationary phase and take longer to elute.

### Using Selectivity to Optimize Resolution

A second approach to improving resolution is to adjust the selectivity, $\alpha$. In fact, for $\alpha \approx 1$ it usually is not possible to improve resolution by adjusting the solute retention factor, $k_B$, or the column efficiency, $N$. A change in $\alpha$ often has a more dramatic effect on resolution than a change in $k_B$. For example, changing $\alpha$ from 1.1 to 1.5, while holding constant all other terms, improves resolution by 267%. In gas chromatography, we adjust $\alpha$ by changing the stationary phase; in liquid chromatography, we change the composition of the mobile phase to adjust $\alpha$.

To change $\alpha$ we need to selectively adjust individual solute retention factors. Figure 26.4.3 shows one possible approach for the liquid chromatographic separation of a mixture of substituted benzoic acids. Because the retention time of a compound's weak acid form and its weak base form are different, its retention time will vary with the pH of the mobile phase, as shown in Figure 26.4.3 a. The intersections of the curves in Figure 26.4.3 a show pH values where two solutes co-elute. For example, at a pH of 3.8 terephthalic acid and *p*-hydroxybenzoic acid elute as a single chromatographic peak.

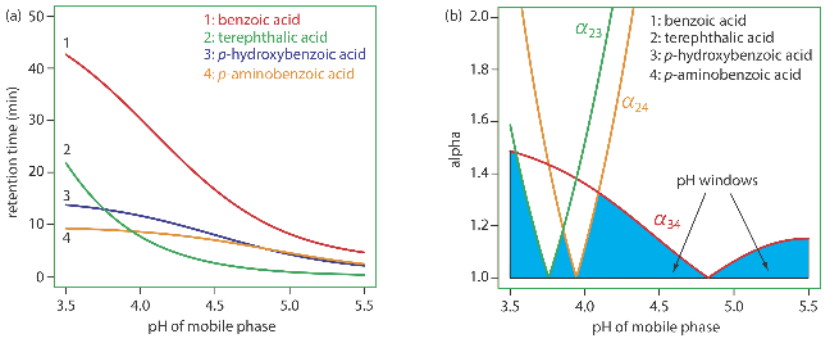



Figure 26.4.3 . Example that shows how the mobile phase pH in liquid chromatography affects selectivity: (a) retention times for four substituted benzoic acids as a function of the mobile phase's pH; (b) alpha values for three pairs of solutes that are difficult to separate. See text for details. The mobile phase is an acetic acid/sodium acetate buffer and the stationary phase is a nonpolar hydrocarbon. Data from Harvey, D. T.; Byerly, S.; Bowman, A.; Tomlin, J. "Optimization of HPLC and GC Separations Using Response Surfaces," *J. Chem. Educ.* **1991**, *68*, 162–168.

Figure 26.4.3 a shows that there are many pH values where some separation is possible. To find the optimum separation, we plot $\alpha$ for each pair of solutes. The red, green, and orange curves in Figure 26.4.3 b show the variation in $\alpha$ with pH for the three pairs of solutes that are hardest to separate (for all other pairs of solutes, $\alpha > 2$ at all pH levels). The blue shading shows windows of pH values in which at least a partial separation is possible—this figure is sometimes called a window diagram—and the highest point in each window gives the optimum pH within that range. The best overall separation is the highest point in any window, which, for this example, is a pH of 3.5. Because the analysis time at this pH is more than 40 min (Figure 26.4.3 a), choosing a pH between 4.1–4.4 might produce an acceptable separation with a much shorter analysis time.

Let's use benzoic acid, $C_6H_5COOH$, to explain why pH can affect a solute's retention time. The separation uses an aqueous mobile phase and a nonpolar stationary phase. At lower pHs, benzoic acid is predominately in its weak acid form, $C_6H_5COOH$, and partitions easily into the nonpolar stationary phase. At more basic pHs, however, benzoic acid is in its weak base form, $C_6H_5COO^-$. Because it now carries a charge, its solubility in the mobile phase increases and its solubility in the nonpolar stationary phase decreases. As a result, it spends more time in the mobile phase and has a shorter retention time.

Although the usual way to adjust pH is to change the concentration of buffering agents, it also is possible to adjust pH by changing the column's temperature because a solute's p$K_a$ value is pH-dependent; for a review, see Gagliardi, L. G.; Tascon, M.; Castells, C. B. "Effect of Temperature on Acid–Base Equilibria in Separation Techniques: A Review," *Anal. Chim. Acta*, **2015**, *889*, 35–57.

## Using Column Efficiency to Optimize Resolution

A third approach to improve resolution is to adjust the column's efficiency by increasing the number of theoretical plates, *N*. If we have values for $k_B$ and $\alpha$, then we can use Equation 26.4.7 to calculate the number of theoretical plates for any resolution. Table 26.4.1 provides some representative values. For example, if $\alpha = 1.05$ and $k_B = 2.0$, a resolution of 1.25 requires approximately 24 800 theoretical plates. If our column provides only 12 400 plates, half of what is needed, then a separation is not possible. How can we double the number of theoretical plates? The easiest way is to double the length of the column, although this also doubles the analysis time. A better approach is to cut the height of a theoretical plate, *H*, in half, providing the desired resolution without changing the analysis time. Even better, if we can decrease *H* by more than 50%, it may be possible to achieve the desired resolution with an even shorter analysis time by also decreasing $k_B$ or $\alpha$.

Table 26.4.1 . Minimum Number of Theoretical Plates to Achieve Desired Resolution for Selected Values of $k_B$ and $\alpha$

| | $R_{AB}$ = 1.00 | | $R_{AB}$ = 1.25 | | $R_{AB}$ = 1.50 | |
|---|---|---|---|---|---|---|
| $k_B$ | $\alpha = 1.05$ | $\alpha = 1.10$ | $\alpha = 1.05$ | $\alpha = 1.10$ | $\alpha = 1.05$ | $\alpha = 1.10$ |
| 0.5 | 63500 | 17400 | 99200 | 27200 | 143000 | 39200 |
| 1.0 | 28200 | 7740 | 44100 | 12100 | 63500 | 17400 |
| 1.5 | 19600 | 5380 | 30600 | 8400 | 44100 | 12100 |
| 2.0 | 15900 | 4360 | 24800 | 6810 | 35700 | 9800 |
| 3.0 | 12500 | 3440 | 19600 | 5380 | 28200 | 7740 |
| 5.0 | 10200 | 2790 | 15900 | 4360 | 22900 | 6270 |
| 10.0 | 8540 | 2340 | 13300 | 3660 | 19200 | 5270 |

## The General Elution Problem

Adjusting the retention factor to improve the resolution between one pair of solutes may lead to unacceptably long retention times for other solutes. For example, suppose we need to analyze a four-component mixture with baseline resolution and with a run-time of less than 20 min. Our initial choice of conditions gives the chromatogram in Figure 26.4.4 a. Although we successfully separate components 3 and 4 within 15 min, we fail to separate components 1 and 2. Adjusting conditions to improve the resolution for the first two components by increasing $k_2$ provides a good separation of all four components, but the run-time is too long (Figure 26.4.4 b). This problem of finding a single set of acceptable operating conditions is known as the general elution problem.

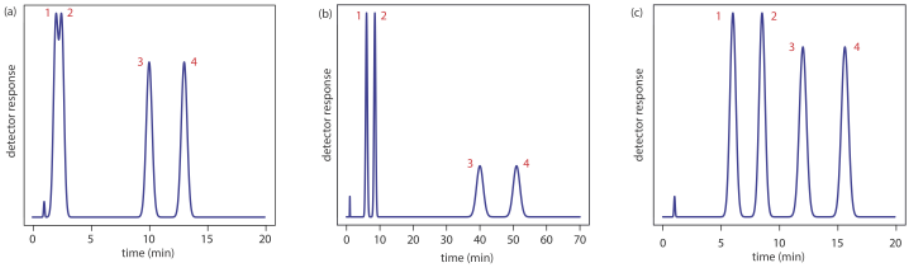



Figure 26.4.4 . Example that shows the general elution problem in chromatography. See text for details.

One solution to the general elution problem is to make incremental adjustments to the retention factor as the separation takes place. At the beginning of the separation we set the initial chromatographic conditions to optimize the resolution for early eluting solutes. As the separation progresses, we adjust the chromatographic conditions to decrease the retention factor—and, therefore, to decrease the retention time—for each of the later eluting solutes (Figure 26.4.4 c). In gas chromatography this is accomplished by temperature programming. The column's initial temperature is selected such that the first solutes to elute are resolved fully. The temperature is then increased, either continuously or in steps, to bring off later eluting components with both an acceptable resolution and a reasonable analysis time. In liquid chromatography the same effect is obtained by increasing the solvent's eluting strength. This is known as a gradient elution. We will have more to say about each of these in later sections of this chapter.

This page titled 26.4: Optimization and Column Performance is shared under a CC BY-NC-SA 4.0 license and was authored, remixed, and/or curated by David Harvey.

# 26.5: Summary of Important Relationships for Chromatography

In this chapter we have introduced many chromatographic variables, some directly measured from the chromatogram, provided by the manufacturer, or from the operating conditions, and some derived from these variables. The following two tables summarize these variables.

Table 26.5.1. Chromatographic Variables Directly Measured From Chromatogram, Provided by Manufacturer, or From Operating Conditions

| variable | name | source |
|---|---|---|
| $t_r$ | retention time for solute | chromatogram |
| $t_m$ | retention time for non-retained solute | chromatogram |
| $w$ | peak width | chromatogram |
| $u$ | mobile phase flow rate | operating conditions |
| $L$ | length of column's stationary phase | manufacturer |
| $d_c$ | diameter of column | manufacturer |
| $d_p$ | diameter of packing material | manufacturer |
| $d_f$ | thickness of stationary phase | manufacturer |
| $V_s$ | volume of stationary phase | operating conditions |

Table 26.5.2. Derived Chromatographic Variables

| variable | name | equation to derive value |
|---|---|---|
| $V_m$ | volume of mobile phase | $V_m = t_m u$ |
| $k$ | retention factor | $k = \frac{t_r - t_m}{t_m}$ |
| $t_r'$ | adjusted retention time | $t_r' = t_r - t_m$ |
| $D$ | distribution ratio | $D = k \times \frac{V_s}{V_m}$ |
| $\alpha$ | selectivity factor | $\alpha = \frac{k_B}{k_A}$ |
| $R_{AB}$ | resolution | $R_{AB} = \frac{\sqrt{N_B}}{4} \times \frac{\alpha - 1}{\alpha} \times \frac{k_B}{1 + k_B}$ |
| $N$ | number of theoretical plates | $N = 16 \left(\frac{t_r}{w}\right)^2$ |
| $H$ | height of theoretical plates | $H = \frac{Lw^2}{16t_r^2} = \frac{L}{N}$ |
| $H_p$ | height due to multiple paths | $H_p = 2\lambda d_p$ |
| $H_d$ | height due to longitudinal diffusion | $H_d = \frac{2\gamma D_m}{u}$ |
| $H_s$ | height due to mass transfer in stationary phase | $H_s = \frac{qkd_f^2}{(1+k)^2 D_s} u$ |
| $H_m$ | height due to mass transfer in mobile phase | $H_m = \frac{fn(d_p^2, d_c^2)}{D_m} u$ |

This page titled 26.5: Summary of Important Relationships for Chromatography is shared under a CC BY-NC-SA 4.0 license and was authored, remixed, and/or curated by David Harvey.

# 26.6: Applications of Chromatography

Although the primary purpose of chromatography is the separation of a complex mixture into its component parts, as outlined here, a chromatographic separation also provides qualitative and quantitative information about our samples. More detailed examples of qualitative and quantitative applications are found in the chapters that follow.

## Qualitative Analysis

As we learned in Section 26.2, solutes migrate through a chromatographic system at rate that is a function of the properties of the mobile phase and the stationary phase. This means that a particular solute will elute with a consistent retention time. If we expect a solute to elute with a retention time of 5.0 min, the presence of a peak at 5.0 min is suggestive of, but not definitive evidence of the solute's presence in our sample; however, the absence of a peak at 5.0 min is strong evidence that the solute is not present in our sample. For a complex mixture, this sort of screening technique is a useful qualitative application of chromatography. As we will see in the chapters that follow, the type of detector used to monitor a chromatographic separation may provide useful qualitative information.

## Quantitative Analysis

A chromatographic separation yields a sequence of peaks that, ideally, represent a single solute. These peak's are characterized by an area that is proportional to the amount of analyte injected into the mobile phase. By injecting a series of standards, a calibration curve of peak area as a function of the analyte's concentration provides a way to determine the analyte's concentration in a sample. Any of the calibration strategies discussed in Chapter 1.5—external standards, standard additions, and internal standards—find use in a quantitative chromatographic analysis. Determining a solute's peak area is relatively straight-forward when using a computer-interfaced instrument with appropriate software. Alternatively, peak height, which is easier to measure, can be used as a substitute, although care must be taken to ensure that the peaks are symmetrical and that peak widths are consistent for the standards and the samples.

This page titled 26.6: Applications of Chromatography is shared under a CC BY-NC-SA 4.0 license and was authored, remixed, and/or curated by David Harvey.

# CHAPTER OVERVIEW

## 27: Gas Chromatography

In gas chromatography (GC) we inject the sample, which may be a gas or a liquid, into a gaseous mobile phase (often called the carrier gas). The mobile phase carries the sample through a packed or capillary column that separates the sample's components based on their ability to partition between the mobile phase and the stationary phase. Because it combines separation with analysis, gas chromatography provides excellent selectivity. By adjusting conditions it usually is possible to design a separation so that analytes elute by themselves, even when the mixture is complex. Additional selectivity is possible by using a detector that does not respond to all analytes.


27.1: Principles of Gas Chromatography
27.2: Instruments for Gas Chromatography
27.3: Gas Chromatographic Columns and Stationary Phases
27.4: Applications of Gas Chromatography


This page titled 27: Gas Chromatography is shared under a CC BY-NC-SA 4.0 license and was authored, remixed, and/or curated by David Harvey.

# 27.1: Principles of Gas Chromatography

In Chapter 26 we covered several important elements of chromatography, including the factors that affect the migration of solutes, the factors that contribute to band broadening, and the factors under our control that we can use to optimize the separation of a mixture. Here we consider two topics that apply to a gas chromatographic separation, both of which are a function of the properties of gases.

## Retention Times and Retention Volumes

Many of the chromatographic variables in gathered in the tables included in Chapter 26.5—both those that are measured directly, provided by the manufacturer, or given by the operating conditions, and those derived from these variables—are given in terms or retention times for the solutes, $t_r$, and for the mobile phase, $t_m$. The product of time and flow rate is a volume

$$V_r = t_r \times u$$

$$V_m = t_r \times u$$

where $V_r$ and $V_m$ are the volume of mobile phase needed to elute a solute and the volume of mobile phase needed to elute a non-retained solute, which allows us to describe the retention in terms of volumes instead of times.

Because the volume of gas is a function of pressure, and the pressure drops across the column from an inlet pressure of $P_i$ to an outlet pressure of $P_o$, the retention times are particularly sensitive to operating condition. We can, however, correct the retention volumes by accounting for the compressibility of the gas

$$V_r^o = jt_r u$$

$$V_m^o = jt_m u$$

where $j$ is a correction factor that accounts for the drop in pressure

$$j = \frac{3 \times (P_i/P_o)^2 - 1}{2 \times (P_i/P_o)^3 - 1}$$

and where $V_r^o$ and $V_m^o$ are the corrected retention volumes for the solute and the non-retained solutes, respectively. The solute's corrected retention volume can be further normalized by dividing the adjusted retention volume, $V_r^o - V_m^o$, by the mass of the stationary phase, $w$, and by adjusting for the column's temperature, $T_c$, relative to 273 K

$$V_g = \frac{V_r^o - V_m^o}{w} \times \frac{273}{T_c}$$

yielding the solute's specific retention volume, $V_g$. This value is reasonably insensitive to operating conditions, which makes it useful for qualitative purposes.

## Effect of Diffusion in the Gas Phase on Band Broadening

In Chapter 26 we considered three factors that affect band broadening—multiple paths, longitudinal diffusion, and mass transfer—expressing the relationship between the height of a theoretical plate, $H$, as a function of the mobile phase's velocity, $u$, using the van Deemter equation

$$H = A + \frac{B}{u} + Cu$$

where $A$ is the contribution from multiple paths, $B$ is the contribution from longitudinal diffusion, and $C$ is the contribution from mass transfer. Because solutes have large diffusion coefficients in the gas phase, the term $B/u$ is often the limiting factor in gas chromatography.

This page titled 27.1: Principles of Gas Chromatography is shared under a CC BY-NC-SA 4.0 license and was authored, remixed, and/or curated by David Harvey.

# 27.2: Instruments for Gas Chromatography

In gas chromatography (GC) we inject the sample, which may be a gas or a liquid, into an gaseous mobile phase (often called the carrier gas). The mobile phase carries the sample through a packed or a capillary column that separates the sample's components based on their ability to partition between the mobile phase and the stationary phase. Figure 27.2.1 shows an example of a typical gas chromatograph, which consists of several key components: a supply of compressed gas for the mobile phase; a heated injector, which rapidly volatilizes the components in a liquid sample; a column, which is placed within an oven whose temperature we can control during the separation; and a detector to monitor the eluent as it comes off the column. Let's consider each of these components.




Figure 27.2.1 . Example of a typical gas chromatograph with insets showing the heated injection ports—note the symbol indicating that it is hot—and the oven that houses the column. This particular instrument is equipped with an autosampler for injecting samples, a capillary column, and a mass spectrometer (MS) as the detector. Note that the carrier gas is supplied by a tank of compressed gas.

## Mobile Phase

The most common mobile phases for gas chromatography are He, Ar, and $N_2$, which have the advantage of being chemically inert toward both the sample and the stationary phase. The choice of carrier gas often is determined by the needs of the instrument's detector. For a packed column the mobile phase velocity usually is 25–150 mL/min. The typical flow rate for a capillary column is 1–25 mL/min.

## Sample Introduction

Three factors determine how we introduce a sample to the gas chromatograph. First, all of the sample's constituents must be volatile. Second, the analytes must be present at an appropriate concentration. Finally, the physical process of injecting the sample must not degrade the separation. Each of these needs is considered in this section.

### Preparing a Volatile Sample

Not every sample can be injected directly into a gas chromatograph. To move through the column, the sample's constituents must be sufficiently volatile. A solute of low volatility, for example, may be retained by the column and continue to elute during the analysis of subsequent samples. A nonvolatile solute will condense at the top of the column, degrading the column's performance.

An attractive approach to isolating analytes is a solid-phase microextraction (SPME). In one approach, which is illustrated in Figure 27.2.2 , a fused-silica fiber is placed inside a syringe needle. The fiber, which is coated with a thin film of an adsorbent material, such as polydimethyl siloxane, is lowered into the sample by depressing a plunger and is exposed to the sample for a predetermined time. After withdrawing the fiber into the needle, it is transferred to the gas chromatograph for analysis.

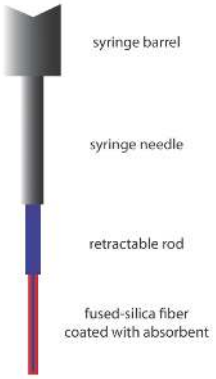


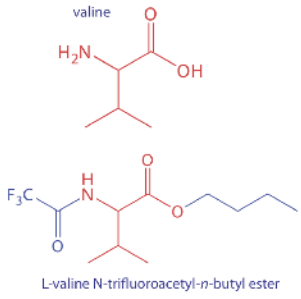

Figure 27.2.2 . Schematic diagram of a solid-phase microextraction device. The absorbent is shown in red.

Two additional methods for isolating volatile analytes are a purge-and-trap and headspace sampling. In a purge-and-trap, we bubble an inert gas, such as He or $N_2$, through the sample, releasing—or purging—the volatile compounds. These compounds are carried by the purge gas through a trap that contains an absorbent material, such as Tenax, where they are retained. Heating the trap and back-flushing with carrier gas transfers the volatile compounds to the gas chromatograph. In headspace sampling we place the sample in a closed vial with an overlying air space. After allowing time for the volatile analytes to equilibrate between the sample and the overlying air, we use a syringe to extract a portion of the vapor phase and inject it into the gas chromatograph. Alternatively, we can sample the headspace with an SPME.

Thermal desorption is a useful method for releasing volatile analytes from solids. We place a portion of the solid in a glass-lined, stainless steel tube. After purging with carrier gas to remove any $O_2$ that might be present, we heat the sample. Volatile analytes are swept from the tube by an inert gas and carried to the GC. Because volatilization is not a rapid process, the volatile analytes often are concentrated at the top of the column by cooling the column inlet below room temperature, a process known as cryogenic focusing. Once volatilization is complete, the column inlet is heated rapidly, releasing the analytes to travel through the column.

> The reason for removing $O_2$ is to prevent the sample from undergoing an oxidation reaction when it is heated.

To analyze a nonvolatile analyte we must convert it to a volatile form. For example, amino acids are not sufficiently volatile to analyze directly by gas chromatography. Reacting an amino acid, such as valine, with 1-butanol and acetyl chloride produces an esterified amino acid. Subsequent treatment with trifluoroacetic acid gives the amino acid's volatile N-trifluoroacetyl-*n*-butyl ester derivative.




## Adjusting the Analyte's Concentration

If an analyte's concentration is too small to give an adequate signal, then we must concentrate the analyte before we inject the sample into the gas chromatograph. A side benefit of many extraction methods is that they often concentrate the analytes. Volatile organic materials isolated from an aqueous sample by a purge-and-trap, for example, are concentrated by as much as $1000\times$.

If an analyte is too concentrated, it is easy to overload the column, resulting in peak fronting and a poor separation. In addition, the analyte's concentration may exceed the detector's linear response. Injecting less sample or diluting the sample with a volatile solvent, such as methylene chloride, are two possible solutions to this problem.

## Injecting the Sample

In Chapter 26 we examined several explanations for why a solute's band increases in width as it passes through the column, a process we called band broadening. We also introduce an additional source of band broadening if we fail to inject the sample into the minimum possible volume of mobile phase. There are two principal sources of this precolumn band broadening: injecting the sample into a moving stream of mobile phase and injecting a liquid sample instead of a gaseous sample. The design of a gas chromatograph's injector helps minimize these problems.

An example of a simple injection port for a packed column is shown in Figure 27.2.3 . The top of the column fits within a heated injector block, with carrier gas entering from the bottom. The sample is injected through a rubber septum using a microliter syringe, such as the one shown in in Figure 27.2.4 . Injecting the sample directly into the column minimizes band broadening because it mixes the sample with the smallest possible amount of carrier gas. The injector block is heated to a temperature at least 50$^{o}$C above the boiling point of the least volatile solute, which ensures a rapid vaporization of the sample's components.

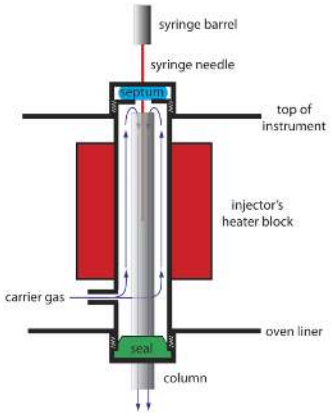



Figure 27.2.3 . Schematic diagram of a heated GC injector port for use with packed columns. The needle pierces a rubber septum and enters into the top of the column, which is located within a heater block.



Figure 27.2.4 . Example of a syringe for injecting samples into a gas chromatograph. This syringe has a maximum capacity of 10 µL with graduations every 0.1 µL.

Because a capillary column's volume is significantly smaller than that for a packed column, it requires a different style of injector to avoid overloading the column with sample. Figure 27.2.5 shows a schematic diagram of a typical split/splitless injector for use with a capillary column.

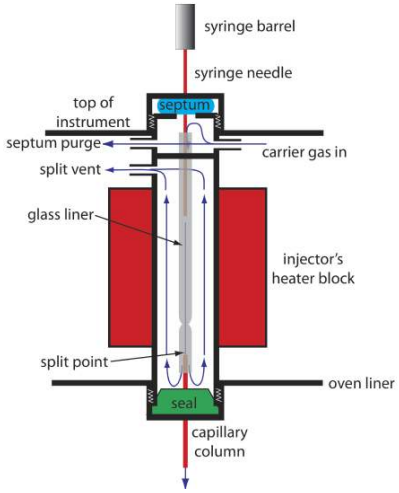



Figure 27.2.5 . Schematic diagram of a split/splitless injection port for use with capillary columns. The needle pierces a rubber septum and enters into a glass liner, which is located within a heater block. In a split injection the split vent is open; the split vent is closed for a splitless injection.

In a split injection we inject the sample through a rubber septum using a microliter syringe. Instead of injecting the sample directly into the column, it is injected into a glass liner where it mixes with the carrier gas. At the split point, a small fraction of the carrier gas and sample enters the capillary column with the remainder exiting through the split vent. By controlling the flow rate of the carrier gas as it enters the injector, and its flow rate through the septum purge and the split vent, we can control the fraction of sample that enters the capillary column, typically 0.1–10%.

> For example, if the carrier gas flow rate is 50 mL/min, and the flow rates for the septum purge and the split vent are 2 mL/min and 47 mL/min, respectively, then the flow rate through the column is 1 mL/min (= 50 – 2 – 47). The ratio of sample entering the column is 1/50, or 2%.

In a splitless injection, which is useful for trace analysis, we close the split vent and allow all the carrier gas that passes through the glass liner to enter the column—this allows virtually all the sample to enters the column. Because the flow rate through the injector is low, significant precolumn band broadening is a problem. Holding the column's temperature approximately 20–25$^{o}$C below the solvent's boiling point allows the solvent to condense at the entry to the capillary column, forming a barrier that traps the solutes. After allowing the solutes to concentrate, the column's temperature is increased and the separation begins.

For samples that decompose easily, an on-column injection may be necessary. In this method the sample is injected directly into the column without heating. The column temperature is then increased, volatilizing the sample with as low a temperature as is practical.

## Temperature Control

Control of the column's temperature is critical to attaining a good separation when using gas chromatography. For this reason the column is placed inside a thermostated oven (see Figure 27.2.1 ). In an isothermal separation we maintain the column at a constant temperature. To increase the interaction between the solutes and the stationary phase, the temperature usually is set slightly below that of the lowest-boiling solute.

One difficulty with an isothermal separation is that a temperature that favors the separation of a low-boiling solute may lead to an unacceptably long retention time for a higher-boiling solute. Temperature programming provides a solution to this problem. At the beginning of the analysis we set the column's initial temperature below that for the lowest-boiling solute. As the separation progresses, we slowly increase the temperature at either a uniform rate or in a series of steps.

## Detectors for Gas Chromatography

The final part of a gas chromatograph is the detector. The ideal detector has several desirable features: a low detection limit, a linear response over a wide range of solute concentrations (which makes quantitative work easier), sensitivity for all solutes or

selectivity for a specific class of solutes, and an insensitivity to a change in flow rate or temperature.

### Thermal Conductivity Detector (TCD)

One of the earliest gas chromatography detectors takes advantage of the mobile phase's thermal conductivity. As the mobile phase exits the column it passes over a tungsten-rhenium wire filament (see Figure 27.2.6 ). The filament's electrical resistance depends on its temperature, which, in turn, depends on the thermal conductivity of the mobile phase. Because of its high thermal conductivity, helium is the mobile phase of choice when using a thermal conductivity detector (TCD).

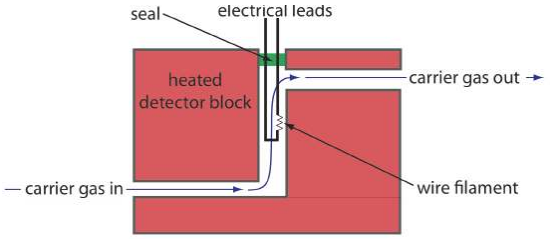



Figure 27.2.6 . Schematic diagram of a thermal conductivity detector showing one cell of a matched pair. The sample cell takes the carrier gas as it elutes from the column. A source of carrier gas that bypasses the column passes through a reference cell.

> Thermal conductivity, as the name suggests, is a measure of how easily a substance conducts heat. A gas with a high thermal conductivity moves heat away from the filament—and, thus, cools the filament—more quickly than does a gas with a low thermal conductivity.

When a solute elutes from the column, the thermal conductivity of the mobile phase in the TCD cell decreases and the temperature of the wire filament, and thus it resistance, increases. A reference cell, through which only the mobile phase passes, corrects for any time-dependent variations in flow rate, pressure, or electrical power, all of which affect the filament's resistance.

Because all solutes affect the mobile phase's thermal conductivity, the thermal conductivity detector is a universal detector. Another advantage is the TCD's linear response over a concentration range spanning $10^4$–$10^5$ orders of magnitude. The detector also is non-destructive, which allows us to recover analytes using a postdetector cold trap. One significant disadvantage of the TCD detector is its poor detection limit for most analytes.

### Flame Ionization Detector (FID)

The combustion of an organic compound in an $H_2$/air flame results in a flame that contains electrons and organic cations, presumably $CHO^+$. Applying a potential of approximately 300 volts across the flame creates a small current of roughly $10^{-9}$ to $10^{-12}$ amps. When amplified, this current provides a useful analytical signal. This is the basis of the popular flame ionization detector, a schematic diagram of which is shown in Figure 27.2.7 .

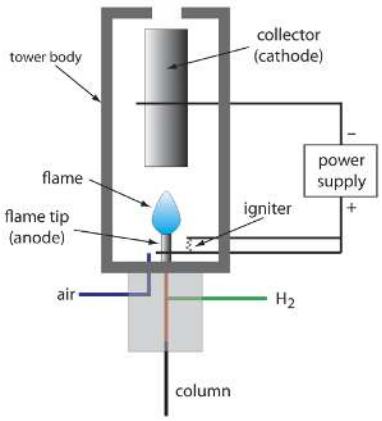



Figure 27.2.7 . Schematic diagram of a flame ionization detector. The eluent from the column mixes with $H_2$ and is burned in the presence of excess air. Combustion produces a flame that contains electrons and the cation $CHO^{+\cdot}$. Applying a potential between the flame's tip and the collector gives a current that is proportional to the concentration of cations in the flame.

Most carbon atoms—except those in carbonyl and carboxylic groups—generate a signal, which makes the FID an almost universal detector for organic compounds. Most inorganic compounds and many gases, such as $H_2O$ and $CO_2$, are not detected, which makes the FID detector a useful detector for the analysis of organic analytes in atmospheric and aqueous environmental samples. Advantages of the FID include a detection limit that is approximately two to three orders of magnitude smaller than that for a thermal conductivity detector, and a linear response over $10^6$–$10^7$ orders of magnitude in the amount of analyte injected. The sample, of course, is destroyed when using a flame ionization detector.

### Electron Capture Detector (ECD)

The electron capture detector is an example of a selective detector. As shown in Figure 27.2.8 , the detector consists of a $\beta$-emitter, such as $^{63}Ni$. The emitted electrons ionize the mobile phase, usually $N_2$, generating a standing current between a pair of electrodes. When a solute with a high affinity for capturing electrons elutes from the column, the current decreases, which serves as the signal. The ECD is highly selective toward solutes with electronegative functional groups, such as halogens and nitro groups, and is relatively insensitive to amines, alcohols, and hydrocarbons. Although its detection limit is excellent, its linear range extends over only about two orders of magnitude.

> A $\beta$-particle is an electron.

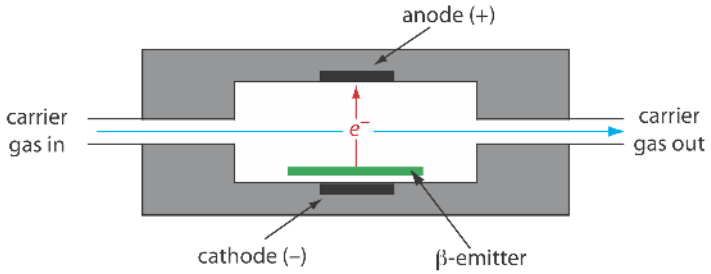



Figure 27.2.8 . Schematic diagram showing an electron capture detector.

### Mass Spectrometer (MS)

A mass spectrometer is an instrument that ionizes a gaseous molecule using sufficient energy that the resulting ion breaks apart into smaller ions. Because these ions have different mass-to-charge ratios, it is possible to separate them using a magnetic field or an electrical field. The resulting mass spectrum contains both quantitative and qualitative information about the analyte. Figure 27.2.9 shows a mass spectrum for toluene.

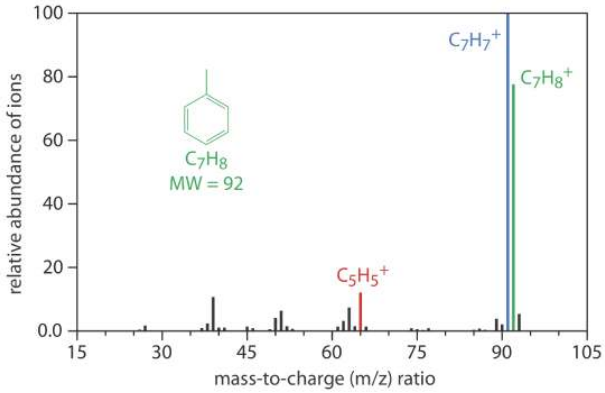



Figure 27.2.9 . Mass spectrum for toluene highlighting the molecular ion in green (m/z=92), and two fragment ions in blue (m/z=91) and in red (m/z= 65). A mass spectrum provides both quantitative and qualitative information: the height of any peak is proportional to the amount of toluene in the mass spectrometer and the fragmentation pattern is unique to toluene.

Figure 27.2.10 shows a block diagram of a typical gas chromatography-mass spectrometer (GC–MS) instrument. The effluent from the column enters the mass spectrometer's ion source in a manner that eliminates the majority of the carrier gas. In the ionization chamber the remaining molecules—a mixture of carrier gas, solvent, and solutes—undergo ionization and fragmentation. The mass

spectrometer's mass analyzer separates the ions by their mass-to-charge ratio and a detector counts the ions and displays the mass spectrum.

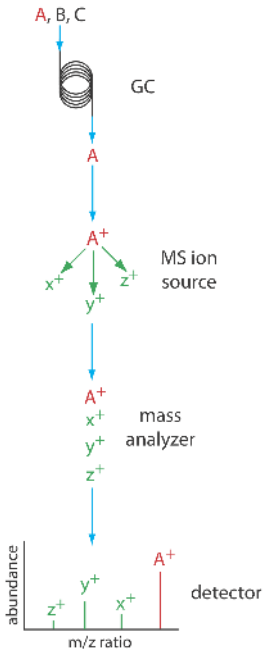



Figure 27.2.10 . Block diagram of GC– MS. A three component mixture enters the GC. When component A elutes from the column, it enters the MS ion source and ionizes to form the parent ion and several fragment ions. The ions enter the mass analyzer, which separates them by their mass-to-charge ratio, providing the mass spectrum shown at the detector.

There are several options for monitoring a chromatogram when using a mass spectrometer as the detector. The most common method is to continuously scan the entire mass spectrum and report the total signal for all ions that reach the detector during each scan. This total ion scan provides universal detection for all analytes. We can achieve some degree of selectivity by monitoring one or more specific mass-to-charge ratios, a process called selective-ion monitoring. A mass spectrometer provides excellent detection limits, typically 25 fg to 100 pg, with a linear range of $10^5$ orders of magnitude. Because we continuously record the mass spectrum of the column's eluent, we can go back and examine the mass spectrum for any time increment. This is a distinct advantage for GC–MS because we can use the mass spectrum to help identify a mixture's components.

## Other Detectors

Two additional detectors are similar in design to a flame ionization detector. In the flame photometric detector, optical emission from phosphorous and sulfur provides a detector selective for compounds that contain these elements. The thermionic detector responds to compounds that contain nitrogen or phosphorous.

A Fourier transform infrared spectrophotometer (FT–IR) also can serve as a detector. In GC–FT–IR, effluent from the column flows through an optical cell constructed from a 10–40 cm Pyrex tube with an internal diameter of 1–3 mm. The cell's interior surface is coated with a reflecting layer of gold. Multiple reflections of the source radiation as it is transmit- ted through the cell increase the optical path length through the sample. As is the case with GC–MS, an FT–IR detector continuously records the column eluent's spectrum, which allows us to examine the IR spectrum for any time increment.

This page titled 27.2: Instruments for Gas Chromatography is shared under a CC BY-NC-SA 4.0 license and was authored, remixed, and/or curated by David Harvey.

# 27.3: Gas Chromatographic Columns and Stationary Phases

There are two broad classes of chromatographic columns: packed columns and capillary columns. In general, a packed column can handle larger samples and a capillary column can separate more complex mixtures.

## Packed Columns

Packed columns are constructed from glass, stainless steel, copper, or aluminum, and typically are 2–6 m in length with internal diameters of 2–4 mm. The column is filled with a particulate solid support, with particle diameters ranging from 37–44 μm to 250–354 μm. Figure 27.3.1 shows a typical example of a packed column.

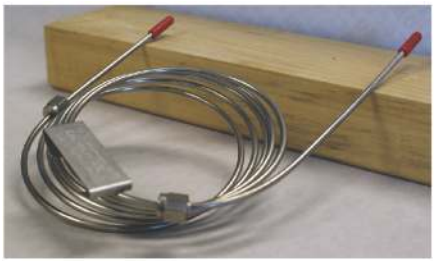
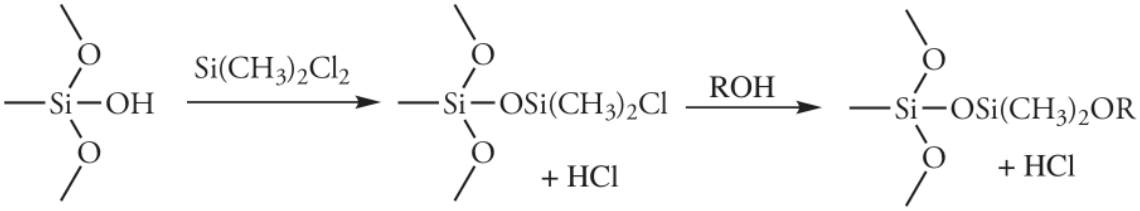


Figure 27.3.1 . Typical example of a packed column for gas chromatography. This column is made from stainless steel and is 2 m long with an internal diameter of 3.2 mm. The packing material in this column has a particle diameter of 149–177 μm. To put this in perspective, beach sand has a typical diameter of 700 μm and the diameter of fine grained sand is 250 μm.

The most widely used particulate support is diatomaceous earth, which is composed of the silica skeletons of diatoms. These particles are very porous, with surface areas ranging from 0.5–7.5 $m^2/g$, which provides ample contact between the mobile phase and the stationary phase. When hydrolyzed, the surface of a diatomaceous earth contains silanol groups (–SiOH), that serve as active sites for absorbing solute molecules in gas-solid chromatography (GSC).

In gas-liquid chromatography (GLC), we coat the packing material with a liquid mobile phase. To prevent uncoated packing material from adsorbing solutes, which degrades the quality of the separation, surface silanols are deactivated by reacting them with dimethyldichlorosilane and rinsing with an alcohol—typically methanol—before coating the particles with stationary phase.




The column in Figure 27.3.1 , for example, has approximately 1800 plates/m, or a total of approximately 3600 theoretical plates.

## Capillary Columns

A capillary, or ***open tubular column*** is constructed from fused silica and is coated with a protective polymer coating. Columns range from 15–100 m in length with an internal diameter of approximately 150–300 μm. Figure 27.3.2 shows an example of a typical capillary column.



Figure 27.3.2 . Typical example of a capillary column for gas chromatography. This column is 30 m long with an internal diameter of 247 μm. The interior surface of the capillary has a 0.25 μm coating of the liquid phase.

Capillary columns are of three principal types. In a wall-coated open tubular column (WCOT) a thin layer of stationary phase, typically 0.25 nm thick, is coated on the capillary's inner wall. In a porous-layer open tubular column (PLOT), a porous solid support—alumina, silica gel, and molecular sieves are typical examples—is attached to the capillary's inner wall. A support-coated open tubular column (SCOT) is a PLOT column that includes a liquid stationary phase. Figure 27.3.3 shows the differences between these types of capillary columns.

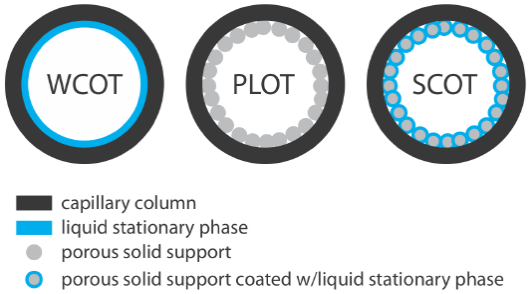



Figure 27.3.3 . Cross sections through the three types of capillary columns.

A capillary column provides a significant improvement in separation efficiency because it has more theoretical plates per meter and is longer than a packed column. For example, the capillary column in Figure 27.3.2 has almost 4300 plates/m, or a total of 129 000 theoretical plates. On the other hand, a packed column can handle a larger sample. Because of its smaller diameter, a capillary column requires a smaller sample, typically less than $10^{-2}$ μL.

## Stationary Phases for Gas-Liquid Chromatography

Elution order in gas–liquid chromatography depends on two factors: the boiling point of the solutes and the interaction between the solutes and the stationary phase. If a mixture's components have significantly different boiling points, then the choice of stationary phase is less critical. If two solutes have similar boiling points, then a separation is possible only if the stationary phase selectively interacts with one of the solutes. As a general rule, nonpolar solutes are separated more easily when using a nonpolar stationary phase, and polar solutes are easier to separate when using a polar stationary phase.

There are several important criteria for choosing a stationary phase: it must not react with the solutes, it must be thermally stable, it must have a low volatility, and it must have a polarity that is appropriate for the sample's components. Table 27.3.1 summarizes the properties of several popular stationary phases.

Table 27.3.1 . Selected Examples of Stationary Phases for Gas-Liquid Chromatography

| stationary phase | polarity | trade name | temperature limit (°C) | representative applications |
|---|---|---|---|---|
| squalane | nonpolar | Squalane | 150 | low-boiling aliphatics hydrocarbons |
| Apiezon L | nonpolar | Apiezon L | 300 | amides, fatty acid methyl esters, terpenoids |
| polydimethyl siloxane | slightly polar | SE-30 | 300–350 | alkaloids, amino acid derivatives, drugs, pesticides, phenols, steroids |
| phenylmethyl polysiloxane (50% phenyl, 50% methyl) | moderately polar | OV-17 | 375 | alkaloids, drugs, pesticides, polyaromatic hydrocarbons, polychlorinated biphenyls |
| trifluoropropylmethyl polysiloxane (50% trifluoropropyl, 50% methyl) | moderately polar | OV-210 | 275 | alkaloids, amino acid derivatives, drugs, halogenated compounds, ketones |
| cyanopropylphenylmethyl polysiloxane (50%cyanopropyl, 50% phenylmethyl) | polar | OV-225 | 275 | nitriles, pesticides, steroids |
| polyethylene glycol | polar | Carbowax 20M | 225 | aldehydes, esters, ethers, phenols |

Many stationary phases have the general structure shown in Figure 27.3.4 a. A stationary phase of polydimethyl siloxane, in which all the –R groups are methyl groups, $–CH_3$, is nonpolar and often makes a good first choice for a new separation. The order of elution when using polydimethyl siloxane usually follows the boiling points of the solutes, with lower boiling solutes eluting first. Replacing some of the methyl groups with other substituents increases the stationary phase's polarity and provides greater selectivity. For example, replacing 50% of the $–CH_3$ groups with phenyl groups, $–C_6H_5$, produces a slightly polar stationary phase. Increasing polarity is provided by substituting trifluoropropyl, $–C_3H_6CF$, and cyanopropyl, $–C_3H_6CN$, functional groups, or by using a stationary phase of polyethylene glycol (Figure 27.3.4 b).

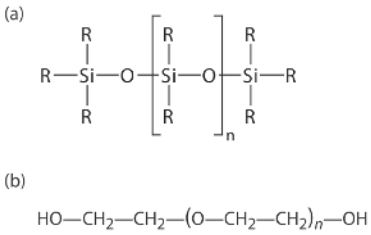



Figure 27.3.4 . General structures of common stationary phases: (a) substituted polysiloxane; (b) polyethylene glycol.

An important problem with all liquid stationary phases is their tendency to elute, or bleed from the column when it is heated. The temperature limits in Table 27.3.1 minimize this loss of stationary phase. Capillary columns with bonded or cross-linked stationary phases provide superior stability. A bonded stationary phase is attached chemically to the capillary's silica surface. Cross-linking, which is done after the stationary phase is in the capillary column, links together separate polymer chains to provide greater stability.

Another important consideration is the thickness of the stationary phase with thinner films of stationary phase improving separation efficiency, as we learned in Chapter 26.4. The most common thickness is 0.25 μm, although a thicker films is useful for highly volatile solutes, such as gases, because it has a greater capacity for retaining such solutes. Thinner films are used when separating low volatility solutes, such as steroids.

A few stationary phases take advantage of chemical selectivity. The most notable are stationary phases that contain chiral functional groups, which are used to separate enantiomers [Hinshaw, J. V. *LC*.*GC* **1993**, *11*, 644–648].

---

This page titled 27.3: Gas Chromatographic Columns and Stationary Phases is shared under a CC BY-NC-SA 4.0 license and was authored, remixed, and/or curated by David Harvey.

# 27.4: Applications of Gas Chromatography

## Quantitative Applications

Gas chromatography is widely used for the analysis of a diverse array of samples in environmental, clinical, pharmaceutical, biochemical, forensic, food science and petrochemical laboratories. Table 27.4.1 provides some representative examples of applications.

Table 27.4.1 . Representative Applications of Gas Chromatography

| area | applications |
|---|---|
| environmental analysis | green house gases ($CO_2$, $CH_4$, $NO_x$) in air<br>pesticides in water, wastewater, and soil<br>vehicle emissions<br>trihalomethanes in drinking water |
| clinical analysis | drugs<br>blood alcohols |
| forensic analysis | analysis of arson accelerants<br>detection of explosives |
| consumer products | volatile organics in spices and fragrances<br>trace organics in whiskey<br>monomers in latex paint |
| petrochemical and chemical industry | purity of solvents<br>refinery gas<br>composition of gasoline |

### Quantitative Calculations

In a GC analysis the area under the peak is proportional to the amount of analyte injected onto the column. A peak's area is determined by integration, which usually is handled by the instrument's computer or by an electronic integrating recorder. If two peak are resolved fully, the determination of their respective areas is straightforward.

> Before electronic integrating recorders and computers, two methods were used to find the area under a curve. One method used a manual planimeter; as you use the planimeter to trace an object's perimeter, it records the area. A second approach for finding a peak's area is the cut-and-weigh method. The chromatogram is recorded on a piece of paper and each peak of interest is cut out and weighed. Assuming the paper is uniform in thickness and density of fibers, the ratio of weights for two peaks is the same as the ratio of areas. Of course, this approach destroys your chromatogram.

Overlapping peaks, however, require a choice between one of several options for dividing up the area shared by the two peaks (Figure 27.4.1 ). Which method we use depends on the relative size of the two peaks and their resolution. In some cases, the use of peak heights provides more accurate results [(a) Bicking, M. K. L. Chromatography Online, April 2006; (b) Bicking, M. K. L. Chromatography Online, June 2006].

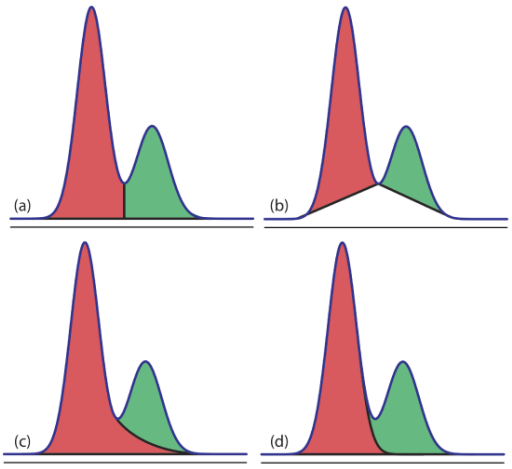



Figure 27.4.1 . Four methods for determining the areas under two overlapping chromatographic peaks: (a) the drop method; (b) the valley method; (c) the exponential skim method; and (d) the Gaussian skim method. Other methods for determining areas also are available.

For quantitative work we need to establish a calibration curve that relates the detector's response to the analyte's concentration. If the injection volume is identical for every standard and sample, then an external standardization provides both accurate and precise results. Unfortunately,even under the best conditions the relative precision for replicate injections may differ by 5%; often it is substantially worse. For quantitative work that requires high accuracy and precision, the use of internal standards is recommended.

## Example 27.4.1

Marriott and Carpenter report the following data for five replicate injections of a mixture that contains 1% v/v methyl isobutyl ketone and 1% v/v *p*-xylene in dichloromethane [Marriott, P. J.; Carpenter, P. D. *J. Chem. Educ.* **1996**, *73*, 96–99].

| injection | peak | peak area (arb. units) |
|---|---|---|
| I | 1 | 48075 |
| | 2 | 78112 |
| II | 1 | 85829 |
| | 2 | 135404 |
| III | 1 | 84136 |
| | 2 | 132332 |
| IV | 1 | 71681 |
| | 2 | 112889 |
| V | 1 | 58054 |
| | 2 | 91287 |

Assume that *p*-xylene (peak 2) is the analyte, and that methyl isobutyl ketone (peak 1) is the internal standard. Determine the 95% confidence interval for a single-point standardization with and without using the internal standard.

### Solution

For a single-point external standardization we ignore the internal standard and determine the relationship between the peak area for *p*-xylene, $A_2$, and the concentration, $C_2$, of *p*-xylene.

$$A_2 = kC_2$$

Substituting the known concentration for *p*-xylene (1% v/v) and the appropriate peak areas, gives the following values for the constant *k*.

$$78112 \quad 135404 \quad 132332 \quad 112889 \quad 91287$$

The average value for *k* is 110 000 with a standard deviation of 25 100 (a relative standard deviation of 22.8%). The 95% confidence interval is

$$\mu = \overline{X} \pm \frac{ts}{\sqrt{n}} = 111000 \pm \frac{(2.78)(25100)}{\sqrt{5}} = 111000 \pm 31200$$

For an internal standardization, the relationship between the analyte's peak area, $A_2$, the internal standard's peak area, $A_1$, and their respective concentrations, $C_2$ and $C_1$, is

$$\frac{A_2}{A_1} = k\frac{C_2}{C_1}$$

Substituting in the known concentrations and the appropriate peak areas gives the following values for the constant *k*.

$$1.5917 \quad 1.5776 \quad 1.5728 \quad 1.5749 \quad 1.5724$$

The average value for *k* is 1.5779 with a standard deviation of 0.0080 (a relative standard deviation of 0.507%). The 95% confidence interval is

$$\mu = \overline{X} \pm \frac{ts}{\sqrt{n}} = 1.5779 \pm \frac{(2.78)(0.0080)}{\sqrt{5}} = 1.5779 \pm 0.0099$$

Although there is a substantial variation in the individual peak areas for this set of replicate injections, the internal standard compensates for these variations, providing a more accurate and precise calibration.

## Exercise 27.4.1

Figure 27.4.2 shows chromatograms for five standards and for one sample. Each standard and sample contains the same concentration of an internal standard, which is 2.50 mg/mL. For the five standards, the concentrations of analyte are 0.20 mg/mL, 0.40 mg/mL, 0.60 mg/mL, 0.80 mg/mL, and 1.00 mg/mL, respectively. Determine the concentration of analyte in the sample by (a) ignoring the internal standards and creating an external standards calibration curve, and by (b) creating an internal standard calibration curve. For each approach, report the analyte's concentration and the 95% confidence interval. Use peak heights instead of peak areas.

**Answer**

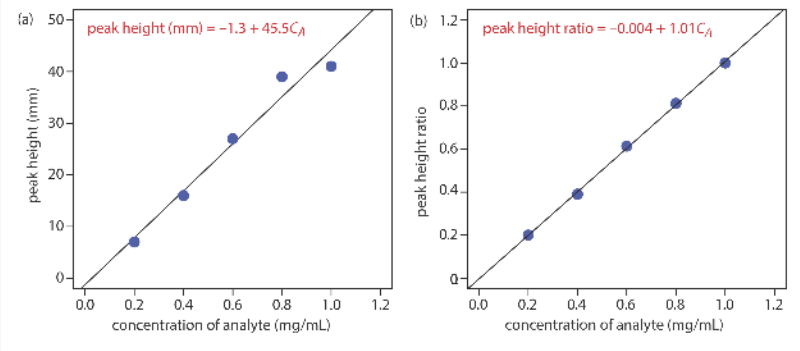
The following table summarizes my measurements of the peak heights for each standard and the sample, and their ratio (although your absolute values for peak heights will differ from mine, depending on the size of your monitor or printout, your relative peak height ratios should be similar to mine).

| [standard] (mg/mL) | peak height of standard (mm) | peak height of analyte (mm) | peak height ratio |
|---|---|---|---|
| 0.20 | 35 | 7 | 0.20 |
| 0.40 | 41 | 16 | 0.39 |
| 0.60 | 44 | 27 | 0.61 |
| 0.80 | 48 | 39 | 0.81 |
| 1.00 | 41 | 41 | 1.00 |
| sample | 39 | 21 | 0.54 |

Figure (a) shows the calibration curve and the calibration equation when we ignore the internal standard. Substituting the sample's peak height into the calibration equation gives the analyte's concentration in the sample as 0.49 mg/mL. The 95%

confidence interval is ±0.24 mg/mL. The calibration curve shows quite a bit of scatter in the data because of uncertainty in the injection volumes.

Figure (b) shows the calibration curve and the calibration equation when we include the internal standard. Substituting the sample's peak height ratio into the calibration equation gives the analyte's concentration in the sample as 0.54 mg/mL. The 95% confidence interval is ±0.04 mg/mL.




The data for this exercise were created so that the analyte's actual concentration is 0.55 mg/mL. Given the resolution of my ruler's scale, my answer is pretty reasonable. Your measurements may be slightly different, but your answers should be close to the actual values.

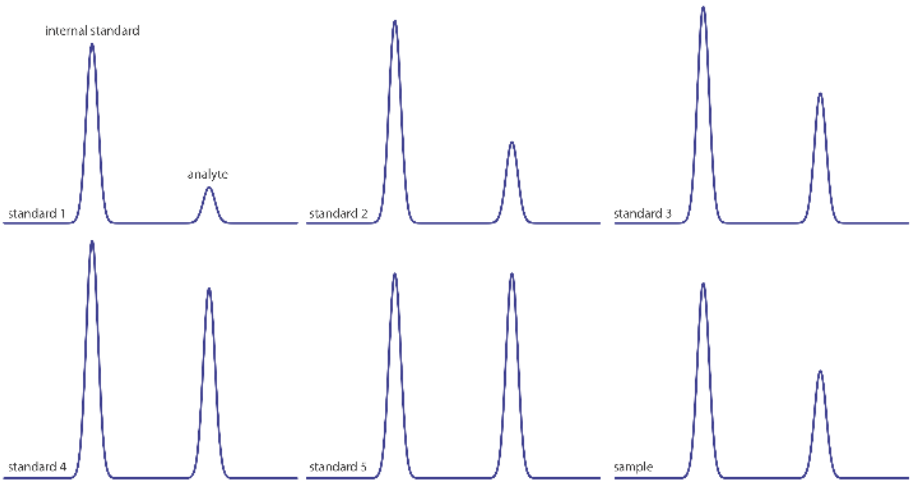



Figure 27.4.2 . Chromatograms for Exercise 27.4.1.

## Qualitative Applications

In addition to a quantitative analysis, we also can use chromatography to identify the components of a mixture. As noted earlier, when we use an FT–IR or a mass spectrometer as the detector we have access to the eluent's full spectrum for any retention time. By interpreting the spectrum or by searching against a library of spectra, we can identify the analyte responsible for each chromatographic peak.

In addition to identifying the component responsible for a particular chromatographic peak, we also can use the saved spectra to evaluate peak purity. If only one component is responsible for a chromatographic peak, then the spectra should be identical throughout the peak's elution. If a spectrum at the beginning of the peak's elution is different from a spectrum taken near the end of the peak's elution, then at least two components are co-eluting.

When using a nonspectroscopic detector, such as a flame ionization detector, we must find another approach if we wish to identify the components of a mixture. One approach is to spike a sample with the suspected compound and look for an increase in peak

height. We also can compare a peak's retention time to the retention time for a known compound if we use identical operating conditions.

Because a compound's retention times on two identical columns are not likely to be the same—differences in packing efficiency, for example, will affect a solute's retention time on a packed column—creating a table of standard retention times is not possible. Kovat's retention index provides one solution to the problem of matching retention times. Under isothermal conditions, the adjusted retention times for normal alkanes increase logarithmically. Kovat defined the retention index, *I*, for a normal alkane as 100 times the number of carbon atoms. For example, the retention index is 400 for butane, $C_4H_{10}$, and 500 for pentane, $C_5H_{12}$. To determine the a compound's retention index, $I_{cpd}$, we use the following formula

$$I_{cpd} = 100 \times \frac{\log t'_{r,cpd} - \log t'_{r,x}}{\log t'_{r,x+1} - \log t'_{r,x}} + I_x \tag{27.4.1}$$

where $t'_{r,cpd}$ is the compound's adjusted retention time, $t'_{r,x}$ and $t'_{r,x+1}$ are the adjusted retention times for the normal alkanes that elute immediately before the compound and immediately after the compound, respectively, and $I_x$ is the retention index for the normal alkane that elutes immediately before the compound. A compound's retention index for a particular set of chromatographic conditions—such as the choice of stationary phase, mobile phase, column type, column length, and temperature—is reasonably consistent from day-to-day and between different columns and instruments.

Tables of Kovat's retention indices are available; see, for example, the NIST Chemistry Webbook. A search for toluene returns 341 values of *I* for over 20 different stationary phases, and for both packed columns and capillary columns.

## Example 27.4.2

In a separation of a mixture of hydrocarbons the following adjusted retention times are measured: 2.23 min for propane, 5.71 min for isobutane, and 6.67 min for butane. What is the Kovat's retention index for each of these hydrocarbons?

### Solution

Kovat's retention index for a normal alkane is 100 times the number of carbons; thus, for propane, *I* = 300 and for butane, *I* = 400. To find Kovat's retention index for isobutane we use Equation 27.4.1.

$$I_{\text{isobutane}} = 100 \times \frac{\log(5.71) - \log(2.23)}{\log(6.67) - \log(2.23)} + 300 = 386$$

## Exercise 27.4.2

When using a column with the same stationary phase as in Example 27.4.2 , you find that the retention times for propane and butane are 4.78 min and 6.86 min, respectively. What is the expected retention time for isobutane?

**Answer**

Because we are using the same column we can assume that isobutane's retention index of 386 remains unchanged. Using Equation 27.4.1, we have

$$386 = 100 \times \frac{\log x - \log(4.78)}{\log(6.86) - \log(4.78)} + 300$$

where *x* is the retention time for isobutane. Solving for *x*, we find that

$$0.86 = \frac{\log x - \log(4.78)}{\log(6.86) - \log(4.78)}$$

$$0.135 = \log x - 0.679$$

$$0.814 = \log x$$

$$x = 6.52$$

> the retention time for isobutane is 6.5 min.

This page titled 27.4: Applications of Gas Chromatography is shared under a CC BY-NC-SA 4.0 license and was authored, remixed, and/or curated by David Harvey.

# CHAPTER OVERVIEW

## 28: High-Performance Liquid Chromatography

In high-performance liquid chromatography (HPLC) we inject the sample, which is in solution form, into a liquid mobile phase. The mobile phase carries the sample through a packed or capillary column that separates the sample's components based on their ability to partition between the mobile phase and the stationary phase. Because it combines separation with analysis, HPLC provides excellent selectivity. By adjusting conditions it usually is possible to design a separation so that analytes elute by themselves, even when the mixture is complex. Additional selectivity is possible by using a detector that does not respond to all analytes.


28.1: Scope of HPLC
28.2: Column Efficiency in Liquid Chromatography
28.3: Instruments for Liquid Chromatography
28.4: Partition Chromatography
28.5: Adsorption Chromatography
28.6: Ion-Exchange Chromatography
28.7: Size-Exclusion Chromatography



This page titled 28: High-Performance Liquid Chromatography is shared under a CC BY-NC-SA 4.0 license and was authored, remixed, and/or curated by David Harvey.

# 28.1: Scope of HPLC

Gas chromatography consists largely of two specific types of interactions, both of which involve the stationary phase: the partitioning of the solute into a polar or a non-polar stationary phase, or the adsorption of the solute onto a solid packing material. The separation of a complex mixture into its component parts is determined primarily by the boiling points of the solutes and differences in the solubility of the solutes in the stationary phase. The properties of the mobile phase, on the other hand, are less important. It is not surprising that there is not much variety in the basic types of gas chromatography.

High-performance liquid chromatography consists of much richer group of techniques, both because the separation depends on the ability of the solutes to partition into the stationary phase **and** to partition into the mobile phase. The range of the possible types of interactions between the solutes and the stationary phase also is greater in HPLC than in GC. In addition to separations based on differences in solubility of the solutes in the stationary phase and the mobile phase (normal and reverse phase partition chromatography) and separations based on the adsorption of solutes on a solid substrate (adsorption chromatography), the separation of ions is possible using ion-exchange resins as stationary phases (ion-exchange chromatography) and the separation of ions by size (size-exclusion chromatography).

This page titled 28.1: Scope of HPLC is shared under a CC BY-NC-SA 4.0 license and was authored, remixed, and/or curated by David Harvey.

# 28.2: Column Efficiency in Liquid Chromatography

In Chapter 26 we considered three factors that affect band broadening—multiple paths, longitudinal diffusion, and mass transfer—expressing the relationship between the height of a theoretical plate, $H$, as a function of the mobile phase's velocity, $u$, using the van Deemter equation

$$H = A + \frac{B}{u} + Cu$$

where $A$ is the contribution from multiple paths, $B$ is the contribution from longitudinal diffusion, and $C$ is the contribution from mass transfer. Unlike gas chromatography, where there is little distance between the point of injection and the column, and little distance between the column and the detector, an HPLC instrument must often include additional tubing to connect together the sample injection port and the column, and the column and the detector. Solutes moving through this tubing, which does not include stationary phase, travel with a velocity that is slower at the walls of the tubing and faster at the center of the tubing; the result is additional band broadening. The magnitude of this contribution to band broadening is minimized by keeping the length of connecting tubing as short as possible. by using tubing with a smaller internal diameter, and by using lower flow rates.

This page titled 28.2: Column Efficiency in Liquid Chromatography is shared under a CC BY-NC-SA 4.0 license and was authored, remixed, and/or curated by David Harvey.

# 28.3: Instruments for Liquid Chromatography

In high-performance liquid chromatography (HPLC) we inject the sample, which is in solution form, into a liquid mobile phase. The mobile phase carries the sample through a packed or capillary column that separates the sample's components based on their ability to partition between the mobile phase and the stationary phase. Figure 28.3.1 shows an example of a typical HPLC instrument, which has several key components: reservoirs that store the mobile phase; a pump for pushing the mobile phase through the system; an injector for introducing the sample; a column for separating the sample into its component parts; and a detector for monitoring the eluent as it comes off the column. Let's consider each of these components.

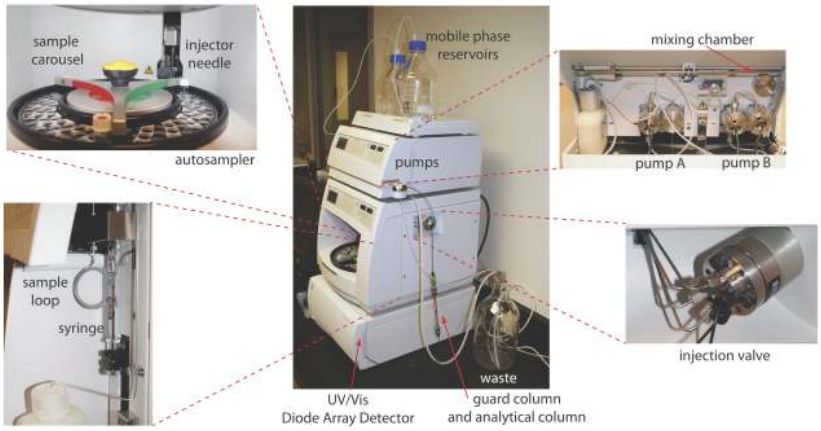



Figure 28.3.1 . Example of a typical high-performance liquid chromatograph with insets showing the pumps that move the mobile phase through the system and the plumbing used to inject the sample into the mobile phase. This particular instrument includes an autosampler. An instrument in which samples are injected manually does not include the features shown in the two left-most insets, and has a different style of loop injection valve.

## HPLC Columns

An HPLC typically includes two columns: an analytical column, which is responsible for the separation, and a guard column that is placed before the analytical column to protect it from contamination.

### Analytical Columns

The most common type of HPLC column is a stainless steel tube with an internal diameter between 2.1 mm and 4.6 mm and a length between 30 mm and 300 mm (Figure 28.3.2 ). The column is packed with 3–10 μm porous silica particles with either an irregular or a spherical shape. Typical column efficiencies are 40 000–60 000 theoretical plates/m. A 25-cm column with 50 000 plates/m has 12 500 theoretical plates.




Figure 28.3.2 . Typical packed column for HPLC. This particular column has an internal diameter of 4.6 mm and a length of 150 mm, and is packed with 5 μm particles coated with stationary phase.

Capillary columns use less solvent and, because the sample is diluted to a lesser extent, produce larger signals at the detector. These columns are made from fused silica capillaries with internal diameters from 44–200 μm and lengths of 50–250 mm. Capillary columns packed with 3–5 μm particles have been prepared with column efficiencies of up to 250 000 theoretical plates [Novotony, M. *Science*, **1989**, *246*, 51–57].

One limitation to a packed capillary column is the back pressure that develops when pumping the mobile phase through the small interstitial spaces between the particulate micron-sized packing material (Figure 28.3.3 ). Because the tubing and the fittings that carry the mobile phase have pressure limits, a higher back pressure requires a lower flow rate and a longer analysis time. Monolithic columns, in which the solid support is a single, porous rod, offer column efficiencies equivalent to a packed capillary column while allowing for faster flow rates. A monolithic column—which usually is similar in size to a conventional packed

column, although smaller, capillary columns also are available—is prepared by forming the mono- lithic rod in a mold and covering it with PTFE tubing or a polymer resin. Monolithic rods made of a silica-gel polymer typically have macropores with diameters of approximately 2 μm and mesopores—pores within the macropores—with diameters of approximately 13 nm [Cabrera, K. Chromatography Online, April 1, 2008].

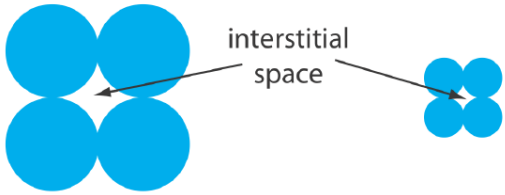



Figure 28.3.3 . The packing of smaller particles creates smaller interstitial spaces than the packing of larger particles. Although reducing particle size by $2\times$ increases efficiency by a factor of 1.4, it also produces a 4-fold increase in back pressure.

### Guard Columns

Two problems tend to shorten the lifetime of an analytical column. First, solutes that bind irreversibly to the stationary phase degrade the column's performance by decreasing the amount of stationary phase available for effecting a separation. Second, particulate material injected with the sample may clog the analytical column. To minimize these problems we place a guard column before the analytical column. A guard column usually contains the same particulate packing material and stationary phase as the analytical column, but is significantly shorter and less expensive—a length of 7.5 mm and a cost one-tenth of that for the corresponding analytical column is typical. Because they are intended to be sacrificial, guard columns are replaced regularly. If you look closely at Figure 28.3.1 , you will see the small guard column just above the analytical column.

## HPLC Plumbing

In a gas chromatograph the pressure from a compressed gas cylinder is sufficient to push the mobile phase through the column. Pushing a liquid mobile phase through a column, however, takes a great deal more effort, generating pressures in excess of several hundred atmospheres. In this section we consider the basic plumbing needed to move the mobile phase through the column and to inject the sample into the mobile phase.

### Moving the Mobile Phase

A typical HPLC includes between 1–4 reservoirs for storing mobile phase solvents. The instrument in Figure 28.3.1 , for example, has two mobile phase reservoirs that are used for an isocratic elution or a gradient elution by drawing solvents from one or both reservoirs.

Before using a mobile phase solvent we must remove dissolved gases, such as $N_2$ and $O_2$, and small particulate matter, such as dust. Because there is a large drop in pressure across the column—the pressure at the column's entrance is as much as several hundred atmospheres, but it is atmospheric pressure at the column's exit—gases dissolved in the mobile phase are released as gas bubbles that may interfere with the detector's response. Degassing is accomplished in several ways, but the most common are the use of a vacuum pump or sparging with an inert gas, such as He, which has a low solubility in the mobile phase. Particulate materials, which may clog the HPLC tubing or column, are removed by filtering the solvents.

> Bubbling an inert gas through the mobile phase releases volatile dissolved gases. This process is called sparging.

The mobile phase solvents are pulled from their reservoirs by the action of one or more pumps. Figure 28.3.4 shows a close-up view of the pumps for the instrument in Figure 28.3.1 . The working pump and the equilibrating pump each have a piston whose back and forth movement maintains a constant flow rate of up to several mL/min and provides the high output pressure needed to push the mobile phase through the chromatographic column. In this particular instrument, each pump sends its mobile phase to a mixing chamber where they combine to form the final mobile phase. The relative speed of the two pumps determines the mobile phase's final composition.

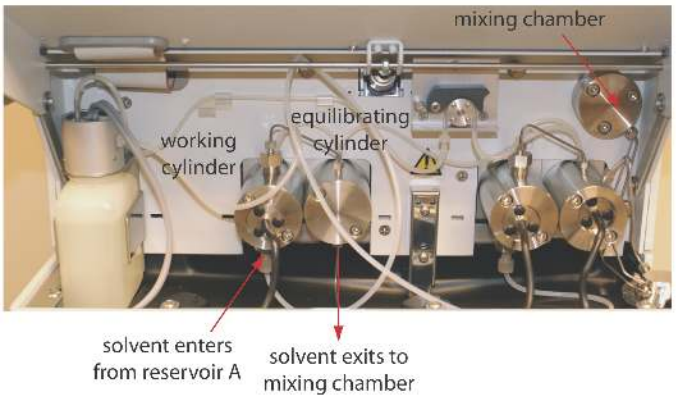



Figure 28.3.4 . Close-up view of the pumps for the instrument shown in Figure 28.3.1 . The working cylinder and the equilibrating cylinder for the pump on the left take solvent from reservoir A and send it to the mixing chamber. The pump on the right moves solvent from reservoir B to the mixing chamber. The mobile phase's flow rate is determined by the combined speeds of the two pumps. By changing the relative speeds of the two pumps, different binary mobile phases can be prepared.

The back and forth movement of a reciprocating pump creates a pulsed flow that contributes noise to the chromatogram. To minimize these pulses, each pump in Figure 28.3.4 has two cylinders. During the working cylinder's forward stoke it fills the equilibrating cylinder and establishes flow through the column. When the working cylinder is on its reverse stroke, the flow is maintained by the piston in the equilibrating cylinder. The result is a pulse-free flow.

There are other ways to control the mobile phase's composition and flow rate. For example, instead of the two pumps in Figure 28.3.4 , we can place a solvent proportioning valve before a single pump. The solvent proportioning value connects two or more solvent reservoirs to the pump and determines how much of each solvent is pulled during each of the pump's cycles. Another approach for eliminating a pulsed flow is to include a pulse damper between the pump and the column. A pulse damper is a chamber filled with an easily compressed fluid and a flexible diaphragm. During the piston's forward stroke the fluid in the pulse damper is compressed. When the piston withdraws to refill the pump, pressure from the expanding fluid in the pulse damper maintains the flow rate.

## Injecting the Sample

The operating pressure within an HPLC is sufficiently high that we cannot inject the sample into the mobile phase by inserting a syringe through a septum, as is possible in gas chromatography. Instead, we inject the sample using a loop injector, a diagram of which is shown in Figure 28.3.5 . In the load position a sample loop—which is available in a variety of sizes ranging from 0.5 μL to 5 mL—is isolated from the mobile phase and open to the atmosphere. The sample loop is filled using a syringe with a capacity several times that of the sample loop, with excess sample exiting through the waste line. After loading the sample, the injector is turned to the inject position, which redirects the mobile phase through the sample loop and onto the column.

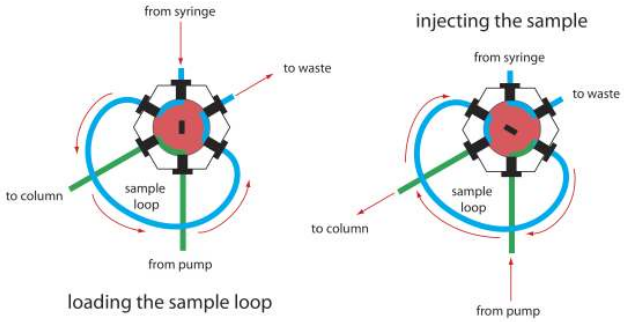



Figure 28.3.5 . Schematic diagram of a manual loop injector. In the load position the flow of mobile phase from the pump to the column (shown in green) is isolated from the sample loop, which is filled using a syringe (shown in blue). Rotating the inner valve (shown in red) to the inject position directs the mobile phase through the sample loop and onto the column.

> The instrument in Figure 28.3.1 uses an autosampler to inject samples. Instead of using a syringe to push the sample into the sample loop, the syringe draws sample into the sample loop.

## Detectors for HPLC

Many different types of detectors have been use to monitor HPLC separations, most of which use spectroscopy or electrochemistry to generate a measurable signal.

### Spectroscopic Detectors

The most popular HPLC detectors take advantage of an analyte's UV/Vis absorption spectrum. These detectors range from simple designs, in which the analytical wavelength is selected using appropriate filters, to a modified spectrophotometer in which the sample compartment includes a flow cell. Figure 28.3.6 shows the design of a typical flow cell when using a diode array spectrometer as the detector. The flow cell has a volume of 1–10 µL and a path length of 0.2–1 cm.

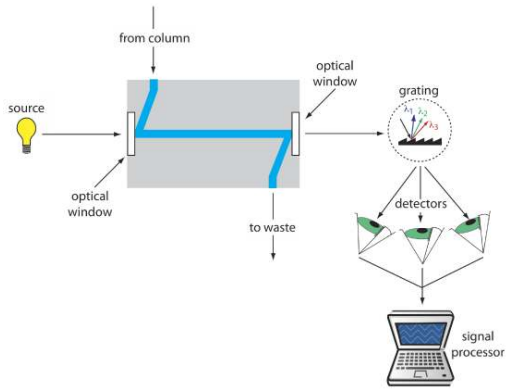



Figure 28.3.6 . Schematic diagram of a flow cell for a detector equipped with a diode array spectrometer.

When using a UV/Vis detector the resulting chromatogram is a plot of absorbance as a function of elution time. If the detector is a diode array spectrometer, then we also can display the result as a three-dimensional chromatogram that shows absorbance as a function of wavelength and elution time. One limitation to using absorbance is that the mobile phase cannot absorb at the wavelengths we wish to monitor. Absorbance detectors provide detection limits of as little as 100 pg–1 ng of injected analyte. If an analyte is fluorescent, we can place the flow cell in a spectrofluorimeter. Detection limits are as little as 1–10 pg of injected analyte.

### Electrochemical Detectors

Another common group of HPLC detectors are those based on electrochemical measurements such as amperometry, voltammetry, coulometry, and conductivity. Figure 28.3.7 , for example, shows an amperometric flow cell. Effluent from the column passes over the working electrode—held at a constant potential relative to a downstream reference electrode—that completely oxidizes or reduces the analytes. The current flowing between the working electrode and the auxiliary electrode serves as the analytical signal. Detection limits for amperometric electrochemical detection are from 10 pg–1 ng of injected analyte.

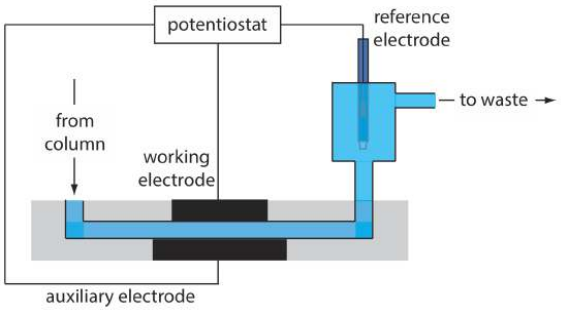



Figure 28.3.7 . Schematic diagram showing a flow cell for an amperometric electrochemical detector.

## Other Detectors

Several other detectors have been used in HPLC. Measuring a change in the mobile phase's refractive index is analogous to monitoring the mobile phase's thermal conductivity in gas chromatography. A refractive index detector is nearly universal, responding to almost all compounds, but has a relatively poor detection limit of 0.1–1 μg of injected analyte. An additional limitation of a refractive index detector is that it cannot be used for a gradient elution unless the mobile phase components have identical refractive indexes.

Another useful detector is a mass spectrometer. Figure 28.3.8 shows a block diagram of a typical HPLC–MS instrument. The effluent from the column enters the mass spectrometer's ion source using an interface the removes most of the mobile phase, an essential need because of the incompatibility between the liquid mobile phase and the mass spectrometer's high vacuum environment. In the ionization chamber the remaining molecules—a mixture of the mobile phase components and solutes—undergo ionization and fragmentation. The mass spectrometer's mass analyzer separates the ions by their mass-to-charge ratio (m/z). A detector counts the ions and displays the mass spectrum.

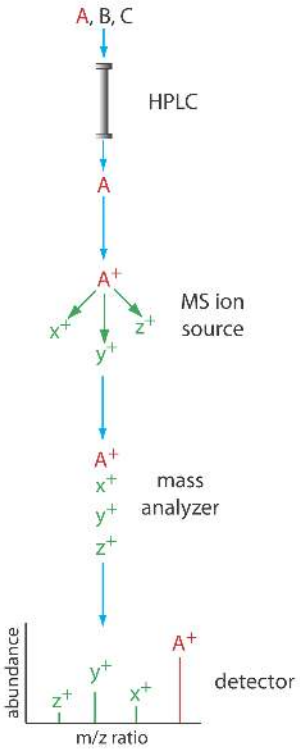



Figure 28.3.8 . Block diagram of an HPLC–MS. A three component mixture enters the HPLC. When component A elutes from the column, it enters the MS ion source and ionizes to form the parent ion and several fragment ions. The ions enter the mass analyzer, which separates them by their mass-to-charge ratio, providing the mass spectrum shown at the detector.

There are several options for monitoring the chromatogram when using a mass spectrometer as the detector. The most common method is to continuously scan the entire mass spectrum and report the total signal for all ions reaching the detector during each scan. This total ion scan provides universal detection for all analytes. We can achieve some degree of selectivity by monitoring only specific mass-to-charge ratios, a process called selective-ion monitoring. The advantages of using a mass spectrometer in HPLC are the same as for gas chromatography. Detection limits are very good, typically 0.1–1 ng of injected analyte, with values as low as 1–10 pg for some samples. In addition, a mass spectrometer provides qualitative, structural information that can help to identify the analytes. The interface between the HPLC and the mass spectrometer is technically more difficult than that in a GC–MS because of the incompatibility of a liquid mobile phase with the mass spectrometer's high vacuum requirement.

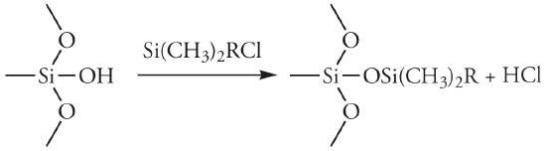
This page titled 28.3: Instruments for Liquid Chromatography is shared under a CC BY-NC-SA 4.0 license and was authored, remixed, and/or curated by David Harvey.

# 28.4: Partition Chromatography

Of the many forms of liquid chromatography, partition chromatography is the most common. In partition chromatography, a solute's retention time is determined by the extent to which it moves from the mobile phase into the stationary phase, and from the stationary phase back into the mobile phase. The extent of this equilibrium partitioning is determined by the polarity of the solutes, the stationary phase, and the mobile phase. In normal-phase partition chromatography, the stationary phase is polar and the mobile phase is non-polar (or of low polarity), with more polar solutes taking longer to elute as they are more strongly retained by the polar stationary phase. In reverse-phase partition chromatography, the stationary phase is non-polar and the mobile phase is polar, with more polar solutes eluting more quickly as they are less strongly retained by the stationary phase. Of the two modes, reverse-phase partition chromatography is the more common.

## Stationary Phases for Partition Chromatography

In partition chromatography the stationary phase is a liquid film coated on a packing material, typically 3–10 μm porous silica particles. Because the stationary phase may be partially soluble in the mobile phase, it may elute, or bleed from the column over time. To prevent the loss of stationary phase, which shortens the column's lifetime, it is bound covalently to the silica particles. Bonded stationary phases are created by reacting the silica particles with an organochlorosilane of the general form $Si(CH_3)_2RCl$, where R is an alkyl or substituted alkyl group.




To prevent unwanted interactions between the solutes and any remaining –SiOH groups, $Si(CH_3)_3Cl$ is used to convert unreacted sites to $–SiOSi(CH_3)_3$; such columns are designated as end-capped.

The properties of a stationary phase depend on the organosilane's alkyl group. If R is a polar functional group, then the stationary phase is polar. Examples of polar stationary phases include those where R contains a cyano ($–C_2H_4CN$), a diol ($–C_3H_6OCH_2CHOHCH_2OH$), or an amino ($–C_3H_6NH_2$) functional group. The most common nonpolar stationary phases use an organochlorosilane where the R group is an *n*-octyl ($C_8$) or *n*-octyldecyl ($C_{18}$) hydrocarbon chain. Most reversed-phase separations are carried out using a buffered aqueous solution as a polar mobile phase, or using other polar solvents, such as methanol and acetonitrile. Because the silica substrate may undergo hydrolysis in basic solutions, the pH of the mobile phase must be less than 7.5.

> It seems odd that the more common form of liquid chromatography is identified as reverse-phase instead of normal phase. One of the earliest examples of chromatography was Mikhail Tswett's separation of plant pigments, which used a polar column of calcium carbonate and a nonpolar mobile phase of petroleum ether. The assignment of normal and reversed, therefore, is all about precedence.

## Mobile Phases for Partition Chromatography

The elution order of solutes in HPLC is governed by polarity. For a normal-phase separation, a solute of lower polarity spends proportionally less time in the polar stationary phase and elutes before a solute that is more polar. Given a particular stationary phase, retention times in normal-phase HPLC are controlled by adjusting the mobile phase's properties. For example, if the resolution between two solutes is poor, switching to a less polar mobile phase keeps the solutes on the column for a longer time and provides more opportunity for their separation. In reversed-phase HPLC the order of elution is the opposite that in a normal-phase separation, with more polar solutes eluting first. Increasing the polarity of the mobile phase leads to longer retention times. Shorter retention times require a mobile phase of lower polarity.

## Choosing a Mobile Phase: Using the Polarity Index

There are several indices that help in selecting a mobile phase, one of which is the polarity index [Snyder, L. R.; Glajch, J. L.; Kirkland, J. J. *Practical HPLC Method Development*, Wiley-Inter- science: New York, 1988]. Table 28.4.1 provides values of the polarity index, $P'$, for several common mobile phases, where larger values of $P'$ correspond to more polar solvents. Mixing together two or more mobile phases—assuming they are miscible—creates a mobile phase of intermediate polarity. For example, a binary mobile phase made by combining solvent *A* and solvent *B* has a polarity index, $P'_{AB}$, of

$$P'_{AB} = \Phi_A P'_A + \Phi_B P'_B \tag{28.4.1}$$

where $P'_A$ and $P'_B$ are the polarity indices for solvents *A* and *B*, and $\Phi_A$ and $\Phi_B$ are the volume fractions for the two solvents.

Table 28.4.1 . Properties of HPLC Mobile Phases

| mobile phase | polarity index ($P'$) | UV cutoff (nm) |
|---|---|---|
| cyclohexane | 0.04 | 210 |
| *n*-hexane | 0.1 | 210 |
| carbon tetrachloride | 1.6 | 265 |
| *i*-propyl ether | 2.4 | 220 |
| toluene | 2.4 | 286 |
| diethyl ether | 2.8 | 218 |
| tetrahydrofuran | 4.0 | 220 |
| ethanol | 4.3 | 210 |
| ethyl acetate | 4.4 | 255 |
| dioxane | 4.8 | 215 |
| methanol | 5.1 | 210 |
| acetonitrile | 5.8 | 190 |
| water | 10.2 | — |

### Example 28.4.1

A reversed-phase HPLC separation is carried out using a mobile phase of 60% v/v water and 40% v/v methanol. What is the mobile phase's polarity index?

**Solution**

Using Equation 28.4.1 and the values in Table 28.4.1 , the polarity index for a 60:40 water–methanol mixture is

$$P'_{AB} = \Phi_{\text{water}} P'_{\text{water}} + \Phi_{\text{methanol}} P'_{\text{methanol}}$$

$$P'_{AB} = 0.60 \times 10.2 + 0.40 \times 5.1 = 8.2$$

### Exercise 28.4.1

Suppose you need a mobile phase with a polarity index of 7.5. Explain how you can prepare this mobile phase using methanol and water.

**Answer**

If we let *x* be the fraction of water in the mobile phase, then 1 – *x* is the fraction of methanol. Substituting these values into Equation 28.4.1 and solving for *x*

$$7.5 = 10.2x + 5.1(1 - x)$$

$$7.5 = 10.2x + 5.1 - 5.1x$$

$$2.4 = 5.1x$$

gives *x* as 0.47. The mobile phase is 47% v/v water and 53% v/v methanol.

As a general rule, a two unit change in the polarity index corresponds to an approximately 10-fold change in a solute's retention factor. Here is a simple example. If a solute's retention factor, *k*, is 22 when using water as a mobile phase ($P'$ = 10.2), then switching to a mobile phase of 60:40 water–methanol ($P'$ = 8.2) decreases *k* to approximately 2.2. Note that the retention factor becomes smaller because we are switching from a more polar mobile phase to a less polar mobile phase in a reversed-phase separation.

## Choosing a Mobile Phase: Adjusting Selectivity

Changing the mobile phase's polarity index changes a solute's retention factor. As we learned in Chapter 26.4, however, a change in *k* is not an effective way to improve resolution when the initial value of *k* is greater than 10. To effect a better separation between two solutes we must improve the selectivity factor, $\alpha$. There are two common methods for increasing $\alpha$: adding a reagent to the mobile phase that reacts with the solutes in a secondary equilibrium reaction or switching to a different mobile phase.

Taking advantage of a secondary equilibrium reaction is a useful strategy for improving a separation [(a) Foley, J. P. *Chromatography*, **1987**, *7*, 118–128; (b) Foley, J. P.; May, W. E. Anal. Chem. 1987, 59, 102–109; (c) Foley, J. P.; May, W. E. Anal. Chem. 1987, 59, 110–115]. Figure 28.4.1 shows the reversed-phase separation of four weak acids—benzoic acid, terephthalic acid, *p*-aminobenzoic acid, and *p*-hydroxybenzoic acid—on a nonpolar $C_{18}$ column using an aqueous buffer of acetic acid and sodium acetate as the mobile phase. The retention times for these weak acids are shorter when using a less acidic mobile phase because each solute is present in an anionic, weak base form that is less soluble in the nonpolar stationary phase. If the mobile phase's pH is sufficiently acidic, the solutes are present as neutral weak acids that are more soluble in the stationary phase and take longer to elute. Because the weak acid solutes do not have identical $pK_a$ values, the pH of the mobile phase has a different effect on each solute's retention time, allowing us to find the optimum pH for effecting a complete separation of the four solutes.

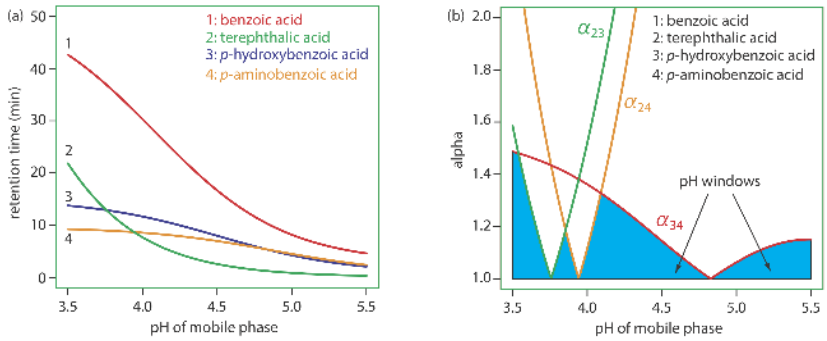



Figure 28.4.1 . Example that shows how the mobile phase pH in liquid chromatography affects selectivity: (a) retention times for four substituted benzoic acids as a function of the mobile phase's pH; (b) alpha values for three pairs of solutes that are difficult to separate. The mobile phase is an acetic acid/sodium acetate buffer and the stationary phase is a nonpolar hydrocarbon. Data from Harvey, D. T.; Byerly, S.; Bowman, A.; Tomlin, J. "Optimization of HPLC and GC Separations Using Response Surfaces," *J. Chem. Educ.* **1991**, *68*, 162–168.

In Example 28.4.1 we learned how to adjust the mobile phase's polarity by blending together two solvents. A polarity index, however, is just a guide, and binary mobile phase mixtures with identical polarity indices may not resolve equally a pair of solutes. Table 28.4.2 , for example, shows retention times for four weak acids in two mobile phases with nearly identical values for $P'$. Although the order of elution is the same for both mobile phases, each solute's retention time is affected differently by the choice of organic solvent. If we switch from using acetonitrile to tetrahydrofuran, for example, we find that benzoic acid elutes more quickly

and that *p*-hydroxybenzoic acid elutes more slowly. Although we can resolve fully these two solutes using mobile phase that is 16% v/v acetonitrile, we cannot resolve them if the mobile phase is 10% tetrahydrofuran.

Table 28.4.2 . Retention Times for Four Weak Acids in Mobile Phases With Similar Polarity Indexes

| retention time (min) | 16% acetonitrile ($CH_3CN$)<br>84% pH 4.11 aqueous buffer ($P'$ = 9.5) | 10% tetrahydrofuran (THF)<br>90% pH 4.11 aqueous buffer ($P'$ = 9.6) |
|---|---|---|
| $t_{r,\,BA}$ | 5.18 | 4.01 |
| $t_{r,\,PH}$ | 1.67 | 2.91 |
| $t_{r,\,PA}$ | 1.21 | 1.05 |
| $t_{r,\,TP}$ | 0.23 | 0.54 |

Key: BA is benzoic acid; PH is *p*-hydroxybenzoic acid; PA is *p*-aminobenzoic acid; TP is terephthalic acid
Source: Harvey, D. T.; Byerly, S.; Bowman, A.; Tomlin, J. "Optimization of HPLC and GC Separations Using Response Surfaces," *J. Chem. Educ.* **1991**, *68*, 162–168.

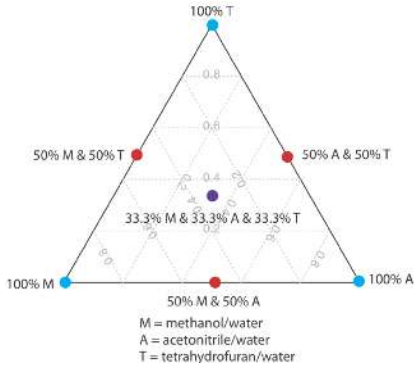



Figure 28.4.2 . Solvent triangle for optimizing a reversed-phase HPLC separation. The three blue circles show mobile phases consisting of an organic solvent and water. The three red circles are binary mobile phases created by combining equal volumes of the pure mobile phases. The ternary mobile phase shown by the purple circle contains all three of the pure mobile phases.

One strategy for finding the best mobile phase is to use the solvent triangle shown in Figure 28.4.2 , which allows us to explore a broad range of mobile phases with only seven experiments. We begin by adjusting the amount of acetonitrile in the mobile phase to produce the best possible separation within the desired analysis time. Next, we use Table 28.4.3 to estimate the composition of methanol/$H_2O$ and tetrahydrofuran/$H_2O$ mobile phases that will produce similar analysis times. Four additional mobile phases are prepared using the binary and ternary mobile phases shown in Figure 28.4.2 . When we examine the chromatograms from these seven mobile phases we may find that one or more provides an adequate separation, or we may identify a region within the solvent triangle where a separation is feasible. Figure 28.4.3 shows a resolution map for the reversed-phase separation of benzoic acid, terephthalic acid, *p*-aminobenzoic acid, and *p*-hydroxybenzoic acid on a nonpolar $C_{18}$ column in which the maximum desired analysis time is set to 6 min [Harvey, D. T.; Byerly, S.; Bowman, A.; Tomlin, J. *J. Chem. Educ.* **1991**, *68*, 162–168]. The areas in blue, green, and red show mobile phase compositions that do not provide baseline resolution. The unshaded area represents mobile phase compositions where a separation is possible.

> The choice to start with acetonitrile is arbitrary—we can just as easily choose to begin with methanol or with tetrahydrofuran.

Table 28.4.3 . Composition of Mobile Phases With Approximately Equal Solvent Strengths

| %v/v $CH_3OH$ | % v/v $CH_3CN$ | %v/v THF |
|---|---|---|
| 0 | 0 | 0 |
| 10 | 6 | 4 |
| 20 | 14 | 10 |
| 30 | 22 | 16 |
| 40 | 32 | 24 |
| 50 | 40 | 30 |
| 6 | 50 | 36 |
| 70 | 60 | 44 |
| 80 | 72 | 52 |
| 90 | 87 | 62 |
| 100 | 99 | 71 |

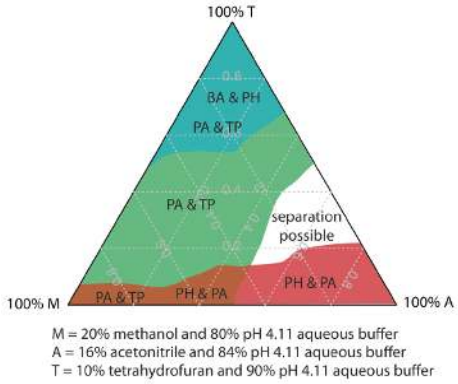



Figure 28.4.3 . Resolution map for the separation of benzoic acid (BA), terephthalic acid (TP), *p*-aminobenzoic acid (PA), and *p*-hydroxybenzoic acid (PH) on a nonpolar $C_{18}$ column subject to a maximum analysis time of 6 min. The shaded areas represent regions where a separation is not possible, with the unresolved solutes identified. A separation is possible in the unshaded area. See Harvey, D. T.; Byerly, S.; Bowman, A.; Tomlin, J. "Optimization of HPLC and GC Separations Using Response Surfaces," *J. Chem. Educ.* **1991**, *68*, 162–168 for details on the mathematical model used to generate the resolution map.

## Choosing a Mobile Phase: Isocratic and Gradient Elutions

A separation using a mobile phase that has a fixed composition is an isocratic elution. One difficulty with an isocratic elution is that an appropriate mobile phase strength for resolving early-eluting solutes may lead to unacceptably long retention times for late-eluting solutes. Optimizing the mobile phase for late-eluting solutes, on the other hand, may provide an inadequate separation of early-eluting solutes. Changing the mobile phase's composition as the separation progresses is one solution to this problem. For a reversed-phase separation we use an initial mobile phase that is more polar. As the separation progresses, we adjust the composition of mobile phase so that it becomes less polar (see Figure 28.4.4 ). Such separations are called gradient elutions.

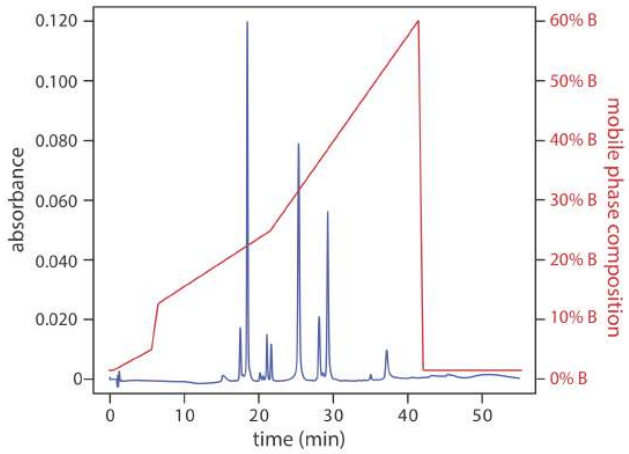



Figure 28.4.4 . Gradient elution separation of a mixture of flavonoids. Mobile phase A is an aqueous solution of 0.1% formic acid and mobile phase B is 0.1% formic acid in acetonitrile. The initial mobile phase is 98% A and 2% B. The percentage of mobile phase B increases in four steps: from 2% to 5% over 5 min, beginning at 0.5 min; from 5% to 12% over 1 min, beginning at 5.5 min; from 12% to 25% over 15 min, beginning at 6.5 min; and from 25% to 60% over 20 min, beginning at 21.5 min. Data provided by Christopher Schardon, Kyle Meinhardt, and Michelle Bushey, Department of Chemistry, Trinty University.

## Choosing a Detector

The availability of different types detectors provides another way to build selectivity into an analysis. Figure 28.4.5 , for example, shows the reverse-phase separation of a mixture of flavonoids using UV/Vis detection at two different wavelengths. In this case, a wavelength of 260 nm increases the method's sensitivity for rutin relative to that for taxifolin.

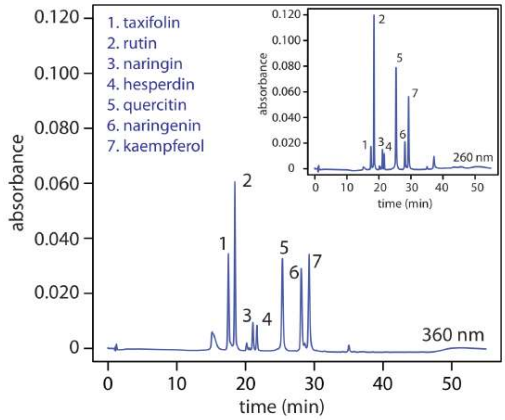



Figure 28.4.5 . HPLC separation of a mixture of flavonoids with UV/Vis detection at 360 nm and, in the inset, at 260 nm. The choice of wavelength affects each analyte's signal. By carefully choosing the wavelength, we can enhance the signal for the analytes of greatest interest. Data provided by Christopher Schardon, Kyle Meinhardt, and Michelle Bushey, Department of Chemistry, Trinty University.

As shown in Figure 28.4.6 , a fluorescence detector provides additional selectivity because only a few of a sample's components are fluorescent.


https://chem.libretexts.org/@go/page/362587

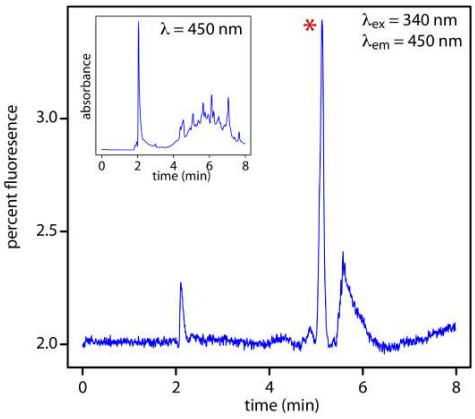



Figure 28.4.6 . HPLC chromatogram for the determination of riboflavin in urine using fluorescence detection with exci-tation at a wavelength of 340 nm and detection at 450 nm. The peak corresponding to riboflavin is marked with a red asterisk (*). The inset shows the same chromatogram when using a less-selective UV/Vis detector at a wavelength of 450 nm. Data provided by Jason Schultz, Jonna Berry, Kaelene Lundstrom, and Dwight Stoll, Department of Chemistry, Gustavus Adolphus College.

With a mass spectrometer as a detector, there are several options for monitoring the chromatogram. The most common method is to continuously scan the entire mass spectrum and report the total signal for all ions reaching the detector during each scan. This total ion scan provides universal detection for all analytes. As seen in Figure 28.4.7 , we can achieve some degree of selectivity by monitoring only specific mass-to-charge ratios, a process called selective-ion monitoring.

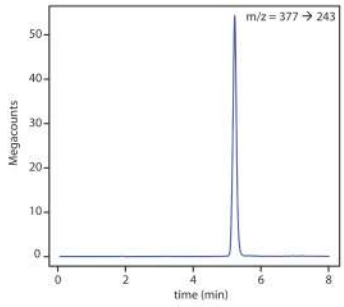



Figure 28.4.7 . HPLC–MS/MS chromatogram for the determination of riboflavin in urine. An initial parent ion with an m/z ratio of 377 enters a second mass spectrometer where it undergoes additional 20 ionization; the fragment ion with an m/z ratio of 243 provides the signal. The selectivity of this detector is evident when you compare this chromatogram to the one in Figure 28.4.7 , which uses fluoresence deterction. Data provided by Jason Schultz, Jonna Berry, Kaelene Lundstrom, and Dwight Stoll, Department of Chemistry, Gustavus Adolphus College.

## Quantitative Applications of Partition Chromatography

Partition chromatography is used routinely for both qualitative and quantitative analyses of environmental, pharmaceutical, industrial, forensic, clinical, and consumer product samples.

### Preparing Samples for Analysis

Samples in liquid form are injected into the HPLC after a suitable clean-up to remove any particulate materials, or after a suitable extraction to remove matrix interferents. In determining polyaromatic hydrocarbons (PAH) in wastewater, for example, an extraction with $CH_2Cl_2$ serves the dual purpose of concentrating the analytes and isolating them from matrix interferents. Solid samples are first dissolved in a suitable solvent or the analytes of interest brought into solution by extraction. For example, an HPLC analysis for the active ingredients and the degradation products in a pharmaceutical tablet often begins by extracting the powdered tablet with a portion of mobile phase. Gas samples are collected by bubbling them through a trap that contains a suitable solvent. Organic isocyanates in industrial atmospheres are collected by bubbling the air through a solution of 1-(2-methoxyphenyl)piperazine in toluene. The reaction between the isocyanates and 1-(2-methoxyphenyl)piperazine both stabilizes them against degradation before the HPLC analysis and converts them to a chemical form that can be monitored by UV absorption.

## Quantitative Calculations

A quantitative HPLC analysis is often easier than a quantitative GC analysis because a fixed volume sample loop provides a more precise and accurate injection. As a result, most quantitative HPLC methods do not need an internal standard and, instead, use external standards and a normal calibration curve.

> An internal standard is necessary when using HPLC–MS because the interface between the HPLC and the mass spectrometer does not allow for a reproducible transfer of the column's eluent into the MS's ionization chamber.

### Example 28.4.2

The concentration of polynuclear aromatic hydrocarbons (PAH) in soil is determined by first extracting the PAHs with methylene chloride. The extract is diluted, if necessary, and the PAHs separated by HPLC using a UV/Vis or fluorescence detector. Calibration is achieved using one or more external standards. In a typical analysis a 2.013-g sample of dried soil is extracted with 20.00 mL of methylene chloride. After filtering to remove the soil, a 1.00-mL portion of the extract is removed and diluted to 10.00 mL with acetonitrile. Injecting 5 µL of the diluted extract into an HPLC gives a signal of 0.217 (arbitrary units) for the PAH fluoranthene. When 5 µL of a 20.0-ppm fluoranthene standard is analyzed using the same conditions, a signal of 0.258 is measured. Report the parts per million of fluoranthene in the soil.

**Solution**

For a single-point external standard, the relationship between the signal, *S*, and the concentration, *C*, of fluoranthene is

$$S = kC$$

Substituting in values for the standard's signal and concentration gives the value of *k* as

$$k = \frac{S}{C} = \frac{0.258}{20.0 \text{ ppm}} = 0.0129 \text{ ppm}^{-1}$$

Using this value for *k* and the sample's HPLC signal gives a fluoranthene concentration of

$$C = \frac{S}{k} = \frac{0.217}{0.0129 \text{ ppm}^{-1}} = 16.8 \text{ ppm}$$

for the extracted and diluted soil sample. The concentration of fluoranthene in the soil is

$$\frac{16.8 \text{ g/mL} \times \frac{10.00 \text{ mL}}{1.00 \text{ mL}} \times 20.00 \text{ mL}}{2.013 \text{ g sample}} = 1670 \text{ ppm fluoranthene}$$

### Exercise 28.4.2

The concentration of caffeine in beverages is determined by a reversed-phase HPLC separation using a mobile phase of 20% acetonitrile and 80% water, and using a nonpolar $C_8$ column. Results for a series of 10-µL injections of caffeine standards are in the following table.

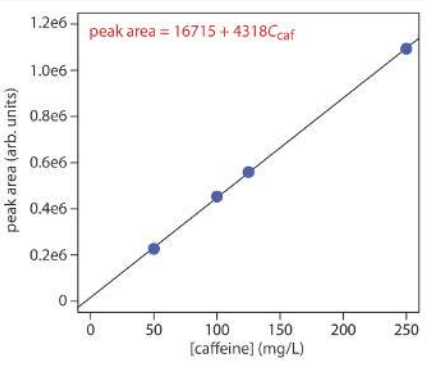
| [caffeine] (mg/L) | peak area (arb. units) |
|---|---|
| 50.0 | 226724 |
| 100.0 | 453762 |
| 125.0 | 559443 |
| 250.0 | 1093637 |

What is the concentration of caffeine in a sample if a 10-µL injection gives a peak area of 424195? The data in this problem comes from Kusch, P.; Knupp, G. "Simultaneous Determination of Caffeine in Cola Drinks and Other Beverages by Reversed-

Phase HPTLC and Reversed-Phase HPLC," *Chem. Educator*, **2003**, *8*, 201–205.

**Answer**

The figure below shows the calibration curve and calibration equation for the set of external standards. Substituting the sample's peak area into the calibration equation gives the concentration of caffeine in the sample as 94.4 mg/L.




This page titled 28.4: Partition Chromatography is shared under a CC BY-NC-SA 4.0 license and was authored, remixed, and/or curated by David Harvey.

# 28.5: Adsorption Chromatography

In adsorption chromatography (or liquid-solid chromatography, LSC) the column packing also serves as the stationary phase. In Tswett's original work the stationary phase was finely divided $CaCO_3$, but modern columns employ porous 3–10 μm particles of silica or alumina. Because the stationary phase is polar, the mobile phase usually is a nonpolar or a moderately polar solvent. Typical mobile phases include hexane, isooctane, and methylene chloride. The usual order of elution—from shorter to longer retention times—is

olefins < aromatic hydrocarbons < ethers < esters, aldehydes, ketones < alcohols, amines < amide < carboxylic acids

Nonpolar stationary phases, such as charcoal-based absorbents, also are used. For most samples, liquid–solid chromatography does not offer any special advantages over liquid–liquid chromatography. One exception is the analysis of isomers, where LSC excels.

This page titled 28.5: Adsorption Chromatography is shared under a CC BY-NC-SA 4.0 license and was authored, remixed, and/or curated by David Harvey.

# 28.6: Ion-Exchange Chromatography

In ion-exchange chromatography (IEC) the stationary phase is a cross-linked polymer resin, usually divinylbenzene cross-linked polystyrene, with covalently attached ionic functional groups (see Figure 28.6.1 and Table 28.6.1 ). The counterions to these fixed charges are mobile and are displaced by ions that compete more favorably for the exchange sites. Ion-exchange resins are divided into four categories: strong acid cation exchangers; weak acid cation exchangers; strong base anion exchangers; and weak base anion exchangers.

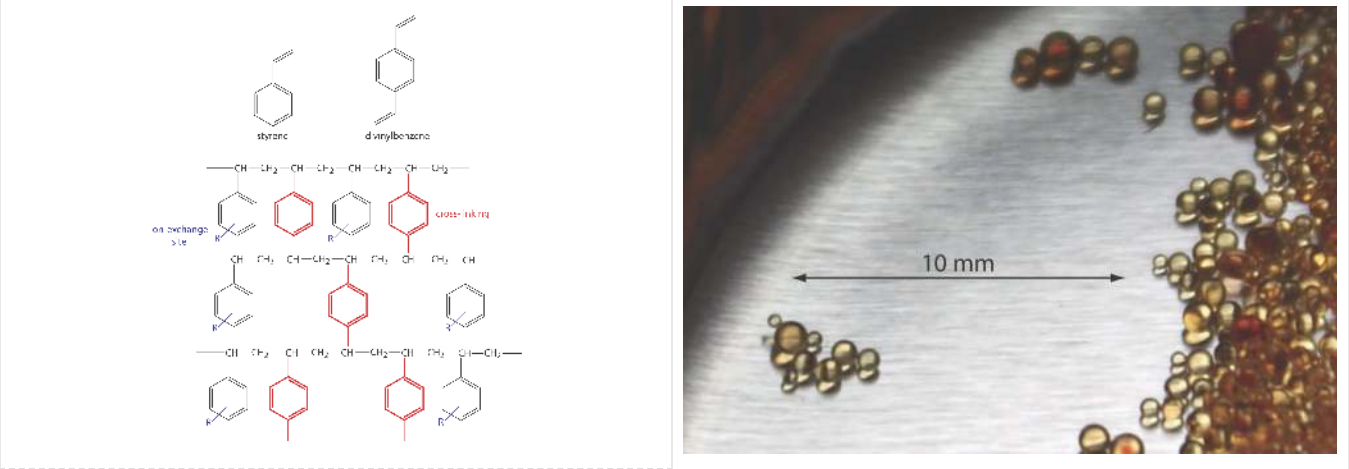



Figure 28.6.1 . Structures of styrene, divinylbenzene, and a styrene–divinylbenzene co-polymer modified for use as an ion-exchange resin are shown on the left. The ion-exchange sites, indicated by R and shown in blue, are mostly in the *para* position and are not necessarily bound to all styrene units. The cross-linking is shown in red. The photo on the right shows an example of the polymer beads. These beads are approximately 0.30–0.85 mm in diameter. Resins for use in ion-exchange chromatography typically are 5–11 μm in diameter.

Table 28.6.1 . Examples of Common Ion-Exchange Resins

| type | functional group | examples |
|---|---|---|
| strong acid cation exchanger | sulfonic acid | $-SO_3^-$<br>$-CH_2CH_2SO_3^-$ |
| weak acid cation exchanger | carboxylic acid | $-COO^-$<br>$-CH_2COO^-$ |
| strong base anion exchanger | quaternary amine | $-CH_2N(CH_3)_3^+$<br>$-CH_2CH_2N(CH_2CH_3)_3^+$ |
| weak base anion exchanger | amine | $-NH_4^+$<br>$-CH_2CH_2NH(CH_2CH_3)_3^+$ |

Strong acid cation exchangers include a sulfonic acid functional group that retains it anionic form—and thus its capacity for ion-exchange—in strongly acidic solutions. The functional groups for a weak acid cation exchanger, on the other hand, are fully protonated at pH levels less then 4 and lose their exchange capacity. The strong base anion exchangers include a quaternary amine, which retains a positive charge even in strongly basic solutions. Weak base anion exchangers remain protonated only at pH levels that are moderately basic. Under more basic conditions a weak base anion exchanger loses a proton and its exchange capacity.

The ion-exchange reaction of a monovalent cation, $M^+$, exchange site is

$$-SO_3^-H^+(s) + M^+(aq) \rightleftharpoons -SO_3^-M^+(s) + H^+(aq)$$

The equilibrium constant for this ion-exchange reaction, which we call the selectivity coefficient, *K*, is

$$K = \frac{\{-SO_3^-M^+\}\,[H^+]}{\{-SO_3^-H^+\}\,[M^+]} \tag{28.6.1}$$

where we use curly brackets, { }, to indicate a surface concentration instead of a solution concentration.

> We don't usually think about a solid's concentration. There is a good reason for this. In most cases, a solid's concentration is a constant. If you break a piece of chalk into two parts, for example, the mass and the volume of each piece retains the same proportional relationship as in the original piece of chalk. When we consider an ion binding to a reactive site on the solid's surface, however, the fraction of sites that are bound, and thus the concentration of bound sites, can take on any value between 0 and some maximum value that is proportional to the density of reactive sites.

Rearranging Equation 28.6.1 shows us that the distribution ratio, *D*, for the exchange reaction

$$D = \frac{\text{amount of } M^+ \text{ in the stationary phase}}{\text{amount of } M^+ \text{ in the mobile phase}}$$

$$D = \frac{\{-SO_3^-M^+\}}{[M^+]} = K \times \frac{\{-SO_3^-H^+\}}{[H^+]} \tag{28.6.2}$$

is a function of the concentration of $H^+$ and, therefore, the pH of the mobile phase.

An ion-exchange resin's selectivity is somewhat dependent on whether it includes strong or weak exchange sites and on the extent of cross-linking. The latter is particularly important as it controls the resin's permeability, and, therefore, the accessibility of exchange sites. An approximate order of selectivity for a typical strong acid cation exchange resin, in order of decreasing *D*, is

$$Al^{3+} > Ba^{2+} > Pb^{2+} > Ca^{2+} > Ni^{2+} > Cd^{2+} > Cu^{2+} > Co^{2+} > Zn^{2+} > Mg^{2+} > Ag^+ > K^+ > NH_4^+ > Na^+ > H^+ > Li^+$$

Note that highly charged cations bind more strongly than cations of lower charge, and that for cations of similar charge, those with a smaller hydrated radius, or that are more polarizable, bind more strongly. For a strong base anion exchanger the general elution order is

$$SO_4^{2-} > I^- > HSO_4^- > NO_3^- > Br^- > NO_2^- > Cl^- > HCO_3^- > CH3COO^- > OH^- > F^-$$

Anions of higher charge and of smaller hydrated radius bind more strongly than anions with a lower charge and a larger hydrated radius.

The mobile phase in IEC usually is an aqueous buffer, the pH and ionic composition of which determines a solute's retention time. Gradient elutions are possible in which the mobile phase's ionic strength or pH is changed with time. For example, an IEC separation of cations might use a dilute solution of HCl as the mobile phase. Increasing the concentration of HCl speeds the elution rate for more strongly retained cations because the higher concentration of $H^+$ allows it to compete more successfully for the ion-exchange sites.

> From Equation 28.6.2, a cation's distribution ratio, *D*, becomes smaller when the concentration of $H^+$ in the mobile phase increases.

An ion-exchange resin is incorporated into an HPLC column either as 5–11 μm porous polymer beads or by coating the resin on porous silica particles. Columns typically are 250 mm in length with internal diameters ranging from 2–5 mm.

Measuring the conductivity of the mobile phase as it elutes from the column serves as a universal detector for cationic and anionic analytes. Because the mobile phase contains a high concentration of ions—a mobile phase of dilute HCl, for example, contains significant concentrations of $H^+$ and $Cl^-$ ions—we need a method for detecting the analytes in the presence of a significant background conductivity.

To minimize the mobile phase's contribution to conductivity, an ion-suppressor column is placed between the analytical column and the detector. This column selectively removes mobile phase ions without removing solute ions. For example, in cation-

exchange chromatography using a dilute solution of HCl as the mobile phase, the suppressor column contains a strong base anion-exchange resin. The exchange reaction

$$\mathrm{H^+}(aq) + \mathrm{Cl^-}(aq) + \mathrm{Resin^+OH^-}(s) \rightleftharpoons \mathrm{Resin^+\,Cl^-}(s) + \mathrm{H_2O}(l)$$

replaces the mobile phase ions $H^+$ and $Cl^–$ with $H_2O$. A similar process is used in anion-exchange chromatography where the suppressor column contains a cation-exchange resin. If the mobile phase is a solution of $Na_2CO_3$, the exchange reaction

$$2\mathrm{Na^+}(aq) + \mathrm{CO_3^{2-}}(aq) + 2\,\mathrm{Resin^-\,H^+}(s) \rightleftharpoons 2\,\mathrm{Resin^-\,Na^+}(s) + \mathrm{H_2CO_3}(aq)$$

replaces a strong electrolyte, $Na_2CO_3$, with a weak electrolyte, $H_2CO_3$.

Ion-suppression is necessary when the mobile phase contains a high concentration of ions. Single-column ion chromatography, in which an ion-suppressor column is not needed, is possible if the concentration of ions in the mobile phase is small. Typically the stationary phase is a resin with a low capacity for ion-exchange and the mobile phase is a very dilute solution of methane sulfonic acid for cationic analytes, or potassium benzoate or potassium hydrogen phthalate for anionic analytes. Because the background conductivity is sufficiently small, it is possible to monitor a change in conductivity as the analytes elute from the column.

A UV/Vis absorbance detector can be used if the analytes absorb ultraviolet or visible radiation. Alternatively, we can detect indirectly analytes that do not absorb in the UV/Vis if the mobile phase contains a UV/Vis absorbing species. In this case, when a solute band passes through the detector, a decrease in absorbance is measured at the detector.

Ion-exchange chromatography is an important technique for the analysis of anions and cations in water. For example, an ion-exchange chromatographic analysis for the anions $F^–$, $Cl^–$, $Br^–$, $NO_2^–$, $NO_3^–$, $PO_4^{3–}$, and $SO_4^{2–}$ takes approximately 15 minutes (Figure 28.6.2 ). A complete analysis of the same set of anions by a combination of potentiometry and spectrophotometry requires 1–2 days. Ion-exchange chromatography also is used for the analysis of proteins, amino acids, sugars, nucleotides, pharmaceuticals, consumer products, and clinical samples.

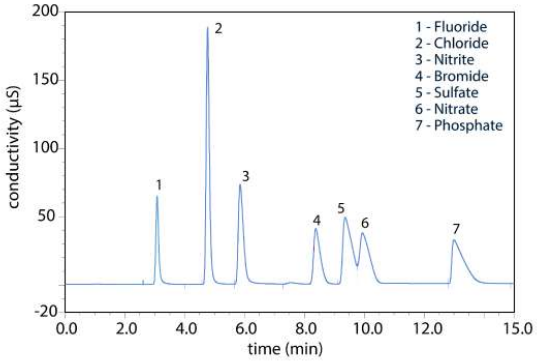



Figure 28.6.2 . Ion-exchange chromatographic analysis of water from Big Walnut Creek in Putnam County, Indiana. Data provided by Jeanette Pope, Department of Geosciences, DePauw University.

This page titled 28.6: Ion-Exchange Chromatography is shared under a CC BY-NC-SA 4.0 license and was authored, remixed, and/or curated by David Harvey.

# 28.7: Size-Exclusion Chromatography

We have considered two classes of micron-sized stationary phases in this chapter: silica particles and cross-linked polymer resin beads. Both materials are porous, with pore sizes ranging from approximately 5–400 nm for silica particles, and from 5 nm to 100 μm for divinylbenzene cross-linked polystyrene resins. In size-exclusion chromatography—which also is known by the terms molecular-exclusion or gel permeation chromatography—the separation of solutes depends upon their ability to enter into the pores of the stationary phase. Smaller solutes spend proportionally more time within the pores and take longer to elute from the column.

A stationary phase's size selectivity extends over a finite range. All solutes significantly smaller than the pores move through the column's entire volume and elute simultaneously, with a retention volume, $V_r$, of

$$V_r = V_i + V_o \tag{28.7.1}$$

where $V_i$ is the volume of mobile phase occupying the stationary phase's pore space and $V_o$ is volume of mobile phase in the remainder of the column. The largest solute for which Equation 28.7.1 holds is the column's inclusion limit, or permeation limit. Those solutes too large to enter the pores elute simultaneously with an retention volume of

$$V_r = V_o \tag{28.7.2}$$

Equation 28.7.2 defines the column's exclusion limit.

For a solute whose size is between the inclusion limit and the exclusion limit, the amount of time it spends in the stationary phase's pores is proportional to its size. The retention volume for these solutes is

$$V_r = DV_i + V_o \tag{28.7.3}$$

where $D$ is the solute's distribution ratio, which ranges from 0 at the exclusion limit to 1 at the inclusion limit. Equation 28.7.3 assumes that size-exclusion is the only interaction between the solute and the stationary phase that affects the separation. For this reason, stationary phases using silica particles are deactivated as described earlier, and polymer resins are synthesized without exchange sites.

Size-exclusion chromatography provides a rapid means for separating larger molecules, including polymers and biomolecules. A stationary phase for proteins that consists of particles with 30 nm pores has an inclusion limit of 7500 g/mol and an exclusion limit of $1.2 \times 10^6$ g/mol. Mixtures of proteins that span a wider range of molecular weights are separated by joining together in series several columns with different inclusion and exclusion limits.

Another important application of size-exclusion chromatography is the estimation of a solute's molecular weight (MW). Calibration curves are prepared using a series of standards of known molecular weight and measuring each standard's retention volume. As shown in Figure 28.7.1 , a plot of log(MW) versus $V_r$ is roughly linear between the exclusion limit and the inclusion limit. Because a solute's retention volume is influenced by both its size and its shape, a reasonably accurate estimation of molecular weight is possible only if the standards are chosen carefully to minimize the effect of shape.

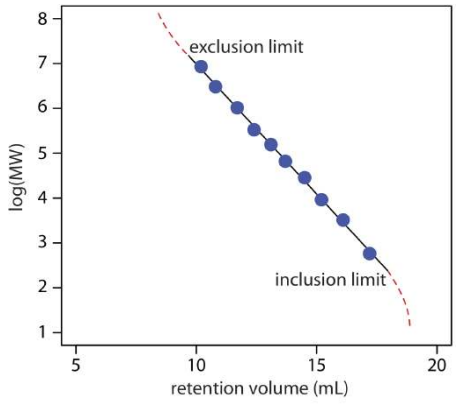



Figure 28.7.1 . Calibration curve for the determination of molecular weight by size-exclusion chromatography. The data shown here are adapted from Rouessac, F.; Rouessac, A. *Chemical Analysis: Modern Instrumentation Methods and Techniques*, Wiley: Chichester, England, 2004, p 141.

Size-exclusion chromatography is carried out using conventional HPLC instrumentation, replacing the HPLC column with an appropriate size-exclusion column. A UV/Vis detector is the most common means for obtaining the chromatogram.

---

This page titled 28.7: Size-Exclusion Chromatography is shared under a CC BY-NC-SA 4.0 license and was authored, remixed, and/or curated by David Harvey.

# CHAPTER OVERVIEW

## 29: Supercritical Fluid Chromatography

Although there are many analytical applications of gas chromatography and liquid chromatography, they can not separate and analyze all types of samples. Capillary column GC separates complex mixtures with excellent resolution and short analysis times. Its application is limited, however, to volatile analytes or to analytes made volatile by a suitable derivatization reaction. Liquid chromatography separates a wider range of solutes than GC, but the most common detectors—UV, fluorescence, and electrochemical— have poorer detection limits and smaller linear ranges than GC detectors, and are not as universal in their selectivity. For some applications, supercritical fluids provide an attractive solution to these limitations.

29.1: Properties of Supercritical Fluids
29.2: Supercritical Fluid Chromatography

---

This page titled 29: Supercritical Fluid Chromatography is shared under a CC BY-NC-SA 4.0 license and was authored, remixed, and/or curated by David Harvey.

# 29.1: Properties of Supercritical Fluids

As shown in Figure 29.1.1 , a supercritical fluid is a species held at a temperature and a pressure that exceeds its critical point. Under these conditions the species is neither a gas nor a liquid. Instead, it is a supercritical fluid.

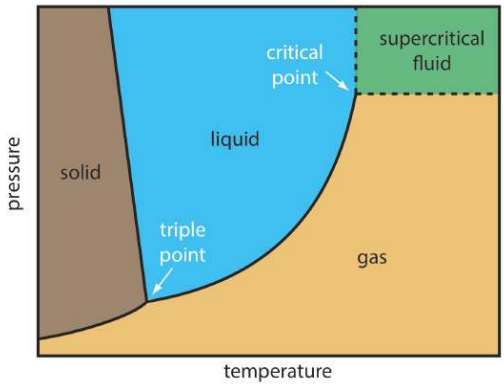



Figure 29.1.1 . Phase diagram showing the combinations of temperature and pressure for which a compound is in its solid state, its liquid state, and its gas state. For pressures and temperatures above the critical point, the compound is a supercritical fluid with properties intermediate between a gas and a liquid.

Some properties of a supercritical fluid, as shown in Table 29.1.1 , are similar to a gas; other properties, however, are similar to a liquid. The viscosity of a supercritical fluid, for example, is similar to a gas, which means we can move a supercritical fluid through a capillary column or a packed column without the need for high pressures. The density of a supercritical fluid, on the other hand, is much closer to that of a liquid, which explains why supercritical fluids are good solvents.

Table 29.1.1 . Typical Properties of Gases, Liquids, and Supercritical Fluids

| phase | density ($g/cm^3$) | viscosity ($g\ cm^{-1}\ s^{-1}$) | diffusion coefficient ($cm^2\ s^{-1}$) |
|---|---|---|---|
| gas | $\approx 10^{-3}$ | $\approx 10^{-4}$ | $\approx 0.1$ |
| supercritical fluid | $\approx 0.1 - 1$ | $\approx 10^{-4} - 10^{-3}$ | $\approx 10^{-4} - 10^{-3}$ |
| liquid | $\approx 1$ | $\approx 10^{-2}$ | $\approx 10^{-3}$ |

The most commonly used supercritical fluid is $CO_2$. Its low critical temperature of 31.1°C and its low critical pressure of 72.9 atm are relatively easy to achieve and maintain. Although supercritical $CO_2$ is a good solvent for nonpolar organics, it is less useful for polar solutes. The addition of an organic modifier, such as methanol, improves the mobile phase's elution strength. Other common mobile phases and their critical temperatures and pressures are listed in Table 29.1.2 .

Table 29.1.2 . Critical Points for Selected Supercritical Fluids

| compound | critical temperature (°C) | critical pressure (atm) |
|---|---|---|
| carbon dioxide | 31.3 | 72.9 |
| ethane | 32.4 | 48.3 |
| nitrous oxide | 36.5 | 71.4 |
| ammonia | 132.3 | 111.3 |
| diethyl ether | 193.6 | 36.3 |
| isopropanol | 235.3 | 47.0 |
| methanol | 240.5 | 78.9 |
| ethanol | 243.4 | 63.0 |
| water | 374.4 | 226.8 |

This page titled 29.1: Properties of Supercritical Fluids is shared under a CC BY-NC-SA 4.0 license and was authored, remixed, and/or curated by David Harvey.

# 29.2: Supercritical Fluid Chromatography

The instrumentation for supercritical fluid chromatography essentially is the same as that for a standard HPLC. The only important additions are a heated oven for the column and a pressure restrictor downstream from the column to maintain the critical pressure. Gradient elutions are accomplished by changing the applied pressure over time. The resulting change in the mobile phase's density affects its solvent strength. Detection is accomplished using standard GC detectors or HPLC detectors. Analysis time and resolution, although not as good as in GC, usually are better than in conventional HPLC. Supercritical fluid chromatography has many applications in the analysis of polymers, fossil fuels, waxes, drugs, and food products.

This page titled 29.2: Supercritical Fluid Chromatography is shared under a CC BY-NC-SA 4.0 license and was authored, remixed, and/or curated by David Harvey.

# CHAPTER OVERVIEW

## 30: Capillary Electrophoresis and Capillary Electrochromatography

Electrophoresis is a class of separation techniques in which we separate analytes by their ability to move through a conductive medium—usually an aqueous buffer—in response to an applied electric field. In the absence of other effects, cations migrate toward the electric field's negatively charged cathode. Cations with larger charge-to-size ratios—which favors ions of greater charge and of smaller size—migrate at a faster rate than larger cations with smaller charges. Anions migrate toward the positively charged anode and neutral species do not experience the electrical field and remain stationary. In this chapter we focus on the most important of these techniques, capillary electrophoresis and a few related variants.


30.1: An Overview of Electrophoresis

30.2: Capillary Electrophoresis

30.3: Applications of Capillary Electrophoresis


---


This page titled 30: Capillary Electrophoresis and Capillary Electrochromatography is shared under a CC BY-NC-SA 4.0 license and was authored, remixed, and/or curated by David Harvey.

# 30.1: An Overview of Electrophoresis

Electrophoresis is a class of separation techniques in which we separate analytes by their ability to move through a conductive medium—usually an aqueous buffer—in response to an applied electric field. In the absence of other effects, cations migrate toward the electric field's negatively charged cathode. Cations with larger charge-to-size ratios—which favors ions of greater charge and of smaller size—migrate at a faster rate than larger cations with smaller charges. Anions migrate toward the positively charged anode and neutral species do not experience the electrical field and remain stationary.

> As we will see shortly, under normal conditions even neutral species and anions migrate toward the cathode.

There are several forms of electrophoresis. In slab gel electrophoresis the conducting buffer is retained within a porous gel of agarose or polyacrylamide. Slabs are formed by pouring the gel between two glass plates separated by spacers. Typical thicknesses are 0.25–1 mm. Gel electrophoresis is an important technique in biochemistry where it frequently is used to separate DNA fragments and proteins. Although it is a powerful tool for the qualitative analysis of complex mixtures, it is less useful for quantitative work.

In capillary electrophoresis the conducting buffer is retained within a capillary tube with an inner diameter that typically is 25–75 μm. The sample is injected into one end of the capillary tube, and as it migrates through the capillary the sample's components separate and elute from the column at different times. The resulting electropherogram looks similar to a GC or an HPLC chromatogram, and provides both qualitative and quantitative information.

This page titled 30.1: An Overview of Electrophoresis is shared under a CC BY-NC-SA 4.0 license and was authored, remixed, and/or curated by David Harvey.

# 30.2: Capillary Electrophoresis

## Theory of Electrophoresis

In capillary electrophoresis we inject the sample into a buffered solution retained within a capillary tube. When an electric field is applied across the capillary tube, the sample's components migrate as the result of two types of actions: electrophoretic mobility and electroosmotic mobility. Electrophoretic mobility is the solute's response to the applied electrical field in which cations move toward the negatively charged cathode, anions move toward the positively charged anode, and neutral species remain stationary. The other contribution to a solute's migration is electroosmotic flow, which occurs when the buffer moves through the capillary in response to the applied electrical field. Under normal conditions the buffer moves toward the cathode, sweeping most solutes, including the anions and neutral species, toward the negatively charged cathode.

### Electrophoretic Mobility

The velocity with which a solute moves in response to the applied electric field is called its electrophoretic velocity, $\nu_{ep}$; it is defined as

$$\nu_{ep} = \mu_{ep} E \tag{30.2.1}$$

where $\mu_{ep}$ is the solute's electrophoretic mobility, and $E$ is the magnitude of the applied electrical field. A solute's electrophoretic mobility is defined as

$$\mu_{ep} = \frac{q}{6\pi\eta r} \tag{30.2.2}$$

where $q$ is the solute's charge, $\eta$ is the buffer's viscosity, and $r$ is the solute's radius. Using Equation 30.2.1 and Equation 30.2.2 we can make several important conclusions about a solute's electrophoretic velocity. Electrophoretic mobility and, therefore, electrophoretic velocity, increases for more highly charged solutes and for solutes of smaller size. Because $q$ is positive for a cation and negative for an anion, these species migrate in opposite directions. A neutral species, for which $q$ is zero, has an electrophoretic velocity of zero.

### Electroosmotic Mobility

When an electric field is applied to a capillary filled with an aqueous buffer we expect the buffer's ions to migrate in response to their electrophoretic mobility. Because the solvent, $H_2O$, is neutral we might reasonably expect it to remain stationary. What we observe under normal conditions, however, is that the buffer moves toward the cathode. This phenomenon is called the electroosmotic flow.

Electroosmotic flow occurs because the walls of the capillary tubing carry a charge. The surface of a silica capillary contains large numbers of silanol groups (–SiOH). At a pH level greater than approximately 2 or 3, the silanol groups ionize to form negatively charged silanate ions ($–SiO^-$). Cations from the buffer are attracted to the silanate ions. As shown in Figure 30.2.1 , some of these cations bind tightly to the silanate ions, forming a fixed layer. Because the cations in the fixed layer only partially neutralize the negative charge on the capillary walls, the solution adjacent to the fixed layer—which is called the diffuse layer—contains more cations than anions. Together these two layers are known as the double layer. Cations in the diffuse layer migrate toward the cathode. Because these cations are solvated, the solution also is pulled along, producing the electroosmotic flow.

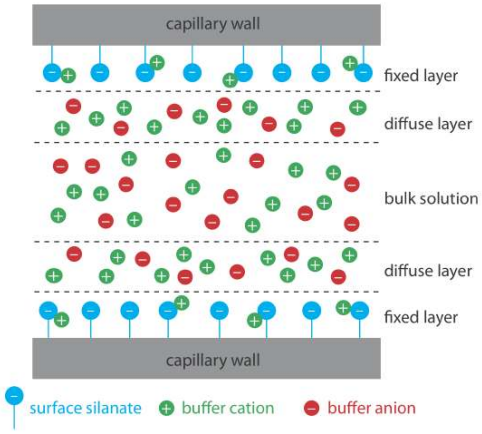



Figure 30.2.1 . Schematic diagram showing the origin of the double layer within a capillary tube. Although the net charge within the capillary is zero, the distribution of charge is not. The walls of the capillary have an excess of negative charge, which decreases across the fixed layer and the diffuse layer, reaching a value of zero in bulk solution.

> The anions in the diffuse layer, which also are solvated, try to move toward the anode. Because there are more cations than anions, however, the cations win out and the electroosmotic flow moves in the direction of the cathode.

The rate at which the buffer moves through the capillary, what we call its electroosmotic flow velocity, $\nu_{eof}$, is a function of the applied electric field, $E$, and the buffer's electroosmotic mobility, $\mu_{eof}$.

$$\nu_{eof} = \mu_{eof} E \tag{30.2.3}$$

Electroosmotic mobility is defined as

$$\mu_{eof} = \frac{\varepsilon \zeta}{4\pi\eta} \tag{30.2.4}$$

where $\epsilon$ is the buffer dielectric constant, $\zeta$ is the zeta potential, and $\eta$ is the buffer's viscosity.

The zeta potential—the potential of the diffuse layer at a finite distance from the capillary wall—plays an important role in determining the electroosmotic flow velocity. Two factors determine the zeta potential's value. First, the zeta potential is directly proportional to the charge on the capillary walls, with a greater density of silanate ions corresponding to a larger zeta potential. Below a pH of 2 there are few silanate ions and the zeta potential and the electroosmotic flow velocity approach zero. As the pH increases, both the zeta potential and the electroosmotic flow velocity increase. Second, the zeta potential is directly proportional to the thickness of the double layer. Increasing the buffer's ionic strength provides a higher concentration of cations, which decreases the thickness of the double layer and decreases the electroosmotic flow.

> The definition of zeta potential given here admittedly is a bit fuzzy. For a more detailed explanation see Delgado, A. V.; González-Caballero, F.; Hunter, R. J.; Koopal, L. K.; Lyklema, J. "Measurement and Interpretation of Electrokinetic Phenomena," *Pure. Appl. Chem.* **2005**, *77*, 1753–1805. Although this is a very technical report, Sections 1.3–1.5 provide a good introduction to the difficulty of defining the zeta potential and of measuring its value.

The electroosmotic flow profile is very different from that of a fluid moving under forced pressure. Figure 30.2.2 compares the electroosmotic flow profile with the hydrodynamic flow profile in gas chromatography and liquid chromatography. The uniform, flat profile for electroosmosis helps minimize band broadening in capillary electrophoresis, improving separation efficiency.

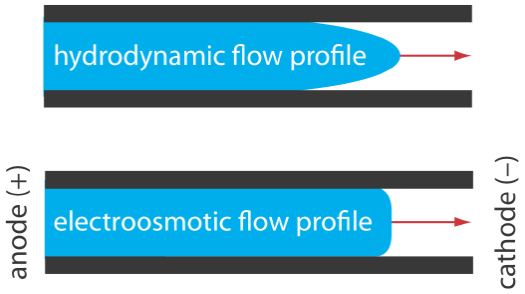



Figure 30.2.2 . Comparison of hydrodynamic flow and electroosmotic flow. The nearly uniform electroosmotic flow profile means that the electroosmotic flow velocity is nearly constant across the capillary.

## Total Mobility

A solute's total velocity, $\nu_{tot}$, as it moves through the capillary is the sum of its electrophoretic velocity and the electroosmotic flow velocity.

$$\nu_{tot} = \nu_{ep} + \nu_{eof}$$

As shown in Figure 30.2.3 , under normal conditions the following general relationships hold true.

$$(\nu_{tot})_{cations} > \nu_{eof}$$

$$(\nu_{tot})_{neutrals} = \nu_{eof}$$

$$(\nu_{tot})_{anions} < \nu_{eof}$$

Cations elute first in an order that corresponds to their electrophoretic mobilities, with small, highly charged cations eluting before larger cations of lower charge. Neutral species elute as a single band with an elution rate equal to the electroosmotic flow velocity. Finally, anions are the last components to elute, with smaller, highly charged anions having the longest elution time.

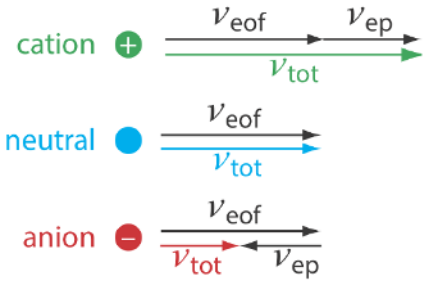



Figure 30.2.3 . Visual explanation for the general elution order in capillary electrophoresis. Each species has the same electroosmotic flow, $\nu_{eof}$. Cations elute first because they have a positive electrophoretic velocity, $\nu_{ep}$. Anions elute last because their negative electrophoretic velocity partially offsets the electroosmotic flow velocity. Neutrals elute with a velocity equal to the electroosmotic flow.

## Migration Time

Another way to express a solute's velocity is to divide the distance it travels by the elapsed time

$$\nu_{tot} = \frac{l}{t_m} \tag{30.2.5}$$

where $l$ is the distance between the point of injection and the detector, and $t_{\mathrm{m}}$ is the solute's migration time. To understand the experimental variables that affect migration time, we begin by noting that

$$\nu_{tot} = \mu_{tot} E = (\mu_{ep} + \mu_{eof}) E \tag{30.2.6}$$

Combining Equation 30.2.5 and Equation 30.2.6 and solving for $t_{\mathrm{m}}$ leaves us with

$$t_{\mathrm{m}} = \frac{l}{(\mu_{ep} + \mu_{eof})\, E} \tag{30.2.7}$$

The magnitude of the electrical field is

$$E = \frac{V}{L} \tag{30.2.8}$$

where $V$ is the applied potential and $L$ is the length of the capillary tube. Finally, substituting Equation 30.2.8 into Equation 30.2.7 leaves us with the following equation for a solute's migration time.

$$t_{\mathrm{m}} = \frac{lL}{(\mu_{ep} + \mu_{eof})\,V} \tag{30.2.9}$$

To decrease a solute's migration time—which shortens the analysis time—we can apply a higher voltage or use a shorter capillary tube. We can also shorten the migration time by increasing the electroosmotic flow, although this decreases resolution.

### Efficiency

As we learned in Chapter 26.3, the efficiency of a separation is given by the number of theoretical plates, $N$. In capillary electrophoresis the number of theoretic plates is

$$N = \frac{l^2}{2Dt_m} = \frac{(\mu_{ep} + \mu_{eof})\,El}{2DL} \tag{30.2.10}$$

where $D$ is the solute's diffusion coefficient. From Equation 30.2.10, the efficiency of a capillary electrophoretic separation increases with higher voltages. Increasing the electroosmotic flow velocity improves efficiency, but at the expense of resolution. Two additional observations deserve comment. First, solutes with larger electrophoretic mobilities—in the same direction as the electroosmotic flow—have greater efficiencies; thus, smaller, more highly charged cations are not only the first solutes to elute, but do so with greater efficiency. Second, efficiency in capillary electrophoresis is independent of the capillary's length. Theoretical plate counts of approximately 100 000–200 000 are not unusual.

> It is possible to design an electrophoretic experiment so that anions elute before cations—more about this later—in which smaller, more highly charged anions elute with greater efficiencies.

### Selectivity

In chromatography we defined the selectivity between two solutes as the ratio of their retention factors. In capillary electrophoresis the analogous expression for selectivity is

$$\alpha = \frac{\mu_{ep,1}}{\mu_{ep,2}}$$

where $\mu_{ep,1}$ and $\mu_{ep,2}$ are the electrophoretic mobilities for the two solutes, chosen such that $\alpha \geq 1$. We can often improve selectivity by adjusting the pH of the buffer solution. For example, $\mathrm{NH_4^+}$ is a weak acid with a p$K_a$ of 9.75. At a pH of 9.75 the concentrations of $\mathrm{NH_4^+}$ and $\mathrm{NH_3}$ are equal. Decreasing the pH below 9.75 increases its electrophoretic mobility because a greater fraction of the solute is present as the cation $\mathrm{NH_4^+}$. On the other hand, raising the pH above 9.75 increases the proportion of neutral $\mathrm{NH_3}$, decreasing its electrophoretic mobility.

### Resolution

The resolution between two solutes is

$$R = \frac{0.177(\mu_{ep,2} - \mu_{ep,1})\sqrt{V}}{\sqrt{D(\mu_{avg} + \mu_{eof})}} \tag{30.2.11}$$

where $\mu_{avg}$ is the average electrophoretic mobility for the two solutes. Increasing the applied voltage and decreasing the electroosmotic flow velocity improves resolution. The latter effect is particularly important. Although increasing electroosmotic flow improves analysis time and efficiency, it decreases resolution.

## Instrumentation

The basic instrumentation for capillary electrophoresis is shown in Figure 30.2.4 and includes a power supply for applying the electric field, anode and cathode compartments that contain reservoirs of the buffer solution, a sample vial that contains the sample, the capillary tube, and a detector. Each part of the instrument receives further consideration in this section.

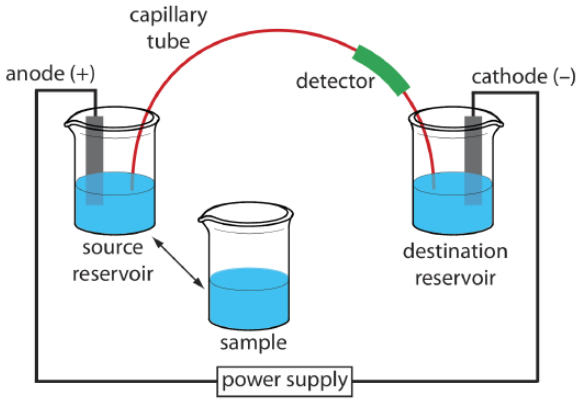



Figure 30.2.4 . Schematic diagram of the basic instrumentation for capillary electrophoresis. The sample and the source reservoir are switched when making injections.

### Capillary Tubes

Figure 30.2.5 shows a cross-section of a typical capillary tube. Most capillary tubes are made from fused silica coated with a 15–35 μm layer of polyimide to give it mechanical strength. The inner diameter is typically 25–75 μm, which is smaller than the internal diameter of a capillary GC column, with an outer diameter of 200–375 μm.

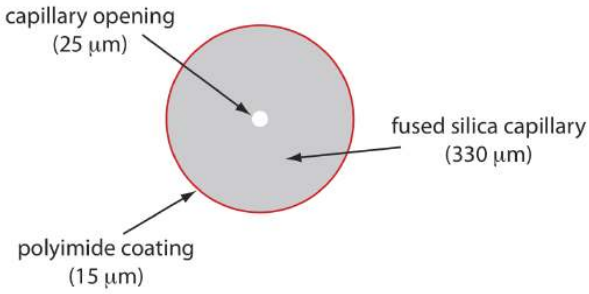



Figure 30.2.5 . Cross section of a capillary column for capillary electrophoresis. The dimensions shown here are typical and are scaled proportionally in this figure.

The capillary column's narrow opening and the thickness of its walls are important. When an electric field is applied to the buffer solution, current flows through the capillary. This current leads to the release of heat, which we call Joule heating. The amount of heat released is proportional to the capillary's radius and to the magnitude of the electrical field. Joule heating is a problem because it changes the buffer's viscosity, with the solution at the center of the capillary being less viscous than that near the capillary walls. Because a solute's electrophoretic mobility depends on its viscosity (see Equation 30.2.2), solute species in the center of the capillary migrate at a faster rate than those near the capillary walls. The result is an additional source of band broadening that degrades the separation. Capillaries with smaller inner diameters generate less Joule heating, and capillaries with larger outer diameters are more effective at dissipating the heat. Placing the capillary tube inside a thermostated jacket is another method for minimizing the effect of Joule heating; in this case a smaller outer diameter allows for a more rapid dissipation of thermal energy.

### Injecting the Sample

There are two common methods for injecting a sample into a capillary electrophoresis column: hydrodynamic injection and electrokinetic injection. In both methods the capillary tube is filled with the buffer solution. One end of the capillary tube is placed in the destination reservoir and the other end is placed in the sample vial.

***Hydrodynamic injection*** uses pressure to force a small portion of sample into the capillary tubing. A difference in pressure is applied across the capillary either by pressurizing the sample vial or by applying a vacuum to the destination reservoir. The volume of sample injected, in liters, is given by the following equation

$$V_{\text{inj}} = \frac{\Delta P d^4 \pi t}{128 \eta L} \times 10^3 \tag{30.2.12}$$

where $\Delta P$ is the difference in pressure across the capillary in pascals, $d$ is the capillary's inner diameter in meters, $t$ is the amount of time the pressure is applied in seconds, $\eta$ is the buffer's viscosity in kg $m^{-1}$ $s^{-1}$, and $L$ is the length of the capillary tubing in meters. The factor of $10^3$ changes the units from cubic meters to liters.

For a hydrodynamic injection we move the capillary from the source reservoir to the sample. The anode remains in the source reservoir. A hydrodynamic injection also is possible if we raise the sample vial above the destination reservoir and briefly insert the filled capillary.

## Example 30.2.1

In a hydrodynamic injection we apply a pressure difference of $2.5 \times 10^3$ Pa (a $\Delta P \approx 0.02$ atm) for 2 s to a 75-cm long capillary tube with an internal diameter of 50 μm. Assuming the buffer's viscosity is $10^{-3}$ kg $m^{-1}$ $s^{-1}$, what volume and length of sample did we inject?

### Solution

Making appropriate substitutions into Equation 30.2.12 gives the sample's volume as

$$V_{inj} = \frac{\left(2.5 \times 10^3 \text{ kg m}^{-1} \text{ s}^{-2}\right)\left(50 \times 10^{-6} \text{ m}\right)^4 (3.14)(2 \text{ s})}{(128)\left(0.001 \text{ kg m}^{-1} \text{ s}^{-1}\right)(0.75 \text{ m})} \times 10^3 \text{L/m}^3$$

$$V_{inj} = 1 \times 10^{-9} \text{ L} = 1 \text{ nL}$$

Because the interior of the capillary is cylindrical, the length of the sample, $l$, is easy to calculate using the equation for the volume of a cylinder; thus

$$l = \frac{V_{\text{inj}}}{\pi r^2} = \frac{\left(1 \times 10^{-9} \text{ L}\right)\left(10^{-3} \text{ m}^3/\text{L}\right)}{(3.14)\left(25 \times 10^{-6} \text{ m}\right)^2} = 5 \times 10^{-4} \text{ m} = 0.5 \text{ mm}$$

## Exercise 30.2.1

Suppose you need to limit your injection to less than 0.20% of the capillary's length. Using the information from Example 30.2.1 , what is the maximum injection time for a hydrodynamic injection?

**Answer**

The capillary is 75 cm long, which means that 0.20% of that sample's maximum length is 0.15 cm. To convert this to the maximum volume of sample we use the equation for the volume of a cylinder.

$$V_{inj} = l\pi r^2 = (0.15 \text{ cm})(3.14)\left(25 \times 10^{-4} \text{ cm}\right)^2 = 2.94 \times 10^{-6} \text{ cm}^3$$

Given that 1 $cm^3$ is equivalent to 1 mL, the maximum volume is $2.94 \times 10^{-6}$ mL or $2.94 \times 10^{-9}$ L. To find the maximum injection time, we first solve Equation 30.2.12 for $t$

$$t = \frac{128 V_{inj} \eta L}{P d^4 \pi} \times 10^{-3} \text{ m}^3/\text{L}$$

and then make appropriate substitutions.

$$t = \frac{(128)\left(2.94 \times 10^{-9}\ \text{L}\right)\left(0.001\ \text{kg}\ \ \text{m}^{-1}\ \text{s}^{-1}\right)(0.75\ \text{m})}{\left(2.5 \times 10^{3}\ \text{kg}\ \text{m}^{-1}\ \text{s}^{-2}\right)\left(50 \times 10^{-6}\ \text{m}\right)^{4}(3.14)} \times \frac{10^{-3}\ \text{m}^{3}}{\text{L}} = 5.8\ \text{s}$$

The maximum injection time, therefore, is 5.8 s.

In an electrokinetic injection we place both the capillary and the anode into the sample and briefly apply an potential. The volume of injected sample is the product of the capillary's cross sectional area and the length of the capillary occupied by the sample. In turn, this length is the product of the solute's velocity (see Equation 30.2.6) and time; thus

$$V_{inj} = \pi r^2 L = \pi r^2 (\mu_{ep} + \mu_{eof}) E' t \tag{30.2.13}$$

where $r$ is the capillary's radius, $L$ is the capillary's length, and $E'$ is the effective electric field in the sample. An important consequence of Equation 30.2.13 is that an electrokinetic injection is biased toward solutes with larger electrophoretic mobilities. If two solutes have equal concentrations in a sample, we inject a larger volume—and thus more moles—of the solute with the larger $\mu_{ep}$.

The electric field in the sample is different that the electric field in the rest of the capillary because the sample and the buffer have different ionic compositions. In general, the sample's ionic strength is smaller, which makes its conductivity smaller. The effective electric field is

$$E' = E \times \frac{\chi_{\text{buffer}}}{\chi_{\text{sample}}}$$

where $\chi_{\text{buffer}}$ and $\chi_{sample}$ are the conductivities of the buffer and the sample, respectively.

When an analyte's concentration is too small to detect reliably, it maybe possible to inject it in a manner that increases its concentration. This method of injection is called stacking. Stacking is accomplished by placing the sample in a solution whose ionic strength is significantly less than that of the buffer in the capillary tube. Because the sample plug has a lower concentration of buffer ions, the effective field strength across the sample plug, $E'$, is larger than that in the rest of the capillary.

We know from Equation 30.2.1 that electrophoretic velocity is directly proportional to the electrical field. As a result, the cations in the sample plug migrate toward the cathode with a greater velocity, and the anions migrate more slowly—neutral species are unaffected and move with the electroosmotic flow. When the ions reach their respective boundaries between the sample plug and the buffer, the electrical field decreases and the electrophoretic velocity of the cations decreases and that for the anions increases. As shown in Figure 30.2.6 , the result is a stacking of cations and anions into separate, smaller sampling zones. Over time, the buffer within the capillary becomes more homogeneous and the separation proceeds without additional stacking.

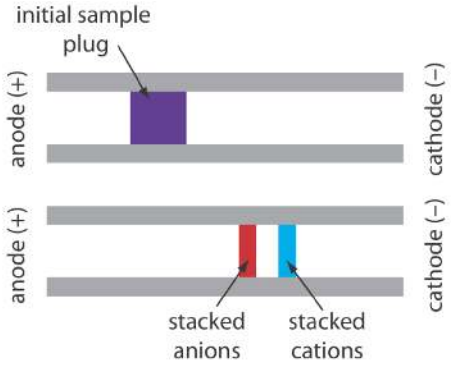



Figure 30.2.6 . The stacking of cations and anions. The top diagram shows the initial sample plug and the bottom diagram shows how the cations and anions are concentrated at opposite sides of the sample plug.

## Applying the Electrical Field

Migration in electrophoresis occurs in response to an applied electric field. The ability to apply a large electric field is important because higher voltages lead to shorter analysis times (Equation 30.2.9), more efficient separations (Equation 30.2.10), and better

resolution (Equation 30.2.11). Because narrow bored capillary tubes dissipate Joule heating so efficiently, voltages of up to 40 kV are possible.

> Because of the high voltages, be sure to follow your instrument's safety guidelines.

## Detectors

Most of the detectors used in HPLC also find use in capillary electrophoresis. Among the more common detectors are those based on the absorption of UV/Vis radiation, fluorescence, conductivity, amperometry, and mass spectrometry. Whenever possible, detection is done "on-column" before the solutes elute from the capillary tube and additional band broadening occurs.

UV/Vis detectors are among the most popular. Because absorbance is directly proportional to path length, the capillary tubing's small diameter leads to signals that are smaller than those obtained in HPLC. Several approaches have been used to increase the pathlength, including a Z-shaped sample cell and multiple reflections (see Figure 30.2.7 ). Detection limits are about $10^{-7}$ M.

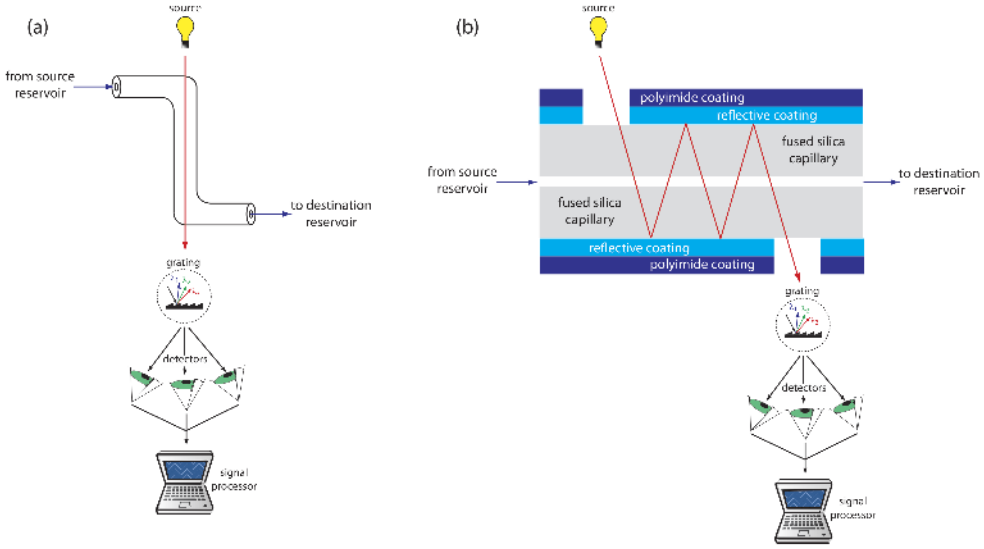



Figure 30.2.7 . Two approaches to on-column detection in capillary electrophoresis using a UV/Vis diode array spectrometer: (a) Z-shaped bend in capillary, and (b) multiple reflections.

Better detection limits are obtained using fluorescence, particularly when using a laser as an excitation source. When using fluorescence detection a small portion of the capillary's protective coating is removed and the laser beam is focused on the inner portion of the capillary tubing. Emission is measured at an angle of $90^{o}$ to the laser. Because the laser provides an intense source of radiation that can be focused to a narrow spot, detection limits are as low as $10^{-16}$ M.

Solutes that do not absorb UV/Vis radiation or that do not undergo fluorescence can be detected by other detectors. Table 30.2.1 provides a list of detectors for capillary electrophoresis along with some of their important characteristics.

Table 30.2.1 . Characteristics of Detectors for Capillary Electrophoresis

| detector | selectivity (universal or analyte must ...) | detection limited (moles injected) | detection limit (molarity) | on-column detection? |
|---|---|---|---|---|
| UV/Vis absorbance | have a UV/Vis chromophore | $10^{-13} - 10^{-16}$ | $10^{-5} - 10^{-7}$ | yes |
| indirect absorbancd | universal | $10^{-12} - 10^{-15}$ | $10^{-4} - 10^{-6}$ | yes |
| fluoresence | have a favorable quantum yield | $10^{-13} - 10^{-17}$ | $10^{-7} - 10^{-9}$ | yes |
| laser fluorescence | have a favorable quantum yield | $10^{-18} - 10^{-20}$ | $10^{-13} - 10^{-16}$ | yes |
| mass spectrometer | universal (total ion) selective (single ion) | $10^{-16} - 10^{-17}$ | $10^{-8} - 10^{-10}$ | no |
| amperometry | undergo oxidation or reduction | $10^{-18} - 10^{-19}$ | $10^{-7} - 10^{-10}$ | no |
| conductivity | universal | $10^{-15} - 10^{-16}$ | $10^{-7} - 10^{-9}$ | no |
| radiometric | be radioactive | $10^{-17} - 10^{-19}$ | $10^{-10} - 10^{-12}$ | yes |

This page titled 30.2: Capillary Electrophoresis is shared under a CC BY-NC-SA 4.0 license and was authored, remixed, and/or curated by David Harvey.

# 30.3: Applications of Capillary Electrophoresis

There are several different forms of capillary electrophoresis, each of which has its particular advantages. Several of these methods are described briefly in this section.

## Capillary Zone Electrophoresis (CZE)

The simplest form of capillary electrophoresis is capillary zone electrophoresis. In CZE we fill the capillary tube with a buffer and, after loading the sample, place the ends of the capillary tube in reservoirs that contain additional buffer. Usually the end of the capillary containing the sample is the anode and solutes migrate toward the cathode at a velocity determined by their respective electrophoretic mobilities and the electroosmotic flow. Cations elute first, with smaller, more highly charged cations eluting before larger cations with smaller charges. Neutral species elute as a single band. Anions are the last species to elute, with smaller, more negatively charged anions being the last to elute.

We can reverse the direction of electroosmotic flow by adding an alkylammonium salt to the buffer solution. As shown in Figure 30.3.1 , the positively charged end of the alkyl ammonium ions bind to the negatively charged silanate ions on the capillary's walls. The tail of the alkyl ammonium ion is hydrophobic and associates with the tail of another alkyl ammonium ion. The result is a layer of positive charges that attract anions in the buffer. The migration of these solvated anions toward the anode reverses the electroosmotic flow's direction. The order of elution is exactly opposite that observed under normal conditions.

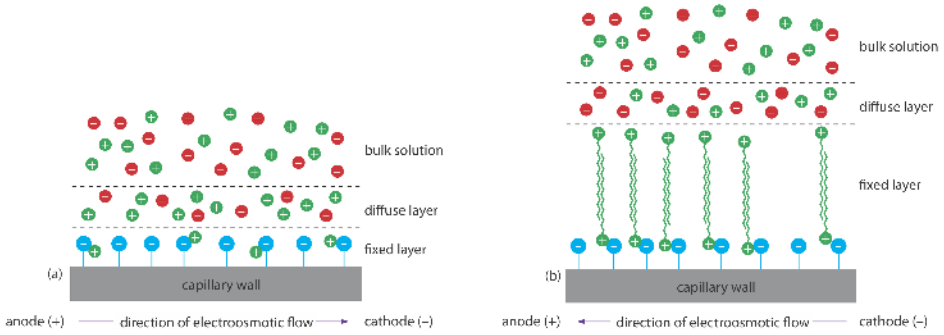



Figure 30.3.1 . Two modes of capillary zone electrophoresis showing (a) normal migration with electroosmotic flow toward the cathode and (b) reversed migration in which the electroosmotic flow is toward the anode.

Coating the capillary's walls with a nonionic reagent eliminates the electroosmotic flow. In this form of CZE the cations migrate from the anode to the cathode. Anions elute into the source reservoir and neutral species remain stationary.

Capillary zone electrophoresis provides effective separations of charged species, including inorganic anions and cations, organic acids and amines, and large biomolecules such as proteins. For example, CZE was used to separate a mixture of 36 inorganic and organic ions in less than three minutes [Jones, W. R.; Jandik, P. *J. Chromatog.* **1992**, *608*, 385–393]. A mixture of neutral species, of course, can not be resolved.

## Micellar Electrokinetic Capillary Chromatography (MEKC)

One limitation to CZE is its inability to separate neutral species. Micellar electrokinetic capillary chromatography overcomes this limitation by adding a surfactant, such as sodium dodecylsulfate (Figure 30.3.2 a) to the buffer solution. Sodium dodecylsulfate, or SDS, consists of a long-chain hydrophobic tail and a negatively charged ionic functional group at its head. When the concentration of SDS is sufficiently large a micelle forms. A micelle consists of a spherical agglomeration of 40–100 surfactant molecules in which the hydrocarbon tails point inward and the negatively charged heads point outward (Figure 30.3.2 b).

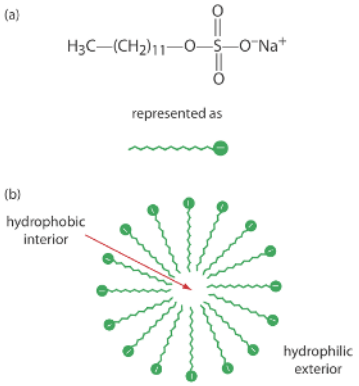



Figure 30.3.2 . (a) Structure of sodium dodecylsulfate and (b) cross section through a micelle showing its hydrophobic interior and its hydrophilic exterior.

Because micelles have a negative charge, they migrate toward the cathode with a velocity less than the electroosmotic flow velocity. Neutral species partition themselves between the micelles and the buffer solution in a manner similar to the partitioning of solutes between the two liquid phases in HPLC. Because there is a partitioning between two phases, we include the descriptive term chromatography in the techniques name. Note that in MEKC both phases are mobile.

The elution order for neutral species in MEKC depends on the extent to which each species partitions into the micelles. Hydrophilic neutrals are insoluble in the micelle's hydrophobic inner environment and elute as a single band, as they would in CZE. Neutral solutes that are extremely hy- drophobic are completely soluble in the micelle, eluting with the micelles as a single band. Those neutral species that exist in a partition equilibrium between the buffer and the micelles elute between the completely hydro- philic and completely hydrophobic neutral species. Those neutral species that favor the buffer elute before those favoring the micelles. Micellar electrokinetic chromatography is used to separate a wide variety of samples, including mixtures of pharmaceutical compounds, vitamins, and explosives.

## Capillary Gel Electrophoresis (CGE)

In capillary gel electrophoresis the capillary tubing is filled with a polymeric gel. Because the gel is porous, a solute migrates through the gel with a velocity determined both by its electrophoretic mobility and by its size. The ability to effect a separation using size is helpful when the solutes have similar electrophoretic mobilities. For example, fragments of DNA of varying length have similar charge-to-size ratios, making their separation by CZE difficult. Because the DNA fragments are of different size, a CGE separation is possible.

The capillary used for CGE usually is treated to eliminate electroosmotic flow to prevent the gel from extruding from the capillary tubing. Samples are injected electrokinetically because the gel provides too much resistance for hydrodynamic sampling. The primary application of CGE is the separation of large biomolecules, including DNA fragments, proteins, and oligonucleotides.

## Capillary Electrochromatography (CEC)

Another approach to separating neutral species is capillary electrochromatography. In CEC the capillary tubing is packed with 1.5–3 µm particles coated with a bonded stationary phase. Neutral species separate based on their ability to partition between the stationary phase and the buffer, which is moving as a result of the electroosmotic flow; Figure 30.3.3 provides a representative example for the separation of a mixture of hydrocarbons. A CEC separation is similar to the analogous HPLC separation, but without the need for high pressure pumps. Efficiency in CEC is better than in HPLC, and analysis times are shorter.

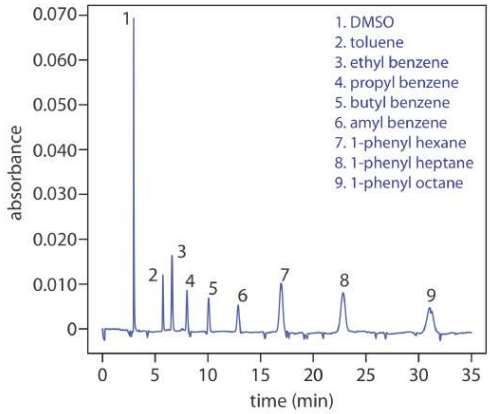



Figure 30.3.3 . Capillary electrochromatographic separation of a mixture of hydrocarbons in DMSO. The column contains a porous polymer of butyl methacrylate and lauryl acrylate (25%:75% mol:mol) with butane dioldacrylate as a crosslinker. Data provided by Zoe LaPier and Michelle Bushey, Department of Chemistry, Trinity University.

---

This page titled 30.3: Applications of Capillary Electrophoresis is shared under a CC BY-NC-SA 4.0 license and was authored, remixed, and/or curated by David Harvey.

# CHAPTER OVERVIEW

## 31: Thermal Methods

A thermal method of analysis is a technique in which measure a physical property of a material as we subject it to a change in temperature. In this chapter we consider three examples of thermal methods: thermogravimetry, differential thermal analysis, and differential scanning calorimetry.


31.1: Thermogravimetry

31.2: Differential Thermal Analysis and Differential Scanning Calorimetry


---


This page titled 31: Thermal Methods is shared under a CC BY-NC-SA 4.0 license and was authored, remixed, and/or curated by David Harvey.

# 31.1: Thermogravimetry

One method for determining the products of a thermal decomposition is to monitor the sample's mass as a function of temperature, a process called a thermogravimetric analysis (TGA) or thermogravimetry. Figure 31.1.1 shows a typical thermogram in which each change in mass—each "step" in the thermogram—represents the loss of a volatile product. As the following example illustrates, we can use a thermogram to identify a compound's decomposition reactions.

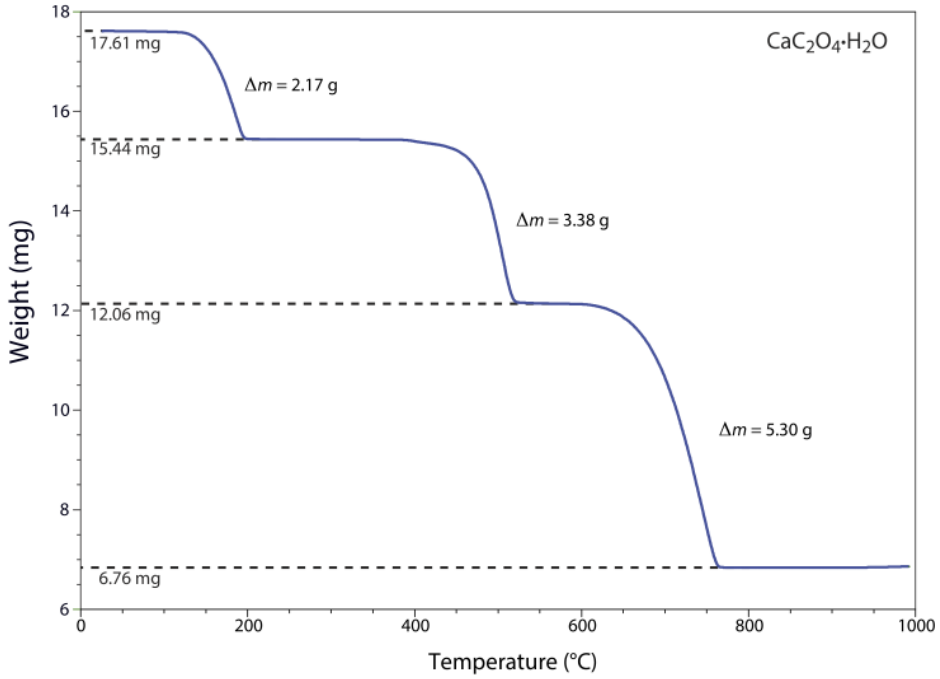



Figure 31.1.1 . Thermogram for $CaC_2O_4{\cdot}H_2O$ obtained by heating a sample from room temperature to 1000°C at a rate of 20°C/min. Each change in mass results from the loss of a volatile product. The sample's initial mass and its mass after each loss are shown by the dotted lines. See Example 31.1.1 for information on interpreting this thermogram.

## Example 31.1.1

The thermogram in Figure 31.1.1 shows the mass of a sample of calcium oxalate monohydrate, $CaC_2O_4{\cdot}H_2O$, as a function of temperature. The original sample of 17.61 mg was heated from room temperature to 1000°C at a rate of 20°C per minute. For each step in the thermogram, identify the volatilization product and the solid residue that remains.

### Solution

From 100–250°C the sample loses 17.61 mg – 15.44 mg, or 2.17 mg, which is

$$\frac{2.17 \text{ mg}}{17.61 \text{ mg}} \times 100 = 12.3\%$$

of the sample's original mass. In terms of $CaC_2O_4{\cdot}H_2O$, this corresponds to a decrease in the molar mass of

$$0.123 \times 146.11 \text{ g/mol} = 18.0 \text{ g/mol}$$

The product's molar mass and the temperature range for the decomposition, suggest that this is a loss of $H_2O(g)$, leaving a residue of $CaC_2O_4$.

The loss of 3.38 mg from 350–550°C is a 19.2% decrease in the sample's original mass, or a decrease in the molar mass of

$$0.192 \times 146.11 \text{ g/mol} = 28.1 \text{ g/mol}$$

which is consistent with the loss of $CO(g)$ and a residue of $CaCO_3$.

Finally, the loss of 5.30 mg from 600-800°C is a 30.1% decrease in the sample's original mass, or a decrease in molar mass of

$$0.301 \times 146.11 \text{ g/mol} = 44.0 \text{ g/mol}$$

This loss in molar mass is consistent with the release of $CO_2$*(g)*, leaving a final residue of CaO. The three decomposition reactions are

$$\begin{aligned} CaC_2O_4 \cdot H_2O(s) &\rightarrow CaC_2O_4(s) + 2H_2O(l) \\ CaC_2O_4(s) &\rightarrow CaCO_3(s) + CO(g) \\ CaCO_3(s) &\rightarrow CaO(s) + CO_2(g) \end{aligned}$$

Identifying the products of a thermal decomposition provides information that we can use to develop an analytical procedure. For example, the thermogram in Figure 31.1.1 shows that we must heat a precipitate of $CaC_2O_4$•$H_2O$ to a temperature between 250 and 400°C if we wish to isolate and weigh $CaC_2O_4$. Alternatively, heating the sample to 1000°C allows us to isolate and weigh CaO.

## ? Exercise 31.1.1

Under the same conditions as Figure 31.1.1 , the thermogram for a 22.16 mg sample of $MgC_2O_4$•$H_2O$ shows two steps: a loss of 3.06 mg from 100–250°C and a loss of 12.24 mg from 350–550°C. For each step, identify the volatilization product and the solid residue that remains. Using your results from this exercise and the results from Example 31.1.1 , explain how you can use thermogravimetry to analyze a mixture that contains $CaC_2O_4$•$H_2O$ and $MgC_2O_4$•$H_2O$. You may assume that other components in the sample are inert and thermally stable below 1000°C.

**Answer**

From 100–250°C the sample loses 13.8% of its mass, or a loss of

$$0.138 \times 130.34 \text{ g/mol} = 18.0 \text{ g/mol}$$

which is consistent with the loss of $H_2O$*(g)* and a residue of $MgC_2O_4$.

From 350–550°C the sample loses 55.23% of its original mass, or a loss of

$$0.5523 \times 130.34 \text{ g/mol} = 71.99 \text{ g/mol}$$

This weight loss is consistent with the simultaneous loss of CO*(g)* and $CO_2$*(g)*, leaving a residue of MgO.

We can analyze the mixture by heating a portion of the sample to 300°C, 600°C, and 1000°C, recording the mass at each temperature. The loss of mass between 600°C and 1000°C, $\Delta m_2$, is due to the loss of $CO_2$*(g)* from the decomposition of $CaCO_3$ to CaO, and is proportional to the mass of $CaC_2O_4$•$H_2O$ in the sample.

$$\text{g } CaC_2O_4 \cdot H_2O = \Delta m_2 \times \frac{1 \text{ mol } CO_2}{44.01 \text{ g } CO_2} \times \frac{146.11 \text{ g } CaC_2O_4 \cdot H_2O}{\text{mol } CO_2}$$

The change in mass between 300°C and 600°C, $\Delta m_1$, is due to the loss of CO*(g)* from $CaC_2O_4$•$H_2O$ and the loss of CO*(g)* and $CO_2$*(g)* from $MgC_2O_4$•$H_2O$. Because we already know the amount of $CaC_2O_4$•$H_2O$ in the sample, we can calculate its contribution to $\Delta m_1$.

$$(\Delta m_1)_{Ca} = \text{g } CaC_2O_4 \cdot H_2O = \Delta m_2 \times \frac{1 \text{ mol CO}}{146.11 \text{ g } CaC_2O_4 \cdot H_2O} \times \frac{28.01 \text{ g CO}}{\text{mol CO}}$$

The change in mass between 300°C and 600°C due to the decomposition of $MgC_2O_4$•$H_2O$

$$(m_1)_{Mg} = \Delta m_1 - (\Delta m_1)_{Ca}$$

provides the mass of $MgC_2O_4$•$H_2O$ in the sample.

$$\text{g } MgC_2O_4 \cdot H_2O = (\Delta m_1)_{Mg} \times \frac{1 \text{ mol } (CO + CO_2)}{130.35 \text{ g } MgC_2O_4 \cdot H_2O} \times \frac{78.02 \text{ g } (CO + CO_2)}{\text{mol } (CO + CO_2)}$$

## Instrumentation

In a thermogravimetric analysis, the sample is placed on a small balance pan attached to one arm of an electromagnetic balance (Figure 31.1.2 ). The sample is lowered into an electric furnace and the furnace's temperature is increased at a fixed rate of a few degrees per minute while monitoring continuously the sample's weight. The instrument usually includes a gas line for purging the volatile decomposition products out of the furnace, and a heat exchanger to dissipate the heat emitted by the furnace.

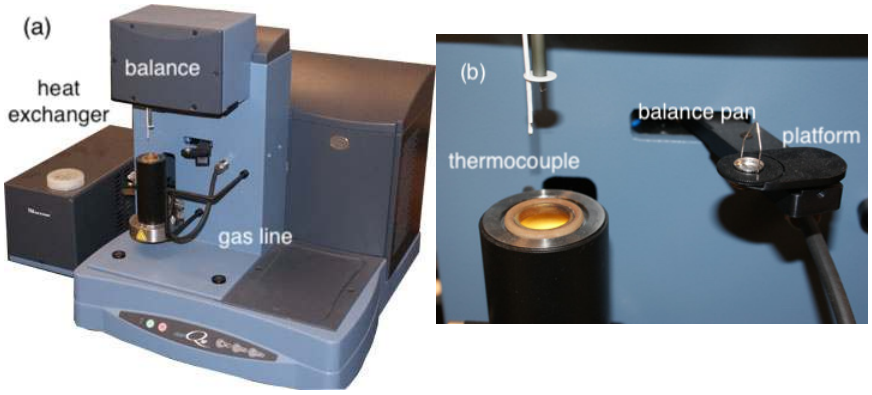



Figure 31.1.2 . (a) Instrumentation for conducting a thermogravimetric analysis. The balance sits on the top of the instrument with the sample suspended below. A gas line supplies an inert gas that sweeps the volatile decomposition products out of the furnace. The heat exchanger dissipates the heat from the furnace to a reservoir of water. (b) Close-up showing the balance pan, which sits on a moving platform, the thermocouple for monitoring temperature, a hook for lowering the sample pan into the furnace, and the opening to the furnace. After placing a small portion of the sample on the balance pan, the platform rotates over the furnace and transfers the balance pan to a hook that is suspended from the balance. Once the balance pan is in place, the platform rotates back to its initial position. The balance pan and the thermocouple are then lowered into the furnace.

## Applications

Perhaps the most important application gravimetry is exploring a compound's thermal stability, as illustrated in Figure 31.1.1 and Exercise 31.1.1 for calcium oxalate hydrate. TGA is particularly useful for studying the thermal stability of polymers.

---

This page titled 31.1: Thermogravimetry is shared under a CC BY-NC-SA 4.0 license and was authored, remixed, and/or curated by David Harvey.

# 31.2: Differential Thermal Analysis and Differential Scanning Calorimetry

Differential thermal analysis (DTA) and differential scanning calorimetry (DSC) are similar methods in which the response of a sample and a reference to a change in temperature. In DTA the temperature applied to the sample is increased linearly and the difference between the temperature of the reference material, $T_{ref}$, and the temperature of the sample, $T_{samp}$, is recorded as function of the sample's temperature

$$\Delta T = T_{ref} - T_{samp}$$

When the sample undergoes an exothermic process, such as a crystallization or a chemical reaction, the temperature of the sample increases more than does the temperature of the reference, resulting in a more negative value for $\Delta T$. For an endothermic process, such as melting of a crystalline material or the loss of waters of hydration, the sample's temperature lags behind that for the reference materials, resulting in a more positive value for $\Delta T$. Figure 31.2.1 shows the general shape of DTA curve with negative peaks signaling an endothermic process and positive peaks signaling an exothermic process. Changes in $\Delta T$ that are not peaks, but shifts in the baseline—as seen at the far left of the curve in Figure 31.2.1—are the result of a simple phase transition for which $\Delta H = 0$.In DSC the temperature applied to the sample is increased linearly and the relative amount of heat needed to maintain the sample and the reference at the same temperature is measured. For an endothermic process, more heat flows into the sample and for an exothermic process, less heat flows into the sample. The result is a DSC curve that looks similar to that for DTA (see Figure 31.2.1).

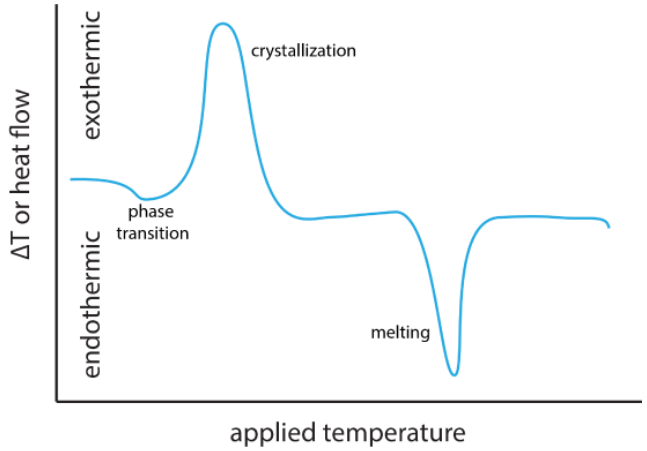



Figure 31.2.1: Illustration showing typical experimental curves for a differential thermal analysis (DTA) or a differential scanning calorimetry analysis (DSC) for a polymeric material. For a DTA analysis, the difference in temperature, $\Delta T$, is measured and for a DSC analysis, the flow of heat is measured. The three responses seen here are, from left-to-right, a phase transition, an exothermic crystallization, and an endothermic melting.

## Instrumentation

Figure 31.2.2 shows the basic components of a heat-flux differential scanning calorimeter. The sample and the reference materials are sealed within small aluminum pans and placed on separate platforms within the sample chamber. The two platforms are connected by a metal disk that provides a low resistance path for moving heat between the sample and the reference to maintain a $\Delta T$ of zero between the two. Another instrumental design for differential scanning calorimetry, which is called power compensation DSC, places the sample and the reference in separated heating chambers and measures the difference in the power applied to the two chambers needed to maintain a $\Delta T$ of zero.

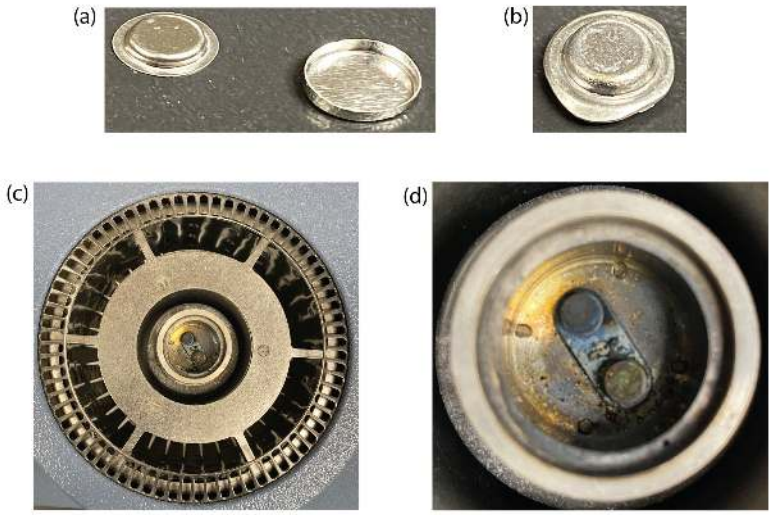



Figure 31.2.2: Components of instrument for a differential scanning calorimetry (DSC) experiment. The sample and the reference material are (a) placed in small aluminum pans, each with a separate lid, and then (b) the lid and the pan are crimped together. The sample chamber in (c) allows for applying heat to the sample and the reference, which are place in the center of the chamber. A close-up of the sample chamber (d) shows two—well-used—platforms on which the sample and the reference are placed. An insulated cap sits on top of the sample chamber. Although the basic set-up shown here is for DSC, it is similar to the instrumentation for a differential thermal analysis. For a sense of scale, the pan in (a) is approximately 5 mm across and has a depth of 1 mm, and the platforms in (d) also are 5 mm across.

## Applications

Integrating a peak in DSC or DTA to determine its its area, $A$, gives a signal that is proportional to $\Delta H$

$$\Delta H = K \times A$$

where the calibration constant, $k$, is determined using an established reference material. Both DSC and DTA find applications in the study of polymers, liquid crystals, and pharmaceutical compounds.

This page titled 31.2: Differential Thermal Analysis and Differential Scanning Calorimetry is shared under a CC BY-NC-SA 4.0 license and was authored, remixed, and/or curated by David Harvey.

# CHAPTER OVERVIEW

## 32: Radiochemical Methods

Radiochemical methods of analysis take advantage of the instability of some elemental isotopes, which decay through the release of alpha particles, beta particles, gamma rays, and/or X-rays, often provide for a selective analysis for one analyte in a complex mixture of other species without the need for a prior separation. In this chapter we review the basics of radioactive decay and its direct application to samples, and two additional methods of importance: neutron activation and isotope dilution.


32.1: Radioactive Isotopes

32.2: Instrumentation

32.3: Neutron Activation Methods

32.4: Isotope Dilution Methods


Thumbnail: Visual representation of alpha decay. (Public Domain; Inductiveload via Wikipedia)


This page titled 32: Radiochemical Methods is shared under a CC BY-NC-SA 4.0 license and was authored, remixed, and/or curated by David Harvey.

# 32.1: Radioactive Isotopes

Atoms that have the same number of protons but a different number of neutrons are isotopes. To identify an isotope we use the notation ${}^{A}_{Z}E$, where $E$ is the element's atomic symbol, $Z$ is the element's atomic number, and $A$ is the element's atomic mass number. Although an element's different isotopes have the same chemical properties, their nuclear properties are not identical. The most important difference between isotopes is their stability. The nuclear configuration of a stable isotope remains constant with time. Unstable isotopes, however, disintegrate spontaneously, emitting radioactive decay particles as they transform into a more stable form.

> An element's atomic number, $Z$, is equal to the number of protons and its atomic mass, $A$, is equal to the sum of the number of protons and neutrons. We represent an isotope of carbon-13 as ${}^{13}_{6}\mathrm{C}$ because carbon has six protons and seven neutrons. Sometimes we omit $Z$ from this notation—identifying the element and the atomic number is repetitive because all isotopes of carbon have six protons and any atom that has six protons is an isotope of carbon. Thus, ${}^{13}\mathrm{C}$ and C–13 are alternative notations for this isotope of carbon.

## Types of Radioactive Decay Particles

The most important types of radioactive particles are alpha particles, beta particles, gamma rays, and X-rays. An alpha particle, $\alpha$, is equivalent to a helium nucleus, ${}^{4}_{2}\mathrm{He}$. When an atom emits an alpha particle, the product is a new atom whose atomic number and atomic mass number are, respectively, 2 and 4 less than its unstable parent. The decay of uranium to thorium is one example of alpha emission.

$$ {}^{238}_{92}\mathrm{U} \longrightarrow {}^{234}_{90}\mathrm{Th} + \alpha $$

A beta particle, $\beta$, comes in one of two forms. A negatron, ${}^{0}_{-1}\beta$, is produced when a neutron changes into a proton, increasing the atomic number by one, as shown here for lead.

$$ {}^{214}_{82}\mathrm{Pb} \longrightarrow {}^{214}_{83}\mathrm{Bi} + {}^{0}_{-1}\beta $$

The conversion of a proton to a neutron results in the emission of a positron, ${}^{0}_{1}\beta$.

$$ {}^{30}_{15}\mathrm{P} \longrightarrow {}^{30}_{14}\mathrm{Si} + {}^{0}_{1}\beta $$

> A negatron, which is the more common type of beta particle, is equivalent to an electron.

The emission of an alpha or a beta particle often produces an isotope in an unstable, high energy state. This excess energy is released as a gamma ray, $\gamma$, or as an X-ray. Gamma ray and X-ray emission may also occur without the release of an alpha particle or a beta particle.

## Radioactive Decay Rates

A radioactive isotope's rate of decay, or activity, follows first-order kinetics

$$ A - t = -\frac{dN}{dt} = \lambda N \tag{32.1.1} $$

where $A$ is the isotope's activity, $N$ is the number of radioactive atoms present in the sample at time $t$, and $\lambda$ is the isotope's decay constant. Activity is expressed as the number of disintegrations per unit time.

As with any first-order process, we can rewrite Equation 32.1.1 in an integrated form.

$$ N_t = N_0 e^{-\lambda t} \tag{32.1.2} $$

Substituting Equation 32.1.2 into Equation 32.1.1 gives

$$ A_t = \lambda N_0 e^{-\lambda t} = A_0 e^{-\lambda t} \tag{32.1.3} $$

If we measure a sample's activity at time $t$ we can determine the sample's initial activity, $A_0$, or the number of radioactive atoms originally present in the sample, $N_0$.

An important characteristic property of a radioactive isotope is its half-life, $t_{1/2}$, which is the amount of time required for half of the radioactive atoms to disintegrate. For first-order kinetics the half-life is

$$t_{1/2} = \frac{0.693}{\lambda} \tag{32.1.4}$$

Because the half-life is independent of the number of radioactive atoms, it remains constant throughout the decay process. For example, if 50% of the radioactive atoms remain after one half-life, then 25% remain after two half-lives, and 12.5% remain after three half-lives.

> Suppose we begin with an $N_0$ of 1200 atoms During the first half-life, 600 atoms disintegrate and 600 remain. During the second half-life, 300 of the 600 remaining atoms disintegrate, leaving 300 atoms or 25% of the original 1200 atoms. Of the 300 remaining atoms, only 150 remain after the third half-life, or 12.5% of the original 1200 atoms.

Kinetic information about a radioactive isotope usually is given in terms of its half-life because it provides a more intuitive sense of the isotope's stability. Knowing, for example, that the decay constant for $^{90}_{38}\text{Sr}$ is 0.0247 $\text{yr}^{-1}$ does not give an immediate sense of how fast it disintegrates. On the other hand, knowing that its half-life is 28.1 yr makes it clear that the concentration of $^{90}_{38}\text{Sr}$ in a sample remains essentially constant over a short period of time.

## Counting Statistics

Radioactivity does not follow a normal distribution because the possible outcomes are not continuous; that is, a sample can emit 1 or 2 or 3 alpha particles (or some other integer value) in a fixed intervale, but it cannot emit 2.59 alpha particles during that same interval. A Poisson distribution provides the probability that a given number of events will occur in a fixed interval in time or space if the event has a known average rate and if each new event is independent of the preceding event. Mathematically a Poisson distribution is defined by the equation

$$P(X, \lambda) = \frac{e^{-\lambda}\lambda^X}{X!}$$

where $P(X, \lambda)$ is the probability that an event happens $X$ times given the event's average rate, $\lambda$. The Poisson distribution has a theoretical mean, $\mu$, and a theoretical variance, $\sigma^2$, that are each equal to $\lambda$.

> **Note**
>
> For a more detailed discussion of the distribution of data, including normal distributions and Poisson distributions, see Appendix 1.

The accuracy and precision of radiochemical methods generally are within the range of 1–5%. We can improve the precision—which is limited by the random nature of radioactive decay—by counting the emission of radioactive particles for as long a time as is practical. If the number of counts, $M$, is reasonably large ($M \geq 100$), and the counting period is significantly less than the isotope's half-life, then the percent relative standard deviation for the activity, $(\sigma_A)_{rel}$, is approximately

$$(\sigma_A)_{\text{rel}} = \frac{1}{\sqrt{M}} \times 100$$

For example, if we determine the activity by counting 10 000 radioactive particles, then the relative standard deviation is 1%. A radiochemical method's sensitivity is inversely proportional to $(\sigma_A)_{rel}$, which means we can improve the sensitivity by counting more particles.

## Analysis of Radioactive Analytes

The concentration of a long-lived radioactive isotope remains essentially constant during the period of analysis. As shown in Example 32.1.1 , we can use the sample's activity to calculate the number of radioactive particles in the sample.

## Example 32.1.1

The activity in a 10.00-mL sample of wastewater that contains $^{90}_{38}\text{Sr}$ is $9.07 \times 10^6$ disintegrations/s. What is the molar concentration of $^{90}_{38}\text{Sr}$ in the sample? The half-life for $^{90}_{38}\text{Sr}$ is 28.1 yr.

### Solution

Solving Equation 32.1.4 for $\lambda$, substituting into Equation 32.1.1, and solving for $N$ gives

$$N = \frac{A \times t_{1/2}}{0.693}$$

Before we can determine the number of atoms of $^{90}_{38}\text{Sr}$ in the sample we must express its activity and its half-life using the same units. Converting the half-life to seconds gives $t_{1/2}$ as $8.86 \times 10^8$ s; thus, there are

$$\frac{\left(9.07 \times 10^6 \text{ disintegrations/s }\right)\left(8.86 \times 10^8 \text{ s}\right)}{0.693} = 1.16 \times 10^{16} \text{ atoms} ^{90}_{38}\text{Sr}$$

The concentration of $^{90}_{38}\text{Sr}$ in the sample is

$$\frac{1.16 \times 10^{16} \text{ atoms } ^{90}_{38}\text{Sr}}{\left(6.022 \times 10^{23} \text{ atoms/mol }\right)(0.01000\text{L})} = 1.93 \times 10^{-6} \text{ M } ^{90}_{38}\text{Sr}$$

The direct analysis of a short-lived radioactive isotope using the method outlined in Example 32.1.1 is less useful because it provides only a transient measure of the isotope's concentration. Instead, we can measure its activity after an elapsed time, $t$, and use Equation 32.1.3 to calculate $N_0$.

One example of a characterization application is the determination of a sample's age based on the decay of a radioactive isotope naturally present in the sample. The most common example is carbon-14 dating, which is used to determine the age of natural organic materials. As cosmic rays pass through the upper atmosphere, some $^{14}_{7}\text{N}$ atoms in the atmosphere capture high energy neutrons, converting them into $^{14}_{6}\text{C}$. The $^{14}_{6}\text{C}$ then migrates into the lower atmosphere where it oxidizes to form C-14 labeled $CO_2$. Animals and plants subsequently incorporate this labeled $CO_2$ into their tissues. Because this is a steady-state process, all plants and animals have the same ratio of $^{14}_{6}\text{C}$ to $^{12}_{6}\text{C}$ in their tissues. When an organism dies, the radioactive decay of $^{14}_{6}\text{C}$ to $^{14}_{7}\text{N}$ by $^{0}_{-1}\beta$ emission ($t$ = 5730 years) leads to predictable reduction in the $^{14}_{6}\text{C}$ to $^{12}_{6}\text{C}$ ratio. We can use the change in this ratio to date samples that are as much as 30000 years old, although the precision of the analysis is best when the sample's age is less than 7000 years. The accuracy of carbon-14 dating depends upon our assumption that the natural $^{14}_{6}\text{C}$ to $^{12}_{6}\text{C}$ ratio in the atmosphere is constant over time. Some variation in the ratio has occurred as the result of the increased consumption of fossil fuels and the production of $^{14}_{6}\text{C}$ during the testing of nuclear weapons. A calibration curve prepared using samples of known age—examples of samples include tree rings, deep ocean sediments, coral samples, and cave deposits—limits this source of uncertainty.

There is no need to prepare a calibration curve for each analysis. Instead, there is a universal calibration curve known as IntCal. The calibration curve from 2013, IntCal13, is described in the following paper: Reimer, P. J., et. al. "IntCal13 and Marine 13 Radiocarbon Age Calibration Curve 0–50,000 Years Cal BP," *Radiocarbon* **2013**, *55*, 1869–1887. This calibration spans 50 000 years before the present (BP).

## Example 32.1.2

To determine the age of a fabric sample, the relative ratio of $^{14}_{6}\text{C}$ to $^{12}_{6}\text{C}$ was measured yielding a result of 80.9% of that found in modern fibers. How old is the fabric?

### Solution

Equation 32.1.3 and Equation 32.1.4 provide us with a method to convert a change in the ratio of $^{14}_{6}\text{C}$ to $^{12}_{6}\text{C}$ to the fabric's age. Letting $A_0$ be the ratio of $^{14}_{6}\text{C}$ to $^{12}_{6}\text{C}$ in modern fibers, we assign it a value of 1.00. The ratio of $^{14}_{6}\text{C}$ to $^{12}_{6}\text{C}$ in the sample, $A$, is 0.809. Solving gives

$$t = \ln \frac{A_0}{A} \times \frac{t_{1/2}}{0.693} = \ln \frac{1.00}{0.809} \times \frac{5730 \text{ yr}}{0.693} = 1750 \text{ yr}$$

Other isotopes can be used to determine a sample's age. The age of rocks, for example, has been determined from the ratio of the number of $^{238}_{92}\text{U}$ to the number of stable $^{206}_{82}\text{Pb}$ atoms produced by radioactive decay. For rocks that do not contain uranium, dating is accomplished by comparing the ratio of radioactive $^{40}_{19}\text{K}$ to the stable $^{40}_{18}\text{Ar}$. Another example is the dating of sediments collected from lakes by measuring the amount of $^{210}_{82}\text{Pb}$ that is present.

---

This page titled 32.1: Radioactive Isotopes is shared under a CC BY-NC-SA 4.0 license and was authored, remixed, and/or curated by David Harvey.

# 32.2: Instrumentation

Alpha particles, beta particles, gamma rays, and X-rays are measured by using the particle's energy to produce an amplified pulse of electrical current in a detector. These pulses are counted to give the rate of disintegration. There are three common types of detectors: gas-filled detectors, scintillation counters, and semiconductor detectors. A gas-filled detector consists of a tube that contains an inert gas, such as Ar. When a radioactive particle enters the tube it ionizes the inert gas, producing an $Ar^+/e^-$ ion-pair. Movement of the electron toward the anode and of the $Ar^+$ toward the cathode generates a measurable electrical current. A Geiger counter is one example of a gas-filled detector. A scintillation counter uses a fluorescent material to convert radioactive particles into easy to measure photons. For example, one solid-state scintillation counter consists of a NaI crystal that contains 0.2% TlI, which produces several thousand photons for each radioactive particle. Finally, in a semiconductor detector, adsorption of a single radioactive particle promotes thousands of electrons to the semiconductor's conduction band, increasing conductivity.

This page titled 32.2: Instrumentation is shared under a CC BY-NC-SA 4.0 license and was authored, remixed, and/or curated by David Harvey.

# 32.3: Neutron Activation Methods

Few analytes are naturally radioactive. For many analytes, however, we can induce radioactivity by irradiating the sample with neutrons in a process called **neutron activation analysis** (NAA). The radioactive element formed by neutron activation decays to a stable isotope by emitting a gamma ray, and, possibly, other nuclear particles. The rate of gamma-ray emission is proportional to the analyte's initial concentration in the sample. For example, if we place a sample containing non-radioactive $^{27}_{13}\text{Al}$ in a nuclear reactor and irradiate it with neutrons, the following nuclear reaction takes place.

$$^{27}_{13}\text{Al} + ^{1}_{0}\text{n} \longrightarrow ^{28}_{13}\text{Al}$$

The radioactive isotope of $^{28}\text{Al}$ has a characteristic decay process that includes the release of a beta particle and a gamma ray.

$$^{28}_{13}\text{Al} \longrightarrow ^{28}_{14}\text{Al} + ^{0}_{-1}\beta + \gamma$$

When irradiation is complete, we remove the sample from the nuclear reactor, allow any short-lived radioactive interferences to decay into the background, and measure the rate of gamma-ray emission.

The initial activity at the end of irradiation depends on the number of atoms that are present. This, in turn, is a equal to the difference between the rate of formation for $^{28}_{13}\text{Al}$ and its rate of disintegration

$$\frac{dN_{^{28}_{13}\text{Al}}}{dt} = \Phi\sigma N_{^{27}_{13}\text{Al}} - \lambda N_{^{28}_{13}\text{Al}} \tag{32.3.1}$$

where $\Phi$ is the neutron flux and $\sigma$ is the reaction cross-section, or probability that a $^{27}_{13}\text{Al}$ nucleus captures a neutron. Integrating Equation 32.3.1 over the time of irradiation, $t_i$, and multiplying by $\lambda$ gives the initial activity, $A_0$, at the end of irradiation as

$$A_0 = \lambda N_{^{28}_{13}\text{Al}} = \Phi\sigma N_{^{27}_{13}\text{Al}}(1 - e^{-kt})$$

If we know the values for $A_0$, $\Phi$, $\sigma$, $\lambda$, and $t_i$, then we can calculate the number of atoms of $^{27}_{13}\text{Al}$ initially present in the sample.

A simpler approach is to use one or more external standards. Letting $(A_0)_x$ and $(A_0)_s$ represent the analyte's initial activity in an unknown and in an external standard, and letting $w_x$ and $w_s$ represent the analyte's weight in the unknown and in the external standard, we obtain the following pair of equations

$$(A_0)_x = kw_x \tag{32.3.2}$$

$$(A_0)_s = kw_s \tag{32.3.3}$$

that we can solve to determine the analyte's mass in the sample.

As noted earlier, gamma ray emission is measured following a period during which we allow short-lived interferents to decay into the background. As shown in Figure 32.3.1 , we determine the sample's or the standard's initial activity by extrapolating a curve of activity versus time back to $t$ = 0. Alternatively, if we irradiate the sample and the standard at the same time, and if we measure their activities at the same time, then we can substitute these activities for $(A_0)_x$ and $(A_0)_s$. This is the strategy used in the following example.

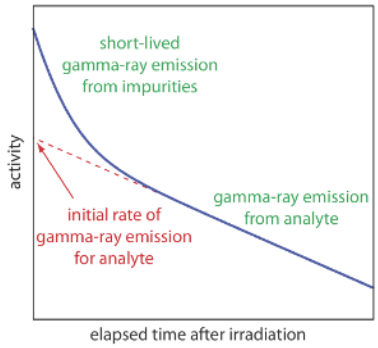



Figure 32.3.1 . Plot of gamma-ray emission as a function of time showing how the analyte's initial activity is determined.

## Example 32.3.1

The concentration of Mn in steel is determined by a neutron activation analysis using the method of external standards. A 1.000-g sample of an unknown steel sample and a 0.950-g sample of a standard steel known to contain 0.463% w/w Mn are irradiated with neutrons for 10 h in a nuclear reactor. After a 40-min delay the gamma ray emission is 2542 cpm (counts per minute) for the unknown and 1984 cpm for the external standard. What is the %w/w Mn in the unknown steel sample?

### Solution

Combining equations 32.3.2 and 32.3.3 gives

$$w_x = \frac{A_x}{A_s} \times w_s$$

The weight of Mn in the external standard is

$$w_s = \frac{0.00463 \text{ g Mn}}{\text{g steel}} \times 0.950 \text{ g steel} = 0.00440 \text{ g Mn}$$

Substituting into the above equation gives

$$w_x = \frac{2542 \text{ cpm}}{1984 \text{ cpm}} \times 0.00440 \text{ g Mn} = 0.00564 \text{ g Mn}$$

Because the original mass of steel is 1.000 g, the %w/w Mn is 0.564%.

Among the advantages of neutron activation are its applicability to almost all elements in the periodic table and that it is nondestructive to the sample. Consequently, NAA is an important technique for analyzing archeological and forensic samples, as well as works of art.

---

This page titled 32.3: Neutron Activation Methods is shared under a CC BY-NC-SA 4.0 license and was authored, remixed, and/or curated by David Harvey.

# 32.4: Isotope Dilution Methods

Another important radiochemical method for the analysis of nonradioactive analytes is isotope dilution. An external source of analyte is prepared in a radioactive form with a known activity, $A_T$, for its radioactive decay—we call this form of the analyte a tracer. To prepare a sample for analysis we add a known mass of the tracer, $w_T$, to a portion of sample that contains an unknown mass, $w_x$ , of analyte. After homogenizing the sample and tracer, we isolate $w_A$ grams of analyte by using a series of appropriate chemical and physical treatments. Because these chemical and physical treatments cannot distinguish between radioactive and nonradioactive forms of the analyte, the isolated material contains both. Finally, we measure the activity of the isolated sample, $A_A$. If we recover all the analyte—both the radioactive tracer and the nonradioactive analyte—then $A_A$ and $A_T$ are equal and $w_x = w_A - w_T$. Normally, we fail to recover all the analyte. In this case $A_A$ is less than $A_T$, and

$$A_A = A_T \times \frac{w_A}{w_x + w_T} \tag{32.4.1}$$

The ratio of weights in Equation 32.4.1 accounts for any loss of activity that results from our failure to recover all the analyte. Solving Equation 32.4.1 for $w_x$ gives

$$w_x = \frac{A_T}{A_A} w_A - w_T \tag{32.4.2}$$

How we process the sample depends on the analyte and the sample's matrix. We might, for example, digest the sample to bring the analyte into solution. After filtering the sample to remove the residual solids, we might precipitate the analyte, isolate it by filtration, dry it in an oven, and obtain its weight.

Given that the goal of an analysis is to determine the amount of nonradioactive analyte in our sample, the realization that we might not recover all the analyte might strike you as unsettling. A single liquid–liquid extraction rarely has an extraction efficiency of 100%. One advantage of isotope dilution is that the extraction efficiency for the nonradioactive analyte and for the tracer are the same. If we recover 50% of the tracer, then we also recover 50% of the nonradioactive analyte. Because we know how much tracer we added to the sample, we can determine how much of the nonradioactive analyte is in the sample.

## Example 32.4.1

The concentration of insulin in a production vat is determined by isotope dilution. A 1.00-mg sample of insulin labeled with $^{14}C$ that has an activity of 549 cpm is added to a 10.0-mL sample taken from the production vat. After homogenizing the sample, a portion of the insulin is separated and purified, yielding 18.3 mg of pure insulin. The activity for the isolated insulin is measured at 148 cpm. How many mg of insulin are in the original sample?

### Solution

Substituting known values into Equation 32.4.1 gives

$$w_x = \frac{549 \text{ cpm}}{148 \text{ cpm}} \times 18.3 \text{ mg} - 1.00 \text{ mg} = 66.9 \text{ mg insulin}$$

Equation 32.4.1 and Equation 32.4.2 are valid only if the tracer's half-life is considerably longer than the time it takes to conduct the analysis. If this is not the case, then the decrease in activity is due both to the incomplete recovery and the natural decrease in the tracer's activity. Table 32.4.1 provides a list of several common tracers for isotope dilution.

Table 32.4.1 . Common Tracers for Isotope Dilution

| isotope | half-life |
|---|---|
| $^{3}H$ | 12.5 years |
| $^{14}C$ | 5730 years |
| $^{32}P$ | 14.3 days |
| $^{35}S$ | 87.1 days |
| $^{45}Ca$ | 152 days |
| $^{55}Fe$ | 2.91 years |
| $^{60}Co$ | 5.3 years |
| $^{131}I$ | 8 days |

An important feature of isotope dilution is that it is not necessary to recover all the analyte to determine the amount of analyte present in the original sample. Isotope dilution, therefore, is useful for the analysis of samples with complex matrices, where a complete recovery of the analyte is difficult.

---

This page titled 32.4: Isotope Dilution Methods is shared under a CC BY-NC-SA 4.0 license and was authored, remixed, and/or curated by David Harvey.

# CHAPTER OVERVIEW

## 33: Automated Methods of Analysis


33.1: Overview of Automated Methods of Analysis

33.2: Flow-Injection Analysis

33.3: Other Automated Methods of Analysis


---

This page titled 33: Automated Methods of Analysis is shared under a CC BY-NC-SA 4.0 license and was authored, remixed, and/or curated by David Harvey.

# 33.1: Overview of Automated Methods of Analysis

An automated method of analysis is one in which the one or more steps in an analysis are completed without the direct action of the analyst. Instead, the instrument itself completes these actions. Some of these actions are carried out discretely, such as an autosampler that can complete all facets of sample preparation, from collecting discrete samples, adding reagents, and diluting the mixture to a desired volume, prior to the analysts analyzing the samples. Another example of a discrete instrument is an automated titrator (see Figure 33.1.1) that relieves the analyst from manually operating a buret. Instead, the analyst introduces the sample into the automated titrator and lets the instrument complete the titration.




Figure 33.1.1 . Typical instrumentation for an automated acid–base titration showing the titrant, the pump, and the titrand. The pH electrode in the titrand's solution is used to monitor the titration's progress. You can see the titration curve in the lower-left quadrant of the computer's display. Modified from: Datamax (commons. Wikipedia.org).

Other automated instruments are continuous in nature, in which samples are injected, either manually or with an autosampler, into a flowing stream of reagents that can serve to transport the samples to a detector and can serve as a source of reagents that convert the analyte into a form suitable for analysis.

Both discrete and continuous automated methods of analysis have the advantage of allowing for a high throughput of samples and providing for greater reproducibility in results by relieving the analyst of the tedium associated with completing repetitive tasks. In general, continuous automated methods can handle more samples per unit time than can a discrete method.

This page titled 33.1: Overview of Automated Methods of Analysis is shared under a CC BY-NC-SA 4.0 license and was authored, remixed, and/or curated by David Harvey.

# 33.2: Flow-Injection Analysis

In this section we consider the technique of flow injection analysis—a continuous automated method—in which we inject the sample into a flowing carrier stream that gives rise to a transient signal at the detector. The shape of this transient signal depends on the physical and chemical kinetic processes that take place in the carrier stream during the time between injection and detection.

## Theory and Practice

Flow injection analysis (FIA) was developed in the mid-1970s as a highly efficient technique for the automated analyses of samples [see, for example, (a) Ruzicka, J.; Hansen, E. H. *Anal. Chim. Acta* **1975**, *78*, 145–157; (b) Stewart, K. K.; Beecher, G. R.; Hare, P. E. *Anal. Biochem.* **1976**, *70*, 167–173; (c) Valcárcel, M.; Luque de Castro, M. D. *Flow Injection Analysis: Principles and Applications*, Ellis Horwood: Chichester, England, 1987]. Unlike the centrifugal analyzer described later in this chapter, in which the number of samples is limited by the transfer disk's size, FIA allows for the rapid, sequential analysis of an unlimited number of samples. FIA is one example of a continuous-flow analyzer, in which we sequentially introduce samples at regular intervals into a liquid carrier stream that transports them to the detector.

A schematic diagram detailing the basic components of a flow injection analyzer is shown in Figure 33.2.1 . The reagent that serves as the carrier is stored in a reservoir, and a propelling unit maintains a constant flow of the carrier through a system of tubing that comprises the transport system. We inject the sample directly into the flowing carrier stream, where it travels through one or more mixing and reaction zones before it reaches the detector's flow-cell. Figure 33.2.1 is the simplest design for a flow injection analyzer, which consists of a single channel and a single reagent reservoir. Multiple channel instruments that merge together separate channels, each of which introduces a new reagent into the carrier stream, also are possible.

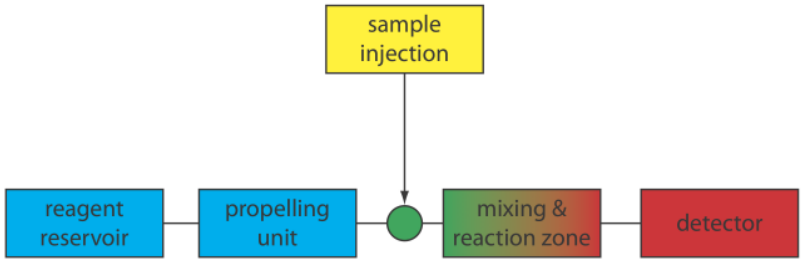



Figure 33.2.1 . Schematic diagram of a simple flow injection analyzer showing its basic components. After its injection into the carrier stream the samples mixes and reacts with the carrier stream's reagents before reaching the detector.

When we first inject a sample into the carrier stream it has the rectangular flow profile of width *w* shown in Figure 33.2.2 a. As the sample moves through the mixing zone and the reaction zone, the width of its flow profile increases as the sample disperses into the carrier stream. Dispersion results from two processes: convection due to the flow of the carrier stream and diffusion due to the concentration gradient between the sample and the carrier stream. Convection occurs by laminar flow. The linear velocity of the sample at the tube's walls is zero, but the sample at the center of the tube moves with a linear velocity twice that of the carrier stream. The result is the parabolic flow profile shown in Figure 33.2.2 b. Convection is the primary means of dispersion in the first 100 ms following the sample's injection.

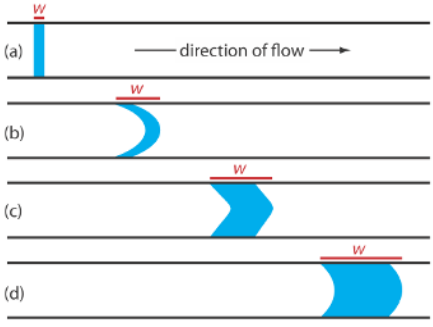



Figure 33.2.2 . Effect of dispersion on the shape of a sample's flow profile, shown in blue, at different times during a flow injection analysis: (a) at injection; (b) when convection dominates dispersion; (c) when convection and diffusion contribute to dispersion; and (d) when diffusion dominates dispersion. The red line shows the width, *w*, of the samples flow profile.

The second contribution to the sample's dispersion is diffusion due to the concentration gradient that exists between the sample and the carrier stream. As shown in Figure 33.2.2 , diffusion occurs parallel (axially) and perpendicular (radially) to the direction in which the carrier stream is moving. Only radial diffusion is important in a flow injection analysis. Radial diffusion decreases the sample's linear velocity at the center of the tubing, while the sample at the edge of the tubing experiences an increase in its linear velocity. Diffusion helps to maintain the integrity of the sample's flow profile (Figure 33.2.2 c) and prevents adjacent samples in the carrier stream from dispersing into one another. Both convection and diffusion make significant contributions to dispersion from approximately 3–20 s after the sample's injection. This is the normal time scale for a flow injection analysis. After approximately 25 s, diffusion is the only significant contributor to dispersion, resulting in a flow profile similar to that shown in Figure 33.2.2 d.

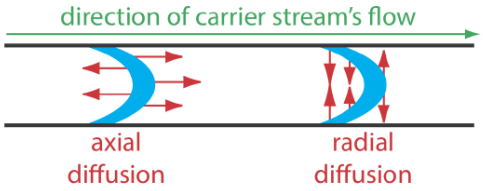



Figure 33.2.3 . Illustration showing axial and radial diffusion. The blue band is the sample's flow profile and the red arrows indicate the direction of diffusion.

An FIA curve, or fiagram, is a plot of the detector's signal as a function of time. Figure 33.2.4 shows a typical fiagram for conditions in which both convection and diffusion contribute to the sample's dispersion. Also shown on the figure are several parameters that characterize a sample's fiagram. Two parameters define the time for a sample to move from the injector to the detector. Travel time, $t_a$, is the time between the sample's injection and the arrival of its leading edge at the detector. Residence time, $T$, on the other hand, is the time required to obtain the maximum signal. The difference between the residence time and the travel time is $t'$, which approaches zero when convection is the primary means of dispersion, and increases in value as the contribution from diffusion becomes more important.

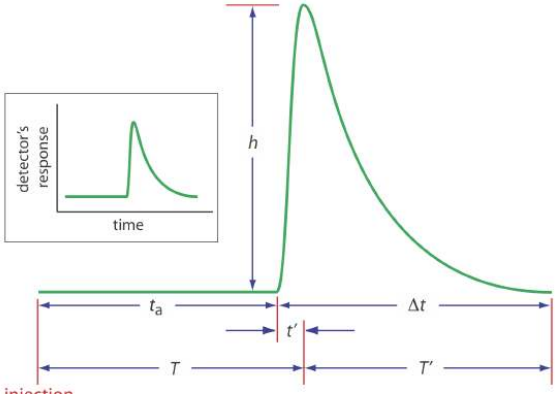



Figure 33.2.4 . Typical fiagram for flow injection analysis showing the detector's response as a function of time. See the text for an explanation of the parameters, $t_a$, $t'$, $\Delta t$, $T'$, and $h$.

The time required for the sample to pass through the detector's flow cell—and for the signal to return to the baseline—is also described by two parameters. The baseline-to-baseline time, $\Delta t$, is the time between the arrival of the sample's leading edge to the departure of its trailing edge. The elapsed time between the maximum signal and its return to the baseline is the return time, $T'$. The final characteristic parameter of a fiagram is the sample's peak height, $h$.

Of the six parameters shown in Figure 33.2.4 , the most important are peak height and the return time. Peak height is important because it is directly or indirectly related to the analyte's concentration. The sensitivity of an FIA method, therefore, is determined by the peak height. The return time is important because it determines the frequency with which we may inject samples. Figure 33.2.5 shows that if we inject a second sample at a time $T'$ after we inject the first sample, there is little overlap of the two FIA curves. By injecting samples at intervals of $T'$, we obtain the maximum possible sampling rate.

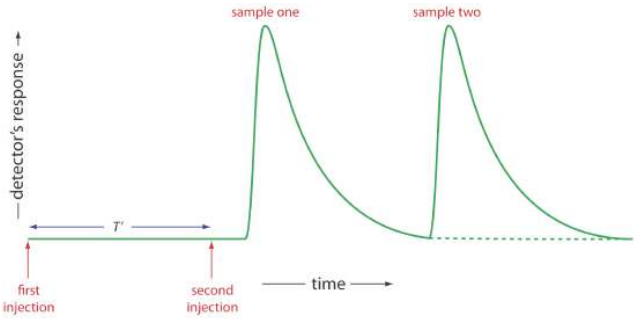



Figure 33.2.5 . Effect of return time, $T'$, on sampling frequency.

Peak heights and return times are influenced by the dispersion of the sample's flow profile and by the physical and chemical properties of the flow injection system. Physical parameters that affect *h* and $T'$ include the volume of sample we inject, the flow rate, the length, diameter and geometry of the mixing zone and the reaction zone, and the presence of junctions where separate channels merge together. The kinetics of any chemical reactions between the sample and the reagents in the carrier stream also influence the peak height and return time.

Unfortunately, there is no good theory that we can use to consistently predict the peak height and the return time for a given set of physical and chemical parameters. The design of a flow injection analyzer for a particular analytical problem still occurs largely by a process of experimentation. Nevertheless, we can make some general observations about the effects of physical and chemical parameters. In the absence of chemical effects, we can improve sensitivity—that is, obtain larger peak heights—by injecting larger samples, by increasing the flow rate, by decreasing the length and diameter of the tubing in the mixing zone and the reaction zone, and by merging separate channels before the point where the sample is injected. With the exception of sample volume, we can increase the sampling rate—that is, decrease the return time—by using the same combination of physical parameters. Larger sample volumes, however, lead to longer return times and a decrease in sample throughput. The effect of chemical reactivity depends on whether the species we are monitoring is a reactant or a product. For example, if we are monitoring a reactant, we can improve sensitivity by choosing conditions that decrease the residence time, *T*, or by adjusting the carrier stream's composition so that the reaction occurs more slowly.

## Instrumentation

The basic components of a flow injection analyzer are shown in Figure 33.2.6 and include a pump to propel the carrier stream and the reagent streams, a means to inject the sample into the carrier stream, and a detector to monitor the composition of the carrier stream. Connecting these units is a transport system that brings together separate channels and provides time for the sample to mix with the carrier stream and to react with the reagent streams. We also can incorporate separation modules into the transport system. Each of these components is considered in greater detail in this section.

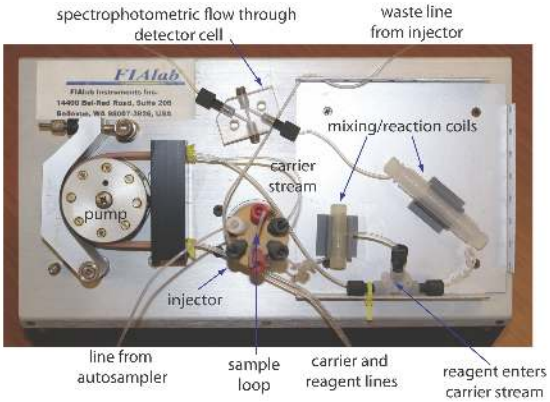



Figure 33.2.6 . Example of a typical flow injection analyzer that shows the pump, the injector, the transport system, which consists of mixing/reaction coils and junctions, and the detector (minus the spectrophotometer). This particular configuration has two channels: the carrier stream and a reagent line.

## Propelling Unit

The propelling unit moves the carrier stream through the flow injection analyzer. Although several different propelling units have been used, the most common is a peristaltic pump, which, as shown in Figure 33.2.7 , consists of a set of rollers attached to the outside of a rotating drum. Tubing from the reagent reservoirs fits between the rollers and a fixed plate. As the drum rotates the rollers squeeze the tubing, forcing the contents of the tubing to move in the direction of the rotation. Peristaltic pumps provide a constant flow rate, which is controlled by the drum's speed of rotation and the inner diameter of the tubing. Flow rates from 0.0005–40 mL/min are possible, which is more than adequate to meet the needs of FIA where flow rates of 0.5–2.5 mL/min are common. One limitation to a peristaltic pump is that it produces a pulsed flow—particularly at higher flow rates—that may lead to oscillations in the signal.

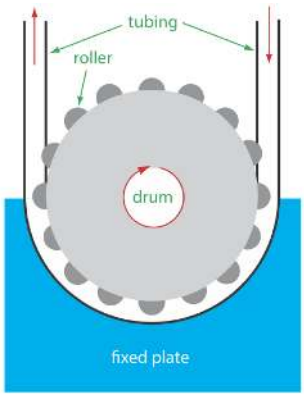



Figure 33.2.7 . Schematic diagram of a peristaltic pump.

## Injector

The sample, typically 5–200 μL, is injected into the carrier stream. Although syringe injections through a rubber septum are possible, the more common method—as seen in Figure 33.2.6 —is to use a rotary, or loop injector similar to that used in an HPLC. This type of injector provides for a reproducible sample volume and is easily adaptable to automation, an important feature when high sampling rates are needed.

## Detector

The most common detectors for flow injection analysis are the electrochemical and optical detectors used in HPLC. These detectors are discussed in Chapter 28 and are not considered further in this section. FIA detectors also have been designed around the use of ion selective electrodes and atomic absorption spectroscopy.

## Transport System

The heart of a flow injection analyzer is the transport system that brings together the carrier stream, the sample, and any reagents that react with the sample. Each reagent stream is considered a separate channel, and all channels must merge before the carrier stream reaches the detector. The complete transport system is called a manifold.

The simplest manifold has a single channel, the basic outline of which is shown in Figure 33.2.8 . This type of manifold is used for direct analysis of analyte that does not require a chemical reaction. In this case the carrier stream serves only as a means for rapidly and reproducibly transporting the sample to the detector. For example, this manifold design has been used for sample introduction in atomic absorption spectroscopy, achieving sampling rates as high as 700 samples/h. A single-channel manifold also is used for determining a sample's pH or determining the concentration of metal ions using an ion selective electrode.

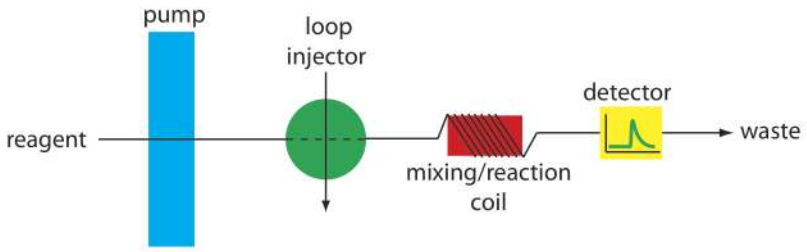



Figure 33.2.8 . Example of a single-channel manifold in which the reagent serves as the carrier stream and as a species that reacts with the sample. The mixing/reaction coil is wrapped around a plastic cylinder.

We can also use the single-channel manifold in Figure 33.2.8 for an analysis in which we monitor the product of a chemical reaction between the sample and a reactant. In this case the carrier stream both transports the sample to the detector and reacts with the sample. Because the sample must mix with the carrier stream, a lower flow rate is used. One example is the determination of chloride in water, which is based on the following sequence of reactions.

$$\mathrm{Hg(SCN)_2}(aq) + 2\mathrm{Cl^-}(aq) \rightleftharpoons \mathrm{HgCl_2}(aq) + 2\mathrm{SCN^-}(aq)$$

$$\mathrm{Fe^{3+}}(aq) + \mathrm{SCN^-}(aq) \rightleftharpoons \mathrm{Fe(SCN)^{2+}}(aq)$$

The carrier stream consists of an acidic solution of $Hg(SCN)_2$ and $Fe^{3+}$. Injecting a sample that contains chloride into the carrier stream displaces thiocyanate from $Hg(SCN)_2$. The displaced thiocyanate then reacts with $Fe^{3+}$ to form the red-colored $Fe(SCN)^{2+}$ complex, the absorbance of which is monitored at a wavelength of 480 nm. Sampling rates of approximately 120 samples per hour have been achieved with this system [Hansen, E. H.; Ruzicka, J. *J. Chem. Educ.* **1979**, *56*, 677–680].

Most flow injection analyses that include a chemical reaction use a manifold with two or more channels. Including additional channels provides more control over the mixing of reagents and the interaction between the reagents and the sample. Two configurations are possible for a dual-channel system. A dual-channel manifold, such as the one shown in Figure 33.2.9 a, is used when the reagents cannot be premixed because of their reactivity. For example, in acidic solutions phosphate reacts with molybdate to form the heteropoly acid $H_3P(Mo_{12}O_{40})$. In the presence of ascorbic acid the molybdenum in the heteropoly acid is reduced from Mo(VI) to Mo(V), forming a blue-colored complex that is monitored spectrophotometrically at 660 nm [Hansen, E. H.; Ruzicka, J. *J. Chem. Educ.* **1979**, *56*, 677–680]. Because ascorbic acid reduces molybdate, the two reagents are placed in separate channels that merge just before the loop injector.

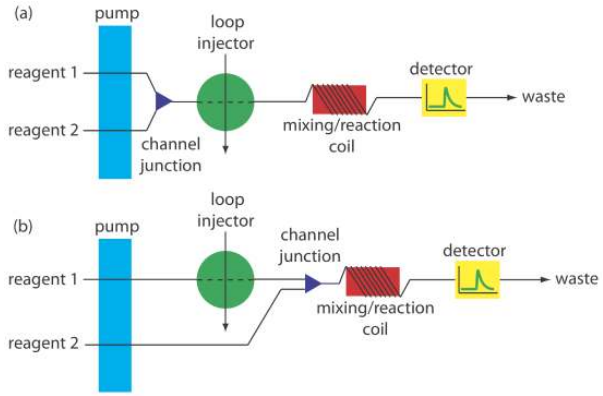



Figure 33.2.9 . Two examples of a dual-channel manifold for flow injection analysis. In (a) the two channels merge before the loop injector, and in (b) the two channels merge after the loop injector.

A dual-channel manifold also is used to add a second reagent after injecting the sample into a carrier stream, as shown in Figure 33.2.9 b. This style of manifold is used for the quantitative analysis of many analytes, including the determination of a wastewater's chemical oxygen demand (COD) [Korenaga, T.; Ikatsu, H. *Anal. Chim. Acta* **1982**, *141*, 301–309]. Chemical oxygen demand is a measure of the amount organic matter in the wastewater sample. In the conventional method of analysis, COD is determined by refluxing the sample for 2 h in the presence of acid and a strong oxidizing agent, such as $K_2Cr_2O_7$ or $KMnO_4$. When refluxing is complete, the amount of oxidant consumed in the reaction is determined by a redox titration. In the flow injection version of this analysis, the sample is injected into a carrier stream of aqueous $H_2SO_4$, which merges with a solution of the oxidant

from a secondary channel. The oxidation reaction is kinetically slow and, as a result, the mixing coil and the reaction coil are very long—typically 40 m—and submerged in a thermostated bath. The sampling rate is lower than that for most flow injection analyses, but at 10–30 samples/h it is substantially greater than the redox titrimetric method.

More complex manifolds involving three or more channels are common, but the possible combination of designs is too numerous to discuss. One example of a four-channel manifold is shown in Figure 33.2.10 .

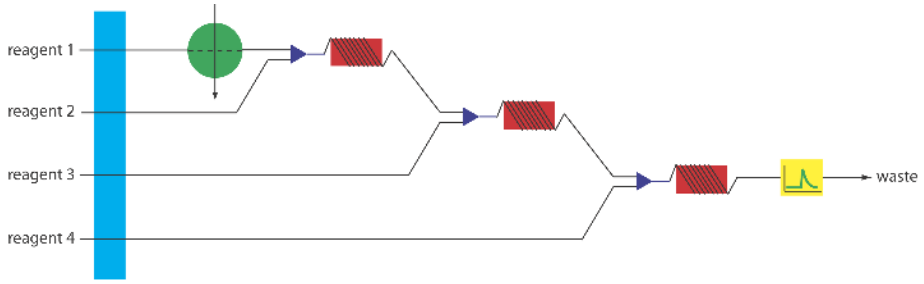



Figure 33.2.10 . Example of a four-channel manifold for a flow injection analysis.

## Separation Modules

By incorporating a separation module into the flow injection manifold we can include a separation—dialysis, gaseous diffusion and liquid-liquid extractions are examples—in a flow injection analysis. Although these separations are never complete, they are reproducible if we carefully control the experimental conditions.

Dialysis and gaseous diffusion are accomplished by placing a semipermeable membrane between the carrier stream containing the sample and an acceptor stream, as shown in Figure 33.2.11 . As the sample stream passes through the separation module, a portion of those species that can cross the semipermeable membrane do so, entering the acceptor stream. This type of separation module is common for the analysis of clinical samples, such as serum and urine, where a dialysis membrane separates the analyte from its complex matrix. Semipermeable gaseous diffusion membranes are used for the determination of ammonia and carbon dioxide in blood. For example, ammonia is determined by injecting the sample into a carrier stream of aqueous NaOH. Ammonia diffuses across the semipermeable membrane into an acceptor stream that contains an acid–base indicator. The resulting acid–base reaction between ammonia and the indicator is monitored spectrophotometrically.

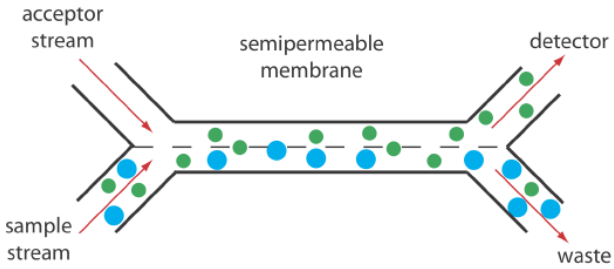



Figure 33.2.11 . Separation module for a flow injection analysis using a semipermeable membrane. The smaller green solutes can pass through the semipermeable membrane and enter the acceptor stream, but the larger blue solutes cannot. Although the separation is not complete—note that some of the green solute remains in the sample stream and exits as waste—it is reproducible if we do not change the experimental conditions.

Liquid–liquid extractions are accomplished by merging together two immiscible fluids, each carried in a separate channel. The result is a segmented flow through the separation module, consisting of alternating portions of the two phases. At the outlet of the separation module the two fluids are separated by taking advantage of the difference in their densities. Figure 33.2.12 shows a typical configuration for a separation module in which the sample is injected into an aqueous phase and extracted into a less dense organic phase that passes through the detector.

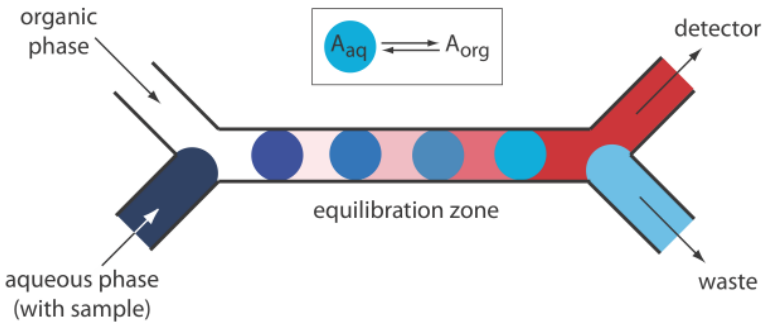



Figure 33.2.12 . Separation module for flow injection analysis using a liquid–liquid extraction. The inset shows the equilibrium reaction. As the sample moves through the equilibration zone, the analyte extracts into the organic phase.

## Quantitative Applications

In a quantitative flow injection method a calibration curve is determined by injecting a series of external standards that contain known concentrations of analyte. The calibration curve's format—examples include plots of absorbance versus concentration and of potential versus concentration—depends on the method of detection.

Flow injection analysis has been used to analyze a wide variety of samples, including environmental, clinical, agricultural, industrial, and pharmaceutical samples. The majority of analyses involve environmental and clinical samples, which is the focus of this section.

Quantitative flow injection methods have been developed for cationic, anionic, and molecular pollutants in wastewater, freshwaters, groundwaters, and marine waters, three examples of which were described in the previous section. Table 33.2.1 provides a partial listing of other analytes that have been determined using FIA, many of which are modifications of standard spectrophotometric and potentiometric methods. An additional advantage of FIA for environmental analysis is the ability to provide for the continuous, in situ monitoring of pollutants in the field [Andrew, K. N.; Blundell, N. J.; Price, D.; Worsfold, P. J. *Anal. Chem.* **1994**, *66*, 916A–922A].

Table 33.2.1 . Selected Flow Injection Analysis Methods for Environmental Samples

| analyte | sample | sample volume (µL) | concentration range | sampling frequency ($h^{-1}$) |
|---|---|---|---|---|
| $Ca^{2+}$ | freshwater | 20 | 0.8–7.2 ppm | 80 |
| $Cu^{2+}$ | groundwater | 70–700 | 100–400 ppb | 20 |
| $Pb^{2+}$ | groundwater | 70–700 | 0–40 ppb | 20 |
| $Zn^{2+}$ | seawater | 1000 | 1–100 ppb | 30–60 |
| $NH_4^+$ | seawater | 60 | 0.18–18.1 ppb | 288 |
| $NO_3^-$ | rainwater | 1000 | 1–10 ppb | 40 |
| $SO_4^{2-}$ | freshwater | 400 | 4–140 ppb | 180 |
| $CN^-$ | industrial | 10 | 0.3–100 ppm | 40 |

*Source*: Adapted from Valcárcel, M.; Luque de Castro, M. D. *Flow-Injection Analysis: Principles and Practice*, Ellis Horwood: Chichester, England, 1987.

Several standard methods for the analysis of water involve an acid–base, complexation, or redox titration. It is easy to adapt these titrations to FIA using a single-channel manifold similar to that shown in Figure 33.2.8 [Ramsing, A. U.; Ruzicka, J.; Hansen, E. H. *Anal. Chim. Acta* **1981**, *129*, 1–17]. The titrant—whose concentration must be stoichiometrically less than that of the analyte—and a visual indicator are placed in the reagent reservoir and pumped continuously through the manifold. When we inject the sample it mixes thoroughly with the titrant in the carrier stream. The reaction between the analyte, which is in excess, and the titrant produces a relatively broad rectangular flow profile for the sample. As the sample moves toward the detector, additional mixing

occurs and the width of the sample's flow profile decreases. When the sample passes through the detector, we determine the width of its flow profile, $\Delta T$, by monitoring the indicator's absorbance. A calibration curve of $\Delta T$ versus log[analyte] is prepared using standard solutions of analyte.

Flow injection analysis has also found numerous applications in the analysis of clinical samples, using both enzymatic and nonenzymatic methods. Table 33.2.2 summarizes several examples.

Table 33.2.2 . Selected Flow Injection Analysis Methods for Clinical Samples

| analyte | sample | sample volume (µL) | concentration range | sampling frequency ($h^{-1}$) |
|---|---|---|---|---|
| ***nonenzymatic methods*** | | | | |
| $Cu^{2+}$ | serum | 20 | 0.7–1.5 ppm | 70 |
| $Cl^-$ | serum | 60 | 50–150 meq/L | 125 |
| $PO_4^{3-}$ | serum | 200 | 10–60 ppm | 130 |
| total $CO_2$ | serum | 50 | 10–50 mM | 70 |
| chlorpromazine | blood plasma | 200 | 1.5–9 $\mu$M | 24 |
| ***enzymatic methods*** | | | | |
| glucose | blood serum | 26.5 | 0.5–15 mM | 60 |
| urea | blood serum | 30 | 4–20 mM | 60 |
| ethanol | blood | 30 | 5–30 ppm | 50 |

*Source*: Adapted from Valcárcel, M.; Luque de Castro, M. D. *Flow-Injection Analysis: Principles and Practice*, Ellis Horwood: Chichester, England, 1987.

## Evaluation

The majority of flow injection analysis applications are modifications of conventional titrimetric, spectrophotometric, and electrochemical methods of analysis; thus, it is appropriate to compare FIA methods to these conventional methods. The scale of operations for FIA allows for the routine analysis of minor and trace analytes, and for macro, meso, and micro samples. The ability to work with microliter injection volumes is useful when the sample is scarce. Conventional methods of analysis usually have smaller detection limits.

The accuracy and precision of FIA methods are comparable to conventional methods of analysis; however, the precision of FIA is influenced by several variables that do not affect conventional methods, including the stability of the flow rate and the reproducibility of the sample's injection. In addition, results from FIA are more susceptible to temperature variations.

In general, the sensitivity of FIA is less than that for conventional methods of analysis for at least two reasons. First, as with chemical kinetic methods, measurements in FIA are made under nonequilibrium conditions when the signal has yet to reach its maximum value. Second, dispersion dilutes the sample as it moves through the manifold. Because the variables that affect sensitivity are known, we can design the FIA manifold to optimize the method's sensitivity.

Selectivity for an FIA method often is better than that for the corresponding conventional method of analysis. In many cases this is due to the kinetic nature of the measurement process, in which potential interferents may react more slowly than the analyte. Contamination from external sources also is less of a problem because reagents are stored in closed reservoirs and are pumped through a system of transport tubing that is closed to the environment.

Finally, FIA is an attractive technique when considering time, cost, and equipment. When using an autosampler, a flow injection method can achieve very high sampling rates. A sampling rate of 20–120 samples/h is not unusual and sampling rates as high as 1700 samples/h are possible. Because the volume of the flow injection manifold is small, typically less than 2 mL, the consumption of reagents is substantially smaller than that for a conventional method. This can lead to a significant decrease in the cost per

analysis. Flow injection analysis does require the need for additional equipment—a pump, a loop injector, and a manifold—which adds to the cost of an analysis.

> For a review of the importance of flow injection analysis, see Hansen, E. H.; Miró, M. "How Flow-Injection Analysis (FIA) Over the Past 25 Years has Changed Our Way of Performing Chemical Analyses," *TRAC, Trends Anal. Chem.* **2007**, *26*, 18–26.

This page titled 33.2: Flow-Injection Analysis is shared under a CC BY-NC-SA 4.0 license and was authored, remixed, and/or curated by David Harvey.

# 33.3: Other Automated Methods of Analysis

In the last two sections we introduced two examples of automated methods of analysis: a brief mention of automated titrators and a more extensive coverage of flow-injection analysis. In this section we consider three additional examples of automated methods of analysis: the stopped-flow analyzer, the centrifugal analyzer, and disposable single-test analyzers based on thin films, screen-printing, and paper.

## Stopped-Flow Analyzer

A variety of instruments have been developed to automate the kinetic analysis of fast reactions. One example, which is shown in Figure 33.3.1 , is the stopped-flow analyzer. The sample and the reagents are loaded into separate syringes and precisely measured volumes are dispensed into a mixing chamber by the action of a syringe drive. The continued action of the syringe drive pushes the mixture through an observation cell and into a stopping syringe. The back pressure generated when the stopping syringe hits the stopping block completes the mixing, after which the reaction's progress is monitored spectrophotometrically. With a stopped-flow analyzer it is possible to complete the mixing of sample and reagent, and initiate the kinetic measurements in approximately 0.5 ms. By attaching an autosampler to the sample syringe it is possible to analyze up to several hundred samples per hour.

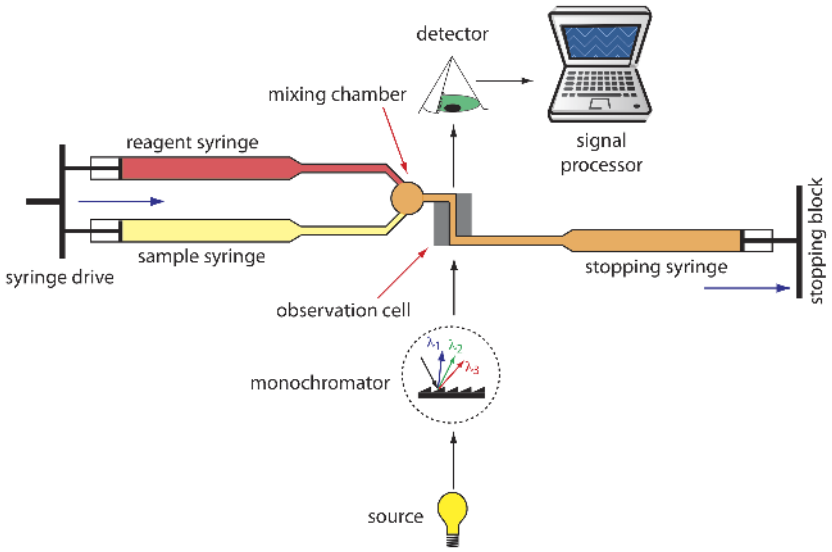



Figure 33.3.7 . Schematic diagram of a stopped-flow analyzer. The blue arrows show the direction in which the syringes are moving.

## Centrifugal Analyzer

Another instrument for kinetic measurements is the centrifugal analyzer, a partial cross section of which is shown in Figure 33.3.2 . The sample and the reagents are placed in separate wells, which are oriented radially around a circular transfer disk. As the centrifuge spins, the centrifugal force pulls the sample and the reagents into the cuvette where mixing occurs. A single optical source and detector, located below and above the transfer disk's outer edge, measures the absorbance each time the cuvette passes through the optical beam. When using a transfer disk with 30 cuvettes and rotating at 600 rpm, we can collect 10 data points per second for each sample.

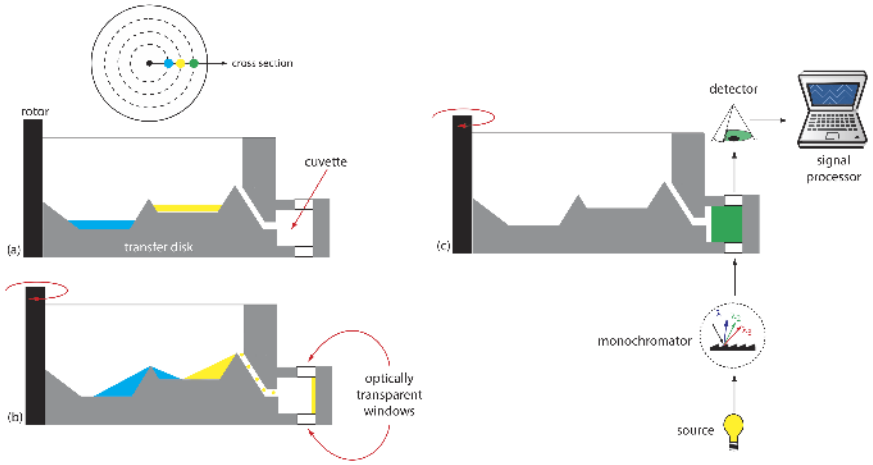



Figure 33.3.2 . Cross sections through a centrifugal analyzer showing (a) the wells that hold the sample and the reagents, (b) the mixing of the sample and the reagents, and (c) the configuration of the spectrophotometric detector.

The ability to collect lots of data and to collect it quickly requires appropriate hardware and software. Not surprisingly, automated kinetic analyzers developed in parallel with advances in analog and digital circuitry—the hardware—and computer software for smoothing, integrating, and differentiating the analytical signal. For an early discussion of the importance of hardware and software, see Malmstadt, H. V.; Delaney, C. J.; Cordos, E. A. "Instruments for Rate Determinations," *Anal. Chem.* **1972**, *44(12)*, 79A–89A.

## Disposable, Single-Test Analyzers

In comparison to other techniques, potentiometry provides a rapid, relatively low-cost means for analyzing samples. The limiting factor when analyzing a large number of samples is the need to rinse the electrode between samples. The use of inexpensive, disposable ion-selective electrodes can increase a lab's sample throughput. Figure 33.3.3 shows one example of a disposable ISE for $Ag^+$ [Tymecki, L.; Zwierkowska, E.; Głąb, S.; Koncki, R. *Sens. Actuators B* **2003**, *96*, 482–488]. Commercial instruments for measuring pH or potential are available in a variety of price ranges, and includes portable models for use in the field.

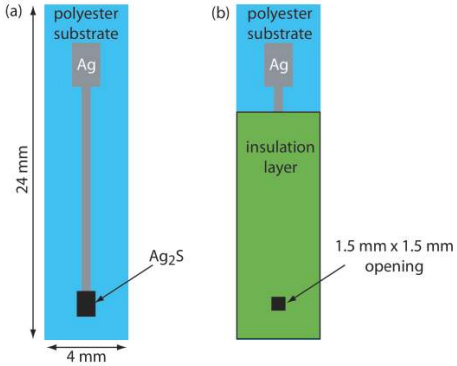



Figure 33.3.3 . Schematic diagram of a disposable ion-selective electrode created by screen-printing. In (a) a thin film of conducting silver is printed on a polyester substrate and a film of $Ag_2S$ overlaid near the bottom. In (b) an insulation layer with a small opening is layered on top exposes a portion of the $Ag_2S$ membrane that is immersed in the sample. The top of the polyester substrate remains uncoated, which allows us to connect the electrode to a potentiometer through the Ag film. The small inset shows the electrode's actual size.

This page titled 33.3: Other Automated Methods of Analysis is shared under a CC BY-NC-SA 4.0 license and was authored, remixed, and/or curated by David Harvey.

# CHAPTER OVERVIEW

## 34: Particle Size Determination

In our coverage of high-performance liquid chromatography (see Chapter 28) we noted that a typical packed column used porous silica particles with a mean diameter between 3-10 μm in size. A column that a manufacturer advertises as using 5 μm particles, however, will contain particles that are smaller and particles that are larger. As the size of the particles has an effect on the pressure it takes to move the mobile phase through the column, knowledge of the distribution of particle sizes is of interest. In this chapter we consider different methods for determining particle size.


34.1: Overview

34.2: Measuring Particle Size Using Sieves

34.3: Measuring Particle Size by Sedimentation

34.4: Measuring Particle Size Using Image Analysis

34.5: Measuring Particle Size Using Light Scattering


---


This page titled 34: Particle Size Determination is shared under a CC BY-NC-SA 4.0 license and was authored, remixed, and/or curated by David Harvey.

# 34.1: Overview

## What Do We Mean By a Particle?

Particles come in many forms. Some are very small, such as nanoparticles with dimensions of 1-100 nm and that might consist of just a few hundred atoms, and some are much larger, as in the beads of ion-exchange resin shown in Figure 34.1.1, which range in size from approximately 300 µm to 850 µm. Or, consider soils, which generally are subdivided into four types of particles: clay, which has particles with diameters smaller than 2 µm, silt, which has particle with diameters that range from 2 µm to 50 µm, sand, which has particle with diameters from 50 µm to 2000 µm, and gravel, which has particles with diameters larger than 2000 µm in size.

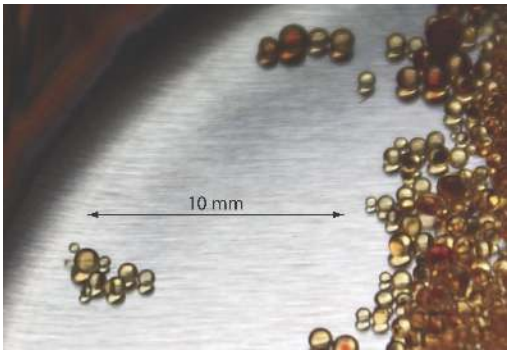



Figure 34.1.1: Example of an ion-exchange resin. The individual beads seen here range in size from approximately 300 µm to 850 µm in diameter.

We often hold as an image that particles are spherical in shape, which means we can characterize them by reporting a single number: the particle's diameter. Many particulate materials, however, are not uniform in shape. Although many of the resin beads in Figure 34.1.1 appear spherical—the largest bead in the small cluster at the left certainly looks spherical—others of the resin beads are distorted in shape, often appearing somewhat flattened. Still, it is not unusual to treat particles as if they are spheres. There are a number of reasons for this. If the method we use to determine size is not based on a static image (as is the case in Figure 34.1.1), but on a suspension of particles that are rotating rapidly on the timescale of our measurement, then the particle's shape averages out to a sphere even if the particle itself is not a sphere. The size we report, in this case, is called an equivalent spherical diameter (ESD), which may vary from method-to-method.

## How do We Report Particle Size?

Suppose we use a method to determine the size of 10000 particles. A simple way to display the data is to use a histogram that reports the frequency of particles in different size ranges, as we see in Figure 34.1.2. We can characterize this distribution by reporting one or more measures of its central tendency and a measure of its spread.

Typical measures of central tendency are the mode, which is the most common result, the median, which is the result that falls exactly in the middle of all recorded values, and the mean, which is the numerical average. For the data in Figure 34.1.2, the mode is 0.255 µm (the center of the bin that begins at 0.200 µm and ends at 0.250 µm), the median is 0.265 µm, and the mean is 0.287 µm. If the distribution was symmetrical, then the mode, median, and mean would be identical; here, the distribution has a long tail to the right, which increases the mean relative to the median, and increases the mean and the median relative to the mode.

A common way to report the spread is to use the width of the distribution at a frequency that is half of the maximum frequency; this is called the full-width-at-half-maximum (FWHM). For the data in Figure 34.1.2, the maximum frequency is 1230 counts. The FWHM is at a frequency of 615 and runs from a diameter of 0.050 µm to 0.450 µm, or FWHM = 0.450 – 0.050 = 0.400 µm.

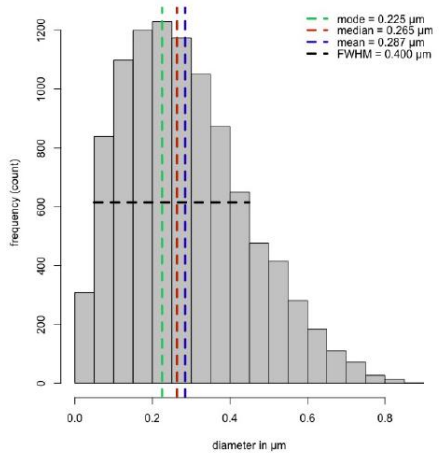



Figure 34.1.2: Histogram that shows the distribution of particle sizes for a sample consisting of 10000 particles. Each bin has a size of 0.05 µm. The mode, median, and mean diameters are shown by the vertical dashed lines. The horizontal dashed line show the data's full-width-at-half-maximum.

Another way to characterize the distribution of particle sizes is to plot the cumulative frequency (as a percent) as a function of the diameter of the particles. Figure 34.1.3 shows this for the data in Figure 34.1.2 using both the binned data for the histogram (shown as the circular black points), and using all of the underlying data (shown as the dashed blue line). The red, purple, and green lines show the particle diameters that include 10% (D10), 50% (D50), and 90% (D90) of all particles. The value of 0.264 µm indicates that half of the particles have diameters less than 0.264 µm and that half have diameters greater than 0.264 µm. One measure of the distribution's relative width is the span, which is defined as

$$\text{span} = \frac{\text{D90} - \text{D10}}{\text{D50}} = \frac{0.511 - 0.093}{0.264} = 1.59$$

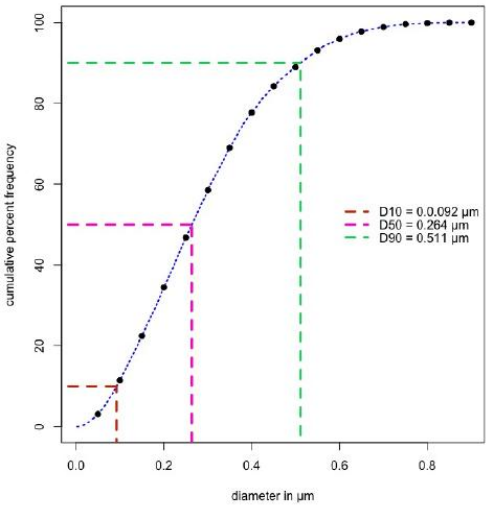



Figure 34.1.3: The cumulative distribution of the data from Figure 34.1.2. The dashed lines show the D10, D50, and D90 values.

## How Can We Measure Particle Size?

There are a variety of methods that we can use to determine the distribution in the sizes of a particulate material, more than we can cover in a single chapter. Instead, we will consider four common methods: sieving, sedimentation, imaging, and light scattering. When choosing a method, the size and form of the particles are important factors. Sieving, for example, is a practical choice when working with solid particulates that have diameters as small as 20 µm and as large as 125 mm (Note the change from µm to mm!).

Sedimentation is useful for particles with diameters of 1 μm, which we can extend to diameters as small as 1 nm by using a centrifuge. Image analysis is useful for particles between 0.5 μm and 1500 μm. Finally, light scattering is useful for particles as small as 0.8 nm.

---

This page titled 34.1: Overview is shared under a CC BY-NC-SA 4.0 license and was authored, remixed, and/or curated by David Harvey.

# 34.2: Measuring Particle Size Using Sieves

The particulates in a solid matrix are separated by size using one or more sieves (Figure 34.2.1). Sieves are available in a variety of mesh sizes, ranging from approximately 25 mm to 40 μm. By stacking together sieves of different mesh size—with the largest mesh at the top and the smallest mesh at the bottom—we can isolate particulates into several narrow size ranges. Using the sieves in Figure 34.2.1, for example, we can separate a solid into particles with diameters >1700 μm, with diameters between 1700 μm and 500 μm, with diameters between 500 μm and 250 μm, and those with a diameter <250 μm. The sample is place in the uppermost sieve and mechanical shaking used to effect the separation.



Figure 34.2.1. Three sieves with, from left to right, mesh sizes of 1700 μm, 500 μm, and 250 μm. Source: BMK (commons.wikimedia.com).

Because we cannot use more than a limited number of sieves in a single stack, the methods for analyzing the particle size data presented in Chapter 34.1 will be discrete in nature instead of continuous; thus, histograms will have a relatively small number of bins and a cumulative distribution will consist of a discrete number of points. One limitation to a sieve is that irregularly shaped particles are sized based on their two smallest dimensions.

This page titled 34.2: Measuring Particle Size Using Sieves is shared under a CC BY-NC-SA 4.0 license and was authored, remixed, and/or curated by David Harvey.

# 34.3: Measuring Particle Size by Sedimentation

When a particle that is larger than 5 μm is placed in suspension it will slowly settle toward the bottom of its container due to the force of gravity, a process called sedimentation. The time it takes for a particle to move a fixed distance is inversely proportional to the difference in the density of the particle and the density of the fluid in which the particles are suspended, and inversely proportional to the square of the particle's diameter. Larger (and denser) particles, therefore settle out more quickly than do smaller particles, as we see in Figure 34.3.1.

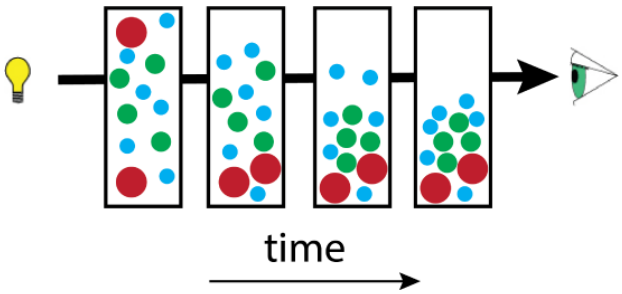



Figure 34.3.1: Schematic illustration of how sedimentation is used to determine particle size. The four rectangular sample cells show the state of sedimentation as a function of time, with the large red particles falling to the bottom of the sample cell more quickly than the medium green particles and the small blue particles. A light source is passed through a narrow cross-section of the sample cell, shown here by the arrow. The light reaching the detector serves as the analytical signal.

To follow the process of sedimentation, a light source is passed through a narrow portion of the sample and the amount of light passing through the sample monitored as a function of time. Once the largest particles pass through the sampling zone, the transmittance of light increases. Standards with well characterized particle sizes are used to calibrate the instrument.

For smaller particles, which may remain suspended due to Brownian motion, sedimentation can be carried out using a centrifuge, a technique known as differential centrifugal separation (DCS). As shown in Figure 34.3.2, the sample is introduced in the center of a disk that contains the fluid through which the particles will move. As the disk spins, larger particles move more quickly, eventually reaching the detector located at the outer edge of the disk.

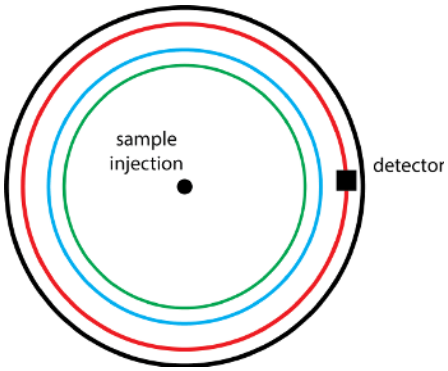



Figure 34.3.2: Schematic diagram of the disc used to separate particles by size in differential centrifugal sedimentation. The sample is injected into the center of the disc, which contains the fluid through which particles will move. As the centrifuge spins, the particles form bands that move toward the edge of the disc. The detector is located near the disc's edge.

This page titled 34.3: Measuring Particle Size by Sedimentation is shared under a CC BY-NC-SA 4.0 license and was authored, remixed, and/or curated by David Harvey.

# 34.4: Measuring Particle Size Using Image Analysis

The chapter overview includes a photograph of an ion-exchange resin's beads. The photograph includes a scale and, in principle, we could use the photograph and scale to estimate the size of the resin's beads. Although the estimates likely are pretty crude, this still serves as an example of image analysis in which we equip an optical microscope or electron microscope with a digital camera that can capture images of the microscope's field of view. Software is used to differentiate the particles from the background, to establish the particle's boundaries, and to determine the particle's size. As shown in Figure 34.4.1*a*, the sample is dispersed on an optical platform and light is passed through the optical platform where it is magnified and focused before capturing the image using a camera. The optical platform can be manually or automatically moved in the *xy*-plane to capture more images, as in Figure 34.4.1*b*. The software then sorts the particles into groups based on size and reports a count of particles in each group, as in Figure 34.4.1*c*. Because the particles remained immobile, this is called a static image analysis.

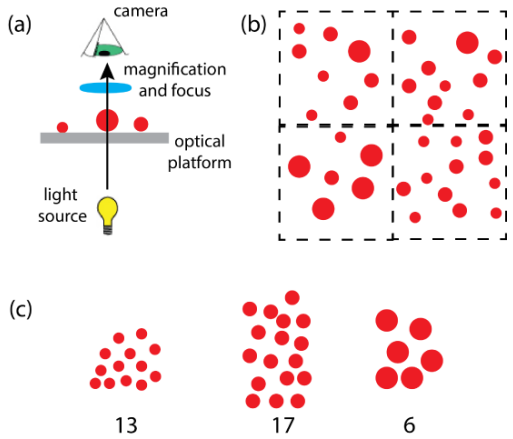



Figure 34.4.1: Illustration of a static image analysis. The basic instrument is shown in (a) and consists of a light source, an movable optical platform, lens for magnifing and focusing the image, and a camera for capturing the image, an example of which appears in (b). The instrument's software returns, in (c), information about the distribution of particles sizes.

One limitation to static imaging analysis is that it generally samples a small number of particles as they must be sufficiently dispersed on the optical platform to allow the individual particles to be imaged, analyzed, and counted. In dynamic imaging analysis, the sample is placed in a flow cell set perpendicular to the camera and the light source. Images are collected by using a high-speed flash and shutter speed to capture a sequence of images that are analyzed. By essentially creating an infinite optical platform, dynamic imaging analysis can achieve analysis rates of 10000 particles per minute.

This page titled 34.4: Measuring Particle Size Using Image Analysis is shared under a CC BY-NC-SA 4.0 license and was authored, remixed, and/or curated by David Harvey.

# 34.5: Measuring Particle Size Using Light Scattering

The blue color of the sky during the day and the red color of the sun at sunset are the result of light scattered by small particles of dust, molecules of water, and other gases in the atmosphere. The efficiency of a photon's scattering depends on its wavelength. We see the sky as blue during the day because violet and blue light scatter to a greater extent than other, longer wavelengths of light. For the same reason, the sun appears red at sunset because red light is less efficiently scattered and is more likely to pass through the atmosphere than other wavelengths of light. The scattering of radiation has been studied since the late 1800s, with applications beginning soon thereafter. The earliest quantitative applications of scattering, which date from the early 1900s, used the elastic scattering of light by colloidal suspensions to determine the concentration of colloidal particles.

## Origin of Scattering

If we send a focused, monochromatic beam of radiation with a wavelength $\lambda$ through a medium of particles with dimensions $< 1.5\lambda$, the radiation scatters in all directions. For example, visible radiation of 500 nm is scattered by particles as large as 750 nm in the longest dimension. Two general categories of scattering are recognized. In elastic scattering, radiation is first absorbed by the particles and then emitted without undergoing a change in the radiation's energy. When the radiation emerges with a change in energy, the scattering is inelastic. Only elastic scattering is considered in this chapter.

Elastic scattering is divided into two types: Rayleigh, or small-particle scattering, and large-particle scattering. Rayleigh scattering occurs when the scattering particle's largest dimension is less than 5% of the radiation's wavelength. The intensity of the scattered radiation is proportional to its frequency to the fourth power, $\nu^4$—which accounts for the greater scattering of blue light than red light—and is distributed symmetrically (Figure 34.5.1 a). For larger particles, scattering increases in the forward direction and decreases in the backward direction as the result of constructive and destructive interferences (Figure 34.5.1 b).

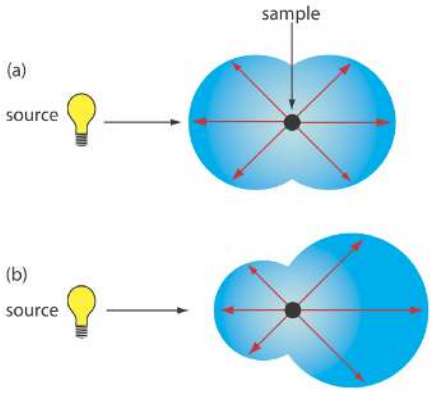



Figure 34.5.1. Distribution of radiation for (a) Rayleigh, or small-particle scattering, and (b) large-particle scattering.

## Rayleigh Scattering

Small particle, or Rayleigh scattering, measured at an angle of $\theta$ is the ratio of the intensity of the scattered light, $I$, to the intensity of the light source, $I_o$, and is expressed as

$$R_\theta = \frac{I}{I_o} = Kr^6$$

where $r_0$ is the radius of the particle and $K$ is a constant that is a function of the angle of scattering, the wavelength of light used, the refractive index of the particle, and the distance to the particle, $R$.

## Dynamic Light Scattering

In dynamic light scattering (DLS), we use a laser as a light source (see Figure 34.5.2 for an illustration). When the light from the source reaches the sample, which is in a sample cell, it scatters in all directions, as shown in Figure 34.5.1.

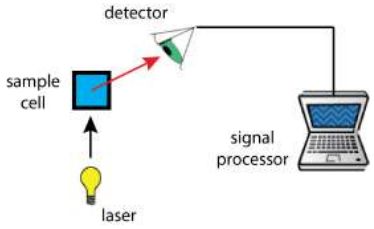



Figure 34.5.2. Basic set-up for a DLS experiment. To avoid saturating the detector, the light from the laser is attenuated before entering the sample cell.

A detector is placed at a fixed angle to collect the light that scatters at that angle. The resulting intensity of scattered light is measure as a function of time. Because the particles in the sample are moving due to Brownian motion, the intensity of light varies with time yielding a noisy signal. Smaller particles diffuse more rapidly than larger particles, which means that fluctuations in intensity with a small particle occurs more rapidly than for a large particle, as seen in Figure 34.5.3.

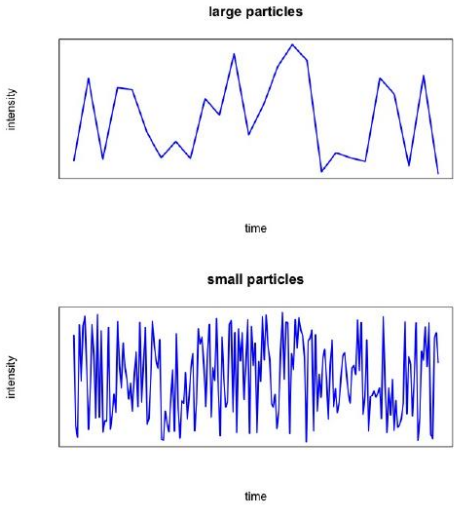



Figure 34.5.3: The time-dependent intensity of scattered light for (top) large particles and for (bottom) small particles.

To process the data in DLS, we examine the correlation of the signal with itself over small increments of time. This is accomplished by shifting the signal by a small amount (we call this the delay time, $\tau$) and computing the correlation between the original signal and the delayed signal. For short delay times, the correlation in intensities is close to 1 because the particles have not had time to move, and for longer delay times the correlation in intensities is close to 0 because the particles have moved significantly; in between these limits, the correlation undergoes an exponential decay. Figure 34.5.4 shows examples of the resulting correlograms for large particles and for small particles. The correlation function, $G(\tau)$, is defined as

$$G(\tau) = A[1 + Be^{-2\Gamma\tau}] \tag{34.5.1}$$

The terms $A$ and $B$ are, respectively, the baseline and the intercept of the correlation function, and $\Gamma = Dq^2$, where $D$ is the translational diffusion coefficient and where $q$ is equivalent to $(4\pi n/\lambda_0)sin(\theta/2)$ where $n$ is the refractive index, $\lambda_0$ is the wavelength of the laser, and $\theta$ is the angle at which scattered light is collected. The relationship between the size of the particles and the translational diffusion coefficient is give by the Stokes-Einstein equation

$$d = \frac{kT}{3\pi\eta D}$$

where $k$ is Boltzmann's constant, $T$ is the absolute temperature, and $\eta$ is the viscosity. Fitting one or more equations for $G(\tau)$ to the correlogram yields the distribution of particle sizes.

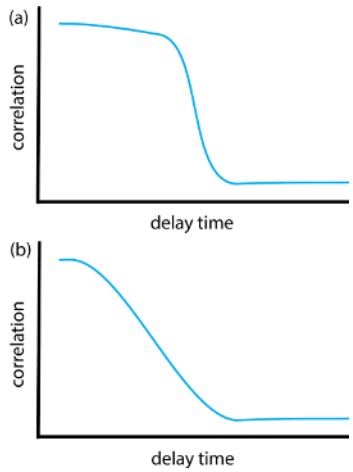



Figure 34.5.4: Correlograms for (a) large and for (b) small particles.

## Static Light Scattering

In dynamic light scattering we are interested in how the intensity of scattering changes with time; in static light scattering, we are interested in how the average intensity of scattered light varies with the concentration of particles, $c$, and the angle, $\theta$, at which scattering is measured. The extent of scattering, $R_\theta$, for each combination of $c$ and $\theta$ is plotted as $Kc/R_\theta$, where $K$ is a constant that is a function of the solvent's refractive index, the change in refracative index with concentration, and Avogadro's number as a function of the angle; the value of $S$ for the x-axis is chosen to maintain a separation between the data. A typical plot, which is known as a Zimm plot, is shown in Figure 34.5.5.

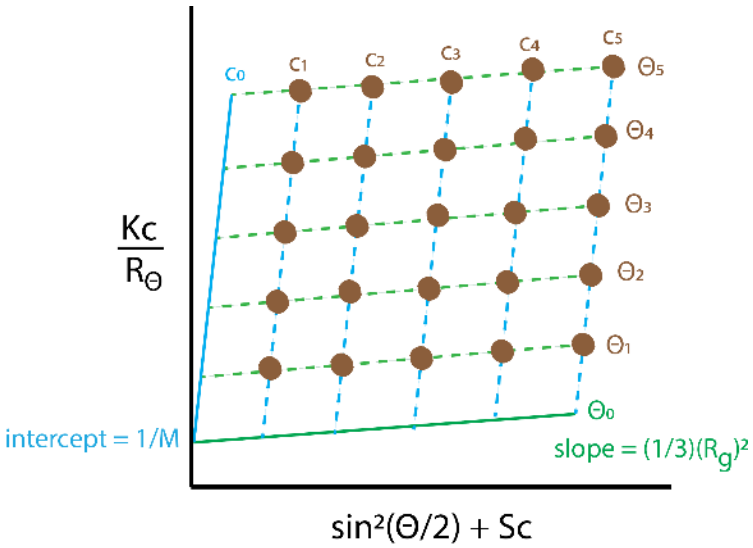



Figure 34.5.5. Zimm plot used to determine the size and molecular weight of particles. Data is collected using concentrations and angles shown in brown. Extrapolating the data to a concentration of zero (dashed green lines) and a scattering angle of zero (dashed blue lines) yields the solid blue and solid green lines that, in turn, yield values for the molecular weight, $M$, and particle size, $R_g$.

Each of the solid brown points gives the value of $Kc/R_\theta$ for a combination of concentration and angle. For each angle, the change in $Kc/R_\theta$ is extrapolated back to a concentration of zero (the dashed green lines) and for each concentration, the change in $Kc/R_\theta$ is extrapolated back to an angle of zero (the dashed blue lines). The resulting extrapolation of $c_0$ to $\theta = 0$ gives an intercept that is the inverse of the particles molecular weight, $M$, and the slope of the extrapolations of $\theta_0$ to a concentration of zero gives $R_g$, which is the particle's radius of gyration (it is moving, after all), which is its effective particle size.

34.5: Measuring Particle Size Using Light Scattering is shared under a not declared license and was authored, remixed, and/or curated by LibreTexts.

# CHAPTER OVERVIEW

## 35: Appendicies

The appendices gathered here provide a lengthy introduction to the analysis of data, a variety of tables that contain critical values for the statistical analysis of data and standard oxidation-reduction potential, a discussion of activity, and a list of acronyms and abbreviations used in this textbook and in other resources for analytical chemistry.


35.1: Evaluation of Analytical Data
35.2: Single-Sided Normal Distribution
35.3: Critical Values for t-Test
35.4: Critical Values for F-Test
35.5: Critical Values for Dixon's Q-Test
35.6: Critical Values for Grubb's Test
35.7: Activity Coefficients
35.8: Standard Reduction Potentials & Polarographic Half-wave Potentials
35.9: Recommended Primary Standards
35.10: Acronyms and Abbreviations


This page titled 35: Appendicies is shared under a CC BY-NC-SA 4.0 license and was authored, remixed, and/or curated by David Harvey.

# 35.1: Evaluation of Analytical Data

The material in this appendix is adapted from the textbook Chemometrics Using R, which is available through LibreTexts using this link. In addition to the material here, the textbook contains instructions on how to use the statistical programming language R to carry out the calculations.

## Types of Data

At the heart of any analysis is data. Sometimes our data describes a category and sometimes it is numerical; sometimes our data conveys order and sometimes it does not; sometimes our data has an absolute reference and sometimes it has an arbitrary reference; and sometimes our data takes on discrete values and sometimes it takes on continuous values. Whatever its form, when we gather data our intent is to extract from it information that can help us solve a problem.

### Ways to Describe Data

If we are to consider how to describe data, then we need some data with which we can work. Ideally, we want data that is easy to gather and easy to understand. It also is helpful if you can gather similar data on your own so you can repeat what we cover here. A simple system that meets these criteria is to analyze the contents of bags of M&Ms. Although this system may seem trivial, keep in mind that reporting the percentage of yellow M&Ms in a bag is analogous to reporting the concentration of $Cu^{2+}$ in a sample of an ore or water: both express the amount of an analyte present in a unit of its matrix.

At the beginning of this chapter we identified four contrasting ways to describe data: categorical vs. numerical, ordered vs. unordered, absolute reference vs. arbitrary reference, and discrete vs. continuous. To give meaning to these descriptive terms, let's consider the data in Table 35.1.1, which includes the year the bag was purchased and analyzed, the weight listed on the package, the type of M&Ms, the number of yellow M&Ms in the bag, the percentage of the M&Ms that were red, the total number of M&Ms in the bag and their corresponding ranks.

Table 35.1.1. Distribution of Yellow and Red M&Ms in Bags of M&Ms.

| bag id | year | weight (oz) | type | number yellow | % red | total M&Ms | rank (for total) |
|---|---|---|---|---|---|---|---|
| a | 2006 | 1.74 | peanut | 2 | 27.8 | 18 | sixth |
| b | 2006 | 1.74 | peanut | 3 | 4.35 | 23 | fourth |
| c | 2000 | 0.80 | plain | 1 | 22.7 | 22 | fifth |
| d | 2000 | 0.80 | plain | 5 | 20.8 | 24 | third |
| e | 1994 | 10.0 | plain | 56 | 23.0 | 331 | second |
| f | 1994 | 10.0 | plain | 63 | 21.9 | 333 | first |

The entries in Table 35.1.1 are organized by column and by row. The first row—sometimes called the header row—identifies the variables that make up the data. Each additional row is the record for one sample and each entry in a sample's record provides information about one of its variables; thus, the data in the table lists the result for each variable and for each sample.

### Categorical vs. Numerical Data

Of the variables included in Table 35.1.1, some are categorical and some are numerical. A categorical variable provides qualitative information that we can use to describe the samples relative to each other, or that we can use to organize the samples into groups (or categories). For the data in Table 35.1.1, bag id, type, and rank are categorical variables.

A numerical variable provides quantitative information that we can use in a meaningful calculation; for example, we can use the number of yellow M&Ms and the total number of M&Ms to calculate a new variable that reports the percentage of M&Ms that are yellow. For the data in Table 35.1.1, year, weight (oz), number yellow, % red M&Ms, and total M&Ms are numerical variables.

We can also use a numerical variable to assign samples to groups. For example, we can divide the plain M&Ms in Table 35.1.1 into two groups based on the sample's weight. What makes a numerical variable more interesting, however, is that we can use it to

make quantitative comparisons between samples; thus, we can report that there are $14.4\times$ as many plain M&Ms in a 10-oz. bag as there are in a 0.8-oz. bag.

$$\frac{333+331}{24+22}=\frac{664}{46}=14.4$$

Although we could classify year as a categorical variable—not an unreasonable choice as it could serve as a useful way to group samples—we list it here as a numerical variable because it can serve as a useful predictive variable in a regression analysis. On the other hand rank is not a numerical variable—even if we rewrite the ranks as numerals—as there are no meaningful calculations we can complete using this variable.

### Nominal vs. Ordinal Data

Categorical variables are described as nominal or ordinal. A nominal categorical variable does not imply a particular order; an ordinal categorical variable, on the other hand, coveys a meaningful sense of order. For the categorical variables in Table $35.1.1$, bag id and type are nominal variables, and rank is an ordinal variable.

### Ratio vs. Interval Data

A numerical variable is described as either ratio or interval depending on whether it has (ratio) or does not have (interval) an absolute reference. Although we can complete meaningful calculations using any numerical variable, the type of calculation we can perform depends on whether or not the variable's values have an absolute reference.

A numerical variable has an absolute reference if it has a meaningful zero—that is, a zero that means a measured quantity of none—against which we reference all other measurements of that variable. For the numerical variables in Table $35.1.1$, weight (oz), number yellow, % red, and total M&Ms are ratio variables because each has a meaningful zero; year is an interval variable because its scale is referenced to an arbitrary point in time, 1 BCE, and not to the beginning of time.

For a ratio variable, we can make meaningful absolute and relative comparisons between two results, but only meaningful absolute comparisons for an interval variable. For example, consider sample e, which was collected in 1994 and has 331 M&Ms, and sample d, which was collected in 2000 and has 24 M&Ms. We can report a meaningful absolute comparison for both variables: sample e is six years older than sample d and sample e has 307 more M&Ms than sample d. We also can report a meaningful relative comparison for the total number of M&Ms—there are

$$\frac{331}{24}=13.8\times$$

as many M&Ms in sample e as in sample d—but we cannot report a meaningful relative comparison for year because a sample collected in 2000 is not

$$\frac{2000}{1994}=1.003\times$$

older than a sample collected in 1994.

### Discrete vs. Continuous Data

Finally, the granularity of a numerical variable provides one more way to describe our data. For example, we can describe a numerical variable as discrete or continuous. A numerical variable is discrete if it can take on only specific values—typically, but not always, an integer value—between its limits; a continuous variable can take on any possible value within its limits. For the numerical data in Table $35.1.1$, year, number yellow, and total M&Ms are discrete in that each is limited to integer values. The numerical variables weight (oz) and % red, on the other hand, are continuous variables. Note that weight is a continuous variable even if the device we use to measure weight yields discrete values.

## Visualizing Data

The old saying that "a picture is worth a 1000 words" may not be universally true, but it true when it comes to the analysis of data. A good visualization of data, for example, allows us to see patterns and relationships that are less evident when we look at data arranged in a table, and it provides a powerful way to tell our data's story. Suppose we want to study the composition of 1.69-oz (47.9-g) packages of plain M&Ms. We obtain 30 bags of M&Ms (ten from each of three stores) and remove the M&Ms from each

bag one-by-one, recording the number of blue, brown, green, orange, red, and yellow M&Ms. We also record the number of yellow M&Ms in the first five candies drawn from each bag, and record the actual net weight of the M&Ms in each bag. Table 35.1.2 summarizes the data collected on these samples. The bag id identifies the order in which the bags were opened and analyzed.

Table 35.1.2. Analysis of Plain M&Ms in 47.9 g Bags.


https://chem.libretexts.org/@go/page/363066

| bag | store | blue | brown | green | orange | red | yellow | yellow_first_five | net_weight |
|---|---|---|---|---|---|---|---|---|---|
| 1 | CVS | 3 | 18 | 1 | 5 | 7 | 23 | 2 | 49.287 |
| 2 | CVS | 3 | 14 | 9 | 7 | 8 | 15 | 0 | 48.870 |
| 3 | Target | 4 | 14 | 5 | 10 | 10 | 16 | 1 | 51.250 |
| 4 | Kroger | 3 | 13 | 5 | 4 | 15 | 16 | 0 | 48.692 |
| 5 | Kroger | 3 | 16 | 5 | 7 | 8 | 18 | 1 | 48.777 |
| 6 | Kroger | 2 | 12 | 6 | 10 | 17 | 7 | 1 | 46.405 |
| 7 | CVS | 13 | 11 | 2 | 8 | 6 | 17 | 1 | 49.693 |
| 8 | CVS | 13 | 12 | 7 | 10 | 7 | 8 | 2 | 49.391 |
| 9 | Kroger | 6 | 17 | 5 | 4 | 8 | 16 | 1 | 48.196 |
| 10 | Kroger | 8 | 13 | 2 | 5 | 10 | 17 | 1 | 47.326 |
| 11 | Target | 9 | 20 | 1 | 4 | 12 | 13 | 3 | 50.974 |
| 12 | Target | 11 | 12 | 0 | 8 | 4 | 23 | 0 | 50.081 |
| 13 | CVS | 3 | 15 | 4 | 6 | 14 | 13 | 2 | 47.841 |
| 14 | Kroger | 4 | 17 | 5 | 6 | 14 | 10 | 2 | 48.377 |
| 15 | Kroger | 9 | 13 | 3 | 8 | 14 | 8 | 0 | 47.004 |
| 16 | CVS | 8 | 15 | 1 | 10 | 9 | 15 | 1 | 50.037 |
| 17 | CVS | 10 | 11 | 5 | 10 | 7 | 13 | 2 | 48.599 |
| 18 | Kroger | 1 | 17 | 6 | 7 | 11 | 14 | 1 | 48.625 |
| 19 | Target | 7 | 17 | 2 | 8 | 4 | 18 | 1 | 48.395 |
| 20 | Kroger | 9 | 13 | 1 | 8 | 7 | 22 | 1 | 51.730 |
| 21 | Target | 7 | 17 | 0 | 15 | 4 | 15 | 3 | 50.405 |
| 22 | CVS | 12 | 14 | 4 | 11 | 9 | 5 | 2 | 47.305 |
| 23 | Target | 9 | 19 | 0 | 5 | 12 | 12 | 0 | 49.477 |
| 24 | Target | 5 | 13 | 3 | 4 | 15 | 16 | 0 | 48.027 |
| 25 | CVS | 7 | 13 | 0 | 4 | 15 | 16 | 2 | 48.212 |
| 26 | Target | 6 | 15 | 1 | 13 | 10 | 14 | 1 | 51.682 |
| 27 | CVS | 5 | 17 | 6 | 4 | 8 | 19 | 1 | 50.802 |
| 28 | Kroger | 1 | 21 | 6 | 5 | 10 | 14 | 0 | 49.055 |
| 29 | Target | 4 | 12 | 6 | 5 | 13 | 14 | 2 | 46.577 |
| 30 | Target | 15 | 8 | 9 | 6 | 10 | 8 | 1 | 48.317 |

Having collected our data, we next examine it for possible problems, such as missing values (Did we forget to record the number of brown M&Ms in any of our samples?), for errors introduced when we recorded the data (Is the decimal point recorded incorrectly

for any of the net weights?), or for unusual results (Is it really the case that this bag has only yellow M&M?). We also examine our data to identify interesting observations that we may wish to explore (It appears that most net weights are greater than the net weight listed on the individual packages. Why might this be? Is the difference significant?) When our data set is small we usually can identify possible problems and interesting observations without much difficulty; however, for a large data set, this becomes a challenge. Instead of trying to examine individual values, we can look at our results visually. While it may be difficult to find a single, odd data point when we have to individually review 1000 samples, it often jumps out when we look at the data using one or more of the approaches we will explore in this chapter.

## Dot Plots

A dot plot displays data for one variable, with each sample's value plotted on the *x*-axis. The individual points are organized along the *y*-axis with the first sample at the bottom and the last sample at the top. Figure 35.1.1 shows a dot plot for the number of brown M&Ms in the 30 bags of M&Ms from Table 35.1.2. The distribution of points appears random as there is no correlation between the sample id and the number of brown M&Ms. We would be surprised if we discovered that the points were arranged from the lower-left to the upper-right as this implies that the order in which we open the bags determines whether they have many or a few brown M&Ms.

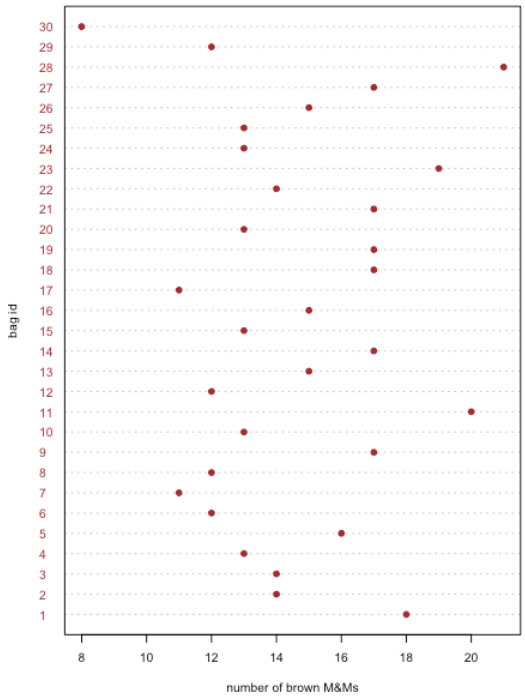



Figure 35.1.1: Dot plot for the brown M&Ms in each of the 30 bags included in Table 35.1.2.

## Stripcharts

A dot plot provides a quick way to give us confidence that our data are free from unusual patterns, but at the cost of space because we use the *y*-axis to include the sample id as a variable. A stripchart uses the same *x*-axis as a dot plot, but does not use the *y*-axis to distinguish between samples. Because all samples with the same number of brown M&Ms will appear in the same place—making it impossible to distinguish them from each other—we stack the points vertically to spread them out, as shown in Figure 35.1.2.

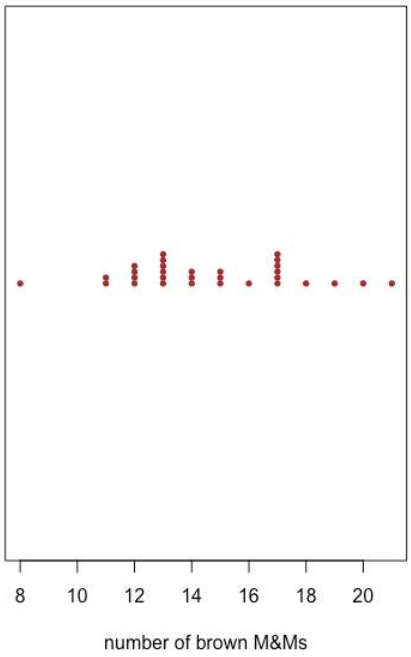



Figure 35.1.2: Stripchart for the brown M&Ms in each of the 30 bags included in Table 35.1.2.

Both the dot plot in Figure 35.1.1 and the stripchart in Figure 35.1.2 suggest that there is a smaller density of points at the lower limit and the upper limit of our results. We see, for example, that there is just one bag each with 8, 16, 18, 19, 20, and 21 brown M&Ms, but there are six bags each with 13 and 17 brown M&Ms.

Because a stripchart does not use the *y*-axis to provide meaningful categorical information, we can easily display several stripcharts at once. Figure 35.1.3 shows this for the data in Table 35.1.2. Instead of stacking the individual points, we jitter them by applying a small, random offset to each point. Among the things we learn from this stripchart are that only brown and yellow M&Ms have counts of greater than 20 and that only blue and green M&Ms have counts of three or fewer M&Ms.

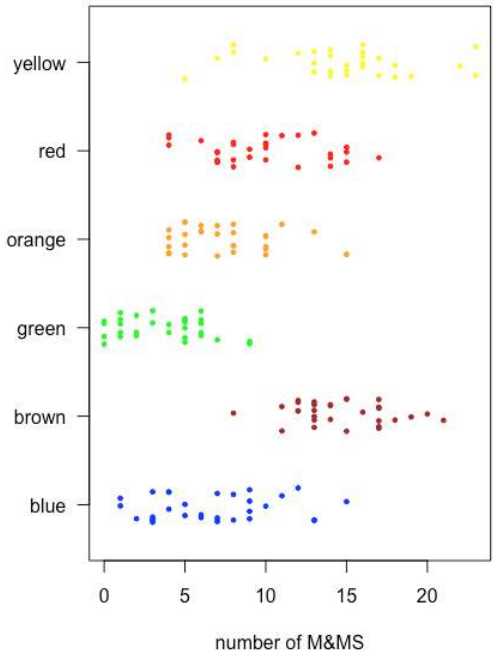



Figure 35.1.3: Stripcharts for each color of M&Ms in each of the 30 bags included in Table 35.1.2.

## Box and Whisker Plots

The stripchart in Figure 35.1.3 is easy for us to examine because the number of samples, 30 bags, and the number of M&Ms per bag is sufficiently small that we can see the individual points. As the density of points becomes greater, a stripchart becomes less useful. A box and whisker plot provides a similar view but focuses on the data in terms of the range of values that encompass the middle 50% of the data.

Figure 35.1.4 shows the box and whisker plot for brown M&Ms using the data in Table 35.1.2. The 30 individual samples are superimposed as a stripchart. The central box divides the *x*-axis into three regions: bags with fewer than 13 brown M&Ms (seven samples), bags with between 13 and 17 brown M&Ms (19 samples), and bags with more than 17 brown M&Ms (four samples). The box's limits are set so that it includes at least the middle 50% of our data. In this case, the box contains 19 of the 30 samples (63%) of the bags, because moving either end of the box toward the middle results in a box that includes less than 50% of the samples. The difference between the box's upper limit (19) and its lower limit (13) is called the interquartile range (IQR). The thick line in the box is the median, or middle value (more on this and the IQR in the next chapter). The dashed lines at either end of the box are called whiskers, and they extend to the largest or the smallest result that is within $\pm 1.5 \times \text{IQR}$ of the box's right or left edge, respectively.

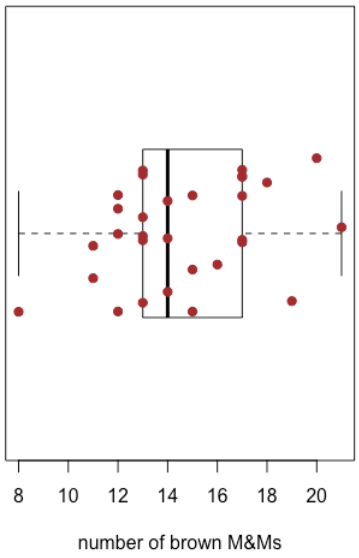



Figure 35.1.4: Box-and-whisker plot for the brown M&Ms in each of the 30 bags included in Table 35.1.2 showing individual samples as a jittered stripchart.

Because a box and whisker plot does not use the *y*-axis to provide meaningful categorical information, we can easily display several plots in the same frame. Figure 35.1.5 shows this for the data in Table 35.1.2. Note that when a value falls outside of a whisker, as is the case here for yellow M&Ms, it is flagged by displaying it as an open circle.

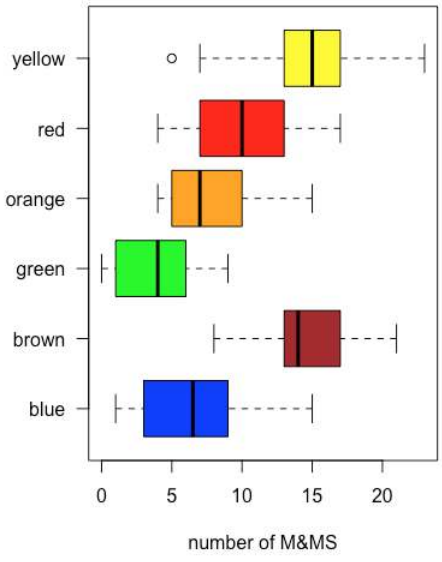



Figure 35.1.5: Box-and-whisker plots for each of the 30 bags included in Table 35.1.2 organized by color.

One use of a box and whisker plot is to examine the distribution of the individual samples, particularly with respect to symmetry. With the exception of the single sample that falls outside of the whiskers, the distribution of yellow M&Ms appears symmetrical: the median is near the center of the box and the whiskers extend equally in both directions. The distribution of the orange M&Ms is asymmetrical: half of the samples have 4–7 M&Ms (just four possible outcomes) and half have 7–15 M&Ms (nine possible outcomes), suggesting that the distribution is skewed toward higher numbers of orange M&Ms (see Chapter 5 for more information about the distribution of samples).

Figure 35.1.6 shows box-and-whisker plots for yellow M&Ms grouped according to the store where the bags of M&Ms were purchased. Although the box and whisker plots are quite different in terms of the relative sizes of the boxes and the relative length of the whiskers, the dot plots suggest that the distribution of the underlying data is relatively similar in that most bags contain 12–18 yellow M&Ms and just a few bags deviate from these limits. These observations are reassuring because we do not expect the choice of store to affect the composition of bags of M&Ms. If we saw evidence that the choice of store affected our results, then we would look more closely at the bags themselves for evidence of a poorly controlled variable, such as type (Did we accidentally purchase bags of peanut butter M&Ms from one store?) or the product's lot number (Did the manufacturer change the composition of colors between lots?).

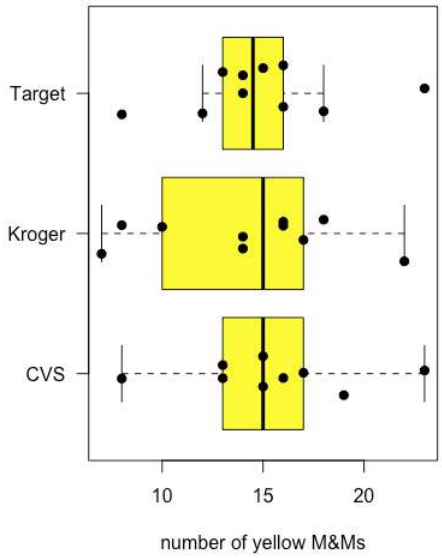



Figure 35.1.6: Box-and-whisker plots for yellow M&Ms for each of the 30 bag in Table 35.1.2 organized by the store where the bags were purchased.

## Bar Plots

Although a dot plot, a stripchart and a box-and-whisker plot provide some qualitative evidence of how a variable's values are distributed—we will have more to say about the distribution of data in Chapter 5—they are less useful when we need a more quantitative picture of the distribution. For this we can use a bar plot that displays a count of each discrete outcome. Figure 35.1.7 shows bar plots for orange and for yellow M&Ms using the data in Table 35.1.2.

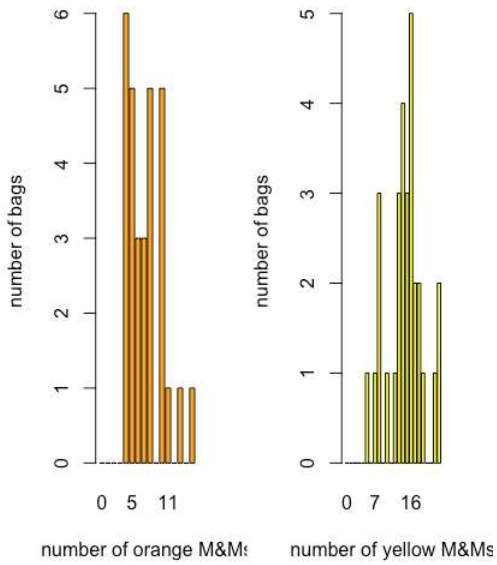



Figure 35.1.7: Bar plots for orange M&Ms and yellow M&Ms using the data in Table 35.1.2.

Here we see that the most common number of orange M&Ms per bag is four, which is also the smallest number of orange M&Ms per bag, and that there is a general decrease in the number of bags as the number of orange M&M per bag increases. For the yellow M&Ms, the most common number of M&Ms per bag is 16, which falls near the middle of the range of yellow M&Ms.

## Histograms

A bar plot is a useful way to look at the distribution of discrete results, such as the counts of orange or yellow M&Ms, but it is not useful for continuous data where each result is unique. A histogram, in which we display the number of results that fall within a sequence of equally spaced bins, provides a view that is similar to that of a bar plot but that works with continuous data. Figure 35.1.8, for example, shows a histogram for the net weights of the 30 bags of M&Ms in Table 35.1.2. Individual values are shown by the vertical hash marks at the bottom of the histogram.

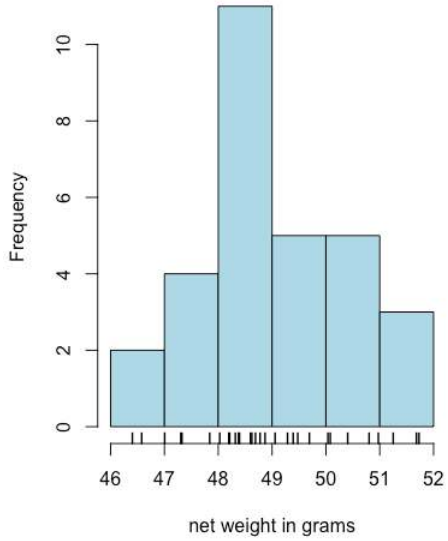



Figure 35.1.8: Histogram of net weights for the data in Table 35.1.2. There are, for example, four bags of M&Ms with net weights between 47 g and 48 g.

## Summarizing Data

In the last section we used data collected from 30 bags of M&Ms to explore different ways to visualize data. In this section we consider several ways to summarize data using the net weights of the same bags of M&Ms. Here is the raw data.

Table 35.1.3: Net Weights for 30 Bags of M&Ms.

| | | | | | |
|---|---|---|---|---|---|
| 49.287 | 48.870 | 51.250 | 48.692 | 48.777 | 46.405 |
| 49.693 | 49.391 | 48.196 | 47.326 | 50.974 | 50.081 |
| 47.841 | 48.377 | 47.004 | 50.037 | 48.599 | 48.625 |
| 48.395 | 51.730 | 50.405 | 47.305 | 49.477 | 48.027 |
| 48.212 | 51.682 | 50.802 | 49.055 | 46.577 | 48.317 |

Without completing any calculations, what conclusions can we make by just looking at this data? Here are a few:

- All net weights are greater than 46 g and less than 52 g.
- As we see in Figure 35.1.9, a box-and-whisker plot (overlaid with a stripchart) and a histogram suggest that the distribution of the net weights is reasonably symmetric.
- The absence of any points beyond the whiskers of the box-and-whisker plot suggests that there are no unusually large or unsually small net weights.

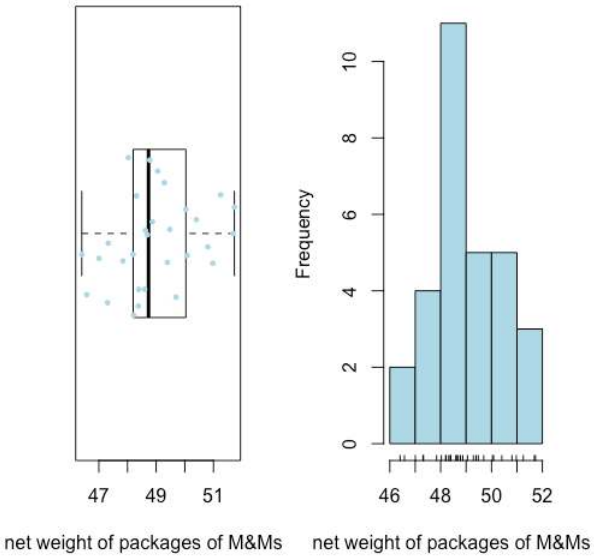



Figure 35.1.9: Two visualizations of the net weights of packages of M&Ms.

Both visualizations provide a good qualitative picture of the data, suggesting that the individual results are scattered around some central value with more results closer to that central value that at distance from it. Neither visualization, however, describes the data quantitatively. What we need is a convenient way to summarize the data by reporting where the data is centered and how varied the individual results are around that center.

## Where is the Center?

There are two common ways to report the center of a data set: the mean and the median.

The mean, $\overline{Y}$, is the numerical average obtained by adding together the results for all *n* observations and dividing by the number of observations

$$\overline{Y} = \frac{\sum_{i=1}^{n} Y_i}{n} = \frac{49.287 + 48.870 + \cdots + 48.317}{30} = 48.980 \text{ g}$$

The median, $\widetilde{Y}$, is the middle value after we order our observations from smallest-to-largest, as we show here for our data.

Table 35.1.4: The data from Table 35.1.3 Sorted From Smallest-to-Largest in Value.

| | | | | | |
|---|---|---|---|---|---|
| 46.405 | 46.577 | 47.004 | 47.305 | 47.326 | 47.841 |
| 48.027 | 48.196 | 48.212 | 48.317 | 48.377 | 48.395 |
| 48.599 | 48.625 | 48.692 | 48.777 | 48.870 | 49.055 |
| 49.287 | 49.391 | 49.477 | 49.693 | 50.037 | 50.081 |
| 50.405 | 50.802 | 50.974 | 51.250 | 51.682 | 51.730 |

If we have an odd number of samples, then the median is simply the middle value, or

$$\widetilde{Y} = Y_{\frac{n+1}{2}}$$

where *n* is the number of samples. If, as is the case here, *n* is even, then

$$\widetilde{Y} = \frac{Y_{\frac{n}{2}} + Y_{\frac{n}{2}+1}}{2} = \frac{48.692 + 48.777}{2} = 48.734 \text{ g}$$

When our data has a symmetrical distribution, as we believe is the case here, then the mean and the median will have similar values.

## What is the Variation of the Data About the Center?

There are five common measures of the variation of data about its center: the variance, the standard deviation, the range, the interquartile range, and the median average difference.

The variance, $s^2$, is an average squared deviation of the individual observations relative to the mean

$$s^2 = \frac{\sum_{i=1}^{n}\left(Y_i - \overline{Y}\right)^2}{n-1} = \frac{\left(49.287 - 48.980\right)^2 + \cdots + \left(48.317 - 48.980\right)^2}{30-1} = 2.052$$

and the standard deviation, *s*, is the square root of the variance, which gives it the same units as the mean.

$$s = \sqrt{\frac{\sum_{i=1}^{n}\left(Y_i - \overline{Y}\right)^2}{n-1}} = \sqrt{\frac{\left(49.287 - 48.980\right)^2 + \cdots + \left(48.317 - 48.980\right)^2}{30-1}} = 1.432$$

The range, *w*, is the difference between the largest and the smallest value in our data set.

$$w = 51.730 \text{ g} - 46.405 \text{ g} = 5.325 \text{ g}$$

The interquartile range, *IQR*, is the difference between the median of the bottom 25% of observations and the median of the top 25% of observations; that is, it provides a measure of the range of values that spans the middle 50% of observations. There is no single, standard formula for calculating the *IQR*, and different algorithms yield slightly different results. We will adopt the algorithm described here:

1. Divide the sorted data set in half; if there is an odd number of values, then remove the median for the complete data set. For our data, the lower half is

Table 35.1.5: The Lower Half of the Data in Table 35.1.4.

| | | | | |
|---|---|---|---|---|
| 46.405 | 46.577 | 47.004 | 47.305 | 47.326 |
| 47.841 | 48.027 | 48.196 | 48.212 | 48.317 |
| 48.377 | 48.395 | 48.599 | 48.625 | 48.692 |

and the upper half is

Table 35.1.6: The Upper Half of the Data in Table 35.1.4.

| | | | | |
|---|---|---|---|---|
| 48.777 | 48.870 | 49.055 | 49.287 | 49.391 |
| 49.477 | 49.693 | 50.037 | 50.081 | 50.405 |
| 50.802 | 50.974 | 51.250 | 51.682 | 51.730 |

2. Find $F_L$, the median for the lower half of the data, which for our data is 48.196 g.

3. Find $F_U$ , the median for the upper half of the data, which for our data is 50.037 g.

4. The *IQR* is the difference between $F_U$ and $F_L$.

$$F_U - F_L = 50.037 \text{ g} - 48.196 \text{ g} = 1.841 \text{ g}$$

The median absolute deviation, *MAD*, is the median of the absolute deviations of each observation from the median of all observations. To find the *MAD* for our set of 30 net weights, we first subtract the median from each sample in Table 35.1.3.

Table 35.1.7: The Results of Subtracting the Median From Each Value in Table 35.1.3.

| | | | | | |
|---|---|---|---|---|---|
| 0.5525 | 0.1355 | 2.5155 | -0.0425 | 0.0425 | -2.3295 |
| 0.9585 | 0.6565 | -0.5385 | -1.4085 | 2.2395 | 1.3465 |
| -0.8935 | -0.3575 | -1.7305 | 1.3025 | -0.1355 | -0.1095 |
| -0.3395 | 2.9955 | 1.6705 | -1.4295 | 0.7425 | -0.7075 |
| -0.5225 | 2.9475 | 2.0675 | 0.3205 | -2.1575 | -0.4175 |

Next we take the absolute value of each difference and sort them from smallest-to-largest.

Table 35.1.8: The Data in Table 35.1.7 After Taking the Absolute Value.

| | | | | | |
|---|---|---|---|---|---|
| 0.0425 | 0.0425 | 0.1095 | 0.1355 | 0.1355 | 0.3205 |
| 0.3395 | 0.3575 | 0.4175 | 0.5225 | 0.5385 | 0.5525 |
| 0.6565 | 0.7075 | 0.7425 | 0.8935 | 0.9585 | 1.3025 |
| 1.3465 | 1.4085 | 1.4295 | 1.6705 | 1.7305 | 2.0675 |
| 2.1575 | 2.2395 | 2.3295 | 2.5155 | 2.9475 | 2.9955 |

Finally, we report the median for these sorted values as

$$\frac{0.7425 + 0.8935}{2} = 0.818$$

## Robust vs. Non-Robust Measures of The Center and Variation About the Center

A good question to ask is why we might desire more than one way to report the center of our data and the variation in our data about the center. Suppose that the result for the last of our 30 samples was reported as 483.17 instead of 48.317. Whether this is an accidental shifting of the decimal point or a true result is not relevant to us here; what matters is its effect on what we report. Here is a summary of the effect of this one value on each of our ways of summarizing our data.

Table 35.1.9: Effect on Summary Statistics of Changing Last Value in Table 35.1.3 From 48.317 g to 483.17 g.

| statistic | original data | new data |
|---|---|---|
| mean | 48.980 | 63.475 |
| median | 48.734 | 48.824 |
| variance | 2.052 | 6285.938 |
| standard deviation | 1.433 | 79.280 |
| range | 5.325 | 436.765 |
| *IQR* | 1.841 | 1.885 |
| *MAD* | 0.818 | 0.926 |

Note that the mean, the variance, the standard deviation, and the range are very sensitive to the change in the last result, but the median, the *IQR*, and the *MAD* are not. The median, the *IQR*, and the *MAD* are considered robust statistics because they are less sensitive to an unusual result; the others are, of course, non-robust statistics. Both types of statistics have value to us, a point we will return to from time-to-time.

## The Distribution of Data

When we measure something, such as the percentage of yellow M&Ms in a bag of M&Ms, we expect two things:

- that there is an underlying “true” value that our measurements should approximate, and
- that the results of individual measurements will show some variation about that "true" value

Visualizations of data—such as dot plots, stripcharts, boxplot-and-whisker plots, bar plots, histograms, and scatterplots—often suggest there is an underlying structure to our data. For example, we have seen that the distribution of yellow M&Ms in bags of M&Ms is more or less symmetrical around its median, while the distribution of orange M&Ms was skewed toward higher values. This underlying structure, or distribution, of our data as it effects how we choose to analyze our data. In this chapter we will take a closer look at several ways in which data are distributed.

### Terminology

Before we consider different types of distributions, let's define some key terms. You may wish, as well, to review the discussion of different types of data in Chapter 2.

### Populations and Samples

A population includes every possible measurement we could make on a system, while a sample is the subset of a population on which we actually make measurements. These definitions are fluid. A single bag of M&Ms is a population if we are interested only in that specific bag, but it is but one sample from a box that contains a gross (144) of individual bags. That box, itself, can be a population, or it can be one sample from a much larger production lot. And so on.

### Discrete Distributions and Continuous Distributions

In a discrete distribution the possible results take on a limited set of specific values that are independent of how we make our measurements. When we determine the number of yellow M&Ms in a bag, the results are limited to integer values. We may find 13 yellow M&Ms or 24 yellow M&Ms, but we cannot obtain a result of 15.43 yellow M&Ms.

For a continuous distribution the result of a measurement can take on any possible value between a lower limit and an upper limit, even though our measuring device has a limited precision; thus, when we weigh a bag of M&Ms on a three-digit balance and obtain a result of 49.287 g we know that its true mass is greater than 49.2865... g and less than 49.2875... g.

### Theoretical Models for the Distribution of Data

There are four important types of distributions that we will consider in this chapter: the uniform distribution, the binomial distribution, the Poisson distribution, and the normal, or Gaussian, distribution. In the previous sections we used the analysis of bags of M&Ms to explore ways to visualize data and to summarize data. Here we will use the same data set to explore the distribution of data.

### Uniform Distribution

In a uniform distribution, all outcomes are equally probable. Suppose the population of M&Ms has a uniform distribution. If this is the case, then, with six colors, we expect each color to appear with a probability of 1/6 or 16.7%. Figure 35.1.10 shows a comparison of the theoretical results if we draw 1699 M&Ms—the total number of M&Ms in our sample of 30 bags—from a population with a uniform distribution (on the left) to the actual distribution of the 1699 M&Ms in our sample (on the right). It seems unlikely that the population of M&Ms has a uniform distribution of colors!

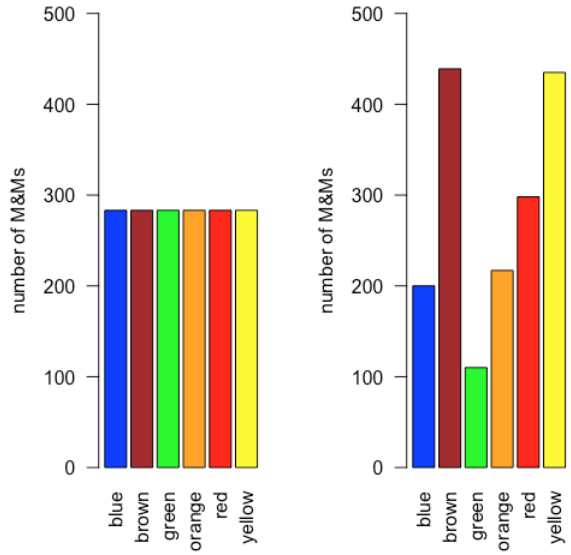



Figure 35.1.10: Comparison of (on the left) a uniform distribution of 1699 M&Ms with (on the right) the actual distribution from the data that make up the sample in Table $PageIndex2$.

## Binomial Distribution

A binomial distribution shows the probability of obtaining a particular result in a fixed number of trials, where the odds of that result happening in a single trial are known. Mathematically, a binomial distribution is defined by the equation

$$P(X,N) = \frac{N!}{X!(N-X)!} \times p^X \times (1-p)^{N-X}$$

where *P*(*X*,*N*) is the probability that the event happens *X* times in *N* trials, and where *p* is the probability that the event happens in a single trial. The binomial distribution has a theoretical mean, $\mu$, and a theoretical variance, $\sigma^2$, of

$$\mu = Np \qquad \sigma^2 = Np(1-p)$$

Figure 35.1.11 compares the expected binomial distribution for drawing 0, 1, 2, 3, 4, or 5 yellow M&Ms in the first five M&Ms—assuming that the probability of drawing a yellow M&M is 435/1699, the ratio of the number of yellow M&Ms and the total number of M&Ms—to the actual distribution of results. The similarity between the theoretical and the actual results seems evident; in a later section we will consider ways to test this claim.

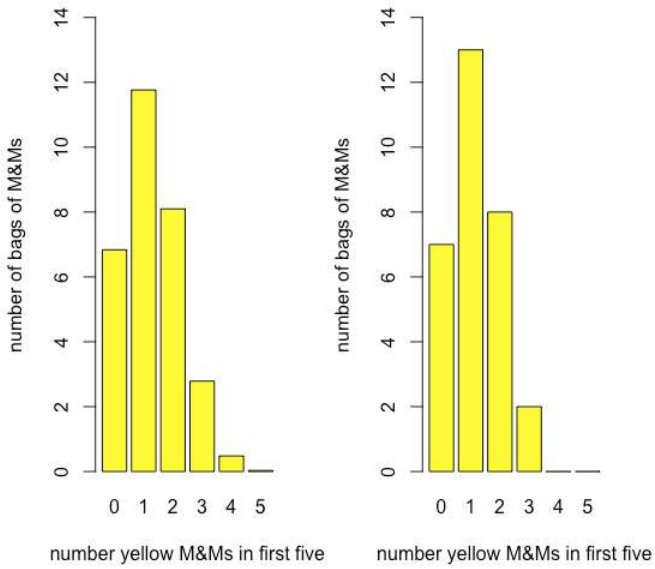



Figure 35.1.11: Comparison of (on the left) the theoretical binomial distribution of yellow M&Ms in the first five selected from a bag of M&Ms and (on the right) the actual distribution of M&Ms.

## Poisson Distribution

The binomial distribution is useful if we wish to model the probability of finding a fixed number of yellow M&Ms in a sample of M&Ms of fixed size—such as the first five M&Ms that we draw from a bag—but not the probability of finding a fixed number of yellow M&Ms in a single bag because there is some variability in the total number of M&Ms per bag.

A Poisson distribution gives the probability that a given number of events will occur in a fixed interval in time or space if the event has a known average rate and if each new event is independent of the preceding event. Mathematically a Poisson distribution is defined by the equation

$$P(X,\lambda) = \frac{e^{-\lambda}\lambda^{X}}{X!}$$

where $P(X,\lambda)$ is the probability that an event happens $X$ times given the event's average rate, $\lambda$. The Poisson distribution has a theoretical mean, $\mu$, and a theoretical variance, $\sigma^2$, that are each equal to $\lambda$.

The bar plot in Figure 35.1.12 shows the actual distribution of green M&Ms in 35 small bags of M&Ms (as reported by M. A. Xu-Friedman "Illustrating concepts of quantal analysis with an intuitive classroom model," Adv. Physiol. Educ. **2013**, *37*, 112–116). Superimposed on the bar plot is the theoretical Poisson distribution based on their reported average rate of 3.4 green M&Ms per bag. The similarity between the theoretical and the actual results seems evident; in Chapter 6 we will consider ways to test this claim.

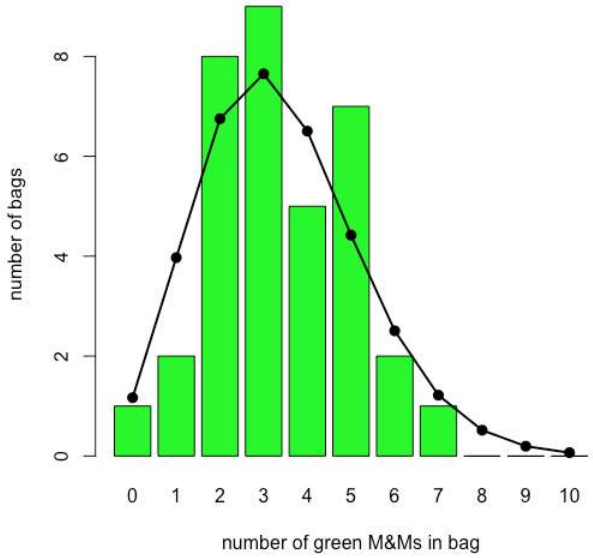



Figure 35.1.12: Comparison of a Poisson distribution for green M&Ms (dots and line) to experimental results (bars). The data are from M. A. Xu-Friedman, "Illustrating concepts of quantal analysis with an intuitive classroom model," Adv. Physiol. Educ. **2013**, *37*, 112–116.

## Normal Distribution

A uniform distribution, a binomial distribution, and a Poisson distribution predict the probability of a discrete event, such as the probability of finding exactly two green M&Ms in the next bag of M&Ms that we open. Not all of the data we collect is discrete. The net weights of bags of M&Ms is an example of continuous data as the mass of an individual bag is not restricted to a discrete set of allowed values. In many cases we can model continuous data using a normal (or Gaussian) distribution, which gives the probability of obtaining a particular outcome, $P(x)$, from a population with a known mean, $\mu$, and a known variance, $\sigma^2$. Mathematically a normal distribution is defined by the equation

$$P(x) = \frac{1}{\sqrt{2\pi\sigma^2}} e^{-(x-\mu)^2/(2\sigma^2)}$$

Figure 35.1.13 shows the expected normal distribution for the net weights of our sample of 30 bags of M&Ms if we assume that their mean, $\overline{X}$, of 48.98 g and standard deviation, $s$, of 1.433 g are good predictors of the population's mean, $\mu$, and standard deviation, $\sigma$. Given the small sample of 30 bags, the agreement between the model and the data seems reasonable.

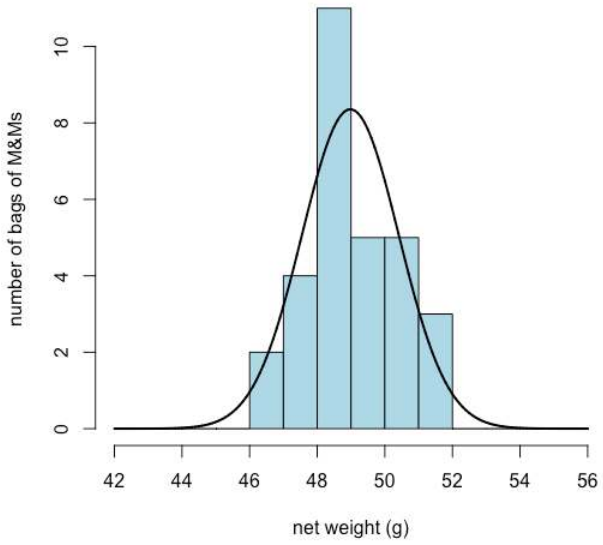



Figure 35.1.13: Comparison of a normal distribution for the net weights of M&Ms (line) to the experimental results (bars).

## The Central Limit Theorem

Suppose we have a population for which one of its properties has a uniform distribution where every result between 0 and 1 is equally probable. If we analyze 10,000 samples we should not be surprised to find that the distribution of these 10000 results looks uniform, as shown by the histogram on the left side of Figure 35.1.14. If we collect 1000 pooled samples—each of which consists of 10 individual samples for a total of 10,000 individual samples—and report the average results for these 1000 pooled samples, we see something interesting as their distribution, as shown by the histogram on the right, looks remarkably like a normal distribution. When we draw single samples from a uniform distribution, each possible outcome is equally likely, which is why we see the distribution on the left. When we draw a pooled sample that consists of 10 individual samples, however, the average values are more likely to be near the middle of the distribution's range, as we see on the right, because the pooled sample likely includes values drawn from both the lower half and the upper half of the uniform distribution.

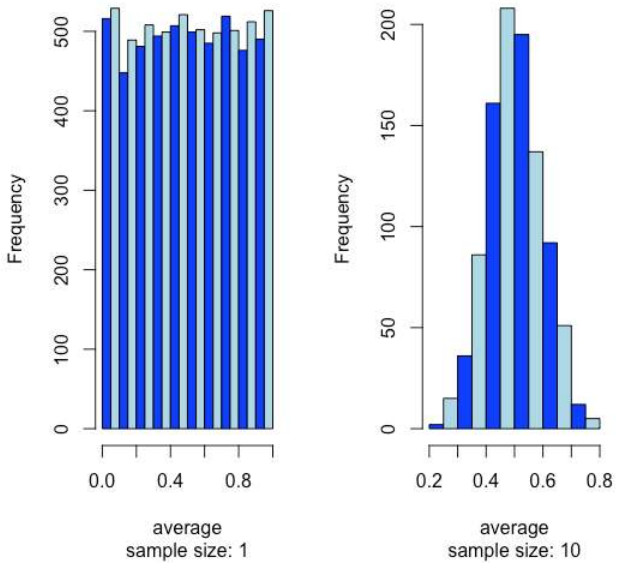



Figure 35.1.14: Distribution of results when analyzing samples of size $n$ = 1 (left) and samples of size $n$ = 10 (right) drawn from a uniform distribution.

This tendency for a normal distribution to emerge when we pool samples is known as the central limit theorem. As shown in Figure 35.1.15, we see a similar effect with populations that follow a binomial distribution or a Poisson distribution.

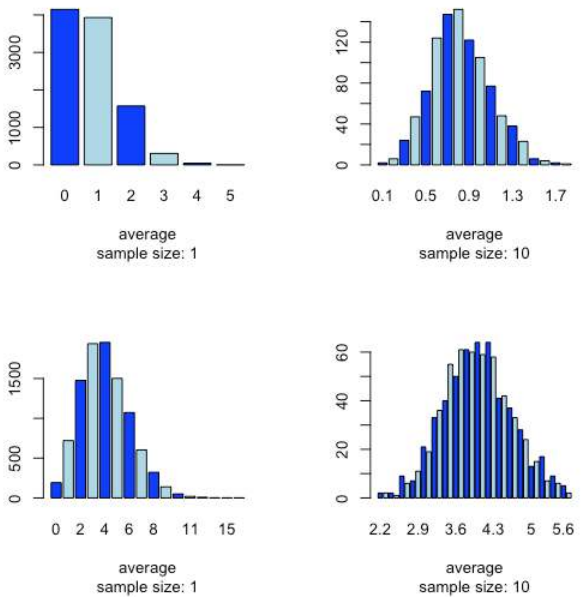



Figure 35.1.15: Distribution of results when analyzing samples of size $n = 1$ (left) and samples of size $n = 10$ (right) drawn from a binomial distribution with $p$ = 0.167 (top) and a Poisson distribution with $\lambda = 4$ (bottom).

You might reasonably ask whether the central limit theorem is important as it is unlikely that we will complete 1000 analyses, each of which is the average of 10 individual trials. This is deceiving. When we acquire a sample of soil, for example, it consists of many individual particles each of which is an individual sample of the soil. Our analysis of this sample, therefore, is the mean for a large number of individual soil particles. Because of this, the central limit theorem is relevant.


https://chem.libretexts.org/@go/page/363066

## Uncertainty of Data

In the last section we examined four ways in which the individual samples we collect and analyze are distributed about a central value: a uniform distribution, a binomial distribution, a Poisson distribution, and a normal distribution. We also learned that regardless of how individual samples are distributed, the distribution of averages for multiple samples often follows a normal distribution. This tendency for a normal distribution to emerge when we report averages for multiple samples is known as the central limit theorem. In this chapter we look more closely at the normal distribution—examining some of its properties—and consider how we can use these properties to say something more meaningful about our data than simply reporting a mean and a standard deviation.

### Properties of a Normal Distribution

Mathematically a normal distribution is defined by the equation

$$P(x) = \frac{1}{\sqrt{2\pi\sigma^2}} e^{-(x-\mu)^2/(2\sigma^2)}$$

where $P(x)$ is the probability of obtaining a result, $x$, from a population with a known mean, $\mu$, and a known standard deviation, $\sigma$. Figure 35.1.16 shows the normal distribution curves for $\mu = 0$ with standard deviations of 5, 10, and 20.

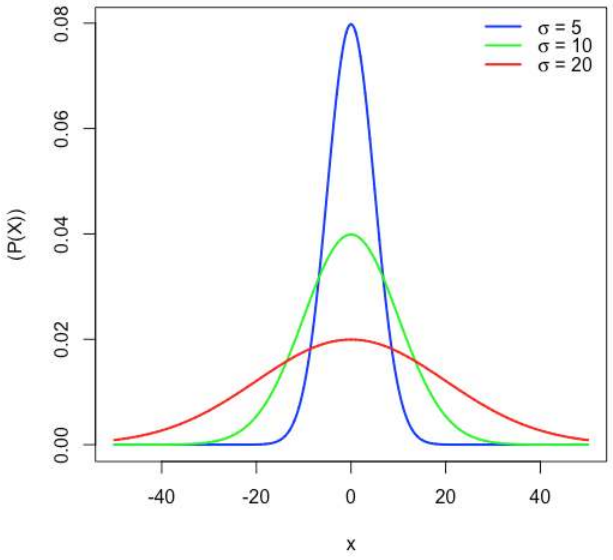



Figure 35.1.16: Three examples of normal distribution curves. Although the height and width are affected by $\sigma$, the area under each curve is the same.

Because the equation for a normal distribution depends solely on the population's mean, $\mu$, and its standard deviation, $\sigma$, the probability that a sample drawn from a population has a value between any two arbitrary limits is the same for all populations. For example, Figure 35.1.17 shows that 68.26% of all samples drawn from a normally distributed population have values within the range $\mu \pm 1\sigma$, and only 0.14% have values greater than $\mu + 3\sigma$.

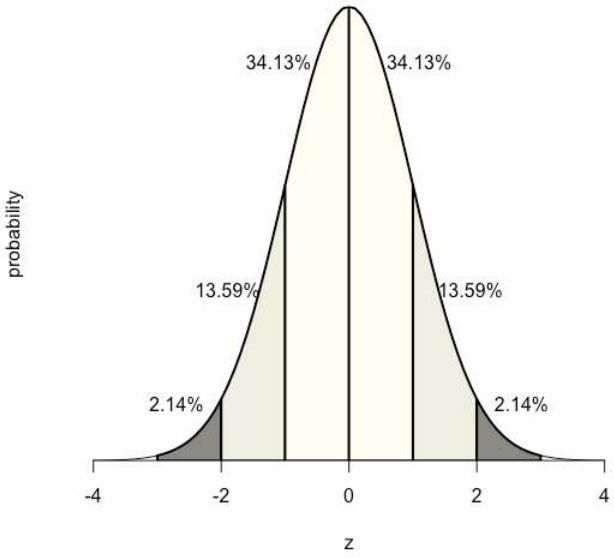



Figure 35.1.17: Normal distribution curve for $\mu = 0$ and $\sigma = 1$ showing area under the curve for various values of $z$ in $\mu \pm z\sigma$.

This feature of a normal distribution—that the area under the curve is the same for all values of $\sigma$—allows us to create a probability table (see Appendix 2) based on the relative deviation, $z$, between a limit, $x$, and the mean, $\mu$.

$$z = \frac{x - \mu}{\sigma}$$

The value of $z$ gives the area under the curve between that limit and the distribution's closest tail, as shown in Figure 35.1.18.

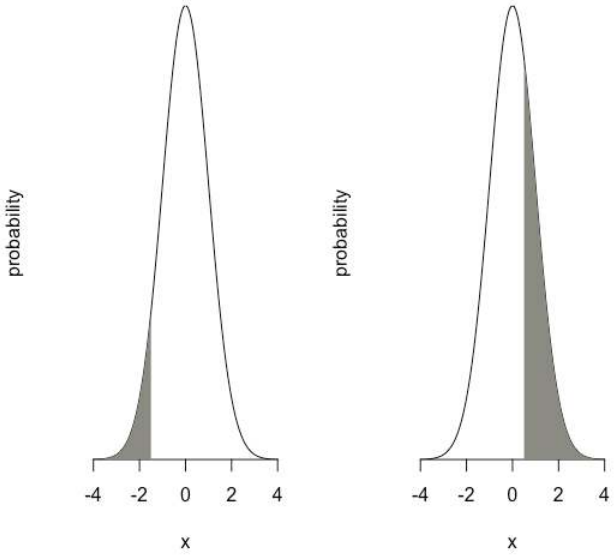



Figure 35.1.18: Normal distribution curve for $\mu = 0$ and $\sigma = 1$ showing (on the left) the area under the curve for $z = -1.5$ and (on the right for $z = +0.5$.


https://chem.libretexts.org/@go/page/363066

## Example 35.1.1

Suppose we know that $\mu$ is 5.5833 ppb Pb and that $\sigma$ is 0.0558 ppb Pb for a particular standard reference material (SRM). What is the probability that we will obtain a result that is greater than 5.650 ppb if we analyze a single, random sample drawn from the SRM?

### Solution

Figure 35.1.19 shows the normal distribution curve given values of 5.5833 ppb Pb for $\mu$ and of 0.0558 ppb Pb $\sigma$. The shaded area in the figures is the probability of obtaining a sample with a concentration of Pb greater than 5.650 ppm. To determine the probability, we first calculate $z$

$$z = \frac{x - \mu}{\sigma} = \frac{5.650 - 5.5833}{0.0558} = 1.195$$

Next, we look up the probability in Appendix 2 for this value of $z$, which is the average of 0.1170 (for $z = 1.19$) and 0.1151 (for $z = 1.20$), or a probability of 0.1160; thus, we expect that 11.60% of samples will provide a result greater than 5.650 ppb Pb.

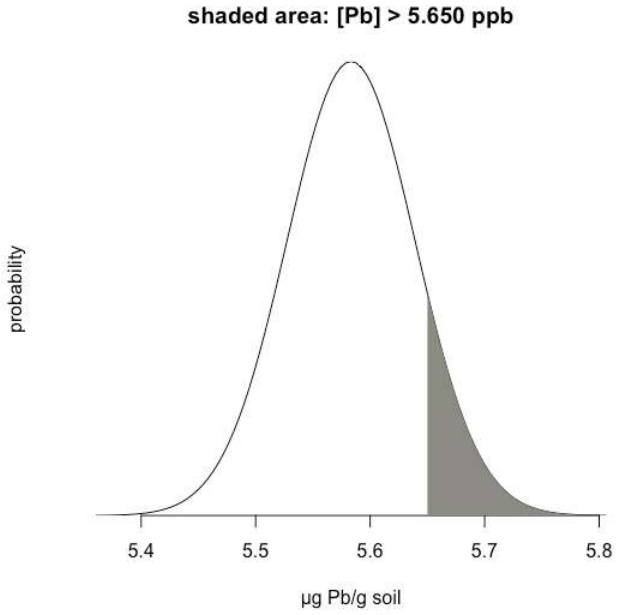



Figure 35.1.19: Normal distribution curve for the amount of lead in a standard reference with $\mu = 5.5833$ ppb and $\sigma = 0.0558$ ppb. The shaded area shows those results for which the concentration of lead exceeds 5.650 ppb.

## Example 35.1.2

Example 35.1.1 considers a single limit—the probability that a result exceeds a single value. But what if we want to determine the probability that a sample has between 5.580 g Pb and 5.625 g Pb?

### Solution

In this case we are interested in the shaded area shown in Figure 35.1.20. First, we calculate $z$ for the upper limit

$$z = \frac{5.625 - 5.5833}{0.0558} = 0.747$$

and then we calculate $z$ for the lower limit

$$z = \frac{5.580 - 5.5833}{0.0558} = -0.059$$

Then, we look up the probability in Appendix 2 that a result will exceed our upper limit of 5.625, which is 0.2275, or 22.75%, and the probability that a result will be less than our lower limit of 5.580, which is 0.4765, or 47.65%. The total unshaded area

is 71.4% of the total area, so the shaded area corresponds to a probability of

$$100.00 - 22.75 - 47.65 = 100.00 - 71.40 = 29.6\%$$

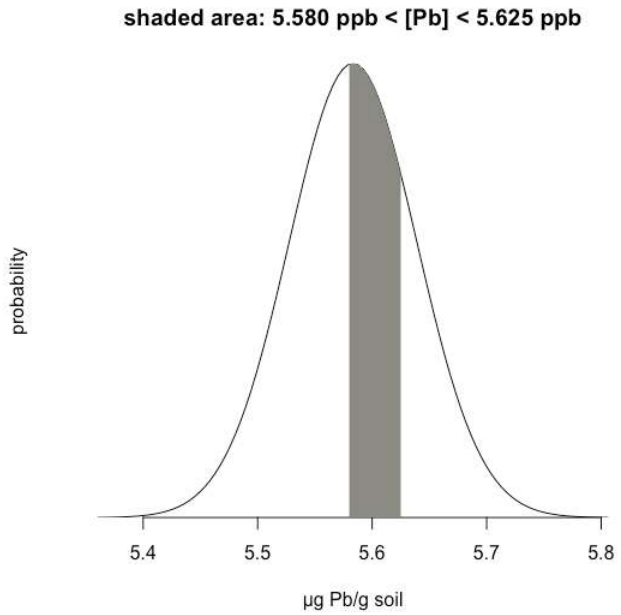



Figure 35.1.20: Normal distribution curve for the amount of lead in a standard reference with $\mu = 5.5833$ ppb and $\sigma = 0.0558$ ppb. The shaded area shows those results for which the concentration of lead is more than 5.580 ppb and less than 5.625 ppb.

## Confidence Intervals

In the previous section, we learned how to predict the probability of obtaining a particular outcome if our data are normally distributed with a known $\mu$ and a known $\sigma$. For example, we estimated that 11.60% of samples drawn at random from a standard reference material will have a concentration of Pb greater than 5.650 ppb given a $\mu$ of 5.5833 ppb and a $\sigma$ of 0.0558 ppb. In essence, we determined how many standard deviations 5.650 is from $\mu$ and used this to define the probability given the standard area under a normal distribution curve.

We can look at this in a different way by asking the following question: If we collect a single sample at random from a population with a known $\mu$ and a known $\sigma$, within what range of values might we reasonably expect to find the sample's result 95% of the time? Rearranging the equation

$$z = \frac{x - \mu}{\sigma}$$

and solving for $x$ gives

$$x = \mu \pm z\sigma = 5.5833 \pm (1.96)(0.0558) = 5.5833 \pm 0.1094$$

where a $z$ of 1.96 corresponds to 95% of the area under the curve; we call this a 95% confidence interval for a single sample.

It generally is a poor idea to draw a conclusion from the result of a single experiment; instead, we usually collect several samples and ask the question this way: If we collect $n$ random samples from a population with a known $\mu$ and a known $\sigma$, within what range of values might we reasonably expect to find the mean of these samples 95% of the time?

We might reasonably expect that the standard deviation for the mean of several samples is smaller than the standard deviation for a set of individual samples; indeed it is and it is given as

$$\sigma_{\bar{x}} = \frac{\sigma}{\sqrt{n}}$$

where $\frac{\sigma}{\sqrt{n}}$ is called the standard error of the mean. For example, if we collect three samples from the standard reference material described above, then we expect that the mean for these three samples will fall within a range

$$\bar{x} = \mu \pm z\sigma_{\bar{X}} = \mu \pm \frac{z\sigma}{\sqrt{n}} = 5.5833 \pm \frac{(1.96)(0.0558)}{\sqrt{3}} = 5.5833 \pm 0.0631$$

that is $\pm 0.0631$ ppb around $\mu$, a range that is smaller than that of $\pm 0.1094$ ppb when we analyze individual samples. Note that the relative value to us of increasing the sample's size diminishes as $n$ increases because of the square root term, as shown in Figure 35.1.21.

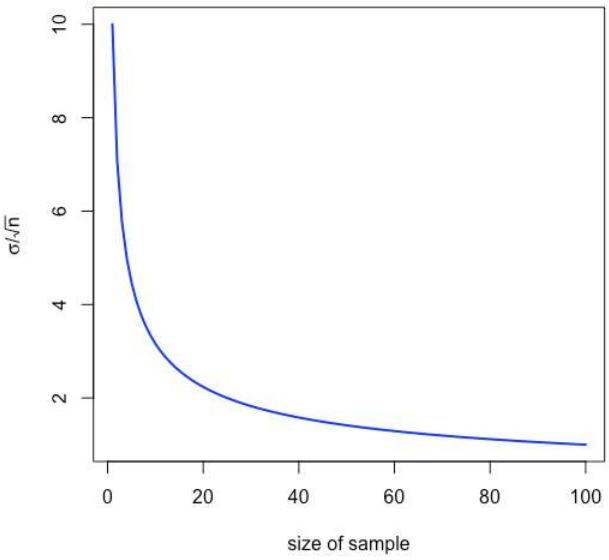



Figure 35.1.21: Plot showing how the standard error of the mean varies with the size of the sample. The value for $\sigma$ is 10.

Our treatment thus far assumes we know $\mu$ and $\sigma$ for the parent population, but we rarely know these values; instead, we examine samples drawn from the parent population and ask the following question: Given the sample's mean, $\bar{x}$, and its standard deviation, $s$, what is our best estimate of the population's mean, $\mu$, and its standard deviation, $\sigma$.

To make this estimate, we replace the population's standard deviation, $\sigma$, with the standard deviation, $s$, for our samples, replace the population's mean, $\mu$, with the mean, $\bar{x}$, for our samples, replace $z$ with $t$, where the value of $t$ depends on the number of samples, $n$

$$\bar{x} = \mu \pm \frac{ts}{\sqrt{n}}$$

and then rearrange the equation to solve for $\mu$.

$$\mu = \bar{x} \pm \frac{ts}{\sqrt{n}}$$

We call this a confidence interval. Values for $t$ are available in tables (see Appendix 3) and depend on the probability level, $\alpha$, where $(1 - \alpha) \times 100$ is the confidence level, and the degrees of freedom, $n - 1$; note that for any probability level, $t \longrightarrow z$ as $n \longrightarrow \infty$.

We need to give special attention to what this confidence interval means and to what it does not mean:

- It **does not** mean that there is a 95% probability that the population's mean is in the range $\mu = \bar{x} \pm ts$ because our measurements may be biased or the normal distribution may be inappropriate for our system.
- It **does provide** our best estimate of the population's mean, $\mu$ given our analysis of $n$ samples drawn at random from the parent population; a different sample, however, will give a different confidence interval and, therefore, a different estimate for $\mu$.

## Testing the Significance of Data

A confidence interval is a useful way to report the result of an analysis because it sets limits on the expected result. In the absence of determinate error, or bias, a confidence interval based on a sample's mean indicates the range of values in which we expect to find the population's mean. When we report a 95% confidence interval for the mass of a penny as 3.117 g ± 0.047 g, for example, we are stating that there is only a 5% probability that the penny's expected mass is less than 3.070 g or more than 3.164 g.

Because a confidence interval is a statement of probability, it allows us to consider comparative questions, such as these:

"Are the results for a newly developed method to determine cholesterol in blood significantly different from those obtained using a standard method?"

"Is there a significant variation in the composition of rainwater collected at different sites downwind from a coal-burning utility plant?"

In this chapter we introduce a general approach that uses experimental data to ask and answer such questions, an approach we call significance testing.

The reliability of significance testing recently has received much attention—see Nuzzo, R. "Scientific Method: Statistical Errors," *Nature*, **2014**, *506*, 150–152 for a general discussion of the issues—so it is appropriate to begin this chapter by noting the need to ensure that our data and our research question are compatible so that we do not read more into a statistical analysis than our data allows; see Leek, J. T.; Peng, R. D. "What is the Question? *Science*, **2015**, *347*, 1314-1315 for a useful discussion of six common research questions.

In the context of analytical chemistry, significance testing often accompanies an exploratory data analysis

"Is there a reason to suspect that there is a difference between these two analytical methods when applied to a common sample?"

or an inferential data analysis.

"Is there a reason to suspect that there is a relationship between these two independent measurements?"

A statistically significant result for these types of analytical research questions generally leads to the design of additional experiments that are better suited to making predictions or to explaining an underlying causal relationship. A significance test is the first step toward building a greater understanding of an analytical problem, not the final answer to that problem!

### Significance Testing

Let's consider the following problem. To determine if a medication is effective in lowering blood glucose concentrations, we collect two sets of blood samples from a patient. We collect one set of samples immediately before we administer the medication, and we collect the second set of samples several hours later. After we analyze the samples, we report their respective means and variances. How do we decide if the medication was successful in lowering the patient's concentration of blood glucose?

One way to answer this question is to construct a normal distribution curve for each sample, and to compare the two curves to each other. Three possible outcomes are shown in Figure 35.1.22. In Figure 35.1.22$a$, there is a complete separation of the two normal distribution curves, which suggests the two samples are significantly different from each other. In Figure 35.1.22$b$, the normal distribution curves for the two samples almost completely overlap each other, which suggests the difference between the samples is insignificant. Figure 35.1.22$c$, however, presents us with a dilemma. Although the means for the two samples seem different, the overlap of their normal distribution curves suggests that a significant number of possible outcomes could belong to either distribution. In this case the best we can do is to make a statement about the probability that the samples are significantly different from each other.

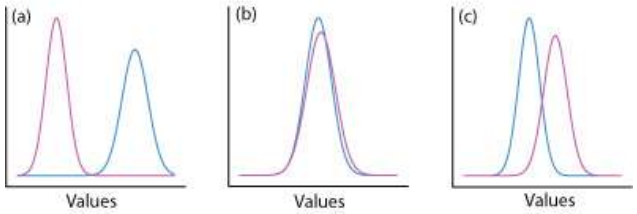



Figure 35.1.22: Three examples of the possible relationships between the normal distribution curves for two samples. In (a) the curves do not overlap, which suggests the samples are significantly different from each other. In (b) the two curves are almost identical, suggesting the samples are indistinguishable. The partial overlap of the curves in (c) means that the best we can do is evaluate the probability that there is a difference between the samples.

The process by which we determine the probability that there is a significant difference between two samples is called significance testing or hypothesis testing. Before we discuss specific examples let's first establish a general approach to conducting and interpreting a significance test.

## Constructing a Significance Test

The purpose of a significance test is to determine whether the difference between two or more results is sufficiently large that we are comfortable stating that the difference cannot be explained by indeterminate errors. The first step in constructing a significance test is to state the problem as a yes or no question, such as

"Is this medication effective at lowering a patient's blood glucose levels?"

A null hypothesis and an alternative hypothesis define the two possible answers to our yes or no question. The null hypothesis, $H_0$, is that indeterminate errors are sufficient to explain any differences between our results. The alternative hypothesis, $H_A$, is that the differences in our results are too great to be explained by random error and that they must be determinate in nature. We test the null hypothesis, which we either retain or reject. If we reject the null hypothesis, then we must accept the alternative hypothesis and conclude that the difference is significant.

Failing to reject a null hypothesis is not the same as accepting it. We retain a null hypothesis because we have insufficient evidence to prove it incorrect. It is impossible to prove that a null hypothesis is true. This is an important point and one that is easy to forget. To appreciate this point let's use this data for the mass of 100 circulating United States pennies.

Table 35.1.10. Masses for a Sample of 100 Circulating U. S. Pennies

| Penny | Weight (g) | Penny | Weight (g) | Penny | Weight (g) | Penny | Weight (g) |
|---|---|---|---|---|---|---|---|
| 1 | 3.126 | 26 | 3.073 | 51 | 3.101 | 76 | 3.086 |
| 2 | 3.140 | 27 | 3.084 | 52 | 3.049 | 77 | 3.123 |
| 3 | 3.092 | 28 | 3.148 | 53 | 3.082 | 78 | 3.115 |
| 4 | 3.095 | 29 | 3.047 | 54 | 3.142 | 79 | 3.055 |
| 5 | 3.080 | 30 | 3.121 | 55 | 3.082 | 80 | 3.057 |
| 6 | 3.065 | 31 | 3.116 | 56 | 3.066 | 81 | 3.097 |
| 7 | 3.117 | 32 | 3.005 | 57 | 3.128 | 82 | 3.066 |
| 8 | 3.034 | 33 | 3.115 | 58 | 3.112 | 83 | 3.113 |
| 9 | 3.126 | 34 | 3.103 | 59 | 3.085 | 84 | 3.102 |
| 10 | 3.057 | 35 | 3.086 | 60 | 3.086 | 85 | 3.033 |
| 11 | 3.053 | 36 | 3.103 | 61 | 3.084 | 86 | 3.112 |
| 12 | 3.099 | 37 | 3.049 | 62 | 3.104 | 87 | 3.103 |
| 13 | 3.065 | 38 | 2.998 | 63 | 3.107 | 88 | 3.198 |
| 14 | 3.059 | 39 | 3.063 | 64 | 3.093 | 89 | 3.103 |
| 15 | 3.068 | 40 | 3.055 | 65 | 3.126 | 90 | 3.126 |
| 16 | 3.060 | 41 | 3.181 | 66 | 3.138 | 91 | 3.111 |
| 17 | 3.078 | 42 | 3.108 | 67 | 3.131 | 92 | 3.126 |
| 18 | 3.125 | 43 | 3.114 | 68 | 3.120 | 93 | 3.052 |
| 19 | 3.090 | 44 | 3.121 | 69 | 3.100 | 94 | 3.113 |
| 20 | 3.100 | 45 | 3.105 | 70 | 3.099 | 95 | 3.085 |
| 21 | 3.055 | 46 | 3.078 | 71 | 3.097 | 96 | 3.117 |
| 22 | 3.105 | 47 | 3.147 | 72 | 3.091 | 97 | 3.142 |
| 23 | 3.063 | 48 | 3.104 | 73 | 3.077 | 98 | 3.031 |
| 24 | 3.083 | 49 | 3.146 | 74 | 3.178 | 99 | 3.083 |
| 25 | 3.065 | 50 | 3.095 | 75 | 3.054 | 100 | 3.104 |

After looking at the data we might propose the following null and alternative hypotheses.

$H_0$: The mass of a circulating U.S. penny is between 2.900 g and 3.200 g

$H_A$: The mass of a circulating U.S. penny may be less than 2.900 g or more than 3.200 g

To test the null hypothesis we find a penny and determine its mass. If the penny's mass is 2.512 g then we can reject the null hypothesis and accept the alternative hypothesis. Suppose that the penny's mass is 3.162 g. Although this result increases our confidence in the null hypothesis, it does not prove that the null hypothesis is correct because the next penny we sample might weigh less than 2.900 g or more than 3.200 g.

After we state the null and the alternative hypotheses, the second step is to choose a confidence level for the analysis. The confidence level defines the probability that we will incorrectly reject the null hypothesis when it is, in fact, true. We can express

this as our confidence that we are correct in rejecting the null hypothesis (e.g. 95%), or as the probability that we are incorrect in rejecting the null hypothesis. For the latter, the confidence level is given as $\alpha$, where

$$\alpha = 1 - \frac{\text{confidence interval (}}{100}$$

For a 95% confidence level, $\alpha$ is 0.05.

The third step is to calculate an appropriate test statistic and to compare it to a critical value. The test statistic's critical value defines a breakpoint between values that lead us to reject or to retain the null hypothesis, which is the fourth, and final, step of a significance test. As we will see in the sections that follow, how we calculate the test statistic depends on what we are comparing.

> The four steps for a statistical analysis of data using a significance test:
>
> 1. Pose a question, and state the null hypothesis, $H_0$, and the alternative hypothesis, $H_A$.
> 2. Choose a confidence level for the statistical analysis.
> 3. Calculate an appropriate test statistic and compare it to a critical value.
> 4. Either retain the null hypothesis, or reject it and accept the alternative hypothesis.

## One-Tailed and Two-tailed Significance Tests

Suppose we want to evaluate the accuracy of a new analytical method. We might use the method to analyze a Standard Reference Material that contains a known concentration of analyte, $\mu$. We analyze the standard several times, obtaining a mean value, $\overline{X}$, for the analyte's concentration. Our null hypothesis is that there is no difference between $\overline{X}$ and $\mu$

$$H_0\text{: } \overline{X} = \mu$$

If we conduct the significance test at $\alpha = 0.05$, then we retain the null hypothesis if a 95% confidence interval around $\overline{X}$ contains $\mu$. If the alternative hypothesis is

$$H_A\text{: } \overline{X} \neq \mu$$

then we reject the null hypothesis and accept the alternative hypothesis if $\mu$ lies in the shaded areas at either end of the sample's probability distribution curve (Figure 35.1.23$a$). Each of the shaded areas accounts for 2.5% of the area under the probability distribution curve, for a total of 5%. This is a two-tailed significance test because we reject the null hypothesis for values of $\mu$ at either extreme of the sample's probability distribution curve.

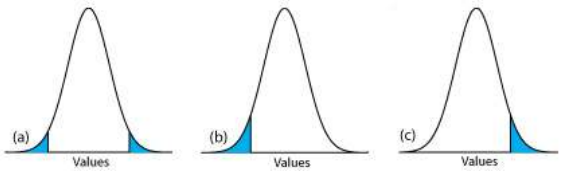



Figure 35.1.23: Examples of (a) two-tailed, and (b, c) one-tailed, significance test of $\overline{X}$ and $\mu$. The probability distribution curves, which are normal distributions, are based on the sample's mean and standard deviation. For $\alpha$ = 0.05, the blue areas account for 5% of the area under the curve. If the value of $\mu$ falls within the blue areas, then we reject the null hypothesis and accept the alternative hypothesis. We retain the null hypothesis if the value of $\mu$ falls within the unshaded area of the curve.

We can write the alternative hypothesis in two additional ways

$$H_A\text{: } \overline{X} > \mu$$

$$H_A\text{: } \overline{X} < \mu$$

rejecting the null hypothesis if $\mu$ falls within the shaded areas shown in Figure 35.1.23$b$ or Figure 35.1.23$c$, respectively. In each case the shaded area represents 5% of the area under the probability distribution curve. These are examples of a one-tailed significance test.

For a fixed confidence level, a two-tailed significance test is the more conservative test because rejecting the null hypothesis requires a larger difference between the results we are comparing. In most situations we have no particular reason to expect that

one result must be larger (or must be smaller) than the other result. This is the case, for example, when we evaluate the accuracy of a new analytical method. A two-tailed significance test, therefore, usually is the appropriate choice.

We reserve a one-tailed significance test for a situation where we specifically are interested in whether one result is larger (or smaller) than the other result. For example, a one-tailed significance test is appropriate if we are evaluating a medication's ability to lower blood glucose levels. In this case we are interested only in whether the glucose levels after we administer the medication are less than the glucose levels before we initiated treatment. If a patient's blood glucose level is greater after we administer the medication, then we know the answer—the medication did not work—and we do not need to conduct a statistical analysis.

### Errors in Significance Testing

Because a significance test relies on probability, its interpretation is subject to error. In a significance test, $\alpha$ defines the probability of rejecting a null hypothesis that is true. When we conduct a significance test at $\alpha = 0.05$, there is a 5% probability that we will incorrectly reject the null hypothesis. This is known as a type 1 error, and its risk is always equivalent to $\alpha$. A type 1 error in a two-tailed or a one-tailed significance tests corresponds to the shaded areas under the probability distribution curves in Figure 35.1.23.

A second type of error occurs when we retain a null hypothesis even though it is false. This is a type 2 error, and the probability of its occurrence is $\beta$. Unfortunately, in most cases we cannot calculate or estimate the value for $\beta$. The probability of a type 2 error, however, is inversely proportional to the probability of a type 1 error.

Minimizing a type 1 error by decreasing $\alpha$ increases the likelihood of a type 2 error. When we choose a value for $\alpha$ we must compromise between these two types of error. Most of the examples in this text use a 95% confidence level ($\alpha = 0.05$) because this usually is a reasonable compromise between type 1 and type 2 errors for analytical work. It is not unusual, however, to use a more stringent (e.g. $\alpha = 0.01$) or a more lenient (e.g. $\alpha = 0.10$) confidence level when the situation calls for it.

### Significance Tests for Normal Distributions

A normal distribution is the most common distribution for the data we collect. Because the area between any two limits of a normal distribution curve is well defined, it is straightforward to construct and evaluate significance tests.

### Comparing $\overline{X}$ to $\mu$

One way to validate a new analytical method is to analyze a sample that contains a known amount of analyte, $\mu$. To judge the method's accuracy we analyze several portions of the sample, determine the average amount of analyte in the sample, $\overline{X}$, and use a significance test to compare $\overline{X}$ to $\mu$. The null hypothesis is that the difference between $\overline{X}$ and $\mu$ is explained by indeterminate errors that affect our determination of $\overline{X}$. The alternative hypothesis is that the difference between $\overline{X}$ and $\mu$ is too large to be explained by indeterminate error.

$$H_0\text{: } \overline{X} = \mu$$

$$H_A\text{: } \overline{X} \neq \mu$$

The test statistic is $t_{\text{exp}}$, which we substitute into the confidence interval for $\mu$

$$\mu = \overline{X} \pm \frac{t_{\text{exp}} s}{\sqrt{n}}$$

Rearranging this equation and solving for $t_{\text{exp}}$

$$t_{\text{exp}} = \frac{|\mu - \overline{X}|\sqrt{n}}{s}$$

gives the value for $t_{\text{exp}}$ when $\mu$ is at either the right edge or the left edge of the sample's confidence interval (Figure 35.1.24$a$).

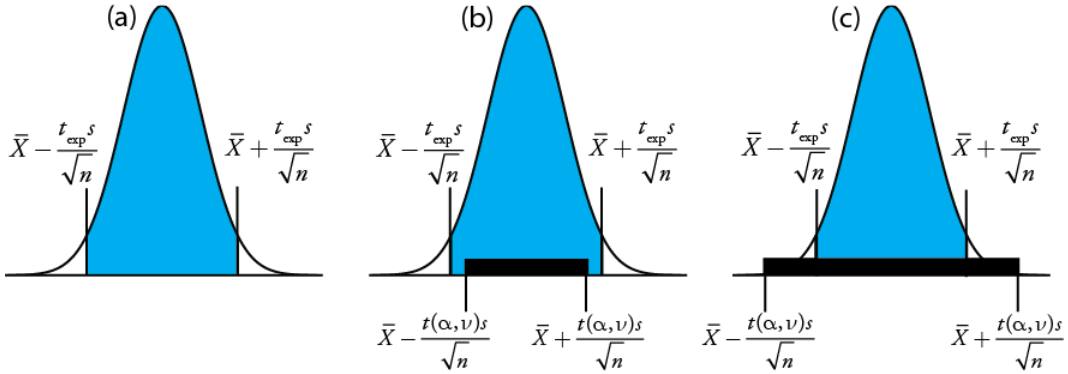



Figure 35.1.24: Relationship between a confidence interval and the result of a significance test. (a) The shaded area under the normal distribution curve shows the sample's confidence interval for $\mu$ based on $t_{exp}$. The solid bars in (b) and (c) show the expected confidence intervals for $\mu$ explained by indeterminate error given the choice of $\alpha$ and the available degrees of freedom, $\nu$. For (b) we reject the null hypothesis because portions of the sample's confidence interval fall outside the confidence interval explained by indeterminate error. In the case of (c) we retain the null hypothesis because the confidence interval explained by indeterminate error completely encompasses the sample's confidence interval.

To determine if we should retain or reject the null hypothesis, we compare the value of $t_{exp}$ to a critical value, $t(\alpha, \nu)$, where $\alpha$ is the confidence level and $\nu$ is the degrees of freedom for the sample. The critical value $t(\alpha, \nu)$ defines the largest confidence interval explained by indeterminate error. If $t_{exp} > t(\alpha, \nu)$, then our sample's confidence interval is greater than that explained by indeterminate errors (Figure 35.1.24b). In this case, we reject the null hypothesis and accept the alternative hypothesis. If $t_{exp} \leq t(\alpha, \nu)$, then our sample's confidence interval is smaller than that explained by indeterminate error, and we retain the null hypothesis (Figure 35.1.24c). Example 35.1.24 provides a typical application of this significance test, which is known as a *t*-test of $\overline{X}$ to $\mu$. You will find values for $t(\alpha, \nu)$ in Appendix 3.

### Example 35.1.3

Before determining the amount of $Na_2CO_3$ in a sample, you decide to check your procedure by analyzing a standard sample that is 98.76% w/w $Na_2CO_3$. Five replicate determinations of the %w/w $Na_2CO_3$ in the standard gives the following results

$$98.71\% \quad 98.59\% \quad 98.62\% \quad 98.44\% \quad 98.58\%$$

Using $\alpha = 0.05$, is there any evidence that the analysis is giving inaccurate results?

**Solution**

The mean and standard deviation for the five trials are

$$\overline{X} = 98.59 \qquad s = 0.0973$$

Because there is no reason to believe that the results for the standard must be larger or smaller than $\mu$, a two-tailed *t*-test is appropriate. The null hypothesis and alternative hypothesis are

$$H_0\text{: } \overline{X} = \mu \qquad H_A\text{: } \overline{X} \neq \mu$$

The test statistic, $t_{exp}$, is

$$t_{exp} = \frac{|\mu - \overline{X}|\sqrt{n}}{2} = \frac{|98.76 - 98.59|\sqrt{5}}{0.0973} = 3.91$$

The critical value for *t*(0.05, 4) from Appendix 3 is 2.78. Since $t_{exp}$ is greater than *t*(0.05, 4), we reject the null hypothesis and accept the alternative hypothesis. At the 95% confidence level the difference between $\overline{X}$ and $\mu$ is too large to be explained by indeterminate sources of error, which suggests there is a determinate source of error that affects the analysis.


https://chem.libretexts.org/@go/page/363066

Note

There is another way to interpret the result of this *t*-test. Knowing that $t_{exp}$ is 3.91 and that there are 4 degrees of freedom, we use Appendix 3 to estimate the value of $\alpha$ that corresponds to a $t(\alpha, 4)$ of 3.91. From Appendix 3, $t(0.02, 4)$ is 3.75 and $t(0.01, 4)$ is 4.60. Although we can reject the null hypothesis at the 98% confidence level, we cannot reject it at the 99% confidence level. For a discussion of the advantages of this approach, see J. A. C. Sterne and G. D. Smith "Sifting the evidence—what's wrong with significance tests?" *BMJ* **2001**, *322*, 226–231.

Earlier we made the point that we must exercise caution when we interpret the result of a statistical analysis. We will keep returning to this point because it is an important one. Having determined that a result is inaccurate, as we did in Example 35.1.3, the next step is to identify and to correct the error. Before we expend time and money on this, however, we first should critically examine our data. For example, the smaller the value of *s*, the larger the value of $t_{exp}$. If the standard deviation for our analysis is unrealistically small, then the probability of a type 2 error increases. Including a few additional replicate analyses of the standard and reevaluating the *t*-test may strengthen our evidence for a determinate error, or it may show us that there is no evidence for a determinate error.

### Comparing $s^2$ to $\sigma^2$

If we analyze regularly a particular sample, we may be able to establish an expected variance, $\sigma^2$, for the analysis. This often is the case, for example, in a clinical lab that analyzes hundreds of blood samples each day. A few replicate analyses of a single sample gives a sample variance, $s^2$, whose value may or may not differ significantly from $\sigma^2$.

We can use an *F*-test to evaluate whether a difference between $s^2$ and $\sigma^2$ is significant. The null hypothesis is $H_0$: $s^2 = \sigma^2$ and the alternative hypothesis is $H_A$: $s^2 \neq \sigma^2$. The test statistic for evaluating the null hypothesis is $F_{exp}$, which is given as either

$$F_{exp} = \frac{s^2}{\sigma^2} \text{ if } s^2 > \sigma^2 \text{ or } F_{exp} = \frac{\sigma^2}{s^2} \text{ if } \sigma^2 > s^2$$

depending on whether $s^2$ is larger or smaller than $\sigma^2$. This way of defining $F_{exp}$ ensures that its value is always greater than or equal to one.

If the null hypothesis is true, then $F_{exp}$ should equal one; however, because of indeterminate errors, $F_{exp}$, usually is greater than one. A critical value, $F(\alpha, \nu_{num}, \nu_{den})$, is the largest value of $F_{exp}$ that we can attribute to indeterminate error given the specified significance level, $\alpha$, and the degrees of freedom for the variance in the numerator, $\nu_{num}$, and the variance in the denominator, $\nu_{den}$. The degrees of freedom for $s^2$ is $n - 1$, where $n$ is the number of replicates used to determine the sample's variance, and the degrees of freedom for $\sigma^2$ is defined as infinity, $\infty$. Critical values of *F* for $\alpha = 0.05$ are listed in Appendix 4 for both one-tailed and two-tailed *F*-tests.

Example 35.1.4

A manufacturer's process for analyzing aspirin tablets has a known variance of 25. A sample of 10 aspirin tablets is selected and analyzed for the amount of aspirin, yielding the following results in mg aspirin/tablet.

$$254 \quad 249 \quad 252 \quad 252 \quad 249 \quad 249 \quad 250 \quad 247 \quad 251 \quad 252$$

Determine whether there is evidence of a significant difference between the sample's variance and the expected variance at $\alpha = 0.05$.

**Solution**

The variance for the sample of 10 tablets is 4.3. The null hypothesis and alternative hypotheses are

$$H_0: s^2 = \sigma^2 \qquad H_A: s^2 \neq \sigma^2$$

and the value for $F_{exp}$ is

$$F_{exp} = \frac{\sigma^2}{s^2} = \frac{25}{4.3} = 5.8$$

The critical value for $F(0.05, \infty, 9)$ from Appendix 4 is 3.333. Since $F_{exp}$ is greater than $F(0.05, \infty, 9)$, we reject the null hypothesis and accept the alternative hypothesis that there is a significant difference between the sample's variance and the

expected variance. One explanation for the difference might be that the aspirin tablets were not selected randomly.

## Comparing Variances for Two Samples

We can extend the *F*-test to compare the variances for two samples, *A* and *B*, by rewriting our equation for $F_{\text{exp}}$ as

$$F_{\text{exp}} = \frac{s_A^2}{s_B^2}$$

defining *A* and *B* so that the value of $F_{\text{exp}}$ is greater than or equal to 1.

### Example 35.1.5

The table below shows results for two experiments to determine the mass of a circulating U.S. penny. Determine whether there is a difference in the variances of these analyses at $\alpha = 0.05$.

| First Experiment | | Second Experiment | |
|---|---|---|---|
| Penny | Mass (g) | Penny | Mass (g) |
| 1 | 3.080 | 1 | 3.052 |
| 2 | 3.094 | 2 | 3.141 |
| 3 | 3.107 | 3 | 3.083 |
| 4 | 3.056 | 4 | 3.083 |
| 5 | 3.112 | 5 | 3.048 |
| 6 | 3.174 | | |
| 7 | 3.198 | | |

**Solution**

The standard deviations for the two experiments are 0.051 for the first experiment (*A*) and 0.037 for the second experiment (*B*). The null and alternative hypotheses are

$$H_0\text{: } s_A^2 = s_B^2 \qquad H_\text{A}\text{: } s_A^2 \neq s_B^2$$

and the value of $F_{\text{exp}}$ is

$$F_{\text{exp}} = \frac{s_A^2}{s_B^2} = \frac{(0.051)^2}{(0.037)^2} = \frac{0.00260}{0.00137} = 1.90$$

From Appendix 4 the critical value for *F*(0.05, 6, 4) is 9.197. Because $F_{\text{exp}} < F(0.05, 6, 4)$, we retain the null hypothesis. There is no evidence at $\alpha = 0.05$ to suggest that the difference in variances is significant.

## Comparing Means for Two Samples

Three factors influence the result of an analysis: the method, the sample, and the analyst. We can study the influence of these factors by conducting experiments in which we change one factor while holding constant the other factors. For example, to compare two analytical methods we can have the same analyst apply each method to the same sample and then examine the resulting means. In a similar fashion, we can design experiments to compare two analysts or to compare two samples.

Before we consider the significance tests for comparing the means of two samples, we need to understand the difference between unpaired data and paired data. This is a critical distinction and learning to distinguish between these two types of data is important. Here are two simple examples that highlight the difference between unpaired data and paired data. In each example the goal is to compare two balances by weighing pennies.

- Example 1: We collect 10 pennies and weigh each penny on each balance. This is an example of paired data because we use the same 10 pennies to evaluate each balance.
- Example 2: We collect 10 pennies and divide them into two groups of five pennies each. We weigh the pennies in the first group on one balance and we weigh the second group of pennies on the other balance. Note that no penny is weighed on both balances. This is an example of unpaired data because we evaluate each balance using a different sample of pennies.

In both examples the samples of 10 pennies were drawn from the same population; the difference is how we sampled that population. We will learn why this distinction is important when we review the significance test for paired data; first, however, we present the significance test for unpaired data.

> **Note**
>
> One simple test for determining whether data are paired or unpaired is to look at the size of each sample. If the samples are of different size, then the data must be unpaired. The converse is not true. If two samples are of equal size, they may be paired or unpaired.

### Unpaired Data

Consider two analyses, *A* and *B*, with means of $\overline{X}_A$ and $\overline{X}_B$, and standard deviations of $s_A$ and $s_B$. The confidence intervals for $\mu_A$ and for $\mu_B$ are

$$\mu_A = \overline{X}_A \pm \frac{ts_A}{\sqrt{n_A}}$$

$$\mu_B = \overline{X}_B \pm \frac{ts_B}{\sqrt{n_B}}$$

where $n_A$ and $n_B$ are the sample sizes for *A* and for *B*. Our null hypothesis, $H_0$: $\mu_A = \mu_B$, is that any difference between $\mu_A$ and $\mu_B$ is the result of indeterminate errors that affect the analyses. The alternative hypothesis, $H_A$: $\mu_A \neq \mu_B$, is that the difference between $\mu_A$ and $\mu_B$ is too large to be explained by indeterminate error.

To derive an equation for $t_{exp}$, we assume that $\mu_A$ equals $\mu_B$, and combine the equations for the two confidence intervals

$$\overline{X}_A \pm \frac{t_{exp}s_A}{\sqrt{n_A}} = \overline{X}_B \pm \frac{t_{exp}s_B}{\sqrt{n_B}}$$

Solving for $|\overline{X}_A - \overline{X}_B|$ and using a propagation of uncertainty, gives

$$|\overline{X}_A - \overline{X}_B| = t_{exp} \times \sqrt{\frac{s_A^2}{n_A} + \frac{s_B^2}{n_B}}$$

Finally, we solve for $t_{exp}$

$$t_{exp} = \frac{|\overline{X}_A - \overline{X}_B|}{\sqrt{\frac{s_A^2}{n_A} + \frac{s_B^2}{n_B}}}$$

and compare it to a critical value, $t(\alpha, \nu)$, where $\alpha$ is the probability of a type 1 error, and $\nu$ is the degrees of freedom.

Thus far our development of this *t*-test is similar to that for comparing $\overline{X}$ to $\mu$, and yet we do not have enough information to evaluate the *t*-test. Do you see the problem? With two independent sets of data it is unclear how many degrees of freedom we have.

Suppose that the variances $s_A^2$ and $s_B^2$ provide estimates of the same $\sigma^2$. In this case we can replace $s_A^2$ and $s_B^2$ with a pooled variance, $s_{pool}^2$, that is a better estimate for the variance. Thus, our equation for $t_{exp}$ becomes

$$t_{exp} = \frac{|\overline{X}_A - \overline{X}_B|}{s_{pool} \times \sqrt{\frac{1}{n_A} + \frac{1}{n_B}}} = \frac{|\overline{X}_A - \overline{X}_B|}{s_{pool}} \times \sqrt{\frac{n_A n_B}{n_A + n_B}}$$

where $s_{pool}$, the pooled standard deviation, is

$$s_{\text{pool}} = \sqrt{\frac{(n_A - 1)s_A^2 + (n_B - 1)s_B^2}{n_A + n_B - 2}}$$

The denominator of this equation shows us that the degrees of freedom for a pooled standard deviation is $n_A + n_B - 2$, which also is the degrees of freedom for the *t*-test. Note that we lose two degrees of freedom because the calculations for $s_A^2$ and $s_B^2$ require the prior calculation of $\overline{X}_A$ amd $\overline{X}_B$.

**Note**

So how do you determine if it is okay to pool the variances? Use an *F*-test.

If $s_A^2$ and $s_B^2$ are significantly different, then we calculate $t_{\text{exp}}$ using the following equation. In this case, we find the degrees of freedom using the following imposing equation.

$$\nu = \frac{\left(\frac{s_A^2}{n_A} + \frac{s_B^2}{n_B}\right)^2}{\frac{\left(\frac{s_A^2}{n_A}\right)^2}{n_A+1} + \frac{\left(\frac{s_B^2}{n_B}\right)^2}{n_B+1}} - 2$$

Because the degrees of freedom must be an integer, we round to the nearest integer the value of $\nu$ obtained from this equation.

**Note**

The equation above for the degrees of freedom is from Miller, J.C.; Miller, J.N. *Statistics for Analytical Chemistry*, 2nd Ed., Ellis-Horward: Chichester, UK, 1988. In the 6th Edition, the authors note that several different equations have been suggested for the number of degrees of freedom for *t* when $s_A$ and $s_B$ differ, reflecting the fact that the determination of degrees of freedom an approximation. An alternative equation—which is used by statistical software packages, such as R, Minitab, Excel—is

$$\nu = \frac{\left(\frac{s_A^2}{n_A} + \frac{s_B^2}{n_B}\right)^2}{\frac{\left(\frac{s_A^2}{n_A}\right)^2}{n_A-1} + \frac{\left(\frac{s_B^2}{n_B}\right)^2}{n_B-1}} = \frac{\left(\frac{s_A^2}{n_A} + \frac{s_B^2}{n_B}\right)^2}{\frac{s_A^4}{n_A^2(n_A-1)} + \frac{s_B^4}{n_B^2(n_B-1)}}$$

For typical problems in analytical chemistry, the calculated degrees of freedom is reasonably insensitive to the choice of equation.

Regardless of whether how we calculate $t_{\text{exp}}$, we reject the null hypothesis if $t_{\text{exp}}$ is greater than $t(\alpha, \nu)$ and retain the null hypothesis if $t_{\text{exp}}$ is less than or equal to $t(\alpha, \nu)$.

**Example 35.1.6**

Example 35.1.3 provides results for two experiments to determine the mass of a circulating U.S. penny. Determine whether there is a difference in the means of these analyses at $\alpha = 0.05$.

**Solution**

First we use an *F*-test to determine whether we can pool the variances. We completed this analysis in Example 35.1.5, finding no evidence of a significant difference, which means we can pool the standard deviations, obtaining

$$s_{\text{pool}} = \sqrt{\frac{(7-1)(0.051)^2 + (5-1)(0.037)^2}{7+5-2}} = 0.0459$$

with 10 degrees of freedom. To compare the means we use the following null hypothesis and alternative hypotheses

$$H_0\text{: } \mu_A = \mu_B \qquad H_A\text{: } \mu_A \neq \mu_B$$

Because we are using the pooled standard deviation, we calculate $t_{\text{exp}}$ as

$$t_{exp} = \frac{|3.117 - 3.081|}{0.0459} \times \sqrt{\frac{7 \times 5}{7 + 5}} = 1.34$$

The critical value for $t(0.05, 10)$, from Appendix 3, is 2.23. Because $t_{exp}$ is less than $t(0.05, 10)$ we retain the null hypothesis. For $\alpha = 0.05$ we do not have evidence that the two sets of pennies are significantly different.

### Example 35.1.7

One method for determining the %w/w $Na_2CO_3$ in soda ash is to use an acid–base titration. When two analysts analyze the same sample of soda ash they obtain the results shown here.

Analyst A: 86.82% 87.04% 86.93% 87.01% 86.20% 87.00%

Analyst B: 81.01% 86.15% 81.73% 83.19% 80.27% 83.93%

Determine whether the difference in the mean values is significant at $\alpha = 0.05$.

**Solution**

We begin by reporting the mean and standard deviation for each analyst.

$$\overline{X}_A = 86.83\% \qquad s_A = 0.32\%$$

$$\overline{X}_B = 82.71\% \qquad s_B = 2.16\%$$

To determine whether we can use a pooled standard deviation, we first complete an $F$-test using the following null and alternative hypotheses.

$$H_0\text{: } s_A^2 = s_B^2 \qquad H_A\text{: } s_A^2 \neq s_B^2$$

Calculating $F_{exp}$, we obtain a value of

$$F_{exp} = \frac{(2.16)^2}{(0.32)^2} = 45.6$$

Because $F_{exp}$ is larger than the critical value of 7.15 for $F(0.05, 5, 5)$ from Appendix 4, we reject the null hypothesis and accept the alternative hypothesis that there is a significant difference between the variances; thus, we cannot calculate a pooled standard deviation.

To compare the means for the two analysts we use the following null and alternative hypotheses.

$$H_0\text{: } \overline{X}_A = \overline{X}_B \qquad H_A\text{: } \overline{X}_A \neq \overline{X}_B$$

Because we cannot pool the standard deviations, we calculate $t_{exp}$ as

$$t_{exp} = \frac{|86.83 - 82.71|}{\sqrt{\frac{(0.32)^2}{6} + \frac{(2.16)^2}{6}}} = 4.62$$

and calculate the degrees of freedom as

$$\nu = \frac{\left(\frac{(0.32)^2}{6} + \frac{(2.16)^2}{6}\right)^2}{\frac{\left(\frac{(0.32)^2}{6}\right)^2}{6+1} + \frac{\left(\frac{(2.16)^2}{6}\right)^2}{6+1}} - 2 = 5.3 \approx 5$$

From Appendix 3, the critical value for $t(0.05, 5)$ is 2.57. Because $t_{exp}$ is greater than $t(0.05, 5)$ we reject the null hypothesis and accept the alternative hypothesis that the means for the two analysts are significantly different at $\alpha = 0.05$.

## Paired Data

Suppose we are evaluating a new method for monitoring blood glucose concentrations in patients. An important part of evaluating a new method is to compare it to an established method. What is the best way to gather data for this study? Because the variation in the blood glucose levels amongst patients is large we may be unable to detect a small, but significant difference between the

methods if we use different patients to gather data for each method. Using paired data, in which the we analyze each patient's blood using both methods, prevents a large variance within a population from adversely affecting a *t*-test of means.

**Note**

Typical blood glucose levels for most non-diabetic individuals ranges between 80–120 mg/dL (4.4–6.7 mM), rising to as high as 140 mg/dL (7.8 mM) shortly after eating. Higher levels are common for individuals who are pre-diabetic or diabetic.

When we use paired data we first calculate the individual differences, $d_i$, between each sample's paired resykts. Using these individual differences, we then calculate the average difference, $\bar{d}$, and the standard deviation of the differences, $s_d$. The null hypothesis, $H_0$: $d = 0$, is that there is no difference between the two samples, and the alternative hypothesis, $H_A$: $d \neq 0$, is that the difference between the two samples is significant.

The test statistic, $t_{exp}$, is derived from a confidence interval around $\bar{d}$

$$t_{exp} = \frac{|\bar{d}|\sqrt{n}}{s_d}$$

where *n* is the number of paired samples. As is true for other forms of the *t*-test, we compare $t_{exp}$ to $t(\alpha, \nu)$, where the degrees of freedom, $\nu$, is *n* – 1. If $t_{exp}$ is greater than $t(\alpha, \nu)$, then we reject the null hypothesis and accept the alternative hypothesis. We retain the null hypothesis if $t_{exp}$ is less than or equal to *t*(a, o). This is known as a paired t-test.

**Example 35.1.8**

Marecek et. al. developed a new electrochemical method for the rapid determination of the concentration of the antibiotic monensin in fermentation vats [Marecek, V.; Janchenova, H.; Brezina, M.; Betti, M. *Anal. Chim. Acta* **1991**, *244*, 15–19]. The standard method for the analysis is a test for microbiological activity, which is both difficult to complete and time-consuming. Samples were collected from the fermentation vats at various times during production and analyzed for the concentration of monensin using both methods. The results, in parts per thousand (ppt), are reported in the following table.

| Sample | Microbiological | Electrochemical |
|---|---|---|
| 1 | 129.5 | 132.3 |
| 2 | 89.6 | 91.0 |
| 3 | 76.6 | 73.6 |
| 4 | 52.2 | 58.2 |
| 5 | 110.8 | 104.2 |
| 6 | 50.4 | 49.9 |
| 7 | 72.4 | 82.1 |
| 8 | 141.4 | 154.1 |
| 9 | 75.0 | 73.4 |
| 10 | 34.1 | 38.1 |
| 11 | 60.3 | 60.1 |

Is there a significant difference between the methods at $\alpha = 0.05$?

**Solution**

Acquiring samples over an extended period of time introduces a substantial time-dependent change in the concentration of monensin. Because the variation in concentration between samples is so large, we use a paired *t*-test with the following null

and alternative hypotheses.

$$H_0\text{: } \overline{d} = 0 \qquad H_A\text{: } \overline{d} \neq 0$$

Defining the difference between the methods as

$$d_i = (X_{\text{elect}})_i - (X_{\text{micro}})_i$$

we calculate the difference for each sample.

| sample | 1 | 2 | 3 | 4 | 5 | 6 | 7 | 8 | 9 | 10 | 11 |
|---|---|---|---|---|---|---|---|---|---|---|---|
| $d_i$ | 2.8 | 1.4 | –3.0 | 6.0 | –6.6 | –0.5 | 9.7 | 12.7 | –1.6 | 4.0 | –0.2 |

The mean and the standard deviation for the differences are, respectively, 2.25 ppt and 5.63 ppt. The value of $t_{\text{exp}}$ is

$$t_{\text{exp}} = \frac{|2.25|\sqrt{11}}{5.63} = 1.33$$

which is smaller than the critical value of 2.23 for $t(0.05, 10)$ from Appendix 3. We retain the null hypothesis and find no evidence for a significant difference in the methods at $\alpha = 0.05$.

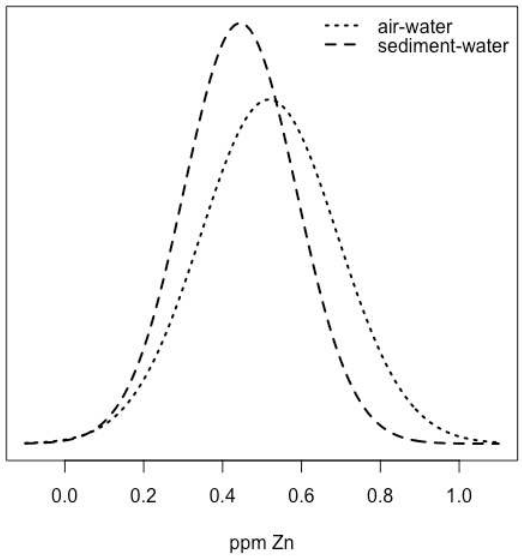
One important requirement for a paired *t*-test is that the determinate and the indeterminate errors that affect the analysis must be independent of the analyte's concentration. If this is not the case, then a sample with an unusually high concentration of analyte will have an unusually large $d_i$. Including this sample in the calculation of $\overline{d}$ and $s_d$ gives a biased estimate for the expected mean and standard deviation. This rarely is a problem for samples that span a limited range of analyte concentrations, such as those in Example 35.1.6 or Exercise 35.1.8. When paired data span a wide range of concentrations, however, the magnitude of the determinate and indeterminate sources of error may not be independent of the analyte's concentration; when true, a paired *t*-test may give misleading results because the paired data with the largest absolute determinate and indeterminate errors will dominate $\overline{d}$. In this situation a regression analysis, which is the subject of the next chapter, is more appropriate method for comparing the data.

**Note**

The importance of distinguishing between paired and unpaired data is worth examining more closely. The following is data from some work I completed with a colleague in which we were looking at concentration of Zn in Lake Erie at the air-water interface and the sediment-water interface.

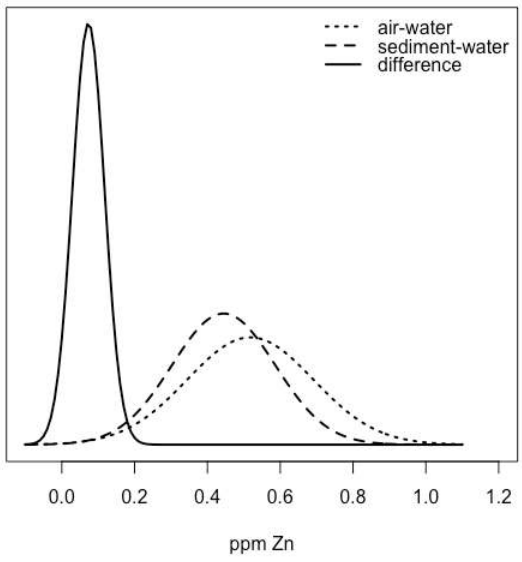
| sample site | ppm Zn at air-water interface | ppm Zn at the sediment-water interface |
|---|---|---|
| 1 | 0.430 | 0.415 |
| 2 | 0.266 | 0.238 |
| 3 | 0.457 | 0.390 |
| 4 | 0.531 | 0.410 |
| 5 | 0.707 | 0.605 |
| 6 | 0.716 | 0.609 |

The mean and the standard deviation for the ppm Zn at the air-water interface are 0.5178 ppm and 0.01732 ppm, and the mean and the standard deviation for the ppm Zn at the sediment-water interface are 0.4445 ppm and 0.1418 ppm. We can use these values to draw normal distributions for both by letting the means and the standard deviations for the samples, $\overline{X}$ and $s$, serve as estimates for the means and the standard deviations for the population, $\mu$ and $\sigma$. As we see in the following figure




the two distributions overlap strongly, suggesting that a *t*-test of their means is not likely to find evidence of a difference. And yet, we also see that for each site, the concentration of Zn at the sediment-water interface is less than that at the air-water interface. In this case, the difference between the concentration of Zn at individual sites is sufficiently large that it masks our ability to see the difference between the two interfaces.

If we take the differences between the air-water and sediment-water interfaces, we have values of 0.015, 0.028, 0.067, 0.121, 0.102, and 0.107 ppm Zn, with a mean of 0.07333 ppm Zn and a standard deviation of 0.04410 ppm Zn. Superimposing all three normal distributions




shows clearly that most of the normal distribution for the differences lies above zero, suggesting that a *t*-test might show evidence that the difference is significant.

## Outliers

Table 35.1.11 provides one more data set giving the masses for a sample of pennies. Do you notice anything unusual in this data? Of the 100 pennies included in our earlier table, no penny has a mass of less than 3 g. In this table, however, the mass of one penny is less than 3 g. We might ask whether this penny's mass is so different from the other pennies that it is in error.

Table 35.1.11. Mass (g) for Additional Sample of Circulating U. S. Penniese

| | | |
|---|---|---|
| 3.067 | 2.514 | 3.094 |
| 3.049 | 3.048 | 3.109 |
| 3.039 | 3.079 | 3.102 |

A measurement that is not consistent with other measurements is called an outlier. An outlier might exist for many reasons: the outlier might belong to a different population

Is this a Canadian penny?

or the outlier might be a contaminated or an otherwise altered sample

Is the penny damaged or unusually dirty?

or the outlier may result from an error in the analysis

Did we forget to tare the balance?

Regardless of its source, the presence of an outlier compromises any meaningful analysis of our data. There are many significance tests that we can use to identify a potential outlier, three of which we present here.

## Dixon's *Q*-Test

One of the most common significance tests for identifying an outlier is Dixon's Q-test. The null hypothesis is that there are no outliers, and the alternative hypothesis is that there is an outlier. The *Q*-test compares the gap between the suspected outlier and its nearest numerical neighbor to the range of the entire data set (Figure 35.1.25).

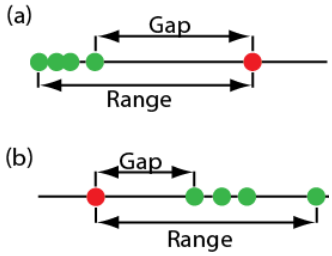



Figure 35.1.25: Dotplots showing the distribution of two data sets containing a possible outlier. In (a) the possible outlier's value is larger than the remaining data, and in (b) the possible outlier's value is smaller than the remaining data.

The test statistic, $Q_{exp}$, is

$$Q_{\text{exp}} = \frac{\text{gap}}{\text{range}} = \frac{|\text{outlier's value} - \text{nearest value}|}{\text{largest value} - \text{smallest value}}$$

This equation is appropriate for evaluating a single outlier. Other forms of Dixon's *Q*-test allow its extension to detecting multiple outliers [Rorabacher, D. B. *Anal. Chem.* **1991**, *63*, 139–146].

The value of $Q_{\text{exp}}$ is compared to a critical value, $Q(\alpha, n)$, where $\alpha$ is the probability that we will reject a valid data point (a type 1 error) and $n$ is the total number of data points. To protect against rejecting a valid data point, usually we apply the more conservative two-tailed *Q*-test, even though the possible outlier is the smallest or the largest value in the data set. If $Q_{\text{exp}}$ is greater than $Q(\alpha, n)$, then we reject the null hypothesis and may exclude the outlier. We retain the possible outlier when $Q_{\text{exp}}$ is less than or equal to $Q(\alpha, n)$. Table 35.1.12 provides values for $Q(\alpha, n)$ for a data set that has 3–10 values. A more extensive table is in Appendix 5. Values for $Q(\alpha, n)$ assume an underlying normal distribution.

Table 35.1.12: Dixon's Q-Test

| $n$ | $Q(0.05, n)$ |
|---|---|
| 3 | 0.970 |
| 4 | 0.829 |
| 5 | 0.710 |
| 6 | 0.625 |
| 7 | 0.568 |
| 8 | 0.526 |
| 9 | 0.493 |
| 10 | 0.466 |

### Grubb's Test

Although Dixon's *Q*-test is a common method for evaluating outliers, it is no longer favored by the International Standards Organization (ISO), which recommends the Grubb's test. There are several versions of Grubb's test depending on the number of potential outliers. Here we will consider the case where there is a single suspected outlier.

> **Note**
>
> For details on this recommendation, see International Standards ISO Guide 5752-2 "Accuracy (trueness and precision) of measurement methods and results–Part 2: basic methods for the determination of repeatability and reproducibility of a standard measurement method," 1994.

The test statistic for Grubb's test, $G_{exp}$, is the distance between the sample's mean, $\overline{X}$, and the potential outlier, $X_{out}$, in terms of the sample's standard deviation, *s*.

$$G_{exp} = \frac{|X_{out} - \overline{X}|}{s}$$

We compare the value of $G_{exp}$ to a critical value $G(\alpha, n)$, where $\alpha$ is the probability that we will reject a valid data point and *n* is the number of data points in the sample. If $G_{exp}$ is greater than $G(\alpha, n)$, then we may reject the data point as an outlier, otherwise we retain the data point as part of the sample. Table 35.1.13 provides values for $G(0.05, n)$ for a sample containing 3–10 values. A more extensive table is in Appendix 6. Values for $G(\alpha, n)$ assume an underlying normal distribution.

Table 35.1.13: Grubb's Test

| $n$ | $G(0.05, n)$ |
|---|---|
| 3 | 1.115 |
| 4 | 1.481 |
| 5 | 1.715 |
| 6 | 1.887 |
| 7 | 2.020 |
| 8 | 2.126 |
| 9 | 2.215 |
| 10 | 2.290 |

## Chauvenet's Criterion

Our final method for identifying an outlier is Chauvenet's criterion. Unlike Dixon's *Q*-Test and Grubb's test, you can apply this method to any distribution as long as you know how to calculate the probability for a particular outcome. Chauvenet's criterion states that we can reject a data point if the probability of obtaining the data point's value is less than $(2n^{-1})$, where *n* is the size of the sample. For example, if *n* = 10, a result with a probability of less than $(2 \times 10)^{-1}$, or 0.05, is considered an outlier.

To calculate a potential outlier's probability we first calculate its standardized deviation, *z*

$$z = \frac{|X_{\text{out}} - \overline{X}|}{s}$$

where $X_{\text{out}}$ is the potential outlier, $\overline{X}$ is the sample's mean and *s* is the sample's standard deviation. Note that this equation is identical to the equation for $G_{\text{exp}}$ in the Grubb's test. For a normal distribution, we can find the probability of obtaining a value of *z* using the probability table in Appendix 2.

### Example 35.1.9

Table 35.1.11 contains the masses for nine circulating United States pennies. One entry, 2.514 g, appears to be an outlier. Determine if this penny is an outlier using a *Q*-test, Grubb's test, and Chauvenet's criterion. For the *Q*-test and Grubb's test, let $\alpha = 0.05$.

#### Solution

For the *Q*-test the value for $Q_{\text{exp}}$ is

$$Q_{\text{exp}} = \frac{|2.514 - 3.039|}{3.109 - 2.514} = 0.882$$

From Table 35.1.12, the critical value for *Q*(0.05, 9) is 0.493. Because $Q_{\text{exp}}$ is greater than *Q*(0.05, 9), we can assume the penny with a mass of 2.514 g likely is an outlier.

For Grubb's test we first need the mean and the standard deviation, which are 3.011 g and 0.188 g, respectively. The value for $G_{\text{exp}}$ is

$$G_{\text{exp}} = \frac{|2.514 - 3.011|}{0.188} = 2.64$$

Using Table 35.1.13, we find that the critical value for *G*(0.05, 9) is 2.215. Because $G_{\text{exp}}$ is greater than *G*(0.05, 9), we can assume that the penny with a mass of 2.514 g likely is an outlier.

For Chauvenet's criterion, the critical probability is $(2 \times 9)^{-1}$, or 0.0556. The value of *z* is the same as $G_{\text{exp}}$, or 2.64. Using Appendix 1, the probability for *z* = 2.64 is 0.00415. Because the probability of obtaining a mass of 0.2514 g is less than the critical probability, we can assume the penny with a mass of 2.514 g likely is an outlier.

You should exercise caution when using a significance test for outliers because there is a chance you will reject a valid result. In addition, you should avoid rejecting an outlier if it leads to a precision that is much better than expected based on a propagation of uncertainty. Given these concerns it is not surprising that some statisticians caution against the removal of outliers [Deming, W. E. *Statistical Analysis of Data*; Wiley: New York, 1943 (republished by Dover: New York, 1961); p. 171].

### Note

You also can adopt a more stringent requirement for rejecting data. When using the Grubb's test, for example, the ISO 5752 guidelines suggest retaining a value if the probability for rejecting it is greater than $\alpha = 0.05$, and flagging a value as a "straggler" if the probability for rejecting it is between $\alpha = 0.05$ and $\alpha = 0.01$. A "straggler" is retained unless there is compelling reason for its rejection. The guidelines recommend using $\alpha = 0.01$ as the minimum criterion for rejecting a possible outlier.

On the other hand, testing for outliers can provide useful information if we try to understand the source of the suspected outlier. For example, the outlier in Table 35.1.11 represents a significant change in the mass of a penny (an approximately 17% decrease in mass), which is the result of a change in the composition of the U.S. penny. In 1982 the composition of a U.S. penny changed from a brass alloy that was 95% w/w Cu and 5% w/w Zn (with a nominal mass of 3.1 g), to a pure zinc core covered with copper (with a nominal mass of 2.5 g) [Richardson, T. H. *J. Chem. Educ.* **1991**, *68*, 310–311]. The pennies in Table 35.1.11, therefore, were drawn from different populations.

## Calibrating Data

A calibration curve is one of the most important tools in analytical chemistry as it allows us to determine the concentration of an analyte in a sample by measuring the signal it generates when placed in an instrument, such as a spectrophotometer. To determine the analyte's concentration we must know the relationship between the signal we measure , $S$, and the analyte's concentration, $C_A$, which we can write as

$$S = k_A C_A + S_{blank}$$

where $k_A$ is the calibration curve's sensitivity and $S_{blank}$ is the signal in the absence of analyte.

How do we find the best estimate for this relationship between the signal and the concentration of analyte? When a calibration curve is a straight-line, we represent it using the following mathematical model

$$y = \beta_0 + \beta_1 x$$

where *y* is the analyte's measured signal, *S*, and *x* is the analyte's known concentration, $C_A$, in a series of standard solutions. The constants $\beta_0$ and $\beta_1$ are, respectively, the calibration curve's expected *y*-intercept and its expected slope. Because of uncertainty in our measurements, the best we can do is to estimate values for $\beta_0$ and $\beta_1$, which we represent as $b_0$ and $b_1$. The goal of a linear regression analysis is to determine the best estimates for $b_0$ and $b_1$.

### Unweighted Linear Regression With Errors in y

The most common method for completing a linear regression makes three assumptions:

1. the difference between our experimental data and the calculated regression line is the result of indeterminate errors that affect *y*
2. any indeterminate errors that affect *y* are normally distributed
3. that indeterminate errors in *y* are independent of the value of *x*

Because we assume that the indeterminate errors are the same for all standards, each standard contributes equally in our estimate of the slope and the *y*-intercept. For this reason the result is considered an unweighted linear regression.

The second assumption generally is true because of the central limit theorem, which we considered earlier. The validity of the two remaining assumptions is less obvious and you should evaluate them before you accept the results of a linear regression. In particular the first assumption is always suspect because there certainly is some indeterminate error in the measurement of *x*. When we prepare a calibration curve, however, it is not unusual to find that the uncertainty in the signal, *S*, is significantly greater than the uncertainty in the analyte's concentration, $C_A$. In such circumstances the first assumption usually is reasonable.

### How a Linear Regression Works

To understand the logic of a linear regression consider the example in Figure 35.1.26, which shows three data points and two possible straight-lines that might reasonably explain the data. How do we decide how well these straight-lines fit the data, and how do we determine which, if either, is the best straight-line?

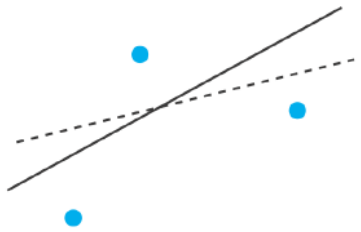


Figure 35.1.26: Illustration showing three data points and two possible straight-lines that might explain the data. The goal of a linear regression is to find the one mathematical model, in this case a straight-line, that best explains the data.

Let's focus on the solid line in Figure 35.1.26. The equation for this line is

$$\hat{y} = b_0 + b_1 x$$

where $b_0$ and $b_1$ are estimates for the *y*-intercept and the slope, and $\hat{y}$ is the predicted value of *y* for any value of *x*. Because we assume that all uncertainty is the result of indeterminate errors in *y*, the difference between *y* and $\hat{y}$ for each value of *x* is the residual error, *r*, in our mathematical model.

$$r_i = (y_i - \hat{y}_i)$$

Figure 35.1.27 shows the residual errors for the three data points. The smaller the total residual error, R, which we define as

$$R = \sum_{i=1}^{n} (y_i - \hat{y}_i)^2$$

the better the fit between the straight-line and the data. In a linear regression analysis, we seek values of $b_0$ and $b_1$ that give the smallest total residual error.

**Note**

The reason for squaring the individual residual errors is to prevent a positive residual error from canceling out a negative residual error. You have seen this before in the equations for the sample and population standard deviations introduced in Chapter 4. You also can see from this equation why a linear regression is sometimes called the method of least squares.

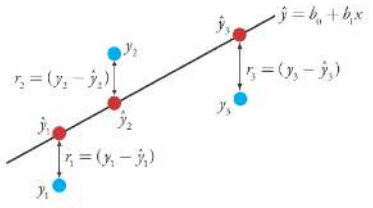



Figure 35.1.27: Illustration that shows the evaluation of a linear regression in which we assume that all uncertainty is the result of indeterminate errors in *y*. The points in blue, *y* , are the original data and the points in red, $\hat{y}_i$, are the predicted values from the regression equation, $\hat{y} = b_0 + b_1 x$.The smaller the total residual error, the better the fit of the straight-line to the data.

## Finding the Slope and *y*-Intercept for the Regression Model

Although we will not formally develop the mathematical equations for a linear regression analysis, you can find the derivations in many standard statistical texts [ See, for example, Draper, N. R.; Smith, H. Applied Regression Analysis, 3rd ed.; Wiley: New York, 1998]. The resulting equation for the slope, $b_1$, is

$$b_1 = \frac{n\sum_{i=1}^{n} x_i y_i - \sum_{i=1}^{n} x_i \sum_{i=1}^{n} y_i}{n\sum_{i=1}^{n} x_i^2 - \left(\sum_{i=1}^{n} x_i\right)^2}$$

and the equation for the *y*-intercept, $b_0$, is

$$b_0 = \frac{\sum_{i=1}^{n} y_i - b_1 \sum_{i=1}^{n} x_i}{n}$$

Although these equations appear formidable, it is necessary only to evaluate the following four summations

$$\sum_{i=1}^{n} x_i \quad \sum_{i=1}^{n} y_i \quad \sum_{i=1}^{n} x_i y_i \quad \sum_{i=1}^{n} x_i^2$$

Many calculators, spreadsheets, and other statistical software packages are capable of performing a linear regression analysis based on this model; see Section 8.5 for details on completing a linear regression analysis using R. For illustrative purposes the necessary calculations are shown in detail in the following example.

**Example 35.1.10**

Using the calibration data in the following table, determine the relationship between the signal, $y_i$, and the analyte's concentration, $x_i$, using an unweighted linear regression.

**Solution**

We begin by setting up a table to help us organize the calculation.

| $x_i$ | $y_i$ | $x_i y_i$ | $x_i^2$ |
|---|---|---|---|
| 0.000 | 0.00 | 0.000 | 0.000 |
| 0.100 | 12.36 | 1.236 | 0.010 |
| 0.200 | 24.83 | 4.966 | 0.040 |
| 0.300 | 35.91 | 10.773 | 0.090 |
| 0.400 | 48.79 | 19.516 | 0.160 |
| 0.500 | 60.42 | 30.210 | 0.250 |

Adding the values in each column gives

$$\sum_{i=1}^{n} x_i = 1.500 \quad \sum_{i=1}^{n} y_i = 182.31 \quad \sum_{i=1}^{n} x_i y_i = 66.701 \quad \sum_{i=1}^{n} x_i^2 = 0.550$$

Substituting these values into the equations for the slope and the *y*-intercept gives

$$b_1 = \frac{(6 \times 66.701) - (1.500 \times 182.31)}{(6 \times 0.550) - (1.500)^2} = 120.706 \approx 120.71$$

$$b_0 = \frac{182.31 - (120.706 \times 1.500)}{6} = 0.209 \approx 0.21$$

The relationship between the signal, $S$, and the analyte's concentration, $C_A$, therefore, is

$$S = 120.71 \times C_A + 0.21$$

For now we keep two decimal places to match the number of decimal places in the signal. The resulting calibration curve is shown in Figure 35.1.28.

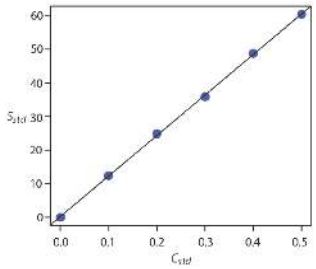



Figure 35.1.28: Calibration curve for the data in Example 35.1.10.

## Uncertainty in the Regression Model

As we see in Figure 35.1.28, because of indeterminate errors in the signal, the regression line does not pass through the exact center of each data point. The cumulative deviation of our data from the regression line—the total residual error—is proportional to the uncertainty in the regression. We call this uncertainty the standard deviation about the regression, $s_r$, which is equal to

$$s_r = \sqrt{\frac{\sum_{i=1}^{n}(y_i - \hat{y}_i)^2}{n-2}}$$

where $y_i$ is the $i^{\text{th}}$ experimental value, and $\hat{y}_i$ is the corresponding value predicted by the regression equation $\hat{y} = b_0 + b_1 x$. Note that the denominator indicates that our regression analysis has $n - 2$ degrees of freedom—we lose two degree of freedom because we use two parameters, the slope and the *y*-intercept, to calculate $\hat{y}_i$.

A more useful representation of the uncertainty in our regression analysis is to consider the effect of indeterminate errors on the slope, $b_1$, and the *y*-intercept, $b_0$, which we express as standard deviations.

$$s_{b_1} = \sqrt{\frac{n s_r^2}{n\sum_{i=1}^{n} x_i^2 - \left(\sum_{i=1}^{n} x_i\right)^2}} = \sqrt{\frac{s_r^2}{\sum_{i=1}^{n}(x_i - \overline{x})^2}}$$

$$s_{b_0} = \sqrt{\frac{s_r^2 \sum_{i=1}^{n} x_i^2}{n\sum_{i=1}^{n} x_i^2 - \left(\sum_{i=1}^{n} x_i\right)^2}} = \sqrt{\frac{s_r^2 \sum_{i=1}^{n} x_i^2}{n\sum_{i=1}^{n}(x_i - \overline{x})^2}}$$

We use these standard deviations to establish confidence intervals for the expected slope, $\beta_1$, and the expected *y*-intercept, $\beta_0$

$$\beta_1 = b_1 \pm t s_{b_1}$$

$$\beta_0 = b_0 \pm t s_{b_0}$$

where we select *t* for a significance level of $\alpha$ and for $n - 2$ degrees of freedom. Note that these equations do not contain the factor of $(\sqrt{n})^{-1}$ seen in the confidence intervals for $\mu$ because the confidence interval here is based on a single regression line.

### ✔ Example 35.1.11

Calculate the 95% confidence intervals for the slope and *y*-intercept from Example 35.1.10.

**Solution**

We begin by calculating the standard deviation about the regression. To do this we must calculate the predicted signals, $\hat{y}_i$ , using the slope and the *y*-intercept from Example 35.1.10, and the squares of the residual error, $(y_i - \hat{y}_i)^2$. Using the last standard as an example, we find that the predicted signal is

$$\hat{y}_6 = b_0 + b_1 x_6 = 0.209 + (120.706 \times 0.500) = 60.562$$

and that the square of the residual error is

$$(y_i - \hat{y}_i)^2 = (60.42 - 60.562)^2 = 0.2016 \approx 0.202$$

The following table displays the results for all six solutions.


https://chem.libretexts.org/@go/page/363066

| $x_i$ | $y_i$ | $\hat{y}_i$ | $(y_i - \hat{y}_i)^2$ |
|---|---|---|---|
| 0.000 | 0.00 | 0.209 | 0.0437 |
| 0.100 | 12.36 | 12.280 | 0.0064 |
| 0.200 | 24.83 | 24.350 | 0.2304 |
| 0.300 | 35.91 | 36.421 | 0.2611 |
| 0.400 | 48.79 | 48.491 | 0.0894 |
| 0.500 | 60.42 | 60.562 | 0.0202 |

Adding together the data in the last column gives the numerator in the equation for the standard deviation about the regression; thus

$$s_r = \sqrt{\frac{0.6512}{6-2}} = 0.4035$$

Next we calculate the standard deviations for the slope and the *y*-intercept. The values for the summation terms are from Example 35.1.10.

$$s_{b_1} = \sqrt{\frac{6 \times (0.4035)^2}{(6 \times 0.550) - (1.500)^2}} = 0.965$$

$$s_{b_0} = \sqrt{\frac{(0.4035)^2 \times 0.550}{(6 \times 0.550) - (1.500)^2}} = 0.292$$

Finally, the 95% confidence intervals ($\alpha = 0.05$, 4 degrees of freedom) for the slope and *y*-intercept are

$$\beta_1 = b_1 \pm t s_{b_1} = 120.706 \pm (2.78 \times 0.965) = 120.7 \pm 2.7$$

$$\beta_0 = b_0 \pm t s_{b_0} = 0.209 \pm (2.78 \times 0.292) = 0.2 \pm 0.80$$

where *t*(0.05, 4) from Appendix 3 is 2.78. The standard deviation about the regression, $s_r$, suggests that the signal, $S_{std}$, is precise to one decimal place. For this reason we report the slope and the *y*-intercept to a single decimal place.

### Using the Regression Model to Determine a Value for *x* Given a Value for *y*

Once we have our regression equation, it is easy to determine the concentration of analyte in a sample. When we use a normal calibration curve, for example, we measure the signal for our sample, $S_{samp}$, and calculate the analyte's concentration, $C_A$, using the regression equation.

$$C_A = \frac{S_{samp} - b_0}{b_1}$$

What is less obvious is how to report a confidence interval for $C_A$ that expresses the uncertainty in our analysis. To calculate a confidence interval we need to know the standard deviation in the analyte's concentration, $s_{C_A}$, which is given by the following equation

$$s_{C_A} = \frac{s_r}{b_1} \sqrt{\frac{1}{m} + \frac{1}{n} + \frac{\left(\overline{S}_{samp} - \overline{S}_{std}\right)^2}{(b_1)^2 \sum_{i=1}^{n} \left(C_{std_i} - \overline{C}_{std}\right)^2}}$$

where *m* is the number of replicates we use to establish the sample's average signal, $S_{samp}$, *n* is the number of calibration standards, $S_{std}$ is the average signal for the calibration standards, and $C_{std_i}$ and $\overline{C}_{std}$ are the individual and the mean concentrations for the calibration standards. Knowing the value of $s_{C_A}$, the confidence interval for the analyte's concentration is

$$\mu_{C_A} = C_A \pm t s_{C_A}$$

where $\mu_{C_A}$ is the expected value of $C_A$ in the absence of determinate errors, and with the value of $t$ is based on the desired level of confidence and $n$ – 2 degrees of freedom.

A close examination of these equations should convince you that we can decrease the uncertainty in the predicted concentration of analyte, $C_A$ if we increase the number of standards, $n$, increase the number of replicate samples that we analyze, $m$, and if the sample's average signal, $\overline{S}_{samp}$, is equal to the average signal for the standards, $\overline{S}_{std}$. When practical, you should plan your calibration curve so that $S_{samp}$ falls in the middle of the calibration curve. For more information about these regression equations see (a) Miller, J. N. *Analyst* **1991**, *116*, 3–14; (b) Sharaf, M. A.; Illman, D. L.; Kowalski, B. R. *Chemometrics*, Wiley-Interscience: New York, 1986, pp. 126-127; (c) Analytical Methods Committee "Uncertainties in concentrations estimated from calibration experiments," AMC Technical Brief, March 2006.

**Note**

The equation for the standard deviation in the analyte's concentration is written in terms of a calibration experiment. A more general form of the equation, written in terms of $x$ and $y$, is given here.

$$s_x = \frac{s_r}{b_1}\sqrt{\frac{1}{m} + \frac{1}{n} + \frac{\left(\overline{Y} - \overline{y}\right)^2}{(b_1)^2 \sum_{i=1}^{n}(x_i - \overline{x})^2}}$$

**Example 35.1.12**

Three replicate analyses for a sample that contains an unknown concentration of analyte, yields values for $S_{samp}$ of 29.32, 29.16 and 29.51 (arbitrary units). Using the results from Example 35.1.10 and Example 35.1.11, determine the analyte's concentration, $C_A$, and its 95% confidence interval.

**Solution**

The average signal, $\overline{S}_{samp}$, is 29.33, which, using the slope and the $y$-intercept from Example 35.1.10, gives the analyte's concentration as

$$C_A = \frac{\overline{S}_{samp} - b_0}{b_1} = \frac{29.33 - 0.209}{120.706} = 0.241$$

To calculate the standard deviation for the analyte's concentration we must determine the values for $\overline{S}_{std}$ and for $\sum_{i=1}^{2}(C_{std_i} - \overline{C}_{std})^2$. The former is just the average signal for the calibration standards, which, using the data in Table 35.1.10, is 30.385. Calculating $\sum_{i=1}^{2}(C_{std_i} - \overline{C}_{std})^2$ looks formidable, but we can simplify its calculation by recognizing that this sum-of-squares is the numerator in a standard deviation equation; thus,

$$\sum_{i=1}^{n}(C_{std_i} - \overline{C}_{std})^2 = (s_{C_{std}})^2 \times (n-1)$$

where $s_{C_{std}}$ is the standard deviation for the concentration of analyte in the calibration standards. Using the data in Table 35.1.10 we find that $s_{C_{std}}$ is 0.1871 and

$$\sum_{i=1}^{n}(C_{std_i} - \overline{C}_{std})^2 = (0.1872)^2 \times (6-1) = 0.175$$

Substituting known values into the equation for $s_{C_A}$ gives

$$s_{C_A} = \frac{0.4035}{120.706}\sqrt{\frac{1}{3} + \frac{1}{6} + \frac{(29.33 - 30.385)^2}{(120.706)^2 \times 0.175}} = 0.0024$$

Finally, the 95% confidence interval for 4 degrees of freedom is

$$\mu_{C_A} = C_A \pm t s_{C_A} = 0.241 \pm (2.78 \times 0.0024) = 0.241 \pm 0.007$$

Figure 35.1.29 shows the calibration curve with curves showing the 95% confidence interval for $C_A$.

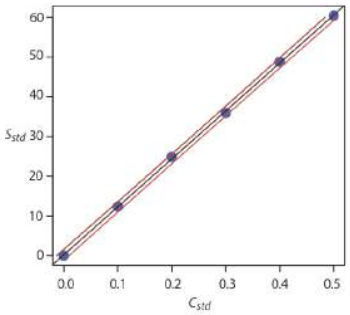



Figure 35.1.29: Example of a normal calibration curve with a superimposed confidence interval for the analyte's concentration. The points in blue are the original data from Table 35.1.10. The black line is the normal calibration curve as determined in Example 35.1.1. The red lines show the 95% confidence interval for $C_A$ assuming a single determination of $S_{samp}$.

## Evaluating a Regression Model

You should never accept the result of a linear regression analysis without evaluating the validity of the model. Perhaps the simplest way to evaluate a regression analysis is to examine the residual errors. As we saw earlier, the residual error for a single calibration standard, $r_i$, is

$$r_i = (y_i - \hat{y}_i)$$

If the regression model is valid, then the residual errors should be distributed randomly about an average residual error of zero, with no apparent trend toward either smaller or larger residual errors (Figure 35.1.30*a*). Trends such as those in Figure 35.1.30*b* and Figure 35.1.30*c* provide evidence that at least one of the model's assumptions is incorrect. For example, a trend toward larger residual errors at higher concentrations, Figure 35.1.30*b*, suggests that the indeterminate errors affecting the signal are not independent of the analyte's concentration. In Figure 35.1.30*c*, the residual errors are not random, which suggests we cannot model the data using a straight-line relationship. Regression methods for the latter two cases are discussed in the following sections.

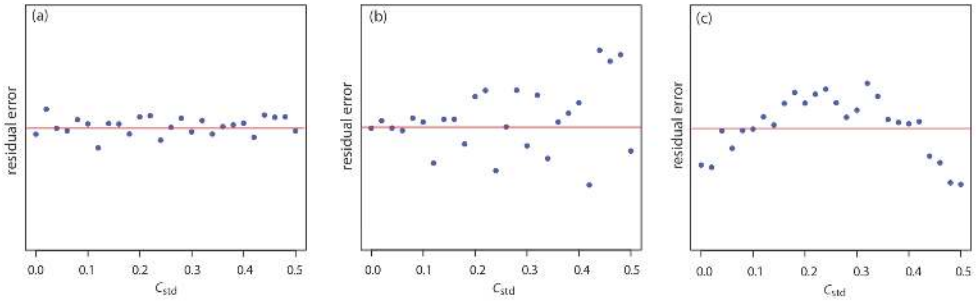



Figure 35.1.30: Plots of the residual error in the signal, $S_{std}$, as a function of the concentration of analyte, $C_{std}$, for an unweighted straight-line regression model. The red line shows a residual error of zero. The distribution of the residual errors in (a) indicates that the unweighted linear regression model is appropriate. The increase in the residual errors in (b) for higher concentrations of analyte, suggests that a weighted straight-line regression is more appropriate. For (c), the curved pattern to the residuals suggests that a straight-line model is inappropriate; linear regression using a quadratic model might produce a better fit.

### Example 35.1.13

Use your results from Exercise 35.1.10 to construct a residual plot and explain its significance.

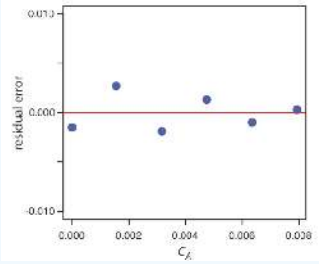
**Solution**

To create a residual plot, we need to calculate the residual error for each standard. The following table contains the relevant information.


https://chem.libretexts.org/@go/page/363066

| $x_i$ | $y_i$ | $\hat{y}_i$ | $y_i - \hat{y}_i$ |
|---|---|---|---|
| 0.000 | 0.000 | 0.0015 | –0.0015 |
| $1.55 \times 10^{-3}$ | 0.050 | 0.0473 | 0.0027 |
| $3.16 \times 10^{-3}$ | 0.093 | 0.0949 | –0.0019 |
| $4.74 \times 10^{-3}$ | 0.143 | 0.1417 | 0.0013 |
| $6.34 \times 10^{-3}$ | 0.188 | 0.1890 | –0.0010 |
| $7.92 \times 10^{-3}$ | 0.236 | 0.2357 | 0.0003 |

The figure below shows a plot of the resulting residual errors. The residual errors appear random, although they do alternate in sign, and they do not show any significant dependence on the analyte's concentration. Taken together, these observations suggest that our regression model is appropriate.




## Weighted Linear Regression With Errors in y

Our treatment of linear regression to this point assumes that any indeterminate errors that affect *y* are independent of the value of *x*. If this assumption is false, then we must include the variance for each value of *y* in our determination of the *y*-intercept, $b_0$, and the slope, $b_1$; thus

$$b_0 = \frac{\sum_{i=1}^{n} w_i y_i - b_1 \sum_{i=1}^{n} w_i x_i}{n}$$

$$b_1 = \frac{n \sum_{i=1}^{n} w_i x_i y_i - \sum_{i=1}^{n} w_i x_i \sum_{i=1}^{n} w_i y_i}{n \sum_{i=1}^{n} w_i x_i^2 - \left(\sum_{i=1}^{n} w_i x_i\right)^2}$$

where $w_i$ is a weighting factor that accounts for the variance in $y_i$

$$w_i = \frac{n(s_{y_i})^{-2}}{\sum_{i=1}^{n} (s_{y_i})^{-2}}$$

and $s_{y_i}$ is the standard deviation for $y_i$. In a weighted linear regression, each *xy*-pair's contribution to the regression line is inversely proportional to the precision of $y_i$; that is, the more precise the value of *y*, the greater its contribution to the regression.

### Example 35.1.14

Shown here are data for an external standardization in which $s_{std}$ is the standard deviation for three replicate determination of the signal.


https://chem.libretexts.org/@go/page/363066

| $C_{std}$ (arbitrary units) | $S_{std}$ (arbitrary units) | $s_{std}$ |
|---|---|---|
| 0.000 | 0.00 | 0.02 |
| 0.100 | 12.36 | 0.02 |
| 0.200 | 24.83 | 0.07 |
| 0.300 | 35.91 | 0.13 |
| 0.400 | 48.79 | 0.22 |
| 0.500 | 60.42 | 0.33 |

Determine the calibration curve's equation using a weighted linear regression. As you work through this example, remember that *x* corresponds to $C_{std}$, and that *y* corresponds to $S_{std}$.

### Solution

We begin by setting up a table to aid in calculating the weighting factors.

| $C_{std}$ (arbitrary units) | $S_{std}$ (arbitrary units) | $s_{std}$ | $(s_{y_i})^{-2}$ | $w_i$ |
|---|---|---|---|---|
| 0.000 | 0.00 | 0.02 | 2500.00 | 2.8339 |
| 0.100 | 12.36 | 0.02 | 250.00 | 2.8339 |
| 0.200 | 24.83 | 0.07 | 204.08 | 0.2313 |
| 0.300 | 35.91 | 0.13 | 59.17 | 0.0671 |
| 0.400 | 48.79 | 0.22 | 20.66 | 0.0234 |
| 0.500 | 60.42 | 0.33 | 9.18 | 0.0104 |

Adding together the values in the fourth column gives

$$\sum_{i=1}^{n} (s_{y_i})^{-2}$$

which we use to calculate the individual weights in the last column. As a check on your calculations, the sum of the individual weights must equal the number of calibration standards, *n*. The sum of the entries in the last column is 6.0000, so all is well. After we calculate the individual weights, we use a second table to aid in calculating the four summation terms in the equations for the slope, $b_1$, and the *y*-intercept, $b_0$.

| $x_i$ | $y_i$ | $w_i$ | $w_i x_i$ | $w_i y_i$ | $w_i x_i^2$ | $w_i x_i y_i$ |
|---|---|---|---|---|---|---|
| 0.000 | 0.00 | 2.8339 | 0.0000 | 0.0000 | 0.0000 | 0.0000 |
| 0.100 | 12.36 | 2.8339 | 0.2834 | 35.0270 | 0.0283 | 3.5027 |
| 0.200 | 24.83 | 0.2313 | 0.0463 | 5.7432 | 0.0093 | 1.1486 |
| 0.300 | 35.91 | 0.0671 | 0.0201 | 2.4096 | 0.0060 | 0.7229 |
| 0.400 | 48.79 | 0.0234 | 0.0094 | 1.1417 | 0.0037 | 0.4567 |
| 0.500 | 60.42 | 0.0104 | 0.0052 | 0.6284 | 0.0026 | 0.3142 |

Adding the values in the last four columns gives

$$\sum_{i=1}^{n} w_i x_i = 0.3644 \quad \sum_{i=1}^{n} w_i y_i = 44.9499 \quad \sum_{i=1}^{n} w_i x_i^2 = 0.0499 \quad \sum_{i=1}^{n} w_i x_i y_i = 6.1451$$

which gives the estimated slope and the estimated *y*-intercept as

$$b_1 = \frac{(6 \times 6.1451) - (0.3644 \times 44.9499)}{(6 \times 0.0499) - (0.3644)^2} = 122.985$$

$$b_0 = \frac{44.9499 - (122.985 \times 0.3644)}{6} = 0.0224$$

The calibration equation is

$$S_{std} = 122.98 \times C_{std} + 0.2$$

Figure 35.1.31 shows the calibration curve for the weighted regression determined here and the calibration curve for the unweighted regression. Although the two calibration curves are very similar, there are slight differences in the slope and in the *y*-intercept. Most notably, the *y*-intercept for the weighted linear regression is closer to the expected value of zero. Because the standard deviation for the signal, $S_{std}$, is smaller for smaller concentrations of analyte, $C_{std}$, a weighted linear regression gives more emphasis to these standards, allowing for a better estimate of the *y*-intercept.

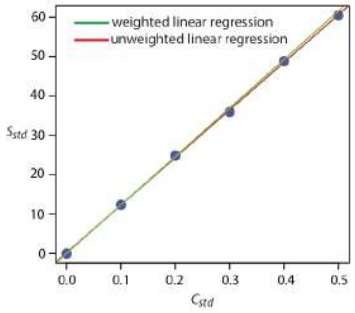



Figure 35.1.31: A comparison of the unweighted and the weighted normal calibration curves. See Example 35.1.11 for details of the unweighted linear regression and Example 35.1.14 for details of the weighted linear regression.

Equations for calculating confidence intervals for the slope, the *y*-intercept, and the concentration of analyte when using a weighted linear regression are not as easy to define as for an unweighted linear regression [Bonate, P. J. *Anal. Chem.* **1993**, *65*, 1367–1372]. The confidence interval for the analyte's concentration, however, is at its optimum value when the analyte's signal is near the weighted centroid, $y_c$ , of the calibration curve.

$$y_c = \frac{1}{n} \sum_{i=1}^{n} w_i x_i$$

### Weighted Linear Regression With Errors in x and y

If we remove our assumption that indeterminate errors affecting a calibration curve are present only in the signal (*y*), then we also must factor into the regression model the indeterminate errors that affect the analyte's concentration in the calibration standards (*x*). The solution for the resulting regression line is computationally more involved than that for either the unweighted or weighted regression lines. Although we will not consider the details in this textbook, you should be aware that neglecting the presence of indeterminate errors in *x* can bias the results of a linear regression.

**Note**

See, for example, Analytical Methods Committee, "Fitting a linear functional relationship to data with error on both variable," AMC Technical Brief, March, 2002), as well as this chapter's Additional Resources.

### Curvilinear, Multivariable, and Multivariate Regression

A straight-line regression model, despite its apparent complexity, is the simplest functional relationship between two variables. What do we do if our calibration curve is curvilinear—that is, if it is a curved-line instead of a straight-line? One approach is to try

transforming the data into a straight-line. Logarithms, exponentials, reciprocals, square roots, and trigonometric functions have been used in this way. A plot of log(*y*) versus *x* is a typical example. Such transformations are not without complications, of which the most obvious is that data with a uniform variance in *y* will not maintain that uniform variance after it is transformed.

**Note**

It is worth noting here that the term "linear" does not mean a straight-line. A linear function may contain more than one additive term, but each such term has one and only one adjustable multiplicative parameter. The function

$$y = ax + bx^2$$

is an example of a linear function because the terms *x* and $x^2$ each include a single multiplicative parameter, *a* and *b*, respectively. The function

$$y = x^b$$

is nonlinear because *b* is not a multiplicative parameter; it is, instead, a power. This is why you can use linear regression to fit a polynomial equation to your data.

Sometimes it is possible to transform a nonlinear function into a linear function. For example, taking the log of both sides of the nonlinear function above gives a linear function.

$$\log(y) = b\log(x)$$

Another approach to developing a linear regression model is to fit a polynomial equation to the data, such as $y = a + bx + cx^2$. You can use linear regression to calculate the parameters *a*, *b*, and *c*, although the equations are different than those for the linear regression of a straight-line. If you cannot fit your data using a single polynomial equation, it may be possible to fit separate polynomial equations to short segments of the calibration curve. The result is a single continuous calibration curve known as a spline function. The use of R for curvilinear regression is included in Chapter 8.5.

**Note**

For details about curvilinear regression, see (a) Sharaf, M. A.; Illman, D. L.; Kowalski, B. R. *Chemometrics*, Wiley-Interscience: New York, 1986; (b) Deming, S. N.; Morgan, S. L. *Experimental Design: A Chemometric Approach*, Elsevier: Amsterdam, 1987.

The regression models in this chapter apply only to functions that contain a single dependent variable and a single independent variable. One example is the simplest form of Beer's law in which the absorbance, $A$, of a sample at a single wavelength, $\lambda$, depends upon the concentration of a single analyte, $C_A$

$$A_\lambda = \epsilon_{\lambda,A} b C_A$$

where $\epsilon_{\lambda,A}$ is the analyte's molar absorptivity at the selected wavelength and $b$ is the pathlength through the sample. In the presence of an interferent, $I$, however, the signal may depend on the concentrations of both the analyte and the interferent

$$A_\lambda = \epsilon_{\lambda,A} b C_A + \epsilon_{\lambda,I} b C_I$$

where $\epsilon_{\lambda,I}$ is the interferent's molar absorptivity and $C_I$ is the interferent's concentration. This is an example of multivariable regression, which is covered in more detail in Chapter 9 when we consider the optimization of experiments where there is a single dependent variable and two or more independent variables.

In multivariate regression we have both multiple dependent variables, such as the absorbance of samples at two or more wavelengths, and multiple independent variables, such as the concentrations of two or more analytes in the samples. As discussed in Chapter 0.2, we can represent this using matrix notation

$$\begin{bmatrix} \cdots & \cdots & \cdots \\ \vdots & A & \vdots \\ \cdots & \cdots & \cdots \end{bmatrix}_{r \times c} = \begin{bmatrix} \cdots & \cdots & \cdots \\ \vdots & \epsilon b & \vdots \\ \cdots & \cdots & \cdots \end{bmatrix}_{r \times n} \times \begin{bmatrix} \cdots & \cdots & \cdots \\ \vdots & C & \vdots \\ \cdots & \cdots & \cdots \end{bmatrix}_{n \times c}$$

where there are $r$ wavelengths, $c$ samples, and $n$ analytes. Each column in the $\epsilon b$ matrix, for example, holds the $\epsilon b$ value for a different analyte at one of $r$ wavelengths, and each row in the $C$ matrix is the concentration of one of the $n$ analytes in one of the $c$ samples. We will consider this approach in more detail in Chapter 11.

**Note**

For a nice discussion of the difference between multivariable regression and multivariate regression, see Hidalgo, B.; Goodman, M. "Multivariate or Multivariable Regression," *Am. J. Public Health*, **2013**, *103*, 39-40.

This page titled 35.1: Evaluation of Analytical Data is shared under a CC BY-NC-SA 4.0 license and was authored, remixed, and/or curated by David Harvey.

# 35.2: Single-Sided Normal Distribution

Table 35.2.1, at the bottom of this appendix, gives the proportion, *P*, of the area under a normal distribution curve that lies to the right of a deviation, *z*

$$z = \frac{X - \mu}{\sigma}$$

where *X* is the value for which the deviation is defined, $\mu$ is the distribution's mean value and $\sigma$ is the distribution's standard deviation. For example, the proportion of the area under a normal distribution to the right of a deviation of 0.04 is 0.4840 (see entry in red in the table), or 48.40% of the total area (see the area shaded blue in Figure 35.2.1). The proportion of the area to the left of the deviation is 1 – *P*. For a deviation of 0.04, this is 1 – 0.4840, or 51.60%.

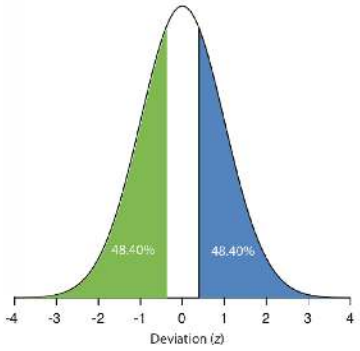



Figure 35.2.1. Normal distribution curve showing the area under a curve greater than a deviation of +0.04 (blue) and with a deviation less than –0.04 (green).

When the deviation is negative—that is, when *X* is smaller than $\mu$—the value of *z* is negative. In this case, the values in the table give the area to the left of *z*. For example, if *z* is –0.04, then 48.40% of the area lies to the left of the deviation (see area shaded green in Figure 35.2.1.

To use the single-sided normal distribution table, sketch the normal distribution curve for your problem and shade the area that corresponds to your answer (for example, see Figure 35.2.2, which is for Example 4.4.2).

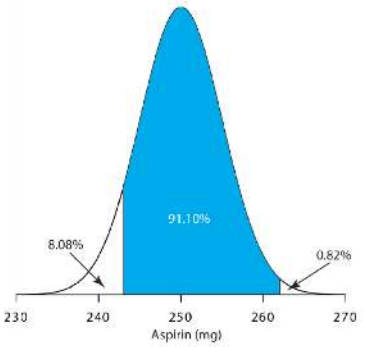



Figure 35.2.2. Normal distribution for the population of aspirin tablets in Example 4.4.2. The population's mean and standard deviation are 250 mg and 5 mg, respectively. The shaded area shows the percentage of tablets containing between 243 mg and 262 mg of aspirin.

This divides the normal distribution curve into three regions: the area that corresponds to our answer (shown in blue), the area to the right of this, and the area to the left of this. Calculate the values of *z* for the limits of the area that corresponds to your answer. Use the table to find the areas to the right and to the left of these deviations. Subtract these values from 100% and, voilà, you have your answer.

Table 35.2.1: Values for a Single-Sided Normal Distribution

| z | 0.00 | 0.01 | 0.02 | 0.03 | 0.04 | 0.05 | 0.06 | 0.07 | 0.08 | 0.09 |
|---|---|---|---|---|---|---|---|---|---|---|
| **0.0** | 0.5000 | 0.4960 | 0.4920 | 0.4880 | 0.4840 | 0.4801 | 0.4761 | 0.4721 | 0.4681 | 0.4641 |
| **0.1** | 0.4602 | 0.4562 | 0.4522 | 0.4483 | 0.4443 | 0.4404 | 0.4365 | 0.4325 | 0.4286 | 0.4247 |
| **0.2** | 0.4207 | 0.4168 | 0.4129 | 0.4090 | 0.4502 | 0.4013 | 0.3974 | 0.3396 | 0.3897 | 0.3859 |
| **0.3** | 0.3821 | 0.3783 | 0.3745 | 0.3707 | 0.3669 | 0.3632 | 0.3594 | 0.3557 | 0.3520 | 0.3483 |
| **0.4** | 0.3446 | 0.3409 | 0.3372 | 0.3336 | 0.3300 | 0.3264 | 0.3228 | 0.3192 | 0.3156 | 0.3121 |
| **0.5** | 0.3085 | 0.3050 | 0.3015 | 0.2981 | 0.2946 | 0.2912 | 0.2877 | 0.2843 | 0.2810 | 0.2776 |
| **0.6** | 0.2743 | 0.2709 | 0.2676 | 0.2643 | 0.2611 | 0.2578 | 0.2546 | 0.2514 | 0.2483 | 0.2451 |
| **0.7** | 0.2420 | 0.2389 | 0.2358 | 0.2327 | 0.2296 | 0.2266 | 0.2236 | 0.2206 | 0.2177 | 0.2148 |
| **0.8** | 0.2119 | 0.2090 | 0.2061 | 0.2033 | 0.2005 | 0.1977 | 0.1949 | 0.1922 | 0.1894 | 0.1867 |
| **0.9** | 0.1841 | 0.1814 | 0.1788 | 0.1762 | 0.1736 | 0.1711 | 0.1685 | 0.1660 | 0.1635 | 0.1611 |
| **1.0** | 0.1587 | 0.1562 | 0.1539 | 0.1515 | 0.1492 | 0.1469 | 0.1446 | 0.1423 | 0.1401 | 0.1379 |
| **1.1** | 0.1357 | 0.1335 | 0.1314 | 0.1292 | 0.1271 | 0.1251 | 0.1230 | 0.1210 | 0.1190 | 0.1170 |
| **1.2** | 0.1151 | 0.1131 | 0.1112 | 0.1093 | 0.1075 | 0.1056 | 0.1038 | 0.1020 | 0.1003 | 0.0985 |
| **1.3** | 0.0968 | 0.0951 | 0.0934 | 0.0918 | 0.0901 | 0.0885 | 0.0869 | 0.0853 | 0.0838 | 0.0823 |
| **1.4** | 0.0808 | 0.0793 | 0.0778 | 0.0764 | 0.0749 | 0.0735 | 0.0721 | 0.0708 | 0.0694 | 0.0681 |
| **1.5** | 0.0668 | 0.0655 | 0.0643 | 0.0630 | 0.0618 | 0.0606 | 0.0594 | 0.0582 | 0.0571 | 0.0559 |
| **1.6** | 0.0548 | 0.0537 | 0.0526 | 0.0516 | 0.0505 | 0.0495 | 0.0485 | 0.0475 | 0.0465 | 0.0455 |
| **1.7** | 0.0466 | 0.0436 | 0.0427 | 0.0418 | 0.0409 | 0.0401 | 0.0392 | 0.0384 | 0.0375 | 0.0367 |
| **1.8** | 0.0359 | 0.0351 | 0.0344 | 0.0336 | 0.0329 | 0.0322 | 0.0314 | 0.0307 | 0.0301 | 0.0294 |
| **1.9** | 0.0287 | 0.0281 | 0.0274 | 0.0268 | 0.0262 | 0.0256 | 0.0250 | 0.0244 | 0.0239 | 0.0233 |
| **2.0** | 0.0228 | 0.0222 | 0.0217 | 0.0212 | 0.0207 | 0.0202 | 0.0197 | 0.0192 | 0.0188 | 0.0183 |
| **2.1** | 0.0179 | 0.0174 | 0.0170 | 0.0166 | 0.0162 | 0.0158 | 0.0154 | 0.0150 | 0.0146 | 0.0143 |
| **2.2** | 0.0139 | 0.0136 | 0.0132 | 0.0129 | 0.0125 | 0.0122 | 0.0119 | 0.0116 | 0.0113 | 0.0110 |
| **2.3** | 0.0107 | 0.0104 | 0.0102 | | 0.00964 | | 0.00914 | | 0.00866 | |
| **2.4** | 0.00820 | | 0.00776 | | 0.00734 | | 0.00695 | | 0.00657 | |
| **2.5** | 0.00621 | | 0.00587 | | 0.00554 | | 0.00523 | | 0.00494 | |
| **2.6** | 0.00466 | | 0.00440 | | 0.00415 | | 0.00391 | | 0.00368 | |
| **2.7** | 0.00347 | | 0.00326 | | 0.00307 | | 0.00289 | | 0.00272 | |
| **2.8** | 0.00256 | | 0.00240 | | 0.00226 | | 0.00212 | | 0.00199 | |
| **2.9** | 0.00187 | | 0.00175 | | 0.00164 | | 0.00154 | | 0.00144 | |
| **3.0** | 0.00135 | | | | | | | | | |
| **3.1** | 0.000968 | | | | | | | | | |

| | | | | | | | | | | |
|---|---|---|---|---|---|---|---|---|---|---|
| **3.2** | 0.000687 | | | | | | | | | |
| **3.3** | 0.000483 | | | | | | | | | |
| **3.4** | 0.000337 | | | | | | | | | |
| **3.5** | 0.000233 | | | | | | | | | |
| **3.6** | 0.000159 | | | | | | | | | |
| **3.7** | 0.000108 | | | | | | | | | |
| **3.8** | 0.0000723 | | | | | | | | | |
| **3.9** | 0.0000481 | | | | | | | | | |
| **4.0** | 0.0000317 | | | | | | | | | |

This page titled 35.2: Single-Sided Normal Distribution is shared under a CC BY-NC-SA 4.0 license and was authored, remixed, and/or curated by David Harvey.

# 35.3: Critical Values for t-Test

Assuming we have calculated $t_{exp}$, there are two approaches to interpreting a *t*-test. In the first approach we choose a value of $\alpha$ for rejecting the null hypothesis and read the value of $t(\alpha, \nu)$ from the table below. If $t_{exp} > t(\alpha, \nu)$, we reject the null hypothesis and accept the alternative hypothesis. In the second approach, we find the row in the table below that corresponds to the available degrees of freedom and move across the row to find (or estimate) the a that corresponds to $t_{exp} = t(\alpha, \nu)$; this establishes largest value of $\alpha$ for which we can retain the null hypothesis. Finding, for example, that $\alpha$ is 0.10 means that we retain the null hypothesis at the 90% confidence level, but reject it at the 89% confidence level. The examples in this textbook use the first approach.

Table 35.3.1: Critical Values of t for the t-Test

| Values of t for… | | | | |
|---|---|---|---|---|
| …a confidence interval of: | 90% | 95% | 98% | 99% |
| …an $\alpha$ value of: | 0.10 | 0.05 | 0.02 | 0.01 |
| Degrees of Freedom | | | | |
| 1 | 6.314 | 12.706 | 31.821 | 63.657 |
| 2 | 2.920 | 4.303 | 6.965 | 9.925 |
| 3 | 2.353 | 3.182 | 4.541 | 5.841 |
| 4 | 2.132 | 2.776 | 3.747 | 4.604 |
| 5 | 2.015 | 2.571 | 3.365 | 4.032 |
| 6 | 1.943 | 2.447 | 3.143 | 3.707 |
| 7 | 1.895 | 2.365 | 2.998 | 3.499 |
| 8 | 1.860 | 2.306 | 2.896 | 3.255 |
| 9 | 1.833 | 2.262 | 2.821 | 3.250 |
| 10 | 1.812 | 2.228 | 2.764 | 3.169 |
| 12 | 1.782 | 2.179 | 2.681 | 3.055 |
| 14 | 1.761 | 2.145 | 2.624 | 2.977 |
| 16 | 1.746 | 2.120 | 2.583 | 2.921 |
| 18 | 1.734 | 2.101 | 2.552 | 2.878 |
| 20 | 1.725 | 2.086 | 2.528 | 2.845 |
| 30 | 1.697 | 2.042 | 2.457 | 2.750 |
| 50 | 1.676 | 2.009 | 2.311 | 2.678 |
| $\infty$ | 1.645 | 1.960 | 2.326 | 2.576 |

The values in this table are for a two-tailed *t*-test. For a one-tailed test, divide the $\alpha$ values by 2. For example, the last column has an $\alpha$ value of 0.005 and a confidence interval of 99.5% when conducting a one-tailed *t*-test.

This page titled 35.3: Critical Values for t-Test is shared under a CC BY-NC-SA 4.0 license and was authored, remixed, and/or curated by David Harvey.

# 35.4: Critical Values for F-Test

The following tables provide values for $F(0.05, \nu_{\text{num}}, \nu_{\text{denom}})$ for one-tailed and for two-tailed *F*-tests. To use these tables, we first decide whether the situation calls for a one-tailed or a two-tailed analysis and calculate $F_{\text{exp}}$

$$F_{\text{exp}} = \frac{s_A^2}{s_B^2}$$

where $S_A^2$ is greater than $s_B^2$. Next, we compare *F*exp to $F(0.05, \nu_{\text{num}}, \nu_{\text{denom}})$ and reject the null hypothesis if $F_{\text{exp}} > F(0.05, \nu_{\text{num}}, \nu_{\text{denom}})$. You may replace *s* with $\sigma$ if you know the population's standard deviation.

Table 35.4.1: Critical Values of F for a One-Tailed F-Test

| $\frac{\nu_{\text{num}} \rightarrow}{\nu_{denom} \downarrow}$ | 1 | 2 | 3 | 4 | 5 | 6 | 7 | 8 | 9 | 10 | 15 | 20 | ∞ |
|---|---|---|---|---|---|---|---|---|---|---|---|---|---|
| **1** | 161.4 | 199.5 | 215.7 | 224.6 | 230.2 | 234.0 | 236.8 | 238.9 | 240.5 | 241.9 | 245.9 | 248.0 | 254.3 |
| **2** | 18.51 | 19.00 | 19.16 | 19.25 | 19.30 | 19.33 | 19.35 | 19.37 | 19.38 | 19.40 | 19.43 | 19.45 | 19.50 |
| **3** | 10.13 | 9.552 | 9.277 | 9.117 | 9.013 | 8.941 | 8.887 | 8.845 | 8.812 | 8.786 | 8.703 | 8.660 | 8.526 |
| **4** | 7.709 | 6.994 | 6.591 | 6.388 | 6.256 | 6.163 | 6.094 | 6.041 | 5.999 | 5.964 | 5.858 | 5.803 | 5.628 |
| **5** | 6.608 | 5.786 | 5.409 | 5.192 | 5.050 | 4.950 | 4.876 | 4.818 | 4.722 | 4.753 | 4.619 | 4.558 | 4.365 |
| **6** | 5.987 | 5.143 | 4.757 | 4.534 | 4.387 | 4.284 | 4.207 | 4.147 | 4.099 | 4.060 | 3.938 | 3.874 | 3.669 |
| **7** | 5.591 | 4.737 | 4.347 | 4.120 | 3.972 | 3.866 | 3.787 | 3.726 | 3.677 | 3.637 | 3.511 | 3.445 | 3.230 |
| **8** | 5.318 | 4.459 | 4.066 | 3.838 | 3.687 | 3.581 | 3.500 | 3.438 | 3.388 | 3.347 | 3.218 | 3.150 | 2.928 |
| **9** | 5.117 | 4.256 | 3.863 | 3.633 | 3.482 | 3.374 | 3.293 | 3.230 | 3.179 | 3.137 | 3.006 | 2.936 | 2.707 |
| **10** | 4.965 | 4.103 | 3.708 | 3.478 | 3.326 | 3.217 | 3.135 | 3.072 | 3.020 | 2.978 | 2.845 | 2.774 | 2.538 |
| **11** | 4.844 | 3.982 | 3.587 | 3.257 | 3.204 | 3.095 | 3.012 | 2.948 | 2.896 | 2.854 | 2.719 | 2.646 | 2.404 |
| **12** | 4.747 | 3.885 | 3.490 | 3.259 | 3.106 | 2.996 | 2.913 | 2.849 | 2.796 | 2.753 | 2.617 | 2.544 | 2.296 |
| **13** | 4.667 | 3.806 | 3.411 | 3.179 | 3.025 | 2.915 | 2.832 | 2.767 | 2.714 | 2.671 | 2.533 | 2.459 | 2.206 |
| **14** | 4.600 | 3.739 | 3.344 | 3.112 | 2.958 | 2.848 | 2.764 | 2.699 | 2.646 | 2.602 | 2.463 | 2.388 | 2.131 |
| **15** | 4.534 | 3.682 | 3.287 | 3.056 | 2.901 | 2.790 | 2.707 | 2.641 | 2.588 | 2.544 | 2.403 | 2.328 | 2.066 |
| **16** | 4.494 | 3.634 | 3.239 | 3.007 | 2.852 | 2.741 | 2.657 | 2.591 | 2.538 | 2.494 | 2.352 | 2.276 | 2.010 |
| **17** | 4.451 | 3.592 | 3.197 | 2.965 | 2.810 | 2.699 | 2.614 | 2.548 | 2.494 | 2.450 | 2.308 | 2.230 | 1.960 |
| **18** | 4.414 | 3.555 | 3.160 | 2.928 | 2.773 | 2.661 | 2.577 | 2.510 | 2.456 | 2.412 | 2.269 | 2.191 | 1.917 |
| **19** | 4.381 | 3.552 | 3.127 | 2.895 | 2.740 | 2.628 | 2.544 | 2.477 | 2.423 | 2.378 | 2.234 | 2.155 | 1.878 |
| **20** | 4,351 | 3.493 | 3.098 | 2.866 | 2.711 | 2.599 | 2.514 | 2.447 | 2.393 | 2.348 | 2.203 | 2.124 | 1.843 |
| ∞ | 3.842 | 2.996 | 2.605 | 2.372 | 2.214 | 2.099 | 2.010 | 1.938 | 1.880 | 1.831 | 1.666 | 1.570 | 1.000 |

Table 35.4.2: Critical Values of F for a Two-Tailed F-Test

| $\nu_{num} \rightarrow$ / $\nu_{denom} \downarrow$ | 1 | 2 | 3 | 4 | 5 | 6 | 7 | 8 | 9 | 10 | 15 | 20 | ∞ |
|---|---|---|---|---|---|---|---|---|---|---|---|---|---|
| **1** | 647.8 | 799.5 | 864.2 | 899.6 | 921.8 | 937.1 | 948.2 | 956.7 | 963.3 | 968.6 | 984.9 | 993.1 | 1018 |
| **2** | 38.51 | 39.00 | 39.17 | 39.25 | 39.30 | 39.33 | 39.36 | 39.37 | 39.39 | 39.40 | 39.43 | 39.45 | 39.50 |
| **3** | 17.44 | 16.04 | 15.44 | 15.10 | 14.88 | 14.73 | 14.62 | 14.54 | 14.47 | 14.42 | 14.25 | 14.17 | 13.90 |
| **4** | 12.22 | 10.65 | 9.979 | 9.605 | 9.364 | 9.197 | 9.074 | 8.980 | 8.905 | 8.444 | 8.657 | 8.560 | 8.257 |
| **5** | 10.01 | 8.434 | 7.764 | 7.388 | 7.146 | 6.978 | 6.853 | 6.757 | 6.681 | 6.619 | 6.428 | 6.329 | 6.015 |
| **6** | 8.813 | 7.260 | 6.599 | 6.227 | 5.988 | 5.820 | 5.695 | 5.600 | 5.523 | 5.461 | 5.269 | 5.168 | 4.894 |
| **7** | 8.073 | 6.542 | 5.890 | 5.523 | 5.285 | 5.119 | 4.995 | 4.899 | 4.823 | 4.761 | 4.568 | 4.467 | 4.142 |
| **8** | 7.571 | 6.059 | 5.416 | 5.053 | 4.817 | 4.652 | 4.529 | 4.433 | 4.357 | 4.259 | 4.101 | 3.999 | 3.670 |
| **9** | 7.209 | 5.715 | 5.078 | 4.718 | 4.484 | 4.320 | 4.197 | 4.102 | 4.026 | 3.964 | 3.769 | 3.667 | 3.333 |
| **10** | 6.937 | 5.456 | 4.826 | 4.468 | 4.236 | 4.072 | 3.950 | 3.855 | 3.779 | 3.717 | 3.522 | 3.419 | 3.080 |
| **11** | 6.724 | 5.256 | 4.630 | 4.275 | 4.044 | 3.881 | 3.759 | 3.644 | 3.588 | 3.526 | 3.330 | 3.226 | 2.883 |
| **12** | 6.544 | 5.096 | 4.474 | 4.121 | 3.891 | 3.728 | 3.607 | 3.512 | 3.436 | 3.374 | 3.177 | 3.073 | 2.725 |
| **13** | 6.414 | 4.965 | 4.347 | 3.996 | 3.767 | 3.604 | 3.483 | 3.388 | 3.312 | 3.250 | 3.053 | 2.948 | 2.596 |
| **14** | 6.298 | 4.857 | 4.242 | 3.892 | 3.663 | 3.501 | 3.380 | 3.285 | 3.209 | 3.147 | 2.949 | 2.844 | 2.487 |
| **15** | 6.200 | 4.765 | 4.153 | 3.804 | 3.576 | 3.415 | 3.293 | 3.199 | 3.123 | 3.060 | 2.862 | 2.756 | 2.395 |
| **16** | 6.115 | 4.687 | 4.077 | 3.729 | 3.502 | 3.341 | 3.219 | 3.125 | 3.049 | 2.986 | 2.788 | 2.681 | 2.316 |
| **17** | 6.042 | 4.619 | 4.011 | 3.665 | 3.438 | 3.277 | 3.156 | 3.061 | 2.985 | 2.922 | 2.723 | 2.616 | 2.247 |
| **18** | 5.978 | 4.560 | 3.954 | 3.608 | 3.382 | 3.221 | 3.100 | 3.005 | 2.929 | 2.866 | 2.667 | 2.559 | 2.187 |
| **19** | 5.922 | 4.508 | 3.903 | 3.559 | 3.333 | 3.172 | 3.051 | 2.956 | 2.880 | 2.817 | 2.617 | 2.509 | 2.133 |
| **20** | 5.871 | 4.461 | 3.859 | 3.515 | 3.289 | 3.128 | 3.007 | 2.913 | 2.837 | 2.774 | 2.573 | 2.464 | 2.085 |
| ∞ | 5.024 | 3.689 | 3.116 | 2.786 | 2.567 | 2.408 | 2.288 | 2.192 | 2.114 | 2.048 | 1.833 | 1.708 | 1.000 |

This page titled 35.4: Critical Values for F-Test is shared under a CC BY-NC-SA 4.0 license and was authored, remixed, and/or curated by David Harvey.

# 35.5: Critical Values for Dixon's Q-Test

The following table provides critical values for $Q(\alpha, n)$, where $\alpha$ is the probability of incorrectly rejecting the suspected outlier and $n$ is the number of samples in the data set. There are several versions of Dixon's *Q*-Test, each of which calculates a value for $Q_{ij}$ where *i* is the number of suspected outliers on one end of the data set and *j* is the number of suspected outliers on the opposite end of the data set. The critical values for *Q* here are for a single outlier, $Q_{10}$, where

$$Q_{\text{exp}} = Q_{10} = \frac{|\text{outlier's value} - \text{nearest value}|}{\text{largest value} - \text{smallest value}}$$

The suspected outlier is rejected if $Q_{\text{exp}}$ is greater than $Q(\alpha, n)$. For additional information consult Rorabacher, D. B. "Statistical Treatment for Rejection of Deviant Values: Critical Values of Dixon's '*Q*' Parameter and Related Subrange Ratios at the 95% confidence Level," *Anal. Chem.* **1991**, *63*, 139–146.

Table 35.5.1: Critical Values for Dixon's Q-Test

| $\frac{\alpha \longrightarrow}{n \downarrow}$ | **0.1** | **0.05** | **0.04** | **0.02** | **0.01** |
|---|---|---|---|---|---|
| **3** | 0.941 | 0.970 | 0.976 | 0.988 | 0.994 |
| **4** | 0.765 | 0.829 | 0.846 | 0.889 | 0.926 |
| **5** | 0.642 | 0.710 | 0.729 | 0.780 | 0.821 |
| **6** | 0.560 | 0.625 | 0.644 | 0.698 | 0.740 |
| **7** | 0.507 | 0.568 | 0.586 | 0.637 | 0.680 |
| **8** | 0.468 | 0.526 | 0.543 | 0.590 | 0.634 |
| **9** | 0.437 | 0.493 | 0.510 | 0.555 | 0.598 |
| **10** | 0.412 | 0.466 | 0.483 | 0.527 | 0.568 |

This page titled 35.5: Critical Values for Dixon's Q-Test is shared under a CC BY-NC-SA 4.0 license and was authored, remixed, and/or curated by David Harvey.

# 35.6: Critical Values for Grubb's Test

The following table provides critical values for $G(\alpha, n)$, where $\alpha$ is the probability of incorrectly rejecting the suspected outlier and *n* is the number of samples in the data set. There are several versions of Grubb's Test, each of which calculates a value for $G_{ij}$ where *i* is the number of suspected outliers on one end of the data set and *j* is the number of suspected outliers on the opposite end of the data set. The critical values for *G* given here are for a single outlier, $G_{10}$, where

$$G_{\text{exp}} = G_{10} = \frac{|X_{out} - \overline{X}|}{s}$$

The suspected outlier is rejected if $G_{\text{exp}}$ is greater than $G(\alpha, n)$.

Table 35.6.1: Critical Values for the Grubb's Test

| $\frac{\alpha \longrightarrow}{n \downarrow}$ | **0.05** | **0.01** |
|---|---|---|
| **3** | 1.155 | 1.155 |
| **4** | 1.481 | 1.496 |
| **5** | 1.715 | 1.764 |
| **6** | 1.887 | 1.973 |
| **7** | 2.020 | 2.139 |
| **8** | 2.126 | 2.274 |
| **9** | 2.215 | 2.387 |
| **10** | 2.290 | 2.482 |
| **11** | 2.355 | 2.564 |
| **12** | 2.412 | 2.636 |
| **13** | 2.462 | 2.699 |
| **14** | 2.507 | 2.755 |
| **15** | 2.549 | 2.755 |

This page titled 35.6: Critical Values for Grubb's Test is shared under a CC BY-NC-SA 4.0 license and was authored, remixed, and/or curated by David Harvey.

# 35.7: Activity Coefficients

Careful measurements on the metal–ligand complex $Fe(SCN)^{2+}$ suggest its stability decreases in the presence of inert ions [Lister, M. W.; Rivington, D. E. *Can. J. Chem.* **1995**, *33*, 1572–1590]. We can demonstrate this by adding an inert salt to an equilibrium mixture of $Fe^{3+}$ and $SCN^-$. Figure 35.7.1 a shows the result of mixing together equal volumes of 1.0 mM $FeCl_3$ and 1.5 mM KSCN, both of which are colorless. The solution's reddish–orange color is due to the formation of $Fe(SCN)^{2+}$.

$$Fe^{3+}(aq) + SCN^-(aq) \rightleftharpoons Fe(SCN)^{2+}(aq) \tag{35.7.1}$$

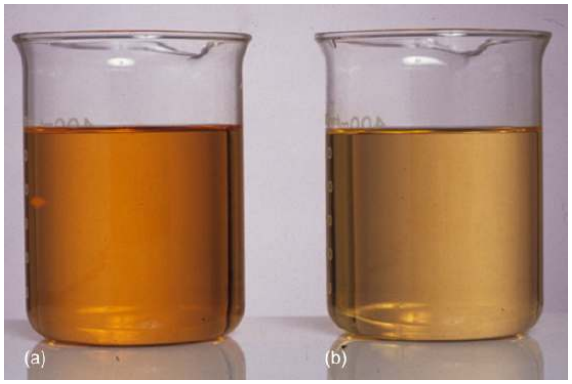



Figure 35.7.1 . The effect of a inert salt on a reaction's equilibrium position is shown by the solutions in these two beakers. The beaker on the left contains equal volumes of 1.0 mM $FeCl_3$ and 1.5 mM KSCN. The solution's color is due to the formation of the metal–ligand complex $Fe(SCN)^{2+}$. Adding 10 g of $KNO_3$ to the beaker on the left produces the result shown on the right. The lighter color suggests that there is less $Fe(SCN)^{2+}$ as a result of the equilibrium in reaction 35.7.1 shifting to the left.

Adding 10 g of $KNO_3$ to the solution and stirring to dissolve the solid, produces the result shown in Figure 35.7.1 b. The solution's lighter color suggests that adding $KNO_3$ shifts reaction 35.7.1 to the left, decreasing the concentration of $Fe(SCN)^{2+}$ and increasing the concentrations of $Fe^{3+}$ and $SCN^-$. The result is a decrease in the complex's formation constant, $K_1$.

$$K_1 = \frac{[Fe(SCN)^{2+}]}{[Fe^{3+}]\,[SCN^-]} \tag{35.7.2}$$

Why should adding an inert electrolyte affect a reaction's equilibrium position? We can explain the effect of $KNO_3$ on the formation of $Fe(SCN)^{2+}$ if we consider the reaction on a microscopic scale. The solution in Figure 35.7.1 b contains a variety of cations and anions: $Fe^{3+}$, $SCN^-$, $K^+$, $NO_3^-$, $H_3O^+$, and $OH^-$. Although the solution is homogeneous, on average, there are slightly more anions in regions near the $Fe^{3+}$ ions, and slightly more cations in regions near the $SCN^-$ ions. As shown in Figure 35.7.2 , each $Fe^{3+}$ ion and each $SCN^-$ ion is surrounded by an ionic atmosphere of opposite charge ($\delta^-$ and $\delta^+$) that partially screen the ions from each other. Because each ion's apparent charge at the edge of its ionic atmosphere is less than its actual charge, the force of attraction between the two ions is smaller. As a result, the formation of $Fe(SCN)^{2+}$ is slightly less favorable and the formation constant in Equation 35.7.2 is slightly smaller. Higher concentrations of $KNO_3$ increase $\delta^-$ and $\delta^+$, resulting in even smaller values for the formation constant.

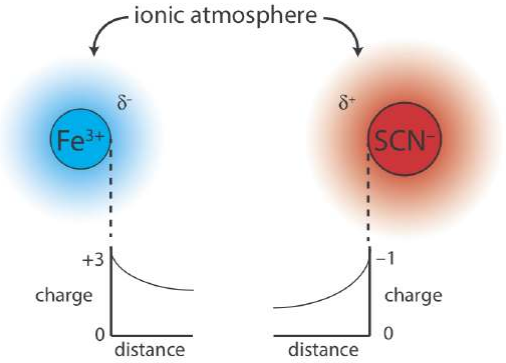



Figure 35.7.2 . Ions of $Fe^{3+}$ and $SCN^-$ are surrounded by ionic atmospheres with net charges of $\delta^-$ and $\delta^+$. Because of these ionic atmospheres, each ion's apparent charge at the edge of its ionic atmosphere is less than the ion's actual charge.

## Ionic Strength

To factor the concentration of ions into the formation constant for $Fe(SCN)^{2+}$, we need a way to express that concentration in a meaningful way. Because both an ion's concentration and its charge are important, we define the solution's ***ionic strength***, $\mu$ as

$$\mu = \frac{1}{2}\sum_{i=1}^{n} c_i z_i^2$$

where $c_i$ and $z_i$ are the concentration and charge of the $i^{th}$ ion.

### Example 35.7.1

Calculate the ionic strength of a solution of 0.10 M NaCl. Repeat the calculation for a solution of 0.10 M $Na_2SO_4$.

**Solution**

The ionic strength for 0.10 M NaCl is

$$\mu = \tfrac{1}{2}\left\{[Na^+] \times (+1)^2 + [Cl^-] \times (-1)^2\right\}$$
$$\mu = \tfrac{1}{2}\left\{(0.10) \times (+1)^2 + (0.10) \times (-1)^2\right\} = 0.10 \text{ M}$$

For 0.10 M $Na_2SO_4$ the ionic strength is

$$\mu = \tfrac{1}{2}\left\{[Na^+] \times (+1)^2 + [SO_4^{2-}] \times (-2)^2\right\}$$
$$\mu = \tfrac{1}{2}\left\{(0.20) \times (+1)^2 + (0.10) \times (-2)^2\right\} = 0.30 \text{ M}$$

In calculating the ionic strengths of these solutions we are ignoring the presence of $H_3O^+$ and $OH^-$, and, in the case of $Na_2SO_4$, the presence of $HSO_4^-$ from the base dissociation reaction of $SO_4^{2-}$. In the case of 0.10 M NaCl, the concentrations of $H_3O^+$ and $OH^-$ are $1.0 \times 10^{-7}$, which is significantly smaller than the concentrations of $Na^+$ and $Cl^-$. Because $SO_4^{2-}$ is a very weak base ($K_b = 1.0 \times 10^{-12}$), the solution is only slightly basic (pH = 7.5), and the concentrations of $H_3O^+$, $OH^-$, and $HSO_4^-$ are negligible. Although we can ignore the presence of $H_3O^+$, $OH^-$, and $HSO_4^-$ when we calculate the ionic strength of these two solutions, be aware that an equilibrium reaction can generate ions that might affect the solution's ionic strength.

Note that the unit for ionic strength is molarity, but that a salt's ionic strength need not match its molar concentration. For a 1:1 salt, such as NaCl, ionic strength and molar concentration are identical. The ionic strength of a 2:1 electrolyte, such as $Na_2SO_4$, is three times larger than the electrolyte's molar concentration.

## Activity and Activity Coefficients

Figure 35.7.1 shows that adding $KNO_3$ to a mixture of $Fe^{3+}$ and $SCN^-$ decreases the formation constant for $Fe(SCN)^{2+}$. This creates a contradiction. Earlier in this chapter we showed that there is a relationship between a reaction's standard-state free energy, $\Delta G^o$, and its equilibrium constant, $K$.

$$\triangle G^\circ = -RT \ln K$$

Because a reaction has only one standard-state, its equilibrium constant must be independent of solution conditions. Although ionic strength affects the *apparent* formation constant for $Fe(SCN)^{2+}$, reaction 35.7.1 must have an underlying *thermodynamic* formation constant that is independent of ionic strength.

The apparent formation constant for $Fe(SCN)^{2+}$, as shown in Equation 35.7.2, is a function of concentrations. In place of concentrations, we define the true thermodynamic equilibrium constant using activities. The activity of species $A$, $a_A$, is the product of its concentration, $[A]$, and a solution-dependent activity coefficient, $\gamma_A$

$$a_A = [A]\gamma_A$$

The true thermodynamic formation constant for $Fe(SCN)^{2+}$, therefore, is

$$K_1 = \frac{a_{Fe(SCN)^{2+}}}{a_{Fe^{3+}} \times a_{SCN^-}} = \frac{[Fe(SCN)^{2+}]\,\gamma_{Fe(SCN)^{2+}}}{[Fe^{3+}]\,\gamma_{Fe^{3+}}\,[SCN^-]\,\gamma_{SCN^-}}$$

> Unless otherwise specified, the equilibrium constants in the appendices are thermodynamic equilibrium constants.

A species' ***activity coefficient*** corrects for any deviation between its physical concentration and its ideal value. For a gas, a pure solid, a pure liquid, or a non-ionic solute, the activity coefficient is approximately one under most reasonable experimental conditions.

> For a gas the proper terms are fugacity and fugacity coefficient, instead of activity and activity coefficient.

For a reaction that involves only these species, the difference between activity and concentration is negligible. The activity coefficient for an ion, however, depends on the solution's ionic strength, the ion's charge, and the ion's size. It is possible to estimate activity coefficients using the extended ***Debye-Hückel equation***

$$\log \gamma_A = \frac{-0.51 \times z_A^2 \times \sqrt{\mu}}{1 + 3.3 \times \alpha_A \times \sqrt{\mu}} \tag{35.7.3}$$

where $z_A$ is the ion's charge, $\alpha_A$ is the hydrated ion's effective diameter in nanometers (Table 6.2), $\mu$ is the solution's ionic strength, and 0.51 and 3.3 are constants appropriate for an aqueous solution at 25°C. A hydrated ion's effective radius is the radius of the ion plus those water molecules closely bound to the ion. The effective radius is greater for smaller, more highly charged ions than it is for larger, less highly charged ions.

Table 35.7.1 . Effective Diameters ($\alpha$) for Selected Ions

| ion | effective diameter (nm) |
|---|---|
| $H_3O^+$ | 0.9 |
| $Li^+$ | 0.6 |
| $Na^+$, $IO_3^-$, $HSO_3^-$, $HCO_3^-$, $H_2PO_4^-$ | 0.45 |
| $OH^-$, $F^-$, $SCN^-$, $HS^-$, $ClO_3^-$, $ClO_4^-$, $MnO_4^-$ | 0.35 |
| $K^+$, $Cl^-$, $Br^-$, $I^-$, $CN^-$, $NO_2^-$, $NO_3^-$ | 0.3 |
| $Cs^+$, $Tl^+$, $Ag^+$, $NH_4^+$ | 0.25 |
| $Mg^{2+}$, $Be^{2+}$ | 0.8 |
| $Ca^{2+}$, $Cu^{2+}$, $Zn^{2+}$, $Sn^{2+}$, $Mn^{2+}$, $Fe^{2+}$, $Ni^{2+}$, $Co^{2+}$ | 0.6 |
| $Sr^{2+}$, $Ba^{2+}$, $Cd^{2+}$, $Hg^{2+}$, $S^{2-}$ | 0.5 |
| $Pb^{2+}$, $SO_4^{2-}$, $SO_3^{2-}$ | 0.45 |
| $Hg_2^{2+}$, $SO_4^{2-}$, $S_2O_3^{2-}$, $CrO_4^{2-}$, $HPO_4^{2-}$ | 0.40 |
| $Al^{3+}$, $Fe^{3+}$, $Cr^{3+}$ | 0.9 |
| $PO_4^{3-}$, $Fe(CN)_6^{3-}$ | 0.4 |
| $Zr^{4+}$, $Ce^{4+}$, $Sn^{4+}$ | 1.1 |
| $Fe(CN)_6^{4-}$ | 0.5 |
| Source: Kielland, J. *J. Am. Chem. Soc.* **1937**, *59*, 1675–1678. | |

Several features of Equation 35.7.3 deserve our attention. First, as the ionic strength approaches zero an ion's activity coefficient approaches a value of one. In a solution where $\mu = 0$, an ion's activity and its concentration are identical. We can take advantage of this fact to determine a reaction's thermodynamic equilibrium constant by measuring the apparent equilibrium constant for several

increasingly smaller ionic strengths and extrapolating back to an ionic strength of zero. Second, an activity coefficient is smaller, and the effect of activity is more important, for an ion with a higher charge and a smaller effective radius. Finally, the extended Debye-Hückel equation provides a reasonable estimate of an ion's activity coefficient when the ionic strength is less than 0.1. Modifications to Equation 35.7.3 extend the calculation of activity coefficients to higher ionic strengths [Davies, C. W. *Ion Association*, Butterworth: London, 1962].

## Including Activity Coefficients When Solving Equilibrium Problems

Earlier in this chapter we calculated the solubility of $Pb(IO_3)_2$ in deionized water, obtaining a result of $4.0 \times 10^{-5}$ mol/L. Because the only significant source of ions is from the solubility reaction, the ionic strength is very low and we can assume that $\gamma \approx 1$ for both $Pb^{2+}$ and $IO_3^-$. In calculating the solubility of $Pb(IO_3)_2$ in deionized water, we do not need to account for ionic strength. But what if we need to know the solubility of $Pb(IO_3)_2$ in a solution that contains other, inert ions? In this case we need to include activity coefficients in our calculation.

### Example 35.7.2

Calculate the solubility of $Pb(IO_3)_2$ in a matrix of 0.020 M $Mg(NO_3)_2$.

**Solution**

We begin by calculating the solution's ionic strength. Since $Pb(IO_3)_2$ is only sparingly soluble, we will assume we can ignore its contribution to the ionic strength; thus

$$\mu = \frac{1}{2}\left\{(0.020)(+2)^2 + (0.040)(-1)^2\right\} = 0.060 \text{ M}$$

Next, we use Equation 35.7.3 to calculate the activity coefficients for $Pb^{2+}$ and $IO_3^-$.

$$\log \gamma_{Pb^{2+}} = \frac{-0.51 \times (+2)^2 \times \sqrt{0.060}}{1 + 3.3 \times 0.45 \times \sqrt{0.060}} = -0.366$$

$$\gamma_{Pb^{2+}} = 0.431$$

$$\log \gamma_{IO_3^-} = \frac{-0.51 \times (-1)^2 \times \sqrt{0.060}}{1 + 3.3 \times 0.45 \times \sqrt{0.060}} = -0.0916$$

$$\gamma_{IO_3^-} = 0.810$$

Defining the equilibrium concentrations of $Pb^{2+}$ and $IO_3^-$ in terms of the variable *x*

| Concentrations | $Pb(IO_3)_2$ (*s*) | $\rightleftharpoons$ | $Pb^{2+}$ (*aq*) | + | $2IO_3^-$ (*aq*) |
|---|---|---|---|---|---|
| initial | solid | | 0 | | 0 |
| change | solid | | +*x* | | +2*x* |
| equilibrium | solid | | *x* | | 2*x* |

and substituting into the thermodynamic solubility product for $Pb(IO_3)_2$ leaves us with

$$K_{sp} = a_{Pb^{2+}} \times a_{IO_3^-}^2 = \gamma_{Pb^{2+}}\left[Pb^{2+}\right] \times \gamma_{IO_3^-}^2\left[IO_3^-\right]^2 = 2.5 \times 10^{-13}$$

$$K_{sp} = (0.431)(x)(0.810)^2(2x)^2 = 2.5 \times 10^{-13}$$

$$K_{sp} = 1.131x^3 = 2.5 \times 10^{-13}$$

Solving for *x* gives $6.0 \times 10^{-5}$ and a molar solubility of $6.0 \times 10^{-5}$ mol/L for $Pb(IO_3)_2$. If we ignore activity, as we did in our earlier calculation, we report the molar solubility as $4.0 \times 10^{-5}$ mol/L. Failing to account for activity in this case underestimates the molar solubility of $Pb(IO_3)_2$ by 33%.

The solution's equilibrium composition is

$$[Pb^{2+}] = 6.0 \times 10^{-5}\ M$$
$$[IO_3^-] = 1.2 \times 10^{-4}\ M$$
$$[Mg^{2+}] = 0.020\ M$$
$$[NO_3^-] = 0.040\ M$$

Because the concentrations of both $Pb^{2+}$ and $IO_3^-$ are much smaller than the concentrations of $Mg^{2+}$ and $NO_3^-$ our decision to ignore the contribution of $Pb^{2+}$ and $IO_3^-$ to the ionic strength is reasonable.

How do we handle the calculation if we can not ignore the concentrations of $Pb^{2+}$ and $IO_3^-$ when calculating the ionic strength. One approach is to use the method of successive approximations. First, we recalculate the ionic strength using the concentrations of all ions, including $Pb^{2+}$ and $IO_3^-$. Next, we recalculate the activity coefficients for $Pb^{2+}$ and $IO_3^-$ using this new ionic strength and then recalculate the molar solubility. We continue this cycle until two successive calculations yield the same molar solubility within an acceptable margin of error.

## Exercise 35.7.1

Calculate the molar solubility of $Hg_2Cl_2$ in 0.10 M NaCl, taking into account the effect of ionic strength. Compare your answer to that from Exercise 6.7.2 in which you ignored the effect of ionic strength.

**Answer**

We begin by calculating the solution's ionic strength. Because NaCl is a 1:1 ionic salt, the ionic strength is the same as the concentration of NaCl; thus $\mu$ = 0.10 M. This assumes, of course, that we can ignore the contributions of $Hg_2^{2+}$ and $Cl^-$ from the solubility of $Hg_2Cl_2$.

Next we use Equation 35.7.3 to calculate the activity coefficients for $Hg_2^{2+}$ and $Cl^-$.

$$\log \gamma_{Hg_2^{2+}} = \frac{-0.51 \times (+2)^2 \times \sqrt{0.10}}{1 + 3.3 \times 0.40 \times \sqrt{0.10}} = -0.455$$

$$\gamma_{Hg_2^{2+}} = 0.351$$

$$\log \gamma_{Cl^-} = \frac{-0.51 \times (-1)^2 \times \sqrt{0.10}}{1 + 3.3 \times 0.3 \times \sqrt{0.10}} = -0.12$$

$$\gamma_{Cl^-} = 0.75$$

Defining the equilibrium concentrations of $Hg_2^{2+}$ and $Cl^-$ in terms of the variable *x*

| concentrations | Hg2Cl2 (*s*) | ⇌ | $Hg_2^{2+}$ (*aq*) | + | $2Cl^-$ (*aq*) |
|---|---|---|---|---|---|
| initial | solid | | 0 | | 0.10 |
| change | solid | | +*x* | | +2*x* |
| equilibrium | solid | | *x* | | 0.10 + 2*x* |

and substituting into the thermodynamic solubility product for $Hg_2Cl_2$, leave us with

$$K_{sp} = a_{Hg_2^{2+}} (a_{Cl^-})^2 = \gamma_{Hg_2^{2+}} \left[Hg_2^{2+}\right] (\gamma_{Cl^-})^2 \left[Cl^-\right]^2 = 1.2 \times 10^{-18}$$

Because the value of *x* likely is small, let's simplify this equation to

$$(0.351)(x)(0.75)^2(0.1)^2 = 1.2 \times 10^{-18}$$

Solving for *x* gives its value as $6.1 \times 10^{-16}$. Because *x* is the concentration of $Hg_2^{2+}$ and 2*x* is the concentration of $Cl^-$, our decision to ignore their contributions to the ionic strength is reasonable. The molar solubility of $Hg_2Cl_2$ in 0.10 M NaCl is

$6.1 \times 10^{-16}$ mol/L. In Exercise 6.7.2, where we ignored ionic strength, we determined that the molar solubility of $Hg_2Cl_2$ is $1.2 \times 10^{-16}$ mol/L, a result that is $5\times$ smaller than the its actual value.

As Example 35.7.2 and Exercise 35.7.1 show, failing to correct for the effect of ionic strength can lead to a significant error in an equilibrium calculation. Nevertheless, it is not unusual to ignore activities and to assume that the equilibrium constant is expressed in terms of concentrations. There is a practical reason for this—in an analysis we rarely know the exact composition, much less the ionic strength of aqueous samples or of solid samples brought into solution. Equilibrium calculations are a useful guide when we develop an analytical method; however, it only is when we complete an analysis and evaluate the results that can we judge whether our theory matches reality. In the end, work in the laboratory is the most critical step in developing a reliable analytical method.

This is a good place to revisit the meaning of pH. In Chapter 2 we defined pH as

$$\text{pH} = -\log [H_3O^+]$$

Now we see that the correct definition is

$$\text{pH} = -\log a_{H_3O^+}$$
$$\text{pH} = -\log \gamma_{H_3O^+} [H_3O^+]$$

Failing to account for the effect of ionic strength can lead to a significant error in the reported concentration of $H_3O^+$. For example, if the pH of a solution is 7.00 and the activity coefficient for $H_3O^+$ is 0.90, then the concentration of $H_3O^+$ is $1.11 \times 10^{-7}$ M, not $1.00 \times 10^{-7}$ M, an error of +11%. Fortunately, when we develop and carry out an analytical method, we are more interested in controlling pH than in calculating $[H_3O^+]$. As a result, the difference between the two definitions of pH rarely is of significant concern.

This page titled 35.7: Activity Coefficients is shared under a CC BY-NC-SA 4.0 license and was authored, remixed, and/or curated by David Harvey.

# 35.8: Standard Reduction Potentials & Polarographic Half-wave Potentials

Standard/Formal Reduction Potentials

The following table provides $E^o$ and $E^{o'}$ values for selected reduction reactions. Values are from the following sources (primarily the first two):

- Bard, A. J.; Parsons, B.; Jordon, J., eds. *Standard Potentials in Aqueous Solutions*, Dekker: New York, 1985
- Milazzo, G.; Caroli, S.; Sharma, V. K. *Tables of Standard Electrode Potentials*, Wiley: London, 1978;
- Swift, E. H.; Butler, E. A. *Quantitative Measurements and Chemical Equilibria*, Freeman: New York, 1972.
- Bratsch, S. G. "Standard Electrode Potentials and Temperature Coefficients in Water at 298.15K, *J. Phys. Chem. Ref. Data*, **1989**, *18*, 1–21.
- Latimer, W. M. *Oxidation Potentials*, 2nd. Ed., Prentice-Hall: Englewood Cliffs, NJ, 1952

Solids, gases, and liquids are identified; all other species are aqueous. Reduction reactions in acidic solution are written using $H^+$ in place of $H_3O^+$. You may rewrite a reaction by replacing $H^+$ with $H_3O^+$ and adding to the opposite side of the reaction one molecule of $H_2O$ per $H^+$; thus

$$H_3AsO_4 + 2H^+ + 2e^- \rightleftharpoons HAsO_2 + 2H_2O$$

becomes

$$H_3AsO_4 + 2H_3O^+ + 2e^- \rightleftharpoons HAsO_2 + 4H_2O$$

Conditions for formal potentials ($E^{o'}$) are listed next to the potential.

For most of the reduction half-reactions gathered here, there are minor differences in values provided by the references above. In most cases, these differences are small and will not affect calculations. In a few cases the differences are not insignificant and the user may find discrepancies in calculations. For example, Bard, Parsons, and Jordon report an $E^o$ value of –1.285 V for

$$Zn(OH)_4^{2-} + 2e^- \rightleftharpoons Zn(s) + 4OH^-$$

while Milazzo, Caroli, and Sharma report the value as –1.214 V, Swift reports the value as –1.22, Bratsch reports the value as –1.199 V, and Latimer reports the value as –1.216 V.

| Aluminum | $E$ (V) | $E^{o'}$ (V) |
|---|---|---|
| $Al^{3+} + 3e^- \rightleftharpoons Al(s)$ | –1.676 | |
| $Al(OH)_4^- + 3e^- \rightleftharpoons Al(s) + 4OH^-$ | –2.310 | |
| $AlF_6^{3-} + 3e^- \rightleftharpoons Al(s) + 6F^-$ | –2.07 | |

| Antimony | $E$ (V) | $E^{o'}$ (V) |
|---|---|---|
| $Sb + 3H^+ + 3e^- \rightleftharpoons SbH_3(g)$ | –0.510 | |
| $Sb_2O_5 + 6H^+ + 4e^- \rightleftharpoons 2SbO^+ + 3H_2O(l)$ | 0.605 | |
| $SbO^+ + 2H^+ + 3e^- \rightleftharpoons Sb(s) + H_2O(l)$ | 0.212 | |

| Arsenic | $E$ (V) | $E^{o'}$ (V) |
|---|---|---|
| $As(s) + 3H^+ + 3e^- \rightleftharpoons AsH_3(g)$ | –0.225 | |
| $H_3AsO_4 + 2H^+ + 2e^- \rightleftharpoons HAsO_2 + 2H_2O(l)$ | 0.560 | |
| $HAsO_2 + 3H^+ + 3e^- \rightleftharpoons As(s) + 2H_2O(l)$ | 0.240 | |

| Barium | $E$ (V) | $E^{o'}$ (V) |
|---|---|---|
| $Ba^{2+} + 2e^- \rightleftharpoons Ba(s)$ | –2.92 | |
| $BaO(s) + 2H^+ + 2e^- \rightleftharpoons Ba(s) + H_2O(l)$ | –2.166 | |

| Beryllium | $E$ (V) | $E^{o'}$ (V) |
|---|---|---|
| $Be^{2+} + 2e^- \rightleftharpoons Be(s)$ | –1.99 | |

| Bismuth | $E$ (V) | $E^{o'}$ (V) |
|---|---|---|
| $Bi^{3+} + 3e^- \rightleftharpoons Bi(s)$ | 0.317 | |
| $BiCl_4^- + 3e^- \rightleftharpoons Bi(s) + 4Cl^-$ | 0.199 | |

| Boron | $E$ (V) | $E^{o'}$ (V) |
|---|---|---|
| $B(OH)_3 + 3H^+ + 3e^- \rightleftharpoons B(s) + 3H_2O(l)$ | –0.890 | |
| $B(OH)_4^- + 3e^- \rightleftharpoons B(s) + 4OH^-$ | –1.811 | |

| Bromine | $E$ (V) | $E^{o'}$ (V) |
|---|---|---|
| $Br_2(l) + 2e^- \rightleftharpoons 2Br^-$ | 1.087 | |
| $HOBr + H^+ + 2e^- \rightleftharpoons Br^- + H_2O(l)$ | 1.341 | |
| $HOBr + H^+ + e^- \rightleftharpoons \frac{1}{2}Br_2 + H_2O(l)$ | 1.604 | |
| $BrO^- + H_2O(l) + 2e^- \rightleftharpoons Br^- + 2OH^-$ | | 0.76 in 1 M NaOH |
| $BrO_3^- + 6H^+ + 5e^- \rightleftharpoons \frac{1}{2}Br_2(l) + 3H_2O(l)$ | 1.5 | |
| $BrO_3^- + 6H^+ + 6e^- \rightleftharpoons Br^- + 3H_2O(l)$ | 1.478 | |

| Cadmium | $E$ (V) | $E^{o'}$ (V) |
|---|---|---|
| $Cd^{2+} + 2e^- \rightleftharpoons Cd(s)$ | –0.4030 | |
| $Cd(CN)_4^{2-} + 2e^- \rightleftharpoons Cd(s) + 4CN^-$ | –0.943 | |
| $Cd(NH_3)_4^{2+} + 2e^- \rightleftharpoons Cd(s) + 4NH_3$ | –0.622 | |

| Calcium | $E$ (V) | $E^{o'}$ (V) |
|---|---|---|
| $Ca^{2+} + 2e^- \rightleftharpoons Ca(s)$ | –2.84 | |

| Carbon | $E$ (V) | $E^{o'}$ (V) |
|---|---|---|
| $CO_2(g) + 2H^+ + 2e^- \rightleftharpoons CO(g) + H_2O(l)$ | –0.106 | |
| $CO_2(g) + 2H^+ + 2e^- \rightleftharpoons HCO_2H$ | –0.20 | |
| $2CO_2(g) + 2H^+ + 2e^- \rightleftharpoons H_2C_2O_4$ | –0.481 | |
| $HCHO + 2H^+ + 2e^- \rightleftharpoons CH_3OH$ | 0.2323 | |

| Cerium | $E$ (V) | $E^{o'}$ (V) |
|---|---|---|
| $Ce^{3+} + 3e^- \rightleftharpoons Ce(s)$ | –2.336 | |
| $Ce^{4+} + e^- \rightleftharpoons Ce^{3+}$ | 1.72 | 1.70 in 1 M $HClO_4$<br>1.44 in 1 M $H_2SO_4$<br>1.61 in 1 M $HNO_3$<br>1.28 in 1 M HCl |

| Chlorine | $E$ (V) | $E^{o'}$ (V) |
|---|---|---|
| $Cl_2(g) + 2e^- \rightleftharpoons 2Cl^-$ | 1.396 | |
| $ClO^- + H_2O(l) + e^- \rightleftharpoons \frac{1}{2}Cl_2(g) + 2OH^-$ | | 0.421 in 1 M NaOH |
| $ClO^- + H_2O(l) + 2e^- \rightleftharpoons Cl^- + 2OH^-$ | | 0.890 in 1 M NaOH |
| $HClO_2 + 2H^+ + 2e^- \rightleftharpoons HOCl + H_2O(l)$ | 1.64 | |

| Chlorine | $E$ (V) | $E^{o'}$ (V) |
|---|---|---|
| $ClO_3^- + 2H^+ + e^- \rightleftharpoons ClO_2(g) + H_2O(l)$ | 1.175 | |
| $ClO_3^- + 3H^+ + 2e^- \rightleftharpoons HClO_2 + H_2O(l)$ | 1.181 | |
| $ClO_4^- + 2H^+ + 2e^- \rightleftharpoons ClO_3^- + H_2O(l)$ | 1.201 | |

| Chromium | $E$ (V) | $E^{o'}$ (V) |
|---|---|---|
| $Cr^{3+} + 3e^- \rightleftharpoons Cr(s)$ | –0.424 | |
| $Cr^{2+} + 2e^- \rightleftharpoons Cr(s)$ | –0.90 | |
| $Cr_2O_7^{2-} + 14H^+ + 6e^- \rightleftharpoons 2Cr^{3+} + 7H_2O(l)$ | 1.36 | |
| $CrO_4^{2-} + 4H_2O(l) + 3e^- \rightleftharpoons Cr(OH)_4^- + 4OH^-$ | | –0.13 in 1 M NaOH |

| Cobalt | $E$ (V) | $E^{o'}$ (V) |
|---|---|---|
| $Co^{2+} + 2e^- \rightleftharpoons Co(s)$ | –0.277 | |
| $Co^{3+} + 3e^- \rightleftharpoons Co(s)$ | 1.92 | |
| $Co(NH_3)_6^{3+} + e^- \rightleftharpoons Co(NH_3)_6^{2+}$ | 0.1 | |
| $Co(OH)_3(s) + e^- \rightleftharpoons Co(OH)_2(s) + OH^-$ | 0.17 | |
| $Co(OH)_2(s) + 2e^- \rightleftharpoons Co(s) + 2OH^-$ | –0.746 | |

| Copper | $E$ (V) | $E^{o'}$ (V) |
|---|---|---|
| $Cu^+ + e^- \rightleftharpoons Cu(s)$ | 0.520 | |
| $Cu^{2+} + e^- \rightleftharpoons Cu^+$ | 0.159 | |
| $Cu^{2+} + 2e^- \rightleftharpoons Cu(s)$ | 0.3419 | |
| $Cu^{2+} + I^- + e^- \rightleftharpoons CuI(s)$ | 0.86 | |
| $Cu^{2+} + Cl^- + e^- \rightleftharpoons CuCl(s)$ | 0.559 | |

| Fluorine | $E$ (V) | $E^{o'}$ (V) |
|---|---|---|
| $F_2(g) + 2H^+ + 2e^- \rightleftharpoons 2HF(g)$ | 3.053 | |
| $F_2(g) + 2e^- \rightleftharpoons 2F^-$ | 2.87 | |

| Gallium | $E$ (V) | $E^{o'}$ (V) |
|---|---|---|
| $Ga^{3+} + 3e^- \rightleftharpoons Ga(s)$ | –0.529 | |

| Gold | $E$ (V) | $E^{o'}$ (V) |
|---|---|---|
| $Au^+ + e^- \rightleftharpoons Au(s)$ | 1.83 | |
| $Au^{3+} + 2e^- \rightleftharpoons Au^+$ | 1.36 | |
| $Au^{3+} + 3e^- \rightleftharpoons Au(s)$ | 1.52 | |
| $AuCl_4^- + 3e^- \rightleftharpoons Au(s) + 4Cl^-$ | 1.002 | |

| Hydrogen | $E$ (V) | $E^{o'}$ (V) |
|---|---|---|
| $2H^+ + 2e^- \rightleftharpoons H_2(g)$ | 0.00000 | |
| $H_2O(l) + e^- \rightleftharpoons \frac{1}{2}H_2(g) + OH^-$ | –0.828 | |

| Iodine | $E$ (V) | $E^{o'}$ (V) |
|---|---|---|
| $I_2(s) + 2e^- \rightleftharpoons 2I^-$ | 0.5355 | |

| Iodine | $E$ (V) | $E^{o'}$ (V) |
|---|---|---|
| $I_3^- + 2e^- \rightleftharpoons 3I^-$ | 0.536 | |
| $HIO + H^+ + 2e^- \rightleftharpoons I^- + H_2O(l)$ | 0.985 | |
| $IO_3^- + 6H^+ + 5e^- \rightleftharpoons \frac{1}{2}I_2(s) + 3H_2O(l)$ | 1.195 | |
| $IO_3^- + 3H_2O(l) + 6e^- \rightleftharpoons I^- + 6OH^-$ | 0.257 | |

| Iron | $E$ (V) | $E^{o'}$ (V) |
|---|---|---|
| $Fe^{2+} + 2e^- \rightleftharpoons Fe(s)$ | –0.44 | |
| $Fe^{3+} + 3e^- \rightleftharpoons Fe(s)$ | –0.037 | |
| $Fe^{3+} + e^- \rightleftharpoons Fe^{2+}$ | 0.771 | 0.70 in 1 M HCl<br>0.767 in 1 M $HClO_4$<br>0.746 in 1 M $HNO_3$<br>0.68 in 1 M $H_2SO_4$<br>0.44 in 0.3 M $H_3PO_4$ |
| $Fe(CN)_6^{3-} + e^- \rightleftharpoons Fe(CN)_6^{4-}$ | 0.356 | |
| $Fe(phen)_3^{3+} + e^- \rightleftharpoons Fe(phen)_3^{2+}$ | 1.147 | |

| Lanthanum | $E$ (V) | $E^{o'}$ (V) |
|---|---|---|
| $La^{3+} + 3e^- \rightleftharpoons La(s)$ | –2.38 | |

| Lead | $E$ (V) | $E^{o'}$ (V) |
|---|---|---|
| $Pb^{2+} + 2e^- \rightleftharpoons Pb(s)$ | –0.126 | |
| $PbO_2(s) + 4H^+ + 2e^- \rightleftharpoons Pb^{2+} + 2H_2O(l)$ | 1.46 | |
| $PbO_2(s) + SO_4^{2-} + 4H^+ + 2e^- \rightleftharpoons PbSO_4(s) + 2H_2O(l)$ | 1.690 | |
| $PbSO_4(s) + 2e^- \rightleftharpoons Pb(s) + SO_4^{2-}$ | –0.356 | |

| Lithium | $E$ (V) | $E^{o'}$ (V) |
|---|---|---|
| $Li^+ + e^- \rightleftharpoons Li(s)$ | –3.040 | |

| Magnesium | $E$ (V) | $E^{o'}$ (V) |
|---|---|---|
| $Mg^{2+} + 2e^- \rightleftharpoons Mg(s)$ | –2.356 | |
| $Mg(OH)_2(s) + 2e^- \rightleftharpoons Mg(s) + 2OH^-$ | –2.687 | |

| Manganese | $E$ (V) | $E^{o'}$ (V) |
|---|---|---|
| $Mn^{2+} + 2e^- \rightleftharpoons Mn(s)$ | –1.17 | |
| $Mn^{3+} + e^- \rightleftharpoons Mn^{2+}$ | 1.5 | |
| $MnO_2(s) + 4H^+ + 2e^- \rightleftharpoons Mn^{2+} + 2H_2O(l)$ | 1.23 | |
| $MnO_4^- + 4H^+ + 3e^- \rightleftharpoons MnO_2(s) + 2H_2O(l)$ | 1.70 | |
| $MnO_4^- + 8H^+ + 5e^- \rightleftharpoons Mn^{2+} + 4H_2O(l)$ | 1.51 | |
| $MnO_4^- + 2H_2O(l) + 3e^- \rightleftharpoons MnO_2(s) + 4OH^-$ | 0.60 | |

| Mercury | $E$ (V) | $E^{o'}$ (V) |
|---|---|---|
| $Hg^{2+} + 2e^- \rightleftharpoons Hg(l)$ | 0.8535 | |
| $2Hg^{2+} + 2e^- \rightleftharpoons Hg_2^{2+}$ | 0.911 | |

| Mercury | $E$ (V) | $E^{o'}$ (V) |
|---|---|---|
| $Hg_2^{2+} + 2e^- \rightleftharpoons 2Hg(l)$ | 0.7960 | |
| $Hg_2Cl_2(s) + 2e^- \rightleftharpoons 2Hg(l) + 2Cl^-$ | 0.2682 | |
| $HgO(s) + 2H^+ + 2e^- \rightleftharpoons Hg(l) + H_2O(l)$ | 0.926 | |
| $Hg_2Br_2(s) + 2e^- \rightleftharpoons 2Hg(l) + 2Br^-$ | 1.392 | |
| $Hg_2I_2(s) + 2e^- \rightleftharpoons 2Hg(l) + 2I^-$ | –0.0405 | |

| Molybdenum | $E$ (V) | $E^{o'}$ (V) |
|---|---|---|
| $Mo^{3+} + 3e^- \rightleftharpoons Mo(s)$ | –0.2 | |
| $MoO_2(s) + 4H^+ + 4e^- \rightleftharpoons Mo(s) + 2H_2O(l)$ | –0.152 | |
| $MoO_4^{2-} + 4H_2O(l) + 6e^- \rightleftharpoons Mo(s) + 8OH^-$ | –0.913 | |

| Nickel | $E$ (V) | $E^{o'}$ (V) |
|---|---|---|
| $Ni^{2+} + 2e^- \rightleftharpoons Ni(s)$ | –0.257 | |
| $Ni(OH)_2(s) + 2e^- \rightleftharpoons Ni(s) + 2OH^-$ | –0.72 | |
| $Ni(NH_3)_6^{2+} + 2e^- \rightleftharpoons Ni(s) + 6NH_3$ | –0.49 | |

| Nitrogen | $E$ (V) | $E^{o'}$ (V) |
|---|---|---|
| $N_2(g) + 5H^+ + 4e^- \rightleftharpoons N_2H_5^+$ | –0.23 | |
| $N_2O(g) + 2H^+ + 2e^- \rightleftharpoons N_2(g) + H_2O(l)$ | 1.77 | |
| $2NO(g) + 2H^+ + 2e^- \rightleftharpoons N_2O(g) + H_2O(l)$ | 1.59 | |
| $HNO_2 + H^+ + e^- \rightleftharpoons NO(g) + H_2O(l)$ | 0.996 | |
| $2HNO_2 + 4H^+ + 4e^- \rightleftharpoons N_2O(g) + 3H_2O(l)$ | 1.297 | |
| $NO_3^- + 3H^+ + 2e^- \rightleftharpoons HNO_2 + H_2O(l)$ | 0.94 | |

| Oxygen | $E$ (V) | $E^{o'}$ (V) |
|---|---|---|
| $O_2(g) + 2H^+ + 2e^- \rightleftharpoons H_2O_2$ | 0.695 | |
| $O_2(g) + 4H^+ + 4e^- \rightleftharpoons 2H_2O(l)$ | 1.229 | |
| $H_2O_2 + 2H^+ + 2e^- \rightleftharpoons 2H_2O(l)$ | 1.763 | |
| $O_2(g) + 2H_2O(l) + 4e^- \rightleftharpoons 4OH^-$ | 0.401 | |
| $O_3(g) + 2H^+ + 2e^- \rightleftharpoons O_2(g) + H_2O(l)$ | 2.07 | |

| Phosphorous | $E$ (V) | $E^{o'}$ (V) |
|---|---|---|
| $P(s, white) + 3H^+ + 3e^- \rightleftharpoons PH_3(g)$ | –0.063 | |
| $H_3PO_3 + 2H^+ + 2e^- \rightleftharpoons H_3PO_2 + H_2O(l)$ | –0.499 | |
| $H_3PO_4 + 2H^+ + 2e^- \rightleftharpoons H_3PO_3 + H_2O(l)$ | –0.276 | |

| Platinum | $E$ (V) | $E^{o'}$ (V) |
|---|---|---|
| $Pt^{2+} + 2e^- \rightleftharpoons Pt(s)$ | 1.188 | |
| $PtCl_4^{2-} + 2e^- \rightleftharpoons Pt(s) + 4Cl^-$ | 0.758 | |

| Potasium | $E$ (V) | $E^{o'}$ (V) |
|---|---|---|
| $K^+ + e^- \rightleftharpoons K(s)$ | –2.924 | |

| Ruthenium | $E$ (V) | $E^{o'}$ (V) |
|---|---|---|
| $Ru^{3+} + 3e^- \rightleftharpoons Ru(s)$ | 0.249 | |
| $RuO_2(s) + 4H^+ + 4e^- \rightleftharpoons Ru(s) + 2H_2O(l)$ | 0.68 | |
| $Ru(NH_3)_6^{3+} + e^- \rightleftharpoons Ru(NH_3)_6^{2+}$ | 0.10 | |
| $Ru(CN)_6^{3-} + e^- \rightleftharpoons Ru(CN)_6^{4-}$ | 0.86 | |

| Selenium | $E$ (V) | $E^{o'}$ (V) |
|---|---|---|
| $Se(s) + 2e^- \rightleftharpoons Se^{2-}$ | | –0.67 in 1 M NaOH |
| $Se(s) + 2H^+ + 2e^- \rightleftharpoons H_2Se(g)$ | –0.115 | |
| $H_2SeO_3 + 4H^+ + 4e^- \rightleftharpoons Se(s) + 3H_2O(l)$ | 0.74 | |
| $SeO_4^{3-} + 4H^+ + e^- \rightleftharpoons H_2SeO_3 + H_2O(l)$ | 1.151 | |

| Silicon | $E$ (V) | $E^{o'}$ (V) |
|---|---|---|
| $SiF_6^{2-} + 4e^- \rightleftharpoons Si(s) + 6F^-$ | –1.37 | |
| $SiO_2(s) + 4H^+ + 4e^- \rightleftharpoons Si(s) + 2H_2O(l)$ | –0.909 | |
| $SiO_2(s) + 8H^+ + 8e^- \rightleftharpoons SiH_4(g) + 2H_2O(l)$ | –0.516 | |

| Silver | $E$ (V) | $E^{o'}$ (V) |
|---|---|---|
| $Ag^+ + e^- \rightleftharpoons Ag(s)$ | 0.7996 | |
| $AgBr(s) + e^- \rightleftharpoons Ag(s) + Br^-$ | 0.071 | |
| $Ag_2C_2O_4(s) + 2e^- \rightleftharpoons 2Ag(s) + C_2O_4^{2-}$ | 0.47 | |
| $AgCl(s) + e^- \rightleftharpoons Ag(s) + Cl^-$ | 0.2223 | |
| $AgI(s) + e^- \rightleftharpoons Ag(s) + I^-$ | –0.152 | |
| $Ag_2S(s) + 2e^- \rightleftharpoons 2Ag(s) + S^{2-}$ | –0.71 | |
| $Ag(NH_3)_2^+ + e^- \rightleftharpoons Ag(s) + 2NH_3$ | –0.373 | |

| Sodium | $E$ (V) | $E^{o'}$ (V) |
|---|---|---|
| $Na^+ + e^- \rightleftharpoons Na(s)$ | –2.713 | |

| Strontium | $E$ (V) | $E^{o'}$ (V) |
|---|---|---|
| $Sr^{2+} + 2e^- \rightleftharpoons Sr(s)$ | –2.89 | |

| Sulfur | $E$ (V) | $E^{o'}$ (V) |
|---|---|---|
| $S(s) + 2e^- \rightleftharpoons S^{2-}$ | –0.407 | |
| $S(s) + 2H^+ + 2e^- \rightleftharpoons H_2S(g)$ | 0.144 | |
| $S_2O_6^{2-} + 4H^+ + 2e^- \rightleftharpoons 2H_2SO_3$ | 0.569 | |
| $S_2O_8^{2-} + 2e^- \rightleftharpoons 2SO_4^{2-}$ | 1.96 | |
| $S_4O_6^{2-} + 2e^- \rightleftharpoons 2S_2O_3^{2-}$ | 0.080 | |
| $2SO_3^{2-} + 2H_2O(l) + 2e^- \rightleftharpoons S_2O_4^{2-} + 4OH^-$ | –1.13 | |
| $2SO_3^{2-} + 3H_2O(l) + 4e^- \rightleftharpoons S_2O_3^{2-} + 6OH^-$ | | –0.576 in 1 M NaOH |
| $2SO_4^{2-} + 4H^+ + 2e^- \rightleftharpoons S_2O_6^{2-} + 2H_2O(l)$ | –0.25 | |
| $SO_4^{2-} + H_2O(l) + 2e^- \rightleftharpoons SO_3^{2-} + 2OH^-$ | –0.936 | |
| $SO_4^{2-} + 4H^+ + 2e^- \rightleftharpoons H_2SO_3 + H_2O(l)$ | 0.172 | |

| Thallium | $E$ (V) | $E^{o'}$ (V) |
|---|---|---|
| $Tl^{3+} + 2e^- \rightleftharpoons Tl^+$ | | 1.25 in 1 M $HClO_4$<br>0.77 in 1 M HCl |
| $Tl^{3+} + 3e^- \rightleftharpoons Tl(s)$ | 0.742 | |

| Tin | $E$ (V) | $E^{o'}$ (V) |
|---|---|---|
| $Sn^{2+} + 2e^- \rightleftharpoons Sn(s)$ | | –0.19 in 1 M HCl |
| $Sn^{4+} + 2e^- \rightleftharpoons Sn^{2+}$ | 0.154 | 0.139 in 1 M HCl |

| Titanium | $E$ (V) | $E^{o'}$ (V) |
|---|---|---|
| $Ti^{2+} + 2e^- \rightleftharpoons Ti(s)$ | –0.163 | |
| $Ti^{3+} + e^- \rightleftharpoons Ti^{2+}$ | –0.37 | |

| Tungsten | $E$ (V) | $E^{o'}$ (V) |
|---|---|---|
| $WO_2(s) + 4H^+ + 4e^- \rightleftharpoons W(s) + 2H_2O(l)$ | –0.119 | |
| $WO_3(s) + 6H^+ + 6e^- \rightleftharpoons W(s) + 3H_2O(l)$ | –0.090 | |

| Uranium | $E$ (V) | $E^{o'}$ (V) |
|---|---|---|
| $U^{3+} + 3e^- \rightleftharpoons U(s)$ | –1.66 | |
| $U^{4+} + e^- \rightleftharpoons U^{3+}$ | –0.52 | |
| $UO_2^+ + 4H^+ + e^- \rightleftharpoons U^{4+} + 2H_2O(l)$ | 0.27 | |
| $UO_2^{2+} + e^- \rightleftharpoons UO_2^+$ | 0.16 | |
| $UO_2^{2+} + 4H^+ + 2e^- \rightleftharpoons U^{4+} + 2H_2O(l)$ | 0.327 | |

| Vanadium | $E$ (V) | $E^{o'}$ (V) |
|---|---|---|
| $V^{2+} + 2e^- \rightleftharpoons V(s)$ | –1.13 | |
| $V^{3+} + e^- \rightleftharpoons V^{2+}$ | –0.255 | |
| $VO^{2+} + 2H^+ + e^- \rightleftharpoons V^{3+} + H_2O(l)$ | 0.337 | |
| $VO_2^+ + 2H^+ + e^- \rightleftharpoons VO^{2+} + H_2O(l)$ | 1.000 | |

| Zinc | $E$ (V) | $E^{o'}$ (V) |
|---|---|---|
| $Zn^{2+} + 2e^- \rightleftharpoons Zn(s)$ | –0.7618 | |
| $Zn(OH)_4^{2-} + 2e^- \rightleftharpoons Zn(s) + 4OH^-$ | –1.285 | |
| $Zn(NH_3)_4^{2+} + 2e^- \rightleftharpoons Zn(s) + 4NH_3$ | –1.04 | |
| $Zn(CN)_4^{2-} + 2e^- \rightleftharpoons Zn(s) + 4CN^-$ | –1.34 | |

## Polarographic Half-Wave Potentials

The following table provides $E_{1/2}$ values for selected reduction reactions. Values are from Dean, J. A. *Analytical Chemistry Handbook*, McGraw-Hill: New York, 1995.

| Element | $E_{1/2}$ (volts vs. SCE) | Matrix |
|---|---|---|
| $Al^{3+}(aq) + 3\,e^- \rightleftharpoons Al(s)$ | –0.5 | 0.2 M acetate (pH 4.5–4.7) |
| $Cd^{2+}(aq) + 2\,e^- \rightleftharpoons Cd(s)$ | –0.6 | 0.1 M KCl<br>0.050 M $H_2SO_4$<br>1 M $HNO_3$ |
| $Cr^{3+}(aq) + 3\,e^- \rightleftharpoons Cr(s)$ | –0.35 $(+3 \longrightarrow +2)$<br>–1.70 $(+2 \longrightarrow 0)$ | 1 M $NH_4Cl$ plus 1 M $NH_3$<br>1 M $NH_4^+/NH_3$ buffer (pH 8–9) |
| $Co^{3+}(aq) + 3\,e^- \rightleftharpoons Co(s)$ | –0.5 $(+3 \longrightarrow +2)$<br>–1.3 $(+2 \longrightarrow 0)$ | 1 M $NH_4Cl$ plus 1 M $NH_3$ |
| $Co^{2+}(aq) + 2\,e^- \rightleftharpoons Co(s)$ | –1.03 | 1 M KSCN |
| $Cu^{2+}(aq) + 2\,e^- \rightleftharpoons Cu(s)$ | 0.04<br>–0.22 | 0.1 M KSCN<br>0.1 M $NH_4ClO_4$<br>1 M $Na_2SO_4$<br>0.5 M potassium citrate (pH 7.5) |
| $Fe^{3+}(aq) + 3\,e^- \rightleftharpoons Fe(s)$ | –0.17 $(+3 \longrightarrow +2)$<br>–1.52 $(+2 \longrightarrow 0)$ | 0.5 M sodium tartrate (pH 5.8) |
| $Fe^{3+}(aq) + e^- \rightleftharpoons Fe^{2+}(aq)$ | –0.27 | 0.2 M $Na_2C_2O_4$ (pH < 7.9) |
| $Pb^{2+}(aq) + 2\,e^- \rightleftharpoons Pb(s)$ | –0.405<br>–0.435 | 1 M $HNO_3$<br>1 M KCl |
| $Mn^{2+}(aq) + 2\,e^- \rightleftharpoons Mn(s)$ | –1.65 | 1 M $NH_4Cl$ plus 1 M $NH_3$ |
| $Ni^{2+}(aq) + 2\,e^- \rightleftharpoons Ni(s)$ | –0.70<br>–1.09 | 1 M KSCN<br>1 M $NH_4Cl$ plus 1 M $NH_3$ |
| $Zn^{2+}(aq) + 2\,e^- \rightleftharpoons Zn(s)$ | –0.995<br>–1.33 | 0.1 M KCl<br>1 M $NH_4Cl$ plus 1 M $NH_3$ |

This page titled 35.8: Standard Reduction Potentials & Polarographic Half-wave Potentials is shared under a CC BY-NC-SA 4.0 license and was authored, remixed, and/or curated by David Harvey.

## 35.9: Recommended Primary Standards

All compounds are of the highest available purity. Metals are cleaned with dilute acid to remove any surface impurities and rinsed with distilled water. Unless otherwise indicated, compounds are dried to a constant weight at 110 $^{o}$C. Most of these compounds are soluble in dilute acid (1:1 HCl or 1:1 $HNO_3$), with gentle heating if necessary; some of the compounds are water soluble.

| Element | Compound | FW (g/mol) | Comments |
|---|---|---|---|
| aluminum | Al metal | 26.982 | |
| antimony | Sb metal | 121.760 | |
| | $KSbOC_4H_4O_6$ | 324.92 | prepared by drying $KSbC_4H_4O_6 \cdot \frac{1}{2} H_2O$ at 100 °C and storing in a desicator |
| arsenic | As metal | 74.922 | |
| | $As_2O_3$ | 197.84 | toxic |
| barium | $BaCO_3$ | 197.84 | dry at 200 ºC for 4 h |
| bismuth | Bi metal | 208.98 | |
| boron | $H_3BO_3$ | 61.83 | do not dry |
| bromine | KBr | 119.01 | |
| cadmium | Cd metal | 112.411 | |
| | CdO | 128.40 | |
| calcium | $CaCO_3$ | 100.09 | |
| cerium | Ce metal | 140.116 | |
| | $(NH_4)_2Ce(NO_3)_4$ | 548.23 | |
| cesium | $Cs_2CO_3$ | 325.82 | |
| | $Cs_2SO_4$ | 361.87 | |
| chlorine | NaCl | 58.44 | |
| chromium | Cr metal | 51.996 | |
| | $K_2Cr_2O_7$ | 294.19 | |
| cobalt | Co metal | 58.933 | |
| copper | Cu metal | 63.546 | |
| | CuO | 79.54 | |
| fluorine | NaF | 41.99 | do not store solutions in glass containers |
| iodine | KI | 166.00 | |
| | $KIO_3$ | 214.00 | |
| iron | Fe metal | 55.845 | |
| lead | Pb metal | 207.2 | |
| lithium | $Li_2CO_3$ | 73.89 | |
| magnesium | Mg metal | 24.305 | |
| manganese | Mn metal | 54.938 | |
| mercury | Hg metal | 200.59 | |

| Element | Compound | FW (g/mol) | Comments |
|---|---|---|---|
| molybdenum | Mo metal | 95.94 | |
| nickel | Ni metal | 58.693 | |
| phosphorous | $KH_2PO_4$ | 136.09 | |
| | $P_2O_5$ | 141.94 | |
| potassium | KCl | 74.56 | |
| | $K_2CO_3$ | 138.21 | |
| | $K_2Cr_2O_7$ | 294.19 | |
| | $KHC_8H_4O_2$ | 204.23 | |
| silicon | Si metal | 28.085 | |
| | $SiO_2$ | 60.08 | |
| silver | Ag metal | 107.868 | |
| | $AgNO_3$ | 169.87 | |
| sodium | NaCl | 58.44 | |
| | $Na_2CO_3$ | 106.00 | |
| | $Na_2C_2O_4$ | 134.00 | |
| strontium | $SrCO_3$ | 147.63 | |
| sulfur | elemental S | 32.066 | |
| | $K_2SO_4$ | 174.27 | |
| | $Na_2SO_4$ | 142.04 | |
| tin | Sn metal | 118.710 | |
| titanium | Ti metal | 47.867 | |
| tungsten | W metal | 183.84 | |
| uranium | U metal | 238.029 | |
| | $U_3O_8$ | 842.09 | |
| vanadium | V metal | 50.942 | |
| zinc | Zn metal | 81.37 | |

Sources:


- Smith, B. W.; Parsons, M. L. *J. Chem. Educ.* **1973**, *50*, 679–681
- Moody, J. R.; Greenburg, P. R.; Pratt, K. W.; Rains, T. C. *Anal. Chem.* **1988**, *60*, 1203A–1218A.



This page titled 35.9: Recommended Primary Standards is shared under a CC BY-NC-SA 4.0 license and was authored, remixed, and/or curated by David Harvey.

# 35.10: Acronyms and Abbreviations


https://chem.libretexts.org/@go/page/362975

| acronym or abbreviation | name |
|---|---|
| AC | alternating current |
| ADC | analog-to-digital convertor |
| AES | atomic emission spectroscopy<br>auger electron spectroscopy |
| AFM | atomic force microscopy |
| AFS | atomic fluorescence spectroscopy |
| ASV | anodic stripping voltammetry |
| ATF | attenuated total reflectance |
| BPC | binary pulse counter |
| CCD | charge-coupled device |
| CE | capillary electrophoresis |
| CEC | capillary electrochromatography |
| CGE | capillary gel electrophoresis |
| CI | chemical ionization |
| CID | charge injection device |
| COSY | correlation spectroscopy |
| CZE | capillary zone electrophoresis |
| CSV | cathodic stripping voltammetry |
| CV | cyclic voltammetry |
| DAC | digital-to-analog convertor |
| DAS | diode array spectrometer |
| DC | direct current |
| DCP | direct current plasma |
| DCS | differential centrifugal separation |
| DL | detection limit |
| DME | dropping mercury electrode |
| DPP | differential pulse polarography |
| DRIFT | diffuse reflectance infrared Fourier transform |
| DSC | differential scanning calorimetry |
| DTA | differential thermal analysis |
| ECD | electron capture detector<br>electrochemical detector |
| EDL | electrical double layer |
| EM | electromagnetic |

| acronym or abbreviation | name |
|---|---|
| ESR | electron spin resonance |
| FAAS | flame atomic absorption spectrometry |
| FIA | flow-injection analysis |
| FID | flame ionization detector<br>free induction decay |
| FIR | far infrared |
| FT | Fourier transform |
| GC | gas chromatography |
| GC-MS | gas chromatography-mass spectrometry |
| GDMS | glow-discharge mass spectrometry |
| HCL | hollow cathode lamp |
| HETCOR | heteronuclear correlation spectroscopy |
| HETP | height-equivalent of theoretical plate |
| HMDE | hanging mercury drop electrode |
| HPLC | high performance liquid chromatography |
| ICP | inductively coupled plasma |
| IEC | ion-exchange chromatography |
| IR | infrared |
| IS | internal standard |
| ISE | ion-selective electrode |
| LC | liquid chromatography |
| LOI | limit-of-identification |
| LOQ | limit-of-quantification |
| LSV | linear sweep voltammetry |
| MALDI | matrix-assisted laser desorption ionization |
| MEKC | micellar electrokinetic capillary chromatography |
| MS | mass spectrometry |
| MW | molecular weight |
| M/Z | mass-to-charge ratio |
| NAA | neutron activation analysis |
| NHE | normal hydrogen electrode |
| NIR | near infrared |
| NMR | nuclear magnetic resonance |

| acronym or abbreviation | name |
|---|---|
| NOSEY | nuclear overhauser and exchange spectroscopy |
| NP | normal polarography |
| NPP | normal pulse polarography |
| ORD | optical rotary dispersion |
| PDA | photodiode array |
| PLOT | porous-layer open tubular column |
| PP | pulse polarography |
| RPC | reverse phase chromatography |
| RRM | resonance Raman spectrosocopy |
| SCE | saturated calomel electrode |
| SCOT | support-coated open tubular column |
| SEC | size-exclusion chromatography |
| SEM | scanning electron microscopy |
| SERS | surface-enhanced Raman spectroscopy |
| SFC | supercritical fluid chromatography |
| SHE | standard hydrogen electrode |
| SIMS | secondary ion mass spectrometry |
| SMDE | static mercury drop electrode |
| S/R (or SNR) | signal-to-noise ratio |
| SSMS | spark-source mass spectrometry |
| STM | scanning tunneling microscopy |
| TCD | thermal conductivity detector |
| TGA | thermal gravimetric analysis |
| TOCSY | total correlation spectroscopy |
| TOF | time-of-flight |
| UV | ultraviolet |
| UV/Vis | ultraviolet/visible |
| Vis | visible |
| WCOT | wall-coated open tubular column |
| XPS | x-ray photoelectron spectroscopy |
| XRF | x-ray fluorescence |

This page titled 35.10: Acronyms and Abbreviations is shared under a CC BY-NC-SA 4.0 license and was authored, remixed, and/or curated by David Harvey.

# Index


## A

abbreviation
- 35.10: Acronyms and Abbreviations

absorbance
- 7: Components of Optical Instruments
- 7.1: General Design of Optical Instruments
- 9.3: Interferences in Absorption Spectroscopy
- 13: Introduction to Ultraviolet/Visible Absorption Spectrometry
- 13.1: Transmittance and Absorbance
- 13.3: Effect of Noise on Transmittance and Absorbance Measurements
- 13.4: Instrumentation
- 14: Applications of Ultraviolet/Visible Molecular Absorption Spectrometry
- 14.5: Photometric Titrations
- 17.1: Mid-Infrared Absorption Spectometry

absorbance spectrum
- 14.2: Absorbing Species

absorbed
- 6.5: Quantitative Considerations

Absorption
- 1.2: Types of Instrumental Methods
- 6: An Introduction to Spectrophotometric Methods
- 6.1: General Properties of Electromagnetic Radiation
- 8: An Introduction to Optical Atomic Spectroscopy
- 13.3: Effect of Noise on Transmittance and Absorbance Measurements
- 14: Applications of Ultraviolet/Visible Molecular Absorption Spectrometry
- 14.2: Absorbing Species
- 14.3: Qualitative and Characterization Applications
- 14.4: Quantitative Applications
- 16: An Introduction to Infrared Spectrometry

Absorption Spectrometry
- 12.4: Other X-Ray Methods
- 17: Applications of Infrared Spectrometry

absorption spectroscopy
- 13: Introduction to Ultraviolet/Visible Absorption Spectrometry
- 15: Molecular Luminescence

accuracy
- 1.4: Selecting an Analytical Method
- 15.5: Evaluation of Molecular Luminescence

acid
- 35.9: Recommended Primary Standards

acidic solution
- 35.8: Standard Reduction Potentials & Polarographic Half-wave Potentials

acronym
- 35.10: Acronyms and Abbreviations

activity coefficients
- 35.7: Activity Coefficients

activitycoefficients
- 35: Appendicies

adsorption
- 26.1: A General Description of Chromatography

adsorption chromatography
- 28: High-Performance Liquid Chromatography
- 28.5: Adsorption Chromatography

adsorptive stripping voltammetry
- 25.6: Stripping Methods

affinity chromatography
- 26.1: A General Description of Chromatography

affordable learning
- InfoPage

AFM
- 21.4: Scanning Probe Microscopes

Ag electrode
- 23.2: Metallic Indicator Electrodes

alpha
- 32: Radiochemical Methods
- 35.3: Critical Values for t-Test

alpha particles
- 32.2: Instrumentation

alternating current
- 2: Electrical Components and Circuits
- 2.3: Alternating Current Circuits

alternatingcurrent
- 2.2: Direct Current (DC) Circuits

alternative hypothesis
- 35.3: Critical Values for t-Test

alumina
- 28.5: Adsorption Chromatography

aluminum
- 35.9: Recommended Primary Standards

American Chemical Society
- About the Author

ammonia
- 1.3: Instruments For Analysis
- 7: Components of Optical Instruments

amperes
- 2.1: Basic Terminology and Laws of Electricity

amperometric sensors
- 25.3: Linear Sweep Voltammetry

amperometry
- 22.6: Types of Electroanalytical Methods
- 25.7: Applications of Voltammetry

amplification
- 3: Operational Amplifiers
- 3.3: Amplification and Measurement of Signals

amplifier circuit
- 3.2: Operational Amplifier Circuits

amplitude
- 6.2: Wave Properties of Electromagnetic Radiation

analog
- 4: Analog and Digital Data

analog signals
- 4.3: Cleaning Up Signals and Counting Events

analysis
- 1.2: Types of Instrumental Methods
- 1.4: Selecting an Analytical Method
- 6.5: Quantitative Considerations
- 7: Components of Optical Instruments
- 21: Surface Characterization by Spectroscopy and Microscopy
- 23: Potentiometry
- 26.5: Summary of Important Relationships for Chromatography
- 28: High-Performance Liquid Chromatography
- 29.2: Supercritical Fluid Chromatography
- 31: Thermal Methods
- 32: Radiochemical Methods
- 33: Automated Methods of Analysis

analysis_time
- 26.4: Optimization and Column Performance

analyte
- 1.4: Selecting an Analytical Method
- 6.5: Quantitative Considerations
- 9: Atomic Absorption Spectrometry
- 9.2: Atomic Absorption Instrumentation
- 12.3: Atomic X-Ray Fluorescence Methods
- 14: Applications of Ultraviolet/Visible Molecular Absorption Spectrometry
- 14.2: Absorbing Species
- 24.2: Controlled-Potential Coulometry
- 25.1: Potential Excitation Signals and Currents in Voltammetry
- 26: Introduction to Chromatographic Separations

analyte concentration
- 9.1: Sample Atomization Techniques
- 25.6: Stripping Methods

analyte extraction
- 9.4: Atomic Absorption Techniques

analyteconcentration
- 27.2: Instruments for Gas Chromatography

analytematrix
- 9.3: Interferences in Absorption Spectroscopy

analytes
- 15.3: Applications and Photoluminescence methods

analytical balance
- 1.3: Instruments For Analysis

analytical chemistry
- About the Author
- 1: Introduction
- 8.3: Sample Introduction Methods
- 9.4: Atomic Absorption Techniques
- 14.4: Quantitative Applications
- 33.1: Overview of Automated Methods of Analysis

analytical instruments
- 33.3: Other Automated Methods of Analysis

analytical method
- 5: Signals and Noise
- 15.3: Applications and Photoluminescence methods
- 24.2: Controlled-Potential Coulometry

Analytical Methods
- 1: Introduction
- 1.4: Selecting an Analytical Method
- 21.1: Introduction to the Study of Surfaces

analytical signal
- 22: An Introduction to Electroanalytical Chemistry

analytical signals
- 22.6: Types of Electroanalytical Methods

analytical techniques
- 25.7: Applications of Voltammetry

analyticalchemistry
- 9.3: Interferences in Absorption Spectroscopy
- 28.3: Instruments for Liquid Chromatography
- 35: Appendicies

analyticalcolumns
- 28.3: Instruments for Liquid Chromatography

analyzers
- 33: Automated Methods of Analysis

anionexchangers
- 28.6: Ion-Exchange Chromatography

anions
- 35.7: Activity Coefficients

anodic stripping voltammetry
- 25.6: Stripping Methods

applications
14.3: Qualitative and Characterization Applications
21.3: Scanning Electron Microscopy
aqueous samples
18.2: Instrumentation
aqueous solutions
35.8: Standard Reduction Potentials & Polarographic Half-wave Potentials
area
35.2: Single-Sided Normal Distribution
argon gas
11: Atomic Mass Spectrometry
aromatic hydrocarbons
28.5: Adsorption Chromatography
arsenic
35.9: Recommended Primary Standards
atomic
8: An Introduction to Optical Atomic Spectroscopy
atomic absorption
9: Atomic Absorption Spectrometry
9.2: Atomic Absorption Instrumentation
10.1: Emission Spectroscopy Based on Flame and Plasma Sources
atomic absorption spectroscopy
9.2: Atomic Absorption Instrumentation
9.4: Atomic Absorption Techniques
atomic emission
10: Atomic Emission Spectrometry
10.2: Emission Spectroscopy Based on Arc and Spark Sources
12.1: Fundamental Principles
atomic emission spectroscopy
35.10: Acronyms and Abbreviations
atomic force microscopy
35.10: Acronyms and Abbreviations
atomic mass spectrometry
11: Atomic Mass Spectrometry
atomic methods
8.2: Atomization Methods
atomic spectra
10.1: Emission Spectroscopy Based on Flame and Plasma Sources
atomic spectroscopic methods
8.3: Sample Introduction Methods
atomic theory
11.1: General Features of Atomic Mass Spectrometry
AtomicSpectroscopy
9.3: Interferences in Absorption Spectroscopy
12.3: Atomic X-Ray Fluorescence Methods
atomization
8.3: Sample Introduction Methods
9: Atomic Absorption Spectrometry
9.1: Sample Atomization Techniques
atomization process
8.2: Atomization Methods
atoms
11.1: General Features of Atomic Mass Spectrometry
attenuated total reflectance spectrometry
17.2: Mid-Infrared Reflection Spectrometry
Auger
21: Surface Characterization by Spectroscopy and Microscopy
automated
33: Automated Methods of Analysis
automated analysis
33.1: Overview of Automated Methods of Analysis
33.3: Other Automated Methods of Analysis
automated titrator
33.1: Overview of Automated Methods of Analysis
autosampler
33.1: Overview of Automated Methods of Analysis

## B

bandbroadening
27.2: Instruments for Gas Chromatography
base peak
20.1: Molecular Mass Spectra
Beer’s Law
13.2: Beer's Law
14.4: Quantitative Applications
Beer's Law
12.1: Fundamental Principles
12.4: Other X-Ray Methods
13: Introduction to Ultraviolet/Visible Absorption Spectrometry
13.3: Effect of Noise on Transmittance and Absorbance Measurements
14: Applications of Ultraviolet/Visible Molecular Absorption Spectrometry
beta
32: Radiochemical Methods
beta particles
32.2: Instrumentation
binary
4: Analog and Digital Data
binary numbers
4.2: Working With Binary Numbers
biochemistry
About the Author
biomolecules
28.7: Size-Exclusion Chromatography
bulk properties
21.1: Introduction to the Study of Surfaces

## C

CaCO3
28.5: Adsorption Chromatography
calibration
1.3: Instruments For Analysis
13.4: Instrumentation
calibration curve
9.4: Atomic Absorption Techniques
10.1: Emission Spectroscopy Based on Flame and Plasma Sources
18.3: Applications of Raman Spectroscopy
23.3: Membrane Ion-Selective Electrodes
26.6: Applications of Chromatography
27.4: Applications of Gas Chromatography
35.1: Evaluation of Analytical Data
calibration curves
15.3: Applications and Photoluminescence methods
calomel electrodes
23.1: Reference Electrodes
cantilever
21.4: Scanning Probe Microscopes
capacitance
2.3: Alternating Current Circuits
capillary columns
27.3: Gas Chromatographic Columns and Stationary Phases
capillary electrochromatography
30: Capillary Electrophoresis and Capillary Electrochromatography
30.3: Applications of Capillary Electrophoresis
capillary electrophoresis
30: Capillary Electrophoresis and Capillary Electrochromatography
30.2: Capillary Electrophoresis
35.10: Acronyms and Abbreviations
capillary gel electrophoresis
30.3: Applications of Capillary Electrophoresis
capillary zone electrophoresis
30.3: Applications of Capillary Electrophoresis
carbohydrates
18.3: Applications of Raman Spectroscopy
carbon dioxide
16.1: Theory of Infrared Absorption Spectrometry
cathodic stripping voltammetry
25.6: Stripping Methods
cationexchangers
28.6: Ion-Exchange Chromatography
cations
35.7: Activity Coefficients
cell potential
22.4: Calculation of Cell Potentials from Electrode Potentials
centrifugal
33: Automated Methods of Analysis
centrifugal analyzer
33.3: Other Automated Methods of Analysis
CGE
30.3: Applications of Capillary Electrophoresis
characterization analysis
1: Introduction
charge
2.1: Basic Terminology and Laws of Electricity
chemical analysis
14.4: Quantitative Applications
17: Applications of Infrared Spectrometry
19.3: NMR Spectrometers
33.3: Other Automated Methods of Analysis
chemical equilibria
35.8: Standard Reduction Potentials & Polarographic Half-wave Potentials
chemical formulas
20.4: Applications of Molecular Mass Spectrometry
chemical identification
1: Introduction
chemical ionization
35.10: Acronyms and Abbreviations
chemical measurements
1: Introduction
chemical reactions
20.1: Molecular Mass Spectra
35.7: Activity Coefficients
chemical reactivity
21.1: Introduction to the Study of Surfaces
chemical selectivity
23.3: Membrane Ion-Selective Electrodes
27.3: Gas Chromatographic Columns and Stationary Phases

chemical shifts
19.2: Environmental Effects on NMR Spectra
19.5: Carbon-13 NMR
chemicalanalysis
27.2: Instruments for Gas Chromatography
chemicalinterferences
9.3: Interferences in Absorption Spectroscopy
chemicalShifts
19.4: Applications of Proton NMR
chemiluminescence
1.2: Types of Instrumental Methods
15: Molecular Luminescence
chemiluminscence
15.4: Chemiluminscence
chemistry
About the Author
11.1: General Features of Atomic Mass Spectrometry
26: Introduction to Chromatographic Separations
chemometrics
35.1: Evaluation of Analytical Data
chromatographic columns
27: Gas Chromatography
chromatography
20.3: Mass Spectrometers
26: Introduction to Chromatographic Separations
26.1: A General Description of Chromatography
26.4: Optimization and Column Performance
26.5: Summary of Important Relationships for Chromatography
26.6: Applications of Chromatography
27.3: Gas Chromatographic Columns and Stationary Phases
28: High-Performance Liquid Chromatography
28.3: Instruments for Liquid Chromatography
29.2: Supercritical Fluid Chromatography
chromatography methods
28.7: Size-Exclusion Chromatography
circuit analysis
3.2: Operational Amplifier Circuits
circuits
2.1: Basic Terminology and Laws of Electricity
3: Operational Amplifiers
3.4: Mathematical Operations Using Operational Amplifiers
clinical analysis
27.4: Applications of Gas Chromatography
CO2
29.1: Properties of Supercritical Fluids
collaboration
InfoPage
colloidal suspensions
34: Particle Size Determination
ColloidalParticles
18.4: Other Types of Raman Spectroscopy
colorimetric
7: Components of Optical Instruments
colorimetric analysis
1.3: Instruments For Analysis
column efficiency
26.3: Zone Broadening and Column Efficiency
combustion gases
9.1: Sample Atomization Techniques
compartment
7.4: Sample Containers
complex
14.3: Qualitative and Characterization Applications
complexcircuits
2.2: Direct Current (DC) Circuits
compounds
11.1: General Features of Atomic Mass Spectrometry
35.9: Recommended Primary Standards
concentration
1.4: Selecting an Analytical Method
6.5: Quantitative Considerations
13.3: Effect of Noise on Transmittance and Absorbance Measurements
14: Applications of Ultraviolet/Visible Molecular Absorption Spectrometry
14.4: Quantitative Applications
14.5: Photometric Titrations
15.3: Applications and Photoluminescence methods
conductivity
22: An Introduction to Electroanalytical Chemistry
conductor
2: Electrical Components and Circuits
confidence level
35.3: Critical Values for t-Test
confidencelevel
35.5: Critical Values for Dixon's Q-Test
conservation of mass
11.1: General Features of Atomic Mass Spectrometry
continuous instruments
33.1: Overview of Automated Methods of Analysis
copper
35.9: Recommended Primary Standards
copper electrode
23.2: Metallic Indicator Electrodes
correlation_spectroscopy
19: Nuclear Magnetic Resonance Spectroscopy
COSY
19.6: Two-Dimensional Fourier Transform NMR
coulometry
22.6: Types of Electroanalytical Methods
24: Coulometry
24.1: Introduction to Coulometry
critical values
35.3: Critical Values for t-Test
35.6: Critical Values for Grubb's Test
criticalvalues
35: Appendicies
35.4: Critical Values for F-Test
35.5: Critical Values for Dixon's Q-Test
Cu2+
14.5: Photometric Titrations
23.2: Metallic Indicator Electrodes
cumulative distribution
34.2: Measuring Particle Size Using Sieves
current
2: Electrical Components and Circuits
2.1: Basic Terminology and Laws of Electricity
2.3: Alternating Current Circuits
25: Voltammetry
25.1: Potential Excitation Signals and Currents in Voltammetry
current efficiency
24.2: Controlled-Potential Coulometry
current measurement
22: An Introduction to Electroanalytical Chemistry
25.2: Voltammetric Instrumentation
current measurements
3.3: Amplification and Measurement of Signals
currentmeasurement
21.4: Scanning Probe Microscopes
customization
InfoPage
cyclic voltammetry
25: Voltammetry
25.4: Cyclic Voltammetry
25.7: Applications of Voltammetry

## D

D2lamp
9.3: Interferences in Absorption Spectroscopy
data
4: Analog and Digital Data
data analysis
4.3: Cleaning Up Signals and Counting Events
5: Signals and Noise
35.1: Evaluation of Analytical Data
35.6: Critical Values for Grubb's Test
data processing
19.3: NMR Spectrometers
dataanalysis
35: Appendicies
35.5: Critical Values for Dixon's Q-Test
David Harvey
About the Author
DC circuits
2: Electrical Components and Circuits
DCCircuits
2.2: Direct Current (DC) Circuits
decay
32: Radiochemical Methods
decimal
4: Analog and Digital Data
degrees of freedom
35.3: Critical Values for t-Test
density
29.1: Properties of Supercritical Fluids
DePauw University
About the Author
depth profiling
21.1: Introduction to the Study of Surfaces
detection
20.3: Mass Spectrometers
29.2: Supercritical Fluid Chromatography
detection limit
1.4: Selecting an Analytical Method
detection limits
15.5: Evaluation of Molecular Luminescence
25.6: Stripping Methods
DetectionLimits
18.4: Other Types of Raman Spectroscopy
detector
1.3: Instruments For Analysis
7.1: General Design of Optical Instruments
7.5: Radiation Transducers
9.2: Atomic Absorption Instrumentation
detectors
28.3: Instruments for Liquid Chromatography
32.2: Instrumentation

deviation
35.2: Single-Sided Normal Distribution
differential amplifier
5.3: Signal-to-Noise Enhancement
differential pulse polarography
25.7: Applications of Voltammetry
differential scanning calorimetry
31: Thermal Methods
31.2: Differential Thermal Analysis and Differential Scanning Calorimetry
35.10: Acronyms and Abbreviations
differential thermal analysis
31: Thermal Methods
31.2: Differential Thermal Analysis and Differential Scanning Calorimetry
diffraction spectrum
12.4: Other X-Ray Methods
diffuse reflectance spectrometry
17.2: Mid-Infrared Reflection Spectrometry
digital
4: Analog and Digital Data
digital camera
34.4: Measuring Particle Size Using Image Analysis
digital data
4.1: Analog and Digital Data
digital signals
4.3: Cleaning Up Signals and Counting Events
dilution
14.5: Photometric Titrations
dipole
16: An Introduction to Infrared Spectrometry
direct current
2: Electrical Components and Circuits
2.3: Alternating Current Circuits
direct current plasma
10: Atomic Emission Spectrometry
directcurrent
2.2: Direct Current (DC) Circuits
discrete analysis
34.2: Measuring Particle Size Using Sieves
discrete instruments
33.1: Overview of Automated Methods of Analysis
dispersive instruments
18.2: Instrumentation
disposable
33: Automated Methods of Analysis
disposable analyzers
33.3: Other Automated Methods of Analysis
disposable card
7.4: Sample Containers
Distribution
34.1: Overview
distribution constant
26.2: Migration Rates of Solutes
division
3.4: Mathematical Operations Using Operational Amplifiers
DixonQTest
35.5: Critical Values for Dixon's Q-Test
dixonstest
35: Appendicies
Doppler broadening
8.1: Optical Atomic Spectra
drugs
29.2: Supercritical Fluid Chromatography
dynamic imaging analysis
34.4: Measuring Particle Size Using Image Analysis
Dynamic Light Scattering
34.5: Measuring Particle Size Using Light Scattering
dynamic techniques
22: An Introduction to Electroanalytical Chemistry
22.6: Types of Electroanalytical Methods

## E

EDTA
14.5: Photometric Titrations
effective nuclear charge
2.4: Semiconductors
elastic scattering
18: Raman Spectroscopy
electric arcs
8.2: Atomization Methods
electrical
16: An Introduction to Infrared Spectrometry
electrical circuits
2.3: Alternating Current Circuits
electrical engineering
3.2: Operational Amplifier Circuits
3.4: Mathematical Operations Using Operational Amplifiers
electrical signal
3.3: Amplification and Measurement of Signals
electricalsignal
3: Operational Amplifiers
electricity
2: Electrical Components and Circuits
2.1: Basic Terminology and Laws of Electricity
electroanalytical
26: Introduction to Chromatographic Separations
electrochemical
23: Potentiometry
25: Voltammetry
25.1: Potential Excitation Signals and Currents in Voltammetry
electrochemical cell
22.1: Electrochemical Cells
23.2: Metallic Indicator Electrodes
23.3: Membrane Ion-Selective Electrodes
electrochemical cells
22: An Introduction to Electroanalytical Chemistry
25.2: Voltammetric Instrumentation
electrochemical experiments
22.6: Types of Electroanalytical Methods
electrochemical techniques
1.2: Types of Instrumental Methods
22: An Introduction to Electroanalytical Chemistry
25.6: Stripping Methods
electrochemistry
22: An Introduction to Electroanalytical Chemistry
22.6: Types of Electroanalytical Methods
24.2: Controlled-Potential Coulometry
25.2: Voltammetric Instrumentation
25.7: Applications of Voltammetry
35.8: Standard Reduction Potentials & Polarographic Half-wave Potentials
electrode
25.1: Potential Excitation Signals and Currents in Voltammetry
electrode oxidation
25.2: Voltammetric Instrumentation
electrode potentials
22: An Introduction to Electroanalytical Chemistry
35.8: Standard Reduction Potentials & Polarographic Half-wave Potentials
electrodes
10.2: Emission Spectroscopy Based on Arc and Spark Sources
22.1: Electrochemical Cells
23: Potentiometry
25.2: Voltammetric Instrumentation
electrolysis
24.2: Controlled-Potential Coulometry
electrolytic cell
22.1: Electrochemical Cells
electromagnetic
6.2: Wave Properties of Electromagnetic Radiation
electromagnetic radiation
6: An Introduction to Spectrophotometric Methods
6.1: General Properties of Electromagnetic Radiation
7: Components of Optical Instruments
14.2: Absorbing Species
14.5: Photometric Titrations
electromagnetic spectrum
12.1: Fundamental Principles
14: Applications of Ultraviolet/Visible Molecular Absorption Spectrometry
Electron
7.5: Radiation Transducers
electron capture detector
35.10: Acronyms and Abbreviations
electron microscope
34.4: Measuring Particle Size Using Image Analysis
electronbeam
12.2: Instrument Components
21.4: Scanning Probe Microscopes
electronic transitions
14.2: Absorbing Species
electronmicroscope
21.3: Scanning Electron Microscopy
electrons
11.1: General Features of Atomic Mass Spectrometry
21.3: Scanning Electron Microscopy
electroosmotic mobility
30.2: Capillary Electrophoresis
electrophoresis
30.1: An Overview of Electrophoresis
electrophoretic mobility
30.2: Capillary Electrophoresis
electrothermal atomization
9: Atomic Absorption Spectrometry
9.1: Sample Atomization Techniques
9.4: Atomic Absorption Techniques
elemental analysis
1: Introduction
9.1: Sample Atomization Techniques
elements
11.1: General Features of Atomic Mass Spectrometry
elution chromatography
26.1: A General Description of Chromatography

elution order
28.5: Adsorption Chromatography
emission
1.2: Types of Instrumental Methods
6: An Introduction to Spectrophotometric Methods
6.1: General Properties of Electromagnetic Radiation
8: An Introduction to Optical Atomic Spectroscopy
10.1: Emission Spectroscopy Based on Flame and Plasma Sources
12.4: Other X-Ray Methods
emission lines
9.2: Atomic Absorption Instrumentation
10.2: Emission Spectroscopy Based on Arc and Spark Sources
emission spectra
6.4: Emission and Absorbance Spectra
emission spectroscopy
10: Atomic Emission Spectrometry
emission spectrum
12.1: Fundamental Principles
emitted
6.5: Quantitative Considerations
energy
6: An Introduction to Spectrophotometric Methods
6.1: General Properties of Electromagnetic Radiation
8: An Introduction to Optical Atomic Spectroscopy
energy states
6.4: Emission and Absorbance Spectra
14.2: Absorbing Species
energy transfer
1.2: Types of Instrumental Methods
EnergyDispersiveInstruments
12.3: Atomic X-Ray Fluorescence Methods
enhancement
5: Signals and Noise
environmental analysis
17.1: Mid-Infrared Absorption Spectometry
27.4: Applications of Gas Chromatography
environmental applications
14.4: Quantitative Applications
environmental noise
5.2: Sources of Instrumental Noise
environmental samples
25.7: Applications of Voltammetry
environmental science
27: Gas Chromatography
environmental_effects
19: Nuclear Magnetic Resonance Spectroscopy
equivalence point
14.5: Photometric Titrations
errors
13.3: Effect of Noise on Transmittance and Absorbance Measurements
ethanol
16.1: Theory of Infrared Absorption Spectrometry
event detection
4.3: Cleaning Up Signals and Counting Events
events
4: Analog and Digital Data
Excellence in Education
About the Author
experimental design
35.1: Evaluation of Analytical Data
external standard
27.4: Applications of Gas Chromatography

## F

faradaic current
22.1: Electrochemical Cells
Fdistribution
35.4: Critical Values for F-Test
feedback
3: Operational Amplifiers
feedback circuit
3.2: Operational Amplifier Circuits
feedback loop
3.3: Amplification and Measurement of Signals
3.4: Mathematical Operations Using Operational Amplifiers
fiber optic probes
18.2: Instrumentation
fiber optics
7: Components of Optical Instruments
7.6: Fiber Optics
field
16: An Introduction to Infrared Spectrometry
fields
6.2: Wave Properties of Electromagnetic Radiation
filtering
5.3: Signal-to-Noise Enhancement
filters
2.3: Alternating Current Circuits
flame aspiration
8.3: Sample Introduction Methods
flame atomization
9: Atomic Absorption Spectrometry
9.1: Sample Atomization Techniques
9.4: Atomic Absorption Techniques
flameatomization
9.3: Interferences in Absorption Spectroscopy
flames
8.2: Atomization Methods
flicker noise
5.2: Sources of Instrumental Noise
flow injection analysis
33.2: Flow-Injection Analysis
flow rate
26.5: Summary of Important Relationships for Chromatography
FlowProportionalCounter
12.2: Instrument Components
fluid
29.1: Properties of Supercritical Fluids
fluorescence
7.1: General Design of Optical Instruments
8: An Introduction to Optical Atomic Spectroscopy
12.3: Atomic X-Ray Fluorescence Methods
15: Molecular Luminescence
15.1: Theory of Fluorescence and Phosphorescence
15.5: Evaluation of Molecular Luminescence
18.2: Instrumentation
fluorescence analysis
15.3: Applications and Photoluminescence methods
fluorescence quantum yield
15.1: Theory of Fluorescence and Phosphorescence
fluorometer
15.2: Instruments for Measuring Fluorescence and Phosphorescence
forensic analysis
27.4: Applications of Gas Chromatography
formal potentials
35.8: Standard Reduction Potentials & Polarographic Half-wave Potentials
formation constant
35.7: Activity Coefficients
Fourier_transform
19: Nuclear Magnetic Resonance Spectroscopy
fragmentation
20: Molecular Mass Spectrometry
20.1: Molecular Mass Spectra
fragmentation patterns
20.4: Applications of Molecular Mass Spectrometry
frequencies
12.1: Fundamental Principles
frequency
2: Electrical Components and Circuits
2.3: Alternating Current Circuits
6.2: Wave Properties of Electromagnetic Radiation
Ftest
35: Appendicies
35.4: Critical Values for F-Test
FWHM
34.1: Overview

## G

gain
3.2: Operational Amplifier Circuits
galvanic cell
22.1: Electrochemical Cells
gamma
32: Radiochemical Methods
gamma rays
32.2: Instrumentation
gas
29.1: Properties of Supercritical Fluids
gas chromatography
20: Molecular Mass Spectrometry
20.4: Applications of Molecular Mass Spectrometry
27: Gas Chromatography
27.3: Gas Chromatographic Columns and Stationary Phases
27.4: Applications of Gas Chromatography
35.10: Acronyms and Abbreviations
gas phase
8.2: Atomization Methods
gaschromatography
27.2: Instruments for Gas Chromatography
GC
27: Gas Chromatography
Geiger counter
4.3: Cleaning Up Signals and Counting Events
32.2: Instrumentation
glass
7.4: Sample Containers
glow discharge mass spectrometry
11.4: Other Forms of Atomic Mass Spectrometry
glucose concentration
1: Introduction

gradient elutions
29.2: Supercritical Fluid Chromatography
Grubbs test
35.6: Critical Values for Grubb's Test
grubbstest
35: Appendicies
guardcolumns
28.3: Instruments for Liquid Chromatography

H

hanging mercury drop
25.6: Stripping Methods
hardware
5: Signals and Noise
high throughput
33.1: Overview of Automated Methods of Analysis
higher education
InfoPage
histogram
34.1: Overview
histograms
34.2: Measuring Particle Size Using Sieves
hollow cathode lamp
9.2: Atomic Absorption Instrumentation
HPLC
28: High-Performance Liquid Chromatography
28.3: Instruments for Liquid Chromatography
29.2: Supercritical Fluid Chromatography
HPLC instrumentation
28.7: Size-Exclusion Chromatography
hypothesis testing
35.1: Evaluation of Analytical Data
35.3: Critical Values for t-Test
35.4: Critical Values for F-Test
35.6: Critical Values for Grubb's Test

I

identification
20.4: Applications of Molecular Mass Spectrometry
IEC
28.6: Ion-Exchange Chromatography
image analysis
34: Particle Size Determination
34.4: Measuring Particle Size Using Image Analysis
image capture
34.4: Measuring Particle Size Using Image Analysis
imaging
34.1: Overview
imagingtechniques
21.4: Scanning Probe Microscopes
impedance
2.3: Alternating Current Circuits
impurities
21.1: Introduction to the Study of Surfaces
35.9: Recommended Primary Standards
indicator electrodes
23.2: Metallic Indicator Electrodes
inductively coupled plasma
10: Atomic Emission Spectrometry
11: Atomic Mass Spectrometry
inelastic scattering
18: Raman Spectroscopy
infrared
14.3: Qualitative and Characterization Applications
16: An Introduction to Infrared Spectrometry
16.1: Theory of Infrared Absorption Spectrometry
infrared spectromters
16.3: Infrared Instruments
infrared spectroscopy
7.4: Sample Containers
16.1: Theory of Infrared Absorption Spectrometry
17: Applications of Infrared Spectrometry
17.1: Mid-Infrared Absorption Spectometry
infrared transducer
16.2: Infrared Sources and Transducers
innovative experiments
About the Author
inorganic compounds
18.3: Applications of Raman Spectroscopy
instrument
3.3: Amplification and Measurement of Signals
instrumental methods
1: Introduction
1.2: Types of Instrumental Methods
12: Atomic X-Ray Spectrometry
instrumental noise
13: Introduction to Ultraviolet/Visible Absorption Spectrometry
13.3: Effect of Noise on Transmittance and Absorbance Measurements
instrumentation
4.3: Cleaning Up Signals and Counting Events
15: Molecular Luminescence
18: Raman Spectroscopy
18.2: Instrumentation
21.3: Scanning Electron Microscopy
32: Radiochemical Methods
instruments
4: Analog and Digital Data
7.1: General Design of Optical Instruments
16: An Introduction to Infrared Spectrometry
23: Potentiometry
insulator
2: Electrical Components and Circuits
integration
3.4: Mathematical Operations Using Operational Amplifiers
intensity ratio
19.2: Environmental Effects on NMR Spectra
interfacial techniques
22.6: Types of Electroanalytical Methods
interference filter
7.3: Wavelength Selectors
interferencecompensation
9.3: Interferences in Absorption Spectroscopy
interferences
9: Atomic Absorption Spectrometry
interferometer
7.7: Fourier Transform Optical Spectroscopy
internal reflection
17.2: Mid-Infrared Reflection Spectrometry
internal standard
1.5: Calibration of Instrumental Methods
27.4: Applications of Gas Chromatography
internalStandard
19.4: Applications of Proton NMR
InternalStandards
12.3: Atomic X-Ray Fluorescence Methods
inverting amplifier
3.2: Operational Amplifier Circuits
ion activity
23.3: Membrane Ion-Selective Electrodes
ionexchangechromatography
28.6: Ion-Exchange Chromatography
ionic strength
35.7: Activity Coefficients
ionicfunctionalgroups
28.6: Ion-Exchange Chromatography
ionization
11: Atomic Mass Spectrometry
20.3: Mass Spectrometers
32.2: Instrumentation
ions
11: Atomic Mass Spectrometry
20: Molecular Mass Spectrometry
20.3: Mass Spectrometers
iR drop
22.5: Currents in Electrochemical Cells
IR radiation
17.1: Mid-Infrared Absorption Spectometry
IR spectrum
16.1: Theory of Infrared Absorption Spectrometry
iron
35.9: Recommended Primary Standards
irregularly shaped particles
34.2: Measuring Particle Size Using Sieves
isotope dilution methods
32.4: Isotope Dilution Methods
isotope ratios
11.3: Inductively Coupled Plasma Mass Spectrometer
isotopes
32: Radiochemical Methods

J

J. Calvin Giddings Award
About the Author
John Dalton
11.1: General Features of Atomic Mass Spectrometry

K

kinetic analysis
33.3: Other Automated Methods of Analysis
Kirchhoff's laws
3.2: Operational Amplifier Circuits
kirchhoffs laws
2.1: Basic Terminology and Laws of Electricity
Kirchoff'slaw
2.2: Direct Current (DC) Circuits

L

laser
7.2: Sources of Radiation
LibreTexts
InfoPage
light
6: An Introduction to Spectrophotometric Methods
6.1: General Properties of Electromagnetic Radiation

light absorption
9: Atomic Absorption Spectrometry
light detection
13.4: Instrumentation
light scattering
34: Particle Size Determination
34.1: Overview
line spectra
6.4: Emission and Absorbance Spectra
linear sweep
25: Voltammetry
Linear Sweep Voltammetry
25.3: Linear Sweep Voltammetry
liquid
29.1: Properties of Supercritical Fluids
liquid chromatography
20.4: Applications of Molecular Mass Spectrometry
Liquid Junction Potentials
22.2: Potentials in Electroanalytical Cells
liquid samples
7.4: Sample Containers
liquidchromatography
28.3: Instruments for Liquid Chromatography
luminescence methods
15: Molecular Luminescence

## M

magnetic field
19.2: Environmental Effects on NMR Spectra
19.3: NMR Spectrometers
magnetogyric ratio
19.5: Carbon-13 NMR
magnification
21.3: Scanning Electron Microscopy
mass
21: Surface Characterization by Spectroscopy and Microscopy
mass analyzers
20.3: Mass Spectrometers
mass spectrometer
11: Atomic Mass Spectrometry
mass spectrometers
20: Molecular Mass Spectrometry
mass spectrometry
1.2: Types of Instrumental Methods
11: Atomic Mass Spectrometry
11.1: General Features of Atomic Mass Spectrometry
20: Molecular Mass Spectrometry
20.3: Mass Spectrometers
20.4: Applications of Molecular Mass Spectrometry
21.1: Introduction to the Study of Surfaces
35.10: Acronyms and Abbreviations
mass spectrum
20.1: Molecular Mass Spectra
massspectrometry
27.2: Instruments for Gas Chromatography
materials analysis
12.4: Other X-Ray Methods
mathematical operations
3.4: Mathematical Operations Using Operational Amplifiers
matrix effect
11.3: Inductively Coupled Plasma Mass Spectrometer
matrix interference
9.4: Atomic Absorption Techniques
MatrixEffects
12.3: Atomic X-Ray Fluorescence Methods
mean
35.2: Single-Sided Normal Distribution
measurement
3: Operational Amplifiers
5: Signals and Noise
measurements
13: Introduction to Ultraviolet/Visible Absorption Spectrometry
25.1: Potential Excitation Signals and Currents in Voltammetry
mechanical shaking
34.2: Measuring Particle Size Using Sieves
MEKC
30.3: Applications of Capillary Electrophoresis
membrane potential
23.3: Membrane Ion-Selective Electrodes
mercury film electrode
25.6: Stripping Methods
metal ion deposition
25.6: Stripping Methods
metal ions
15.3: Applications and Photoluminescence methods
metallic electrodes
23.2: Metallic Indicator Electrodes
metals
10.2: Emission Spectroscopy Based on Arc and Spark Sources
18.4: Other Types of Raman Spectroscopy
35.9: Recommended Primary Standards
method
34.1: Overview
methods
33: Automated Methods of Analysis
micellar electrokinetic capillary chromatography
30.3: Applications of Capillary Electrophoresis
microscopy
21: Surface Characterization by Spectroscopy and Microscopy
mineral calcite
12.4: Other X-Ray Methods
minerals
18.3: Applications of Raman Spectroscopy
mobile phase
26: Introduction to Chromatographic Separations
26.1: A General Description of Chromatography
26.5: Summary of Important Relationships for Chromatography
26.6: Applications of Chromatography
27: Gas Chromatography
28: High-Performance Liquid Chromatography
28.5: Adsorption Chromatography
29.1: Properties of Supercritical Fluids
29.2: Supercritical Fluid Chromatography
mobile_phase
26.4: Optimization and Column Performance
mobilephase
28.3: Instruments for Liquid Chromatography
modulation
5.3: Signal-to-Noise Enhancement
molar absorptivity
14: Applications of Ultraviolet/Visible Molecular Absorption Spectrometry
14.1: What is Molar Absorptivity?
molecular analysis
13.4: Instrumentation
15: Molecular Luminescence
molecular fluorescence
15.3: Applications and Photoluminescence methods
molecular ion
20.1: Molecular Mass Spectra
molecular mass spectra
20: Molecular Mass Spectrometry
molecular orbitals
14.2: Absorbing Species
Molecular Structure
19.5: Carbon-13 NMR
molecular vibrations
16.1: Theory of Infrared Absorption Spectrometry
molecular weight
20.4: Applications of Molecular Mass Spectrometry
28.7: Size-Exclusion Chromatography
monochromator
7.3: Wavelength Selectors
9.2: Atomic Absorption Instrumentation
multielemental analysis
10.1: Emission Spectroscopy Based on Flame and Plasma Sources
multiple standard additions
1.5: Calibration of Instrumental Methods
multiplication
3.4: Mathematical Operations Using Operational Amplifiers

## N

NAA
32.3: Neutron Activation Methods
nanoparticles
34: Particle Size Determination
34.1: Overview
nanotechnology
21.4: Scanning Probe Microscopes
nanowires
21.3: Scanning Electron Microscopy
natural pigments
18.3: Applications of Raman Spectroscopy
nebulizer
9.1: Sample Atomization Techniques
negative feedback
3.2: Operational Amplifier Circuits
Nernst
23: Potentiometry
Nernst equation
24.2: Controlled-Potential Coulometry
Nernst_equation
25.1: Potential Excitation Signals and Currents in Voltammetry

Nessler's method
1.3: Instruments For Analysis
neutron activation analysis
32.3: Neutron Activation Methods
NH3
14.5: Photometric Titrations
nitrophenols
19.5: Carbon-13 NMR
NMR
19: Nuclear Magnetic Resonance Spectroscopy
19.2: Environmental Effects on NMR Spectra
19.3: NMR Spectrometers
NMR_spectra
19: Nuclear Magnetic Resonance Spectroscopy
NMR_spectrometers
19: Nuclear Magnetic Resonance Spectroscopy
NMRpeak
19.4: Applications of Proton NMR
noise
5: Signals and Noise
5.1: The Signal-to-Noise Ratio
noise reduction
4.3: Cleaning Up Signals and Counting Events
nonmetals
10.2: Emission Spectroscopy Based on Arc and Spark Sources
nonpolar solvent
28.5: Adsorption Chromatography
nonpolar stationary phase
27.3: Gas Chromatographic Columns and Stationary Phases
normal distribution
35.2: Single-Sided Normal Distribution
nuclear magnetic resonance
19.2: Environmental Effects on NMR Spectra
nuclear magnetic resonance spectroscopy
19.1: Theory of Nuclear Magnetic Resonance
nuclear overhauser enhancement
19.5: Carbon-13 NMR
nuclear_magnetic_resonance
19: Nuclear Magnetic Resonance Spectroscopy
null hypothesis
35.3: Critical Values for t-Test
nullhypothesis
35.4: Critical Values for F-Test

O

OER
InfoPage
ohms law
2.1: Basic Terminology and Laws of Electricity
Ohmslaw
2.2: Direct Current (DC) Circuits
onetailedtest
35.4: Critical Values for F-Test
online learning
InfoPage
opamp
3: Operational Amplifiers
operational amplifier
3.1: Operational Amplifiers
3.2: Operational Amplifier Circuits
3.4: Mathematical Operations Using Operational Amplifiers
4.3: Cleaning Up Signals and Counting Events
operational amplifiers
3.3: Amplification and Measurement of Signals
operationalamplifiers
3: Operational Amplifiers
optical
8: An Introduction to Optical Atomic Spectroscopy
optical bench
18.2: Instrumentation
optical benches
9: Atomic Absorption Spectrometry
10.2: Emission Spectroscopy Based on Arc and Spark Sources
optical filter
7.3: Wavelength Selectors
optical instruments
7: Components of Optical Instruments
optical measurement
1.3: Instruments For Analysis
optical methods
15.5: Evaluation of Molecular Luminescence
optical microscope
34.4: Measuring Particle Size Using Image Analysis
optical path
13: Introduction to Ultraviolet/Visible Absorption Spectrometry
optical platform
34.4: Measuring Particle Size Using Image Analysis
optical spectroscopy
12: Atomic X-Ray Spectrometry
opticalbenches
9.3: Interferences in Absorption Spectroscopy
opticalmicroscopy
21.3: Scanning Electron Microscopy
OpticalSpectroscopy
12.2: Instrument Components
optimization
5: Signals and Noise
26.4: Optimization and Column Performance
optrodes
7.6: Fiber Optics
organic compounds
15.3: Applications and Photoluminescence methods
organic molecules
17: Applications of Infrared Spectrometry
organicchemistry
19.4: Applications of Proton NMR
oscillation
6.2: Wave Properties of Electromagnetic Radiation
16: An Introduction to Infrared Spectrometry
outlier detection
35.6: Critical Values for Grubb's Test
outlierdetection
35.5: Critical Values for Dixon's Q-Test
oxidation
22.1: Electrochemical Cells
35.8: Standard Reduction Potentials & Polarographic Half-wave Potentials

P

packed column
34: Particle Size Determination
packed columns
27.3: Gas Chromatographic Columns and Stationary Phases
parallel
2.2: Direct Current (DC) Circuits
particle
34.1: Overview
particle properties
6: An Introduction to Spectrophotometric Methods
particle size
34: Particle Size Determination
34.4: Measuring Particle Size Using Image Analysis
particle size separation
34.2: Measuring Particle Size Using Sieves
particles
32: Radiochemical Methods
particulates
34.2: Measuring Particle Size Using Sieves
partition chromatography
28: High-Performance Liquid Chromatography
28.4: Partition Chromatography
peak area
26.6: Applications of Chromatography
27.4: Applications of Gas Chromatography
peak splitting
19.2: Environmental Effects on NMR Spectra
peak width
26.5: Summary of Important Relationships for Chromatography
petrochemical analysis
27.4: Applications of Gas Chromatography
pH
23: Potentiometry
23.3: Membrane Ion-Selective Electrodes
pH measurement
3.3: Amplification and Measurement of Signals
22: An Introduction to Electroanalytical Chemistry
pharmaceutical laboratories
27: Gas Chromatography
pharmaceuticals
25.7: Applications of Voltammetry
phase diagram
29.1: Properties of Supercritical Fluids
phosphorescence
15: Molecular Luminescence
15.1: Theory of Fluorescence and Phosphorescence
15.3: Applications and Photoluminescence methods
phosphorescence quantum yield
15.1: Theory of Fluorescence and Phosphorescence
photodiode
4.3: Cleaning Up Signals and Counting Events
photoelectric effect
6.3: Quantum Mechanical Properties of Electromagnetic Radiation
photoelectron
12.1: Fundamental Principles
21: Surface Characterization by Spectroscopy and Microscopy

photoluminescence
1.2: Types of Instrumental Methods
15.5: Evaluation of Molecular Luminescence
photometer
13.4: Instrumentation
photometry
15: Molecular Luminescence
photomultiplier
7.5: Radiation Transducers
photon absorption
18: Raman Spectroscopy
photon emission
18: Raman Spectroscopy
photon's
16: An Introduction to Infrared Spectrometry
PhotonCounting
12.2: Instrument Components
photons
6: An Introduction to Spectrophotometric Methods
6.1: General Properties of Electromagnetic Radiation
6.5: Quantitative Considerations
12.1: Fundamental Principles
21.3: Scanning Electron Microscopy
photovoltaic cell
7.5: Radiation Transducers
physical properties
31: Thermal Methods
piezoelectric
21.4: Scanning Probe Microscopes
plasma
10.2: Emission Spectroscopy Based on Arc and Spark Sources
plasmas
8.2: Atomization Methods
plastic
7.4: Sample Containers
polar stationary phase
27.3: Gas Chromatographic Columns and Stationary Phases
polarization
6.2: Wave Properties of Electromagnetic Radiation
polarography
25: Voltammetry
25.1: Potential Excitation Signals and Currents in Voltammetry
25.5: Polarography
polymer resins
28.7: Size-Exclusion Chromatography
polymerresin
28.6: Ion-Exchange Chromatography
polymers
29.2: Supercritical Fluid Chromatography
population mean
35.2: Single-Sided Normal Distribution
populationstandarddeviation
35.4: Critical Values for F-Test
porous silica
34: Particle Size Determination
potential
25: Voltammetry
25.1: Potential Excitation Signals and Currents in Voltammetry
25.2: Voltammetric Instrumentation
potential control
22: An Introduction to Electroanalytical Chemistry
potentiometer
22.1: Electrochemical Cells
23.5: Instruments for Measuring Cell Potentials
potentiometry
22.6: Types of Electroanalytical Methods
23: Potentiometry
23.2: Metallic Indicator Electrodes
23.3: Membrane Ion-Selective Electrodes
potentiostat
24.2: Controlled-Potential Coulometry
25.2: Voltammetric Instrumentation
power law
2.1: Basic Terminology and Laws of Electricity
precision
1.4: Selecting an Analytical Method
9.4: Atomic Absorption Techniques
13: Introduction to Ultraviolet/Visible Absorption Spectrometry
13.3: Effect of Noise on Transmittance and Absorbance Measurements
15.5: Evaluation of Molecular Luminescence
probability
35.2: Single-Sided Normal Distribution
35.6: Critical Values for Grubb's Test
probe
21: Surface Characterization by Spectroscopy and Microscopy
professional development
About the Author
propagation
6.2: Wave Properties of Electromagnetic Radiation
propanal
19.4: Applications of Proton NMR
propane
19.2: Environmental Effects on NMR Spectra
proton decoupling
19.5: Carbon-13 NMR
protonNMR
19.4: Applications of Proton NMR
pulse polarography
25.5: Polarography
pumps
28.3: Instruments for Liquid Chromatography
pure compounds
20.4: Applications of Molecular Mass Spectrometry
purity
35.9: Recommended Primary Standards

## Q

Qexp
35.5: Critical Values for Dixon's Q-Test
quadrupole
20.3: Mass Spectrometers
qualitative
14.3: Qualitative and Characterization Applications
20.4: Applications of Molecular Mass Spectrometry
qualitative analysis
1: Introduction
12: Atomic X-Ray Spectrometry
14: Applications of Ultraviolet/Visible Molecular Absorption Spectrometry
15: Molecular Luminescence
16.1: Theory of Infrared Absorption Spectrometry
17: Applications of Infrared Spectrometry
17.1: Mid-Infrared Absorption Spectometry
18: Raman Spectroscopy
20: Molecular Mass Spectrometry
26.6: Applications of Chromatography
27: Gas Chromatography
qualitative applications
18.3: Applications of Raman Spectroscopy
qualitative data
35.1: Evaluation of Analytical Data
qualitative identification
10.2: Emission Spectroscopy Based on Arc and Spark Sources
12.4: Other X-Ray Methods
qualitativeAnalysis
12.3: Atomic X-Ray Fluorescence Methods
19.4: Applications of Proton NMR
quantitative
6.5: Quantitative Considerations
15.3: Applications and Photoluminescence methods
quantitative analysis
1: Introduction
10.1: Emission Spectroscopy Based on Flame and Plasma Sources
12: Atomic X-Ray Spectrometry
12.4: Other X-Ray Methods
14: Applications of Ultraviolet/Visible Molecular Absorption Spectrometry
14.4: Quantitative Applications
15: Molecular Luminescence
16.1: Theory of Infrared Absorption Spectrometry
17: Applications of Infrared Spectrometry
17.1: Mid-Infrared Absorption Spectometry
18: Raman Spectroscopy
19.3: NMR Spectrometers
20: Molecular Mass Spectrometry
25: Voltammetry
26: Introduction to Chromatographic Separations
26.6: Applications of Chromatography
27: Gas Chromatography
27.4: Applications of Gas Chromatography
quantitative applications
18.3: Applications of Raman Spectroscopy
quantitative data
35.1: Evaluation of Analytical Data
quantitative potentiometry
23.6: Quantitative Potentiometry
quantitative reduction
24.2: Controlled-Potential Coulometry
quantitativeAnalysis
12.3: Atomic X-Ray Fluorescence Methods
19.4: Applications of Proton NMR
quantum mechanics
6.1: General Properties of Electromagnetic Radiation
quantum yield
15.5: Evaluation of Molecular Luminescence
quantum_mechanics
19: Nuclear Magnetic Resonance Spectroscopy
quartz
7.4: Sample Containers

## R

radiation
- 6.2: Wave Properties of Electromagnetic Radiation
- 7.4: Sample Containers
- 8: An Introduction to Optical Atomic Spectroscopy
- 9: Atomic Absorption Spectrometry
- 12.2: Instrument Components

radiation detection
- 13: Introduction to Ultraviolet/Visible Absorption Spectrometry

radiation transducers
- 7: Components of Optical Instruments

radical cation
- 20.1: Molecular Mass Spectra

Radioactive
- 32: Radiochemical Methods

radioactive decay
- 32.1: Radioactive Isotopes

radioactive isotopes
- 32.1: Radioactive Isotopes

radioactivity
- 12.1: Fundamental Principles

radiochemical
- 32: Radiochemical Methods

Raman spectroscopy
- 6.5: Quantitative Considerations
- 18: Raman Spectroscopy
- 18.1: Theory of Raman Spectroscopy
- 18.2: Instrumentation
- 18.3: Applications of Raman Spectroscopy

Raman spectrum
- 18: Raman Spectroscopy

RamanSpectroscopy
- 18.4: Other Types of Raman Spectroscopy

Rayleigh scattering
- 18: Raman Spectroscopy
- 34.5: Measuring Particle Size Using Light Scattering

redox
- 23: Potentiometry
- 25.7: Applications of Voltammetry

redox reaction
- 23.2: Metallic Indicator Electrodes

redox reactions
- 22.1: Electrochemical Cells

redox_reaction
- 25.1: Potential Excitation Signals and Currents in Voltammetry

reduction
- 22.1: Electrochemical Cells

reduction reactions
- 35.8: Standard Reduction Potentials & Polarographic Half-wave Potentials

reference
- 23: Potentiometry

reference electrodes
- 23.1: Reference Electrodes

reference spectra
- 18.3: Applications of Raman Spectroscopy

reflection spectrometry
- 17: Applications of Infrared Spectrometry

refraction
- 6: An Introduction to Spectrophotometric Methods
- 6.1: General Properties of Electromagnetic Radiation

regression analysis
- 35.1: Evaluation of Analytical Data

reproducibility
- 33.1: Overview of Automated Methods of Analysis

research
- 23.3: Membrane Ion-Selective Electrodes
- 35.5: Critical Values for Dixon's Q-Test

resistance
- 2.1: Basic Terminology and Laws of Electricity

resistive heating
- 8.2: Atomization Methods
- 8.3: Sample Introduction Methods

resistor
- 2.3: Alternating Current Circuits

resistors
- 2: Electrical Components and Circuits
- 2.2: Direct Current (DC) Circuits

resolution
- 20.3: Mass Spectrometers
- 21: Surface Characterization by Spectroscopy and Microscopy
- 21.3: Scanning Electron Microscopy
- 26.4: Optimization and Column Performance
- 26.5: Summary of Important Relationships for Chromatography
- 29.2: Supercritical Fluid Chromatography

ResonanceRamanSpectroscopy
- 18.4: Other Types of Raman Spectroscopy

retention factor
- 26.2: Migration Rates of Solutes

retention time
- 26.2: Migration Rates of Solutes
- 26.5: Summary of Important Relationships for Chromatography
- 26.6: Applications of Chromatography
- 27.1: Principles of Gas Chromatography

retention volume
- 27.1: Principles of Gas Chromatography
- 28.7: Size-Exclusion Chromatography

retention_time
- 26.4: Optimization and Column Performance

RF_radiation
- 19: Nuclear Magnetic Resonance Spectroscopy

robustness
- 1.4: Selecting an Analytical Method

Rorabacher
- 35.5: Critical Values for Dixon's Q-Test

## S

salt bridge
- 22.1: Electrochemical Cells

sample
- 26: Introduction to Chromatographic Separations

sample analysis
- 11: Atomic Mass Spectrometry

sample handling
- 17.1: Mid-Infrared Absorption Spectometry

sample holder
- 7.1: General Design of Optical Instruments

sample inlet systems
- 20: Molecular Mass Spectrometry

sample introduction
- 9.1: Sample Atomization Techniques

sample preparation
- 9.4: Atomic Absorption Techniques
- 33.1: Overview of Automated Methods of Analysis

sample probe
- 19.3: NMR Spectrometers

sample size
- 35.6: Critical Values for Grubb's Test

sample throughput
- 33.3: Other Automated Methods of Analysis

sampleintroduction
- 27.2: Instruments for Gas Chromatography

sampling
- 4: Analog and Digital Data

saturated calomel reference electrode
- 23.2: Metallic Indicator Electrodes

scanning
- 21: Surface Characterization by Spectroscopy and Microscopy

scanning tunneling microscopy
- 21.1: Introduction to the Study of Surfaces

scanningelectronmicroscopy
- 21.3: Scanning Electron Microscopy

scattered
- 6.5: Quantitative Considerations

scattering
- 18.4: Other Types of Raman Spectroscopy

scattering intensity
- 18.2: Instrumentation

scintillation counters
- 32.2: Instrumentation

ScintillationCounter
- 12.2: Instrument Components

seawater analysis
- 8.2: Atomization Methods
- 8.3: Sample Introduction Methods

sedimentation
- 34.1: Overview
- 34.3: Measuring Particle Size by Sedimentation

selectivity
- 1.4: Selecting an Analytical Method
- 26.4: Optimization and Column Performance
- 27: Gas Chromatography

selectivity coefficient
- 23.3: Membrane Ion-Selective Electrodes

selectivity factor
- 26.2: Migration Rates of Solutes
- 26.5: Summary of Important Relationships for Chromatography

semiconductor
- 7.5: Radiation Transducers

semiconductor detectors
- 32.2: Instrumentation

semiconductors
- 2: Electrical Components and Circuits

SemiconductorTransducers
- 12.2: Instrument Components

Sensitivity
- 1.4: Selecting an Analytical Method
- 1.5: Calibration of Instrumental Methods
- 7.5: Radiation Transducers
- 9.1: Sample Atomization Techniques
- 9.2: Atomic Absorption Instrumentation
- 15.5: Evaluation of Molecular Luminescence
- 18.4: Other Types of Raman Spectroscopy

sensor
1.3: Instruments For Analysis
separation
26.1: A General Description of Chromatography
26.4: Optimization and Column Performance
27: Gas Chromatography
28: High-Performance Liquid Chromatography
28.6: Ion-Exchange Chromatography
separation efficiency
27.3: Gas Chromatographic Columns and Stationary Phases
separation technique
26.6: Applications of Chromatography
separation techniques
28.7: Size-Exclusion Chromatography
series
2.2: Direct Current (DC) Circuits
SERS
18.4: Other Types of Raman Spectroscopy
shaded area
35.2: Single-Sided Normal Distribution
shielding
19.2: Environmental Effects on NMR Spectra
shot noise
5.2: Sources of Instrumental Noise
sieves
34: Particle Size Determination
34.2: Measuring Particle Size Using Sieves
signal
5: Signals and Noise
signal averaging
13.4: Instrumentation
signal intensity
19.5: Carbon-13 NMR
signal processing
1.3: Instruments For Analysis
3.4: Mathematical Operations Using Operational Amplifiers
4.3: Cleaning Up Signals and Counting Events
19.3: NMR Spectrometers
signal processor
3.3: Amplification and Measurement of Signals
7.1: General Design of Optical Instruments
signal transducer
12: Atomic X-Ray Spectrometry
signals
3: Operational Amplifiers
4: Analog and Digital Data
significance testing
35.1: Evaluation of Analytical Data
silica
28.5: Adsorption Chromatography
silica particles
28.7: Size-Exclusion Chromatography
silicon photodiode
7.5: Radiation Transducers
size
34.1: Overview
size ranges
34.2: Measuring Particle Size Using Sieves
slit width
7.3: Wavelength Selectors
sodium concentration
8.2: Atomization Methods
sodium ions
8.3: Sample Introduction Methods
software
4: Analog and Digital Data
5: Signals and Noise
software analysis
34.4: Measuring Particle Size Using Image Analysis
solid matrix
34: Particle Size Determination
34.2: Measuring Particle Size Using Sieves
solid samples
8.3: Sample Introduction Methods
solidphasemicroextraction
27.2: Instruments for Gas Chromatography
solubility
35.7: Activity Coefficients
35.9: Recommended Primary Standards
solute
26.1: A General Description of Chromatography
26.4: Optimization and Column Performance
26.6: Applications of Chromatography
Solution
8.3: Sample Introduction Methods
solutions
14.4: Quantitative Applications
solvents
29.1: Properties of Supercritical Fluids
spectra
6: An Introduction to Spectrophotometric Methods
8: An Introduction to Optical Atomic Spectroscopy
spectral
14.3: Qualitative and Characterization Applications
spectral searching
17.1: Mid-Infrared Absorption Spectometry
spectrometry
17.1: Mid-Infrared Absorption Spectometry
spectrophotometer
9.1: Sample Atomization Techniques
13.4: Instrumentation
Spectrophotometers
9.2: Atomic Absorption Instrumentation
Spectrophotometry
14.5: Photometric Titrations
33.3: Other Automated Methods of Analysis
spectroscopic
6.5: Quantitative Considerations
spectroscopy
1.2: Types of Instrumental Methods
7: Components of Optical Instruments
7.1: General Design of Optical Instruments
7.5: Radiation Transducers
9: Atomic Absorption Spectrometry
10.1: Emission Spectroscopy Based on Flame and Plasma Sources
13.3: Effect of Noise on Transmittance and Absorbance Measurements
13.4: Instrumentation
14.3: Qualitative and Characterization Applications
14.4: Quantitative Applications
15.5: Evaluation of Molecular Luminescence
16: An Introduction to Infrared Spectrometry
19: Nuclear Magnetic Resonance Spectroscopy
19.2: Environmental Effects on NMR Spectra
19.3: NMR Spectrometers
19.5: Carbon-13 NMR
21: Surface Characterization by Spectroscopy and Microscopy
26: Introduction to Chromatographic Separations
splitinjector
27.2: Instruments for Gas Chromatography
splitlessinjector
27.2: Instruments for Gas Chromatography
stability
35.7: Activity Coefficients
standard additions
9.4: Atomic Absorption Techniques
standard deviation
35.2: Single-Sided Normal Distribution
standard hydrogen electrode
22.3: Electrode Potentials
standard reduction potentials
35.8: Standard Reduction Potentials & Polarographic Half-wave Potentials
standardreductionpotentials
35: Appendicies
static image analysis
34.4: Measuring Particle Size Using Image Analysis
static techniques
22.6: Types of Electroanalytical Methods
stationary phase
26: Introduction to Chromatographic Separations
26.1: A General Description of Chromatography
26.5: Summary of Important Relationships for Chromatography
26.6: Applications of Chromatography
27.3: Gas Chromatographic Columns and Stationary Phases
28: High-Performance Liquid Chromatography
28.5: Adsorption Chromatography
stationary phases
28.7: Size-Exclusion Chromatography
stationaryphase
28.3: Instruments for Liquid Chromatography
28.6: Ion-Exchange Chromatography
statistical analysis
35.6: Critical Values for Grubb's Test
statistical methods
35.3: Critical Values for t-Test
statisticalanalysis
35.5: Critical Values for Dixon's Q-Test

statistics
35: Appendicies
35.1: Evaluation of Analytical Data
35.2: Single-Sided Normal Distribution
35.4: Critical Values for F-Test
35.5: Critical Values for Dixon's Q-Test
STM
21.4: Scanning Probe Microscopes
stoichiometry
14.3: Qualitative and Characterization Applications
stripping methods
25: Voltammetry
strongacid
28.6: Ion-Exchange Chromatography
subatomic particles
11.1: General Features of Atomic Mass Spectrometry
supercritical
29.1: Properties of Supercritical Fluids
supercritical fluid chromatography
29: Supercritical Fluid Chromatography
29.2: Supercritical Fluid Chromatography
surface analysis
21.1: Introduction to the Study of Surfaces
surface properties
21.1: Introduction to the Study of Surfaces
SurfaceEnhancedRamanSpectroscopy
18.4: Other Types of Raman Spectroscopy
surfaceimaging
21.4: Scanning Probe Microscopes
Surfaces
21: Surface Characterization by Spectroscopy and Microscopy
synthetic organic pigments
18.3: Applications of Raman Spectroscopy

T

tandem mass spectrometry
20.4: Applications of Molecular Mass Spectrometry
techniques
7.1: General Design of Optical Instruments
temperature
31: Thermal Methods
test_values
35.4: Critical Values for F-Test
textbooks
InfoPage
theoretical plates
26.5: Summary of Important Relationships for Chromatography
27.3: Gas Chromatographic Columns and Stationary Phases
theoretical_plates
26.4: Optimization and Column Performance
thermal energy
8.2: Atomization Methods
thermal excitation
10.1: Emission Spectroscopy Based on Flame and Plasma Sources
thermal methods
31: Thermal Methods
thermal noise
5.2: Sources of Instrumental Noise
thermodynamics
35.7: Activity Coefficients
thermogravimetry
31: Thermal Methods
31.1: Thermogravimetry
thin films
33: Automated Methods of Analysis
titration
14.5: Photometric Titrations
33.1: Overview of Automated Methods of Analysis
titrators
33: Automated Methods of Analysis
TOCSY
19.6: Two-Dimensional Fourier Transform NMR
trace analysis
15.5: Evaluation of Molecular Luminescence
trace metals
10.1: Emission Spectroscopy Based on Flame and Plasma Sources
25.7: Applications of Voltammetry
transducer
1.3: Instruments For Analysis
3: Operational Amplifiers
3.3: Amplification and Measurement of Signals
7.5: Radiation Transducers
transmission
13.1: Transmittance and Absorbance
transmittance
13: Introduction to Ultraviolet/Visible Absorption Spectrometry
13.3: Effect of Noise on Transmittance and Absorbance Measurements
16.1: Theory of Infrared Absorption Spectrometry
ttest
35: Appendicies
TunableLaser
18.4: Other Types of Raman Spectroscopy
tunnelingcurrent
21.4: Scanning Probe Microscopes
twotailedtest
35.4: Critical Values for F-Test

U

ultraviolet
8: An Introduction to Optical Atomic Spectroscopy
14.3: Qualitative and Characterization Applications
uncertainty
5: Signals and Noise
13.3: Effect of Noise on Transmittance and Absorbance Measurements
UV
14.2: Absorbing Species
uv vis spectroscopy
18.2: Instrumentation
UV/Vis
7.4: Sample Containers
13.4: Instrumentation
UV/Vis analysis
26: Introduction to Chromatographic Separations
UV/Vis radiation
13: Introduction to Ultraviolet/Visible Absorption Spectrometry
UV/Vis Spectroscopy
14: Applications of Ultraviolet/Visible Molecular Absorption Spectrometry
UVVis
14.4: Quantitative Applications

V

vacuum
20.3: Mass Spectrometers
valence electrons
14.2: Absorbing Species
van Deemter equation
27.1: Principles of Gas Chromatography
28.2: Column Efficiency in Liquid Chromatography
velocity
6.2: Wave Properties of Electromagnetic Radiation
vibrational
16: An Introduction to Infrared Spectrometry
vibrational energy states
16.1: Theory of Infrared Absorption Spectrometry
viscosity
29.1: Properties of Supercritical Fluids
visible
8: An Introduction to Optical Atomic Spectroscopy
14.3: Qualitative and Characterization Applications
visible radiation
14.2: Absorbing Species
visible spectrum
6.1: General Properties of Electromagnetic Radiation
volatilecompounds
27.2: Instruments for Gas Chromatography
voltage
2.1: Basic Terminology and Laws of Electricity
2.2: Direct Current (DC) Circuits
2.3: Alternating Current Circuits
3: Operational Amplifiers
voltage comparison
3.4: Mathematical Operations Using Operational Amplifiers
voltage follower
3.2: Operational Amplifier Circuits
voltage measurements
3.3: Amplification and Measurement of Signals
voltammetric techniques
25.2: Voltammetric Instrumentation
25.6: Stripping Methods
voltammetry
22.6: Types of Electroanalytical Methods
25: Voltammetry
25.1: Potential Excitation Signals and Currents in Voltammetry
25.2: Voltammetric Instrumentation
25.7: Applications of Voltammetry
voltammogram
25: Voltammetry

W

wave
6.2: Wave Properties of Electromagnetic Radiation
wave properties
6: An Introduction to Spectrophotometric Methods
waveform generator
25.2: Voltammetric Instrumentation

wavelength isolation
7.1: General Design of Optical Instruments
wavelength selectors
7: Components of Optical Instruments
WavelengthDispersiveInstruments
12.3: Atomic X-Ray Fluorescence Methods
wavelengths
12.1: Fundamental Principles
waves
6.1: General Properties of Electromagnetic Radiation
weakacid
28.6: Ion-Exchange Chromatography
working electrode
24.2: Controlled-Potential Coulometry
X
XPS
21.2: Spectroscopic Surface Methods
XrayFluorescence
12.3: Atomic X-Ray Fluorescence Methods
XRaySpectrometry
12.2: Instrument Components
XRayTube
12.2: Instrument Components
Z
Zeemaneffect
9.3: Interferences in Absorption Spectroscopy

# Detailed Licensing

## Overview

**Title:** Instrumental Analysis (LibreTexts)

**Webpages:** 200

**Applicable Restrictions:** Noncommercial

**All licenses found:**

- CC BY-NC-SA 4.0: 98% (196 pages)
- Undeclared: 2% (4 pages)

## By Page


- Instrumental Analysis (LibreTexts) - *CC BY-NC-SA 4.0*
  - Front Matter - *CC BY-NC-SA 4.0*
    - TitlePage - *CC BY-NC-SA 4.0*
    - InfoPage - *CC BY-NC-SA 4.0*
    - Table of Contents - *Undeclared*
    - Licensing - *Undeclared*
    - About the Author - *CC BY-NC-SA 4.0*
  - 1: Introduction - *CC BY-NC-SA 4.0*
    - 1.1: Classification of Analytical Methods - *CC BY-NC-SA 4.0*
    - 1.2: Types of Instrumental Methods - *CC BY-NC-SA 4.0*
    - 1.3: Instruments For Analysis - *CC BY-NC-SA 4.0*
    - 1.4: Selecting an Analytical Method - *CC BY-NC-SA 4.0*
    - 1.5: Calibration of Instrumental Methods - *CC BY-NC-SA 4.0*
  - 2: Electrical Components and Circuits - *CC BY-NC-SA 4.0*
    - 2.1: Basic Terminology and Laws of Electricity - *CC BY-NC-SA 4.0*
    - 2.2: Direct Current (DC) Circuits - *CC BY-NC-SA 4.0*
    - 2.3: Alternating Current Circuits - *CC BY-NC-SA 4.0*
    - 2.4: Semiconductors - *CC BY-NC-SA 4.0*
  - 3: Operational Amplifiers - *CC BY-NC-SA 4.0*
    - 3.1: Operational Amplifiers - *CC BY-NC-SA 4.0*
    - 3.2: Operational Amplifier Circuits - *CC BY-NC-SA 4.0*
    - 3.3: Amplification and Measurement of Signals - *CC BY-NC-SA 4.0*
    - 3.4: Mathematical Operations Using Operational Amplifiers - *CC BY-NC-SA 4.0*
  - 4: Analog and Digital Data - *CC BY-NC-SA 4.0*
    - 4.1: Analog and Digital Data - *CC BY-NC-SA 4.0*
    - 4.2: Working With Binary Numbers - *CC BY-NC-SA 4.0*
    - 4.3: Cleaning Up Signals and Counting Events - *CC BY-NC-SA 4.0*
  - 5: Signals and Noise - *CC BY-NC-SA 4.0*
    - 5.1: The Signal-to-Noise Ratio - *CC BY-NC-SA 4.0*
    - 5.2: Sources of Instrumental Noise - *CC BY-NC-SA 4.0*
    - 5.3: Signal-to-Noise Enhancement - *CC BY-NC-SA 4.0*
  - 6: An Introduction to Spectrophotometric Methods - *CC BY-NC-SA 4.0*
    - 6.1: General Properties of Electromagnetic Radiation - *CC BY-NC-SA 4.0*
    - 6.2: Wave Properties of Electromagnetic Radiation - *CC BY-NC-SA 4.0*
    - 6.3: Quantum Mechanical Properties of Electromagnetic Radiation - *CC BY-NC-SA 4.0*
    - 6.4: Emission and Absorbance Spectra - *CC BY-NC-SA 4.0*
    - 6.5: Quantitative Considerations - *CC BY-NC-SA 4.0*
  - 7: Components of Optical Instruments - *CC BY-NC-SA 4.0*
    - 7.1: General Design of Optical Instruments - *CC BY-NC-SA 4.0*
    - 7.2: Sources of Radiation - *CC BY-NC-SA 4.0*
    - 7.3: Wavelength Selectors - *CC BY-NC-SA 4.0*
    - 7.4: Sample Containers - *CC BY-NC-SA 4.0*
    - 7.5: Radiation Transducers - *CC BY-NC-SA 4.0*
    - 7.6: Fiber Optics - *CC BY-NC-SA 4.0*
    - 7.7: Fourier Transform Optical Spectroscopy - *CC BY-NC-SA 4.0*
  - 8: An Introduction to Optical Atomic Spectroscopy - *CC BY-NC-SA 4.0*
    - 8.1: Optical Atomic Spectra - *CC BY-NC-SA 4.0*

- 8.2: Atomization Methods - *CC BY-NC-SA 4.0*
- 8.3: Sample Introduction Methods - *CC BY-NC-SA 4.0*

9: Atomic Absorption Spectrometry - *CC BY-NC-SA 4.0*
- 9.1: Sample Atomization Techniques - *CC BY-NC-SA 4.0*
- 9.2: Atomic Absorption Instrumentation - *CC BY-NC-SA 4.0*
- 9.3: Interferences in Absorption Spectroscopy - *CC BY-NC-SA 4.0*
- 9.4: Atomic Absorption Techniques - *CC BY-NC-SA 4.0*

10: Atomic Emission Spectrometry - *CC BY-NC-SA 4.0*
- 10.1: Emission Spectroscopy Based on Flame and Plasma Sources - *CC BY-NC-SA 4.0*
- 10.2: Emission Spectroscopy Based on Arc and Spark Sources - *CC BY-NC-SA 4.0*

11: Atomic Mass Spectrometry - *CC BY-NC-SA 4.0*
- 11.1: General Features of Atomic Mass Spectrometry - *CC BY-NC-SA 4.0*
- 11.2: Mass Spectrometers - *CC BY-NC-SA 4.0*
- 11.3: Inductively Coupled Plasma Mass Spectrometer - *CC BY-NC-SA 4.0*
- 11.4: Other Forms of Atomic Mass Spectrometry - *CC BY-NC-SA 4.0*

12: Atomic X-Ray Spectrometry - *CC BY-NC-SA 4.0*
- 12.1: Fundamental Principles - *CC BY-NC-SA 4.0*
- 12.2: Instrument Components - *CC BY-NC-SA 4.0*
- 12.3: Atomic X-Ray Fluorescence Methods - *CC BY-NC-SA 4.0*
- 12.4: Other X-Ray Methods - *CC BY-NC-SA 4.0*

13: Introduction to Ultraviolet/Visible Absorption Spectrometry - *CC BY-NC-SA 4.0*
- 13.1: Transmittance and Absorbance - *CC BY-NC-SA 4.0*
- 13.2: Beer's Law - *CC BY-NC-SA 4.0*
- 13.3: Effect of Noise on Transmittance and Absorbance Measurements - *CC BY-NC-SA 4.0*
- 13.4: Instrumentation - *CC BY-NC-SA 4.0*

14: Applications of Ultraviolet/Visible Molecular Absorption Spectrometry - *CC BY-NC-SA 4.0*
- 14.1: What is Molar Absorptivity? - *CC BY-NC-SA 4.0*
- 14.2: Absorbing Species - *CC BY-NC-SA 4.0*
- 14.3: Qualitative and Characterization Applications - *CC BY-NC-SA 4.0*
- 14.4: Quantitative Applications - *CC BY-NC-SA 4.0*
- 14.5: Photometric Titrations - *CC BY-NC-SA 4.0*

15: Molecular Luminescence - *CC BY-NC-SA 4.0*
- 15.1: Theory of Fluorescence and Phosphorescence - *CC BY-NC-SA 4.0*
- 15.2: Instruments for Measuring Fluorescence and Phosphorescence - *CC BY-NC-SA 4.0*
- 15.3: Applications and Photoluminescence methods - *CC BY-NC-SA 4.0*
- 15.4: Chemiluminscence - *CC BY-NC-SA 4.0*
- 15.5: Evaluation of Molecular Luminescence - *CC BY-NC-SA 4.0*

16: An Introduction to Infrared Spectrometry - *CC BY-NC-SA 4.0*
- 16.1: Theory of Infrared Absorption Spectrometry - *CC BY-NC-SA 4.0*
- 16.2: Infrared Sources and Transducers - *CC BY-NC-SA 4.0*
- 16.3: Infrared Instruments - *CC BY-NC-SA 4.0*

17: Applications of Infrared Spectrometry - *CC BY-NC-SA 4.0*
- 17.1: Mid-Infrared Absorption Spectometry - *CC BY-NC-SA 4.0*
- 17.2: Mid-Infrared Reflection Spectrometry - *CC BY-NC-SA 4.0*
- 17.3: Near-Infrared and Far-Infrared Spectroscopy - *CC BY-NC-SA 4.0*

18: Raman Spectroscopy - *CC BY-NC-SA 4.0*
- 18.1: Theory of Raman Spectroscopy - *CC BY-NC-SA 4.0*
- 18.2: Instrumentation - *CC BY-NC-SA 4.0*
- 18.3: Applications of Raman Spectroscopy - *CC BY-NC-SA 4.0*
- 18.4: Other Types of Raman Spectroscopy - *CC BY-NC-SA 4.0*

19: Nuclear Magnetic Resonance Spectroscopy - *CC BY-NC-SA 4.0*
- 19.1: Theory of Nuclear Magnetic Resonance - *CC BY-NC-SA 4.0*
- 19.2: Environmental Effects on NMR Spectra - *CC BY-NC-SA 4.0*
- 19.3: NMR Spectrometers - *CC BY-NC-SA 4.0*
- 19.4: Applications of Proton NMR - *CC BY-NC-SA 4.0*
- 19.5: Carbon-13 NMR - *CC BY-NC-SA 4.0*
- 19.6: Two-Dimensional Fourier Transform NMR - *CC BY-NC-SA 4.0*

20: Molecular Mass Spectrometry - *CC BY-NC-SA 4.0*
- 20.1: Molecular Mass Spectra - *CC BY-NC-SA 4.0*
- 20.2: Ion Sources - *CC BY-NC-SA 4.0*

- 20.3: Mass Spectrometers - *CC BY-NC-SA 4.0*
- 20.4: Applications of Molecular Mass Spectrometry - *CC BY-NC-SA 4.0*

- 21: Surface Characterization by Spectroscopy and Microscopy - *CC BY-NC-SA 4.0*
  - 21.1: Introduction to the Study of Surfaces - *CC BY-NC-SA 4.0*
  - 21.2: Spectroscopic Surface Methods - *CC BY-NC-SA 4.0*
  - 21.3: Scanning Electron Microscopy - *CC BY-NC-SA 4.0*
  - 21.4: Scanning Probe Microscopes - *CC BY-NC-SA 4.0*
- 22: An Introduction to Electroanalytical Chemistry - *CC BY-NC-SA 4.0*
  - 22.1: Electrochemical Cells - *CC BY-NC-SA 4.0*
  - 22.2: Potentials in Electroanalytical Cells - *CC BY-NC-SA 4.0*
  - 22.3: Electrode Potentials - *CC BY-NC-SA 4.0*
  - 22.4: Calculation of Cell Potentials from Electrode Potentials - *CC BY-NC-SA 4.0*
  - 22.5: Currents in Electrochemical Cells - *CC BY-NC-SA 4.0*
  - 22.6: Types of Electroanalytical Methods - *CC BY-NC-SA 4.0*
- 23: Potentiometry - *CC BY-NC-SA 4.0*
  - 23.1: Reference Electrodes - *CC BY-NC-SA 4.0*
  - 23.2: Metallic Indicator Electrodes - *CC BY-NC-SA 4.0*
  - 23.3: Membrane Ion-Selective Electrodes - *CC BY-NC-SA 4.0*
  - 23.4: Molecular-Selective Electrode Systems - *CC BY-NC-SA 4.0*
  - 23.5: Instruments for Measuring Cell Potentials - *CC BY-NC-SA 4.0*
  - 23.6: Quantitative Potentiometry - *CC BY-NC-SA 4.0*
- 24: Coulometry - *CC BY-NC-SA 4.0*
  - 24.1: Introduction to Coulometry - *CC BY-NC-SA 4.0*
  - 24.2: Controlled-Potential Coulometry - *CC BY-NC-SA 4.0*
  - 24.3: Controlled-Current Coulometry - *CC BY-NC-SA 4.0*
- 25: Voltammetry - *CC BY-NC-SA 4.0*
  - 25.1: Potential Excitation Signals and Currents in Voltammetry - *CC BY-NC-SA 4.0*
  - 25.2: Voltammetric Instrumentation - *CC BY-NC-SA 4.0*
  - 25.3: Linear Sweep Voltammetry - *CC BY-NC-SA 4.0*
  - 25.4: Cyclic Voltammetry - *CC BY-NC-SA 4.0*
  - 25.5: Polarography - *CC BY-NC-SA 4.0*
  - 25.6: Stripping Methods - *CC BY-NC-SA 4.0*
  - 25.7: Applications of Voltammetry - *CC BY-NC-SA 4.0*
- 26: Introduction to Chromatographic Separations - *CC BY-NC-SA 4.0*
  - 26.1: A General Description of Chromatography - *CC BY-NC-SA 4.0*
  - 26.2: Migration Rates of Solutes - *CC BY-NC-SA 4.0*
  - 26.3: Zone Broadening and Column Efficiency - *CC BY-NC-SA 4.0*
  - 26.4: Optimization and Column Performance - *CC BY-NC-SA 4.0*
  - 26.5: Summary of Important Relationships for Chromatography - *CC BY-NC-SA 4.0*
  - 26.6: Applications of Chromatography - *CC BY-NC-SA 4.0*
- 27: Gas Chromatography - *CC BY-NC-SA 4.0*
  - 27.1: Principles of Gas Chromatography - *CC BY-NC-SA 4.0*
  - 27.2: Instruments for Gas Chromatography - *CC BY-NC-SA 4.0*
  - 27.3: Gas Chromatographic Columns and Stationary Phases - *CC BY-NC-SA 4.0*
  - 27.4: Applications of Gas Chromatography - *CC BY-NC-SA 4.0*
- 28: High-Performance Liquid Chromatography - *CC BY-NC-SA 4.0*
  - 28.1: Scope of HPLC - *CC BY-NC-SA 4.0*
  - 28.2: Column Efficiency in Liquid Chromatography - *CC BY-NC-SA 4.0*
  - 28.3: Instruments for Liquid Chromatography - *CC BY-NC-SA 4.0*
  - 28.4: Partition Chromatography - *CC BY-NC-SA 4.0*
  - 28.5: Adsorption Chromatography - *CC BY-NC-SA 4.0*
  - 28.6: Ion-Exchange Chromatography - *CC BY-NC-SA 4.0*
  - 28.7: Size-Exclusion Chromatography - *CC BY-NC-SA 4.0*
- 29: Supercritical Fluid Chromatography - *CC BY-NC-SA 4.0*
  - 29.1: Properties of Supercritical Fluids - *CC BY-NC-SA 4.0*
  - 29.2: Supercritical Fluid Chromatography - *CC BY-NC-SA 4.0*

- 30: Capillary Electrophoresis and Capillary Electrochromatography - *CC BY-NC-SA 4.0*
  - 30.1: An Overview of Electrophoresis - *CC BY-NC-SA 4.0*
  - 30.2: Capillary Electrophoresis - *CC BY-NC-SA 4.0*
  - 30.3: Applications of Capillary Electrophoresis - *CC BY-NC-SA 4.0*
- 31: Thermal Methods - *CC BY-NC-SA 4.0*
  - 31.1: Thermogravimetry - *CC BY-NC-SA 4.0*
  - 31.2: Differential Thermal Analysis and Differential Scanning Calorimetry - *CC BY-NC-SA 4.0*
- 32: Radiochemical Methods - *CC BY-NC-SA 4.0*
  - 32.1: Radioactive Isotopes - *CC BY-NC-SA 4.0*
  - 32.2: Instrumentation - *CC BY-NC-SA 4.0*
  - 32.3: Neutron Activation Methods - *CC BY-NC-SA 4.0*
  - 32.4: Isotope Dilution Methods - *CC BY-NC-SA 4.0*
- 33: Automated Methods of Analysis - *CC BY-NC-SA 4.0*
  - 33.1: Overview of Automated Methods of Analysis - *CC BY-NC-SA 4.0*
  - 33.2: Flow-Injection Analysis - *CC BY-NC-SA 4.0*
  - 33.3: Other Automated Methods of Analysis - *CC BY-NC-SA 4.0*
- 34: Particle Size Determination - *CC BY-NC-SA 4.0*
  - 34.1: Overview - *CC BY-NC-SA 4.0*
  - 34.2: Measuring Particle Size Using Sieves - *CC BY-NC-SA 4.0*
  - 34.3: Measuring Particle Size by Sedimentation - *CC BY-NC-SA 4.0*
  - 34.4: Measuring Particle Size Using Image Analysis - *CC BY-NC-SA 4.0*
  - 34.5: Measuring Particle Size Using Light Scattering - *Undeclared*
- 35: Appendicies - *CC BY-NC-SA 4.0*
  - 35.1: Evaluation of Analytical Data - *CC BY-NC-SA 4.0*
  - 35.2: Single-Sided Normal Distribution - *CC BY-NC-SA 4.0*
  - 35.3: Critical Values for t-Test - *CC BY-NC-SA 4.0*
  - 35.4: Critical Values for F-Test - *CC BY-NC-SA 4.0*
  - 35.5: Critical Values for Dixon's Q-Test - *CC BY-NC-SA 4.0*
  - 35.6: Critical Values for Grubb's Test - *CC BY-NC-SA 4.0*
  - 35.7: Activity Coefficients - *CC BY-NC-SA 4.0*
  - 35.8: Standard Reduction Potentials & Polarographic Half-wave Potentials - *CC BY-NC-SA 4.0*
  - 35.9: Recommended Primary Standards - *CC BY-NC-SA 4.0*
  - 35.10: Acronyms and Abbreviations - *CC BY-NC-SA 4.0*
- Back Matter - *CC BY-NC-SA 4.0*
  - Index - *CC BY-NC-SA 4.0*
  - Glossary - *CC BY-NC-SA 4.0*
  - Detailed Licensing - *Undeclared*